

U.S. DEPARTMENT OF THE INTERIOR  
U.S. GEOLOGICAL SURVEY

**NATIONAL EARTHQUAKE HAZARDS REDUCTION PROGRAM  
ANNUAL PROJECT SUMMARIES: XXXVI**

**VOLUME I**

Prepared by Participants in

**NATIONAL EARTHQUAKE HAZARDS REDUCTION PROGRAM**

Compiled by

**Muriel L. Jacobson**

The research results described in the following summaries were submitted by the investigators in September 1994 and cover the period from October 1993 through October 1, 1994. These reports include both work performed under contracts administered by the Geological Survey and work by members of the Geological Survey. The report summaries are grouped into the four major goals of the National Earthquake Hazards Reduction Program.

Open File Report No. 95-210

This report has not been reviewed for conformity with U.S. Geological Survey editorial standards or with the North American Stratigraphic Code. Parts of it were prepared under contract to the U.S. Geological Survey and the opinions and conclusions expressed herein do not necessarily represent those of the USGS. Any use of trade, product, or firm names is for descriptive purposes only and does not imply endorsement by the U.S. Government.

The data and interpretations in these progress reports may be reevaluated by the investigators upon completion of the research. Readers who wish to cite findings described herein should confirm their accuracy with the author.

## EARTHQUAKE HAZARDS REDUCTION PROGRAM

### CONTENTS - VOLUME I

#### Goal I - Understanding what happens at the earthquake source

Why and how does a segment of a geologic fault suddenly slip and produce an earthquake? What physical conditions within the Earth control where and when an earthquake occurs?

Aki	1
Andrews	3
Arabasz	4
Beroza	7
Boatwright	13
Boatwright	17
Bohlen	21
Catchings	23
Catchings	25
Chen	27
Chester	31
Clayton	37
Crosson	42
Delaney	47
Dmowska	51
Ebel	58
Ellsworth	64
Forster	71
Gomberg	85
Hall	87
Harris	89
Hartzell	91
Herrmann	95
Herrmann	99
Hickman	101
Hyndman	108
Johnson	122
King, C-Y	126
Logan	131
Marone	134
McMechan	135
McMechan	140
Oppenheimer	144
Pollard	149
Powell	158
Rice	162
Rudnicki	168
Satake	172
Sleep	176

Smalley	179
Smalley	181
Smith	176
Snoke	189
Teng	195
Toksoz	201
Tullis	208
Tworzydlo	216
Williams, C	223

## Goal II - Evaluating the potential of future earthquakes

Where are future earthquakes likely? How large will they be? How often will they occur? When will they occur? Where are future earthquakes unlikely?

Braile	277
Agnew	234
Breckenridge	286
Bucknam	288
Butler	290
Campbell	291
Chiu	307
Clark, M.M	310
Crone	312
Crosson	317
Dreger	319
Endo	329
Engdahl	331
Galehouse	335
Genrich	347
Gephart	352
Gephart	360
Gladwin	364
Guccione	373
Haeussler	386
Hall	389
Harris, J	393
Harty	399
Hauksson	401
Healy	406
Heaton	407
Helmburger	414
Hengesh	417
Hildenbrand	428
Hill	432
Hill	435
Hoffman	437

Holt . . . . .	440
Howard . . . . .	446
Hudnut . . . . .	449
Jachens . . . . .	451
Jachens . . . . .	454
Jacoby . . . . .	455
Jacoby . . . . .	459
Jensen . . . . .	462
Jibson . . . . .	463
Johnston, M.J.S. . . . .	465
Kanamori . . . . .	476
Kanamori . . . . .	479
Keaton . . . . .	481
Kelson . . . . .	483
Kelson . . . . .	486
Klein . . . . .	489
Kulm . . . . .	493
Lahr . . . . .	503
Lajoie . . . . .	510
Langbein . . . . .	514
Langbein . . . . .	522
Lay . . . . .	526
Lee . . . . .	534
Li . . . . .	536
Lienkaemper . . . . .	545
Lisowski . . . . .	547
Machette . . . . .	557
Madin . . . . .	560
Malone . . . . .	561
Mann . . . . .	564
McCrory . . . . .	571

# **Southern California Earthquake Center**

## **Cooperative Agreement 14-08-0001-A0899**

**Keiiti Aki**  
**Southern California Earthquake Center**  
**University of Southern California**  
**Los Angeles, CA 90089-0740**  
**e-mail: aki@coda.usc.edu**

### **Program Element: Southern California**

The Southern California Earthquake Center research program and many of its intellectual activities are structured around eight disciplinary working groups. These groups and their leaders are:

- A) Master Model Construction (Keiiti Aki, USC)
- B) Ground Motion Prediction (Steve Day, San Diego State)
- C) Earthquake Geology (Kerry Sieh, Caltech)
- D) Subsurface Imaging and Tectonics (Robert Clayton, Caltech)
- E) Crustal Deformation (Duncan Agnew, UCSD)
- F) Seismicity and Source Processes (Egill Hauksson, Caltech)
- G) Physics of Earthquakes (Leon Knopoff, UCLA)
- H) Engineering Applications (Geoff Martin, USC)

Group A guides development of the master model and integrates the results from the other seven groups. Group H provides an interface between earth scientists and geotechnical engineers. The addition of this group to the center following a major grant from the California Department of Transportation and City and County of Los Angeles has provided the first links between center scientists, earthquake engineers, and our user community.

During the 1993 annual meeting, the center agreed on the following tasks for the 1994 research effort:

- Task 1: First generation maps of probabilistic seismic hazard analysis for southern California.
- Task 2: Plausible future earthquake scenarios with emphasis on the Los Angeles Basin.
- Task 3: Fundamental studies on seismogenic structures, earthquake dynamics and recurrence, to develop physical basis for the hazard master model constructed in Task 1.
- Task 4: Intermediate-term earthquake prediction.
- Task 5: Real time earthquake information.
- Task 6: Response to future earthquakes.

As a major accomplishment in Task 1, we have completed the Phase II report titled "Seismic Hazards in Southern California: Probable Earthquakes, 1994-2024" and submitted to the Bulletin of Seismological Society of America. We have responded to the Northridge earthquake by coordinating post-earthquake research under Task 6. A major accomplishment in Task 2 in this year was a consensus report on earthquake potentials in

the greater Los Angeles Metropolitan area by a group of geologists to be published shortly in Science. We also recently successfully completed the Los Angeles Region Seismic Experiment (LARSE) as a part of Task 3. How the multi-disciplinary approach of SCEC is working this year can be seen in the task-discipline matrix of funding shown below.

**SCEC 1994 Discipline Task Matrix for Science and Northridge Response  
(in thousands)**

	Group A	B	C	D	E	F	G	Sub-Total
Task 1	158	14	134	28	28			362
Task 2	43	215	108	24	45		32	467
Task 3	173	11	223	447	54	138	83	1,129
Task 4	55					10	36	101
Task 5	3			7	14	57		81
Task 6	35	80	22		132	446		715
Sub-Total	467	320	487	506	273	651	151	2,855

Consistent with the six key tasks developed at SCEC, the education and knowledge transfer functions of the Center link it with a wide spectrum of audiences and user groups.

The goal of SCEC is to integrate research findings from various disciplines in earthquake-related science to develop a prototype probabilistic seismic hazard model (master model) for southern California. During the first three years, we made considerable progress in developing both methodology and prototype products. The 1992 Landers/Big Bear earthquakes, early in our second year, helped provide a research focus and accelerate work toward our goal.

The Phase II report is, in effect, the center's first generation master model. It addresses earthquake source characterization in southern California. The report integrates information from paleoseismic, GPS-derived geodetic and regional seismicity data to develop a regional model of earthquake hazard potential. For this purpose, we divided southern California into 65 source zones, and integrated the above three data sources in terms of the seismic moment rate which can be evaluated from the three data sources independently. In fact, the recent Northridge earthquake occurred in a source zone which ranked at the top 13% of the whole of southern California in the seismic moment rate per unit area. The zone, in which the Northridge earthquake occurred, had recent seismic activity (San Fernando in 1971), a high rate of strain accumulation observed by GPS, and the active faults geology group working for the Phase II report assigned a maximum magnitude of earthquake in this zone to be 6.7.

The next target in Task 1 is the Phase III report, in which we shall include the propagation path and local site effects in the probabilistic seismic hazard analysis. We have organized 5 subgroups responsible for each chapter of the Phase III report, and each subgroup has already started working.

## Modeling Fault Slip

9960-10296, 9960-12296

D. J. Andrews

Branch of Earthquake Geology and Geophysics  
U.S. Geological Survey  
345 Middlefield Road, MS 977  
Menlo Park, California 94025  
(415) 329-5606

Program elements I.2, II.4

### INVESTIGATIONS

Modeling geologic deformation rates in the San Francisco Bay region

### RESULTS

I modified a finite element program in order to calculate models of long-term geologic deformation in the San Francisco Bay region. Major strike-slip faults can be prescribed in the finite element mesh as slip surfaces having a small coefficient of friction. The upper crust is not elastic but is treated as a layer of sand; it has a Coulomb yield condition with a larger coefficient of friction than do the major faults. Yielding simulates faulting on unmodeled faults, in particular, dip slip in strike-slip stepovers.

To achieve this objective I modified Jay Melosh's finite element code, Tecton. I preserved the same input and output, so that my modification is accessible to an existing body of users. I solve for stress equilibrium by explicit iteration rather than by matrix inversion. The reason for this fundamental change is to be able to introduce nonlinear rheologies easily.

In the coming year the model will be fit to geologic fault slip rates in the San Francisco Bay region, and it can provide an interpolation of those rates. Geometric complications in the strike-slip fault system, such as bends and stepovers, will produce yielding, which will be interpreted as faulting on subsidiary faults. In this way the geometry of the major faults will be used to predict locations of blind thrust faulting.

### REPORT

D. J. Andrews, 1994, Modeling tectonic deformation with yielding in the upper crust (abstract): EOS Transactions AGU, vol. 75, p. 681.

## Regional Seismic Monitoring Along The Wasatch Front Urban Corridor And Adjacent Intermountain Seismic Belt

1434-92-A-0966

W. J. Arabasz, R. B. Smith, J. C. Pechmann, and S. J. Nava

Department of Geology and Geophysics

University of Utah

Salt Lake City, Utah 84112

(801) 581-6274

### Investigations

This cooperative agreement partially supports the operation of the University of Utah's 100-station telemetered regional seismic network. USGS support focuses on the seismically hazardous Wasatch Front urban corridor of north-central Utah, but also encompasses neighboring areas of the Intermountain Seismic Belt. Primary products for this USGS support are quarterly bulletins, periodic earthquake catalogs, and the services of a regional earthquake recording and information center.

### Results (October 1, 1993 - September 30, 1994)

**General accomplishments.** During the report period, significant efforts related to:

(1) continued fine tuning of data acquisition and analysis software, including local modifications to autopicking software ("cpick", developed by University of Washington and U.S. Bureau of Reclamation); (2) continued upgrading of field equipment at stations that have been operating since the mid-1970's, including the implementation of a new temperature-compensated solar regulator; (3) implementation of public access to local earthquake information via Internet, including: (a) the listing of recent earthquakes locations using the command "finger quake@eqinfo.seis.utah.edu", (b) anonymous ftp access to earthquake catalogs for the Utah region on the machine ftp.seis.utah.edu, and (c) a local Mosaic server on the World Wide Web (<http://www.seis.utah.edu>) including information about the seismograph network, seismicity maps, and general earthquake information; (4) replacement of local paper recording of Wood-Anderson records at station DUG by use of USNSN data from DUG to determine local magnitudes; and (5) extended operation of six temporary telemetered stations and four portable digital seismographs in and around the source region of a  $M_w$  5.9 earthquake which occurred near the Idaho-Wyoming border in SE Idaho on February 3, 1994, just north of our region of monitoring responsibility.

**Network Seismicity.** Figure 1 shows the epicenters of 1,928 earthquakes ( $M_c < 4.7$ ) located in part of the University of Utah study area designated the "Utah region" (lat.  $36.75^{\circ}$  -  $42.5^{\circ}$ N, long.  $108.75^{\circ}$ - $114.25^{\circ}$ W) during the period October 1, 1993 to September 30, 1994. The seismicity sample includes 35 shocks of magnitude 3.0 or greater and 9 felt earthquakes. The largest earthquake to occur within the Utah region proper during the report period was a shock of  $M_c$  4.7 on September 6, 1994 (03:48 UTC), located 7 miles south of Circleville, in central Utah. Approximately half of the seismicity detected during the report period was associated with areas of ongoing coal-mining-related seismicity, located within 60 km radius of

Price in east-central Utah (820 shocks,  $0.9 \leq M \leq 3.3$ ).

On February 3, 1994, the  $M_w$  5.9 Draney Peak, Idaho, earthquake occurred near the Idaho-Wyoming border in a "gap" between three regional seismograph networks operated respectively by the Idaho National Engineering Laboratory, the U.S. Bureau of Reclamation, and the University of Utah. The University of Utah responded to the earthquake, deploying a 10-station, temporary network to record aftershocks. Supplemental monitoring equipment was borrowed from IRIS, the University of Memphis, and the U.S. Bureau of Reclamation. During the five months following the mainshock, over 3200 aftershocks were recorded, including three with magnitudes greater than 5.0 (Figure 2).

The mainshock had a normal-faulting mechanism and occurred in a region of complex subsurface geology involving the superposition of basin-range extension upon Cretaceous-early Tertiary thrustbelt structure. No surface rupture has been observed. Despite proximity to the active west-dipping Star Valley normal fault, preliminary data appear to restrict the earthquake sequence to some unknown structure on the hangingwall side of the Star Valley fault (Figure 2). The mainshock was preceded by foreshocks as large as  $M_L$  4.7 and has been followed by the most energetic aftershock sequence (relative to the size of the mainshock) ever observed instrumentally in the Intermountain Seismic Belt.

## Reports and Publications

- Arabasz, W.J. (1994). Idaho-Wyoming Border Area Jolted, *EERI Newsletter*, 10, no. 3, 7.
- Arabasz, W.J., J.C. Pechmann, S.J. Nava, and R.B. Smith (1994). The Magnitude ( $M_w$ ) 5.8-5.9 Earthquake in SE Idaho of February 3, 1994, and Associated Shocks, *University of Utah Seismograph Stations Preliminary Earthquake Report*, 5 p.
- Nava, S.J., W.J. Arabasz, and J.C. Pechmann (1994). The  $M$  5.9 Draney Peak Idaho (Idaho-Wyoming border) Earthquake of February 3, 1994—A preliminary report (abstract), Seismological Society of America, *Late Abstracts for the 1994 Meeting*, Pasadena.
- Pechmann, J.C., W.J. Arabasz, and S.J. Nava (1994). Refined analysis of the 1992  $M_L$  5.8 St. George, Utah, earthquake and its aftershocks (abstract), *Seismological Research Letters* 65, 32.
- Nava, S.J. (1994). Earthquake Activity in the Utah Region, July 1 - September 30, 1993, *Fault Line Forum (Utah Geological Survey)* 10, no. 1, 8.
- Nava, S.J. (1994). Earthquake Activity in the Utah Region, July 1 - September 30, 1993, *Fault Line Forum (Utah Geological Survey)* 10, no. 2, 8.
- Nava, S.J., W.J. Arabasz, and J.C. Pechmann (1994). The  $M$  5.9 Draney Peak, Idaho Earthquake of February 3, 1994—A preliminary report, *Fault Line Forum (Utah Geological Survey)* 10, no. 1, p. 5-6.
- Nava, S.J., (1994). Earthquake Activity in the Utah Region January 1, 1993 - June 30, 1993, *Survey Notes (Utah Geological Survey)* 26, no. 2, 3.
- Nava, S.J., (1993). Earthquake Activity in the Utah Region January 1, 1993 - June 30, 1993, *Wasatch Front Forum (Utah Geological Survey)* 9, no. 3-4, p. 2-3.
- Nava, S.J., (1993). Earthquake Activity in the Utah Region, July 1 - December 31, 1992, *Survey Notes (Utah Geological Survey)* 26, no. 1, p. 26-27.

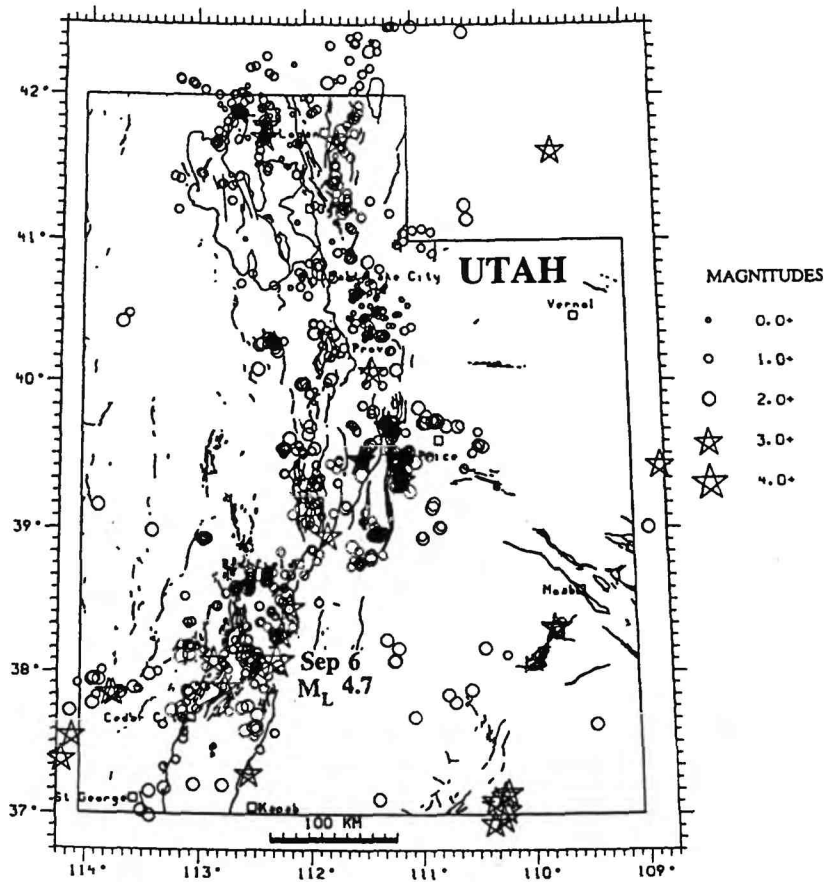


**Figure 1.** Earthquakes in the Utah Region, October 1, 1993 through September 30, 1994. Shocks of magnitude 3.0 and larger are plotted as stars, those less than magnitude 3.0 as circles.

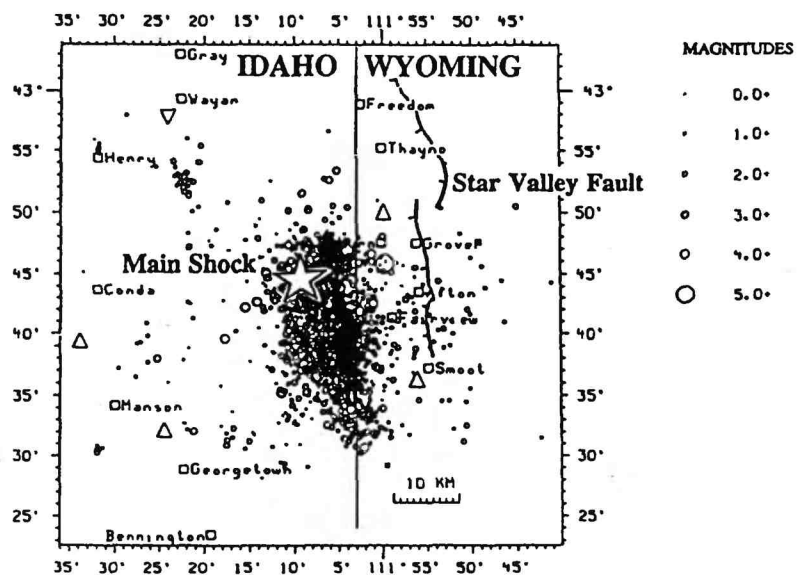


**Figure 2.** Preliminary epicenter map of the February 3, 1994 M<sub>W</sub> 5.9 Draney Peak, Idaho, earthquake sequence (circles scaled by magnitude) for the five months following the main shock. The seismicity appears too shallow to have occurred on a downdip projection of the active Star Valley normal fault.

# Modeling Loma Prieta Strong Ground Motion Using Interpolated Empirical Green's Functions

Grant Number 1434-93-G-2312

Greg Beroza  
Brian Cohee  
Department of Geophysics  
Stanford University  
Stanford, CA 94305-2215  
beroza or brian@pangea.stanford.edu

ELEMENT I.2

## Investigations

At high frequency ( $>1$  Hz), theoretical Green's functions are too inaccurate to allow either recovery of short-wavelength earthquake rupture characteristics or forward-prediction of high frequency ground motion from a known source. In principle, theoretical Green's functions can be computed to high frequency using complex 3D models, but in practice the velocity structure is not known with enough detail to produce an accurate result. Empirical Green's functions (corrected small earthquake seismograms) include the high-frequency Earth response, but are difficult to use directly as Green's functions because they sample the source volume unevenly, have variable mechanisms, and finite source dimensions.

One method for addressing these difficulties is an interpolation technique that accounts for known variations in location, mechanism, and magnitude (Spudich and Miller, *BSSA*, 1990). In this method the site transfer-function is represented as a time-varying response with simple dependencies on azimuth and incidence angle.

We find the site response for an incident *S*-wave and use cross-validation to quantify the model's ability to predict missing data. If the cross-validation test shows the model can reliably predict missing seismograms, we can calculate the response of point sources with arbitrary mechanism and location within the aftershock volume and use the interpolated Green's functions to study high frequency ground motion during the mainshock.

## Results

### *Loma Prieta Aftershock Data*

We apply the method to aftershocks of the 1989 Loma Prieta earthquake recorded at five strong-motion sites that also recorded the mainshock:

- KOI - Corralitos (107 aftershocks)
- SAR - Saratoga (73 aftershocks)
- GA2 - Gavilan College, Gilroy (27 aftershocks)
- DMD - Anderson Dam, Downstream (35 aftershocks)
- CAP - Capitola (24 aftershocks).

The station and aftershock locations are shown in Figure 1. The number of aftershocks available at each station is limited by deployment duration, the low *snr* of small events, and the subset occurring on or adjacent to the mainshock fault plane. At each site seismometers were deployed adjacent to a strong-motion accelerometer. Three components recorded both ground velocity (L-22D 2-Hz geophone) and acceleration (FBA-13 accelerometer). We use the smaller ( $M < 4$ ) well-recorded aftershocks, and

bandpass filter the seismograms with corners at 0.2 and 3.0 Hz. The corner frequencies of these aftershocks should be well above the 3.0 Hz corner, which should minimize source-finiteness effects. The high-pass corner at 0.2 Hz is used to minimize integration noise. The band-limited character of the recording instrument also attenuates signal at frequencies below 1.0 Hz. The data are integrated to displacement, and aligned on the S-wave arrival.

### *Evaluating Models Using Cross-Validation*

We define a good model as one capable of predicting missing data, and use delete-one cross-validation to quantify this property. The ability to predict missing data is the best measure of the usefulness of the interpolation method. Using cross-validation, each datum is removed from the set, the system is solved and a prediction is made from the model for the absent datum. In our case we delete one seismogram at a time from the data used in the inversion and measure the misfit between the model prediction and the missing waveform. When comparing the two vectors model prediction ( $s$ ) with data ( $d$ ), we define the misfit:

$$\left( \frac{\sum_{i=1}^n (d_i - s_i)^2}{\sum_{i=1}^n d_i^2 + \sum_{i=1}^n s_i^2} \right)^{\frac{1}{2}}$$

which varies from 1.4 (anti-correlated) to 0 (perfect fit).

### *Green's Function Interpolation*

Repeated aftershocks occurring in the same location with the same focal mechanism (e.g. doublets) produce seismograms that are identical, even at high-frequencies. This reproducibility underscores the ability of empirical recordings to characterize the Earth's response to an earthquake source. In practice, aftershocks unevenly sample the fault plane and have varied mechanisms. Given the aftershock and station coordinates, the fault mechanism and magnitude, and a layered velocity model, it is possible to correct the recorded seismogram and theoretically remove these effects. Once this correction is made, the common features of the seismograms should be evident.

We used an approach developed by Spudich and Miller (*BSSA*, 1990). Each horizontal component at each seismic station is treated separately. The S-wave arrival and coda is windowed and corrected for source mechanism, magnitude and travel-time. In the inverse problem, a time-varying transfer-function (model) is found having  $\cos\theta$  and  $\cos 2\theta$  dependencies on azimuth and incidence angle. The description of the transfer-function can vary; multi-scatterer models include the effect of neighboring heterogeneity, a single-scatterer model solves for site-response only.

We find that multi-scatterer models have many degrees of freedom and fit the data very well; however, these models fail to predict data not included in the inversion. In order to increase the stability, we reduced the model complexity and defined only one scatterer located at the site. The single-scatterer models are less complex and fit the data appreciably worse. They also do poorly in the cross-validation test. Example data and predicted seismograms are shown in Figure 2, and the cross-validation results are summarized in Figure 3. Thus, the ability of the interpolated seismograms to accurately predict Green's functions for point sources with arbitrary mechanism and location is suspect.

We examined residuals to determine why some aftershocks are predicted by the model and others are not. Errors in the focal mechanism or aftershock locations are examples of effects that might cause problems in the modeling. We did not find any significant trends that could be correlated with the aftershock source parameters or their location in the fault zone. Thus we attempted to isolate the site effects using a different approach.

### ***Isolating Site Effects Using SVD Reconstruction***

To isolate site response from source and path effects, we performed a singular value decomposition (SVD) of the data seismograms. All recordings for one component at a station are gathered in a matrix. The row dimension is the number of points in the seismogram, and the column dimension is the number of aftershocks. After computing the SVD of this waveform matrix, we use an F-test of significance, or a fixed percentage of the largest singular value, to retain only the largest singular values in a partial reconstruction of the original seismograms.

The common features of the data (presumably the site response) are contained in the largest singular values. These are retained in the reconstruction. Dissimilar properties of the seismograms are discarded. Using the simplified data, it is possible to predict missing data and produce a satisfactory cross-validation result using the site-only transfer-function (see Figures 2 and 3); however, because the data contain only a fraction of the original aftershock complexity, their utility for modeling the mainshock data is greatly diminished.

### **Conclusions**

The site model fits the data reasonably well, but does a poor job of predicting missing seismograms in the cross-validation analysis. SVD reconstruction emphasizes the site-response and suppresses source and path effects, allowing an improved cross-validation result, but does this at the expense of useful interpolations. Two possible explanations for these results are that the quantity of data is insufficient to characterize the site, and uncertainties in the source parameters degrade model resolution. However, our residual analysis suggests it is more likely that uncorrelated path effects are important, or that the model is an inadequate representation of the site response. In summary we find *i*) cross-validation is a useful tool for testing models, *ii*) a simple site response model is inadequate for Green's function interpolation with this data, *iii*) SVD reconstruction is an easy method to isolate common effects associated with the site response.

### **References**

Spudich P. and D.P. Miller (1990). Seismic site effects and the spatial interpolation of earthquake seismograms: results using aftershocks of the 1986 North Palm Springs, California, earthquake, *Bulletin Seismological Society of America*, 80, 1504-1532.

### **Reports**

Cohee, B.P., G.C. Beroza and D.A. Dodge (1994). Modeling Loma Prieta strong motion seismograms with interpolated empirical Green's functions, *EOS Transactions AGU*, 75.

Cohee, B.P. and G.C. Beroza (1994). A comparison of two methods for earthquake source inversion using strong-motion seismograms, in *Earthquake Source Mechanics, Annali di Geofisica*, Istituto Nazionale di Geofisica, Rome (in press).

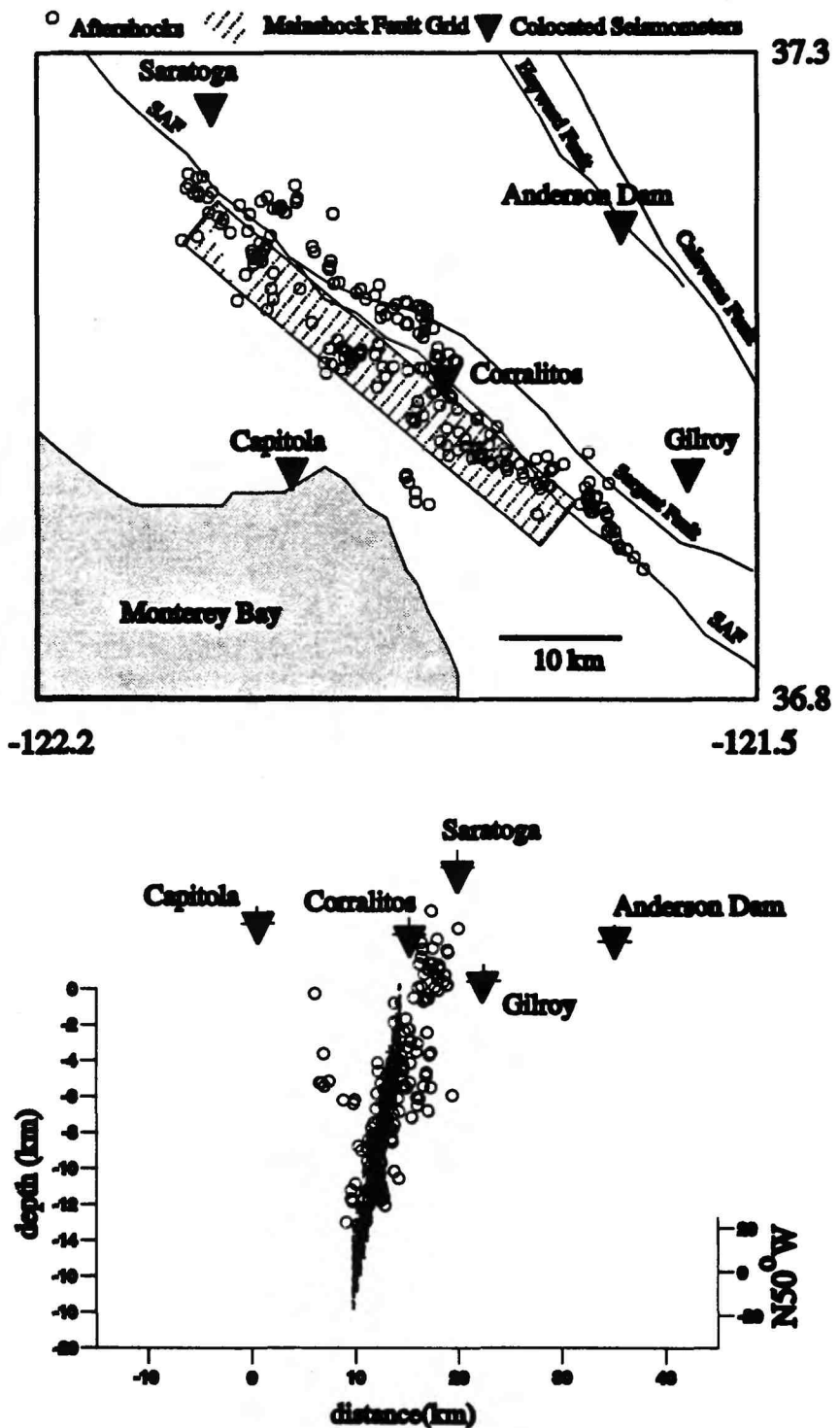
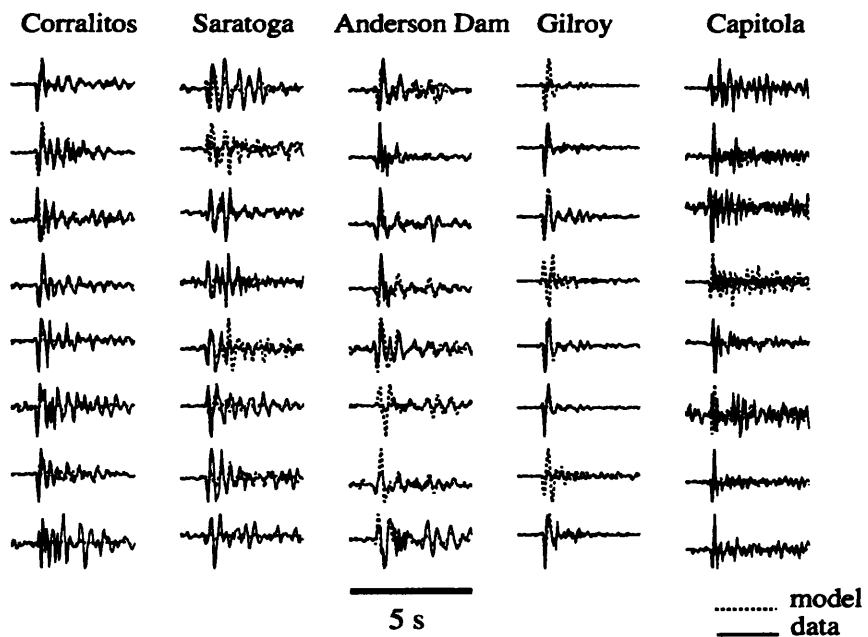


Figure 1. Map (top) and cross-section (bottom) views of the seismometer and aftershock locations.

### Prediction using complete data



### Prediction using reconstructed data

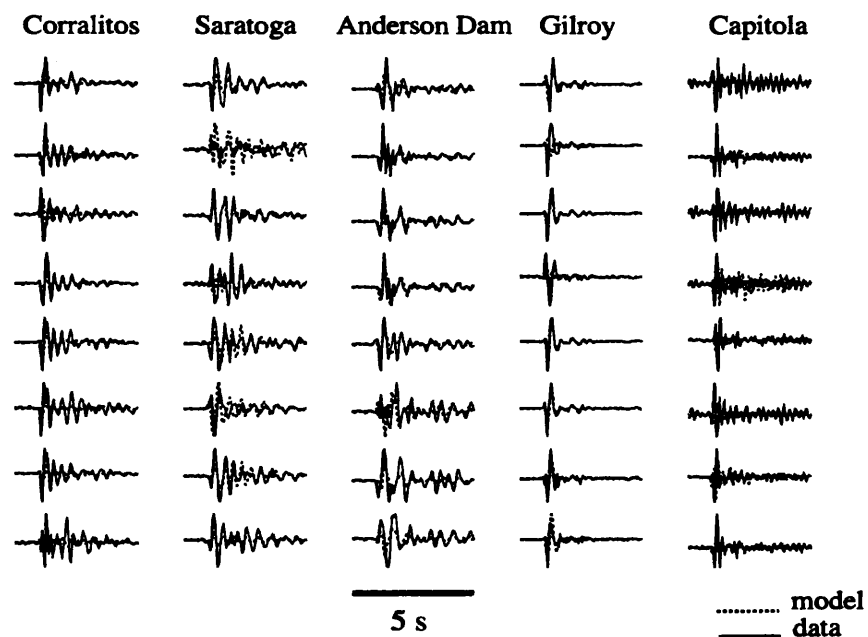


Figure 2. Selected horizontal displacement aftershock seismograms. All eigenvalues are retained in the *top* panel. The *bottom* panel shows the reconstructed data using only the largest eigenvalues.

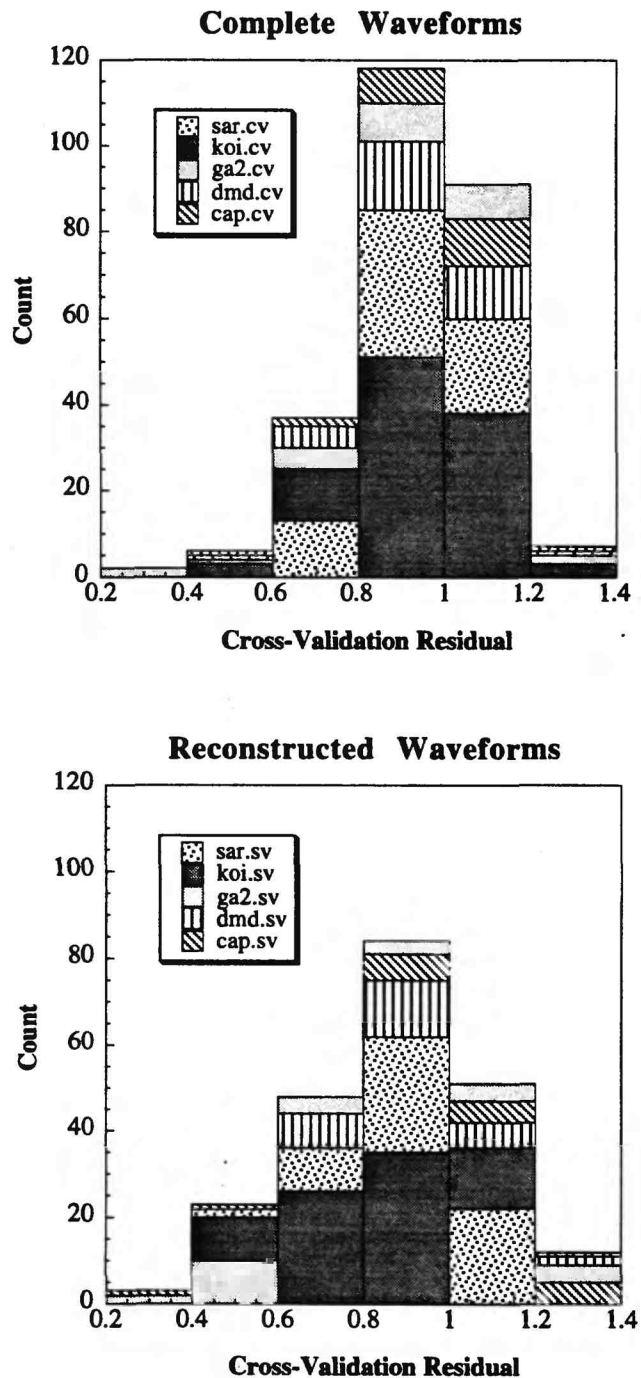


Figure 3. Histograms showing cross-validation residuals obtained using complete waveforms (top) and partially reconstructed waveforms (bottom) obtained using the largest singular values.

# FRICTIONAL CONSTRAINTS ON CRUSTAL FAULTING

9930-10343

John Boatwright

Branch of Seismology  
 U.S. Geological Survey  
 345 Middlefield Road, MS 977  
 Menlo Park, California 94025  
 (415) 329-5609, BOAT@samoawr.usgs.gov

## Objectives

The goal of this project is to devise a 2D numerical method for modelling the entire seismic cycle that encompasses both dynamic rupture processes and quasi-static interseismic slip. An ancillary goal is to determine appropriate constitutive laws and ranges for the constitutive parameters of the model by analyzing the phenomenology (microseismicity, dynamic slip distributions, aftershocks, and interseismic slip) of crustal faulting.

## Results

Boatwright and Cocco (1995) proposed a comprehensive frictional model for crustal faulting that uses the state and rate-variable constitutive law. Their faulting model generally resembles the asperity model proposed by Kanamori (1981), but emphasizes the coupling of the asperity to the surrounding weak-seismic and compliant fault areas through the process of rapid afterslip. They test this model using the microseismicity and geodetic data presented by Oppenheimer et al. (1992), concluding that weak-seismic zones can inhibit or stop dynamic rupture, that compliant zones can have aftershocks but not foreshocks or interseismic activity, and that aftershocks can occur on the main shock rupture area through a reloading process associated with rapid aseismic slip outside the dynamic rupture area. These “reloaded” aftershocks are evident in Figure 1, which shows the response of a set of spring sliders to a load with an abrupt onset which continues to grow for 30 days, tapering to a constant value.

In August, 1994, both Paul Okubo and Massimo Cocco visited Menlo Park for an extended collaboration. During their visits, we were able to program the dynamic part of the 2D numerical method. We have incorporated a simple Runge-Kutta solution of the non-linear constitutive law directly into the boundary integral code of Boatwright and Quin (1986). The solution of the constitutive law at the vertex of the causality

cone in the Hamano technique is equivalent to solving the spring slider without inertia: consequently, the algorithm is unstable for either a state variable law with velocity-independent friction for steady-state sliding (Dieterich, 1978) or velocity-strengthening friction (Weeks, 1992) at high slip velocity. To stabilize the Runge-Kutta algorithm, we simply limit the slip velocity: we intend to thoroughly test this modification for its dynamic appropriateness.

At the present time, the rupture is initiated on 8 grid points by setting the initial friction and velocity values for these points equal to those of a spring slider at the initiation of dynamic failure. The friction drops on these "nucleation" points in  $t = 5\Delta t$ . By  $t = 12\Delta t$ , the rupture begins to extend beyond the nucleation zone, and by  $t = 30\Delta t$ , it has accelerated to the Rayleigh-wave speed in the in-plane direction. As the rupture continues to grow, the interior of the fault continues to slip. In general, this slip is smooth, but there are some secondary slip accelerations that may result from the discretization of the rupture front in the numerical solution.

## References

- Boatwright, J., and H. Quin (1986). The seismic radiation from a 3-D dynamic model of a complex rupture process. Part I: confined ruptures, *Earthquake Source Mechanics*, Maurice Ewing Series, **6**, edited by S. Das, J. Boatwright, and C.H. Scholz, AGU, Washington, D.C., 97-109.
- Dieterich, J.H. (1978). Time dependent friction and the mechanics of stick slip, *Pure and Appl. Geophys.*, **116**, 790-806.
- Kanamori, H. (1981). The nature of seismicity patterns before large earthquakes, in *Earthquake Prediction - An International Review*, Maurice Ewing Series, **4**, edited by D. Simpson and P.G. Richards, AGU, Washington, D.C., 1-19.
- Oppenheimer, D.H., W.H. Bakun, and A.G. Lindh (1990). Slip partitioning of the Calaveras fault, California, and prospects for future earthquakes, *J. Geophys. Res.*, **95** B6, 8483-8498.
- Weeks, J.D. (1993). Constitutive laws for high-velocity frictional sliding and their influence on stress drop during unstable slip, *J. Geophys. Res.*, **98**, B10, 17637-17648.

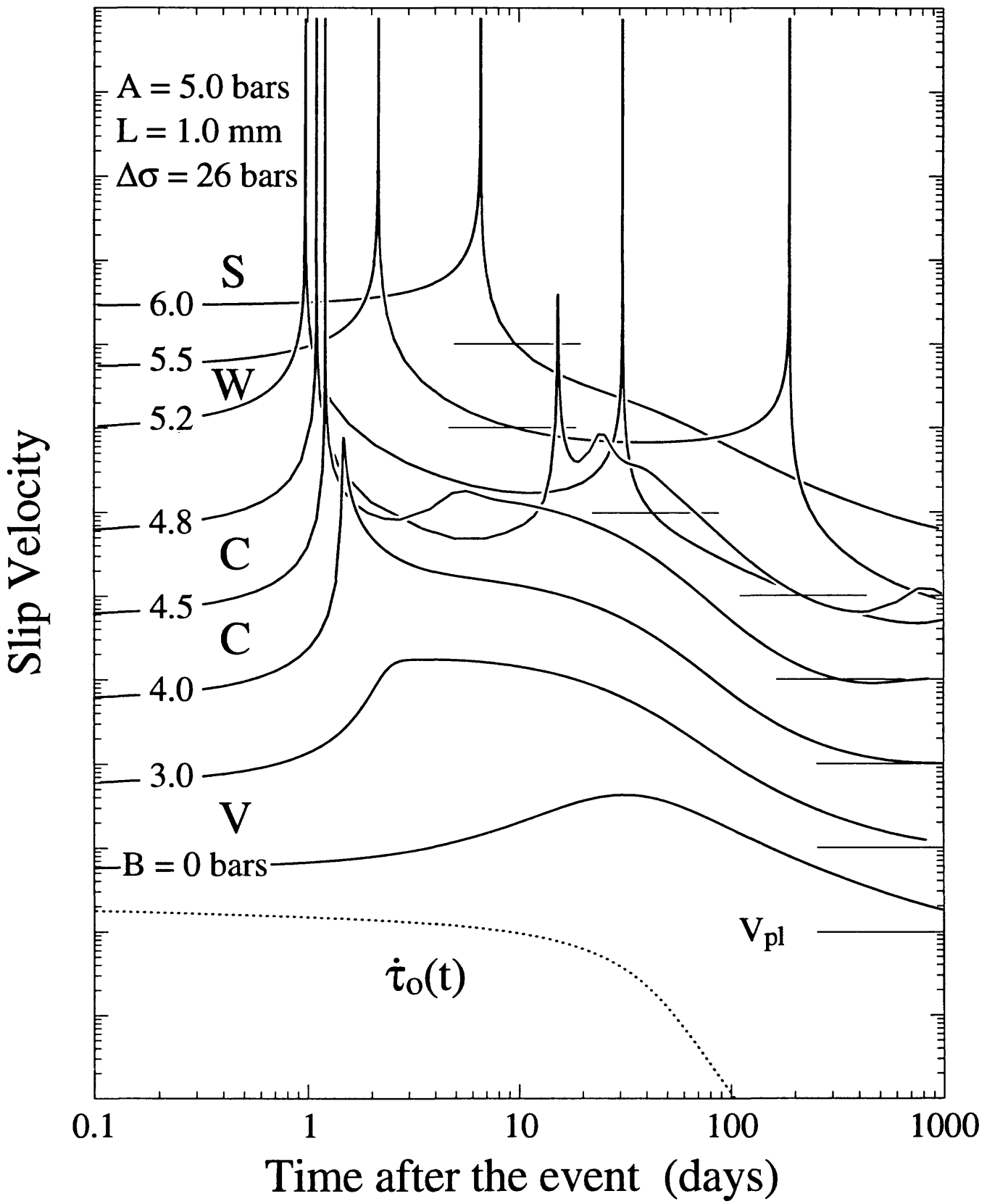
## Products with Director's Approval in FY 1994

- Boatwright, J. and M. Cocco, 1995, Frictional constraints on crustal faulting, submitted to *J. Geophys. Res.*

## Figure Captions

Figure 1. Spring slider responses for an abruptly applied and continued load, reprinted from Boatwright and Cocco (1995). The load rate  $\dot{\tau}_o$  grows for 30 days, after which it tapers to a constant value.  $A = 5.0$  bars,  $L = 1$  mm, and  $k = 0.05$  bars/mm. The slider velocities are offset by a decade: the thin horizontal lines indicate the common plate velocity  $V_{pl}$ . The curves labelled W refer to the weak-seismic sliders ( $B > A$ ) for which  $B = 5.5$  and 5.2 bars. The secondary instabilities for these weak sliders are the “reloaded” aftershocks. The “weakest” of the compliant sliders (that is, the  $B = 4.8$  bar slider) exhibits a secondary slip episode, but doesn’t accelerate to dynamic instability. The  $B = 4.5$  and 4.0 bar compliant sliders show broad pulses of accelerated afterslip instead of the “reloaded” accelerated slip events of the weak sliders.

# Spring Slider Models for Afterslip and Aftershocks



# GROUND MOTION MAPS FOR LARGE EARTHQUAKES ANTICIPATED FOR THE BAY AREA

**9930-12343**

John Boatwright, Linda C. Seekins, and Leif Wennerberg

Branch of Seismology  
U.S. Geological Survey  
345 Middlefield Road, MS 977  
Menlo Park, California 94025  
(415) 329-5609, BOAT@samoa.wr.usgs.gov  
(415) 329-5661, SEEKINS@samoa.wr.usgs.gov  
(415) 329-5659, LWENNERBERG@isdmnl.wr.usgs.gov

## Objectives

This project encompasses the seismological research necessary for calculating scenario maps of ground motion and damage for large earthquakes that have been anticipated for the Bay Area. The range of critical research topics includes source scaling and directivity, near-fault amplification of ground motion, regional propagation characteristics, site amplification, and the relation of structural damage to ground shaking.

## Results

1. Margheriti, Wennerberg, and Boatwright (1994) analyzed site response in the South Bay, comparing S-wave and coda techniques. They correlated these results with the surficial geology, and with the amplification factors determined by Borcherdt and Glassmoyer (1993) for the set of four rock types (hard and soft rock, alluvium and bay mud). They conclude that for sites in sedimentary basins, the relative amplifications obtained from the direct S-waves underestimate the relative amplifications obtained from the coda waves. In general, the coda samples provide a better estimate of the relative amplification observed from 20 s recordings of the main shock than do short windows of the direct S-waves.

2. Boatwright (1994) has developed a source model for mapping seismic hazard that incorporates source scaling, source finiteness, and directivity. An initial description and analysis of this model was presented at the ATC-35 talks. A version of this model has now been used to fit the damage from the 1983 Morgan Hill and 1989 Loma Prieta earthquakes, in a collaborative work with Jeanne Perkins of ABAG. The Loma Prieta

damage is best fit using a rupture velocity of  $0.85\beta$  to the northwest, combined with an amplification at 75 to 95 km associated with the coherence arrival of waves reflected from the Moho.

3. Seekins and Boatwright (1994) have transferred their results on the relation of geology to site amplification in San Francisco into a poster of the City of San Francisco showing areas of relative seismic risk, by superimposing a simplified (four color) geologic map onto a high altitude photograph of the city. The poster is being prepared by Stuart Allen, of Allen Cartography in Medford, Oregon. We are presently negotiating with BWTR to have this poster published as a Department of Interior Special Publication.

4. Wennerberg (1995) has analyzed aftershock recordings to test Chin and Aki's (1991) assertion of "pervasive non-linear effects" in the recordings of the Loma Prieta earthquake, and concluded that their assertions are unjustified for all but one of the stations for which he was able to obtain aftershock recordings from co-located instruments. Figure 1 shows the results of his analysis as corrections to Chin and Aki's (1991) inferences of non-linearity.

## References

- Chin, B.-H. and K. Aki, 1991, Simultaneous study of the source, path, and site effects on strong ground motion during the Loma Prieta earthquake: a preliminary result on pervasive nonlinear effects, *Bull. Seismol. Soc. Am.* 81, 1859-1884.
- Seekins, L.C., and J. Boatwright, 1994, Ground motion amplification, geology, and damage in the city of San Francisco from the 1989 Loma Prieta earthquake, *Bull. Seismol. Soc. Am.*, 84, 16-30.

## Products that received Director's approval in FY94:

- Margheriti, L., L. Wennerberg, and J. Boatwright, 1994, A comparison of coda and S-wave spectral ratio as estimates of site response in the southern San Francisco bay area, *Bull. Seismol. Soc. Am.*, in press.

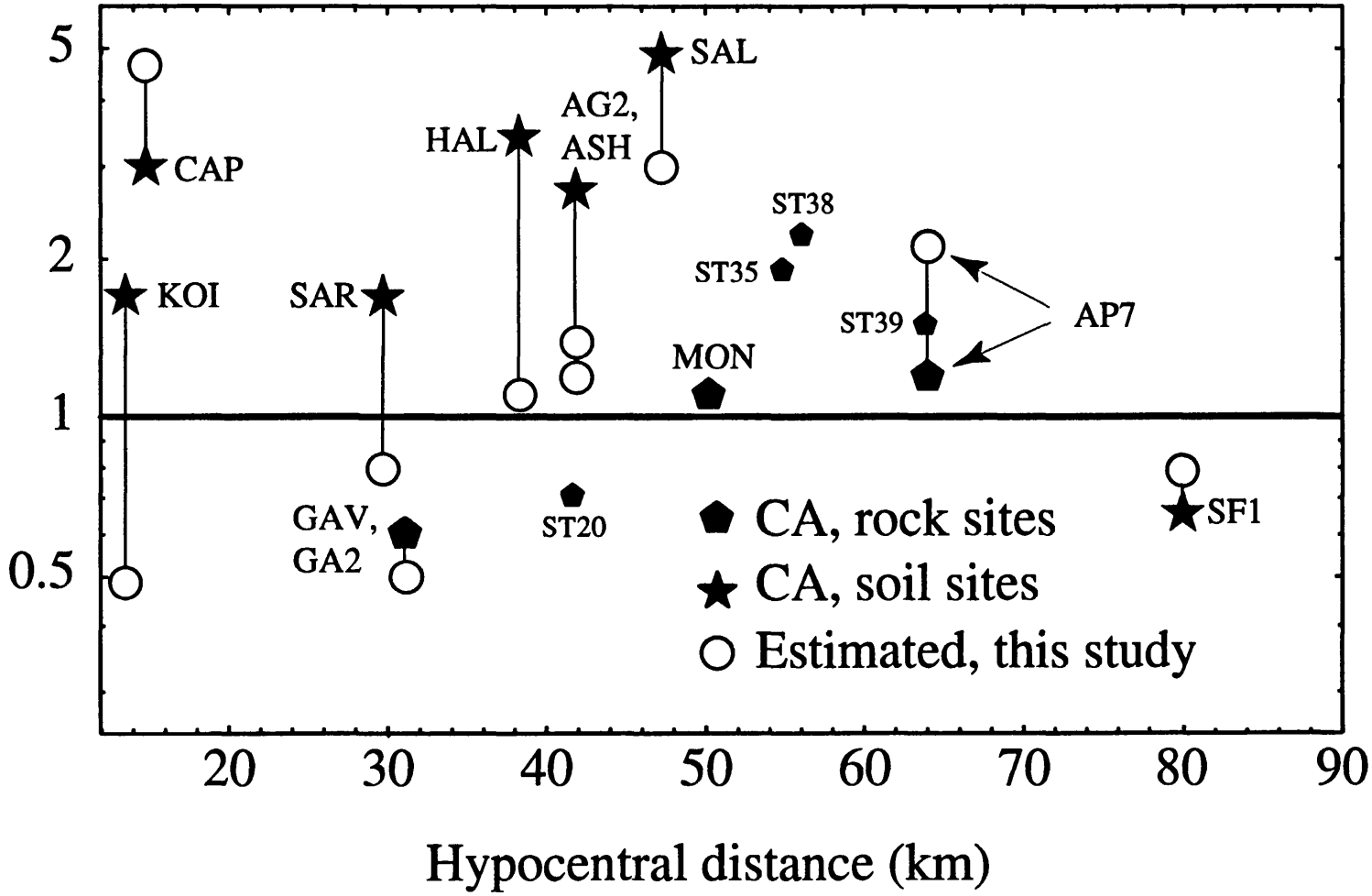
- Boatwright, J., 1994, Calculating ground motions in the near-field of rupturing faults, ATC-35.

- Wennerberg, L., 1995, Comment on "Simultaneous study of the source, path, and site effects on strong ground motion during the Loma Prieta earthquake: a preliminary result on pervasive nonlinear effects" by Byau-Heng Chin and Keiti Aki, submitted to *Bull. Seismol. Soc. Am.*

## Figure Caption

Figure 1. Ratios of estimated peak accelerations to observed peak accelerations. Solid symbols are from Chin and Aki's (1991) modeling. Open symbols are estimates from random vibration theory using spectral ratios obtained from aftershock cudas, and assuming that the site amplification of MON estimated by Chin and Aki was appropriate. Chin and Aki (1991) overestimate the peak accelerations at station KOI, SAR, HAL, ASH, and SAL. Only station CAP remains consistent with the interpretation of significant non-linearity. No aftershock data are available for the rock sites ST20, ST35, ST38 and ST39: these stations presented for comparison with AP7 and SAL. ST38 and ST39 are near AP7 and have similar discrepancies between observed peak acceleration and modeling, indicating that Chin and Aki's crustal propagation model gives amplitudes which are too high for these stations. ST20, MON and ST35 are at hypocentral distances that are roughly comparable to the distance to SAL, but their back-azimuths differ. The discrepancy at SAL is arguably within the scatter of discrepancies for these three rock sites.

20  
Modeled/Observed Peak Acc.  
Log scale



## The Role of Reaction Kinetics in Earthquake Generation

9980-10448

Steven R. Bohlen

US Geological Survey

345 Middlefield Road MS-910, Menlo Park CA 94025

329-5341, fax 329-5203, [sbohlen@mojave.wr.usgs.gov](mailto:sbohlen@mojave.wr.usgs.gov)

Program Element 1

### Investigations undertaken

The basalt (gabbro)-to-eclogite transition is likely to play a major role in altering the states of stress near the subducted crust-mantle boundary as a result of the volume change (- 20%) of the transition. The volume change and the accompanying deformation is likely to generate slab earthquakes. Experiments are underway to understand the details of the various reactions that occur during the conversion of gabbro to eclogite and to quantify the kinetics of these reactions under both wet and dry conditions. The main objective of our work is to better understand the tectonic and seismic implications of kinetically-controlled metamorphic processes that occur in subduction zones as they relate to the physics of faulting. Specifically we seek to understand the kinetics of the conversion of gabbro to eclogite by conducting a series of experiments to elucidate the kinetics and reaction mechanisms of a few fundamental metamorphic reactions and on gabbros with a bulk composition approaching MORB.

The relative seismic risk that accompanies slab deformation in subduction zones is well known, but a heretofore unheralded and potentially very important mechanism for slab deformation is the volume reduction (- 20%) resulting from the transformation of gabbro to eclogite. We have proposed that the gabbro-eclogite transformation may play a major role in altering the states of stress near the subducted crust-mantle boundary and may therefore generate slab earthquakes.

The locus of the transformation depends on the kinetics of eclogite-forming reactions and hence the thermal state of the descending slab. Our initial studies of one of the key eclogite-forming reactions indicates that reaction rates are markedly higher in the presence of free water than in its absence. This result suggests that eclogite formation may be delayed (kinetically hindered) in subducting crust until large-scale dehydration occurs. Most igneous petrologists think that this dehydration occurs at the roots of arc volcanoes where the liberated water causes melting in the overlying asthenospheric wedge in the range of depths between 85 and 150 km, most likely related to the dehydration of amphibole. This is the same the same range of depths wherein a population of earthquakes worldwide have been identified that have focal mechanisms consistent with stretching deformation from a reduction of volume within the slab.

### Results

Work on the kinetics of the reaction of albite to jadeite + quartz has been completed for both wet and dry conditions. A paper is now being written and should be completed sometime in the summer. The experimental data document the enormous affect of H<sub>2</sub>O on the transformation rate and the reaction mechanism. In terms of a subducting slab, the formation of jadeitic pyroxene should be kinetically hindered in the absence of H<sub>2</sub>O, but it will proceed very rapidly should H<sub>2</sub>O migrate through the rock, a likely scenario given that amphibole dehydrates even in the absence of vapor at roughly 75-100 km depth.

As a prerequisite for understanding the kinetics of the gabbro to eclogite transition under H<sub>2</sub>O-saturated conditions, we have completed the phase diagram for gabbro (MORB) + H<sub>2</sub>O (See figure 1). Even though there have been numerous attempts to outline the phase relationships in this

system, our data are the first *reversed* data proving the stability of various phase assemblages, and disproving the stability of phases such as those containing chloritoid and lawsonite that appeared in the *unreversed* experimental products of Pawley and Holloway (Science, v. 260, p. 664-667, 1994). The results of our work will be prepared for publication this summer.

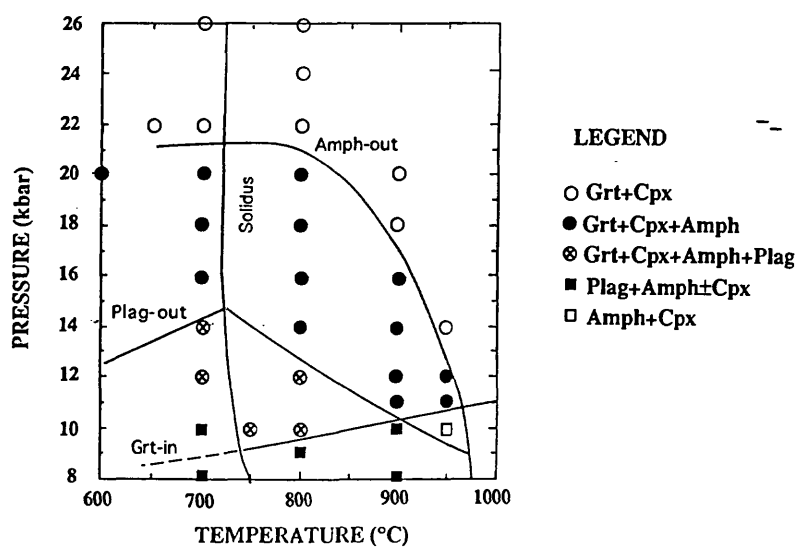
Reconnaissance experiments have been performed on a fine-grained gabbro from the lava lake at Kilauea Iki. The gabbro contains principally olivine, cpx, and plagioclase. The initial experiments performed at 1000 °C and 20, 25, and 30 Kbar show the incipient formation of pyroxene within plagioclase grains and the formation of garnet as thin rims around oxide minerals and at the interface of pyroxene and plagioclase. Such textures mimic those observed in our products from experiments investigating equilibria 1 and 2. Furthermore, the formation of garnet and pyroxene is significant because stable phase relationships for the chemically complex system represented by the gabbro would require the formation of spinel-bearing assemblages from which the garnet-bearing assemblages would grow at higher pressures. By overstepping the garnet-forming reactions by 10-15 Kbars, it appears from our very initial results that gabbro converts directly to eclogite without the formation of assemblages of intermediate density containing spinel. These experiments imply that in a downgoing slab, the conversion of gabbro or basalt to eclogite will be kinetically hindered, and the overstepping of the garnet-forming reaction allows the direct transformation to eclogite with the attendant -20 % reduction in volume. In turn, these findings have fundamental significance for the sudden increase in the state of stress in the slab that leads to earthquakes.

#### Reports Published

Bohlen, S. R., Mosenfelder, J. L., Hacker, B. R., and Hankins, W. B. (1994) Mineral reactions as drivers and recorders of continental dynamics (abstract). Geological Society of America Abstract with Programs, v. 26, p. A260.

Mosenfelder J. L., Bohlen, S. R., and Hankins, W. B. (1994) New method for making synthetic "rocks" for use in phase transformation studies, and initial results on the quartz = coesite transformations (abstract). Geological Society of America Abstract with Programs, v. 26, p. A260.

Fig. 1 PRELIMINARY PHASE DIAGRAM IN BASALTIC SYSTEM



## Evaluation of Seismic Propagation Effects Along and Across the Hayward and San Andreas Faults

9930 12283

R. D. Catchings, W. M. Kohler, and G. S. Fuis

U. S. Geological Survey, Branch of Seismology  
345 Middlefield Rd. MS 977, Menlo Park, CA 94025  
(415) 329-5163 Fax # (415) 329-5163  
[catching@andreas.wr.usgs.gov](mailto:catching@andreas.wr.usgs.gov)

### Elements I and III

#### Investigations Undertaken

Our investigations of seismic hazards in the San Francisco Bay region included both analysis of existing seismic data and acquisition of new seismic data. Explosive-source seismic data acquired in 1993 were analyzed to determine the velocity structure and to calculate weak ground motion measurements along the San Francisco Peninsula and along the Hayward Fault in the East Bay. Analysis of aftershocks of the 1989 Loma Prieta earthquake was also completed to compare those ground motion measurements with those from the explosive sources. New seismic data were acquired in the Los Angeles region following the 1994 Northridge earthquake in order to make comparisons of ground motion and damage between the San Francisco region and the Los Angeles region. In the San Francisco Bay area, new high-resolution (~1m) seismic reflection data that were acquired near the shore of the San Francisco Bay, along the San Mateo Bridge in search of faulting hazards associated with the transportation system.

#### Results

Our results indicate that the velocity structure (geometry of crustal layers and the Moho) of the San Francisco Peninsula largely controls the distribution of severe shaking for future earthquakes along the San Francisco Peninsula and for the 1989 Loma Prieta earthquake. Our explosive sources, aftershocks, and the mainshock of the 1989 Loma Prieta earthquake produce the same pattern of increased shaking in discrete locations along the San Francisco Peninsula. Synthetic seismograms were generated with sources located in high-probability zones along the Peninsula, and these data suggest that the city of San Francisco will be very severely shaken regardless of the location of the earthquake along the Peninsula and that discrete locations along the Peninsula will be severely shaken, depending on the location of the earthquake. The new high-resolution seismic reflection data indicate that shallow depth faults are present along the western end of the San Mateo bridge, in the city of Foster City, CA. Earthquakes along these faults may present a particular

danger to important life lines (transportation, water, etc.) in the San Francisco Bay area.

### **Reports Published**

Catchings, R. D., and W. M. Kohler, submitted, Reflected seismic waves and their effect on strong shaking during the 1989 Loma Prieta, California, earthquake, *Seis. Soc. Am. Bull.*

Catchings, R. D., W. M. Kohler, M. Rymer, and W. H. K. Lee, 1994, A search for San Francisco Bay faults using on-shore high-resolution seismic imaging along the San Mateo bridge, Foster City, CA, *EOS, Transactions, AGU*, 75, p. 684

Seismic Propagation, Attenuation and Ground Motion  
Measurements in Central U. S. (New Madrid) Region  
9930 14283

R. D. Catchings and W. M. Kohler

U. S. Geological Survey, Branch of Seismology  
345 Middlefield Rd. MS 977, Menlo Park, CA 94025  
(415) 329-4749 Fax #: 415) 329-5163  
catching@andreas.wr.usgs.gov

Elements I and III

### Investigations Undertaken

Investigations for the New Madrid region in FY 94 consisted of (1) analysis of existing seismic data to determine the likely extent of strong shaking from future large-magnitude earthquakes in that region and (2) acquisition of additional seismic data from other regions for comparison with the New Madrid region. Because large-magnitude earthquakes have not occurred in the New Madrid region since the region has been instrumented with modern seismographs, characteristics of wave propagation, attenuation, and strong shaking from large-magnitude earthquakes are not well known. These characteristics are, however, largely known for the San Francisco and Los Angeles regions in California, which have experienced recent large-magnitude earthquakes. By comparing wave propagation, attenuation, and strong shaking from the regions that have experienced recent large-magnitude earthquakes with those characteristics of the New Madrid region, we estimate the impact of future large-magnitude earthquakes on that region. We determined the seismic characteristics for each region by measuring seismic waves from explosive sources for all three regions. The relation between the explosive sources and large-magnitude earthquakes were determined for the San Francisco and Los Angeles regions. Seismic data for the Los Angeles region were acquired during 1994 following the Northridge earthquake.

### Results

Our measurements indicate that for an earthquake or explosion of the same size, seismic waves propagate more than four times greater distances in the Central U. S. than in the San Francisco region. Preliminary inspection of data from the Los Angeles region indicates that seismic energy also attenuates much more rapidly there than in the New Madrid region. These data indicate that the effects of a damaging earthquake will cover an area at least 16 times greater in size in the New Madrid region than would a similar earthquake in the San Francisco region. We expect that shaking can be as severe at 150 km from a New Madrid earthquake epicenter as within 15 km of the epicenter.

## Reports Published

Catchings, R. D., and W. M. Kohler, submitted, The hazard New Madrid earthquake pose for St. Louis, Memphis, and the central United States, Bull., Seism. Soc. Am.

Lee, W. H. K., R. D. Catchings, J. F. Gibbs, P. Spudich, and R. A. White, 1994, Observations of Northridge aftershocks and artificial sources in Tarzana, California, using a dense seismic array, EOS, Transactions, AGU, 75, p. 166

# Thermal Modeling of the Cascadia Subduction Zone

1434-93-G2330

Y. John Chen

College of Oceanic and Atmospheric Sciences  
 Oregon State University  
 Corvallis, OR 97331  
 (503) 737-0500  
 (503) 737-2064 (fax)  
 cheny@ucs.orst.edu (e-mail)

Program Element I.2

## Investigations Undertaken

This project is designed to develop thermal models to examine the thermal structure of the Cascadia subduction zone and is aimed at emphasizing the effect the thermal state may have on coupling of the subducting Juan de Fuca plate with the overlying North American plate. The overall objective of this numerical study is to estimate the thermal regime beneath this convergent margin, thus to contribute a better understanding of its unusual behavior, particularly the lack of large shallow thrust earthquakes in this important Pacific Northwest region. We have developed two-dimensional finite element thermal models for the Cascadia subduction zone across the central Oregon. The model includes realistic subducting slab geometry (with varying dip angle) and a thin layer of elements to examine various properties associated with the contact between the subducting slab and the overriding plate.

## Results

The mesh of the finite element model is shown at the top of Figure 1 which includes the trench at the origin and the Juan de Fuca plate subducting at an angle of 15° beneath the continental slope and the coast, and at a steeper angle of 40° beyond 200 km distance east of the deformation front. The right hand side of the model domain is chosen to be 520 km from the trench and the boundary condition there is a prescribed thickness of the North American plate corresponding to the depth of the 1325°C.

The predicted flow field and thermal structure from one numerical experiment is shown in Figures 1b and 1c, respectively. It shows a strong

asthenospheric flow in the wedge of the overriding plate. This secondary flow was found to be quite important in maintaining the hotter thermal structure of the overriding plate. One another interesting result is that the thickness of the subducting slab (in terms of its thermal contours) does not change much at least down to the 400 km depth. This finding lends support to the assumption of a uniform temperature at the base of the subducting slab used in a previous thermal study of the Cascadia forearc across the Vancouver Island [Hyndman and Wang, 1993].

The temperature at the plate contact is shown in Figure 2 as a function of the horizontal distance from the trench. The top panel compares the results for two continental plate thickness of 50 km and 100 km at the right side of the model domain; the results are not sensitive to this boundary condition as long as there is a significant asthenospheric flow in the plate wedge. Our results suggest that frictional heating plays an important role in elevating the plate interface temperature as shown in Figure 2b. If stick slip occurs below 350°C then the seismogenic zone has a width of about 150 km if no significant frictional heating takes place; it is limited within a narrow zone of less than 60 km from the deformation front if significant heat is generated by friction at the plate interface.

We are still in the stage of digesting these preliminary modeling results and refining our finite element models to calibrate with the seismic studies across the central Oregon margin [Trehu *et al.*, 1994; Nabelek *et al.*, 1993]. The preliminary modeling results will be reported in the 1994 Fall AGU Meeting in San Francisco [Ding and Chen, 1994] and the details of our results and interpretations will be reported later in a JGR paper.

## References

- Hyndman, R.D., and K. Wang, Thermal constraints on the zone of major thrust earthquake failure: The Cascadia subduction zone, *J. Geophys. Res.*, 98, 2039-2060, 1993.
- Nabelek, J., X.-Q. Li, S. Azevedo, J. Braunmiler, A. Fabritius, B. Leitner, A. Trehu, A high-resolution image of the Cascadia Subduction Zone from teleseismic converted phases recorded by a broadband seismic array, *EOS Trans. Am. Geophys. Union*, 74, 431, 1993.
- Trehu, A. M., I. Asudeh, T. M. Brocher, J. H. Luetgert, W. D. Mooney, J. L. Nabelek, Y. Nakamura, Crustal architecture of the Cascadia forearc, *Science*, 266, October 14, 1994.

## Reports Published

- Ding, R., and Y. J. Chen, Implications to Cascadia convergent margin (abstract), *Eos, Trans. Am. Geophys. Union*, 75, 641, 1994.

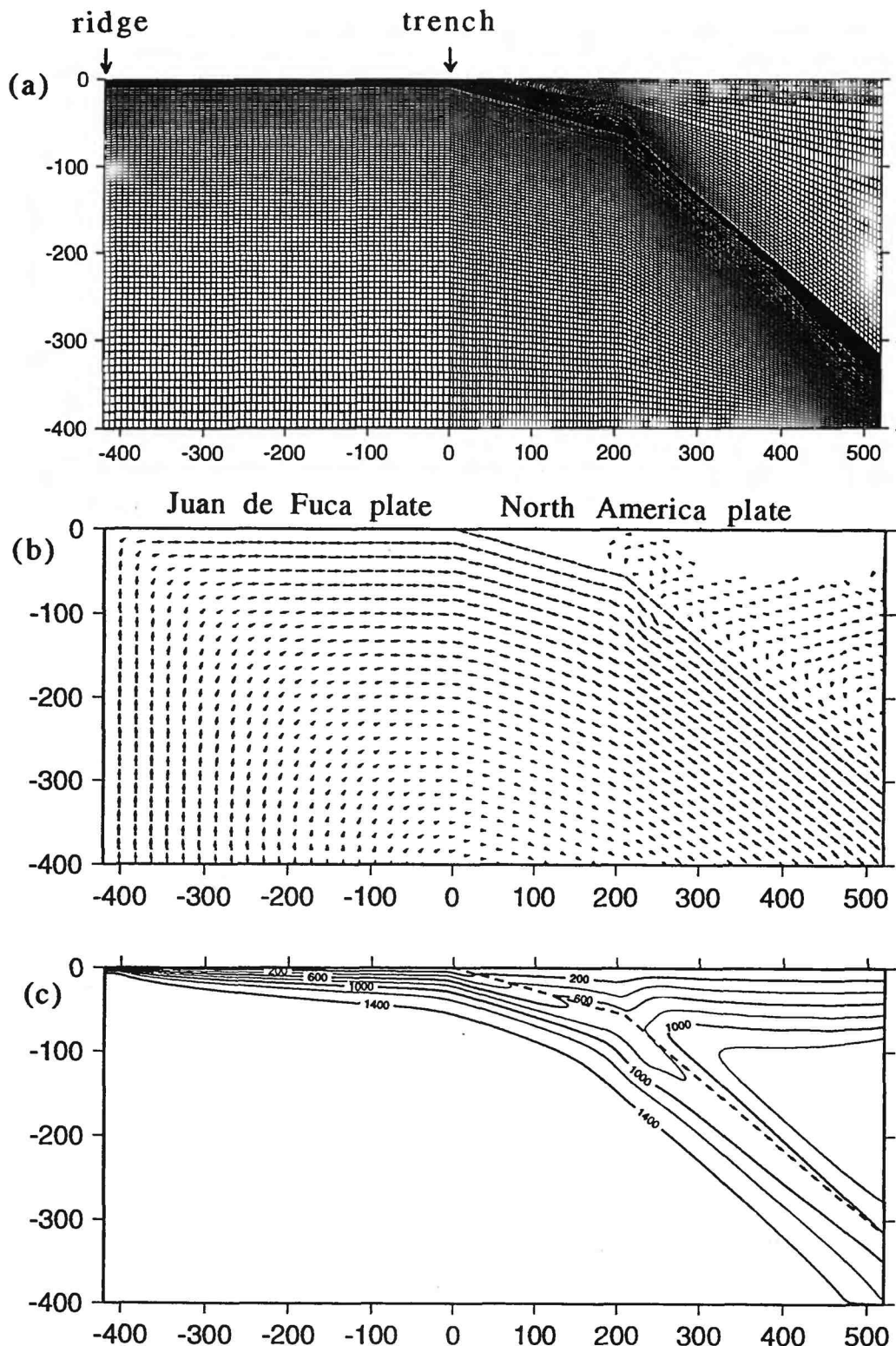


Fig. 1. Two-dimensional finite element models. (top) The finite element mesh of a model domain of 520 by 400 km. (middle) The calculated flow field shows mantle upwelling at the Juan de Fuca ridge and downwelling at the subduction zone. Note a strong asthenospheric flow in the wedge of the overriding plate. (bottom) Model thermal structure is shown in contours with an interval of 200°C. The plate interface is shown as a dashed line.

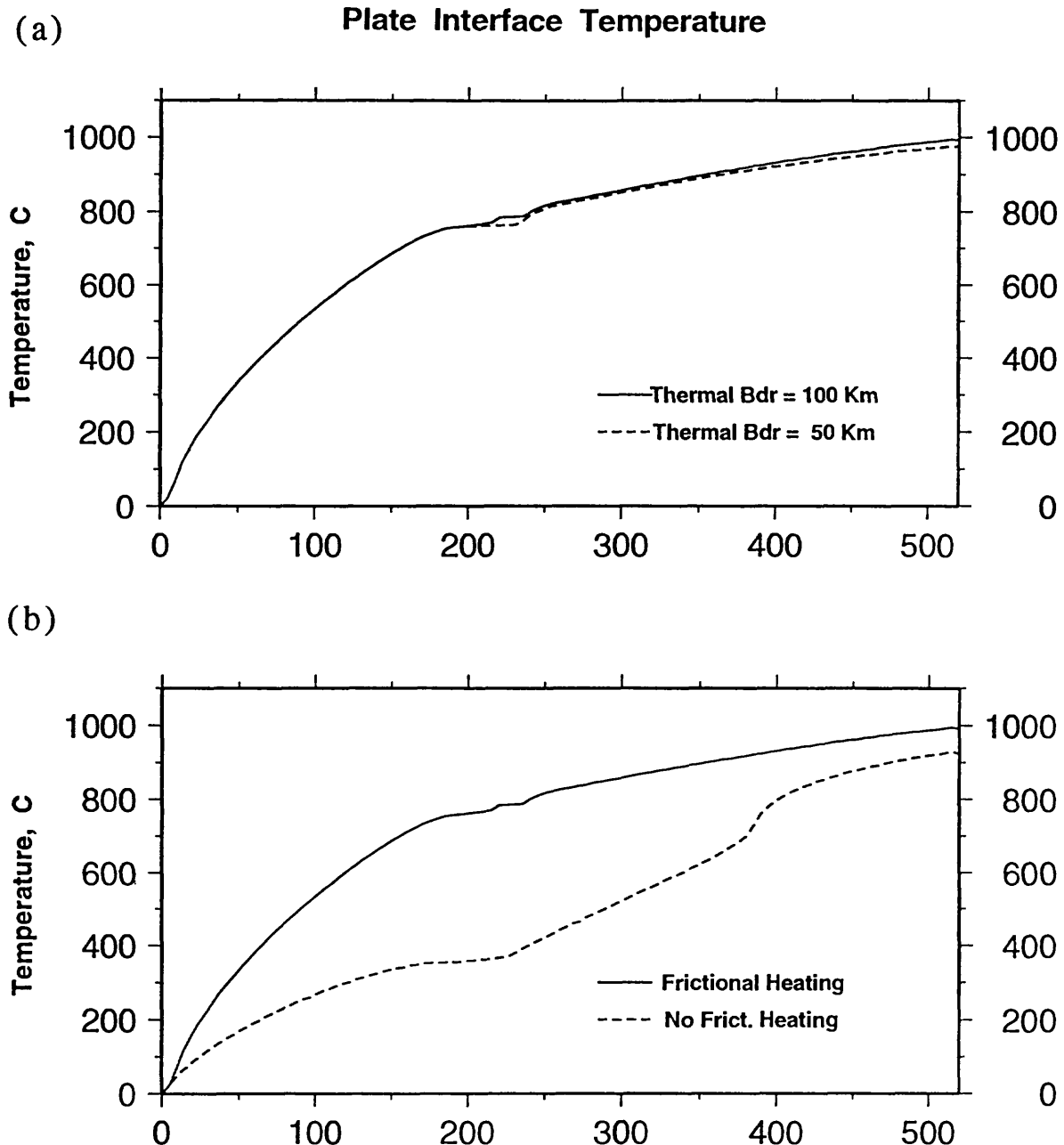


Fig. 2. Predicted plate interface temperatures versus distance from the trench are shown at the top panel for two different plate thicknesses (50 and 100 km) of the North America plate and at the bottom panel for the comparison between the case with significant frictional heating and the case without it.

**Collaborative Research (Saint Louis University and Utah State University):  
Geologic Studies of Deeply Exhumed Faults of the San Andreas System, Southern  
California**

**Project Number: 1434-94-G-2457**

**Frederick M. Chester**

Department of Earth & Atmospheric Sciences  
Saint Louis University  
3507 Laclede Ave.  
St. Louis, MO 63103

Voice: (314)977-3124

FAX: (314)977-3117

E-mail: [chester@slueas.slu.edu](mailto:chester@slueas.slu.edu)

**Project Number: 1434-94-G-2468**

**James P. Evans**

Department of Geology  
Utah State University  
Logan, UT 84322-4505

Voice: (801)797-1267

FAX: (801)797-1588

E-mail: [jpevans@cc.usu.edu](mailto:jpevans@cc.usu.edu)

**Program Element:**

**I. Understanding the earthquake source.**

**I.1: Physical properties and mechanical behavior of active crustal fault zones and surroundings.**

**INVESTIGATIONS**

Previous examinations of exhumed faults of the San Andreas system have helped to: 1] define fault zone properties, relative fault strength, weakening mechanisms, and processes of rupture initiation, propagation, and localization within the fault; 2] determine the amount of fluids in and near faults, and the role of fluids in fault zone processes; and 3] provide insight into fault morphology at depth [e.g., Chester et al., 1993; Evans and Chester, 1994]. However, faults exhumed to only several kilometers depth have been studied to date. To further our understanding of the physical and chemical processes of fault weakening and earthquake rupture nucleation and propagation along the San Andreas fault system, it is critical that fault zones and deformed rocks from deeper crustal levels well within the seismogenic regime are examined. In this project we continue our geologic investigations of faults that may represent the most deeply exhumed portions of the San Andreas system: the Sawpit Canyon fault and the deformed basement rocks of the Punchbowl fault. This work will allow us to evaluate whether the findings from studies of the San Andreas fault system at shallower levels and findings from studies of deeper fault exposures from different tectonic settings are generally applicable to the deeper portions of the San Andreas fault.

The Sawpit Canyon and Punchbowl faults are located in the San Gabriel basement complex of the San Gabriel Mountains, southern California. In general, the basement complex consists of Proterozoic, Jurassic, and Cretaceous crystalline rocks and Cretaceous schists cut by numerous faults of the San Andreas system [e.g., Ehlig, 1981; Powell, 1993; Morton and Matti, 1993]. The San Gabriel basement complex was a site of high relief throughout the Miocene and significant uplift has occurred on the northward-dipping Sierra Madre-Cucamonga thrust system since the Pliocene. Erosion and the desert climate produces excellent exposure of the ancient faults exhumed to seismogenic depths. The present geologic studies have two primary goals: to define the petrologic/geochemical characteristics of the fault rocks and to examine the structural/morphological properties of the fault zone. We also will use subsidiary fault fabric, cross cutting relations, and kinematic indicators to define movement history for the faults, and conduct a pilot geochronology study of hydrothermal minerals which formed during faulting to constrain the history of slip on the faults.

## RESULTS

Total right-lateral separation across the Punchbowl-Nadeau fault system is approximately 44 km and occurred largely during the latest Miocene and Pliocene. In many places the fault system consists of a broad zone of brittle deformed rock containing one or more principal fault surfaces. In the vicinity of the Devil's Punchbowl Los Angeles County Park, the Punchbowl fault (*sensu stricto*) is defined by a narrow brown gouge layer between the deformed basement and the Pliocene Punchbowl Formation. Previous work focused on the brown gouge layer and deformation in the Punchbowl Formation [Chester and Logan, 1986, 1987].

The Sawpit Canyon fault trends east-northeast joining the Sierra Madre thrust to the southwest and the North Branch of the San Gabriel fault to the northeast. At the western end two faults exist, the Clamshell and Sawpit Canyon faults. These have subparallel trends and appear to merge with the Sierra Madre thrust. There is no consensus regarding the geometry, history of slip, or kinematics of the Sawpit/Clamshell faults [Ehlig, 1981, pers. comm., 1992; Dillon and Ehlig, 1993; Powell, 1993; Ziony and Jones, 1989].

The FY1994 project involved three tasks: 1) study of the deformed rock and other principal faults south of the brown gouge layer in the vicinity of the Devil's Punchbowl County Park by the Saint Louis University group under the direction of F. Chester, 2) a characterization of the along-strike variation in structure and style of deformation along the Punchbowl fault system to the southeast of the Devil's Punchbowl County Park by the Utah State University group under the direction of J. Evans, and 3) preliminary analysis of structural data and samples collected from the Sawpit Canyon-Clamshell faults.

**Task 1.** Two months of field mapping and sample collection in the vicinity of the Devil's Punchbowl County Park was completed June and July of 1994 by the Saint Louis University group. Extent of intense brittle deformation, location of principal faults, and igneous and metamorphic rock contacts were mapped at 1:12000 along the fault system between Pallet Creek and Holcomb Creek. In this area the deformed zone of basement is generally between 0.5 and 1 km thick. The southern boundary is marked by principal faults oriented subparallel to the brown gouge layer of the Punchbowl fault. However, the southern boundary faults are neither as well developed or as continuous as the fault surface marked by the brown gouge. In addition, the overall structure of the bounding principal faults varies with host rock type. Where contrasting rock types are juxtaposed, the principal faults are typically a single continuous layer of cataclasite that marks localized fault slip. Within more homogeneous granitic igneous rock bodies the principal faults are characterized by many smaller faults distributed over a broad zone. The slice of basement rock between the southern boundary faults and the brown gouge layer of the Punchbowl fault to the north displays penetrative but heterogeneous brittle deformation. Some domains are deformed by dense networks of subsidiary faults and fractures, and in many cases the faults and fractures are mineralized.

Preliminary structural and petrologic data suggests the principal faults and brittle deformation in the basement rocks represent earlier and deeper episodes of deformation than that recorded in the Punchbowl Formation and brown gouge layer of the Punchbowl fault. Chester and Logan [1986] found only very low-grade alteration products of smectite and clinoptillolite in the brown gouge. In contrast, rock from within the zone of deformed basement and from the principal faults along the southern boundary of the deformed basement show higher-grade synfaulting mineral assemblages of chlorite, biotite, calcite and albite. During the field mapping we collected upwards of 100 oriented samples along traverses across the deformed zone of basement and across selected principal faults within the basement for petrographic and geochemical study.

Subsidiary fault geometries within the basement are consistent with right-lateral strike-slip movement on the principal faults of the Punchbowl fault system (Figure 1). In total, the subsidiary faults define a quasi-conjugate geometry of steeply dipping faults. Preferred orientation of B-axes indicate the faults are primarily strike-slip faults. The preferred orientation of right-lateral faults is a strike of N27°W and of left-lateral faults is a strike of N09°E. The bisector of the conjugate set forms an angle of approximately 60° with the overall N70°W strike of the Punchbowl fault system. The geometry of faults implies that during deformation and slip along the Punchbowl fault system, the maximum principal compressive stress was at high angles to the Punchbowl fault. This angular relation implies the Punchbowl fault was weak similar to the inferred stress state and strength of the active traces of the San Andreas fault [e.g., Hickman, 1991]. The subsidiary fault geometry in the deformed basement rock is similar to the quasi-conjugate geometry found for subsidiary faults in the deformed Punchbowl Formation along the brown gouge layer of the Punchbowl fault [Chester & Logan, 1987]. However, the bisector of the conjugate faults in the Punchbowl Formation is at a larger angle to the Punchbowl fault than observed for the subsidiary faults in the basement. Because the deformation of the Punchbowl Formation is thought to reflect the latest stages of deformation associated with the Punchbowl system, the larger angle between the conjugate bisector and the Punchbowl fault for the Punchbowl Formation relative to the basement could imply the Punchbowl fault progressively weakened with slip.

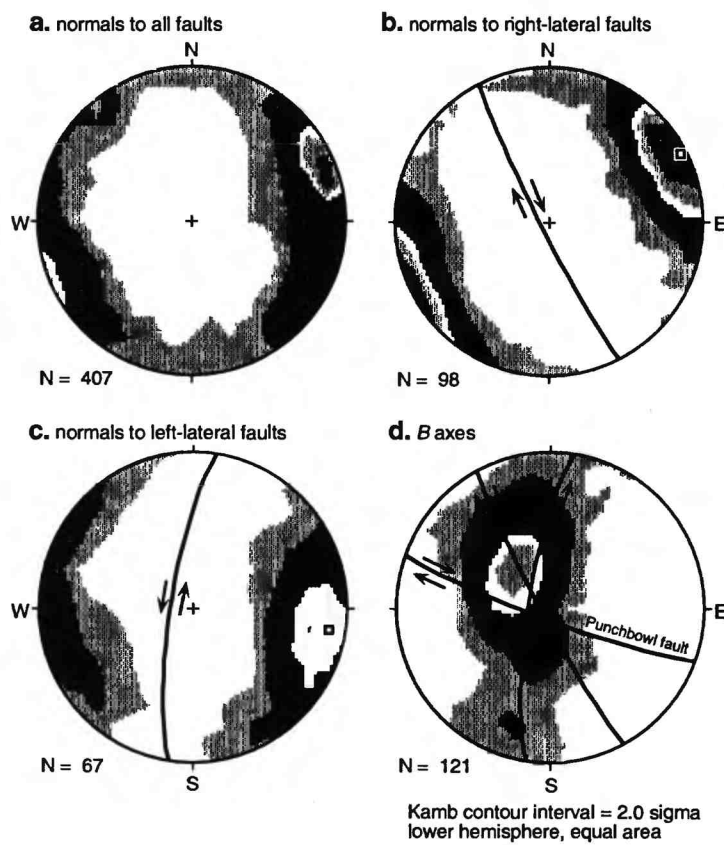


Figure 1. Subsidiary fault fabric in the slice of brittle faulted basement between the northern and southern boundary faults of the Punchbowl fault system in the Devil's Punchbowl area. Lower hemisphere, equal area projection with north at top. Number of measurements, N, is indicated at the bottom of each plot. All plots are contoured using the Kamb method for a contour interval of 2 sigma; concentrations greater than 4 sigma are considered statistically significant for point maxima. a) Normals to all subsidiary faults show that the subsidiary faults strike in all directions and are generally steeply dipping. b) Normals to all faults with a right-lateral sense of separation viewed in the horizontal plane; preferred orientation (shown) is a vertical plane striking northwest. c) Normals to all faults with a left-lateral sense of separation viewed in the horizontal plane; preferred orientation (shown) is a vertical plane striking north northeast. d) B-axes, defined as the imaginary lines that lie in the fault planes and are normal to the slip direction, are preferentially steeply plunging to the northwest. This preferred orientation indicates the faults are dominantly strike-slip. The right- and left-lateral faults define a quasi-conjugate fault geometry having bisector at approximately 60° from the plane of the Punchbowl fault (shown).

**Task 2.** Two months of field mapping and sample collection along the Punchbowl fault system between Vincent Gap and Cajon Pass (to the southeast of the Devil's Punchbowl County Park) was completed July and August of 1994 by the Utah State University group. This work focused on the Punchbowl fault where it cuts the Pelona Schist, and expands our investigations into different rock types. We have carried out detailed study along traverses spanning the fault zone

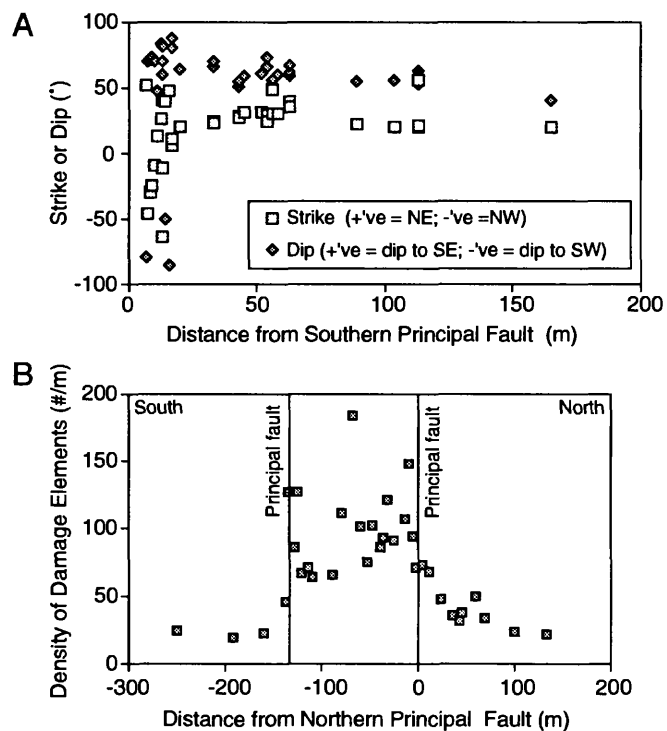
and typically several hundred meters in length. Measurements were made of small fault density and orientation, fracture density and orientation, and schistosity and other foliation orientations near the fault. In addition, over 200 samples for petrographic and geochemical analyses were collected.

Consistent with findings from other study areas, preliminary results show that the Punchbowl fault in the Pelona Schist is a relatively narrow zone as defined by changes in foliation orientation and in fracture and fault density (Figure 2). Data suggests that the majority of fault displacement was localized to a 10 to 50 m thick zone of shear. Within this zone the slip was further localized to one or more narrow layers of cataclasite and ultracataclasite. Thus, unlike our previous work on the North Branch San Gabriel fault, where the principal fault is typically defined by a single layer of ultracataclasite, the Punchbowl fault within the Pelona Schist contains several distinct layers recording multiple sites of localized slip. Preliminary analysis suggests subsidiary faulting within the fault zone is different than that outside the zone (Figure 3). Small faults outside the zone record right-lateral slip with a component of reverse motion on a set of ordered faults. Subsidiary fault kinematics is less organized within the fault zone. This could reflect an internal rotation of faults during progressive shear.

Figure 2. Measures of localization along the Punchbowl fault.

A) Orientation of the foliation of Pelona Schist as measured on the southern side of the Punchbowl fault, Blue Cut (Old Highway 66) exposure, Cajon Pass. The foliation is unaffected by the fault zone up to about 20 m from the southern edge of the fault.

B) Density of damage elements (fractures, veins, and faults) across the Punchbowl fault south of Big Pines. Logarithmic sampling was used to focus on the fault zone and adjacent regions, and shows that there is a small increase in damage elements within towards the boundaries of the fault, but that most of the damage is accumulated within the fault.



To extend our studies of the influence of protolith on fault structure, we also investigated the variation in morphology of the San Andreas fault in granites and granitic gneisses between the region southeast of Cajon Pass to Big Pines (near Wrightwood). The development of fine-grained foliated cataclasites appears strongly dependent on the presence of mica-rich gneisses. In regions where the fault cuts the gneisses, narrow layers of foliated cataclasite dominate the fault zone. In equigranular granites the fault consists of gouge zones with less obvious layers of cataclasite recording localized slip. These preliminary results indicate that protolith composition may play a critical role in the nature of slip localization within the seismogenic regime.

**Task 3.** Previous mapping of the eastern Sawpit fault (Ehlig, unpublished mapping) and our investigations suggest that this portion of the fault zone consists of a relatively thick zone of greenschist facies chlorite-epidote-albite mineral assemblage of mylonitic fault-rocks. In some

localities there is extensive greenschist facies neomineralization in veins that are spatially associated with the Sawpit Canyon fault. Later-stage deformation is brittle and involves mineralogic alteration to clays and laumontite similar to that observed in our studies of the North Branch San Gabriel fault and adjacent to the San Andreas fault [e.g., Chester et al., 1993]. We find the distinct clay-lined fault surfaces of both the Sawpit and Clamshell faults and the associated brittle deformation are well exposed in deeply cut canyons on the southern margin of the San Gabriel Mountains.

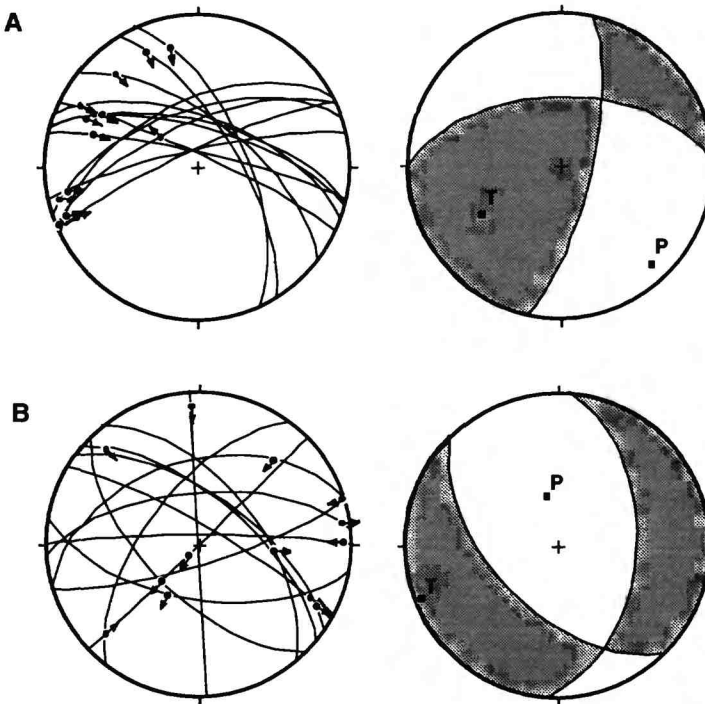


Figure 3. Preliminary kinematic analyses of small faults near the Punchbowl fault, Blue Cut.

A) Small faults with well defined slip vectors are rare in the Pelona Schist. Kinematic analysis of 13 small faults show a set of right-lateral faults. A quasi-focal mechanism solution yields a preferred fault plane of striking east-west with a component of reverse slip.

B) Small faults within the fault zone show a more complex pattern. Analysis of 13 small faults show a wide array of fault orientations and slip directions. This may reflect internal rotation in the fault zone, or a complex slip system within the fault zone to accommodate shear.

The fault rocks are extremely fine grained and foliated, and cut diabase dikes inferred to be of Miocene age (Hazelton and Nourse, 1994; Ehlig, pers. comm., 1992). Very limited outcrop-scale sense of shear indicators suggest left-lateral slip during the earliest stages of mylonitization. Preliminary field work on the western Sawpit/Clamshell faults revealed numerous small faults displaying good to excellent slip indicators. In general, the small faults suggest that an early, epidote-coated set of faults with right-lateral strike-slip motion were cut by later, polished hematitic surfaces which display a large component of reverse dip-slip movement. Numerous diabase dikes are exposed in the area, and appear to be cut and locally reoriented by the faults. Based on the fault rock fabrics and mineralogic assemblage, we believe that the Sawpit Canyon fault may be exhumed to significantly greater depths than the North Branch San Gabriel fault and well within the seismogenic regime. However, the faults record several distinct episodes of deformation and additional work is necessary to define fault history. Some of the preliminary field work and mapping also suggests that parts of the Sawpit/Clamshell faults have been active in the Quaternary, perhaps as a result of slip on the frontal thrust. We are carrying out exploratory petrographic study of samples from the Sawpit Canyon fault in preparation for the field mapping planned for the summer of 1995.

## Reports Published

- Chester, F. M., G. Li, and J. P. Evans, Thickness and strain distribution of the San Gabriel fault, an exhumed fault of the San Andreas system, *Eos Trans. AGU*, 75, 342, 1994.
- Evans, J. P., and F. M. Chester, Fluid-Rock Interaction in faults of the San Andreas system: Inferences from San Gabriel Fault-Rock Geochemistry and Microstructures, *J. Geophys. Res.*, in press, 1994.
- Evans, J. P., Chester, F. M., and Li, G., Characterization of exhumed faults of the San Andreas fault system, southern California, in: Tectonic Studies Group, special meeting on fault populations, Edinburgh, Scotland, 1994

## Other References

- Chester, F.M., and J.M. Logan, Implications for mechanical properties of brittle faults from observations of the Punchbowl fault zone, California, *Pure Appl. Geophys.*, 124, 79-106, 1986.
- Chester, F.M., and J.M. Logan, Composite planar fabric of gouge from the Punchbowl fault, California, *J. Struct. Geol.*, 9, 621-634, 1987.
- Chester, F. M., Evans, J. P., and Biegel, R. L., Internal structure and weakening mechanisms of the San Andreas fault, *J. Geophys. Res.* 98, 771-786, 1993.
- Dillion, J. T., and P. L. Ehlig, Displacement on the southern San Andreas fault, in: The San Andreas Fault System, *Geol. Soc. Am. Mem.* 178, 199-217, 1993.
- Ehlig, P.L., Origin and tectonic history of the basement terrane of the San Gabriel Mountains, central Transverse Ranges, in *The Geotectonic Development of California, Rubey* Vol. 1, edited by W.G. Ernst, pp. 253-283, Prentice-Hall, Englewood Cliffs, N. J., 1981.
- Evans, J. P., and F. M. Chester, Fluid-Rock Interaction in faults of the San Andreas system: Inferences from San Gabriel Fault-Rock Geochemistry and Microstructures, *J. Geophys. Res.*, in press, 1994.
- Hazelton, G. B., and Nourse, J. A., Constraints on the direction of Miocene extension and degree of crustal tilting in the eastern San Gabriel Mountains, Southern California, *Geol. Soc. Am. Abst.*, 26, #2, 58, 1994.
- Hickman, S. H., Stress in the lithosphere and the strength of active faults, *Reviews of Geophysics, Supplement to* 29, 759-775, 1991.
- Morton, D.M., and J.C. Matti, Paleogeographic evolution of the San Andreas fault in southern California, in: in: The San Andreas Fault System, *Geol. Soc. Am. Mem.* 178, R. E. Powell, R. J. Weldon, II, and J. C. Matti, eds., p. 107-160, 1993.
- Powell, R. E., Balanced palinspastic reconstruction or Pre-late Cenozoic paleogeography, southern California, in: The San Andreas Fault System, *Geol. Soc. Am. Mem.* 178, R. E. Powell, R. J. Weldon, II, and J. C. Matti, eds., p. 1-107, 1993.
- Ziony, J. I., and L. M. Jones, Map showing Late Quaternary faults and 1978-1984 seismicity of the Los Angeles region, California, U. S. Geol. Survey Map MF-1964.

## Partial Support of Joint USGS-CALTECH Southern California Seismographic Network

#1434-92-A-0960

Robert W. Clayton  
Egill Hauksson

Seismological Laboratory,  
California Institute of Technology  
Pasadena, CA 91125  
[hauksson@seismo.gps.caltech.edu](mailto:hauksson@seismo.gps.caltech.edu)  
Tel: 818-395 6954  
FAX: 818-564 0715

### INVESTIGATIONS

This Cooperative Agreement provides partial support for the joint USGS-Caltech Southern California Seismographic Network. The purpose is to record and analyze data from more than 29,300 local earthquakes from October 1993 to September 1994 and generate a data base of phase data and digital seismograms. The primary product derived from the data base is a joint USGS-Caltech catalog of earthquakes in the southern California region. We also provide rapid response to media and public inquiries about earthquakes.

For more detailed information about data access, please contact:  
Dr. Kate Hutton at (818)-395-6959;  
or with E-mail: [kate@bombay.gps.caltech.edu](mailto:kate@bombay.gps.caltech.edu).

### RESULTS

#### Network Operation

*Southern California Seismographic Network.* The SCSN has 250 remote sites (with 330 components) and gathers data from local, regional and teleseismic earthquakes. These data are used for earthquake hazards reduction as well as for basic scientific research. The earthquake hazards reduction effort has become more important as moderate-sized earthquakes continue to occur within densely populated areas in southern California. The largest damaging earthquake to occur was the ( $M_w$ 6.7) Northridge earthquake of 17 January 1994, located 30 km west-northwest of downtown Los Angeles.

The average rate of 15 publications per year over the last 10 years using the network data illustrates the strength of the ongoing research activities that use the network data. Continued efforts to improve data quality and accessibility have created the arguably best regional earthquake data base in the world. The ongoing upgrading of the quality of the waveforms recorded by the short-period network and the addition of low-gain seismometers and accelerometers provide numerous new avenues of research. Most important of these is analysis of on-scale waveforms to determine source, path and site effects.

The USGS operates most of the remote stations in the SCSN. Caltech operates: 1) 24 short period telemetered stations; 2) 17 very broadband TERRAscope stations; in 1995 we plan to install 3 more TERRAscope stations. Caltech also maintains drum recorders and other equipment at the central site located in the Seismological Laboratory at Caltech.

The SCSN data are recorded by two microVAX-III computers and the data processing is done on six VAX workstations using a VAX-4000 as a central server. The operation of this equipment is shared by Caltech and USGS personnel. To avoid duplication, software development is done in cooperation with the USGS in Menlo Park.

More than 29,300 earthquakes will be entered into the southern California earthquake catalog for this reporting period. Approximately 5.0-10.0 Mbytes of phase data and 50-75 Gbytes of seismograms will be archived. In addition to the data analysis we carry out software maintenance, hardware maintenance, and other tasks necessary to complete the catalog. Caltech and USGS maintain a data base that includes: 1) earthquake catalog (1932-present); 2) phase data (1932-present); 3) photographic paper seismograms (1930-1992); and 4) digital seismograms (1977-present). The earthquake catalog (1932-present) and phase data (1932-present) are available via dial-up and over INTERNET. Other data are available upon request. This data base has been made available to the DC/SCEC and is the most voluminous part of the data stored in the DC/SCEC.

Near real-time reporting to USGS in Reston and the Governor's Office of Emergency Services and other response to any felt or damaging earthquake activity is provided by network personnel.

*The Data Center of the Southern California Earthquake Center.* This center has significantly increased the use of the data from SCSN for scientific research. The mass-store system, which became operational on 1 October 1991, provides on-line storage for more than 600 Gbytes of data. The availability of 60 years of catalog, 60 years of phase data, and 15 years of digital seismograms on both UNIX and VMS computers and on-line over INTERNET/NSFNET improves the access to the data.

#### Seismicity October 1993- September 1994

The Southern California Seismographic Network (SCSN) recorded approximately 29,300 earthquakes during the 12 months from October 1993 through September 1994, an average of 2440 per month, making it the second most active reporting period ever (Figure 1). The largest earthquake to occur was the M6.7 Northridge earthquake. In addition to the Northridge sequence, three earthquakes of  $5.0 < M < 6.0$  occurred during the last 12 months. One of these was a Landers aftershock, while one occurred near Eureka Valley (Figure 1).

The  $M_w 6.7$  Northridge earthquake occurred on January 17, 1994 beneath the San Fernando Valley (Figure 2). Two seismicity clusters, located 25 km to the south and 32 km to the north-northwest, preceded the mainshock by 7 days and 16 hours, respectively. The mainshock hypocenter was relatively deep, at 19 km depth in the lower crust. It had a thrust faulting focal mechanism with the actual fault plane dipping  $35^\circ$  to the south, striking  $N75^\circ W$  with a rake of  $100^\circ$ . Because the mainshock did not rupture the surface, its association with surficial geological features remains difficult to resolve. Nonetheless, its occurrence reemphasized the seismic hazard of concealed faults associated with the contractional deformation of the Transverse Ranges. The Northridge earthquake is part of the temporal increase in earthquake activity in the Los Angeles area since 1970.

The mainshock was followed by an energetic aftershock sequence. Eight aftershocks of  $M \geq 5.0$  and 48 aftershocks of  $4 \leq M < 5$  occurred between January 17 and September 30, 1994. The aftershocks extend over most of the western San Fernando Valley and Santa Susana Mountains. They form a diffuse spatial distribution around the mainshock rupture plane, illuminating a previously unmapped thrust ramp, extending from 7-10 km depth into the lower crust to a depth of 23 km.

Other regions of high activity are the San Jacinto fault, the most active fault in southern California, Coso geothermal area, Eureka Valley, and Long Valley. The activity along the San Jacinto fault extended more than 100 km south of the US Mexico border. The Coso seismicity has remained at a high level since the 28 June 1992 Landers earthquake. This high rate of seismicity is anomalous for southern California when compared with the previous decade (Figure 1).

## PUBLICATIONS USING NETWORK DATA (ABSTRACTS EXCEPTED)

- Abercrombie, R., and J. Mori, Local observations of the onset of a large earthquake: 28 June 1992, *Bull. Seismo. Soc. Amer.*, 84, 725-734, 1994.
- Benz, H. M., J. E. Vidale, and J. Mori, Using regional seismic networks to study the Earth's deep interior, *Eos Transactions*, 75, 225-229, 1994.
- Dreger, D., Investigations of the rupture process of the 28 June 1992 Landers earthquake utilizing TERRAscope, *Bull. Seismo. Soc. Amer.*, 84, 713-724, 1994.
- Dreger, D. S., Empirical Green's function study of the January 17, 1994 Northridge, California earthquake (Mw6.7), *Geophys. Res. Lett.*, submitted, 1994.
- Hartse, H. E., M. C. Fehler, R. C. Aster, J. S. Scott, and F. L. Vernon, Small-scale stress heterogeneity in the Anza seismic gap, southern California, *J. Geophys. Res.*, 99, 6801-6818, 1994.
- Hauksson, E., and L. M. Jones, The Northridge Earthquake of January 17, 1994 SPECTRA Special Report (contributed), Seismological Aspects, J. Hall (ed), EERI, December 1994.
- Hauksson, E., The 1991 Sierra Madre earthquake sequence in southern California: Seismological and tectonic analysis, *Bull. Seismol. Soc. Amer.*, 84, 1058-1074, 1994b.
- Hauksson, E., State of stress from focal mechanisms before and after the 1992 Landers earthquake sequence, *Bull. Seismo. Soc. Amer.*, 84, 917-934, 1994.
- Jones, C. H., H. Kanamori, and S. W. Roecker, Missing roots and mantle "drips": Regional  $P_n$  and teleseismic arrival times in the southern Sierra Nevada and vicinity, California, *J. Geophys. Res.*, 99, 4567-4601, 1994.
- Jones, L. M., Foreshocks, aftershocks, and earthquake probabilities: Accounting for the Landers earthquake, *Bull. Seismo. Soc. Amer.*, 84, 892-899, 1994.
- Jones, L. M., and E. Hauksson, Review of potential earthquake sources in southern California, in *ATC-35 Seminar on New Developments in Earthquake Ground Motion Estimation and Implications for Engineering Design Practice*, U. S. Geological Survey, Los Angeles, California, 1994.
- Roquemore, G. R., and G. W. Simila, Aftershocks from the 28 June 1992 Landers earthquake: Northern Mojave desert to the Coso Volcanic Field, California, *Bull. Seismo. Soc. Amer.*, 94, 854-862, 1994.
- Scientists of the U. S. Geological Survey and the Southern California Earthquake Center, The magnitude 6.7 Northridge, California, earthquake of January 17, 1994, *Science*, 266, 389-397, 1994.
- Scott, J., E. Hauksson, and H. Kanamori, Global positioning system re-survey of Southern California seismic network stations, in press, 1994.
- Wald, D. J., and T. H. Heaton, Spatial and temporal distribution of slip for the 1992 Landers, California, earthquake, *Bull. Seismo. Soc. Amer.*, 84, 668-691, 1994.
- Wiemer, S., and M. Wyss, Seismic quiescence before the Landers (M = 7.5) and Big Bear (M = 6.5) 1992 earthquakes, *Bull. Seismo. Soc. Amer.*, 84, 900-916, 1994.
- Zhao, L.-S., and D. V. Helmberger, Source estimation from broadband regional seismograms, *Bull. Seismo. Soc. Amer.*, 84, 91-104, 1994.

Southern California  
October 1993 -- September 1994

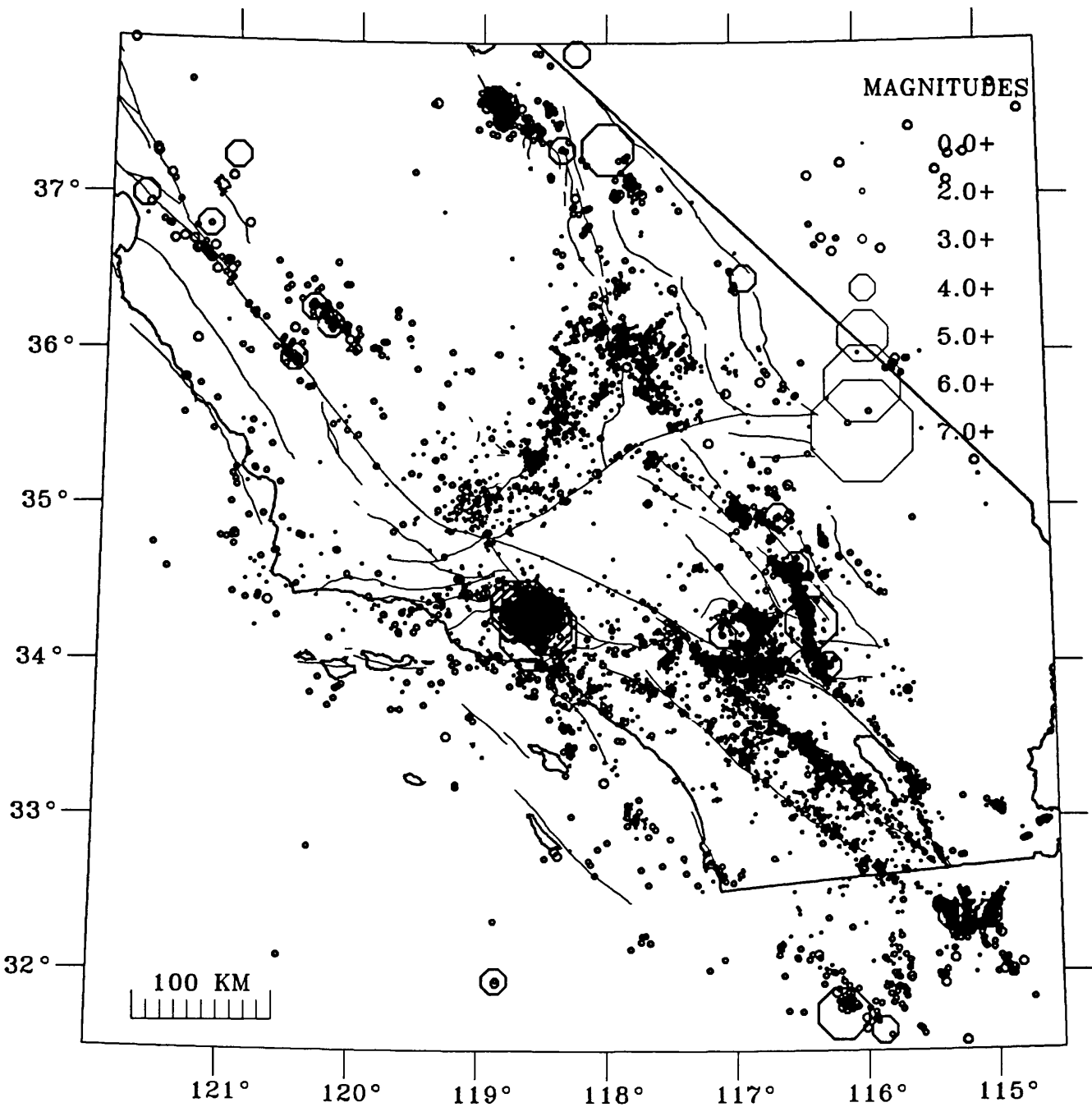


Figure 1. Map of epicenters of earthquakes in the southern California region, 1 October 1993 to 30 September 1994.

# Northridge Sequence

January – July 1994

I-N

34° 30'

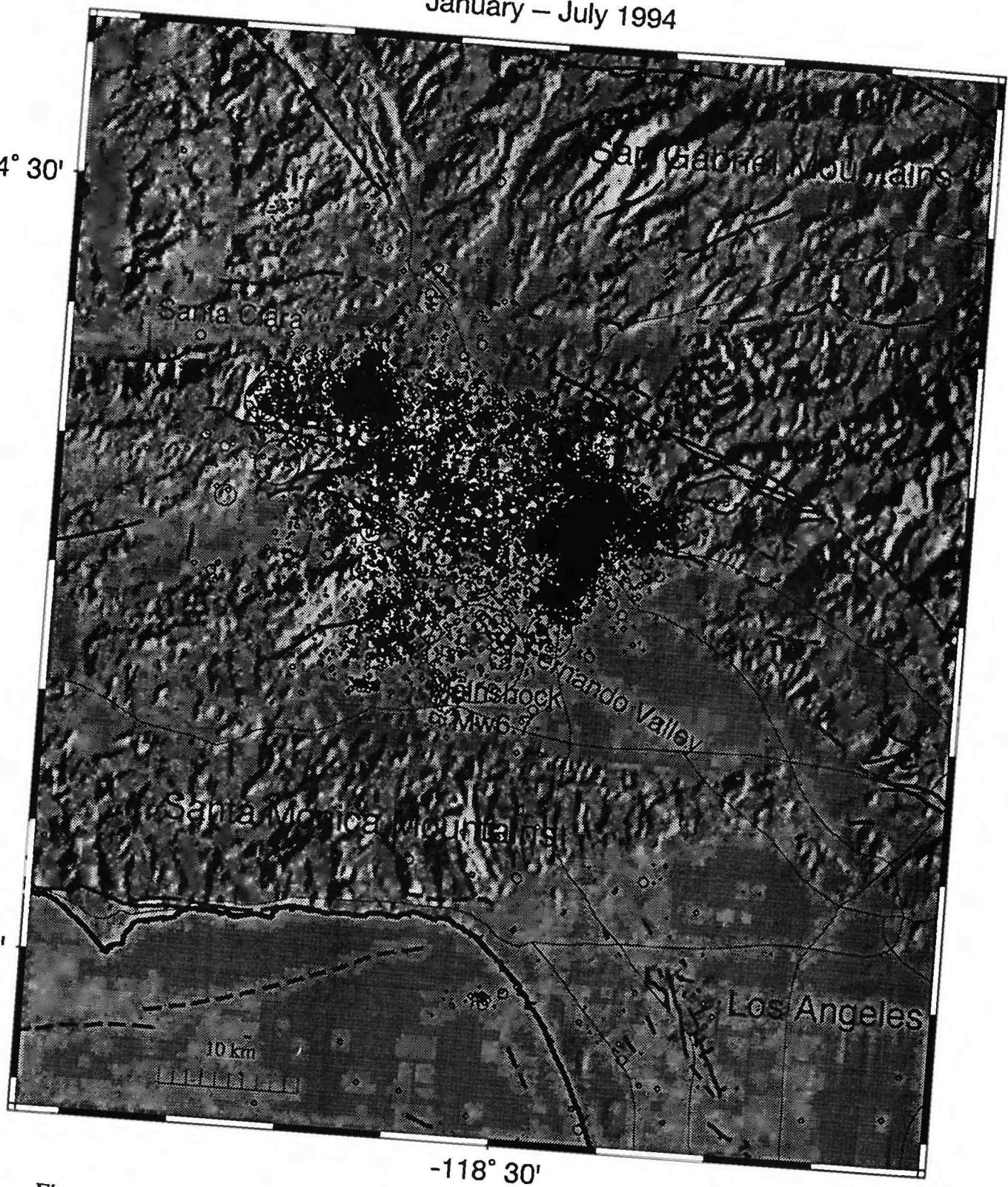


Figure 2. Map of the 1994 Northridge earthquake, its aftershocks and major late Quaternary faults (dashed or dotted where inferred). Symbol size is scaled with magnitude.

## Pacific Northwest Seismograph Network Operations

1434-92-A-0963 R.S. Crosson, S.D. Malone and A.I. Qamar, P.I.s

R.S. Crosson, S.D. Malone, A.I. Qamar and R.S. Ludwin

Geophysics Program

University of Washington

Seattle, WA 98195

(206) 543-8020

e-mail: bob, steve, tony, or ruth@geophys.washington.edu

Oct. 1, 1993 - Sept. 30, 1994

### Investigations

Operation of the Pacific Northwest Seismograph Network (PNSN) (formerly known as the Washington Regional Seismograph Network or WRSN) and preliminary analysis of earthquakes in Washington and Oregon continues under this agreement. Quarterly bulletins which provide operational details and descriptions of seismic activity in Washington and Oregon are available from 1984 through the third quarter of 1994. Final published catalogs are available from 1970, when the network began operation, though 1989.

The University of Washington operates 96 stations west of 120 degrees west longitude under this agreement. This report includes a brief summary of significant seismic activity. Additional details are included in our Quarterly bulletins.

### Information - Emergency Notification and Public Education and Outreach

In addition to monitoring earthquake activity in Washington and much of Oregon, the staff of the PNSN participates in outreach projects to inform and educate the public about seismicity and natural hazards. Our outreach includes lab tours, lectures, educational classes and workshops, TV and radio interviews, field trips, and participation in regional earthquake planning efforts. We answer from 5-40 questions per day on Pacific Northwest seismicity and seismic hazards, and give about a half-dozen lab tours or presentations each month for a wide variety of groups, including elementary through post-graduate students, retirees, science teachers, emergency educators, and many others. We provide a taped telephone message describing the seismic hazards in Washington and Oregon and a separate taped message on current seismic activity ((206) 543-7010). Both these services are heavily used. We provide a one-page information and resource sheet on seismic hazards in Washington and Oregon that we encourage others to reproduce and further distribute.

For significant local events, our automatic processing includes an alarm that initiates electronic mail (e-mail) or faxes to local emergency response agencies, operators of adjacent seismograph networks, and the National Earthquake Information Center in Colorado. When the event has been fully processed, updated final information on it is also faxed or e-mailed.

Locations of recent earthquakes of magnitude 2 or larger can be obtained via modem by dialing (206)685-0889 and logging in as **quake** with password **quake**, by sending e-mail to **quake@geophys.washington.edu** or via ethernet using the UNIX utility **finger quake@geophys.washington.edu**. Summary lists for all earthquakes located by the PNSN since 1969 are available via anonymous ftp on **ftp.geophys.washington.edu** in the **pub/seis net** sub-directory. In addition, special sub-directories; **pub/kfalls** and **pub/woodburn**; include locations, focal mechanisms, and local station lists for the Klamath Falls and Scotts Mills, Oregon earthquake sequences. This information is also available via the **World-Wide-Web (WWW)** which provides text and graphics for anyone connected to the Internet running a version of "Mosaic" (available for workstations, PC-Windows, and Macintoshes with anonymous ftp at **ftp.ncsa.uiuc.edu**). Our **WWW** server contains text about earthquakes in the Pacific Northwest, maps of stations, catalogs and maps of recent earthquake activity, and maps and text about recent interesting sequences. It

also contains links into other sources of earthquake information around the country and world. To access it use mosaic <http://www.geophys.washington.edu>.

Seismic trace data are being reformatted to the IRIS-SEED format, and submitted to the IRIS Data Management Center, where they will be made available over Internet through the IRIS database system. We have also recently acquired a very large (18 gigabyte) on-line storage disk, which will allow us to store all PNSN digital seismic trace data (since 1980).

### Network Operations

A station map and a discussion of recently installed three-component broad-band instrumentation is included in the summary for agreement 1434-92-G-2195.

This year, we modified both our seismic trace data and pickle (phase arrival times) formats (and associated data-processing software). The old formats, in use since 1980, did not allow broad-band data to be merged into our network data stream. The modifications were developed and tested in the context of SNAPS (Seismic Network Automated Processing System), a software package for processing network data that allows automated processing steps to be integrated with steps controlled by an analyst.

Our new working seismic trace data format (UW-2) allows us to accommodate data of varying durations, sample rates, start times, and formats; is extensible without affecting existing processing programs; and is backward-compatible with our original (UW-1) format. Conversion programs allow easy conversion between UW-2 and other commonly used trace-data formats such as AH and SEED. The new UW-2 pickle format provides full support for three-component stations, flexibility to represent arbitrary phase types (our old UW-1 format could only represent P and S phases) such as Pn and PmP, and a number of other advantages, and is also backward compatible. Interactive viewing of both trace and pickle data is provided through **Xped** (X pickle editor), an X window application that allows the user to display trace and pick information, modify picks, run location programs, and perform other data analysis functions.

In addition to the extensive modifications of data-processing software required by the change to UW-2 data formats, we are also updating our data acquisition hardware and software. Since 1988, we have used a Concurrent 5600 computer running *HAWK* software, a derivative of the *CEDAR* system developed at Cal Tech by Carl Johnson. Now, in 1994, rapid advances in computer speed enable us to enhance and streamline data acquisition while lowering our computer costs. The new data acquisition software is called *SUNWORM*. It is being developed in cooperation with the *EARTHWORM* project at the USGS in Menlo Park, and is currently running in test mode on a SUN-SparcStation-5 workstation. *SUNWORM* will replace the *HAWK* system by the end of 1994.

### Seismicity

Figure 1 shows earthquakes of magnitude 2.0 or larger located in Washington and Oregon during this reporting period. The PNSN processed 8,457 events between Oct. 1, 1993 and Sept. 30, 1994. Of these, 7,588 were earthquakes or blasts within the network (1,701 of which were too small to locate). The remaining events were regional earthquakes (274) or teleseisms (595). Within our network area, 5,305 earthquakes were located west of 120.5 degrees west longitude, (including 383 near Mount St. Helens, which has not erupted since 1986), and 187 east of 120.5 degrees west longitude.

During this reporting period there were 21 earthquakes reported felt west of the Cascades, and 4 reported felt east of the Cascades. The largest earthquake was magnitude 5.1, and occurred on December 4, 1993 (22:15 UCT) near Klamath Falls, Oregon. This was the largest aftershock following a main-shock pair (magnitudes 5.9 and 6.0) on September 21, 1993 (UCT). The sequence, which had diminished rapidly after the September, 1993 mainshocks, resurged following the December 4 aftershock. Table 1 gives the number of Klamath Falls earthquakes of magnitude 2.0 or greater in each month since the mainshock. Following the December 4 aftershock, five additional shocks of magnitude 4 or larger in the Klamath Falls area followed during December 1993 and January 1994, and smaller earthquakes continued throughout this reporting period.

Articles on the Klamath Falls, Oregon sequence have been published in the USGS publication **Earthquakes and Volcanos** (Vol. 24, No. 3, 1993) which can be ordered from: USGS Map Distribution, Box 25286, Bldg. 810, Denver Federal Center, Denver, CO 80225.

**Table 1: Klamath Falls earthquakes;  
Number per month, magnitude 2.0 or larger**

Month	Number of events
September, 1993	105
October, 1993	16
November, 1993	12
December, 1993	112
January, 1994	110
February, 1994	11
March, 1994	15
April, 1994	12
May, 1994	10
June, 1994	6
July, 1994	3
August, 1994	4
September, 1994	1
October, 1994	1

Two other notable felt earthquakes, magnitudes 4.0 and 4.3, occurred within a few days of one another in June and are apparent in Fig. 1. The earlier event, on June 15 at 8:22 UCT, was a deep earthquake (about 45 km) west south-west of Bremerton, Washington. It was widely felt around the south Puget Sound region. Earthquakes of this type (deeper than 30 km and within the subducting Juan de Fuca plate) are well known, and include the damaging earthquakes of 1949 and 1965 (magnitudes 7.1 and 6.5 respectively). Magnitude 4 or larger earthquakes within the subducting plate have occurred about every two years, on average, since 1970 (preceding this event, the last such earthquakes were in 1989, when two deep events larger than magnitude 4 occurred). The other earthquake, magnitude 4.3 on June 18th at 07:01 UCT, was located near Skykomish, Washington with an estimated depth of 6 km, and was followed by 8 aftershocks within the next few days. This event was unusual because, historically, Skykomish is not known to be the source of any significant earthquakes, and no other felt earthquakes, nor any larger than magnitude 2.5, have been located within 10 km of the mainshock since we began locating earthquakes with our regional network in 1970.

PNSN Quarterly Reports for 1994 have included moment-tensor focal mechanisms for earthquakes larger than magnitude 3.5. These have been provided to us by Dr. John Nabelek of Oregon State University (OSU) under support from USGS NEHRP Grant 1434-93-G-2326. OSU also provides broad-band data from station COR, which we archive with our trace-data files. The University of Oregon (UO) also provides broad-band data (from stations PIN and DBO), which is likewise archived.

#### Reports and Articles

- Braunmiller, J., J. Nabelek, B. Leitner, and A.I. Qamar, 1994 (in press), The 1993 Klamath Falls, Oregon, earthquake sequence: Source mechanisms from regional data, submitted to *Geophys. Res. Lett.*
- Jonientz-Trisler, C. B. Myers, and J. Power, 1994, Seismic identification of gas-and-ash explosions at Mount St. Helens: capabilities, limitations, and regional application, in *Proceeding Volume, First International Symposium on Volcanic Ash and Aviation Safety, T.J. Casedevall, editor, USGS Bulletin 2047.*
- Ludwin, R.S., A.I. Qamar, S.D. Malone, C. Jonientz-Trisler, R.S. Crosson, R. Benson, and S. Moran, 1994, Earthquake Hypocenters in Washington and Northern Oregon, 1987-1989 and the Washington Regional Seismograph Network; Operations and Data Processing, Washington State Dept. of Natural Resources, Information Circular 89, 40 p.
- Ludwin, R.S., A.I. Qamar, S.D. Malone, R.S. Crosson, S. Moran, G.C. Thomas, and W.P.

- Steele (in preparation), Earthquake Hypocenters in Washington and Oregon, 1990-1994, Washington State Dept. of Natural Resources Information Circular
- Qamar, A.I. and K. L. Meagher, 1993, Precisely Locating the Klamath Falls, Oregon, Earthquakes, Earthquakes and Volcanos, V. 24, N. 3, pp. 129-139.
- Thomas, G.T. and R.S. Crosson, (in preparation), The 25 March 1993 Scotts Mills, Oregon earthquake and aftershock sequence; spatial distribution, focal mechanisms, and the Mount Angel Fault Zone, to be submitted to BSSA.
- Univ. of Wash. Geophysics Program, 1994, Quarterly Network Reports; 93-D, 94-A, 94-B, and 94-C; Seismicity of Washington and Western Oregon
- Wiley, T.J., D.R. Sherrod, D.K. Keefer, A.I. Qamar, R.L. Schuster, J.W. Dewey, M.A. Mabey, G. E. Black, and R.E. Wells, 1993, Klamath Falls earthquakes, September 20, 1993 - including the strongest quake ever measured in Oregon, Oregon Geology, Vol. 55, No. 6, pp. 127-134.

#### Abstracts

- Khazaradze, G. and S.D. Malone, 1994, Determination of local magnitude using Pacific Northwest Seismic Network Broadband Data, EOS, Vol. 75, Supplement to No. 44, p. 460.
- Ludwin, R.S., S.D. Malone, A.I. Qamar, and R.S. Crosson, 1993, Operation of the Washington Regional Seismograph Network, Seis. Res. Lett., V. 64, No. 3, p. 262.
- Malone, S.D., 1994, A review of seismic data access techniques over the Internet, EOS, Vol. 75, Supplement to No. 44, p. 429.
- Moran, S.C., and S.D. Malone, 1994, A Seismic refraction profile across the central Washington Cascades: Preliminary Results, EOS, Vol. 75, Supplement to No. 44, p. 621.
- Qamar, A.I., and K.L. Meagher, 1993, The 1993 Klamath Falls, Oregon Earthquake Sequence, Special Session, Fall 1993 AGU meeting at-meeting program, p. 219.

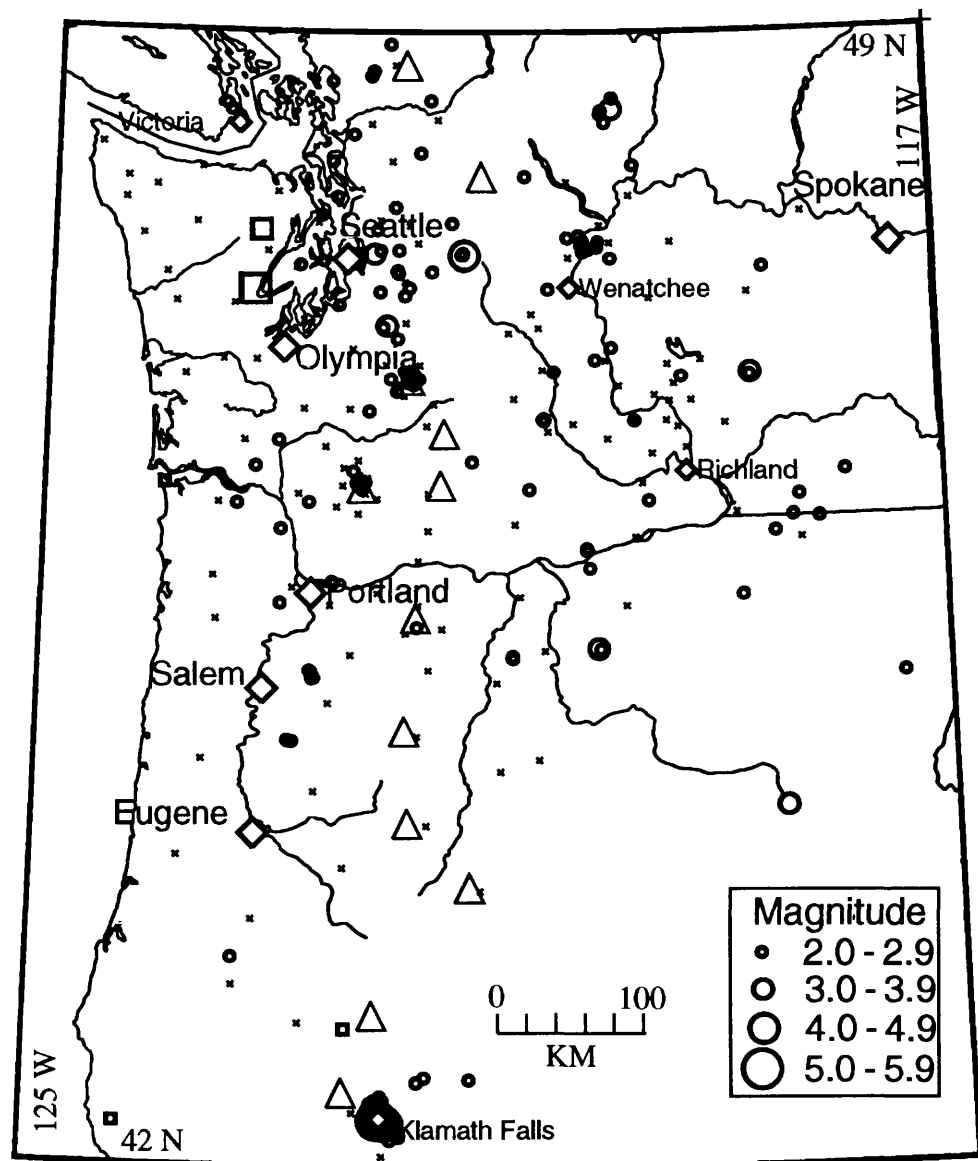


Figure 1. Earthquakes larger than magnitude 2.0 between Oct. 1, 1993 and Sept. 30, 1994. Locations of a few cities are shown as white-filled diamonds. Earthquakes are indicated by filled circles or squares; circles represent earthquakes at depths shallower than 30 km, and squares represent earthquakes at 30 km or deeper. Small "x" symbol indicate locations of seismometers operated by the PNSN at the end of Sept. 1994. More information on stations is included in the report on grant 1434-92-G-2195 in this volume.

## Deformation of Hawaiian Volcanic Systems

9980-10128

Paul Delaney  
U.S. Geological Survey  
2255 North Gemini Drive  
Flagstaff, Arizona, 86001  
602/556-7270, fax -7169  
delaney@aa.wr.usgs.gov

### *Investigations Undertaken*

1. The era of modern terrestrial geodetic data collection is coming to an end, having begun in Hawaii during the mid 1950s with the development by Jerry Eaton of water-tube tilt instruments and the completion of a 3rd-order leveling across east Hawaii. Subsequent leveling-, ranging-, and tilt-measurement procedures were specific to the staff and equipment at HVO; they suffer accordingly from a number of peculiarities. Most of these data have not been critically examined for accuracy and precision, and have not been interpreted using modern techniques.
2. The stresses that dilate Kilauea's rift system are greatly uncertain, as is the thermal structure that permits its mobility. The state of stress responsible for motions accumulated during the 15 years after the M7.2 earthquake of 1975 was investigated using a two-dimensional boundary-element technique. The thermal structure was investigated using a parameterization developed as part of a Geothermal Studies project. An abstract was submitted to the fall meeting of the American Geophysical Union; a short paper is in Branch Review and will be sent to the proceedings volume of the World Geothermal Congress 1995.
3. The relation between dike injection and seaward motions of the south flank of Kilauea remains controversial and critical to understanding of the related seismicity. With my post-doctoral investigator, Michelle Wallace, I reexamined the events leading to and accompanying the 1983 east-rift-zone dike injection, one of the best recorded such events. We summarized the observational, seismic, and geodetic data and completed dislocation analyses of both the June 1982 injection in the southwest rift zone and the January 1983 injection in the east rift. A paper is in review at Journal of Geophysical Research.
4. I examined the methods used to calculate volumes of accumulation in, or withdrawal from, magma reservoirs. I applied results to geodetic data collected during 1960 collapse of Kilauea volcano, the largest since 1924. A paper is in press at Bulletin of Volcanology.

## Results

1. I delved into the water-tube and spirit-level tilt data collected by HVO since about 1958. Two results emerge. The first is that all stations tilt more-or-less perpendicular to nearby structures, be they faults in the Hilina or Koae systems, the rift zones, or the summit magma reservoir. This result shouldn't be surprising, but has not, to my knowledge, been documented. Second, tilts were everywhere directed away from the summit and rift zones of Kilauea prior to the M7.2 earthquake of 1975 and have been directed toward them ever since. This result is consistent with level data and emphasizes the difference between the present pattern of motion and that taking place prior to that earthquake.
2. The primary active structures of young Hawaiian volcanoes are rifts and low-angle fault systems at the base of the volcanic pile at depths that increase from 8–9 km to 12–13 km toward the island center beneath Mauna Loa. Using the boundary-element method, I modeled these structures as a near-vertical dilatant crack and a near-horizontal slipping crack. Some have argued, myself included, that rift-zone dilation pushes the south flank of Kilauea seaward. Others suggest that ongoing gravitational instability of the edifice produces a relative tension across the rift system which is relieved by magma accumulation there. In the crack model, ambient stresses are assumed to be lithostatic; the low-angle fault is frictional and sensitive to pore pressure. A load attributable to the increased density of magmatic cumulates along the rift system is applied to the dilatant crack. This density contrast,  $150 \text{ kg/m}^3$ , is consistent with gravimetric and aeromagnetic interpretations. This loading alone, however, cannot account for the observed motions of Kilauea, no matter how slippery the fault and no matter what the vertical extent of the rift system. I then added a fault traction estimated from the critical-wedge approximations for basal and surface slopes of  $2^\circ$  and  $7^\circ$ , respectively, of the volcanic edifice. Adjusting the pore pressure to 80% of lithostatic, fault slip extends from the rift system seaward for about 30 km. The displacements are consistent with the subsidence and extension of the summit (more than 1.5 m and 2.25 m, respectively) and the uplift of the south flank (more than 0.5 m). The displacements, however, cannot be matched if the only loading is the critical-wedge traction.

Geothermal exploration along the lower east rift zone is providing important data related to the mobility of this distal subaerial section of Kilauea's rift system. A simple heat-transfer model shows that the hydrothermal reservoir can be maintained at temperatures of  $\sim 300^\circ\text{C}$  by magmatic replenishment at a rate consistent with the ongoing extension and the rate of dike intrusion and eruption over the past 1500 years, less than 2 cm/yr.

2. The east-rift-zone dike injection of 1983 followed a year of heightened earthquake activity, as measured by both the persistent seismicity beneath the south flank and the frequency and duration of the rift-zone swarms that accompany magma migration. At the same time, extension of Kilauea summit accelerated to 35 cm/yr; this rate is a good

estimate of the seaward migration of the south flank. The June 1982 earthquake swarm is well modeled with geodetic data to solve for a dislocation extending along 15 km of the southwest rift zone from 2–3-km to 10–11-km depth and opening about 1 m. The dislocation coincides with the earthquake locations. More complex models, with sources to account for summit subsidence and south-flank fault slip, were more successful in the sense that estimated station motions were more consistently directed seaward. The January 1983 dike injection in the east rift zone is modeled with an opening dislocation that coincides with the seismicity and eruptive fissures. We find that the geodetic data support the presence of a magma reservoir beneath Makaopuhi, where the seismic activity initiated. Deflation at Makaopuhi, therefore, was caused by the magma withdrawal that fed dike propagation. As more elements are added to models the amount of estimated opening of the rift-zone dikes decreases. Geodetic data sets that allow development of dislocation-source models for the June 1982 and January 1983 dike intrusions suffer from extremely narrow network apertures. There is substantial covariance, for instance, among opening displacement, depth, and dip of the dikes. Moreover, we show that the data lack resolving power, and so sources of motion other than or in addition to the rift-zone dikes are difficult to identify. Arguments to the contrary notwithstanding, these data are incapable of uniquely determining the relation between rift-zone dike intrusions and south flank migration.

3. There exists a widespread misconception in volcanology that the volume of ground-surface uplift or subsidence equals the volume of magma accumulation or withdrawal in the underlying reservoir. We show that for the most commonly used model, the Mogi model, the uplift volume is 50% *greater* than the accumulation volume for the most commonly used value of Poisson's ratio. We also show that there is no general factor relating these volumes; the uplift volume above a vertical dislocation, for instance, is 25% *less* than the accumulation volume. Finally, we demonstrate that unambiguous identification of the appropriate magma-reservoir model is problematic and conclude that volumes of magma transfer estimated from geodetic data are much more poorly constrained than has been supposed. For the 1960 collapse of Kilauea, estimates that account for the data equally well vary by a factor of three.

### ***Reports Published***

Delaney, P.T., and D.F. McTigue, *in press*, Volume of magma accumulation or withdrawal estimated from surface uplift or subsidence, with application to the 1960 collapse of Kilauea volcano: *Bulletin of Volcanology*, 19 ms pages, 2 tables, 4 figures.

Wallace, M.H., and P.T. Delaney, *submitted*, Deformation of Kilauea volcano during 1982 and 1983: a transition period: *Journal of Geophysical Research*, 35 ms pages, 8 tables, 15 figures.

Wallace, M.H., and P.T. Delaney, 1994, Rift zone and south flank motions of Kilauea volcano during 1982: Geological Society of America Abstracts with Programs, v. 26, p. A-220.

Delaney, P.T., M.H. Wallace, and A.M. Rubin, 1994, Origin of coincident subsidence and extension of Kilauea summit and uplift of its south flank since 1976: Transactions of the American Geophysical Union, v. 75, p. 712.

Wallace, M.H., P.T. Delaney, and C.A. Williams, 1994, A critical wedge model of the south flank of Kilauea volcano: Transactions of the American Geophysical Union, v. 75, p. 718.

Delaney, P.T., J.H. Sass, W.A. Duffield, and J.P. Kauahikaua, *in review*, Characteristic temperatures and response times of geothermal systems, with an example from Kilauea, Hawaii: Proceedings World Geothermal Conference 1995, 16 ms pages, 5 figures.

# Integrated Approach to Earthquake Hazard Assessment of a Subduction Segment: A Case Study of the Shumagin Islands Region, Alaska (grant 1434-93-G-2325)

Renata Dmowska and James R. Rice (PI)

Division of Applied Sciences and Department of Earth and Planetary Sciences,  
Harvard University, Cambridge, MA 02138

(617) 495-3452 dmowska@geophysics.harvard.edu, (617) 495-3445 rice@esag.harvard.edu  
Program element:

## Investigations:

An integrated approach is being used to understand the seismic potential of the Shumagin Islands, Alaska, subduction. It consists of using: (1) seismicity data to understand the maturity of the segment by analysis of outer-rise and intermediate-depth seismicity, as it depends on time in the cycle, and to predict the areas of highest slip in future earthquakes; (2) seismicity in the thrust contact zone to anticipate the coming earthquake if an accelerated seismic moment release is observed; (3) local seismicity data to understand the local geometry of the descending slab and to constrain the geometry for finite element modeling; (4) 2D finite element modeling to investigate the strain and deformation changes during the earthquake cycle and compare them with geodetic strain, tilt and vertical displacement observations if available; (5) 3D extensions of the modeling to specifically address geodetic and seismicity implications of non-uniform locking along the thrust interface, having the form of most severe inhibition of slip in regions that will manifest themselves as "asperities" in the pattern of seismic moment release in a future ruptures.

## Results:

The most recent results are directed to improving our 2D modeling to fit newly available geodetic data for the Shumagins (Larson and Lisowski, *Geophys. Res. Lett.*, 1994) consisting of GPS 1987, 1989 and 1991 surveys, and their integration with the EDM data (Lisowski et al., *J. Geophys. Res.*, 1988) for 1981-1987. We also continue to analyze our 3D generic model of a subduction segment with asperities, to better understand the influence of asperities on deformation of the upper plate, stress channeling effects on nearby seismicity, etc.; ultimately we hope to develop a family of 3D asperity(ies) models, tailored to the Shumagins segment, which are consistent with along-strike variations of seismicity and geodetic measurements.

The Shumagin Islands subduction segment has been identified as a seismic gap between the 1938 earthquake to the east ( $M_w = 8.2$ ) and the 1946 earthquake ( $M_s = 7.3$ ) to the west (Kelleher, *J. Geophys. Res.*, 1970; Davies et al., *ibid*, 1981). Previous large or great earthquakes which ruptured that part include 22 July 1788, 16 April 1847 (see, e.g. Estabrook et al., *ibid*, 1994), and the most recent one of 31 May 1917 ( $M_s = 7.4$ , Estabrook and Boyd, *Bull. Seism. Soc. Amer.*, 1989). Based on these events the average repeat time is  $65 \pm 10$  years (Nishenko, *Pure Appl. Geophys.*, 1991). The accumulated seismic moment release rate of shallow (0-50 km depth) earthquakes in this area increases markedly, and much faster than linearly with time, since approximately 1980, as we show in figure 1 (Dmowska, Spring 93 AGU special session on the  $M_s = 6.9$  event of May 13, 1993). Also, we find (figure 2) a cessation since 1977 of the previously abundant, generally tensional, outer-rise seismicity, which we interpret as a sign of significant coupling, leading to a decrease of tensional stresses there as the seismic cycle matures. Both these signs suggest maturity of this segment.

However, the strain measurements available there seemed, as first reported based on EDM for 1980-87, to not show any significant strain accumulation, suggesting that aseismic slip is occurring (Lisowski et al., *J. Geophys. Res.*, 1988). Subsequent GPS for 1987-1991 data (Larson and Lisowski, *Geophys. Res. Lett.*, 1994) showed, when combined with EDM data, a somewhat stronger indication of strain accumulation, with trench-perpendicular compression rate of  $0.026 \pm 0.012 \mu\text{strain/yr}$  averaged over the network. Our previous modeling had been directed to trying to rationalize the (Lisowski et al., 1988) inference of a strain rate reported, from the EDM data, as  $0.00 \pm 0.03 \mu\text{strain/yr}$ , and now we seek models which are consistent with the new interpretation of the strain measurements and also with the more detailed structure of the variation in trench-perpendicular velocity component within the network, as reported by Larson and Lisowski (1994). The uplift data and tilt data (Beavan, *USGS Open-file Rept. 92-258*, 1992) do suggest observable variation which might be related to a seismically coupled subduction zone. With these observations in mind we have been addressing the following question: Given the seismic and geodetic constraints, can we judge if the Shumagin segment is seismically coupled or not, and what magnitude earthquake might be expected in the future there, if at all?

The basic 2D finite element model has been described previously; figure 3 shows the coupled part of the thrust zone (heavy line); either free-slip or flow with a short relaxation time are allowed along the fault up-dip and in the two elements immediately down-dip from it. Slip is imposed along the heavy line by the standard sawtooth history, using a superposition into steady and cyclic response described by Dmowska et al. (*J. Geophys. Res.*, 1988); we deal only with the cyclic variations of deformation and stress here and, for that purpose, we assume that a fraction  $\alpha$  of the incoming plate motion is seismically coupled, so that the amplitude of the sawtooth variation in imposed slip, for calculation of the cyclic response, is  $\alpha V_{\text{plate}} T_{\text{cycle}}$ . The interface has been chosen based on seismicity locations (Beavan et al., *J. Geophys. Res.*, 1984; Hauksson, *ibid*, 1985), but modest variations in interface position near the bend can cause significant changes in surface deformation predictions. The model shown evolved in an attempt to rationalize the pre-GPS deformation data, and that work must be repeated in light of the newer data. The mantle and, especially, mantle wedge are made viscoelastic. Previously, to keep strains low in the region of the network, and also to fit a possibly too large estimate of relative uplift between stations (see footnote 3 of the Table), we had considered mantle relaxation times as short as  $T_{\text{cycle}}/12$ . It now appears that longer relaxation times, of order  $T_{\text{cycle}}/3$ , may be acceptable.

If  $M_0 = 1.7 \times 10^{27}$  dyne cm (Estabrook and Boyd, 1992) for the 1917 event is used, based on shear modulus  $\mu = 3.0 * 10^{11}$  dyne/cm<sup>2</sup>, average recurrence time  $T_{\text{cycle}} = 70$  years (which would mean the region is overdue), relative convergent rate  $V_{\text{plate}} = 64$  mm/yr and a rupture area 85 to 90 km long, combined with the 97.6 km is the down-dip width in our model, we get a seismic coupling factor  $\alpha = 0.15$ . Estabrook and Boyd (1992) suggested a rupture length 75 km and down-dip width of 100 km, which results in  $\alpha = 0.17$ . The distribution of coupling factor with depth could be variable; seismic observations suggest that the lower part of the coupled zone is the dominant area. This kind of variation can be described by assigning various seismic coupling factors. The ratio was fixed as 1 : 1.5 : 2 for the upper part, bend and lower part of the locked zone in the modeling results shown, but we will be reviewing such distribution in light of the more recent data.

Results for area-averaged seismic coupling factors  $\alpha = 0.15$  and 0.20 are shown in the Table; the latter,  $\alpha = 0.20$ , gives a very good account of the data. The assumption of zero seismic coupling could not fit the data. Thus, we have a tentative interpretation of the seismic data which is

consistent with our inferences from seismicity (figures 1 and 2) that this region is strongly coupled and is likely to produce a future event comparable to the 1917 earthquake.

Figure 4 shows a comparison, for the case of relaxation time  $T_{re} = T_{cycle}/3$ , of the horizontal velocity distribution predicted by the model and the newly available (Larson and Lisowski, 1994) trench-perpendicular velocity data. We will be trying alterations of the coupling factor distribution and interface geometry near the bend to achieve a better description of that data.

### Reports:

Dmowska R., "Interplate coupling and trench-outer-rise earthquakes" (abstract), SUBCON, An Interdisciplinary Conference on the Subduction Process, Catalina Island, California, June 12-17, 1994.

Dmowska, R., G. Zheng and J. R. Rice, "Rheological and Tectonic Controls on Stressing History and Seismicity in the Outer-rise During the Earthquake Cycle: Oaxaca 1978, Mexico, Segment" (abstract), *EOS Trans. Amer. Geophys. Union*, 75, no. 44, Fall Meeting Supplement, 1994, p. 449.

Dmowska, R., G. Zheng and J. R. Rice, "Earthquake cycles in a subduction segment with a row of asperities" (abstract), *EOS, Trans. Am. Geophys. Un.*, 74, N. 43, supplement, p. 91, 1993.

Zheng, G., R. Dmowska and J. R. Rice, "Deformation during the earthquake cycle in an oblique subduction segment with asperities" (abstract), *EOS, Trans. Am. Geophys. Un.*, 74, N. 43, supplement, p. 91, 1993.

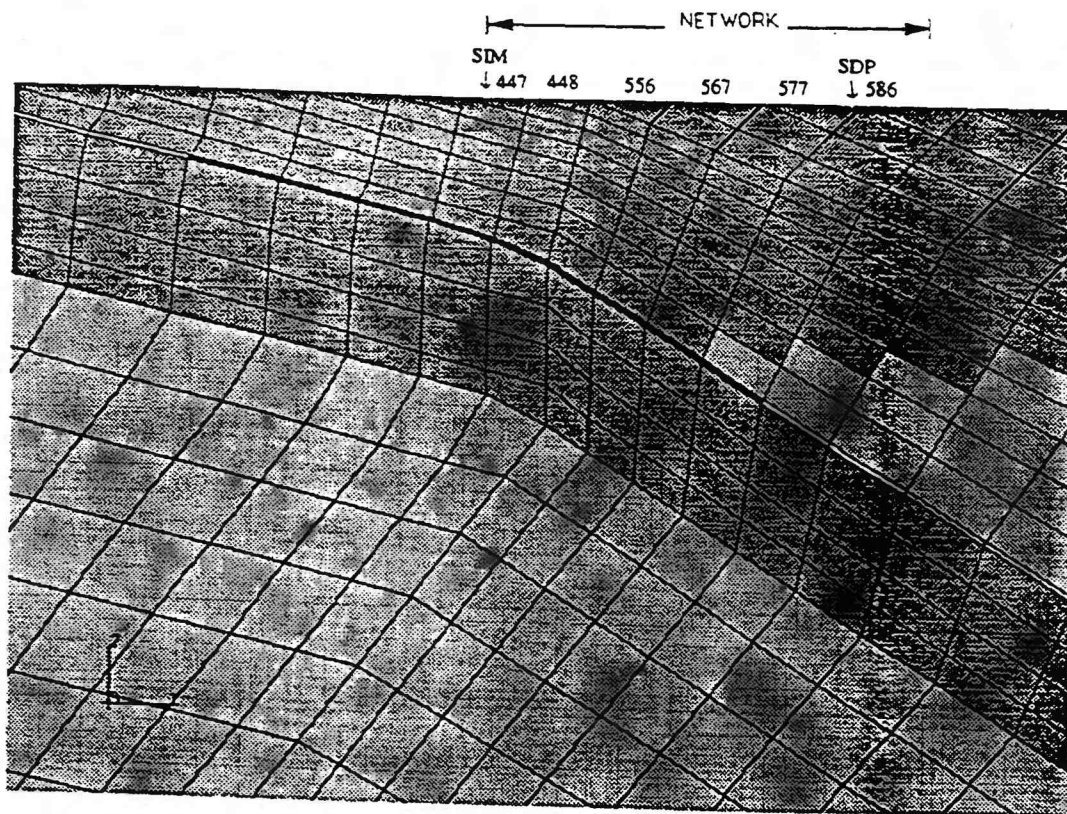


Figure 3. Finite-element mesh, and network for deformation data. (Figures 1 and 2 appear later).

$T_{re} = T_{cycle}/6$ 

Deformation Parameter	Model Predictions		Observations
	$\alpha = 0.15$	$\alpha = 0.20$	
Strain ( $\mu$ strain/yr) 1981-1991 Averaged over network <sup>1</sup>	-0.0184	-0.0245	-0.026 $\pm$ 0.012
Tilt ( $\mu$ rad/yr) 1981-1991 Inner Shumagins <sup>2</sup> Outer Shumagins <sup>2</sup>	0.0718 -0.0677	0.0957 -0.0903	0.10 $\pm$ 0.05 -0.11 $\pm$ 0.07
Uplift (mm/yr) SIM relative to SDP 1976-1991 <sup>3</sup> SIM relative to SDP 1985-1991 <sup>3</sup> SDP absolute 1970-1990 <sup>4</sup>	-2.69 -2.69 -1.85	-3.58 -3.58 -2.46	-4.0 $\pm$ 1.0 -1.8 $\pm$ 1.2 -2.2 $\pm$ 1.4

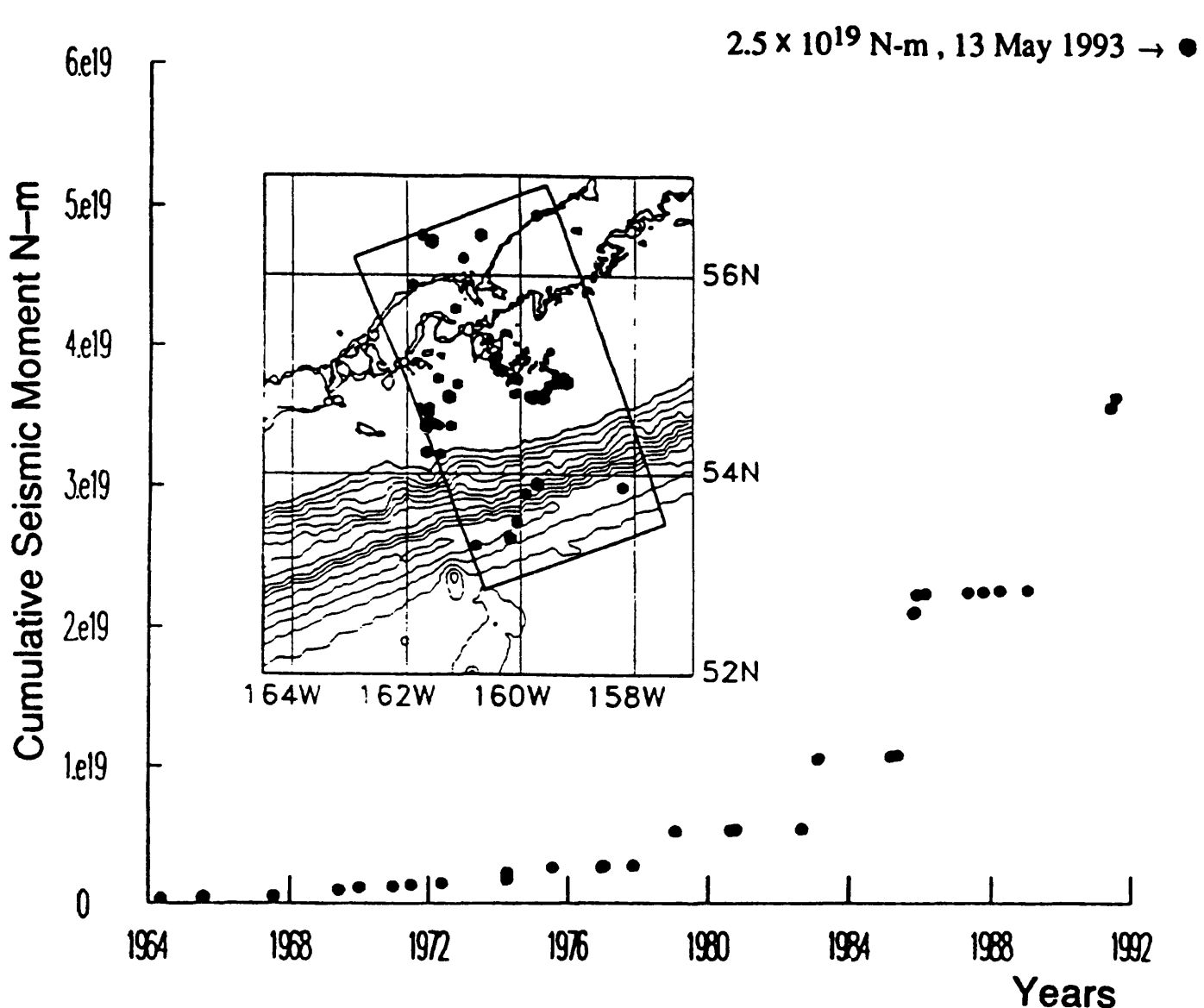
 $T_{re} = T_{cycle}/3$ 

Deformation Parameter	Model Predictions		Observations
	$\alpha = 0.15$	$\alpha = 0.20$	
Strain ( $\mu$ strain/yr) 1981-1991 Averaged over network <sup>1</sup>	-0.0192	-0.0256	-0.026 $\pm$ 0.012
Tilt ( $\mu$ rad/yr) 1981-1991 Inner Shumagins <sup>2</sup> Outer Shumagins <sup>2</sup>	0.0646 -0.0677	0.0861 -0.0903	0.10 $\pm$ 0.05 -0.11 $\pm$ 0.07
Uplift (mm/yr) SIM relative to SDP 1976-1991 <sup>3</sup> SIM relative to SDP 1985-1991 <sup>3</sup> SDP absolute 1970-1990 <sup>4</sup>	-2.21 -2.21 -1.67	-2.94 -2.94 -2.23	-4.0 $\pm$ 1.0 -1.8 $\pm$ 1.2 -2.2 $\pm$ 1.4

**Notes:**

1. Larson & Lisowski (*Geophys. Res. Lett.*, 1994), combining results of GPS survey for 1987-1991 and earlier (Lisowski et al., *J. Geophys. Res.*, 1988) EDM survey for 1980-1987.
2. Beavan (*USGS Open-file Rept. 92-258*, 1992), tilt measurement, for 1981-1991.
3. Beavan (*op cit*, 1992), based on sea level data: if the 1976-91 differential sea level data are interpreted as constant tilt rate, then SIM appears to be subsiding relative to SDP at  $4 \pm 1$  mm/yr; if however the fit is made only to higher quality post-1985 data, then SIM is subsiding relative to SDP at  $1.8 \pm 1.2$  mm/yr.
4. Savage and Plafker (*J. Geophys. Res.*, 1991), based on sea level change (1970-1990), adjusted to account for postglacial rebound rate and eustatic rate.

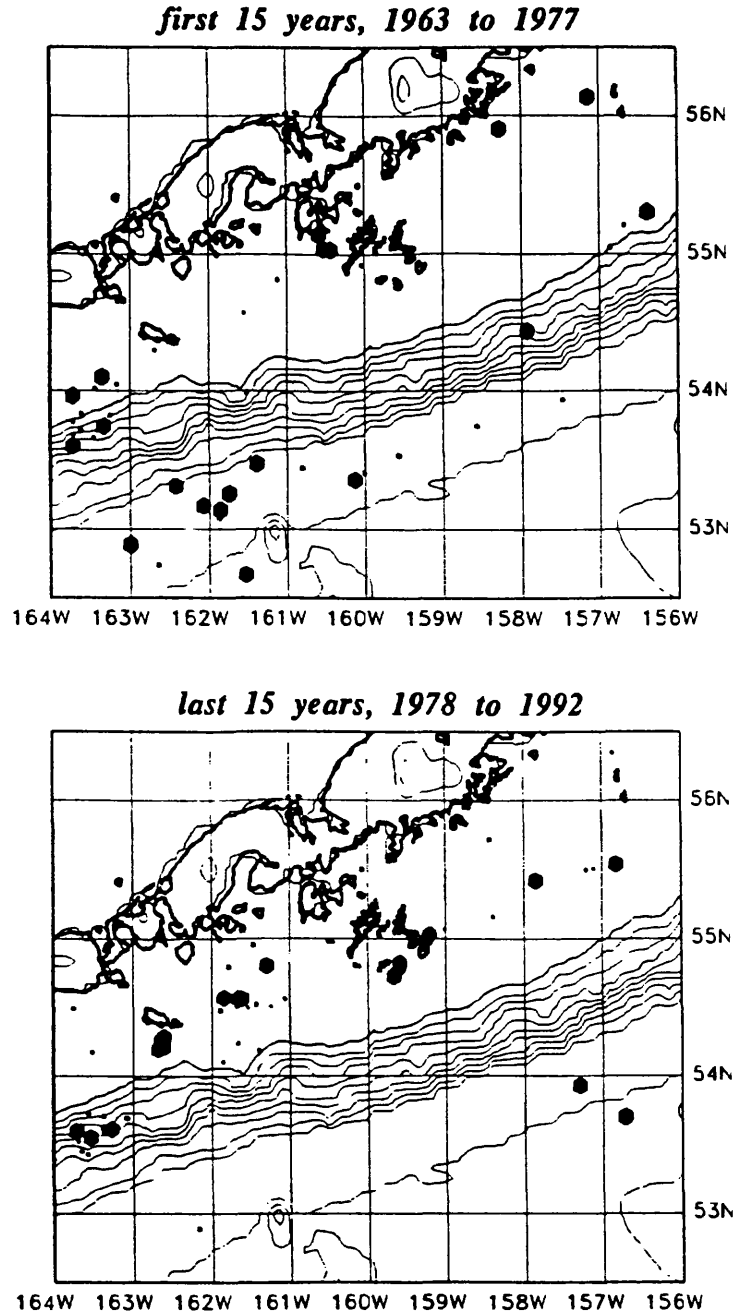
Table: Summary of models, assuming different relaxation times  $T_{re} = T_{cycle}/6$  and  $T_{cycle}/3$ , and different seismic coupling factors  $\alpha = 0.15$  and  $0.20$



Cumulative moment for events with depth  $\leq 50$  km in box shown  
*(portion of box along thrust zone coincides with 1917 rupture;*  
*marked events:  $m_b \geq 5.0$  for 1963.0 to 91.5)*

Figure 1. Accelerated moment release in the Shumagins area.

**30 Years of Seismicity in Shumagins Region, 1963 to 1992**  
 ( Depths  $\leq$  50 km ; Small symbols:  $5.0 \leq m_b \leq 5.4$  ; Large symbols:  $m_b \geq 5.5$  )



**Consistency with maturing of cycle in coupled subduction segment:**

- **Outer rise:** Decreased activity in last versus first period; building of stress in compression shuts off the (presumably) extensional seismicity.
- **Thrust region:** Increased activity in last 15 year period; see moment release.

Figure 2. Reduction since 1977 of the previously abundant outer-rise seismicity along the Shumagins segment.

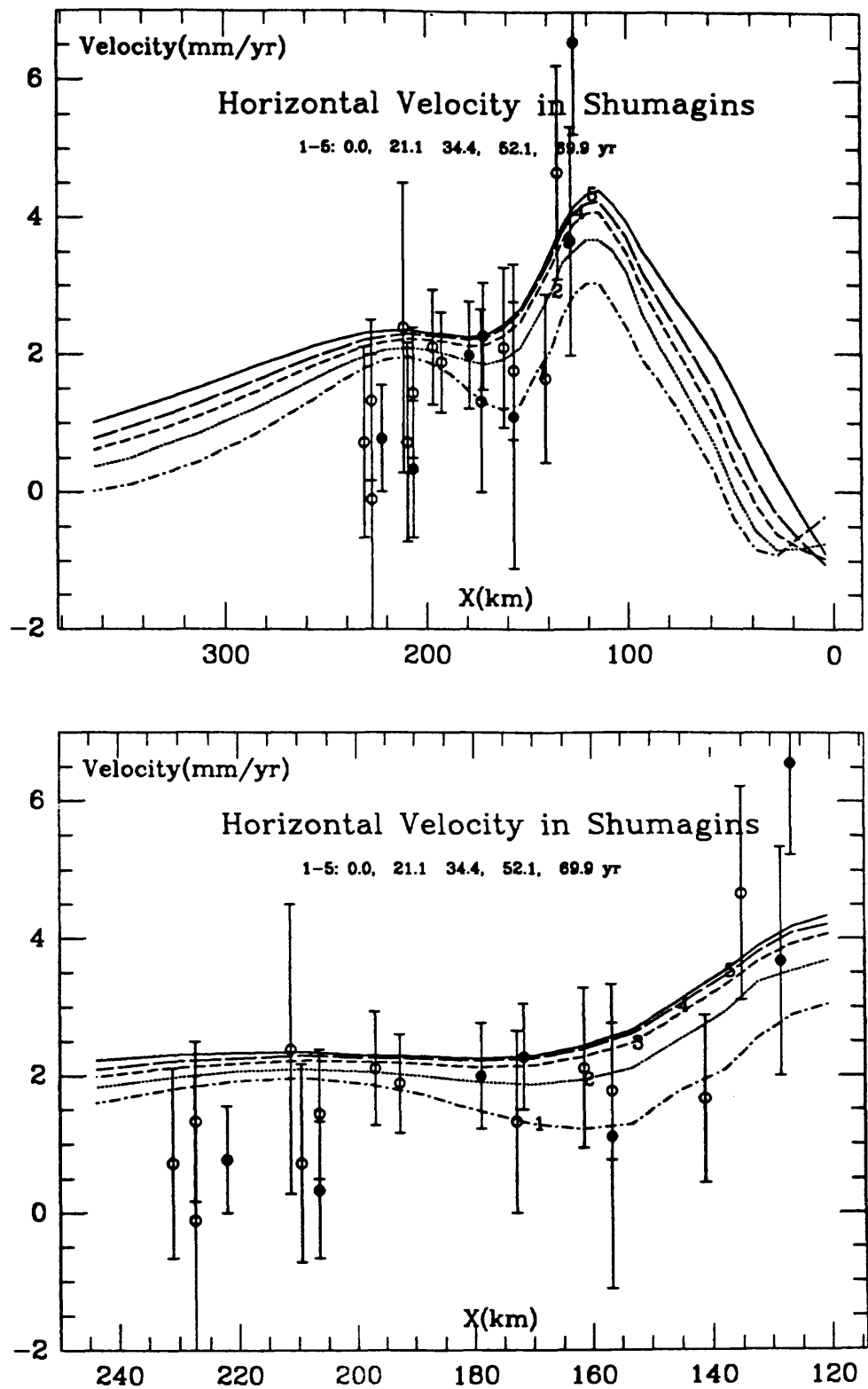


**Figure 4:** Prediction, for  $T_{re} = T_{cycle}/3$ , of trench-perpendicular velocity components from the model, as compared to the recent data of Larson and Lisowski (Geophys. Res. Lett., 1994). The lines are for different times and the solid line corresponds to 70 years after the previous event, i.e., to 1987.

## The New England Seismic Network

Award Number 1434-92-A-0972

John E. Ebel  
Weston Observatory  
Department of Geology and Geophysics  
Boston College  
Weston, MA 02193  
(617) 552-8300  
Fax: (617) 552-8388  
EBEL@BCVMS.BC.EDU

Program Element: Seismic Network Operations

## Investigations

The operation of a regional seismic network to monitor earthquake activity in New England and vicinity is supported under this project. The purpose of this earthquake monitoring is to compile a complete database of earthquake activity in New England to as low a magnitude as possible in order to understand the causes of the earthquakes in the region, to assess the potential for future damaging earthquakes, and to better constrain the patterns of strong ground motions from earthquakes in the region. The New England Seismic Network (NESN) is cooperatively operated by Weston Observatory of Boston College and the Earth Resources Laboratory of the Massachusetts Institute of Technology (MIT).

## Network Status

On October 1, 1993 the U.S. Nuclear Regulatory Commission terminated the analog telephone for the stations of the NESN, reducing the Weston Observatory network to the station at Weston Observatory plus remote stations with PC recording systems at Milo, Maine and Gaze, New Hampshire. In August of 1993 Boston College received a \$300,000 grant from the Federal Emergency Management Agency to purchase and fabricate equipment for 15 new seismic stations. Each of these new stations, to be operated jointly by Weston Observatory and by MIT, is to be comprised of a three-component set of broad-band sensors (peak sensitivity in the 30 sec to .03 sec period range), a 16-bit A/D system, a PC capable of recording both individually triggered events and 7-days continuous data, and a modem for dial-up telephone telemetry to the

central recording sites (Weston Observatory and the Earth Resources Laboratory at MIT). Initial equipment orders were placed in September and October, 1994. It was decided to purchase the station digitizing systems from Nanometrics, Inc., the recording computers from IBM, and the seismic sensors from Guralp, Ltd.

Installation of the new stations has been delayed due to hardware delivery delays, software bugs in the data acquisition and transmission software, and thorough testing of the new systems. Shortages in the inventories of the first computers which were ordered left the initial orders unfilled for several months. Some initial problems with the communications software were fixed by the manufacturer, as were some other minor bugs in earlier versions of the acquisition software. The first seismometers were about two months late in being delivered. These were then shipped to the data acquisition manufacturer to test compatibility with their hardware and to perform initial calibrations. Due to the long-period part of the instrument response, the instruments needed a long time period (several weeks) to settle down before they could be calibrated.

The first data acquisition system was installed at Weston Observatory for testing in the spring of 1994. Because the Guralp seismometers were not yet available, the acquisition equipment was connected to a vertical-component, 1-Hz HS-10 velocity transducer geophone. After a few months of testing and debugging, this first station was installed at Milo, Maine in July, 1994. It operated well for about 2 months, collecting the signals from several earthquakes. The station went down briefly in September, 1994, necessitating a trip to the station for repairs. Overall, the equipment has operated very well, providing reliable, high-quality data. At the time of the writing of this report, equipment for a second new station at Gaza, New Hampshire has been assembled and prepared for installation, and preparations for the installation of a new station at Hanover, New Hampshire have begun.

In addition to the Weston Observatory NESN stations, MIT continues to operate 5 analog seismic stations in New Hampshire and Massachusetts. These stations provide important data for locating earthquakes centered within New England. Also, there are now 4 USNSN stations operating in New England. A USNSN satellite receiver is installed atop Weston Observatory, and in some preliminary tests USNSN data have been successfully received via from the USGS at Golden, Colorado. The present plans are to develop software to receive at Weston Observatory satellite transmissions of the triggered waveform data from the 4 New England

USNSN stations. However, the software for receiving and storing these data will not be ready before 1995.

Weston Observatory has begun routinely requesting local earthquake data from the USGS via the USNSN AUTODRM system. This has proven to be a very speedy and satisfactory way to procure USNSN waveforms of local and regional earthquakes. The USNSN stations are viewed as one important component of regional seismic network monitoring in New England and vicinity.

Weston Observatory and MIT continue to archive independently the waveform data for the seismic stations which they are operating. Each institution has the capability to convert these waveforms to SAC format for external distribution, and ftp accounts are available at each institution for easy external access to the waveforms as well as the event location data. For the Weston Observatory data, both location files (with .XX extensions) and station waveforms in SAC format (the file name prefixes are the date, day of year and time of the record and the extension is the station name), one connects via ftp to BCINFO.BC.EDU, username: ANONYMOUS, password: GUEST. The files are in a subdirectory named [FTP.EBEL].

## Seismicity

Figure 1 shows the local and regional earthquakes recorded by the NESN seismic stations of Weston Observatory from October 1, 1993 to September 30, 1994. A total of 26 local earthquakes from New England and vicinity with magnitudes from 2.0 to 4.6 were detected and located by the network, nine of which were felt. In addition to these events, a number of microearthquakes and suspected events, too small to be located, were detected by the network. Several significant earthquakes during this time period, including several earthquakes above magnitude 4.0. The largest earthquake detected was a  $m_{bLg}=4.6$  earthquake centered near Reading, PA. This event, combined with a  $m_{bLg}=4.2$  aftershock, caused some minor damage in the epicentral area. These earthquakes occurred at the edge of a recently abandoned quarry, leading to some speculation that water infilling the quarry pit could have induced these earthquakes. Other earthquakes above magnitude 4.0 occurred in the Charlevoix seismic zone on September 25, 1994 ( $m_{bLg}=4.3$ ), near Montreal on November 11, 1993 ( $m_{bLg}=4.4$ ), and in the aftershock zone of the 1982 Miramichi, New Brunswick earthquakes on July 14, 1994 ( $m_{bLg}=4.1$ ). The former was felt in the Charlevoix area, while the latter was felt in New Brunswick and at Presque Isle, Maine. A swarm of at least 11 earthquakes, ranging in magnitude up to  $m_{bLg}=3.8$ , were centered near Springfield, Maine between

September 16 and September 22, 1994. Several of these earthquakes were felt by persons in the towns near the epicenters. In addition to these felt earthquakes, an intriguing event took place east of Cape Ann, Massachusetts on June 14, 1994. While only  $m_{bLg}=2.5$ , this event is of interest because of it may be an indicator of the source region of the strong earthquake of 1755. The 1755 event, estimated to have been about  $m_{bLg}=6$ , is thought to have been centered somewhere east of Cape Ann.

## Publications

Ebel, J.E., Bollinger, G.A., and Herrmann, R.B., Historic and Recent Seismicity, Chapter 2 in Earthquake Hazard Assessment in the Central and Eastern United States, in press, 1994.

Klotz, L.H. and J.E. Ebel, Earthquakes in the Eastern U.S.: How Vulnerable are We?, Proceedings of the First Annual Congress on Natural Disaster Loss Reduction, Boston, MA, June 17, 1994, in press, 1994.

Zhu, H. and J.E. Ebel, Tomographic inversion for the seismic velocity structure beneath northern New England using seismic refraction data, J. Geophys. Res., 99, 15,331-15,357, 1994.

## Abstracts

Ebel, J., Analysis of Spectral Attenuation Functions in New England for Seismic Hazard Analyses, EOS, Trans. Amer. Geophys. U., vol. 75, No. 44, p. 450, Supplement, 1994.

Ebel, J.E., A Reexamination of the Seventeenth Century Earthquakes in Northeastern North America, Seism. Res. Lett., vol. 65, in press, 1994.

Ebel, J.E. and R. Hon, The Upper Mantle Boundary Between Grenville and Avalon in New England: Seismic Evidence and Petrologic Implications, Seism. Res. Lett., vol. 65, p. 16, 1994.

Ebel, J., Focal Depth Constraint of New England Earthquakes from Regional Seismic Network Seismograms, EOS, Trans. Amer. Geophys. U., vol. 74, No. 43, p. 401, Supplement, 1993.

Feng, Q. and J.E. Ebel, Determination of Rupture Duration and Stress Drop for Earthquakes in New England, Seism. Res. Lett., vol. 64, p. 259, 1993.

Ebel, J.E. and R. Bedell, A Seismic Hazard Study for the State of Vermont,  
Seism. Res. Lett., vol. 64, p. 259, 1993.

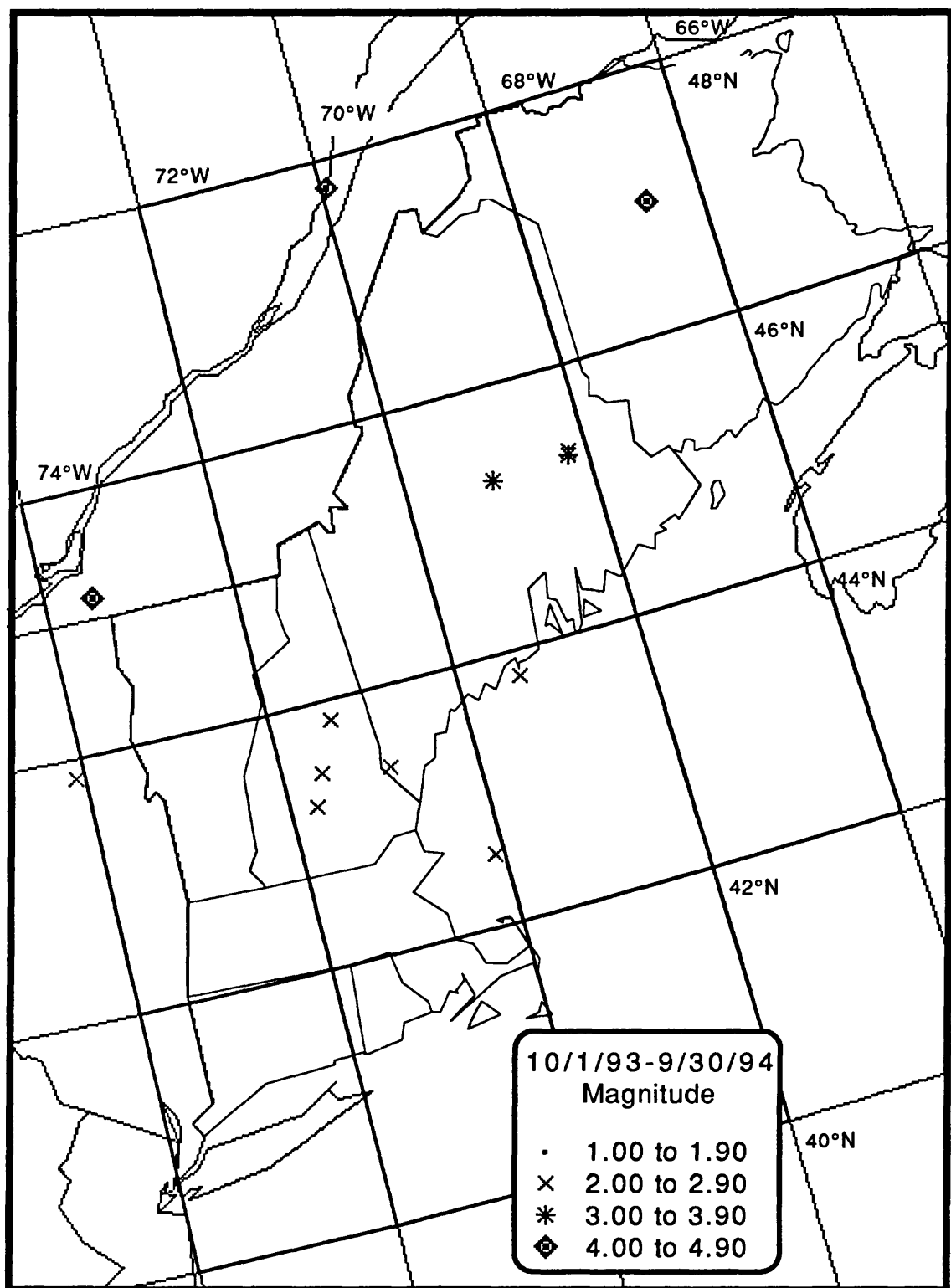


Figure 1. Seismicity recorded by the New England Seismic Network stations of Weston Observatory of Boston College from October 1, 1993 to September 30, 1994.

# Seismic Studies of Fault Mechanics

9930-12123

William L. Ellsworth  
Alex Cole and Lynn Dietz

Branch of Seismology  
U.S. Geological Survey  
345 Middlefield Road - MS 977  
Menlo Park, California 94025  
415-329-4784; 415-329-5163 (Fax)  
ellswrth@andreas.wr.usgs.gov

Program Elements I.1, I.2, II.6, II.7, II.8, and IV.1

## Investigations

1. Earthquake nucleation.
2. Characteristic earthquakes.
3. Real-time earthquake notification system (Earthworm) for the San Francisco Bay Area.

## Results

1. When an earthquake occurs, a fault accelerates from a locked state to one where slip occurs at speeds of up to several m/s and propagates along the fault at a rupture velocity of several km/s. The onset of rupture, as revealed by seismic waves, has generally been interpreted as consistent with self-similar solutions for crack growth, in which the rate of moment release grows as the square of the elapsed time. We have compiled an extensive set of broadband, on-scale, near-field observations of earthquakes from a wide range of tectonic environments that span the magnitude range 1 to 8. We analyze these data by deconvolving complete Green's functions from the P-wave seismograms to determine the moment-rate function.

In all events examined we find that rupture initiates with a distinct phase of slow growth in the moment rate. We term this initial phase the seismic nucleation phase, and the phase of quadratic growth, the breakout phase. The properties of the seismic nucleation phase vary somewhat, in some cases returning to zero before the breakout phase and in other cases smoothly accelerating into the breakout phase. In some cases the seismic nucleation phase has been interpreted as an "immediate foreshock" (e.g. the Loma Prieta, Landers, and Northridge earthquakes). We also find that the distance between the hypocenter, where the nucleation phase begins to be radiated, and the point on the fault where the breakout phase initiates is small. This suggests that the seismic nucleation phase may represent slip growing in place, i.e. without the slipping region propagating along the fault. We find a systematic correlation of the duration of the nucleation phase and the magnitude of the entire earthquake. The duration of the seismic nucleation phase follows a scaling similar to that of constant stress drop (slope of 1/3 on a log-log scale) over 13 orders of magnitude of seismic moment (~3 msec for M=1 to ~5 s for M=8).

The observed scaling suggests that the process responsible for the nucleation phase has a strong influence on the size of the resulting earthquake. Figure 1 shows the seismic nucleation phase for the 1994 Northridge, California, earthquake.

The routine observation of a distinct phase of slow moment growth at the start of earthquakes, M 1-8, suggests that this process is a fundamental part of the earthquake nucleation process. This seismic nucleation phase typically accounts for ~0.5% of the total seismic moment. Its duration, when normalized by the main shock duration, is approximately log-normally distributed about a mean value of 0.16. If we assume that the stress drop during the seismic nucleation phase equals the dynamic stress drop during the breakout phase, then both the size of the nucleation zone and amount of slip can be determined. We find that both of these nucleation zone quantities follow constant stress drop scaling with the main shock moment. We also find that the slip in the nucleation zone represents approximately 20% of the average slip in the main shock.

The characteristics of the seismic nucleation are consistent with two contrasting models of the nucleation process. In one interpretation, which we call the cascade model, the earthquake instability initiates at a point and there is no difference between the beginnings of large and small earthquakes. In this case, the seismic nucleation phase represents a stochastic accumulation of earthquakes. Another interpretation, which we call the pre-slip model,

proposes that the earthquake instability begins within a finite area and that the beginnings of small and large earthquakes differ. We find that the seismic nucleation phase bears the signature of the very end of the nucleation process predicted by theoretical models of earthquake nucleation. It suggests that what we call the beginning of an earthquake — the instant when high frequency waves first radiate into the far field — represents the transition from stable sliding to dynamic rupture. According to theory, failure begins with stable sliding in a confined region that continues until the stiffness falls below a critical value. When dynamic rupture occurs, it is initially confined to this nucleation zone. The rupture breaks out of the zone and propagates along the fault as an earthquake only after a critical stress concentration is achieved. Because the slip in the nucleation zone is a large fraction of the average slip in the main shock, the eventual size of the earthquake may be determined by the amplitude of the stress concentration at breakout. In simple terms, the size of the earthquake is set by how hard it is pushed at the beginning.

2. Waveform analysis of seismicity in central California reveals the routine occurrence of families of repeating earthquakes, events that rupture the same fault area in events of similar seismic moment. These repeating earthquakes share many of the attributes proposed under the characteristic earthquake hypothesis for recurrence of large earthquakes including: a probability distribution for recurrence intervals with a central mean and a long-tail; an inverse proportionality between the length of recurrence interval and the mean rate of strain accumulation; and an absence of evidence for repetition before the recovery of most of the released elastic strain energy.

We are focussing on three sequences of repeating earthquakes that illustrate the variability of the earthquake cycle (Figure 2). One sequence on the San Andreas fault northwest of Parkfield displays remarkably little variation in the length of the recurrence interval (10% coefficient of variation), which is in excellent correlation with the surface record of

steady fault creep at this location. In contrast, the intervals between repetitions for two sources on the Calaveras fault near the southern end of the M 6.2 1984 Morgan Hill earthquake rupture vary from 3 days to over 3 years. These recurrence intervals are not random, however, but are inversely proportional to the geodetically-determined strain rate across the Calaveras fault, which is precisely the prediction of the elastic rebound theory of H.F. Reid (1910).

These observations suggest a probabilistic approach to predicting the time of the next earthquake in each series, in which the independent variable in the model is the stress acting on the source. Because this cannot be measured directly, we must rely upon surrogates, including geodetic measurements of strain and fault creep rate, and the stressing effect of other earthquakes to estimate the time of the next earthquake.

3. Larva 2.0, a functional replacement for the aging Allen/Ellis Real-Time Processor (RTP), is nearing completion. This system is an application of the modular Earthworm signal processing system (Bittenbinder et al., 1994); it features an extremely flexible architecture for both the hardware and software components that will permit us to add new analysis capabilities and new data types (e.g. real-time data from the broad-band digital stations) without interfering with established functionality. Larva software is written in the C programming language and operates on DOS and Unix computers. The main modules of Larva are two network digitizers, two P-wave pickers, and a phase associator. Support modules include a player routine that reads historic trace files, simulating the digitizer module, and a plotting module for visual display of trace data.

In its current implementation, Larva divides the Northern California Seismic Network into two groups of 256 channels; analog signals for each group are digitized on a 486/50MHz computer at a rate of 100 samples/sec. A guide signal is tracked to ensure time-series integrity. Multiplexed digital data are packaged into messages, time-stamped by decoding an IRIG-E time signal, and transmitted over a dedicated ethernet line once per second. In our application we have one Ethernet line per digitizer. Any number of modules attached to these Ethernet lines can receive and process the waveform data independently.

One such "receiver" module is the seismic phase picker. Larva uses two P-wave pickers, each processing data from one of the digitizers on its own 60 Mhz PC. For each phase detected, the picker reports pick time, quality, polarity, station code, coda length, and amplitude information. This information is packaged into messages and sent via serial line to a Sun workstation. Here, a phase associator (Johnson, 1994) receives picks from the entire network and groups them into arrivals from individual earthquakes. It then spools picks from each individual event to a series of programs which locate the earthquake, calculate its magnitude, and send out notifications and alarms. An earthquake in the network is reported about 2-5 minutes after its seismic waves are recorded at the station closest to its epicenter.

Very-rapid reporting of significant earthquakes will be tested this summer with our retrospective "player" system for archived events and the Pacific Gas and Electric Co. (PG&E) prototype earthquake monitor and display computer.

## Reports

- Beroza, G.C., Cole, A.T., and Ellsworth, W.L., in press, Stability of coda-wave attenuation during the Loma Prieta, California earthquake sequence: *Journal of Geophysical Research*, 19 p.
- Beroza, G.C., and Ellsworth, W.L., 1994, The seismic nucleation phase: evidence from near-source seismograms: *EOS, American Geophysical Union Transactions*, v. 75, p. 426.
- Dietz, L., Kohler, W., Bittenbinder, A., Bogaert, B., and Hirshorn, B., 1994, Larva: an implementation of Earthworm on the USGS northern California seismic network: *EOS, American Geophysical Union Transactions*, v. 75, p. 430.
- Dodge, D.A., Beroza, G.C., and Ellsworth, W.L., in press, The foreshock sequence of the 1992 Landers, California earthquake and its implications for earthquake nucleation: *Journal of Geophysical Research*, 30 p.
- Dodge, D.A., Beroza, G.C., and Ellsworth, W.L., 1994, The foreshock sequence of the 1992 Landers, California earthquake and its implications for earthquake nucleation: *EOS, American Geophysical Union Transactions*, v. 75, p. 426.
- Ellsworth, W.L., 1994, Characteristic earthquakes and long-term forecasts: implications of central California seismicity: *Proceedings of the International Conference on Earthquake Prediction and Hazard Mitigation Technology*, March 1-4, 1994, Tsukuba, Japan, Science and Technology Agency, Japan, National Research Institute for Earth Science and Disaster Prevention, p. 71-93.
- Ellsworth, W.L., and Beroza, G.C., 1994, Nucleation and initial growth of the Northridge, California, earthquake: 89th Annual Meeting of the Seismological Society of America Program for Northridge Abstracts, p. 9.
- Ellsworth, W.L., and Beroza, G.C., 1994, The seismic nucleation phase: implications for earthquake rupture dynamics: *EOS, American Geophysical Union Transactions*, v. 75, p. 426.
- Ellsworth, W.L., and Beroza, G.C., submitted, Seismic evidence for an earthquake nucleation phase: *Science*, 12 p.
- Ellsworth, W.L., Cole, A.T., and Vidale, J.E., 1994, Characteristic earthquakes: probabilistic models and testable predictions: *EOS, American Geophysical Union Transactions*, v. 75, p. 461.
- Ellsworth, W.L., Kissling, E., and Maurer, H., 1994, Errors in traveltimes tomography and robust estimation of tomographic models (abs.): *International Association of Seismology and Physics of the Earth's Interior 27th General Assembly Abstracts*, W4.9.
- Kissling, E., Ellsworth, W.L., Eberhart-Phillips, D., and Kradolfer, U., 1994, Initial reference models in local earthquake tomography: *Journal of Geophysical Research*, v. 99, p. 19635-19646.
- Marone, C., Vidale, J.E., and Ellsworth, W.L., 1994, Physical interpretation of source variations in repeating earthquakes: *EOS, American Geophysical Union Transactions*, v. 75, p. 435.
- Vidale, J.E., Ellsworth, W.L., Cole, A., and Marone, C., 1994, Variation in rupture process with recurrence interval in a repeated small earthquake: *Nature*, v. 368, p. 624-626.

## References

- Bittenbinder, A., Johnson, C.E., and Bogaert, B., 1994, Earthworm: a modular distributed processing approach to seismic network processing: EOS, American Geophysical Union Transactions, v. 75, p. 430.
- Johnson, C.E., 1994, Rapid association of regional network phases: EOS, American Geophysical Union Transactions, v. 75, p. 430.

## Digital Recordings of the Northridge Earthquake Nucleation

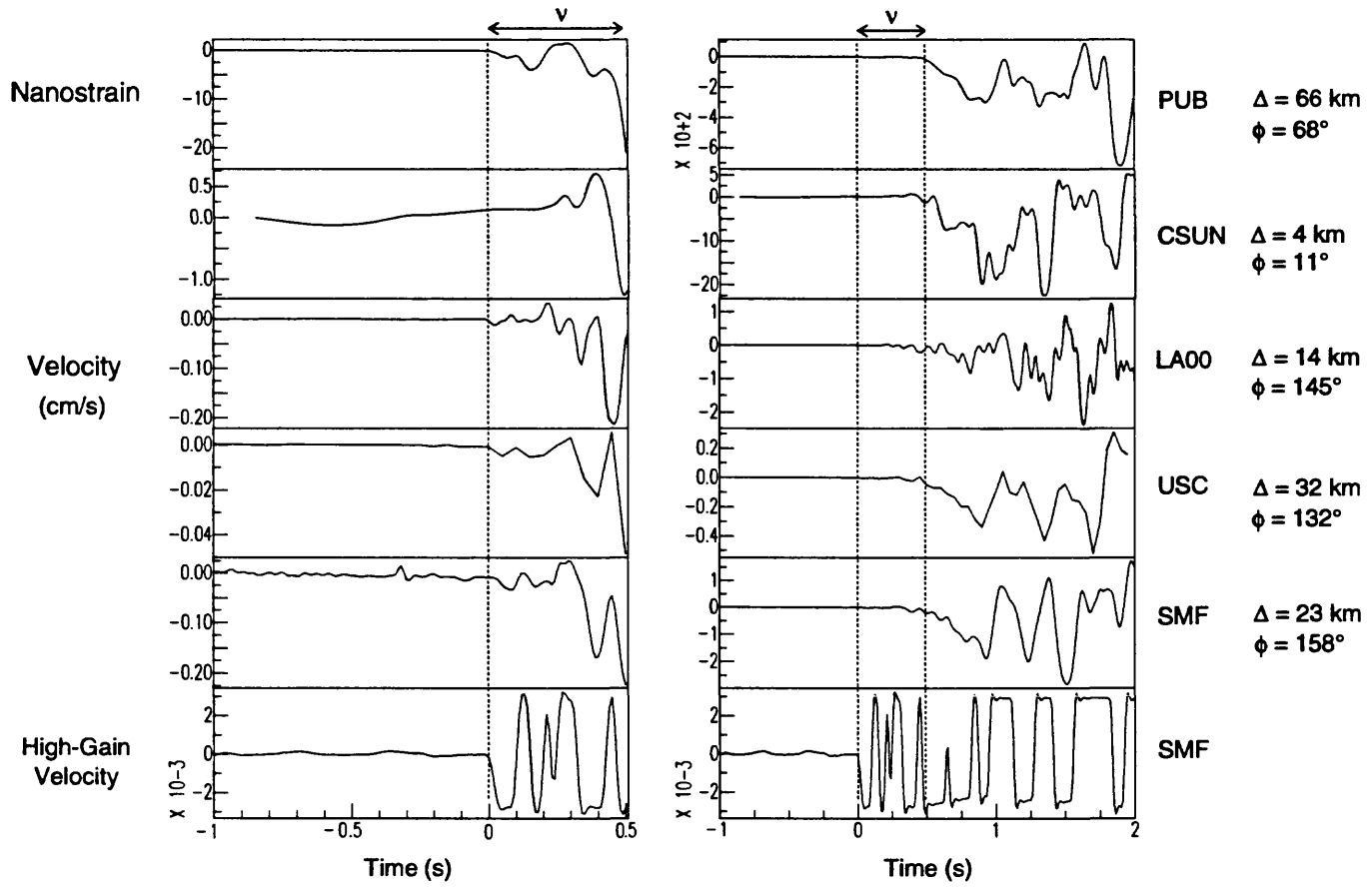


Figure 1. Near-source recordings of the Northridge, California, earthquake (M 6.7). The first arrival from the main shock occurs at  $t=0$  (vertical dashed line). The left panel shows the first 0.5 s of the earthquake, which corresponds to the seismic nucleation phase. The right panel shows the first 1.5 s, which shows the nucleation phase in relation to the much larger arrivals that follow (after the second dashed line). Note the similarity in waveforms during the first 0.5 s, suggesting that the source of the nucleation phase is quite compact. The large ramp in ground velocity beginning on all stations at  $+0.5$  s corresponds to a dynamic stress drop of 40 MPa and is interpreted as the rupture breaking away from the nucleation zone.

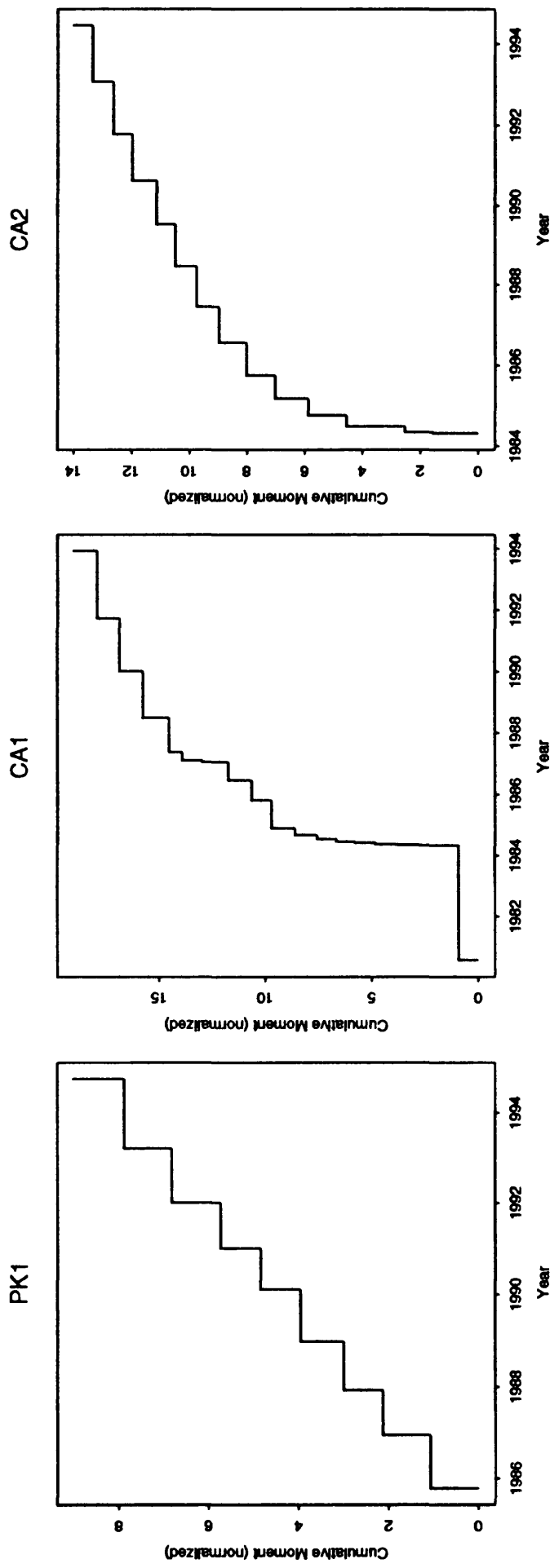


Figure 2. Cumulative seismic moment versus time for repeating earthquake sources. Left: Multiplet PK1, located to the northwest of the 1966 Parkfield earthquake. Center: Multiplet CA1, located on the Calaveras fault at the southern end of the 1984 Morgan Hill earthquake aftershock zone. Right: Multiplet CA2, located on the Calaveras fault 4 km southeast of CA1 and further from the Morgan Hill earthquake. The Parkfield multiplet shows a remarkably steady rate of recurrence and is located on a part of the fault where geodetic data show a steady rate of fault creep. In contrast, the two Calaveras multiplets show a clear response to the April 24, 1994 M 6.2 Morgan Hill earthquake; each event acted as an aftershock of this earthquake.

**Field and Laboratory Study of the Spatial and Temporal Variability in  
Hydromechanical Properties of an Active Normal Fault Zone, Dixie Valley,  
Nevada**

Award Number 1434-93-G-2280

*Craig B. Forster (co-P.I.)*  
*Ronald L. Bruhn (co-P.I.)*  
*Jonathan Caine (Graduate Student)*  
*Department of Geology and Geophysics*  
*University of Utah*  
*Salt Lake City, Utah 84112*  
*(801) 581-3864*  
*E-mail: cforster@geofluid.esri.utah.edu*

*Joanne Fredrich (co-P.I.)*  
*Sandia National Laboratory*

## INTRODUCTION

Spatial and temporal variations in mechanical and hydraulic properties of faulted rocks are postulated to exert a profound influence on both the mechanics of faulting and post-seismic deformation [Sibson, 1989; Byerlee, 1990; Rice, 1992]. Enhanced knowledge of the detailed variations in mechanical and hydraulic properties of fault zones is thus critical for furthering our understanding of earthquake source processes. This report describes a survey of fracturing in the Dixie Valley fault zone, a large normal fault in the Central Nevada Seismic Belt. The spatial distribution, geometry, and intensity of fracturing is described, and fracture permeability is estimated for stress states that may be representative of pre-rupturing and post-rupturing regimes in large normal faults. Finally, we present a preliminary analysis that treats fracture networks as potential reservoirs of high pressure fluid, and consider the effects of injecting this fluid between fault surfaces during the onset of rupturing. This report summarizes progress in our study of how the permeability structure of a large normal fault might influence the fluid dynamical processes operating during faulting.

## PROJECT OUTLINE

The primary purpose of this project is to investigate the physical and mechanical properties of a large, seismically active normal fault system. The first year of our 2-year project emphasized obtaining the field-based data needed to characterize fault zone architecture, collect rock samples, and drill cores from the samples. The second year of study emphasizes the systematic correlation of field-structural observations with laboratory-based rock mechanics and hydraulic data.

Field work has focused on detailed mapping of fracture networks found at two locations on the Dixie Valley and Stillwater fault zones. These data have helped to revise our conceptual model of fault zone architecture (Figure 1) and yield constraints on efforts to simulate fluid flow within and near the fault zone. Contacts between fault core (identified as a distinctive breccia zone), damage zone, and protolith were mapped over a region extending over tens of square kilometers. Fracture data are tied together over several scales by centimeter-scale petrographic fracture analyses, meter-scale outcrop fracture analyses, and tens to hundreds of meters-scale fracture analyses using field mapping and low-elevation aerial photographs. In spite of the complicated fracture network found in this large fault zone, distinct kinematically-related fracture sets can be identified. From these and the other fracture data, fracture permeability models are generated for each component of the fault.

Laboratory testing of faulted rock samples are providing a quantitative basis for ongoing numerical simulations of the impact of fault architecture on fluid flow properties of the fault zone.

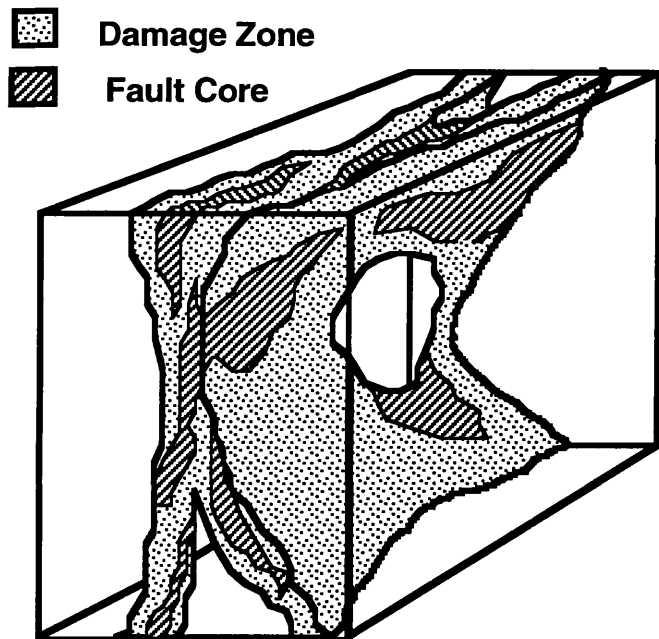


**Figure 1:** Conceptual model of a fault zone with protolith removed to reveal the anastamosing, interleaved character of the core and damaged zone (after Smith et al., 1990).

## GEOLOGIC SETTING

The Dixie Valley and Stillwater fault zones are part of a 300 km long belt of normal and normal-oblique slip faulting in central Nevada [Wallace, 1984]. Historic earthquakes that generated scarps within the belt include (from north to south): Pleasant Valley (1915), Fairview Peak - Dixie Valley (1954), Wonder (1903), Cedar Mountains (1932), Excelsior Mountain (1934), Mammoth Lakes (1980), and Owens Valley (1872) [Wallace & Whitney, 1984]. One of the largest normal faulting earthquakes in history ( $M_o \sim 0.7 \times 10^{20}$  Nm) occurred along this belt in 1915 [Jackson & White, 1989].

The Dixie Valley and Stillwater faults are located along the eastern side of the Stillwater range. Several features motivate us to study these faults:

- These are active normal faults capable of generating  $M > 6$  earthquakes. The 1954  $M = 6.8$  earthquake rupture on the Dixie Valley fault was 30 to 40 km long; the hypocenter was located at a depth in excess of 12 km.
- Granitic and gabbroic rock found in the footwall of the fault zones are representative of a large percentage of the rock types found in the continental crust. The rocks at the Dixie Valley fault exposures contain minerals which provide excellent indicators of the pressure and temperature conditions present during fluid circulation and fluid-assisted alteration within the fault zone. Thus, the results of

- our study are expected to be directly applicable to active normal faults found elsewhere in the U.S.
- The Dixie Valley and Stillwater faults are some of the best exposed faults in the continental U.S.

The Stillwater range comprises Mesozoic metasedimentary rocks intruded by the Jurassic gabbroic Humboldt lopolith, Cretaceous granite, a multiphase Oligocene granodiorite-quartz monzonite-granite intrusive complex intruded at 28 Ma, and volcanic rocks of Oligocene and Miocene age [Page, 1965; Wilden and Speed, 1974; Speed and Armstrong, 1971; Speed, 1976]. Hydrothermal alteration in the Oligocene granitic complex along the base of the Stillwater Range reflects cataclasis and fluid circulation within the Dixie Valley fault zone; alteration minerals include an early biotite-feldspar assemblage that is overprinted by Fe-chlorite and epidote. These latter minerals are in turn partly replaced by hydrothermal sericite and the rock is cut by calcite-hematite and quartz-calcite veins. Biotite is partly replaced by prehnite. The latest hydrothermal mineral assemblage includes stilbite, laumontite, kaolinite, alunite, smectite, illite and fine-grained quartz, chalcedony, and opal [Parry et al., 1991].

**Locality 1 - Little and Big Box Canyons:** The Dixie Valley fault zone (DVF) lies at the eastern base of the Stillwater Range. Total vertical displacement (or throw) across the fault zone is about 6 km. Approximately 2.0 to 2.5 km of displacement occurred between 23 and 15 Ma, and an additional 3.5 km of displacement occurred between 10-13 Ma and the present. Extension during the first phase of faulting was directed N68E-S68W; however, the latter phase is characterized by extension oriented at N65W-S65E [Parry et al., 1991]. Stream canyons eroded through the Oligocene granodiorite at Little and Big Box Canyons expose natural cross sections through the fault zone (from foliated cataclasite, through a fractured and hydrothermally altered damage zone developed immediately below the primary slip planes, into lesser deformed and little-altered footwall rock). The damage zone of intense hydrothermal alteration developed through fracturing and fluid circulation within the Dixie Valley fault zone and varies from several meters to several tens of meters in width. The dominant hydrothermal alteration minerals are chlorite and epidote, but veins and patches of younger, lower temperature alteration minerals also occur, including fine-grained quartz which has partly silicified the rock (thus making it suitable for drilling). The multiple phases of hydrothermal alteration found at the site were developed during uplift of the footwall by normal faulting [Parry et al., 1991]. Fault rock exposed at this site has been uplifted from depths of approximately 6 km within the Dixie Valley fault zone.

**Locality 2 - "The Mirrors":** The "Mirrors" locality is found in the footwall of the Stillwater fault (SWF). The Stillwater fault is a proposed seismic gap located along the base of the Stillwater Range immediately north of the 1954 Dixie Valley rupture. Holocene scarps within the fault zone probably formed during a major earthquake within the last 12,000 years [Wallace & Whitney, 1984]. Total displacement on the Stillwater fault is estimated at 3 to 6 km [Power & Tullis, 1989]. Large, striated and polished fault surfaces up to 25 m<sup>2</sup> in area are exposed over a strike distance of about 100 m in silicified, brecciated gabbroic rock of the Humboldt lopolith at the "Mirrors" locality [Power & Tullis, 1989]. The fault surfaces are encased in hydrothermally cemented breccia in a zone several meters thick. This zone grades into metamorphosed gabbro in the footwall of the fault zone. Silicification of the gabbro resulted from fluid circulation and mineral precipitation within the Stillwater fault zone. The footwall rock probably was uplifted from depths of 3 to 6 km, but formation of the striated fault surfaces occurred at depths less than 2 km and temperatures less than 270°C (this estimate is based on the stability of kaolinite and quartz, which occur in the fault rock). Power and Tullis [1989] found evidence for intervals of continuous (slow) deformation and discontinuous (rapid) brittle cataclasis which alternated in time.

## FIELD WORK

Field work yields a hydrogeological conceptualization of the physical characteristics of the SWF zone. These characteristics include a fault core composed of cataclastic and brecciated host rocks, a damage zone composed of highly fractured host rock surrounding the core (filled in part with precipitated minerals and cataclasite), and the surrounding protolith. The transition between damaged zone and unaffected protolith is discerned by a visible decrease in fracture density and intensity of the protolith. Pods of brecciated protolith generally occur as isolated units close to slip surfaces suggesting that they are intimately related to dynamic slip processes (discussed in detail below). The damage, core, and protolith zones are mappable units that form the conceptual basis (Figure 1) for our subsequent sampling program. Block samples were collected for later petrographic, mechanical, and permeability analyses.

Work at the two field sites reveals the absence of a fault core at the Box Canyon area and excellent exposures of the fault core at the Mirrors locality. The Mirrors site also exhibits large panels, several square meters in dimensions, of highly polished and striated slip surfaces. These surfaces are in contact with highly disturbed fault gouge and breccia pods (a more detailed description of these features follows). Both localities provide excellent exposures of both damage zone and protolith rocks. Oriented samples of each of the three fault components and several unoriented blocks (generally one cubic foot in size) of breccia zone float were collected for both petrographic analysis and permeability studies. This sampling strategy is designed to provide clues regarding the magnitude and variation of permeability as a function of orientation within representative samples of each of the fault zone components. Coring of the rock blocks is complete and permeability tests are underway. Cores will also provide samples for cutting composite petrographic thin sections from transition zones where breccia grades into less deformed rock.

The three main fault zone components are viewed not only as distinct structural entities that reflect changes in formative deformation mechanisms, but also as distinct hydrogeological units. The hydraulic effect of these units (i.e., whether they are barriers or conduits to fluid flow) depends upon the stage in the evolution of the fault zone. Contacts between each unit were determined by mapping macroscopic changes in the structural character of the outcrop (i.e. degree of cataclasis for fault cores, and fracture density for the damaged zone and the protolith). Mapping fault cores along the SWF zone was fairly easy because abrupt changes from breccia or cataclasite to highly fractured rock is generally easy to discern. The contact between the damaged zone and protolith, however, is less obvious.

In addition to mapping internal fault zone contacts, an attempt was made to characterize and determine the structural origin of geometrically distinct fracture sets. This was done to distinguish fault-related fractures from pre-existing and overprinted magmatic and regional fracture sets as well as to gain a field-based understanding of the permeability structure of the SWF zone. Different fracture types can be genetically grouped as shear fractures, extensional fractures, slip surfaces, and fractures of unknown origin. Assuming that the mountain front is the erosional remnant of the footwall of the SWF zone, and is sub-parallel to the average orientation of the fault core, the origin of the different fracture sets identified above can be kinematically associated by their orientation relative to this surface.

An understanding of the geometry and spatial variability of the different fault components is gained by mapping the contacts of the fault core, damage zone, and protolith. Detailed fracture mapping and characterization was done to facilitate field-based fracture permeability modeling. Data collected in the fracture analysis included fracture orientation, trace length, scale of spacing, density, and observation of aperture opening and macroscopic filling (if present). Photographs of selected fractured faces were taken for later enlargement. The resulting photos assisted in the detailed fracture mapping carried out in the summer of 1994. Field observations indicate that

fracturing is similar at both the Mirrors and Box Canyon areas. Thus, the fracture density, trace length, and fracture aperture data obtained in the Box Canyon area can also be used in characterizing fault rocks at the Mirrors locality.

The results of our field mapping at the Box Canyon locality indicate that the contacts of the structural/hydrogeologic domains occur as spatially variable and curviplanar surfaces with anisotropic topography. The damage zone protolith contacts strike roughly north-northeast and dip 23 to 60 degrees to the south-southeast. By inspection of the outcrop patterns it is observed that the contacts dip in symmetrical opposition to topographic stream valley contours. The contacts were generally best observed in these stream cuts. These features indicate that the structural anisotropy is elongated parallel to the slip direction of the SWF zone. Field observations indicate that the damage zone ranged from several meters up to thirty meters in thickness. It was not possible from this field work or data set to delineate a quantitatively rigorous anisotropy factor or ratio of fault topography amplitude to wavelength.

The primary difference between the Mirrors and the Box Canyon areas is the excellent exposure of fault core at the Mirrors locality. The fault zone at the Mirrors strikes northeast to east northeast, dips from 32 to 70 degrees and comprises slip-parallel, elongated and anastomosing pods of breccia separated by up to 1 meter thick curviplanar layers of fault gouge. These outcrop-scale fabric relationships suggest that fault slip was distributed throughout a wide, heterogeneous zone. The interleaved and lenticular nature of the breccia pods and gouge layers, each with differing hydromechanical properties, likely cause significant hydrogeologic and mechanical anisotropy within the fault.

Locally, the fault gouge likely acts as a low permeability unit based on the clay content and tight structural texture typical of fault gouge. In contrast both breccia pods and the fracture networks observed in the fault zone damage zone may have acted as significant conduits for fluid flow during an earthquake. Thus, this system may be interpreted as a complex conduit-barrier flow system that changes through time. In order to work out the timing relationships of fluid flow it may be necessary to invoke the use of light stable isotopes and other elemental tracers and their spatial distribution in different components of the fault zone.

## **PETROGRAPHIC OBSERVATIONS OF STILLWATER FAULT ZONE ROCKS**

Samples were collected from representative portions of fault zone core, damage zone, and protolith for compositional and textural petrographic and XRD analyses during both field excursions to Dixie Valley. Fourteen large format thin sections have been made from these samples. These samples include representatives of the breccia pods, associated slip surfaces, and the damage zone.

### **Petrographic Features of Breccia Samples**

A “transect” of thin sections were cut to encompass the region between the slip surface and the outer edge of a breccia pod. Sections parallel and perpendicular to slip were made in an attempt to document and evaluate the relationships between the microstructures and rock composition found along the traverse from the slip surface to the breccia pod.

XRD and petrographic analyses of the breccia zone samples indicate that the bulk average composition is 90% quartz, 10% clay minerals (predominantly kaolinite from XRD analysis), and less than 1% sericite, iron oxide, calcite, and amphibole fragments. Compared with samples from the damage zone and protolith breccia pod samples do not show similar alteration products such as

abundant chlorite. This may be due to the destruction of mafic phases during fluid-assisted alteration within the breccia pod zones.

The predominant texture of the breccia samples is that of angular clasts within a fine-grained matrix. In the two dimensional view that thin sections afford the samples suggest a matrix supported fabric. The porphyroclast to matrix grain size distribution ranges from bimodal to multimodal. The distribution tends to be multimodal closer to slip surfaces and bimodal within the breccia pods. Porphyroclasts range in size from less than 1 millimeter to several centimeters in diameter. "Intact" porphyroclasts are generally strained angular quartz grains with a few calcite grains. The quartz porphyroclasts are interpreted to be relicts from the protolith that have survived the deformation processes responsible for pod emplacement. Calcite occurs as a precipitate that fills void spaces and small stringer like veins. Euhedral boundaries on calcite grains suggest that this is likely a post-tectonic mineral (i.e. the grains have not undergone cataclasis nor they have been totally recrystallized).

The breccia clasts show a high degree of internal brecciation that indicates multiple episodes of deformation and leads to the observed multimodal grain size distribution. Other evidence for multiple episodes of deformation can be observed on polished and striated outcrop surfaces. Distinct layered sheets of polished and striated quartz show different lineation directions from one layer to another and several of the individual surfaces show abrupt changes in lineation direction causing striation interference patterns.

### Petrographic Features of Damage Zone and Protolith Samples

Several samples of damage zone and protolith rocks were analyzed. Compositinally these rocks are granodiorites with approximately 60% calcic plagioclase, 20% quartz, 10% hornblende, 5% biotite, and 5% alteration products and accessory minerals which include chlorite, epidote, and sericite.

Petrographic analysis indicates that both the degree of rock alteration and fracture intensity decrease with increasing distance from the fault core and associated breccia zone. Alteration primarily includes chloritization and albitization as suggested previously by Parry [1991]. The reader is referred to this paper for detailed descriptions of the mineralogy and subsequent alteration of these rocks. Fracture orientations observed in the thin sections are similar to those observed at the macroscopic scale. Mixed mode fracturing is strikingly evidenced by the abundant presence of horsetail fractures bleeding from shear fractures. These microscopic structures may yield significant zones of higher permeability because they add significant porosity. Scaling the impact of this microscale porosity enhancement up to the macroscale forms an important step in defining the equivalent porous media properties needed to model the hydraulic properties of the damage zone.

Petrographic evidence for fluid flow increases with increased proximity to the fault core. The consequences of fluid flow are evidenced by mineral infilling, iron stained quartz, dilated fractures, and the presence of cataclastic porphyroclasts within the finer grained fracture filling. The common presence of cataclastic porphyroclasts can be interpreted as evidence that the fracture infill was associated with faulting processes and not earlier magmatic processes. Because microscopic fracture infill is found within all fractures without being restricted to a particular fracture orientation, fluid flow appears to have been pervasive throughout the fault zone.

### ESTIMATES OF PERMEABILITY

Fluid transport properties of the fractured rock mass are estimated using the model and algorithms of Oda et al. [1987]. Permeability tensor  $\mathbf{K}$  is defined by

$$K_{ij} = \lambda (P_{kk} \delta_{ij} - P_{ij}) \quad (1)$$

$$P_{ij} = (\Pi/4 \cdot V) \sum_{k=1, N} (L_k^2 [t_k^3] n_{ik} n_{jk}) \quad (2)$$

Fractures are modeled as discs of diameter  $L$ .  $L_k$  is the diameter and  $t_k$  is the aperture of the  $k^{\text{th}}$  fracture in the model network.  $n_{ik}$  are the three components of the direction cosine of the  $k^{\text{th}}$  fracture.  $\delta_{ij}$  is the Kroenecker delta function, and  $V$  is the volume of the fractured rock mass.  $N$  is the number of fractures in the network.  $\lambda$  varies from 1/12 for flow between parallel plates of infinite extent to zero for a non-percolating fracture network.  $\lambda$  is defined as 1/16 (0.064) for calculations in this study, based on the discussion and numerical simulations of Oda et al. [1987].

Fracture aperture ( $t$ ) is difficult to assign with any degree of confidence. Aperture decreases rapidly with increasing effective normal stress, and is also a function of the surface roughness and fracture size [Oda et al., 1987]. However, none of these functional relationships are well established for fractures at elevated temperature and pressure in natural fault zones. In this study, the initial or 'zero effective stress' aperture ( $t_0$ ) of each fracture is proportional to the fracture diameter, using the ratio  $(t_0/L) = 1 \times 10^{-3}$ . The decrease in aperture caused by effective normal stress is computed using the algorithm and coefficients proposed by Oda [1986].

Implementation of equations (1) and (2) requires simulation of a fracture network based on field measurements of fracture intensity, orientation and trace length. The number of fractures in a rock volume is estimated from the scan-line measurements and detailed fracture mapping discussed previously. The density of fracture poles expressed as % per 1% area on a lower hemisphere stereoplot provides the probability density distribution from which we generate a sample of fractures with the appropriate angular dispersion. Trace length measurements are corrected for sampling bias (Warburton, 1980) and used to assign mean diameters to fractures falling within the orientation ranges of the three prominent fracture sets. Fracture diameters are generated with a negative exponential distribution and the mean diameter specified for each fracture set.

The above procedure is automated in a computer program. The code generates an interpolation table of fracture pole orientation density based on field measurements. The operator specifies the total number of fractures to be modeled within a volume of rock, and the mean diameter of fractures in various sets defined by restricted ranges in orientation. A list of fractures is created with the appropriate distribution in orientation and diameter. The fracture list (fracture network) is entered into another computer program which implements equations (1) and (2). This latter code computes the initial aperture ( $t_0$ ) of each fracture as a function of diameter, corrects  $t_0$  for closure caused by the specified stress state, and determines the principal magnitudes and directions of the permeability tensor. Oda et al. [1987] provide a thorough discussion and numerical tests of this 'equivalent porous media' algorithm.

At the Box Canyon study locality the contacts of the fault core (breccia zone in this case), damage zone, and protolith were mapped over a region extending over tens of square kilometers. Fracture data are tied together over several scales by the centimeter-scale petrographic fracture analyses, meter-scale outcrop fracture analyses, and tens to hundreds of meters-scale fracture analyses described previously. In spite of the complicated fracture network found in this large fault zone, distinct kinematically-related fracture sets emerge when the data are plotted on an equal area net. From these and the other fracture data, a fracture network model is generated and the equivalent permeability tensor is estimated. We expect to use the approach outlined above to compute average bulk permeabilities for each component of the fault zone.

Laboratory tests are underway to augment the fracture-based permeability estimates by providing insight into the magnitude of matrix permeabilities and bulk permeability of faulted rocks at the scale of 2 inch and 1 inch diameter cores. Testing is performed at two scales in order to obtain a first order estimate of the possible impact of sample size on our attempt to estimate small-scale permeabilities for each component of the fault zone. 4 sets of cores are being tested. Each sample set comprises cores drilled in three orthogonal directions. This provides core samples with three distinct alignments: 1) parallel to slip within the fault plane, 2) perpendicular to slip within the fault plane, and 3) normal to the fault plane. Altered granite forms the dominant lithology represented in the samples. Fracture mapping carried out in three orthogonal planes complement the oriented core samples. As will be discussed in a subsequent section, the fracture maps and core test results provide a basis for estimating permeability anisotropy within the fault zone.

Core samples submitted for testing include representative samples of damage zone, fault core breccia, and protolith. Two breccia types are represented. One breccia is a cataclastic rock dominated by altered granite clasts that exhibits a high degree of interclast pore space. The matrix is similar for both breccia types and is dominated by bone white, finely-crystalline quartz. In contrast, the second breccia type is matrix dominated. This sample may represent an implosion breccia formed within a breccia pod that formed at a dialational jog in the fault zone. This breccia type is typical of the central fault core material found at the Mirrors locality. Damage zone samples illustrate an array of extensional, shear, and cross fracturing that are typical of damage zone structures found in the SWF. The macroscopic fracturing found in these samples suggests that permeabilities will be fracture-dominated, even at the small scale of the samples tested. The protolith samples are fine-grained, altered granites. These samples differ from those obtained from the damage zone and the fault core because they lack the veins, small faults, brecciation, and any other macroscopic signs of deformation. Although some fracturing was observed in outcrop, fracture densities in the protolith are much less than those found within the damage zone rocks. These fractures are inferred to result from strain release fractures during exhumation.

## **IMPACT OF FAULT ZONE ARCHITECTURE ON FLUID FLOW WITHIN A FAULT**

We are incorporating the results of our field and laboratory work in a series of numerical simulations designed to evaluate how fault architecture changes during faulting and how the permeability structure of a fault might influence fluid flow both before and after an earthquake. Although our analyses are still at a relatively early stage, the following paragraphs outline some preliminary results.

### **Response of Fault Permeability to Changes in Stress State**

We use the approach discussed above to estimate the impact of partial closure of fractures between pre- and post-rupture stress states associated with an earthquake. In this case we use observations of fracturing found within the damage (transition) zone obtained from a number of different locations along the SWF as the basis for the analysis. First, a 'generic' fracture network model is created using representative fracture intensity measurements, orientation, and trace length data. The general characteristics of the model are summarized in Table 1, for a 1 m<sup>3</sup> rock volume. This model is used in subsequent calculations to estimate fracture network permeability and fluid reservoir characteristics. Fracture network heterogeneity is not considered in this preliminary study.

TABLE 1. FRACTURE SET PARAMETERS

Fracture Type	Pole Direction (°)		Mean Trace Length (m)	Fracture Density (r = #/m <sup>3</sup> ) *
	Trend	Plunge		
<b>Extension</b>				255
Set #1a	260-320	0-29	0.2	
Set #1b	105-141	0-30	0.2	
<b>Shear Fractures</b>				26
Set #2	250-315	30-65	0.5	
<b>Cross Fractures</b>				164
Set #3a	180-245	30-70	0.25	
Set #3b	003-050	40-75	0.25	

\* Computed from scan-line intensity for each fracture set. Total # of mesoscopic fractures in 1 m<sup>3</sup> of rock is 445.

The number of fractures per unit volume ( $\rho$ ) is estimated from scanline intensity values (eqn. 25, Oda et al., 1987).

$$\rho \langle L^2 \rangle = 4I_S / [\pi \langle |n \cdot q| \rangle] \quad (3)$$

$\langle L^2 \rangle$  is the mean squared fracture diameter,  $I_S$  is scanline intensity (#/m), and  $\langle |n \cdot q| \rangle$  is the mean value of the dot product between the poles to fractures in a specific set (defined by unit vectors  $n$ ) and the unit vector parallel to the scanline ( $q$ ). Using data obtained in this study, we assign  $I_S = 8/m$  for both extension and cross fractures, and  $5/m$  for shear fractures (set 2). These are average intensities for each fracture set. Trace length measurements for each set yield in sequence,  $\langle L \rangle = 0.2$  m (set 1),  $0.5$  m (set 2) and  $0.25$  m (set 3) (Table 1). Fracture density is estimated from (3) with  $\langle |n \cdot q| \rangle = 1.0$ .  $\rho_1 = 255/m^3$ ,  $\rho_2 = 26/m^3$ ,  $\rho_3 = 164/m^3$ , for a total mesoscopic fracture density of 445 fractures/m<sup>3</sup>. As discussed above, field and microscopic studies indicate multiple episodes of fracture sealing and filling by hydrothermal minerals. We account for the possible effects of hydrothermal alteration and cementation by assuming that only 1/3 of these fractures are open and transport fluid at any given time. This proportion of open fractures is only a guess, and is not based on any quantitative information. The real value may be significantly higher, or much lower.

The fluid flow and reservoir properties of fault zone fracture networks are important in theories of rupture initiation and modeling of earthquake precursors [Sibson, 1989; Byerlee, 1993]. Most large, normal faulting earthquakes initiate at depth  $\geq 10$  km. For purposes of modeling we impose stress conditions and fluid pressures that may exist in parts of a normal fault zone at a depth of 10 km, based on studies of fluid inclusions and mineral alteration assemblages [Parry and Bruhn, 1990; Bruhn et al., 1990]. In the pre-rupture state, the ratio of fluid pressure ( $P_f$ ) to lithostatic

pressure ( $P_L$ ) is defined as  $P_f/P_L = 0.9$ . The vertical principal stress ( $S_v$ ) =  $\rho_r g z (1 - P_f/P_L) = 27$  MPa, for  $\rho_r = 2700$  Kg/m<sup>3</sup>. The major fault surfaces have a coefficient of friction  $\mu = 0.6$ , no cohesion, and dip 45°. The least principal stress  $S_{h\min} = 6.8$  MPa at failure. For simplicity, we assume that  $S_{h\max} = S_{h\min}$ , or

$$\phi_s = [S_{h\max} - S_{h\min}]/[S_v - S_{h\min}] = 0.0 \quad (4)$$

Fluid pressure presumably drops within the damage zone either during or after rupturing because permeability increases, and newly formed fractures provide connections to the surface [Sibson, 1989; Parry and Bruhn, 1990; Bruhn et al., 1990]. Assume that the post-rupture fluid pressure becomes hydrostatic, that the shear stress is completely relaxed, and the three principal stresses become equal, with a magnitude of 170 MPa. These pre- and post-rupture stress states are chosen to provide upper bounds on fracture volume changes and fluid production from the damage zone at seismogenic depths.

Partial closure of fractures between pre- and post-rupture stress states has a marked effect on fracture permeability (Table 2). The maximum and intermediate permeability axes ( $K_1$  and  $K_2$ ) plunge more steeply than the plane of the fault zone, and the least principal axis ( $K_3$ ) plunges more gently than the pole to the fault zone in the pre-rupture stress state. The average fracture aperture is 19 microns, and total fracture volume is 0.52 liter. Fracture permeability is large in the pre-rupture state due to low effective normal stress across most fractures. Permeability magnitudes are  $\approx 10^{-13}$  m<sup>2</sup>, about 4 orders of magnitude greater than in the post-rupturing stress state (Table 2).

A marked reduction in permeability in the post-rupture stress state is accompanied by a rotation in permeability axes. Thus, the permeability anisotropy that influences flow within the damage zone likely changes in both magnitude and orientation during the transition from pre- to post-rupture states.  $K_1$  and  $K_2$  are located essentially within the plane of the fault zone, and  $K_3$  is almost parallel to the fault zone pole (Table 2). Average aperture is 1.5 microns, and fracture volume is 0.04 liter. Permeability magnitude is  $\approx 10^{-17}$  m<sup>2</sup>.

The increase in effective stress between pre- and post-rupture stress states could produce about 0.5 liter of fluid from a cubic meter of fractured, transition-zone rock because of partial closure of fracture apertures. If fluid expulsion occurs during the initial phase of rupturing, this fluid may be injected between fault surfaces and act to trigger an earthquake [Byerlee, 1993]. The fluid also acts as a mineralizing agent, carrying ionic species in solution into fractures and voids between fault surfaces, where chemical reactions produce cement and mineral filling that ultimately reduces permeability, and partially heals fault surfaces.

Byerlee [1993] proposes a 'fluid compartment' model for fault zones and the triggering of earthquakes. Fluid sealed under high pressure in one compartment is partially drained into an adjacent compartment of initially lower fluid pressure. We use this model to investigate the potential effect of draining fluid from the transition-zone fracture network into the space between opposing walls of faults or 'slip-surfaces'. Assume the following initial conditions at a depth of 10 km: 1) fluid is initially trapped at hydrostatic pressure in the fault, and 2) fluid is trapped at 0.9  $P_L$  in the adjacent fracture network. The fault and fracture network are hydraulically isolated until the onset of rupturing, when the seal between the two compartments is broken. Fault permeability is much less than that of the fracture network, and we neglect changes in fluid compressibility during pressure changes.

TABLE 2. ESTIMATED FRACTURE-INDUCED PERMEABILITY

Case	Principal Stresses (MPa)			†Permeability x 10 <sup>-13</sup> m <sup>2</sup>			Fracture Volume (liters)
	S <sub>v</sub>	*S <sub>hmax</sub>	S <sub>hmin</sub>	K1	K2	K3	
1 Pre-Rupture	27	6.8@020°	6.8	1.2 (023/38)	1.1 (178/49)	0.3 (283/130)	0.52
			†Permeability x 10 <sup>-17</sup> m <sup>2</sup>				
2 Post-Rupture	170	170@020°	170	5.0 (032/23)	4.7 (142/38)	1.3 (278/43)	0.04

† Trend and plumb of permeability tensor axes indicated by bracketed values.

S<sub>v</sub> = vertical principal stress

S<sub>hmax</sub> = maximum horizontal stress

S<sub>hmin</sub> = minimum horizontal stress

\* Maximum Horizontal Stress trends 020°, parallel to fault zone

The final fluid pressure, after equalization of pressure between the two compartments is [Byerlee, 1993]:

$$P_f = [V_{dz}P_{dz} + V_{sz}P_{sz}]/[V_{dz} + V_{sz}] \quad (5)$$

V and P are the fracture volumes and initial fluid pressures in the damage zone (dz) and fault (sz), respectively. We assign V<sub>dz</sub> = 0.52 x 10<sup>-3</sup> m<sup>3</sup>, and P<sub>dz</sub> = 0.9 lithostatic pressure (P<sub>dz</sub> = 243 MPa) based on the stress and transition-zone structural parameters summarized in Tables 1 and 2.

How large a section of fault surface is affected by injection of fluid from 1 m<sup>3</sup> of damage zone rock? Consider the situation where P<sub>f</sub> = 171.5 MPa, half the difference between P<sub>tz</sub> and P<sub>sz</sub>. Rearranging equation 5 to solve for V<sub>sz</sub> gives:

$$V_{sz} = V_{dz}[P_{dz} + P_f]/[P_f - P_{sz}] \quad (6)$$

The fault area that can be pressurized from P<sub>sz</sub> = 100 MPa to P<sub>f</sub> = 171.5 MPa is V<sub>sz</sub>/t<sub>sz</sub>, where t<sub>sz</sub> is the average aperture between opposing walls of the fault. t<sub>sz</sub> ≈ 1 to 5 microns for the specified stress conditions according to the joint aperture constitutive law of Oda [1986]. A fault surface area ≥ 100 m<sup>2</sup> is affected by the fluid injected from 1 m<sup>3</sup> of transition-zone rock. This preliminary result is intriguing because fluid from only a small volume of over-pressured rock may apparently reduce the effective normal stress over a large fault surface area. Only small, heterogeneously distributed patches of over-pressured fracture network are required to make the fluid pressure compartment model viable. This conclusion is consistent with observations that the structural and fluid pressure properties of fractured rock are spatially and temporally heterogeneous [Bruhn et al., 1990; Parry and Bruhn, 1990].

## Fluid Pressure Dissipation

Preliminary estimates of the time required to dissipate a fluid pressure pulse generated by localized rupture are made using a simple groundwater flow model (MODFLOW). In this case, the fault zone is assumed to be a layer of variable thickness filled with porous granular material (Figure 2). The thickness pattern is created by computing the distance between two computer-generated, synthetic, rough fault surfaces. Thicknesses range from 0 to 0.1 m with a median value of about 0.05 m. The intervening zone, assumed to comprise a mix of both gouge and damage zone, is assigned a bulk permeability of  $10^{-16} \text{ m}^2$  and a storage coefficient of 0.001. The surrounding rock mass is assumed to be both impermeable and incompressible.

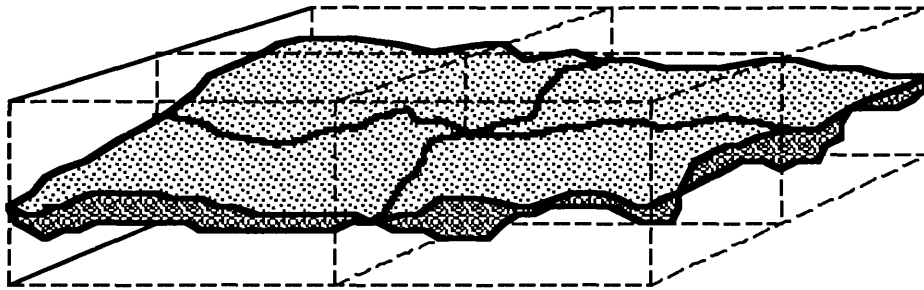


**Figure 2:** Schematic view of the numerical modeling domain used to compute the dissipation of fluid pressure within a fault zone. The stippled and shaded structure is the region modeled as an equivalent porous media sandwiched between rocks that are assumed to be both impermeable and incompressible.

A localized pressure pulse associated with fault rupture is simulated by instantaneously injecting  $0.1 \text{ m}^3$  of water into a  $0.1 \text{ m}^2$  area of the fault zone. A 10 m by 10 m patch within the fault plane is represented in the model. Given the relatively small thickness of the fault zone (on average about 0.05 m) and the incompressible-impermeable protolith, the resulting pressure pulse rises to 100 MPa above the ambient pre-rupture fluid pressure. This fluid pressure exceeds lithostatic pressure for depths shallower than about 30 km. For the purposes of this illustration, however, we assume that the pressure pulse site is located deeper than 30 km.

Simulation results indicate that the fluid pressure will be reduced to 10% of the original value after a period of about 5 years as the injected fluid moves away from the pulse site within the fault zone. Thus, for the geometry simulated we find that fluid pressure compartments might maintain pressures elevated well above ambient (perhaps close to lithostatic) for time periods on the order of 10 years. Assigning a much higher fault zone permeability of  $10^{-13} \text{ m}^2$  produces a much shorter time of about 1.5 days to dissipate the same pressure pulse. Additional simulations that mimic a very thin region of the fault ( $1 \mu\text{m}$ ) suggest that about 50 years would be required to dissipate the same fluid pressure pulse to 10% of the initial value. Using the semi-quantitative data that we are collecting from rock samples and cores of the SWF we will explore how different patterns of fault thickness, various fault permeabilities, and different pressure pulse locations influence the dissipation of fluid pressure pulses within faults and the transfer of fluid pressure between different fault compartments.

## CONCLUSIONS

Field studies of faulted rocks exposed at the surface in Dixie Valley, Nevada are complete. Field mapping has produced a detailed image of the internal structure of the Stillwater Fault Zone at two localities. Our conceptual model for fault architecture seems to apply at these locations as we see distinct fault components represented by the damage zone, fault core, and protolith. The different zones are distinguished by distinctive variations in fracture intensity, rock alteration, and rock fabric.

Detailed mapping of fracture networks in thin-section and outcrop provide a geometrical basis for estimating effective bulk permeabilities for the fault zone. An automated computer code is used to construct synthetic fracture networks which are then used as input for a second code that computes the effective permeability of the specified fractured rock mass. Laboratory testing is underway to obtain quantitative insight into the hydraulic and mechanical properties of each fault component.

Field observations and measurements of fracture networks surrounding large fault surfaces provide important constraints on structural and mechanical properties of large normal fault zones. Large fault surfaces that rupture during earthquakes are encased within intensely fractured rock. The fracture networks provide pathways for fluid flow within the fault zone, and also form fluid reservoirs. High pressure fluid trapped in isolated, fractured-rock reservoirs may bleed into voids between fault surfaces, possibly triggering instability by the reduction of effective normal stress, as envisaged by Byerlee (1993). Estimates of fracture permeability vary from as high as  $10^{-13} \text{ m}^2$  in the modeled pre-rupture stress state, to as low as  $10^{-17} \text{ m}^2$  in the post-rupture state. If an impermeable host rock is assumed, fluid pressure pulses generated within a low-permeability ( $10^{-16} \text{ m}^2$ ) fault zone with average thickness of 0.5 m might persist for periods on the order of 1 to 10 years.

## REFERENCES

- Bruhn, R.L., Yonkee, W. T., and Parry, W. T., 1990, Structural and fluid-chemical properties of seismogenic normal faults. *Tectonophysics*, V. 175, p.139-157.
- Byerlee, J.D., 1993, Model for episodic flow of high-pressure  $\text{H}_2\text{O}$  in fault zones before earthquakes. *Geology*, V. 21, p. 289-304.
- Byerlee, J.D., 1990, Friction, overpressure and fault normal compression. *Geophys. Res. Letts.*, V. 17, p. 2109 - 2112.
- Jackson, J.A., and N.J. White, 1989, Normal faulting in the upper continental crust: Observations from regions of active extension, *J. Struct. Geol.*, 15-36.
- Oda, M., Hatsuyama, Y., and Ohnishi, Y., 1987, Numerical experiments on permeability tensor and its application to jointed granite at the Stripa Mine, Sweden. *J. Geophys. Res.*, V. 92, p. 8037-8048.
- Oda, M., 1986, An equivalent continuum model for coupled stress and fluid flow analysis in jointed rock masses. *Water Resources Res.*, V. 22, p. 1845-1856.
- Page, B.M., 1965, Preliminary geologic map of a part of the Stillwater Range, Churchill County, Nevada, Map 28, Nevada Bureau of Mines and Geology, Reno, Nevada.
- Parry, W.T., Hedderly-Smith, D., and Bruhn, R.L., 1991, Fluid inclusions and hydrothermal alteration on the Dixie Valley Fault, Nevada: *J. Geophys. Res.*, v. 96, p. 19,733-19,748.
- Parry, W. T., and Bruhn, R. L., 1990, Fluid pressure transients on seismogenic normal faults: *Tectonophysics*, v. 179, p. 335-344.
- Power, W.L., and T.E. Tullis, 1989, The relationship between slickenside surfaces in fine-grained quartz and the seismic cycle, *J. Struct. Geol.*, 11, 879-893.

- Rice, J.R., 1992, Fault stress states, pore pressure distributions, and the weakness of the San Andreas fault: *in* Fault Mechanics and Transport Properties of Rocks, B. Evans and T. -F. Wong (eds.), p. 475-504 (Academic Press).
- Sibson, R.H., 1989, Earthquake faulting as a structural process. *J. Struct. Geol.*, V. 11, p. 1-14.
- Smith, L., Forster, C.B., and Evans, J.P., 1990, Interaction of fault zones, fluid flow and heat transfer at the basin scale: *in* Hydrogeology of permeability environments. Inter. Assoc. of Hydrogeologists, V. 2, p. 41-67.
- Speed, R.C., 1976, Geologic map of the Humboldt Lopolith, Geol. Soc. Amer. Map & Chart Series MC-14, Scale 1:81050.
- Speed, R.C., and Armstrong, R.L., 1971, Potassium-Argon ages of some minerals from igneous rocks of western Nevada. *Isochron/West*, V. 71-1, p. 1-8.
- Wallace, R.E., 1974, Patterns and timing of late Quarternary faulting in the Great Basin Province and relation to some regional tectonic features, *J. Geophys. Res.*, 89, 5763-5769.
- Wallace, R.E., and R.A. Whitney, 1984, Late Quarternary history of the Stillwater seismic gap, Nevada, *Bull. Seism. Soc. Am.*, 74, 301-314.
- Warburton, P.M., 1980, A stereological interpretation of joint trace data. *Int. J. Rock Mech. Min. Sci. & Geomech. Abstr.*, V. 17, p. 181-190.
- Wilden, R., and Speed, R.C., 1974, Geology and mineral resources of Churchill County, Nevada. Nevada Bureau of Mines and Geology Bulletin 83, 95 p.

# Earthquake Triggering

Project Number 995011395

Joan Gomberg  
 U.S. Geological Survey  
 CERI, University of Memphis  
 Memphis, TN 38152  
 901-678-4858  
 gomberg@ceri.memphis.edu

## Element I: Components I.1,I.2

### PROJECT SUMMARY:

This study consisted of several parts, all pertaining to earthquakes triggering on varying spatial and temporal scales. The first part deals primarily with the role of dynamic strains (those associated with seismic waves) and triggering by distant earthquakes. To fully understand the triggering process we also look at triggering in the near field as manifest in earthquake foreshock/mainshock/aftershock sequences. The last part pertains to the actual measurement of dynamic strains.

### PROJECT RESULTS:

*Dynamic strains and triggering.* Seismicity triggered at The Geysers geothermal field and by the Ms7.4 Landers earthquake in California provide strong constraints on the physical process of earthquake triggering. Results of analysis of seismicity catalogs and broad-band seismograms suggest a physical model of triggering in which strain-rate dependent processes elevate pore pressures to failure levels due to compaction of fault gouge. The dynamic strains themselves do not significantly elevate stresses in the fault zone but rather they initiate secondary processes that lead to increased pore pressures. Although the physics may be the same, the absolute threshold level differs from site to site, apparently reflecting differences in fault rheology. In addition to being relevant to triggering at remote distances, dynamic strains may also be important at near distances (aftershock zone) where previously seismicity has been attributed primarily to static strain changes.

*Foreshock/mainshock/aftershock triggering.* The relationship between mainshocks and foreshock/aftershock activity requires accurate characterization of mainshock slip patterns. We examine slip distributions for the 3 Oct., 1974 (M<sub>w</sub>=8.0) Peru earthquake and its largest aftershock on 9 Nov. (M<sub>s</sub>=7.1) using teleseismic, long-period waveforms. We demonstrate that erroneous results are obtained if the parameterization used does not allow for a sufficiently complex source. Slip during the main shock is shallow (<15 km) and extends up-dip from the hypocenter. Prior to the 9 Nov. event, aftershocks are shown to cluster near the event's hypocenter. These aftershocks locate generally down-dip from the major zones of main shock slip, with two obvious clusters apparent. One cluster extends 20 km down-dip from the 9 Nov. aftershock hypocenter suggesting that the region was near failure with local strain relaxation culminating in the 9 Nov. event. The second cluster is located at a much greater depth (45-65 km) and is far removed from any major slip or subsequent large aftershock. Its location indicates that it may be the result of down-dip compressional strain accumulation due to the large amount of shallow plate displacement. This explanation is consistent with the plate stress model of Astiz et al. (1989).

*Dynamic strain measurement.* Investigations undertaken include testing of the capability of a novel rotational sensor to record strong-ground motions, continued development of low-cost PC-based computer systems for processing seismic-waveform data, and interpretation of the significance of the Northridge strong-ground-motion dataset with respect to dynamic strains. The waveforms of a

regional magnitude 5 earthquake recorded in San Bernardino, California, suggest that a significant component of rotational ground motion was produced by the conversion of P-waves to S-waves at the dipping alluvium/rock interface beneath the site. PC-based computer systems have now attained a level of processing capability that is comparable to that of the computer systems traditionally used for seismological research, e.g., SUNs and VAXs, and the former are significantly less expensive than the latter. Although the strong-ground-motion dataset of the Northridge Earthquake mainshock/aftershock sequence is unprecedently large, it is nonetheless severely spatially aliased by approximately two orders of magnitude relative to the observed variation of building damage and ground motion waveforms over distances of a city block.

## PRODUCTS:

- Cranswick, E., 1994, Damage done by the 1994 Northridge, California, Earthquake and the spatial density of sampling strong ground motions: Program for Northridge Abstracts, 89th Annual Meeting of the Seismological Society of America, 5-7 April 1994, Pasadena, California.
- Cranswick, E., Meremonte, M., Frankel, A., 1994, Correlation of waveform incoherence with site amplification of Northridge aftershocks recorded by small-aperture arrays: *Eos*, v. 75, p. 168.
- Cranswick, E., Overturf, D., Bice, T., Hough, S., Abramovich, I., 1994, Recordings of ground motion rotation in San Bernardino, California, produced by a magnitude 5 earthquake: *Seismological Research Letters*, v. 65, p. 39.
- Gomberg, J., Stress/strain changes and seismicity following the Ms7.4 Landers, California earthquake, in preparation.
- Gomberg, J. and D.C. Agnew, The accuracy of seismic estimates of dynamic strains from Piñon Flat Observatory, California, strainmeter and seismograph data, in preparation.
- Gomberg, J. and S. Davis, Stress/Strain changes and seismicity at The Geysers, California, in preparation.
- Frankel, A., Meremonte, M., Cranswick, E., Carver, D., Worley, D., Odum, J., Williams, R., and Bodin, P., 1994, Observations from Northridge aftershocks recorded by seismometers deployed in the San Fernando Valley and at the Interstate-10 collapse: Program for Northridge Abstracts, 89th Annual Meeting of the Seismological Society of America, 5-7 April 1994, Pasadena, California.
- Hartzell, S., and Langer, C. (1993). Importance of model parameterization in finite fault inversion: application to the 1974 Mw 8.0 Peru earthquake, *J. Geophys. Res.*, 98, 22123-22134.
- Meremonte, M., Cranswick, E., Carver, D., Worley, D., Odum, J., Williams, R., Frankel, A., Overturf, D., Bice, T., Van Dreser, T., Shedlock, K., and Banfill, R., 1994, Processing digital seismograms of aftershocks of the Northridge Earthquake in a motel at Pasadena, California: Program for Northridge Abstracts, 89th Annual Meeting of the Seismological Society of America, 5-7 April 1994, Pasadena, California.
- Meremonte, M., Frankel, A., and Cranswick, E., 1994, Observations of basin surface waves from Northridge aftershocks recorded by small-aperture arrays: *Eos*, 75, p. 168.

## Central California Network Operations

9930-10093  
9930-15093  
9930-57093

Wes Hall  
Branch of Seismology  
U.S Geological Survey  
345 Middlefield Road-Mail Stop 977  
Menlo Park, California 94025  
(415) 329-4730  
FAX (415) 329-5143  
hall@andreas.wr.usgs.gov

### Investigations

Maintenance and recording of 356 seismograph stations (453 components) located in Northern California, Central California and Oregon. Also recording 71 components from other agencies. The area covered is from Southern Oregon, south to Santa Maria.

### Results

- |  |     |
|--|-----|
| 1. Site maintenance visits   | 331 |
| 2. Bench Maintenance Repair  |     |
| A. seismic VCO units   | 307 |
| B. summing amplifiers  | 36  |
| C. seismic test units  | 05  |
| D. VO2H/VO2L VCO units   | 137 |
| E. dc-dc converters  | 22  |
| 3. Production/Fabrication  |     |
| A. J512A VCO units   | 27  |
| B. J512B VCO units   | 03  |
| C. summing amplifier units   | 12  |
| D. lithium battery packs   | 126 |
| E. seismometer housing/cable   | 36  |
| 4. Rehabilitation:   |     |
| VCO enclosures   | 28  |
| 5. Computer site map plots   |     |
| A. new   | 06  |
| B. update  | 109 |
| 6. GPS recordings recorded   | 150 |
| 7. Seismometers replaced   | 54  |
| 8. Discriminator repair and tuning (J120)  | 78  |
| 9. Installed and documented hardwire interface for eartworm project (512 channels) |     |
| 10. Installed and documented 256 channels to PC System.                            |     |
| 11. Installed 5 new sites in Southern California after Nortridge Earthquake        |     |

12. Revised and updated documentation on all wiring from telco input to discriminator output.  
(cusp, RTP, Motorola, PC, helicorder, etc).

13. Ordered parts for 100 ea. V02 rack mount VCO's

14. Equipment Shipped:

A. Cal Tech, Pasadena  
a. 5 ea J120 discriminators

B. University Washington  
a. 5 ea. J120 discriminators

E. Lawrence Livermore National Laboratory  
a. 1ea J110 discriminator

I. University of Utah  
a. 21 ea. J120 discriminators

15. New installations

A. NBO (Bolinas)  
B. CVPI, CVPJ, CVPK (3 component FBA at Vollmer Peak)

16. Stations discontinued.

A. PG1, PGS (Gold Hill Dilatometers)  
B. GMO (Moffet Ranch)

17. Discontinued recording on Bell and Howell 1 inch tape recorders.

18. Supplied support for Refraction Experiments.

## 3D Dynamic Modeling of Earthquakes and Segmented Faults

9960-10446

Principal Investigator  
**Ruth A. Harris**

United States Geological Survey  
Mail Stop 977, 345 Middlefield Road, Menlo Park, CA 94025  
(415) 329-4842  
email: [harris@jog.wr.usgs.gov](mailto:harris@jog.wr.usgs.gov)  
Program Element I

### Investigations Undertaken:

During FY94 I continued my investigation into the roles of dynamic and static stresses in determining the sizes and locations of future large earthquakes. For the dynamic stress analyses I used 2D and 3D finite-difference simulations of spontaneously propagating earthquakes. The simulations incorporate a slip-weakening fracture criterion and allow the physics of the stress waves to determine the rupture behavior. The static stress analyses are a collaborative effort with Robert Simpson and Paul Reasenberg (USGS). We evaluated the effects of 25 years of large southern California earthquakes, including the 1994 M6.7 Northridge, California earthquake, on future large earthquakes in California.

### Results:

In FY94 I showed how the 1992 M7.3 Landers earthquake cascaded from fault to fault as it evolved from a 'predicted' [Wesnousky, 1986] M6 event on the Johnson Valley fault into a much larger multi-fault earthquake. This earthquake demonstrated that parallel faults spaced closer than 2-3 km may fail in single events. The lesson from Landers is that we may need to reassign the magnitude estimates for future large strike-slip earthquakes in California.

I also initiated a study on the effects of a fault-parallel low-velocity zone (fault gouge) on the rupture velocity of an earthquake. Evidence of these zones is provided by studies of shear waves recorded after the Landers earthquake, and on the San Andreas fault near Parkfield [e.g. Li et al., 1994]. Preliminary 2D numerical simulations show that a large propagating earthquake rupture may not 'sense' a narrow, 200 meter wide gouge zone, but as the gouge zone widens, the rupture velocity will be affected by the low-velocity material.

In FY94 we showed that the Northridge earthquake is following a pattern observed for the previous 25 years of magnitude>5 southern California earthquakes; most large ( $M>5$ ) aftershocks occur on faults that were loaded towards Coulomb failure by the mainshock. This relationship appears to last for less than 2 years, after which it is equally likely to have a subsequent large earthquake on a loaded or relaxed fault.

## **3D Dynamic Modeling of Earthquakes and Segmented Faults**

### **P.I.: Ruth A. Harris**

**Reports Published:**

Harris, R.A., and R.W. Simpson, In the shadow of 1857; an evaluation of the static stress changes generated by the M8 Ft. Tejon, California earthquake (abstract), EOS Trans. AGU, vol. 74, page 427, 1993.

Harris, R.A., A new method for defining fault segment boundaries in strike-slip faults (abstract), Seism. Res. Lett., 65, 54, 1994.

Harris, R.A., and R.W. Simpson, Earthquake interactions among moderate and large earthquakes in the Landers region (abstract), Seism. Res. Lett., 65, 54, 1994.

Harris, R.A., R.W. Simpson, and P.A. Reasenberg, Static stress changes influence future earthquake locations in southern California, (abstract), EOS Trans. AGU, vol. 75, page 169, 1994.

Harris, R.A., S.M. Day, Y-G Li, and J.E. Vidale, Numerical Simulations of an Earthquake Spontaneously Propagating in Fault Gouge (abstract), EOS Trans. AGU, vol. 75, page 442, 1994.

Pollard, D.D., and R.A. Harris, Quasi-static and dynamic stress changes during faulting: Implications for paleoearthquake identification (abstract), Presented at the Geological Society of America Annual Meeting, Boston, Mass., October 1993.

Scientists of the US Geological Survey and the Southern California Earthquake Center, The Magnitude 6.7 Northridge, California, Earthquake of January 17, 1994, Science, vol. 266, pages 389-397, 1994.

Simpson, R.W., and R.A. Harris, A model of active faults in southern California for calculating static stress changes after earthquakes (abstract), EOS Trans. AGU, vol. 74, page 428, 1993.

Simpson, R.W., D.A. Castillo, R.A. Harris, L.K. Hutton, and L.M. Jones, Faults in southern California with increased coulomb failure load after ML>5 earthquakes are more likely to have ML>5 events in the year following (abstract), Seism. Res. Lett., 65, 63, 1994.

Simpson, R.W., R.A. Harris, and P.A. Reasenberg, Stress changes caused by the 1994 Northridge, California earthquake (abstract), Northridge Abstract Program for the 1994 SSA Meeting, page 8, 1994.

## **EARTHQUAKE SOURCE AND EFFECT STUDIES**

**9950-11255**

**S. H. Hartzell, D. Carver, E. Cranswick**

**Branch of Earthquake and Landslide Hazards  
U.S. Geological Survey  
Box 25046, MS 966, Denver Federal Center  
Denver, CO 80225  
(303) 273-8572**

### **Main Program Elements I.2, II.2, III.2**

#### **Investigations**

- 1) Aftershocks of the 1989 Loma Prieta, Calif., earthquake are used to estimate site response in an area of 12 square kilometers centered on downtown Santa Cruz. We also use waveforms from a three station array located in the flood plain to calculate the apparent velocity and azimuth of propagation of coherent arrivals within moving windows of the S-wave coda.
- 2) A previously-developed hybrid, global search algorithm is extended for use in calculation of finite-fault rupture histories, where both the rupture time and the slip amplitude are free parameters. The new method is applied to the 1992 Landers, California, earthquake.
- 3) Site response is calculated for the Los Angeles urban area using aftershocks of the 1994 Northridge earthquake.
- 4) Tested capability of a novel rotational sensor to record strong-ground motions.
- 5) Development of new techniques for obtaining detailed site response information from surface sources.
- 6) Continued development of low-cost, PC-based computer systems for processing seismic-waveform data.
- 7) Interpretation of the significance of the Northridge strong-ground-motion dataset with respect to building damage.
- 8) Exploration of strategies for mass-distribution of low-cost strong motion instrumentation in urban environments in cooperation with members of the general public.

#### **Results**

- 1) A total of 259 shear-wave records from 36 aftershocks are used in a linear inversion for site response spectra. The shear-wave site responses correlate well with the surficial geology and observed damage pattern of the main shock. In the frequency band from 1 to 4 Hz, sites on or near crystalline basement have site response amplification factors from 1.0 to 1.6, sites on marine terrace deposits have factors from 2.1 to 3.4, and sites on the alluvium-filled flood plain have factors from 5.0 to 12.1. Amplification factors

are progressively lower for frequency bands of 4-7 Hz and 7-10 Hz. For example, the factors range from 1.8 to 6.5 at flood-plain sites in the 7-10 Hz frequency band. Results of the apparent velocity and azimuth calculations show that the direct S-waves come from azimuths consistent with the source locations and have higher velocities than later arrivals. Waves arriving later than 2 sec after the direct S-waves have apparent velocities less than 2 km/sec, arrive from divergent azimuths, and have nearly horizontal angles of incidence. These results indicate that the large amplitude waves that arrive after the direct S-wave arrival are surface waves generated and trapped in the flood-plain basin alluvial sediments.

2) Many interesting inverse problems in geophysics are nonlinear and multimodal (having many local minima). By combining simulated annealing with the downhill simplex method, a hybrid global search algorithm is obtained for solving these problems. One such interesting problem is the retrieval of finite-fault rupture histories. The hybrid global search method is used to determine the rupture history of the 1992 Landers earthquake by the inversion of teleseismic waveform data. Traditional approaches to this problem using iterative least squares are dependent on the starting model and converge to local minima. The hybrid global method converges to the global minimum of the prescribed objective function.

Application of the global search method to the Landers earthquake yields a very heterogeneous distribution of slip. Each of the three main segments of the rupture (Johnson Valley, Homestead Valley, Emerson/Camp Rock) has one or two large slip patches. Major slip lies above 14 km depth for all three fault segments. Slip on the Emerson/Camp Rock Fault shallows northward to include just near-surface faulting (top 2 to 4 km). Large offsets at the surface generally occur north of (in the direction of rupture propagation) large slip zones at depth. Moment release is the greatest on the Homestead Valley Fault, followed by the Emerson/Camp Rock Fault, and least on the Johnson Valley Fault where the earthquake initiated. Rupture times from the global search inversion indicate an average rupture velocity of about 3.0 km/sec. Local variations in rupture velocity vary from about 2.5 to 3.5 km/sec. The total rupture duration is 22 sec. Jumping of the rupture from one segment to another as faulting progressed from south to north occurs before the rupture has reached the end of a given segment, but is variable in its timing.

3) A linear-inversion technique is used in which the recorded aftershock spectra are decomposed into source and site spectra after correction for propagation-path attenuation and geometric spreading. No assumptions are made about the shape of the source spectra. The inversion is constrained by requiring the site response at a hard-rock site in the Santa Monica Mountains to have an approximate value of 1.0 with a kappa of 0.02. Sparse-matrix techniques are used to rapidly calculate a solution. Site response is estimated using both the direct S-wave and the S-wave coda. Over 60 sources are used, many recorded at 20 or more sites, to determine the site response at 90 locations throughout the Los Angeles urban area. Most of the strong-motion sites within 30 km of the epicenter of the Northridge earthquake were co-located with aftershock recorders. Determination of the site response at these locations adds insight into the distribution of mainshock ground motion. Site response values are also compared between the damaged and non-damaged areas in an attempt to explain the observed damage pattern. The distribution of sites allows us to

compare site-response values over different length scales, including on a block-by-block basis up to the dimensions of an entire sediment-filled basin like the San Fernando Valley. Comparisons are also made between the calculated site response and surficial geology and topography and the depth to basement. This information is used to suggest ways that site response can be estimated at locations where no aftershock recordings exist.

4) The waveforms of a regional magnitude 5 earthquake recorded in San Bernardino, California, suggest that a significant component of rotational ground motion was produced by the conversion of P-waves to S-waves at the dipping alluvium/rock interface beneath the site.

5) The ground motions recorded 5 m from the impact points of vertical impulses (i.e., weight drops) correlate well with the site response independently estimated from the examination of the local geology, shallow reflection/refraction surveys, and analysis of aftershock waveforms recorded at those sites; however, because of problems of source coupling, the ground motions produced by horizontal impulses (i.e., shear impacts) do not show such good correlation.

6) PC-based computer systems have now attained a level of processing capability that is comparable to that of the computer systems traditionally used for seismological research, e.g., SUNs and VAXs, and the former are significantly less expensive than the latter.

7) Although the strong-ground-motion dataset of the Northridge Earthquake main-shock/aftershock sequence is unprecedently large, it is nonetheless severely spatially aliased by approximately two orders of magnitude relative to the observed variation of building damage and ground motion waveforms over distances of a city block.

8) The technology presently exists for the low-cost and reliable acquisition, telemetry, and database management of strong-ground-motion data from sites with a spatial density comparable to population density, but since public interest in participating in such a program depends upon the recent experience of a locally destructive earthquake, e.g., Northridge (since the the 1989 Loma Prieta Earthquake, public interest in earthquakes in the San Francisco Bay Area has already largely waned), a government initiative related to earthquake insurance and hazard mitigation is necessary to sustain the development of dense urban seismic arrays.

## Reports

Carver, D. L., and S. H. Hartzell, 1994, Mapping earthquake site response in Santa Cruz, California, Bull. Seism. Soc. Am., submitted.

Carver, D. L., and S. H. Hartzell, 1994, Mapping earthquake site response in Santa Cruz, California, EOS, v. 75, no. 44, 447.

Cranswick, E., 1994, Damage done by the 1994 Northridge, California, Earthquake and the spatial density of sampling strong ground motions: Program for Northridge

Abstracts, 89th Annual Meeting of the Seismological Society of America, 5-7 April 1994, Pasadena, California.

Cranswick, E., Meremonte, M., Frankel, A., 1994, Correlation of waveform incoherence with site amplification of Northridge aftershocks recorded by small-aperture arrays: *Eos*, v. 75, p. 168.

Cranswick, E., Overturf, D., Bice, T., Hough, S., Abramovich, I., 1994, Recordings of ground motion rotation in San Bernardino, California, produced by a magnitude 5 earthquake: *Seismological Research Letters*, v. 65, p. 39.

Darby, D., Darby, J., and Hammond, S., (Sponsor: E. Cranswick), 1994, The Public Seismic Network (PSN) of Pasadena, HAM radio and the 17 January 1994 Northridge Earthquake: Program for Northridge Abstracts, 89th Annual Meeting of the Seismological Society of America, 5-7 April 1994, Pasadena, California. [NOTE: this abstract was sponsored as part of the USGS/PSN Seismology Education Project, E. Cranswick, project chief]

Frankel, A., Meremonte, M., Cranswick, E., Carver, D., Worley, D., Odum, J., Williams, R., and Bodin, P., 1994, Observations from Northridge aftershocks recorded by seismometers deployed in the San Fernando Valley and at the Interstate-10 collapse: Program for Northridge Abstracts, 89th Annual Meeting of the Seismological Society of America, 5-7 April 1994, Pasadena, California.

Hartzell, S., and P. C. Liu, 1994, Inversion of earthquake rupture histories using a hybrid global search algorithm: application to the 1992 Landers, California, earthquake, *Phys. Earth Plant. Int.*, submitted.

Hartzell, S., and P. C. Liu, 1994, Inversion for fault rupture history using a hybrid global search algorithm: application to the Landers, California earthquake, *Seism. Res. Lett.*, v. 65, no. 1, 52.

Hartzell, S., A. Leeds, and A. Frankel, 1994, Calculation of site response for urban Los Angles using aftershock records from the Northridge earthquake, *EOS*, v. 75, no. 44, 168.

Meremonte, M., Cranswick, E., Carver, D., Worley, D., Odum, J., Williams, R., Frankel, A., Overturf, D., Bice, T., Van Dreser, T., Shedlock, K., and Banfill, R., 1994, Processing digital seismograms of aftershocks of the Northridge Earthquake in a motel at Pasadena, California: Program for Northridge Abstracts, 89th Annual Meeting of the Seismological Society of America, 5-7 April 1994, Pasadena, California.

Meremonte, M., Frankel, A., and Cranswick, E., 1994, Observations of basin surface waves from Northridge aftershocks recorded by small-aperture arrays: *Eos*, v. 75, p. 168.

Williams, R.A, Pratt, T.L., Cranswick, E., Carver, D.L., Worley, D.M., and Lee, W.H.K., 1994. Preliminary site response in Santa Cruz, California, using controlled seismic sources: *Eos*, v. 75, p. 447.

## Regional Microearthquake Network in the Central Mississippi Valley

14-08-0001-A0619

Robert B. Herrmann  
Department of Earth and Atmospheric Sciences  
Saint Louis University  
3507 Laclede Ave.  
St. Louis, MO 63103  
(314) 977-3131

### **Investigations**

The purpose of the network is to monitor seismic activity in the Central Mississippi Valley Seismic zone, in which the large 1811-1812 New Madrid earthquakes occurred. The following section gives a summary of network observations from October 1993 through September 1994.

### **Results**

During this time, 55 earthquakes were located by the regional telemetered microearthquake network operated by Saint Louis University for the U.S. Geological Survey. Figure 1 shows 52 earthquakes located within a  $4^\circ \times 5^\circ$  region centered on  $36.5^\circ\text{N}$  and  $89.5^\circ\text{W}$ . The magnitudes are indicated by the size of the open symbols. Figure 2 shows the locations and magnitudes of 38 earthquakes located within a  $1.5^\circ \times 1.5^\circ$  region centered at  $36.25^\circ\text{N}$  and  $89.75^\circ\text{W}$ .

From October 1, 1993 through September 30, 1994, 91 teleseisms were recorded by the PC clone running the VENIX operating system. Epicentral coordinates were determined by assuming a plane wave front propagating across the network and using travel-time curves to determine back azimuth and slowness, and by assuming a focal depth of 15 kilometers using spherical geometry. Arrival time information for teleseismic P and PKP phases has been published in the quarterly earthquake bulletin.

The significant earthquakes occurring during this time include the following:

February 5, 1994 (1455 UTC). Cape Girardeau, Missouri region.  $M_D$  4.2 (SLM).  $m_{bLg}$  4.2 (GS). Felt (V) at Scott City and Ste. Genevieve, Missouri. Also felt (V) at Dongola and Johnson City, Illinois. Felt (IV) at Carbondale, Cobden, De Soto, Goreville, Jonesboro, Makanda, Metropolis, Tamms and Royalton, Illinois. Also felt (IV) at Benton, Cape Girardeau, Fredericktown and Perryville, Missouri. Felt in southern Illinois, southeastern Missouri and western Kentucky. Broadband waveform modeling (Herrmann and Ammon, 1995) of the BB waveforms at the IRIS station at Cathedral Cave, Missouri, yielded a focal depth of 15 km, a strike of  $25^\circ$ , a rake of  $170^\circ$  and a dip of  $70^\circ$  for the focal mechanism, and a seismic moment of  $6.0 \times 10^{21}$  dyne-cm. This focal mechanism is shown in relation to others in Figure 3, which include the

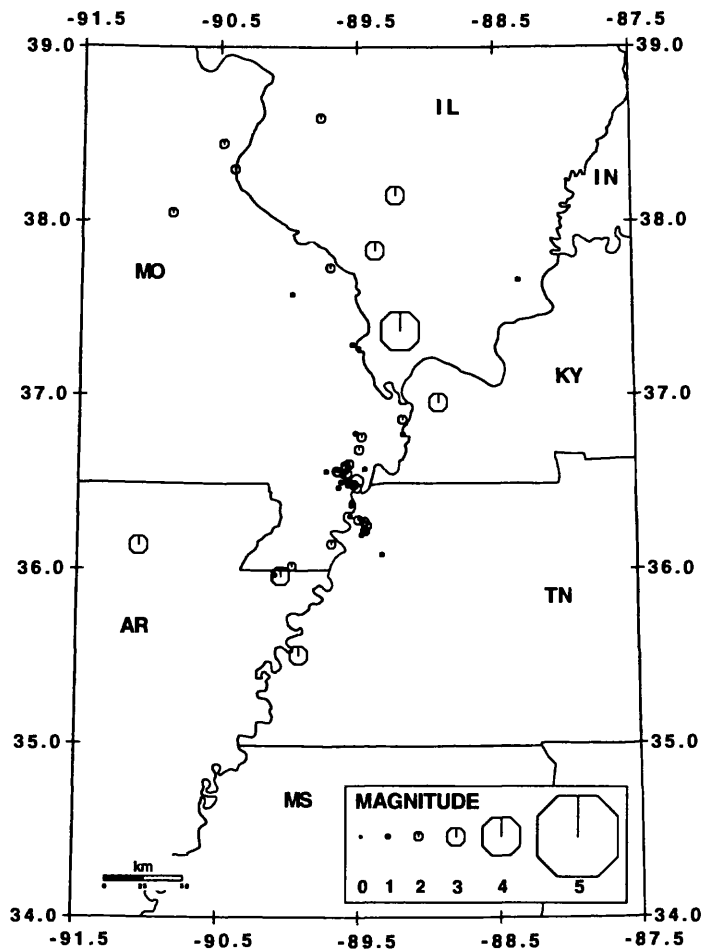


FIGURE 1  
CUMULATIVE EVENTS 01 OCT 1993 TO 30 SEP 1994  
LEGEND : ▲ STATION ◊ EPICENTER

revised focal mechanisms for the March 3, 1963 and July 21, 1967 events (Herrmann, 1995).

February 28, 1994 (1829 UTC). Cape Girardeau, Missouri region.  $M_D$  3.0 (SLM).  $m_{bLg}$  2.6 (GS). Felt (V) at Carbondale and (IV) at Cambria, Illinois. Also felt at Murphysboro, Illinois.

March 21, 1994 (1734 UTC). New Madrid, Missouri region.  $M_D$  2.9 (SLM).

April 6, 1994 (1738 UTC). Southern Illinois.  $m_{bLg}$  3.1 (GS).  $M_D$  3.1 (SLM). Felt (IV) at Carbondale and Oakdale. Felt (II) at Benton.

April 23, 1994 (1946 UTC). Arkansas.  $M_D$  3.0 (SLM).  $m_{bLg}$  2.8 (GS).

May 4, 1994 (0912 UTC). Alabama.  $m_{bLg}$  3.0 (GS). Felt (IV) at Addison; (III) at Decatur, Houston and Madison; (II) at Arley. Also felt at Double Springs and Jones Chapel.

August 20, 1994 (1045 UTC). Missouri-Arkansas border region.  $m_{bLg}$  3.5

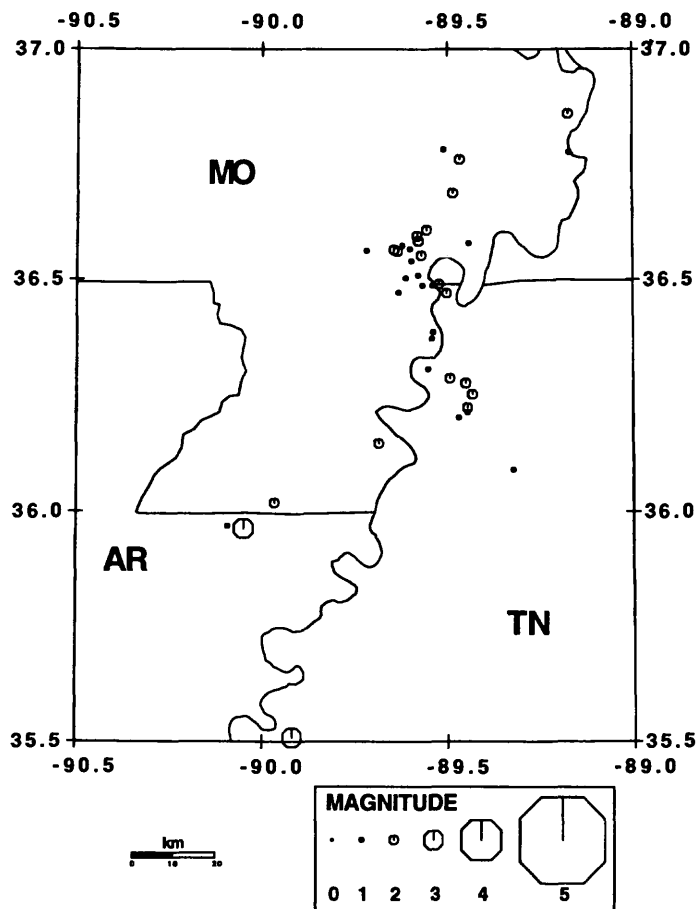


**FIGURE 2**  
**CUMULATIVE EVENTS 01 OCT 1993 TO 30 SEP 1994**  
**LEGEND :** ▲ STATION ◉ EPICENTER

(GS). Felt (IV) at Jonesboro, Lynn, Portia, Tuckerman and Walnut Ridge; (III) at Ravenden Springs and Smithville; (II) at Minturn, Powhatan and Ravenden, Arkansas.

September 26, 1994 (1423 UTC). Tennessee.  $m_{bLg}$  3.6 (GS).  $M_D$  3.5 (SLM). Felt (V) at Bardwell, Paducah and Wickliffe; (III) at Clinton and La Center, Kentucky. Also felt (III) at Brookport, Illinois.

### Publications

Herrmann, R. B. (1995). Broadband seismology and small regional seismic networks in, K. M. Shedlock and A. C. Johnston, eds., *Investigations of the New Madrid Seismic Zone*, U. S. Geological Survey Prof. Paper 1538 (in review).

Herrmann, R. B., and C. J. Ammon (1995). Waveform modeling as a tool for focal mechanism determination and validation, *Bull. Seism. Soc. Am.* (in revision).

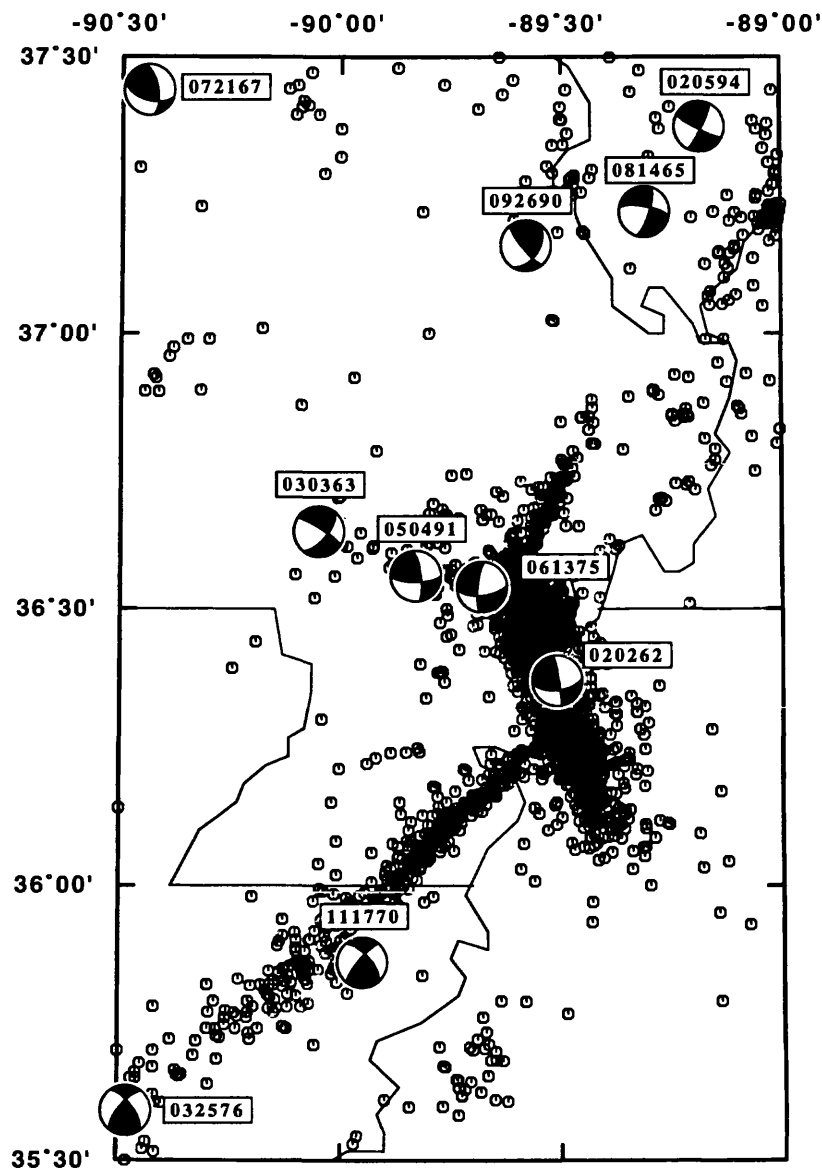


Fig. 3. Focal mechanisms of larger events in the New Madrid seismic zone, 1962 - 1995. The focal mechanisms of the March 3, 1963 (030363) and the July 21, 1967 (072167) are recent revisions.

## Cooperative New Madrid Seismic Network

14-08-0001-G1922

Robert B. Herrmann

Department of Earth and Atmospheric Sciences

Saint Louis University

3507 Laclede Avenue

St. Louis, MO 63103

(314) 977-3131

[rbh@slueas.slu.edu](mailto:rbh@slueas.slu.edu)

### Introduction

The object of this effort is to upgrade the regional seismic networks in the central Mississippi Valley to provide the data sets necessary for future research in the earthquake process and in earthquake generated ground motion.

### Status

#### *Network Design*

This cooperative network has two aspects: detailed monitoring of seismicity in the region of New Madrid, Missouri, and an emphasis on regional monitoring. In the division of responsibilities, the University of Memphis will install a dense array of short period instruments in the New Madrid region proper, while Saint Louis University will install a backbone broadband network. Figure 1 shows the proposed locations of the broadband stations.

#### *RFP*

An RFP was released to manufacturers for equipment bids in late autumn, 1993. The RFP reflected the evolution of the seismic network design. The requirement is that the stations indicated in Figure 1, be modern broadband digital stations with dialup capability - e.g., open stations. These stations will be interrogated daily and also following an earthquake.

The RFP's were evaluated, and the decision was to purchase 15 systems consisting of Quanterra 380LX data acquisition and Guralp CMG-40T sensors. One station, on the campus of Saint Louis University, will be connected to Internet. All stations have sufficient disk capacity to store 7 days data online.

#### *Data Center*

Using internal university funds and a grant from the Union Pacific Foundation, a major effort was directed to improve the appearance and functionality of the *Saint Louis University Earthquake Center*. The central hallway has been remodeled, seismograph drum recorders are placed on top of exhibit cases which present a collection of seismic instruments from the turn of the century. An adjoining side room, formerly used for photographic recording of the French Village, Missouri, WWSSN station, has been made the network operations room, and has the VSAT control, a SparcStation 5, and PC data acquisition of the remaining analog telemetry data. Finally, an additional UPS has been constructed to keep the data center functioning in case of power failure.

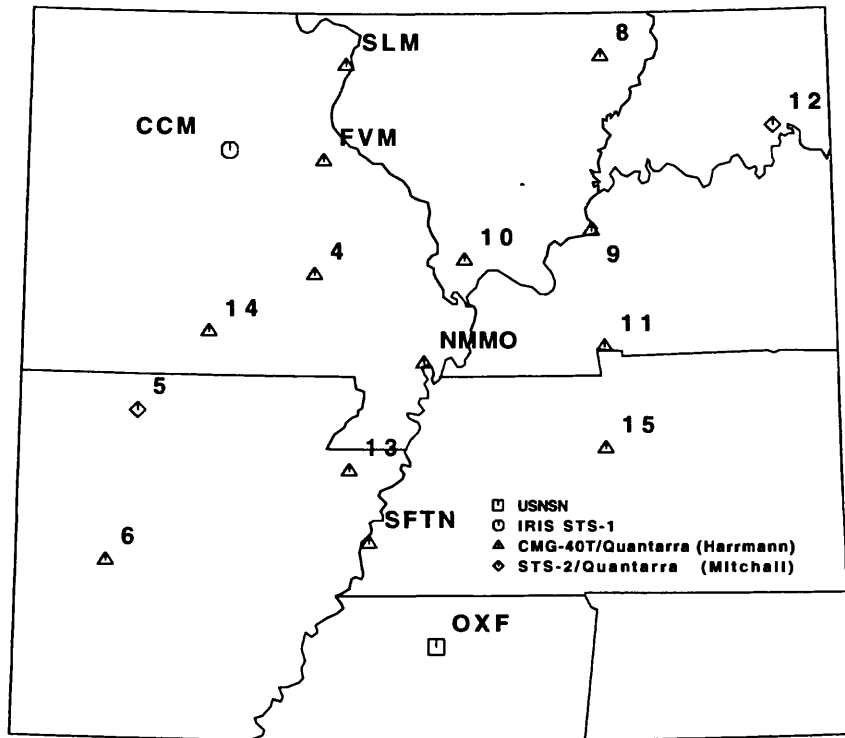


Fig. 1. Proposed distribution of 24 bit broadband stations in the New Madrid region: USNSN (squares), IRIS (circle), SLU STS-2/Quanterra by Harrmann (triangle) and under this grant SLU Guralp/Quanterra (diamond).

### Public Interaction

The network currently participates in the [finger quake@slueas.slu.edu](mailto:finger quake@slueas.slu.edu), initiated by the University of Washington. in addition, a Mosaic server has been established to provide earthquake history in the region, basic concepts, and also software and databases for use on UNIX workstations and PC's. The pointer to these products will be found on <ftp://geophys.washington.edu/HTML/seismosurfing.html>

### Continuing Efforts

Efforts are now directed toward assembling the broad band field stations and establishing a data base procedure for storing digital data.

# PRESSURE SOLUTION, CRACK HEALING AND CRUSTAL STRESS

Project Number: 9960-10226

Stephen H. Hickman  
 U.S. Geological Survey  
 345 Middlefield Rd., MS 977  
 Menlo Park, CA 94025  
 Phone: (415) 329-4807  
 Fax: (415) 329-5163  
 E-Mail: Hickman@thepub.wr.usgs.gov

## Program Element I

### INVESTIGATIONS UNDERTAKEN

#### *1. Laboratory Studies of Solution-Transport Deformation*

Solution-transport processes such as pressure solution, crack healing, and neck growth are quite important in determining the rheology of fault zones and the evolution of rock physical properties. In this laboratory investigation we are studying deformation at individual mineral-to-mineral contacts to provide fundamental constraints on the mechanisms and kinetics of these processes in quartzose rocks. These single-contact experiments are important because they allow unambiguous identification of the deformation mechanisms, the sources and sinks of material, and the effect of both contact geometry and second phases on neck growth, crack healing, and pressure solution (e.g., Hickman and Evans, 1992, 1994). These experiments are being performed in a unique apparatus that allows us to continually observe the contact region or crack while under load at hydrothermal conditions ( $P_{H_2O} \leq 200$  MPa,  $T \leq 600^\circ C$ ). By employing reflected-light interferometry, we are also able to monitor both the rate at which the lenses approach one another (i.e., converge) and the evolution of contact topology or crack aperture with time. In this manner we can independently determine the rates of pressure solution, neck growth, and crack healing as a function of temperature, effective normal stress, contact geometry, grain-boundary orientation and second-phase mineralogy.

#### *2. Improvement of Wireline Packer System*

To formulate a more viable and cost-effective in-situ stress program, we have used NEHRP funds to build a wireline packer system that can be used to make stress, permeability, and pore-pressure measurements without requiring a drilling rig on site. This system incorporates real-time digital telemetry of down-hole test-interval pressure, packer pressure, and flow rate. Motivated by the need to make permeability measurements in wells in which the water level is deeper than several tens of meters below ground level (as in the Ben Lomond well, discussed below), in FY 1994 we modified this packer system to provide downhole electronic control of fluid flow into the packers and test interval.

#### *3. In-situ Study of Physical Mechanisms for Permeability changes Associated with the 1989 Loma Prieta Earthquake*

The 1989 Loma Prieta, California, earthquake ( $M \sim 7.0$ ) caused significant changes in the shallow hydrology of the nearby Santa Cruz Mountains. These changes, which consisted of streamflow increases that persisted for several months after the earthquake and long-lived post-seismic lowering of the water table, are most readily explained by an increase in the permeability of the near-surface aquifers and aquitards during the Loma Prieta earthquake (Rojstaczer and Wolf, 1992). Historic water-level data from the Santa Cruz Mountains suggests that the permeability

created during earthquakes then gradually decreases during the interseismic period, perhaps by the infilling of fractures or faults with low-temperature hydrothermal deposits or weathering products. To determine the physical mechanisms responsible for this coseismic permeability enhancement, we are currently conducting measurements of stress, natural fracture orientation, and permeability in an approximately 170-m-deep borehole drilled in granodiorite at the crest of the Ben Lomond Ridge in the Santa Cruz Mountains, California. This project is being performed in collaboration with Stuart Rojstaczer of Duke University.

#### *4. Coupled Tectonic and Hydrologic Processes in Fractured Rock, Yosemite National Park*

This study, which involved hydrologists, geophysicists and geochemists from the USGS (Geologic and Water Resources Divisions) and the U.S. Department of Energy, was conducted to understand the nature, timing and extent of ground water flow in the fractured granitic aquifer beneath Yosemite National Park. Our role in this study was to make hydraulic fracturing stress measurements in two shallow wells drilled by the National Park Service near the town of Wawona to understand the nature and origin of the shallow stress field in this area. In coordination with in-situ permeability and geochemical studies by other investigations, our investigations will help determine if and in what manner these stresses might control the orientations of permeable fractures and faults in this aquifer.

#### *5. Planning and Coordination of San Andreas Fault Zone Drilling Project*

For the past three years we have been working with an international team of scientists and engineers in proposing a long-term, integrated program of surface-based geological and geophysical investigations and deep scientific drilling along the San Andreas fault system. This project would provide data essential to understanding the structure, composition, mechanical behavior, and physical state of an active, major plate-boundary fault. Our ultimate goal is to core inclined holes through the San Andreas fault zone at one location at depths of about 1, 3, 6, and 9 km and conduct extensive investigations in the holes and on the recovered materials. Upon completion of drilling, seismometers and other instruments will be placed in the holes for long-term monitoring of earthquake locations and source parameters, seismic wave propagation, electromagnetic radiation, fluid pressure, fluid chemistry, temperature, and deformation. The scientific objectives, experimental strategy, and site-selection process for the San Andreas Fault Zone Drilling Project (FZDP) are described in Hickman et al. (1994e and f). A key aspect of the funding strategy for this project, which would most likely occur as part of the International Continental Drilling Program currently under development (see Zoback and Emmermann, 1994), is to obtain new money for a broad range of geological and geophysical investigations of the San Andreas fault zone as well as for drilling and technology development.

The first stage of the FZDP is now well underway, with about 20 reconnaissance field investigations – incorporating geologic mapping, active and passive seismology, potential field methods (aeromagnetics, gravity, and magnetotellurics), hydrology, and borehole geophysics – being conducted along four segments of the San Andreas fault potentially suitable for drilling of the 10-km-deep hole. Our goal in site selection is to build a suite of comparative models of the geologic, hydrologic, and geodynamic settings of the San Andreas fault along these candidate segments, located in the Mojave Desert, Carrizo Plain, San Francisco Peninsula, and Northern Gabilan Range. These studies are being conducted by individual investigators, each of whom will contribute their results to a common data base, and will provide information necessary both to select the best site for the deep hole and to extend results from this hole to other segments of the San Andreas fault and to faults in other tectonic environments.

#### *6. USGS Red-Book Conference on the Mechanical Involvement of Fluids in Faulting*

With Rick Sibson (University of Otago, New Zealand) and Ron Bruhn (University of Utah) we convened a NEHRP-sponsored "Red-Book" conference on the Mechanical Involvement of

Fluids in Faulting at Fish Camp, California, from June 6-10, 1993 (see Hickman et al., 1994a). This conference drew together a diverse group of 45 scientists, whose expertise included electrical and magnetic methods, geochemistry, hydrology, ore deposits, rock mechanics, seismology, and structural geology. Some of the topics addressed included the pressures, compositions, and origins of fluids at different depths within active fault zones; the physical involvement of crustal fluids in the overall process of stress accumulation, release, and transfer during the earthquake cycle; and the roles of faults in distributing fluids in the crust and in altering fluid pressure domains. Also discussed were the chemical roles of fluids in facilitating fault creep; the chemical effects of aqueous fluids on constitutive response, frictional stability, and long-term fault strength; and the processes by which porosity and permeability are either created or destroyed in the mid to lower crust.

## RESULTS

### *1. Laboratory Studies of Solution-Transport Deformation*

In FY 1993, we performed an initial series of experiments using a convex quartz lens and a flat quartz lens pressed together under a load of 5.2 Newtons in distilled water at 150 MPa fluid pressure and a temperature of 520°C. In-situ monitoring of contact geometry and interference fringes showed no discernible convergence (pressure solution) but did show the development of a contact spot, or neck, between the two lenses. Interestingly, however, the rate at which the neck grew with time in our experiments was about 10-20 times slower than expected based upon simple extrapolations of intragranular crack healing rates for quartz determined by Brantley et al. (1990). We believe that the slow neck growth rates we observed are due either to: 1) a systematic overestimation of crack apertures used in the Brantley et al. reconnaissance study, or 2) the retarding effects of grain boundary energy on neck-growth rates. The latter effect has been theoretically predicted as a consequence of the balance of interfacial tensions at the intersection between a grain boundary and two solid-liquid interfaces and has been experimentally confirmed in the halite/brine system (Hickman and Evans, 1992).

To systematically examine this effect, in FY 1994 we initiated a series of crack healing experiments in quartz single crystals at  $T = 400\text{--}600^\circ\text{C}$  and  $P_{\text{H}_2\text{O}} = 100\text{--}200\text{ MPa}$ . These experiments will provide data on the rate of crack healing as a function of crack aperture, temperature, and fluid pressure in the absence of any retarding effects due to grain boundary energy. In spite of USGS hiring restrictions which prevented us from hiring a new laboratory technician, we have been able to make some progress on these experiments during FY 1994. We moved into a new laboratory; installed a vibration isolation system; established procedures for preparing oriented cracks in quartz single crystals; and modified the seals on the fluid input to the hydrothermal vessel to improve high-temperature creep resistance and prevent leaks (a recurring problem, now solved). We have just finished construction of a gold liner to be used inside the pressure vessel and are beginning our first crack healing experiments. We also submitted a journal article on pressure solution experiments conducted earlier using halite single crystals (Hickman and Evans, 1994).

### *2. In-situ Study of Physical Mechanisms for Permeability Changes Associated with the 1989 Loma Prieta Earthquake*

Our borehole televiewer and television logging in the Ben Lomond well has revealed numerous fractures and faults with thicknesses of up to several cm. The great majority of these fractures and faults strike N-NW and dip 40-70° to the east. We conducted four hydraulic fracturing stress measurements in this well at depths of 30-100 m using our new wireline packer system. Packer tests at greater depths were not possible because of a blockage in the hole associated with a pronounced fault zone at 103 m depth. Analysis of these data show that the magnitude of the least horizontal principal stress ( $S_{\text{Hmin}}$ ) is equal to or slightly less than the calculated vertical stress ( $S_{\text{V}}$ ) and that the direction of the maximum horizontal principal stress ( $S_{\text{Hmax}}$ ) is  $\text{N}10^\circ\text{W} \pm 20^\circ$ . This  $S_{\text{Hmax}}$  direction is parallel to the ridge axis (suggesting topographic control of the stress field) and

the strike of most of the natural fractures and faults in this well. Thus, these fractures/faults are favorably oriented for normal faulting. Analysis of the potential for frictional failure on these planes using simple frictional faulting theory indicates that normal faulting could be induced at this site by a reduction in  $S_{H\min}$  of about 0.5-1.0 MPa. Calculations of the magnitude and approximate orientations of dynamic (i.e. strong-ground-motion induced) stress perturbations expected during the 1989 Loma Prieta earthquake indicate that cyclic reductions in  $S_{H\min}$  of this order are indeed possible at this location. In contrast, calculations by Robert Simpson (USGS, Menlo Park) of the static (i.e., long-term) stress perturbations expected at this site from the 1989 Loma Prieta earthquake indicate that static stress changes would have little effect on the propensity for frictional failure on the faults/fractures observed. Thus, we propose that these features are shallow normal faults reactivated by earthquake-induced dynamic stress perturbations and that these faults, in turn, are responsible for the permeability enhancement associated with the Loma Prieta earthquake.

To further test this hypothesis, we are currently measuring the permeabilities of individual fractures and fault zones in the Ben Lomond well and conducting detailed resistivity, full-waveform sonic, and temperature logging to determine the extent of permeability anisotropy and the manner in which this anisotropy, if it exists, is aligned with the in-situ stresses. Since modifying our wireline packer system (see above) we have made 12 permeability measurements on faults intersected by this well at depths above 103 m. Preliminary analysis of these data – when compared to similar measurements conducted over intact (i.e., unfractured) intervals of the Ben Lomond well – indicate that the permeability of these shallow faults is probably not high enough to explain the 10-fold increase in *average* permeability inferred to have occurred in the shallow bedrock of the Santa Cruz Mountains during the Loma Prieta earthquake. To see if more permeable faults exist at depth, we are currently conducting a suite of cased-hole geophysical logs across and below the fault zone at 103 m and will be drilling and testing an approximately 350-m-deep well at a nearby location in the Santa Cruz Mountains next year.

### 3. Coupled Tectonic and Hydrologic Processes in Fractured Rock, Yosemite National Park

In FY 1994 we completed analysis of the hydraulic fracturing data obtained earlier using our wireline packer system in two 300-m-deep wells drilled near Wawona, California. In both wells the relative magnitudes of the principal stresses indicate a reverse-faulting stress regime at depths less than about 200 m that is transitional to a strike-slip faulting at greater depths. The magnitudes of the horizontal principal stresses in the upper 100 m of these wells are extremely high, with  $S_{H\max}$  attaining a maximum magnitude of about 13 MPa at a depth of 50 m. The corresponding differential stresses ( $S_{H\max} - S_v$ ) are roughly twice as great as predicted using laboratory coefficients of friction of 0.6 to 1.0 and simple frictional faulting theory (i.e. Byerlee's law). Based on borehole televiewer logs conducted in these wells, we hypothesize that these high differential stresses can be maintained because of the paucity of natural fractures or faults that are favorably oriented for reverse faulting. Orientations of the hydraulic fractures created during our tests indicate that  $S_{H\max}$  at Wawona is directed  $N55^\circ W \pm 10^\circ$ . This orientation departs significantly from the roughly north-south to northeast  $S_{H\max}$  directions observed on either side of the Sierra Nevada (Zoback and Zoback, 1989), but is subparallel to the overall trend of the valley of the South Fork Merced River at Wawona.

In FY 1994 we used the three-dimensional topographic stress model of Liu and Zoback (1992) to see if the gravitational loading by the Sierran Nevada Mountains might explain both the anomalous stress orientations seen at Wawona and the extremely high near-surface stress magnitudes. This model was applied to a 21 x 21 km square digital topographic grid centered on the town of Wawona, with a 100 m grid spacing. A variety of stress boundary conditions were assumed in this modeling, making geologically reasonable assumptions about the orientations and relative magnitudes of the far-field (i.e., tectonic) stresses acting on the Sierra Nevada. Although several of these models were able to fit our measured stress *orientations* very closely, none of them were able to reproduce the high near-surface horizontal stress *magnitudes* observed in these wells. Near-surface residual or thermal stresses due to the extremely rapid erosion of the Merced River

valley might thus be responsible, at least in part, for the high horizontal stress magnitudes observed (see McGarr, 1988).

Analysis of pumping tests conducted in these wells by Morin and Borchers (1993) indicates that the most permeable fractures are roughly perpendicular to the least principal stress, suggesting that the permeability tensor is controlled by the present-day in-situ stress field. Our hydraulic fracturing tests in the deepest of these two wells were conducted while borehole seismometer and tiltmeter arrays were deployed in nearby shallow boreholes by House and Phillips (1993) and Snaman et al. (1993). The microseismic event locations and shallow tilts determined from these arrays agreed with our interpretation of the orientations and relative magnitudes of the in-situ stresses in this area. These and other results of the Wawona experiment were presented at the 1993 Fall AGU meeting as part of the special session on *Coupled Hydrologic and Tectonic Processes in Fractured Rock* co-convened by Jim Borchers (USGS Water Resources Division, Sacramento) and Stephen Hickman.

#### 4. Planning and Coordination of San Andreas Fault Zone Drilling Project

Over the past year it has become clear that the current level of site characterization activity will be inadequate to characterize all four segments of the San Andreas fault in sufficient detail to make an intelligent selection of the deep drilling site before 1997, as originally proposed. Moreover, we feel that an accelerated site characterization program does not provide us with the kind of detailed, three-dimensional information needed to extend the information gained in the deep hole into the adjacent crust. Thus, we are now operating under a new strategy and time table that divides site characterization into two successive stages. The first stage, currently being funded by existing programs within the USGS, National Science Foundation (NSF), and Department of Energy (DOE), consists of reconnaissance-scale geophysical and geological studies along the four segments. The second stage of site characterization, which would be funded using new money raised in support of the FZDP, would consist of much more detailed studies of the crust and upper mantle along two of these segments. These investigations will incorporate seismology, geophysical imaging, geodesy, geologic mapping, hydrology, geochemistry, shallow drilling, geodynamic modeling, and other disciplines. The subsequent deep drilling phase of the project would make it possible to conduct the in-situ investigations that are crucial to the success of this project and, when integrated with site characterization studies, would provide three-dimensional information on the fault zone and the surrounding lithosphere on an unparalleled scale.

From March 28-30, 1994, we held a workshop at the Marconi Conference Center in northern California to discuss site characterization activities associated with the FZDP. The primary purposes of this workshop were to: (1) discuss the present state of knowledge regarding the structure, behavior, and physical properties of the San Andreas fault zone along the four segments being considered for the 10-km hole; (2) present preliminary results and research plans from the first round of site characterization studies currently funded by the USGS, NSF, and DOE; (3) identify and discuss gaps in the current site characterization effort to help in preparation of new proposals; and (4) begin preparation of a science plan for detailed site characterization studies in the two finalist segments. The workshop was attended by 68 people and was quite successful in illustrating the diversity and quality of work going on along the four segments of the San Andreas and in stimulating discussions which led to the evolution of the revised long-term plan mentioned above. Moreover, it provided extremely useful overviews of outstanding scientific questions about each area's suitability for deep drilling and the variety of techniques that could be used to answer these questions.

During this past year, the NSF Continental Dynamics Panel strongly suggested that we consider drilling a 3 km borehole into the fault zone as soon as possible. In part, their logic was that we should do this to avoid appreciable expenditures for site selection studies if deep drilling into the fault zone proves to be impractical. Although a 3 km hole is not deep enough to address many of the key scientific questions about the physics of faulting that are driving this project, we have decided to follow the Panel's recommendation for several reasons. First, it enables us to obtain direct information on the structure, physical properties, and mechanical behavior of the fault

at intermediate depth. This information will improve current knowledge tremendously and help with all aspects of further planning. Second, it enables us to identify and begin dealing with the technical problems of drilling, coring, casing, downhole measurements, and long-term monitoring in and near the active fault zone. The drilling, sampling, and down-hole measurements programs we are proposing for the 3-km experiment (see Hickman et al., 1994f) are similar to those for the 10-km hole, with the exception that the fault will be crossed at a depth of only 3 km. As with the 10-km hole, an important aspect of the 3-km experiment is instrumentation of the borehole for long-term monitoring of seismicity, deformation, fluid pressure, and temperature directly within and adjacent to the fault zone.

We convened a workshop on the scientific goals, experimental design, and site selection for the 3-km borehole from July 11-12, 1994, at the USGS in Menlo Park. At this workshop about 45 people discussed the current state of knowledge on the subsurface geology and geophysics at several candidate segments. As there are strong arguments in favor of siting the 10-km-deep hole along a section of the San Andreas that is "locked" and likely to produce great earthquakes, we propose drilling the shallow hole where the fault is currently slipping through a combination of small-to-moderate sized earthquakes and fault creep. A key consideration in selecting the site for the 3-km hole is our ability to accurately target a seismically active patch of the fault at 3 km depth. By choosing an "active" segment of the fault for the 3-km hole we will also be able to broaden the overall scope of the FZDP by eventually comparing conditions in and around the fault zone in two areas where fault behavior is markedly different. As a result of the July workshop, the primary localities being considered for the 3-km hole are the Parkfield and Northern Gabilans segments of the San Andreas fault. The selection of the final site for the 3 km hole will be based on information – including limited new geological, seismological, and potential-field data – that we as a group are able to gather over the next six months to fill the gaps identified during this workshop.

### 5. USGS Red Book Conference on the Mechanical Involvement of Fluids in Faulting

During FY 1994, we co-edited the proceedings volume from this conference (Hickman et al., 1994c). The 43 contributors to this "Red Book" included researchers on electrical and magnetic methods, geochemistry, hydrology, ore deposits, rock mechanics, seismology, and structural geology. The Red Book is divided into four chapters: 1) Evidence for Fluid Involvement in Faulting and Deep Crustal Fluid Reservoirs, 2) Fault-Zone Transport Properties and Composition of Fault-Zone Fluids, 3) Coupled Mechanical and Hydrological Processes in Faulting and 4) Chemical Effects of Fluids on Fault-Zone Rheology. We are also co-editing a *J. Geophys. Res.* special issue on this same topic, to appear early in 1995.

### REFERENCES CITED (see also FY 1994 Publications)

- Brantley, S. L., B. Evans, S. H. Hickman, and D. A. Crerar, 1990, Healing of microcracks in quartz: Implication for fluid flow. *Geology* 18, 136-139.
- Hickman, S. and B. Evans, 1992, Growth of grain contacts in halite by solution-transfer: Implications for diagenesis, lithification, and strength recovery, in *Fault Mechanics and Transport Properties of Rocks*, B. Evans and T-f. Wong (eds.), Academic Press, London, 253-280.
- House, L., and W.S. Phillips, 1993, Earthquakes induced by hydraulic injections at Yosemite National Park, *EOS, Trans. AGU*, 74, No. 43, 582.
- Liu, L., and M. D. Zoback, 1992, The effect of topography on the state of stress in the crust: Application to the site of the Cajon Pass scientific drilling project, *J. Geophys. Res.*, 97, 5095-5108.
- McGarr, A., 1988, On the state of lithospheric stress in the absence of applied tectonic forces, *J. Geophys. Res.*, 93, 13609-13617.
- Morin, R., and J. Borchers, 1993, Hydrologic characterization of fractures in granitic bedrock from analysis of geophysical well logs, Yosemite National Park, Wawona, California, *EOS, Trans. AGU*, 74, No. 43, 582.

- Rojstaczer, S., and Wolf, S., 1992, Permeability changes associated with large earthquakes: An example from Loma Prieta, California, *Geology*, 20, 211-214.
- Snaman, D.K., R.J. Hunter, and M.D. Wood, 1993, Tiltmeter mapping of fractures in granitic rock at Wawona, Yosemite National Park, California, *EOS, Trans. AGU*, 74, No. 43, 582.
- Zoback, M.D., and R. Emmermann, 1994, Toward establishing an International Continental Scientific Drilling Program, *Eos, Trans. AGU*, 75, p. 461.
- Zoback, M. L., and M. D. Zoback, 1989, Tectonic stress field of the continental United States, *Geol. Soc. Am. Mem.*, 172, 523-539.

## FY 1994 PUBLICATIONS

- Borchers, J., S. Hickman, and G. Nimz, G., 1993, In-situ stress and ground-water flow in fractured granite at Wawona, Yosemite National Park, California: A model for the west-central Sierra Nevada, *Eos, Trans. AGU*, 74, 581.
- Borchers, J., R. Morin, and S. Hickman, 1993, Characterization of fractures in granitic rocks at Wawona, Yosemite National Park, California: A comparison of borehole geophysical and downhole visualization tools, *Eos, Trans. AGU*, 74, 567.
- Hickman, S., and B. Evans, 1994, The kinetics of pressure solution at halite-silica interfaces and intergranular clay films, in *Proceedings USGS Red Book Conference on the Mechanical Involvement of Fluids in Faulting*, S. Hickman, R. Sibson, and R. Bruhn (eds), USGS Open-File Report 94-228, pp. 540-575 (also in press for *J. Geophys. Res.*).
- Hickman, S., and S. Rojstaczer, 1994, In-situ study of physical mechanisms for permeability changes associated with the 1989 Loma Prieta earthquake, *Proceedings VIIth International Symposium on Observation of the Continental Crust Through Drilling*, Santa Fe, NM, April 24-29 (abstract).
- Hickman, S., J. Svitek, J. Borchers, and E. Scholz, 1993, In-situ stress measurements at Wawona, Yosemite National Park, California, *Eos, Trans. AGU*, 74, 581.
- Hickman, S., R. Sibson, and R. Bruhn, 1994a, Conference explores mechanical involvement of fluids in faulting, *Eos, Trans. AGU*, 75, pp. 426 and 428 (meeting report).
- Hickman, S., R. Sibson, and R. Bruhn, 1994b, Introduction: USGS Red Book Conference on the Mechanical Involvement of Fluids in Faulting in *Proceedings USGS Red Book Conference on the Mechanical Involvement of Fluids in Faulting*, S. Hickman, R. Sibson, and R. Bruhn (eds), USGS Open-File Report 94-228, pp. 1-3.
- Hickman, S., R. Sibson, and R. Bruhn (eds), 1994c, *Proceedings USGS Red Book Conference on the Mechanical Involvement of Fluids in Faulting*, USGS Open-File Report 94-228, 615 pp. (similar volume in review as special issue of *J. Geophys. Res.*).
- Hickman, S., L. Younker, M. D. Zoback, and G. Cooper, 1994d, The San Andreas fault zone drilling project: Scientific objectives and technological challenges, in *Drilling Technology—1994*, J. P. Vozniak (ed.), Am. Soc. Mech. Eng. PD Vol. 56, pp. 263-271.
- Hickman, S., M. D. Zoback, L. Younker, and W. Ellsworth, 1994e, Deep scientific drilling in the San Andreas fault zone, *Eos, Trans. AGU*, 75; pp. 137, 140 and 142 (similar article appeared in *The IRIS Newsletter*, v. XII, No. 3, pp. 9-11, 1993).
- Hickman, S., M. D. Zoback, W. Ellsworth, and L. Younker, 1994f, Update on the San Andreas Fault Zone Drilling Project, *Physical Properties of Earth Materials Newsletter*, October 1994, pp. 7-10.
- Rojstaczer, S., S. Hickman, and J. Svitek, 1993, Permeability changes associated with the 1989 Loma Prieta Earthquake, San Lorenzo River basin, California, *Eos, Trans. AGU*, 74, 565.
- Rojstaczer, S., and S. Hickman, 1994, In-situ study of physical mechanisms for permeability changes associated with the 1989 Loma Prieta earthquake, *Eos, Trans. AGU*, 75, 147.
- Zoback, M. D., S. Hickman, and L. Younker, 1994, Scientific drilling into the San Andreas fault zone, *Proceedings VIIth International Symposium on the Observation of the Continental Crust Through Drilling*, Santa Fe, NM, April 24-29 (abstract).

# **Cascadia Megathrust Earthquake Potential: Constraints from Current Deformation and the Thermal Regime**

**USGS NHERP Project No. 1434-94-G-PN4054**

**R.D. Hyndman, K. Wang and H. Dragert**

**Pacific Geoscience Centre  
P.O. Box 6000, Sidney B.C. V8L 4B2, Canada**

Tel. (604) 363-6428; Fax. (604) 363-6565; email [hyndman@pgc.emr.ca](mailto:hyndman@pgc.emr.ca)

External Investigators, National Earthquake Hazard Reduction Program (NHERP)

**USGSREPT**  
This version November 24, 1994

# Cascadia Megathrust Earthquake Potential: Constraints from Current Deformation and the Thermal Regime

USGS NHERP Project No. 1434-94-G-PN4054

R.D. Hyndman, K Wang and H. Dragert

## Abstract

An important but poorly known part of the earthquake hazard at near-coastal cities of western North America from northern California to southern British Columbia is from great thrust earthquakes on the Cascadia subduction zone. Although there have been no historical such events, there is good evidence that they have occurred in the past. In this NHERP supported study, we have, (1) analyzed the evidence that along the whole Cascadia margin the subduction thrust fault is locked at present and accumulating elastic strain toward future great earthquakes, (2) estimated the downdip landward limit of the seismic source zone on the subduction thrust fault through modelling of the pattern of current deformation from repeated geodetic surveys, and from the thermal regime, taking the down-dip limit of seismic behaviour on the fault to be controlled by temperature. An important hazard factor is the down-dip landward limit of the seismogenic zone. (3) confirmed the validity of our analysis methods by a study of the SW Japan Nankai subduction zone, wherein we have compared the present downdip locked zone estimated from interseismic geodetic data and thermal models, with the actual rupture zone in the 1944 and 1946 ( $M=8.2$ ) great subduction earthquakes. We have also made an initial comparison of the predicted Cascadia great earthquake coseismic vertical motion from our elastic deformation models with that estimated from coastal marsh subsidence, and we are developing viscoelastic models in an attempt to describe the earthquake deformation cycle more accurately than with simple elastic models.

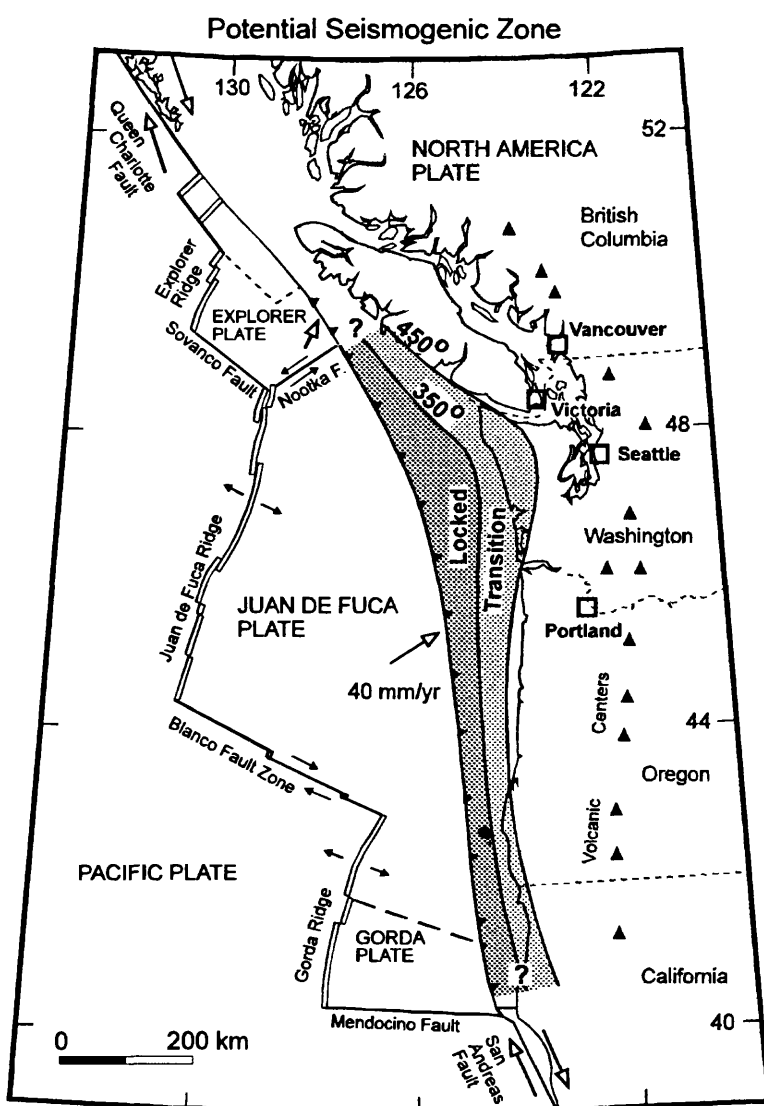


**Figure 1** Estimated width of the seismogenic zone along the Cascadia subduction zone as determined from current deformation and from thermal constraints. The model great earthquake rupture decreases across the transition zone.

The first phase of our study was a detailed analysis of geodetic data and deformation and thermal modelling of the northern Cascadia region of S. British Columbia and N. Washington. We have now extended the analysis to the whole Cascadia margin from southern British Columbia to northern California. The geodetic data include long term tide gauges at 6 locations, 10 repeated levelling lines, 7 horizontal strain arrays and several continuously recording GPS stations. For most of the coast there is present uplift at a rate of a few mm/a, decreasing inland, and shortening across the coastal region at about  $0.1 \mu\text{strain/a}$  (mm/a per km). The present interseismic uplift is consistent with the abrupt subsidence at the time of great earthquakes inferred from buried coastal salt marshes. The modeled width of the locked zone that is accumulating elastic strain averages 60 km fully locked plus 60 km transition; it is wider, about 90 + 90 km off the Olympic Peninsula of northern Washington where a bend in the coastline causes the plate dip to be anomalously shallow; it is narrower, about 35 + 35 km, off central Oregon. The unusually narrow downdip extent for the Cascadia margin is a consequence of high temperatures associated with the young oceanic plate and thick blanket of insulating sediments on the incoming crust. The variations in the modelled locked zone width in general correspond to variations along the margin of downdip temperatures on the fault as estimated from numerical thermal models. The landward limit to the seismogenic zone, extending little if at all beneath the coast, limits the ground motion from great subduction earthquakes at the major Cascadia cities of Vancouver, Seattle and Portland that lie 100-200 km inland. The narrow width also limits the maximum earthquake size somewhat (the actual maximum depends on the along-margin length) but events of well over magnitude 8 are expected. If the whole estimated seismogenic zone along the Cascadia margin breaks at once, empirical fault area versus magnitude relations give earthquakes as large as  $M_w=9$ .

## INTRODUCTION

The Cascadia subduction zone margin of western North America is unusual in having experienced no historical great thrust earthquakes. However, most comparable margins globally have had such very damaging events and extensive paleoseismicity data from sites along the coast from southern Vancouver Island to northern California indicate that they have occurred here at irregular intervals averaging about 600 years, the last 300 years ago (e.g., Atwater et al., 1995; Adams, 1990). Geodetic data has also shown that the coast region is shortening in the direction of plate convergence as expected for a locked subduction thrust fault (e.g., Savage et al., 1991). In this study we have analyzed the evidence that along the whole Cascadia margin the subduction thrust fault is locked at present

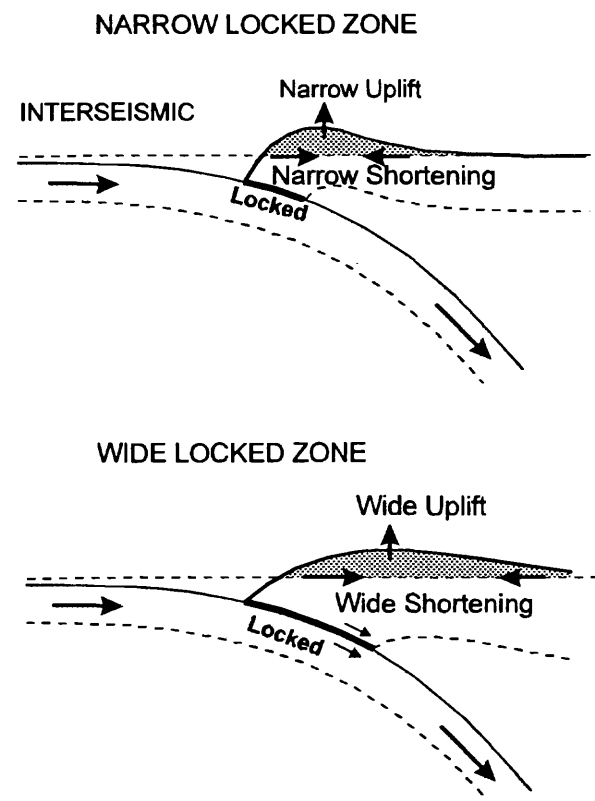


**Figure 2** Schematic diagram illustrating the interseismic deformation associated with a subduction thrust fault. The wider the locked seismogenic zone the wider the zone of interseismic uplift and of horizontal shortening.

and accumulating elastic strain toward future great earthquakes, and estimated the downdip landward limit of the seismic source zone on the subduction thrust fault (Figure 1). The width has been estimated from:

(1) the present locked zone determined through modelling of the pattern of current deformation from repeated levelling surveys, long term trends in tide gauge records, repeated precision gravity surveys and repeated positional surveys (e.g., Dragert et al., 1994).

(2) the thermal regime, taking the down-dip limit of seismic behaviour on the fault to be thermally controlled (e.g., Hyndman and Wang, 1993).

## "LOCKED ZONE" FROM CURRENT DEFORMATION

If a portion of the subduction thrust fault is locked, ongoing convergence results in the toe of the continent being dragged down and of flexural uplift further inland, along with elastic shortening in the direction of plate motion (Figure 2). The abrupt collapse of the flexural uplift (which is located near the coast for most of the Cascadia margin) at the time of great earthquakes gives the coastal subsidence inferred from buried coastal salt marshes and other paleoseismic data (e.g., Atwater et al., 1995 and references therein). The wider the locked zone, the further landward are the flexural uplift and the hinge line marking the transition between interseismic subsidence and uplift. Matching the spatial pattern of current deformation across the

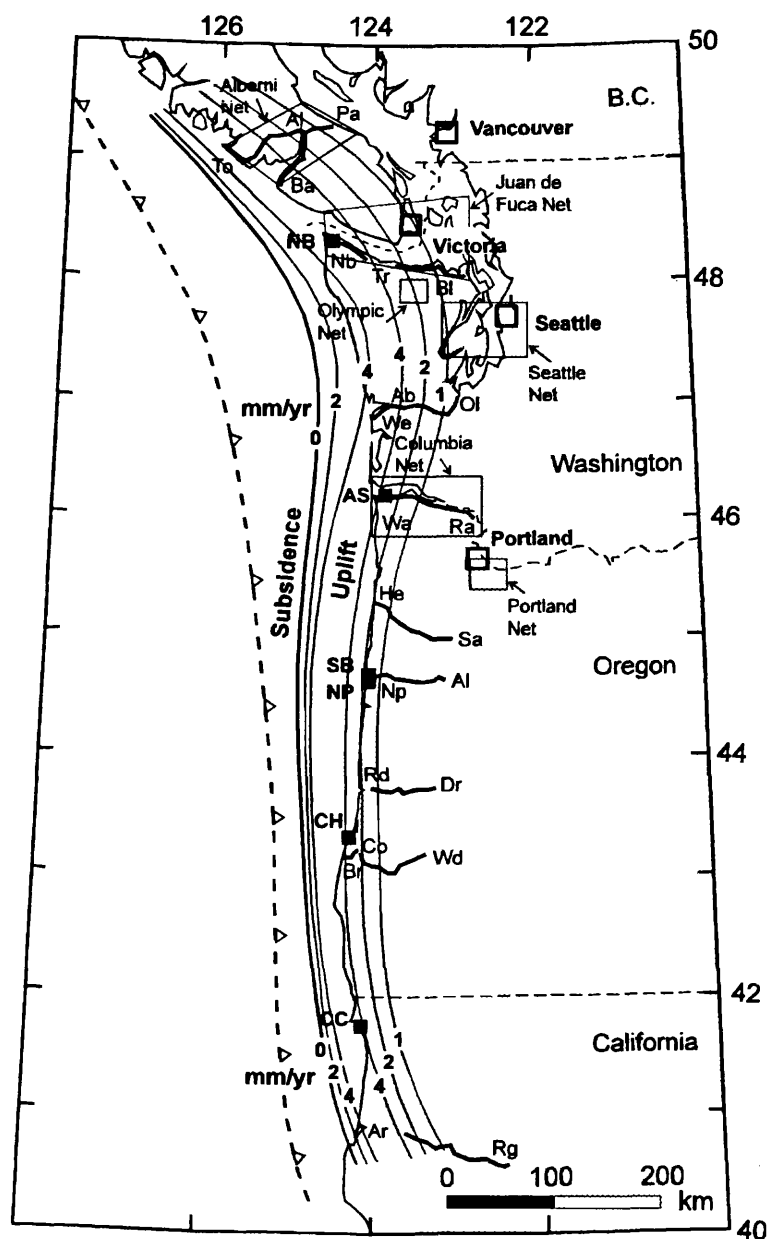


**Figure 3** Locations of Cascadia levelling lines (thick lines), tide gauges (square dots) and horizontal positioning networks (boxes). The contours of present uplift rate are based on the best fitting elastic dislocation models to the corrected data. The coseismic subsidence is approximately this rate times the interseismic period (~600 yrs).

margin with that from deformation models allows estimation of the width of the locked (and transition) and thus seismogenic zone. Great earthquakes may rupture all or some portion of the locked and transition zones. The geodetic data for vertical motion include tide gauges at 6 locations and 10 repeated levelling lines running inland from the coast (Figure 3). The horizontal shortening is constrained by repeated measurements of 7 horizontal strain arrays and continuous Global Positioning (GPS) monitoring of one coastal site (Dragert and Hyndman, 1994).

The repeated levelling and gravity data provide only relative levels and they have been referenced to the tide gauge data and to margin parallel levelling lines. The vertical data have also been corrected for postglacial rebound and the tide gauge data for global eustatic sealevel rise. The corrected data show present uplift for most of the coast at a rate of a few mm/yr decreasing inland (Figure 3), and shortening across the coastal region at about  $0.1 \mu\text{strain/yr}$  (mm/yr shortening per km perpendicular to the margin) (e.g., Savage et al., 1991; Dragert et al., 1994; Mitchell et al., 1994; Dragert and Hyndman, 1994). Through comparison with the predictions of elastic dislocation models, we find that the thrust is locked everywhere along the margin and that the width of the present locked zone that is accumulating elastic strain averages about 60 km fully locked plus a 60 km transition zone to completely free downdip (90 km fully locked with no transition gives similar deformation); it is wider, 90 + 90 km off the Olympic Peninsula of northern Washington and narrower, 35 + 35 km off central and southern Oregon (Figure 1). Examples of the repeat levelling and strain results are given in Figures 9 & 10 (Appendix Figures at the end) (also Figures 4 and 5). The landward motion of ALBH (Victoria) in the coastal zone with respect to DRAO (Penticton) on stable North America (in S. British Columbia just to the right off Figure 1) from Global Positioning (GPS) is shown in Figures 8 (Appendix Figures at the end) The GPS measured motion fits a model with a 80+80 km to 100+100 km locked plus transition zone.

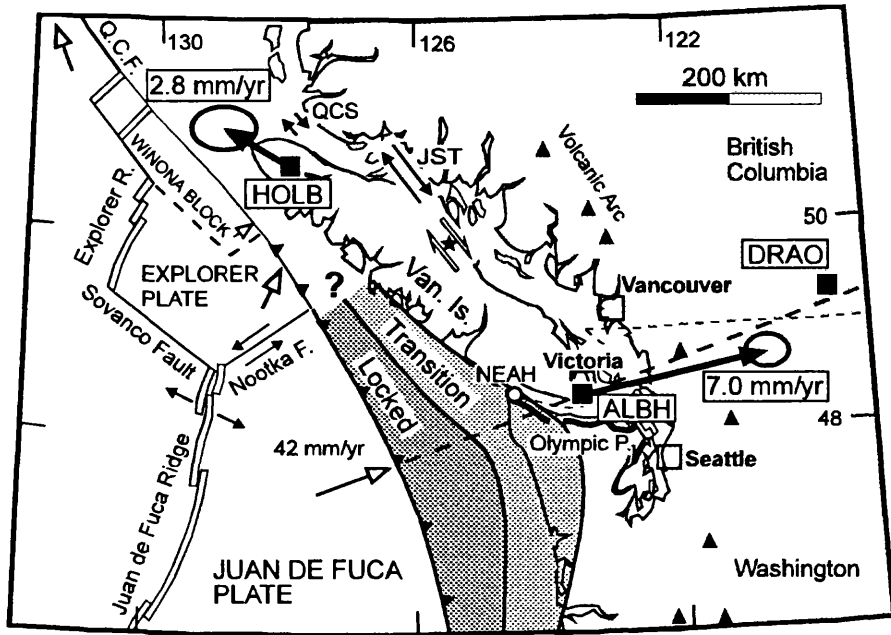


**Figure 4** Global Positioning System (GPS) data showing the landward motion of ALBH (Victoria) relative to DRAO (Penticton) at a rate in agreement with the model prediction for a 100 km locked and 100 km transition zone subduction thrust. The HOLB station at the north end of the subduction zone is moving parallel to the margin which indicates that there is not locked subduction in that area.

## THERMAL CONSTRAINTS TO SEISMOGENIC ZONE

Temperature appears to be the primary constraint on the downdip width of the locked seismogenic zone (e.g., Tichelaar and Ruff, 1991; Savage et al., 1991; Hyndman and Wang, 1993). Certainly at some depth a temperature is reached where rocks exhibit ductile or plastic behaviour and no earthquakes can occur. Both laboratory data for seismic (velocity weakening) behaviour in crustal rocks and the observed maximum depth for crustal earthquakes indicate that the critical temperature for earthquake initiation is about 350°C (see discussion by Hyndman and Wang, 1993). In our models we have included a transition zone between completely locked and completely free that extends to where the temperature reaches 450°C. Great earthquake rupture may extend with decreasing displacement downdip to where the latter temperature is reached. The seaward limit of the seismogenic zone may be controlled by temperature through the dehydration of stable-sliding clays in the fault zone that occurs at about 150°C. However, other factors such as sediment consolidation and pore pressure may be important.

We have generated finite element numerical thermal models for a series of profiles across the Cascadia margin constrained by heat flow and other thermal data. Both the model and the observed heat flow decrease landward because of the heat sink provided by the underthrusting oceanic lithosphere beneath the margin. The observed heat flow can be matched by the numerical models only if the frictional heating on the fault is very small. Hence the subduction thrust must be very weak as is also inferred from seismicity data (Wang et al., 1994).

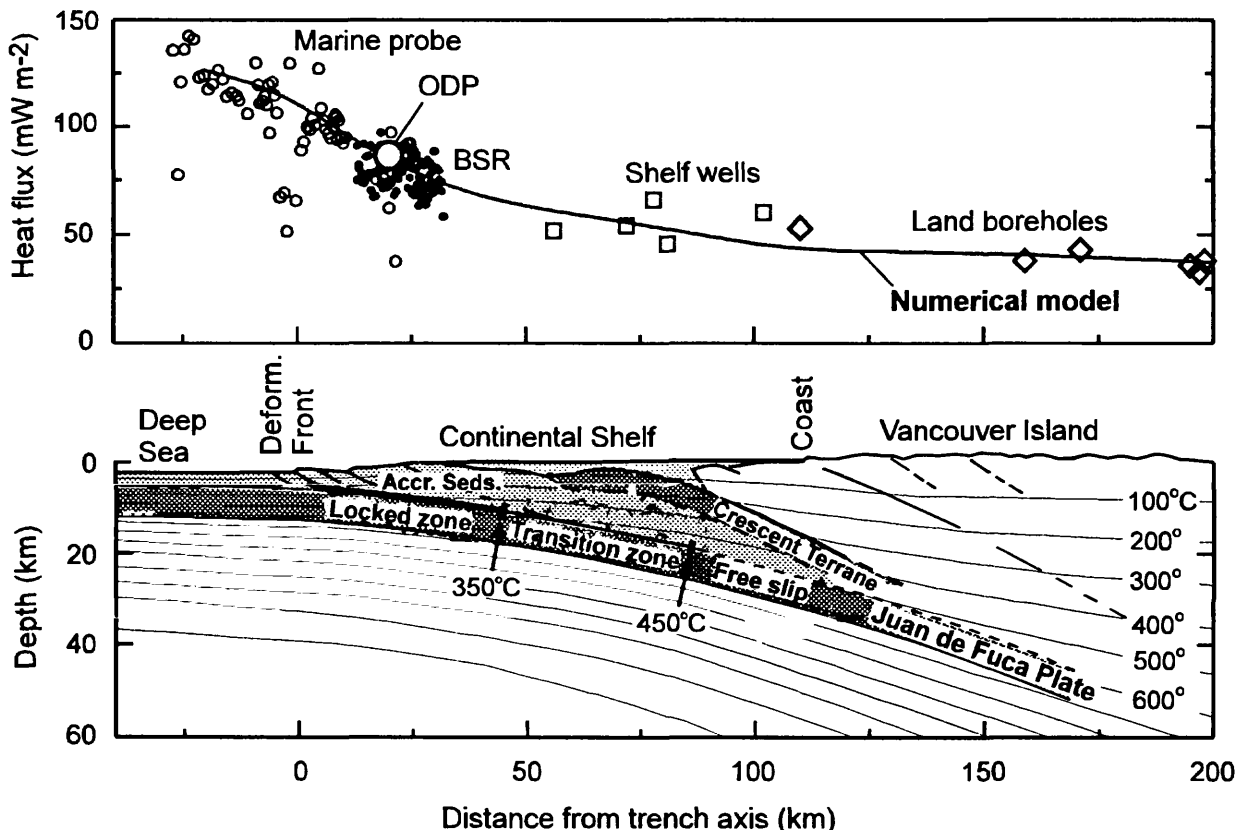


**Figure 5** Top: Heat flow data across the N. Cascadia margin at southern Vancouver Island and the best fitting thermal model heat flow. Bottom: Model temperatures on a seismic section across the N. Cascadia margin showing the positions on the subduction thrust fault of the 350 and 450°C downdip limits that define the locked and transition zones.

**Figure 5 (top)** shows the heat flow data compared to the model results for the southern Vancouver Island profile. The model temperatures are superimposed on the cross-section structure in **Figure 5 (bottom)**, illustrating the positions of the 350 and 450°C points on the subduction thrust fault. **Figure 6** shows the thermally predicted locked and transition zones compared to those from dislocation modelling of the current deformation data. The thermally predicted widths of the locked seismogenic zone average about 60 km with a 60 km transition zone (e.g., ). The thermally estimated widths have a lower resolution than those from the deformation data, about  $\pm 20$  km compared to  $\pm 10$  km. The thermally estimated widths agree in general with those from the current deformation data; the widest zones from the deformation data and also to the 350° and 450°C temperature limits are beneath the northern Washington margin where the bend in the coastline causes an upbowing of the underthrusting oceanic plate and shallowing of the thrust dip. The narrower locked and transition zones off central Oregon are a consequence of the steeper plate dip and the increase in temperature on the subduction thrust fault caused by the low thermal conductivity Siletz/Crescent basalts that extend across the continental shelf.

The unusually narrow downdip extent for the Cascadia margin is a consequence of high temperatures associated with the young oceanic plate and thick blanket of thermally insulating sediments on the incoming crust; the temperature at the top of the oceanic crust is greater than 200°C at the deformation front (trench axis). The high temperatures also mean that stable-sliding clays should not be present and the seismogenic zone may extend to the deformation front. The main parameters that control temperatures and thus the downdip extent of the locked seismogenic zone on the subduction thrust fault are: (1) the dip angle profile of the fault, (2) the age of the subducting plate, (3) the plate convergence rate and, (4) the thickness of sediments on the incoming crust.

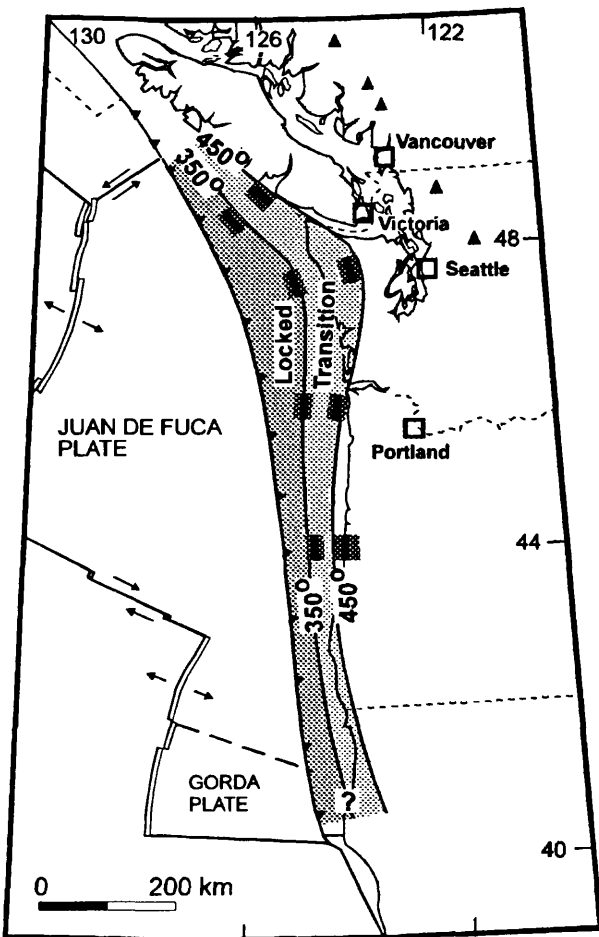


**Figure 6** The positions of the locked and transition zones defined by the 350 and 450°C limits from numerical thermal models on four sections, compared to the estimates from current deformation data.

## A COMPARISON WITH S.W. JAPAN

Since the Cascadia margin has had no historical great subduction earthquakes, the seismogenic zone must be estimated from present interseismic data. To provide a calibration of our procedure for estimating the Cascadia megathrust seismogenic zone, we have applied the same methods in a study of the Nankai margin of southwest Japan. The Nankai subduction zone has a history of great earthquakes to the 7th century, and has extensive geodetic and thermal data. At both margins young oceanic crust is being subducted at a rate of about 4 cm/yr and there is a thick blanket of insulating sediments on the incoming oceanic crust. The deformation and thermal analyses for the SW Japan margin give widths for the fully locked plus transition seismogenic zones that are in agreement, and both estimates agree well with the rupture area for two great earthquakes, Nankaido of 1946 and Tonankai of 1944 (Hyndman et al., 1995). This agreement gives support to the use of the locked (and transition) seismogenic zone from dislocation modelling of current deformation and thermal constraints to estimate the maximum rupture zone for future Cascadia great subduction thrust earthquakes. The seismogenic zone for the Nankai margin is about twice as wide as that for Cascadia as a consequence of the shallower plate dip, the slightly

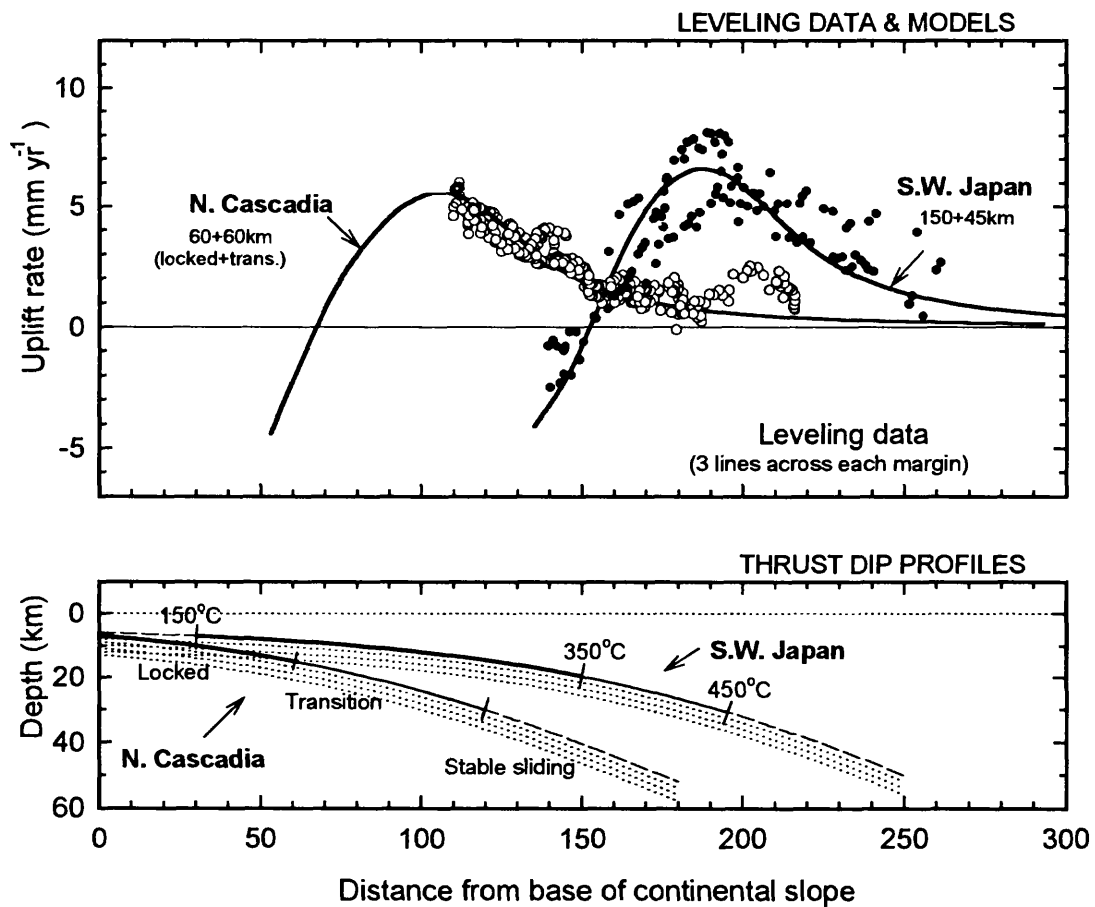


**Figure 7 Top:** The measured current vertical motion from levelling surveys across the margins of northern Cascadia and southwest Japan compared to the predictions for elastic dislocation models (60 km wide locked plus 60 km transition for Cascadia, 150 plus 45 km for SW Japan).

**Bottom:** The locked and transition zones that give the model vertical profiles above, shown on the dip profiles for the two subducting plates, and the estimated temperature limits.

older incoming crust, and the thinner layer of insulating sediments on the incoming crust. The difference in widths is seen clearly in both the thermal and deformation data (Figure 7).

## DISCUSSION

Modelling of geodetic data across the Cascadia margin has provided estimates of the locked and transition zones that range from 35 km + 35 km to 90 km + 90 km. The thermal constraints are in general agreement although the uncertainties are larger. Our analysis shows that each subduction zone must be modelled in detail to accurately estimate the width of the seismogenic zone from the thermal regime. However, thermal modelling allows the widths of the locked seismogenic zone to be estimated where there are no seismic or geodetic data. In general, margins with steep thrust dip, young subducting lithosphere, slow convergence, and thick insulating sediments on the incoming oceanic crust should have the narrowest locked seismogenic zones. The comparison with SW Japan provides support that these interseismic analyses do constrain the maximum downdip extent of the seismic rupture zone (Figure 7). The seaward limit to the Cascadia great earthquake rupture zone is poorly known but the high fault temperatures ( $>200^{\circ}\text{C}$  at the deformation front) may mean that stable sliding clays are not present and that the seismogenic zone extends to the deformation front (trench).

The landward limit to the Cascadia seismogenic zone, extending little if at all beneath the coast, limits the ground motion from great subduction earthquakes for the major Cascadia cities that lie 100-200 km inland. The narrow width also limits the maximum earthquake size (the actual maximum depends on the along-margin length) but events of well over magnitude 8 are expected. If the whole estimated seismogenic zone breaks at once, empirical fault area versus magnitude relations (e.g., Wyss, 1979) give earthquakes as large as  $M_w=9$ .

## REFERENCES CITED

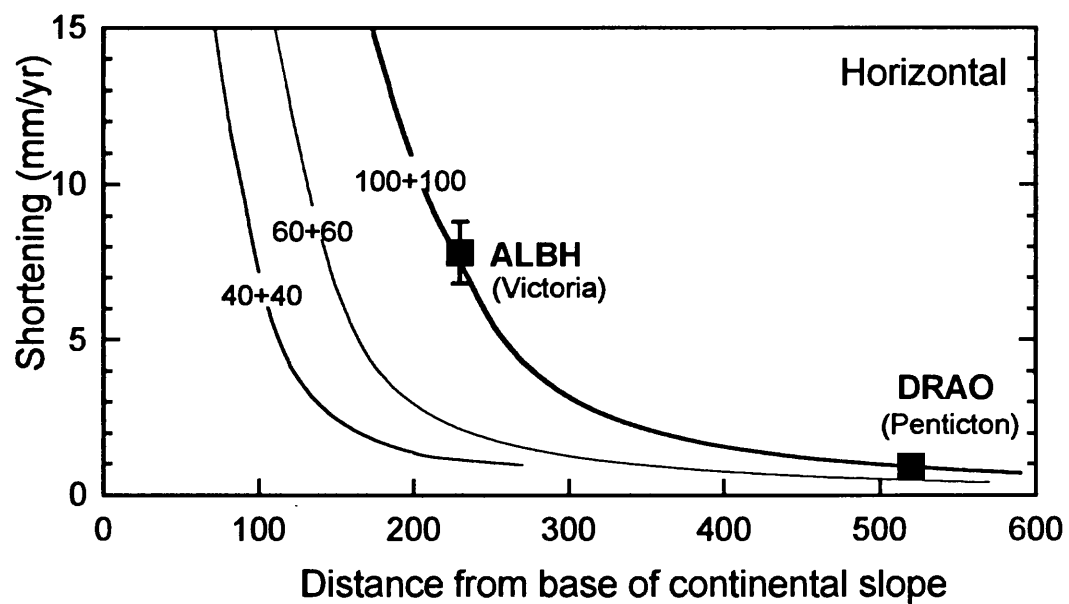
- Adams, J., Paleoseismicity of the Cascadia subduction zone: Evidence from turbidites off the Oregon-Washington margin, *Tectonics*, 9, 569-583, 1990.
- Atwater, B.F., et al., Consensus about past great earthquakes at the Cascadia subduction zone, *Earthquake Spectra*, in press, 1995.
- Dragert, H., R.D. Hyndman, G.C. Rogers, and K. Wang, Current deformation and the width of the seismogenic zone of the northern Cascadia subduction thrust, *J. Geophys. Res.*, 99, 653-668, 1994.
- Dragert, H., and R.D. Hyndman, Continuous GPS monitoring of strain in the northern Cascadia subduction zone, *Geophys. Res. Lett.*, submitted, 1994.
- Hyndman, R.D. and K. Wang, Thermal Constraints on the zone of major thrust earthquake failure: The Cascadia subduction zone, *J. Geophys. Res.*, 98, 2039-2060, 1993.
- Hyndman, R.D., K. Wang, and M. Yamano, Thermal constraints to the seismogenic portion of the southwestern Japan subduction thrust, *J. Geophys. Res.*, in press, 1995.
- Mitchell, C.E., P. Vincent, R.J. Weldon II, and M.A. Richards, Present-day vertical deformation of the Cascadia margin, Pacific Northwest, U.S.A., *J. Geophys. Res.*, 99, 12,257-12,277, 1994.
- Savage, J.C., M. Lisowski, and W.H. Prescott, Strain accumulation in western Washington, *J. Geophys. Res.*, 96, 14,493-14,507, 1991.
- Tichelaar, B.W., and L.J. Ruff, Depth of seismic coupling along subduction zones, *J. Geophys.*

Res., 98, 2017-2037, 1993.

Wang, K., T. Mulder, G.C. Rogers, and R.D. Hyndman, Case for very low coupling stress on the Cascadia subduction fault, *J. Geophys. Res.*, in press, 1994.

Wyss, M., Estimating maximum expectable magnitude of earthquakes from fault dimensions, *Geology*, 7, 336-340, 1979

## Appendix Figures



CASH&W

**Figure 8** Horizontal landward motion of the Victoria (ALBH) Global Positioning Station with respect to the inland Penticton (DRAO) station. The Penticton station is taken to be on stable North America. The data fit dislocation model locked and transition zones of width  $100 + 100$  km. The two GPS stations lie along a line through the Juan de Fuca strain network and the northern Washington levelling data which indicate similar widths.

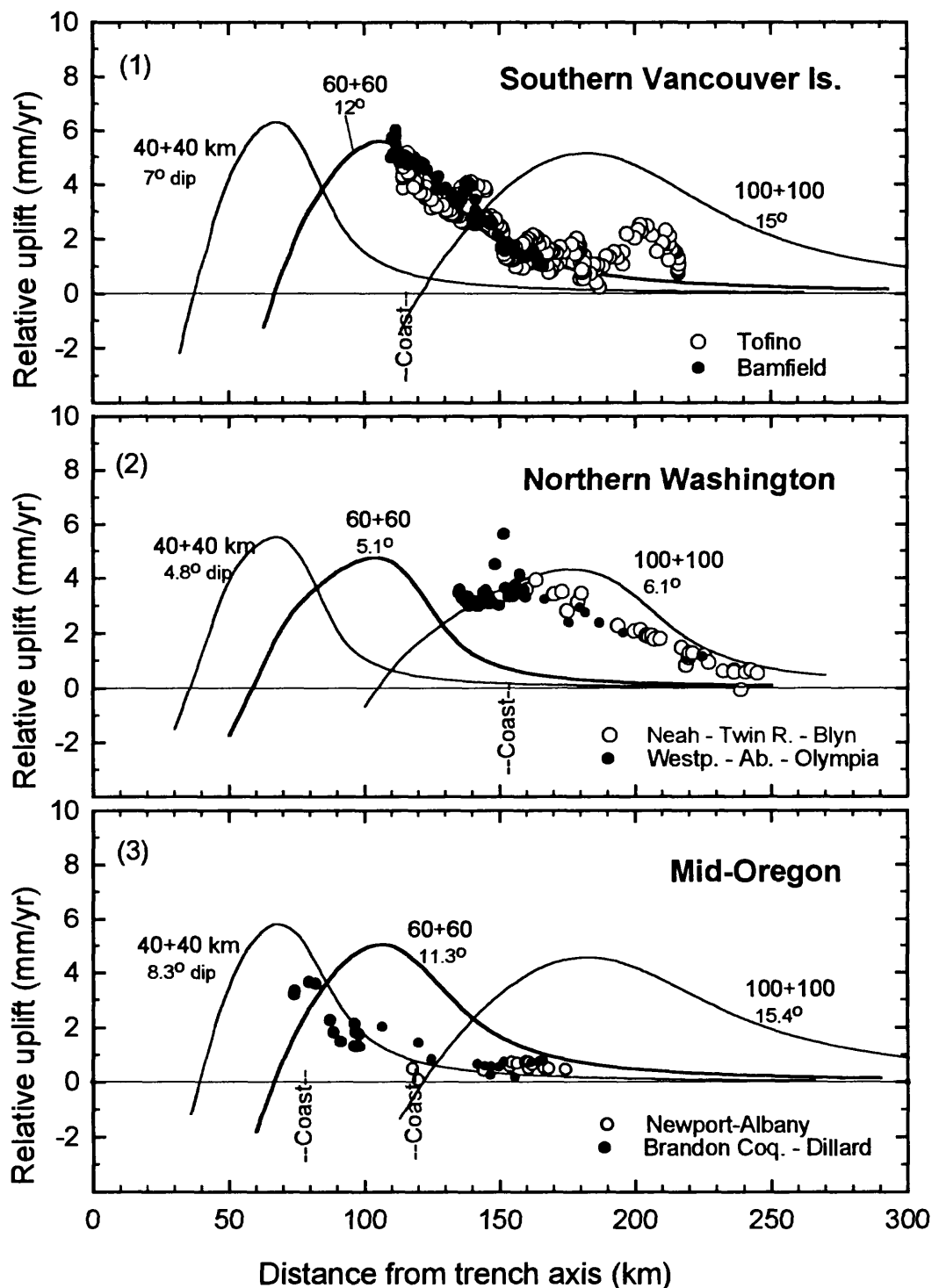


**Figure 9** Grouped levelling data across the Cascadia margin. Group 1 (top) compares the results of two repeat levelling lines across southern Vancouver Island to three dislocation model vertical motion profiles. The data best fit locked and transition zone of intermediate width, 60 + 60 km. Group 2 (middle) is for two lines across northern Washington (Olympic Peninsula); the best fit is for wide zones, a little narrower than 100 + 100 km. Group 3 (bottom) is for two lines across central Oregon; the best fit is for narrow zones, a little narrower than 40 + 40 km.

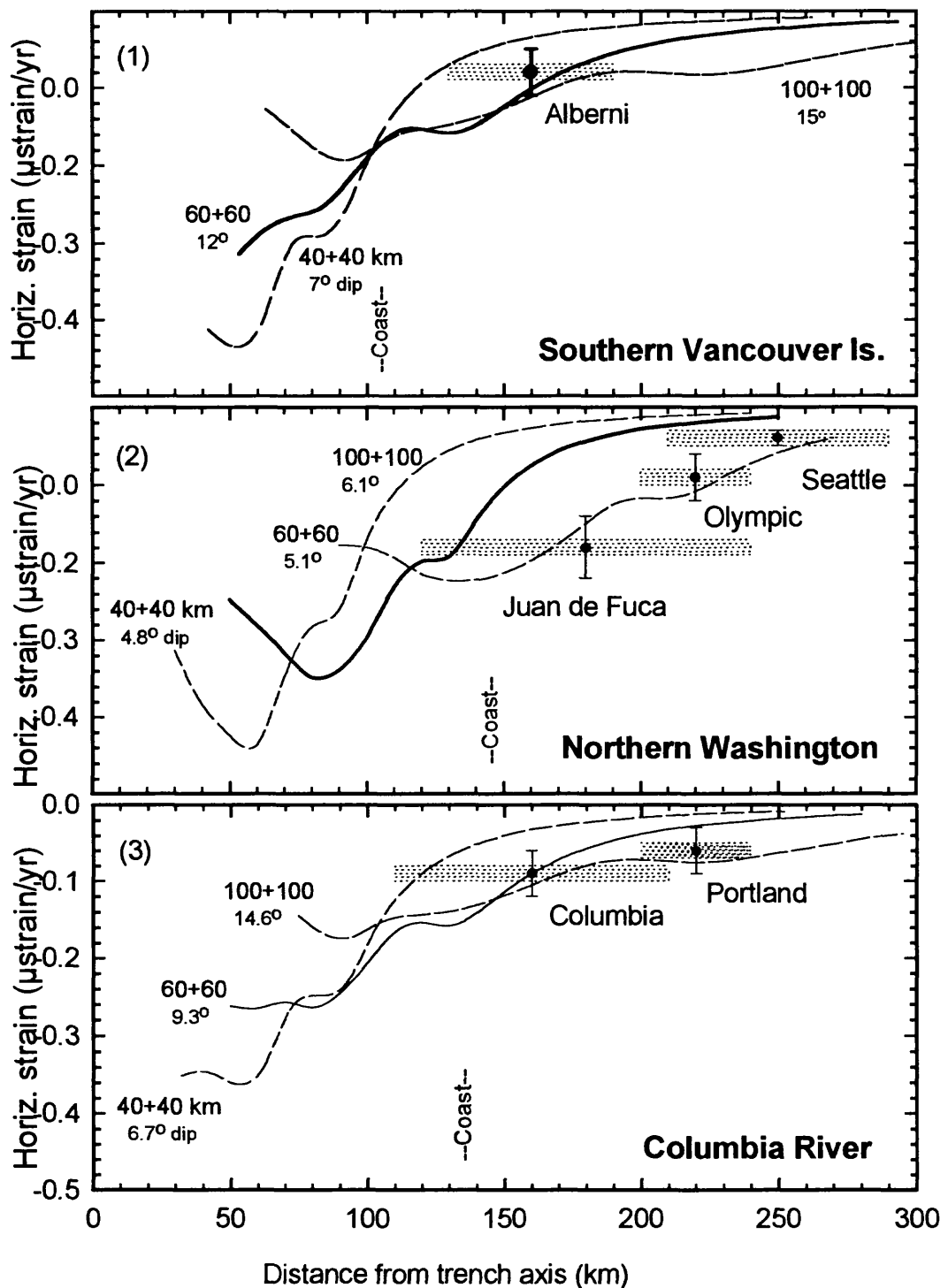


**Figure 10.** Horizontal strain network data across the Cascadia margin. Group 1 (top) compares the results of one network on southern Vancouver Island to three dislocation model horizontal strain profiles. The data fit locked and transition zones of width,  $60 + 60$  km or  $100 + 100$  km. Group 2 (middle) is for three networks on the northern Washington margin (Olympic Peninsula); the best fit is for wide zones, about  $100 + 100$  km. Group 3 (bottom) is for two networks on the northern Oregon (Columbia River) margin; the best fit is for narrow zones,  $40 + 40$  km or  $60 + 60$  km.

## Reports Published

### This project

- Dragert, H., Hyndman, R.D., G.C. Rogers, and K. Wang, Constraints on the seismogenic zone of the northern Cascadia subduction thrust from current deformation, *J. Geophys. Res.*, 99, 653-668, 1994.
- Dragert, H., and R.D. Hyndman, Continuous GPS monitoring of strain in the northern Cascadia subduction zone, *Geophys. Res. Lett.*, submitted, 1994.
- Dragert, H., M. Schmidt, and X. Chen, The use of continuous GPS tracking for deformation studies in southwestern British Columbia, *in* Proc. ION GPS-94, Salt Lake City, Utah, Sept. 20-23, 1994.
- Dragert, H., X. Chen, and J. Kouba, GPS monitoring of crustal strain in southwestern British Columbia with the Western Canada Deformation Array, *Geomatica*, submitted, 1994.
- Hyndman, R.D., and K. Wang, Thermal constraints on the zone of major thrust earthquake failure: the Cascadia subduction zone, *J. Geophys. Res.*, 98, 2039-2060, 1993.
- Hyndman, R.D., Widespread fluids in the lower crust: A source to crustal penetrating faults?, U.S. Geological Survey (Redbook Series), 178-189, 1994.
- Hyndman, R.D., and K. Wang, The rupture width of Cascadia subduction zone great earthquakes, U.S. Geological Survey, SUBCON Conference (Redbook Series), in press, 1994.
- Hyndman, R.D., K. Wang, and M. Yamano. Thermal constraints to the seismogenic portion of the southwestern Japan subduction thrust, *J. Geophys. Res.*, in press, 1994.
- Hyndman, R.D. and K. Wang, Current deformation and thermal constraints on the zone of potential great earthquakes on the Cascadia subduction thrust, *J. Geophys. Res.*, submitted, 1994.
- Wang, K., Coupling of tectonic loading and earthquake fault slips at subduction zones, *Pure Appl. Geophys.*, submitted, 1994..
- Wang, K., R. D. Hyndman, and M. Yamano, Thermal regime of the Southwest Japan subduction zone: effects of age history of the subducting plate, *Tectonophysics*, submitted, 1994.
- Wang, K. and G. C. Rogers, An explanation for the double seismic layers north of the Mendocino Triple Junction, *Geophys. Res. Lett.*, 21, 121-124, 1994.
- Wang, K., H. Dragert, and H.J. Melosh, Finite element study of strain and uplift across southern Vancouver Island, *Can. J. Earth. Sci.*, in press, 1994.
- Wang, K., T. Mulder, G.C. Rogers, and R.D. Hyndman, Case for very low coupling stress on the Cascadia subduction fault, *J. Geophys. Res.*, in press, 1994.

### Related work

- Davis, E. E., K. Becker, K. Wang, and B. Carson, Long-term observations of pressure and temperature in hole 892B, Cascadia accretionary prism, *ODP Proceedings, Scientific Results* Vol. 146, in press.
- Hyndman, R.D., K. Wang, T. Yuan, and G.D. Spence, Tectonic sediment thickening, fluid expulsion, and the thermal regime of subduction zone accretionary prisms: The Cascadia margin off Vancouver Island, *J. Geophys. Res.*, 98, 21,865-21,876, 1993.
- Hyndman, R.D., G.D. Spence, T. Yuan, and E.E. Davis, Regional geophysics an structural framework of the Vancouver Island margin accretionary prims, *in*, Proceedings of the Ocean

- Drilling Program, Initial Reports, 146, College Station, TX (Ocean Drilling Program), 399-419, 1994.
- Hyndman, R.D., A review of geoscience studies on the LITHOPROBE corridor across the Vancouver Island continental margin, *Can. J. Earth Sci.*, submitted, 1994.
- Hyndman, R.D., G.D. Spence, T. Yuan, and K. Wang, Seismic velocity and thermal measurements across the N. Cascadia accretionary sedimentary prism: tectonic consolidation and fluid expulsion, U.S. Geological Survey, SUBCON Conference (Redbook Series), in press, 1994.
- Hyndman, R.D., and T.S. Lewis, A review of the thermal regime along the southern Canadian Cordillera LITHOPROBE corridor, *Can. J. Earth Sci.*, submitted, 1994.
- Wang, K., Kinematic models of dewatering accretionary prisms, *J. Geophys. Res.* 99, 4429-4438, 1994.
- Wang, K., R.D. Hyndman, and E.E. Davis, Thermal effects of sediment thickening and fluid expulsion in accretionary prisms: Model and parameter analysis, *J. Geophys. Res.*, 9975-9984, 1993
- Yuan, T., G.D. Spence, and R.D. Hyndman, Seismic velocities and inferred porosities in the accretionary wedge sediments at the Cascadia margin, *J. Geophys. Res.*, 99, 4413-4427, 1994.

## Cenozoic tectonic and paleogeographic evolution, Puget Lowland seismic zone, Washington

Project 9450-50551

Samuel Y. Johnson  
U.S. Geological Survey  
MS 939, Box 25046, DFC  
Denver, CO 80225  
(303) 236-1545 - voice  
(303) 236-0459 - fax  
sjohnson@sedproc.cr.usgs.gov - E-mail

### NEHRP Element 1 Understanding the earthquake source

#### Investigations undertaken

This research addresses Element 1, Component 1.1, of the FY1994 NEHRP Prospectus. The regional focus task involves identification and characterization of active seismotectonic structures in the Seattle area. Research concentrates on reconstructing the Tertiary and Quaternary geologic history of the Puget Lowland seismic zone. This history is poorly understood because most important geologic features are either submerged in Puget Sound or are mantled by a thick cover of glacial deposits and vegetation. In particular, the histories and geometries of active and potentially active fault zones have not been adequately described. Integration and synthesis of data collected from petroleum industry seismic-reflection data, surface exposures, and boreholes provides the basis for a greatly improved understanding of these fault zones. This understanding contributes to reliable assessment of the local and regional earthquake hazards in the Puget Sound region. During FY 1994, research concentrated on examination of the Seattle fault, the southern Whidbey Island fault, and the western Rainier seismic zone (fig. 1).

#### Results

Seattle fault. A report on the origin and evolution of the Seattle fault and Seattle basin was published in *Geology* (see below). This report used petroleum-industry seismic reflection data to show that the Seattle basin is markedly asymmetric and consists of ~8-9 km of Eocene and younger deposits. The basin began as a discrete geologic element in the late Eocene (~40 Ma), the result of a reorganization in regional fault geometry and kinematics. In this reorganization, dextral offset on the Puget fault southeast of Seattle stepped eastward, and the Seattle fault began as a restraining transfer zone. North-vergent thrusting on the Seattle fault forced flexural subsidence in the Seattle basin to the north. Offset on the Seattle fault and subsidence of the Seattle basin have continued to the present. I have also been working with Tom Pratt and others (see abstracts below, manuscript in review) in formulating a model which interprets the Seattle fault as one component of a regional thrust system that underlies the Puget Lowland from the southern Whidbey Island fault on the north to at least the Black Hills on the south.

Southern Whidbey Island fault. Information from seismic reflection profiles, outcrops, boreholes, and potential field surveys has been used in an abstract (published) and manuscript (in review) to interpret the structure and history of the southern Whidbey Island fault in the Puget Lowland of western Washington. This northwest-trending fault comprises a broad (as wide as 6 to 7 km), steep northeast-dipping zone that includes splays interpreted as thrusts and backthrusts, and fault-propagation folds. Along-strike variations in structural style and geometry, positive flower structure, local unconformities, out-of-plane displacements, and juxtaposition of correlative sedimentary units with different

histories, indicate the southern Whidbey Island fault has a transpressional history with both strike-slip and thrust offset.

The southern Whidbey Island fault represents a segment of a boundary between two major crustal blocks. The Cascade block to the northeast is underlain by diverse assemblages of pre-Tertiary rock, and the Coast Range block to the southwest is underlain by lower Eocene marine basaltic rocks of the Crescent Formation. The fault originated as a dextral strike-slip fault along the eastern side of a continental-margin rift in which the basalt of the Crescent Formation was erupted. Eocene dextral offset resulted in juxtaposition of sedimentologically and petrologically disparate lower and middle Eocene sedimentary rocks. Bending of the fault and transpressional deformation began in the late middle Eocene and continues to the present. In the late middle and late Eocene, this deformation was manifested by uplift and erosion on the northeast side of the fault while subsidence apparently continued on its southwest side. Movement apparently slowed in the late Eocene and Oligocene when a regional fault reorganization led to initiation of the nearby Seattle and Devils Mountain faults. During the Neogene, the southern Whidbey Island fault formed the active boundary between thrust-related deformation to the south-southwest and relative tectonic quiescence to the north-northeast. The driving forces for progressive bending of the southern Whidbey Island fault and ongoing transpressional deformation are inferred to be clockwise rotation of western Washington and oblique convergence along the continental margin.

Evidence for Quaternary movement on the southern Whidbey Island fault includes (1) offset and disrupted upper Quaternary strata imaged on seismic-reflection profiles; (2) about 420 m of offset of the Tertiary-Quaternary boundary in boreholes in the fault zone; (3) several meters of displacement along exposed faults in upper Quaternary sediments; (4) late Quaternary folds with dips of ~7-8°; (5) large-scale liquefaction features in upper Quaternary sediments within the fault zone; and (6) minor historical seismicity. The southern Whidbey Island fault should be considered capable of generating large earthquakes ( $M_s \geq 7$ ) and represents a potential seismic hazard to residents of the Puget Lowland.

Mount Rainier seismic zone. I have collaborated with W.D. Stanley on a manuscript (now in review) that describes and interprets the sources of seismicity in the southern Washington Cascades region with a focus on the western Rainier seismic zone. We propose that the region is a distributed right lateral shear zone that includes two significant transfer zones. Ongoing transpressional deformation within this zone is resulting in earthquakes with focal mechanisms that indicate both thrust and strike-slip displacement.

### Reports Published

Johnson, S.Y., Potter, C.J., and Armentrout, J.M., 1994, Origin and evolution of the Seattle basin and Seattle fault: *Geology*, v. 24, p. 71-74 and large-format insert.

Johnson, S.Y., Potter, C.J., Amentrout, J.M., Finn, C., and Weaver, C.S., 1994, The southern Whidbey Island fault, Puget Lowland, Washington: *Geological Society of America Abstracts with Programs*, v. 26, p. A-188.

Johnson, S.Y., and Yount, J.C., 1994, Toward a better understanding of the Paleogene paleogeography of the Puget Lowland, western Washington, in Lasmanis, R., and Cheney, E.S., eds., *Regional geology of Washington State: Washington Division of Geology and Earth Resources Bulletin 80*, p. 225 (abstract).

Pratt, T.L., Johnson, S.Y., Potter, C.J., and Stephenson, W.J., 1994, The Puget lowland thrust sheet: *Seismological Research Letters*, V. 65, p. 31.

Pratt, T.L., Johnson, S.Y., Potter, C.J., and Stephenson, W.J., 1994, The Puget lowland thrust sheet: *Geological Society of America Abstracts with Programs*, v. 26, p. A-187.

Pratt, T.L., Johnson, S.Y., Potter, C.J., and Stephenson, W.J., 1994, The Puget Lowland thrust sheet: EOS, v.75, p. 621 (abstract).

Stanley, W.D., Johnson, S.Y., and Nuccio, V.F., 1994, Analysis of deep seismic reflection and other data from the southern Washington Cascades: U.S. Geological Survey Open-File Report 94-159, 145 p.

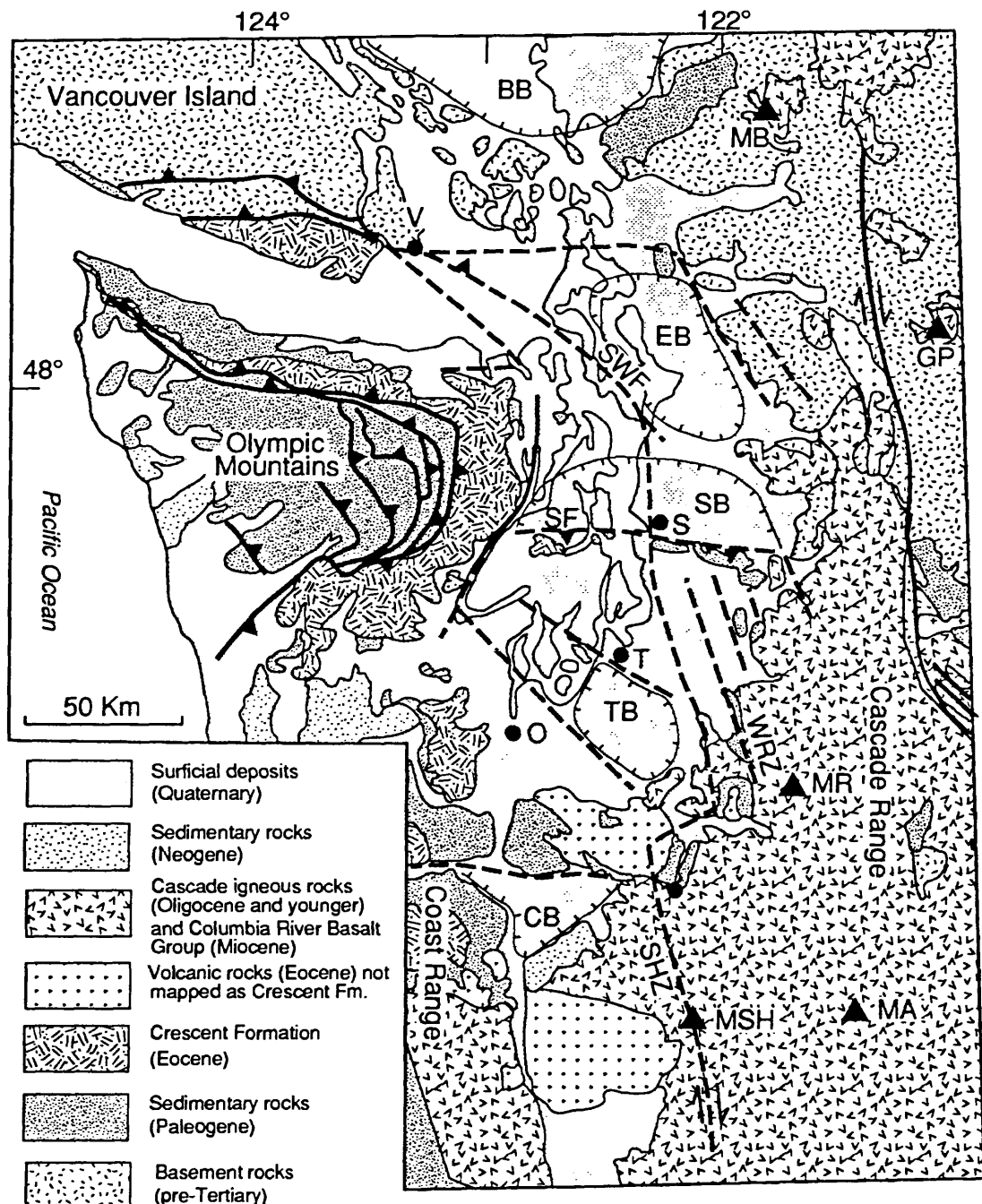


Figure 1. Schematic geologic map of western Washington. Abbreviations for cities and locations: O = Olympia; S = Seattle; T = Tacoma; V = Victoria. Abbreviations for faults (heavy lines): SF = Seattle fault; SHZ = Saint Helens zone; SWF = southern Whidbey Island fault; WRZ = West Rainier zone. Abbreviations for sedimentary basins (enclosed hachured areas) in Puget Lowland: BB = Bellingham basin; CB = Chehalis basin; EB = Everett basin; SB = Seattle basin; TB = Tacoma basin. Abbreviations for modern Cascade volcanoes (triangles): GP = Glacier Peak; MA = Mount Adams; MB = Mount Baker; MR = Mount Rainier; MSH = Mount Saint Helens.

## FAULT MECHANICS AND CHEMISTRY

9960-12106

C.-Y. King

Branch of Earthquakes Geology and Geophysics  
U.S. Geological Survey  
345 Middlefield Road, MS/977  
Menlo Park, California 94025  
(415) 329-4838

### Investigations

- (1) Continued soil-gas geochemical survey across active faults in California.
- (2) Continued continuous radon monitoring at four wells in Oakland, San Juan Bautista, and Parkfield.
- (3) Analyzed temporal variation of soil-gas radon data recorded at 60 stations in central California during 1975-1983.
- (4) Initiated a study of satellite thermal-infrared images in search of possible ground-surface temperature increases before some California earthquakes.

### Results

#### Spatial Soil-Gas Geochemical Anomalies on Active Faults

Radon emanation has been observed to vary greatly along transects across active faults in many parts of the world. We tested this relationship by conducting and repeating soil-air radon surveys with a portable radon meter across several faults in California. The results confirm the existence of fault-associated radon anomalies, which show characteristic features that may be related to fault structures but vary in time due to other environmental changes, such as rainfall. Across two creeping faults in San Juan Bautista and Hollister, the radon anomalies showed prominent double peaks straddling the fault-gouge zone during dry summers, but the peak-to-background ratios diminished after significant rainfall during winter. Across a locked segment of the San Andreas fault near Olema, the anomaly has a single peak located several meters southwest of the slip zone associated with the 1906 San Francisco earthquake. Across two fault segments that ruptured during the magnitude 7.5 Landers earthquake in 1992, anomalously high radon concentration was found in the fractures three weeks after the earthquake. We attribute the fault-related anomalies to a slow vertical gas flow in or near the fault zones. Radon generated locally in subsurfaces soil has a concentration profile that increases three orders of magnitude from the surface to a depth of several meters; thus an upward flow that brings up deeper and radon-richer soil air to the detection level can cause a significantly higher concentration reading. This

explanation is consistent with concentrations of carbon dioxide and oxygen, measured in soil-air samples collected during several surveys.

#### Anomalous Radon Emanation Associated with the 1983 Coalinga Earthquake?

Radon emanations monitored by a Track-Etch method during 1975–83 at 60 sites (Figure 1) along the San Andreas fault system between Santa Rosa and Cholame in central California have been found to show several different patterns of seasonal variations largely attributable to water-saturations and moisture-retention characteristics of the shallow part of the soil. When such effects are removed by a statistic method, the emanations at 45 of the 60 sites show significant increases starting as early as late 1980. Figures 2 and 3 show two examples of the original data (recorded at sites #1 and 11, respectively), their rainfall responses, the corrected and smoothed data (trend), and the residual irregular variations. The possibility that these anomalous radon increases are related to the magnitude 6.5 Coalinga earthquake of May 2, 1983 is investigated.

#### Reports

- King, C.-Y., Zhang, W., and King, B.-S., 1993, Radon anomalies on three kinds of faults in California, *Pure and Applied Geophysics*, **141**, 111-124.
- King, C.-Y., Basler, D., Minissale, A., Presser, T.S., Evans, W.C., and White, L.D., 1993, In search of earthquake related hydrologic and chemical changes along the Hayward fault, *Applied Geochemistry*, **9**, 83-91.
- King, C.-Y., 1993, Earthquake mechanism and predictability shown by a laboratory fault, *Earthquake Research in China*, **7**(1), 1-18.
- King, C.-Y., 1994, Seasonal variability of soil-gas radon concentration in central California, *Nuclear Tracks and Radiation Measurements*, **23**, 683-692.
- Xie, J., and King, C.-Y., 1994, Comparison of U.S. and Chinese research progress on strain changes along fault zones, *Seismogeology Translations*, **16**, 1-15 (in Chinese).
- Zhang, W., and King, C.-Y., 1994, Measurement of radon gas on major faults in California, USA, *Aeta Seismologica Simica*, **7**(1), 159-165.
- King, C.-Y., Zhang, W., King, B.-S., and Evans, W.C., 1994, Spatial radon anomalies on active faults in California, *Journal of Geophysical Research* (submitted).
- King, C.-Y., 1994, Spatial radon anomalies on active faults (abstract), *Seismological Research Letters*, **65**, 70.
- King, C.-Y., Evans, W.C., and Zhang, W., 1994, Spatial radon variations near active faults in California, *Eos, American Geophysical Union, 1994 Fall Meeting Supplement*, 471.

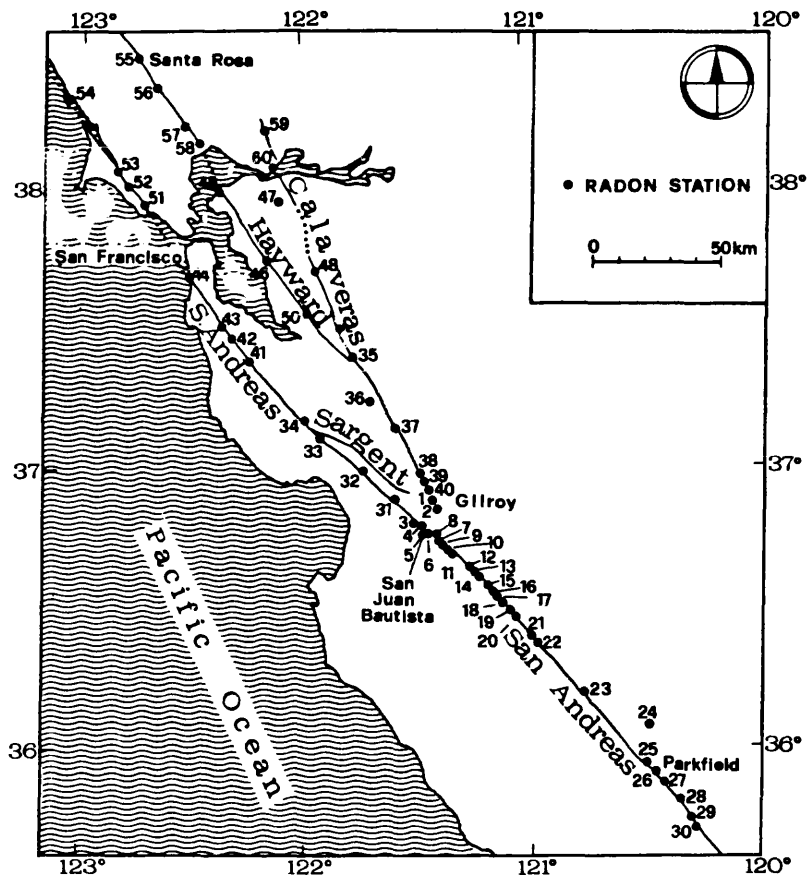
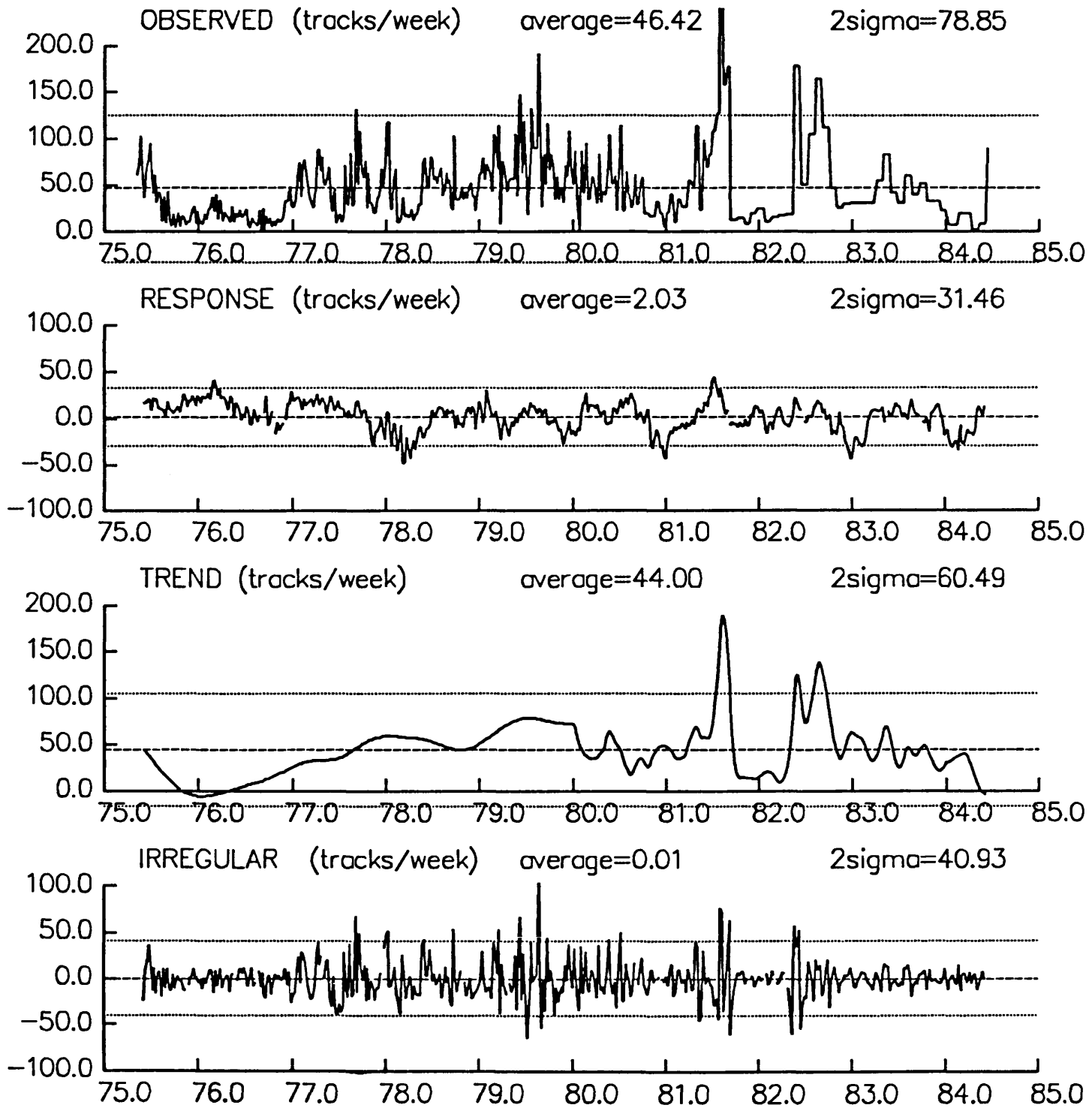


FIG. 1. Location of soil-gas radon monitoring sites in central California.

Figure 1.

Site 01



Site 11

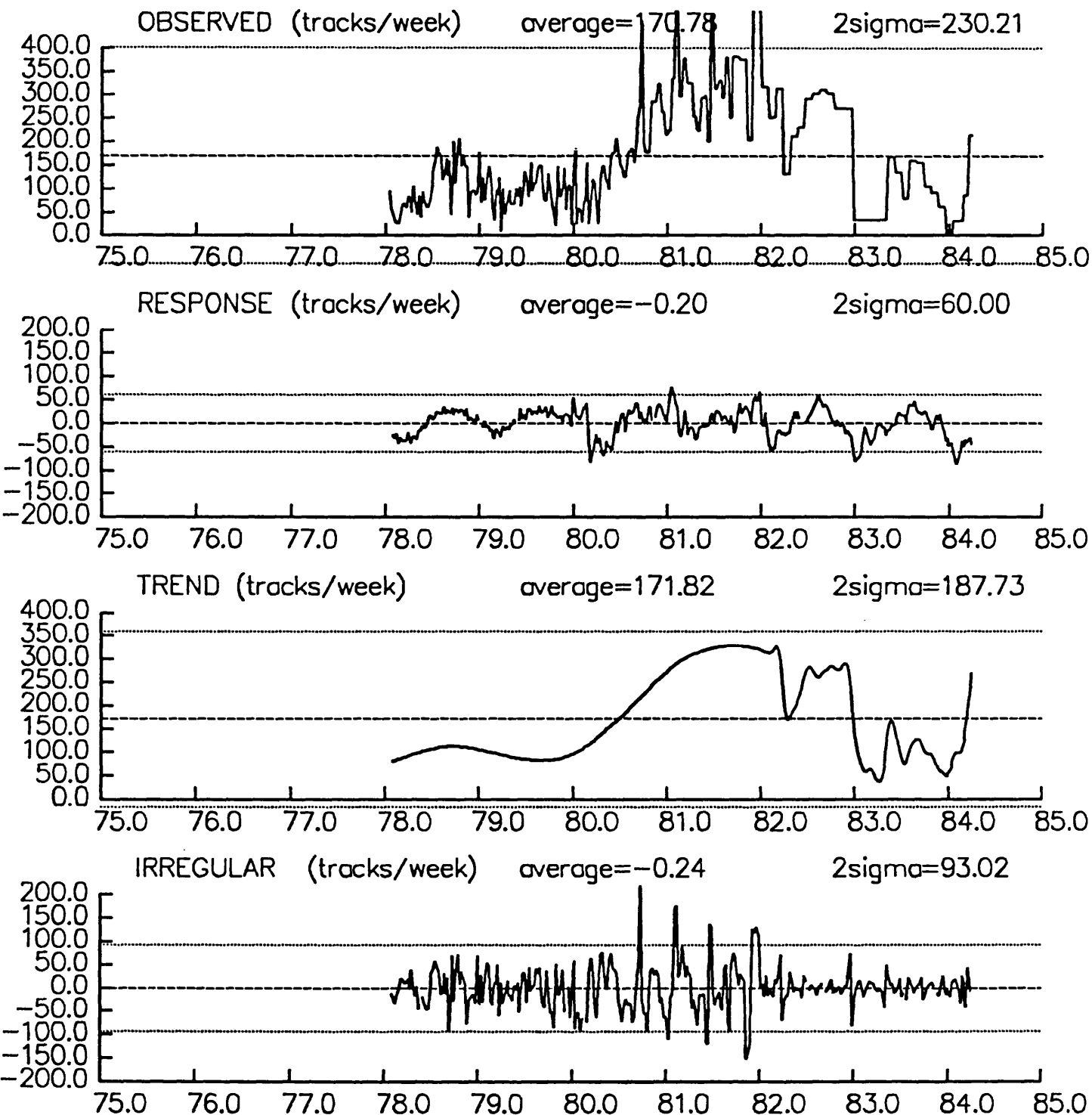


Figure 3.

## PORE FLUID CHEMISTRY AND MECHANICAL BEHAVIOR OF FAULTS

1434-94-G-2445

John M. Logan  
 Center for Tectonophysics  
 Department of Geology and Geophysics  
 Texas A&M University  
 College Station, TX 77843  
 409-845-0312

### Investigations

Our goal is to examine the role of chemical weakening caused by the interaction of pore fluids with fault-zone materials. We are focusing on clay-rich fault zones. This is because the presence of clays apparently enhance chemical effects and they have been argued to significantly change the physical properties of faults. An integrated field and experimental program is being pursued. The results of this research should help to fill a major gap in developing constitutive characterizations of fault zones thus enhancing efforts to better predict earthquakes.

During this contract period we have: (1) petrologically and chemically analyzed samples collected from the Hunter Valley Thrust, Southern Appalachians; (2) sampled critical portions of the Lewis Thrust, Montana and McConnell Thrust, Canada for comparison to the Hunter Valley; (3) Completed analysis of field studies of faults from the Somerset coast of the UK; and (4) Completed experiments on intact specimens of shale in preparation for frictional tests on that material.

### Results

*Hunter Valley Thrust* The Hunter Valley Thrust has been postulated to have displacements from 15 to 25 km, been deformed at depths from 3,000 to 4,500 m, at temperatures between 80 and 110°C, and at confining pressures from 70 to 100 MPa. It is characterized by limestone in the hangingwall, cataclasites developed within the fault zone and shales in the footwall. Two distinct cataclasites separate Cambrian carbonates from Devonian shales: an upper carbonate cataclasite and a lower shale cataclasite. Near the cataclasite the hangingwall is heavily faulted, fractured, veined and moderately folded. The carbonate cataclasite is banded, contains numerous stylolites, many generations of folded, boudined veins and primarily hangingwall-derived clasts. The underlying shale cataclasite is also banded, but contains less clasts (primarily from the FWS) and veins than the carbonate cataclasite. The footwall shales (FWS), near the cataclasite are well-cleaved and extremely hard.

The bulk mineralogy reflects the influence of the fault: the undeformed hangingwall is composed of calcite and minor dolomite; the hangingwall cataclasite (in order of decreasing abundance): calcite, muscovite, quartz, pyrite; the footwall cataclasite: calcite, quartz illite, pyrite; and the footwall shale: quartz, illite/muscovite and pyrite. That there is little change in mineralogy between the footwall cataclasites and footwall shales is notable.

Hangingwall limestones show macroscopic evidence for the presence of fluids, e.g. stylolites and veins. Footwall shales are practically devoid of these features. The hangingwall veins are composed of calcite; at the fault contact they are mixtures of calcite and siderite. Where present in the footwall the veins contain siderite and iron hydroxides (?).

Bulk rock chemistry was undertaken on the cataclasites and footwall shales to determine changes in chemistry accompanying deformation. XRF data suggests an enrichment of CaO and Sr and depletion in SiO<sub>2</sub>, Ba, Zr, Rb and Fe<sub>2</sub>O<sub>3</sub> in the shale cataclasite relative to the footwall shales. These chemical changes are only slight, however, compared to the changes between the cataclasites. The shale cataclasite is markedly enriched in SiO<sub>2</sub>, and depleted in CaO compared to the carbonate cataclasite. The estimated volume loss from the footwall shales/shale cataclasite system during deformation is zero, which is an unexpected result.

Along a traverse across strike, the footwall shales are remarkably constant in their major oxide chemistry. This depletion of SiO<sub>2</sub> in the shale cataclasites with respect to the FWS, in conjunction with the zero volume loss between the two, and the constant chemistry of the FWS suggests that after initial mechanical deformation to form the shale cataclasite, the footwall shales were essentially chemically isolated from the overlying rocks. The base of the footwall cataclasite apparently operated as a barrier towards fluids migrating toward the footwall shales. This barrier appears to have been mechanical in origin, formed during localization of displacement along a Y-shear within the fault zone.

These analyses suggest migration of fluids through the hangingwall and fault zone, but absent from the footwall due to a mechanical barrier within the fault zone. The fluid presence resulted in significant mineralogical differences across the fault. Their influence on mechanical properties remains for our laboratory experiments.

*Lewis Thrust, Montana and McConnell Thrust, Canada* These two faults were sampled across and along the fault contacts. Data were also collected at the macroscopic scale on fracture and vein orientations, geometries, density and other relevant information. The samples will be examined for structural and geochemical differences and the two faults compared with the Hunter Valley Thrust. The field work involved two person months during the summer.

*Faulting Along the Somerset Coast, U. K.* The excellent fault exposures and mineralization confined to the fault zones indicating significant fluid migration lead us to examine these faults in detail. They cut limestones, shales and siltstones. Several distinct vein characteristics have been identified. (1) Carbonate veins in limestones and shales have geometries that are distinct from geometries of gypsum/anhydrite veins in siltstones. (2) Fault-zones with veins of different geometries appear to be spatially distributed across the region. (3) Faults with little or no mineralization are oriented generally N-S, while faults with at least a five-centimeter wide zone of mineralization are oriented generally E-W. (4) The width of mineralized fault zones cannot be correlated with fault displacement.

Two fault-zone vein geometries, laminated vein (LV) and duplexes vein (DV), have been characterized in detail; most calcite-mineralized faults with an E-W orientation have one or the other of these geometries. Fault-zone vein geometry (LV or DV) may be correlated with the spacing and orientation of fractures, and the width of an intensely fractured and folded deformation halo adjacent to the fault zone. In DV fault zones, it appears that the geometry of fault-zone veins changes with increasing displacement; the DV geometry is inferred to be an early-stage, low-displacement fabric, which may be overprinted by brecciation with increasing displacement.

Episodic fluid flow is suggested by both DV and LV fault-zone textures, and several generations of fluids have been identified along a DV fault. There is evidence that DV and LV faults act as seals during late-stage fluid flow and basin inversion. Based on mineralogical and elemental compositional analysis, fault-zone shales are altered by fluid/rock interaction. In country rock adjacent to the DV fault, alteration may also occur immediately adjacent to veins. Organic and/or water content of the shale also appears to vary between the fault zone and country rock. Shale composition

varies in different ways in LV or DV fault-zones. Different types of fluid-rock interactions accompanied deformation along the two different kinds of faults.

*Laboratory Tests on Intact Shale Specimens* In preparation for laboratory experiments on simulated fault gouge and frictional sliding of shales, tests have been completed on intact specimens. Samples of shale having a composition of illite-kaolinite-chlorite in ratios of 13:13:28% with about 40-45% quartz and feldspar were deformed in the laboratory. Triaxial compression tests were done at effective pressures to 100 MPa, temperatures to 250°, and strain rates from  $10^{-4}$  to  $10^{-7}$  sec $^{-1}$  were used. These preliminary experiments show: (1) The material does not follow effective stress law over strain rates of  $10^{-4}$  to  $10^{-7}$ /sec. (2) The strength is inversely proportion to absolute value of pore pressure. (3) At the same temperature, the strength of saturated specimens is only 6 to 25% that of "dry" ones. This behavior differs from data on other rock types for reasons that are not clear at this time. (4) Brittle shear fractures, the failure mode at fast strain rates, are replaced by shear bands at lower rates. (5) With increasing temperatures to 225° C, failure changes from shear fracture to shear bands. (6) When "dry", strength decreases with temperature as expected, but when saturated no change with temperature is observed, which again differs from other rock types. (7) The morphology of failure surface in specimens is significantly different with transition in behavior so that in either tensile failure or in shear bands (which involve very little displacement)--little change in material on either side of the failure zone is found. (8) With shear fractures, however, SEM studies show highly indurated material occurs along the surfaces which is expected to impede fluid flow normal to them. (9) This, combined with the very low strengths when saturated makes localized shear more likely and may be a cause of decreased permeability commonly associated with shales. Observations of common "disturbances" in texture of shales which now appear to frequently be the result of localized shearing, supports hypothesis.

## Reports

Kennedy, L. A. and Logan, J. M., 1994, Cataclasites and the development of seals to fluid migration: Geol. Soc. Am. Abstracts with Programs, v. 26, no. 7, p. A-210.

The Effects of Lithification and Healing in Fault Gouge on Friction  
Constitutive Properties and Fault Stability

Award Number: 1434-94-G-2417

Chris Marone

Brian Evans

Department of Earth, Atmospheric, and Planetary Sciences  
Massachusetts Institute of Technology  
Cambridge, MA 02139

617-253-4352 (phone) 617-253-1699 (fax)  
cjm@westerly.mit.edu

This is an experimental study of fault strengthening at elevated temperature and pressure. The effect of healing on frictional strength is assessed by measuring changes in peak strength and constitutive parameters as a function of hold time. Experiments involve shearing 1mm-thick layers of quartz powder within sawcut quartzite samples at 200-700°C, effective normal stress of 200-300MPa, and fluid pressure of 100MPa. Healing times range from  $10^1$ - $10^5$ s. Higher temperatures are used to access longer healing times. The effects of healing and elevated temperature are assessed independently by shearing at a standard temperature after healing in some cases. A major goal has been to relate laboratory observations of fault strengthening to seismic observations of fault properties and variations in earthquake source parameters with recurrence time.

Publications

- Li, Y. G., Vidale, J. E., Aki, K., Marone, C. J., and W. H. K. Lee, Fine structure of the Landers fault zone: segmentation and the rupture process, *Science*, 265, 367-370, 1994.
- Marone, C., Mechanics and scaling of the critical slip distance for seismic faulting, *Seismological Society of America, Conference Proceedings*, 1994.
- Marone, C., Mechanics of the critical slip distance for seismic faulting and effects of fault zone structure on fault stability and rupture dynamics, *Int. Assoc. of Seismology and Phys. Earth's Inter.*, 1994
- Marone, C., Fault zone strength and failure criteria, submitted to *Geophys. Res. Lett.* 8/29/94.
- Marone, C., Failure criteria for fault zones and intact rock, *Eos, Transactions, American Geophysical Union*, 75, 625, 1994.
- Marone, C. and S. J. D. Cox, Scaling of rock friction constitutive parameters: the effects of surface roughness and cumulative offset on friction of gabbro, *Pure and Applied Geophysics*, 143, 359-386, 1994.
- Marone, C., Vidale, J. E., William L. Ellsworth, Physical interpretation of source variations in repeating earthquake, *Eos, Transactions, American Geophysical Union*, 75, 435, 1994.
- Roy, M., and Marone, C., Pre-seismic slip on faults with rate and state dependent friction, *Eos, Transactions, American Geophysical Union*, 75, 442, 1994.
- Vidale, J. E., Ellsworth, W., Cole, A., and C. Marone, Rupture variation with recurrence interval in eighteen cycles of a small earthquake, *Nature*, 368, 624-626, 1994.
- Vidale, J. E., Ellsworth, W., Marone, C., and A. Cole, Rupture variation with recurrence interval in eighteen cycles of a small earthquake, *Seismological Society of America, Conference Proceedings*, 1994.

APPLICATION OF GROUND-PENETRATING RADAR TO INVESTIGATION OF  
NEAR-SURFACE FAULT PROPERTIES IN THE SAN FRANCISCO BAY REGION

1434-93-G-2335

George A. McMechan  
Center for Lithospheric Studies  
The University of Texas at Dallas  
Richardson, TX 75083-0688  
(214) 690-2419

Program Element 1.1

Objectives

-----

Ground penetrating radar (GPR) provides, in many geologic environments, very detailed images of near-surface earth structure beneath the GPR survey line. GPR is non-destructive and very economical (compared to trenching) and therefore a potentially useful adjunct to trenching for neotectonic studies. The purpose of this project was to evaluate the potential of GPR by recording profiles near existing trenches, for correlation with the trench records. Sixty-two profiles were collected at twelve sites around the San Francisco Bay region.

Preliminary results indicate that features in GPR images do correlate with existing trench observations, can be used to locate faults where they are buried or where their positions are not well known, and can identify previously unknown faults. GPR data potentially provide a valuable adjunct to trenching, by extending trench data laterally, and to depths greater than those to which trenching can be done.

Data Acquisition

-----

In July of 1993, personnel from The University of Texas at Dallas conducted ground penetrating radar (GPR) surveys at a number of sites around San Francisco Bay. The sites were chosen in consultation with people at the USGS office in Menlo Park (Drs. M. Fisher, M.G. Bonilla, and E. Brabb) to allow investigation of a variety of geologic situations and to give control by collecting data at previously trenched sites.

GPR data were collected at five main locations:

- 1) the San Andreas fault near Olema,
- 2) the San Andreas near Millbrae in the San Francisco watershed,
- 3) the Greenville fault, near Altamont Pass, Livermore,
- 4) the San Gregorio fault, near Pescadero, on the coast, and
- 5) the Hayward fault at the Freemont City Hall.

In the field, the trenches were located as accurately as possible from maps made at the time they were dug. GPR data were then collected along a line parallel to the trench, about 2 m away, to avoid the disturbed region associated with the trench. At each site, common-midpoint surveys were done first, to help to select the best offset to perform the constant-offset surveys, and for velocity analysis. This step was repeated at 50, 100, and 200 Mhz. The GPR equipment used was a pulseEKKO IV system. We also collected topography information along the survey lines.

#### Data Processing and Analysis

---

Because of the large number of profiles collected, data processing is still in progress; one PhD graduate student (Jun Cai) is spending 100% of his time on this project. Processing includes filtering, editing, adding topographic data, velocity analysis, normal moveout (NMO) corrections, migration, coherency enhancement, and plotting with various trace and gray-scale formats.

#### Representative Results

---

For the purpose of illustration, we here present two examples of GPR and trench data.

Fig. 1 contains raw and processed 200 Mhz data at 2 m offset, acquired along a trench across the San Andreas fault in the San Francisco Watershed. The trench profile (trench A in Bonilla et al., 1978) is in Fig. 1a; the corresponding GPR data, after NMO and topographic corrections, are in Fig. 1b. Faults are visible in the GPR data as truncations of geologic features and zones of increased scattering, but are not directly visible as GPR reflectors as they are too steep. Also, the resolution of the GPR is necessarily lower than that of the information in the trench profile; only the larger scale features are visible. Perfect correlation is not expected as the GPR lines are beside, not right at the trenches, and trench maps do not contain information on the electrical properties that GPR is sensitive to; thus only the main structural features are seen in both. These characteristics are typical of all the GPR-trench correlations.

Fig. 2 contains a profile at a site near Olema; the data were recorded at 50 MHz, with 3 m antenna separation. This location is near the maximum displacement occurred in the 1906 San Andreas event. There is no trench here, but a whole series of faults are visible in the GPR data. The most obvious break in the GPR data occurs on the trace of the 1906 event. The current position of the active fault as mapped by Hall et al. (labeled A) is a broader zone of diffuse scattering that extends off the bottom of the profile.

The data shown above are 2 of the 62 profiles that were collected; Analysis is continuing.

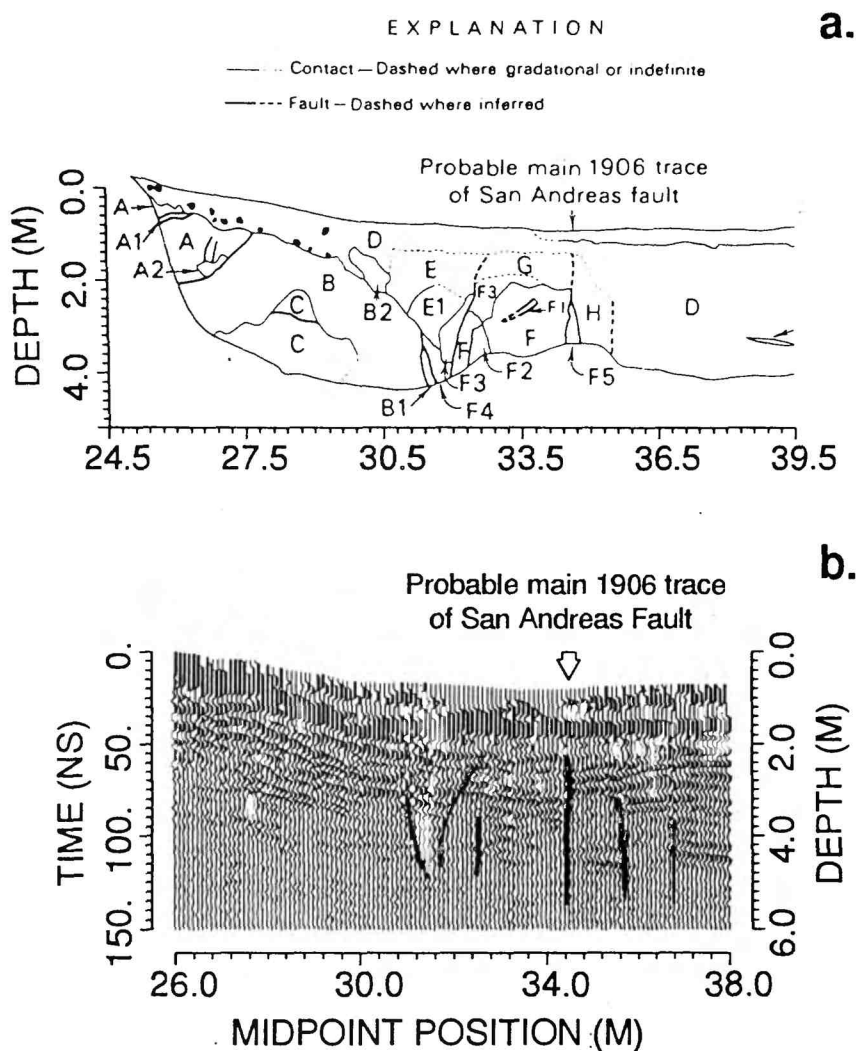


Fig. 1. The trench profile (a), and the corresponding 200 MHz GPR data (b) collected every 10 cm, with 2 m antenna separation; acquired in the San Francisco Watershed. (a) is trench A from Bonilla et al. (1978). (b) has both NMO and elevation corrections, and has the same spatial scales as (a). Heavy lines superimposed on (b) are interpreted fault positions; these generally correspond well with those in (a). Perfect correspondence is not expected as the GPR line is about 2 m away from the trench (to avoid the disturbance associated with the trench itself).

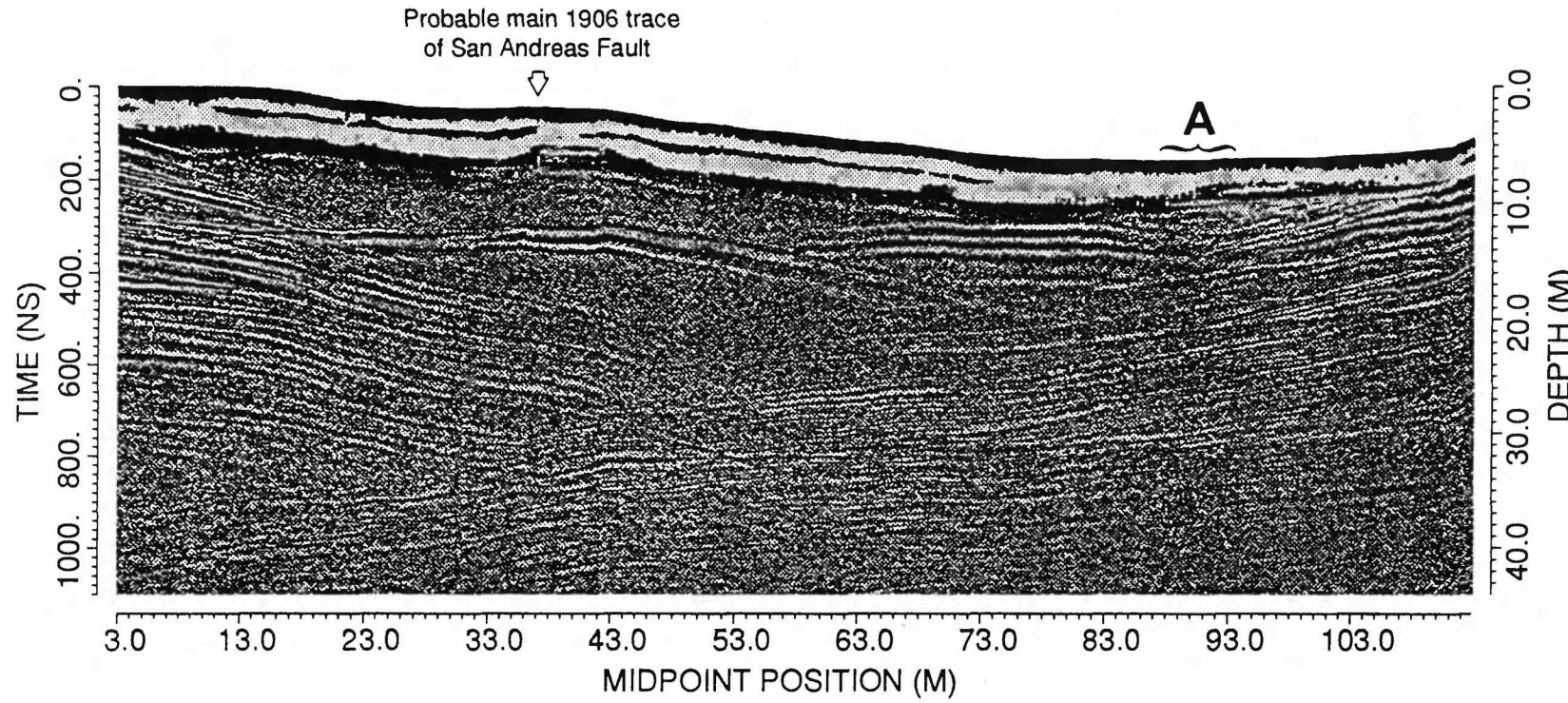


Fig. 2. NMO-corrected data collected at a site near Olema with 50 Mhz antennas, 20 cm between traces, and 3 m antenna separation. 'A' is the currently active portion of the fault zone.

## Conclusions

---

The GPR technique is a useful approach for mapping faults; correlation with trench data is demonstrated; the main 1906 trace of the San Andreas fault is clearly shown in the profiles. The resolution of GPR is sufficient for fault location, but not enough for detailed neotectonic analysis, as the fault themselves are only indirectly evident through layer truncation and scattering. GPR will be useful for initial reconnaissance and to determine optimal placement of trenches, but will not replace trenching.

Larger scale studies of fault geometries are possible with GPR. Its depth of penetration is much larger than that to which trenching can be done. Also, it is a low cost and convenient tool for doing long lines (kilometers or more) and even 3-D surveys of complex faulted regions. These will be the subjects of future projects.

## Data format and availability

---

Field data are in the format designed by the equipment manufacturer (Sensors & Software, Inc.). This consists of a file header containing survey parameter information, followed by each trace; each trace has its own header followed by the data samples in 16 bit integers. Field data are available from the P.I. at

Center for Lithospheric Studies  
The University of Texas at Dallas  
P.O. Box 830688 (FA31)  
Richardson, TX 75083-0688

Edited data and plotted sections will be delivered to the USGS as part of the final project report.

## References

---

- Bonilla, M. G., Alt, J. N., and Hodgen, L. D., 1978, Trenches across the 1906 trace of the San Andreas Fault in northern San Mateo county, California, J. Res. U.S. Geol. Survey, Vol. 6, No. 3, 347-358.
- Fisher, E., McMechan, G. A., Annan, A. P., 1992, Acquisition and processing of wide-aperture ground-penetrating radar data. Geophysics, 57, 495-504.
- Hall, Cotton, and Hay, Detailed analysis of 1906 faulting in Marin County, CA, USGS Contract Report, 14-68-0001-21242.
- Irwin, W. P., 1990, Earthquake History, 1769-1989, in The San Andreas Fault System, California, U.S. Geological Survey Professional Paper 1515, 153-188.

## ANALYSIS OF 1991 USGS REFRACTION DATA FOR VISCOELASTIC PROPERTIES OF THE NEW MADRID SEISMIC ZONE

1434-94-G-2456

George A. McMechan  
Center for Lithospheric Studies  
The University of Texas at Dallas  
Richardson, TX 75083-0688  
(214) 690-2419

### Program Element I.1

#### Objectives

-----

The corellation of the New Madrid axial seismic zone with the Blytheville and Pascola Arches brings us closer to a fundamental understanding of the physical causes of seismicity in the New Madrid Seismic Zone (NMSZ). It appears that the geologic structures are weak due to effects that may include high pore pressure, repeated deformation, igneous intrusion, diapirism, and/or thermal and hydrothermal alteration (Johnson and Shedlock, 1992). The tectonic setting as a rift complex (Braile et al., 1992) underlies the contemporary seismicity (Kane et al., 1981; Chiu et al., 1992; Hildenbrand et al., 1992). The details of the structure/seismicity relationship are not yet clear, but seismic waves that pass through the NMSZ are strongly attenuated (Hamilton and Mooney, 1990).

The goal of this project is to determine, with high resolution, the seismic attenuation ( $Q$ ) distribution for both P and S waves along with their velocities, in the Blytheville Arch, through direct measurement and through detailed viscoelastic modeling of the 1991 USGS refraction profiles across the New Madrid Seismic Zone. This will provide constraints on the physical properties of the NMSZ, and thereby to shed light on the cause of the seismicity. The practical objective is to define criteria for delimiting high-risk zones in the NMSZ, and throughout the eastern U.S.

#### Data Acquisition

-----

In October/November 1991, a pair of refraction profiles were recorded by the USGS across the notrthern end of the Blytheville Arch in the NMSZ. Eight shots were fired into a N-S line and ten shots were fired into an E-W line. The recording aperture for both lines was about 60 km; receivers were spaced at an average of 100 m. The preprocessed data were provided by the USGS in SEG-Y format.

## Data Processing and Analysis

---

Data processing and interpretation involves two parts. The first, direct measurement of Q in the near-surface, is now complete. The second, detailed modeling, is now in progress; one PhD graduate student (Qingbo Liao) is spending 100% of his time on this project.

Direct Q estimates were made from in-situ measurements of energy loss per cycle from transmitted P and S waves, as a function of frequency. Assuming that intrinsic Q is frequency-independent and scattering Q is frequency-dependent, the relative contributions of each are estimated. Figure 1 shows a representative portion of the data, and figure 2 shows the fit to the Q model. The resulting parameters and their uncertainties are:

Intrinsic Q for P-waves	220	(+16, -2)
Intrinsic Q for S-waves	68	(+6, -9)
Dominant scatterer size	100 m	(+20, -6)
Velocity deviation for P-wave scattering	20.0%	(+6, -3)
Velocity deviation for S-wave scattering	11.4%	

These are consistent, both internally, and with the geologic environment. An independent estimate of Q for P-waves of 231 by R. Catchings of the USGS from other data in the area is consistent with our estimate of 220.

With these parameters as a starting point, we are proceeding with the modeling. Recent developments in viscoelastic theory based on superposition of relaxation mechanisms (Liu et al., 1976; Day and Minster, 1984) allow time domain computations of synthetic seismograms for viscoelastic media. The algorithm to be used here is based on Carcione et al. (1988) and Tal-Ezer et al. (1990). Scattered waves may be included by locally perturbing the parameters of the input model to provide a distribution of scatterers of known statistical properties. The model we are using is described by the Von Karman correlation function (Frankel and Clayton, 1986; Crossley and Jensen, 1989).

## References

---

- Carcione, J.M., Kosloff, D., and Kosloff, R., 1988. Wave propagation in a linear viscoelastic medium, *Geophys. J.*, 95, 597-611.

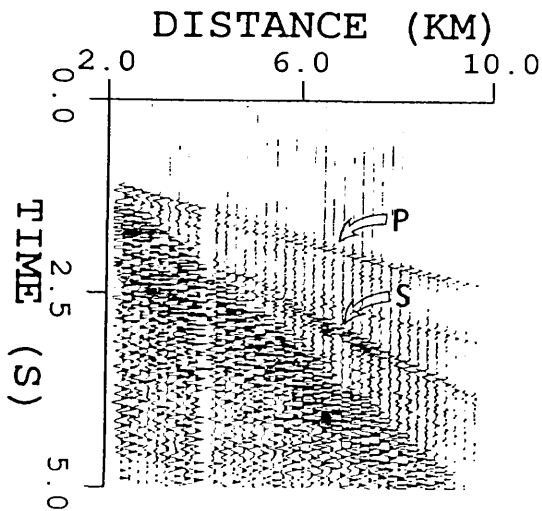


Figure 1: Refraction seismic data from shot point 14 on the E-W line in the 1991 USGS experiment across the Blytheville Arch (Mooney et al., 1993). The direct (labeled) P- and S- wave branches are input to produce the Q estimates in figure 2. From Kang and McMechan (1995).

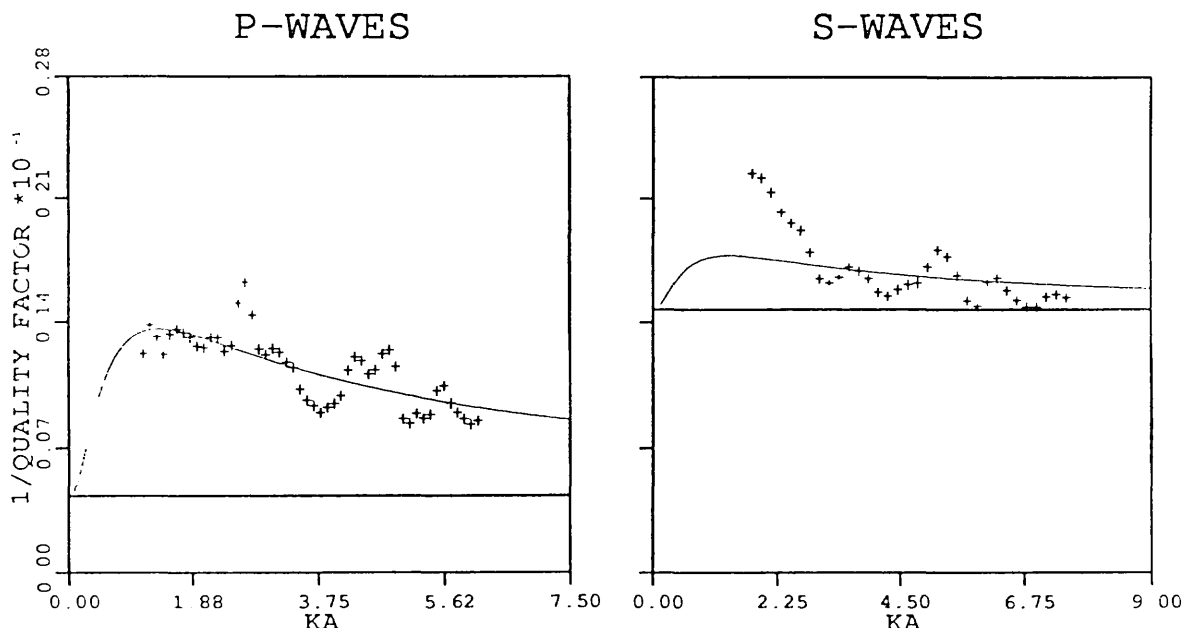


Figure 2: Composite intrinsic/scattering model fitting for the New Madrid data in figure 1. Symbols (+) are (slightly smoothed) estimates of total Q as a function of dimensionless wavenumber (KA). The rms uncertainty in the data points is fairly constant at about 0.08. In each plot, the heavy horizontal line is the best fit (constant) intrinsic Q contribution and the light solid line is the best-fit frequency-dependent) scattering Q contribution. The corresponding parameters are in the text. From Kang and McMechan (1995).

- Chiu, J.M., Johnson, A.C., and Yang, Y.T., 1992. Imaging the active faults of the central New Madrid seismic zone using Panda Array data, *Seis. Res. Lett.*, 63, 375-393.
- Crossley, D.J., and Jensen, O.G., 1989. Fractal models in refraction seismolgy, *Pure Appl. Geophys.*, 131, 61-76.
- Day, S.M., and Minster, J.B., 1984. Numerical simulation of attenuated wavefields using a Pade approximant method, *Geophys. J. R. Astr. Soc.*, 78, 105-118.
- Frankel, A., and Clayton, R.W., 1986. Finite-difference simulation of seismic scattering: Implications for the propagation of short-period waves in the crust and models of crustal heterogeneity, *J. Geophys. Res.*, 91, 6465-6489.
- Hildenbrand, S.G., and Hendricks, J.D., 1992. Geophysical setting of the Reelfoot Rift and relations between rift structures and the New Madrid seismic zone, USGS Professional Paper, preprint.
- Johnson, A.C., and Shedlock, K.M., 1992. Overview of research in the New Madrid Seismic Zone, *Seis. Res. Lett.*, 63, 193-208.
- Kane, M.F., Hildenbrand, T.G., and Hendricks, J.D., 1981. Model for the tectonic evolution of the Mississippi embayment and its contemporary seismicity, *Geology*, 9, 563-568.
- Liu, H.P., Anderson, D.L., and Kanamori, H., 1976. Velocity dispersion due to anelasticity; implications for seismology and mantle composition, *Geophys. J. R. Astr. Soc.*, 47, 41-58.
- Mooney, W.D., Murphy, J., Li, S.L., McCarthy, J., and Ammon, C., 1993. Seismic properties of the New Madrid fault from high resolution seismic refraction profiles (abstract), *EOS Trans. AGU*, 74, 411-412.
- Tal-Ezer, H., Carcione, J.M., and Kosloff, D., 1990. An accurate and efficiant scheme for wave propagation in linear visco-elastic media, *Geophysics*, 55, 1366-1379.

Papers in press

-----

- Kang, I.B. and McMechan, G.A., 1995. Separation of intrinsic and scattering Q based on frequency-dependent amplitude ratios of transmitted waves, *J. Geophys. Res.*, in press.

**Array Studies of Seismicity**  
**David H. Oppenheimer**  
**Branch of Seismology**  
**United States Geological Survey**  
**345 Middlefield Road - MS 977**  
**Menlo Park, California 94025**  
**415-329-4792 / [oppen@alum.wr.usgs.gov](mailto:oppen@alum.wr.usgs.gov)**  
**NEHRP: NC:I, II, III, IV**

## **Investigations**

1. Operation and data management for the Northern California Seismic Network.
2. Prototype development of GIS-based seismicity maps.
3. Replacement of the Real Time (Earthquake) Picker.
4. Rapid pager notification
5. Map of Seismicity of California and Nevada
6. Seismicity and deformation near Hollister, California
7. Seismic evidence for faulting in the western Sacramento Delta
8. Microearthquake activity as indicators of blind thrust faulting in the San Francisco Bay region

## **Results**

1. The Northern California Seismic Network (NCSN) recorded and processed nearly 21,000 earthquakes that occurred in central and northern California during FY94. These events were timed, located and archived at the U.C. Berkeley/USGS Northern California Earthquake Data Center (NCEDEC), where all users with access to the Internet can retrieve the data. Earthquake locations were updated at the NCEDEC on a daily basis. We completed the transcription of all digital waveform data recorded since 1984 from over 2000 9-track magnetic tapes to the optical mass storage device at the data center. We responded to public inquiries about earthquake activity and provided earthquake information about any  $M>4.0$  earthquake occurring within the NCSN to emergency response agencies, like the California Office of Emergency Services, within 20 minutes of occurrence.

We continue to prepare and distribute a report of seismicity recorded by the NCSN each week. This report is sent by e-mail and fax to more than 400 recipients, including the media, emergency response officials, government agencies, and academicians. The report is also posted to public access bulletin boards read by thousands of individuals. The report is a regular feature in many newspapers in California and is also distributed by a commercial enterprise. We also provide a daily telephone message of significant seismicity in the preceding 24 hours.

We have assembled a catalog of seismicity for release on a CD-ROM that contains all earthquakes recorded by the NCSN, Southern California Seismic Network (SCSN), University of Nevada-Reno Seismic Network (UNRN), and Southern Great Basin Seismic Network (SGBSN) for the period 1969-1993. Software for selecting subsets of the data and creating maps of seismicity is also provided.

2. The catalog of earthquakes recorded by the NCSN between 1967 and 1993 now exceeds 330,000 earthquakes, and each year an additional 15,000 earthquakes are added to the catalog. Consequently, it is no longer practical nor desirable to publish bulletins of all earthquakes recorded by the network. Instead, most seismologists prefer to have the data in digital form. However, for the non-seismologist, there is a need for maps of earthquakes recorded by the network. To address this need, we have imported raster-scan images of the 1:250,000 scale USGS topographic base maps for central California into a GIS system so that we can portray seismicity at the same scale and boundaries as the maps of the Geologic Atlas of California published by C.D.M.G. For the map view, we portray seismicity using color to indicate earthquake depth. Well constrained focal mechanisms are also depicted in map view. For the cross sections, we portray each aftershock sequence with its own color and make the color shade a function of the time of each event relative to the mainshock occurrence. Thus, it is possible to recognize both individual earthquake sequences and their time dependent aftershock behavior.

We originally planned to release the San Jose sheet first. Completion of this map has been delayed because we subsequently decided to release the combined San Jose and adjacent San Francisco sheets together. This required obtaining new raster scans of the combined cultural and drainage as well as revising all of the map views and many cross sections. In addition, a full time ARC/INFO technician working on this project resigned. We now expect to release the project in early 1995.

3. Development of a computer system (LARVA) to replace the Real Time (Earthquake) Pickers (RTP) continued this year. The new generation of hardware uses multiple computers (DOS PC's and Unix machines) connected by Ethernet to digitize, detect, and locate earthquakes in real time. LARVA has three principal modules. The first module is the data acquisition computer. This machine digitizes 256 channels of analog seismic data at 100 sps in real time while simultaneously reading time code, checking for channel skipping in the A/D, and broadcasting the time-stamped data onto an Ethernet cable for reception by the 'picker' module. The 'picker' computer receives the Ethernet broadcasts of 256 channels of data in real time while simultaneously calculating the arrival time, first motion, and coda duration of any detected earthquakes. The picker module, at present, broadcasts its picks via RS232 to the locator module. This third machine runs a prototype pick associator developed by Carl Johnson of the University of Hawaii at Hilo. The associator distinguishes earthquakes from independent noise triggers and reports earthquake picks to existing Unix software that locates the event and issues an alarm if the event meets prescribed criteria.

Technical direction of this project is provided by Alex Bittenbinder, who has been responsible for all of the hardware development and most of the software development. This year software development was directed toward error reporting design, system Q/A, shared memory management, documentation, and integration of 24-bit digital data from the Hayward digital telemetered network. Digital data for a set of 39 earthquake sequences was assembled for testing of the software. This set included examples of earthquake swarms, main shocks, robust after-

shock sequences, telemetry problems, teleseisms, and regional earthquakes. By comparing the performance of LARVA software for this set to the performance of both the original RTP and CUSP systems, we have been able to diagnose problems in advance of implementation. Revisions based on the Q/A tests are completed, and we anticipate release of LARVA with supporting documentation by the end of 1994. Installation of LARVA is planned for early 1995 when wiring for 587 analog channels and assembly of corresponding anti-aliasing filters are completed.

Initial tests to receive 24-bit digital telemetered data from the 4-station Southern Hayward Fault Network were completed. Software is being modified to be able to process this data stream using 32-bit architecture together with external triggering notification by the CUSP system. We are attempting to ultimately integrate this data with the traditional analog-telemetered data that is processed by the CUSP system, so that it can be accessed by the public at the NCEDC.

4. Most seismic networks in the U.S. now have the ability to automatically detect and locate earthquakes within minutes of their occurrence. We are attempting to make this information available to the public as rapidly as possible so that critical decisions can be made without having to rely on access to seismologists. For instance, emergency response officials need to know both the location, magnitude, and distribution of aftershocks so that resources can be rationally allocated and directed. Governmental officials need to be apprised of significant earthquake activity. The news media would like to have authoritative information to provide to the public. Educational institutions would find this information valuable for teaching about tectonics. Power, water, and telephone agencies need accurate information to re-route their networks following earthquakes. Railroad companies need to stop trains if there is a danger of derailment.

Since many of these customers are not connected to the Internet, we have chosen to provide this information via wireless alphanumeric paging devices. Using software called "SEISMIC", developed by Alan Jones of the State University of New York at Binghamton, we have established a prototype system that provides nationwide paging of earthquake information through a commercial paging company. The SEISMIC software operates on inexpensive PC platforms and provides map, cross-section, and 3-D views of seismicity received by the pager device, which connects to the PC's serial interface. Currently local earthquake information is being provided within minutes of earthquake occurrence by the NCSN, SCSN, and University of Washington. The National Earthquake Information Center (NEIC) is also providing nationwide and teleseismic information, though all NEIC data is first reviewed by seismologists.

5. This project provided technical guidance for a new version of the map, "Seismicity of California and Nevada" by Goter et al. This new map will differ from the 1988 version in that it depicts 1) more than 300,000 earthquakes recorded by the SCSN, NCSN, UNRN, and SGBSN from 1980-1994 as small dots that clearly image the location of current seismically active faults, 2) the location of all M>5.5 earthquakes as larger symbols to denote activity on faults that were not seismogenic during the last 15 years, and 3) the surface projection of rupture zones for significant earthquakes to illustrate the extent of rupture in contrast to a quake's epicentral location. The map clearly demonstrates that deformation of the brittle crust occurs over a broader region that encompasses all of California and Nevada. The map is scheduled for release in December, 1994.

6. Seismologists (Dorbath, Amelung, and King) at the Institut de Physique du Globe in Strasbourg, France have been collaborating with David Oppenheimer on an integrated analysis of the deformation occurring near Hollister, California, where the San Andreas fault bifurcates into the Calaveras fault. The goal of this research is to understand the relationship of contemporary faulting, as expressed by microseismicity, to topography. We have used traveltimes data recorded by the NCSN to generate a 3-D velocity model of this complex region through inverse methods. This model is used to relocate the earthquakes in the region to obtain an accurate map of active faults. We use a fault geometry based on these earthquake locations together with slip rates based on independent studies to compute the deformation at the earth's surface.

We find that many features of the topography can be explained by a simple model. The overall form of the Hollister Valley is reproduced together with the subsidence extending towards Monterey Bay. Bends in the fault predict local uplift that are also observed in the topography. By using faults imaged only through microseismicity in conjunction with faults mapped at the surface, we demonstrate how it is possible to model topography and perhaps infer where blind thrust faults may exist. A manuscript is in preparation

7. In an effort to identify the faults of the San Francisco Bay area, the BASIX experiment was conducted to acquire marine seismic reflection surveys in the shallow waters of the San Francisco Bay and western Sacramento Delta. Both the shallow (100 meter) and deeper (2 km) seismic profiles image faulting and deformation in the vicinity of Pittsburg, California. David Oppenheimer collaborated with Jill McCarthy to provide a companion analysis of earthquakes recorded by the NCSN in the vicinity of the BASIX seismic lines. Earthquake locations based on a new velocity model developed from inversion of traveltimes data occur at depths between 17 and 25 km. These unusually great depths place this activity just above the Moho, the boundary between the crust and mantle. In addition, the earthquakes locate directly beneath the shallow deformation imaged in the seismic reflection data. The pattern of earthquake locations and mechanisms reveal a complex pattern of right-lateral faulting, right step-overs, and attendant reverse faulting in the region of the Kirby Hills. The link between surface deformation and very deep seismicity suggests that this fault presents a significant earthquake hazard for the Pittsburg region.
8. Over the last century significant earthquakes in the S.F. Bay region have exhibited predominantly strike-slip motion on near-vertical faults, and geodetic studies confirm that the plate motion is being accommodated on these same faults. However, the topographic relief in this region exhibits significant variation that is not easily explained by the strike-slip faulting. The age of these mountain ranges indicates uplift rates on the order of ~1mm/yr, suggesting that active reverse faults analogous to faults which slipped during the Loma Prieta and Northridge earthquakes may underlie these ranges. Robert Simpson and David Oppenheimer have examined first-motion focal mechanisms for 7610 earthquakes recorded since 1984 to assess whether earthquakes with reverse mechanisms define significant seismogenic structures in regions of uplift, and conversely whether those with normal mechanisms occur in regions of low topography.

Most earthquakes with reverse and normal mechanisms are scattered throughout the region and do not clearly define though-going faults. The Loma Prieta and Northridge earthquakes demonstrated, however, that "blind" faults exhibit little background seismicity, suggesting that the period of seismic observation is too short to image them. We conducted a systematic analysis

of the earthquake focal mechanisms to determine whether the first-motion observations for the reverse and normal mechanisms could also be explained by motion occurring on fault planes with orientations typical of the right-lateral strike-slip faults in the region. We found that unambiguous reverse faulting occurs only adjacent to the Calaveras, Hayward, and San Andreas faults. Normal earthquakes occur only adjacent to the San Andreas fault near the Golden Gate and at the Geysers geothermal area. Little evidence of reverse faulting is observed in the recent seismicity beneath the topographically elevated regions of the S.F. Bay region. Consequently, active blind thrust faults in this region are presumably locked and not currently generating microearthquake activity.

## Reports

1. Oppenheimer, D., B. Bogaert, A. Michael, and A. Jones, Rapid reporting of hypocentral information via nationwide pagers, *EOS, Trans. Amer. Geophys. Union*, 75, 430, 1994.
2. Simpson, R.W., K.R. Lajoie, and D.H. Oppenheimer, Inferring blind thrusts in the San Francisco Bay region from earthquake focal mechanisms and averaged topography, *EOS, Trans. Amer. Geophys. Union*, 75, 681, 1994.
3. McCarthy, J., P.E. Hart, R. Anima, D. Oppenheimer, and T. Parsons, Seismic evidence for faulting in the western Sacramento Delta region, Pittsburg, California, *EOS, Trans. Amer. Geophys. Union*, 75, 684, 1994.
4. Amelung, F., G.C.P. King, and D. Oppenheimer, Summation of seismic moment: applications to microearthquakes in central California, *EOS, Trans. Amer. Geophys. Union*, 75, 478, 1994.
5. Goter, S., D. Oppenheimer, J. Mori, and M. Savage, Seismicity Map of California and Nevada, Open-File Report 94-647, in press, 1994.

# The Temporal and Spatial Development of Deformation and Degradation along Strike-slip Fault Bends

**1434-94-G-2464**

David D. Pollard [(415) 723-4679; dpollard@pangea.stanford.edu]  
 Ramón Arrowsmith [(415) 725-0573; ramon@pangea.stanford.edu]

Department of Geological and Environmental Sciences, Stanford University, Stanford, CA  
 94305-2115; Fax: (415) 725-0979

This report summarizes research from 2/1/94 to 10/15/94.

## **PROBLEM**

Topography results from the competition between the tectonic processes of uplift and deformation, and the geomorphic processes of erosion, transport, and sedimentation. Tectonic landforms can retain information about the tectonic history of a particular region, and their analysis provides information that bridges the gaps between geodetic (< 100 yrs) and geologic (>0.5 Ma) timescales, and between the spatial scales of trenching and regional mapping. Development of an explicit linkage in physical-process-based models between deformation and degradation along a major strike-slip fault is the focus of the this research.

Combining detailed geologic mapping and geomorphic analysis with numerical models of deformation and degradation, this field and computer modeling based project tests the hypothesis that the geometry and magnitude of deformation along a portion of the San Andreas Fault (SAF) is consistent with the transition from a straight segment to a restraining segment. We expect that the partitioning of deformation among reverse and normal faults and folds changes as a function of the counterclockwise deviation of the strike of this fault from the direction of plate motion.

## **INVESTIGATIONS**

- 1) Completion of geologic and geomorphologic mapping of an approximately 12 km<sup>2</sup> area adjacent to the SAF in the Elkhorn Hills, southeastern Carrizo Plain, San Luis Obispo County, California at 1:6,000.
- 2) Identification of deformed surfaces of known age, as well as morphologic analysis of degraded fault scarps, to provide timelines for the understanding of the temporal and spatial development of restraining bends and the structures associated with them.
- 3) Compilation of structural, geologic, topographic, and geomorphic observations and modeled results using a geographic information system (GIS).
- 4) Continued analysis of the data by developing and testing mechanical (numerical) models to evaluate the interaction and direct coupling between the deformation (uplift, folding, and faulting), and the subsequent degradation (hillslope processes).

## **PROGRESS**

- 1) Field work for this portion of the project is complete. In the next year, we will extend our mapping along the SAF to further test our hypothesis. We are compiling the field observations and expect to prepare a ~1:6000 geologic and geomorphic map. These data will be incorporated into our GIS database (see 3). The geologic observations of this portion of the SAF zone where we observe strike-slip, *and* normal & reverse dip-slip faulting are detailed, and their description and interpretation based upon quantitative tectonic and geomorphic models will be presented in a manuscript to be completed before 12/31/94 and submitted to *Tectonics*. A portion of this research was presented at the San Andreas Site Characterization Workshop by R. Arrowsmith (3/94; see full citation below).

- 2) We are calibrating the geomorphic model parameters at two sites in the central Carrizo Plain. Along with the scarp immediately southeast of Wallace Creek where our primary calibration effort is focused, we have identified a site on the Van Maitre Ranch at which a scarp has been exposed as a result of the ~15 m of lateral offset inferred to have accumulated in the last two large earthquakes along the SAF [Grant and Donnellan, 1994; Grant and Sieh, 1993]; *Figure 1*. The association of offset and exposure with these two events provides a good age constraint on the history of the landforms. At that site, we have selected 2 profiles for calibration: A) a scarp over which animal burrowing, rainsplash and soil creep dominate the material transport (indicating "diffusive conditions") and B) knickpoint in a small channel over which concentrated soil wash transports material. These processes are included in our geomorphic model (see 4) and the site will add an important test of the calibration at Wallace Creek. The results from these investigations will be presented at the Fall American Geophysical Union Meeting [Arrowsmith *et al.*, 1994b], and documented in a manuscript to be completed before 11/31/94 and submitted to *Geology*.
- 3) The GIS laboratory at Stanford will be fully operational in late fall, 1994. In this laboratory, we will compile structural, geologic, topographic, and geomorphic observations and modeled results. We have purchased a panchromatic SPOT satellite image of the Carrizo Plain. With its 10 meter ground resolution cells, this image forms a portion of the background for our geologic and geomorphologic analyses.
- 4) We have developed a quantitative model for geomorphic and tectonic displacements that is applied to hillslope profile development in areas of active tectonics. This has been the primary project effort in the last 8 months.

In our model, transient finite difference solutions to the continuity equation for material transport determine geomorphic displacements. The material transport rate is a function of distance from the divide to the power  $m$ , local slope to the power  $n$ , and a rate constant. Values of  $m$  and  $n$  may change to simulate threshold independent processes varying from rainsplash and creep (i.e., diffusive;  $m = 0, n = 1$ ) to slope wash and river flow ( $m > 0, n > 0$ ; [Carson and Kirkby, 1972]; *Figure 2*). Specifying a critical flux for channel formation includes the transition from diffusive hillslope conditions to converging flow and stream incision. The actual geomorphic displacements may be transport- or weathering-limited, depending on soil profile development (*Figure 3*).

Superimposed edge dislocations in an elastic half-plane are used to model tectonic displacements. Slip along a normal or reverse fault of any dip, depth and length may be incremental (earthquake) or continuous (creep). We consider faults of spatial scale much less than crustal thickness so isostatic responses to topographic loading are not important, but could be easily included.

We model profile development by identifying an initial profile shape and boundary conditions; soil production and process parameters; age; and fault geometry and slip rate. Model tectonic landforms are sensitive to the ratio of geomorphic and tectonic displacement distributions in space and time. Considering climate and material properties constant, it is roughly the ratio of the material transport rate constant ( $\alpha$ ) and the fault slip rate that determines form. Profile responses to tectonic displacements relate directly to the surface displacement gradient and are greatest when the fault ruptures the surface. This model extends existing morphologic diffusion erosion analyses of tectonic landforms to include other geomorphic processes and realistic distributions of tectonic displacement. The simulations serve to develop intuition, and to indicate which parameters or processes should be the focus of detailed field observations. Calibration of these parameters and processes provides a quantitative approach to modeling landform development, determining deformation rates, and inferring earthquake hazard.

Below, we present two examples demonstrating the utility of this geomorphic and tectonic model in the evaluation of surficial deformation associated with slip along faults.

## Fault Scarp Incision

In previous models of fault scarp development, care was taken to choose fault scarps in areas that have minimum contour curvature (ideally to avoid converging flow in gullies; e.g., [Hanks *et al.*, 1984]). On the other hand, our analysis permits the investigation of profiles that cross a fault scarp and may be dominated by gully processes or a transition thereto (*Figure 4*). The initial shape is a planar 5° slope. The boundary conditions are constant elevation (upper) and zero flux lower. This simulation might represent one half of a graben that has formed in an alluvial fan--the zero flux lower boundary causes the expected deposition and filling of the graben. The profile that is purely diffusive is shown (gray). The faulting parameters are 2 mm/yr along a 45° dipping 500 m long normal fault, and all examples are for a duration of 10 ka &  $\alpha = 1 \text{ m}^2/\text{ka}$ .

In the examples in which there is no channel head, discharge dependent ( $m > 0$ ) processes contribute to the transport capacity through the profile. This represents a case in which a well established drainage cuts across the active fault. If we permit channel head formation above a critical flux, we can model the incision of the fault scarp as greater relief and slope develop with continued fault slip. The smaller plot under these profiles uses the same horizontal axis as the profiles, but shows the channel head location with time. For the examples with higher flux, it takes some time (2 - 3 ka) for enough slip to accumulate and permit the establishment of a channel. As the channel grows headward, it incises the scarp. This is an important alternative to the diffusive (with extremely high rate constant) gully development of [Begin, 1988]. With proper calibration and determination of appropriate transport process behavior and rate, gullies may be included in the morphologic dating of fault scarps, and possibly provide more robust results. Weathering-limited conditions could be included to contribute to dating of landforms in areas of higher erosion rates or lower weathering rates.

## Active thrust faults, river channel profiles and fluvial terraces: fault slip rate vs. geomorphic rate constant

As an example of the conclusion that the tectonic landforms owe their shapes to the ratio between the geomorphic and tectonic displacement rates over the landform profile and over the time period of interest, we provide the following scenario (*Figure 5A & B*). The initial shape is a  $m = 2$ ,  $n = 2$  characteristic small river profile 1000 m long and with a maximum elevation of 50 m (small dashes). Such a choice minimizes the response to a disequilibrium initial shape and emphasizes responses to tectonic displacements. The geomorphic boundary conditions are constant elevation (the ends of the profiles are tectonically displaced), and transport-limited conditions persist. Two sets of profiles at 1, 5, and 10 ka are shown. The only difference between the plots is that the rate constant ( $\alpha$ ) is 0.1 above and it is 1 below. The upper (less erosive) profiles are more sensitive to the tectonic displacements,. We simulate the deformation of abandoned fluvial terraces by assuming that the initial topographic profile is abandoned at time 0, and then is deformed along with the active channel. The terrace profiles include geomorphic displacements due to diffusive processes only (the grayed lines in *Figure 5*).

*Figure 5A* illustrates the effects of tectonic displacements due to a 500 m long buried thrust fault dipping upstream. The top of the fault is 50 m below the surface and 750 m downstream from the divide. The slip rate along the thrust is 1 mm/yr. Notice that the displacement field varies greatly along the profile. These profiles have a remarkable similarity in age, scale, form and setting to fluvial terraces over the active thrust fault and fold at Wheeler Ridge, California (Salt Creek profiles of [Keller *et al.*, 1988]). *Figure 5B* shows a similar result for a much longer surface rupturing fault with the same slip rate and the same distance from the top to the divide. The displacement field is much less variable. These profiles are similar to many flights of terraces upstream from active range-bounding faults (e.g., [Rockwell, 1988]). Each terrace forms as a result of a variety of factors and probably not solely because of an earthquake.

*Figure 6* is an extreme example of the inclusion of soil production into the above scenario. All other parameters are the same as in *Figure 5A*, but the slip rate along the buried thrust is 5 mm/yr. The material is uplifted so fast that the soil cannot be produced quickly enough, and conditions become weathering limited. A steep reach--possibly a waterfall--forms along the channel profile in the area above the fault tip.

A manuscript describing this model has been submitted to the *Journal of Geophysical Research*, Special Section on Paleoseismology [Arrowsmith *et al.*, 1994a]. It has been presented at the International Lithosphere Program-USGS Workshop on Paleoseismology, 9/94; and the geomorphic portion of the model described in the associated Workshop Proceedings volume: [Arrowsmith, 1994]. It will be presented at the Fall Meeting of the Geological Society of America: [Arrowsmith *et al.*, 1994c].

The model has been written in the FORTRAN 77 computer language. The code is available for other researchers by contacting Ramón Arrowsmith. It will be submitted for publication as either a *USGS Open File Report* or in *Computers & Geosciences*. As the results shown in *Figures 4, 5, & 6* suggest, this model has wide application in the investigation of the deformation history of the landscape and in the inference of earthquake hazards based upon analysis of the resultant landforms.

### **PRESENTATIONS OF THIS RESEARCH**

International Lithosphere Program-USGS Workshop on Paleoseismology, Marconi Conference Center, Marshall, California: *A model for geomorphic displacements applied to hillslope development in areas of active tectonics* (9/94).

San Andreas Site Characterization Workshop, NSF/DOE/USGS, *The geologic and geophysical framework of the San Andreas fault in the Carrizo Plain* (3/94).

### **ABSTRACTS AND PUBLICATIONS RESULTING FROM THIS RESEARCH**

Arrowsmith, R., A model for geomorphic displacements applied to hillslope development in areas of active tectonics, in *Proceedings of the Workshop on Paleoseismology: USGS Open File Report 94-568*, edited by C. S. Prentice, D. P. Schwartz and R. S. Yeats, pp. 11-13, 1994.

Arrowsmith, R., D. D. Pollard and D. D. Rhodes, A model for tectonic and geomorphic displacements applied to hillslope development in areas of active tectonics, *Submitted to Journal of Geophysical Research, Special Section on Paleoseismology*, 9/30/94, 1994a.

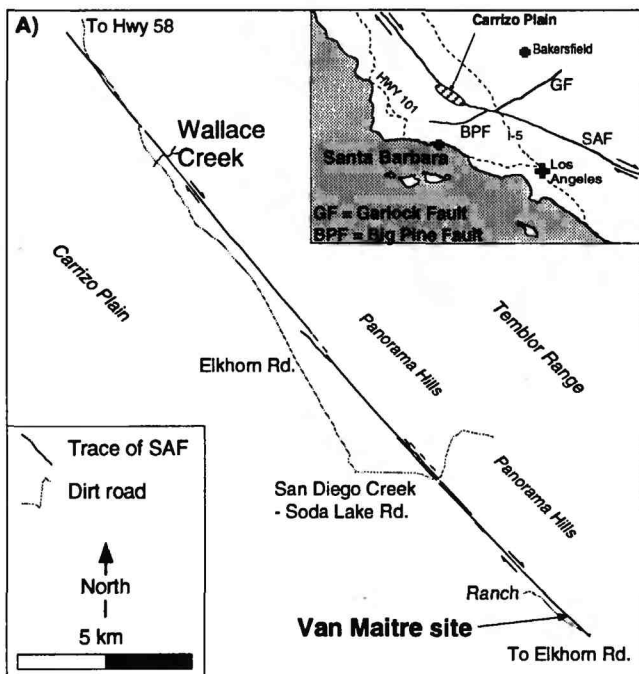
Arrowsmith, R., D. D. Pollard and D. D. Rhodes, A model for geomorphic and tectonic displacements applied to hillslope development in areas of active tectonics, *EOS Transactions AGU, 1994 Fall AGU Meeting*, 1994b.

Arrowsmith, R., D. D. Pollard and D. D. Rhodes, A quantitative model for geomorphic and tectonic displacements applied to hillslope development in areas of active tectonics, *Geological Society of America Abstracts with Programs, 1994 Annual meeting*, 1994c.

### **REFERENCES**

- Begin, Z. B., Application of a diffusion-erosion model to alluvial channels which degrade due to base-level lowering, *Earth Surface Processes and Landforms*, 13, 487-500, 1988.
- Carson, M. A. & M. J. Kirkby, *Hillslope form and process*, 475 p., Cambridge University Press, Cambridge, 1972.
- Grant, L. B. and A. Donnellan, 1855 and 1991 surveys of the San Andreas Fault; implications for fault mechanics, *Bulletin of the Seismological Society of America*, 84, 241-246, 1994.
- Grant, L. B. and K. E. Sieh, Stratigraphic evidence for several meters of dextral slip on the San Andreas fault during the 1857 earthquake in the Carrizo Plain, *Bulletin of the Seismological Society of America*, 83, 619-635, 1993.
- Grant, L. B. and K. E. Sieh, Paleoseismic evidence of clustered earthquakes on the San Andreas Fault in the Carrizo Plain, California, *Journal of Geophysical Research*, 1994.
- Hanks, T. C., R. C. Bucknam, K. R. Lajoie and R. E. Wallace, Modification of wave-cut and fault-controlled landforms, *Journal of Geophysical Research*, 89, 5771-5790, 1984.
- Keller, E. A., D. L. Johnson, D. M. Laduzinsky, T. K. Rockwell, D. B. Seaver, R. L. Zepeda and X. Zhao, Tectonic geomorphology and late pleistocene soil chronology of the Wheeler Ridge, San Emigdio Mountains, and Frazier Mountains areas, in *Friends of the Pleistocene Field Trip Guidebook*, 1988.
- Rockwell, T., Neotectonics of the San Cayetano fault, Transverse Ranges, California, *Geological Society of America Bulletin*, 100, 500-513, 1988.
- Sieh, K. E. and R. H. Jahns, Holocene activity of the San Andreas Fault at Wallace Creek, California, *Geological Society of America Bulletin*, 95, 883-896, 1984.
- Vedder, J. G. and R. E. Wallace, *Map showing recently active breaks along the San Andreas and related faults between Cholame Valley and Tejon Pass, California*, U.S. Geol. Survey Misc. Geol. Inv. Map I-574, 1970.

Figure 1. Location map and reconstruction of offset at Van Maitre site, Carrizo Plain, CA. A) The location of the Carrizo Plain in Southern California is shown in the inset. The locations of Wallace Creek and the Van Maitre site along the SAF in the Carrizo Plain are illustrated along with dirt roads and apparently active fault traces. Fault traces are from Vedder and Wallace, 1970. B) Reconstruction of offset at Van Maitre site. The lateral offset of the shutter ridge changes the lower boundary elevations for various portions of the scarp. The slip rate, slip per event, and event time are from Sieh and Jahns, 1984; Grant & Sieh, 1993; and Grant & Sieh, 1994. Aggradation and terrace formation are caused by shutter ridge offset raising the channel elevations at the SAF. The exposure of the scarp is thus constrained, and we calibrate our geomorphic models along profiles of the ungullied scarp and the gully (see PRESENT contour map). Contour interval is 1 m. Topographic data was surveyed using digital surveying equipment.



**B) Reconstruction of offset at Van Maitre site**

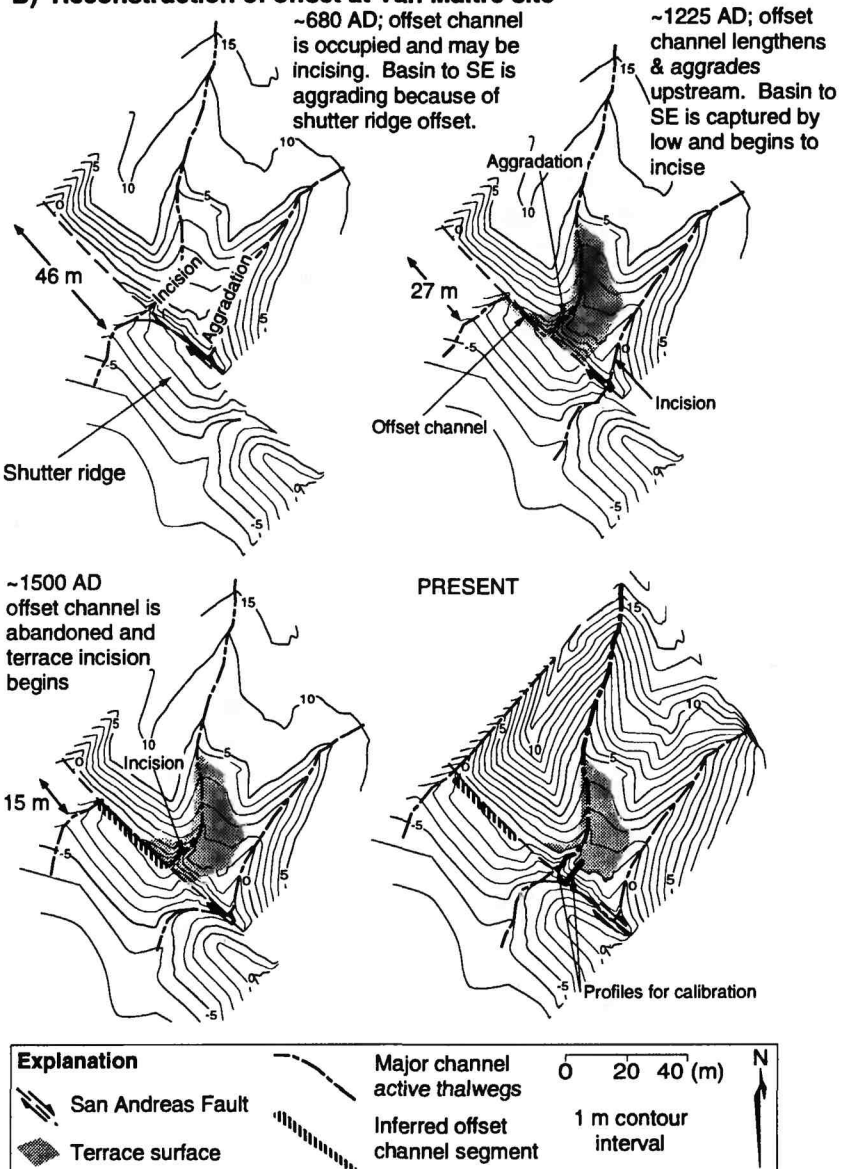


Figure 2. Approximate "characteristic forms" to which hillslope profiles tend with transport-limited conditions, no tectonic displacements, and constant elevation boundary conditions. The resultant form depends upon the process: convex for slope dependent processes such as creep, rainsplash and animal induced disturbances ( $m = 0$ ), straight for sheetwash ( $m = 1$ , all  $n$ ), and concave for gullyling and rivers ( $m > 1$ ,  $n > 0$ ). After Carson & Kirkby, 1972.

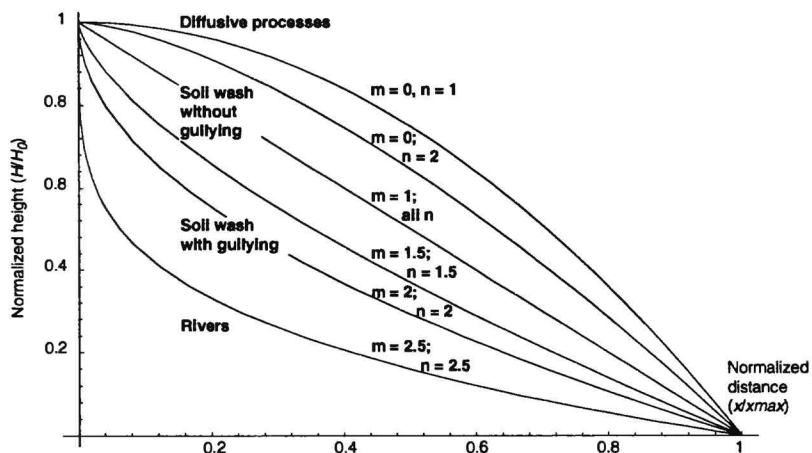


Figure 3. Simulations of hillslope development with variable soil production rates showing the transition from transport-limited to weathering-limited conditions. All parameters and initial conditions are the same except for  $B_a$  (weathering rate of bare bedrock) and  $B_b$  (weathering rate sensitivity to soil depth--exponential decrease with increasing soil depth) which vary from 1 and 1 to 0.01 and 100 respectively. Age is 10 ka and boundary conditions are constant elevation.

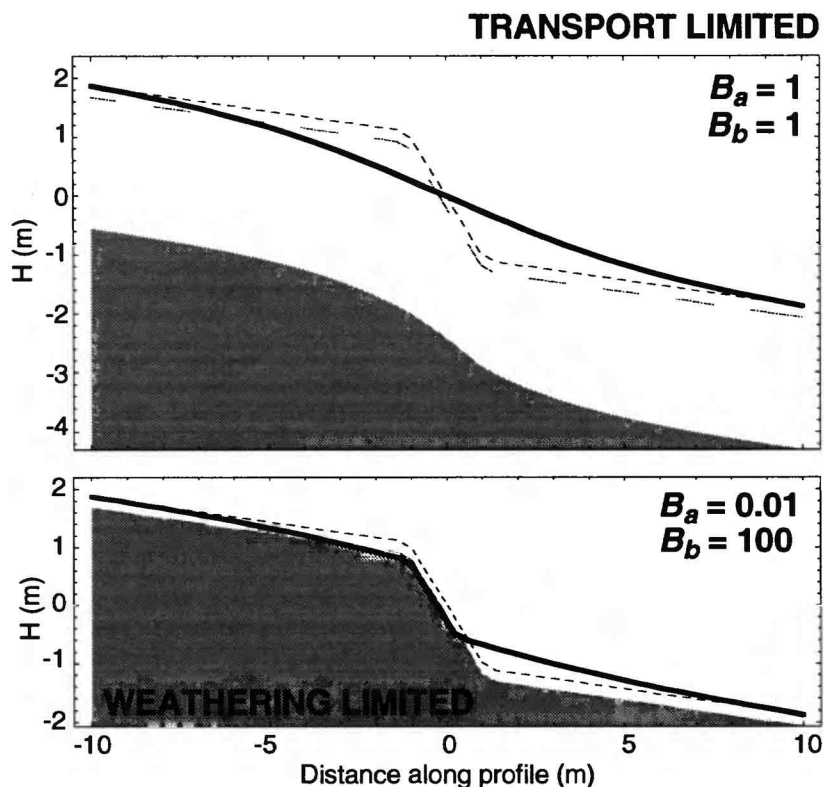


Figure 4. Illustration of fault scarp incision. These plots show the initially planar fan surface that is cut by a short normal fault. Compare the profile modified by diffusive processes (gray) only with those that include overland flow and thus may be gullies incising the scarp as it forms (solid). Those plots that indicate a critical flux above which the profile becomes channelized include the channel-head-with-time plot that uses the same horizontal axis as the profiles.

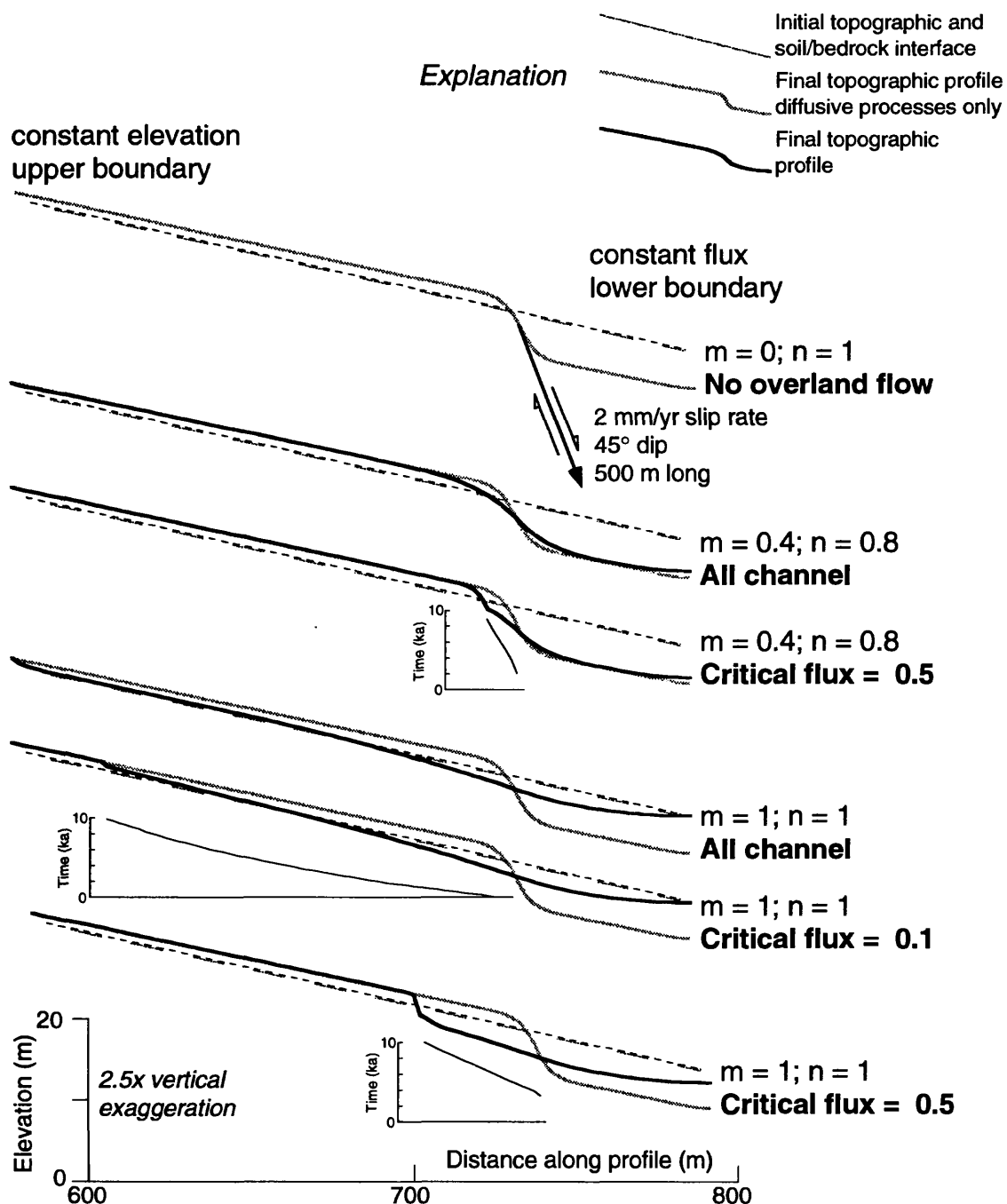


Figure 5. Investigations of the ratio of geomorphic and tectonic displacement rate distributions and the deformation of fluvial terraces. Each set of three plots shows profiles for 1, 5 and 10 ka. The upper profiles result from lower  $\alpha$  and are influenced more by the tectonic displacements. A) Tectonic displacements result from a short and buried thrust fault. B) Tectonic displacements result from a long surface rupturing thrust fault.

156

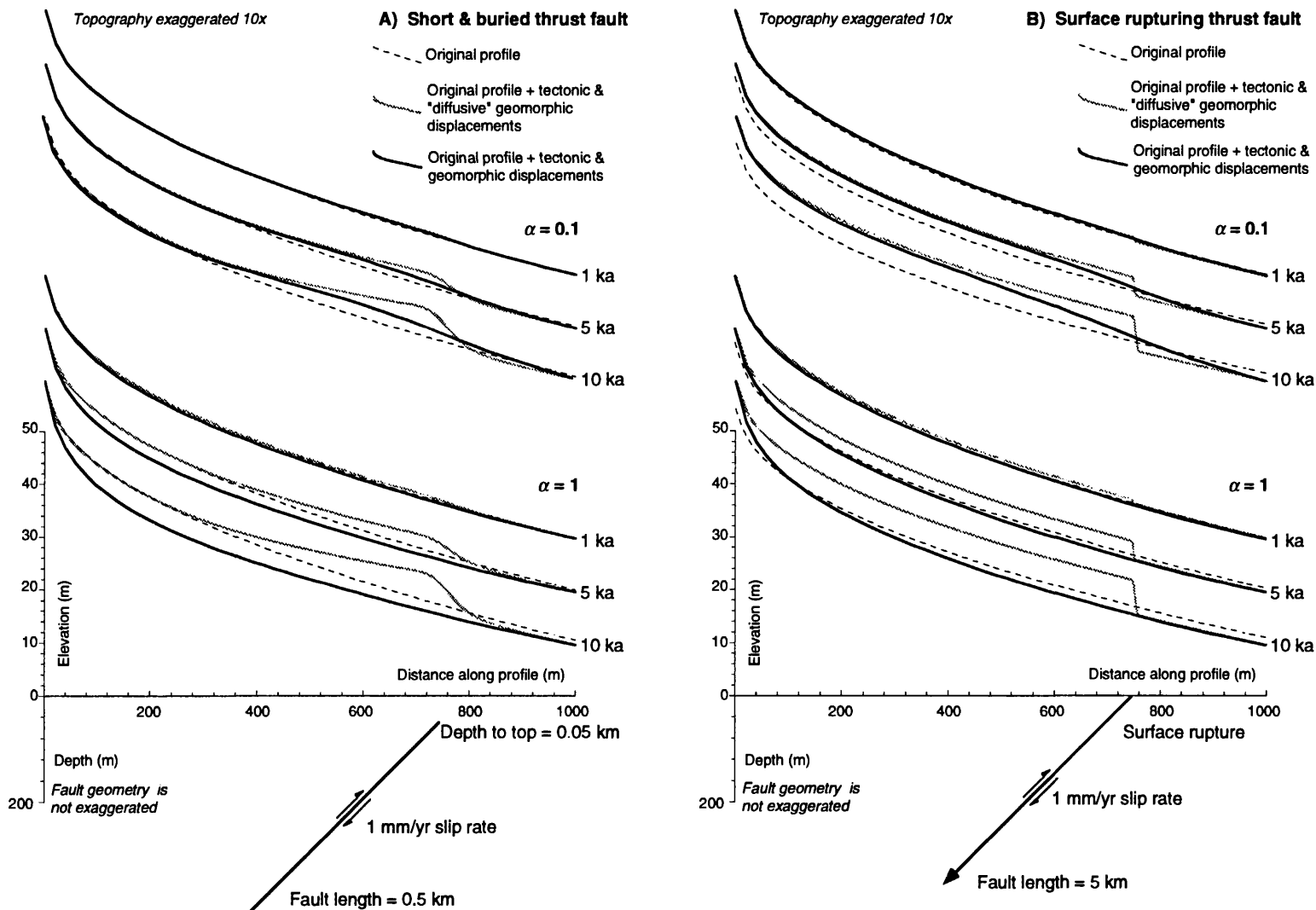
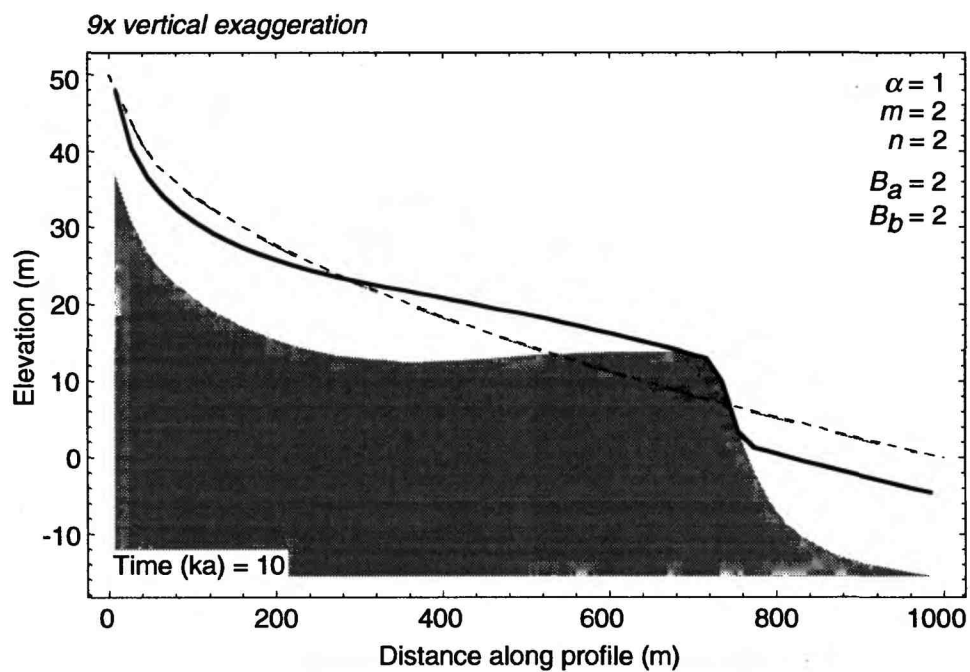


Figure 6. Effect of variable material properties on longitudinal profile development. Parameters are the same as in *Figure 5A* except for 5 mm/yr slip rate along the buried thrust fault. The increased uplift rate caused the material to erode faster than the soil could be produced so bedrock is exposed and conditions are weathering limited for a portion of the profile.



**A COMPREHENSIVE STUDY OF THE EASTERN TENNESSEE SEISMIC ZONE**  
**1434-94-G-2431**  
**Christine A. Powell**  
**UNC Chapel Hill**  
**Department of Geology**  
**CB#3315**  
**Chapel Hill, NC 27599-3315**  
**(919) 962-0705, FAX (919) 966-4519, [cap@geosci.unc.edu](mailto:cap@geosci.unc.edu)**  
**Program Element: 1.2**

**Investigations Undertaken:**

During recent decades, the eastern Tennessee seismic zone has produced the second highest release of seismic strain energy east of the Rocky Mountains. Only the New Madrid seismic zone is more seismogenic. Unlike the New Madrid zone, eastern Tennessee has not experienced a large, destructive earthquake in historic time. The potential for a destructive event in this intraplate region is poorly understood. The eastern Tennessee seismic zone (ETSZ) covers an area of roughly 300 by 50 km (Figure 1). The large, linear extent of the zone and its proximity to a prominent potential field anomaly implies an association with a major crustal structural boundary. This is unique in eastern North America in the sense that no other seismic zone exhibits such a clear spatial association with a major geophysical anomaly. The need to understand and properly assess the hazard associated with seismicity in eastern Tennessee is compelling. Contained within the zone are numerous Tennessee Valley Authority nuclear power reactors and hydroelectric projects, the Oak Ridge National Labs, and population centers including Knoxville and Chattanooga.

The primary goal of the proposed research effort is increased understanding of seismotectonics in eastern Tennessee. Specifically, 1) a crustal velocity model for the ETSZ is being developed using the entire arrival-time data set obtained during the past decade of seismic network monitoring in the region and 2) the apparent association of seismicity with the New York - Alabama (NY-AL) magnetic lineament is being investigated by determining the origin of this prominent potential field anomaly. The results of this effort will greatly improve our understanding of the locations and orientations of rupture surfaces in the ETSZ and will serve as the observational framework needed to develop seismotectonic models and properly assess seismic hazard.

**Results:**

Investigation of crustal velocity structure was initiated by selecting the initial arrival-time data set from the Southeastern United States Seismic Network Bulletins (SEUSSN Bulletins; e.g. Sibol et al., 1992). An initial data base consisting of P and S arrival times from 148 well-located events was obtained with the assistance of M. Sibol and M. Chapman, both at the Seismological Observatory, VPI&SU. Criteria used to select events included a minimum of eight recorded phases, one S phase, and high-quality arrival times as indicated by the original analyst. Events were relocated and a careful analysis was made to distinguish P from Pn. Selected events occur within the study area shown in Figure 2. Development of the final data base is still underway.

Considerable time was devoted to preparation of software for the development of one- and three-dimensional crustal velocity models and for focal mechanism solutions. The inversion technique used was developed by Roecker (1982). Preparation involved 1) testing the inversion code with data sets provided by S. Roecker and with a small, preliminary data set provided by VPI&SU and 2) modifying the code for the specific problem at hand (i.e. retaining information from seismic stations outside of the inversion volume).

One dimensional inversions were performed using a three-layer starting velocity model developed by Moore (1980) for southwestern Virginia. Initially, only stations located above the inversion volume were used. This station-event geometry produced roughly 3,000 raypaths. The inversion technique is iterative. Events are relocated after each iteration and unacceptable events are eliminated. Strict criteria were imposed for retention of events. The inversion stabilized after

three iterations. After the first iteration, thirteen events were eliminated, four were eliminated after the second, and two were eliminated after the third. Resolution was not high in the first (top) layer which extended to a depth of 5.7 km but excellent resolution was obtained in the two lower layers (0.96 in layer two and 0.99 in layer three). Velocity increased in the second layer (depth 5.7 to 14.7 km) by 2.8% relative to the Moore model while velocity decreased in the third layer (depth 14.7 to 50.7 km) by 1.7%. The primary effect on event relocations was to change focal depth. We are now in the process of running three-dimensional inversions and will expand the number of raypaths by incorporating more data from the SEUSSN bulletins and using stations lying outside of the inversion volume.

Investigation of the NY-AL magnetic lineament has been initiated. Potential field data has been collected from various sources (e.g. USGS, TVA) and a consistent data set, suitable for forward and inverse modeling, is being compiled. Preliminary forward modeling of profiles obtained from contours on the TVA aeromagnetic map suggest that the origin for the NY-AL lineament is located below the decollement. This result was anticipated and is consistent with results obtained previously (e.g. King and Zietz, 1980; Hopkins et al., 1994). The implication is that mid-crustal magnetically susceptible sources occur over a tectonically significant distance. Preliminary interpretation of gravity profiles does not support the presence of mafic bodies as the source for the NY-AL lineament. This result is also in agreement with results obtained by Hopkins et al. (1994). Preliminary interpretation of potential field data is encouraging and suggests that it can be used in conjunction with crustal velocity inversions to derive a viable seismotectonic model for the ETSZ.

**Published Results:**

Powell, C.A., Bollinger, G.A., Chapman, M.C., Sibol, M.S., Johnston, A.C., and Wheeler, R.L., 1994, A seismotectonic model for the 300-km long eastern Tennessee seismic zone, *Science*, vol. 264, p. 686-688.

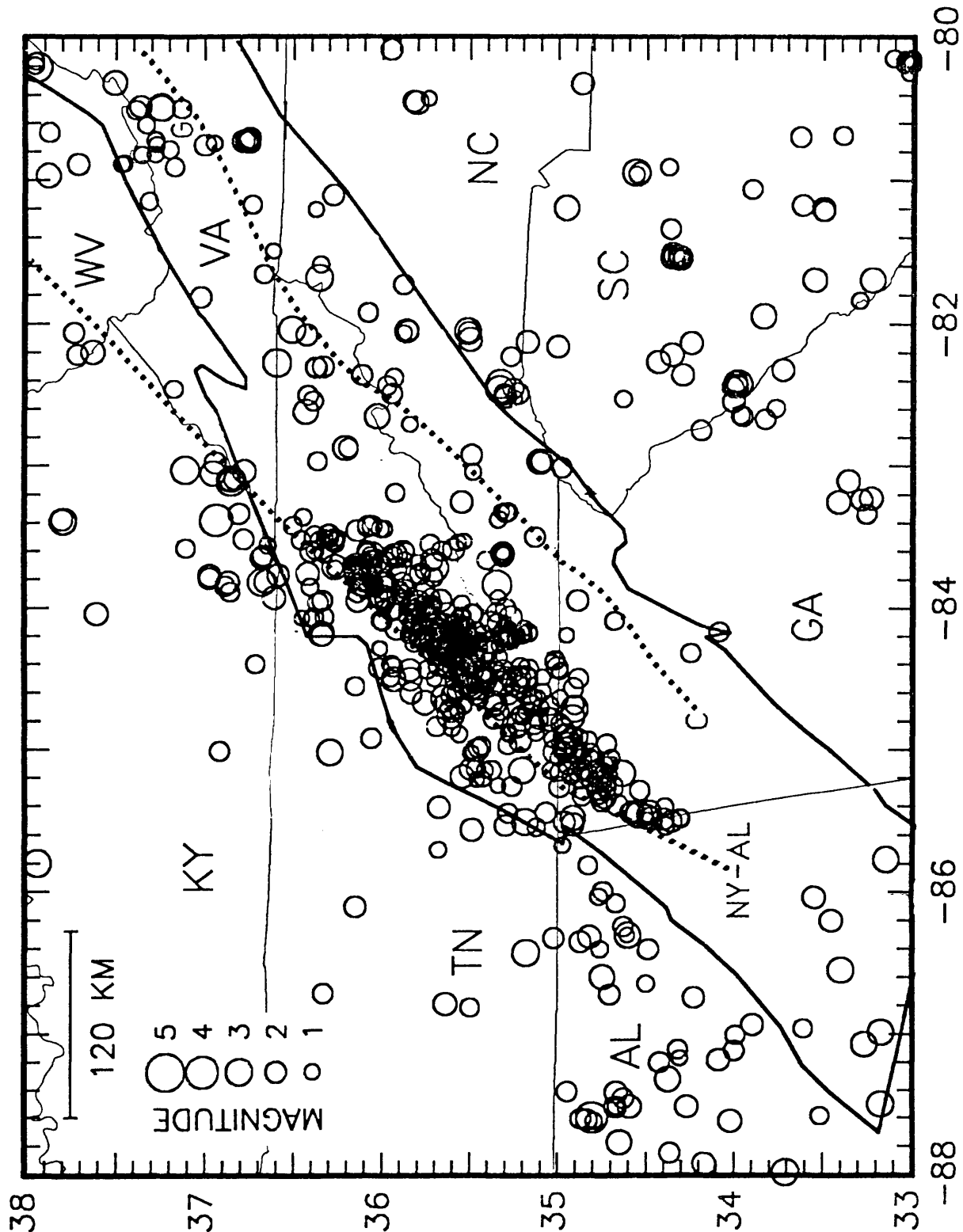


Figure 1 Seismicity in eastern Tennessee and surrounding regions for 1981 - 1992. The ETSZ covers eastern Tennessee and parts of North Carolina and Georgia. The Valley and Ridge and Blue Ridge physiographic provinces are enclosed by the heavy line. The dotted lines indicate the NY-AL and Clingman magnetic lineaments.

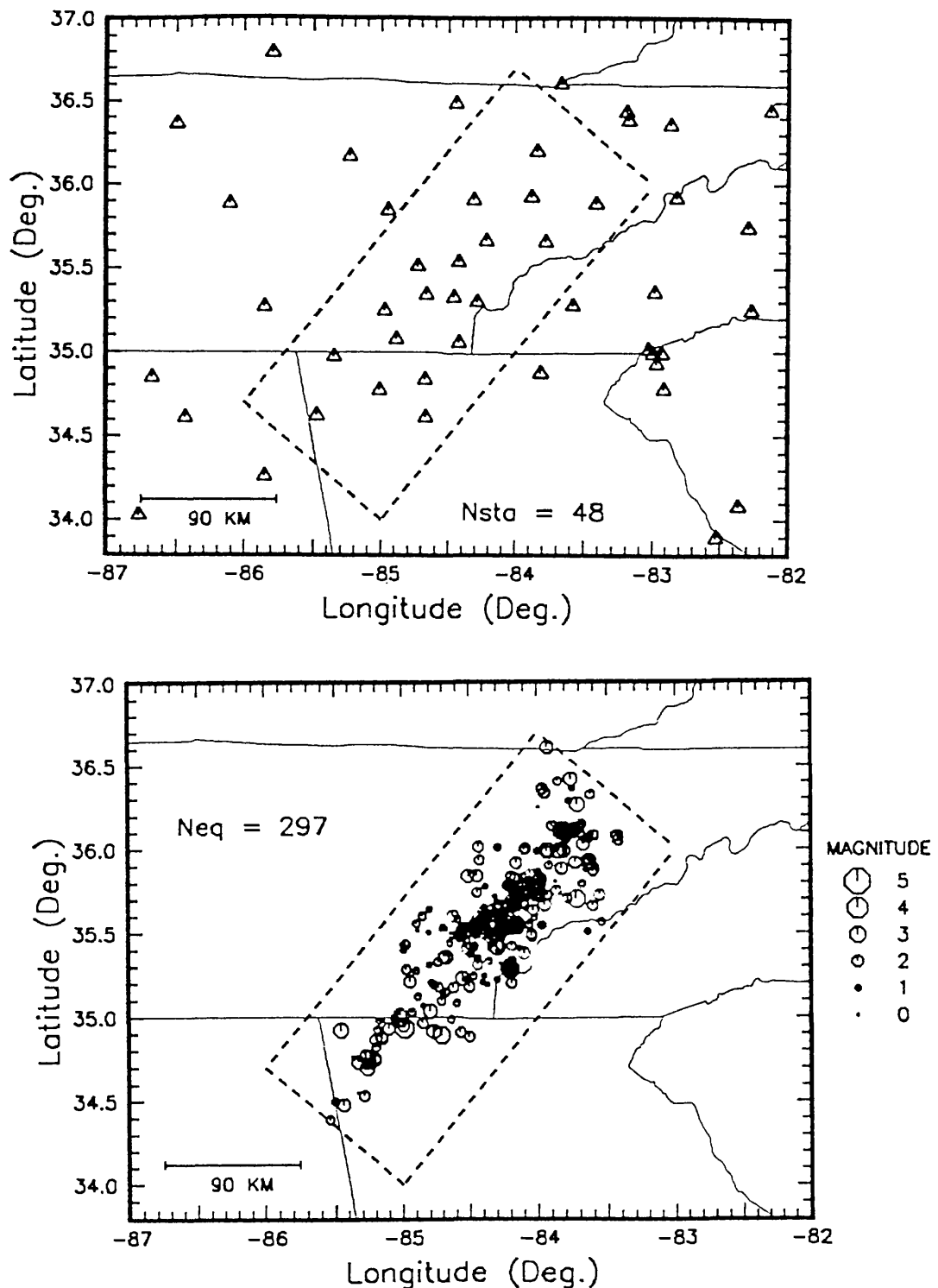


Figure 2 Station location map (upper) showing the approximate network configuration (triangles) for 1983-1990. Epicenter map (lower) showing 297 well located earthquakes reported in the SEUSSN Bulletin for that period. The study area is shown as a dashed box.

## Physical Basis for Seismicity Associated with the Earthquake Cycle and Development of Asperities (grant 14-08-0001-G2450)

James R. Rice (PI) and Renata Dmowska

Department of Earth and Planetary Sciences and Division of Applied Sciences

Harvard University, Cambridge, MA 02138

(617) 495-3445 rice@esag.harvard.edu, (617) 495-3452 dmowska@geophysics.harvard.edu

Program element:

### Investigations:

**1.1** Rheological and tectonic controls on stressing history and seismicity in the outer-rise during the earthquake cycle are being studied. Focusing on the Oaxaca 1978, Mexico, segment, the timing of a recent event near the trench is being used to constrain the rheology of the shallow aseismic part of the thrust interface between the trench and the upper border of the aftershock zone.

**1.2** Slip complexity in repetitive earthquakes is being studied in 3D and 2D fault modeling, with special reference on how the friction law adopted may influence the results. Also, we continue to explore how heterogeneity of fault zones may control earthquake statistics and estimates of future large events.

**1.3** We have studied dynamic fault rupture to understand which type of constitutive laws, loading, and rupture nucleation conditions will lead to propagation in a self-healing Heaton (*Phys. Earth Planet. Int.*, 1990) pulse mode and when, instead rupture propagates in a mode like that of a classical crack. This work has also led to a versatile elastodynamic numerical method, thus far for 2D anti-plane rupture, but which is being extended to 3D problems of rupture along planar faults.

**1.4** Mechanisms of fault weakness are being studied, with particular attention to understanding high-strength but low-toughness mechanisms, particularly including, in recent work, shear heating in a fluid-infiltrated fault zone.

### Results:

**2.1** It is well known that large and great subduction earthquakes are often followed by prolonged periods of tensional seismicity in the adjacent outer-rise. The present work is directed towards understanding what rheological and tectonic controls (shallow mantle viscosity, rheology of the interplate interface, slip in the subduction event, dip of the interplate interface, thickness of the subducting plate, etc.) are influencing periods of occurrence as well as the spatial distribution (e.g., how far from the trench) of such earthquakes.

The case considered here is the central Oaxaca (Mexico) segment that ruptured in  $M_w = 7.8$  on Nov. 29, 1978, followed by a tensional outer-rise event of  $M_w = 6.4$  on July 4, 1994. Along that segment the Cocos Plate, approximately 20 m.y. old, dips at  $14^\circ$  under the North American Plate. The average repeat time of large earthquakes there is  $54 \pm 8$  years (Nishenko, *Pure Appl. Geophys.*, 1991).

Without assuming that the July event ends the tensional seismicity period following the 1978 Oaxaca subduction earthquake, we model in 2D the current earthquake cycle in that segment and investigate the stressing history of the outer-rise under different model conditions.

We assume that tensional outer-rise earthquakes occur only in periods of time when, and in areas where, the tensional stresses caused by the earthquake cycle along the main interplate interface are not decreasing. Our model results indicate that for shallow (0-15 km) outer-rise events occurring near the trench, like the July 1994 event did, the most important factors controlling the stressing history are the dip of the subducting slab and the rheological behavior of the interplate interface between the top of the seismogenic zone and trench. The relevant rheological property for a thin fault zone is  $\eta/h$ , where  $\eta$  is viscosity and  $h$  is thickness. The occurrence of the July event is consistent with  $\eta/\mu h \geq 0.2$  yr/km, and values in the range 0.2 to 0.8 yr/km are acceptable, but not conditions of free slip ( $\eta = 0$ ) there. Here  $\mu$  is shear modulus of the adjoining material.

Somewhat less important for the stressing history of the shallow outer-rise near the trench is the rheology of the underlying asthenosphere; that is more important for locations further from the trench and also for the deeper outer-rise, where, sometimes, compressional events occur. The modeling also indicates that the occurrence of the July event is consistent with a relaxation time of the upper asthenosphere that is not shorter than approximately 5 years.

By assuming that the shallow aseismic part of the thrust interface responds to stress perturbations in the earthquake cycle by stable frictional slip, with Coulomb strength  $\tau = f(\sigma_n - p)$ , with  $f = f_0 + (a - b) \ln(V/V_{plate})$ , we can attempt to relate the  $\eta/\mu h$  range cited above to these parameters. Then  $\eta/\mu h$ , which comes from a linearized rheological model, is to be identified with  $(1/\mu) d\tau/dV = (a - b)(\sigma_n - p)/\mu V$ , or approximately with  $(a - b)(\sigma_n - p)/\mu V_{plate}$ . Assuming  $(\sigma_n - p) = 540$  bars, which is the difference between overburden and hydrostatic pore pressure at the average 3 km depth of the aseismic part of the interface in central Oaxaca,  $\mu = 3 \times 10^5$  bars, and  $V_{plate} = 76$  mm/yr as appropriate for the region, we find that range cited above for  $\eta/\mu h$ , namely, 0.2 to 0.8 yr/km, is consistent with values of  $a - b$  in the range 0.01 to 0.03. That is, in fact, coincident with the experimental range  $a - b = 0.02 \pm 0.01$  shown for serpentine powder by Reinen et al. (*Geophys. Res. Lett.*, 1990, 91) under effective stress of order 500 bars and low slip rates; it is larger than the  $a - b = 0.005 \pm 0.002$  found for granite gouge (Marone and Scholz, *ibid*, 1988; Marone et al., *J. Geophys. Res.*, 1990) under the same conditions.

**2.2.1** Characteristics of repetitive earthquakes on a vertical strike slip fault in an elastic half-space are compared for two friction laws. For both laws the friction coefficient  $f = f_0 + a \ln(v/v_0) + b \ln(v_0 \theta/d_c)$  where  $v$  is slip rate and  $f_0$ ,  $a$ ,  $b$ ,  $v_0$  and  $d_c$  are constants. The laws differ in the evolution of state variable  $\theta$ , and are: (1) The Ruina-Dieterich "slip" law,  $d\theta/dt = -(v\theta/d_c) \ln(v\theta/d_c)$ , in which state evolves only during slip. This law is most often written with  $\psi = \ln(v\theta/d_c)$  so that  $d\psi/dt = -(v/d_c)[\psi + \ln(v/v_0)]$ . (2) The Dieterich-Ruina "slowness" law,  $d\theta/dt = 1 - v\theta/d_c$ , which is a true "ageing" law in that state evolves with time even without slip. Both laws give identical expressions for steady state strength,  $f_{ss} = f_0 + (a - b) \ln(v/v_0)$ , and give identical response for linearized perturbations from steady state.

Predictions are compared for a depth-variable  $a$  and  $b$  distribution over a 24 km thick crust (Rice, *J. Geophys. Res.*, 1993, based on experiments by Blanpied et al., *Geophys. Res. Lett.*,

1991). Slip is imposed at a uniform rate (35 mm/yr) on the portion of the fault below that depth. The modelled region consists of a certain distance along strike (taken variously as 240, 480 and 960 km in cases to be shown) and the calculated slip pattern in that region is repeated periodically along strike. The methodology is that of Rice (1993), including 3D elastostatic stress transfers and a seismic radiation term to limit slip speeds during instabilities. A new explicit numerical method is used. The standard  $a$  and  $b$  distribution noted is given  $\pm 5$  to 10% variations along strike to trigger possible complexity of response.

In all cases considered, simulations based on law (1) show a sequence of large, nearly identical ruptures which span the entire distance modeled along strike and repeat in a nearly periodic manner. Such is consistent with the results of Rice (1993), who used the same law. In contrast, simulations based on law (2) show highly variable rupture lengths that rarely or never span the entire region modelled, and the history of events at any given location along strike is strongly aperiodic. Still, events with length along-strike shorter than about 20 to 25 km, and with depth extent less than the 15 km extent of the "brittle" depth range of the crust, are never observed in the modeling. Following Rice (93) and Ben-Zion and Rice (*J. Geophys. Res.*, 1993; *USGS Redbook*, 1994; *J. Geophys. Res.*, 1995), some representation of geometric disorder of fault zones at smaller scales may be necessary to explain smaller events.

One may not, however, conclude that law (1) can never give complex slip in a continuum fault model; Horowitz and Ruina (*J. Geophys. Res.*, 1989) found complex response using exactly that law, albeit with an added viscous term that prevented large variation in slip velocity.

**2.2.2** A longstanding focus of our studies has been to understand how much of the slip complexity of natural earthquakes be generated by the nonlinear dynamics of stressing and rupture on a smooth fault, and the extent to which the observable geometric disorder of fault zones (step-overs, branching), and perhaps other strong property heterogeneity, is central to the process. We have continued 3D and 2D modeling of earthquake sequences on smooth faults, like in the work just discussed, with numerical models have a well defined limit with refinement of the computational grid. Continuum elastodynamic response is included either approximately by use of a radiation damping term (Rice, 1993), or rigorously in some 2D modeling that involves special choice of parameter ranges and grid density for computational tractability. The rigorous elastodynamic modeling adopts a new spectral numerical formulation with modal convolutions to relate stress and slip histories on the fault (Perrin, Rice and Zheng, manuscript submitted, 1994), but adapts the formulation in such a way that we are able to deal accurately, within a single computational procedure, with long nearly-quasistatic intervals, of order 100 years, between the intervals of a few seconds duration during which inertial and wave effects become significant.

We find that all such smooth fault models as thus far examined fail to produce complex slip sequences like those of realistic frequency-size statistics of earthquakes, at least for events with a maximum rupture dimension that is comparable to or less than the seismogenic depth. Rather, the responses involve sequences of large earthquakes, repeating either periodically or chaotically; the models do not simulate the multitude of small- and intermediate-size earthquakes occurring in nature in the size range smaller than the seismogenic thickness of the crust.

In contrast, Ben-Zion and Rice (1993, 1994, 1995) have shown that models which do approximately incorporate fault zone geometric disorder can produce frequency-size distributions of earthquakes with features that are comparable to observed response. Those models represent

disorder by using over-sized cells in the computational grid, or by adopting classical friction laws without a length scale so that no continuum limit exists and the computational model is "inherently discrete". Such inherently discrete cells of a computational grid may represent arrays of quasi-independent fault segments that are capable of failing independently of one another. The generic response of such inherently discrete models seems to involve self-similar frequency-size statistics for, at least, some range of smaller event sizes.

Our results indicate that, owing to the scaling of stress concentration with rupture size in elastic solids, fault systems with brittle properties (i.e., geometrical irregularities) characterized by a narrow range of size scale can have self-similar frequency-size earthquake statistics only for events smaller than a critical size. In such systems, the statistics of larger earthquakes, sometimes fitting the description of "characteristic earthquakes", are strongly enhanced with respect to the Gutenberg-Richter power law distribution. This is compatible with observations of seismicity along mature fault systems with large cumulative slip and with relatively small number and size of geologically mapped offsets of fault trace per unit length along strike (Wesnousky, *Bull. Seismol. Soc. Amer.*, 1994). On the other hand, when the distribution of fault heterogeneities is characterized by a broad spectrum of size scales, the range of Gutenberg-Richter power law statistics is broad. This is compatible with observations of seismicity along young, strongly disordered, fault systems with more prominent and highly variable offsets along strike, such as the San Jacinto fault in Southern California (Wesnousky, 1994).

**2.3** Guided by observations of short-duration radiated pulses in earthquake ruptures, Heaton (1990) has postulated a mechanism for the frictional sliding of two identical elastic solids that consists in the subsonic propagation of a self-healing slip-velocity pulse of finite duration along the interface. We analyzed such pulses, first as steady traveling waves which move at constant speed, and without alteration of shape, on the interface between joined elastic half-spaces, and later as transient disturbances along such an interface, arising as slip rupture propagates spontaneously from an over-stressed nucleation site. The study was conducted in the framework of antiplane elastodynamics; normal stress was uniform and alteration of it was not considered. We showed that not all constitutive models allow for steady traveling wave pulses: the static friction threshold subsequent to the relocking of the fault must increase with time. That is, such solutions do not exist for pure velocity-dependent constitutive models, in which the stress resisting slip on the ruptured surface is a continuously decreasing function of the instantaneous sliding rate (but not of its previous history or of other measures of the evolving state of the surface). Further, even for constitutive models that include both the rate-and state-dependence of friction, such as the laboratory based constitutive models for friction as developed by Dieterich and Ruina, steady pulse solutions do not exist for versions, like the Ruina-Dieterich "slip" version, which do not allow (rapid) restrengthening in truly stationary contact. For a particular class of rate- and state-dependent laws which includes such restrengthening, we established parameter ranges for which steady pulse solutions exist, and used a numerical method stabilized by a Tikhonov-style regularization to construct the solutions. This class involved a regularized form of the Dieterich-Ruina "slowness" law, written in terms of a time and history dependent strength  $\tau_{\max}$ :

$$\begin{cases} \tau_{\max}(t) = \tau_o + A \ln\{[V_o + V(t)]/[V_{\infty} + V(t)]\} + B \ln[1 + \theta(t)(V_{\infty} - V_o)/L], \\ d\theta(t)/dt = 1 - \theta(t)[V_o + V(t)]/L. \end{cases}$$

Here, slip ( $V > 0$ ) can occur only when stress  $\tau = \tau_{\max}$ ;  $V_o$  is a characteristic speed over which

velocity weakening occurs,  $V_\infty$  is an upper cut-off to velocity dependence, and the contact-time-like variable  $\theta$  has an upper bound of  $L/V_o$ .

The numerical method used for the transient analysis adopts Fourier series representations for the spatial dependence of stress and slip along the interface, with the (time dependent) coefficients in those Fourier series being related to one another in a way which obtains from exact solution to the equations of elastodynamics. This allows an efficient numerical method, based on use of the Fast Fourier Transform in each time step, with the frictional constitutive law enforced at the FFT sample points along the interface. Solutions based on a law that includes restrengthening in stationary contact show that spontaneous rupture propagation will occur either in the self-healing slip pulse mode (but not generally as a steady pulse) or in the classical enlarging-crack mode, depending on the values of parameters which enter the constitutive law. In general, we find that when the speed of the steady, traveling wave, pulse solution which exists under a given set of conditions falls below about  $0.6 c_s$ , then rupture propagation in response to nucleation by a localized stress pulse takes the form of the classical crack mode rather than the self-healing pulse mode. This results suggest that the strictly steady, traveling wave pulse solutions may either be unstable or have a limited basin of attraction. For  $A/B = 0.2$ , the transition from self-healing pulse to crack-like rupture mode occurs as  $V_o$  decreases below a number 0.2 to 0.5  $Bc_s/\mu$ ; the value within that range depends on the load level.

**2.4** Crustal earthquakes seem often to occur under driving stress that is low compared to expectations based on typical rock friction coefficients and hydrostatic pore pressure. Some possible explanations are: (1) Fault *strength* is low due to unusually weak materials or because pore-pressure is elevated well above hydrostatic; (2) Fault strength, at least at the onset of slip, is high but *toughness* is low because strength decreases significantly during rupture, due to strong *velocity weakening* and/or strong *slip weakening* (e.g., Sibson/Lachenbruch/Mase/Smith shear heating of a fluid-infiltrated fault zone); (3) Nonlinear constitutive properties, or heterogeneity of property distributions, outside the fault cause slip to induce a reduction in normal stress near a rupture tip (e.g., a generic nonlinear elastic effect is that simple shear deformation alters normal stress). The recent work on this area has attempted to quantify mechanisms of type (2), particularly shear heating.

A highly simplified first model was used so that pore pressure at any particular place within the fault zone satisfies  $dp/dt = - (p - p_{amb}) / T_p + \tau V / f_0 L_p$ , up to limiting  $p$  values at which hydraulic cracking intervenes, where  $p_{amb}$  is a given ambient pore pressure, typically hydrostatic, in the nearby crust, the constant  $T_p$  is a characteristic time for achieving fluid pressure equilibrium,  $\tau$  is shear stress,  $V$  is slip rate,  $f_0$  is the constant part of friction coefficient in laws like discussed above, and [writing  $\tau = f_0 (\sigma_n - p)$ ] the constant  $L_p$  can be interpreted as a characteristic slip weakening distance over which  $p$  is driven towards normal stress  $\sigma_n$  during rapid slip. Continuing dilatancy during shear alters the model and mitigates or eliminates the weakening. A depth variable strike-slip fault model is then analyzed. This consists of a vertical surface in an elastic half space with slip imposed at a uniform rate below 24 km like in Rice (1993). *Both frictional and creep slippage are allowed, the latter assumed proportional to  $\tau^3$*  and becoming increasingly easy with depth, so that a classical pine-tree strength envelope results.

Ignoring dilatancy and hydraulic cracking limits, results for values of  $L_p$  of order of 2 to 10 mm, and  $T_p = 0.25$  yr, show sometimes chaotic sequences of great earthquakes with negligible

heat generation and slips of order 5 to 15 m. The average stress over 15 km depth at the time of their nucleation is of order 40 to 100 bars, much less than the 1300 bar average of the strength envelope for hydrostatic  $p_{amb}$  (and creep transition below 15 km) over the same depth. However, in versions of the model with hydrostatic  $p_{amb}$ , the ruptures nucleate near the earth's surface where the local stress first reaches the strength. This seems to be unrealistic and suggests that the shear-heating mechanism would have to be complemented with some trigger, perhaps consisting of elevated pore pressure over some isolated patch at depth, to agree with typical earthquake nucleation depths.

## Reports:

- Ben-Zion, Y., and J. R. Rice, "Quasi-Static Simulations of Earthquakes and Slip Complexity along a 2D Fault in a 3D Elastic Solid", in *The Mechanical Involvement of Fluids in Faulting, Proceedings of June 1993 National Earthquake Hazards Reduction Program Workshop LXIII*, USGS Open-File Report 94-228, Menlo Park, CA, 1994, pp. 406-435.
- Ben-Zion, Y., and J. R. Rice, "Slip Patterns and Earthquake Populations along Different Classes of Faults in Elastic Solids", *J. Geophys. Res.*, in press, 1995
- Dmowska, R., G. Zheng and J. R. Rice, "Rheological and Tectonic Controls on Stressing History and Seismicity in the Outer-rise During the Earthquake Cycle: Oaxaca 1978, Mexico, Segment", *EOS Trans. Amer. Geophys. Union*, vol. 75, no. 44, Fall Meeting Supplement, 1994, p. 449.
- Perrin, G., J. R. Rice and G. Zheng, "Self-healing Slip Pulse on a Frictional Surface", manuscript submitted to *J. Mech. Phys. Solids*, 1994.
- Rice, J. R., Y. Ben-Zion and K.-S. Kim, "Three-Dimensional Perturbation Solution for a Dynamic Planar Crack Moving Unsteadily in a Model Elastic Solid", *J. Mech. Phys. Solids*, vol. 42, 1994, pp. 813-843
- Rice, J. R., "Earthquakes at Low Driving Stress in a High Strength, Low Toughness Fault Zone: Shear-Heating Example", *EOS Trans. Amer. Geophys. Union*, vol. 75, no. 44, Fall Meeting Supplement, 1994, p. 426.
- Rice, J. R., "Comparison of Slip Complexity Produced by Two Rate- and State-Dependent Friction Laws", *EOS Trans. Amer. Geophys. Union*, vol. 75, no. 44, Fall Meeting Supplement, 1994, p. 441.
- Segall, P. and J. R. Rice, "Dilatancy, Compaction, and Slip Instability of a Fluid-Infiltrated Fault", *EOS Trans. Amer. Geophys. Union*, vol. 75, no. 44, Fall Meeting Supplement, 1994, p. 425.
- Zheng, G. and J. R. Rice, "Rupture Propagation in Classical Enlarging Crack Mode Versus Short-Duration Heaton Slip Pulse Mode", *EOS Trans. Amer. Geophys. Union*, vol. 75, no. 44, Fall Meeting Supplement, 1994, p. 441.

## Green's functions for an Inhomogeneous Parkfield Model

Grant 1434-94-G-2435  
 J. W. Rudnicki, Mingdong Wu  
 Department of Civil Engineering,  
 Northwestern University,  
 Evanston, IL 60208;  
 (708)-491-3411, (708)-491-8439  
 Fax: (708)-491-4011  
 E-mail: mwu@taml.mech.nwu.edu

### Objectives

Present simulations of the earthquake cycle at Parkfield idealize the San Andreas fault as a vertical plane in a uniform elastic half-space [e.g., Tullis and Stuart, 1992]. But it is well known that the subsurface at Parkfield is not homogeneous. Seismic velocities, and hence elastic moduli at Parkfield increase dramatically with depth and are not the same on opposite sides of the San Andreas fault [Michael and Eberhart-Phillips, 1991a; Eberhart-Phillips and Michael, 1993]. We investigate the effect of nonuniform elastic properties on simulations of the earthquake cycle. Currently, we are doing three-dimensional analysis of fault behavior near the interface of two welded dissimilar elastic half-spaces using a theoretical solution for material nonuniformity [Lee et al., 1987] or quarter spaces using the finite element method. The purposes of these studies are to get a qualitative understanding of the material nonuniformity effect and to help select the mesh size for elaborate finite element calculations for more realistic models.

Michael and Eberhart-Phillips [1991a] have identified subsurface zones of complex seismic velocity variations at Parkfield and near other seismogenic faults in California. They have hypothesized that such features control the locations where earthquake ruptures initiate and terminate. But the physical mechanisms by which bodies of differing elastic properties might influence rupture have not been established. One possibility is that frictional properties are different where these bodies abut the fault surface. Another possibility is that the nonuniform stiffness of the material containing the fault focuses the stress field nonuniformly on the fault. The identification of fault segments that rupture with a characteristic interevent interval is a cornerstone of seismic risk estimation [eg., Working Group on California Earthquake Probabilities, 1988]. Because recent work at Parkfield has shown that the surface fault features thought to delineate such segments [Lindh and Boore, 1981] do not always extend to seismogenic depths [Nishioka and Michael, 1990; Michael and Eberhart-Phillips, 1991b], it is important to investigate other bases for fault segmentation. Ultimately, we will consider the behavior of a fault embedded in a material whose elastic property distribution is consistent with the seismic velocity structure near Parkfield. For this nonuniform medium, we will use the finite element method to calculate the stress state on the fault plane as well as deformation at the surface caused by slip.

### Results

The effect of the material nonuniformity on the perturbation stress field due to slip has been examined by comparing the normal and shear

stresses in the slip plane for various material properties for a model in which a rupture is approximated as a stress drop slip zone (crack) near the interface of two welded dissimilar elastic half-spaces. The two half spaces,  $S_1$  and  $S_2$ , may have different Poisson's ratios,  $\nu_1$  and  $\nu_2$ , and/or shear moduli,  $G_1$  and  $G_2$ , respectively. For simplicity, however, we assume  $\nu_1=\nu_2$  and that the slip zone is parallel to the interface. To simulate an earthquake about the size of a representative Parkfield foreshock, a slip zone 1 km in radius is embedded in  $S_1$  and 1 m from the interface and a uniform shear stress of 10 MPa is applied at great distance from and parallel to the slip zone, while constraining the normal relative displacement across the slip zone to be zero. Michael and Eberhart-Phillips [1991a] have shown that near the epicenter of the 1966 Parkfield earthquake,  $V_p$  at 5 km depth is 20% higher on the southwest side of the fault than on the northeast side of the fault. This suggests that the shear modulus or Young's modulus could differ by as much as 40% at these two locations. Thus, we consider the effects on the post-seismic stress field as the ratio of the shear moduli  $G_2/G_1$  is varied from 1.1 to 1.5, corresponding to a seismic velocity contrast of 10% to 25% across the fault.

The normal and shear stresses in the plane of the slip zone and the relative shear displacement (slip) are calculated using the solution of Lee et al. [1987], developed to analyze cracks in bimaterials. For a Poisson's ratio of 0.25 and an average shear modulus,  $(G_1+G_2)/2$ , of  $3 \times 10^4$  MPa, the average relative displacement across the slip zone varies from 26 to 31 cm, yielding moments varying from  $2.5$  to  $3.0 \times 10^{23}$  dyne-cm. Thus this problem is an idealized representation of a magnitude 5 earthquake, about the size of a Parkfield foreshock. Although the shear stress ahead of the slip zone does not differ significantly from that for the case  $G_2/G_1=1$  (uniform elastic full space), the normal stress ahead of the slip zone no longer vanishes as it does in the uniform medium. For example, the normal stress is about  $5 \times 10^{-2}$  MPa (tension) at 0.2 km ahead of the slip zone's front for  $G_2/G_1=1.5$ . The normal stress becomes larger at locations closer to the slip zone's front. If the slip zone is embedded in  $S_2$  instead of  $S_1$ , the normal stress reverses its sign.

The largest effect is on the normal stress within the slip zone. For  $G_2/G_1=1.5$ , the normal stress is about 4 MPa at 0.1 km behind the front of the slip zone. The average normal stress across the slip zone is about 1.2 MPa. For right-lateral slip in the less stiff half-space, this is a decrease in compressive normal stress across the slip zone, which will reduce its frictional resistance and cause it to slip at a lower stress if loading continues. Conversely, if the slip zone were moved to the stiffer half-space, the fault-normal compression would increase, "clamping" the slip zone so that it would require a higher level of shear stress to re-rupture. Recent laboratory work by Linker and Dieterich [1992] has documented the effects of variable normal stress on the stability of sliding on faults with frictional behavior described by rate and state dependent constitutive models.

The effect of the material nonuniformity on the surface deformation due to slip has also been examined by considering a material consisting of two welded elastic quarter-spaces  $q_1$  and  $q_2$ . Surface displacements

for different ratios of  $G_2/G_1$  are calculated for a point strike-slip source using the finite element method. By choosing the free surface to coincide with the  $xy$  plane and the interface with the  $xz$  plane, the strike-slip source is located at  $(0, 0, d)$  along the  $x$  direction. For the finite element calculations, the problem domain is represented by a finite cubic body with a horizontal length  $L (>>d)$ , a vertical height  $H (>>d)$  and a horizontal thickness  $W (>>d)$ . Thus  $q_1$  and  $q_2$  are represented by two  $LxHx(W/2)$  cuboids. The finite element meshes are constructed so that elements become smaller as the slip is approached. The average diagonal length of the near-field elements is about 1/15 that of the far field elements. A relative slip  $b$  is imposed by specifying the displacement of the dislocation node belonging to  $q_1$  as  $-b/2$  and that belonging to  $q_2$  as  $b/2$ . The far-field boundary conditions are specified by pinching the problem domain at a few selected boundary nodes.

A striking result indicated by the finite element calculations is that the slip induced surface displacement field is very sensitive to the variation of  $G_2/G_1$ . For  $G_2/G_1 \neq 1$ , profiling  $u_x(0,y,0)$  against  $y$  shows that  $u_x$  is no longer antisymmetric ( $u_x(0,y,0) = -u_x(0,-y,0)$  for a uniform half-space), where  $u_x$  is the  $x$  component of the surface displacement field. More specifically, the magnitude of  $u_x$  decreases in  $q_1$  but increases in  $q_2$  when  $G_2/G_1$  increases from unity. For a mesh with 8064 elements and 9406 nodes, for example, the maximum magnitude of  $u_x$  is about 10% larger (smaller) than that for a uniform medium in  $q_2$  ( $q_1$ ) for  $G_2/G_1 = 1.05$ . For  $G_2/G_1 = 1.15$ , the nonuniformity effect is so large that the maximum magnitude of  $u_x$  is increased about 40% in  $q_2$  and is decreased nearly to zero in  $q_1$ . Similar results are observed for other meshes with about the same size. However, because the far-field displacements are somewhat sensitive to the boundary conditions specified at the far-field boundary nodes for all the meshes used, we are now refining these finite element meshes. In addition, we are also carrying out the first- and second-order derivatives on the potentials of Rongved [1955] for a point force in a bimaterial so that the displacements at the plane  $z=0$  can be calculated analytically. By assuming that the free surface effect on the far-field displacements can be neglected for deep sources, we can determine the mesh size for the finite element calculations by comparison between the theoretical and finite element results.

#### References

- Eberhart-Phillips, D., and A.J. Michael, Three-dimensional velocity structure, seismicity, and fault structure in the Parkfield region, central California, *J. Geophys. Res.*, v. 98, 15,337-15,758, 1993.
- Lee, J.C., T.N. Farris, and L.M. Keer, Stress intensity factors for cracks of arbitrary shape near an interfacial boundary, *Eng. Fract. Mech.*, 27, 27-41, 1987.
- Lindh, A.G., and D.M. Boore, Control of rupture by fault geometry during the 1966 Parkfield earthquake, *Bull. Seismol. Soc. Am.*, 71, 95-116, 1981.

Linker, M.F., and J.H. Dieterich, Effects of variable normal stress on rock friction: Observations and constitutive equations, *J. Geophys. Res.*, 92, 4923-4940, 1993.

Michael, A.J., and D. Eberhart-Phillips, Relationships between fault behavior, subsurface geology, and three-dimensional velocity models, *Science*, 253, 1991a.

Michael, A.J., and D. Eberhart-Phillips, Fault geometry at the surface and at seismogenic depth near Parkfield, California, *EOS, Trans. Am. Geophys. Union*, 72, 1991b.

Nishioka, G.K., and A.J. Michael, A detailed seismicity study of the Middle Mountain zone at Parkfield, California, *Bull. Seismol. Soc. Am.*, 80, 577-588, 1990.

Rongved, L., Force interior to one of two jointed semi-infinite solid, *Proceedings, Second Midwestern Conference on Solid Mechanics*, 1-13, 1955.

Tullis, T.E., and W.D. Stuart, Premonitory changes prior to a model Parkfield earthquake, *EOS, Trans. Am. Geophys. Union*, 73, 397, 1992.

Working Group on California Earthquake Probabilities, Probabilities of large earthquakes occurring in California on the San Andreas Fault, *U.S. Geological Survey Open-File Report 88-398*, 1988.

#### Publications

Wu, M., Effect of Material Nonuniformity on Fault Behavior Simulations at Parkfield (Abstract), for presentation at the 1994 AGU Fall Meeting.

# Earthquake source process and tsunami generation in Aleutian-Alaska-Cascadia

Agreement 1434-93-G-2320

Kenji Satake and Larry J. Ruff

Dept of Geological Sciences, University of Michigan  
Ann Arbor, MI 48109  
(313) 764-7385

Program Element 1.1

## Investigations Undertaken

We continued our investigation of earthquakes and tsunamis in the Aleutian-Alaska-Cascadia region. In addition to the four earthquakes (the 1938 Alaska, 1957 Aleutian, 1992 Petrolia, and 1993 Shumagin Islands earthquakes) described in the last year's report (Satake and Ruff, 1994), we studied slip distribution of two great earthquakes (the 1964 Alaskan and 1965 Rat Islands earthquakes) using geodetic and tsunami data. We also calculated the possible tsunami heights from several hypothetical earthquakes in the Cascadia Subduction Zone.

## Results

### 1. 1964 Alaska earthquake

The great Alaskan (Prince William Sound) earthquake of March 28, 1964,  $M_w=9.2$ , ruptured a large area beneath the Gulf of Alaska from southern Alaska to Kodiak Island. The source process has been studied by using seismic waves (e.g., Kanamori, 1970; Ruff and Kanamori, 1983; Christensen and Beck, 1994) and geodetic data (e.g., Holdahl and Sauber, 1994). We made a joint inversion of tsunami waveforms and geodetic data (both vertical displacements and horizontal vectors) to estimate a detailed slip distribution on the fault. Two areas of high slip correspond to seismologically determined areas of high moment release: the Prince William Sound asperity with average slip of 18 m, and the Kodiak asperity with average slip of 10 m. The average slip on the fault is 8.6 m and the seismic moment is estimated as  $6.3 \times 10^{22}$  Nm, or over 75% of the seismic moment determined from long-period surface waves.

### 2. 1965 Rat Islands earthquake

The February 4, 1965 Rat Islands earthquake,  $M_w=8.7$ , was studied by several researchers by using seismic waves (e.g., Wu and Kanamori, 1973, Beck and Christensen, 1991). These studies have identified areas along the rupture zone on which moment release and, by implication, slip was high. These areas of high moment release, or asperities, have been correlated with the tectonic blocks of the western Aleutians.

We invert tsunami waveforms to determine the slip distribution using tide gauge records from Japan, N. America, and the Pacific Islands. We develop a model based on the tectonic structures in the Rat Islands earthquake rupture zone. Our results show a broad area of moment release in the eastern half of the aftershock zone and a smaller area with high slip in the western half. The eastern slip only generally follows the tectonic structures while the eastern slip correlated well with the Near Block where an asperity has been identified. Our results are therefore only partially consistent with the asperity model and we cannot accept or reject the asperity model based on this data.

### 3. Tsunami Heights from Hypothetical Earthquakes in Cascadia Subduction Zone

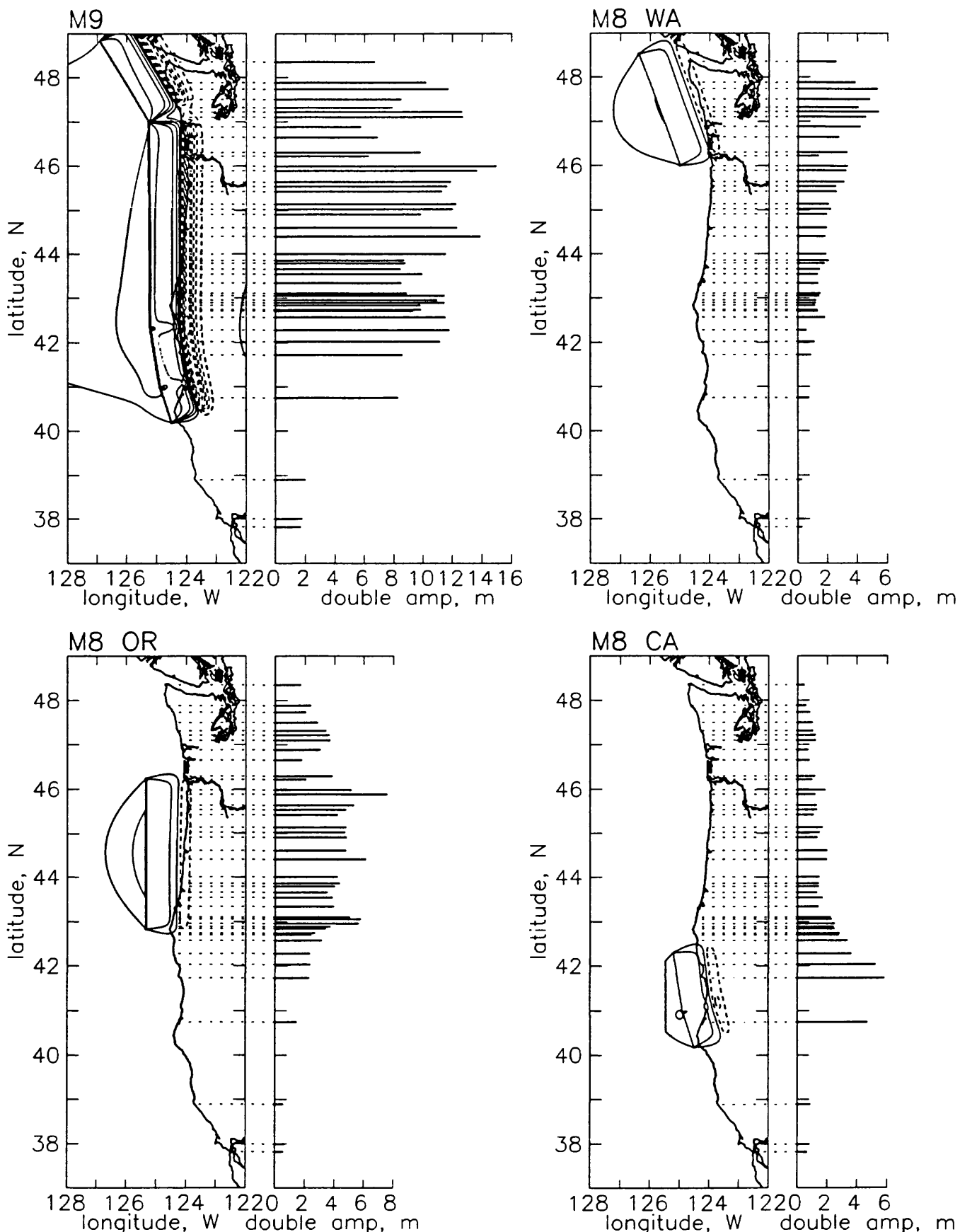
We made numerical computations of crustal deformation and tsunamis from hypothetical earthquakes in order to compare with paleo-seismological data and to estimate the time-space distribution of the subduction earthquakes in Cascadia. We consider four different earthquakes. The case M9 represents a single earthquake rupturing almost the entire Cascadia Subduction Zone, in a way similar to the 1960 Chilean earthquake (slip is 24 m). The cases M8 represent smaller (M~8) earthquakes that rupture smaller segments of the Cascadia Subduction Zone. The case M8 CA is for a segment south of the Blanco Fracture Zone and corresponds to the Gorda plate. The case M8 OR is for a segment offshore Oregon, from off Cape Blanco to off the Columbia River mouth. The Case M8 WA is for a segment offshore Washington, from the Columbia River mouth to near off Vancouver Island. The slip amount for the M~8 events is assumed to be 8 m, which suggests a recurrence interval of 200 to 270 years.

Figure in the next page shows the crustal deformation and tsunami heights along the coast calculated from the four scenario earthquakes. Depending on the fault width, more precisely if the fault extends below the coastline, the coast may be uplifted or subsided. In the above four cases, the northern California coast near Cape Mendocino and the Oregon coast near Cape Blanco are uplifted and other places are subsided, which is consistent with geological observations (e.g. Atwater, 1992). The maximum subsidence is nearly 2 m for the M~8 events and nearly 6 m for the M~9 event.

Generation and propagation of tsunamis are numerically computed using the above crustal deformation as the initial conditions. Finite-difference computations of non-linear shallow water equations are made with a grid size of 1 minute (about 1.6 km). Tsunami heights along the coast are affected by coseismic crustal deformation; the tsunami inundation would be more significant if the coast is coseismically subsided rather than uplifted. Figure shows the double (peak-to-trough) amplitude of tsunamis, which is independent of datum (i.e., not affected by coseismic deformation). To a first order approximation, the plotted heights are similar to run-up heights; detailed run-up calculations would provide more accurate estimations. The tsunami heights from the M9 event are more than 10 m along the Pacific coast of Northern California, Oregon and Washington, whereas an M8 event would cause about 5 m tsunamis in coastal areas facing to the source.

### References

- Atwater, B.F., Geologic evidence for earthquakes during the past 2000 years along the Copalis River, southern coastal Washington, *J. Geophys. Res.*, 97, 1901-1919, 1992.
- Beck, S.L., and D.H. Christensen, Rupture process of the February 4, 1965, Rat Islands earthquake, *J. Geophys. Res.*, 96, 2205-2221, 1991.
- Christensen, D. and S. Beck, The 1964 Prince William Sound earthquake: rupture process and plate segmentation, *Pure and Applied Geophysics*, 142, 29-53, 1994.
- Holdahl, S.R. and J. Sauber, Coseismic slip in the 1964 Prince William Sound earthquake: a new geodetic inversion, *Pure and Applied Geophysics*, 142, 55-82, 1994.
- Kanamori, H., The Alaska earthquake of 1964: radiation of long-period surface waves and source mechanism, *J. Geophys. Res.*, 75, 5029-5040, 1970.
- Ruff, L., and H. Kanamori, The rupture process and asperity distribution of three great earthquakes from long-period diffracted P-waves, *Phys. Earth Planet. Inter.*, 31, 202-230, 1983.
- Satake, K. and L.J. Ruff, Earthquake source process and tsunami generation in Aleutian-Alaska-Cascadia, National Earthquake Hazards Reduction Program, Summaries of Technical Reports XXXV, *U.S.G.S. Open-file Report 94-176*, p.112-114, 1994.
- Wu, F.T., and H. Kanamori, Source mechanism of February 4, 1965, Rat Island earthquake, *J. Geophys. Res.*, 78, 6082-6092, 1973.



**Figure.** Crustal deformation and tsunami amplitudes along the Pacific coast from four scenario earthquakes (M9, M8 WA, M8 OR and M8 CA). The contour interval for ground deformation is 1m (solid curves are uplift and dashed are subsidence).

## Reports Published

### 1. Abstracts

- Johnson, J.M., K. Satake, S.R. Holdahl, and J.M. Sauber, Slip distribution of the 1964 Alaska earthquake from joint inversion of tsunami and geodetic data, *AGU Spring Meeting*, G41B-6 (*Eos*, 75, Suppl. p. 112), 1994.
- Johnson, J.M. and K. Satake, Slip Distribution of the 1965 Rat Islands Earthquake: A Test of the Asperity Model, *AGU Fall Meeting*, S51D-8, (*Eos*, 75, suppl. p. 479), 1994.
- Satake, K., Numerical computation of tsunamis from hypothetical Cascadia earthquakes, *Seismological Society of America, 89th Annual Meeting* (*Seism. Res. Lett.* 65, p.25), 1994.
- Satake, K., Predicting Tsunami Heights for Future Earthquakes in the Pacific Northwest, *AGU Spring Meeting*, S41A-9 (*Eos*, 75, Suppl. p. 236), 1994.
- Satake, K., M.A. Reinhart and J. Bourgeois, A comparison of computed tsunamis with analysis of tsunami deposits for the 300-year-old Cascadia event, SW Washington. *Geological Society of America, 1994 Annual Meeting* (Abstract Volume p. 523), 1994.

### 2. Papers

- Johnson, J.M. and K. Satake, Source parameters of the 1957 Aleutian earthquake from tsunami waveforms, *Geophys. Res. Lett.*, 20, 1487-1490, 1993.
- Johnson, J.M. and K. Satake, Rupture extent of the 1938 Alaska earthquake as inferred from tsunami waveforms, *Geophys. Res. Lett.*, 21, 733-736, 1994.
- Johnson, J. M. and K. Satake, Source parameters of the 1957 Aleutian and 1938 Alaskan earthquakes from tsunami waveforms, Y. Tsuchiya (editor), *Recent Developments in Tsunami Research*, Kluwer Academic Publishers (in press).
- Johnson, J.M., Y. Tanioka, L.J.Ruff, K. Satake, H. Kanamori and L. Sykes, The 1957 Aleutian earthquake, *Pure and Applied Geophysics*, 142, 3-28, 1994.
- Satake, K., J. Bourgeois, and M.A. Reinhart, Tsunami Heights in the Pacific Northwest from Cascadia Subduction Earthquakes, Proceedings of the Workshop on Paleoseismology, *U.S.G.S. Open-file Report 94-568*, p.163-165, 1994.
- Tanioka, Y., K. Satake, L.Ruff and F. Gonzalez, Fault parameters and tsunami excitation of the May 13, 1993, Shumagin Islands earthquake, *Geophys. Res. Lett.*, 21, 967-970, 1994.
- Tanioka, Y., K. Satake and L.Ruff, Seismotectonics of the April 25, 1992 Petrolia earthquake and the Mendocino triple junction region. submitted to *Tectonics*.

# Macroscopic Rheology and Molecular Processes Within Major Strike-Slip Fault Zones: Creep, Compaction, and Elevated Fluid Pressures

# 1434-94-G-2390

Norman H. Sleep

Department of Geophysics, Stanford University  
 Stanford, California 94305  
 (415) 723-0882  
 norm@pangea.stanford.edu

## Investigations

The grain-scale physics of creep within fine-grained rocks at low-temperature hydrothermal conditions within fault zones was investigated. This work is applicable to the depth range of a few to about 20 km where major earthquakes begin on strike-slip faults. At such depths, the coarse-grained country rock is probably elastic on the time scale of earthquake recurrence while the fine-grained material in the fault fault may flow ductily.

This work quantifies the hypothesis by *Sleep and Blampied* (1992) that creep within fault zones leads to compaction and hence transient elevation of fluid pressures. The high fluid pressure reduces the effective normal traction (normal stress minus fluid pressure) on the fault zone. The fault is weakened because earthquake failure (or frictional creep) can then occur at lower shear tractions. Cyclic evolution where the fluid within the fault zone is in equilibrium with hydrostatic pressure in the country rock is possible with this mechanism because frictional slip creates pore space in low-porosity rocks. This allows, fluid pressure to drop below hydrostatic following earthquakes and to increase above hydrostatic as compaction occurs.

The purpose of this project was to investigate physical processes that control the ductile creep rate and hence the compaction rate within fault zones. Two papers discussing our progress to date appear in a special issue of *Pure and Applied Geophysics* on the behavior of fault zones (*Sleep*, 1994; *Sleep and Blampied*, 1994). A paper unifying compaction theory with rate and state theory for time-dependent frictional creep has been submitted to *Journal Geophysical Research* and is currently in review.

## Results

Our most important results involve the grain-scale physics of creep. Significant progress was obtained as proposed in determining the evolution of grain size with time. In addition, a grain-scale unification of ductile creep theory and rate and state frictional theory was obtained.

The evolution of grain-size within a fault zone as a function of frictional slip was investigated. Fault zones theoretical should self-adjust so that some ductile creep occurs. The logic is simple. Fracturing decreases grain size. For example, grains and amorphous material smaller than 10 nm in diameter are produced efficiently within laboratory fault zones (*Yund et al.*, 1990). However, such very small grains have significant surface free energy and thus are more soluble than large grains. In addition, the small grain size increases reaction area and decreases diffusion distances. The small grains dissolve and reprecipitate on large grains—a process called Ostwald ripening. For continuous frictional slip at constant shear traction, an equilibrium is reached when small grains are removed as fast as they are created by fracture. Pressure solution creep is then expected because molecular transport between grains is kinetically efficient.

This reasoning was quantified to obtain the dynamic equilibrium grain size distribution within a continuously sliding fault zone as well as dimensional relationships and numerical equations applicable to grain growth following earthquakes. The viscosity of fine-grained material within a fault zone was obtained from a balance between the energy associated with new grain surfaces created by faults and the free energy released as grains grow by Ostwald

ripening.

For example, The creep rate in fault zones and Ostwald ripening are both likely to be accommodated by pressure solution limited by diffusion along hard load-bearing grain-grain contacts. Then the viscosity for an equilibrium grain size distribution is then

$$\eta = \left[ \frac{12W}{\beta_F \tau_F v_F} \right]^{3/5} \left[ \frac{\sigma RT}{\Xi V_m} \right]^{2/5} \quad (3)$$

where  $W$  is fault zone width,  $\beta_F$  is the fraction of elastic strain release that goes into creating new grain surfaces,  $\tau_F$  is the shear traction on the fault,  $v_F$  is the long term velocity of frictional movement on the fault,  $R$  is the gas constant,  $T$  is absolute temperature,  $V_m$  is molecular volume, and  $\sigma$  is the surface free energy of grain-grain surfaces.

In practice, this theory yielded viscosities appropriate for significant creep at temperatures from 100°C to 300°C. However, predictive constraints on faults zones were not obtained because the relevant physics properties are poorly constrained. In particular, the effective diffusion coefficient  $\Xi$  is proportional the molecular diffusivity of the grain boundary fluid times effective thickness of the grain boundary channel has been measured at relevant conditions only for simple materials like quartz. The rate which grain surface is produced  $\beta_F$  is constrained by experiments for other purposes and it is not clear how these measurements should be extrapolated to low-temperature hydrothermal conditions.

Frictional dilatancy within a mostly sealed fault zone, decreases fluid pressure and increases effective normal stress thus stabilizing preseismic frictional creep (*Lockner and Byerlee, 1994*). To study this effect, we have unified our compaction theory with rate and state theory which is commonly used to model time dependent friction along fault surfaces. We identify the different between a critical porosity for cracks that aids failure and the actual porosity of such failure cracks with the state variable. The rate and state equation for the coefficient of friction is

$$F = F_0 + a (V/V_0) + b \ln(\psi/\psi_0) \quad (4)$$

where  $F$  is the instantaneous coefficient of friction,  $V$  is slip velocity,  $a$  and  $b$  are empirical constants,  $\psi$  is the state variable, and  $V_0$  and  $\psi_0$  are normalizing constants. The evolution equation is

$$\frac{\partial \psi}{\partial t} = \frac{\Delta P}{\eta} - \frac{V\psi}{D_c} \quad (5)$$

where  $t$  is time,  $\Delta P$  is the effective normal stress,  $\eta$  the effective viscosity for closing failure cracks, and  $D_c$  a critical displacement for producing failure crack by frictional dilatancy. In drained ( $\Delta P = \text{constant}$ ) cases, the formalism reduces to traditional rate and state theory (see (*Linker and Dieterich, 1992*, for a review of rate and state theory.) An equation similar to (5) is obtained for porosity that does not significantly affect failure.

Once a fault is sliding rapidly, two additional mechanisms may produce pore space (that can compact slowly until the next earthquake) without immediately locking the fault by decreasing the fluid pressure are evident: (1) Frictional heating during rapid slip leads to elevated temperatures within the fault zone. The pore fluid expands relative to the matrix. An increase in porosity, for example, equal to this expansion would not change fluid pressure. After the earthquake, the fault zone cools to the temperature of the country rock. The pore fluid then contracts relative to the matrix decreasing the fluid pressure. (2) Slip may create isolated voids that do not immediately decrease fluid pressure throughout the fault zone. After the earthquake, fluid within the fault zone drains into these voids decreasing the fluid pressure throughout the zone. The amount of porosity production from both these mechanisms can be constrained by considering energy balances.

### References

- Linker, M. F., and J. H. Dieterich, Effects of variable normal stress on rock friction: Observations and constitutive equations, *J. Geophys. Res.*, 97, 4923-4940, 1992.
- Lockner, D. A., and J. D. Byerlee, Dilatancy in hydraulically isolated faults and the suppression of instability, *Geophys. Res. Lett.*, 21, 2353-2356, 1994.
- Sleep, N. H., Grain size and chemical controls on the ductile properties of mostly frictional faults at low-temperature hydrothermal conditions, *Pure Applied Geophys.*, 143, 41-60, 1994.
- Sleep, N. H. and M. L. Blanpied, Creep, compaction and the weak rheology of major faults, *Nature*, 359, 687-692, 1992.
- Sleep, N. H., and M. L. Blanpied, Ductile creep and compaction: A mechanism for transiently increasing fluid pressure in mostly sealed fault zones, *Pure Applied Geophys.*, 143, 9-40, 1994.
- Yund, R. A., M. L. Blanpied, T. E. Tullis, and J. D. Weeks, Amorphous material in high strain experimental fault gouges, *J. Geophys. Res.*, 95, 15589-15602, 1990.

### Reports

- Sleep, N. H., and M. L. Blanpied, Ductile creep and compaction: A mechanism for transiently increasing fluid pressure in mostly sealed fault zones, *Pure Applied Geophys.*, 143, 9-40, 1994.

- Sleep, N. H., Grain size and chemical controls on the ductile properties of mostly frictional faults at low-temperature hydrothermal conditions, *Pure Applied Geophys.*, 143, 41-60, 1994.

**The Cooperative New Madrid Seismic Network**

Agreement No. USGS 1434-92-A-0968

Robert Smalley, Jr.

Center for Earthquake Research and Information

University of Memphis

Memphis, TN 38152

(910) 678-4929, (901) 678-4734, [smalley@ceri.memst.edu](mailto:smalley@ceri.memst.edu)**Annual Project Summary:**

The Cooperative New Madrid Seismic Network (CNMSN) is being jointly developed by the Center for Earthquake Research and Information (CERI) at University of Memphis (U of M) and Saint Louis University (SLU) to both replace and upgrade the previous Memphis Area Regional Seismic Network (MARSN) and the Central Mississippi Valley Seismic Network. The new network will be fully integrated into the National Seismic Network (NSN). Activity during the past year has concentrated on design and testing of hardware and software to meet the monitoring goals of the network.

The new network will be composed of two complementary components, a dense distribution of ~80 short period seismometers focusing on the most active region of the New Madrid Seismic Zone and a sparser distribution of 15 broad-band seismometers covering a geographically larger area. All stations will be 3-component. The broad-band sensors will provide state-of-the-art digital seismic data for advanced scientific research of topics such as the wave propagation properties of the Mississippi Embayment and the deep structure of the Central U.S. These studies will be important for the estimation of ground shaking in cities such as Memphis and the results will be immediately useful in seismic zoning, development of building codes, etc. Digital broad-band data will be collected at CERI/U OF M through several technologies including satellite telemetry through the USGS NSN and two way digital telemetry using new communication technologies through existing FM radios. Several VSATs have been installed and tested and the parts of the digital telemetry hardware have been tested but still lack integration. The short-period stations have been designed and several prototypes installed. The short-period element of the network will provide high quality location and magnitudes for seismic activity in the

New Madrid Seismic Zone area. These systems will use analog telemetry with a single gain step to increase total dynamic range. The data will be recorded digitally and be available in real-time, which is important to meet the goal of providing timely information about earthquakes to the public and to emergency response services.

We have also continued with the upgrade of the old WWSSN site at Oxford, MS, into an NSN station. This station had been closed for almost 20 years. Data from this instrument are now being sent in real time directly to the USGS in Golden Colorado through a satellite link and "looped" back to CERI over another satellite link.

The last year has seen the finalizing of the short period station design and the testing of prototype units, several of which have been installed. Significant work still remains to be done, but the plan that we are now implementing can be substantially completed by the end of the final year of funding.

**The Southern Appalachian Cooperative Seismic Network**

Agreement No. USGS 1434-92-A-00973

Robert Smalley, Jr.

Center for Earthquake Research and Information

University of Memphis

Memphis, TN 38152

(910) 678-4929, (901) 678-4734, [smalley@ceri.memst.edu](mailto:smalley@ceri.memst.edu)**Annual Project Summary:**

The Southern Appalachian Cooperative Seismic Network (SACSN) is being developed by the Center for Earthquake Research and Information (CERI) at University of Memphis (U of M) and the Seismological Observatory at Virginia Polytechnic Institute and State University (VPI) to upgrade the previous Southern Appalachians Regional Seismic Network (SARSN). The new network will be integrated into the National Seismic Network (NSN). The University of North Carolina at Chapel Hill (UNC) also participates in SACSN through a sub-contract with CERI. Activity during the past year has concentrated on solving telecommunications problems associated with the increased bandwidth for the upgrade of all stations to 3 component instruments, the testing and development of hardware and software, and the purchase and installation of equipment to implement the network.

The design of the new network had several important goals:

- ending dependence on expensive dedicated telephone lines.
- upgrading the network from single component stations to three component stations.
- integration of the new network into the NSN through satellite telemetry.

The new network configuration uses analog telemetry to send the seismic data in real-time to data collection nodes in eastern Tennessee and UNC. The real-time data arriving at UNC will be processed there and the Internet will be used to move triggered data from UNC to CERI. Some of the data from eastern Tennessee will return to CERI over a microwave link between TVA and CERI that has been to be installed and is in the process of being tested. The remaining data from eastern Tennessee will return to CERI by a mix of methods that include the Internet.

Pending solution of the telecommunications problems, the next step is the upgrading of all stations to 3 components. This will be accomplished by using both S-13 1 Hz instruments and L-28 4.5 Hz geophones. A gain ranging analog telemetry system, developed at CERI, will be used to increase the total dynamic range of the network. The total range of the system is over 140 db. The dynamic range within any single gain step is 60 db.

Finally the network will be integrated into the NSN through several satellite communication links (VSAT).

Significant work still remains to be done. There are no new untried technologies in the plan but there will be a large mix of telecommunications technologies. We should have the upgrade basically finished by the end of the final year of funding.

**ANNUAL REPORT ON THE OPERATION AND MAINTENANCE OF THE  
YELLOWSTONE SEISMOGRAPH NETWORK FOR:  
October 1, 1993 to September 31, 1994**

**USGS Cooperative Agreement #1434-92-A-0975.**

Robert B. Smith and Susan J. Nava  
 University of Utah Seismograph Stations (UUSS)  
 Department of Geology and Geophysics  
 University of Utah  
 Salt Lake City, Utah, 84112  
 (801) 581-6274

November 30, 1994

**Investigations**--The Yellowstone seismograph network (YSN) is operated by the University of Utah through a cooperative agreement with the U. S. Geological Survey and is supported under the NEHRP and Volcano Hazards programs with support from the National Park Service (NPS). The Yellowstone network covers the volcanically active Pleistocene Yellowstone Plateau and its 45 km by 70 km, 0.6 Ma caldera including several active scarp-forming Quaternary faults, encompassing more than 10,000 km<sup>2</sup>. The Yellowstone Seismic Network (YSN) operates primarily on land under the jurisdiction of the National Park Service and is a joint operation of the University of Utah--USGS--NPS with support for aspects of the fieldwork in Yellowstone from the NPS. This report covers the third year of a planned 5 yr. upgrade and expansion of the YSN to enhance seismographic coverage of the YNP region. This year, for the first time three-component seismograph stations provided the ability to monitor S wave propagation through the caldera and to provide more uniform coverage of the Yellowstone Plateau and surrounding Quaternary fault zones.

This project provides real-time earthquake surveillance by a newly upgraded and expanded 18-station, single- and three-component, short period seismic network telemetered via four FAA microwave links (via the Sawtelle Peak FAA radar site 20 km west of Yellowstone and at no cost to the project) to Salt City, Utah for digital recording at the University of Utah. The cooperative agreement provides a service to the U. S. Geol. Survey and is not a direct contract for scientific research, although the data are routinely distributed and used for diverse volcanic, earthquake and ancillary investigations by a federal, state, and University users. The cooperative agreement supports the network operations (maintenance, recording and routine data analysis) of the Yellowstone seismograph network. Note that the MS thesis of Doug Miller was supported primarily under a Graduate NSF Fellowship, while data acquisition using the RefTek data loggers, for S wave recording was in part supported by this grant.

The University of Utah produces an on-line catalog of earthquake data and provides map(s) of epicenters, a summary of earthquake information, status of network operations, station maps, a catalog of felt reports of earthquakes (compiled by the NPS), etc. to all interested users. In the event of unusual seismic activity, additional reports and telephone communications summarizing the seismicity. Our primary contacts for such information is our scientific liaison officer, Dr. Dan Dzurisin, USGS Johnson Cascade Volcano Observatory, and the Yellowstone National Park, Superintendent, Research Manager and Public Affairs officers. The U. S. Bureau of Reclamation kindly provides data from the Jackson Lake seismic network for better earthquake locations in the southern part of the YSN. For unusual seismicity outside of the park, we also notify local and state officials as well as the U. S. Forest Service and Bureau of Reclamation officials.

Due to the remote location of most of the Yellowstone stations, helicopter, boat, and horseback support is required. Also because of the very difficult operating conditions with several

meters of snow, temperatures as low as -60° F, and inaccessibility 6 to 8 months per year the network requires highly reliable equipment and telemetry links built to withstand the rigorous conditions.

**Yellowstone Seismotectonics**--More than 16,529 earthquakes of  $0 \leq M_S \leq 6$  have been located by the Yellowstone network from 1973-1981 and 1983-1994<sup>1</sup>. Annual rates of occurrence average ~700 locatable events per year. However, in several cases, intense swarms have produced thousands of correlatable events per month.

Focal depths of earthquakes within the Yellowstone caldera show sharp variations across the caldera. Maximum foci outside the caldera are generally less than 18 km, but within the caldera, foci seldom exceed 5 km. This pattern of shallowing beneath the caldera suggests the presence of a thin upper-crustal seismogenic brittle layer that is considered capable of sustaining  $M < 6$  earthquakes. At depths below ~ km, the crust appears to be in a quasi-plastic ductile state at temperatures in excess of ~400°C, incapable of supporting large stresses owing to high temperatures. The high temperatures are suggested to reflect deeper magma or hot, but solid bodies, related to the Yellowstone volcanism.

**Network Upgrade Accomplishments**--This year was the third year of the planned Yellowstone network upgrade. In the previous two years we concentrated on preparing and upgrading seismograph sites. This year we concentrated on: 1) changing the location of one station, replacing solar panel voltage regulators and batteries at remote telemetry sites, installation of additional solar panels at key sites to provide adequate (>50 watt) power for winter operations and tuning and hardening telemetry links from the FAA Sawtelle Peak site to SLC.

Our 1994 efforts were enhanced significantly by the assignment of National Park Service housing at the Lake Junction ranger station which provided a semi-permanent engineering/work base for our field efforts. Our summer field efforts consisted of a very intense 1.5-month period of hard field work by a two person field team. Early summer 1993 was devoted to ordering and making the necessary equipment for the field implementation. We worked closely with the Yellowstone NPS Center for Resources as well as with the district rangers in selection of sights which represented minimal or no environmental problems.

---

<sup>1</sup>Note that the Yellowstone network was not in operation for 18 months in 1982 and 1983.

Our primary field accomplishments are as follows (see Fig. 1 for seismic station locations, telemetry links, and radio frequencies).

**Table 1. List 1993-1994 Yellowstone Network Equipment Modifications and Upgrades**

Station	Single Battery Upgrade	Double Battery Upgrade	Solar Panel Modification	Other
YWB	x		New 30 watt panel	Installed 2" mast, new seismometer housing, new concrete pad and new UUSS VCO
YFT		x		
YML		x	New 50 watt panel	Installed new transmitter.
YGC		x		Installed 21' mast for relay receivers, mast mounted enclosures for receivers and transmitters, new transmitter, new seismometer housing, concrete pad and new VCO.
YMV	x		New 18 watt panel	Installed new solar panel voltage regulator and new VCO.
YTC				Closed station and reclaimed ground
YTP	x		New 30 watt panel	Replacement station for YTC. New tree mounted antenna, and new VCO.
YHH		x		Changed transmitter from VHF to UHF
YMC	x		New 30 watt panel	New seismometer housing, new concrete pad, and new VCO
YJC		x		New transmitter
YSB				Change site to less noisy location and installed new VCO
YLA		x	New 50 watt panel	Replaced receive antennas and redirected towards Mt. Washburn, new transmitter, new relay receiver, new lightning protection, new seismometer barrel,
YPM		x		Changed transmitter to UHF
YIT	x		New 30 watt panel	New seismometer housing, new VCO
YDC	x		New 30 watt panel	New seismometer housing, new VCO, new antenna mast.
YBE	x		New 30 watt panel	New seismometer housing, new VCO, and new mounted enclosure for transmitter.
Mt. Washburn Relay Site				Replaced one UHF transmitter and antenna for a VHF system, installed new receivers for YLA and YTP.
Sawtelle Peak FAA receive site				Installed two side arm assemblies, reinstalled all VHF antennas on side arms, installed a UHF antenna and installed YMC receiver.

Because of the remote nature of the YSN field work extensive backpacking, horse packing, and helicopter access was required. Our personnel hiked into most sites with NPS horse packing and helicopter transport of the heavy and sensitive electronic equipment. We especially thank the NPS and the personnel at the Sawtelle Peak site for their cooperation and work supporting our operation.

**Yellowstone Seismicity (October 1, 1993-September, 1994)**--Fig. 2 shows the epicenter map for the Yellowstone study area (latitude  $44^{\circ} 07'N$  to  $45^{\circ} 07'N$ , and longitude  $109^{\circ} 40'W$  to  $111^{\circ} 30'$ ) for the  $M_C \leq 4.4$  events located for the Yellowstone recording area during the reporting period, October 1, 1993-September, 1994.

#### Summary of Yellowstone Earthquakes October 1, 1993--September 30, 1994

Number of analyst located earthquakes of  $M_C < 2.0$ : 418  
 Number of analyst located earthquakes of  $M_C \geq 2.0$ : 261  
 Number of analyst located earthquakes of  $M_C \geq 3.0$ : 39  
 Number of analyst located earthquakes of  $M_C \geq 4.0$ : 3  
Total number of located earthquakes 679

**Table of Magnitude 3.5 and Larger Earthquakes in the Yellowstone National Park Region**

Local Date	Local Time	Mag. $M_C$	Location
Jan 1, 1994	2:52 pm MST	3.7	21 m. ENE of Fishing Bridge, WY.
Mar 26, 1994	1:41 pm MST	4.9	10 m. NNW of Madison Junction, WY
Mar 26, 1994	10:37 pm MST	3.6	10 m. NNW of Madison Junction, WY
Apr 5, 1994	1:43 am MDT	3.8	3 m. NNE of West Yellowstone, MT.
Apr 5, 1994	4:03 pm MDT	4.3	3 m. NNE of West Yellowstone, MT.
Apr 29, 1994	11:57 pm MDT	3.7	1 m. SW of Canyon Junction, WY.
May 19, 1994	12:45 pm MDT	3.5	4 m. NW of West Yellowstone, MT.
Jul 3, 1994	10:17 am MDT	3.6	4 m. NE of Tower Junction, WY.
Jul 11, 1994	5:25 pm MDT	3.9	8 m. NNE of West Yellowstone, MT.
Jul 31, 1994	8:45 am MDT	3.8	14 m. S of West Thumb, WY.
Jul 31, 1994	9:03 am MDT	4.0	15 m. SSE of West Thumb, WY
Aug 18, 1994	9:32 pm MDT	3.7	16 m. SSE of West Thumb, WY
Aug 18, 1994	10:04 pm MDT	3.7	9 m. WSW of Old Faithful, WY.
Aug 31, 1994	6:46 pm MDT	3.6	3 m. ESE of Norris Junction, WY.
Sep 24, 1994	9:04 am MDT	4.8	4 m. SSE of Canyon Junction, WY.

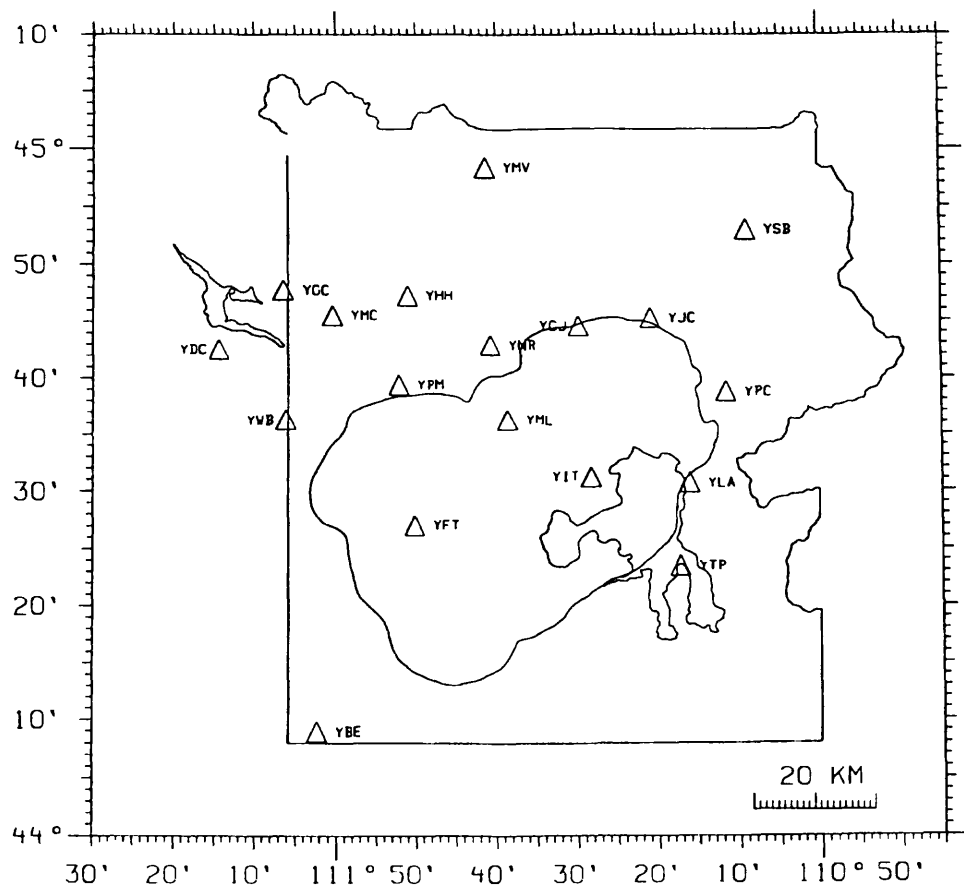
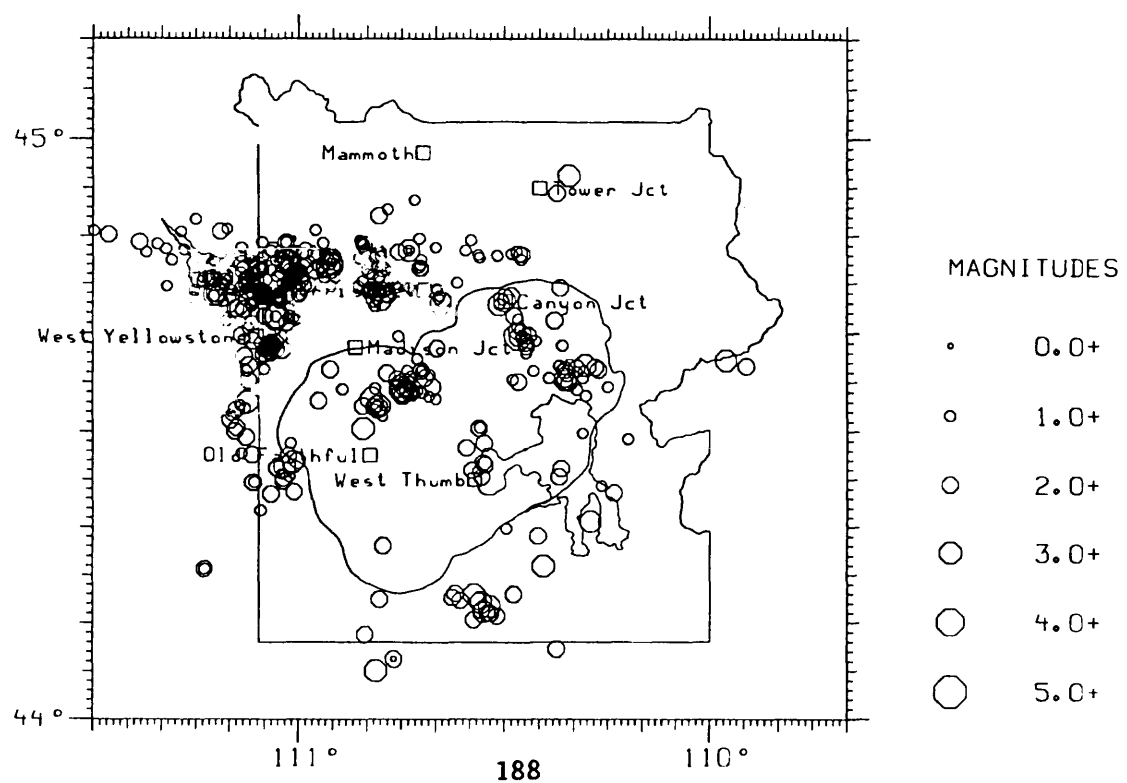
**Reports and Publications Reporting or Substantially Using Yellowstone Seismograph Network Data From The Univ. of Utah**

- Lowry, A. R. and Smith, R. B., 1994, Elastic thickness and earthquake focal depth, *Eos, Trans. Amer. Geophys. Un.*, 75, no. 14, Supplement, 445.
- Miller, D. S. and R.B. Smith, 1994, Three-dimensional velocity structure of the Yellowstone Plateau from local earthquake tomography, *Seismol. Res. Lettrs.*, SSA 89th Ann. Meeting, Pasadena, Calif., 65:57.
- Nava, S. J., W. J. Arabasz, J. C. Pechmann and Smith, R. B. 1994, Status and developments in data distribution and exchange—University of Utah Regional Seismic Network, *Eos, Trans. Amer. Geophys. Un.*, 75, no. 14, Supplement, 430.
- Smith, R. B. and L. W. Braile, 1993, Topographic signature, space-time evolution, and physical properties of the Yellowstone-Snake River Plain volcanic system: the Yellowstone hotspot, in A. W. Snare, J. Steidtmann, and S. M. Roberts, editors, "Geology of Wyoming", Geological Survey of Wyoming Memoir No. 5, p. 694-754.
- Smith, R. B., and L. W. Braile, 1994, The Yellowstone Hotspot, in *J. Volcanology and Geotherm. Resesearch*, eds. D.P. Hill, P. Gasparini, S. McNutt and H. Rymer, H., 61:121-188.
- Smith, R. B. and A. M. Rubin, 1994, Rapid reversal of uplift to subsidence at the Yellowstone caldera by magmatic processes image by earthquakes, *Seismol. Res. Letters, Abstracts*, 89th Annual Meeting, *Seismol. Soc. Am.*, v. 65, no. 1, 56.
- Smith, R. B., C. M. Meertens, A. M. Rubin and N. M. Ribe, 1994, Active tectonic processes of the Yellowstone hotspot imaged by topography, earthquakes and GPS, *Geol. Soc. Amer., Abstracts With Programs, Annual Meeting*, v. 26, no. 7, A-313.
- Smith, R. B., D. S. Miller, and C. M. Meertens, 1994, Active tectonics of the Yellowstone hotspot imaged by earthquakes and GPS, *Eos, Trans. Amer. Geophys. Un.*, 75, no. 14, Supplement, 65.

**Figure 1**

## Yellowstone Seismic Network, 1994

I-N

**Figure 2**Yellowstone Seismicity  
October 1, 1993 - September 30, 1994

## THE SOUTHERN APPALACHIAN COOPERATIVE SEISMIC NETWORK: VIRGINIA TECH COMPONENT

Agreement No. 1434-92-A-0971

J. A. Snoke, M. C. Chapman, and M. S. Sibol  
Virginia Tech Seismological Observatory  
Virginia Polytechnic Institute and State University  
Blacksburg, Virginia 24061-0420  
(703) 231-6729

### OBJECTIVES

A major goal of this 1991-1994 cooperative project involving Virginia Tech, University of Memphis, the Tennessee Valley Authority (TVA), and the University of North Carolina at Chapel Hill (UNC) is to provide modern instrumental coverage of seismicity in the southern Appalachians. Stations of the Virginia Tech and University of Memphis networks are being upgraded with three-component sensors, high dynamic range electronics, and radio telemetry. Incorporation of the TVA and UNC networks will bring on-line the fully integrated Southern Appalachian Cooperative Seismic Network (SACSN). Calibrated digital waveform data recorded by each SACSN member institution network will be made available in near real-time via the Internet to the other member institutions and the general seismological community. This cooperative regional network is scheduled to be integrated into the U. S. National Seismic Network.

Research objectives for the SACSN are focused on seismic activity in the southern Appalachian region (Figure 1). Research areas include earthquake monitoring (in part to maintain continuity of earthquake catalogs), seismic hazard assessment, studies of the seismotectonics of the region, earthquake source studies, wave propagation at local and regional distances, crustal structure studies, and the temporal/spatial behavior of seismicity. Service objectives of the SACSN include the publication of an annual seismicity bulletin for the southeastern United States; the development and maintenance of regional earthquake catalogs; and informational service to federal/state/local governments, the engineering community, and the general public.

This report summarizes only the Virginia Tech portion of the SACSN project.

### NETWORK OPERATIONS

#### Current Status:

For the past several years, Virginia Tech has operated a calibrated network comprised currently of ten short-period stations (Figure 2). The telemetry is analog, mostly via phone lines, to the data collection center on the Virginia Tech campus in Blacksburg (near BLA; Figure 2). Each channel is then digitized by a 12-bit sampler at a rate of 100 sps. The effective dynamic range of the entire system is approximately 40 dB. The Giles County subnetwork consists of six stations (3 three-component stations), and the central Virginia subnetwork has four stations (1 three-component station).

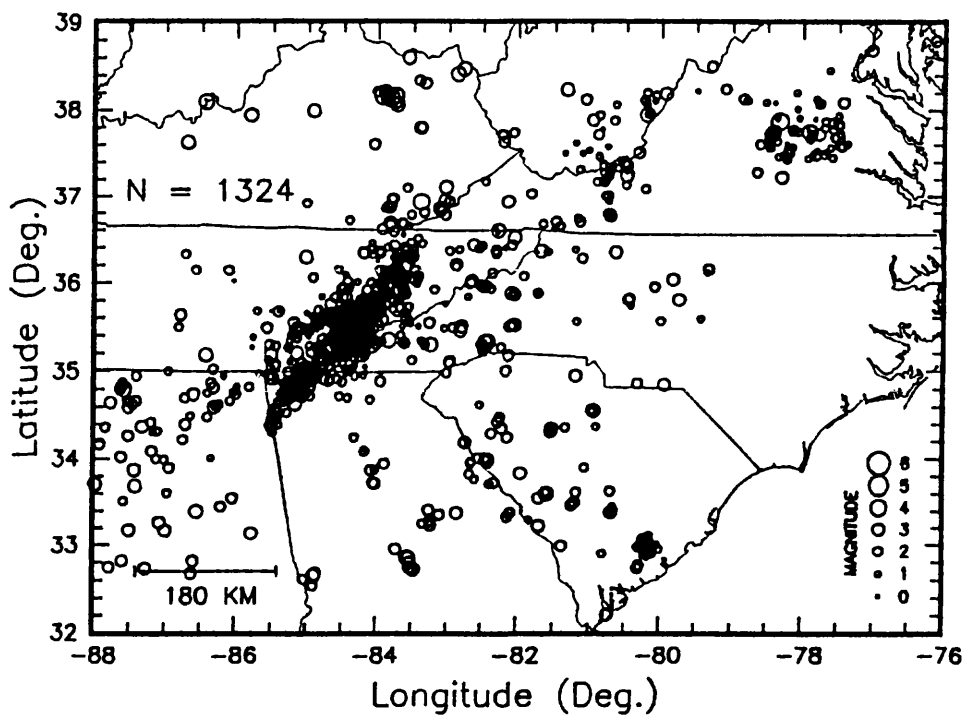
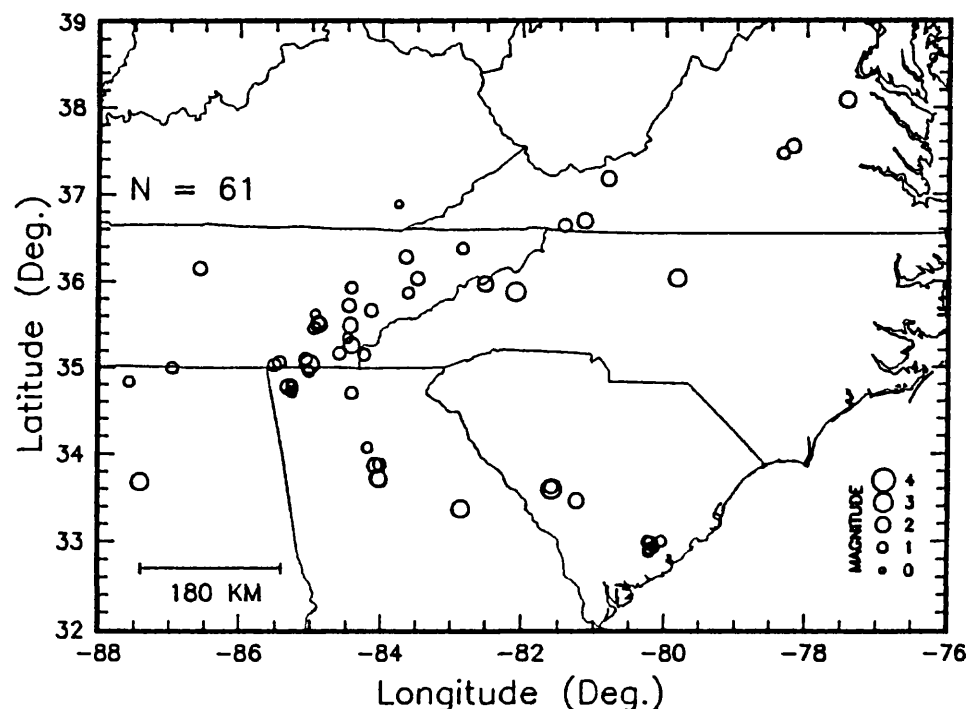


Figure 1. (Upper) Epicenters for 1993 earthquakes reported in Southeastern U. S. Seismic Network Bulletin 28. (Bottom) Epicenters for earthquakes during the period July 1977 through December 1993.

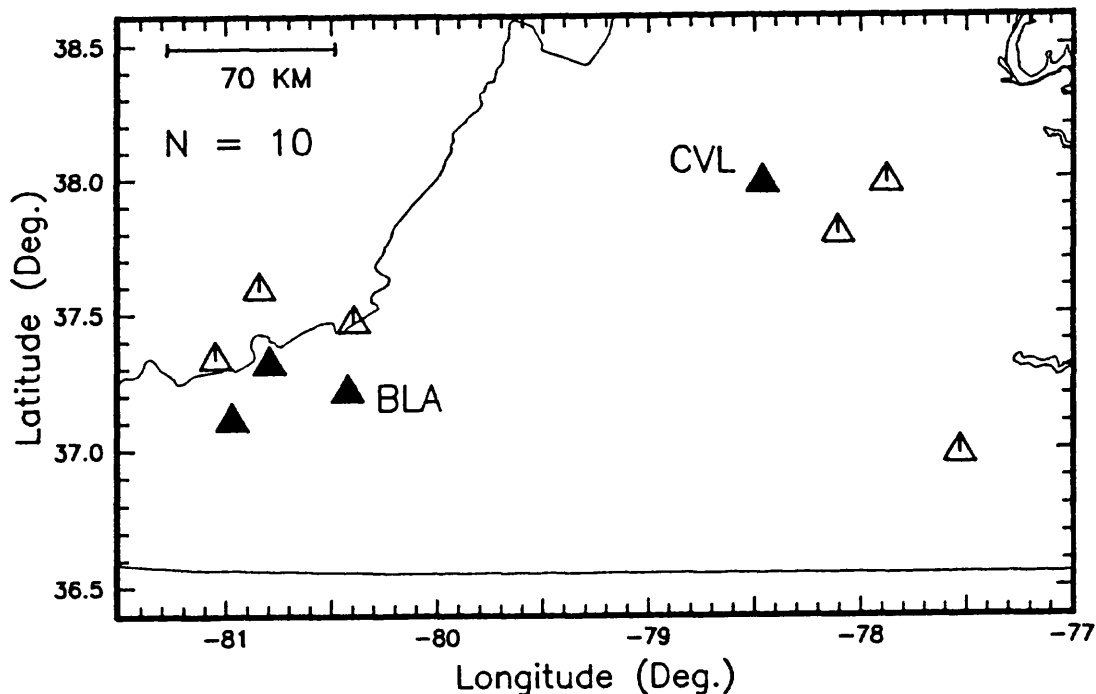


Figure 2. Current configuration of the Virginia Tech seismic network (solid triangles are three-component stations). The Giles County subnetwork is in western Virginia and southern West Virginia. The central Virginia subnetwork is the more diffuse cluster of stations in the central portion of Virginia. The upgraded network configuration will be approximately the same as shown here, except for one additional station in the central Virginia subnetwork, and with three component sensors at all stations. BLA and CVL are near the data collection nodes for the upgraded network.

An anonymous ftp account and a gopher server have been established for providing access to waveform data recorded by Virginia Tech. Special waveform data sets recorded by the network and/or the high dynamic range six-component GSE seismograph system at BLA, can be accessed. In addition to the special waveform data sets, triggered event files from the digitizing system are put on the anonymous ftp account within 20 minutes of the trigger time. A description of how to access waveform files, calibration files, and other information, was published in *Southeastern U. S. Seismicity Bulletin 28* (July 1994).

The U. S. National Seismic Network station has been installed at BLA (Blacksburg, Virginia). Digital data from surface broadband instruments are now available. Downhole broadband instruments are scheduled to be installed in December 1994.

#### Network Upgrade:

The upgraded network will have 11 stations (six in the Giles County subnetwork and five in the central Virginia subnetwork) with essentially the same

configuration as existed prior to the upgrade. All stations will have three-component sensors, 24-bit field digitizers (REF TEK model 72-07A), and radio telemetry to transmit digital data back to one of two collection nodes. Data from the Giles County subnetwork will be collected in Blacksburg, and data from the central Virginia subnetwork will be collected at the Virginia Division of Mineral Resources in Charlottesville (near CVL; Figure 2). The Charlottesville and Blacksburg data collection nodes will be connected using the Internet. New three-component sensors for the Giles County subnetwork have been installed and will be operating when the upgrade for that subnetwork is completed at the end of calendar year 1994. The central Virginia subnetwork upgrade will take place when funds become available.

## RESEARCH

### Probabilistic Seismic Hazard Assessment:

A comparison of probabilistic seismic hazard estimates for the Giles County, Virginia, area was made using two models for fault rupture in the seismic zone. The source was envisioned as a 40 km long, vertical fault. Hazard was calculated at the 475 and 2373 year return period levels, for 1 and 5 Hz oscillator PSRV response. The first of the two fault models was a simple line source, assuming that earthquakes occur as point sources at a constant depth on the fault plane. The other, more complex, model is similar to the fault-contained rupture model described by Bender (1984). In this case, the earthquakes were modeled as finite ruptures, with areas determined from the Brune (1970) source model, as a function of moment and stress drop (specified as 100 bars). The thickness of the brittle crust was assumed to be 25 km, and the fault length was specified from the source model by determining a rectangular fault rupture with equivalent circular area, given a specified aspect ratio (length/width). In both cases, ground motion prediction was made using the model of Atkinson and Boore (1990) for rock site condition in eastern North America.

The results show that the finite rupture model produces an increase in the ground motions associated with a given hazard level, relative to those calculated using the simple line source. The degree of this relative increase depends on the chosen return period, oscillator frequency, and site location. The general trend is for the difference to be greatest for low frequency oscillators located near the center of the fault at the longer return periods. In detail, for 1 Hz oscillators at the 2373 year return period, an increase in ground motion of 50-60% occurs for sites near the center of the fault. This decreases to 30-40% for sites near the ends of the fault. For the 475 year return period, 1 Hz oscillator response levels increase by only 10-20% for sites near the fault center and by less than 10% at the ends of the fault. For 5 Hz oscillators, the difference between the results of the two models is as follows. At the 2373 year return period: 30-40% at the fault center; 20-30% at the ends. For the 475 year return period: 20-30% at the center, 10% at the ends.

### The August 6, 1994, Eastern North Carolina Earthquake:

A small earthquake occurred in coastal North Carolina on August 6, 1994, at 19:54:11.1 UTC. The epicenter, determined from arrival times at 11 stations, is 35.1°N, 76.8°W. The NEIC reported the magnitude as 3.6 mb(L<sub>g</sub>). Although the shock was recorded by stations at regional distances in North Carolina, South Carolina, and Virginia, the nearest station (CEH - Chapel Hill, NC) is at a distance of 227 km. The

instrumental epicenter of the shock is uncertain by several kilometers, and the depth is unconstrained.

The earthquake is the first to have occurred in the North Carolina Coastal Plain since regional network monitoring began during the mid 1970's. It was felt over an area of 24,000 km<sup>2</sup>. Intensity effects reached V MM in and near the towns of New Bern and Washington. The intensity data, obtained from responses to requests for information published in local newspapers, establishes the epicenter of the shock approximately 20 km to the north of the instrumentally determined epicenter, close to a large phosphate mine. The open-pit mining operation pumps 30-40 million gallons of water per day from wells penetrating the Castle Hayne formation which is competent limestone at a depth of less than 200 m. The macroseismic epicenter is within the 5000 km<sup>2</sup> groundwater cone of depression, suggesting the possibility of induced seismicity.

The instrumental data at the closer stations are remarkable for their large spectral amplitudes at the higher frequencies. At CEH, the displacement amplitude spectrum of the L<sub>g</sub> phase (uncorrected for attenuation) is essentially flat throughout the bandwidth of the recording system, from less than 0.5 Hz to greater than 12 Hz. Path correction of data from CEH and stations in the central Virginia network at distances less than 300 km indicate a source spectrum greatly enhanced at the high frequencies (>10 Hz), relative to a "standard"  $\omega^{-2}$ , 100 bar stress drop source model. The high frequency spectral amplitudes as well as the absence of R<sub>g</sub> surface waves suggest a focus in the Paleozoic basement rock, well below the shallow aquifer in the overlying Tertiary Coastal Plain sediments. However, the fact that the event was very audible as an explosive sound near the epicenter points toward a shallow source. At this time, the possibility that the shock was induced cannot be ruled out.

## SERVICE

The *Southeastern U. S. Seismicity Bulletin* 28 for calendar year 1993 was distributed this past July to over 200 institutions and individuals. There were 78 tectonic (i.e., non-reservoir related) earthquakes reported in the Bulletin for 1993 (Figure 1). The current southeastern U. S. catalog now includes 1348 tectonic earthquakes and 691 reservoir-related events for the period from July 1977 through December 1993 (Figure 1). The largest 1993 shock was on 8 August near Aiken, South Carolina ( $mb(L_g) = 3.2$ ,  $I_0 = V$ ). In addition to reporting the usual hypocentral parameters, magnitudes, etc. for the report period, the Bulletin included a report on the Aiken earthquake, a report on a sequence of 20+ small (magnitudes  $\leq 2.8$ ) but strongly felt ( $I_0$  up to V) earthquakes near Columbia, Maryland, a summary of a county-by-county probabilistic seismic hazard analysis of Virginia, a report on strong motion instruments in the region, and an abstract on seismic wave attenuation in Florida. A description of how to access digital waveform data at Virginia Tech via anonymous ftp over the Internet has become a regular feature of the Bulletin, and it is planned that future Bulletins will contain similar information from other contributors. Contributors to the Bulletin 28 included:

- Charleston Southern University,
- Delaware Geological Survey,
- Georgia Institute of Technology,
- Maryland Geological Survey,
- Tennessee Valley Authority,
- National Earthquake Information Center,

- University of Florida,
- University of Memphis (formerly Memphis State University,
- University of South Carolina,
- Virginia Department of Mines, Minerals and Energy,
- Virginia Tech, and
- Westinghouse Savannah River Company.

Two members of the VTSO staff were invited by the U. S. Geological Survey to present research results at the Northeastern U.S. Seismic Hazard Workshop at Lamont-Doherty Earth Observatory on August 2-3, 1994. Matthew Sibol presented his work on converting epicentral intensity and felt area data to magnitude, and Martin Chapman presented his work on a probabilistic seismic hazard assessment for Virginia.

Virginia Tech is also in the process of providing the Virginia Department of Environmental Quality and various engineering firms information necessary to evaluate siting permits.

## RELATED PUBLICATIONS AND REPORTS

- Chapman, M. C., and F. Krimgold (1994). *Seismic Hazard Assessment for Virginia*, Virginia Tech Seismological Observatory, Blacksburg, VA, 62 p.
- Chapman, Martin C. (1994). Seismic hazard estimates for Giles County, Virginia: comparing a magnitude dependent finite rupture model with a simple line source, 66th Meeting of the Eastern Section of the Seism. Soc. of Am., Oct. 16-18, 1994, Columbia, South Carolina (abstract).
- Chapman, Martin C., Christine A. Powell, and Ginger Castle (1994). The August 6, 1994 coastal North Carolina earthquake: large high-frequency spectral amplitudes from an event in a region of low seismicity, 66th Meeting of the Eastern Section of the Seism. Soc. of Am., Oct. 16-18, 1994, Columbia, South Carolina (abstract).
- Chapman, M. C. (1995). A probabilistic approach to ground motion selection for engineering design, *Bull. Seism. Soc. Am.*, accepted for publication.
- Sibol, M. S., M. C. Chapman, and E. C. Mathena (1994). *Appendix A: Bibliography*, in Chapman, M. C., and F. Krimgold (1994). *Seismic Hazard Assessment for Virginia*, Virginia Tech Seismological Observatory, Blacksburg, VA, 62 p.
- Sibol, M. S., M. C. Chapman, and E. C. Mathena (1994). *Appendix B: Seismic History of Virginia by County*, in Chapman, M. C., and F. Krimgold (1994). *Seismic Hazard Assessment for Virginia*, Virginia Tech Seismological Observatory, Blacksburg, VA, 62 p.
- Sibol, M. S., J. A. Snoke, and E. C. Mathena (1994). *Southeastern U. S. Seismic Network Bulletin No. 28*, Virginia Tech Seismological Observatory, Blacksburg, VA, 71 p.

## REFERENCES CITED

- Atkinson, G. M., and D. M. Boore (1990). Recent trends in ground motion and spectral response relations for eastern North America, *Earthquake Spectra*, 6, pp. 15-35.
- Bender, Bernice (1970). Modeling source zone boundary uncertainty in seismic hazard analysis, *Bull. Seism. Soc. Am.*, 76, pp. 329-341.
- Brune, J. N. (1970). Tectonic stress and the spectra of seismic shear waves from earthquakes, *J. Geophys. Res.*, 75, pp. 4997-5009

## **Earthquake Hazard Research in the Greater Los Angeles Basin and Its Offshore Area**

**Agreement # 14-08-0001-A0620**

**Ta-liang Teng and Thomas L. Henyey**  
**Department of Earth Sciences**  
**University of Southern California**  
**Los Angeles, CA 90089-0740**  
**E-mail: lteng@coda.usc.edu**

### **Program Element: Seismic Networks**

**INVESTIGATION UNDERTAKEN:** The Los Angeles Basin Seismic Network (LABNET) is a principal participant in the monitoring and subsequent field study of the 1994 Northridge earthquake. Data output of LABNET contributes significantly to the location and fault-plane solutions of the mainshock and the long aftershock sequence. As one of the regions in the U.S. subject to a high potential for earthquake loss, the Los Angeles area warrants the close attention of a special-purpose seismic monitoring network -- one which can cope with the high background noise problem in a coastal urban area. This objective is achieved through the deployment of 3-component downhole and surface seismometers, through a diligent field instrument maintenance program, and through data processing making use of up-to-date software and velocity information derived from active research. Presently, the LABNET at USC digitizes 65 channels of telemetered data from land (surface and downhole) and offshore island stations. Data from this network is transmitted in realtime to the Southern California Seismic Network (SCSN) at Caltech/USGS, where it becomes a critical part of routine earthquake locations and information for the greater Los Angeles urban area. Data from the network stored at USC also serves as an important backup to the SCSN operation at Caltech for events in the Los Angeles urban area. This network is also an important part of the research activity coordinated by the Southern California Earthquake Center (SCEC), and the network output enters the SCEC database at Caltech from which data can be accessed by investigators easily through a FTP procedure.

**RESULTS:** The principal tasks accomplished are:

- (1) Operate a high-performance special-purpose network and obtain broadband on-scale seismic data necessary for earthquake hazard reduction studies in the greater Los Angeles basin and its offshore area. Figure 1 shows the events recorded and located by LABNET during the current reporting period; Figure 2 shows events from the last reporting period. Figure 3 is a LABNET station map, with single-component and 3-component stations indicated by different symbols given in the insert. Signal channels from the USGS/CIT SCSN are also indicated.

- (2) Perform diligent maintenance and calibrations of all downhole seismic stations and OTS telemetry equipment to insure high data quality.
- (3) Perform network data analysis to prepare regular bulletins for distribution to the scientific community and public agencies.
- (4) Keep up with the close data exchange and communication between LABNET and the USGS/CIT SCSN. Coordinate closely with the USGS/CIT SCSN regarding the concentrated monitoring and aftershock field work for the 1994 Northridge earthquake sequence. Currently, 16 channels of seismic data are exchanged in realtime between these two networks. This exchange augments the seismic coverage for both networks. Figure 4 shows the locations of events ( $M \geq 3.0$ ) and portable instruments deployed in the Northridge area in 1994.
- (5) Any significant changes in the pattern of local seismicity will be brought to the attention of the USGS.
- (6) Continue to update the Los Angeles basin network data in the SCEC database at Caltech. This SCEC database is freely accessed by all scientists for research on seismotectonics, earthquake hazards, and earthquake prediction in the Los Angeles basin and its offshore area.
- (7) Continue to improve the reliability and the data quality of the remote field stations through R/D on seismic instrumentation. This activity includes:
  - an upgrade of the recording system to a much faster Vax 3900 workstation with USGS CUSP 2.6 software upgrade;
  - a backup dual PC recording system (16-bit 64-channel and expandable to 256 channels);
  - a thorough calibration of the entire network response, making sure that all 3-component seismometers have matched responses for waveform-oriented studies;
  - installation of radio-links to reduce telephone cost;
  - preliminary R/D work on a broadband and large dynamic range seismic network; and
  - refinement of seismic triggering by application of artificial neural network to detection and classification.

Besides the above accomplishments related to the network operation, we have concentrated on seismotectonic analysis based on data recorded in the Los Angeles basin during the past 21 years. Comprehensive studies have been completed of:

- (1) Artificial neural network-based seismic detector, including the S-picking for local and teleseismic events.
- (2) Seismic response of a 2-D and 3-D sedimentary basin, and the propagation of short-period surface waves in 3-D basins by a Gaussian beam synthesis.

- (3) Evaluation of the displacement and dynamic strain fields in the Los Angeles basin.
- (4) Development of a fast recursive stochastic deconvolution scheme in the estimation of earthquake source parameters.

## NEW RESEARCH FINDINGS:

### SHORT-PERIOD SURFACE WAVES IN SOUTHERN CALIFORNIA 3-D BASINS

The occurrence of the  $M = 7.4$  Landers earthquake offers an unusual opportunity for the study of relatively long wavelength energy propagation in southern California basins, where large man-made structures are exposed to potentially damaging shaking as a consequence of focusing effects due to crustal heterogeneities. We have approached this hazard problem by constructing an initial 3-D model of southern California based on available crustal velocity models, from which phase and group velocity maps are generated. Dynamic ray tracing is applied to the generation and propagation of surface waves due to the Landers twin event (a  $M = 7.4$  and a  $M = 6.5$  events 10 sec apart). The bending of rays due to local heterogeneities displays remarkable focusing and defocusing effects, which directly affect the local strong shaking amplitudes. Observations in the Los Angeles basin (Inglewood station) and over southern California are simulated by applying the surface-wave Gaussian beam method that is particularly useful in calculating waves in a 3-D basins. A forward modeling procedure is applied that successfully perturbed the southern California crustal structure in order to obtain an excellent fit to the observations. The result also shows that a twin source is required that is in excellent agreement with near source observations. Implication of this type of study is the development of the ability of a quantitative evaluation of shaking hazard in the Los Angeles basin if and when the so-called Big One does come.

### REAL-TIME SEISMOLOGY USING ARTIFICIAL NEURAL NETWORK

This application is particularly appropriate for the LABNET in the Los Angeles basin where the signal-to-noise ratio is low and the types of ambient noise are numerous. We have been, as part of our effort for improvement in network operation, experimenting an application of a neural network-based pattern classification system to the seismic event detection. Two types of AAN are designed for realtime earthquake monitoring in the Los Angeles basin: Type A uses a recursive STA/LTA ratio as input feature, and Type B uses moving window spectrogram as input feature. Further development along this line should significantly improve the automation of the LABNET operation.

### MAPPING THE STRESS FIELD

We have systematically calibrated the LABNET and have conducted a thorough examination of 3-component seismograms recorded since 1988 for evidence of shear-wave splitting for crustal rock at depth beneath the Los Angeles basin. We observed 20-120 ms travelttime difference between the two split shear waves for earthquakes occurring in the crystalline basement at depths of 6-18 km beneath the Los Angeles basin. We interpret the observed shear-wave splitting to be caused by a stress-induced crustal anisotropy. We suggest that the seismic anisotropy is mainly the result of microcracks aligned in the direction of maximum principal stress at the crustal depth.

Based on analyses of shear-wave splitting data in the Los Angeles basin, we did not find significant temporal variation of shear-wave splitting before and after the M5.5 Upland earthquake

(on Feb. 28, 1990), M5.8 Sierra Madre earthquake (on June 28, 1991), and the Joshua-Landers-Big Bear earthquake sequence (on April 22 and June 28, 1992, respectively). These three big earthquakes occurred with epicenters about 60 km, 40 km and 120 km away, respectively, from the network center.

We shall continue to search for evidence of shear-wave splitting in the Los Angeles basin area using LABNET data and the data recorded by portable instruments set up in the basin area. Based on analysis of shear-wave splitting data, we shall produce two maps: one map shows the distribution of the directions of principal stresses at depth in the Los Angeles basin, inferred by polarizations of shear waves, and the other map shows the distribution of stress levels or the degree of crustal rock fracturing in the Los Angeles basin, inferred by time differences between the two split shear waves.

## PUBLICATIONS:

- Huang, B. S., Teng, T. L. and Yeh, Y. T. (1994) Numerical modeling of fault zone trapped waves: I. Acoustic case, in review, *Bull. Seis. Soc. Am.*
- Wang, J. and T. L. Teng (1994) Surface-wave profiling of the lithosphere beneath the Mojave desert using TERRAscope data, *J. Geophys. Res.*, Vol. 99, No. B1, 743-750.
- Qu, J., T. L. Teng and J. Wang (1994) Modeling of short-period surface waves propagation in Southern California, *Bull. Seis. Soc. Am.*, Vol. 84, No. 3, 596-612.
- Qu, J. and T. L. Teng (1994) Recursive stochastic deconvolution in the estimation of earthquake source parameters: synthetic waveforms, in press, *Phys. Earth Plan. Int.*
- Wang, J. and T. L. Teng (1994) Artificial neural network-based seismic detector, in press, *Bull. Seis. Soc. Am.*
- Li, Y. G., T. L. Teng, T. L. Henyey (1994) Shear-wave splitting observation in Los Angeles basin, Southern California, *Bull. Seis. Soc. Am.*, Vol. 84, No. 2, 307-323.
- Zeng, Y., K. Aki, and T. L. Teng (1993) Mapping of high frequency source radiation for the Loma Prieta earthquake, California, *J. Geophys. Res.*, 98, No. B7, 11,981-11,993
- Zeng, Y., K. Aki, and T. L. Teng (1993) Source inversion of the 1989 Loma Prieta earthquake, California using isochron method, Accepted, *Geophys. Res. Letters*.
- Kato, K., K. Aki, and T. L. Teng (1993) 3-D simulation of the surface wave propagation in the Kanto sedimentary basin, Japan (Part 1), *Bull. Seis. Soc. Am.*, Vol. 83, No. 6, 1676-1699.
- Hisada, Y., K. Aki, and T. L. Teng (1993) 3-D simulation of the surface wave propagation in the Kanto sedimentary basin, Japan (Part 2), *Bull. Seis. Soc. Am.*, Vol. 83, No. 6, 1700-1720.

# LOS ANGELES BASIN EARTHQUAKES

November 1993 – October 1994

I-N

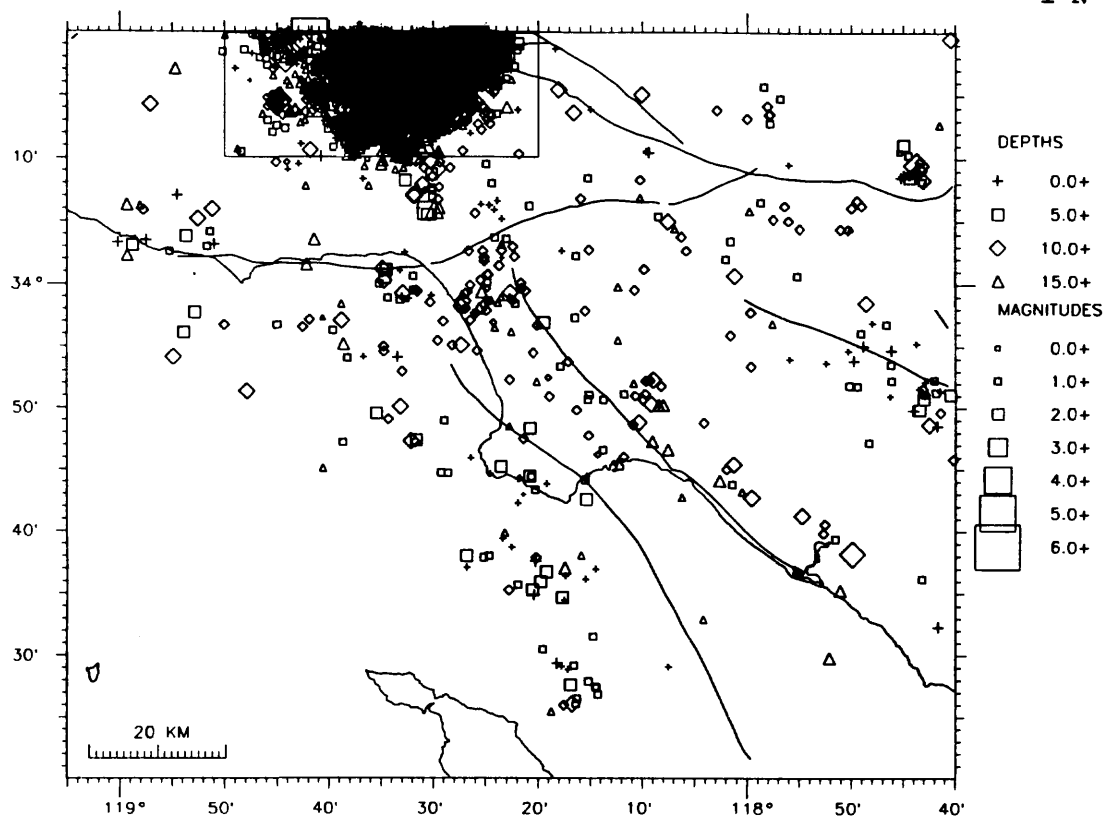


Figure 1. Seismicity recorded by LABNET between November 1, 1993 and October 31, 1994. Locations of events within the Northridge region were provided by the SCEC Data Center.

# LOS ANGELES BASIN EARTHQUAKES

November 1992 – October 1993

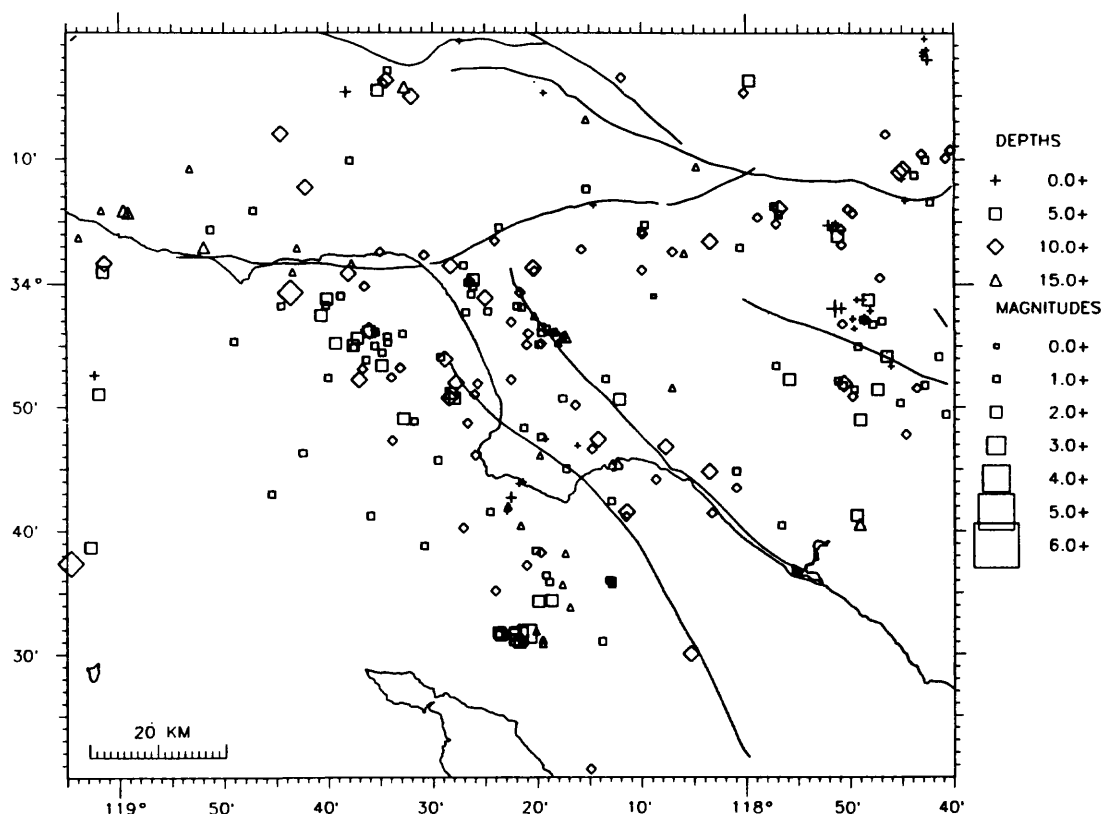


Figure 2. Seismicity recorded by LABNET between November 1, 1992 and October 31, 1993.

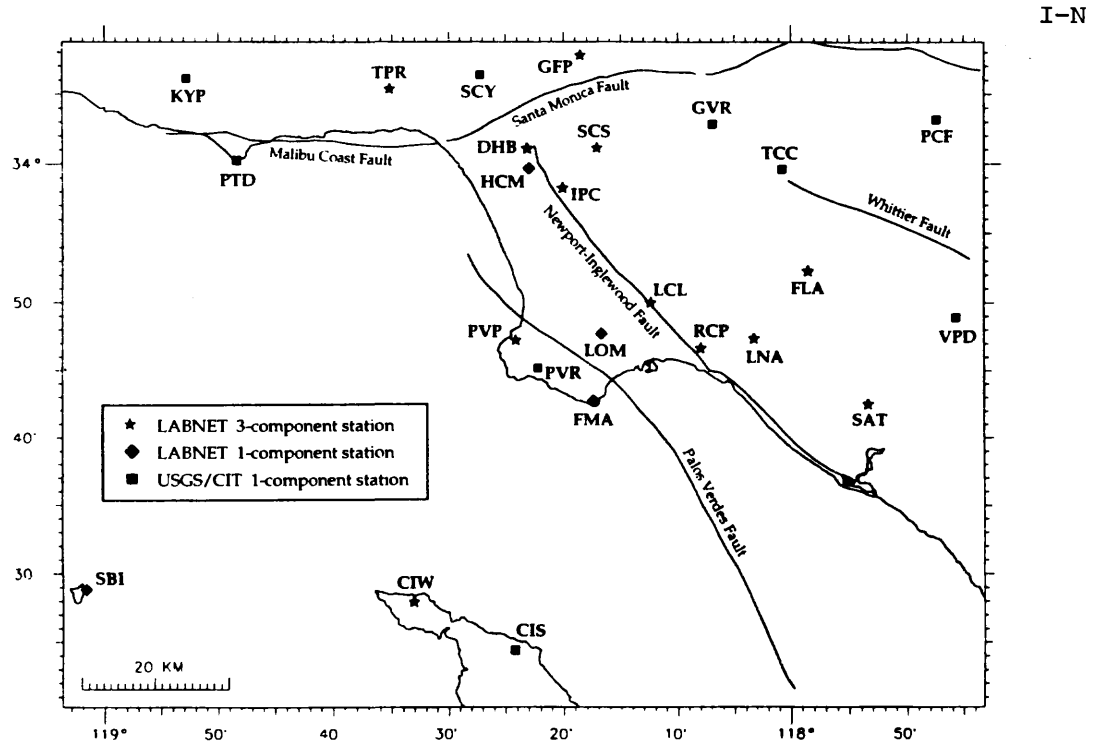


Figure 3. Seismic stations in the Los Angeles basin and its peripherals monitored by LABNET.

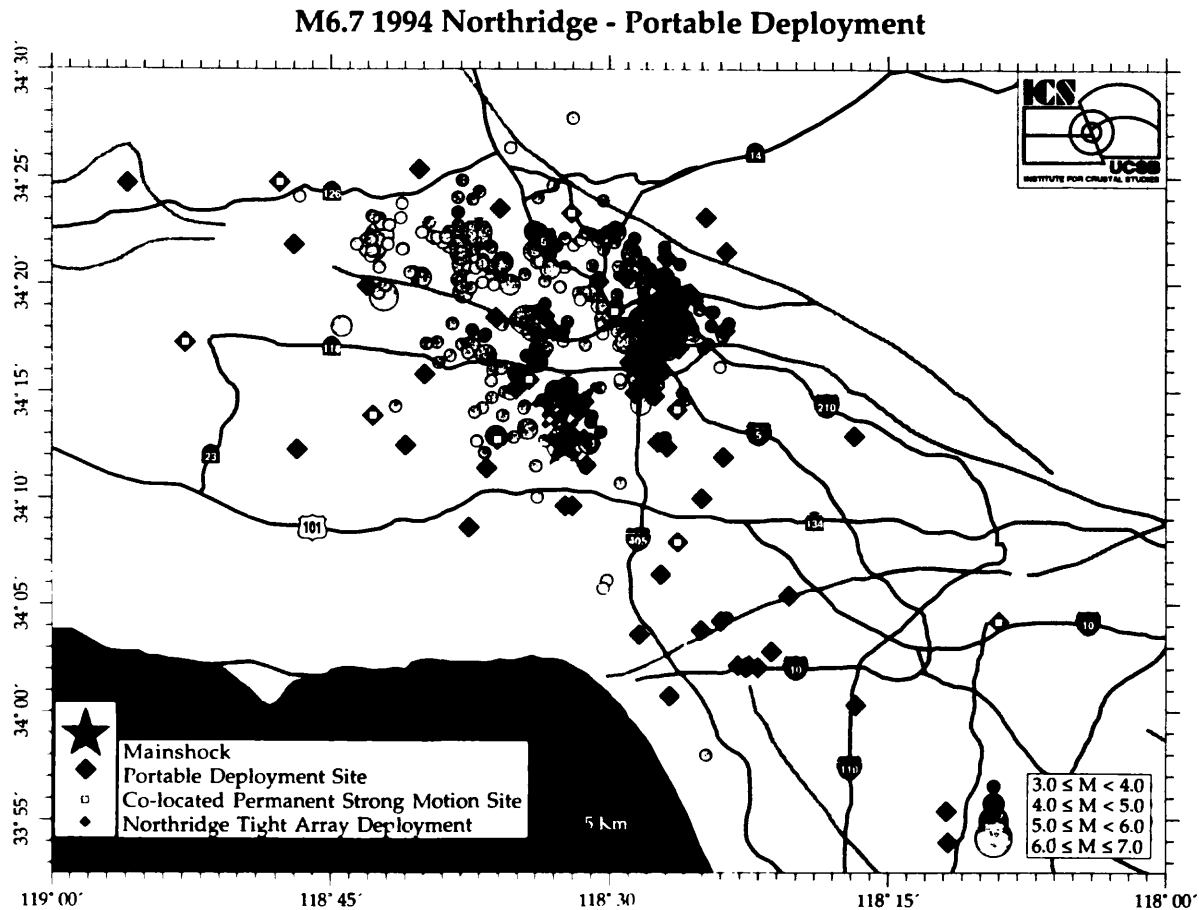


Figure 4. Locations of the M6.7 1994 Northridge earthquake and its aftershock sequence (M>3.0). Also shown are locations of portable instruments deployed by USC, UCSB, UCSD, USGS/CIT, and other SCEC institutions.

**THE NEW ENGLAND SEISMIC NETWORK  
(Operated Collaboratively by M.I.T. and Boston College)**

Contract no. 1434-92-A-0974

M. Nafi Toksöz  
Massachusetts Institute of Technology  
Earth Resources Laboratory  
42 Carleton Street  
Cambridge, Massachusetts 02142  
(617)-253-7852  
email: nafi@erl.mit.edu

### NETWORK OPERATIONS

The Earth Resources Lab (ERL) of MIT and the Weston Observatory (WO) of Boston College operate collaboratively the New England Seismic Network (NESN). The ERL at MIT currently operates five seismic stations in New Hampshire and eastern Massachusetts as part of the NESN. Presently, these stations, together with Stations WES, MIM and NH0 (operated by the Weston Observatory of Boston College) and four USGS National Seismic Network stations, are providing continuous earthquake monitoring in New England (Figure 1). The NESN is in a major transition from older recording equipment using analog telemetry to new seismic systems with digital recording at the field sites. To date two of the "new-generation" stations (MIM and WES) have been installed and are acquiring data routinely. The WO and the ERL are working together to site a total of approximately fifteen new stations to optimize the regional monitoring coverage of earthquakes in New England. The new stations record three-component broadband seismic data, resulting in a significant improvement in the quality of the seismic waveforms compared to the older short-period, mostly vertical component stations. A modem-to-modem dial-up procedure is used to transfer the data to the central facility (*i.e.*, the ERL or the WO) and to check the health status of the field recording system. The five MIT stations in New Hampshire and eastern Massachusetts serve to help maintain a regional network monitoring presence during the conversion of the NESN to new field recording systems, and to provide a baseline to assess the performance of and tune the new NESN seismic stations. The operating expenses for these MIT stations are shared between MIT and the USGS.

In a project completed in 1994, all regional earthquakes recorded digitally by the MIT Seismic Network (database beginning in 1981) have been sorted from the event database and converted to SAC format. In addition, the hypocentral locations, origin times (relative to event reference time) and magnitudes of these earthquakes have been included in the SAC files. An FTP anonymous account is available to provide on-line access to the digital waveforms and phase data files for the most recent local earthquakes recorded by the MIT stations. Older data is available through the FTP account by special request. Details on accessing this account can be obtained by contacting Charles Doll at 617-253-7863 or [doll@erl.mit.edu](mailto:doll@erl.mit.edu).

The ERL and the WO exchange regional earthquake data in SAC format using FTP via the Internet. The MIT waveform and arrival time data for new regional earthquakes are routinely transferred in SAC format via Internet to the primary NESN data archive at Weston Observatory. Future plans call for establishing an on-line facility at the WO to access the complete NESN (MIT and Weston) data archive of regional earthquakes.

Toward this end, the ERL is currently developing a Mosaic-based data management and dissemination program named SESAME (Seismic Event Server at MIT ERL) to interface clients with the NESN data archive at the WO. The SESAME home page is displayed in Figure 2. Many of the basic functions of SESAME have been written and a prototype is operating at the ERL (Matarese *et al.*, 1994). A principal feature of SESAME is the "interactive browser" (database search engine) which enables clients to search for events using parameters such as location, depth, origin time and magnitude, and then download waveform data to the client's local disk. Search parameters are chosen by clicking on search keys presented in menus of the browser. In Figure 3, a flow chart is displayed which illustrates the sequence of programs, known as CGI (Common Gateway Interface) scripts, which interpret and execute the menu choices made by the client using the browser. The SESAME home page (Figure 2) is generated by the CGI script **newsflash** when the client first accesses the ERL web site and clicks on the SESAME icon of the NESN home page. The sequence of programs to perform the data search begins with the script **searchkey** by clicking on the hypertext link Interactive query form on the SESAME home page (see Figure 2). Search capabilities include previewing and downloading waveform data, extracting hypocenter, available source, and instrument parameters for the selected events, and saving postscript files of waveforms or epicenter maps (*e.g.*, for hardcopy) on the client's local disk. Static information in the form of text (catalogs, reports, SESAME tutorial, etc.) and NESN seismicity maps is accessed by the links to hypertext documents on the SESAME home page.

SESAME is being designed to meet two objectives. First, it will serve as a research tool for seismologists working on regional earthquake problems in northeastern North America. As described above, SESAME will provide the flexibility to researchers to search the complete NESN waveform archive for data satisfying specific parameters important to their study requirements. Aside from waveform data, hypocentral and available source information about specific events and general information about New England seismicity (*e.g.*, seismicity maps, earthquake catalogs, etc.) will also be accessible to researchers. Second, SESAME will include a simple mode of operation to permit easy and timely access to basic seismic information about current earthquakes in and around New England, which might be requested by the National Earthquake Information Center, the US National Seismic Network, the Canadian Geological Survey, or other regional seismic networks. In the near future, the CGI script **newsflash** (Figure 3), will display hypocentral information about current regional earthquakes directly on the SESAME home page, with the option of clicking on a hypertext link to call up arrival time picks and other information from the hypocenter solution file.

## SEISMICITY

The ERL of MIT is currently operating five digitally recorded short-period stations located in central and southern New Hampshire and eastern Massachusetts. Data from these stations are routinely analyzed to provide hypocentral and arrival time information for regional earthquakes in and adjacent to New England. This information is published in quarterly seismic bulletins currently available for the period October 1979 - June 1994.

The epicentral locations of all regional earthquakes recorded by the MIT Seismic Network for the period October 11, 1993 - October 10, 1994 are displayed in Figure 4. Twenty-nine earthquakes, with magnitudes of 1.7 - 4.6, occurred during this period. Nineteen of these events were located inside or within 50 km of the MIT Seismic Network. Two significant earthquake swarms, one in eastern Maine and another in central Massachusetts, are represented by the multiple events plotted in Figure 4. Additional small aftershocks of

these two swarms, four in Maine and two in Massachusetts, were recorded on analog recorders.

## CURRENT RESEARCH

Two research projects, involving the application of high precision relative event location (HPREL) and empirical Green's function (EGF) techniques to seismicity in eastern North America, have been continued in 1994. HPREL has been used to refine the hypocentral locations of the seismicity of the Charlevoix Seismic Zone (CSZ) of Quebec with the objective of correlating well defined spatial patterns of relocated hypocenters with potentially active faults (Li *et al.*, 1994a). To date, results show good correlation of hypocenter distributions of relocated seismicity with some mapped faults and with fault orientations suggested by polarization angles of split shear-waves (Doll *et al.*, 1994) in specific subregions of the CSZ. This work is ongoing and the results are preliminary. The EGF method (*e.g.*, Li and Thurber, 1988) has been used to derive a relative source time function (STF) for the larger earthquakes of event multiplets or pairs in the CSZ (Li *et al.*, 1994b). The STF has been analyzed to estimate important source parameters including fault length, stress drop, seismic moment, rupture directivity and rupture velocity. Rupture directivity has been combined with P focal mechanisms for larger events to identify which nodal plane is the probable fault plane. This work has been completed for the CSZ (Li *et al.*, 1994c) and is summarized along with the preliminary HPREL results in a separate report under another USGS contract.

## REFERENCES

- Doll, Jr., C., Y. Li, M.N. Toksöz, 1994. Spatial variation in shear-wave splitting in the Charlevoix Seismic Zone of Quebec and its relationship to the local and regional stress fields, *EOS, Trans., AGU, Spring Meeting Supplement*, 75, no. 16, 235.
- Li, Y., C. Doll, Jr., W. Rodi, and M.N. Toksöz, 1994a. Precise relative location of earthquakes for characterizing seismicity and its geological association in the Charlevoix Seismic Zone, Quebec, *Seism. Res. Lett.*, 65, SSA Abstract 201, 60.
- Li, Y., C. Doll, Jr., and M.N. Toksöz, 1994b. Estimates of source time functions and associated paraameters using the EGF method for M=1.5 - 4.5 earthquakes in the Charlevoix, Miramichi, and New Hampshire seismic zones, *Seism. Res. Lett.*, 65, SSA Abstract 81, 32.
- Li , Y., C. Doll, Jr., and M.N. Toksöz, 1994c. Source characterization and fault plane determinations for  $M_b L_g = 1.2$  to 4.4 earthquakes in the Charlevoix Seismic Zone, Quebec, Canada, submitted to *Bull. Seism. Soc. Am.*
- Li, Yingping, and C. H. Thurber, 1988. Source Properties of Two Microearthquakes at Kilauea Volcano, Hawaii, *Bull. Seis. Soc. Am.*, 78, 1123-1132.
- Matarese, J.R., C. Doll, Jr., J. McIver, S. Park, and S. Woo, 1994. Serving regional seismic data to the Internet community, *EOS, Trans., AGU, Fall Meeting Supplement*, 75, no. 44, 429.

## New England Seismic Network and USNSN Stations

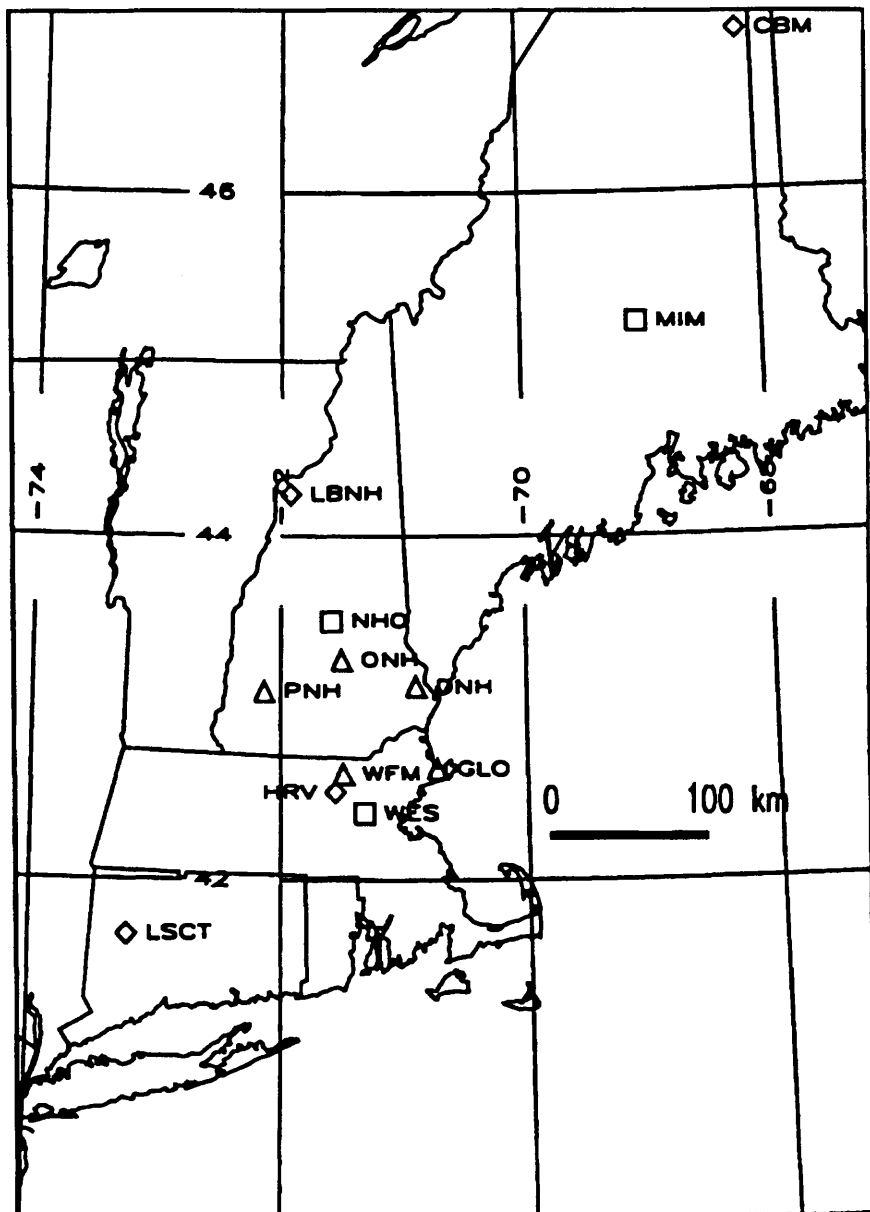


Figure 1: NESN (MIT = triangles, Weston Observatory = boxes) and US National Seismic Network (diamonds) stations operating in New England in 1994. Stations WES and MIM have been instrumented with the new broadband, three-component seismic systems as part of the conversion of the NESN.



## Seismic Event Server at MIT ERL (SESAME)

### Welcome to SESAME!

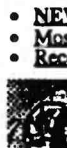


*Warning! This server is under construction.*

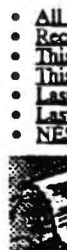
SESAME is a Web-savvy data service that provides information about seismic events in New England. SESAME has been designed to appeal to a wide audience, presenting general information about New England seismicity to the public while at the same time offering detailed information to the seismological community. We hope you enjoy using SESAME, and we have put together a [tutorial](#) to help you get started. If you have any comments or suggestions, feel free to contact [Chuck.Doll <doll@erl.mit.edu>](mailto:Chuck.Doll<doll@erl.mit.edu>)



#### Earthquakes in New England



#### Maps



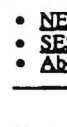
#### Reports (in gzipped PostScript format)



#### Catalogs



#### Help and Information



#### Custom Materials

- [Interactive query form](#)
- [Mailing list form \(unimplemented\)](#)



[NESN / MIT home page](#)



[MIT ERL home page](#)

*Joe Matarrese*

*created: Mon Jun 27 16:15:38 EDT 1994*

*updated: Tue Nov 29 18:55:16 EST 1994*

Figure 2: Home page of SESAME, showing the hypertext links to text, map, and waveform information for New England earthquakes. SESAME is a Mosaic-based seismic event server which features on-line access to NESN waveform data.

# Implementation

## Organization of SESAME's CGI Scripts

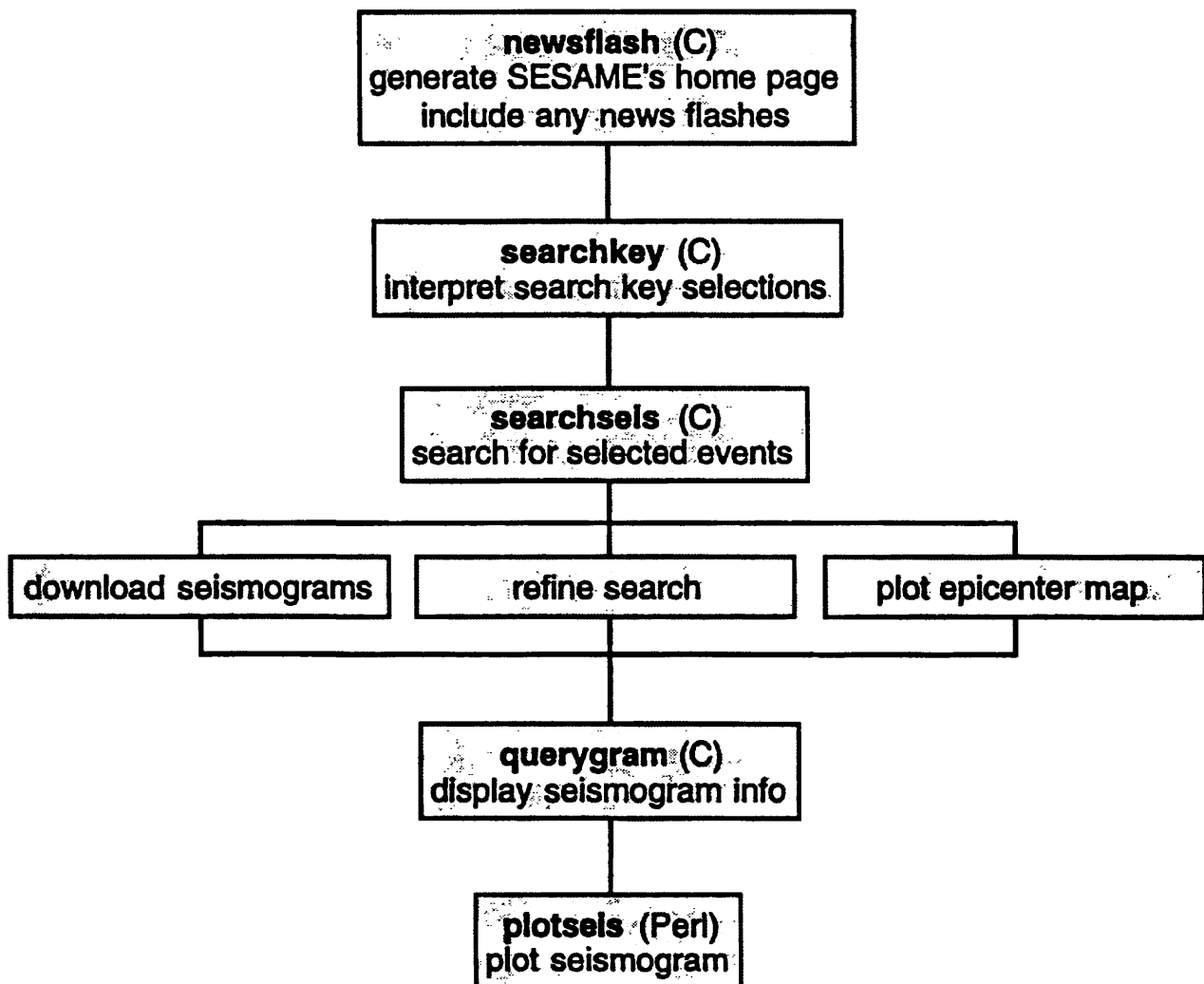


Figure 3: Flow chart illustrating the sequence of CGI scripts executed when a client uses SESAME's "interactive browser" to search the seismic database with specified search parameters. The CGI scripts are programs which interpret the client's search parameters chosen from menu options of SESAME and perform the data search.

## MIT Network Seismicity, 10/11/93 - 10/10/94

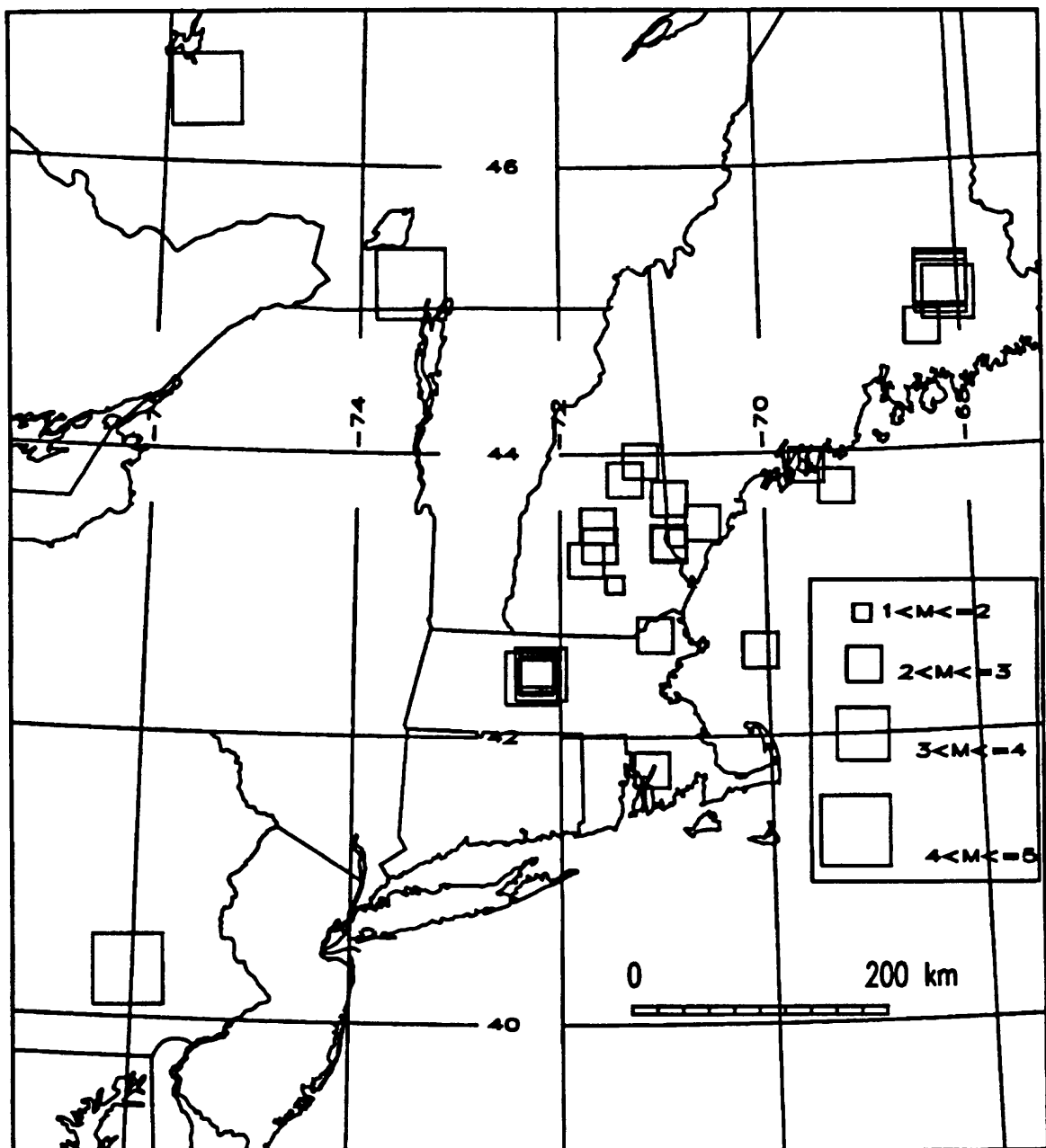


Figure 4: Seismicity of New England and adjacent regions recorded by the MIT Seismic Network for the period October 11, 1993 - October 10, 1994. Note the two swarms in eastern Maine and central Massachusetts.

# EXPERIMENTS ON ROCK FRICTION CONSTITUTIVE LAWS APPLIED TO EARTHQUAKE INSTABILITY ANALYSIS

USGS Contract 14-08-0001-21227

Terry E. Tullis  
 John D. Weeks  
 Department of Geological Sciences  
 Brown University  
 Providence, Rhode Island 02912  
 (401) 863-3829

## INVESTIGATIONS:

1. Frictional behavior of feldspar, quartz and mica as components in granite.
2. Frictional behavior of olivine.
3. Frictional behavior of large displacement experimental granite faults.
4. Dynamic Rupture.
5. Indentation tests on quartz under varying chemical environments

## RESULTS:

1. Westerly granite has been the subject of many investigations of rock friction. Granite is an aggregate made up of several phases ( 28% quartz, 35% microcline, 32% plagioclase (An17), 5% mica (biotite and minor muscovite) and < 1% magnetite), each with its own frictional properties. A simple view of granite friction is that it is the sum of its constituent's behavior. However, inhomogeneous deformation is likely if the constituents have significantly different strengths, in which case weak phases may have a disproportionate effect. Experiments were conducted at room temperature and 25 MPa on bare surface Cheshire quartzite, Tanco albite, Westerly granite and powdered muscovite. The change in friction with displacement is displayed in figure 1. Note the higher strength of feldspar as compared to the strength of granite and quartz. Muscovite is found to be considerably weaker than any of the framework silicates. Since feldspars make up 67% of the volume fraction of Westerly granite, one might expect the strength of granite and feldspar to be similar. However, the strength of granite is lower than that of feldspar, and may be affected by the presence of weaker minerals such as mica.

The velocity dependence ( $d\mu_{ss}/d\ln V$ ) versus displacement ( $\delta$ ) for each experiment is shown in figure 2. Due to irreproducibility of friction at the beginning of the experiment, we focus on the velocity dependence at large displacements after  $\mu$  has reached steady state. Since the velocity dependence for both bare quartz and feldspar are more negative than that for bare granite, mica must contribute positively to the velocity dependence. However, the ratio of mica in the granite is smaller than the ratio needed to explain the difference in velocity dependence between the value expected for granite and the data; the mica must be disproportionately contributing to the velocity dependence.

This can be understood more quantitatively, by fitting the details of the frictional response to changes in sliding velocity to a constitutive law of the form

$$\mu = \mu_0 + a \ln(V/V_0) + \sum b_i \ln(\theta_i V_0 / D_{ci}) \quad (1)$$

where the state variable  $\theta$  is defined by

$$d\theta_i/dt = (\theta_i V / D_{ci}) \ln(\theta_i V / D_{ci}), \quad (2)$$

(*Ruina* , 1983). Averaged frictional parameters  $\mu_0$ ,  $a$ ,  $b_i$ , and  $a - \sum b_i$  ( $= d\mu_{ss} / d\ln V$ ) are given in Table 1. We assume that the behavior of feldspar in granite is adequately represented by albite and that the behavior of muscovite is representative for mica. The values expected for granite are calculated by multiplying the component values by the percentage of each component in Westerly granite. By comparing the expected values with the actual parameters for granite, one can see that the frictional behavior of granite lies between the behavior of quartz and mica and has values of  $\mu_0$ ,  $a$ ,  $b_i$ , and  $a - \sum b_i$  that are lower than those of its major component, feldspar. These results suggest that granite is preferentially deforming on micas, which is not unexpected.

2. Although olivine is a major component of oceanic lithosphere, there are relatively few studies of its frictional behavior. The strength of olivine has important implications for the transition from brittle to ductile behavior and the locations of earthquakes in the lithosphere. We report results from a bare surface experiment of Balsam Gap dunite prepared under humid conditions. The experiment was conducted at room temperature and 25 MPa normal stress. We found a strength for olivine that was lower than the strength associated with most framework silicates. The coefficient of friction at the beginning of the experiment peaked at 0.5 and then decayed to 0.25 with continued displacement to 100 mm. The sample was found to be velocity weakening for the duration of the experiment. The sample slid by both stick-slip and stable sliding at velocities in the range of 10  $\mu\text{m/sec}$  to 0.001  $\mu\text{m/sec}$ . A small amount of alteration product, presumably serpentine, was observed at the grain boundaries of the undeformed sample. These products may be acting to reduce the overall coefficient of friction, but may not be affecting the velocity dependence since serpentine shows velocity strengthening behavior or a transition to velocity strengthening behavior at lower velocities.

3. We have conducted experiments to determine the origin of the difference between the velocity dependence of gouge ( $< 90 \mu\text{m}$ ) and bare surfaces and the origin and nature of displacement dependence of gouge for displacements to  $> 400 \text{ mm}$  at room temperature and 25 MPa normal stress. The results detailed in previous reports are summarized in the remainder of this paragraph. Initially bare surfaces attain a steady-state negative velocity dependence, a steady-state fault zone microstructure and a constant strength after a few tens of millimeters. These faults are constrained to be localized by the fault geometry and fault surface roughness. Velocity weakening is the characteristic response of such a localized fault (Figure 2). Simulated gouges at low displacement are strong and velocity strengthening, but with continued displacement become progressively weaker and less velocity strengthening (Figure 3a and b). This behavior coincides with localization of deformation into a narrow basal shear which at its most localized is observed to be velocity weakening. With subsequent displacement, the fault restrengthens and returns to velocity strengthening to velocity neutral; this behavior coincides with delocalization of the deformation.

In the gouge experiments, the variation in the observed degree of localization and hence in the velocity dependence results from displacement dependence of strength and probably not from variations in the velocity dependence per se. Localization is initiated in the vicinity of the peak strength, when the velocity dependence is positive. Positive velocity dependence in the absence of displacement dependence would lead to delocalization. Therefore the eventual negative velocity dependence seen when the fault is most localized is not the cause of the localization, but somehow is simply characteristic of the localized condition. Similarly, beyond the strength minimum the velocity dependence is negative, a condition which, if acting alone, would result in localization. Instead, subsequent delocalization occurs, resulting from the displacement dependence of fault zone strength. The change in the velocity dependence is not the cause of the delocalization, but

instead more positive velocity dependence is apparently characteristic of delocalized deformation.

When the gouge has a more positive velocity dependence, changes in sliding velocity are accompanied by changes in fault-normal strain rate  $d\epsilon_n/d\gamma = dL/d\delta$  (Figure 3c insets) which contribute to the measured friction through the well known work balance

$$\mu^A = \mu^f - d\epsilon_n/d\gamma, \quad (3)$$

(e.g. *Edmond and Paterson*, 1972) where  $\mu^A = \tau^A/\sigma_n$  is the measured friction and  $\mu^f$  is the intrinsic frictional resistance to shear in the absence of normal strain. Therefore normal strain contributes to the measured steady-state velocity dependence through the velocity dependence of the fault normal strain rate  $d(d\epsilon_n/d\gamma)/d\ln V$ . This contribution is not large enough to account for the difference between the steady-state velocity dependence of bare surfaces and gouge (Figure 3d and e). However there is a positive correlation between velocity dependence and changes in fault-normal strain rate and both appear to measure the degree of localization.

Variations in the intrinsic friction ( $\approx \mu^A$ ) reflect changes in the micro-mechanisms of deformation within the gouge, and as the micro-mechanics change so may the intrinsic velocity dependence of friction. An important contribution of our experiments is that they convincingly demonstrate that as the intrinsic friction changes, the intrinsic velocity dependence of friction also changes (Figure 3). Furthermore because we observe the intrinsic velocity dependence to vary with the velocity dependence of fault-normal strain rate, we conclude that dilation and compaction themselves involve or result from processes which change the energy of the system, e.g. the dissipative process of inter-particle slip and the creation of surface area by grain fracture, both of which are velocity dependent. A description of gouge deformation that emerges from this study is that intrinsic friction, the velocity dependence of fault-normal strain rate and velocity dependence correlate in these experiments, because dilation and compaction themselves contribute to or result from processes which contribute to the intrinsic velocity dependence.

4. Seismological observations of short slip duration (short rise time on seismograms) on faults during earthquakes are not consistent with conventional crack models of dynamic rupture. In these models, the leading edge of rupture stops only when a strong region is encountered, and slip at an interior point ceases only when waves from the stopped edge of slip propagate back to that point. In contrast, some seismological evidence suggests that the duration of slip is too short for waves to propagate from the nearest edge of the rupture surface, perhaps even if the distance used is an asperity size instead of the entire rupture. What controls slip duration, if not dimensions of the fault or of asperities?

In this study, dynamic earthquake rupture is represented as a propagating, rate-dependent mode II shear crack. For all propagating shear cracks, slip velocity is highest at the rupture front, and immediately behind the rupture front the slip velocity decreases. As pointed out by *Heaton* (1990), if the crack obeys a negative rate-dependent strength relation, the lower slip velocity behind the rupture front will lead to fault strengthening which further reduces the velocity, and under certain circumstances healing of the crack can occur. The boundary element method was used in a program adapted from *Andrews* (1985) for numerical simulations of mode II rupture with two different velocity-dependent strength functions. For the first function, after a slip-weakening displacement, the fault follows an exponential velocity-weakening relation. The characteristic velocity  $V_0$  of the exponential determines the magnitude of the velocity-dependence at dynamic velocities. The velocity-dependence at high velocity is zero when  $V_0$  is small and the result is similar to slip-weakening. If  $V_0$  is larger, rupture propagation resembles slip-weakening, but spontaneous healing occurs behind the rupture front (Figure 4a). The rise time and propagation velocity depend on the choice of constitutive parameters. The second strength function is a natural log velocity-dependent form similar equations (1) and (2) which fit experimental rock friction data well. Slip pulses also arise with this function (Figure 4b). For a reasonable choice of constitutive

parameters, slip pulses with this function do not propagate at speeds greater than the Raleigh wave velocity.

The results of this study of mode II rupture are in general agreement with a similar study of mode III rupture (Perrin *et al.*, 1994). Healing rupture is apparently a general consequence of negative velocity-dependent strength provided that fault strength increases when sliding velocity is zero (Figure 4). The calculated slip pulses are similar in many aspects to the seismic observations. In all cases of healing rupture, the residual stress increases with distance behind the trailing edge of the pulse so that the final stress drop is much less than the dynamic stress drop, in agreement with some recent seismological observations of rupture.

5. The friction evolution effect causes surfaces to become stronger during stationary contact and leads to a tendency for them to be weaker as sliding velocity increases. This effect is the most important factor in the time and velocity dependence of rock friction because it can lead to unstable sliding and may explain the occurrence of earthquakes. Previous experiments have shown that the evolution effect disappears for quartz when experiments are done in a weak acid solution at a pH of 2.6, the point of zero charge for quartz. This was predicted, based on the idea that time-dependent removal of contaminants is responsible for the evolution effect, and that contaminants would be absent for uncharged surfaces. However, time-dependent increase of the real area of contact due to dislocation motion or microfracturing is an alternative hypothesis for the evolution effect; this might also be reduced at the point of zero charge. Consequently we performed nanoindentation experiments on quartz to see how much indentation creep occurs and to see if it is reduced at the point of zero charge.

We chose a natural milky quartz because its plastic deformation is most similar to the quartz found in common rocks. We used indentation depths of about 200 nm and loads of about 7 mN. These are sufficiently small to be within the surface layer previously found by others to be anomalously weak in the presence of water during microindentation experiments on other materials. We made replicated indentations in normal humidity laboratory air, in double deionized water, and in dilute nitric acid at a pH of 2.6. In all three cases, creep indentation did occur, but it was not significantly reduced at the point of zero charge. The increase of the indentation area with time is not linear when plotted vs. log time and is much greater than the increase of frictional resistance with time for quartzite. This, plus the difference in the role played by the pH 2.6 solution, suggests that the process involved in indentation is not responsible for the evolution effect. One possibility is that the mean stress is high enough during indentation that dislocation motion occurs, but that the mean stress is lower at frictional contacts and so fracture dominates there.

## REFERENCES

- Andrews, D. J., Dynamic plane-strain shear rupture with a slip-weakening friction law calculated by a boundary integral method, *Bull. Seis. Soc. Am.*, 75, 1-21, 1985.
- Edmond, J. M. and Paterson, M. S., Volume changes during the deformation of rocks at high pressures, *Int. J. Rock Mech. Min. Sci.*, 9, 161-182, 1972.
- Heaton, T. H., Evidence for and implication of self-healing pulses of slip in earthquake rupture, *Phys. Earth and Planet. Inter.*, 64, 1-20, 1990.
- Perrin, G., Rice, J. R., and Zheng, G., Self-healing slip pulse on a frictional surface, submitted to *J. Mech. Phys. Sol.*, 1994.
- Ruina, A. L., Slip instability and state variable friction laws, *J. Geophys. Res.*, 88, 10359-10370, 1983.

## REPORTS:

*Papers:*

Beeler, N. M., Tullis, T. E. and Weeks, J. D., The roles of time and displacement in the evolution effect in rock friction, *Geophys. Res. Lett.*, 21, 1987-1990, 1994.

Tullis, T. E., Predicting earthquakes and the mechanics of fault slip, *Geotimes*, 39, 19-21, 1994.

Reinen, L. A., Weeks, J. D., and Tullis, T. E., The frictional behavior of lizardite and antigorite serpentinites: Experiments, constitutive models, and implications for natural faults, *Pure Applied Geophys.*, 143, 317-358, 1994.

Beeler, N. M., and Tullis, T. E., Implications of Coulomb plasticity for the velocity dependence of experimental faults, *Pure Applied Geophys.*, in press, 1994.

Beeler, N. M., Blanpied, M. L., Tullis, T. E., and Weeks, J. D., Evolution of frictional behavior in experimental granite faults with and without simulated gouge, *J. Geophys. Res.*, in preparation.

Beeler, N.M., Tullis, T.E., Self-healing slip pulses in dynamic rupture models due to velocity dependent friction, *Bull. Seis. Soc. Am.*, submitted.

Blanpied, M. L., Weeks, J. D., and Tullis, T. E., The effects of displacement, sliding rate and shear heating on the friction constitutive behavior of granite, *J. Geophys. Res.*, in preparation.

Stuart, W. D. and Tullis, T. E., Fault model for preseismic deformation at Parkfield, California, *J. Geophys. Res.*, submitted.

Beeler, N. M., and Tullis, T. E., On the role of fault-normal strain in velocity-dependent friction., *J. Geophys. Res.*, in preparation.

*Abstracts:*

Tullis, T. E., What determines the maximum strength of crustal earthquakes and what are the implications of this for the strength of the crust?, *Eos Trans. AGU*, 75, Spring Meeting Abs. Supp., 328, 1994.

Tullis, T. E., The implications of microhardness measurements of quartz for the friction evolution effect, *Eos Trans. AGU*, 75, Spring Meeting Abs. Supp., 328, 1994.

Tullis, T. E., Cooper, C., Sanford, D., and Lochhead, A., The influence of fluid chemistry on nanoindentation of quartz: relevance for the friction evolution effect, *Eos Trans. AGU*, 75, Fall Meeting Abs. Supp., 443, 1994.

Scruggs, V., Beeler, N. M., Tullis, T. E., and Weeks, J. D., Frictional behavior of feldspar, quartz and mica as components in granite, *Eos Trans. AGU*, 75, Fall Meeting Abs. Supp., 443, 1994.

Beeler, N. M., and Tullis, T. E., Is the "direct effect" in rock friction due to dilation?, *Eos . AGU*, 75, Fall Meeting Abs. Supp., 443, 1994.

## FIGURES AND TABLES:

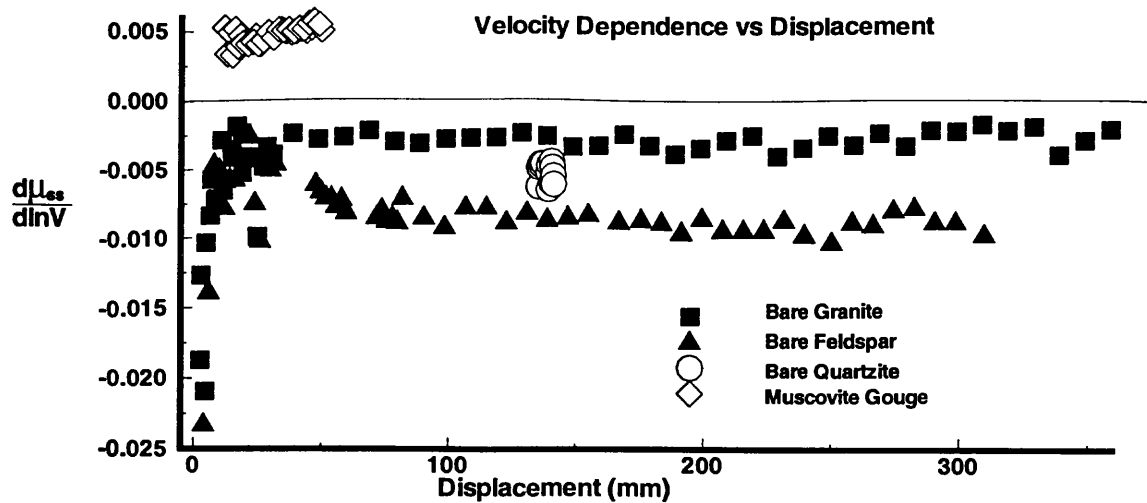


Figure 1. The overall change in friction with displacement for the constituent phases of granite. The peaks in  $\mu$  superimposed on the overall trend are due to imposed velocity changes and strengthening during periods of no sliding. The drops in  $\mu$  are stick-slip events or periods during the experiment where the torque was removed. Friction is shown for two separate quartzite experiments, one sliding to a displacement of 68 mm and a second from 89 to 160 mm. Both show a similar level of  $\mu$  at steady state.

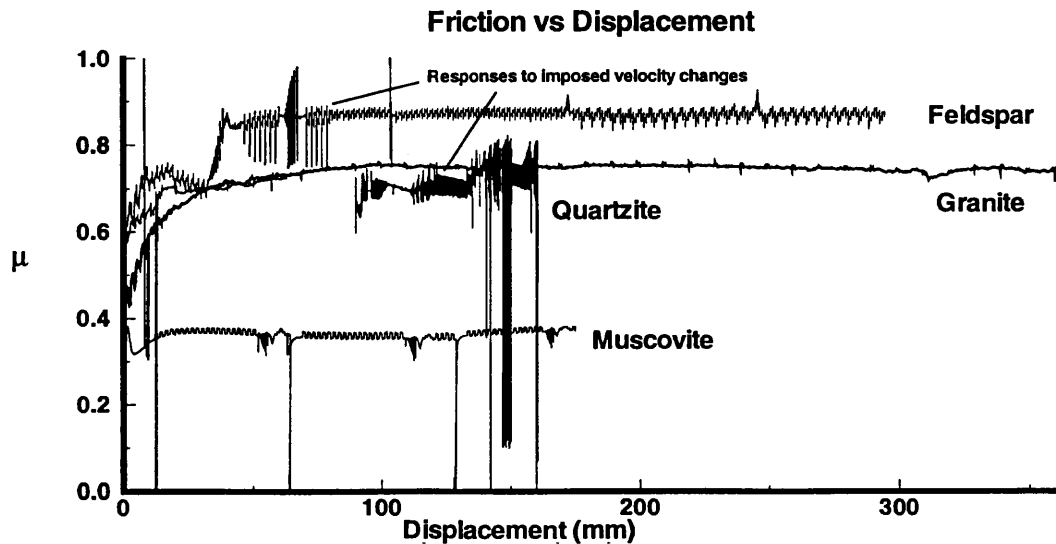


Figure 2. The velocity dependence versus displacement for the constituent phases of granite. The velocity dependence is calculated from step tests in velocities ranging from 0.0316  $\mu\text{m/sec}$  to 10  $\mu\text{m/sec}$ . Due to irreproducibility of friction at the beginning of the experiment, we focus on the velocity dependence at large displacements after  $\mu$  has reached steady state.

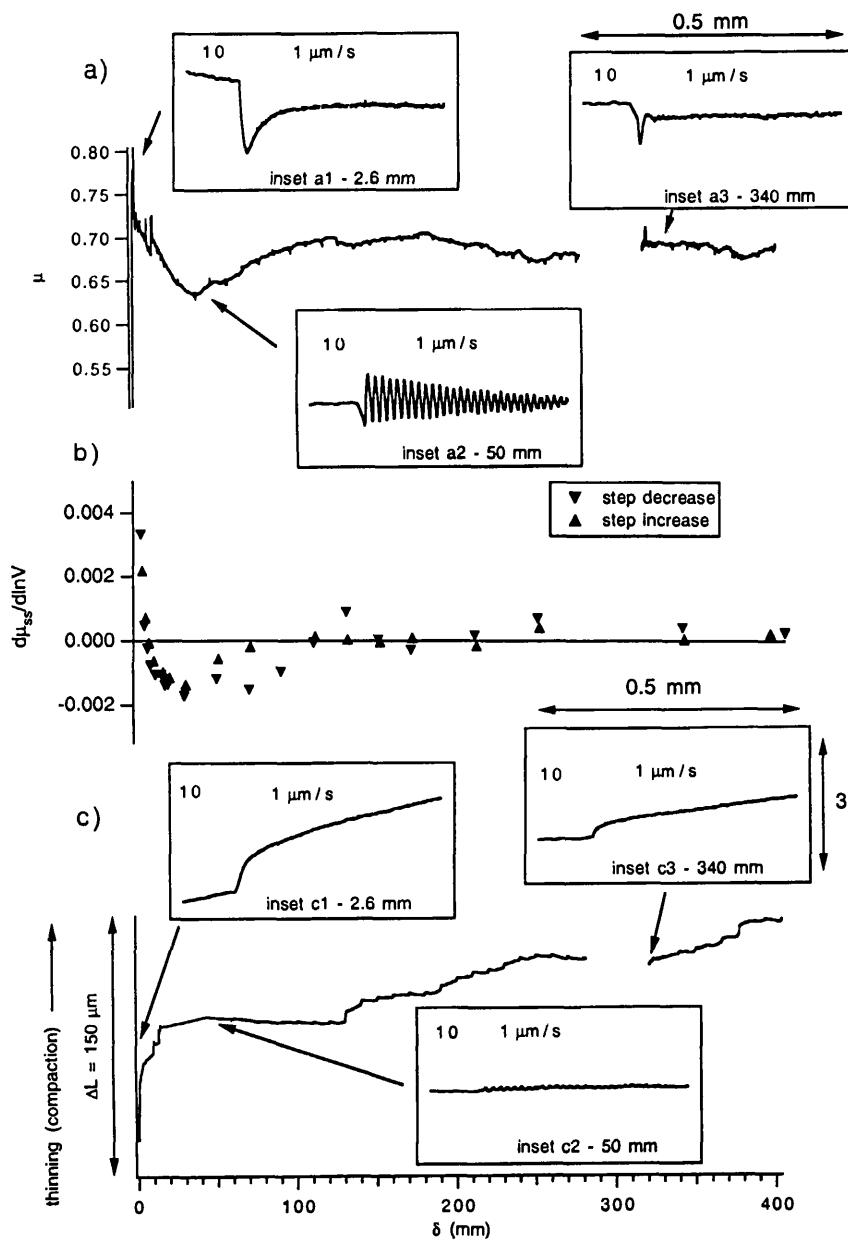
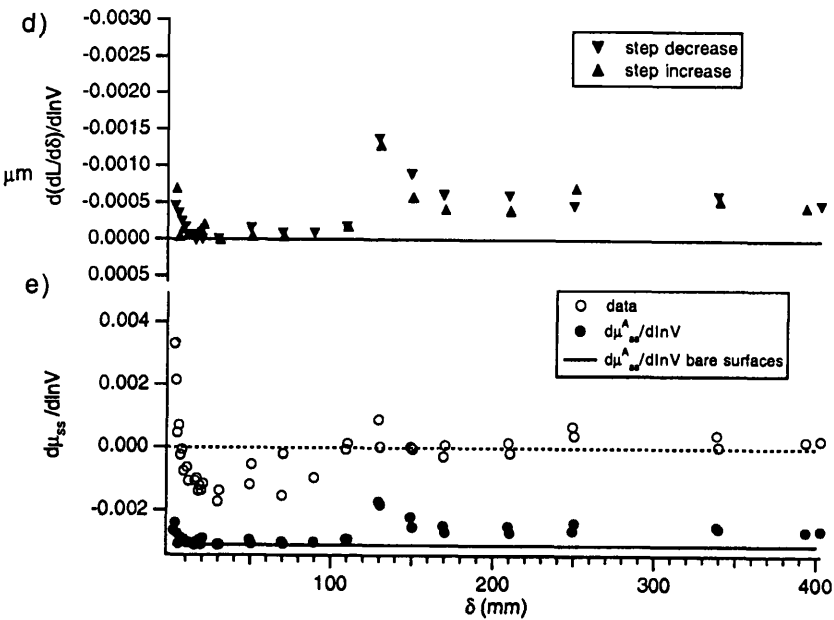


Figure 3. Mechanical observations for a typical simulated gouge experiment. a) Friction vs. displacement  $\delta$ . Insets show the details of the response to decreases in sliding velocity at four different displacements. b) Velocity dependence vs.  $\delta$ . c) Changes in sample column length  $L$  vs.  $\delta$ . Changes in  $L$  are attributed to strain within the fault zone, normal to the fault plane. Insets show the details of the response of  $L$  to decreases in sliding velocity at the four different displacements, all at the same scale as shown in a). d) Velocity dependence of fault-normal strain rate vs.  $\delta$ . e) Summary of the role of fault-normal strain rate in measured velocity dependence as suggested by equation 3. Shown is the measured velocity dependence (open circles, same as b) ), the velocity dependence of bare surfaces (line, same as Figure 2) and the predicted velocity dependence of gouge assuming that velocity dependence of gouge is the sum of an intrinsic velocity dependence equal to the bare surface value; minus the observed contribution from the velocity dependence of fault normal strain rate (solid circles).



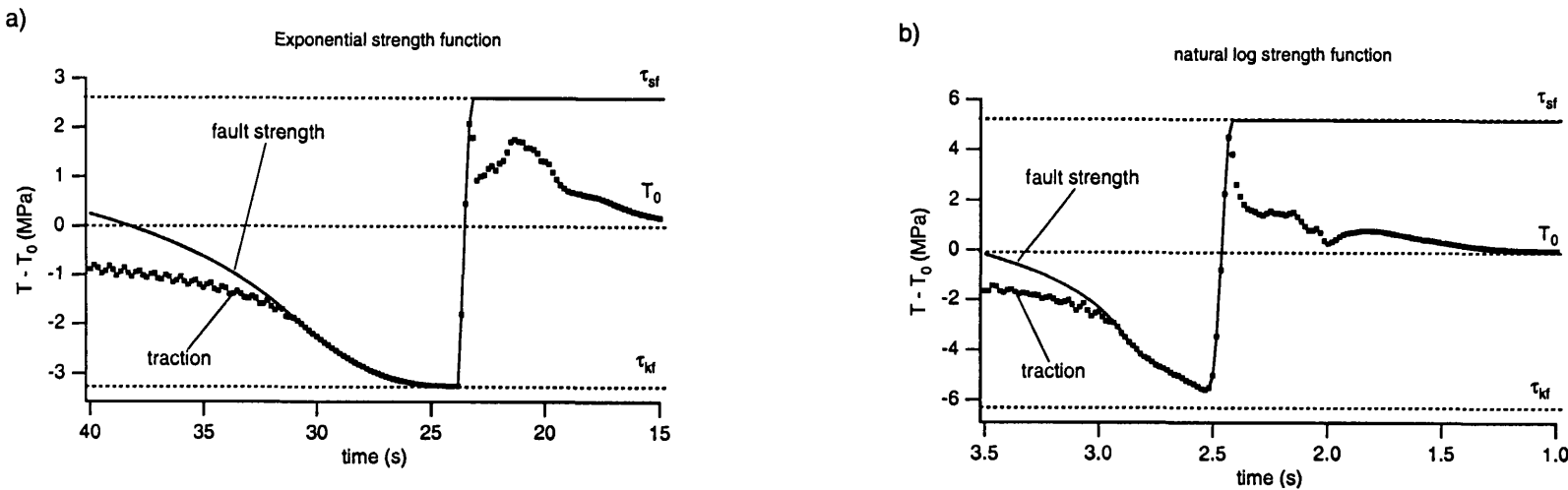


Figure 4. Calculated distribution in time of fault strength (line) and traction (squares) around propagating slip pulses. a) Results for a strength function which has an exponential velocity dependence.  $\tau_{sf}$  is the static strength of the fault,  $\tau_{kf}$  is the minimum allowed sliding strength of the fault and  $T_0$  is the remote stress. The pulse starts when the traction exceeds the fault strength (at  $\sim 24$  s) and ceases when the fault strength becomes larger than the traction (at  $\sim 31$  s). b) same as a) for a log velocity dependent strength function which resembles equations (1) and (2).

	Quartzite	Albite	Muscovite	Expected Granite	Westerly Granite
$\mu_0$	0.75	0.89	0.38	0.83	0.75
<b>a</b>	0.01	0.024	0.006	0.019	0.011
<b>b<sub>1</sub></b>	0.01	0.015	0.001	0.013	0.009
<b>D<sub>c1</sub></b>	0.6	2.1	50.0	(4.1)	4.9
<b>b<sub>2</sub></b>	0.005	0.014	0.0003	0.011	0.005
<b>D<sub>c2</sub></b>	11.0	12.2	115.0	(17.0)	17.0
<b>a-<math>\Sigma b_j</math></b>	-0.005	-0.008	0.005	-0.006	-0.003

Table 1. The averaged parameters for equation 1 from velocity step tests. The values expected for granite are calculated by multiplying the component values by the percentage of each component in Westerly granite. By comparing the expected values with the actual parameters for granite, one can see that the frictional behavior of granite is more similar to quartz and mica than to its major component, feldspar. Mica contributes to frictional behavior than its abundance would predict.

# Modeling and Prediction of Earthquakes as Unstable Phenomena of Dynamic Friction

*USGS Award: 1434-94-G-2414*

W.W. Tworzydlo, S. Sharma and J.T. Oden

*The Computational Mechanics Company,  
7701 N. Lamar, ste 200, Austin, TX 78752*

*Ph: (512) 467-0618  
Fax: (512) 467-1382  
E-mail: woytek@comco.com*

*Program Element I: Understanding the Earthquake Source*

## 1. Introduction

The primary objective of this project is to extend the present state of understanding of earthquake phenomena by recognition of importance of normal compliance of the fault surface as one of the primary factors affecting the dynamic instability of tectonic plates and, as a consequence, earthquakes. This new factor strongly interacts with such well-recognized fault properties as friction, slip weakening, wave propagation etc.

The above new approach stems from our previous research in the area of dynamic friction [2,5,6], wherein the recognition of importance of normal deformation of the frictional interface resulted in a breakthrough in understanding of friction-induced oscillations, stick-slip motion and other related phenomena. The resulting new models of contact and friction were used successfully in computational modeling of friction-induced oscillations in mechanical systems [5,6], which compared favorably with experimental observations.

Notably, the scale problems typical of the earthquake phenomena introduce additional complexities, not present in small technological systems addressed in our previous work. This includes, in particular, wave propagation, very slow overall motion of the plates, presence of fluid in the crust and gauge layers on the fault surface. It can still be reasoned, however, that the effect of normal deformation on the dynamic instability of the fault is as pronounced here as it was discovered to be the case in technological systems. Indeed, it can be logically expected that even a small increase of separation of contacting fault surfaces will produce a reduction of the local friction force compatible or exceeding the direct effects of slip weakening or velocity weakening of friction.

This project is focused on proving the correctness of the above postulate for rock formations (blocks) in relative sliding motion. When proven successful, this work will be followed by development of corresponding new constitutive models of contact and friction and by implementation of computational models capable of simulating more realistic fault systems.

## 2. Progress Summary

The innovative idea presented in this project has not yet been explored in the context of earthquake modeling (although it has been successfully demonstrated for technological systems). Similarly, the team working on the project is new to the area of earthquake-oriented research. Therefore our effort in the first year of the project was dedicated to a literature survey, to getting acquainted with intricacies of friction in the context of crustal faults, to testing our ideas on simplified examples, and to preparation of computer software that will be used in our further studies. A brief summary of this work is presented in this section.

**1. A literature survey** was performed, focusing primarily on previous research dedicated to understanding and modeling of earthquakes originating in the upper crust. It appears to be generally agreed (see references [1,3,4] and many others) that the primary source of these earthquakes is a dynamic instability of frictional sliding on fault surfaces. While there exist a large variety of specific friction formulas and computational models, the primary factors considered as earthquake sources are: slip weakening and velocity weakening of friction.

In the context of this project it is of importance to note that, up to date, there have been no theoretical or experimental works considering the normal deformation on the fault as an important factor directly contributing to dynamic instability and earthquake origination.

**2. Introductory numerical studies** of dynamic stability of a simple rigid block sliding on a plane (fig. 1) were performed. In contrast with majority of previous such studies, the block has not one but three degrees of freedom, namely sliding, normal motion and rotation. The friction law is that of Oden–Martins [2]. It includes both friction and normal compliance of the interface, and has no explicit slip-dependence or velocity-dependence of the coefficient of friction. With these

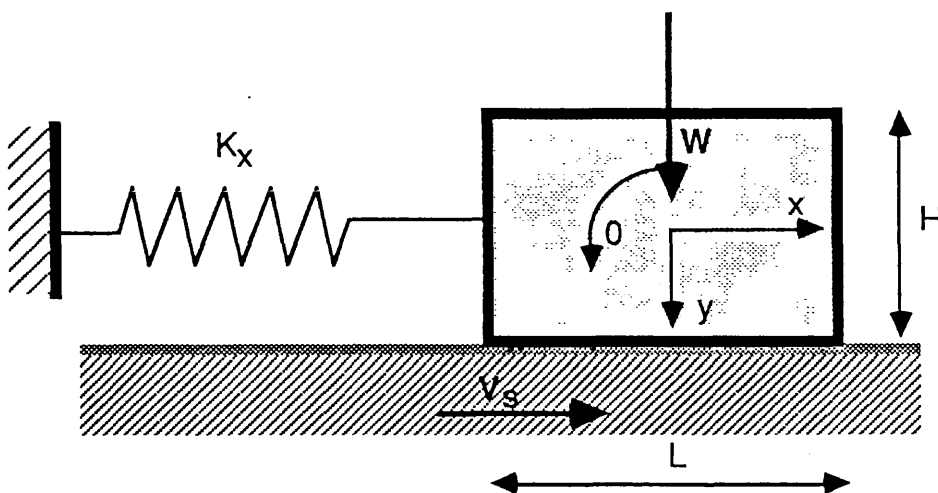


Fig. 1. A block sliding with friction on a moving belt

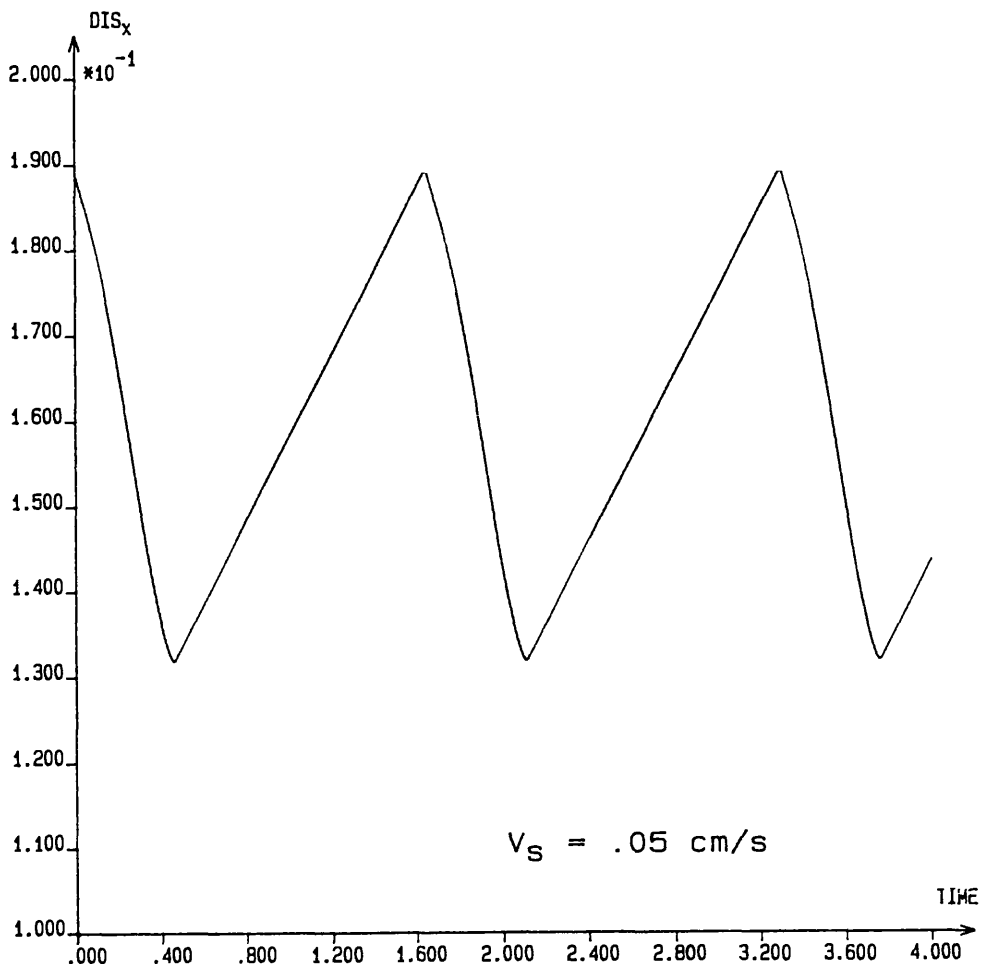
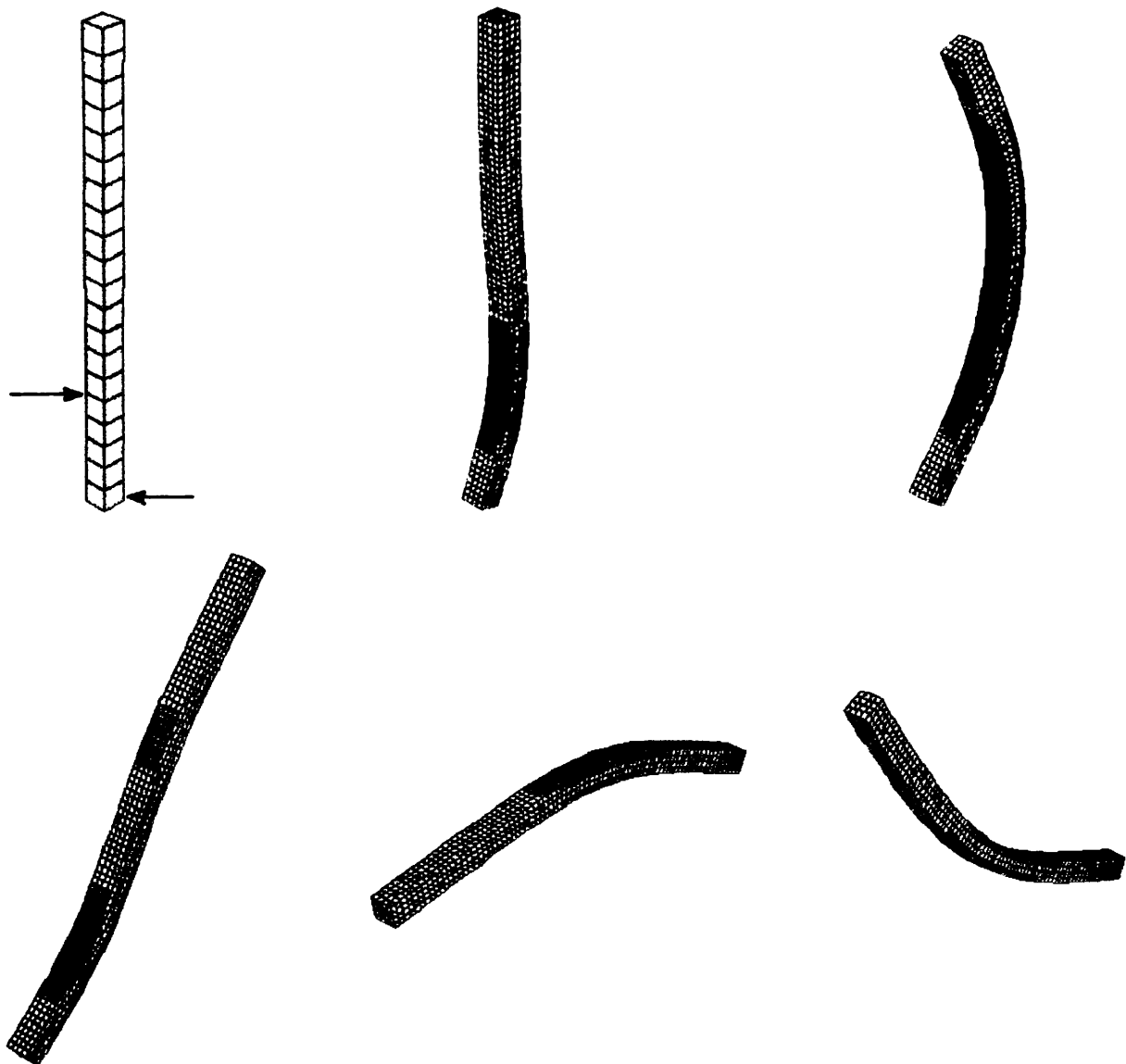


Fig. 2. Reduction of the apparent coefficient of friction and stick-slip motion (low sliding velocity).

parameters, under certain circumstances the motion of the slider is dynamically unstable and produces stick-slip motion, with the apparent macroscopic kinematic coefficient of friction lower than the static value. To illustrate this, a computed time-history of velocity of the center of mass is shown in figure 2 – a typical saw-tooth pattern of stick-slip motion is clearly visible. Importantly, it is both the coefficient of friction and the dynamic characteristics of the slider that determine the occurrence of instability.

This simple example illustrates the importance of the normal degree of freedom and of the compliance of the interface in predicting friction-induced instabilities. Our effort in the next year of the project will focus on extending these studies to deformable bodies (granite blocks) in sliding motion.

**3. The numerical simulation capability** is being extended to address the problem of simulation of unstable frictional sliding of elastic bodies (rock formations). We began extensions and modifications of the generic hp-adaptive finite element kernel PHLEX, which was our in-kind contribution to this project. In particular, a family of Newmark implicit methods



*Fig. 3. Test of the transient finite element algorithm – free motion of an elastic body.*

was implemented for time-dependent simulation of motion of elastic bodies. This includes, as an additional option, large deformation kinematics. For the purpose of present effort, the hp-adaptive mesh adaptation capability is of secondary importance and will not be discussed here. The numerical algorithm has been tested on several classical vibration problems with analytical solutions. As a more illustrative example of the performance of this algorithm, we present transient analysis of a slender deformable body, which was subjected to a transient moment load and "ejected" into space. Figure 3 shows several consecutive positions of the body, colored by von Mises stress intensity.

In the forthcoming second year of the project the above algorithm will be extended to dynamic frictional contact of elastic bodies (rock blocks) sliding on a flat surface.

### 3. Discussion

The majority of our effort in the first year of the project was dedicated to literature survey and to preparation of computer software that will be used in our further studies. Only a few examples were solved to clearly illustrate the merit of our innovation for simple sliding systems.

In the next year of the project our work will focus on extensive numerical studies of elastic blocks sliding on flat surfaces. The major objective will be to definitely prove the importance of the normal compliance of the frictional interface (fault surface) for the dynamic instability of sliding and for occurrence of stick-slip motion. To accomplish that, we will study both elastic and rigid body systems with various size scales. We will also experiment with extension of our contact and friction laws to incorporate specific effects characteristic of earthquake simulation.

### 4. References

- [1] Dieterich, J., "Modeling of Rock Friction: 1 Experimental Results and Constitutive Equations, 2. Simulation of Preseismic Slip", *Journ. of Geoph. Research*, **84**, pp. 21612175, 1979.
- [2] Oden, J. T. and Martins, J., "Models and Computational Methods for Dynamic Friction Phenomena", *Comp. Meth. Appl. Mech. Engng.*, **52**, pp. 527–634, 1985.
- [3] Rice, J.R., "Spatio-Temporal Complexity of Slip on a Fault", *Journ. of Geoph. Research*, **98**, pp. 9885–9907, 1993.
- [4] Stuart, W.D. and Aki. K., eds. **Intermediate Term Earthquake Prediction**, Birkhäuser, 1988.
- [5] Tworzydlo, W. W., and Becker, E., "Influence of Forced Vibrations on the Static Coefficient of friction – Numerical Analysis", *Wear*, **143**, pp. 175–186, 1991.
- [6] Tworzydlo, W. W., Becker, E. B. and Oden, J. T., "Numerical Modeling of Friction-Induced Vibrations and Dynamic Instabilities", in Ibrahim, R. A. and Soom, A., Editors, **Friction-Induced Vibration, Chatter, Squeal and Chaos**, ASME, De-Vol. 49, New York, 1992, pp. 13–32.

**Earthquake Preparedness Educational Program for Nurses  
Practicing in the New Madrid Seismic Zone**

1434-94-G-2508

**Stephanie VanArsdale, Ed.D., CCRN, Associate Professor  
Loewenberg School of Nursing  
University of Memphis  
Memphis, Tennessee 38152  
901-678-3080  
FAX 901-678-4906**

**Roy VanArsdale, Ph.D., Professor  
Department of Geological Sciences  
University of Memphis  
Memphis, Tennessee 38152  
901-678-4356**

**FAX 901-678-2178/E-Mail RBVanArsdale@cc.Memphis.EDU**

**Investigations Undertaken**

In the event of a damaging earthquake, health care facilities within the New Madrid Seismic Zone (NMSZ) will need to respond simultaneously to the needs of the victims in the community while dealing with major problems within their own facilities. To do so will require considerable preparation and participation in emergency planning, education, and disaster drills (Haynes et al., 1992; Walker & Gatzert-Snyder, 1991). As Saliger and Simoneau (1986) point out, there is a clear positive correlation between the extent of planning and preparedness training and effective response.

An important component of a hospital's response team in any large scale disaster is the nursing department, which includes registered nurses, licensed practical nurses, and nursing assistants practicing in the roles of patient caregivers and managers. The nursing staff is present in health care facilities 24 hours a day. In fact, in small hospitals and other health care facilities such as nursing homes, the nursing staff may be the only employees on duty during the evening and night shifts. Quite often a registered nurse is the designated person responsible for the management of the facility. These nurse managers and their colleagues must be able to manage the facility under normal circumstances and, in the event of natural disasters, they must be able to respond quickly and efficiently. Key components to their ability to respond are education and training.

The purpose of this project is to educate nursing staff members within the NMSZ about the principles of earthquake preparedness. An educational outreach program has been developed and includes a pretest, instruction on principles of earthquakes - the earthquake experience - emergency preparedness, and a posttest. This outreach program has formed the basis for a study to

evaluate the effectiveness of two instructional modalities. One includes the use of a videotape followed by a slide presentation and question and answer period. The first modality is used for nursing staff members that can attend a one to two hour oral presentation. The second modality involves the use of two self-instructional modules that have been demonstrated to be effective (VanArsdale & Hammons, 1994) for nursing staff who are not able to attend the classes. The same information is included in both approaches.

### Results

Effectiveness of the teaching modalities is being measured through use of a pretest and posttest which are the same for both teaching modalities. During the first 6 months of the project over 200 nurses and nursing staff members have attended the educational classes and 75 have completed the self-instructional modules. General interest in earthquake preparedness in health care facilities has been impressive. Specialized groups such as regional chapters of the American Association of Critical Care Nurses and the Association of Operating Room Nurses have requested oral presentations at their professional meetings. Additionally, presentations have been made at a research conference and a state nurses convention. At the completion of data collection statistical analysis of effectiveness of the two teaching modalities will be completed.

This work will continue for the remaining 6 months of the project period. A major goal of the project is to emphasize the need and encourage registered nurses to become more involved in earthquake mitigation and planning in their health care facilities.

### References Cited

Haynes, B.E., Freeman, C., Rubin, J.L., Koehler, G.A., Enriquez, S.M. & Smiley, D.R. (1992). Medical response to catastrophic events: California's planning and the Loma Prieta earthquake. *Annals of Emergency Medicine*, 21, pg. 368-374.

Seliger, J.S. & Simoneau, J.K. (1986). *Emergency preparedness: Disaster planning for health care facilities*. Rockville, Maryland: Aspen Publishers.

VanArsdale, S.K. & Hammons, J.O. (1994). Preparing for the inevitable: The New Madrid earthquake. *Journal of Continuing Education in Nursing*, 25 (6), pg. 224-229.

Walker, V. & Gatzert-Snyder, S. (1991). When disaster strikes: The concern of staff nurses. *Journal of Psychosocial Nursing*, 29 (6), pg. 9-13.

### Reports Published

None (project in progress)

## Heat Flow and Tectonic Studies

9960-10026, -11026, -12026

Colin F. Williams  
 Arthur H. Lachenbruch  
 Earthquake Geology and  
 Geophysics Branch  
 U.S. Geological Survey  
 345 Middlefield Road  
 Menlo Park, CA 94025  
 (415) 329-4881/4879  
 e-mail: colin@hq.wr.usgs.gov

John H. Sass  
 Earthquake Geology and  
 Geophysics Branch  
 U.S. Geological Survey  
 2255 North Gemini Drive  
 Flagstaff, AZ 86001  
 (602) 556-7226  
 e-mail: jsass@iflag2.wr.usgs.gov

### Investigations

This project obtains, assembles and interprets thermal data in an effort to understand the tectonic processes that lead to destructive earthquakes, constrain the factors that control the thickness of the seismogenic zone, and contribute insights into the nature and structure of major active faults. These objectives are accomplished through a series of studies focused on the thermal aspects of tectonics in the western United States.

#### Heat Flow and the San Andreas Fault System -

As part of a continuing effort to understand processes controlling earthquakes along the San Andreas fault (SAF), new thermal data were acquired from two holes on the San Francisco Peninsula west of the SAF, a deep (4.5 km) oil well in the Elk Hills field east of the Carrizo Plain segment of the SAF, and twelve idle oil wells in the Eastern Ventura Basin near the Northridge Earthquake rupture. In addition new heat-flow values were determined for four holes in the northern Gabilan Range west of the SAF and four holes in the East Bay hills near the Hayward Fault. One of the two holes on the San Francisco Peninsula was continuously cored to a depth of 200 meters, and collaborative investigations are focusing on relations among fluid movement and stress perturbations near an active fault. A paper revisiting heat flow in the Cajon Pass scientific drillhole is in press for JGR.

#### Heat Flow and the Tectonics of the Great Basin -

Active faulting and recent magmatism in the Basin and Range lead to a convergence of interests for the Earthquake Hazards Reduction Program and the Volcano Hazards and Geothermal Research Program. Project activities in this region included acquiring temperature and thermal conductivity data from a geothermal test well near the southern edge of the Colorado Plateau, investigating conductive and advective heat transfer in the 2.3 kilometer-deep Long Valley Exploratory well, and determining conductive heat flow in geothermal exploration wells near Ft. Irwin, 29 Palms and China Lake, California. Existing

data from oil wells in Railroad Valley, Nevada are being integrated with a regional study of the thermo-tectonics of the northern Basin and Range. A cooperative research effort among the USGS (both the Water Resources and Geologic Divisions), the Department of Energy, Stanford University, and Industrial partners is being planned to study fracture-controlled permeability anisotropy in Dixie Valley, the site of an  $M > 7$  earthquake in 1954. Two papers summarizing the thermal regime of the southern Basin and Range were published in JGR.

#### Thermal Processes in the Deep Crust and in Active Hydrothermal Systems -

The project continued its involvement in continental scientific drilling programs and in laboratory measurements of the thermal properties of rocks at elevated temperature. Heat and mass transfer at seismogenic depths (approximately 5 to 15 km for the San Andreas fault system) takes place at temperatures (200 to 400 °C) found at the base of shallow geothermal systems (typically 3 to 5 km) and often encountered in deep scientific drillholes. Investigating these processes both *in situ* and in the laboratory supports valuable contributions to the Earthquake Hazards Reduction Program, the Deep Continental Studies Program, and the Volcano Hazards and Geothermal Energy Program. Project activities in the past year included research on the high temperature thermal conductivity of Franciscan graywacke from The Geysers geothermal field and core samples from the 9 kilometer-deep German KTB hole, an investigation of techniques for determining *in situ* thermal conductivity in deep drillholes, and an evaluation of a Russian technique for rapid, high resolution laser-scanning for thermal conductivity.

#### Yucca Mountain Project -

In a related effort, the project conducts thermal research in support of the Yucca Mountain Project. A paper on the regional thermal setting of the Yucca Mountain area is in press as a chapter in a USGS Professional Paper on the geophysics of Yucca Mountain. Ongoing temperature logging in the deep well USW G-2 is focused on the evaluating aspects of the complex hydraulic gradients north of the proposed repository. Equipment is being prepared for the temperature logging of horizontal holes drilled across fault zones within Yucca Mountain. These logs will provide information on the magnitude and direction of fluid movement along active fault planes.

## Results

### Heat Flow and the San Andreas Fault System -

#### Thermal Studies in the Vicinity of the Northridge Earthquake:

The USGS Geothermal Studies Project is acquiring new subsurface heat-flow data from oil fields in the eastern Ventura and northern Los Angeles basins to investigate the thermal state of the crust in the vicinity of the Northridge earthquake. The primary objectives of this study are to (1) define crustal temperature and rheology at the nucleation depth of the Northridge rupture, (2) provide thermal constraints on regional tectonic models used to estimate future seismic events, and (3) search for evidence of seismically-triggered subsurface fluid movement. Preliminary estimates of heat flow from these oil fields show an increase in heat flow from  $43 \text{ mW/m}^2$  west of the Northridge rupture to  $60 \text{ mW/m}^2$  within the rupture zone delineated by aftershocks. The western termination of Northridge seismicity is approximately coincident with the decreasing heat flow and deepening isotherms (Figure 1). These results suggest that the nucleation depth of the Northridge earthquake is coincident with the  $400 \text{ }^{\circ}\text{C}$  isotherm and that a throughgoing rupture of the western segment of the Oak Ridge fault system could nucleate at depths as great as 25 km.

#### Heat Flow Measurements in the Vicinity of the Hayward Fault, California:

In 1991 and 1992, temperature and thermal conductivity data were acquired from five borehole strainmeter exploratory pilot holes and one borehole strainmeter installation hole drilled near the southern segment of the Hayward fault. Although thermal disturbances due to locally rugged topography and shallow groundwater flow are substantial, reliable conductive heat flow measurements have been obtained from four of the six holes. The average heat flow is approximately  $85 \text{ mW/m}^2$ , a value similar to an  $84 \text{ mW/m}^2$  value measured in the Berkeley Hills to the north and an average of  $89.2 \text{ mW/m}^2$  from six sites on the southern San Francisco Peninsula. This places the Hayward fault well within the region of elevated heat flow that characterizes most of the California Coast Ranges.

#### Heat Flow at Cajon Pass, California, Revisited:

In recent studies of a 3.5 km borehole near Cajon Pass we showed that the observed high heat flow and its sharp decrease with depth are predictable effects of independently determined erosion history, topography, and radioactivity, leaving little room for the large contribution from frictional heat required by conventional faulting models for the nearby San Andreas fault. We have since discovered an error in our analysis that lowers the predicted surface heat flow from the upper end ( $\sim 100 \text{ mW/m}^2$ ) to the lower end ( $\sim 90 \text{ mW/m}^2$ ) of the range of measurement uncertainty at this site. Better agreement between the prediction and observations at depth confine the permissible extra heat flow to the upper part of the hole, making it difficult to attribute it to a deep frictional source. In any

case, such a frictional source would be too small to attribute to conventional high-strength faulting models, and the basic conclusion of the original study is unchanged.

### Heat Flow and the Tectonics of the Great Basin -

#### Temperatures, Thermal Conductivities and Heat Flow in the Long Valley Exploratory Well:

A total of 41 high-resolution temperature profiles have been obtained during hiatuses in drilling in the Long Valley (California) Exploratory Well (LVEW). Despite evidence indicating near-magmatic temperatures within 7 or 8 km of the surface of the resurgent dome, no evidence for such temperatures has been found to date from temperature profiles in LVEW or other wells drilled on the resurgent dome (the bottom-hole temperature is 103°C at 2310 m). Temperature profiles indicate significant hydrologic disturbances to the thermal regime, both above 300 m and below depths of 1500 m. Vertical conductive heat flow ranges from 120  $\text{mW m}^{-2}$  in the Bishop Tuff between depths of 600 and 900 m, through 100  $\text{mW m}^{-2}$  between 900 and 1500 m, to 0 in an effectively isothermal open-hole section of corehole in the depth range 2100 to 2300 m. Hydrologic testing in this section indicates that permeabilities may be sufficiently high for hydrologic recharge to depress the measured temperatures. The near-surface conductive heat flow of  $\sim 100 \text{ mW m}^{-2}$ , while high in a regional sense, is small compared to the estimated combined conductive/convective flux of about 600  $\text{mW m}^{-2}$  for the caldera as a whole and is inconsistent with other indications of high temperatures at shallow depths. Extrapolation of temperature profiles from Phases I and II predicts temperatures in the range 200 to 250°C at a depth of 4.3 km. Other physical observations suggest temperatures approaching 400°C at that depth. This apparent paradox will be resolved by measurements to 4.3 km, the projected depth of the Phase III corehole.

#### Thermal Regime of the Great Basin and Its Implications for Hydrocarbon Occurrence:

The Great Basin is a province of high average heat flow ( $92 \pm 9 \text{ mW m}^{-2}$ ), but it contains sub-provinces of both higher and lower heat flow. Higher heat flow ( $>100 \text{ mW m}^{-2}$ ) is characteristic of the north-central Great Basin (the Battle Mountain High, BMH) and several smaller areas along its margins. There is also a large area of lower heat flow ( $<60 \text{ mW m}^{-2}$ , the Eureka Low, EL) in the south-central portion of the province. There is hydrologic and thermal evidence that the EL is a shallow ( $\sim 3 \text{ km}$ ) hydrologically controlled heat sink associated with interbasin water flow. On the other hand, seismic and magnetic studies suggest that the heat sink in the EL extends to at least mid-crustal depths. Temperatures in the deeper parts of many basins in the BMH are higher than considered favorable for generation or stability of oil. Paradoxically, temperature-gradients as high as  $100^\circ\text{C km}^{-1}$  and an underlying hydrothermal system are found within the EL in Railroad Valley, the site of the most productive oil-fields in the Great Basin. The heat source driving this hydrothermal system is a combination of local upward flow from the Paleozoic carbonate aquifer and possible thermal input from nearby igneous activity. If the presence of hydrothermal systems are required for the formation of significant hydrocarbon reservoirs

in the EL, then such reservoirs will occur only where regional groundwater flow in the carbonate aquifer is not removing heat from the basins.

### Thermal Processes in the Deep Crust and in Active Hydrothermal Systems -

#### Determination of Thermal Conductivity for Deep Boreholes:

Thermal conductivity determinations on rock cores and fragments and estimates of thermal conductivity using the mineral composition of the rock and physical well logs have been reviewed and tested on a suite of samples from the KTB superdeep drillhole and compared with in-situ thermal conductivity measurements. Laboratory methods provide precise determinations of the thermal conductivities of both solid core ( $\pm 5\%$ ) and drill cuttings ( $\pm 10\%$ ) at room temperature and pressure. For isotropic rocks, there is little to choose from between the steady-state 'divided-bar' (DB) and the transient 'halfspace' line-source (LS) techniques, both of which provide reliable values of vertical conductivity. The LS is the preferred method for field reconnaissance, and the DB is the preferred method to obtain both principal thermal conductivities. For deep research wells, the difficulties of extrapolating laboratory results to in-situ conditions present additional obstacles to determining heat flow. Laboratory measurements of water-saturated samples under in-situ conditions, combined with in-situ measurements and judicious use of calculations based on mineralogy and well-log derived physical properties can all aid in the accurate determination of thermal conductivity. In situ determinations are rare because they involve long and costly periods of drill-rig standby and the radial symmetry of cylindrical probe methods results in the measurement of only the horizontal component of conductivity. These difficulties notwithstanding, in-situ determinations of thermal conductivity remain a desirable and potentially valuable adjunct.

#### The Role of Temperature-Dependent Thermal Conductivity in Heat Transfer at The Geysers Geothermal Field, California:

The Geysers geothermal field, located in the northern California Coast Ranges, produces more than 1500 MW of steam-generated electricity. Almost all of the steam production is from a nearly-isothermal ( $\sim 240$  °C) vapor-dominated reservoir underlying a low permeability, liquid-saturated caprock. We have acquired thermal data from 3 deep production wells at The Geysers for the first continuous heat-flow profiles through the entire thickness of the caprock. We have also measured caprock and reservoir thermal conductivities under simulated in situ conditions in a newly constructed apparatus for the measurement of saturated rock thermal properties under elevated temperatures and pressures. The high temperatures encountered in The Geysers have a significant impact on the in situ thermal conductivity. An observed reduction in conductivity with temperature, when combined with measured temperature gradients, reveals a 20 to 40% decrease in heat flow with depth. The available data suggest that the variation in heat flow with depth is a transient effect of temperature changes within the system over the past 5000 to 10,000 years

and may provide a thermal record of recent intrusive or tectonic activity beneath the reservoir.

### Characteristic Temperatures and Response Times of Geothermal Systems, with an Example from Kilauea, Hawaii:

Hydrothermal cooling models predict that heat is removed quickly in comparison to the longevity of much silicic volcanic activity, which may persist for 10 Ma or more in many instances. It is probably more realistic, therefore, to examine systems that are continuously resupplied with heat. Such systems attain a steady-state temperature; the time required to reach that temperature is proportional to the inverse of the square-root of a "heat-flux" Rayleigh number. The temperature itself exhibits that same proportionality. In the geothermal field of the lower east rift zone on Kilauea volcano, Hawaii, we find that intermittent dikes that invade the shallow (2–4 km) rift zone to feed eruptions are probably inadequate to maintain the geothermal reservoir. Rather, we postulate that heat supplied by magma intruded at greater depths maintains temperatures in excess of about 300°C at depths reached by drilling. This deeper hot-rock-and-magma system can maintain itself with a magma accumulation rate that is small in comparison to the eruption rate of Kilauea. Absence of high ground-surface heat flow is explained by the vigorous groundwater flow across the top of the reservoir.

### Yucca Mountain Project -

#### Regional Thermal Setting of Yucca Mountain:

Over most of the southwestern United States, heat flow is high, between 60 and 100  $\text{mW m}^{-2}$ . There are significant areas of both higher and lower heat flow, however, and these heat sources and sinks generally can be explained in terms of the tectonic history of the area under consideration. Yucca Mountain is located near the southern boundary of the "Eureka Low," a region of low heat flow ( $< 60 \text{ mW m}^{-2}$ ) in eastern-central Nevada. From both deep temperature profiles and hydrologic studies, the primary cause of the low heat flow is thought to be interbasin water flow with a downward component of a few millimeters per year. For this reason, measurements of heat flow near Yucca Mountain do not provide unambiguous indications of tectonic processes. Within the area of the proposed repository, the thermal regime appears to be dominated by water flow in the Paleozoic carbonate rocks underlying the Tertiary section. For this reason, the interpretation of existing shallow thermal data is more relevant to hydrologic characterization than to identifying tectonic hazards. Proposed deep holes at Yucca Mountain and at Crater Flat might well provide thermal data that bear on both tectonic and hydrologic investigations.

## Is There Perched Water Under Yucca Mountain in Borehole USW G-2?

Borehole USW G-2 (Figure 2) was drilled to 1.8 km through Tertiary volcanic rocks in order to characterize the lithology and stratigraphy of a potential site for a radioactive waste repository. The borehole is one of two on the upgradient side of a feature referred to as the "large hydraulic gradient" – an area where the apparent horizontal hydraulic gradient is at least 0.15. Because USW G-2 penetrated more than 1.3 km of saturated rock, the measured water level was thought to reflect the water level of the saturated zone. Since initial measurements in 1981, water levels in USW G-2 have declined almost 12 meters. This decline may be the result of drainage from a perched or semi-perched water body in or above the Calico Hills Formation. Temperature logs from USW G-2 and other holes in the area reveal a complex thermal regime influenced by vertical fluid movement. Downward flow could explain an isothermal section observed in temperature logs obtained over a 150-meter interval in the Calico Hills Fm. Heat flow above the interval (mostly in the unsaturated zone) was low ( $44 \text{ mW/m}^2$ ). Heat flow below it was significantly higher ( $71 \text{ mW/m}^2$ ). A temperature log of USW G-2 obtained in 1992 indicates a marked decrease in the presumed vertical water flow and an overall cooling of the borehole over the same 150-meter interval. Spinner and tracejector surveys completed during fluid injection into USW G-2 showed transmissive zones within the Calico Hills Fm and the Crater Flat Tuff. One transmissive zone identified from these surveys is nearly coincident with the bottom of the 150-meter interval. If the water level measured in USW G-2 reflects a perched or semi-perched system, the significance of the "large hydraulic gradient" diminishes considerably.

### Reports

- Barton, C.A., Zoback, M.D., Moos, D., Sass, J.H., and Goldberg, D.S., 1994, In-situ stress and permeability in fractured and faulted rock, EOS, v. 75, n. 44, p. 625.
- Czarnecki, J.B., O'Brien, G.M., Nelson, P.H., Sass, J.H., Bullard, J.W., and Flint, A.L., 1994, Is there perched water under Yucca Mountain in borehole USW G-2?, EOS, v. 75, n. 44, p. 249.
- Delaney, P.T., Sass, J.H., Duffield, W.A., and Kauahikaua, J.P., 1994, Characteristic temperatures and response times of geothermal systems, with an example from Kilauea, Hawaii, in press, Proceedings of the World Geothermal Congress.
- Lachenbruch, A.H., Sass, J.H., Clow, G.D., and Weldon, R., 1994, Heat flow at Cajon Pass, California, revisited: in press, J. Geophys. Res.
- Lachenbruch, A.H., Sass, J.H., and Morgan, P., 1994, Thermal regime of the southern Basin and Range Province: II. Implications of heat flow for regional extension and metamorphic core complexes, J. Geophys. Res., v. 99, p. 22,121-22,133.
- Pribnow, D.F.C., and Sass, J., 1994, Determination of thermal conductivity for deep research boreholes, EOS, v. 75, n. 11, p. 592.
- Pribnow, D.F.C., and Sass, J., 1994, Determination of thermal conductivity for deep research boreholes, J. Geophys. Res., in review.
- Rundle, J.B., Sass, J., Finger, J., and Eichelberger, J.C., 1994, Deep exploration of an active silicic caldera: A search for magma in the crust beneath Long Valley, California: VIIth International Symposium on the Observation of the Continental

- Crust Through Drilling, Santa Fe, New Mexico.
- Sass, J.H., 1994, Downhole experiments in the U.S. Continental Scientific Drilling Program: Proceedings, VIIth International Symposium on the Observation of the Continental Crust Through Drilling, Santa Fe, New Mexico.
- Sass, J.H., and Jacobson, R., 1994, Temperatures, thermal conductivities and heat flow in the Long Valley Exploratory Well: Proceedings, VIIth International Symposium on the Observation of the Continental Crust Through Drilling, Santa Fe, New Mexico.
- Sass, J.H., Lachenbruch, A.H., Galanis, S.P., Jr., Morgan, P., Priest, S.S., Moses, T.H., Jr., and Munroe, R.J., 1994, Thermal regime of the southern Basin and Range Province: I. Heat-flow data from Arizona and the Mojave Desert of California and Nevada, *J. Geophys. Res.*, v. 99, p. 22,093-22,119.
- Williams, C.F., and Galanis, S.P., Jr., 1994, Heat-flow measurements in the vicinity of the Hayward Fault, California: U.S. Geological Survey Open-File Report 94-xxx.
- Williams, C.F., Moses, T.H., Jr., and Grubb, F.V., 1994, Thermal studies in the vicinity of the Northridge earthquake, *EOS*, v. 75, n. 44, p. 171.
- Williams, C.F., and Pribnow, D., 1994, The determination of thermal conductivity from well logs in crystalline rocks penetrated by deep scientific drillholes, Proceedings, VIIth International Symposium on the Observation of the Continental Crust Through Drilling, Santa Fe, New Mexico.
- Williams, C.F., and Sass, J.H., 1994, The role of temperature-dependent thermal conductivity in heat transfer at The Geysers geothermal field, California: 27th General Assembly of the International Association of Seismology and Physics of the Earth's Interior.

Figure 1 - East-West cross section through Northridge aftershocks showing locations of heat flow data (solid squares) and estimated depths to selected isotherms (dashed lines).

Figure 2 - Map of the Yucca Mountain area showing heat-flow and water-level contours.  
(Light shading - outcrops of Yucca Mountain Tuffs. Dark shading - area of proposed repository.)

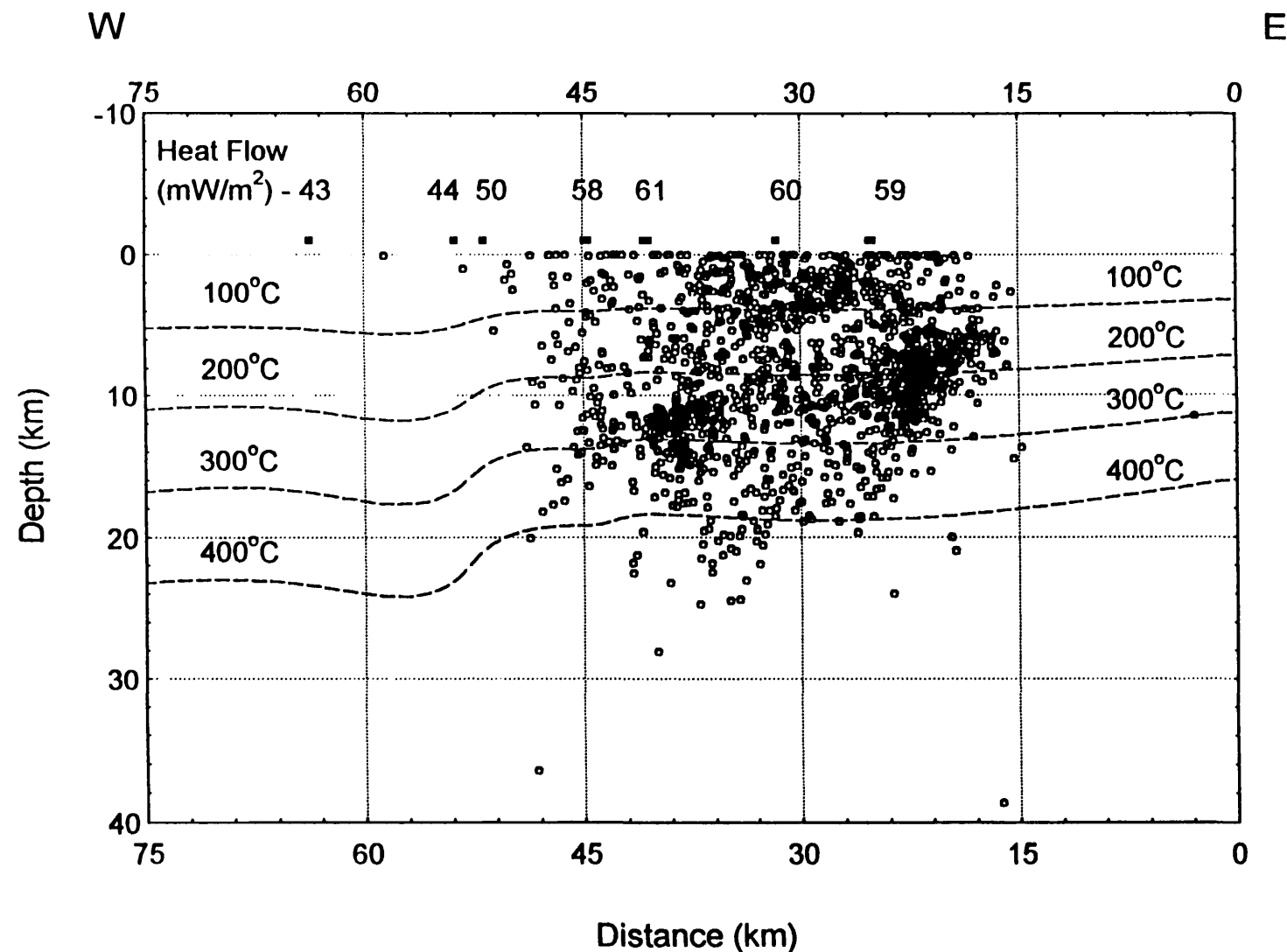


Figure 1 - East-West cross section through Northridge aftershocks showing locations of heat flow data (solid squares) and estimated depths to selected isotherms (dashed lines).

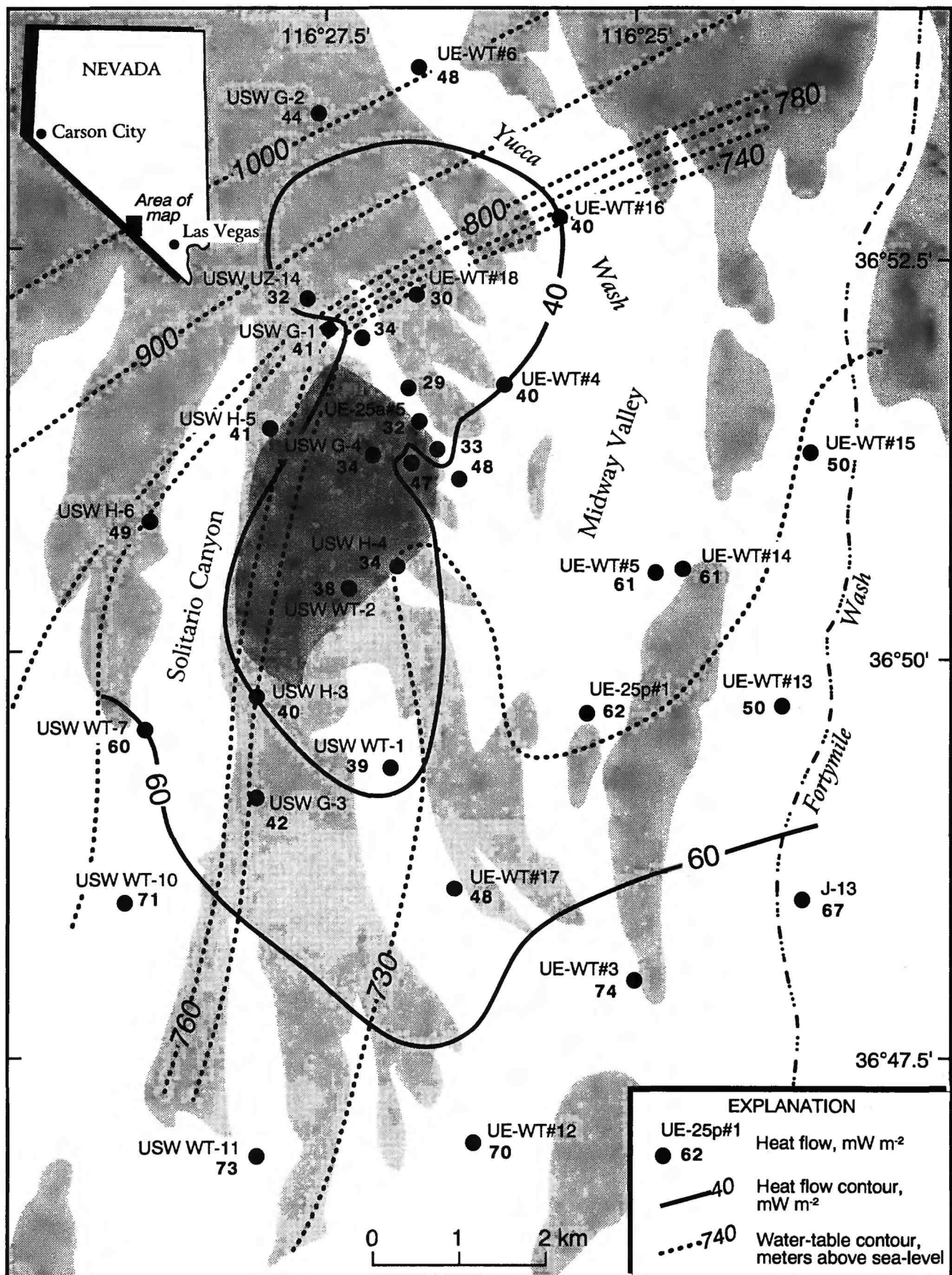


Figure 2 - Map of the Yucca Mountain area showing heat-flow and water-level contours. (Light shading — outcrops of Yucca Mountain Tuffs. Dark shading — area of proposed repository.)

**Piñon Flat Observatory:  
Studies in Crustal Deformation Measurement and Interpretation**

Award Number: 1434-93-G2307

Duncan C. Agnew, Hadley Johnson,  
and Frank K. Wyatt

Institute of Geophysics and Planetary Physics  
Scripps Institution of Oceanography  
University of California, San Diego  
La Jolla, CA 92093-0225

(619) 534-2590; FAX 534-2332; [dagnew@ucsd.edu](mailto:dagnew@ucsd.edu)

Program Element: II.3

This grant—ending with this submission—provides support for research on crustal deformation, including collaborative studies with USGS-sponsored investigators doing research at or near Piñon Flat Observatory (PFO), though our studies have extended well beyond this location.

**Fault-scale Continuous GPS**

Most studies of GPS errors have concentrated on distances of tens to thousands of kilometers. But for studies of fault behavior, especially in transcurrent environments, this scale is much too large: deformations over lengths of 1 to 50 km are what describe the pattern of strain accumulation around a fault. This realization is part of what is driving the current push to densify GPS stations to these scales. It then becomes important to understand the error spectrum, and error sources, of GPS over tens of km and less. At a scale of 10 km, a continuous GPS system begins to look a lot like a long-base strainmeter: indeed, the ratio of this length to the strainmeter length is only a factor of 14. (For comparison, the ratio of scale between borehole strain and longbase strain is 3000–4000). We thus have considerable experience in the errors and problems associated with measurements on this scale. Knowing these errors is important in planning how best to combine, not just GPS measurements and other data, but also different modes of observation with GPS. For example, a lower-cost alternative to continuous GPS would be occasional, unattended occupation of the same locations. This could not of course detect fluctuations, but could still determine, in a longer time, the secular strain rate. To decide how much longer, and thus how cost-effective this mode would be, we need to know the errors in the data. Any short-term correlation would imply that measurements could be spaced a few days apart with little loss; any long-term correlation (redness of the spectrum) would imply that having many measurements would not in fact gain as much as might be thought compared to fewer over a longer time (see below); and any non-normality (especially large outliers) would argue for more frequent observations, to make the results more robust.

In order to have data with which to address this question, we have been running continuous GPS over a 14-km baseline since the summer of 1991, with the support of the predecessors of this grant.<sup>1</sup>

---

<sup>1</sup> This experiment has been possible because of the assistance of Dr. David Jackson (UCLA) in providing equipment, and of Dr. Yehuda Bock (IGPP) in providing advice, data storage, and data processing.

This effort is similar to one being carried out by the USGS Crustal Strain Group in Menlo Park, under the direction of Dr. Nancy King. This GPS line extends west from PFO to a site at Pine Meadow (ROCH); while this intentionally does not cross the San Jacinto fault, it is within the region of strain accumulation.<sup>2</sup> At both ends of the line we have installed Trimble 4000 SST receivers, each connected to a PC so as to operate as a continuous trackers; a modem is used to download the data over a dialup phone line. At ROCH the antenna is mounted on a post set into a massive granite outcrop; at PFO (site PIN2), the antenna is mounted on one of our deeply-anchored monuments. At PFO there is also data available from P-code receivers operated at the main PGGA mark, PIN1. We first planned to measure the PIN2-ROCH baseline for a year and a half; because of the occurrence of the Landers earthquake, we have extended this to the present, and plan to continue it at least to the end of 1994, in order to look for possible response to the stress change imposed on the San Jacinto fault, and any other reactions to the Landers sequence.

Figure 1 shows the data so far processed (the data available are essentially continuous). Unfortunately, the processing was the project of a graduate student who eventually left; additional processing, though planned, will take still longer due to the fact that funding of this project has been ended. Figure 1 does contain enough data from before and after the Landers earthquake to confirm the results of dislocation modeling (shown, along with the values already mentioned for the interseismic motions, as the "Theoretical" lines). A more tantalizing result is the apparent change in rate between the period before the Landers earthquake and that after it; though since the rate before was much higher than expected, and that after (though closer to the model) is based on few points, we are suspicious of the reality of this signal. When the whole data set is processed this question should be cleared up.

One result from our processing of the data is that over the very short (50 m) line from PIN1 to PIN2 the error is less than 0.5 mm for  $L1/L2$ , and about 3 times this for  $LC$ : presumably the noise floor for this class of receivers. Over 14 km the 1991 data show a scatter in both the horizontal and vertical components that is about four times as large. We attribute this increased scatter to the effect of different tropospheric delays at PIN2 and ROCH. This scatter is not much greater than what was then seen on the 100+ km lines of the PGGA, implying that the troposphere is just as uncorrelated over a 14-km distance as it is over longer lines.<sup>3</sup> The fluctuations also appear to be correlated, perhaps over times longer than a week, though more data will be needed to be sure of this.

### Monument Stability in Practice

One of our long-running concerns has been the stability of geodetic monuments: a major factor in the quality of data from strainmeters and tiltmeters, and with the move toward closely-spaced GPS, probably a major influence on this dataset as well. At the moment the best data for this purpose comes from the 2-color EDM instrument at Parkfield, which collects daily data with better precision than expected from GPS. In cooperation with Dr. John Langbein of the USGS, we have been looking at these data—and more importantly, constructing stable monuments to see if we can improve the results. The standard marks at Parkfield are conventional piers, sunk ~2 m deep into the soil and isolated from the top 0.75 m of the ground; this is the conventional approach to building survey monuments, and is clearly insufficient, as many of these marks show seasonal movements of up to 1 cm. We have constructed several marks in which the position of the mark relative to points at depth is continuously monitored using optical interferometers. This works well, but even the low-maintenance versions of

<sup>2</sup> Assuming 1 cm/yr motion at depth on the San Jacinto fault, with no motion above 5–10 km, we expect ROCH to be moving 1.3 mm/yr westerly away from PFO, and 0.9 mm/yr to the north.

<sup>3</sup> Perhaps due to the increased number of satellites, more recent PGGA data shows decreased scatter.

these (using optical fibers) are not engineered to the level where they are suitable for general use—though a modest amount of development funds would go a long way toward rectifying this.

The compromise approach we have followed, where the highest stability ( $< 1$  mm/yr) is not needed, is to construct deeply-anchored monuments in which the anchoring is provided by a trusswork of pipes cemented to depth in drilled holes. Table 1 gives a list of those deep monuments we have built so far. While the initial impetus was to provide high-quality monuments for the stations of the PGGA, we have also built marks at PFO and at Parkfield to be used in the two-color net there.

Table 1: Deeply Anchored Marks

Name	Built	Type	Location	Purpose	Comments
PIN1	1989	A	PFO	PGGA	First deep-anchored mark
PIN2	1989	B	PFO	GPS	Auxiliary mark for permanent GPS at PFO
VAND	1991	A	Pt. Conception	PGGA	
PIN3c	1992	C	PFO	2-color	First ground-level mark
GREENc	1992	C	Pinyon Flat	2-color	
PF5c	1992	C	Pinyon Flat	2-color	
SIO3	1993	A	La Jolla	PGGA	Replacement for mark destroyed by new building.
MNPK	1993	B	Monument Pk.	PGGA	
MIDA	1993	B	Parkfield	2-color	
POMM	1993	B	Parkfield	2-color	

Types: A—removable tripod; B—fixed tripod, mark elevated; C—mark at ground level.

We feel that the construction of these marks has educated us about this technique, to the point that we can generate clear specifications for future constructions of this type, with good assurance that the marks built will be long-lived. It has also, we think, been a stimulus to the rest of the community. As evidence of this we can point to the angled-rod installation developed by Dr. Ken Hudnut for use at the PGGA site in Blythe; this, by using driven rods rather than drilled ones, offers a less costly method of installation that should work about as well in deep alluvium.

One of the difficulties of this research has been the problem of how to test the results: this requires a known stable point and highly accurate surveys between it and the other marks. We have built some marks at PFO for testing stability; we also constructed, in the summer of 1993, two monuments at Parkfield, both to help in the strain-monitoring work there and to serve as a test of our techniques. The marks selected, POMO and MIDE, are both known to be unstable ( $\sim 10$  mm level) and are also particularly important, since they are both on Middle Mountain, directly above the anticipated initiation zone.

The data from the new marks (MIDA and POMM), collected by Dr. Langbein, shows much higher stability than that from the old marks, even though there was little rainfall (the main driver of mark motion) in 1993-94. The line-lengths to MIDA and POMM do show fluctuations of a few mm, but since these are correlated we suspect them to arise from instability of the central instrument, a suspicion recently confirmed by data from other marks near the same azimuth.

### Analysis of Crustal Deformation: Monument Stability in Theory

In a recent study of the effect of geodetic network design on determining fault parameters, Johnson and Wyatt (1994) found that, of all the changes one could make, the least effective was to increase the frequency of surveys. This result seemed counter to the expectation that more frequent surveys would give about  $N^{1/2}$  improvement. Some simple (but realistic) numerical experiments show how this result comes about. As a model of errors, we assume that the position of a point at time  $t_i$  is given by

(in one direction)

$$p(i) = a\alpha(i) + b\beta(i) \quad (1)$$

where  $\alpha$  is an independently-distributed Gaussian random variable, with standard deviation of 1 mm, representing the measurement error for a day of data (we can vary  $a$  to scale this); and  $\beta$  is a random-walk process, representing monument wander. The scaling of  $\beta$  is such that, for  $b$  equal to 1, the wander is 1 mm per  $\text{yr}^{1/2}$ . For this error model the random-walk monument motion introduces a long-term correlation.

We now fit a model  $p(t) = p_0 + rt$  to these synthetic data;  $r$  is of course the rate we seek. Since we know the error model, we can compute the standard error of  $r$ ,  $\sigma_r$ , taking the full covariance structure into account. When we do this, we can find  $\sigma_r$  (in mm/yr), for different observation schedules, depending on  $T$  (the total span of observations) and  $\Delta$  (the sample interval). The solid lines in Figure 2 show the results as a function of  $\Delta$  for different values of  $b/a$ , given a total survey time  $T$  of 5 years. The box to the right, with symbols corresponding to values of  $b/a$ , shows the results for  $T = 20$  years,  $\Delta = 1$  year (the annual-survey mode referred to above).

What is clear is that when the monument motion dominates ( $b \geq a$ ) the benefits of frequent sampling are slight; only for  $b$  one-tenth of  $a$  is there a significant improvement for weekly as opposed to monthly data, and  $b$  must be less than  $a$  for there to be any advantage in making surveys more than annually. The reason is that the covariance structure of the errors means that the correlation between closely-spaced data is high, so that more frequent sampling does not produce as many additional “independent” data as might be thought. Only if the correlated errors are small relative to the independent ones do we see the  $N^{1/2}$  improvement expected. On the other hand, since monument motion grows only slowly with time, it is much less deleterious when considering its effect on the total survey time: the gain from making 20 years of annual measurements, as opposed to 5 years, is about the same whether  $b/a$  is 3 or 0.3.

An important point from these simulations is that if this error structure exists, and we ignore the correlated part, we will be led, especially for frequent data, to grossly underestimate the true error in our rate estimate. Any correlation between data will cause such a bias in the error estimates. This bias can be accounted for when error estimates are determined if we assume we know the error structure (as we have done in Figure 2), but we must know this in order to make realistic error estimates.

Another reason that has been given for wanting frequent measurements is to protect against the occasional bad data point. As a first check on this, we added to the error model (1) a 10% chance of an (independent) error with standard deviation 5 mm. We then found  $\sigma_r$  directly from 10000 realizations of the error process, for the same observation schedules as before. These results are plotted as the dashed lines (and symbols marked “ $5\sigma$ ”) in Figure 2. For the case when  $b$  is small (negligible monument instability), annual surveys are more affected than weekly ones by the presence of bad data (a factor of 2 in  $\sigma_r$  for annual, as against 1.5 for weekly); on the other hand, even in this case, monthly surveys would be almost as good. Clearly this needs more thorough examination, including more realistic error models and some consideration of the use of more robust techniques for estimating the rate especially when considering the effect of bad data points.

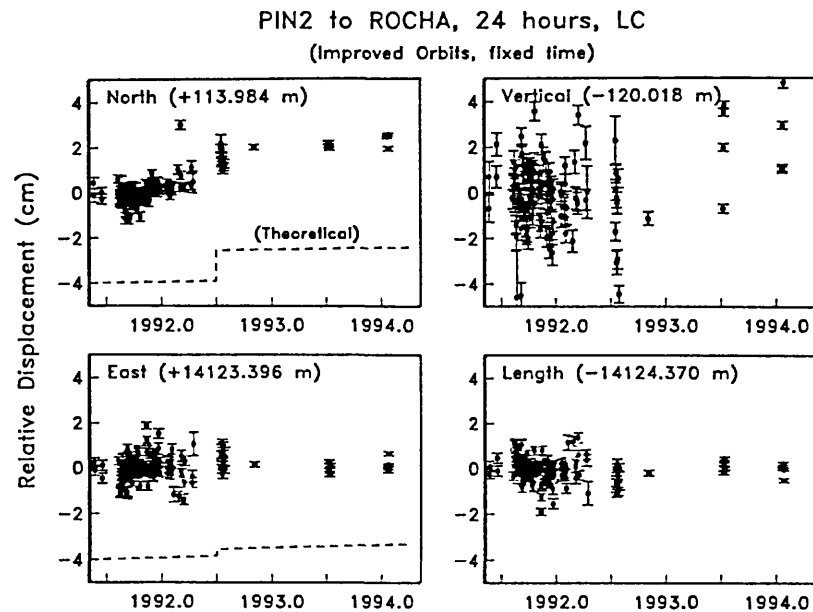


Figure 1.

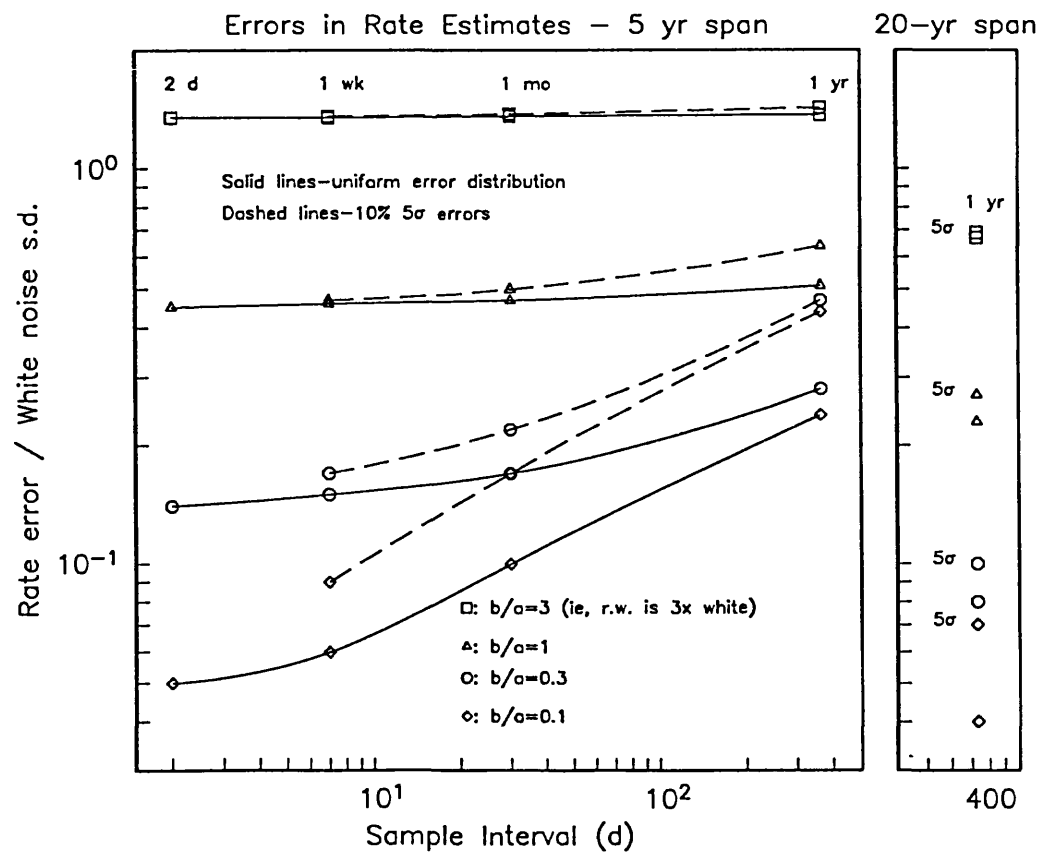


Figure 2.

## Analysis of Similar Earthquakes in Seismic Gaps

Award number: 1434-92-G-2202

Richard C. Aster

Department of Geoscience/Geophysical Research Center  
New Mexico Institute of Mining and Technology  
Socorro, NM 87801

Office: (505) 835-5924; Fax: (505) 835-6436; email: aster@jupiter.nmt.edu  
Program Element: II

### Investigations Undertaken

A large but conflicting literature exists which suggests that the scattering properties of the Earth in seismogenic areas may be temporally variable and could be correlated with the nucleation times of moderate to large earthquakes. To search for temporal variations in coda  $Q$  in the vicinity of an expected moderate earthquake nucleation region along the San Andreas fault zone, pairs and clusters of earthquakes recorded by the digital Anza Seismic Network between 1982 and 1992 and by the Parkfield downhole High resolution seismic network between 1987 and 1994 are examined. To minimize differences arising from path and source variability, only the most similar examples of microearthquake wavefields are intercompared. Such similar event catalogues are comprehensively identified using 3-component networks crosscorrelation coefficient via a method outlined in Aster and Scott (1992).

To assess source and coda  $Q$  differences between similar microearthquake signals, we estimate moving-window log amplitude spectral ratios and search for any systematic temporal changes. For similar microearthquake signals propagating through an Earth with temporally varying scattering and/or attenuation properties, an increase/decrease in coda attenuation,  $Q_c^{-1}$ , would be indicated by a progressive increase/decrease, respectively, in the coda spectral ratio between the first and second events with advancing time and frequency. In contrast, source differences preferentially map into a spectral ratio term which is constant with respect to advancing time. For a single-scattering coda model with an envelope decay function of the form

$$t^{-m} e^{-\pi f t / Q_c} \quad (1)$$

the relationship between the log amplitude spectral ratio and

$$\Delta Q^{-1} = Q_c^{-1} - Q_c^{-1} \quad (2)$$

is linear, i.e.,

$$\ln r(f, t) = \pi f t \Delta Q^{-1} + W(f) \quad (3)$$

where  $W(f)$  is a time-independent relative source term. To obtain robust uncertainty estimates, we utilize multitaper spectral techniques (Thomson, 1982; Park et al., 1987) coupled with a non-Gaussian Monte Carlo error estimation procedure. This algorithm was applied to comprehensive sets of similar earthquakes observed in both regions.

### Results

For the most similar events available from the Anza region (Figure 1; coda crosscorrelation values of approximately 0.7 for approximately 16 s of coda), we find that it is possible to constrain differences in coda  $Q$  as a function of time with this technique at a typical  $1\sigma$  resolution of only approximately (-25%, +50%) in the best-constrained frequency bands. Analysis of short time base event pairs suggests that essentially all of this variability can be attributed to random fluctuations in the coda driven by source variability and does not reflect any systematic temporal variability in coda  $Q$ . This indicates that the moving-window spectral ratio analysis technique requires significantly more similar earthquakes than are produced

by seismogenic processes in the Anza region in order to produce estimates of relative coda  $Q$  which are more precise than approximately  $\pm 10\%$ .

Such earthquakes have, however, been observed to occur in other regions of the San Andreas Fault system. Remarkable similar microearthquake clustering coupled with a high degree of likelihood for a moderate to large earthquake in the near future make the Parkfield, California, segment of the San Andreas fault system a prime location at which to search for temporal variations in coda  $Q$  associated with lithospheric changes which may occur during the earthquake cycle. We comprehensively examine 21 of the more than 250 clusters observed to date which exhibit nearly identical waveforms across the network (Figure 2; coda crosscorrelation values of approximately 0.98 for approximately 12 s of coda; Nadeau et al., 1994a,b). The restriction of the data set to only the most highly similar sources is found to be critical, as small differences in source processes, even for event pairs with centroid locations within approximately 20 m, are shown to significantly increase the spurious noise level in the parameter estimates. Absolute 68% confidence bounds obtained on the repeatability of coda  $Q$  for all microearthquake pairs are conservatively estimated to be approximately  $\pm 10\%$  for frequencies below 20 Hz. Tighter constraints than those found for individual pairs of microearthquakes are obtainable by reconstructing the temporal history of coda  $Q$  from all  $N \cdot (N-1)$  first difference measurements within  $N$ -event multiplets. These functional reconstructions unambiguously indicate that the mean value of coda  $Q$  has not varied by more than approximately  $\pm 5\%$  from 3-30 Hz, at the  $1\sigma$  level (Figure 3). The estimated variability in coda  $Q$  during the study period thus shows no sign of systematic change during this period. This is in sharp contrast to other observables, such as an increased level of microseismicity, which suggest that a preparatory stage for the next Parkfield earthquake has begun.

## Reports Published

### *Publications in Refereed Journals*

- Antolik, M., Nadeau, R., Aster, R., McEvilly, T.V., Differential analysis of coda  $Q$  using similar microearthquakes in seismic gaps Part 2: Application to seismograms recorded by the Parkfield High Resolution Seismic Network, 1994. *Bull Seism. Soc. Am.*, submitted.
- Aster, R., Scott, J., Comprehensive Identification of Similar Earthquakes in Microearthquake Data Sets, 1993. *Bull. Seism. Soc. Am.*, 83, 1307-1314.
- Aster, R., Slad, G., Henton, J., Antolik, M. Differential analysis of coda  $Q$  using similar microearthquakes in seismic gaps Part 1: Techniques and application to seismograms recorded in the Anza seismic gap, 1994. *Bull Seism. Soc. Am.*, submitted.
- Scott, J., Shearer, P., Aster, R., Constraints on temporal variations in velocity near Anza, California, from analysis of similar event pairs, 1993. *Bull Seism. Soc. Am.*, in press.

### *Abstracts of Meeting Presentations*

- Aster, R., Antolik, M., Nadeau, R., McEvilly, T.V., Differential analysis of coda  $Q$  using similar microearthquakes in seismic gaps, 1994. *EOS trans. AGU*, 75, no 44, p. 454.
- Aster, R., Scott, J., Shearer, P., Vernon, F.L., Analysis of near-repeating earthquake wavefields in the San Jacinto fault zone, southern California, 1991. *EOS trans. AGU*, 72, no 44, p. 352.
- Aster, R., Scott, J., Shearer, P., Vernon, F.L., Similar earthquakes in the Anza Seismic Gap, 1992. *Seism. Res. Lett.*, 63, p. 63.
- Aster, R., Henton, J., Scott, J., Shearer, P., Vernon, F.L., Comparative coda analysis using similar earthquakes in the Anza seismic gap, 1993. *Seism. Res. Lett.*, 64, p. 35.
- Aster, R., Slad, G., Nadeau, R., Antolik, M., Coda stability analysis of similar earthquakes in seismic gaps, 1993. *EOS trans. AGU*, 74, no 43, p. 397.
- Aster, R., Henton, J., Scott, J., Shearer, P., Vernon, F.L., Comparative coda analysis of similar earthquakes with large temporal separations near the Anza seismic gap, southern

- California, 1992. *EOS trans. AGU*, **73**, no 43, p. 361.
- Nadeau, R., Aster, R.C., McEvilly, T.V., Analysis of P and S wave polarizations at the Parkfield high-resolution seismic network (HRSN), 1991. *EOS trans. AGU*, **72**, no 44, p. 483.
- Scott, J., Shearer, P., Aster, R., Constraints on temporal variations in velocity near Anza, California, from analysis of similar event pairs, 1992. *EOS trans. AGU*, **73**, no 43, p. 360.
- Slad, G., Aster, R., Coda analysis using similar earthquakes in the hypocentral area of the Landers main shock, 1994. *EOS trans. AGU*, **75**, no 44, p. 462.

### References

- Hellweg, M., P. Spudich, J. B. Fletcher, and L. M. Baker (1994). Stability of coda  $Q$  in the region of Parkfield, California: The view from the USGS Parkfield dense seismograph array, submitted to *J. Geophys. Res.*.
- Nadeau, R., M. Antolik, P. Johnson, W. Foxall, and T. McEvilly (1994a). Seismological studies at Parkfield III: Microearthquake clusters in the study of fault-zone dynamics, *Bull. Seism. Soc. Am.*, **84**, 247-263.
- Nadeau, R., W. Foxall, and T. V. McEvilly (1994b). Periodic recurrence and spatial clustering in characteristic microearthquakes on the San Andreas fault, submitted to *Science*.
- Park, J., C. Lindberg, and F. Vernon (1987). Multitaper spectral analysis of high-frequency seismograms, *J. Geophys. Res.*, **92**, 12,675-12,684.
- Thomson, D. (1982). Spectrum estimation and harmonic analysis, *IEEE Proc.*, **70**, 1055-1096.

PFO 88206005916 90053082315

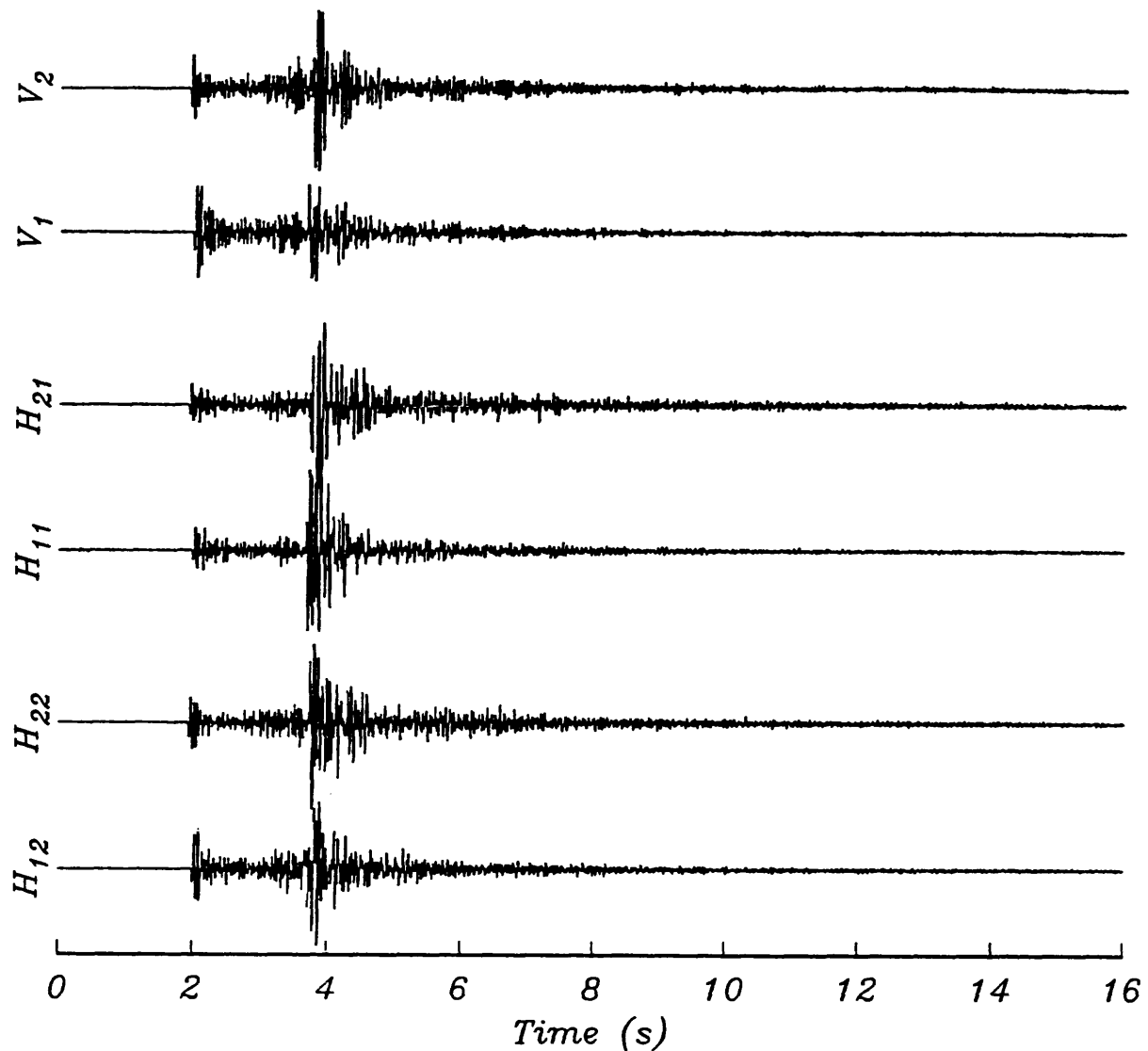


Figure 1. Similar event pair three-component seismograms (time separation of approximately 624 days) from the Toro Peak swarm zone of the Anza region recorded at Anza network station PFO. The three-component crosscorrelation of the entire seismogram coda is approximately 0.75.

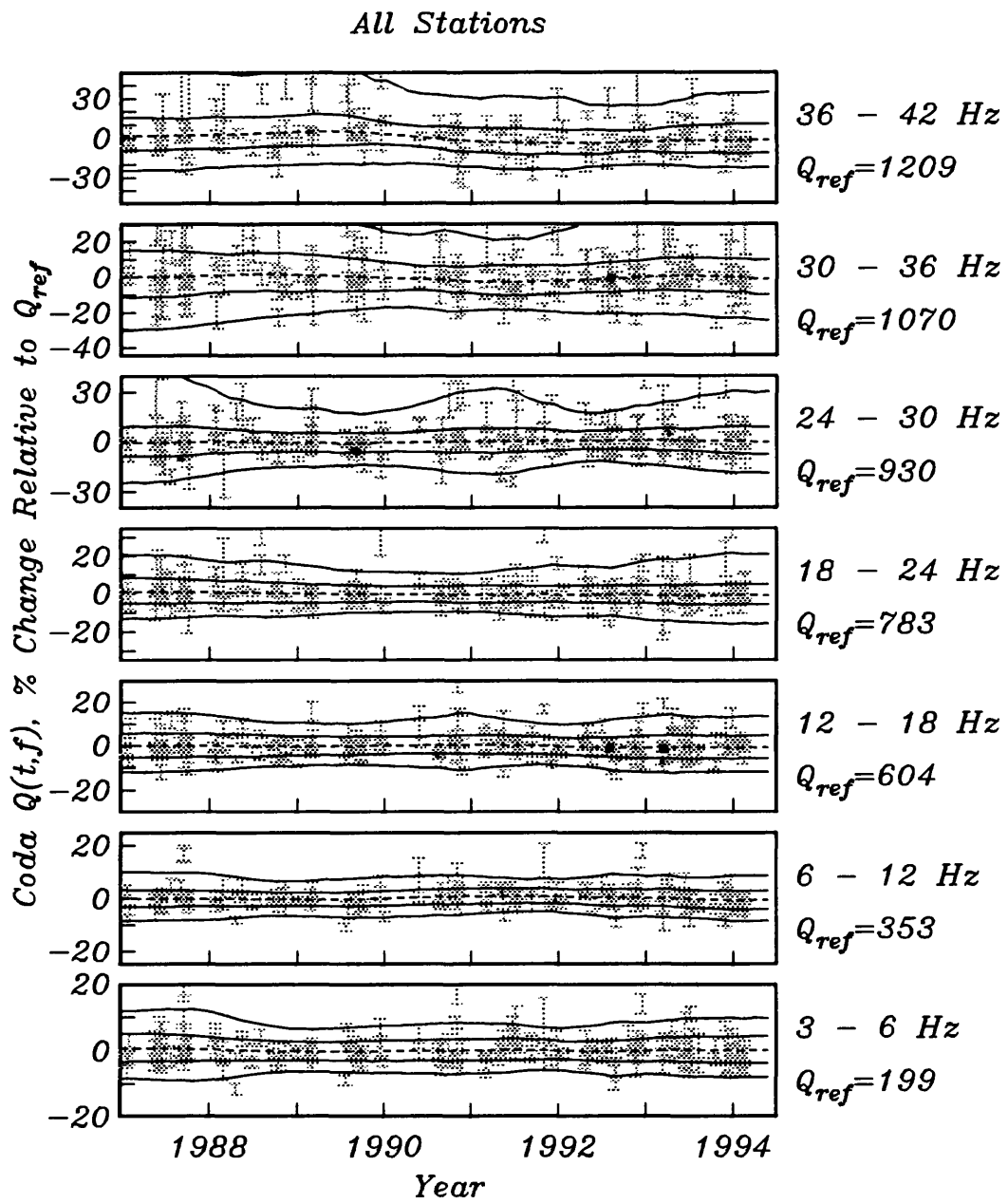


Figure 3. Coda  $Q$  as a function of time obtained from combining functional reconstructions from all observed clusters (e.g., Figure 2) at all stations in the Parkfield High Resolution Seismic Network. The regional coda  $Q$  estimates of Hellweg et al. (1994) were used as reference levels to convert  $\Delta Q$  (equation 2) to coda  $Q$ . The mean value of coda  $Q$ , fixed to the reference value, is shown as a dashed line. Solid curved indicate 68% and 95% confidence bounds for deviations from the reference value. Note that there is no indication of a regional change in coda  $Q$  during the 7-year observation period.

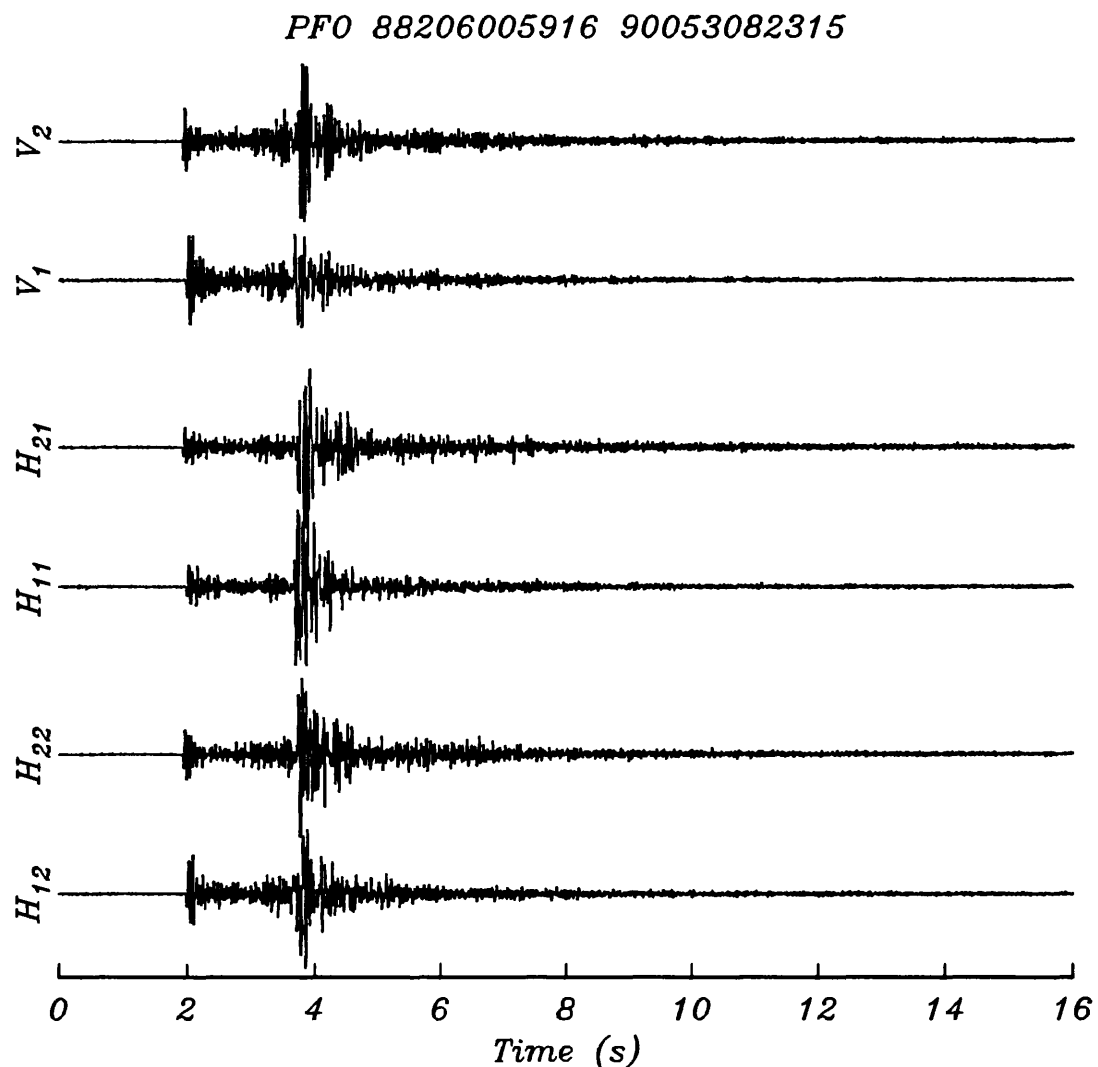


Figure 1. Similar event pair three-component seismograms (time separation of approximately 624 days) from the Toro Peak swarm zone of the Anza region recorded at Anza network station PFO. The three-component crosscorrelation of the entire seismogram coda is approximately 0.75.

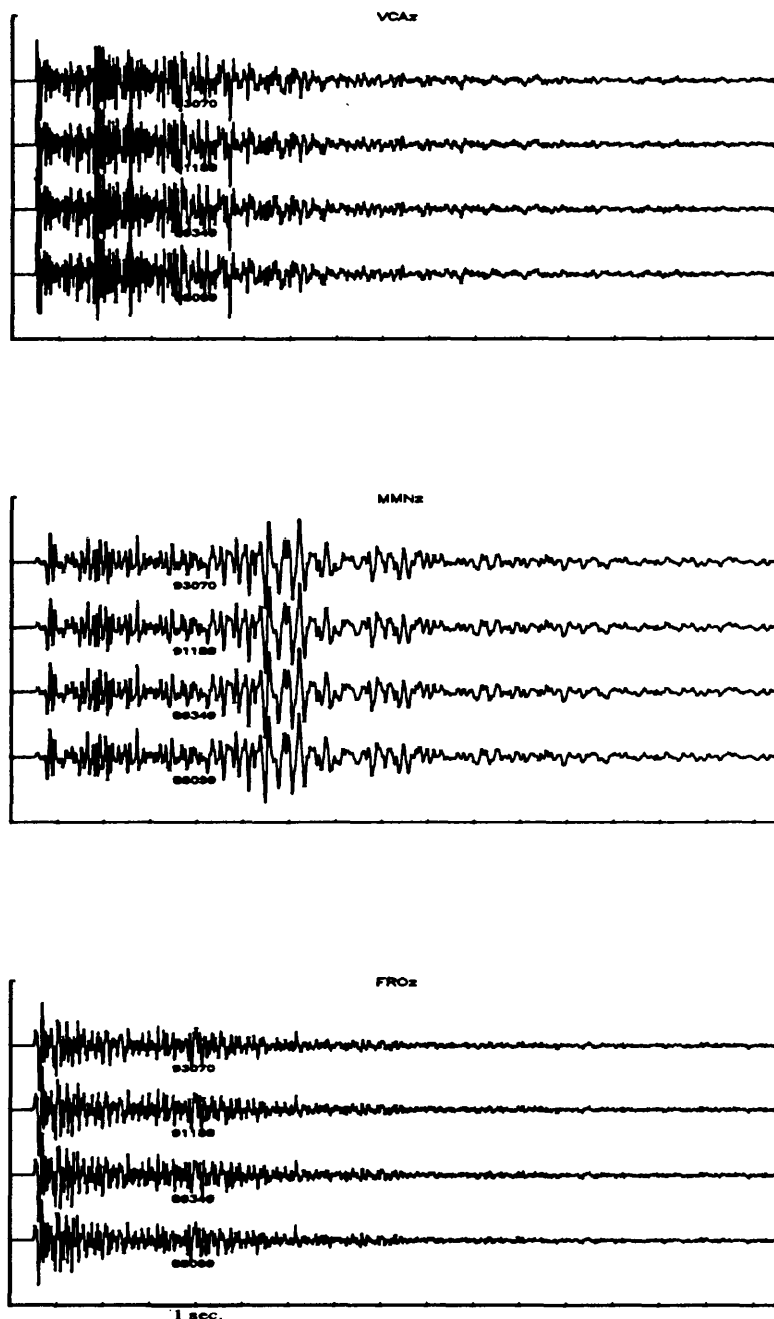


Figure 2. Similar event cluster vertical-component seismograms from a typical similar event multiplet spanning approximately 5 years from the Parkfield region recorded at three of the Parkfield High Resolution Seismic Network borehole stations. The three-component crosscorrelation of the entire seismogram coda is approximately 0.97 between any two pairs in such multiplets

## Holocene Paleoseismology in Western Washington State

Brian F. Atwater

5-9540-10180

U.S. Geological Survey at Department of Geological Sciences  
University of Washington AJ-20  
Seattle, Washington 98195  
206-553-2927 (voice), -8350 (fax), [atwater@u.washington.edu](mailto:atwater@u.washington.edu)

### INVESTIGATIONS UNDERTAKEN

In summer of 1994 I spent a month at Willapa Bay investigating the history of sudden land-level changes in an area of net Cenozoic uplift. This area is an antiform defined by outcrops of the Eocene Crescent Formation, which is the basement rock of the Washington and Oregon coast ranges, and by dips of overlying Tertiary units. Continued uplift in the Quaternary is shown by Pleistocene estuarine deposits as much as 180 m above sea level. I studied Holocene estuarine deposits on the antiform to determine whether or not they, like other such coastal deposits along much of the Cascadia subduction zone, record coseismic subsidence attributable to flexure of the North America plate during great (magnitude 8 or larger) plate-boundary earthquakes. I chose the antiform to test the alternative hypothesis that lesser earthquakes on crustal structures have limited the coseismic subsidence to synclines in the North America plate. The field work--chiefly surveys of evidence for land-level change exposed at low tide in banks of tidal streams--was done with many collaborators, including David Lewis, John Shulene, Jaime Hill, and Eileen and Mark Hemphill-Haley.

The summer work also included several weeks of study of earthquake-induced liquefaction along the lower Columbia River. The goal of this study was to measure the properties of sand that probably liquefied about 300 years ago, during the most recent major plate-boundary earthquake in the area. The study entailed measurements of penetration resistance and subsequent coring beside the penetrometer holes. The penetrometer came from the Oregon Department of Transportation, courtesy of Mei Mei Wang of the Oregon Department of Geology and Mineral Industries. The coring was done mainly with a vibracore operated by a Portland State University team headed by Curt Peterson. Others active in the work included Stephen Palmer of the Washington Division of Geology and Earth Resources.

### RESULTS

The field studies on the antiform showed little if any difference in Holocene stratigraphy between two large outcrops near the axis of the antiform and two large outcrops along the western flank of the antiform. The similarities include details of stratigraphic sequence that suggest one-for-one correlation between subsidence events

near the axis and subsidence events on the flank. These similarities imply that great plate-boundary earthquakes, not lesser upper-plate earthquakes, account for most or all of the geologic evidence for earthquakes at northern Willapa Bay during the past 3500 years. This finding reduces an uncertainty about the size and frequency of great earthquakes at the Cascadia subduction zone.

Field studies on the antiform also led to an unexpected finding about interseismic uplift. According to simple models of cyclic earthquake-related deformation, interseismic uplift should complement the coseismic subsidence from whole-plate flexure at the Cascadia subduction zone. However, an archaeological site on the antiform at Willapa Bay may have undergone little or no uplift during the final decades or centuries before the site subsided coseismically about A.D. 1700. The archaeological site is marked by camp debris exposed in vertical outcrop at the edge of a modern salt marsh, and by remains of two fish weirs on an adjoining mudflat. Coseismic subsidence of the site about A.D. 1700 probably accounts for the burial of a soil above the camp debris. But 5-20 cm of mud accumulated on the camp debris before the subsidence, and the paleoecology of this mud implies negligible preseismic emergence. The implication is that rapid interseismic emergence, such as the 1-2 mm/yr estimated from tide gages along the Pacific coast of Vancouver Island and northern Washington, need not occur at Willapa Bay throughout the final centuries before a great earthquake on the southern Washington part of the Cascadia subduction zone.

The work along the Columbia River led to two sobering findings about methods for the estimating the intensity of shaking responsible for paleoliquefaction features: (1) The sand with the lowest present-day resistance to penetration is sand that both liquefied and flowed in the past. Such reconstituted sand can be identified in core by a combination of lack of bedding, presence of mud clasts, and continuity with intrusions into mud. Its penetration resistance is unsuitable for setting upper bounds on the strength of prehistoric shaking. (2) Sand that has not flowed—that is, sand that retains its primary bedding--may have escaped liquefaction, or it may have liquefied but failed to flow. This ambiguity adds to the difficulty of identifying sand whose penetration resistance can yield estimates of the strength of prehistoric shaking.

#### REPORTS PUBLISHED

Atwater, B.F., compiler, 1994, Geology of liquefaction features about 300 years old along the lower Columbia River at Marsh, Brush, Price, Hunting, and Wallace Islands, Oregon and Washington: U.S. Geological Survey Open-File Report 94-209, 64 p.

Atwater, B.F., Nelson, A.R., Clague, J.J., Carver, G.A., Bobrowsky, P.T., Bourgeois, J., Darienzo, M.E., Grant, W.C., Hemphill-Haley, E., Kelsey, H.M., Jacoby, G.C., Nishenko, S.P., Palmer, S.P., Peterson, C.D., Reinhart, M.A., and Yamaguchi, D.K., 1995, Summary of coastal geologic evidence about past great earthquakes at the Cascadia subduction zone: *Earthquake Spectra* (in press).

Surface Geologic Mapping of Part of the Bootheel Lineament Area  
A Pilot Project in the New Madrid Seismic Zone

Project number 1434 - 94 - G - 2475

Whitney J. Autin  
Institute for Environmental Studies  
Louisiana State University  
Baton Rouge, LA 70803

(504) 388 - 3420  
(504) 388 - 4286 (FAX)  
WAUTIN@LSUVM.SNCC.LSU.EDU

Surficial geological mapping in the Bootheel Lineament area of the New Madrid Seismic Zone is in progress. The mapping area includes the USGS 7.5-minute quadrangles of Bragg City, Wardell, Stanley, Deering, and Hayti Heights. At this writing, the project data collection is in progress, with an anticipated project completion date of February 28, 1995.

Field data acquisition and photogeologic analysis has been completed. Cores and auger borings from approximately 75 locations have been described in the project area. The cores are generally aligned along transects to produce cross sections of relevant landform, soils, and lithofacies associations.

Data reduction and synthesis will be completed in the next phase of the project. The final report of February 1995 will include a set of 7.5-minute geologic quadrangle maps depicting the distribution of Holocene and Pleistocene sediments. Accompanying cross sections will illustrate the relation of surface landscape features to underlying surficial sediments. The report will discuss lithologic and pedologic properties of map units, and relate the distribution of surficial materials to relevant neotectonic data existing for the area.

## **Analysis of Crustal Deformation Along the Southernmost Segment of the San Andreas Fault System, Imperial Valley, California: Implications for Earthquake Prediction**

1434-94-G-2162

Richard Bennett  
Robert Reilinger  
Earth Resources Laboratory  
Dept. of Earth, Atmospheric, and Planetary Sciences  
Massachusetts Institute of Technology  
Cambridge, Massachusetts 02142  
(617) 253-7868  
bennett@erl.mit.edu

### **INVESTIGATIONS**

Since 1988, a consortium of universities and government agencies has been using the Global Positioning System (GPS) to monitor crustal deformation in the vicinity of the Salton Trough, southern California and northern Mexico. As of 1993, the observation network includes over one hundred stations, extending from the Big Bend segment of the San Andreas fault to the Gulf of California (Figure 1). We use these geodetic observations in conjunction with other geophysical and geological information to investigate active tectonic processes along the southernmost segment of the San Andreas fault system. Our primary efforts during the present contract period have been in the analysis and interpretation of 1988 to 1993 GPS measurements in the Imperial and Coachella Valleys with emphasis on

1. Isolation of earthquake-associated (episodic) and interseismic (secular) deformation.
2. The distribution of strain accumulation along and across the fault systems comprising the Pacific-North American plate boundary in southern California and northern Mexico.
3. Understanding the active tectonics of the complex transition from ocean spreading in the Gulf of California to continental transform faulting along the San Andreas fault system.

### **RESULTS**

Crustal deformation derived from the 1988-1993 observations have been used to investigate coseismic deformation for the 1992 Joshua Tree earthquake [Bennett et al., 1995], far field deformation associated with the Landers earthquake [Bennett et al., 1994], and contemporary interseismic deformation [Bennett et al., 1994; Sung et al., 1994].

While the Landers earthquake sequence adds significant uncertainty to the secular velocity estimates for sites in the northern part of the network, there is little effect on velocities to the south.

We mitigate the effects of the 1992 earthquakes (Joshua Tree and Landers) by estimating coseismic displacements at those sites for which the history of observations is sufficient. (For the Landers earthquake, coseismic displacement estimates at PGGA sites were constrained to agree with their well determined values [Bock et al., 1993; Blewitt et al., 1993]). We then fit the resulting coseismic displacement estimates to an earthquake model. For the case of the Joshua Tree earthquake, we included estimates of trilateration station displacements [Dong, 1993] in determining the earthquake model parameters. Coseismic displacement estimates for sites which were poorly determined by the data due to insufficient observation histories were then predicted from the model. Assuming that the model is accurate to within 10%, we then simultaneously estimated corrections to these model displacements along with the secular site velocities.

The resulting velocity field is shown in Figure 2. Velocities are computed in a North America fixed reference frame. The velocity field is clearly dominated by right-lateral shear, with no significant motion (relative to the uncertainties) beyond about 30 km northeast of the San Andreas fault. There are apparently significant, fault normal motions near fault offsets and associated basins. We are currently investigating the implications of such motions for models of continental plate boundary deformation.

Figures 3-5 show velocity profiles relative to North America along three transects across the plate boundary (see Figure 1 for location of transects). The profiles are oriented perpendicular to the strike of the local faults. Arctangent trends predicted from geologically reasonable screw dislocation models are also shown for comparison. Based on these profiles, we make the following observations:

1. While the uncertainties for the velocity estimates at most sites in the northern half of the network are still quite large, profile A-A' does provide useful constraints on the relative motions about the San Andreas ( $\sim 28$  mm/yr) and San Jacinto ( $\sim 10$  mm/yr) faults; the southernmost San Andreas apparently accommodates the lion's share of Pacific-North American plate motion ( $\sim 60\%$ ). This result is consistent with geologic and geomorphic evidence for a long term slip rate along the southernmost San Andreas of 23 to 35 mm/yr [Keller et al., 1982; Weldon and Sieh, 1985]. With the recurrence interval inferred to be about 300 years and with last major rupture having occurred in 1680 [Sieh, 1986], a large earthquake on the southernmost San Andreas appears to be due.
2. Across the Imperial Valley, a large amount of the plate motion (40 mm/yr) is accommodated by the Imperial fault. The shallow locking depth required by the data (7.5 km) is consistent with high temperatures and the shallow seismicity cut off.
3. Across the Cerro Prieto fault, we determine a slip rate nearly identical to the NUVEL-1A estimate (46 mm/yr). The difference between the rates along the Cerro Prieto fault and the fault systems to the north can be explained by about 6 mm/yr of motion along the Agua Blanca system which transfers motion to the faults of the southern California Borderlands. This interpretation is consistent with the results of Farina et al., [1994], and Larson [1993].

## REFERENCES

- Blewitt et al., Absolute far-field displacements from the 28 June 1992 Landers earthquake sequence, *Nature*, 361, 340-342, 1993.
- Bock et al., Detection of crustal deformation from the Landers earthquake sequence using continuous geodetic measurements, *Nature*, 361, 337-340, 1993.
- Dong, D., The horizontal velocity field in southern California from a combination of terrestrial and space-geodetic data, *Ph. D. Thesis, Massachusetts Institute of Technology*, p. 157, 1993.
- Farina, F., T. Dixon, F. Suarez, E. Humphreys, M. Miller, Preliminary GPS results bearing on motion of the Agua Blanca fault zone, Baja California, Mexico, *EOS, Trans. Am. Geophys. Union*, 75, 182, 1994.
- Keller et al., Tectonic geomorphology of the San Andreas fault zone in the southern Indio Hills, Coachella Valley, California, *Geol. Soc. Am. Bull.*, 93, 46-56, 1982.
- Larsen, K. M., Application of the Global Positioning System to crustal deformation measurements 3. Results from the southern California Borderlands, *J. Geophys. Res.*, 98, 21,713-21,726, 1993.
- Sieh, K. E., Slip rate across the San Andreas and prehistoric earthquakes at Indio, California, *EOS, Trans. Am. Geophys. Union*, 67, 1200, 1986.
- Weldon, R. J., and Sieh, K. E., Holocene rate of slip and tentative recurrence interval for large earthquakes on the San Andreas fault, Cajon Pass, southern California, *Geo. Soc. Am. Bull.*, 96, 793-812, 1985.

## PUBLICATIONS

- Bennett, R. A., R. Reilinger, W. Rodi, Y. Li, N. Toksöz, and K. Hudnut, Coseismic Fault Slip Associated with the 1992  $M_w$  6.1 Joshua Tree, California Earthquake: Implications for the Joshua Tree-Landers Earthquake Sequence, *J. Geophys. Res.*, *in press*, 1995.
- Bennett, R. A., R. Reilinger, J. Gonzalez, GPS Measurements in Southernmost California/Northern Baja-Mexicali Valley: Continental Deformation in a Trans-Current/Extensional Environment, *EOS, Trans. Am. Geophys. Union*, 75, 164, 1994.
- Sung, L., Z. Shen, R. Reilinger, D. Jackson, K. Hudnut, T. Herring, B. Hager, B. Ge, J. Freymueller, Aseismic crustal velocity estimation of southern California, *EOS, Trans. Am. Geophys. Union*, 75, 179, 1994.

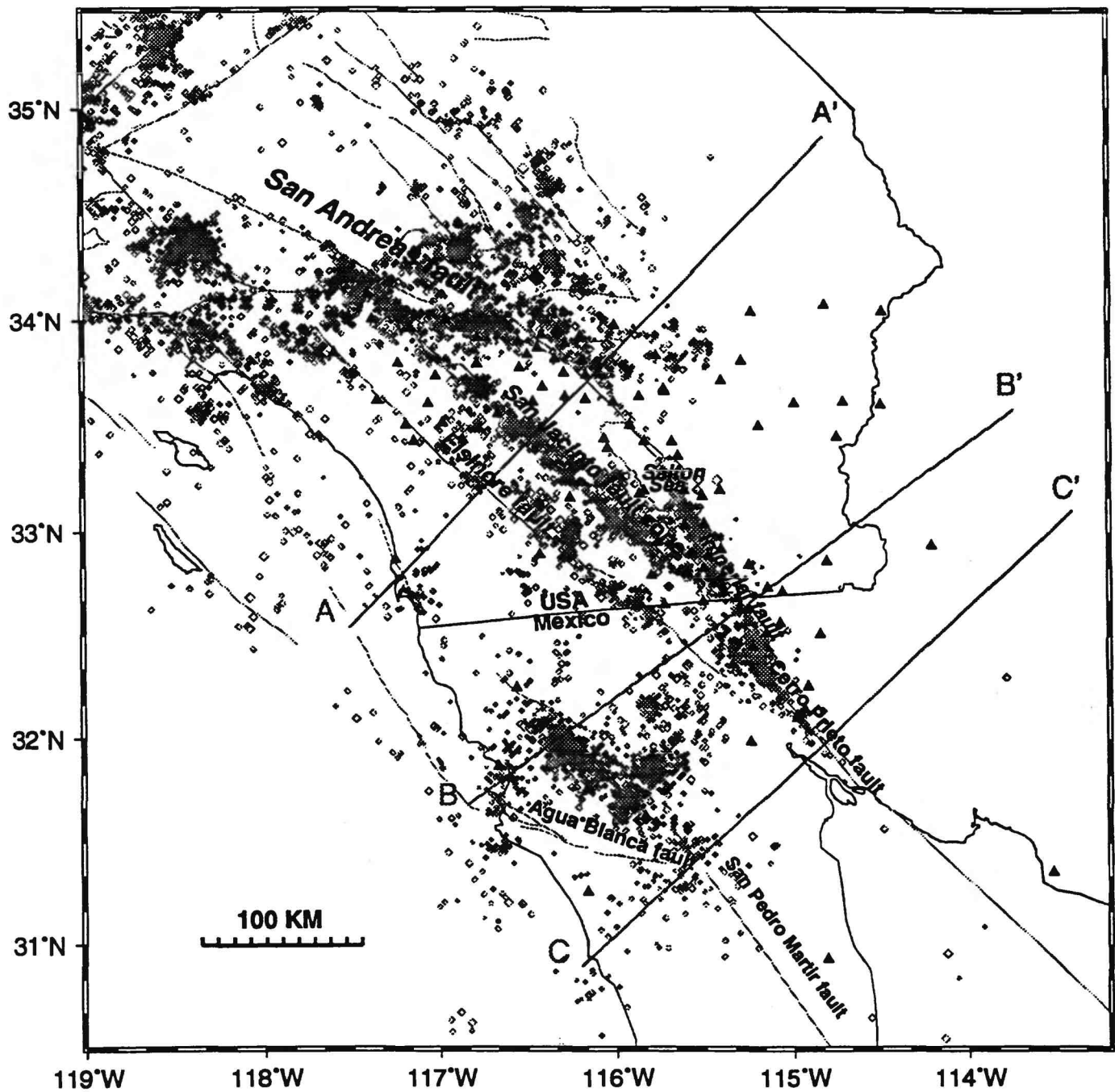


**Figure 1.** GPS stations established by a consortium of university groups and government agencies during the period 1988 - 1993 (triangles). Lines show the location of velocity profiles presented in Figures 3-5.

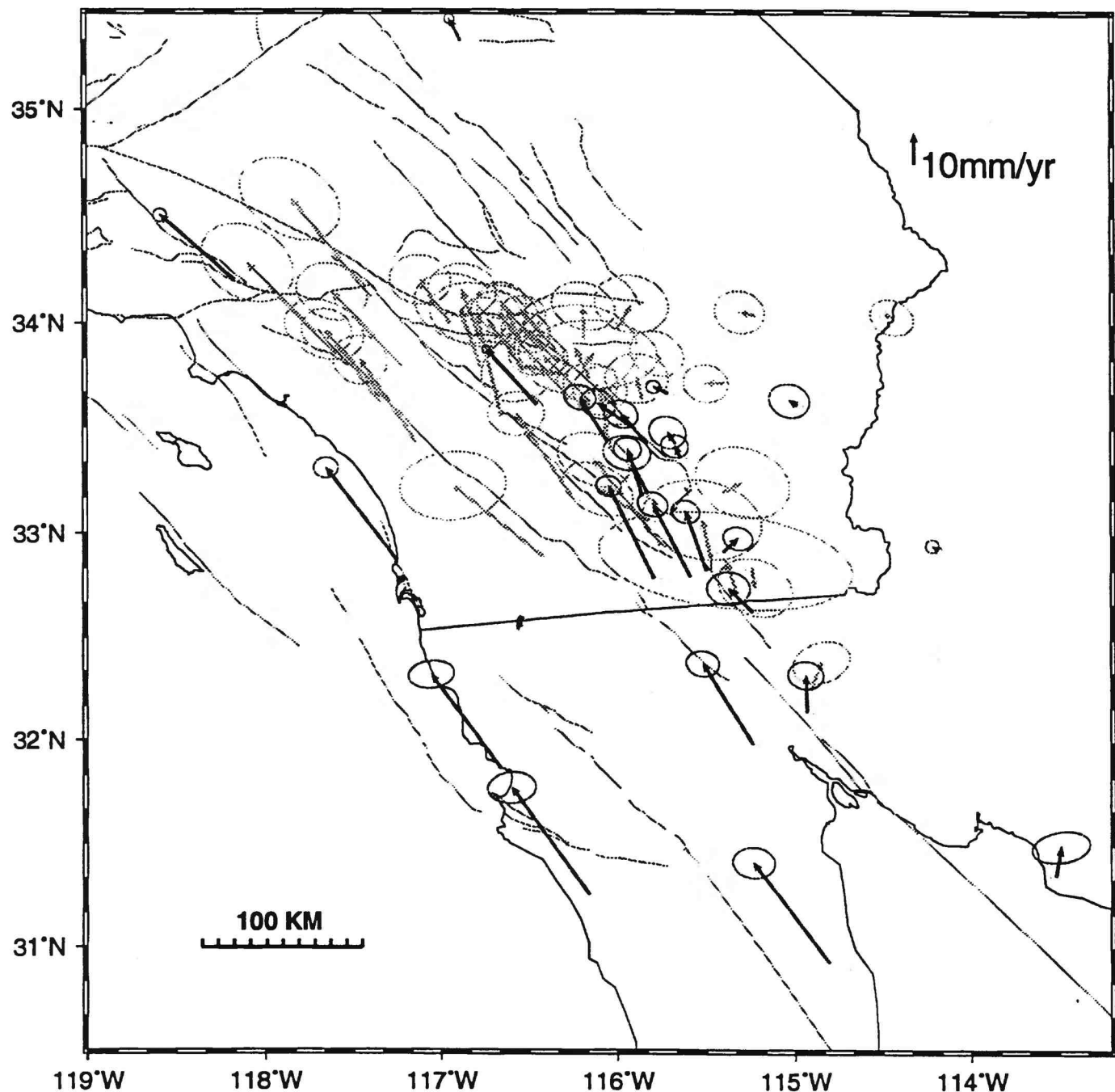


**Figure 2.** The southern California - northern Mexico velocity field inferred from GPS data collected over the period of 1988 to 1993. Error ellipses represent the 95% confidence level after rescaling the formal uncertainties by a factor of 2. Dark arrows show velocities determined with uncertainties less than 6 mm/yr. Light arrows show velocity estimates for the remaining sites within the network. That the velocity estimates for sites in the southern half of the network are better determined is a result of the large uncertainties introduced by the occurrence of the 1992 earthquakes.

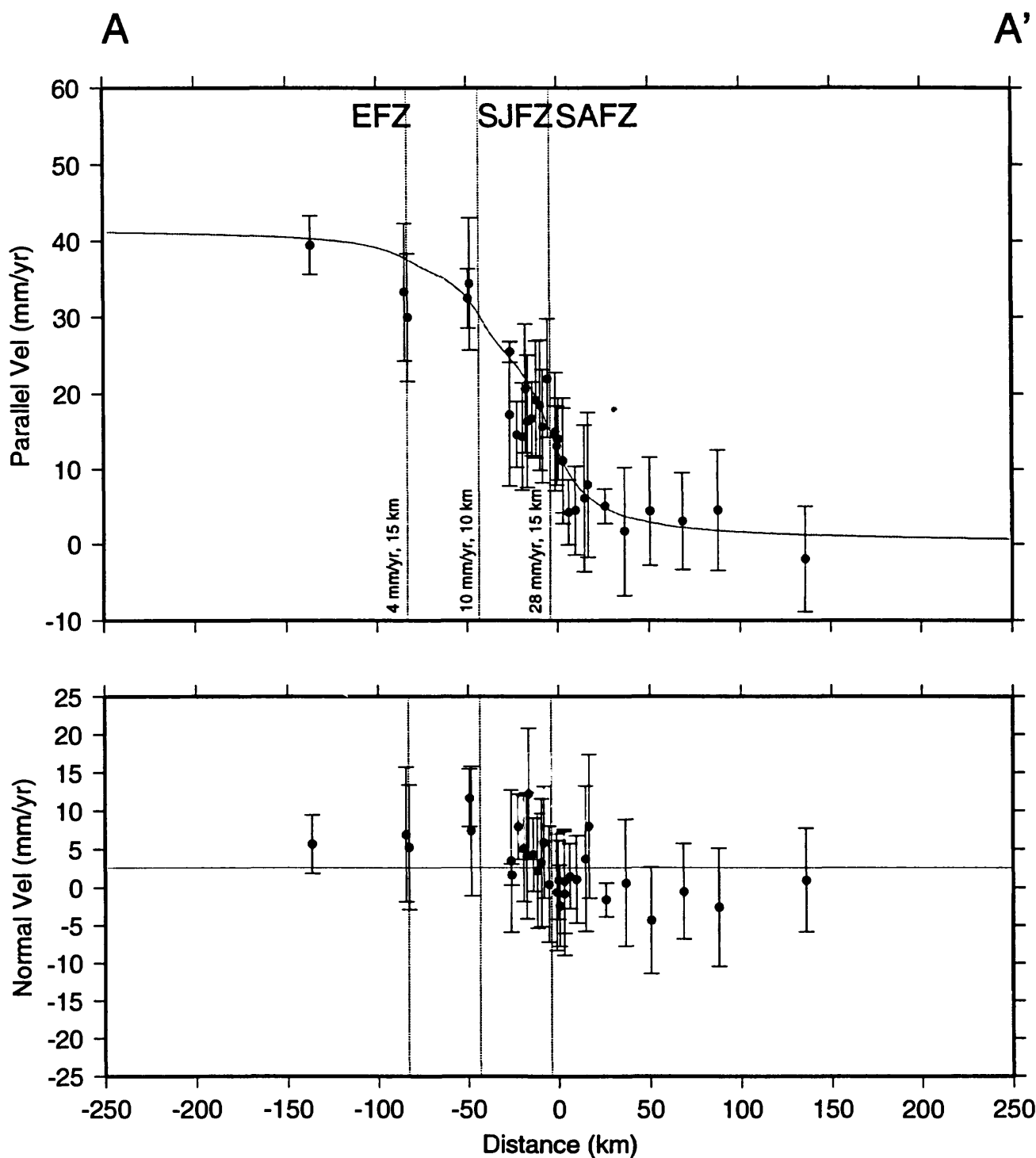


**Figure 3.** Velocity profile A-A' across the southern San Andreas, San Jacinto, and Elsinore faults in southern California. The model curve represents the net effect of screw dislocations for the San Andreas (28 mm/yr, 15 km), San Jacinto (10 mm/yr, 10 km), and Elsinore (4 mm/yr, 15 km) faults.

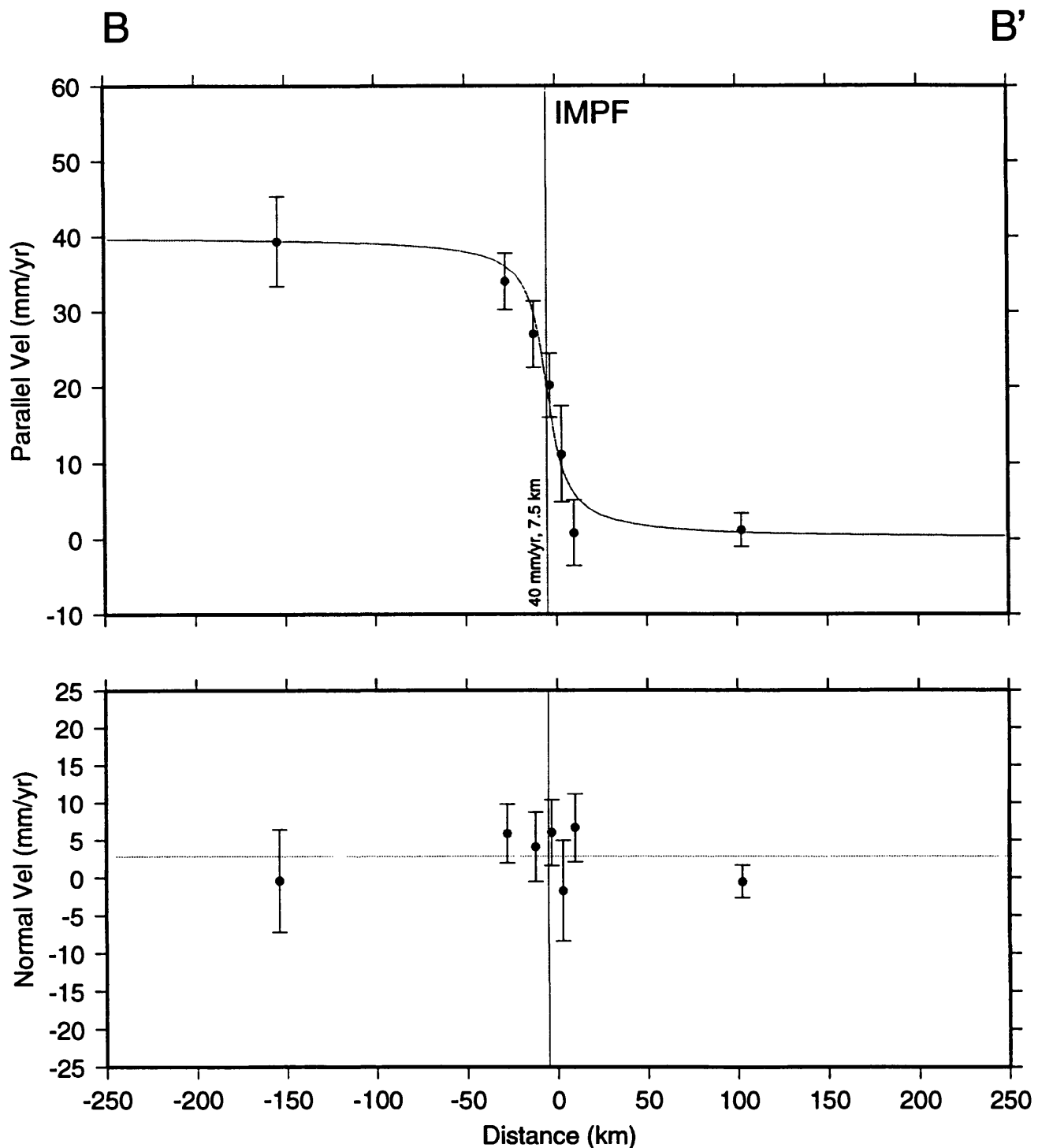


**Figure 4.** Velocity profile B-B' across the Imperial, Laguna-Salada, and San Miguel-Vallacitos faults, southern California and northern Mexico. The arctangent curve is a screw dislocation model of the Imperial fault (40 mm/yr, 7.5 km).

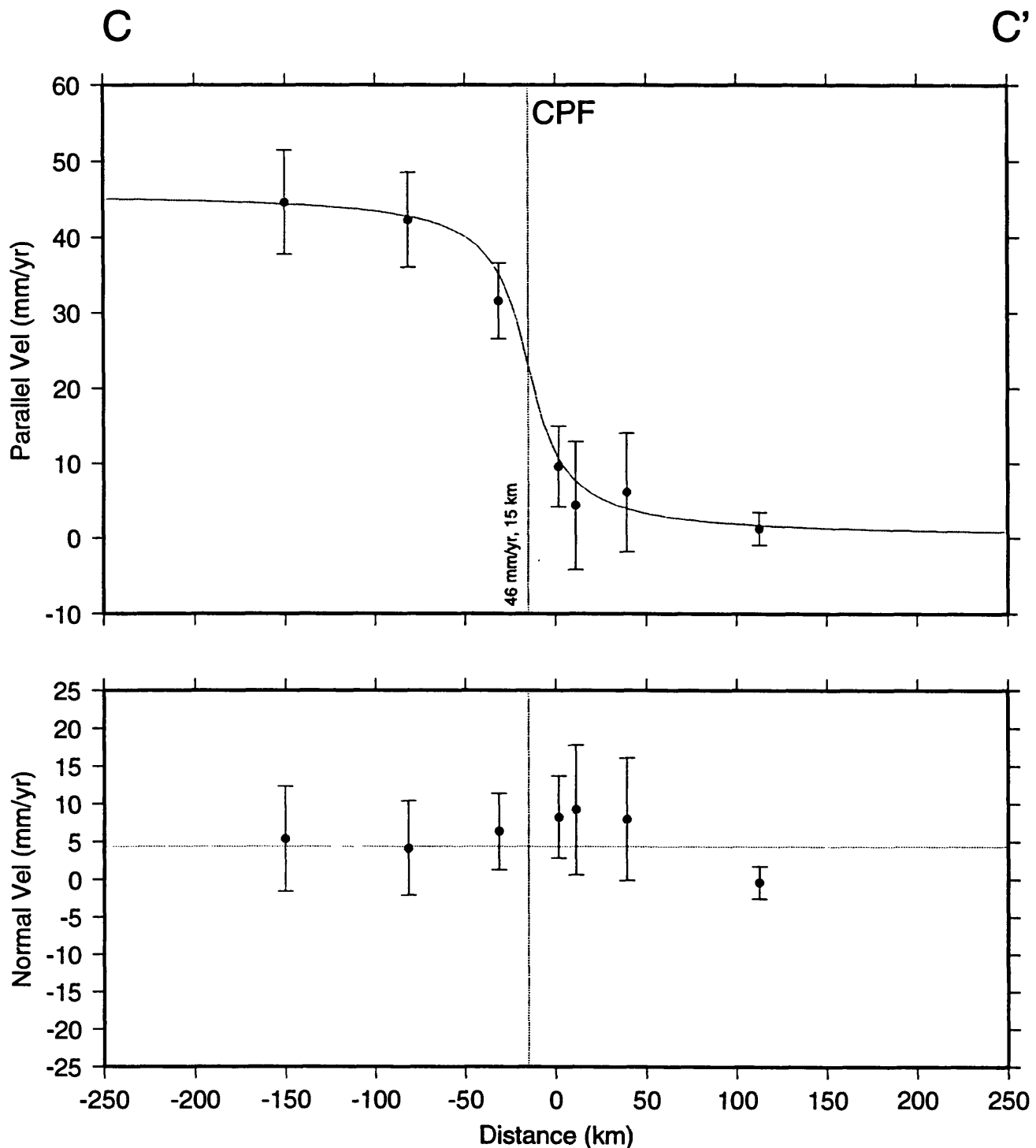


**Figure 5.** Velocity profile C-C' across the Cerro Prieto and Agua Blanca faults in northern Mexico. The arctangent curve is a screw dislocation model of the Cerro Prieto fault (46 mm/yr, 15 km).

# Seismic Source Evaluation of the Salt Lake City segment of the Wasatch fault zone, Central Wasatch Front, Utah

**Award No. 1434-94-G-2495**

**Bill D. Black, William R. Lund, and Bea H. Mayes**  
**Utah Geological Survey**  
**2363 South Foothill Drive**  
**Salt Lake City, Utah 84109-1491**  
**(801) 467-7970**

## INTRODUCTION

The Wasatch fault zone (WFZ) is the longest and most active normal-slip fault in North America, and has long been recognized as a potential source of large-magnitude earthquakes that could affect over 80 percent of Utah's 2.3 million residents. The WFZ is divided into 10 independent, seismogenic segments based on scarp morphology, surface-fault-rupture patterns, range-crest morphology, geophysical evidence, and trenching investigations (Schwartz and Coppersmith, 1984; Machette and others, 1992). The Salt Lake City segment of the WFZ trends through the densely populated Salt Lake Valley (figure 1) and poses a significant earthquake risk to citizens living in the Salt Lake City metropolitan area.

The Holocene chronology of surface-rupturing earthquakes on the Salt Lake City segment of the WFZ has been the subject of paleoseismic studies for more than a decade. The current faulting chronology is based on data from several incompletely investigated trench sites at Little Cottonwood Canyon (LCC) in 1979, South Fork Dry Creek (SFDC) in 1985, and Dry Gulch (DG) in 1991 (figure 1; Lund and Schwartz, 1987; Schwartz and Lund, 1988; Lund, 1992). Because of this, questions remain regarding timing and recurrence of large-magnitude, surface-rupturing earthquakes on this segment. The purpose of this investigation is to establish a complete earthquake chronology from at least the mid-Holocene for the Salt Lake City segment at a single site. The investigation consists of detailed logging of five new trenches excavated across the fault zone at the SFDC site (figure 1), and radiocarbon dating of material from key stratigraphic units in the trenches to constrain the timing of prehistoric surface-rupturing earthquakes.

## INVESTIGATION RESULTS

**(May 1, 1994 through October 1, 1994)**

At the SFDC site (figure 1), the WFZ consists of six sub-parallel, west-dipping faults, and a single westernmost east-dipping antithetic fault, in a zone a few hundred meters wide (Lund and Schwartz, 1987; Personius and Scott, 1992). Three of the six west-dipping faults displace a

debris-flow levee along South Fork Dry Creek, estimated to be 2,000 to 4,000 years old based on soil profile development (Scott and Shroba, 1985); the two easternmost faults merge south of the debris-flow levee and continue southward for a short distance (Personius and Scott, 1992). A fourth fault is buried by the levee; a fifth is also probably buried but does not reappear north of South Fork Dry Creek. The sixth fault is represented by a short, single-event scarp that does not intersect the debris-flow levee. Road construction destroyed the antithetic fault scarp.

Five new trenches have been excavated across five of the fault scarps at the SFDC site. A sixth fault scarp was trenched in 1992, at the location of a trench previously investigated in 1985, and was not trenched again as the data obtained confirmed the earlier results. Three of these trenches are across scarps trenched in previous investigations. The remaining trenches are across scarps not previously trenched.

### **Trench DC2-1**

Trench DC2-1 was excavated across a short, single-event fault scarp, north of trench DC3 excavated in 1985, and did not expose any new stratigraphic relationships. The trench exposes a single fault trace displacing alluvial-fan deposits 1.3 meters (4.3 ft) (0.8 meters [2.6 ft] approximate net slip) down to the west. The most recent event on this fault produced a wide crack that rapidly filled with organic-rich material from the degrading scarp free face, followed by formation of a 0.8-meter (2.6-ft) thick colluvial wedge. The wedge buried an A-horizon soil forming on the alluvial-fan deposits, and is overlain by slope-wash colluvium on which the soil is forming. Radiocarbon samples (dates pending) were taken from the crack-fill material and paleosol A horizon to determine timing for this event.

### **Trench DC2-2**

Trench DC2-2 was excavated across a multiple-event fault scarp, just north of trench DC4 excavated in 1985, and shows similar stratigraphic relationships. The trench exposes a single main fault trace and smaller subsidiary fault, which displace alluvial-fan deposits 1.6 meters (5.2 ft) (0.8 meters [2.6 ft] approximate net slip) down to the west. The lower portion of these deposits has been altered and masked by calcium carbonate deposition from ground water; they are overlain by slope-wash colluvium and the modern soil.

Trench DC2-2 contains evidence for two earthquakes, and indirect evidence for a third event. The colluvial wedge and fault trace for the antepenultimate event are not exposed, but are evidenced by a degraded scarp free face which truncates the alluvial-fan deposits and A-horizon soil. The penultimate event on the main fault trace formed a 0.6-meter (2.0-ft) thick colluvial wedge, which buried the alluvial-fan deposits, A-horizon soil, and the degraded scarp free face from the antepenultimate event. The most recent event was followed by formation of a 0.7-meter (2.3-ft) thick colluvial wedge stacked on top of the penultimate-event wedge, overlain by additional slope-wash colluvium and the modern soil.

Bulk sediment samples were taken from: (1) the paleosol A horizon, and (2) organic-rich material deposited in a crack at the base of the scarp free face from the most recent event.

Results of radiocarbon dating (pending) will determine timing for the penultimate and most recent events on this fault scarp.

### Trench DC2-3

Trench DC2-3 was excavated across a fault scarp not previously trenched. The scarp is buried by the younger debris-flow levee to the north, and has been modified by excavation for a water-tank pad. The trench exposes a debris-flow deposit containing numerous, large, grusified quartz monzonite boulders and two earthquake-related colluvial wedges.

In trench DC2-3, a single fault trace has displaced the debris-flow deposit a total of 2.1 meters (6.9 ft) (1.3 meters [4.3 ft] approximate net slip) down to the west during the past two surface-rupturing earthquake events. The penultimate event formed a 1.7-meter (5.6-ft) thick colluvial wedge, burying the debris-flow deposit and an A-horizon soil formed on it. The most recent event sheared the penultimate-event wedge, and formed a 0.9-meter (3.0-ft) thick colluvial wedge stacked on top of the penultimate-event wedge.

Bulk-sediment samples were taken from: (1) the paleosol A horizon, (2) a block of the paleosol A horizon incorporated in the penultimate-event wedge, and (3) organic-rich crack-fill material associated with the most recent event. Results of radiocarbon dating (pending) will define timing for the last two events.

### Trench DC2-4

Trench DC2-4 was excavated across the multiple-event fault scarp trenched at the nearby Dry Gulch site (DG, figure 1) in 1991. The trench shows evidence for multiple large earthquake events on two fault traces. The amount of offset on these faults is difficult to determine due to complex stratigraphic relationships and the lack of correlative stratigraphy across the faults.

The western fault trace shows evidence for two earthquakes, and indirect evidence for a third event. This fault trace displaces alluvial-fan deposits at least 3.4 meters (11.2 ft) (net slip undetermined) down to the west below the floor of the trench, and bounds a deep graben to the west filled with dark-gray, organic-rich alluvium. Although the colluvial wedge for the antepenultimate event on the fault is not exposed, that event is evidenced by a degraded scarp free face formed on the alluvial-fan deposits. The free face is mantled by the colluvial wedge formed following the penultimate event, which in turn was partially eroded and buried by graben-fill sediments. The most recent event on this fault trace formed a 1.7-meter (5.6-ft) thick colluvial wedge, which buried the graben-fill deposits and penultimate-event wedge and is in turn overlain by additional graben fill.

The eastern fault trace shows evidence for two earthquakes, which may be distinct from or the same as those on the western fault trace. The eastern fault trace displaces alluvial-fan deposits roughly 3.3 meters (10.8 ft) (net slip undetermined) down to the west. On the downthrown side of the fault, the alluvial-fan deposits are buried by a 1.5-meter (4.9-ft) thick colluvial wedge formed after the penultimate event. The distal portion of the penultimate-event wedge, and an A-

horizon soil formed on it, have been eroded by a degrading-scarp free face formed after the most recent event on the western fault trace. The most recent event on the eastern fault trace sheared the penultimate-event wedge, and formed a 2.7-meter (8.9-ft) thick colluvial wedge stacked on top of the penultimate-event wedge and A-horizon soil.

Bulk sediment samples were taken from: (1) the paleosol A horizon buried by the colluvial wedge formed after the most recent event on the eastern fault trace, (2) organic-rich crack-fill deposits resulting from the most recent event on the western fault trace, and (3) the lowermost portion of the graben-fill deposits exposed in the trench. Results of radiocarbon dating (pending) will determine timing for the most recent event on both fault traces and the age of the graben-fill deposits. A sample will also be taken from the lower colluvial wedge on the western fault trace to hopefully further constrain the timing for this older event. No suitable material was found to date the older event on the eastern fault trace.

### Trench DC2-5

Trench DC2-5 was excavated across the easternmost fault scarp at the SFDC site, which crosses the debris-flow levee to the north. This fault scarp had not been previously trenched, but merges with the scarp trenched at DC2-3. The trench exposes two main fault traces and an antithetic fault which offset alluvial-fan deposits and discontinuous hillslope colluvium. The eastern fault trace has evidence for one earthquake, and displaces these deposits 1.0 meters (3.3 ft) (0.7 meters [2.3 ft] approximate net slip) down to the west. The western fault trace bounds a shallow graben to the west and also has evidence for one event, displacing the deposits 2.9 meters (9.5 ft) (2.0 meters [6.6 ft] approximate net slip) down to the west. The western end of the graben is bounded by a small antithetic fault with 0.2 meters (0.7 ft) of offset (down to the east).

Stratigraphic relations exposed in the trench are complex and difficult to interpret. The most recent event on the eastern fault trace formed a 1.1-meter (3.6-ft) thick colluvial wedge, burying the alluvial-fan deposits and an A-horizon soil. To the west, these deposits are truncated by the degraded scarp free face formed after the most recent event on the western fault trace. The most recent event on the western fault trace, followed by post-event slumping, produced a large and complex colluvial wedge 3.5 meters (11.5 ft) thick consisting of several intact slump blocks surrounded by organic-rich crack-fill material. This wedge also buries the alluvial-fan deposits and A-horizon soil, and is bounded by the antithetic fault to the west. Both colluvial wedges are overlain by slope-wash colluvium on which soil is forming.

Bulk sediment samples were taken from: (1) the paleosol A horizon buried by the easternmost colluvial wedge, (2) organic-rich crack-fill material resulting from the most recent event on the western fault trace, and (3) the paleosol A horizon buried by the westernmost colluvial wedge. Results of radiocarbon dating (pending) will determine timing for the two events.

## REPORTS

The following brief report was prepared presenting the preliminary results of the Salt Lake City segment seismic source evaluation:

Black, B.D., Lund, W.R., and Mayes, B.H., 1994, Large earthquakes on the Salt Lake City segment of the Wasatch fault zone - A preliminary summary of new information from the South Fork Dry Creek site, Salt Lake County, Utah: Unpublished Utah Geological Survey Report, 9 p.

## REFERENCES

- Lund, W.R., 1992, New information on the timing of earthquakes on the Salt Lake City segment of the Wasatch fault zone - Implications for increased earthquake hazard along the central Wasatch Front: Utah Geological Survey, Wasatch Front Forum, v. 8, no. 3, p. 12-13.
- Lund, W.R., and Schwartz, D.P., 1987, Fault behavior and earthquake recurrence at the Dry Creek site, Salt Lake City segment, Wasatch fault zone, Utah [abs.]: Geological Society of America Abstracts with Programs, v. 19, no. 5, p. 317.
- Machette, M.N., Personius, S.F., and Nelson, A.R., 1992, Paleoseismology of the Wasatch fault zone - A summary of recent investigations, interpretations, and conclusions, *in* Gori, P.L., and Hays, W.W., editors, Assessment of regional earthquake hazards and risk along the Wasatch Front, Utah: U.S. Geological Survey Professional Paper 1500, p. A1-A71.
- Personius, S.F., and Scott, W.E., 1992, Surficial geologic map of the Salt Lake City segment and parts of adjacent segments of the Wasatch fault zone, Davis, Salt Lake, and Utah Counties, Utah: U.S. Geological Survey Miscellaneous Investigation Series Map I-2106, scale 1:50,000.
- Schwartz, D.P., and Coppersmith, K.J., 1984, Fault behavior and characteristic earthquakes - Examples from the Wasatch and San Andreas fault zones: *Journal of Geophysical Research*, v. 89, no. B7, p. 5681-5698.
- Schwartz, D.P., and Lund, W.R., 1988, Paleoseismicity and earthquake recurrence at Little Cottonwood Canyon, Wasatch fault zone, Utah, *in* Machette, M.N., editor, In the footsteps of G.K. Gilbert - Lake Bonneville and neotectonics of the eastern Basin and Range Province: Utah Geological and Mineral Survey Miscellaneous Publication 88-1, p. 82-85.
- Scott, W.E., and Shroba, R.R., 1985, Surficial geologic map of an area along the Wasatch fault zone in the Salt Lake Valley, Utah: U.S. Geological Survey Open-File Report 85-448, scale 1:24,000, 18 p.

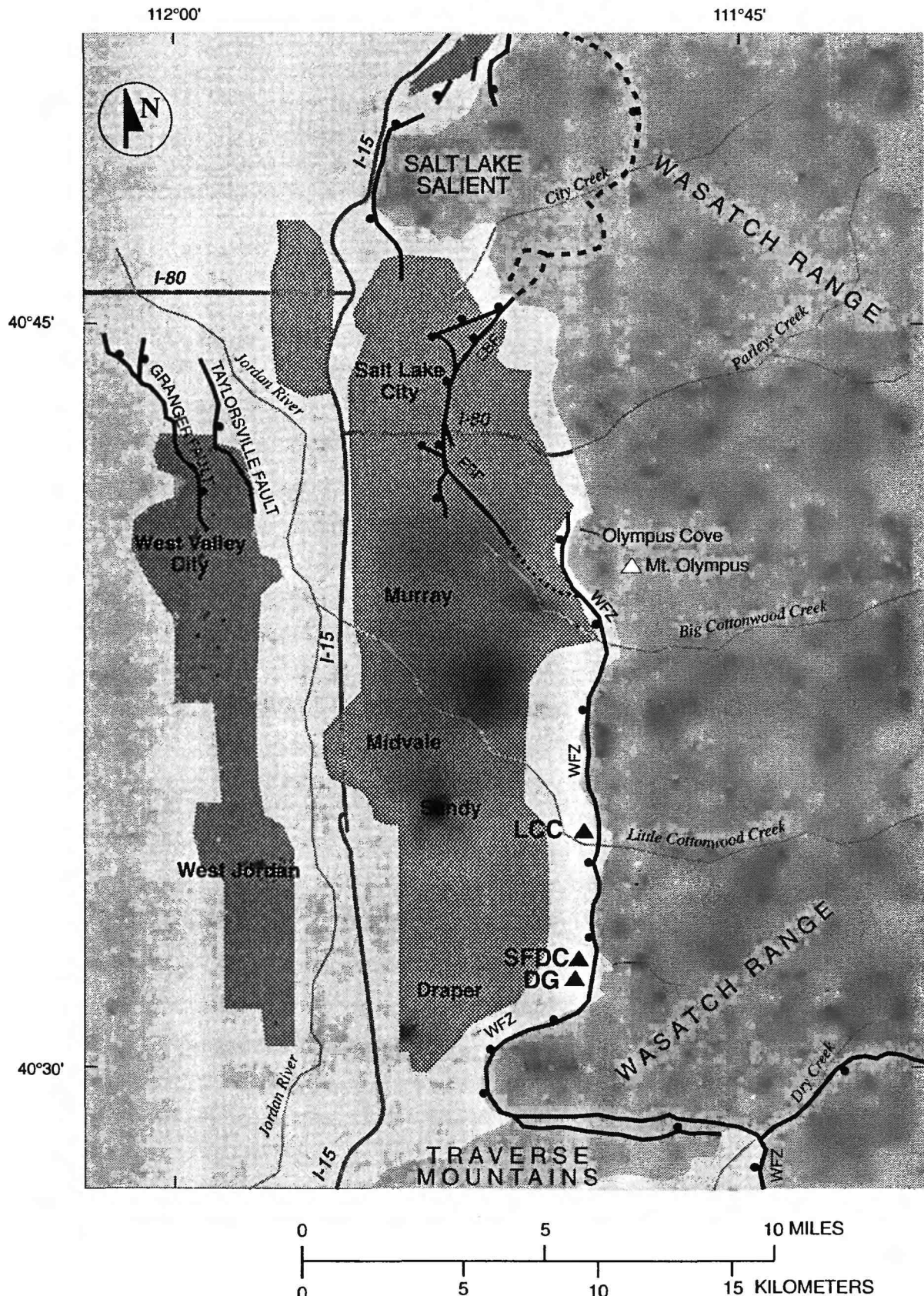


Figure 1. Salt Lake City segment of the Wasatch fault zone showing location of the Little Cottonwood Canyon (LCC), South Fork Dry Creek (SFDC), and Dry Gulch (DG) trench sites (Lund, 1992).

## High-Resolution Geophysical Studies in the Pacific Northwest

9380-10104

Richard J. Blakely  
 U.S. Geological Survey, MS 989  
 345 Middlefield Road  
 Menlo Park, CA 94025

415-329-5316 (voice)  
 415-329-5133 (fax)  
 blakely@gauss.wr.usgs.gov

### Element II

#### Investigations Undertaken

*Portland area.* This project focused its FY 1994 efforts on completion of interpretations based on new, high-resolution aeromagnetic data from the Portland Basin and surrounding areas. Two abstracts, an Open-File Report, and a journal article are now published or in review, each written in cooperation with USGS, Oregon Department of Geology and Mineral Industries, and Portland State University scientists.

*Salem area.* A new aeromagnetic survey will be acquired in FY 1994 adjacent to the Portland survey discussed above. This survey, funded by the National Earthquake Hazard Reduction Program, will be flown in early FY 1995 in order to investigate the structure responsible for the M=5.6 earthquake that struck Scotts Mills, Oregon, in March 1993.

*Klamath Falls Area.* The association between faulting, volcanism, gravity anomalies, and recent earthquakes at Klamath Falls was investigated in cooperation with Ray Wells, Craig Weaver, Tony Qamar, and other earth scientists.

#### Results

*Portland area.* The U.S. Geological Survey conducted a high-resolution aeromagnetic survey of the Portland-Vancouver area in September 1992 to help locate and understand concealed hazards in the area. These data indicate that the Portland Basin is underlain by several strongly magnetic blocks, part of a chain of sources that extend south through the Willamette Valley and north into Washington. We interpret these blocks to be accreted oceanic crust of Eocene age. Several northwest-trending anomalies reflect faulting in the underlying basaltic basement. Most notable is a pronounced northwest-striking magnetic gradient in downtown Portland clearly correlated with the location of a mapped fault (Fig. 1). This fault lies beneath Quaternary sedimentary deposits, its existence and location based previously on data from a few shallow wells. The correlation between the magnetic anomaly and the mapped fault confirms the existence of the fault. More important, our models indicate that the fault may have a total vertical offset of nearly 1 km and that it may extend significantly beyond its mapped extent, a total distance of at least 50 km. If seismically active along this entire length, seismic risk to the Portland-Vancouver metropolitan area may be greater than previously suspected. We interpret this and other northwest-trending faults to be

part of a former pull-apart zone now occupied by the Portland Basin. This pull-apart zone is now reactivated by compressional stresses and is apparently the source of diffuse earthquake activity at the  $M \leq 4$  level throughout this area.

*Salem area.* As noted above, data are being collected from this area in early FY 1995; results will not be available until after data acquisition.

*Klamath Falls area.* We found that the  $M \leq 6.0$  Klamath Falls earthquakes of September 1993 occurred at an inflection point in the trend of normal faults bounding the Klamath Falls graben. This change in fault trend is mirrored in the focal mechanisms of the two mainshocks and in the pronounced curvature of the aftershock distribution. It also coincides with a northeast trending residual gravity gradient previously recognized in regional gravity data (Blakely and Jachens, 1990), which in turn correlates with boundaries between segments in the Quaternary Cascade arc that were recognized by Guffanti and Weaver (1988) based on the distribution of volcanic vents. The northeast-trending gravity anomalies appear fundamentally related to crustal stress, recent seismicity, and volcanism. They may reflect in a broad sense the relative strength of the middle and upper crust; i.e., crustal strength is a function of its lithology and thermal state. The high gravity regions, which have experienced essentially no volcanism during the Quaternary, may be cooler, composed of more consolidated crustal materials, and possess greater elastic strength than the neighboring low gravity regions with abundant volcanism.

## References

- Beeson, M.H., Tolan, T.L., and Madin, I.P., 1991, Geologic map of the Portland quadrangle, Multnomah and Washington Counties, and Clark County, Washington: Oregon Department of Geology and Mineral Industries Geologic Map Series GMS-75, scale 1:24,000.
- Blakely, R.J., and Jachens, R.C., Volcanic, isostatic residual gravity, and regional tectonic setting of the Cascade volcanic province: *Journal of Geophysical Research*, v. 95, p. 19,439–19,451.
- Guffanti, M. and Weaver, C.S., 1988, Distribution of late Cenozoic volcanic vents in the Cascade Range: Volcanic arc segmentation and regional tectonic considerations: *Journal of Geophysical Research*, v. 93, p. 6513–6529.

## Reports Published

- Snyder, S.L., Felger, T.J., Blakely, R.J., and Wells, R.E., 1993, Aeromagnetic map of the Portland–Vancouver metropolitan area, Oregon and Washington: U.S. Geological Survey Open-File Report 93-211, scale 1,100,000.
- Blakely, R.J., Beeson, M.H., Madin, I.P., Popowski, T., Wells, R.E., and Yelin, T.S., 1993, Tectonic implications of a high-resolution aeromagnetic survey of the Portland basin, Oregon and Washington: Abstracts with Programs, 89th Annual Meeting of the Cordilleran Section, Geological Society of America, Reno, Nevada, March 1993, p. 11.
- Blakely, R.J., Yelin, T.S., Wells, R.E., Beeson, M.H. and Madin, I.P., 1993, Active high-angle faults in the Portland–Vancouver area, Oregon and Washington: A tectonic application of high-resolution aeromagnetic data: *EOS, Transactions of the American Geophysical Union*, v. 74, p. 223.

Blakely, R.J., Wells, R.E., Yelin, T.S., Madin, I.P., and Beeson, M.H., 1995, Tectonic setting of the Portland–Vancouver area, Oregon and Washington: Constraints from low-altitude aeromagnetic data: *Geological Society of America Bulletin*, in journal review.

Guffanti, M., Blakely, R.J., Christiansen, R.L., Clynne, M.A., Donnelly-Nolan, J.M., Muffler, L.J.P., and Smith, J.G., Spatial correlation of gravity anomalies, volcanic vents, and young faulting in the Cascade Range, California, and implications for crustal stress and structure: *Abstracts with Programs*, 1994 Annual Meeting, Geological Society of America, Seattle, Washington, October 24–27, 1994, p. A-145.

Blakely, R.J., Sherrod, D.R., and Wells, R.E., Where is the margin of the Columbia embayment beneath the Cascade Range in central Oregon?: *Abstracts with Programs*, 1994 Annual Meeting, Geological Society of America, Seattle, Washington, October 24–27, 1994, p. A-145.

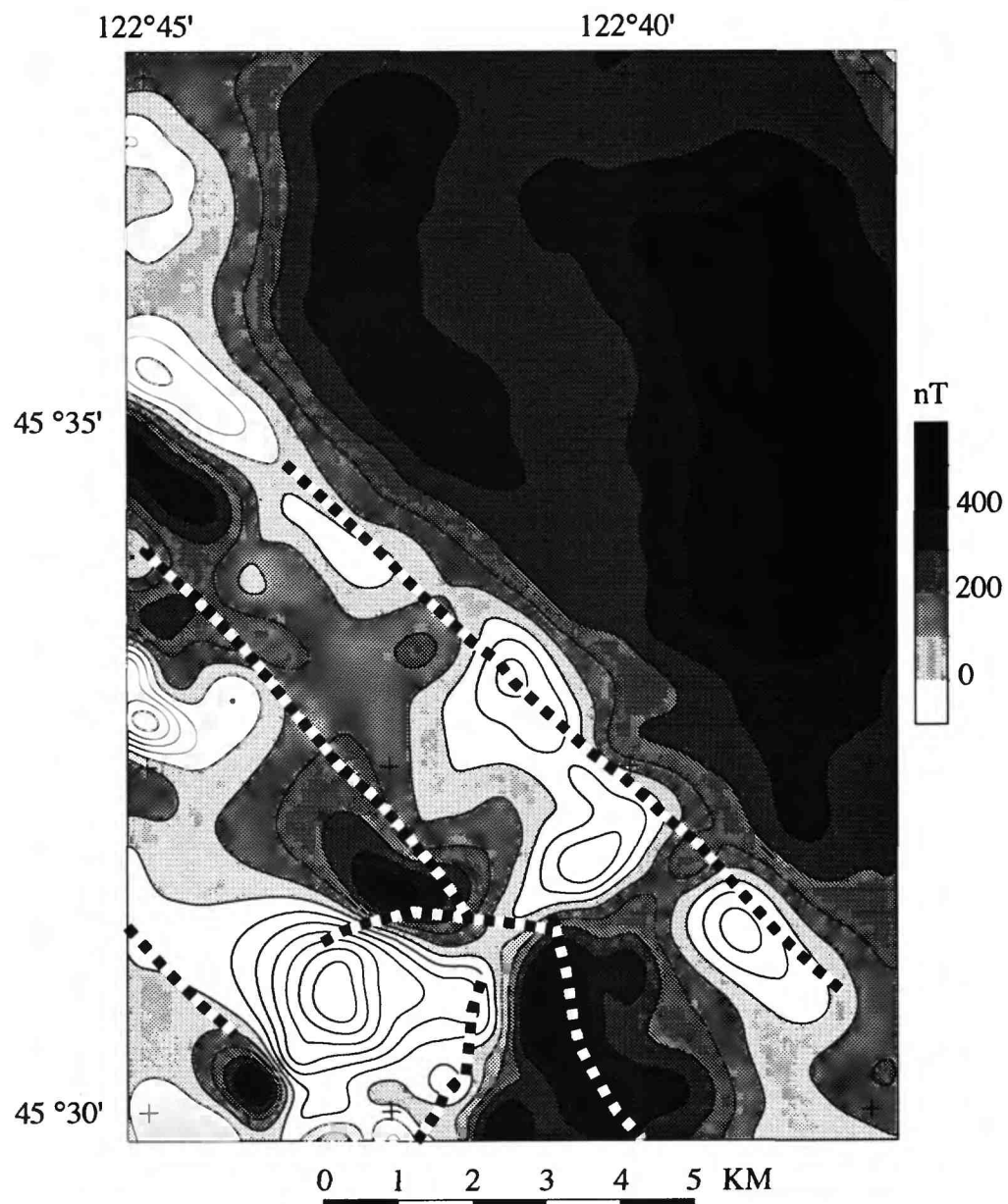


Figure 1. – Total-field magnetic anomaly over the Portland quadrangle. This map represents only a small part of the 1992 survey. Dashed lines indicate mapped faults from Beeson and others (1991). Note the pronounced northwest-trending magnetic gradient associated with the northeastern-most fault.

# A Strategy for Obtaining High Spatial and Temporal Resolution of Crustal Deformation using GPS

USGS 1434-92-G2196

Yehuda Bock  
 Institute of Geophysics and Planetary Physics  
 Scripps Institution of Oceanography  
 La Jolla, CA 92093  
 Tel: (619) 534-5292  
 Fax: (619) 534-9873  
 E-Mail: bock@pgga.ucsd.edu

Program Element II.3: Determine the Nature and Rates of Crustal Deformation

## Objectives

GPS geodesy in continuous and campaign modes provides *frequent and dense* monitoring of interseismic, coseismic and postseismic displacements which add to our fundamental understanding of the physics of the earthquake process. GPS also has the potential to provide crustal deformation precursors for the prediction of large earthquakes. The goal of this research is to develop and evaluate the capability of surveying *spatially dense, local to regional scale, three-dimensional geodetic networks, in near real-time with millimeter-level accuracy*.

## Investigations Undertaken and Data Collected

The Permanent GPS Geodetic Array (PGGA) has been operated in southern California since the spring of 1990 by SIO and JPL with assistance from MIT, UCLA, Caltech and USGS (Pasadena Office). Funding for the operations and analysis of the network is provided by SCEC, NASA, NSF and USGS. The goals of the PGGA are to monitor crustal deformation related to the earthquake cycle in California, continuously, in near real-time and with millimeter accuracy. The PGGA also provides reference sites to support detailed GPS geophysical surveys in southern California. In response to the Northridge earthquake a dense GPS array was initiated in the Los Angeles Basin. This dense network and the regional-scale PGGA are part of the Southern California Integrated GPS Network (SCIGN). The current distribution of continuous GPS stations is shown in Figure 1.

We have developed an automated system to collect, analyze and archive data from the PGGA sites and from a globally distributed set of about 32 GPS tracking stations of the International GPS Service for Geodynamics (IGS). We collect data at a 30 second sampling rate to all visible satellites, 24 hours a day, 7 days a week. We have been estimating the position of the PGGA stations daily since August 1991. We perform, at twenty-four hour intervals, a simultaneous weighted least squares adjustment of the station positions and improved satellites ephemerides. We also generate precise satellite ephemerides and improved earth orientation parameters (polar motion) in support of GPS surveys in southern California. These products are available via anonymous ftp over Internet within 5-7 days of collection. We evaluate the precision of our satellite parameters based on overlapping orbital arcs and baseline repeatability. Our orbital ephemerides are sufficiently precise to support any crustal deformation GPS survey in California, thereby eliminating the time consuming and costly need for each investigator and/or analysis center to compute their own orbit improvements. Since the coordinates of the PGGA sites are computed with respect to the International Terrestrial Reference Frame (ITRF), realized through the positions and velocities of the global IGS stations, crustal motion can be determined in a reference frame external to California.

In FY94 we have concentrated on:

- (1) re-analyzing the PGGA data collected prior to the Northridge earthquake in a search for pre-seismic signals
- (2) improving geodetic accuracy
- (3) developing distributed processing techniques to allow us analyze the growing number of global and regional GPS stations, efficiently and accurately.

## Results

*Northridge earthquake studies.* The Northridge earthquake of 17 January 1994 caused small coseismic displacements at the (then) two PGGA sites in the Los Angeles Basin, Palos Verdes and JPL (Figure 1). We estimated, within 3 days of the earthquake, a coseismic contraction of the Basin of  $11.5 \pm 3.2$  mm, with displacements at PVEP of  $10.4 \pm 3.2$  mm N,  $0.9 \pm 3.8$  mm E and at JPL of  $5.1 \pm 3.2$  mm S,  $6.5 \pm 3.9$  mm E. In addition, we recognized possible anomalous variations in the daily time series of position at both sites several months prior to the earthquake which were not apparent at the other PGGA sites (outside the area of permanent deformation) [Bock, 1994]. To exclude the possibility that apparent signals were just processing artifacts from our operational, near real-time analysis, we embarked on a re-analysis of the PGGA data using improved physical models and processing algorithms. The recomputed time series for the baseline between Palos Verdes and JPL is shown in Figure 2 [Zhang et al., 1994] for the period before and shortly after the Northridge earthquake (indicated by a vertical line), in terms of north, east, up components and length. Each point represents a 24-hour solution and error bars are one-sigma. The anomalous signals are essentially eliminated, except for small variations in the east component (which turns out to be at Palos Verdes from an examination of its individual time series), indicating that they were, in fact, an artifact of our initial analysis of the data. Nevertheless, the new time series provides the interseismic rate of deformation of the Los Angeles for the 8 months prior to the earthquake (unfortunately we only started collecting data at Palos Verdes in June 1993). The rate of  $8.1 \pm 0.9$  mm/yr which is higher by 2-3 mm/yr than previous estimates from geology and space geodesy [Feigl et al., 1993]. We are continuing with the PGGA re-analysis to compute the deformation rate after the Northridge earthquake.

*Improved Geodetic Accuracy.* Improved physical models and processing algorithms have significantly increased the geodetic accuracy of the PGGA time series, in both horizontal and vertical components. In Figure 3 we show a recent time series for the PGGA site at Piñon Flat Observatory using the distributed processing scheme described below. Each point represents a 24-hour solution and error bars are one-sigma. Daily horizontal precision (one-sigma) for all the PGGA sites is typically 2-3 mm, and the vertical precision is about 4-6 mm.

*Distributed Processing.* We have implemented a distributed processing scheme for the PGGA and IGS analysis since the numbers of global and PGGA stations have increased steadily. Currently we are analyzing about 60 global and regional sites per day. We divide the processing into two steps. In the first step, we analyze a well distributed set of global stations to compute precise satellite orbits and earth orientation. We save the least squares adjustment and the full covariance matrix from this daily solution [Behr et al., 1994; Blewitt et al., 1994]. Constraining the satellite orbits, we then analyze data from the California sites and 3-5 IGS sites from North America and Hawaii (used in the first step). We then combine the solutions and covariance matrices from these two solutions using the GLOBK Kalman Filter program [T.A. Herring]. The distributed approach is nearly rigorous since the global and regional coordinates in a simultaneous analysis of all the sites are found to be very weakly correlated.

## Reports published (1993-1994)

### Journal articles

- Blewitt, G. and Y. Bock, Landers earthquake: Seeing California move with Global Positioning Satellites, *Geophysics News*, Amer. Geophys. Union, 23-24, 1993.
- Blewitt, G., Y. Bock and G. Gendt, Global GPS network densification: A distributed processing approach, submitted to *Manuscripta Geodaetica*, 1994.
- Bock, Y., D.C. Agnew, P. Fang, J.F. Genrich, B.H. Hager, T.A. Herring, K.W. Hudnut, R.W. King, S. Larsen, J.B. Minster, K. Stark, S. Wdowinski and F.K. Wyatt, Detection of crustal deformation from the Landers earthquake sequence using continuous geodetic measurements, *Nature*, 361, 337-340, 1993.
- Bock, Y., Crustal deformation and earthquakes, *Geotimes*, 39, 16-18, 1994.
- Feigl, K.L., D.C. Agnew, Y. Bock, D. Dong, A. Donnellan, B.H. Hager, T.A. Herring, D.D. Jackson, T.H. Jordan, R.W. King, S. Larsen, K.M. Larsen, M.H. Murray, Z. Shen and F.H. Webb, Measurement of the velocity field of central and southern California, 1984-1992, *J. Geophys. Res.*, 98, 21,677-21,712, 1993.
- Hudnut, K.W., Y. Bock, M. Cline, P. Fang, Y. Feng, J. Freymueller, X. Ge, W.K. Gross, D. Jackson, M. Kim, N.E. King, S.C. Larsen, M. Lisowski, Z-K. Shen, J. Svarc and J. Zhang, Coseismic displacements of the 1992 Landers earthquake sequence, *Bull. Seismol. Soc. Amer.*, Special Issue on the Landers earthquake sequence, 84, 625-645, 1994.
- King, R.W. and Y. Bock, Documentation of the GAMIT GPS analysis software v. 9.3, Mass. Inst. of Technology and Scripps Inst. of Oceanography, unpublished, 1994.
- Schaffrin, B. and Y. Bock, Geodetic deformation analysis based on robust inverse theory, *Manuscripta Geodaetica*, 19, 31-44, 1994.
- Shen, Z-K., D.D. Jackson, Y. Feng, M. Cline, M. Kim, P. Fang and Y. Bock, Postseismic deformation following the Landers Earthquake, California, June 28, 1992, *Bull. Seismol. Soc. Amer.*, Special Issue on the Landers earthquake sequence, 84, 780-791, 1994.

### Invited Abstracts (1994)

- J. Zhang, Y. Bock, P. Fang, J. Behr, J. Genrich and K. Hudnut, Surface Deformation in the Northridge Earthquake and the Los Angeles Basin from the PGGA Time Series, *Eos Trans. AGU*, 75, 166, 1994.
- P. Fang, Y. Bock, S. McClusky, R.W. King, and T.A. Herring, Modeling atmospheric delays with continuous GPS measurements in southern California, *Eos Trans. AGU*, 75, 174, 1994.
- G. Blewitt and Y. Bock, Global GPS network densification: A distributed processing approach, *Eos Trans. AGU*, 75, 182 1994.
- J. Behr, Y. Bock, P. Fang, J. Zhang and K. Stark, Distributed processing of global, regional and local GPS data: techniques and results, *Eos Trans. AGU*, 75, 182 1994.
- K. Hudnut, M.H. Murray, A. Donnellan, Y. Bock, P. Fang, Y. Feng, Z. Shen, B. Hager, T. Herring, R. King, Co-Seismic displacements of the 1994 Northridge, California, Earthquake, *Eos Trans. AGU*, 75, 176, 1994.

# Southern California Integrated GPS Network (SCIGN)

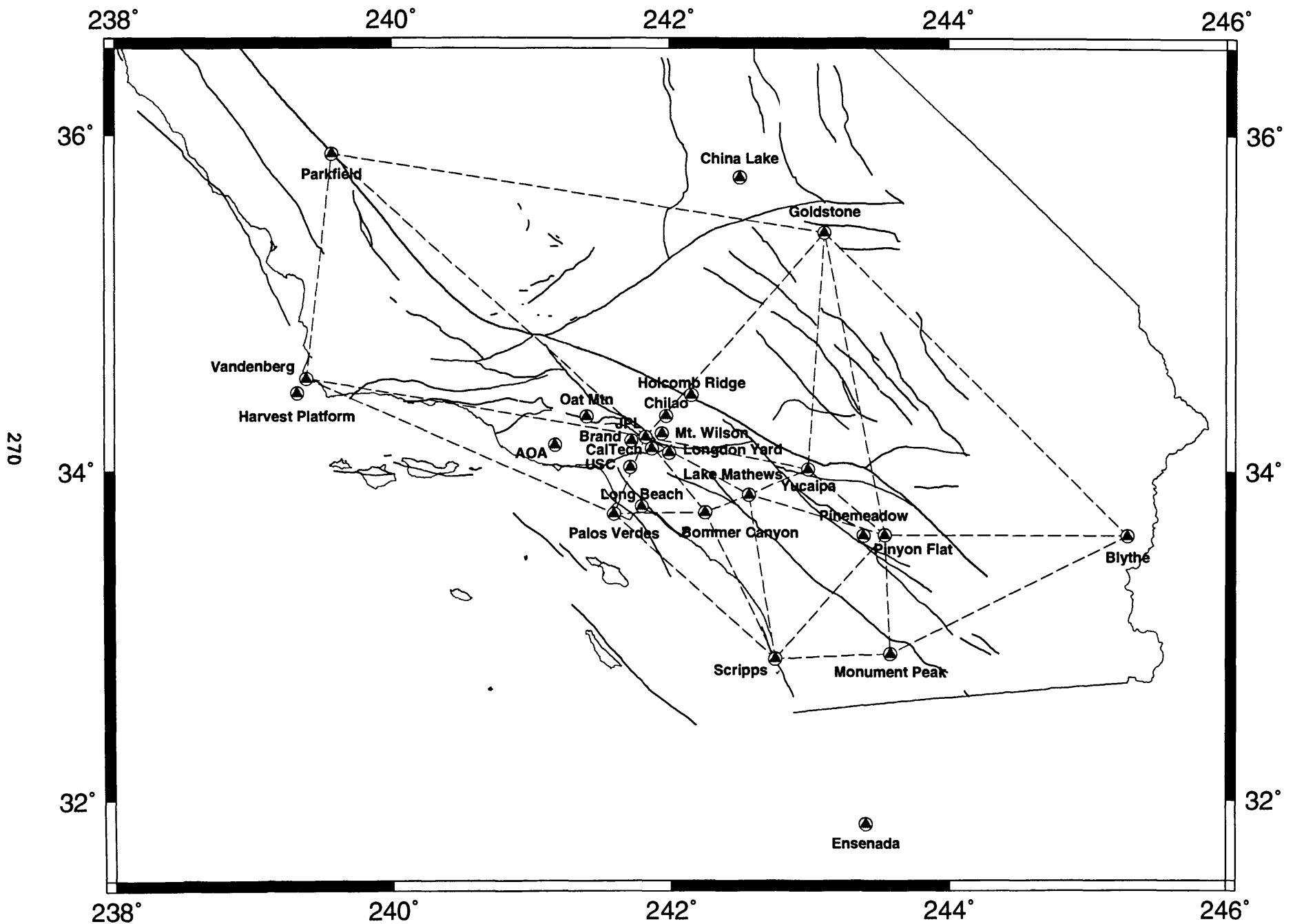
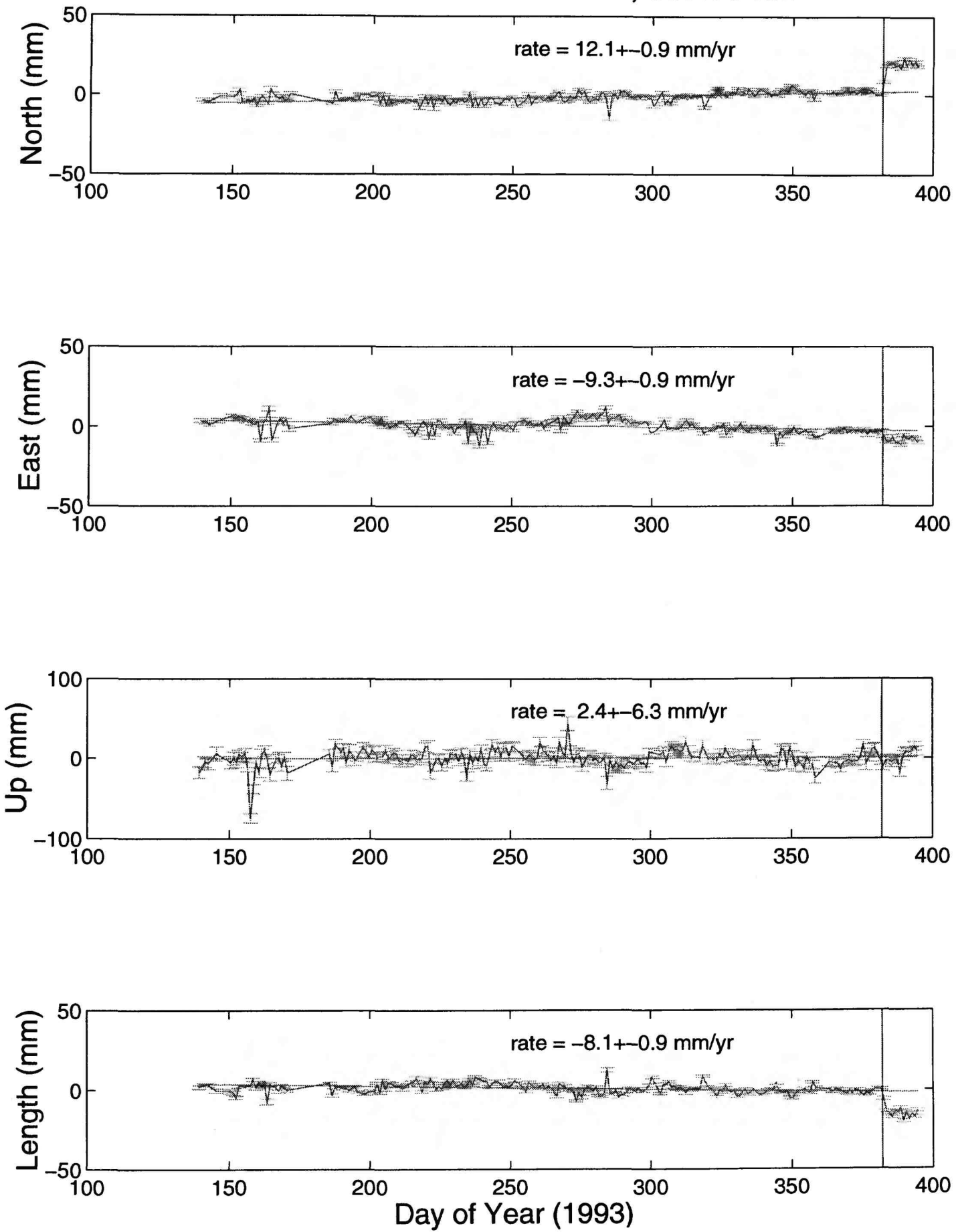


FIGURE 1

# Baseline JPL1-PVEP, 55.470 km II



# PIN1 Position Time Series (Filtered)

II

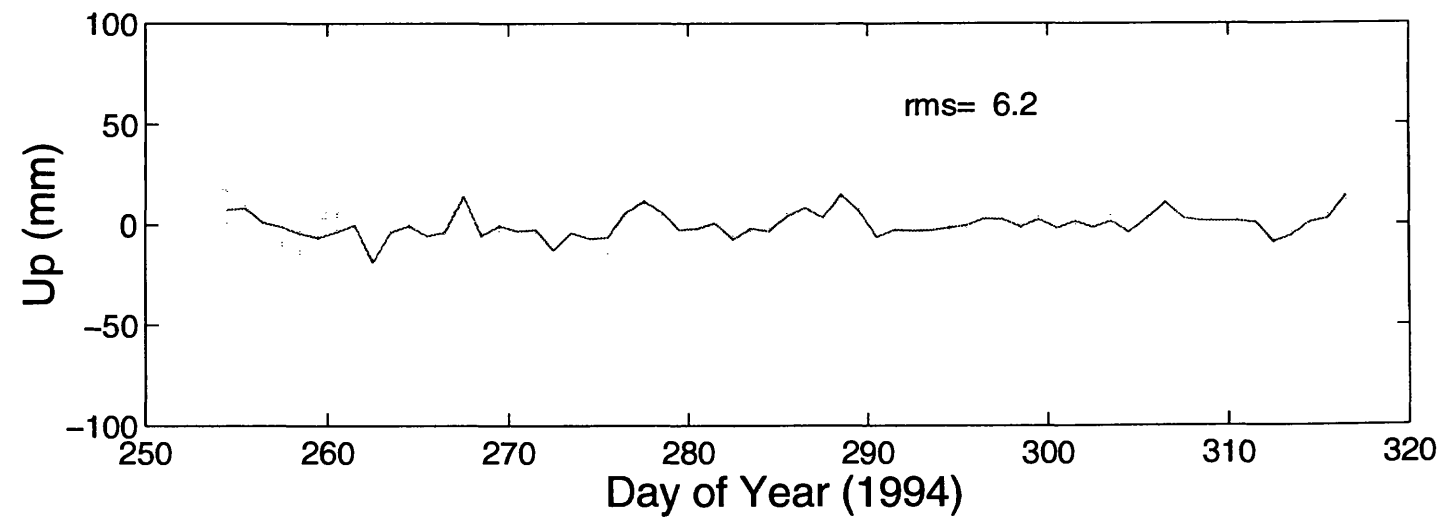
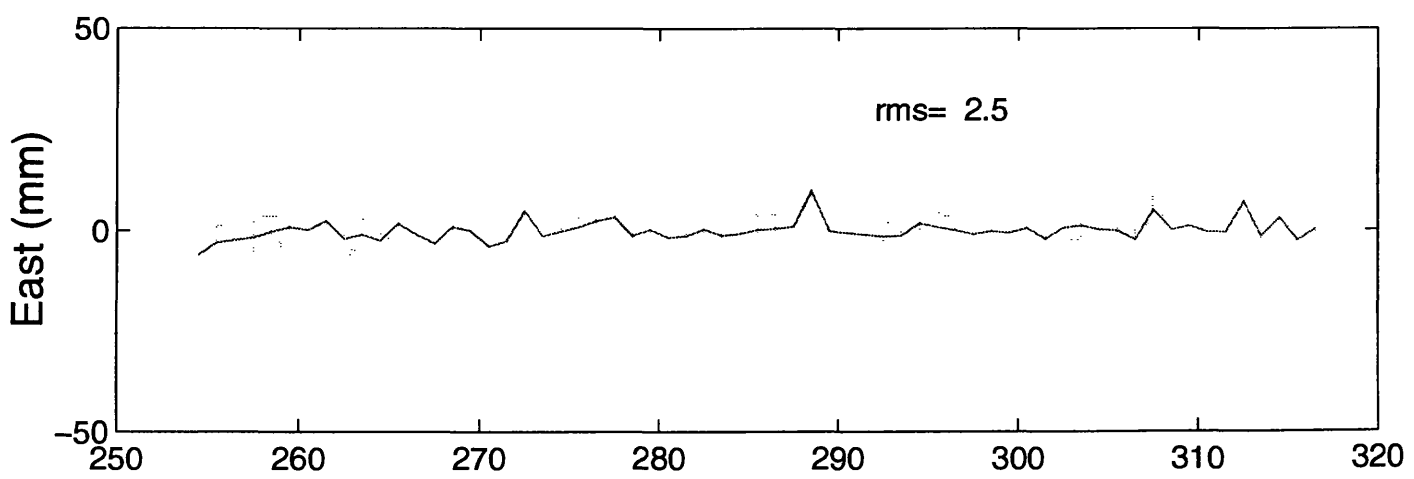
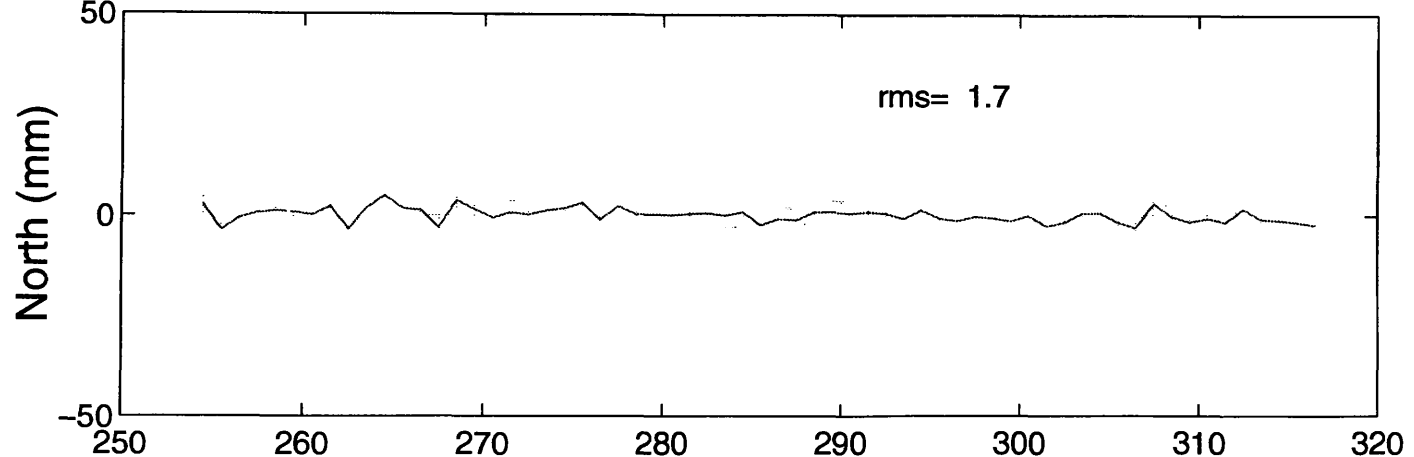


Figure 3

**SLIP RATE OF THE NORTHERN HAYWARD FAULT  
AT POINT PINOLE, CALIFORNIA**

1434-93-G-2333

Glenn Borchardt  
Soil Tectonics  
P.O. Box 5335

Berkeley, California 94705  
510-654-1619; Fax 510-654-4551

Component II.3: "Determine the nature and rates of crustal deformation"

**Investigations Undertaken**

This project is an attempt to produce the first Quaternary slip rate for the northern end of the Hayward fault. Because this end of the fault has great crustal stability, it records evidence of the last highstand of San Francisco Bay during the Sangamon at 122 ka. The highstand, about +8 m, crossed the fault in the southwestern part of Point Pinole Regional Shoreline, planating the bedrock and removing older surficial deposits for a distance of over 1 km along the fault. Most of the planated surface of an embayment that crossed the fault now lies beneath regressive sediments and colluvial deposits. The objective of this project is to gather field evidence to determine the precise configuration and age of the offset embayment and its associated features.

The first phase of the work involved the preparation of a log of the Sangamon wave-cut platform and its overlying marine and continental sediments and soils where it is exposed at Pinole Point. The second phase involved trenching, logging, and studying a suspect alluvial fan that appears to overlie the Sangamon wave-cut platform southwest of the fault. The third phase involved drilling and sampling a series of boreholes designed to determine the elevation of the abrasion platform along the fault.

**Results**

**Pinole Point Exposure**

A log of the 115-m long exposure at Pinole Point shows that the abrasion platform in the Garrity Member of the Contra Costa Group is exposed for about 55 m. The platform reaches a maximum elevation of about 8 m, and has an easterly slope of about 5%. The soil in the overlying colluvium is similar to those described in alluvium above Sangamon coquinas elsewhere along the south shore of San Pablo Bay. An analysis of all possible candidates (oxygen isotope stages 3, 5a, 5c, 5e, and 7) showed that oxygen isotope stage 5e (122 ka) was the only global highstand fitting the low uplift at Point Pinole. These

data were used to produce a speculative model of the Sangamon platform for refining the selection of drill sites along the fault.

#### Suspect Alluvial Fan

The fan-shaped geomorphic feature in the southwestern part of the park contains no alluvium. Two trenches here revealed fine-grained sediments no coarser than very fine sand (<100 um) to depths up to 7 m. Early speculations that this was an alluvial fan offset from Parchester Creek 880 m to the southeast thus were placed in doubt. The absence of alluvium at this point indicated that the slip on this end of the fault must have been less than the 8±1 mm/yr rate we found on the southern part of the fault at Union City.

#### Drilling Program

Continuous cores drilled to depths as great as 24 m provided data for three fault-normal cross sections and one fault-parallel cross section. Although more drilling and trenching is necessary to confirm these results, our evolving model of the offset Sangamon wave-cut platform suggests the following tentative conclusions derived from detailed soil descriptions of over 100 1-m core samples:

1. Inner edge platform gradients for the base of the regressive section in the deepest part of the offset embayment in the southwestern part of the park were about 5%--similar to those at Pinole Point.
2. Vertical movement along the Hayward fault at Point Pinole was apparently limited to about 2.6 m of subsidence on the southwest during the last 122 ka.
3. Preliminary measurements of the buried embayment, along with other permissive evidence suggest that the Sangamon platform may have been offset right-laterally by about  $626\pm173$  m in the last  $112\pm4$  ka and  $674\pm21$  m in the last  $121\pm4$  ka. Thus, the tentative slip rate of the Hayward fault at Point Pinole is about  $5.6\pm1.5$  mm/yr for the last 122 ky.
4. The above measurement is equivalent to the aseismic slip measured on street curbs just south of the study site.
5. The possible equivalence of the geologic slip rate and the creep rate would explain the lack of evidence for catastrophic surface rupture in previous studies of the Hayward fault at Point Pinole and in offshore sediments on strike to the northwest.
6. A 2.4-mm/yr slip deficit at Point Pinole might be taken up in a 6-km right stepover to the Pinole fault, the probable

southeast extension of the Rodgers Creek fault.

7. A stepover would imply that the hazard of catastrophic surface rupture decreases on the northwestern 7 km of the Hayward fault as it increases on the northwestern 4 km of the Pinole fault (Figure 1).

8. The northernmost 4 km of the Pinole fault should be investigated for possible Holocene activity.

#### Reports Published

Borchardt, Glenn, 1994, The Sangamon strandline in northern San Francisco Bay and its significance for paleoseismic studies [abs.], in Prentice, C.S., Schwartz, D.P., and Yeats, R.S., eds., Proceedings of the Workshop on Paleoseismology: U.S. Geological Survey Open-File Report 94-568, p. 24-25.

Borchardt, Glenn, and Lienkaemper, J.J., 1994, Pedogenic calcite as an indicator of an early Holocene dry period in the San Francisco Bay Area [abs.], in Lanphere, M.A., Dalrymple, G.B., and Turrin, B.D., eds., Abstracts of the Eighth International Conference on Geochronology, Cosmochronology, and Isotope Geology: U.S. Geological Survey Circular 1107, p. 36.

Borchardt, Glenn, and Lienkaemper, J.J., 1994, Pedogenic calcite as an indicator of the early Holocene dry period in the San Francisco Bay Area [abs.]: EOS, Transactions of the American Geophysical Union, v. 75, no. 44, p. 371.

Dwyer, M.J., and Borchardt, Glenn, 1994, Paleoseismicity and liquefaction potential of a Sangamon marine terrace near the San Andreas fault, Sonoma County, California [abs.], in Prentice, C.S., Schwartz, D.P., and Yeats, R.S., eds., : Proceedings of the Workshop on Paleoseismology, U.S. Geological Survey Open-File Report 94-568, p. 59-61.

Lienkaemper, J.J., and Borchardt, Glenn, 1994, Holocene slip rate of the Hayward fault at Union City, California [abs.], in Prentice, C.S., Schwartz, D.P., and Yeats, R.S., eds., : U.S. Geological Survey Open-File Report 94-568, Proceedings of the Workshop on Paleoseismology, p. 108-109.

Lienkaemper, J.J., and Borchardt, Glenn, 1994 (submitted), Holocene slip rate of the Hayward fault at Union City, California: Journal of Geophysical Research.

## Hypothesized Hayward-Rodgers Creek-Pinole Fault Stepover

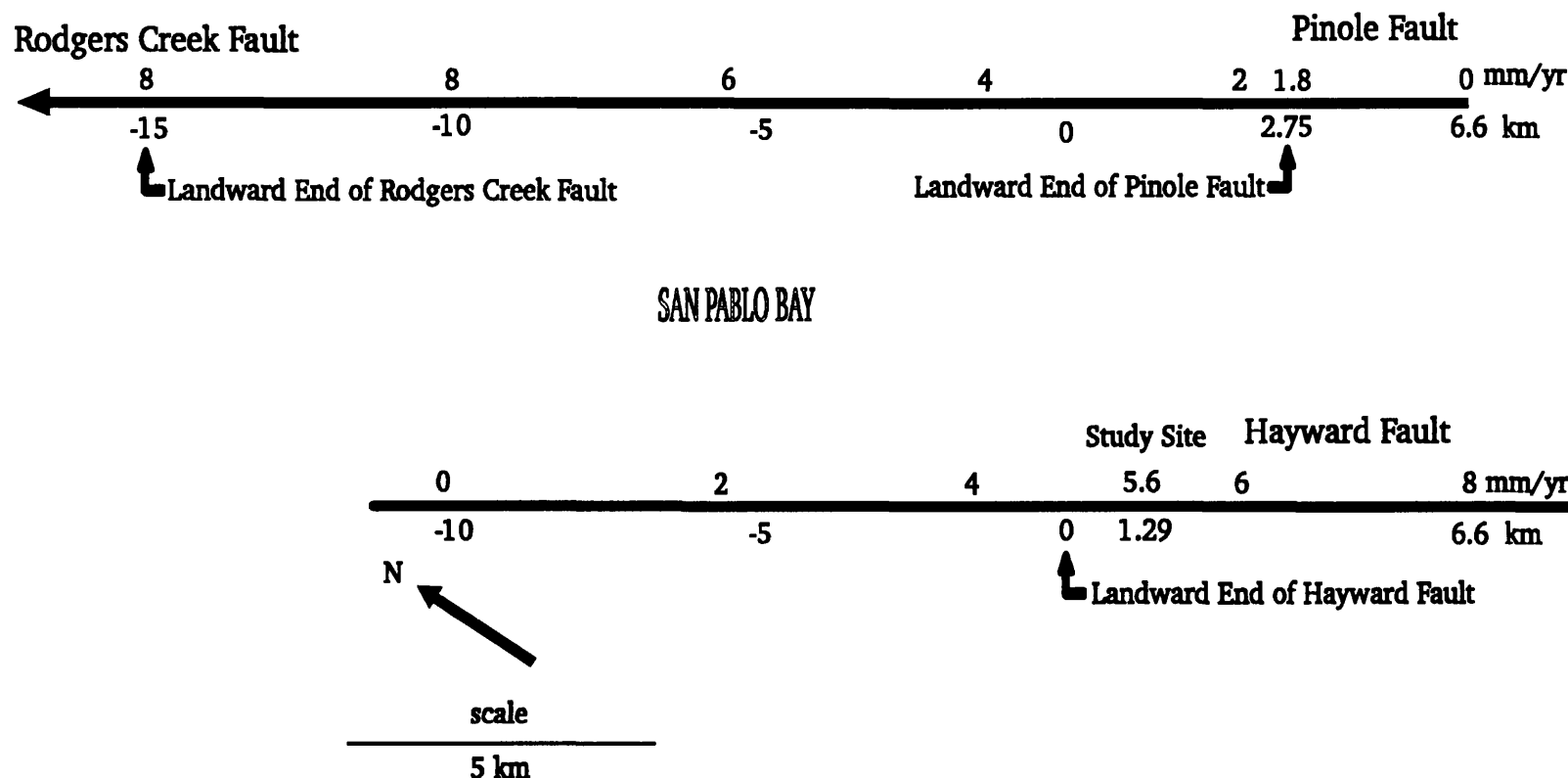


Figure 1. Hypothesized model of the Hayward-Rodgers Creek-Pinole fault stepover. Confirmation of the 5.6-mm/yr slip rate would imply that slip decreases on the Hayward fault as it increases on the Pinole fault.

**Project Title:** Evaluation of the Time-of-Failure Method for Intermediate-Term Earthquake Prediction in the New Madrid Area

**Project Number:** 1434-94-G-2413

**Investigator:** PI: Professor Lawrence W. Braile

**Institution:** Purdue University

**Address:** Department of Earth & Atmospheric Sciences  
1397 Civil Engineering Building  
West Lafayette, IN 47907-1397

**Telephone:** (317) 494-5979 (Office)  
(317) 496-1210 (FAX)

**E-Mail:** braile@vm.cc.purdue.edu

**Program Element:** Element II. Evaluating Earthquake Potential  
Component II.8. Develop and evaluate short- and intermediate-term earthquake prediction methods  
Central United States (CU)

#### Investigations Undertaken:

This project consists of performing a detailed evaluation of the time-of-failure method (Varnes, 1989; Bufe and Varnes, 1990) for intermediate-term earthquake prediction for the New Madrid area. The method utilizes an exponential relationship to model the accelerating strain release of precursory earthquake sequences preceding a larger-magnitude main shock. The equation of the curve is given by

$$\sum E^{1/2} = \Delta - k / m(T_f - t)^m \quad (1)$$

where delta is the square root of the total cumulative energy released up to and including the main shock, t is time,  $T_f$  is the estimated time-of-failure, and k and m are constants. The solution to the equation yields estimates of the time of failure ( $T_f$ ) and the magnitude (from  $\Delta$ ) of the main shock. Input data consist of times and magnitudes for "precursory" events in a selected region surrounding the area of the main shock. Magnitudes of precursory events are converted to seismic moment (Nuttli, 1983) and then energy (Kanamori, 1983), and the cumulative square-root of energy is plotted versus time. A non-linear least squares fit to the observed precursory data, using equation 1, is then calculated to estimate  $T_f$  and  $\Delta$ . A significant aspect of this analysis and an objective of our research project is to define an objective approach to determining the size of the area around a main shock for which preceding events should be considered. An additional emphasis of our project is to develop a procedure for error analysis of the time-of-failure method for application in the New Madrid area.

## Results:

We have utilized two historical earthquake data files for the New Madrid area: the "Nuttli" file (1813-1977) (Figure 1) and the "Network" file (1974-1994) (Figure 2). Data from the Nuttli file was used in preliminary analysis of the  $m_b = 6.2$ , 1895 New Madrid earthquake. Based on encouraging results of this analysis, we are analyzing data for additional New Madrid earthquakes. Because of incompleteness of the historical earthquake data in the Nuttli file, the lack of data for earthquakes with magnitudes less than three, and possible uncertainties in magnitudes assigned to each event, only limited study of additional main shocks and precursory sequences in the Nuttli file has been conducted.

We are presently analyzing the Network file data which contains a fairly complete data set for earthquakes with magnitudes greater than about 1.5 for the 1974-94 time period. The network file contains only nine earthquakes with magnitudes greater than four because of the relatively short time period covered by the data set. In order to increase the number of sequences analyzed, we have evaluated all earthquake sequences in the network file which have a main shock magnitude greater than 3.5. Identifying events of magnitude greater than 3.5 as "main shocks" is reasonable for this data set because the file is reasonably complete for earthquake magnitudes greater than about 1.5.

The network data file contains a total of 25 events with a magnitude greater than 3.5. At present, we have studied nine sequences which appear to provide an adequate curve for modeling the possible accelerated energy release before a main shock. The sequences for the remaining 16  $m_b > 3.5$  events will be subjected to further study. However, it appears that, for these events, the accelerated energy release is not readily apparent for one or more of the following reasons: main shocks occurring on the edge of the network coverage area; nearby interfering main shocks; inadequate precursory data due to the limited time span of the data file (1974-1994); and apparent poor distribution of precursory events around a main shock location.

For the nine  $m_b > 3.5$  events which show an apparent acceleration of energy release before the main shock, several criteria (distance from main shock, time before main shock, and limiting the magnitude range of precursory events) were varied to test the sensitivity of the method.

Two examples are used to demonstrate the potential of the time-of-failure method. The first example is a  $m_b = 4.1$  event which occurred on 6-13-87 (1987.455 decimal years) located at  $36.54^\circ\text{N}$ ,  $89.67^\circ\text{W}$ . The precursory data (14 events) consisted of events within a 2.5 km radius of the main shock. The cumulative square root of energy is plotted versus time and the best fit non-linear least squares solution is calculated (Figure 3). The least squares solution yields a calculated magnitude of 4.39, and predicted time of failure of 1987.420 (6-2-87) which is very close to the actual time and magnitude.

The second example (Figure 4) is a  $m_b = 4.0$  event which occurred on 9-29-87 (1987.748) located at  $36.84^\circ\text{N}$ ,  $89.21^\circ\text{W}$ . The precursory data (12 events) consisted of events within a 20 km radius of the main shock. The solution provided a predicted magnitude of 4.89, and a time-of-failure of 1987.605 (8-8-87). Both estimates are close to the actual parameters of this event, magnitude 4.0 and time 9-29-87.

Error analysis of these solutions and other analyses for the New Madrid earthquakes from the Network file are being evaluated with a Monte Carlo method. The method consists of calculating uniformly distributed random numbers over a particular interval for each of the four parameters (delta, k, m, and  $T_f$ ). The four coefficients are inserted into the equation, and the resulting theoretical curve is compared to the observed cumulative energy release data. Solutions with an RMS error between the observed and calculated cumulative square root of energy which are less than a specified value are accepted. Solutions with a high RMS are rejected. The method provides a histogram of values for each coefficient. The preliminary application of this method to the two examples described above has given some insight into the range of "acceptable" coefficients for the equation. Defining acceptable RMS error bounds will require further analysis of the possible contributions of magnitude uncertainty. Once the RMS error limits are established, the Monte Carlo solutions provide a useful approach to determining uncertainties of the coefficients of equation 1. Of course, we are most interested in the uncertainties of the estimated failure time and the estimated magnitude. At present, adequate solutions have tentatively been defined, for the examples shown, as solutions with RMS values within 4 units of those provided by the non linear least squares solution. This selection results in a set of Monte Carlo test solutions (curves) which display a substantial mis-fit as compared to the least-squares solutions shown in Figures 3 and 4. Further consideration of the acceptable RMS error criterion will require analysis of the possible effects of magnitude uncertainty on the fit of the theoretical line. The error analyses are similar for the two examples. Acceptable solutions from the Monte Carlo calculations provide a range in the time-of-failure of 1987.400-1987.500 years for the 6-13-87 (1987.455) event and 1987.530-1987.840 years for the 9-29-87 (1987.748) event. Thus, for these two examples, the method predicts the time-of-failure to a surprising degree of accuracy. However, the uncertainty estimates for the magnitude for each event are not as encouraging. The "acceptable" solutions yield a magnitude range of 3.0-5.6 for both examples.

In addition to further study of all of the  $m_b \geq 3.5$  events and precursory sequences in the network file, future error analysis will investigate the RMS error range for acceptable solutions. In addition, further analysis is required to determine the optimum radial distance from the main shock to search for precursory events. In the first example, a high rate of seismicity and the presence of "competing", nearby larger events in the time series necessitated a small search radius. In the second example, precursory events were included for distances up to 20 km from the main shock. After reviewing the other precursory sequences, it appears that precursory events located as far as 100 km may contribute to the energy release sequence for larger events. However, the limiting factor in practical application of the method is the presence of a nearby main shock of similar magnitude and time of occurrence. That is, when two larger (main shock) events are close to each other in time and space, it may be difficult to recognize precursory energy release associated with an individual event.

The application of the time-of-failure method to the relatively accurate and consistent earthquake data set provided by the Network file for the New Madrid area has produced encouraging results for the possible use of this method in intermediate-term earthquake prediction. Research currently being conducted will provide an analysis of all available and appropriate data in the Network file and further study of the effects of uncertainties in the data.

## References:

- Bufe, C.G., and D.J. Varnes, Time-to-failure analysis of seismicity preceding the 1989 Loma Prieta earthquake, U.S. Geol. Surv. Open-File Rpt. 90-666, 18 pp., 1990.
- Hamilton, R.M., and A.C. Johnston (Eds.), Tecumseh's Prophecy: Preparing for the Next New Madrid Earthquake, U.S. Geol. Surv. Circular 1066, 30 pp., 1990.
- Kanamori, H., Magnitude scale and quantification of earthquakes, *Tectonophysics*, 93, 185-199, 1983.
- Mitchell, B.J., O.W. Nuttli, R.B. Herrmann, and W. Stauder, Seismotectonics of the central United States, in Slemmons, D.B., Engdahl, E.R., Zoback, M.D., and Blackwell, D.D., eds., *Neotectonics of North America*: Boulder, Colorado, Geol. Soc. Am., Decade Map Volume 1, 245-260, 1991.
- Nuttli, O.W., Seismicity in the central United States, *Geol. Soc. Am. Rev. Eng. Geol.*, 4, 67-93, 1979.
- Nuttli, O.W., Average seismic source-parameter relations for mid-plate earthquakes, *Bull. Seis. Soc. Am.*, 73, 519-535, 1983.
- Varnes, D.J., Predicting earthquakes by analyzing accelerating precursory seismic activity, *Pageoph.*, 130, 661-686, 1989.

**Figure 1.** Earthquakes (mostly  $m_b \geq 3$ ) from 1816-1989 for the New Madrid area from the "Nuttli file" (Nuttli, 1979) for events through 1976 and from the USGS from 1976 to 1989. Event locations have been slightly "randomized" by adding a random number (mean = 0; standard deviation = 5 km) to the x and y locations in order to avoid alignment along even latitude and longitude lines.

**Figure 2.** Earthquakes from 1974 to 1994 for the New Madrid area from the "Network file" (Arch Johnston, personal communication, 1994). Locations were determined from the data recorded by the seismograph networks operated by St. Louis University and the University of Memphis (Hamilton and Johnston, 1990; Mitchell et al., 1991).

**Figure 3.** Application of the time-of-failure method to the June 13, 1987,  $m_b = 4.1$  event in the New Madrid seismic zone (location is  $36.54^\circ\text{N}$ ,  $89.67^\circ\text{W}$ ). The vertical scale is in units of  $\text{sqrt (N-m)}$ . The best fit line (using equation 1) to the "precursory" events (circles) within 2.5 km of the main shock results in estimated time of failure parameters corresponding to a predicted time of June 2, 1987 and magnitude of  $m_b = 4.39$ .

**Figure 4.** Application of the time-of-failure method to the September 29, 1987,  $m_b = 4.0$  event in the New Madrid seismic zone (location is  $36.84^\circ\text{N}$ ,  $89.21^\circ\text{W}$ ). The vertical scale is in units of  $\text{sqrt (N-m)}$ . The best fit line (using equation 1) to the "precursory" events (circles) within 20 km of the main shock results in estimated time of failure parameters corresponding to a predicted time of August 8, 1987 and magnitude of  $m_b = 4.89$ .

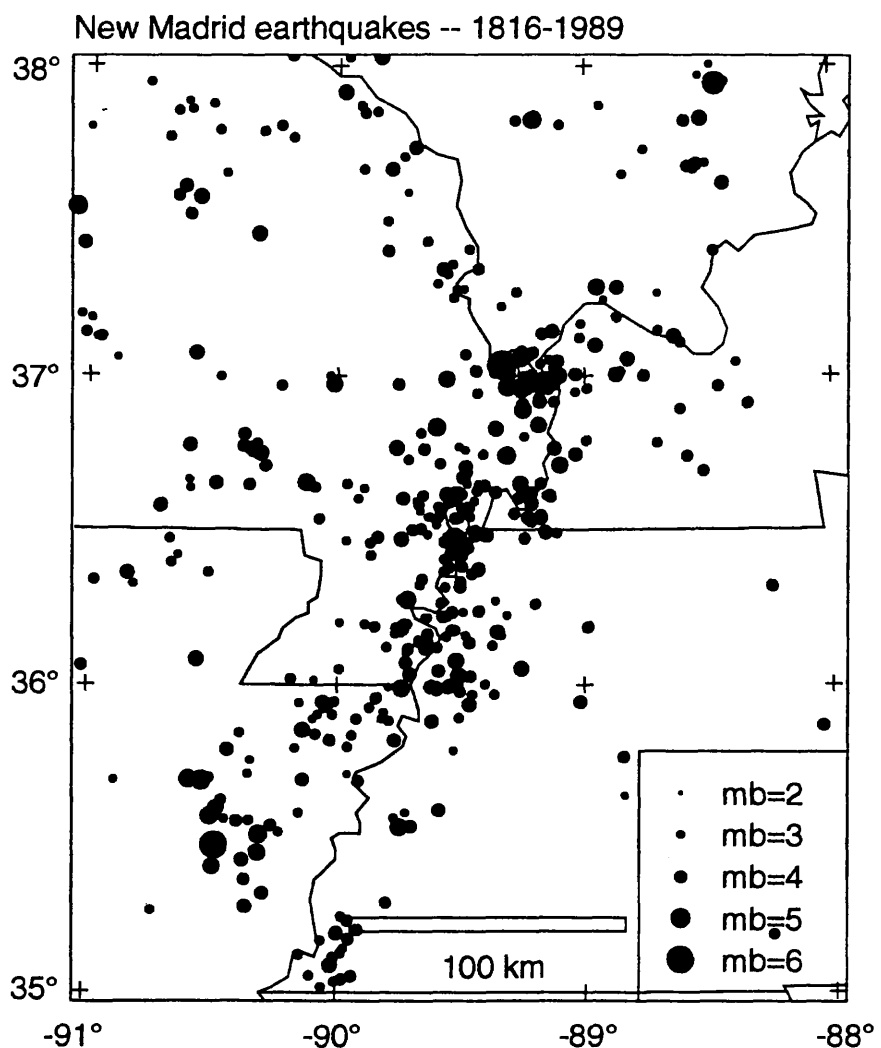


Figure 1. Earthquakes (mostly  $m_b \geq 3$ ) from 1816-1989 for the New Madrid area from the "Nuttli file" (Nuttli, 1979) for events through 1976 and from the USGS from 1976 to 1989. Event locations have been slightly "randomized" by adding a random number (mean = 0; standard deviation = 5 km) to the x and y locations in order to avoid alignment along even latitude and longitude lines.

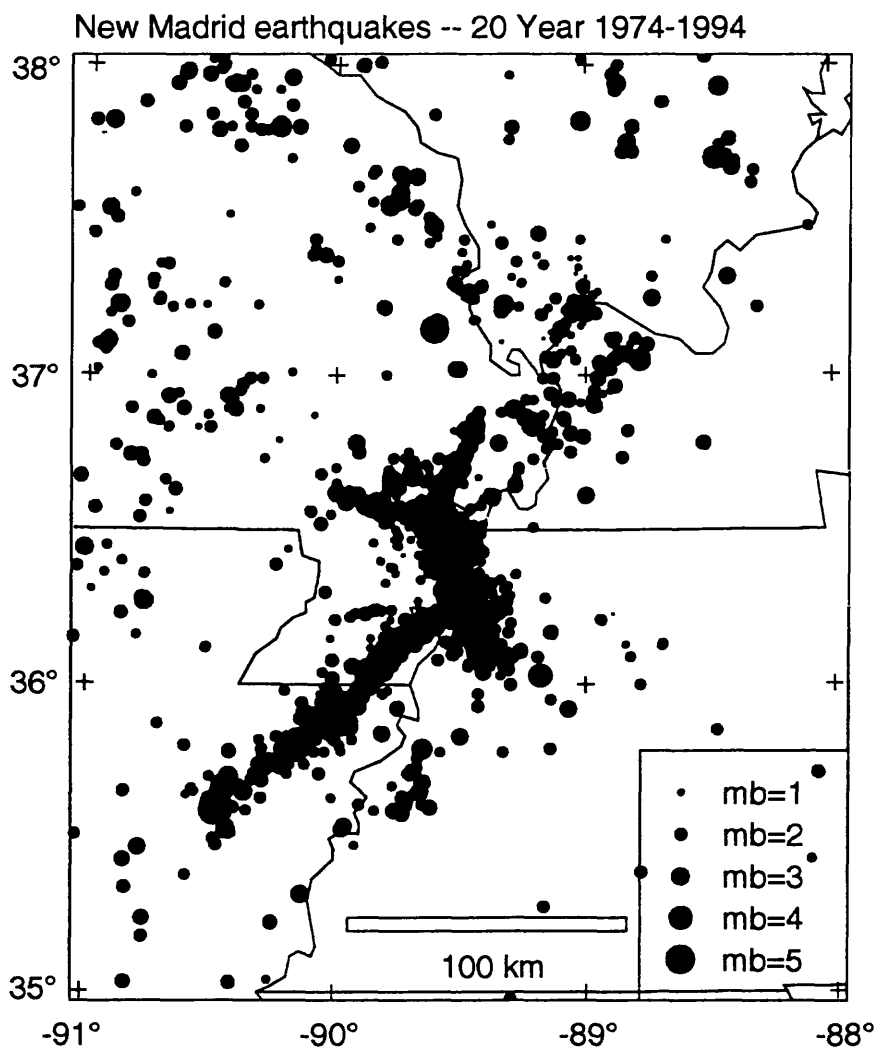


Figure 2. Earthquakes from 1974 to 1994 for the New Madrid area from the "Network file" (Arch Johnston, personal communication, 1994). Locations were determined from the data recorded by the seismograph networks operated by St. Louis University and the University of Memphis (Hamilton and Johnston, 1990; Mitchell et al., 1991).

## 6-13-87 Earthquake Event -- Magnitude = 4.1

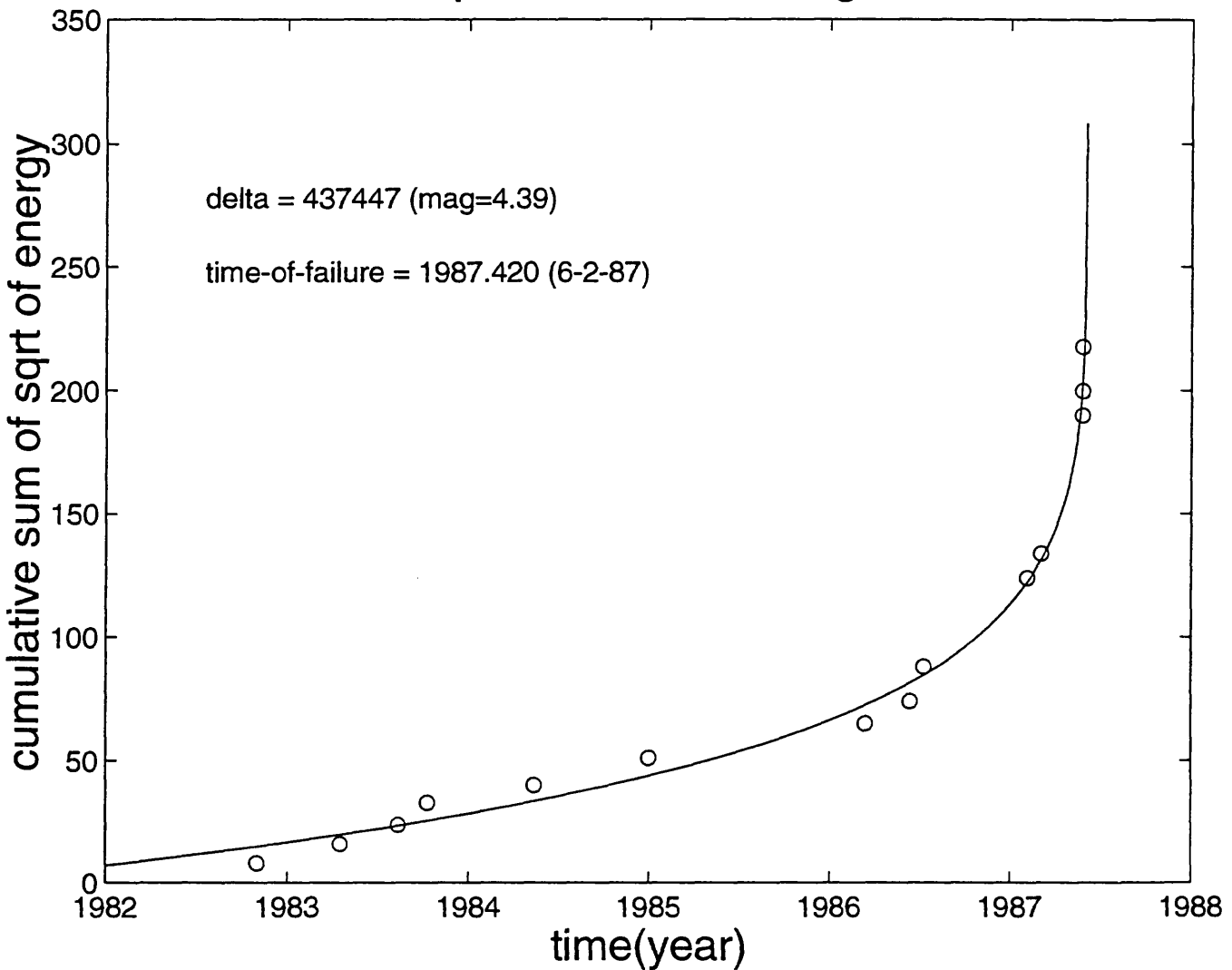


Figure 3. Application of the time-of-failure method to the June 13, 1987,  $m_b = 4.1$  event in the New Madrid seismic zone (location is  $36.54^\circ\text{N}$ ,  $89.67^\circ\text{W}$ ). The vertical scale is in units of  $\text{sqrt}(N\text{-m})$ . The best fit line (using equation 1) to the "precursory" events (circles) within 2.5 km of the main shock results in estimated time of failure parameters corresponding to a predicted time of June 2, 1987 and magnitude of  $m_b = 4.39$ .

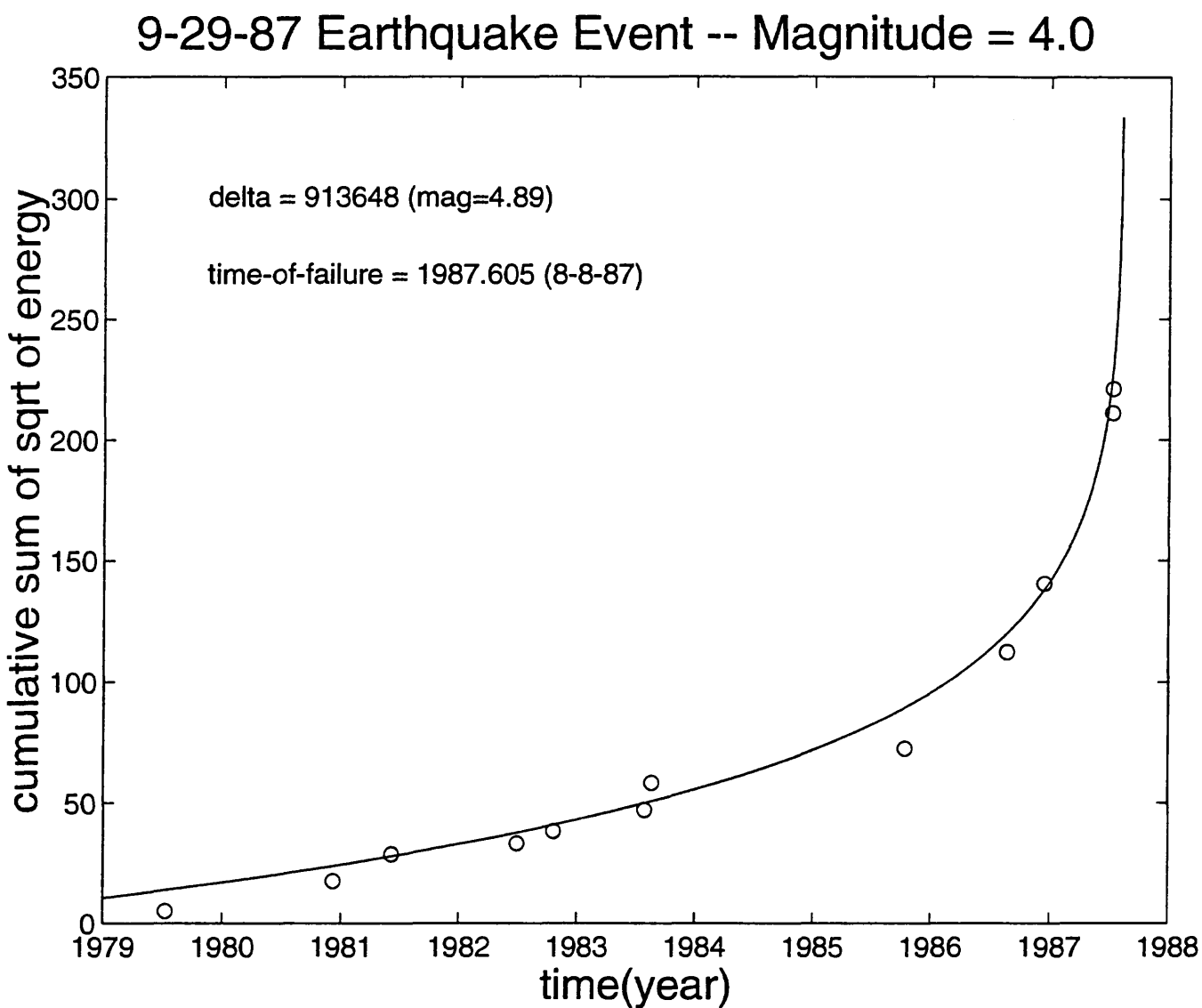


Figure 4. Application of the time-of-failure method to the September 29, 1987,  $m_b = 4.0$  event in the New Madrid seismic zone (location is  $36.84^\circ\text{N}$ ,  $89.21^\circ\text{W}$ ). The vertical scale is in units of  $\text{sqrt}(N\cdot\text{m})$ . The best fit line (using equation 1) to the "precursory" events (circles) within 20 km of the main shock results in estimated time of failure parameters corresponding to a predicted time of August 8, 1987 and magnitude of  $m_b = 4.89$ .

SEISMIC POTENTIAL OF THE LEWIS AND CLARK ZONE,  
MONTANA AND IDAHO

1434-94-G-2515 Idaho Geological Survey  
1434-94-G-2516 Montana Bureau of Mines and Geology

Roy M. Breckenridge  
Kenneth F. Sprence  
Idaho Geological Survey  
Room 332, Morrill Hall  
University of Idaho  
Moscow, ID 83844-33014  
(208) 885-7991  
fax (208) 885-5826  
email breckenridge@aspen.csrv.uidaho.edu

Michael C. Stickney  
Montana Bureau of Mines and Geology  
Montana Tech of the University of Montana  
1300 W Park St.  
Butte, MT 59701  
(406) 496-4332  
fax (406) 496-4451  
email mcstickney@mtvms2.mtech.edu

PROGRAM ELEMENT: II

On September 17, 1994, the Idaho Geological Survey and the Montana Bureau of Mines and Geology received funding from the National Earthquake Hazards Reduction Program to study earthquake hazards associated with the Lewis and Clark Zone. The Lewis and Clark Zone is a fundamental, WNW-trending shear zone active since Precambrian time, extending over 400 km from Coeur d'Alene, Idaho to Helena, Montana and encompassing genetically related extensional faults to the north. A sequence of destructive earthquakes within the eastern Lewis and Clark Zone in 1935 with magnitudes up to 6 1/4 resulted in serious damage to over 60% of the buildings in Helena and four fatalities. More recent earthquakes with magnitudes ranging up to 5.0 within the Lewis and Clark Zone have fault plane solutions compatible with continued dextral slip on WNW-trending faults within the zone. Despite significant levels of historic seismicity, the Lewis and Clark Zone has never been monitored by a permanent seismograph network.

The grant contract began late in fiscal year 94 and we have just begun working on deployment of the seismic network. New seismograph sites are being selected and the necessary permits secured. The addition of these monitoring stations to existing regional seismograph networks will provide critical coverage of regions lacking any instrumentation. To control telemetry costs, PC-based data acquisition systems will be installed at several locations and waveform data down loaded to the Earthquake Studies Office via modem or Internet for analysis.

We will conduct field investigations for evidence of faulting and seismic activity in 1995. We began an inventory of exposures of Pleistocene Glacial Lake Missoula sediments for possible liquefaction features. We are in the process of acquiring the engineering properties of the section from several studies including the Bureau of Reclamations seismotectonic study of the Flathead Lake Basin. The liquefaction potential of the Pleistocene section has been verified by the U.S. Bureau of Reclamation (Dan Levish, oral communication). We have also started compilation of a digital base map of the Lewis and Clark line for preparation of an integrated geologic map of the Idaho and Montana portions of the study area.

Results: none

Reports published: none

## PUGET SOUND PALEOSEISMICITY

9950-13175

Robert C. Bucknam  
 U.S. Geological Survey  
 M.S. 966, Box 25046  
 Denver, Colorado 80225  
 (303) 273-8566  
 bucknam@gldvxa.cr.usgs.gov

### PROGRAM ELEMENT II

#### INVESTIGATIONS

The primary objective of this project is to document and characterize Holocene deformation in the Puget Sound, Washington, region and develop an understanding of its structural and tectonic origins. Work during the reporting period (October 1993-September 1994) focused on refining the extent and age of late Holocene uplift in central and southwest Puget Sound (Fig. 1) that has been inferred to have been the site of a large earthquake about 1000 years ago (Bucknam and others, 1992). An important component of the work is the paleoecological analysis of sites near sea level using fossils to infer changes in relative sea level during the late Holocene in the Puget Sound region. Plant macrofossil and pollen studies are being carried out by Estella Leopold at the University of Washington, assisted by Dan Ekblaw, Gengwu Liu, and Tracy Fuentes; diatom studies are being carried out by Eileen Hemphill-Haley, U.S. Geological Survey at the University of Oregon.

#### INVESTIGATIONS AND RESULTS:

1) *Determine the extent and elevation of a well-expressed marine platform lying south of the Seattle fault. The work is expected to provide unusually detailed information on the distribution and spatial variation of the amount of uplift associated with a prehistoric earthquake and will constrain models of the structure(s) responsible for the uplift.* To date uplift has been measured at 6 sites in an 80 km<sup>2</sup> area on southern Bainbridge Island and the coast of the Kitsap Peninsula to the south, where uplift ranges between 5 and 7 meters. A shell midden that was deposited above the abandoned raised shoreline in Blakeley Harbor about 3 km south of the Seattle fault and that is now about 9 m above present high tide, provides upper limit for the amount of uplift at the site. The midden, which was deposited about 1-2 m above the preuplift shoreline, was in existence prior to uplift as shown by an analysis of charcoal from the base of the midden gave a conventional radiocarbon age of  $1490 \pm 70$   $^{14}\text{C}$  yr B.P. (Beta-57447).

2) *Reconnaissance studies of coastal Puget Sound. Continued reconnaissance of sites adjacent to the area already under study to further define the extent and character of the zone of uplift.* Reconnaissance study of a marsh at Thorndyke Bay near the northern end of Hood shows no obvious stratigraphic evidence of an abrupt change in relative sea level 1,100 years ago at the time of uplift and slip on the Seattle fault, 25 km to the southeast. Leaf bases of *Triglochin maritima* in growth position in mud 1.8 m below the present Thorndyke Bay marsh surface

gave a conventional radiocarbon age of  $1360 \pm 55$  yr. The mud containing scattered leaf bases of *Triglochin maritima* grades upward into peat containing conspicuous salt marsh macrofossils at a gradational contact 40 cm higher in the section. The Thorndyke Bay marsh is 40 km north of an area at the southern end of Hood Canal and adjacent Puget Sound that was uplifted several meters 1,000 years ago. The marsh is about 7 km southwest of a marsh on Hood Canal studied by Eronen and others (1987), who analysed an 8.5-m-long core that sampled 8,000 years of deposits that formed near sea level. They, also, saw no sudden changes in relative sea level in that record to attribute to tectonic deformation.

3) *Stratigraphic studies of existing* Continued stratigraphic studies of existing sites to more closely constrain the age and amount of uplift. Continued field study and analysis of a sand sheet at Lynch Cove (discussed in more detail in NEHRP Summaries of Technical Reports, January 1994, v. 35, p. 260-262) that is interpreted to be a tsunami deposit. Additional effort is being expended on this deposit and wood incorporated within it because it offers an opportunity for testing (possibly with a resolution of several months) whether or not uplift in the southwestern uplift area was synchronous with the 1,100-year-old uplift (and earthquake) near Seattle. Existing limiting radiocarbon ages of samples from this site were analyzed in collaboration with Glenn Biasi, University of Nevada, Reno, using Bayesian probabilistic methods to reduce the variance in the estimated time of uplift. Bayesian analysis of the calibrated ages of the stratigraphically ordered samples gives a mean estimate for the time of uplift of A.D. 885 (with a 95% range of A.D. 775-965). This estimate is concordant with the  $2\sigma$  calibrated age ranges from high-precision radiocarbon analyses of trees and herbaceous plants killed by the effects of an earthquake that produced up to 7 m of uplift along the Seattle fault 35 km to the northeast (A.D. 894-997; Jacoby, G.C., and others, 1992, *Science*, v. 258, p. 1621-1623; A.D. 885-990; Atwater, B.F., and Moore, A.L., 1992, *Science*, v. 258, p. 1614-1617). Despite the similar ages from the two areas, the uplifts are too widely separated to have resulted from slip on a single fault, which suggests that the uplifts were produced by two earthquakes that were closely spaced in time.

## REPORTS PUBLISHED

Bucknam, R.C., and Biasi, Glenn P., 1994, An improved estimate of the time of a prehistoric earthquake in the southwest Puget Sound region, Washington: Geological Society of America Abstracts with Programs, v. 26, no. 7, p. A-522.

Bucknam, R.C., Leopold, E.B., Hemphill-Haley, Ekblaw, D.E., Atwater, B.F., Benson, B.E. and Phipps, J.B., 1994, Holocene tectonics in western Washington, in Swanson, D.A., and Haugerud, R.A., eds., Geologic field trips in the Pacific Northwest—1994 Geological Society of America Annual Meeting:

9920-10162

Howell M. Butler

Branch of Earthquake and Geomagnetic Information

U.S. Geological Survey

Building 10002, Kirtland AFB-East

Albuquerque, New Mexico 87115-5000

Telephone: (505) 846-5646, FAX: (505) 846-6973, E-mail: butler@asl.cr.usgs.gov

### Investigations

The Global Seismograph Network (GSN) presently consists of the Incorporated Research Institutions for Seismology Network (IRIS/GSN) 37 stations and the Worldwide Standardized Seismograph Network (WWSSN) 55 stations. Support is furnished at a level needed to keep the GSN at the highest percentage of operational time in order to provide the improved geographical coverage with analog and digital data from highly sensitive short-period and very broadband seismic sensor seismograph systems. This support includes provision of operational supplies, replacement parts, repair services, modifications, on-site system installation, maintenance, training and system calibration.

### Results

The GSN continues with a combined total of 92 WWSSN/IRIS-1/IRIS-2 stations. Global seismic data coverage is provided to the National Earthquake Information Center (NEIC) and to other data centers and research organizations throughout the world.

IRIS-2 seismograph systems were installed at eight locations: Honiara, Solomon Islands (HNR); Grafenberg, Germany (GRFO); Kipapa, Hawaii (KIP); Bogota, Colombia (BOCO); Lusaka, Zambia (LSZ); Santo Domingo, Venezuela (SDV); Tsumeb, Namibia (TSUM); and Cathedral Caves, Missouri (CCM).

On-site maintenance visits were required at the following locations: Albuquerque, New Mexico (ANMO); Charters Towers, Australia (CTAO); South Karori, New Zealand (SNZO); Rarotonga, Cook Islands (RAR); Afiamalu, Western Samoa (AFI); Kipapa, Hawaii (KIP); Ankara, Turkey (ANTO); San Pablo, Spain (PAB); Taipei, Taiwan (TATO); Chiang Mai, Thailand (CHTO); and Adak, Alaska (ADK).

Site visits/surveys were performed at the following locations: Nairobi, Kenya; Lusaka, Zambia; Tsumeb, Namibia; Kiev, Ukraine; Mopti, Mali; Galapagos Islands, Ecuador; Antofagasta, Chile; Addis Ababa, Ethiopia; Franceville, Gabon; Davao, Philippines; Ulaanbaatar, Mongolia; and Santa Lucia, Brazil.

**TITLE:** Earthquake Hazard Study in the Vicinity of  
Toppenish Basin, South-Central Washington

**AWARD NUMBER:** 1434-94-G-2490

**INVESTIGATORS:** Newell P. Campbell, Tom Ring, Ted Repasky

**INSTITUTION:** Yakama Indian Nation

**ADDRESS:** Department of Natural Resources  
P.O. Box 151  
Toppenish, WA 98948

**TELEPHONE NUMBER:** (509) 877-6121  
**FAX NUMBER:** (509) 877-6907

## INVESTIGATIONS UNDERTAKEN

Work plans for the Toppenish Basin Earthquake Study encompassed five components. The first four, involving known fault scarps on Toppenish Ridge, included:

- installing a seismometer on Toppenish Ridge.
- constructing trenches across fault scarps on an undisturbed area of Toppenish Ridge.
- running a 2 km seismic line across the scarp system.
- establishing and monitoring a trilateration survey net across the faults.

The fifth component involved an initial investigation of scarps occurring on Ahtanum Ridge near a population center (Yakima) to determine if these faults might represent a hazard (Fig. 1).

Our initial investigation attempted to answer three fundamental questions:

- What is the nature and timing of the fault scarps on Toppenish Ridge?
- Are these faults capable of producing a magnitude 7 earthquake?
- Does the faulting on Ahtanum Ridge mimic that of Toppenish Ridge and potentially produce large seismic events?

Our schedule called for completion of all field work by October 1, 1994. However the Yakama Indian Reservation suffered a series of large fires resulting in restricted access for several weeks in the summer. As a result, the seismic line project was delayed until mid-November. All other field work was completed as scheduled.

## RESULTS

### Seismometer Installation

The Ahtanum Ridge seismometer was relocated in order to improve telemetry (new name - Yakima 2). A new seismometer was installed on Toppenish Ridge (named TRW) and became operational on October 20, 1994. The Washington State seismic net began receiving and routinely processing data from the site. Installation of this new instrument not only fills a former gap in the Columbia Basin network but also places a seismometer within 0.5 km of the Mill Creek Thrust System on Toppenish Ridge (Fig. 2).

TRW has recorded ten local earthquakes (as well as many larger non-local events). On four local events, TRW was a significant contributor to the ability to detect and locate the events. TRW was the first arrival station on one small (1.3) event about halfway between TRW and the Goldendale station. Without TRW, this event would not have triggered the automatic locating system because the event would not have been recorded on the required minimum of three stations.

### Trilateration Survey

The first set of measurements of the trilateration survey was completed October 19, 1994. Figure 2 shows the locations of the 5-point survey net. This net was tied into a first order triangulation station on Pumphouse Road approximately 10 km to the east. Because the high relief on Toppenish Ridge caused line-of-sight problems for a conventional survey, we employed a high resolution Global Positioning System. Reid-Middleton Corporation used Trimble 4000 SSE, dual frequency, geodetic receivers; they report accuracy in the sub-centimeter range. GPS was also chosen because the net can be expanded more easily than conventional surveys.

The survey will be repeated in one year to measure for evidence of creep along the fault system. The reinforced concrete piers provide permanent stations that should be stable for at least five more years. Trilateration survey data are available from the Yakama Nation Water Resources Branch (Tom Ring, (509) 877-6121).

### Trenching

Four trenches were dug across faults along Toppenish Ridge, one trench across a 2-meter-high scarp of the Mill Creek Thrust and three trenches in an extensional graben (Fig. 2). The trenches show evidence of four periods of seismic activity.

Trench 1, through the thrust, shows 3.5 meters of fault plane offset involving modern A and B soil zones, L-1 loess, and an older dark-brown clayey "chocolate" soil. L-1 loess contains shards of Mt. St. Helens "S" tephra (age approximately 13,000 yrs BP) and is the horizon locally on which modern soils develop (Figs. 3 and 4). Returns from radiocarbon (RC) and thermoluminescence (TL) sampling in Trench 1 are not yet available; however the event probably correlates with 500-700 yrs BP dates from elsewhere on Toppenish Ridge (Campbell & Bentley, 1981) and with a local Indian legend involving loss of life in a landslide (approximately 500 yrs BP). Geomatrix (1993) proposed a maximum seismic event of 6.0-7.3 for Toppenish Ridge (depending on coupling). The latest movement observed in Trench 1 fits their calculations.

Trench 1 also shows evidence for two older events (Fig. 4). Clastic wedges involving gravel and soil indicate the fault was active at least twice prior to deposition of the "chocolate" soil (more than 40,000 yrs BP). TL dates are not yet available for the oldest of these wedges (Unit 2-A) and the amount of offset caused by these older events is unknown.

Trench 4, across a sag pond in an extensional graben, provides evidence of two seismic events (Fig. 5). Two periods of extension are visible in the north end of the trench. Initial extension caused by an underlying thrust created offset in Pliocene Ellensburg Formation sediments of about 3 m. A second extensional event down-dropped the Ellensburg Formation another meter; the resulting depression is filled with disrupted soil and rock. Modern A & B zones, L-1 loess, the Washtucna soil (20,000-40,000 yrs BP), and fan gravels are offset by formation of this inner graben. Datable materials that were collected will probably show that the inner graben was formed during the 500-700 yr BP seismic event seen in Trench 1.

Evidence for an earlier event occurs at the south end of Trench 4. A buried A-zone lies within the L-1 loess, above a layer of Mt. St. Helens "S" tephra. Buried A-zones are rare in the Columbia Basin and, when present, tend to be rapidly destroyed by organic activity. Such soils are unlikely to be older than 3000 yrs BP (Alan Busacca, personal communication, 1994). A radiocarbon date on the buried A-zone is pending. In summary, Trench 4 shows evidence for two seismic events, both younger than 13,000 yrs and probably younger than 3000 yrs.

Trench 2 and Trench 3 show further evidence for two periods of movement within the extensional graben (Figs. 6 and 7). In Trench 2 (Trench 3 mimics the upper part of Trench 2), the Ellensburg Fm is offset at least 6 m (!) by graben extension. Fan gravels of at least 2 ages are involved as graben fill. An older, yellow gravel displaying tilted carbonate pendants was down-dropped and tilted during the first period of extension. A second extensional event offsets the yellow gravel an additional 1 m and fills the extensional opening with imbricated, dark gravel. The darker gravel thickens into the graben center and was probably deposited after the graben became active a second time. Although there is no way to date these gravels, Trench 2 and Trench 3 lend credibility to the events postulated in Trench 4.

In conclusion, trenching demonstrated evidence for four seismic events. Table 1 summarizes the events and proposed ages. There remain several untrenched scarps on Toppenish Ridge associated with other thrust plates. Future trenching may show that additional seismic events occurred along the fault system. Figure 9 is a diagrammatic profile of the bench area on Toppenish Ridge in the vicinity of this study. This composite figure was drawn from the data collected in trenches 1-4.

**TABLE 1. Tabulation of Seismic Events on Toppenish Ridge**

<u>Event</u>	<u>Age (yrs BP)</u>	<u>Exposed</u>	<u>Evidence</u>
1	500-700	Trench 1 & 4	inner graben fill; 3.5 m. offset of loess and soil; RC dates from previous work; Indian legend
2	1000-3000	Trench 2 & 4	buried A-zone in graben; 2 offsets in fan gravels
3	more than 40,000	Trench 1 & 4	fault-caused clastic gravel wedge below thrust; pre-"chocolate" and Washtucna soil age
4	more than 40,000	Trench 1	clastic soil wedge; wedge below thrust and under event 3

#### Seismic Line Survey

Figure 2 shows the location of our scheduled seismic survey. The line passes by Trenches 2 & 3 and is tied into a nearby trilateration survey station. The line will involve shots of approximately 2-meter-spacing using either a "Betsy" seisgun or hammer energy source. We expect to locate Columbia River Basalt and Ellensburg Fm units buried beneath the gravel and loess cover. Shooting will begin in mid-November.

#### Ahtanum Ridge Investigation

Our initial investigation of the Ahtanum Ridge scarps shows surprising similarity to those on Toppenish Ridge (Fig. 8). Both feature ridgeline grabens that cut down slope (and down structure) to the base of the ridge. Both grabens involve surface scarps that cut loess and fan gravel. The Toppenish Ridge system is longer and more complex with thrust scarps and graben scarps tapering together toward the west.

Ahtanum Ridge may also have recent thrusting but agriculture and urban development have destroyed the surface scarps. Bentley and others (1983, 1993) indicate a buried thrust at the base of Ahtanum Ridge in a similar position to those on Toppenish Ridge.

In short, faults on Ahtanum Ridge seem to mimic those on Toppenish Ridge but on a smaller scale. The Ahtanum graben passes under a trailer development and water tank; a buried thrust may lie under the city of Union Gap and numerous houses south of Yakima. The Yakima area would be seriously affected by a magnitude 5.0 or greater event. Clearly, faults on Ahtanum Ridge warrant further investigation.

## REPORTS PUBLISHED

Campbell, N.P., Repasky, T.R., Ring, T.E., Becenti, T.C., and Busacca, A.J., 1994, Recurrent Holocene to Recent Movement in the Toppenish Ridge Fault System, South-central Washington (Abs.): Geological Society of America Abstracts with programs, Vol. 26, No. 7, Page 187.

## REFERENCES CITED

Bentley, R.D., Campbell, N.P., and Powell, J. E., 1993, Geologic Maps of the Yakima Fold Belt, Northeastern Yakima County, Washington: Washington Division of Geology and Earth Resources Open File Report 93-3, 13 p.

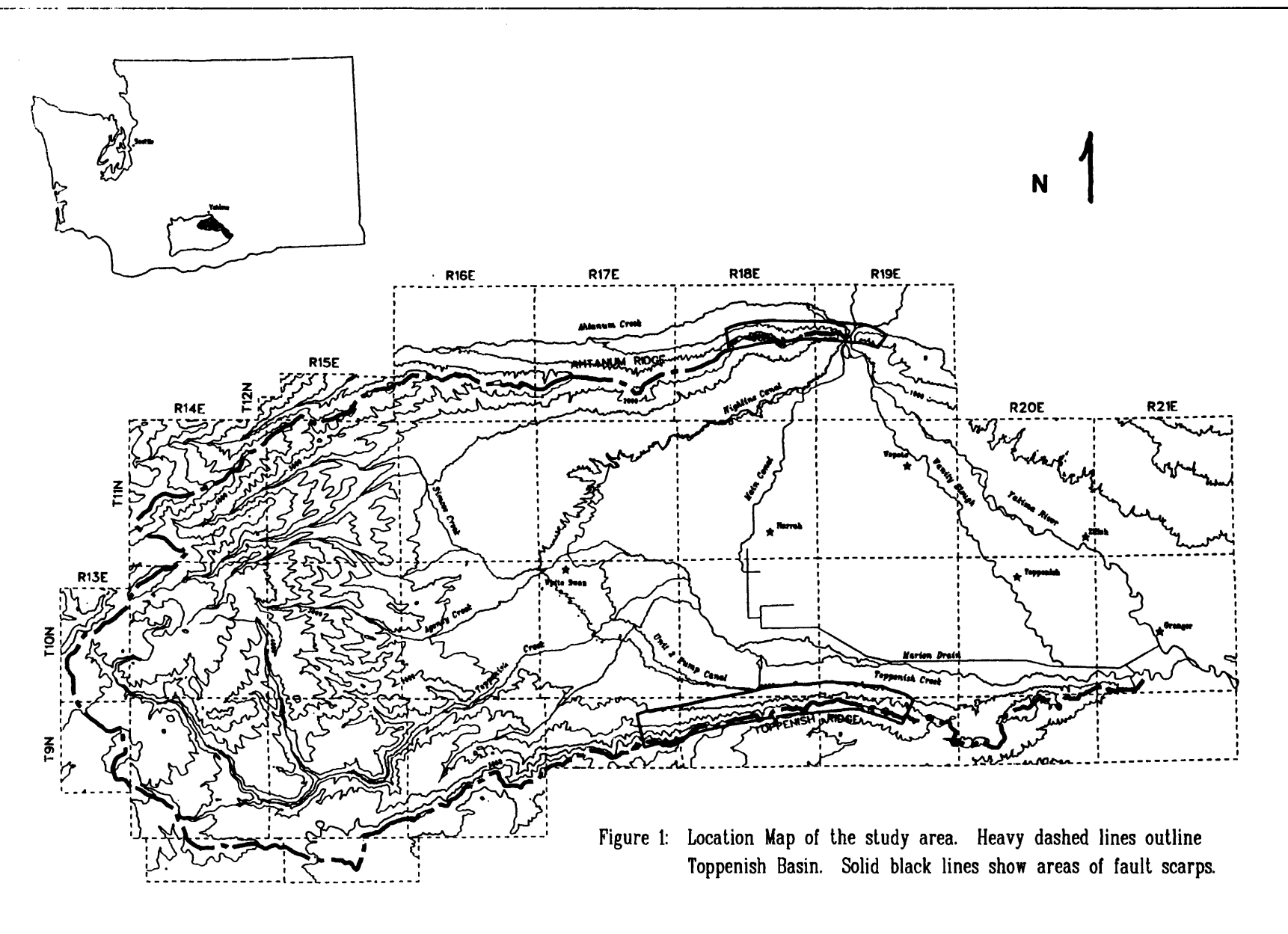
Bentley, R.D. and Campbell, N.P., 1983, Geologic Map of the Yakima Quadrangle, Washington: Washington Division of Geology and Earth Resources Geologic Map GM-29.

Campbell, N.P. and Bentley, R.D., 1981, Late Quaternary Deformation of the Toppenish Uplift in South-Central Washington: Geology, V. 9, p. 579-524.

Geomatrix Consultants, 1993, Probabilistic Seismic Hazard Analysis, DOE Hanford Site, Washington: WHC-50-W236A-TI-002, Revision O, prepared for Westinghouse Hanford Company, Richland, Washington, 60 p.

## LIST OF FIGURES

- Figure 1.** Location map of the study area. Heavy dashed lines outline Toppenish Basin. Solid black lines show areas of fault scarps.
- Figure 2.** Location map of trenches (T), trilateration survey points (N), seismometer (S) and seismic line (L).
- Figure 3.** Photo of thrust fault in Trench 1. Rock units are labeled in Figure 4.
- Figure 4.** Trench 1 profile, east wall.
- Figure 5.** Trench 4 profile, east wall.
- Figure 6.** Trench 2 profile, east wall.
- Figure 7.** Trench 3 profile, east wall.
- Figure 8.** Comparison of graben and thrust on Ahtanum Ridge with those on Toppenish Ridge.
- Figure 9.** Diagrammatic profile in vicinity of 1994 trenches showing relationships between thrust faults, grabens, critical rock units & proposed seismic events. Composite figure from trenches 1-4.



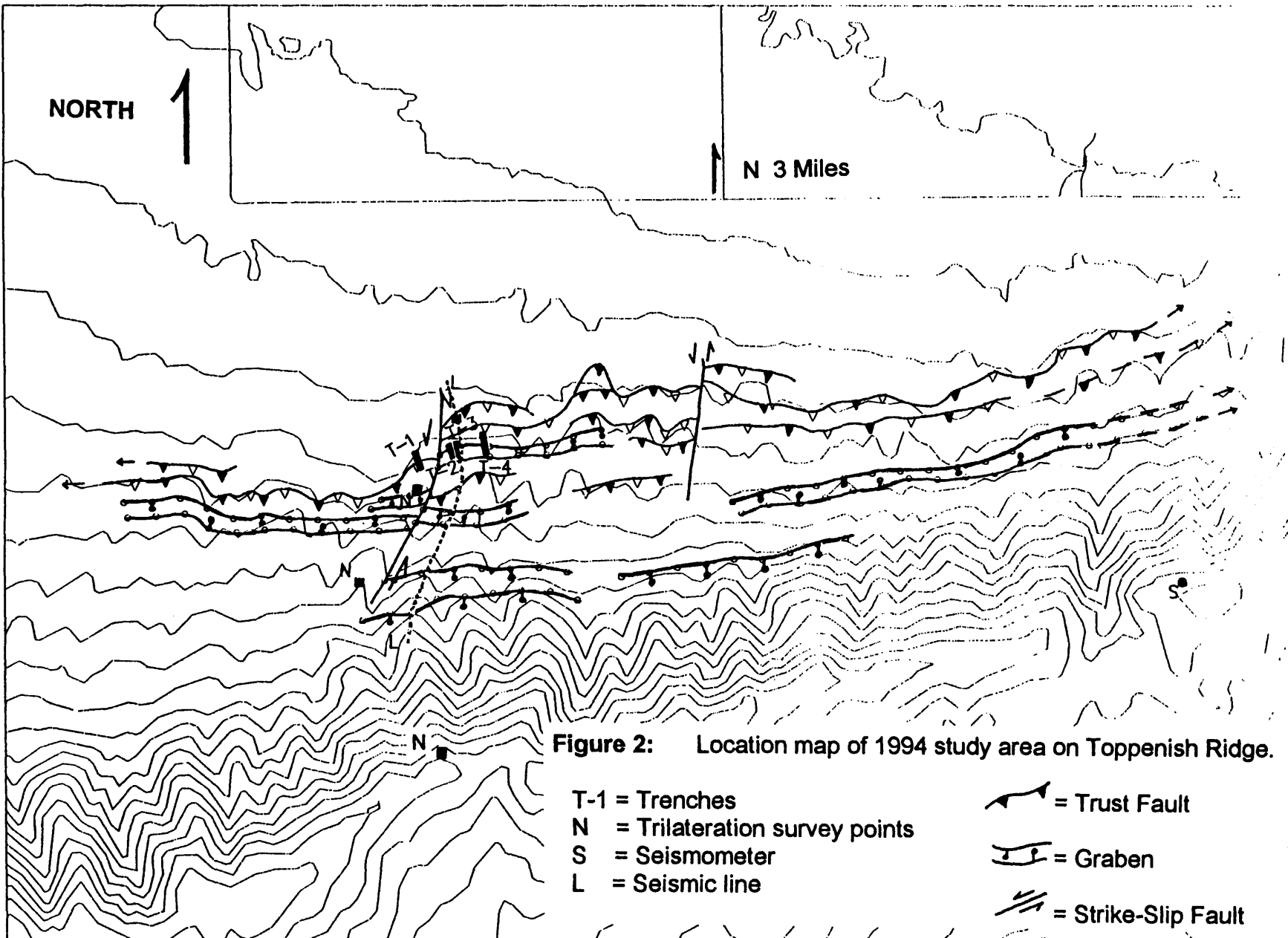


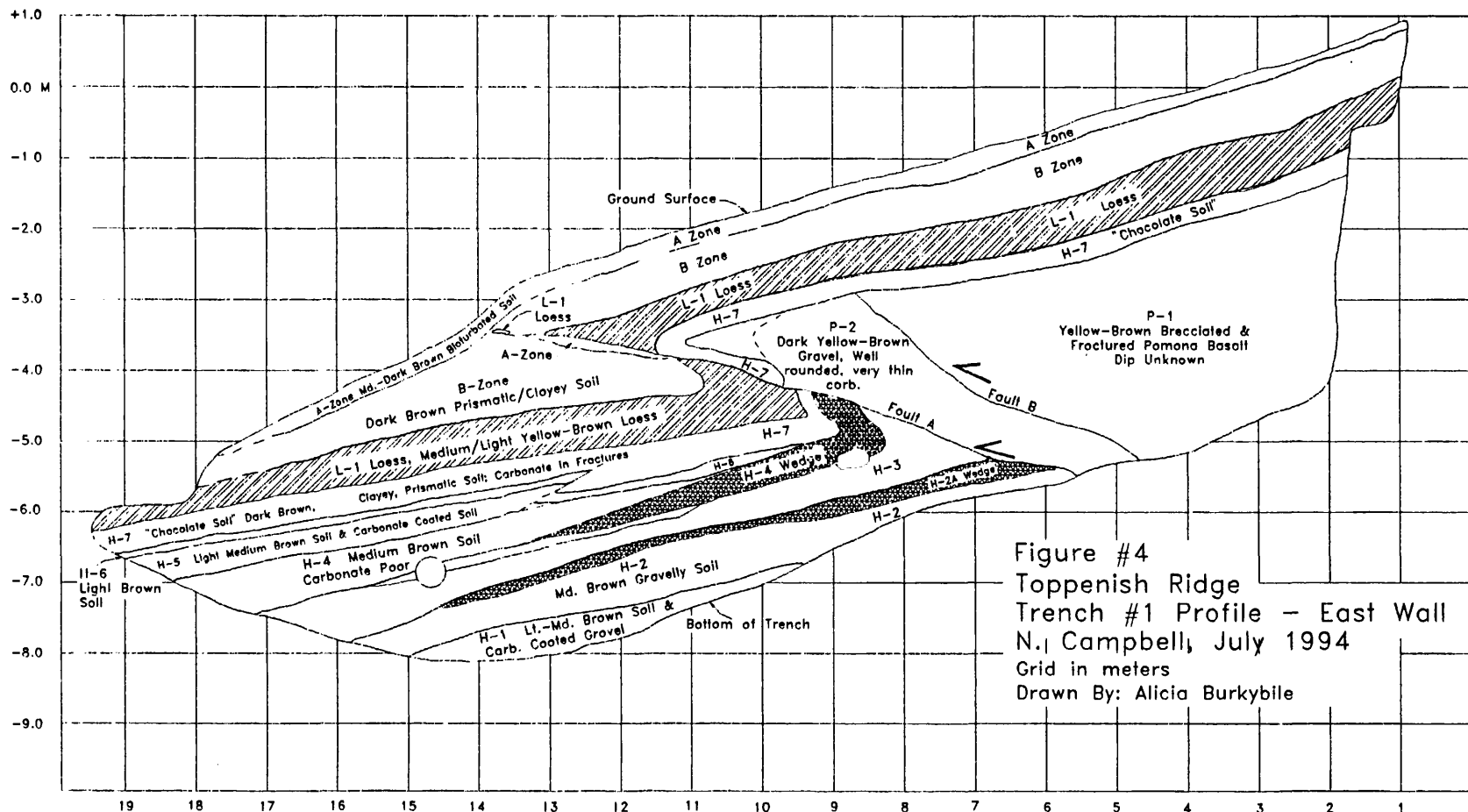


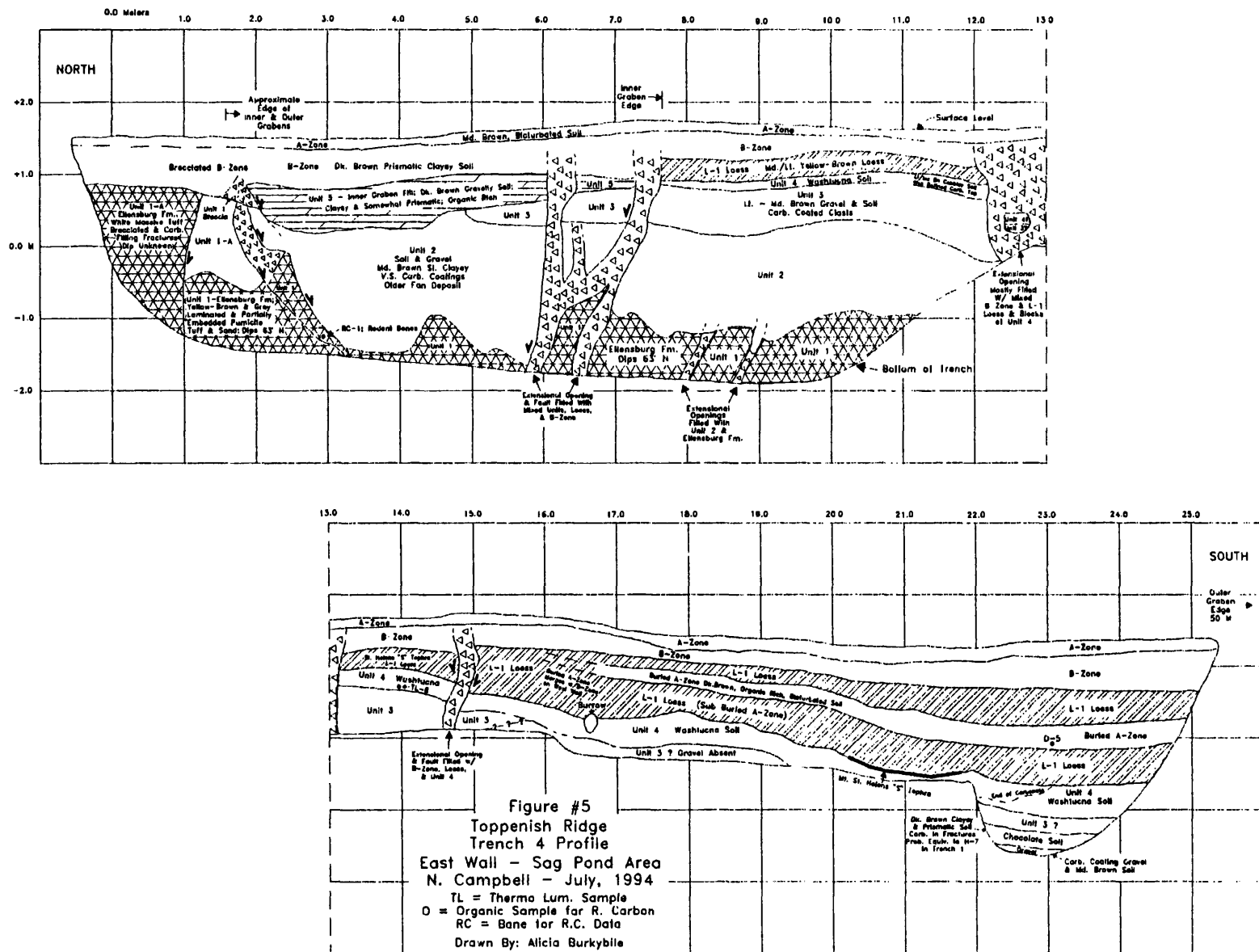
**Figure 3:** Photo of thrust fault in Trench 1. Rock units are labeled in Figure 4.

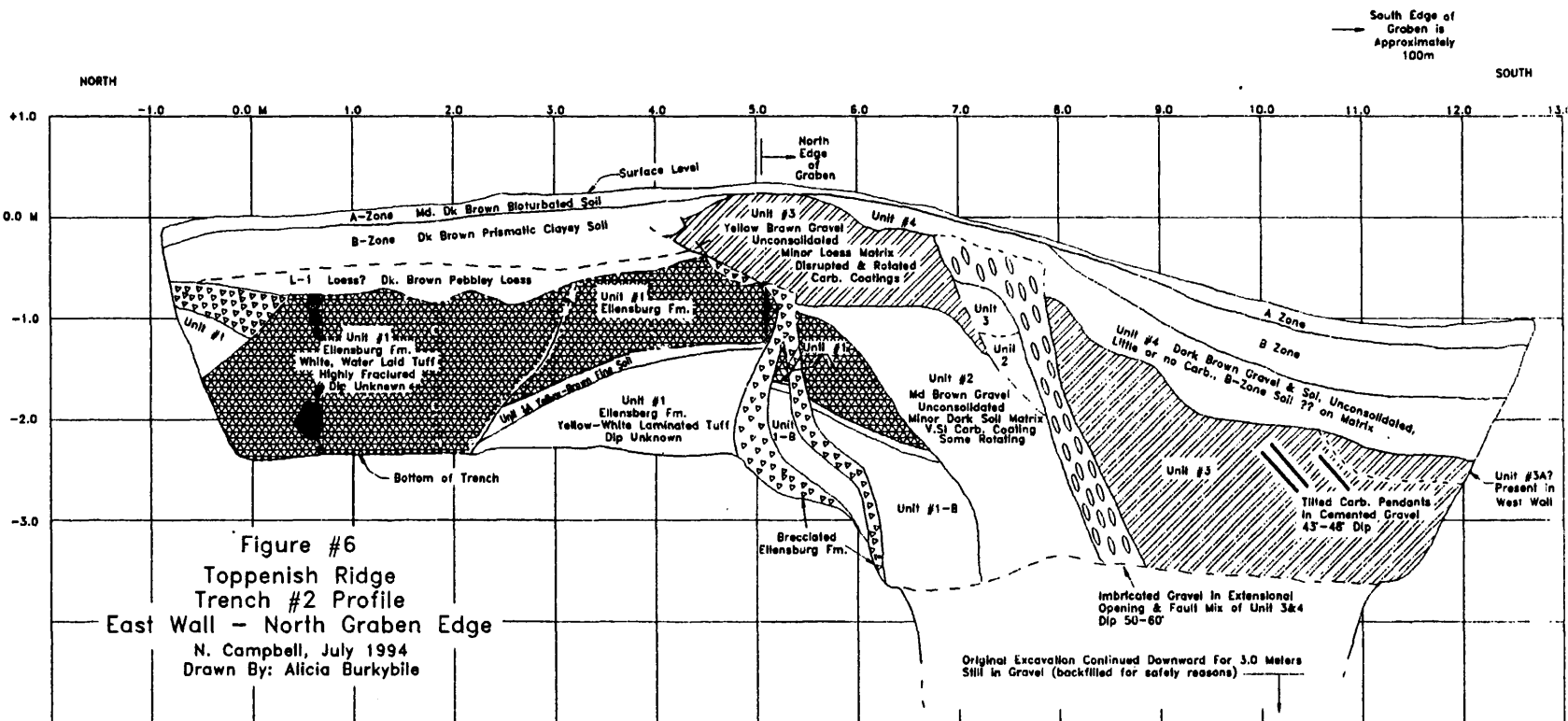
NORTH

SOUTH

301







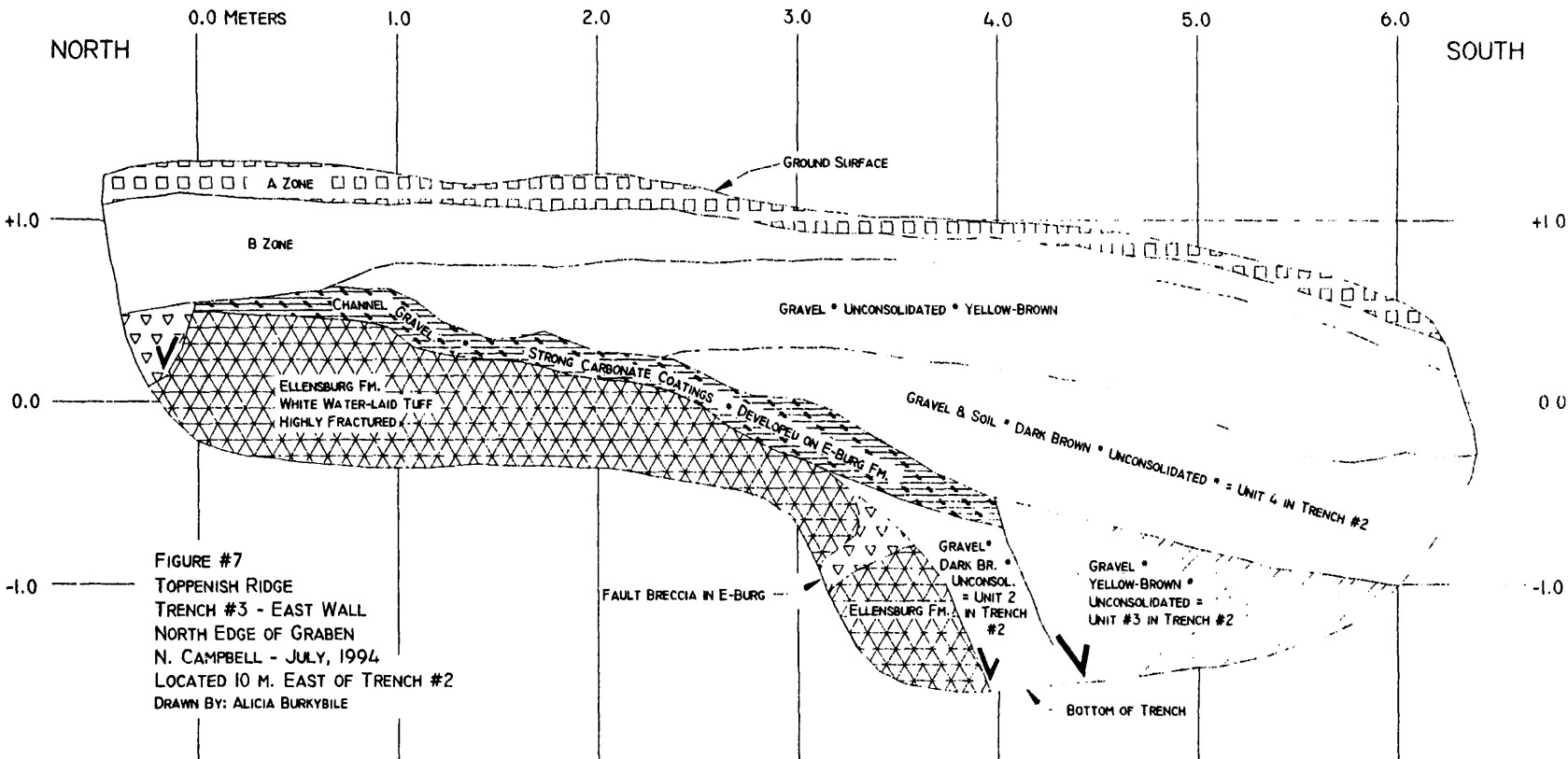
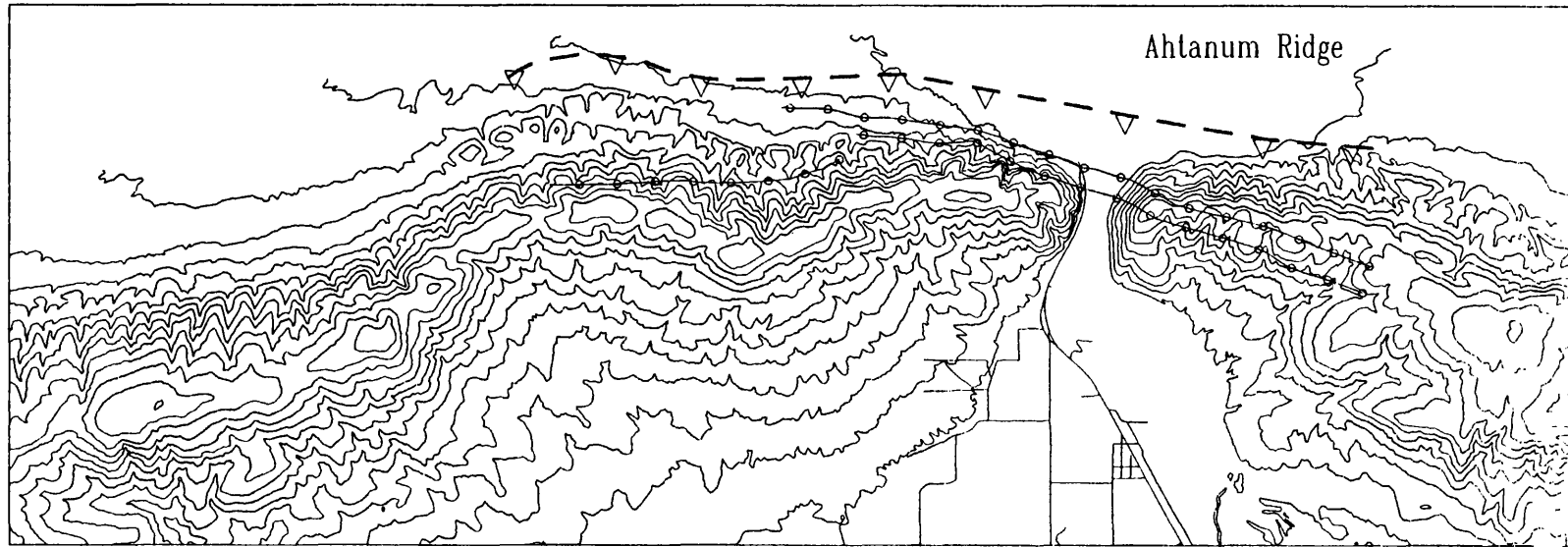
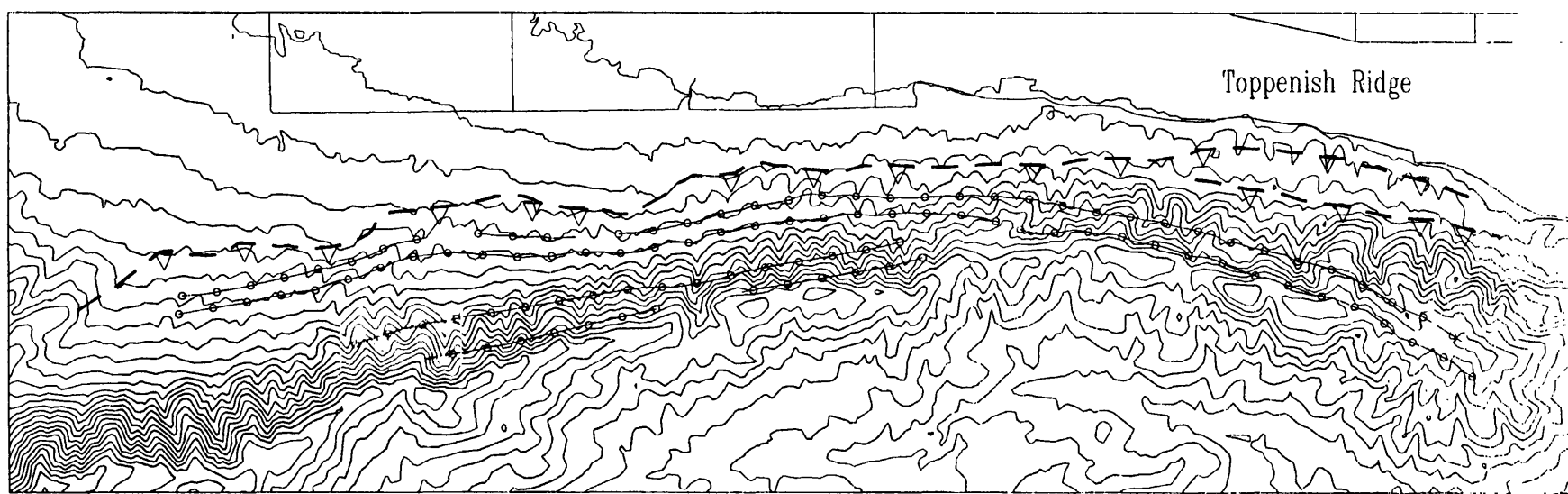


FIGURE #7  
 TOPPENISH RIDGE  
 TRENCH #3 - EAST WALL  
 NORTH EDGE OF GRABEN  
 N. CAMPBELL - JULY, 1994  
 LOCATED 10 M. EAST OF TRENCH #2  
 DRAWN BY: ALICIA BURKBILE



305

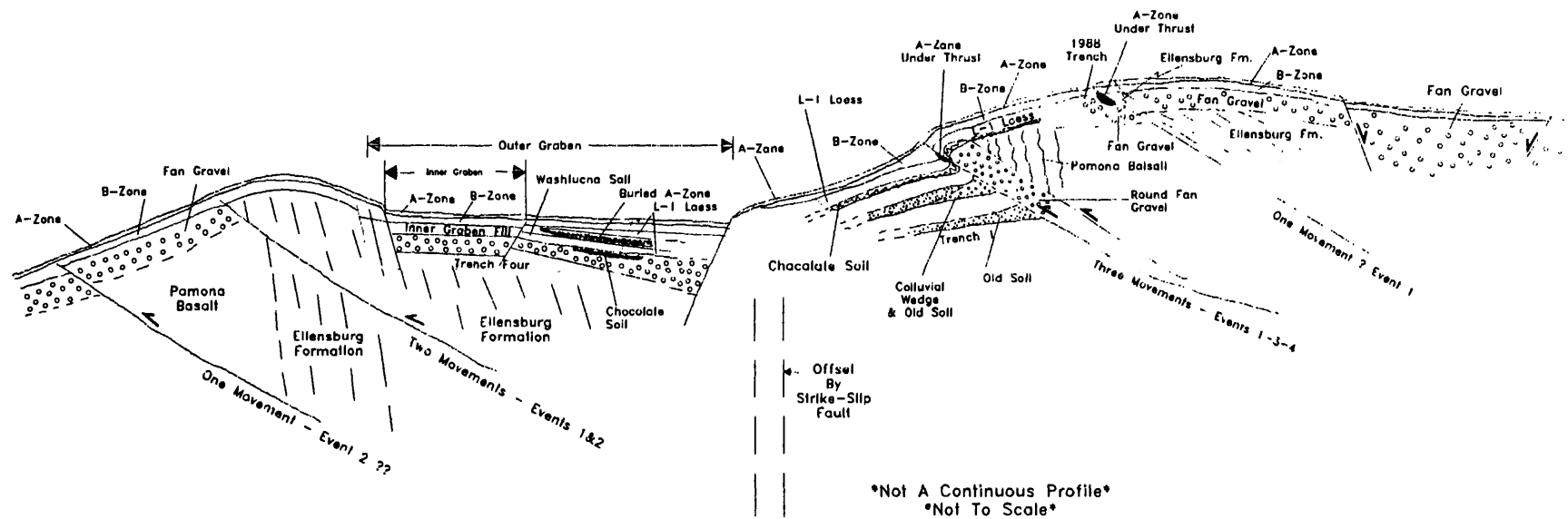


II

**Figure 8:** Comparison of graben and thrust fault on Ahtanum Ridge with those on Toppenish Ridge

NORTH

SOUTH



306

Figure #9  
Toppenish Ridge  
Diagrammatic Profile in Vicinity of 1994 Trenches  
Showing Relationships Between Thrust Faults, Grabens,  
Critical Rock Units & Proposed Seismic Events.

N. Campbell - August 1994  
Drawn By: Alicia Burkybile

**Seismotectonics Studies of the New Madrid Seismic Zone  
using Data Collected by the PANDA Array**

**#1434-94-G2398**

**Jer-Ming Chiu, Jose Pujol, and Arch C. Johnston**

**University of Memphis**

**Center for Earthquake Research and Information**

**Memphis, TN 38152**

**Tel : 901-678-2007, Fax : 901-678-4734**

**E-mail : chiu@ceri.memphis.edu**

**Program Element : CU**

**Investigations**

Our research works during this supporting period are mainly concentrated on the cleanup of PANDA database, on the 3-dimensional tomographic inversions of P and S wave velocity models in the upper crust, on the study of attenuation features of P and S waves inside the sedimentary basin in the upper Mississippi embayment, and on the image of 3-dimensional configurations of the sedimentary basin. The PANDA database has been carefully cleaned and updated. It has been reduced to about 1/3 of its original volume. We anticipate to be able to release final PANDA data via USGS at the end of the current funding period. P wave velocity profiles from the available well-log data in the upper Mississippi embayment and a  $V_p/V_s$  of 3.2 obtained from preliminary linear velocity inversion are used to provide constraints on the initial model for 3-D tomographic inversion. Time differences between the direct P and converted S and between the direct S and the converted P are used in an attempt to determine the thickness of sediments beneath each PANDA station. Spectra ratio between the direct S and the converted P waves are used to determine the  $Q_p/Q_s$  relationship in the sediments.

**Results**

Principal results obtained from the analysis of PANDA data during this project period include:

- (a) Using travel time differences between the direct P and P to S converted waves and between the direct S and the S to P converted waves to determine the depth of the sediments beneath each PANDA station. 3-dimensional configuration of the sedimentary basin in the upper Mississippi embayment is thus constructed.
- (b) spectra differences between the direct S and the converted P waves from the bottom of the sedimentary basin are used to determine the attenuation characteristics of seismic waves inside the sedimentary basin.  $Q_p$  and  $Q_s$  are estimated to be in the range from 25 to 60 and from 25 to 30 respectively.
- (c) A high-resolution crustal structure image in the NMSZ becomes possible with unambiguous identifications of both P and S arrivals from earthquakes recorded by the 40 3-component PANDA stations supplemented by the regional seismic networks which were mostly single-component. Three-dimensional tomographic inversion method by Liu et al., (1990 and 1993) has been applied to P and S velocity inversions independently. Information obtained from well logs and seismic reflection/refraction were used to provide control on the P-wave velocity, especially in the uppermost sedimentary basin. Additional P and S velocity information from previous layered inversion constitute the initial velocity model for the inversion. Since Only local earthquakes are used which extend from 3 to 15 km in depth, therefore only the upper crust in the NMSZ shallower than 15 km is imaged. Results of P and S images at different depths show

apparent lateral velocity perturbations throughout the entire NMSZ (Figures 1 and 2). Some correlations can be identified between the regions of faster velocity anomaly and some known mafic intrusions identified from magnetic anomalies (Hildenbrand et al., 1992). Cross-sectional views suggest that some anomalous regions may be extended into lower crust. The uppermost sedimentary basin is characterized by water saturated unconsolidated sediments with a  $V_p/V_s$  ratio of 3.0. A low velocity zone at depth from 2.5 to 5 km, however, is characterized by a  $V_p/V_s$  of 1.51 which may be interpreted as a stratigraphic unit of low  $V_p$  (probably shale) but also with elevated  $V_s$  relative to  $V_p$  due to the presence of fluid- or vapor-filled cracks and/or pores, probably under elevated pore pressures.

## References

- Liu, F., H. Wu, and J. Liu, (1990), 3-D velocity image beneath the Chinese continent and adjacent regions, *Geophys. J. Int.*, 101, 379-394.
- Liu, F. and A. Jin, (1993), Seismic tomography of China, *Seismic Tomography, Theory and Practice*, edited by H.M. Iyer and K. Hirahara, published by Chapman& Hall, 299-318.
- Hildenbrand, T.G., J.G. Rosenbaum, and R.L. Reynolds, (1992), High-resolution aeromagnetic study of the New Madrid seismic zone: a preliminary report, *Seismol. Res. Let.*, 63(3), 209-222.

## Papers Published and/or in Press

- Rowlands, H., D.C. Booth, and J.M. Chiu, (1993), Shear-wave splitting from micro-earthquakes in the New Madrid seismic zone, *Can. J. Expl. Geophys.*, 29, 352-362.
- Chen, K.C., J.M. Chiu, and Y.T. Yang, (1994),  $Q_p - Q_s$  relations in the sedimentary basin of the upper Mississippi embayment from the spectra ratio between the direct and the converted waves, December issue of *Bull. Seismol. Soc. Am.*.

## Abstracts

- Liu, F.T., J.M. Chiu, Y.T. Yang and S.C. Chiu, (1994), Upper crustal structure in the NMSZ from 3-dimensional P and S tomographic inversions, presented October 1994 at the annual meeting of the ESSSA in Columbia, South Carolina.

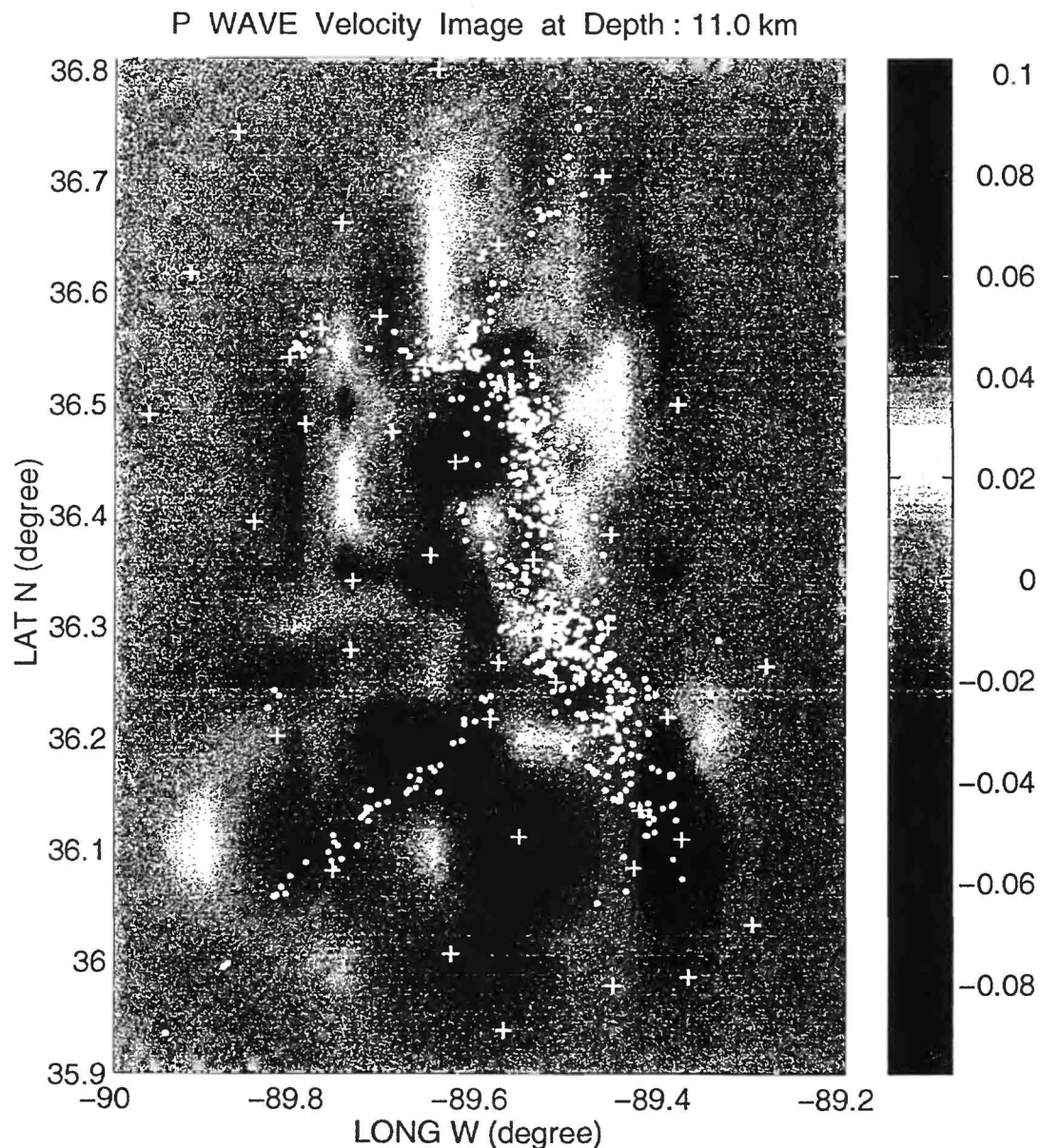


**Figure 1.** Example of P wave velocity perturbations at depth of 11 km from a 3-dimensional tomographic inversion of P waves using PANDA data from the New Madrid seismic zone (Liu et al., 1994). P and S data are used independently in the inversion in order to determine 3-dimensional P and S velocity structures independently. Travel time data from local, regional, and teleseismic earthquakes as well as from airgun shots can be used in the 3-D tomographic inversion.

## Late Quaternary slip rates on active faults of California

9960-10316, 11316, 12316

Malcolm M. Clark

Branch of earthquake geology and geophysics  
345 Middlefield Road, MS 977  
Menlo Park, CA 94025-3591

415 329 5624 /FAX 415 329 5163 /email: mclark@isdmnl.wr.usgs.gov

### Program element II

#### Investigations

1. Recently active traces of the Calaveras fault zone at Tres Pinos and San Felipe Creeks, California (K.J. Kendrick, J.W. Harden, M.M. Clark).
2. Recently active traces of Owens Valley fault zone, California (Sarah Beanland, EDS, IGNS, New Zealand; Clark).
3. Degradation of fluvial terrace risers along Lone Pine Creek, San Bernardino County (Kendrick, with J.B.J. Harrison, L.D. McFadden [UNM] and R.J. Weldon [UOR]).
4. Late Quaternary evolution of the San Timoteo Badlands region, southern California (Kendrick, with S.G. Wells [UCR], D.M. Morton, and L.D. McFadden [UNM]).

#### Results

2. Owens Valley fault zone. See v. 33, p. 202-3 of this publication for results summarized from our report, USGS Bulletin 1982, in press, listed below. This Bulletin features a 1:24,000-scale strip map of the Owens Valley fault zone, a table of characteristics and measurements of active traces at 40 sites along the fault zone from Owens Lake to north of Big Pine, and text.
3. Prepare report, K.J. Kendrick, J.B.J. Harrison, R.J. Weldon, and L.D. McFadden, An evaluation of a non-linear diffusion equation model for determining the rate of scarp degradation in Cajon Pass, southern California (intended for journal publication).
4. Kendrick described 20 soils in San Timoteo and Reche Canyons in San Timoteo Badlands. She analysed these soils in the lab and estimated their soil development and rubification indices. She used these indices and the amount and composition of iron oxides to estimate ages of geomorphic

surfaces associated with these soils. Total elemental analyses, combined with silica extraction, help to constrain the age estimates of the surfaces. These ages, combined with offsets of clasts determined by D.M. Morton and J.C. Matti, yield slip rates of  $10 \pm 3$  and  $19 \pm 6$  mm/yr for this part of the San Jacinto fault. These slip rates are larger than previous estimates for this part of the San Jacinto fault zone.

Prepare report, K.J. Kendrick, L.D. McFadden, and D.M. Morton, Soil development in the San Timoteo Badlands region; implications for slip on the San Jacinto fault (intended for GSA Bulletin).

### Reports

Beanland, Sarah, and Clark, M.M., The Owens Valley fault zone, eastern California, and surface rupture associated with the 1872 earthquake: U.S. Geological Survey Bulletin 1982, in press.

Harrison, J.B.J., Kendrick, K.J., McFadden, L.D., and Weldon, R.J. III, The influence of terrace scarp degradation on soil-profile development, Cajon Pass, southern California: Catena, in press.

Kendrick, K.J., McFadden, L.D., and Morton, D.M., 1994, Soils and slip rates for the northern San Jacinto Fault; Geologic Investigations of an Active Margin, 1994 GSA Cordilleran Section Guidebook, p. 146-151.

# TECTONICS OF SEISMIC SOURCE ZONES, CENTRAL INTERIOR OF THE UNITED STATES

9950-14235

ANTHONY J. CRONE

U.S. Geological Survey

Branch of Earthquake and Landslide Hazards

Box 25046, MS 966,  
Denver, Colorado 80225

(303) 273-8591

Fax: (303) 273-8600

E-mail: [crone@gldvxa.cr.usgs.gov](mailto:crone@gldvxa.cr.usgs.gov)

Program Element II

## PURPOSE OF PROJECT

This project focuses on studies that provide basic geologic information on the distribution, characteristics, and frequency of large earthquakes in the central interior of the United States, including particular emphasis on the New Madrid seismic zone. The overall objective is to contribute to a better understanding of the structural features that might produce large, potentially damaging intraplate earthquakes. Project members during this reporting period include Donley S. Collins, Anthony J. Crone, and John A. Michael.

## INVESTIGATIONS

D.S. Collins has completed a detailed lithologic log for the Dow Chemical No. 1 B.L. Garrigan drill hole. Previously published logs of this drill hole are inconsistent in terms of the quantity and types of rock present in the drill hole. This detailed log helps eliminate the confusion and refines the stratigraphy of Lower Paleozoic rocks in the Reelfoot basin.

D.S. Collins also began searching pre-1912 navigation charts and reports to obtain information on the location of surface deformation associated with the 1811-1812 New Madrid earthquakes. The information from this search helps clarify the location of towns and the channel position of the Mississippi River before and after the New Madrid earthquakes. The purpose of this investigation is to reduce the confusion created by the reiteration of the 1811-1812 earthquake events by various eyewitnesses and by second- or third-party authors. This information helps restrict the location(s) of surface deformation associated with the 1811-1812 earthquakes, which will help focus future investigations. This historical information can also be used as a guide to the style and extent of deformation that might result from future large earthquakes in the New Madrid region.

D.S. Collins has designed—and with the aid of J.A. Michael and Lee-Ann Bradley—has nearly completed a free-standing public relation display of earthquake information for the New Madrid seismic zone. The display is designed to educate and inform the general public about the nature of earthquake hazards and the progress that is being made in understanding earthquake processes. This display provides useful information to the general public and will improve the rapport between the USGS and an informed public.

A.J. Crone, in collaboration with E.S. Schweig (USGS, Memphis) and M. Giardino (Univ. of Torino, Italy), completed their analysis of four trenches that were excavated in search of evidence of large prehistoric earthquakes in the New Madrid seismic zone (NMSZ). We excavated three trenches across the Bootheel lineament at a site about 7.4 km (4.6 mi) west-southwest of Steele, Missouri ( $N^{1/2}$ , NW, SW, T. 17 N, R. 11 E, Pemiscot Co., Missouri; USGS Denton, MO  $7^{1/2}$ -minute topographic quadrangle). Here, the Bootheel lineament is narrow and easily recognized in the field. We also excavated a 49-m-long, east-west-trending trench across the Crittenden County fault zone in northeastern Arkansas (NW, NW, SE, Sec. 22, T. 8 N., R 7 E., Crittenden Co.,

Arkansas; USGS Heafer, Ark. 7 1/2-minute topographic quadrangle) where high-resolution seismic-reflection data indicate the presence of very shallow subsurface deformation.

### Related Investigations

Although not directly funded by NEHRP, Crone and M.N. Machette (Branch of Earthquake and Landslide Hazards), have continued their paleoseismic studies of suspected Quaternary faults in the stable interior of the U.S. As part of this effort, we have conducted studies of the Fowler and Cheraw faults in southeastern Colorado and the Harlan County fault in south-central Nebraska. These investigations are part of our on-going effort to examine the long-term behavior of faults in stable continental settings.

## RESULTS

### (Collins)

The revised lithologic log of the Dow Chemical B.L. Garrigan No. 1 drill hole divides the stratigraphic section into six primary units from oldest to youngest: 103 m (338 ft) of quartzite, 762 m (2,500 ft) of shaly siltstone to silty shale, 530 m (1,740 ft) of silty sandstone to siltstone, 950 m (3,120 ft) of shaly siltstone to silty shale, 183 m (600 ft) of limestone, and 293 m (960 ft) of siltstone. Results of this study show that the rocks in the Garrigan drill hole are predominantly siliciclastic rocks as reported by Howe, (1984) and suggested by Swolfs (1992), and are not dominantly carbonate rocks as indicated by McKeown and others (1990). Stratigraphic and biostratigraphic correlations by Collins and others (1992) and Taylor and others (1992) demonstrate that rocks in the Garrigan drill hole are not correlative with strata in the lower part of the Dow Chemical No. 1 Wilson drill hole as suggested by Howe (1984); rather rocks in the Garrigan drill hole are a deeper-water siliciclastic facies whereas the rocks in the Wilson drill hole are relatively shallow-water carbonate rocks. Other significant nearby drill holes in the northern Mississippi embayment that contain similar siliciclastic rocks include the Strake Petroleum No. 1 T.P. Russell and the O.W. Killam No. 1 Pattinson drill holes. This revised log is being assembled for publication in a U.S. Geological Survey Chart Series.

Preliminary searches of old literature, navigation charts, and archived reports have yielded the following observations, which are commonly not cited or are frequently overlooked in post-1912 publications:

1. Descriptions of deformation of Islands 10, 12, 25, and 32 in the Mississippi River, which span the reach of the river between about 19 km (12 mi) upstream of New Madrid to about 152 km (95 mi) downstream.
2. The pre-earthquake locations of the towns of New Madrid and Little Prairie are in the present channel of the Mississippi River.
3. It is possible that the present location of Caruthersville is not the same as the old town of Little Prairie, which was located on the opposite side of the river "loop" and to the north of Caruthersville..
4. Several sets of northeast-trending fissures, at least 1.5 m (5 ft) deep and spaced about 0.6 km (1/2 mi) apart existed in the Little Prairie area. At present, it is not known if these fractures formed during the earthquakes.
5. Reports of earthquake lights may have been the result of ignition of methane gas, which was derived from swampy areas near New Madrid.

In addition, this preliminary study has found that Land Survey Reports may contain exact locations and descriptions of surface fractures created by the earthquakes of 1811-1812. This source of information has not yet been accessed.

A free-standing display unit has been purchased. It stands 2.4 m (8 ft) high and consists of two 1.2 m x 1.2 m (4 ft x 4 ft) display panels. Both sides of each panel can be used to display

information. These panels are protected by clear plexiglass and are mounted in free-standing aluminum frame. The themes of the four panels in the are:

- Effects of the 1811-1812 earthquakes
- What scientists are doing in the New Madrid region
- What scientists know about the 1811-1812 earthquakes
- Earthquake preparedness information

The final product will be displayed in museums, county offices, city halls, and high traffic public areas such as shopping malls throughout the New Madrid region.

(Crone)

#### *Bootheel Lineament Trenches*

At the trench site, the Bootheel lineament has a general trend of N. 24° E. (024°) and is marked by an area of light-colored, relatively well-drained soil to the west and an area of dark-colored, poorly drained soil to the east. Topographically, the western side of the lineament is about 30 cm higher than the eastern side. We excavated three subparallel, east-west-trending trenches that were spaced approximately 15 m apart. The deposits in the Bootheel lineament trenches consisted of a fining-upward sequence fluvial sediments that are overlain by a sequence of sand-blow deposits. We interpret this fining-upward sequence as deposits from a low-energy meandering stream system in which the basal coarse-grained deposits are buried by progressively finer overbank and slack-water sediment that fill the abandoned channel and were deposited on the floodplain adjacent to the main channel. The fluvial deposits are overlain by well-sorted, coarse- to fine-grained sands that are sand-blow deposits. The basal contact of the sand-blow deposits is sharp and planar, although locally the erupting sand eroded the pre-earthquake ground surface.

The fluvial deposits, which are buried by the sand-blow deposits, are late Holocene in age. Geologic and archaeological evidence, which was described in the preceding (FY 1993) annual report, suggest that the fluvial sediments were probably no more than a few thousand years old. One trench exposed an ancient hearth in the fluvial deposits that contained charcoal. Charcoal fragments from the hearth have a calibrated radiocarbon age of 1,313-1,419 yr B.P. (Geochron sample GX-19872-AMS). Based on the age of these underlying fluvial sediments and the lack of significant weathering and oxidation in the sand-blow sand, the sand blows that define the Bootheel lineament at this site most likely formed during the 1811-12 earthquakes.

We found no evidence of faulting or brittle deformation that we attribute to tectonic causes in any of these trenches. The top of the fluvial deposits was vertically offset across three of the largest dikes, and, in all cases, the downthrown side of the dike is on the east. We found no evidence that these vertical offsets were related to near-surface faulting, and we found no evidence that lateral slip had occurred along these features. Instead, we attribute these vertical offsets to subsidence that resulted from the large volume of sand that was extruded from below onto the surface.

The lack of conclusive evidence of near-surface tectonic deformation associated with the Bootheel lineament at this site makes it difficult to directly associate the Bootheel lineament with underlying seismogenic faults, including those that could have slipped during the 1811-12 earthquakes. The geologic evidence from these trenches suggest that, during the past approximately 1,300 years, liquefaction has occurred at this site only during the 1811-12 earthquakes. The extensive liquefaction that did occur here in 1811-12 suggests that site conditions were very favorable for liquefaction. Given the apparent favorable conditions but lack of evidence of prehistoric liquefaction, we conclude that the site was not been subjected to sustained shaking as strong as that which occurred in 1811-12 for at least 1,300 years.

#### *Crittenden County Trench*

We also excavated a trench across the Crittenden County fault zone (CCFZ) where previous geophysical studies had shown evidence of deformation in very shallow sediments. Seismic-reflection data show that the deformation associated with the CCFZ can be traced from the middle crust to within 6-7 m of the surface (Crone, 1992; Luzietti and others, 1992; Williams and others,

1993). Thus, exploratory trenches, which can extend about 3 m below the surface, offered an opportunity to document very shallow deformation associated with a crustal-scale fault zone.

Our trench was located in the area between two drill holes that provided the original evidence of the presence of the fault. The surficial deposits at the site are composed almost exclusively of Holocene Mississippi River alluvium, and the trench exposed a sequence of fluvial silts that contain varying amounts of sand and clay. We found no evidence of faulting in the trench. The most significant structural feature was an unconformity that separated the two depositional sequences of fluvial deposits. The unconformity progressively rose toward the western end of the trench, and stratigraphic units in the upper sequence pinched-out against the unconformity or thinned greatly to the west as the unconformity became shallower. This unconformity is evidence of a buried feature that had about 1.2 m of topographic relief at the time that the upper sequence of sediments were deposited.

Data from the trench do not yield conclusive evidence about the origin of this buried topographic feature. Much of the present landscape in Crittenden County is the product of fluvial processes, and river channels with several meters of relief are common. Thus, in the absence of evidence of faulting or other tectonic causes, it is reasonable to attribute the relief to fluvial processes. However, the coincidence of the buried feature with the shallow subsurface deformation imaged in the high-resolution reflection data suggests that the buried topography could be related to tectonism (Williams and others, 1993). Because Holocene sediments are involved in the deformation, determining the origin of the buried feature is important for earthquake hazard assessments.

The full documentation of the Bootheel lineament trenches and the Crittenden County trench is being published as a U.S. Geological Survey Miscellaneous Field Studies map.

#### Related Investigations

The long-term behavior of seismogenic faults in stable continental regions is poorly known despite the threat that these faults pose to populated regions. The objective of Crone and Machette's studies is to provide paleoseismic data on three suspected, but unstudied Quaternary faults in the stable interior of the United States in Colorado and Nebraska. In collaboration with geoscientists at the University of Kansas and the Kansas Geological Survey, we mapped the only known exposure of the Harlan County fault in south-central Nebraska and collected samples for grain-size analysis and radiocarbon age determinations. In southeastern Colorado, we examined the Fowler and Cheraw faults. Our study of the Fowler fault indicates that it is a terrace riser associated with an ancient course of the Arkansas River rather than a fault scarp as previously reported. However, our studies show that the Cheraw fault is a *bona fide* fault that has had repeated Quaternary movement. We have conducted a general reconnaissance of the surface trace of the Cheraw fault, measured several topographic profiles to characterize the amount of surface offset, and drilled a series of shallow auger holes to investigate the subsurface materials on both sides of the fault at two important sites. At one of these sites, we will excavate an exploratory trench with the hope of better characterizing the fault's long-term behavior including its recurrence interval, slip rate, and the time of most recent movement. This study will contribute to a better understanding the occurrence of rare but large-magnitude earthquakes in the stable continental regions.

## REFERENCES CITED

- Collins, D.S., Taylor, M.E., Repetski, J.E., and Palmer, A.R., 1992, New sedimentologic and paleontologic data for the Dow Chemical #1 B.L. Garrigan drill hole, Mississippi County, Arkansas: U.S. Geological Survey Open-File Report 92-6, 38 p.
- Crone, A.J., 1992, Structural relations and earthquake hazards of the Crittenden County fault zone, northeastern Arkansas: Seismological Research Letters, v. 63, no. 3, p. 249-262.
- Dart, R.L., 1992, Catalog of pre-Cretaceous geologic drill-hole data from the upper Mississippi embayment--A revision and update of Open-File Report 90-260: U.S. Geological Survey Open-File Report 92-685, 253 p.
- Howe, J.R., 1984, Tectonics, sedimentation, and hydrocarbon potential of the Reelfoot aulacogen: University of Oklahoma, Master of Science Thesis, Oklahoma City, Oklahoma, 75 p.
- Luzietti, G.A., Kanter, L.R., Schweig, E.S., Shedlock, K.M., and VanArsdale, R.B., 1992, Shallow deformation along the Crittenden County fault zone near the southeastern boundary of the Reelfoot rift, northeast Arkansas: Seismological Research Letters, v. 63, no. 3, p. 263-275.
- McKeown, F.A., Hamilton, R.M., Diehl, S.F., and Glick, E.E., 1990, Diapiric origin of the Blytheville and Pascola arches in the Reelfoot rift, east central United States—Relation to New Madrid seismicity: Geology, v. 18, p. 1158-1162.
- Swolfs, H.S., 1992, Structural characteristics in the Dow Chemical B.L. Garrigan #1, Mississippi County, Arkansas, in Louis Unfer Jr. Conference of the Geology of the mid-Mississippi Valley—Extended abstracts: Southeast Missouri State University, Cape Girardeau, Missouri: Missouri Department of Natural Resources, Division of Geology and Land Survey Special Publication No. 8, 81 p.
- Taylor, M.E., Collins, D.S., Palmer, A.R., and Repetski, J.E., 1992, Upper Cambrian biostratigraphic correlations in the Reelfoot basin, northeastern Arkansas, in Louis Unfer, Jr. Conference on Geology of the mid-Mississippi Valley—Extended abstracts, Southeast Missouri State University, Cape Girardeau, Missouri: Missouri Department of Natural Resources, Division of Geology and Land Survey Special Publication No. 8, 81 p.
- Williams, R.A., Luzietti, E.A., and Carver, D.L., 1993, Quaternary faulting on the Crittenden County fault zone, New Madrid seismic zone, northeast Arkansas: EOS (Transactions, American Geophysical Union), The 1993 Fall Meeting abstract supplement, October, 26, 1993, p. 437-438.

## REPORTS

- Crone, A.J., Giardino, Marco, and Schweig, E.S., III, Paleoseismic studies of the Bootheel lineament, southeastern Missouri, and the Crittenden County fault zone, northeastern Arkansas, New Madrid seismic zone, central United States: U.S. Geological Survey Miscellaneous Field Studies Map (MF series).
- Giardino, Marco, Collins, D.S., Michael, J.A., and Crone, A.J., 1994, Earthquake awareness in the New Madrid seismic zone--A public information display by the U.S. Geological Survey [abs.]: Journees Internationales sur L'education Scientifique, presented at Centre Jean Franco, Chamonix, France, 4-8 April 1994.
- Odum, J.K., Stephenson, W.J., Shedlock, K.M., Pratt, T.L., Collins, D.S., Rhea, S.B., Williams, R.A., 1994, Possible fault(s) associated with the February 7, 1812 earthquake-induced Mississippi River waterfalls near New Madrid, Missouri: Geological Society of America Abstracts with Programs, v. 26, no. 7, p. A-471.

**Earthquake Hazard Research  
in the Pacific Northwest using Pacific Northwest Seismograph Network data**

14-08-0001-G1803

R.S. Crosson  
Geophysics Program  
University of Washington  
Seattle, WA 98195  
(206) 543-8020  
e-mail: bob@geophys.washington.edu

October 1, 1993 - September 30, 1994

**Investigations**

This research focuses on regional earthquake hazards in the Pacific Northwest, including effects of large scale plate interactions, through the study of regional structure, earthquake sources, and tectonics. Investigations include a cross-Cascade "refraction" profile using reflected and refracted rays from earthquake sources, investigations of P-wave reverberations from teleseismic observations, investigation of the Scotts Mills earthquake sequence in northwestern Oregon, and initiation of a project to reexamine earthquake location and 3-D structure effects in the Puget Sound region of western Washington in light of recently postulated tectonic models.

**Results**

*East-west cross-Cascades structural profile*

This project was completed in the previous contract period, and reported in a paper delivered at the Fall 1993 AGU meeting (Schultz and Crosson, 1993) and a thesis entitled: "A 2-D Velocity Structure for a Cross-Cascades Profile using Earthquake Sources with Application of Reflectivity Synthetic Modeling" by Andreas Schultz. The research used direct P, PmP, and Pn arrivals recorded on the PNSN regional network to infer the structure across the central Cascade Range of Washington. The final model indicates a depressed Moho beneath the central Cascades, with a relief of about 12 km from west to east. An article is currently in preparation for journal publication. This study indicates the feasibility of using earthquakes as sources for conventional refraction interpretation, and should complement the current emphasis on active source seismic experiments in the Pacific Northwest.

*Crust and Upper Mantle Structure*

In this continuing study, we have been using seismic signals (mainly direct P) from distant earthquakes to search for structure markers produced by P and S wave reverberations in the lithosphere. Using more conventional deconvolution methods, we have found that "receiver functions" can be constructed from vertical component, short-period data alone, but that these receiver functions vary significantly from station to station indicating rapid lateral variation of structure that produces strong scattering and rapid lateral loss of signal coherence. We are presently completing the characterization of the spatial variation of receiver functions and their implications for structure variations. Preliminary results of these investigation was presented at the 1993 Fall AGU meeting (Dewberry and Crosson, 1993).

In a related recent development, we are working on a new deconvolution method which may enhance our ability to detect and interpret crustal reverberations. The method uses joint deconvolution for many sources and many receivers in the Cepstral transform domain. It has the potential to greatly increase the quality of the deconvolution process and thus provide higher quality receiver functions for structure interpretation. The method is still under investigation and active development.

*Scotts Mills Earthquake of 25 March, 1993*

The Scotts Mills earthquake (M 5.6) was the largest earthquake in the crust of western Oregon's Willamette Valley region in recent time. With excellent aftershock data from portable instrument deployment, it offers a unique opportunity to investigate the structure and tectonics of this region. The mainshock and aftershock sequence are consistent with a mid-crustal fault plane that strikes west-northwest, and dips about 60 degrees to the northeast. The mainshock appears to have involved oblique reverse or thrust motion in response to north-south tectonic stress. This stress is consistent with other evidence from earthquake and well data. A paper given at the 1993 Fall AGU meeting (Thomas, et al., 1993) presented the preliminary results

of our aftershock analysis. An article containing these results is currently being prepared for journal publication.

#### *Additional Activities*

We have submitted an article on a new method of moment/magnitude estimation using short period regional network coda amplitude data. Another article by Ma et al. on focal mechanism and stress analysis in western Washington is in the final stages of publication in a USGS Professional Paper.

Recently, USGS investigators (Pratt and others, 1994) have proposed a very specific tectonic model for the Puget Sound region primarily based on industry seismic reflection data. These models elucidate the thrust nature of the "Seattle Fault" and include a decollement at approximately 15 km depth. Most central Puget Sound earthquakes appear to lie deeper than the proposed decollement and questions have been raised about the depth uncertainties of the mid-crustal Puget Sound earthquakes in light of these models. For example, could lack of depth control cause an apparent vertical smearing of hypocenters that are actually on the decollement surface? To address such questions, we are beginning a project to use a true 3-D structure for studying the location uncertainties of western Washington earthquakes.

#### **References**

Pratt, T.L., S.Y. Johnson, C.J. Potter, and W.J. Stephenson, 1994 (abstract), The Puget Lowland Thrust Sheet, EOS, V. 75, No. 44, p. 621.

#### **Publications**

##### **Articles**

Chiao, L.-Y., and K. C. Creager (in preparation) Geometry and lateral membrane rate of the subducting Cascadia slab, to be submitted to JGR

Dewberry, S.R. and R.S. Crosson, (submitted), Source scaling and moment estimation for the Washington Regional Seismograph Network using coda amplitudes, submitted to BSSA.

Ma, L., R.S. Crosson, and R.S. Ludwin, (in press), Focal Mechanisms of western Washington earthquakes and their relationship to regional tectonic stress, \$roman {in} under\\$: USGS Professional Paper "Assessing and Reducing Earthquake Hazards in the Pacific Northwest")

VanDecar, J.C., M.G. Bostock, R.S. Crosson, K.C. Creager, (in preparation), How does subduction cease?: Reconciling the dynamic and kinematic observations of Cascadia tectonic evolution, (to be submitted to Science).

VanDecar, J.C., R.S. Crosson, and K.C. Creager, (in preparation), Nonlinear traveltimes inversion for subduction zone structure: The upper-mantle beneath Cascadia, (to be submitted to J. Geophys. Res.).

##### **Abstracts**

Dewberry, S.R., and R.S. Crosson, 1994, Comparison of stacking and cepstral deconvolution in estimation of receiver functions from short-period regional network teleseismic data, EOS, V. 75, No. 44, p. 485.

Dewberry, S.R., and R.S. Crosson, 1993, Crustal and upper mantle structure beneath Washington state from array analysis of short-period network data, EOS, V. 74, N. 43, p. 201.

Crosson, R.S., and Dewberry, S.R., 1994, Receiver function estimation from short-period regional network teleseismic data using cepstral deconvolution, EOS, V. 75, No. 44, p. 485.

Schultz, A.P. and R.S. Crosson, 1993, A 2-dimensional P-wave velocity profile across the Cascade Range of Washington State using earthquake sources and regional network observations, EOS, V. 74, N. 43, p. 202.

Thomas, G.C., R.S. Crosson, S. Dewberry, J. Pullen, T. Yelin, R. Norris, W.T. Bice, D. Carver, M. Meremonte, D. Overturf, D. Worley, E. Sembera, and T. MacDonald, 1993, The 25 March, 1993 Scotts Mills, Oregon earthquake: aftershock analysis from combined permanent and temporary digital stations, EOS, V. 74, N. 43, p. 201.

VanDecar, J.C., Bostock, M.G., R.S. Crosson, and K.C. Creager, 1993, How does a subduction zone die?: Reconciling the dynamic and kinematic observations of Cascadia tectonic evolution, EOS, V. 74, N. 43, p. 92.

# Source Characteristics of Events in the San Francisco Bay Region

Contract No. 1434-93-G2311

DOUGLAS DREGER AND BARBARA ROMANOWICZ

*Seismographic Station*

*University of California*

*Berkeley, CA 94720*

*(510) 643-5690*

## INVESTIGATIONS

- 1) The continued analysis of moderate to large earthquakes in the San Francisco bay area, and northern and central California to estimate one-dimensional velocity models suitable for use in routine moment tensor studies.
- 2) Compile a catalog of theoretical Green's functions to facilitate source analyses.
- 3) Utilize the Green's function catalog to analyze historic earthquakes recorded on varied instrumentation operated by UC Berkeley since the turn of the century.
- 4) Begin to develop near-realtime methodologies and automation of the moment tensor procedure.

## RESULTS

### *Northern California Seismicity*

Central and northern California has been quite active during the past year. Of particular interest are 16 events with  $M_w > 3.8$  which illustrate the complexity of the active fault structures in the northern two thirds of the state (Figure 1). Of the seven events in the Central Coast Ranges (CCR) and San Francisco bay area four are right lateral mechanisms consistent with their locations on the San Andreas and Hayward-Calaveras fault systems. Three earthquakes had predominantly thrust mechanisms consistent with the fault normal compressive stress observations of Zoback et al. (1987).

The most seismically active region in California is the Mendocino Triple Junction (MTJ) and offshore Gorda plate. Figure 1 shows the range of earthquake mechanisms recorded. Events 5 and 9 occurred within the Gorda plate and exhibit a north-south compressive stress caused by the buttressing of the Gorda plate by the Pacific and the Juan de Fuca plates. Event 16 occurred at relative large depth and was located within the subducting Gorda plate. The normal-slip mechanism suggests that the descended Gorda plate east of the MTJ is no longer subject to the north-south compression observed for events located offshore and is consistent with the observations of McPherson (1987). The largest earthquake during the project period was a  $M_w 6.9$  event (number 12) that occurred on the

Mendocino fault. The reorientation of the principal stress axis locally along the Mendocino fault is suggestive that this fault is weak (e.g. Zoback et al., 1987).

Southern Oregon experienced two Mw5.9-6.0 mainshocks on September 23, 1993 (events 1 & 2, Figure 1). These earthquakes caused extensive damage in the epicentral area and were widely felt to a range of approximately 150 km. We studied this sequence in detail and source mechanisms were obtained for 20 of the largest events which show a east-northeast striking tension axis consistent with deformation occurring in the northwestern Basin and Range province. The mechanisms of the aftershocks indicate a pronounced change in the strike of the causative fault structure. The change in strike is also manifest in the mapped surface faulting. Our analysis of mainshock source kinematics revealed that the pronounced bend in the fault may have acted as a barrier to a through-going Mw 6.2 event. The results of this study will appear shortly as an article in *Geophysical Research Letters*.

The eastern margin of the state became active with a Mw 5.9 event located SE of the Tahoe valley. This sequence is located within a transitional region subject to both strike-slip and normal-slip earthquakes (Zoback and Zoback, 1980). The analysis of approximately 20 aftershocks reveal that the stress field is dominantly east-west striking tension. The mainshock ruptured a vertically dipping strike-slip plane and the largest aftershock ruptured a north-south striking normal-slip fault. It appears that the strike-slip events are occurring at greater depth than the normal events, but more work is needed to fully realize the relationship. Our current efforts are focussed at trying to resolve which of the two possible mainshock nodal planes was the causative structure since there is no clear correlation with surface mapped faults in the region. Of particular interest is to better understand the spatial relationship of the near vertically dipping strike-slip mainshock and the normal-slip structures which were subsequently activated.

### *Moment Tensor Methodology*

The mechanisms in Figure 1 were determined by the time domain inversion of three-component, complete, long-period waveforms. The frequency band in which the inversion is performed is between 0.01 Hz and 0.05-0.1 Hz. The upper corner depends upon the earthquake size and the distance to the recording stations. In this frequency band relatively simple velocity models are found to adequately model wave propagation. To facilitate the moment tensor studies we have regionalized California into two principal domains, namely, the CCR and the Sierra Nevada (Figure 1). We have compiled a catalog of Green's functions for each of the domains which is maintained online.

Figure 2a illustrates the level of fit that is commonly obtained at low frequencies. Paths which cross the San Joaquin valley remain problematic as two- and three-dimensional velocity structures will be needed to model the data. Figure 3a illustrates the need for further refinement of the velocity structures for cross-domain paths by comparing tangential component displacement data with synthetics computed with the Coast Range model (GIL7) and the Sierra Nevada model (SoCal). The body waves are clearly better modeled by the thicker crust of the SoCal model, where as, the dispersed Love wave is predicted by the substantial near surface velocity gradient of model GIL7. At long-periods ( $f < 0.05$  Hz) the differences in the synthetics for the two models are not large. To extend the

capability of our analysis to small events, apply the method to historic data sets, and to improve source depth resolution shorter period waves need to be used, necessitating the refinement of the Green's function catalog.

Table 1 lists the events in Figure 1 and compares the complete waveform results with those from regional surface waves, first-motions, and Harvard Centroid Moment Tensor (CMT) solutions for the largest earthquakes. First-motion solutions were not available for events located outside the dense short-period Northern California Seismic Network.

Generally, we find good agreement between each of the methods, however some events show relatively large discrepancies. Figure 2b compares the focal mechanisms obtained from the different methodologies for event 13 (Figure 1). In this example the strike and dip of the north dipping plane are relatively well constrained, however the rake angle appears to tradeoff with the strike and dip of the conjugate plane. The formal uncertainties estimated for the complete waveform method are  $2^\circ$ ,  $6^\circ$  and  $1^\circ$  for the strike, rake and dip parameters of the north dipping plane. Thus the rake does have the largest uncertainty but it is significantly smaller than the range defined by the different methodologies. This illustrates the need for the application of multiple methodologies to properly evaluate the full range of possible mechanisms, and to evaluate the true uncertainties due to velocity model and inverse method assumptions.

There are also notable differences in the solutions for the Mw 4.2 earthquake north of Berkeley (event 10). In this case there is a  $21^\circ - 52^\circ$  range in the rake angle. The two moment tensor solutions compare reasonably well (within  $4^\circ$ ,  $15^\circ$  and  $21^\circ$  for the strike, dip and rake parameters) however the first-motion mechanism has a significantly different rake. It is noted that first-motion mechanisms in this region are affected by multipathing due to lateral velocity gradients across the Hayward fault (David Oppenheimer, personal communication, 1994).

### *Historic Seismogram Analysis*

During this project period we began searching the historic catalog for events suitably recorded to apply the methodology discussed above. An event that we studied occurred on March 9, 1949 near Gilroy, California. This event was recorded at Berkeley on a smoked paper recorded Bosch-Omori instrument. In collaboration with David Oppenheimer the data was digitized using our newly acquired scanner system.

As was discussed in the previous reporting period the path from Gilroy to BKS was the focus of an extensive modeling effort to determine a suitable one-dimensional velocity model for the San Francisco bay area. Figure 4a demonstrates the fit to a 1993 calibration event which occurred near Gilroy, California. This model fits the waveform data to a frequency of 1 to 2 Hz. Figure 2a attests to the performance of this model at long-periods. The similarity of the 1949 and 1993 events (Figure 4b) indicates these earthquakes occurred in close proximity to one another. We inverted the two horizontal components of the 1949 earthquake using the calibrated Green's functions (Figure 4c). The fit to the tangential data is quite good. The mechanisms of both the 1949 and 1993 events (Figure 4d) indicate that the radial component should be nodal however there is a late arriving Rayleigh wave evident in the data. This phase was also observed in the 1993 data, and filtering revealed that at long-periods the radial component was nodal. Thus it appears

that the short-period Rayleigh wave is a multipath through the Santa Clara valley and San Francisco bay sediments. Because of the bandwidth of the Bosch-Omori instrumentation it was necessary to include 5 s data in the inversion. The general application of the Green's function catalog and moment tensor analysis to the historic waveform data set will require refinement of the models to fit shorter period waves.

#### *Near-realtime Analysis*

We have developed an algorithm to automate the moment tensor procedure using the initial source location determined by REDI (Rapid Earthquake Data Integration). It is now possible to obtain a preliminary Mw and fault plane solution within 8 minutes of receiving notification of the earthquake. The automated codes are now operational and further refinement of the algorithm is underway to reduce processing time and to improve the quality of the automated solutions.

#### REFERENCES

- McPherson, R. C., Seismicity and Focal Mechanisms Near Cape Mendocino, Northern California, *masters thesis, Humboldt State University*, pp 75, 1987.
- Zoback, M. L. and M. D. Zoback, State of Stress in the Conterminous United States, *Journ. Geophys. Res.*, 85, 6113-6156, 1980.
- Zoback, M. D., M. L. Zoback, V.S. Mount, J. Suppe, J. P. Eaton, J. H. Healy, D. Oppenheimer, P. Reasenberg, L. Jones, C. B. Raleigh, I. G. Wong, O. Scotti, and C. Wentworth, New Evidence on the State of Stress of the San Andreas Fault System, *Science*, 238, 1105-1111, 1987.

#### REPORTS

- Dreger, D. S., Ritsema, J., and M. Pasyanos, Broadband Analysis of the 21 September, 1993 Klamath Falls, Oregon, Earthquake Sequence, *In press Geophys. Res. Lett.*, 1994.
- Romanowicz, B., D. Dreger, M. Pasyanos, and R. Uhrhammer, Monitoring of Strain Release in Central and Northern California Using Broadband Data, *Geophys. Res. Lett.*, 20, 1643-1646, 1993.
- Dreger, D. S., Velocity Model Regionalization and Moment Tensor Inversion in Central and Northern California, *EOS*, 74, pp 430, 1993.
- Uhrhammer, R., D. Dreger, M. Pasyanos, and B. Romanowicz, Rapid Moment Tensor Estimation using Regional Data, *submitted to Fall Agu meeting*, 1994.
- Dreger, D. S., Velocity Model Regionalization and Moment Tensor Determination in Central and Northern California, *In preparation*, 1993.

### FIGURE CAPTIONS

Figure 1. Map showing the locations of the 11 operational broadband stations of the Berkeley Digital Seismic Network (triangles) and focal mechanisms of 16 significant earthquakes. determined by inverting complete, three-component, long-period ( $f < 0.05-0.1$  Hz) waveforms recorded at one or more of the stations. The dashed lines show the demarcation of the velocity model domains used in the analysis.

Figure 2. a) Comparison of complete, three-component, long-period ( $0.02 < f < 0.1$  Hz) displacement data and synthetic seismograms for event 13 (Figure 1). b) Comparison of reported focal mechanisms for this event (see Table 1).

Figure 3. a) Comparison of tangential component data for a  $M_w 4.8$  event near San Jose, California recorded at CMB (distance of 140 km) and synthetics computed for the Coast Range model (GIL7) and the Sierra Nevada model (SoCal). b) The one dimensional velocity models for the two domains.

Figure 4. a) Compares the tangential displacement record for the 930116 Gilroy earthquake (solid) with a synthetic (dashed) computed with the GIL7 model. b) Compares a synthetic Bosch-Omori seismogram for the 930116 event (dashed) with a digitized representation of an actual Bosch-Omori seismogram (solid) of an event which occurred on March 9, 1949. c) Compares lowpass filtered ( $f < 0.2$  Hz) Bosch-Omori data (solid) and synthetics (dashed) for the 1949 event. d) Shows the relative locations and focal mechanisms of the two events.

TABLE 1. Comparison of Fault Plane Solutions

Index	Date	Lat. (N)	Lon. (W)	Mag.	$M_o$	Z(km)	Strike/Dip/Rake	Method
1	9309210329	42.316	122.027	5.9	$7.6 \times 10^{24}$	8	332/55/-94	(1)
				5.9	$8.4 \times 10^{24}$	12	353/37/-59	(2)
				6.0	$1.1 \times 10^{25}$	15	334/60/-98	(4)
2	9309210545	42.358	122.058	5.9	$7.9 \times 10^{24}$	8	346/46/-89	(1)
				6.0	$1.4 \times 10^{25}$	12	9/37/-46	(2)
				6.0	$1.0 \times 10^{25}$	15	357/34/-85	(4)
3	9311141225	35.950	120.500	4.8	$2.0 \times 10^{23}$	14	142/83/-179	(1)
				4.8	$1.9 \times 10^{23}$	8	142/88/-174	(2)
				4.6		12	149/81/-165	(3)
4	9401111053	36.988	121.722	4.1	$1.4 \times 10^{22}$	11	270/93/-125	(1)
				4.1	$2.0 \times 10^{22}$	8	269/79/-65	(2)
				4.2		15	270/90/-120	(3)
5	9401201542	40.508	124.824	4.8	$4.5 \times 10^{22}$	11	296/86/176	(1)
6	9402211340	40.424	125.605	4.4	$5.2 \times 10^{22}$	11	97/81/-172	(1)
				4.5	$7.3 \times 10^{22}$	24	88/87/-159	(2)
7	9404211637	36.292	120.432	4.4	$4.9 \times 10^{22}$	5	159/61/122	(1)
				4.4	$4.6 \times 10^{22}$	8	168/30/132	(2)
				4.4		11	125/50/50	(3)
8	9405191645	36.533	121.267	4.0	$1.3 \times 10^{22}$	11	144/71/177	(1)
				4.1	$1.9 \times 10^{22}$	8	133/69/177	(2)
				3.9		8	317/81/160	(3)
9	9406191039	40.364	124.575	4.9	$2.9 \times 10^{23}$	18	126/65/171	(1)
				4.9	$2.7 \times 10^{23}$	18	120/86/-177	(2)
10	9406260842	37.900	122.317	4.2	$2.0 \times 10^{22}$	11	229/88/12	(1)
				4.2	$2.1 \times 10^{22}$	8	234/73/-9	(2)
				4.0		7	215/75/-40	(3)
11	9408280122	36.812	121.222	3.8	$5.6 \times 10^{21}$	5	60/87/2	(1)
				4.0	$9.7 \times 10^{21}$	10	227/66/8	(2)
				3.9		8	50/85/10	(3)
12	9409011515	40.375	125.999	6.9	$2.6 \times 10^{26}$	14	278/88/-164	(1)
				6.9	$2.9 \times 10^{26}$	8	271/77/169	(2)
				7.0	$3.4 \times 10^{26}$	15	273/66/-180	(4)
13	9409071909	37.538	121.271	4.0	$1.2 \times 10^{22}$	11	158/47/133	(1)
				4.0	$1.1 \times 10^{22}$	8	138/33/119	(2)
				4.1		3	170/50/150	(3)
14	9409121223	38.856	119.768	5.9	$7.2 \times 10^{24}$	14	129/84/-163	(1)
				6.1	$1.4 \times 10^{25}$	12	306/88/-167	(2)
				5.9	$1.0 \times 10^{25}$	15	137/57/-164	(4)
15	9409122357	38.765	119.725	5.1	$5.2 \times 10^{23}$	5	361/57/-91	(1)
				5.3	$8.8 \times 10^{23}$	6	356/59/-87	(2)
16	9409271125	40.647	124.074	3.9	$6.8 \times 10^{21}$	14	34/65/-72	(1)
				3.8	$6.1 \times 10^{21}$	24	30/68/-82	(2)

## Key to methods:

- (1) Complete, three-component, long-period ( $f < 0.1$ - $0.05$  Hz) waveform moment tensor inversion (Mag. is  $M_w$ ).
- (2) Regional surface wave inversion (Mag. is  $M_w$ ).
- (3) USGS first motion mechanism from UCB Data Center October 10, 1994 (Mag. is duration magnitude)
- (4) Harvard CMT solution (Mag. is  $M_w$ )

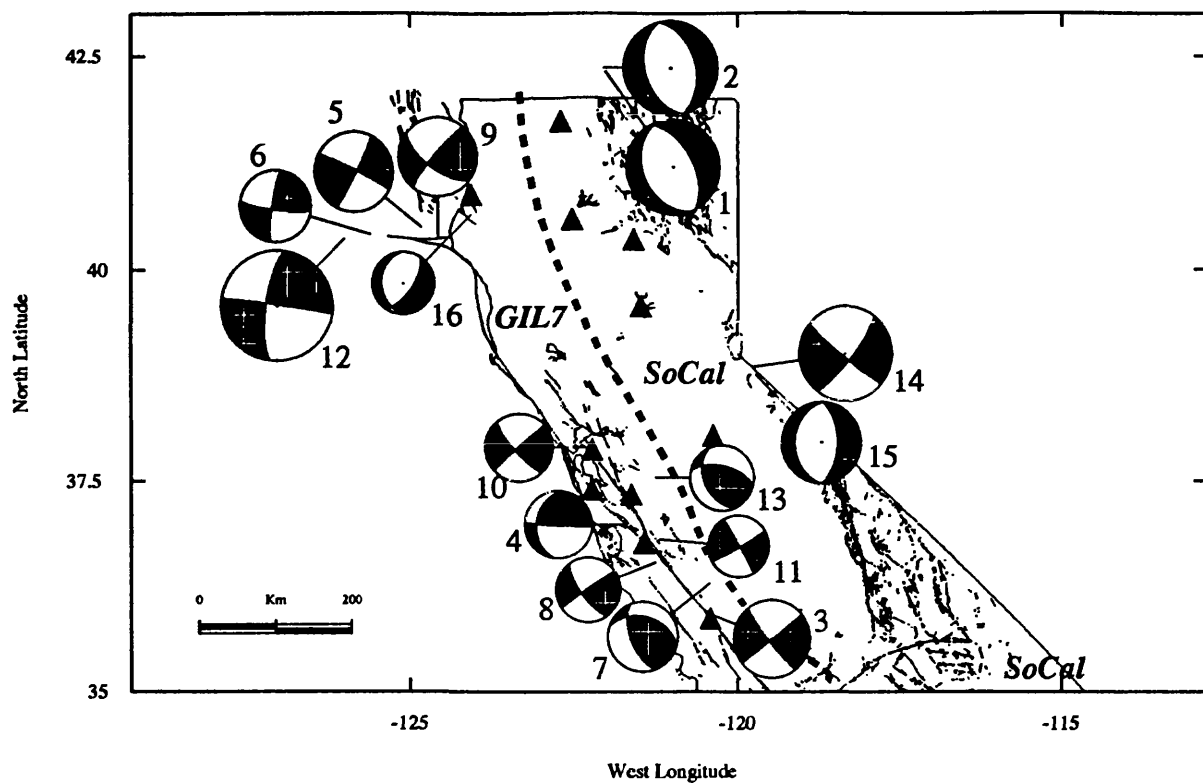


Figure 1. Map showing the locations of the 11 operational broadband stations of the Berkeley Digital Seismic Network (triangles) and focal mechanisms of 16 significant earthquakes determined by inverting complete, three-component, long-period ( $f < 0.05-0.1$  Hz) waveforms recorded at one or more of the stations. The dashed lines show the demarcation of the velocity model domains used in the analysis.

## Complete, Three-Component Waveform Inversion for Event 13

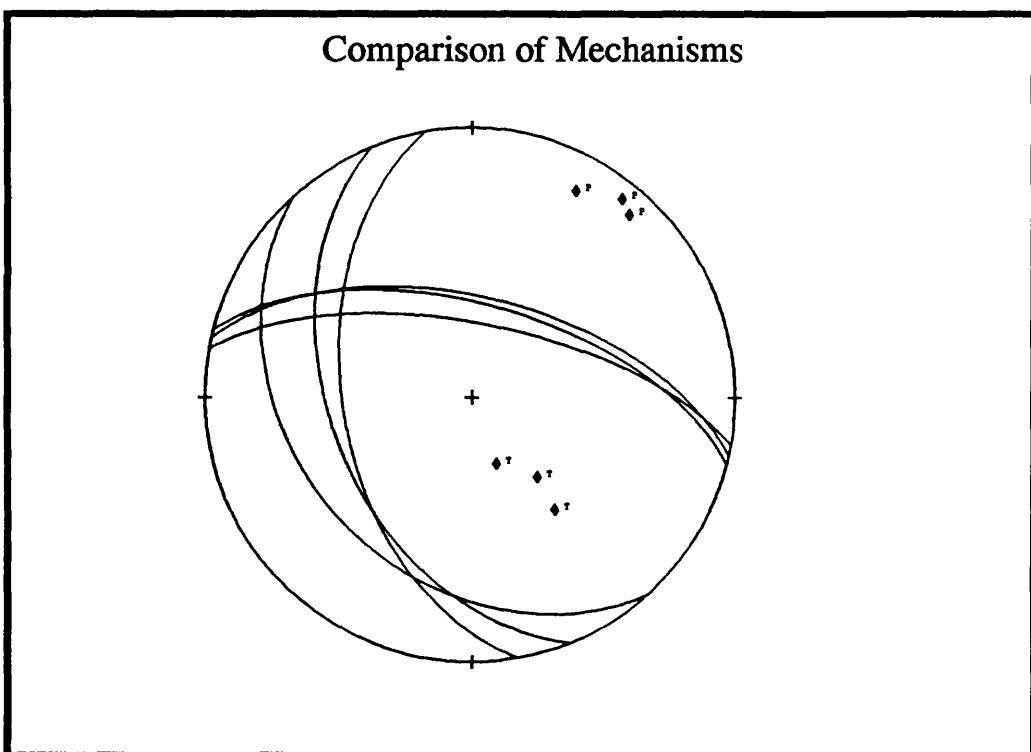
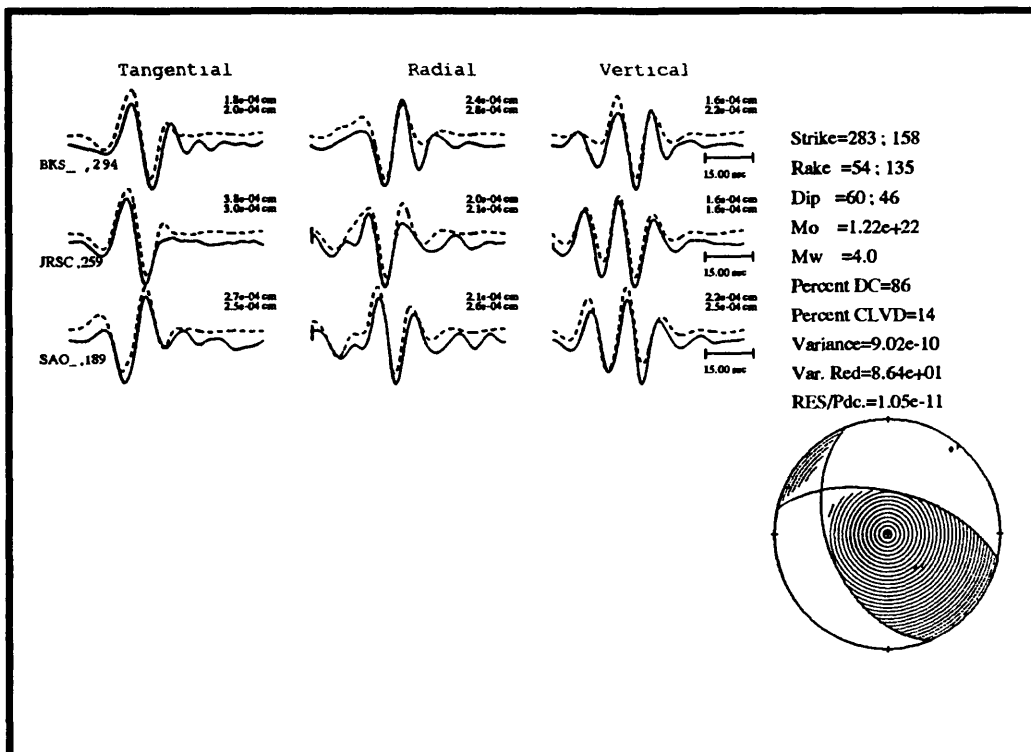


Figure 2. a) Comparison of complete, three-component, long-period ( $0.02 < f < 0.1$  Hz) displacement data and synthetic seismograms for event 13 (Figure 1). b) Comparison of reported focal mechanisms for this event (see Table 1).

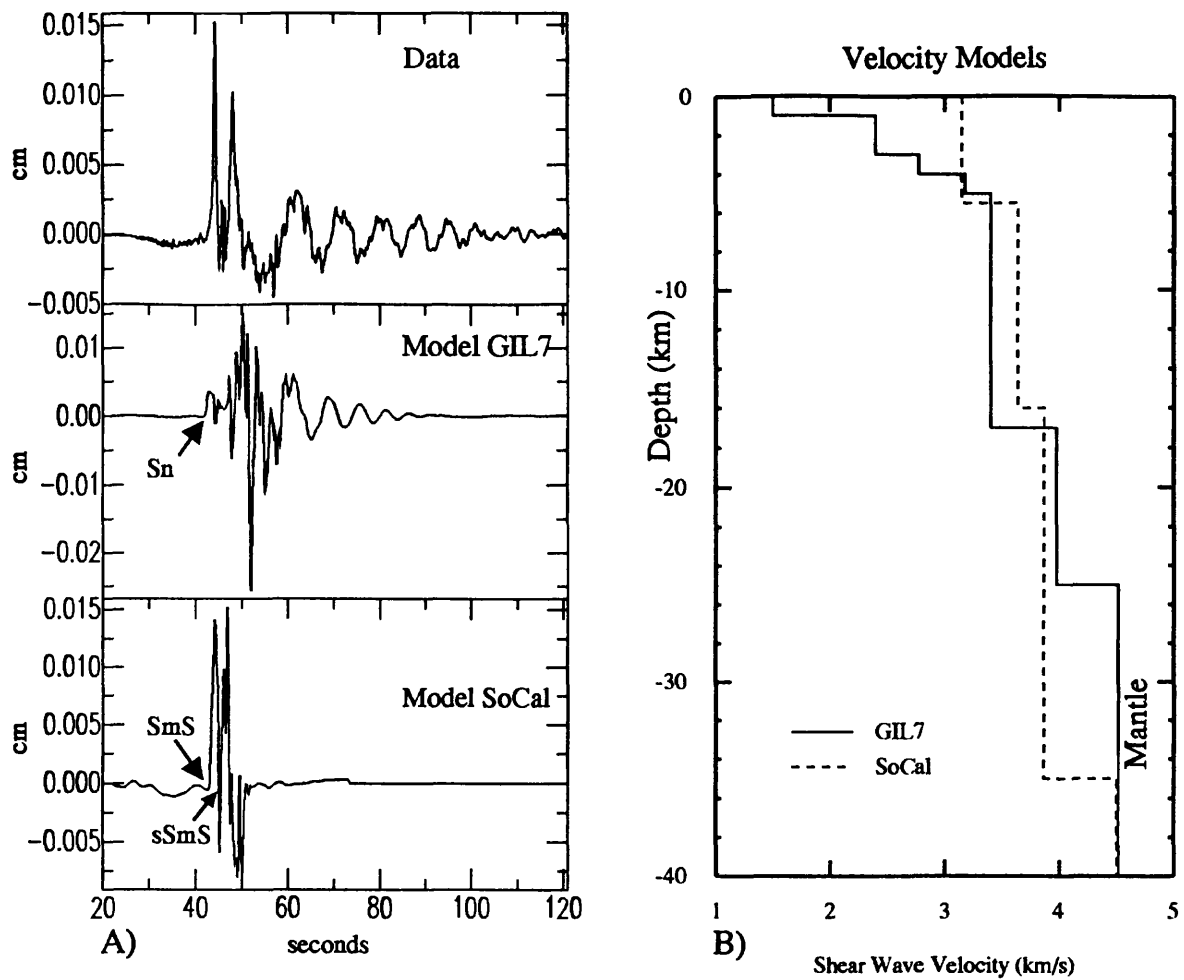


Figure 3. a) Comparison of tangential component data for a  $M_w 4.8$  event near San Jose, California recorded at CMB (distance of 140 km) and synthetics computed for the Coast Range model (GIL7) and the Sierra Nevada model (SoCal). b) The one dimensional velocity models for the two domains.

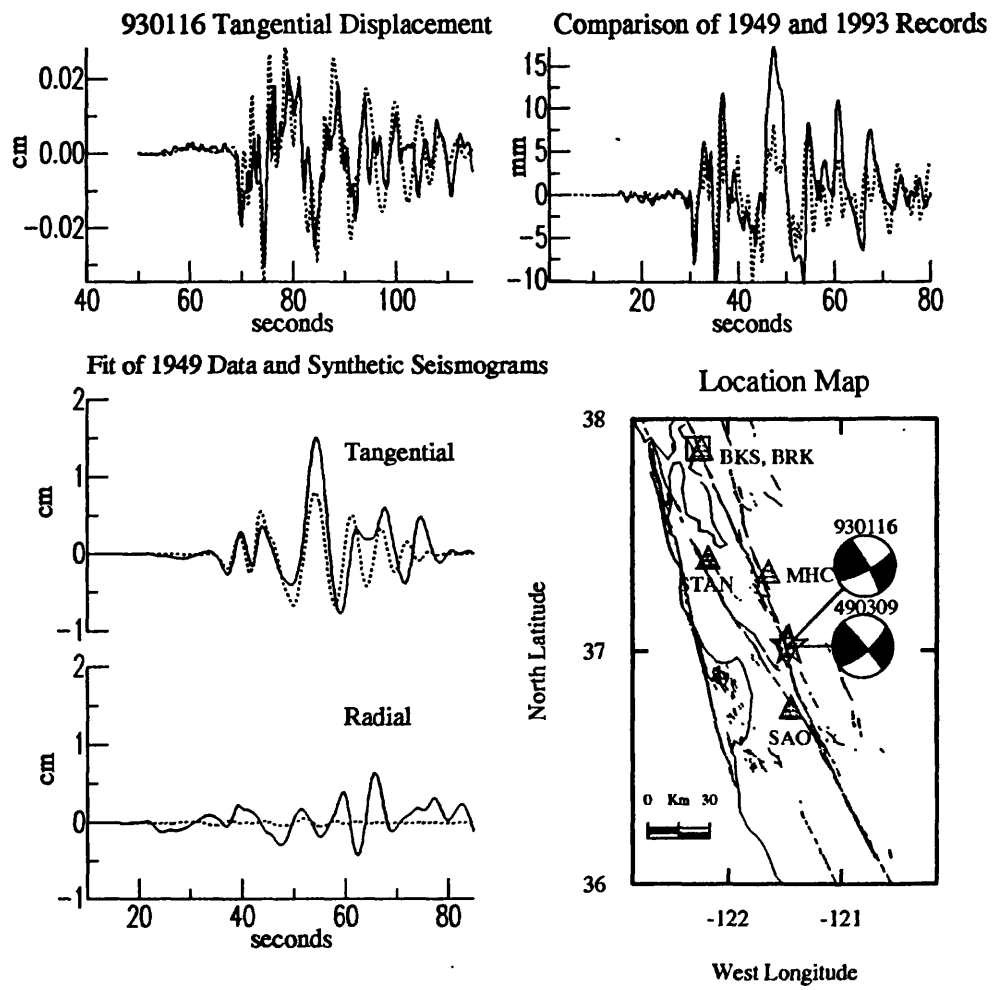


Figure 4. a) Compares the tangential displacement record for the 930116 Gilroy earthquake (solid) with a synthetic (dashed) computed with the GIL7 model. b) Compares a synthetic Bosch-Omori seismogram for the 930116 event (dashed) with a digitized representation of an actual Bosch-Omori seismogram (solid) of an event which occurred on March 9, 1949. c) Compares lowpass filtered ( $f < 0.2$  Hz) Bosch-Omori data (solid) and synthetics (dashed) for the 1949 event. d) Shows the relative locations and focal mechanisms of the two events.

## Physical Processes in Large Silicic Magma Systems

9980-23

Elliot T. Endo, Dan Dzurisin, and Eugene Y. Iwatsubo  
Branch of Volcanoes and Geothermal Process  
Cascades Volcano Observatory  
5400 MacArthur Blvd.  
Vancouver, WA 98661  
(206) 696-7891  
e-mail: etendo@pwavan.wr.usgs.gov

## Program Element II.3

Investigations

The principal objective of this project was the establishment of a baseline regional GPS network in western Washington and NW Oregon that extends from the Pacific coast to a north-south line just east of the Cascades. Special emphasis was given to selecting stations on or close to the major volcanoes of the Cascades. The project was first funded by NEHRP for a regional GPS survey in NW Oregon and SW Washington in 1992 (June and September). Additional funding was provided by NEHRP 1993 and 1994 to extend the network into NW Washington.

Results

## Observations

In August of 1994 the third phase of baseline GPS measurements was completed. During a period of 8 days, 24 stations (Figure 1) were occupied in western Washington and Oregon. Of the 24 stations, six were new marks installed by the Cascades Volcano Observatory. One new mark was located west of Tillamook, Oregon, a second at Port Angeles, Wash., a third at Sunrise (Mt. Rainier), a fourth at Reflection Lake (Mt. Rainier), a fifth at Mowich Lake (Mt Rainier), and a sixth at La Push, Wash. The University of Washington Geophysics program occupied two sites on the Olympic Peninsula. 1994 was the first year that the project had access to 6 P-code receivers from the Hawaiian Volcano Observatory in addition to the two used by the University of Washington. All sites were observed for two eight hour sessions(15 second epochs) on separate days.

## GPS data reduction

In the spring of 1994 the project's UNIX workstation was transported to the UNAVCO facility in Boulder, Colorado. Bernese 3.5 and related UNAVCO software was installed on the workstation. With the help of John Braun from UNAVCO, a June 1992 precise orbit problem was solved and June and September 1992 GPS processing was completed. GPS data for the 1993 campaign was also reduced this past year. With the exception of June 1992, we used CODE precise orbits. NGS orbits were used for June 1992 data. GPS data for the August 1994 campaign will be processed for solutions in late 1994.

Reports

Endo, E.T., and Iwatsubo, E.Y., Preliminary results of the 1992 NW Oregon - SW Washington GPS survey, USGS Open File report, in review.

Endo, E.T., and Iwatsubo, E.Y., Preliminary Bernese results of the 1992 and 1993 NW Oregon - SW Washington GPS surveys, USGS Open File report, in preparation.

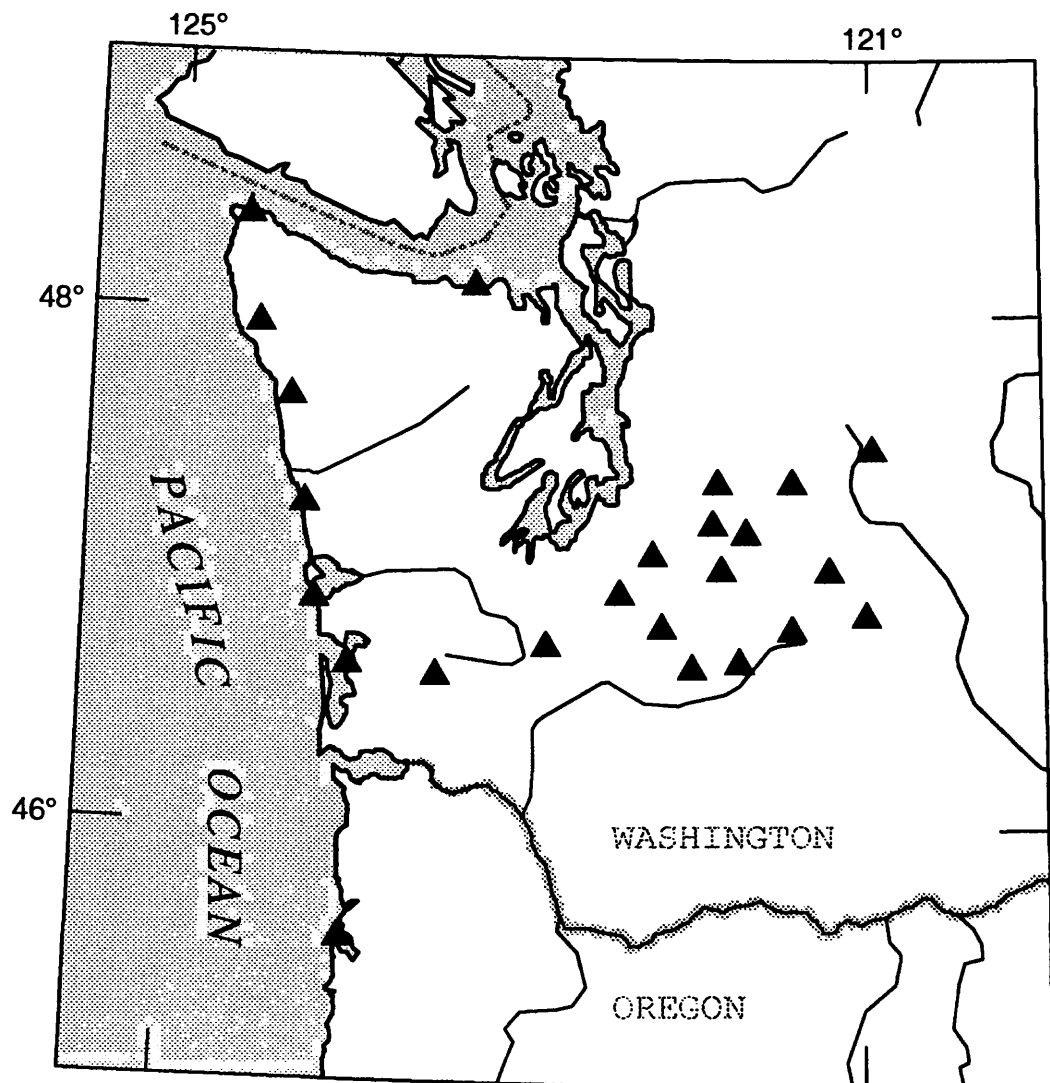


Figure 1. Map showing GPS stations occupied during the August 1994 GPS campaign. Stations selected for observations are indicated by triangles. The cluster of stations near the center of the figure is approximately centered on Mt. Rainier.

## Global Seismology

9920-10212

E. R. Engdahl

and

E. A. Bergman

Branch of Earthquake and Geomagnetic Information

U.S. Geological Survey

Denver Federal Center

Box 25046, Mail Stop 967

Denver, Colorado 80225

(303) 273-8422

### Investigations

1. **Travel-Time Tables.** Develop new standard global travel-time tables to locate earthquakes.
2. **Arrival-Time Data.** Coordinate planning for an International Seismological Observing Period (ISOP)—a time interval during which there would be enhanced reporting of arrival-time data.
3. **Earthquake Location in Island Arcs.** Develop practical methods to accurately locate earthquakes in island arcs.
4. **Subduction Zone Structure.** Develop techniques to invert seismic travel times simultaneously for earthquake locations and subduction zone structure.

### Results

1. **Travel-Time Tables.** New empirical travel-time curves for the major seismic phases have been derived from the catalogues of the International Seismological Centre by relocating events by using P readings, depth phases, and the iasp91 travel times, and then re-associating phase picks. A smoothed set of travel-time tables is extracted by a robust procedure which gives estimates of the variance of the travel times for each phase branch. This set of smoothed empirical times is then used to construct a range of radial velocity profiles which are assessed against a range of different measures of the level of fit between the empirical times and the predictions of the models. These measures are constructed from weighted sums of  $L_2$  misfits for individual phases. The weights are chosen to provide a measure of the likely reliability of the picks for the different phases.

A preferred model ak135 is proposed which gives a significantly better fit to a broad range of phases than is provided by the iasp91 and sp6 models. The differences in velocity from these models are generally quite small except at the boundary of the inner core where reduced velocity gradients are needed to achieve satisfactory performance for the PKP differential time data.

The potential resolution of velocity structure we have been assessed with the aid of a nonlinear search procedure in which 5,000 models have been generated in bounds about ak135. Misfit calculations are performed for each of the phases in the empirical travel-time sets, and the models are then sorted using different overall measures of misfit. The best 100 models for each criterion are displayed in a model density plot which indicates the consistency of the different models. By comparison of different misfit measures, the interaction of information from different phases can be displayed. Structure in the mantle is well resolved except at the base, and ak135 provides a good representation of core velocities.

2. **Arrival-Time Data.** A highlight of the year was a Workshop on Upgrading Seismological Practice at the IASPEI General Assembly held at Wellington, New Zealand, 10-21 January 1994. This full-day workshop focused on ways in which digital technology is being used to improve the effectiveness of seismological observatories. Presentations were grouped into four categories for the quarter-day sessions: (1) Initiatives in Global Seismology; (2) New Concepts in Seismological Practice and Data Processing; (3) Applications of Personal Computers and Workstations; and (4) Automated Station/Array/Network Operation. An ISOP Special Interest Group Meeting was held following the Workshop at which many aspects of the project were discussed with a large group of interested scientists.

In conjunction with the IASPEI Committee on Developing Countries, ISOP also organized a Training Course on Interactive Analysis of Digital Seismic Data, which immediately followed the Regional Seismological Assembly in South America held at Brasilia, Brazil, 22-26 August 1994. The week long course was designed to acquaint participants with the basic principles of digital signal processing which must be understood in order to work effectively with the digital seismograph systems which are increasingly widely deployed in South America. A second goal of the course was to provide background information and resources which would help the course participants understand how the global seismological infrastructure is organizing itself to take advantage of digital seismometry and modern communications, and how they can become involved in this process.

3. **Earthquake Location in Island Arcs.** We use our current Earth model (ak135) and procedures to relocate about 100,000 events which are well-constrained teleseismically by arrival-time data reported to the International Seismological Centre (ISC) and the National Earthquake Information Center during the period 1964-19924 We compare our relocations to the hypocenters reported in the ISC and NEIC catalogues. Differences in epicenter location are generally small, primarily due to the differences in upper mantle travel times between these models and the Jeffreys-Bullen model used by the ISC and NEIC. Focal depths, however, are dramatically improved over those determined by the ISC, demonstrating how regional structures such as downgoing slabs can severely bias depth estimation when only regional and teleseismic P arrivals are used to

determine the hypocenter. This new global hypocenter data base is complete to at least moment magnitude ( $M_w$ ) 5.25 and includes all events for which moment tensor solutions are available. Thus, the depth distribution of global seismicity can be accurately portrayed and, in particular, the depth distributions of intermediate-depth earthquakes within major subduction zones worldwide can be compared. These distributions reveal discontinuous depth variations within and between subduction zones which appear to correlate with such factors as subduction rate and age of lithosphere entering their trenches.

Cross-sections of relocated hypocenters for intermediate-depth (50-300 km) intraslab earthquakes are constructed in true curvilinear distance and depth by projecting about the local center of curvature of either the volcanic front, the trench axis, or a best fit to the dipping seismic plane. Arc-normal and arc-strike cross-sections are presented for major subduction zones worldwide. As an example of this method of analysis, six such centers of curvature (or poles) are required to represent the seismicity in western South America. The new data set and methods of presentation reveal geometrical aspects of slab geometry over this depth range which heretofore had remained hidden or poorly defined. In particular, the fine structure of intermediate-depth seismicity in the vicinity of the Arica bend reveals curvilinear clusters at depths greater than 130 km that appear to be in alignment with offshore island and seamount chains. Moreover, the apparent thickness of the Wadati-Benioff Zone as measured in cross section is greatly reduced compared to previous studies.

4. **Subduction Zone Structure.** The use of a proper reference model and unbiased starting hypocenters are particularly important for relating slab seismicity to seismic velocity anomalies based on tomographic methods. An inadequate reference model and mislocated hypocenters can often result in loss of structural signal in the data and mapping of spurious non-linear effects into the tomographic images. High-resolution tomographic imaging of major subduction zones (Van der Hilst et al., 1991) and the distribution of intraslab intermediate-depth earthquakes within these images were examined. This study revealed that intraslab earthquakes do not necessarily occur within the coldest slab interiors, as previously believed, but within a region of subducted crust just below the upper surface of the slab.

## Reports

- Boyd, T.M., Engdahl, E.R., and Spence, W., 1994, Seismic cycles along the Aleutian arc—Analysis of seismicity from 1957 through 1991: *Journal of Geophysical Research* (in press).
- Hwang, L.J., and Clayton, R.W., 1991, A station catalog of ISC arrivals—Seismic station histories and station residuals: U.S. Geological Survey Open-File Report 91-295, 3187 p.
- Kennett, B.L.N., and Engdahl, E.R., 1991, Travel times for global earthquake location and phase identification: *Geophysical Journal International*, v. 105, p. 429–465.

- Kennett, B.L.N., Engdahl, E.R., and Buland, R.P., 1994, Constraints on seismic velocities in the Earth from travel times: *Geophysical Journal International* (submitted).
- Van der Hilst, R.D., and Engdahl, E.R., 1991, On the use of PP and pP data in delay time tomography: *Geophysical Journal International*, v. 106, p. 169-188.
- Van der Hilst, R.D., Engdahl, E.R., Spakman, W., and Nolet, G., 1991, Tomographic imaging of subducted lithosphere below northwest Pacific island arcs: *Nature*, v. 353, p. 37-42.

# THEODOLITE MEASUREMENTS OF CREEP RATES ON SAN FRANCISCO BAY REGION FAULTS

Award Number 1434-94-G2420

Jon S. Galehouse  
Department of Geosciences  
San Francisco State University  
San Francisco, California 94132

Phone: (415) 338-1204 FAX: (415) 338-7705 galehous@sfsu.edu

## Program Element II

We continued measuring creep (aseismic slip) rates on San Francisco Bay region active faults. Over the past 15 years, we have made over 1550 creep measurements, with over 700 of these occurring in the five years following the Loma Prieta earthquake (LPEQ). Amount of slip is determined by noting changes in angles between sets of measurements taken across a fault at different times. This triangulation method uses a theodolite to measure the angle formed by three fixed points to the nearest tenth of a second of arc. The amount of slip between measurements can be calculated trigonometrically using the change in average angle. The precision of our measurement method is such that we can detect with confidence any movement more than 1-2 mm between successive measurement days.

We presently have regular measurement sites at 29 localities on active faults, including 26 in the San Francisco Bay region (see Figure 1). We also have one measurement site on the San Andreas fault in the Point Arena area and two on the Maacama fault in Willits and Ukiah that do not appear on Figure 1. During 1994 we remeasured most sites with a history of creep about once every two to three months and most sites without any creep history about every three to four months. In addition to our ten regular sites on the Hayward fault, we established 15 additional sites in conjunction with J. Lienkaemper of the USGS. We measured each of these additional sites once during 1994. These measurements will help to document in detail any surface slip on the Hayward fault resulting from any future seismic event(s).

Most measurement sites span a fault width of about 50-225 m, but a few must span a greater width because of site considerations. The fault width spanned (W) is noted on Figures 2 through 6 and represents the distance from the theodolite on one side of a fault to a target on the other side of the fault. The figures also show the average rate of movement at each site as determined by the slope of the least-squares line which also appears on each of the graphs. The graphs also show the time of the 17 October 1989 LPEQ as a vertical line. The following is a brief fault-by-fault summary of our results through the end of 1994.

**SAN ANDREAS FAULT** (see Figure 2) - We have been measuring horizontal slip on the San Andreas fault at Site 18 near Point Arena for 14.0 years, at Site 14 at the Point Reyes National Seashore Headquarters for 9.8 years, and at Site 10 in South San Francisco for 14.6 years. All three sites have shown virtually no net slip and none was affected by the LPEQ.

In November 1989, we began measuring a USGS site (our Site 22) in Woodside that had not been remeasured for many years. Our results compared to unpublished USGS measurements in 1977 show that virtually no surface slip occurred between 16 February 1977 and 4 November 1989 and very little has occurred since. We also established in November 1989 Site 23 on the San Andreas fault near the southeastern end of the LPEQ aftershock zone and northwest of San Juan Bautista. Very little net slip has occurred at this site in the past 4.9 years.

In July 1990, we established Site 25 on the San Andreas fault just southeast of San Juan Bautista and the LPEQ aftershock zone. This site is on the central creeping portion of the fault and has been moving at a rate of about 14 mm/yr for the past 4.3 years. This is considerably faster than the longer-term pre-LPEQ rate of about 7-8 mm/yr as determined by a USGS creepmeter at this site (Schulz, 1989; Gladwin and others, 1991).

In summary, the San Andreas fault at five measurement sites (18, 14, 10, 22, 23) along the previously locked portion of the fault both northwest and southeast of the LPEQ aftershock zone does not appear to have been affected by the LPEQ in the five years since October 1989. This portion of the San Andreas fault has remained virtually locked, with 1 mm/yr or less of creep occurring along it. In contrast, the post-LPEQ creep rate on the northwestern portion of the central creeping segment of the fault at Site 25 near San Juan Bautista is about twice the longer-term, pre-LPEQ creepmeter average.

**HAYWARD FAULT** (see Figure 3) - We have been measuring horizontal slip at five sites along the Hayward fault for 14.3 to 15.2 years and have determined that the overall right-lateral creep rate is about 4.4 to 4.9 mm/yr. Although the creep characteristics (steady or episodic) differ from site to site, the overall rates are quite similar. A detailed analysis of our results indicates that the LPEQ caused an overall slowdown in the rate of right-lateral creep along the Hayward fault, particularly near the southeastern end of the fault in Fremont. A detailed discussion of the pre-LPEQ and post-LPEQ creep rates on the Hayward fault is beyond the scope of this summary but can be found in Galehouse (1995).

In the 14.4 years since we began measurements in August 1980 in San Pablo (Site 17) near the northwesterly end of the Hayward fault, the overall average rate of right slip (about 4.4 mm/yr) has been similar to the overall rates at the other Hayward fault sites. However, superposed on the overall slip rate in San Pablo are changes between some measurement days of up to nearly a cm in either a right-lateral (more common) or left-lateral (less common) sense. It is probable that the results at this site are influenced by the seasonal distribution of rainfall (Lienkaemper and others, 1993).

The Hayward fault at Site 13 on Rose Street in Hayward also moves somewhat episodically, but not as pronounced as in San Pablo. With J. Lienkaemper of the USGS, we remeasured curb offsets and old City of Hayward arrays at Rose Street in late 1992 and determined that the overall creep rate there since 1930 is 5 mm/yr. This is virtually the same rate (4.9 mm/yr) that we have measured for the past 14.3 years (see Figure 3).

Extremely uniform movement characterizes Site 12 on D Street in Hayward. Two active traces of the Hayward fault occur here and their combined movement rate has been about 4.5 mm/yr for the 14.3 years since we began measurements in June 1980.

Movement along the Hayward fault at Site 2 in Union City has also been fairly uniform but somewhat more episodic than movement at Site 12. Site 2 has been moving at a rate of about 4.8 mm/yr for the 15.1 years since we began measurements in September 1979.

Since we began measuring Site 1 in Fremont in September 1979, the fault has moved rather episodically. Typical surface movement characteristics are relatively rapid right slip of about a cm over a few months time alternating with relatively slower slip over a period of two or more years. The fault at Site 1 was in one of the relatively slower phases of movement prior to the LPEQ and the slower phase persisted for a total of about five years, including about three and one-half years following the LPEQ. The average rate of right-lateral creep during this slow period was less than 1 mm/yr. The creep rate before the LPEQ was 5.4 mm/yr but the extended slow phase has brought the overall average down to 4.6 mm/yr for the past 15.2 years. The slow phase ended here between March and May of 1993 when more than a cm of right slip occurred.

In February 1990 we established Site 24 on the Hayward fault on Camellia Drive in Fremont, about four km southeast of Site 1 (see Figure 1). Although relatively rapid right-lateral creep had been reported for this site in recent years, we have measured very little net slip. In fact, our results indicate a slight amount (0.6 mm/yr) of left-lateral creep since the LPEQ. Measurements since April 1992 at Parkmeadow Drive in Fremont (Site 27) only 0.4 km southeast of Site 24 also indicate that very little net slip is occurring (not shown on Figure 3).

In summary, the right-lateral creep rates on the Hayward fault from Site 17 in San Pablo to Site 1 in Fremont are now about the same as they were before the LPEQ. However, the southeasternmost portion of the fault in Fremont at Site 24 and Site 27 still shows very little post - LPEQ slip thus far. All these changes are consistent with Reasenberg and Simpson's (1992) calculations of static stress changes due to the LPEQ ( also see Galehouse, 1995).

In order to fill in the large data gap between Site 17 in San Pablo and Site 13 in Hayward, we began measuring three new sites on the Hayward fault in early 1993. Site 28 is on Encina Way and Site 29 on La Salle Avenue, both in Oakland. Site 30 is on Florida Avenue in Berkeley (see Figure 1). Preliminary results suggest typical Hayward fault creep rates of about 5 mm/yr at Sites 28 and 29, but a much slower than typical rate at Site 30. It is possible that we are not spanning the active fault trace(s) at Site 30.

**CALAVERAS FAULT** (see Figure 4) - We have been measuring horizontal slip at two sites on the Calaveras fault in the Hollister area for more than 15 years. Slip at both sites has been episodic with intervals of relatively rapid right slip typically lasting a couple months or less alternating with longer periods of time when little net slip occurs. The LPEQ occurred during an interval of slower movement that had persisted for about a year at Site 4. The earthquake apparently triggered up to 14 mm of right slip at Seventh Street (see Figure 4). Overall the rate of right slip is about 6.8 mm/yr for the past 15.1 years.

Slip at Site 6 along Wright Road just 2.3 km northwest of Site 4 is also episodic. The LPEQ occurred during an interval of slower movement that had persisted for about a year at Wright Road (similar to the situation at Seventh Street). The earthquake apparently triggered up to 12 mm of right slip. The overall rate of slip at Wright Road is 9.6 mm/yr. This rate is nearly 3 mm/yr faster than the rate at nearby Seventh Street.

Either the creep rate decreases significantly from Wright Road southeast to Seventh Street or undetected surface movement is occurring outside our 89.7 m-long survey line at Seventh Street.

After the rapid slip triggered by the LPEQ, both sites in the Hollister area returned to a slower mode of movement which has now persisted for about five years. The slowdown was not as pronounced at Site 4 and the pre- and post-LPEQ rates are now about the same. At Site 6, however, the slip rate decreased from a pre-LPEQ rate of about 12.2 mm/yr to a post-LPEQ rate of about 3 mm/yr. This has brought the overall average down to 9.6 mm/yr which has resulted in what appears to be a "slip deficit" of about 2 cm at Site 6 at the present time (see Figure 4). A more detailed discussion of the effect of the Loma Prieta earthquake on the Calaveras fault in the Hollister area is in Galehouse (1990). This paper also discusses the effect of the Morgan Hill earthquake in 1984. No immediate surface displacement had occurred at either of the Hollister area sites when they were measured the day after the Morgan Hill earthquake. However, within the following 2.5 months, both sites showed over a cm of right slip which was followed by a relatively long interval of slower slip (see Figure 4). A more detailed discussion of the longer-term effect of the LPEQ on the Calaveras fault is in Galehouse (1995).

In contrast to the sites in the Hollister area, Site 19 in San Ramon near the northwesterly terminus of the Calaveras fault was not affected by the LPEQ. It has remained virtually locked throughout our 14.0 years of measurements.

**CONCORD - GREEN VALLEY FAULT** (see Figure 5) - We began our measurements at Site 3 and Site 5 on the Concord fault in the City of Concord in September 1979. It appears that typical movement characteristics at both sites are intervals of relatively rapid right slip of about 7-10 mm over a period of a few months alternating with intervals of relatively slower right slip of about 1-2 mm/yr over a period of several years. For the past 15.2 years, the overall average creep rate along the Concord fault in the City of Concord is about 3 mm/yr (3.5 at Site 3 and 2.7 at Site 5).

It appears that the LPEQ had little or no effect on the Concord fault at the measurement sites in the City of Concord. As shown in Figure 5, the latest phase of relatively rapid right slip occurred at both sites on the Concord fault in late 1992 - early 1993. It does not appear to be related to any seismic event(s).

We began measuring Site 20 on the Green Valley fault near Cordelia in June 1984. Large variations tend to occur at this site between measurement days, possibly because of the seasonal effects of rainfall and because logistical considerations resulted in our survey line being particularly long (335.8 m). However, our results suggest that the Green Valley fault behaves similarly to the Concord fault i.e., relatively rapid right slip in a short period of time (months) alternating with relatively slower slip over a longer period of time (years). The Green Valley fault was in a period of relatively slower movement for the first 20 months of our measurements, averaging a few mm/yr of right slip. In early 1986, however, the fault slipped right-laterally more than a cm. This was followed by about three years in which the net slip was less than 1 mm/yr. Sometime after 6 August 1989, the Green Valley fault entered into another phase of relatively rapid right slip that had totaled about 2 cm by late 1990. Since then, however, the overall net slip has been left-lateral which has brought the overall average down to 3.4 mm/yr for the past 10.5 years and has resulted in a "slip deficit" of about 1-2 cm.

Regarding the relationship between the Green Valley and Concord faults, the episodes of relatively rapid slip and relatively slower slip do occur at different times; however, the episodic nature of the slip and the overall average rates are similar. Based on these similarities and the small step between their respective trends, we consider the Concord and Green Valley faults to be different names for the southeastern and northwestern segments of the same fault system.

**MAACAMA FAULT** (see Figure 6) - The Maacama fault extends from northern Sonoma County to north of Laytonville in Mendocino County and is the northwesterly continuation of the Hayward-Rodgers Creek fault trend (Galehouse and others, 1992). We began measurements at Site 26 in Willits in November 1991. Results over the past 3.0 years indicate that the Maacama fault is creeping right-laterally at about 7 mm/yr which is about 2 mm/yr faster than the creep rate on the Hayward fault to the southeast. We established a second site (31) on the Maacama fault just east of Ukiah in May 1993. It has also shown about 7 mm/yr of right slip for the past 1.5 years.

**RODGERS CREEK FAULT** - We measured a site (16) on the Rodgers Creek fault in Santa Rosa from August 1980 until we had to abandon it for logistical reasons in January 1986. During these 5.4 years of measurements, no significant surface slip occurred and we concluded that the Rodgers Creek fault was not creeping at this site.

In September 1986, we established Site 21 on the Rodgers Creek fault near Penngrove (see Figure 1). The average at Site 21 has been about 2 mm/yr for the past eight years. However, in mid-1993, we discovered that one of our triangulation points had become unstable. At present, it is difficult to know whether or not the Rodgers Creek fault is really creeping slowly or whether the low rate is due to the "noise" level at this particular measurement site. The LPEQ does not appear to have had any effect on the Rodgers Creek fault at Site 21.

**WEST NAPA FAULT** - We began measurements at Site 15 in the City of Napa in July 1980. Similarly to the situation at Site 21 on the Rodgers Creek fault, there tends to be a lot of surface "noise" at this measurement site. However, the average rate of right slip on the West Napa fault over the past 14.4 years is less than 1 mm/yr. In other words, the West Napa fault is virtually locked at the surface with no creep occurring. The LPEQ does not appear to have had any effect on our results for the West Napa fault.

**SEAL COVE-SAN GREGORIO FAULT** - We began measurements at Site 7 on the Seal Cove fault segment in Princeton in November 1979. The least-squares average indicates that virtually no creep has occurred at this site over the past 15.1 years. We began measuring Site 8 on the San Gregorio fault segment in May 1982. This site shows very large variations from one measurement day to another, probably due in part to the particularly large fault width (455 m) measured. The least-squares average shows virtually no creep for the past 12.6 years. Therefore, the Seal Cove-San Gregorio fault is not presently creeping and the LPEQ does not appear to have had any noticeable effect on the rate of movement at either of the sites on this fault system.

**ANTIOCH FAULT** - We began measurements at Site 11 in the City of Antioch in May 1980. The average rate of movement has been virtually zero for the past 14.6 years. Site 9 just south of town showed 1.7 mm/yr of right slip for the 7.6 years from 21 November 1982 to 1 July 1990. New construction then destroyed our measurement array at this site. We have noted that much subsidence and mass movement creep occur both inside and outside the Antioch fault zone in the area of our two measurement sites and it is probable that these nontectonic movements are influencing our measurement results. If any tectonic creep is occurring along the Antioch fault, it is probably at a very low rate. The LPEQ does not appear to have had any noticeable effect at either of the sites on the Antioch fault.

---

## REFERENCES CITED

- Galehouse, J.S., 1990, Effect of the Loma Prieta earthquake on surface slip along the Calaveras fault in the Hollister area: *Geophysical Research Letters*, v. 17, no. 8, p. 1219-1222.
- Galehouse, J.S., Sowma-Bawcom, J. A., and Prentice, C. S., 1992, The Maacama fault: Preliminary creep and paleoseismic data, Mendocino County, California (abs.): *EOS (American Geophysical Union Transactions)*, v. 73, no. 43, p. 123.
- Galehouse, J.S., 1995, Effect of the Loma Prieta earthquake on fault creep rates in the San Francisco Bay region: in U.S. Geological Survey Professional Paper (Postseismic Effects), in review.
- Gladwin, M.T., Breckenridge, K.S., Hart, R.H.G., and Gwyther, R.L., 1991, Recent acceleration of characteristic creep-strain events at San Juan Bautista (abs.): *EOS (American Geophysical Union Transactions)*, v. 72, no. 44, p. 484.
- Lienkaemper, J.J., Galehouse, J.S., Simpson, R.W., and Breckenridge, K.S., 1993, Creep slowdown since the 1989 Loma Prieta earthquake (LPEQ) continues on the Hayward fault (abs.): *EOS (American Geophysical Union Transactions)*, v. 74, no. 43, p. 192.
- Reasenberg, P.A. and Simpson, R.W., 1992, Response of regional seismicity to the static stress change produced by the Loma Prieta earthquake: *Science*, v. 255, p. 1687-1690.
- Schulz, S.S., 1989, Catalog of creepmeter measurements in California from 1966 through 1988: *U.S. Geological Survey Open-File Report 89-650*, 193 p.

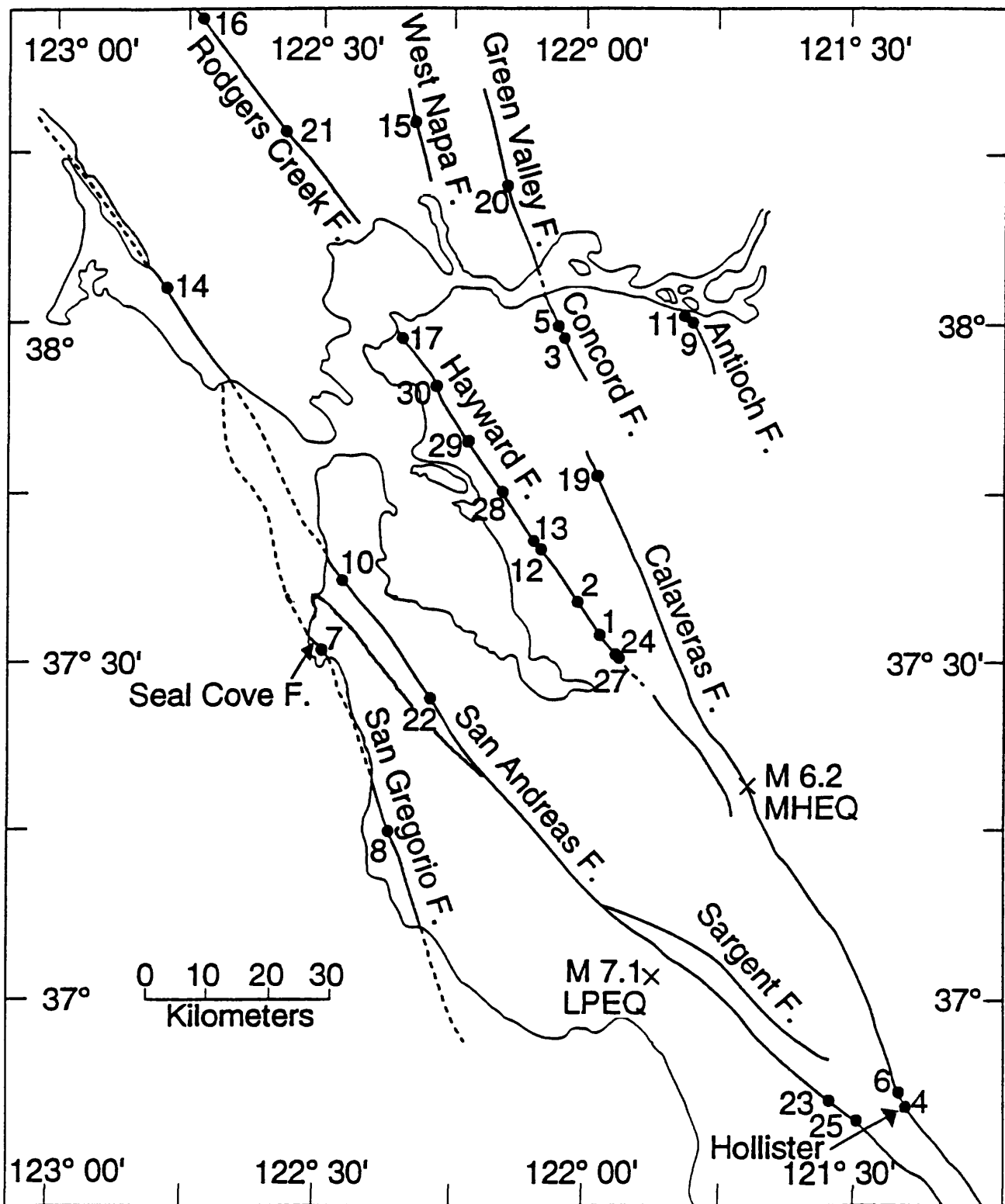


Figure 1. Numbered dots are San Francisco State University theodolite measurement sites. Epicenters and magnitudes are indicated for the 24 April 1984 Morgan Hill earthquake (MHEQ) and the 17 October 1989 Loma Prieta earthquake (LPEQ).

# SAN ANDREAS FAULT

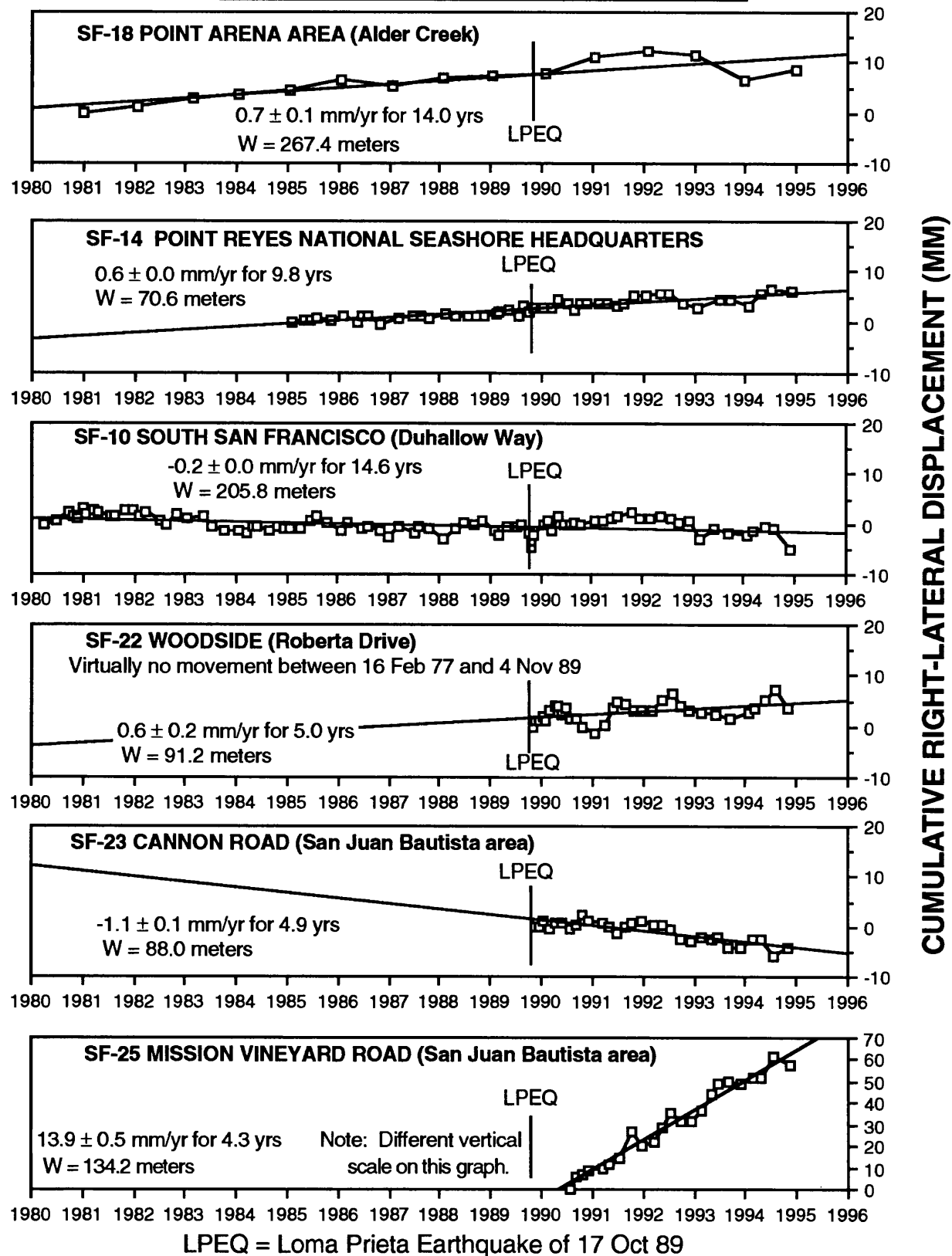
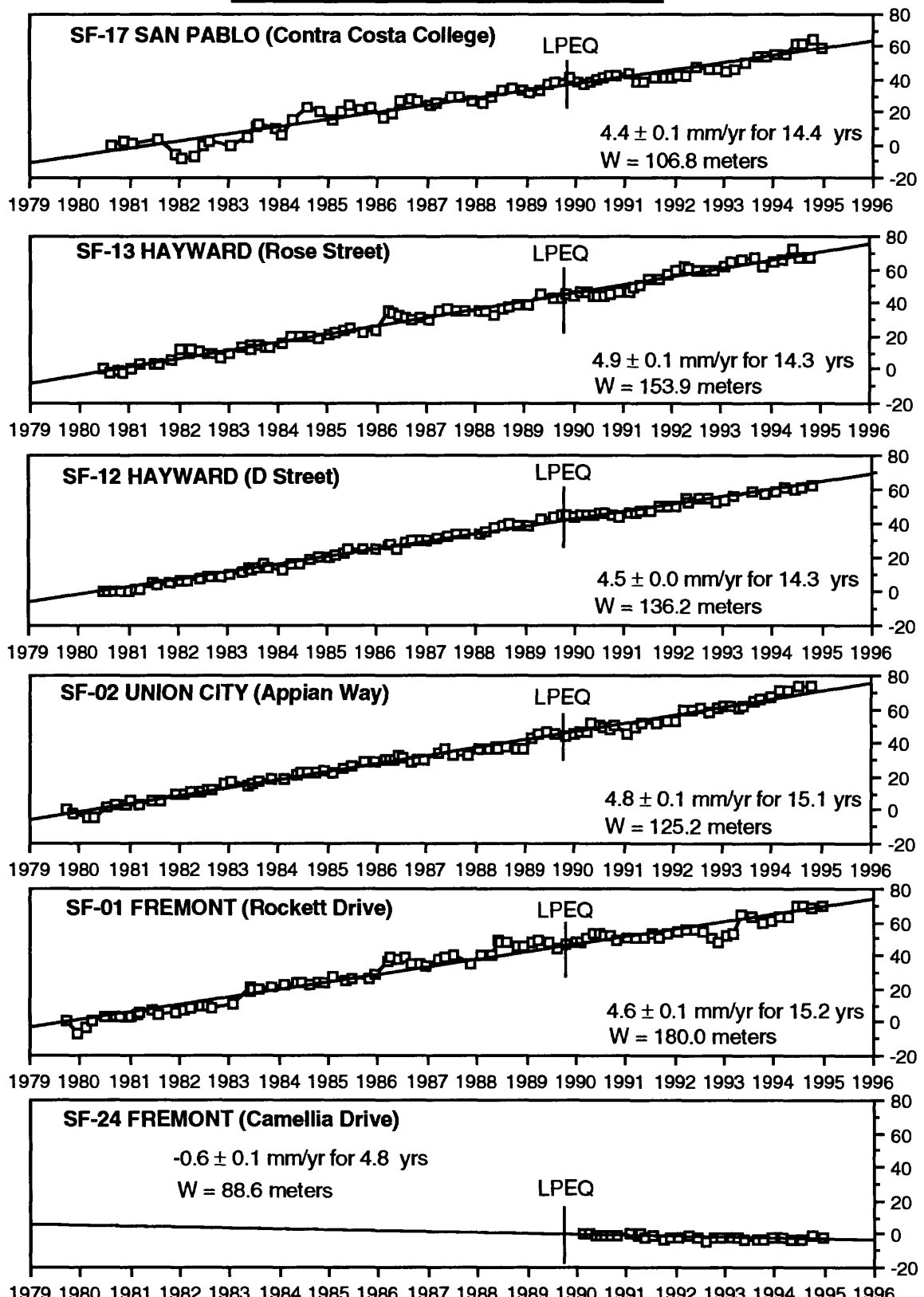


Figure 2. San Andreas Fault Displacement (1980 - 1994)

# HAYWARD FAULT

CUMULATIVE RIGHT-LATERAL DISPLACEMENT (MM)



LPEQ = Loma Prieta Earthquake of 17 Oct 89

**Figure 3. Hayward Fault Displacement (1979 - 1994)**

# CALAVERAS FAULT

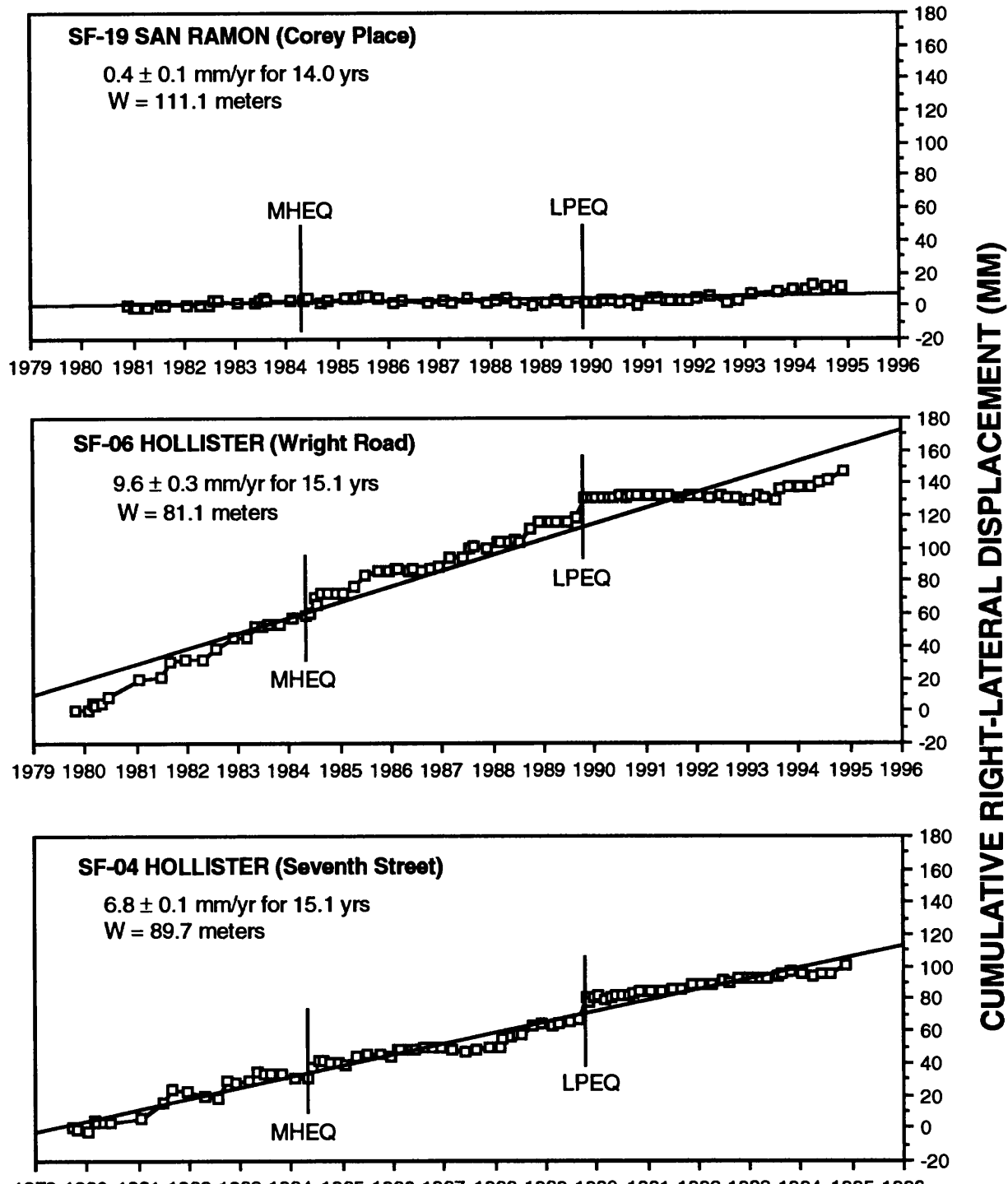


**Figure 4. Calaveras Fault Displacement (1979 - 1994)**

# CONCORD - GREEN VALLEY FAULT

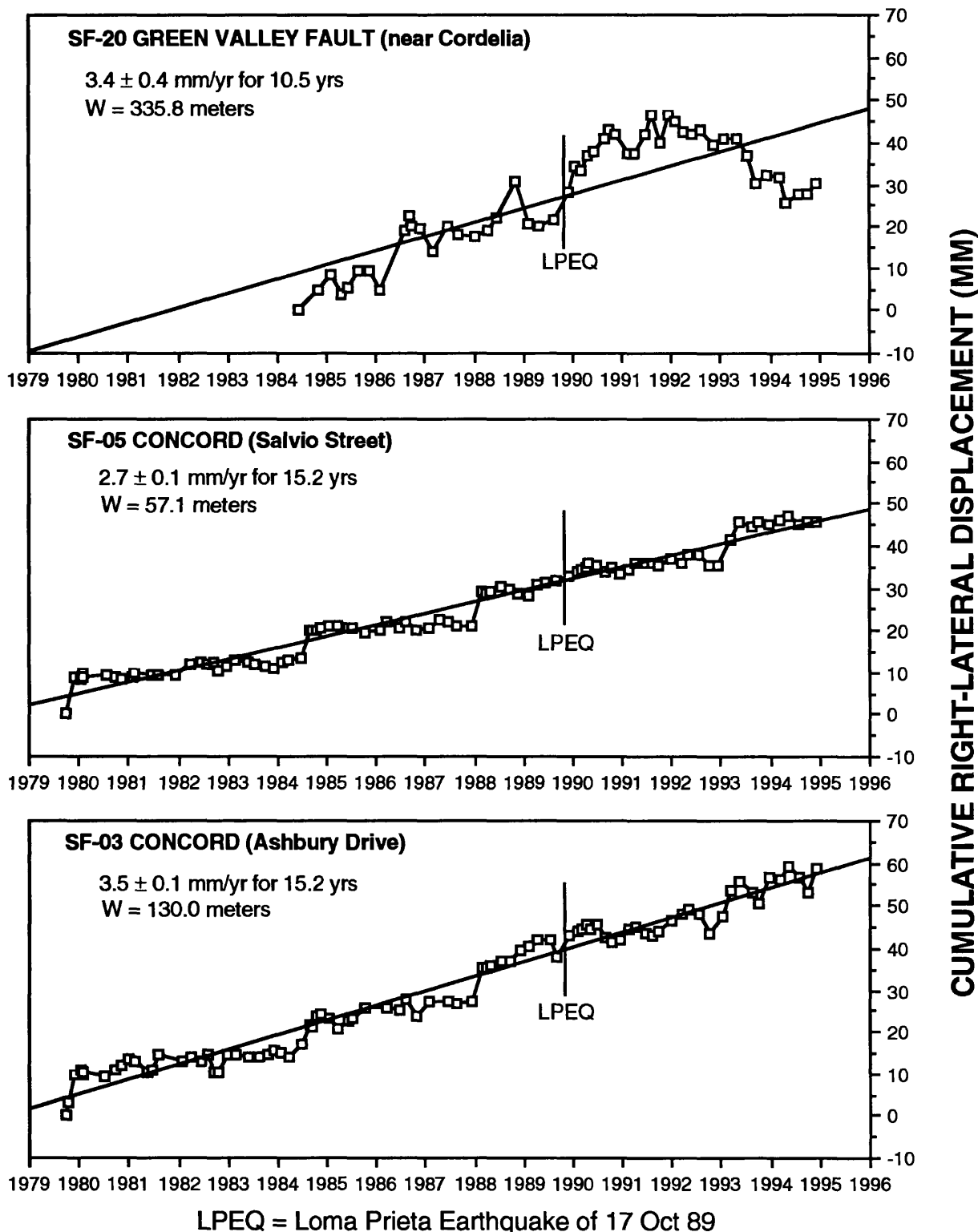


**Figure 5. Concord - Green Valley Fault Displacement (1979 - 1994)**

## **MAACAMA FAULT**

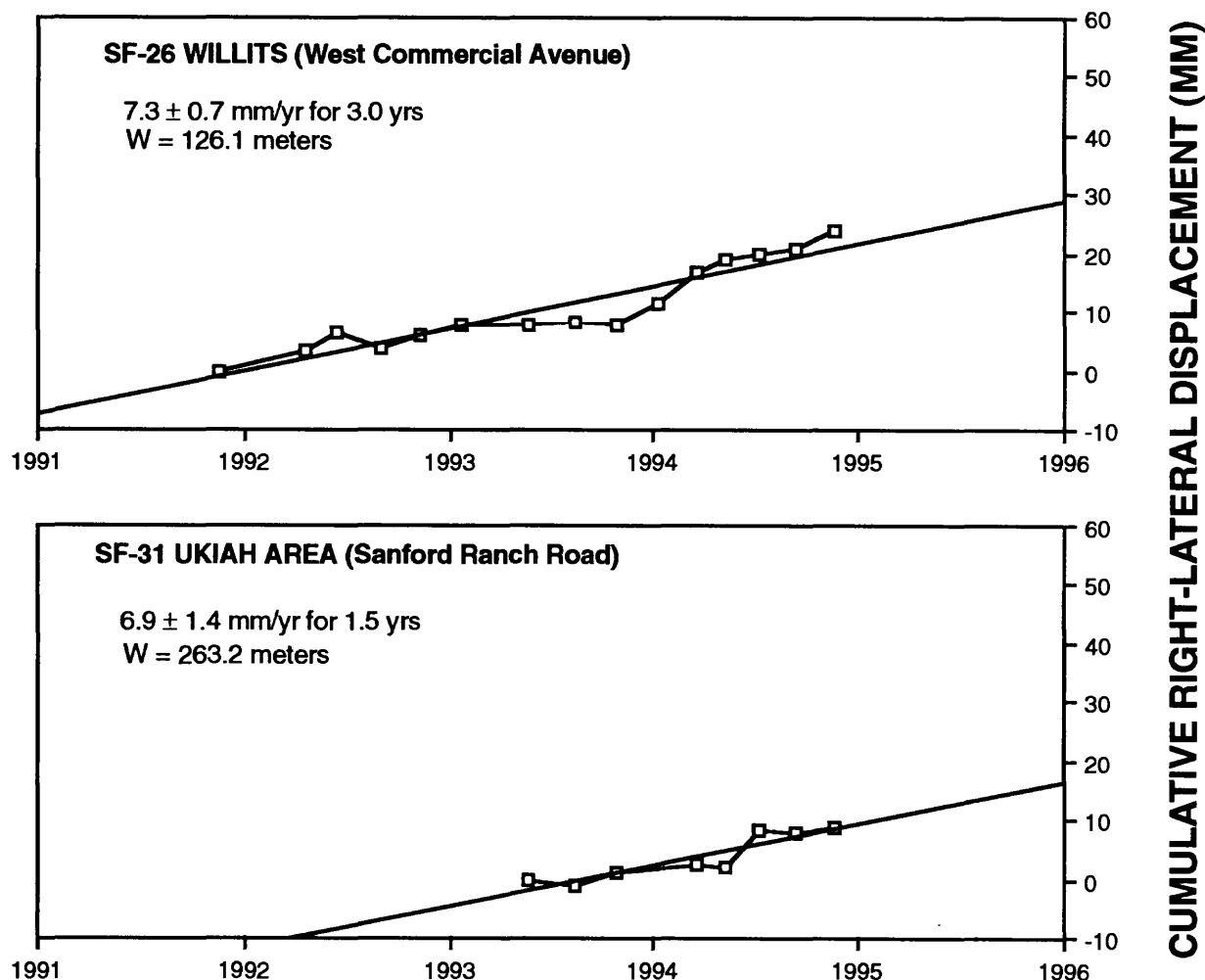


**Figure 6. Maacama Fault Displacement (1991 - 1994)**

## A Dense Geodetic Survey of the Southern Landers Fault Rupture: Implications for Paleoseismology and Segmentation

Jeff Genrich and Hadley O. Johnson

1434-93-G-2396

Institute of Geophysics & Planetary Physics  
Scripps Institution of Oceanography  
University of California, San Diego  
9500 Gilman Dr.  
La Jolla, CA 92093-0225

(619) 534-2445 Fax: (619) 534-5332  
jgenrich@ucsd.edu

### Program Element II.3

This grant has supported a repeat kinematic-GPS survey of a dense network of sites near the southern section of the Landers earthquake rupture. The pre-earthquake survey appears to be one of the highest-density horizontal surveys of high precision to be done close to an earthquake rupture. That it exists is no tribute to a successful earthquake prediction, but rather to good luck and the capabilities of the GPS system. The luck is that the Mojave Water Authority needed a survey done for a new pipeline into Yucca Valley, with a route that followed the fault rupture for about 7 km before crossing it. The capabilities of GPS are such that it can give much higher precision than was attainable before, even when used by a commercial firm (Hunsaker and Associates) for a routine survey such as this; without much effort, the precision can be a few parts in  $10^6$ , a level only attained in the past by first-order classical methods.

Many GPS surveys have been made near this earthquake, mostly to trilateration points and high-precision GPS points observed before the earthquake (Figure 1). Why then repeat another survey, and of relatively low precision at that? The answer lies in the high spatial density of the survey network. Most of the points occupied were public-land section corners and quarter-corners, giving a spacing of 0.8 to 1.6 km. In past studies of crustal motion, such a high density of data has only been available from leveling, in which it was a necessary byproduct of the technique; only rarely have classical geodetic methods provided accurate horizontal measurements over tight spacings, simply because of the costs involved. The result has been a gap in the spatial scales covered by measurements of crustal motion: we know a lot about horizontal deformation over lengths of tens of km and more, and also over a few meters (rupture and creep right on a fault), but not over lengths in between. As an example of what can be missed without measurements over intermediate lengths, consider the blind thrust faults associated with the Coalinga and Whittier Narrows earthquakes; only the fine spatial sampling provided by leveling made possible the convincing correlation between coseismic motion and geologic structure that now guides much thinking on earthquake hazard in Los Angeles.

GPS, especially if used in kinematic mode, promises to reduce the cost of dense surveys to the point that we may expect them to gradually cover many active faults. The existence of such a survey across the Landers rupture can only be regarded as a very fortunate windfall, one upon which we have tried to capitalize.

In the spring of 1994 we conducted the primary field work for this project. Five dual-frequency geodetic GPS receivers (Ashtech Z-12) were deployed during a three-day period in March on a total of

68 stations across and along the southern Landers rupture near the intersection of Highway 246 and Reche Road (**Figure 2**). The surveying was split into five sessions; commencing with a single five-hour static-mode segment of five receivers evenly distributed within the over-all network (the primary points) and followed by four half-day kinematic-mode sessions to densify the number of observed sites within the network (the secondary points). In connection with permanently operating geodetic GPS stations in southern California the initial static-mode session provides an accurate local coordinate system within which to conduct the short-occupation kinematic sessions. This framework of sites also allows us to tie into the other surveys done in the area after the earthquake since several of these sites are common to these larger scale networks. The kinematic sessions were conducted as follows: (1) Stationary receivers were located at three of the nearby primary sites and left in place for the duration of the session, (2) Two kinematic teams (two crew members each) set up antennas on fixed-height poles (borrowed from JPL) at sites near at least one of the primary stations and recorded data for approximately one hour, (3) Each kinematic team then packed the receiver equipment into a vehicle and drove to the next site (typically  $\frac{1}{2}$  mile) while continuing to record data by holding the fixed-height pole out the window to maintain a steady position of the antenna above the vehicle's roof, (4) Each site visited by the kinematic teams from this point on was occupied for 10-15 minutes (the two teams coordinated all movements via hand-held radios). In addition to the five surveying teams (two kinematic teams and three stationary-receiver "baby sitters") we deployed an additional two-person advance team who stayed ahead of the kinematic teams to prepare the next set of sites. The majority of sites surveyed were public-land section markers which meant most sites were buried  $\frac{1}{2}$  to 1 foot below ground level in the middle of hard-packed dirt roads. A number of sites were located below pavement near the center of uncomfortably busy roads thus requiring the use of traffic control equipment (cones and road-side signs which we were able to borrow from the San Diego County Surveyors office). These sites had been located with metal detectors and flagged for easy recovery by a reconnaissance team two weeks before the survey. In all, we had nine people in the field for a total of three days of surveying.

We are now beginning to process both the 1991 pre-earthquake measurements collected by Hun-saker and Associates and our 1994 post-earthquake data. (Our delay in processing is due mainly to the absence of one of us for an extended GPS survey in a foreign country during the summer months.) Processing will be done in two steps. For each observation day, data from the local primary sites (that were observed for several hours) are combined with concurrent measurements at permanent regional sites in Goldstone (DS10), Pinyon (PIN1), Pasadena (JPL) and Lake Mathews (RCFC). These daily solutions will yield accurate local reference frames for the kinematic surveys and provide the deformation field of the static core network. Coordinates and displacements of all sites observed in kinematic mode are then derived by processing individual sessions using tight constraints on the static core sites. With the data processed, we will be able to produce a detailed map of the surface deformation field within our network of stations. There are two primary topics we plan to address with this set of measurements:

1. We will analyze the estimated displacements to look for significant surface strain (beyond that expected from elastic rebound) away from the surface rupture. Any such additional strain, showing up either as distributed strain, or as zones of relatively high shear from "blind strike-slip faults", is of considerable importance both for engineering purposes and even more for paleoseismic studies; substantial off-fault coseismic displacements that do not result in rupture would be undetectable in paleoseismic data, and therefore would imply possible systematic errors in them. This is no small matter given the extent to which paleoseismic and geological slip-rate estimates control our thinking about long-term earthquake risk. The strains resolvable through this

kinematic survey should be between  $10^{-4}$  and  $10^{-5}$ , several orders of magnitude lower than the strain that would produce a mappable rupture.

2. We will also analyze the displacements to attempt to constrain the nature of slip on the northern end of the Johnson Valley fault. This is an area of special interest because this part of the fault is all one segment, and so would have been expected to rupture as a unit; but what is seen at the surface is that the rupture ends within the segment and then transfers to a new fault to the northeast (the Kickapoo). We expect to use these coseismic displacements to determine if the pattern seen at the surface also applies at greater depths, and so contribute to our understanding of how segmentation works (or in this case didn't).

## Geodetic Coverage Around Landers

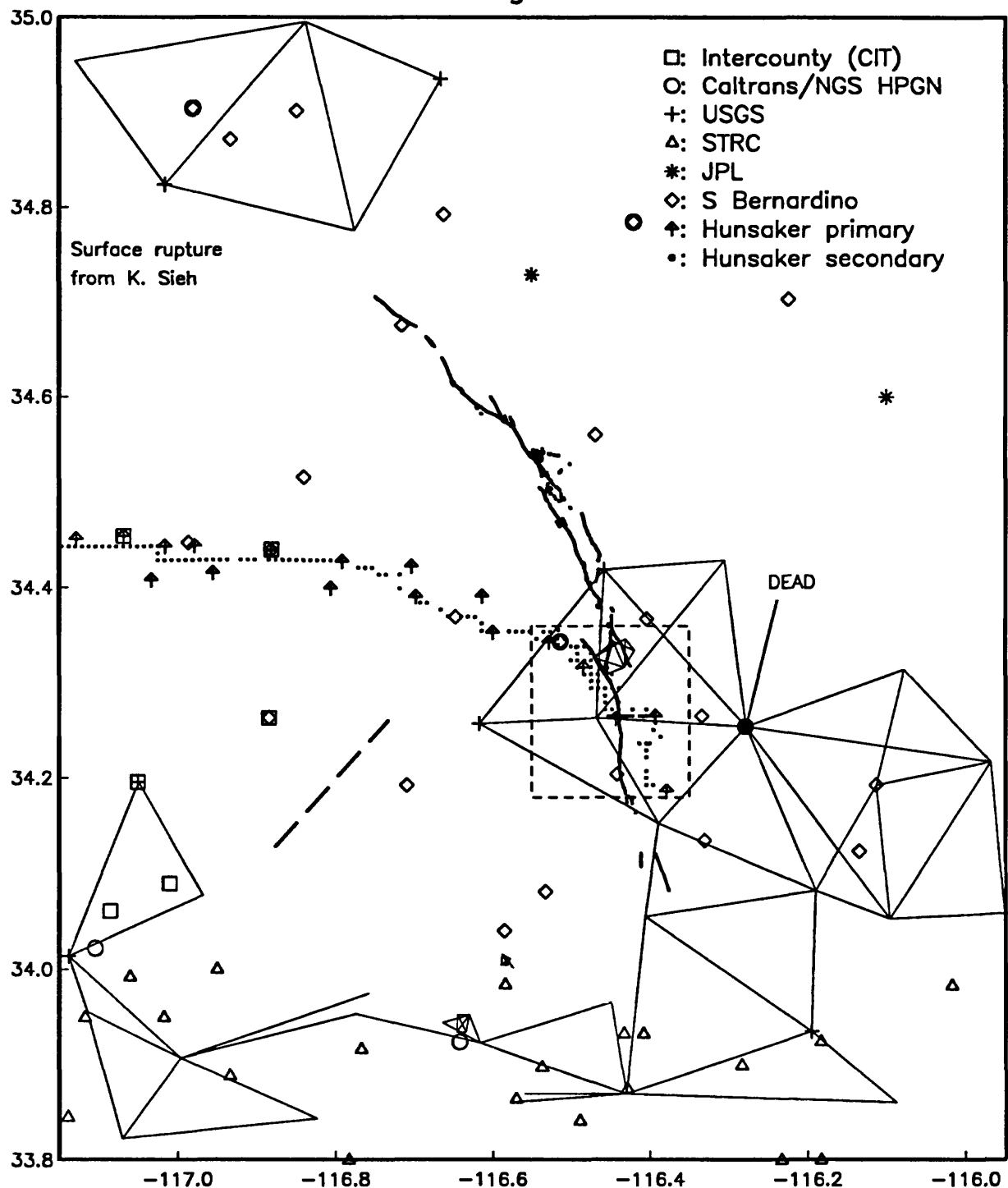
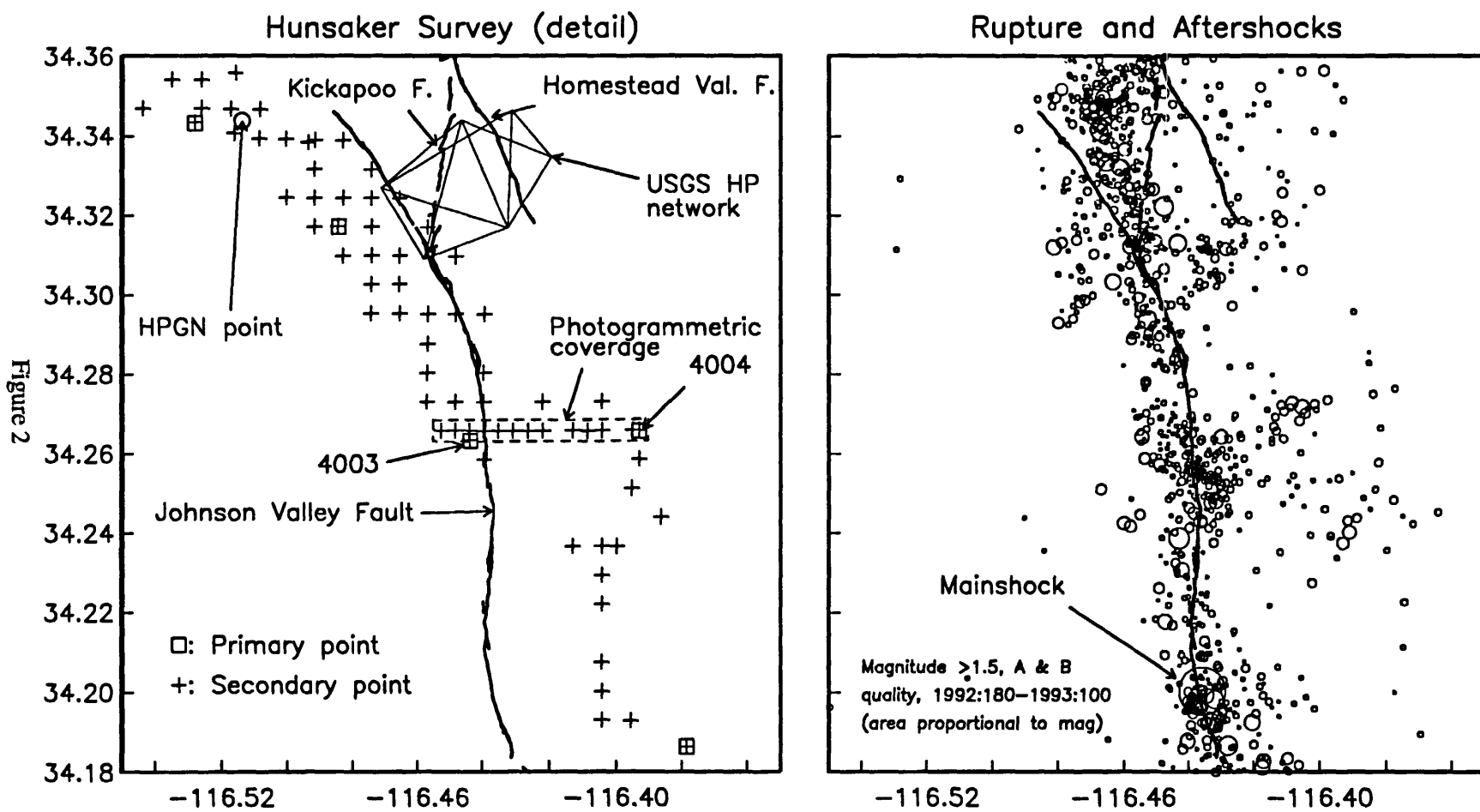


Figure 1



**Investigating Temporal Variations in Stress from Focal  
Mechanisms of Aftershocks of the Loma Prieta Earthquake**

Project Number USGS 1434-94-G-2401

Program Element: II.2

*John W. Gephart*

INSTOC, Snee Hall, Cornell University, Ithaca NY 14853

Phone: (607) 255-3538, Fax: (607) 254-4780

Email: [gephart@geology.cornell.edu](mailto:gephart@geology.cornell.edu)

## Investigations Undertaken

This study investigates the state of stress around the Loma Prieta rupture zone for the period of about four years following the mainshock, based on the focal geometries of aftershocks. Previous work had indicated a distinct spatial variation in stress within the source region among the very early aftershocks [Gephart, in press]. The analysis is based on an established procedure for estimating a four-parameter (partial) stress tensor from populations of well-constrained focal mechanisms, assuming that the shear stress and slip directions are aligned on at least one of the two nodal planes of each event [Gephart, 1990a, 1990b]. The focal mechanism data were obtained from the USGS/UC Berkeley Seismological Data Center.

## Results

Out of several thousand focal mechanisms of Loma Prieta aftershocks spanning the mainshock rupture zone compiled by the USGS/UCB Data Center through 1993, about 1800 were selected as very well constrained based on compilation parameters reported in the database. In this study these data were divided among 47 space-time groups. Because one of the goals is to identify possible spatial variations in stress following mainshock failure, the spatial sorting was performed about coordinates defined by the mainshock hypocenter and focal mechanism. By defining as many as 47 data bins, the time and (especially) space windows were small. Independent inversions were performed on each group, each involving a search over a grid of stress models defined by four independent parameters.

Typically, two exhaustive searches were performed over the range of all stress space (on a nominal  $10^\circ$  grid of principal stress directions and in increments of the stress magnitude parameter,  $R \equiv (\sigma_2 - \sigma_1)/(\sigma_3 - \sigma_1)$ , of 0.1). The regions around local minima were then searched on a denser grid to locate the best-fitting stress model. Adjacent data sets were tested on common grids, so that the results of merged data sets could be found by superimposing the results of the independent inversions, thus avoiding the need to reexecute the inversion for the combined data set. This approach proved to be useful because many of the neighboring small data sets (in space or time) yielded very similar results, suggesting that stress was uniform between them; conversely, some others suggested significant variations, which might have been obscured had the data been grouped in larger bins. The only disadvantage of this strategy is that it requires greater storage capacity to manage a large volume of output, but this is not an overwhelming problem.

The results illustrated in this report reflect some of the "homogeneous" data groupings that

emerged—that is, further division of the data sets on objective (i.e., spatial or temporal) grounds did not seem to lead to better resolved stresses. While preliminary results for the whole data set of ~1800 mechanisms are now compiled, and interpretation of those results continues, only those from some of the peripheral regions are presented here. The division of the data set is illustrated in Figure 1, with examples for three time periods and three spatial clusters. Initially, the data were divided into three temporal domains, with roughly equal numbers of data (divisions shown by columns in Figure 1). Each of these was divided among five spatial domains, based on clustering relative to the mainshock focal mechanism coordinates (of which three are shown by irregular polygons in Figure 1). Within each of the resulting subgroups, additional divisions were made, either in space or time, depending on the number of data available, such that each final subgroup comprised a minimum of 16 (and preferably about 40) events. The point was to divide the data set systematically in space and time, allowing for the fact that there was not an even distribution of data. The three spatial divisions are shown in Figure 1: LPN (Loma Prieta rupture zone-north), SAR (Sargent fault), and CSA (creeping section of the San Andreas fault). Of these, LPN and CSA are composites of smaller data subsets. The results of the tests on these data sets are illustrated in Figures 2 and 3.

Figure 2 is a series of seteronets showing: (1) the data, described by the orientations of P and T axes, and (2) the ranges of acceptable stress models determined in the stress inversion, as indicated by the  $\sigma_1$  and  $\sigma_3$  directions and a histogram of R values, within certain prescribed confidence limits [Gephart, 1990a]. The focal mechanism of the Loma Prieta mainshock is superimposed on each of these figures for reference (the mainshock mechanism was not used in any of the inversions). The results illustrate apparent variations of stress in space (that is, *between* regions LPN, SAR, and CSA) and time (at least for region CSA, for which there was sufficient data to test six different time intervals). In all cases for regions SAR and CSA, the optimum stress model fits the data very well, with average misfits of 4-6°, while in region LPN the fits are only moderately good, with misfits of about 8-10° for all time intervals; this may suggest the occurrence of some local heterogeneity in LPN (consistent with Michael *et al.* [1990] and Gephart [in press]). Regions LPN and SAR appear to indicate stable stresses through time, as the best-fitting stresses remain nearly constant in orientation and there is substantial overlap in the confidence limits from different time intervals. In region CSA, it appears that the stresses remain stable for some time, but then drift to a new (and possibly stable) configuration (discussed below). That the confidence limits tend to broaden with time for LPN and narrow with time for SAR is apparently reflects the number of data in each bin—the later bins have fewer data in LPN, and more in SAR, than earlier ones.

Figure 3, based on the Mohr Sphere construction [Gephart, 1990a], illustrates the results for each datum, the mainshock fault plane, and some hypothetical fault geometries, relative to the best-fitting stresses in each case. These figures can be used to interpret the *relative* magnitudes of normal and shear stress acting on each fault plane, subject to the uncertainty of *absolute* magnitudes, as constrained by the analysis. Each datum is indicated by a point on each of three orthogonal projections; a perfect fit between an observation and model is indicated by a coincidence between the corresponding point and the  $[\tau_b = 0, \tau_s > 0]$  half-plane. To the extent that  $\tau_b = 0$  for any fault geometry, then the magnitude of  $\tau_s$  reflects the *total* shear stress on the fault plane, and thus the  $\tau_s$  versus  $\sigma$  plot can be treated as a conventional Mohr Circle diagram. This enables us to regard the (normalized) magnitudes of shear and normal stress acting on any particular fault

plane.

In LPN, the tendency for  $\sigma_1$  to align with the pole of the mainshock fault plane and for  $\sigma_3$  to be poorly constrained along directions parallel to the fault plane (Figure 2a) is consistent with the earlier findings of *Gephart* [in press], based on much fewer data. This suggests that immediately following the mainshock rupture, the fault plane was essentially relieved of shear stress, leaving only compression perpendicular to the fault plane, generally consistent with the interpretation of *Zoback and Beroza* [1993] from their analysis of 21 months of aftershocks spanning the entire rupture zone. This circumstance is reflected on the Mohr Sphere plots (Figure 3a) by the persistent near-coincidence of the mainshock fault pole and  $\sigma_1$  axis. The present study indicates that this condition did not significantly vary for a period of a few years following the mainshock. Presumably, this state of stress did not exist immediately prior to the main event, although there was little seismicity preceding the mainshock in this region [Olson, 1990; Michael *et al.*, 1990]. Although the population of focal mechanisms and best-fitting stresses each appear to remain qualitatively unchanged throughout the aftershock sequence in region LPN (Figure 2a), there may be a tendency for the late fault planes to occur in higher normal stress orientations (i.e., closer to the right side of the Mohr Sphere) than the early ones, as suggested in Figure 3a. This is also observed in region CSA, discussed below.

Region SAR, including events along the Sargent fault, also appears to exhibit stable stresses through time (Figure 2b), in spite of an apparent slight change in focal mechanisms—with late events tending to have more nearly horizontal P and T axes than early ones. From Figure 3b, for most of the sequence many of the aftershocks and a hypothetical vertical strike-slip fault (parallel to the alignment of aftershock hypocenters) occur in orientations of relatively high shear stress ( $\tau_s \approx$  regional maximum); the mainshock fault plane also occupies an orientation of relatively high shear stress, but such that the predicted shear stress is not aligned with the observed oblique slip direction. In all three time intervals the inferred stresses are consistent with a roughly horizontal slip vector on the mainshock fault plane (not shown in Figure 3b). Thus, in region SAR it appears that any reasonable major fault geometry—of ~NW trend and moderate or steep dip—is probably *not* completely relieved of stress stress (although we cannot know the absolute magnitudes of stress, but only as normalized in the Mohr Sphere). This might suggest that the behavior of the Sargent fault is different from that of a well-evolved fault zone, like the San Andreas, with inherent low material strength or high pore pressure [Rice, 1992; *Zoback and Beroza* [1993]].

At the southeast end of the aftershock zone, in region CSA, there are enough data to invert for stress in six different time intervals (Figures 2c and 3c) and several different subareas (the latter are not shown here, as they indicate spatially uniform stresses). Throughout the aftershock sequence, the focal mechanisms exhibit only limited variability, but apparently of a kind sufficient to achieve reasonably strong constraints on the stress tensor. The analysis suggests a striking pattern of time-varying stresses through the aftershock sequence.

For the first three time intervals, the stress tensor remains stable, both in orientation and R, with  $\sigma_1$  shallowly plunging N,  $\sigma_3$  shallowly plunging E, and  $R \approx 0.5$ . During the fourth and fifth time intervals, the stress directions deviate from their earlier orientation (and may be somewhat less resolved, though the optimum models are very consistent with the data), and the preferred R value

decreases. From the fifth to the sixth time interval, both the stress directions and R value appear to stabilize, with stress directions about 15-20° clockwise from their original position of the first three intervals, and a low value of R. On the Mohr Sphere diagrams (Figure 3c), the aftershock fault planes exhibit a systematic behavior relative to the changing stress tensor. During the first three time intervals most aftershocks have orientations of high shear stress (high  $\tau_s$ ), but during the later intervals occur in orientations of relatively lower shear stress (and relatively higher normal stress). This behavior may reflect a transient pore pressure effect [e.g., *Byerlee, 1990, 1992; Rice, 1992; Blanpied et al., 1992; Zoback and Beroza, 1993*].

## References

- Blanpied, M. L., Lockner, D. A., and Byerlee, J. D., An earthquake mechanism based on rapid sealing of faults, *Nature*, 358, 574-576, 1992.
- Byerlee, J., Friction, overpressure and fault normal compression, *Geophys. Res. Lett.*, 17, 2109-2112, 1990.
- Byerlee, J., The change in orientation of subsidiary shears near faults containing pore fluid under high pressure, *Tectonophys.*, 211, 295-303, 1992.
- Gephart, J. W., Stress and the direction of slip on fault planes, *Tectonics*, 9, 845-858, 1990a.
- Gephart, J. W., FMSI: A FORTRAN program for inverting fault/slickenside and earthquake focal mechanism data to obtain the regional stress tensor, *Computers & Geosci.*, 16, 953-989, 1990b.
- Gephart, J. W., Spatial variations in stress from the first six weeks of aftershocks of the Loma Prieta earthquake: in *The Loma Prieta, California Earthquake of October 17, 1989 - Chapter D, Postseismic Effects, Aftershocks and Other Phenomena*, U. S. Geol. Surv. Prof. Paper 1550, edited by P. Reasenberg, U. S. Geological Survey, in press.
- Gephart, J. W., and D. W. Forsyth, An improved method for determining the regional stress tensor using earthquake focal mechanism data: Application to the San Fernando earthquake sequence, *J. Geophys. Res.*, 89, 9305-9320, 1984.
- Michael, A. J., Ellsworth, W. L., and Oppenheimer, D. H., Coseismic stress changes induced by the 1989 Loma Prieta, California earthquake, *Geophys. Res. Lett.*, 17, 1441-1444, 1990.
- Olson, J. A., Seismicity in the twenty years preceding the Loma Prieta, California earthquake, *Geophys. Res. Lett.*, 17, 1429-1432, 1990.
- Rice, J. R., Fault stress states, pore pressure distributions, and the weakness of the San Andreas fault, in: Fault mechanics and transport properties of rock, B. Evans and T.-F. Wong (eds.), London, Academic Press, 475-503, 1992.
- Zoback, M. D., and Beroza, G. C., Evidence for near-frictionless faulting in the 1989 (M 6.9) Loma Prieta, California, earthquake and its aftershocks, *Geology*, 21, 181-185, 1993.

## Reports

- Gephart, J. W., Spatial and temporal variations in stress from four years of aftershocks of the Loma Prieta earthquake [abstr.], *Eos*, 75, no. 44, 682, 1994.

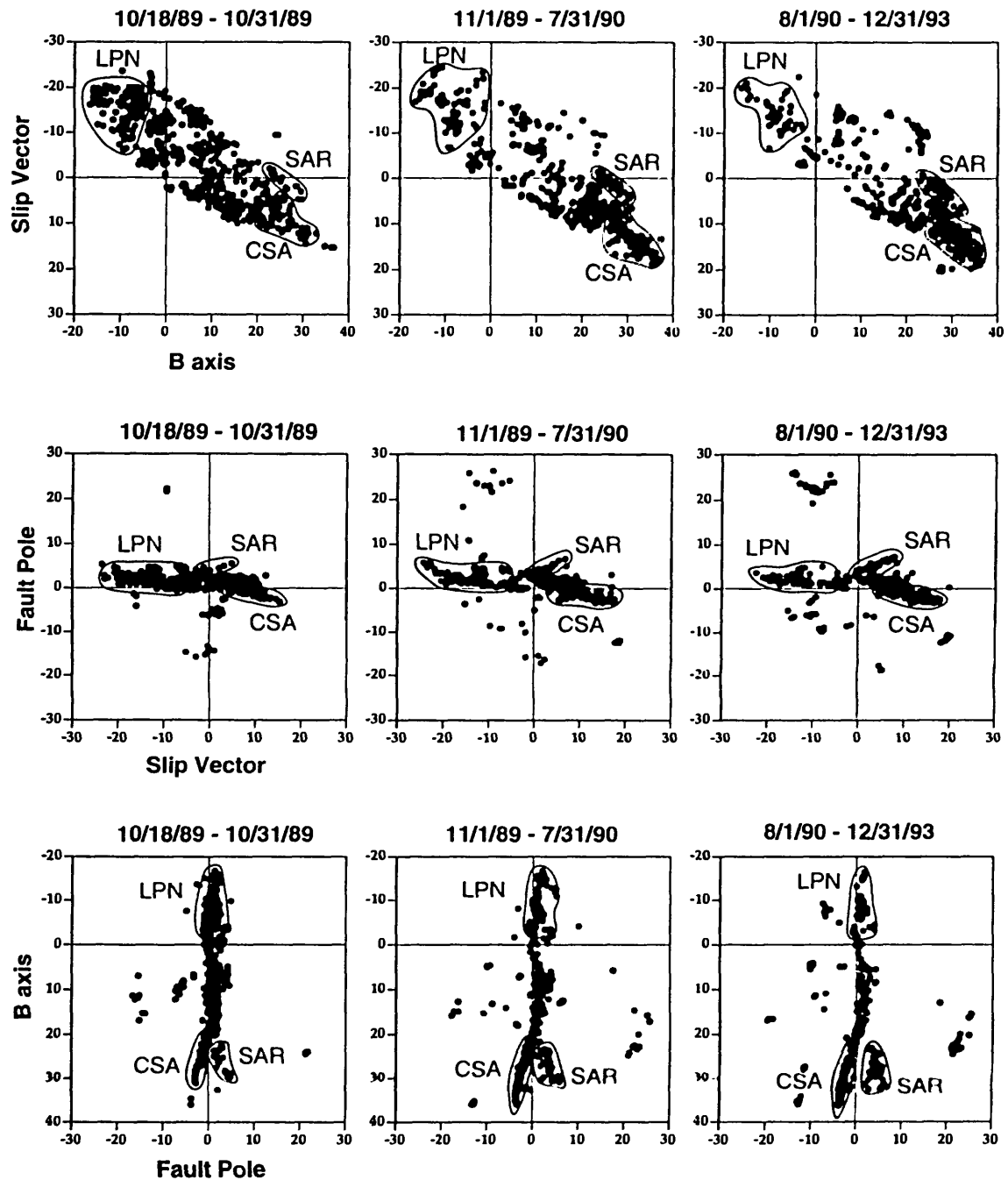


**Figure 1.** Orthogonal sections constructed on mainshock focal mechanism coordinates, for each of three time intervals. These are viewed in the direction of: (top) downward fault pole, (middle) downward B axis, and (bottom) downward slip vector. Scales in kilometers. As examples, three data subsets are indicated by irregular polygons.

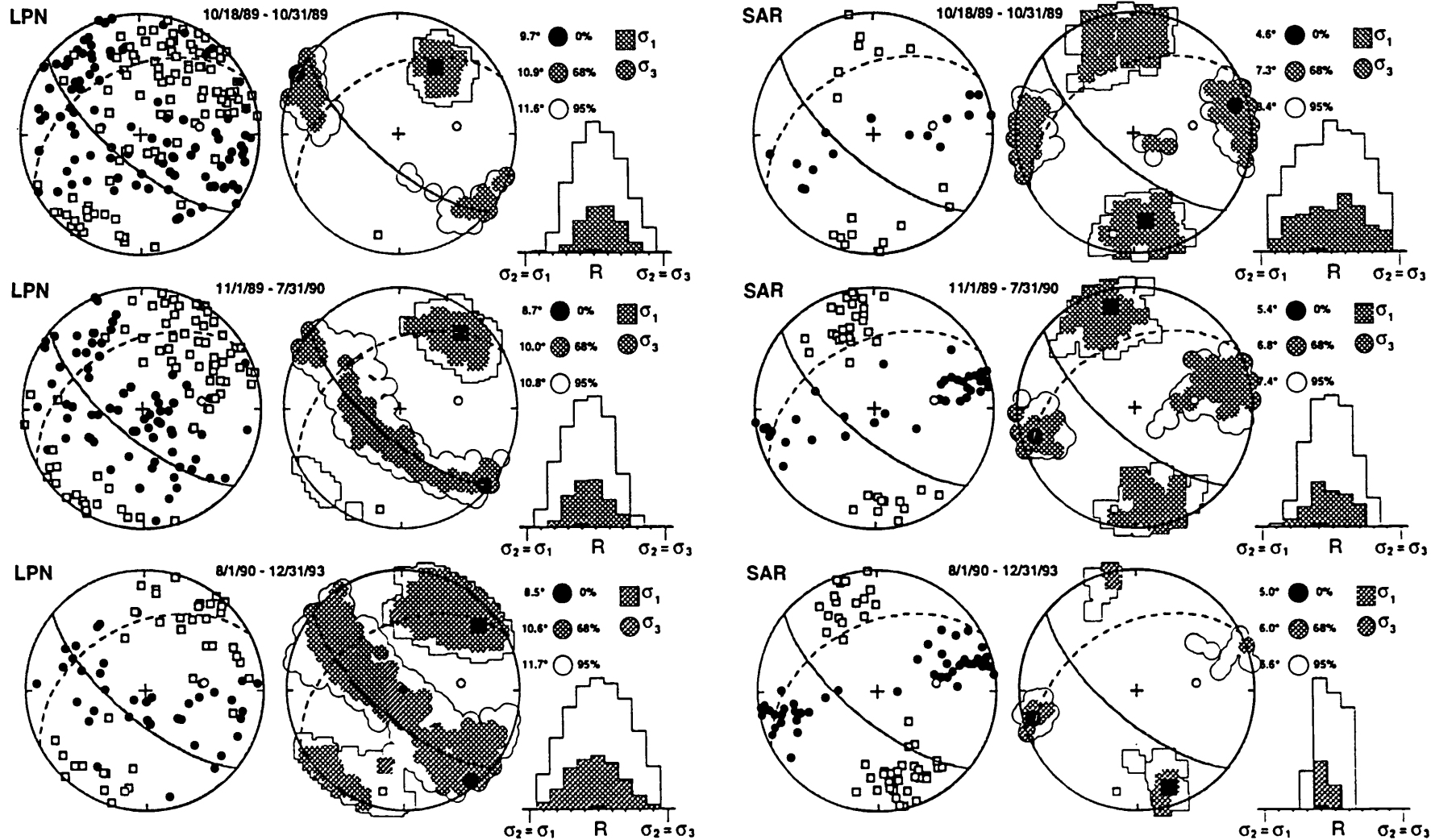


**Figure 2.** Data and results for each of three regions: (a) LPN (3 time intervals), (b) SAR (3 time intervals), and (c) CSA (6 time intervals). In each case, on the left are shown the P and T axes (open squares and filled circles, respectively) of the focal mechanisms, along with the mainshock mechanism (for reference only—mainshock datum was not used in the inversions); on the right are shown the acceptable models, indicated by a stereonet of  $\sigma_1$  and  $\sigma_3$  directions and a histogram of R values. Degrees of shading indicate the best model ("0%"), and ranges of the 68% and 95% confidence limits; the corresponding magnitude of average rotation misfits is shown at the upper right. The mainshock focal mechanism is shown on each plot for reference.

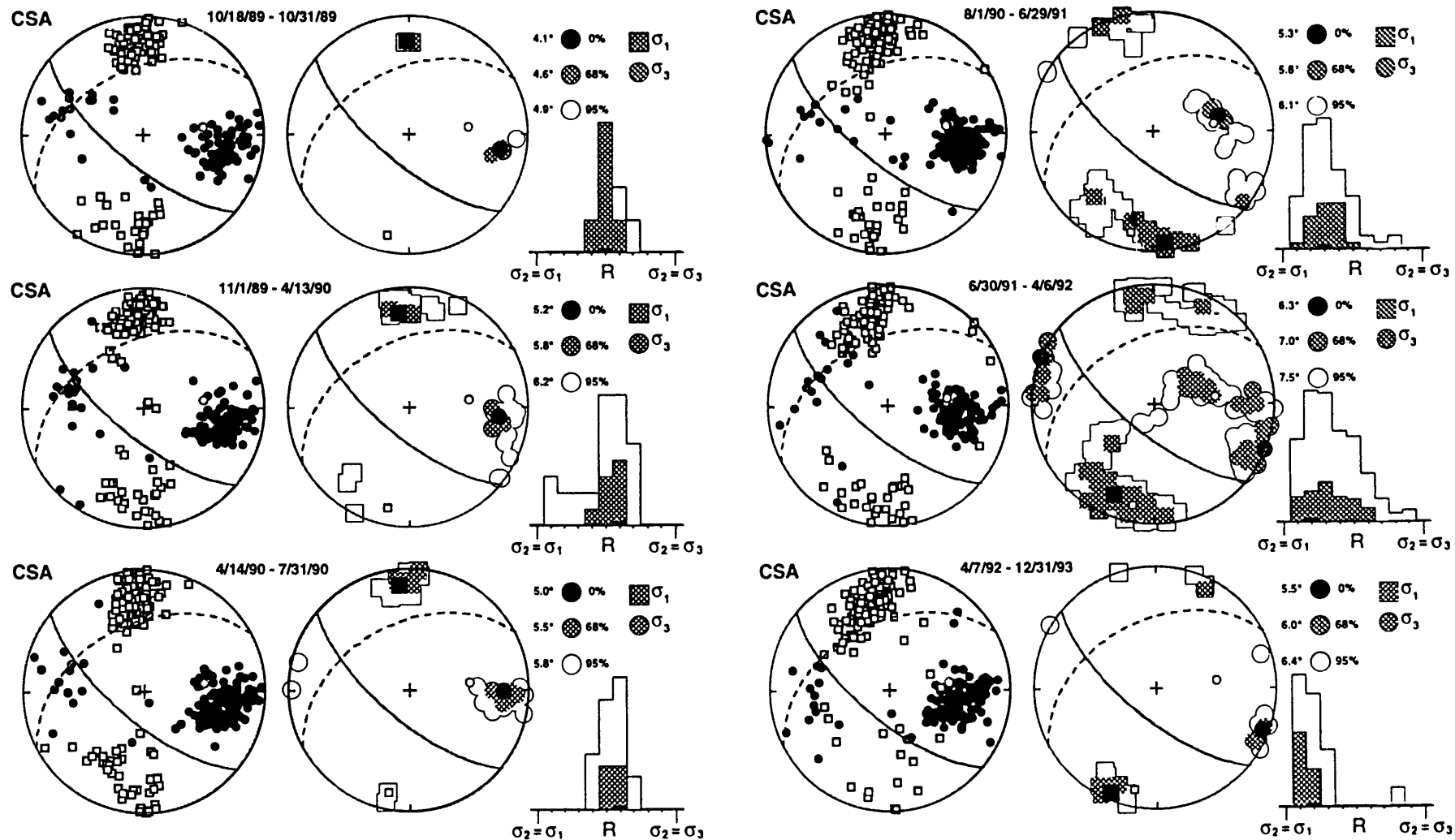
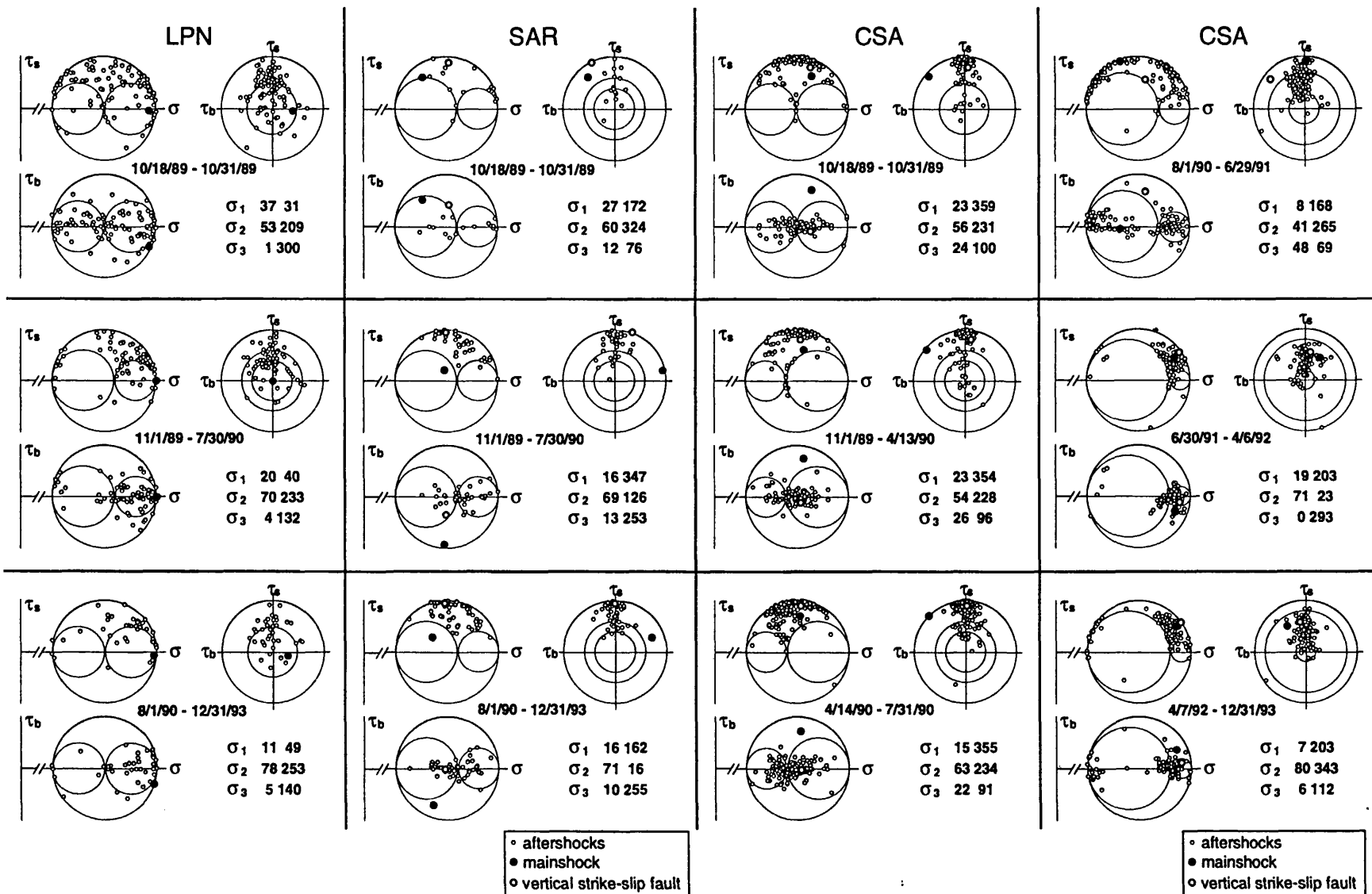


Figure 2. (continued)



**Figure 3.** Three orthogonal projections of the Mohr Sphere construction for each of the three regions in Figure 2, corresponding to the best-fitting stresses in each case. Fault geometries that are consistent with the stress model fall on the  $[\tau_b = 0, \tau_s > 0]$  half-plane. Both aftershock and mainshock mechanisms are shown. For areas SAR and CSA, a hypothetical vertical strike slip fault geometry is also shown—in each case, aligned with the earthquake epicenters (it is presumed that these reflect a realistic main fault geometry).

**Constraining the Regional Stress Tensor Directly  
from Seismic First-Motion Observations**  
Project Number USGS 1434-94-G-2412, -2439  
Program Element: II.2  
*J. W. Gephart<sup>1</sup>, G. A. Abers<sup>2,3</sup>*

<sup>1</sup>INSTOC, Snee Hall, Cornell University, Ithaca NY 14853

Phone: (607) 255-3538, Fax: (607) 254-4780, Email: [gephart@geology.cornell.edu](mailto:gephart@geology.cornell.edu)

<sup>2</sup>Lamont-Doherty Earth Observatory of Columbia University, Palisades NY 10964

<sup>3</sup>now at: Department of Geology, 120 Lindley Hall, University of Kansas, Lawrence KS 66045

Phone: (913) 864-2724, Fax: (913) 864-5276, Email: [abers@kuhub.cc.ukans.edu](mailto:abers@kuhub.cc.ukans.edu)

## Investigations Undertaken

The goal of this project is to devise a procedure for constraining the regional stress tensor from seismic first-motion observations. This approach follows the principles used in earlier work for inferring stresses from earthquake focal mechanisms, based on the assumptions that each mechanism is well-known and that the shear stress and slip directions are aligned on each failure plane (e.g., Gephart and Forsyth [1984], Gephart [1990a, 1990b]). This new inverse procedure is an improvement over the previous ones because it more realistically treats the uncertainty of the focal mechanism determinations from body wave first motions.

## Results

Our main effort to date has been to develop the inversion code; we are working to debug, streamline, and test it. The procedure is designed to execute two nested grid searches: (1) an outer loop which explores a prescribed range of the 4-parameter stress model space (defined by three principal stress directions and a value of  $R \equiv (\sigma_2 - \sigma_1)/(\sigma_3 - \sigma_1)$ ), and (2) an inner loop (performed at each node of the outer one) which compares the first-motion data of each event to completely diverse set of focal mechanisms (i.e., spanning the full range of possible ones) relative to the stress model at hand, which is passed down from the outer loop. The former is adapted from the original Focal Mechanism Stress Inversion algorithm (Gephart [1990b]); the latter is original to this study and is illustrated in Figure 1. Within the inner loop, each admissible focal mechanism is tested against each set of first motions (the data), and a fit statistic is calculated for each mechanism-event pair. Relative to a particular stress model, the best-fitting mechanism for each event is the one which minimizes the misfit among the first motions. The ensemble of these best-fitting mechanisms is then used to calculate a single statistic that characterizes the goodness of fit of each stress model to all of the data. We have attempted to modularize the code among the search strategies and statistical tests of fitness, so that we may debug and modify it efficiently.

In order to properly formulate an inverse problem of first motions, we are evaluating different minimization schemes and different formalisms for the statistics of first motion data. Brillinger *et al.* [1980] devised schemes for evaluating first motion solutions, and we attempt to follow their

formulation to some degree. A somewhat different, although related, approach has been taken by Reasenberg and Oppenheimer [1985]. In general, a given first motion observation  $d_{ij}$  (the  $i^{\text{th}}$  observation for the  $j^{\text{th}}$  event) has an a priori probability  $p_{ij}$  of being correct. The  $d_{ij}$  are treated as Bernoulli trials which have binomial distributions. The number of correct observations (picks that are matched by a given model) can then be used as a simple statistic with well-known properties. Provided that reasonable estimates of  $p_{ij}$  can be made one can estimate the variance associated with the (approximately normal) statistic, and standard  $F$  tests can be used to compare different models. Although such a formulation is normally used to evaluate a single focal mechanism it easily can be applied to a more complex model (such as a stress state) for a suite of events. Hypothesis testing is used to determine confidence limits on stress tensors and to test the resolvability of spatial/temporal changes in stress tensors. Also, we can test whether the number of correct picks is significantly less than expected for the best-fitting stress tensor, allowing us to evaluate whether our assumptions (e.g., a homogeneous stress field) are consistent. The approach for dealing with the error model is general, so that other kinds of data (e.g., S-wave polarities, misfits to waveform modeling) could be easily added in the future. Such an approach requires reasonable *a priori* estimates of picking probabilities  $p_{ij}$ , and we have put some effort into evaluating different ways to quantify variations in  $p_{ij}$ . Our approach has been to examine how picking success (number of correct picks ÷ number of picks; an estimate of  $p$ ) varies with different quantifiable parameters that are likely to influence their success (Figure 2). The Southern California data set is examined because it is very large and the number of well-constrained events are high, and because we are interested in stress variations here. We find that the simplest useful error models are parameterized by two numbers: a uniform probability of a picking blunder (instrument reversed, operator error, etc.) and a scaling term that quantifies how picking success varies with radiated amplitude or distance of a ray from nodal plane (Figure 2a). Because downgoing and refracted rays are problematical, a distance-dependent term may also be useful. It is interesting to note that the fraction of unpicked arrivals also varies systematically, and may form another source of information in more elaborate statistical models.

## References

- Brillinger, D.R., A. Udiás, and B.A. Bolt, A probability model for regional focal mechanism solutions, *Bull. Seismol. Soc. Am.*, 70, 149-170, 1980.
- Gephart, J. W., Stress and the direction of slip on fault planes, *Tectonics*, 9, 845-858, 1990a.
- Gephart, J. W., FMSI: A FORTRAN program for inverting fault/slickenside and earthquake focal mechanism data to obtain the regional stress tensor, *Computers & Geosci.*, 16, 953-989, 1990b.
- Gephart, J. W., and D. W. Forsyth, An improved method for determining the regional stress tensor using earthquake focal mechanism data: Application to the San Fernando earthquake sequence, *J. Geophys. Res.*, 89, 9305-9320, 1984.
- Reasenberg, P., and D. Oppenheimer, FPFIT, FPPLLOT, and FPPAGE: Fortran computer programs for calculating and displaying earthquake fault-plane solutions, *U.S. Geol. Surv. Open-File Rep.*, 85-739, 1985.

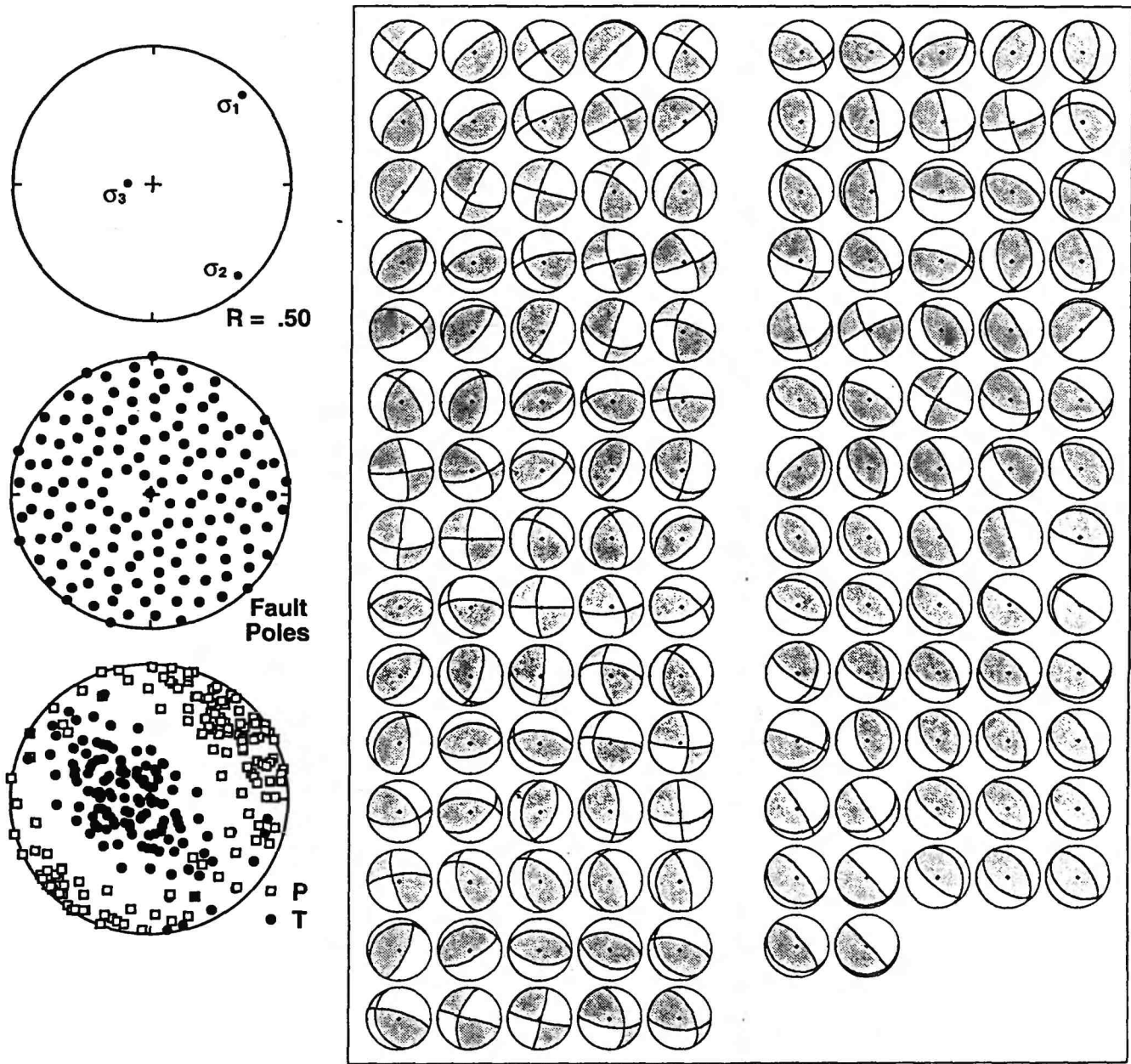


Figure 1. Example of gridding of focal mechanisms relative to a particular stress model, as performed in the inner loop of the inverse procedure. (Top left) A stress model, described by three principal stress directions and a value of  $R$ . (Middle left) A population of 142 fault poles, evenly distributed about the principal stress directions. (Bottom left) P and T axes of 142 focal mechanisms generated by predicting the slip direction on the 142 fault planes under the stress model in question. (Because the grid of fault poles is symmetric about the principal planes, the distribution of mechanisms is also symmetric, allowing for some efficiencies in computation.) (Right) 142 focal mechanisms spanning the range of all ones that are consistent with the stress model. For each event (and stress model), each of the first motion data is compared against each of the 142 mechanisms.

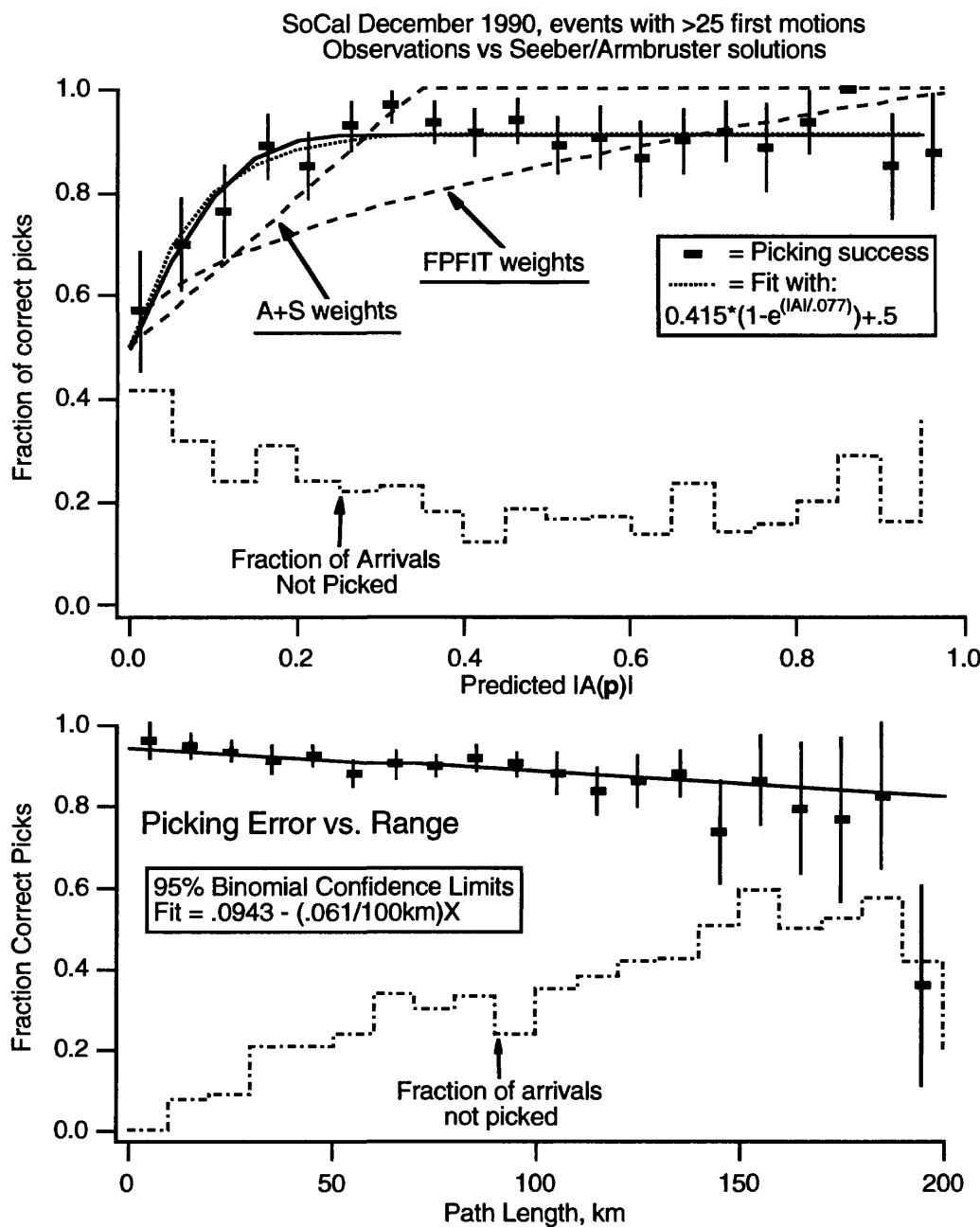


Figure 2. Variation of first motion picking success with  $P$  radiation amplitude (top) and with source-receiver distance (bottom). First motions from Southern California networks for December, 1990, and solutions from Seeber and Armbruster [1994, submitted to JGR]. Top figure uses all events with 25 or more first motions (41 events, 1761 picks), and bottom uses events with ten or more first motions (148 events, 3377 picks). Probabilities of correct picks and 95% confidence limits are estimated by assuming probability of incorrect pick (correct picks/total picks) has binomial distribution. Top figure shows an 8% chance of having an incorrect pick for most calculated  $P$  amplitudes  $|IA(p)|$ , increasing to 50% at nodes when predicted  $|IA(p)|$  is  $<0.2$  of peak values (rays  $<8^\circ$  from nodes). Also shown for top figure are best-fit exponential function, and predictions of weighting schemes for two programs that automatically fit first motions [Seeber and Armbruster, submitted 1994; Reasenberg and Oppenheimer, 1985], with weights scaled between 0.5 and 1.0. Note an increase in frequency of unpicked arrivals near nodes (arrival times without reported first motions), presumably reflecting low-amplitude arrivals; because these data show sensitivity to focal mechanism, it may be possible to incorporate them as weak constraints in inversions. Bottom data show deterioration in pick quality at distances past  $\sim 150$  km, where refracted arrivals become prevalent, and show necessity for downweighting these arrivals.

# DEEP BOREHOLE PLANE STRAIN MONITORING

## 1434-94-G2493

*Michael T Gladwin,*

Department of Physics  
 University of Queensland  
 St.Lucia, 4067  
 AUSTRALIA.  
 ph. (+ 617) 212 4562  
 fax (+ 617) 212 4455

### ACTIVITIES

(1) The seven year baseline of data now available from the array of three BTSM instruments at Parkfield has allowed investigation of BTSM strain data in conjunction with adjacent water well and rainfall data, to identify significant regional long term strain. These data have been compared with other data sets from dilatometers and the 2-color geodetic network.

(2) The continuing long term anomaly in shear strain data measured at San Juan Bautista was monitored, and an emerging anomaly in  $\gamma_2$  shear strain evident since 1993 has been identified.

(3) The effects of cross coupling of areal and shear strains on borehole strain measurements were studied using comparison of data from the BTSM and the Laser strainmeter at Pinon Flat observatory. These investigations are necessary to achieve accurate calibration of the BTSM instruments. Tidal calibration using only ocean load corrected earth tides as references has been found to be inadequate because of the considerable influence of topography and geology.

(4) Routine processing of strain data from the seven BTSM instruments in California was continued. In particular, the archive of strain data in the Menlo Park system was updated, and reports were prepared for consideration at each of the regular Parkfield experiment meetings.

### RESULTS

(1) Strain data from two Borehole Tensor Strain instruments at Parkfield shows a significant anomaly emerging in 1993, continuing until at least mid- 1994. This data is shown in Figure 1. Other Parkfield data (Dilatometers, water well levels, and two-color geodetic measurements) show anomalies over the same period - see Figure 2. Since 1977, four  $M_L > 4$  earthquakes have occurred near Parkfield. Three of these occurred in Oct. 1992, April and Nov. 1993, during the anomaly. Possible hydrologic influence in the strain data due to recharge of the aquifer level after the 1993 rainfall was considered but was found to be unlikely to account for the strain changes observed, particularly the alteration in  $\gamma_1$  gradient at Eades in mid 1993, and in  $\gamma_2$  gradient at Frolich in late 1993. The relationship of this anomaly to the December 1994  $M_L 5$  earthquake at Parkfield is under investigation.

Consideration of a wide range of possible models of fault behaviour to account for these strain observations suggested that a model with aseismic slip of 15 mm/year on a 4km long by 1 km wide surface propagating to the northwest and towards the surface (5 km to 0.5 km depth) over the course of 18 months best predicts the measured shear strain anomalies. This patch is shown in Figure 3, and is broadly consistent with the microearthquake anomaly (P. Malin, *personal comm.*), and velocity anomaly determined from vibroseismic imaging (E. Karageorgi, *personal comm.*) which were both reported at Fall 1994 AGU.

(2) Data from the BTSM near San Juan Bautista show a continuing accumulation of  $\gamma_1$  shear strain at approximately 1.9 microstrain/year, which has been relatively constant since the Loma Prieta earthquake in 1989. The  $\gamma_2$  shear strain was close to zero for two years after that event, and is now increasing at 0.7 microstrain per year, as shown in Figure 7. This change in shear strain indicates an increase in fault normal extension, and would be expected to increase the probability of a medium sized earthquake in this region.

(3) Calibration of the Pinon Flat BTSM instrument, taking cross coupling of areal and shear strains into account, was achieved by the derivation of a general calibration equation relating the regional strain field being measured to the observed instrument transducer readings. This process brings earth tides from the Pinon Flat Borehole Tensor Strainmeter into very good agreement with tides from the co-located Laser Strainmeter. A typical result is shown in Figure 4, in which diagram (a) indicates a comparison of the  $O_1$  and  $M_2$  tidal components of  $\gamma_1$  from the BTSM and Laser (LS) instruments, using only ocean load corrected earth tides to calibrate the BTSM. (b) indicates the similar comparison using a full cross coupling calibration of the BTSM. This result demonstrates the intrinsic inadequacy for calibration purposes of ocean load correction algorithms provided by the literature.

(4) Incorporating cross-coupling and the effects of layers with differing modulus allows borehole strain to provide good discrimination of earthquake source parameters. The Pinon Flat BTSM observations of the Landers earthquake support the Hudnut et al (1994) model. For the Big Bear earthquake, they support the Harvard CMT moment ( $M_L = 6.5$ ). They indicate deep slip for the Joshua Tree earthquake. These results are shown in Figure 5. It was found that beyond epicentral distances of several crustal thicknesses, the effects of crustal layering must be considered for accurate (~10%) modelling of earthquake strain steps. Neglect of cross-coupling at the Pinon Flat BTSM would produce errors of 10% to 20% for comparable strain components, and proportionately larger errors if strain components are not comparable. Such effects may be expected at all borehole strainmeter sites.

(5) The new deployments in the San Francisco (Hayward fault) area are now providing useful shear data. Examples of the strain data from the Garin site are shown in Figure 6, for the period following the installation of mains power at the site as required by the site owners. Performance of the Chabot site is under review, with coupling of one gauge component not yet characterised. Tides on both instruments are less than normal expectations. This is certainly not a topographic effect, and is also evident on colocated dilatometer data.

(6) Two papers were published during the year, one detailing results of strain changes observed during the Landers earthquake, and one paper analysing the series of episodic strain/creep events detailed in earlier volumes, and presenting a modelled slip region which accounts for these results. Both the Parkfield anomaly and the Pinon Flat calibration results described above were presented at the Fall AGU meeting. Two further papers were also jointly presented at this meeting.

## RELEVANT PUBLICATIONS.

### 1994 Publications

- Gladwin, M.T., Gwyther, R.L. and Hart, R.H.G. A Shear Strain Anomaly Following the Loma Prieta Earthquake. *U.S. Geol. Surv. Prof. Pap.* (in press).
- Gladwin, M. T., Breckenridge, K.S., Gwyther, R. L. and Hart, R. Measurements of the Strain Field Associated with Episodic creep events at San Juan Bautista, California. *J. Geophys. Res.*, Vol 99 (B3), 4559-4565, 1994.
- Gwyther R.L., Gladwin M.T. and Mee M.W. A Continuing Strain Anomaly Observed on Parkfield Borehole Tensor Strain Array. *EOS. (Trans. Am. Geo. Un.)* 75(44), p 438, 1994.
- Hart R., Gladwin, M.T., Gwyther R.L., Wyatt F.K. and Agnew D.C. Improved Interpretation of borehole strain data from recent Californian events by inclusion of cross-coupling between strain components. *EOS. (Trans. Am. Geo. Un.)* 75(44), p 438, 1994.
- Linde, A.T., Johnston M.J.S., Gladwin, M.T., and Breckenridge K.S. Modelling of a Slow Earthquake Sequence near San Juan Bautista, California, in December 1992 *EOS. (Trans. Am. Geo. Un.)* 75 No 16 ,p 113, 1994.
- Linde, A.T., Johnston M.J.S., Gladwin, M.T., and Breckenridge K.S. A Sequence of Three Slow Earthquakes Near San Juan Bautista and Related Seismicity *EOS. (Trans. Am. Geo. Un.)* 75(44), p 447, 1994.
- Wyatt, F.K, Agnew, D.C. and Gladwin M.T. Continuous Measurements of Crustal Deformation for the 1992 Landers Earthquake Sequence. *Bull. Seis. Soc. Am.*, Vol 84, No 3, 768-779, 1994.

### Previous Publications

- Gladwin, M. T., High Precision multi component borehole deformation monitoring. *Rev.Sci.Instrum.*, 55, 2011-2016, 1984.
- Gladwin, M.T., Gwyther, R., Hart, R., Francis, M., and Johnston, M.J.S., Borehole Tensor Strain Measurements in California. *J. Geophys. Res.* 92. B8 pp7981-7988, 1987.
- Gladwin, M. T. and Hart, R. Design Parameters for Borehole Strain Instrumentation. *Pageoph.*,123, 59-88, 1985.
- Gladwin, M. T. and Wolfe, J. Linearity of Capacitance Displacement Transducers. *J.Sc.Instr.* 46, 1099-1100, 1975.
- Gladwin, M.T., Gwyther, R.L., Higbie, J.W. and Hart, R.G., A Medium Term Precursor to the Loma Prieta Earthquake? *Geo. Res. Let.* 18 #8 pp 1377-1380, 1991.
- Gladwin, M.T., Gwyther, R.L. and Hart, R.H.G. A Shear Strain Precursor. *U.S. Geol. Surv. Prof. Pap.* 1550-C, 59-66, 1993.
- Gladwin, M.T., Linde A.T., Gwyther, R.L. and Hart, R.H.G. Triggering of Slow Strain Events at San Juan Bautista. *EOS. (Trans. Am. Geo. Un.)* 74(43), p 182, , 1993.
- Gwyther, R. L., Gladwin, M.T. and Hart, R., A Shear Strain Anomaly Following the Loma Prieta Earthquake. *Nature* 356, 142-144, 1992

- Johnston M.J.S., Linde A.T., Myren D., Gladwin M.T. and Breckenridge K. A Slow Earthquake on the San Andreas Fault near San Juan Bautista, California, December 1992. *EOS, (Trans. Am. G. Un.)* 74(43), p 182, 1993.
- Johnston, M.J.S., Gladwin, M.T., and Linde, A.T. Preseismic Failure and Moderate Earthquakes. *I.A.S.P.E.I.*, Tokyo, August 19-30, S7-65, 35, 1985.
- Johnston, M. J. S., Linde, A.T., Gladwin, M.T., and Borcherdt, R.D. Fault Failure with Moderate Earthquakes. *Tectonophysics*. 144, 189-206, 1987.
- Linde, A.T., Gladwin, M.T. and Johnston, M.J.S. The Loma Prieta Earthquake, 1989 and Earth Strain Tidal Amplitudes: An Unsuccessful search for Associated Changes. *Geo. Res. Lett.* 19(3), 317-320, 1992.
- Linde, A.T., Gladwin, M.T. and Johnston, M.J.S. Borehole Strain Measurements of Solid-Earth-Tidal Amplitudes. *U.S. Geol. Surv. Prof. Pap.* 1550-C, 81-85, 1993.
- Lindh, A.G, Breckenridge K. and Gladwin M.T. Seismicity and Creep at Parkfield *Proc. 8th Joint Meeting of US-Japan Conf. Natural Res., Panel Earthquake Pred.Tech.*, p 214, 1993.
- Lindh, A.G., Breckenridge K, Johnston, M.J.S. and Gladwin, M.T. Seismicity and Creep at Parkfield: Building a Better Relationship. *Seis. Res. Lett.* 64(1), p 32, 1993.
- Wyatt F.K., Agnew D.H., Johnson H. and Gladwin M.T. Postseismic Strains and Tilts from the Landers Earthquakes: Fault Afterslip, Crustal Anelasticity, or Local Hydrology? *EOS. (Trans. Am. Geo. U.)* 74(43), p 183, 1993.

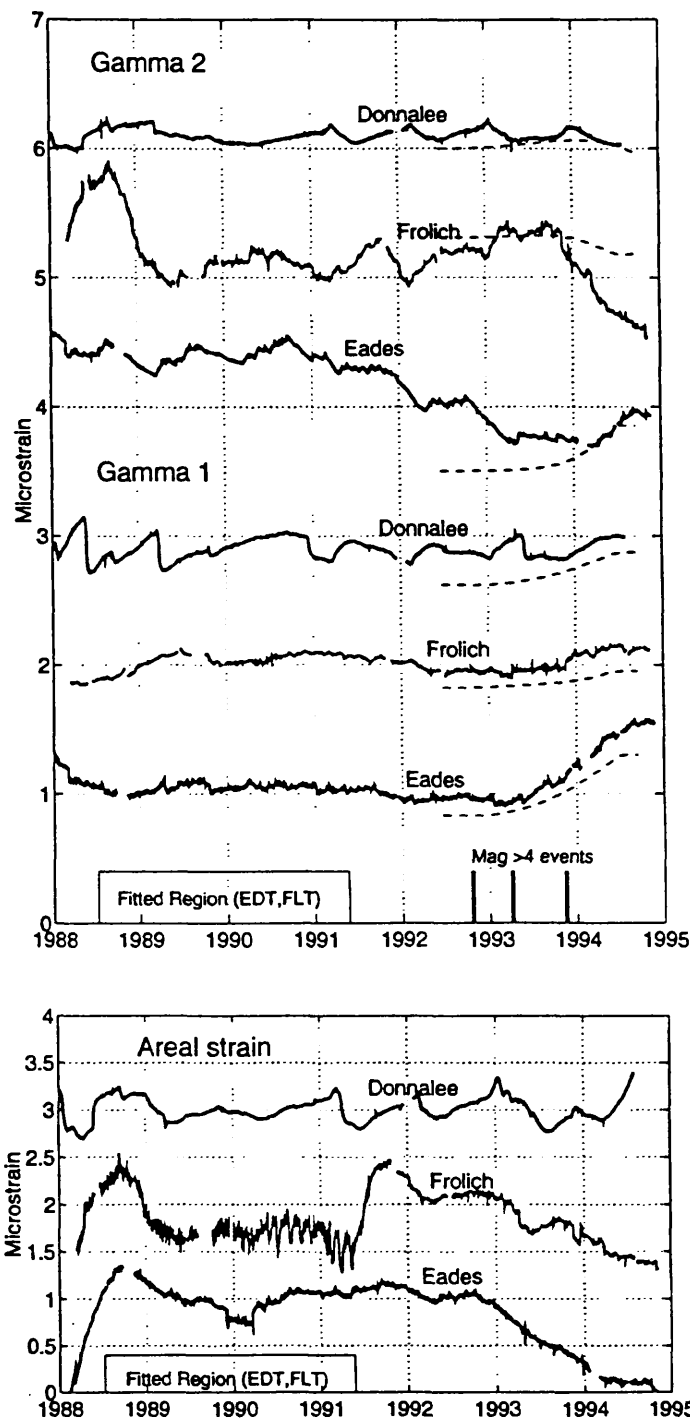


*Figure 1.*

Strain data  $\epsilon_a$ ,  $\gamma_1$  and  $\gamma_2$  from the BTSM instruments at Donalee, Frolich and Eades at Parkfield. The data from Frolich and Eades have been processed by removal of exponentials to account for long term creep of the borehole inclusion, and setting of expansive grout. The Donalee data was also fitted to the rate of change of the water level at nearby WJC water well. This BTSM instrument is situated close to an active aquifer and is consequently sensitive to water level changes during each rainy season. Note the predominant changes in  $\gamma_1$  at Eades in mid 1993, and in  $\gamma_2$  at Frolich in late 1993. Earthquakes with a magnitude  $> 4$  during the period shown in the graph are indicated by vertical lines. Dotted lines above the shear strain curves indicate the modelled strain changes.

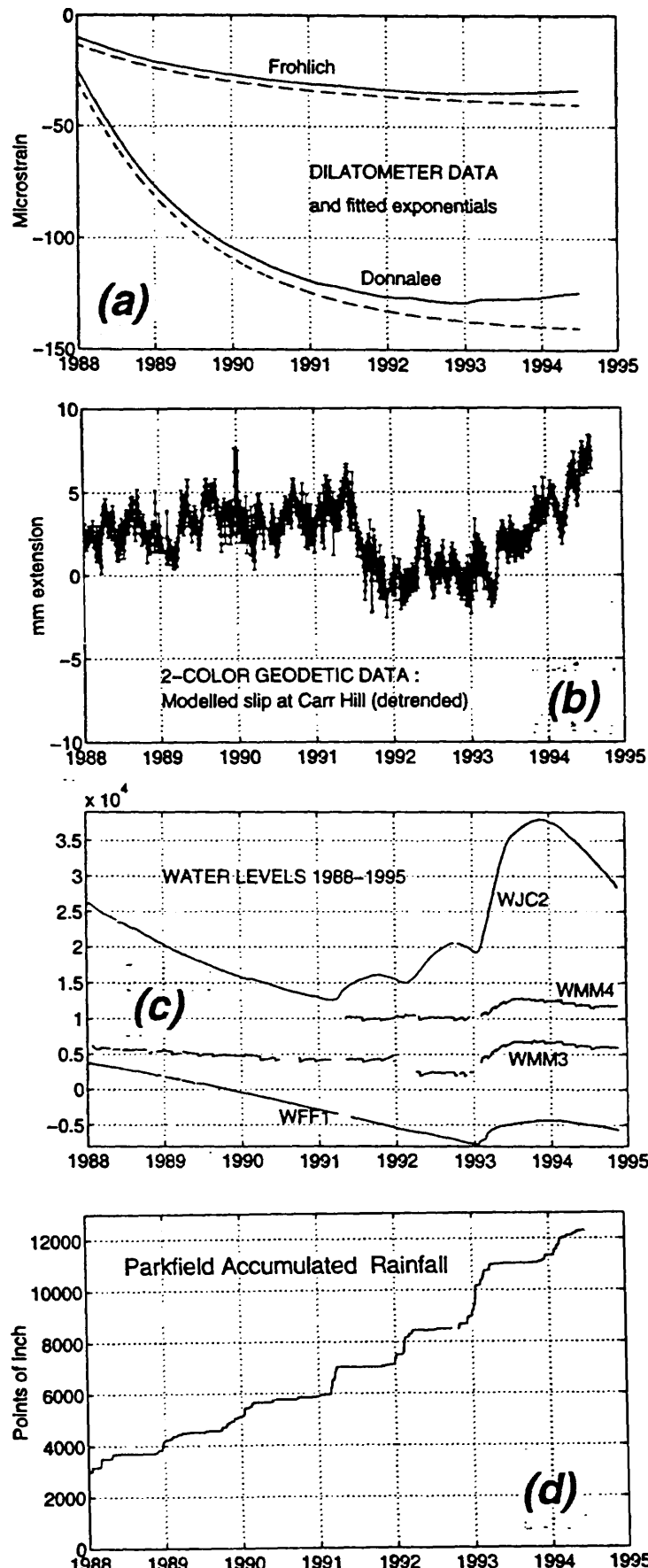


**Figure 2.**  
 Data from Dilatometers at Frolich and Donalee, and geodetic data from the 2-color laser array centred at Carr Hill, resolved as slip on a 5km region of the fault extending downwards 20 km. Rainfall and water well data is also shown.

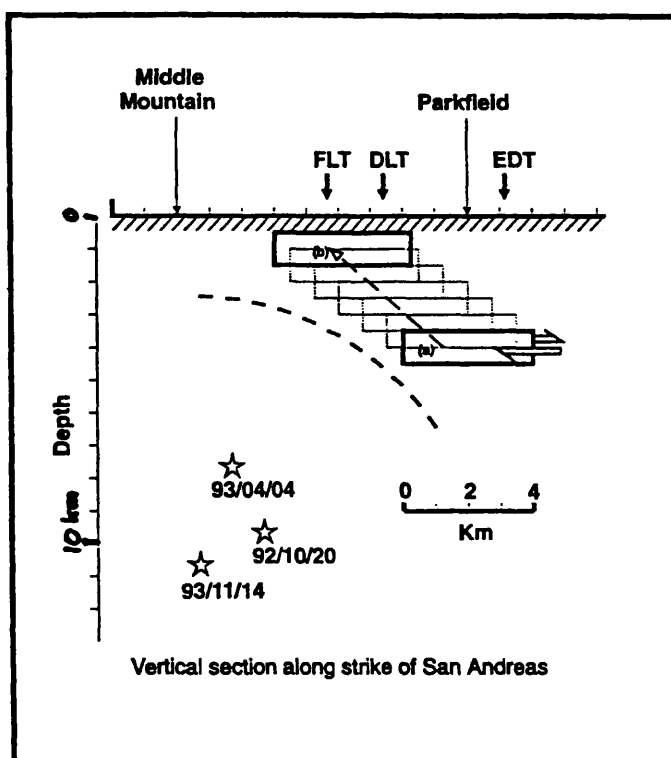


*Figure 3.*

Proposed model to account for the observed shear strain changes. The patch shown is taken to have a total of 15 mm aseismic slip per year, and propagates over 12-18 months from position (a) to position (b).

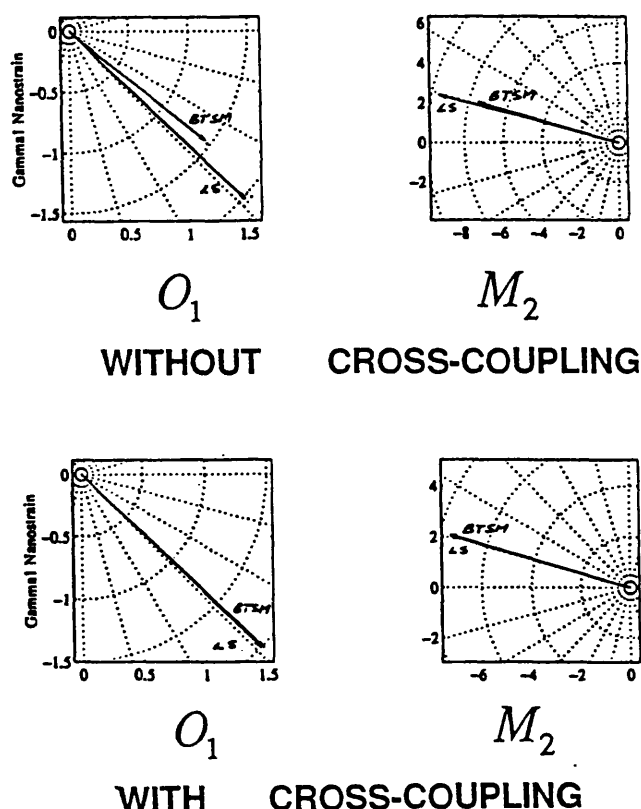


*Figure 4.*

A comparison of the  $O_1$  and  $M_2$  tidal components of  $\gamma_1$  shear strain from the BTSM and the Laser Strainmeter. Section (a) shows the BTSM data using only ocean load corrected theoretical earth tidal strain for calibration, whilst section (b) shows BTSM data using the full cross-coupling calibration result.

## BIG BEAR (strains in nanostrain)

	BTSM (no Xcoupling)	BTSM (with Xcoupling)	BTSM (with Xcoupling & layer correction)	Model $M_o = 7 \times 10^{18} \text{ Nm}$ (geodetic -Hudnut et al 1994 - moment $\sim 2$ )
$e_a$	80	98 $\pm$ 7	112 $\pm$ 7	112
$\gamma_1$	-60	-22 $\pm$ 6	-24 $\pm$ 6	-22
$\gamma_2$	-118	-148 $\pm$ 4	-145 $\pm$ 4	-173
$S$ (max shear)	132	150 $\pm$ 4	147 $\pm$ 4	174
$e_a / S$	0.606	0.654 $\pm$ 0.05	0.755 $\pm$ 0.05	0.641
$\phi_{PA}$ (E of N)	-31.5°	-40.7° $\pm$ 1.2°	-49.7° $\pm$ 1.2°	-41°

## LANDERS (strains in nanostrain)

	BTSM (no Xcoupling)	BTSM (with Xcoupling)	BTSM (with Xcoupling & layer correction)	Model (geodetic -Hudnut et al 1994)
$e_a$	796	757 $\pm$ 34	890 $\pm$ 34	864
$\gamma_1$	-1281	-1188 $\pm$ 17	-1246 $\pm$ 17	-1171
$\gamma_2$	-228	-601 $\pm$ 19	-636 $\pm$ 19	-718
$S$ (max shear)	1301	1332 $\pm$ 18	1399 $\pm$ 18	1374
$e_a / S$	0.612	0.569 $\pm$ 0.027	0.636 $\pm$ 0.027	0.629
$\phi_{PA}$ (E of N)	175°	166.6° $\pm$ 0.4°	166.5° $\pm$ 0.4°	164°

## JOSHUA TREE (strains in nanostrain)

	BTSM (no Xcoupling)	BTSM (with Xcoupling)	BTSM (with Xcoupling & layer correction)	Model $M_o = 1.6 \times 10^{18} \text{ Nm}$ L=10km, Strike = N9W, Dip=90 D=9-15km
$e_a$	145	114 $\pm$ 6	120 $\pm$ 6	120
$\gamma_1$	-213	-235 $\pm$ 3	-231 $\pm$ 3	-241
$\gamma_2$	88	38 $\pm$ 4	41 $\pm$ 4	56
$S$ (max shear)	230	238 $\pm$ 4	234 $\pm$ 4	248
$e_a / S$	0.630	0.447 $\pm$ 0.027	0.478 $\pm$ 0.027	0.486
$\phi_{PA}$ (E of N)	11.2°	4.6° $\pm$ 0.4°	4.9° $\pm$ 0.4°	6.5°

Figure 5.

Observed strain steps at Pinon Flat BTSM, using (1) ocean load corrected tidal stral calibration, (2) cross-coupling calibration, and (3) cross-coupling calibration with a two layer model of high and low rigidity modulus, for the three earthquakes Landers, Big Bear and Joshua Tree. Comparison is with geodetically determined models of these earthquakes.

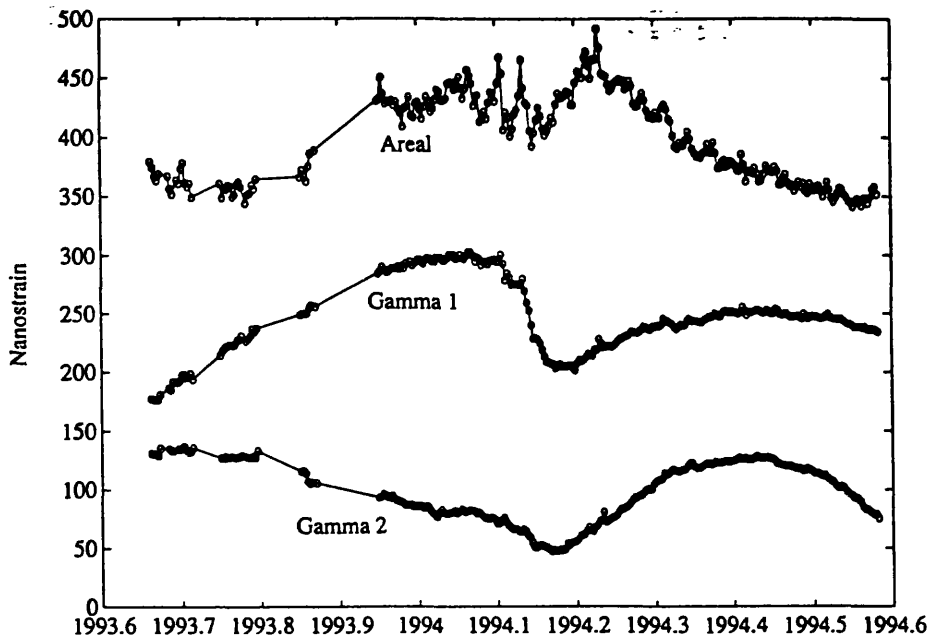


*Figure 6.*

Daily averages of data from the Garin site for twelve months after installation of mains power (with appropriate exponentials removed to account for grout cure and borehole stress recovery as usual). The stability at the 100 Nanostrain level is already apparent, together with a possible anomaly during January 1994.

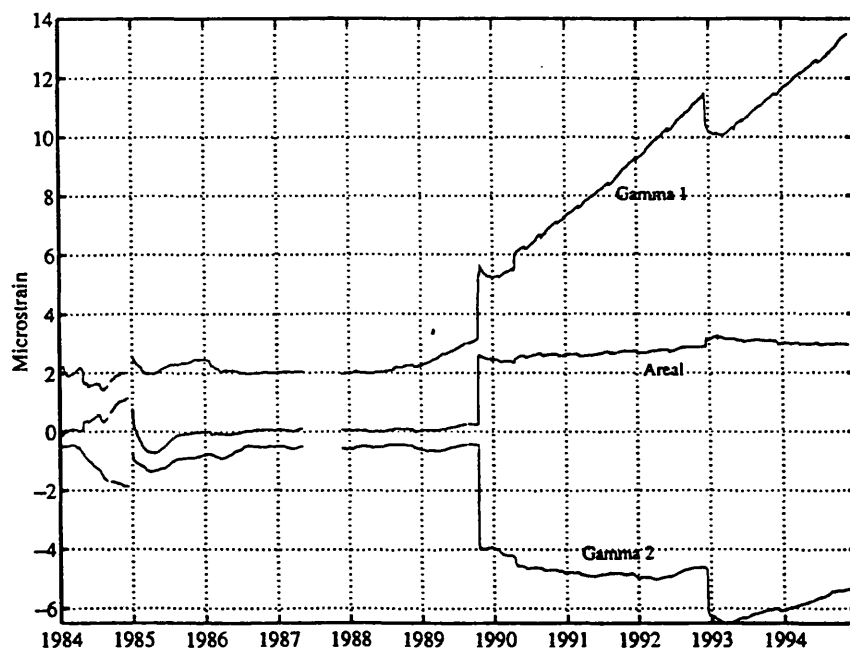


*Figure 7.*

Areal strain  $\epsilon_a$  and shear strains  $\gamma_1$  and  $\gamma_2$  measured near San Juan Bautista. Note the change in  $\gamma_2$  gradient in late 1992, which continued after the slow earthquake sequence in December 1992.

**ORIGIN AND AGE OF THE ST. FRANCIS SUNKLANDS  
USING DRAINAGE PATTERNS, SEDIMENTOLOGY, AND  
DENDROCHRONOLOGY**

Margaret J. Guccione

University of Arkansas  
Geology Department OZARK-118  
Fayetteville, AR 72701

(501) 575-3354  
(501) 575-3846 FAX  
GUCCIONE@COMP.UARK.EDU

Roy B. Van Arsdale

University of Memphis  
Department of Geological Sciences  
Memphis, TN

(901) 678-4356  
(901) 678-2178 FAX  
RBVARSDALE@CC.MEMPHIS.EDU

David W. Stahle  
Malcolm K. Cleaveland  
University of Arkansas  
Geography Department OZAR-108A  
Fayetteville, AR 72701

(501) 575-3159  
(501) 575-3846 FAX  
DS27527@UAFSYSB.UARK.EDU  
MC25095@UAFSYSB.UARK.EDU

**Element II.5**

**Identify active faults, their geometry, their characteristics,  
and dates of past earthquakes.**

**INVESTIGATIONS UNDERTAKEN**

The St. Francis Sunklands is a an open-water to swampy area along the St. Francis River, and is located a few km upstream of the confluence of the St. Francis River with the Left Hand Chute of the Little River in northeastern Arkansas (Fig. 1). This area was referred to as a "sunkland" and its origin was attributed to deformation during the 1811-1812 New Madrid earthquakes (Fuller, 1912). More recently Saucier (1970) attributed the origin of the St. Francis Sunklands to alluvial drowning of relict braided stream channels where a major crevasse channel of the Mississippi River (Left Hand Chute of the Little River) had aggraded faster than its tributary streams. The first purpose of this project was to determine when the lake had been formed and to determine if its

time of origin is consistent with that of the 1811-1812 seismic events. The second purpose of the project was to determine if earlier lakes had existed that may also have resulted from surface deformation and drainage disruption by earlier seismic events. The third purpose was to determine the response of baldcypress in the lake to the 1811-1812 earthquakes and identify any similar signatures in the tree ring record prior to 1811.

This project included describing and sampling 22 cores from Lake St. Francis, the St. Francis River, and adjacent sunkslands (Fig. 2). Fourteen additional cores from two north-south transects, one east and one west of Lake St. Francis, were also described and sampled (Fig. 3). Samples were analyzed for grain size, total carbon content, and pollen. Eleven samples of wood from these cores were dated using radiocarbon analysis. One hundred and six trees living at the time of the 1811-1812 seismic event were sampled for dendrochronological analyses along the northern margins of the lake to search for a possible tree growth response to that event. The annual rings of these cores were exactly dated by matching climatically controlled patterns of annual tree growth in the Lower Mississippi Valley (Stokes and Smiley, 1968).

## RESULTS

Bathymetric and sedimentologic data allowed us to map the former course of the St. Francis River channel through the present sunkland (Fig 4). Within this channel the lacustrine sediment that overlies bedded sand is thin to absent apparently because currents pass through the old channel and continue to prevent deposition. Adjacent to the channel, lacustrine sediment buries a poorly developed, slightly mottled soil marked by large roots and thin, discontinuous clay films. In one core a deposit of liquefied sand separates the lacustrine sediment from the underlying overbank alluvium (Fig. 4B). Twentieth century deposition, as a result of ditch/levee construction projects, is up to 2.5 m thick in the channel of the St. Francis River just south of the lake (Fig. 5).

Basal lacustrine sediment at 2 sites and sediment buried by liquefied sand is radiocarbon dated  $160 \pm 60$  to  $240 \pm 130$  radiocarbon years BP, consistent with the 1811-1812 New Madrid earthquakes (Fig. 4B and C). Thus, the most recent sunkland origin is attributed to subsidence caused by these earthquakes. Based on landsurface elevations, total Holocene subsidence is estimated to be 3.2 m over a distance of 2.8 km, though maximum flexure is 2.5 m in 1 km immediately south of the Sunkslands (Fig. 6). This down-to-the-north deformation is opposite the direction of the regional southerly slope and appears to have partially caused impoundment of the St. Francis River.

There is evidence that the southern margin of the lake may have been impounded prior to the present drowning. Three organic-rich horizons, similar to the organic mat at the base of the

lacustrine sediment, are present in the sunklands southwest of the lake (Fig. 4D). The upper dates are in stratigraphic order and suggest sudden drowning of the site, perhaps caused by seismic events  $4040 \pm 170$  and  $8130 \pm 60$  years BP. The date on the oldest organic mat is stratigraphically inverted and the age of this unit is uncertain.

Tree-ring data from bald cypress trees in the lake area clearly indicate that the St. Francis Sunklands site experienced severe ground motion during the 1811-1812 earthquakes. This disturbance is manifested by severely suppressed radial growth in the surviving trees for up to 40 years after 1811 (Fig. 7). Most of these cores were too traumatized to permit exact dating, and the numerical chronology actually derived is based on trees which were not as severely impacted as most. Therefore the St. Francis tree-ring chronology definitely underestimates the tree growth effects of the 1811-1812 earthquakes.

The baldcypress growth suppression at Lake St. Francis probably reflects physical trauma to the trees caused by major ground shaking. Tree-ring chronologies derived from baldcypress trees therefore provide an excellent tool in the search for ancient earthquakes in the New Madrid seismic zone. The four decades following 1811 stand out as the most severe episode of growth suppression in the entire 668-year long chronology for the St. Francis Sunklands (Fig. 8). This suggests that the Sunklands site did not experience any other earthquakes comparable in magnitude to the 1811-1812 events between 1321 and 1811 AD.

These tree-ring data do not clearly support or refute the tectonic or geomorphic theories for the origin of Lake St Francis in particular, and the St. Francis Sunklands in particular. However, the absence of severe trauma between 1321 and 1811 AD is consistent with the radiocarbon dates of the most recent prior drowning event in the lake area ( $4030 \pm 170$  B.P.). This is date considerably older than the 1321 AD date of the baldcypress chronology.

#### REPORTS PUBLISHED

1. Guccione, M. J., Miller, Jonathan Q., Van Arsdale, Roy B., 1994. Amount and timing of deformation near the St. Francis "Sunklands", northeastern Arkansas: Geological Society of America Abstracts with Programs, v. 26, no. 1, p. 21.
2. Van Arsdale, Roy B., Stahle, David W., and Cleaveland, Malcolm K., 1994. New Madrid earthquake signals in baldcypress at Reelfoot Lake, TN, and Lake St. Francis, ARK: Geological Society of America Abstracts with Programs, v. 26, no. 1, p. 20.

## REFERENCES CITED

- Fuller, M. L., 1912, The New Madrid Earthquake, U. S. Geological Survey Bull. 494: U. S. Printing Office, Washington D. C., 119 p.
- Saucier, R. T., 1970, Origin of the St. Francis Sunk Lands, Arkansas and Missouri, Geological Society of America Bulletin, v. 81, p. 2847-2854.
- Stokes, M. A. and Smiley, T. L., 1968, An Introduction to Tree-Ring Dating: Chicago, University of Chicago Press, 73 p.

**PLEASE REPLACE THE FOLLOWING FIGURE TITLES**

**Figure 4.** Cross sections of cores at A) northern portion of Lake St. Francis, B) central portion of Lake St. Francis, C) southern portion of Lake St. Francis and D) south end of Lake St. Francis. Location of selected radiocarbon dates is shown. Vertical exaggeration = 20x.

**Figure 5.** Cross section of the St. Francis River at first bend south of Lake St. Francis. Vertical exaggeration = 5x.

**Figure 6.** Cross section along the St. Francis River from the southern end of Lake St. Francis to 1 km south of the Siphons. Cross section is oblique to inferred trend of deformation (Figure 3). Vertical exaggeration = 630x.

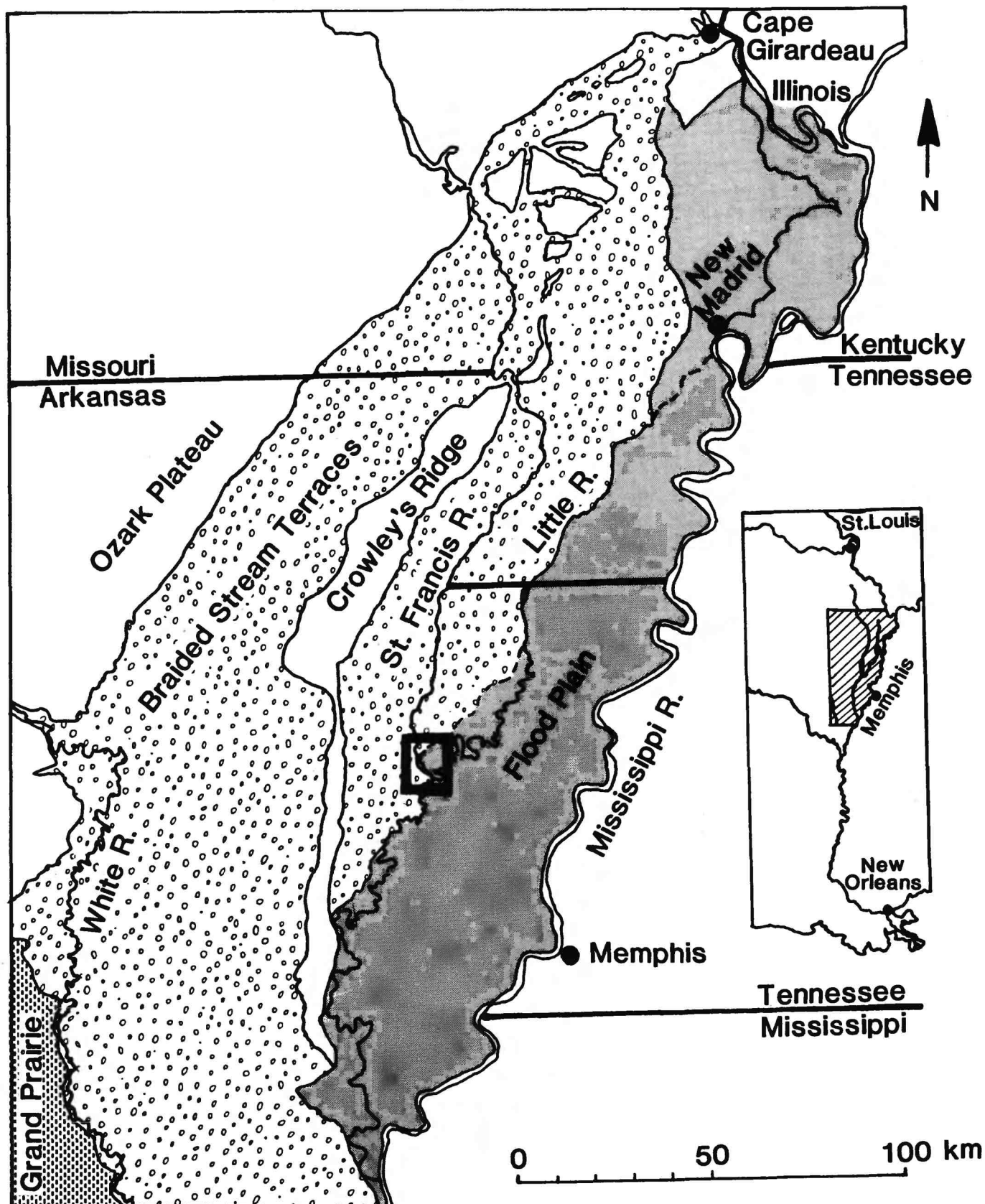


Figure 1. Geomorphic map of the northern portion of the Lower Mississippi Valley. Study area is outlined in box. Locations of cores are shown in Figures 2 and 3.

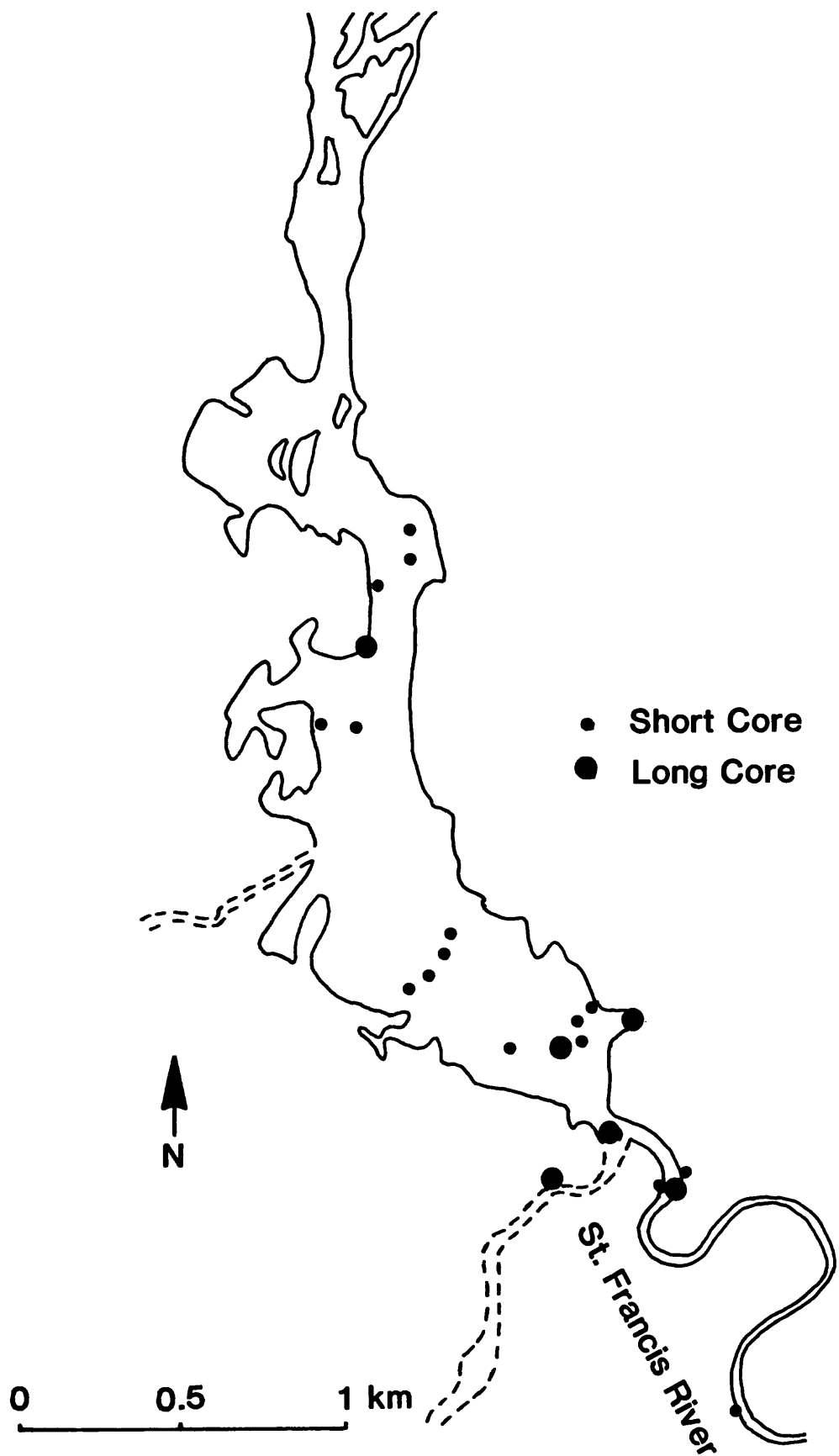


Figure 2. Location of cores in Lake St. Francis and the St. Francis River.

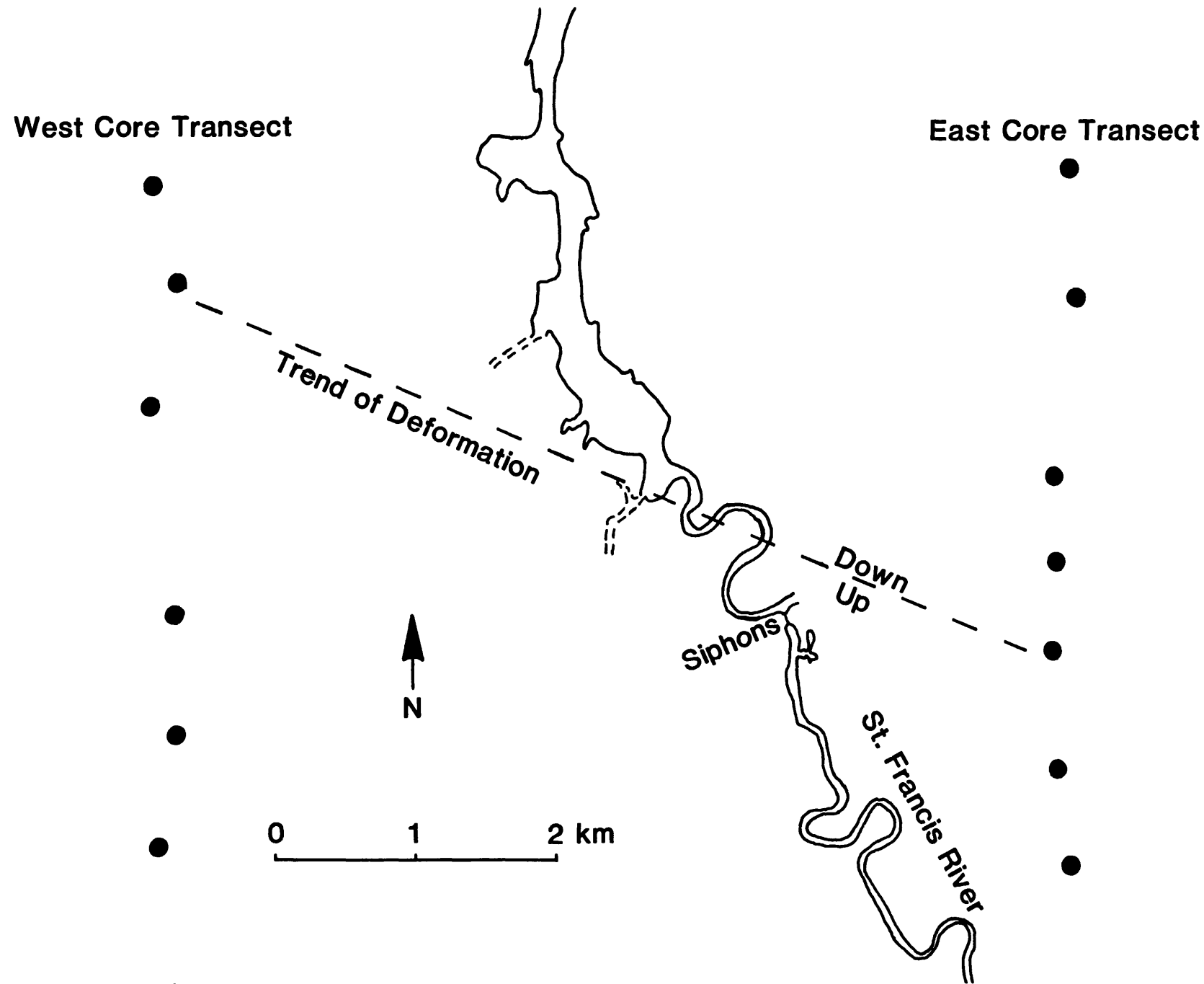


Figure 3. Location of cores in north-south transects east and west of Lake St. Francis. Inferred location of deformation is shown.

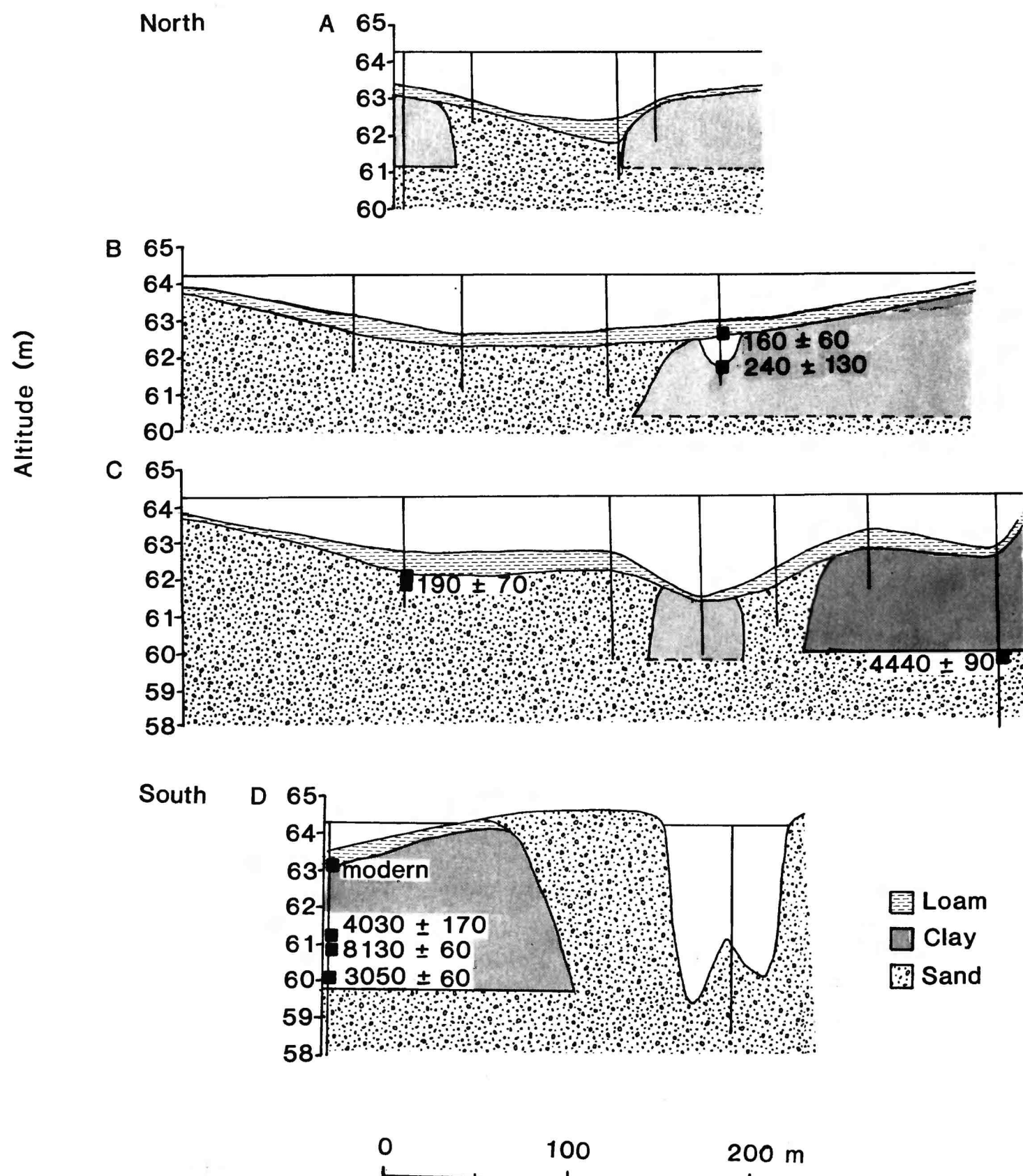


Figure 4. Cross sections of cores at A) northern portion of Lake St. Francis, B) central portion of Lake St. Francis, C) southern portion of Lake St. Francis and D) south end of Lake St. Francis. Location of selected radiocarbon dates is shown.

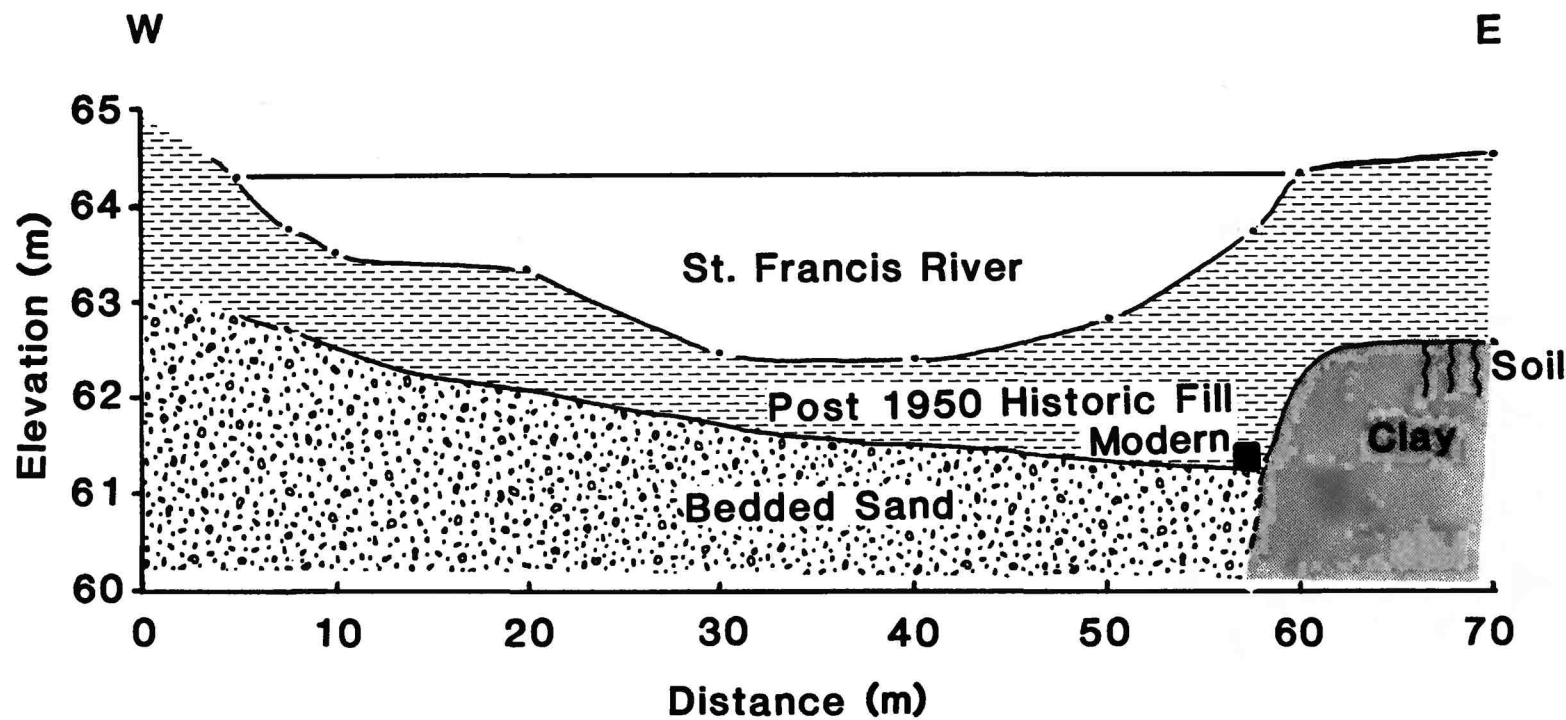


Figure 5. Cross section of the St. Francis River at first bend south of Lake St. Francis.

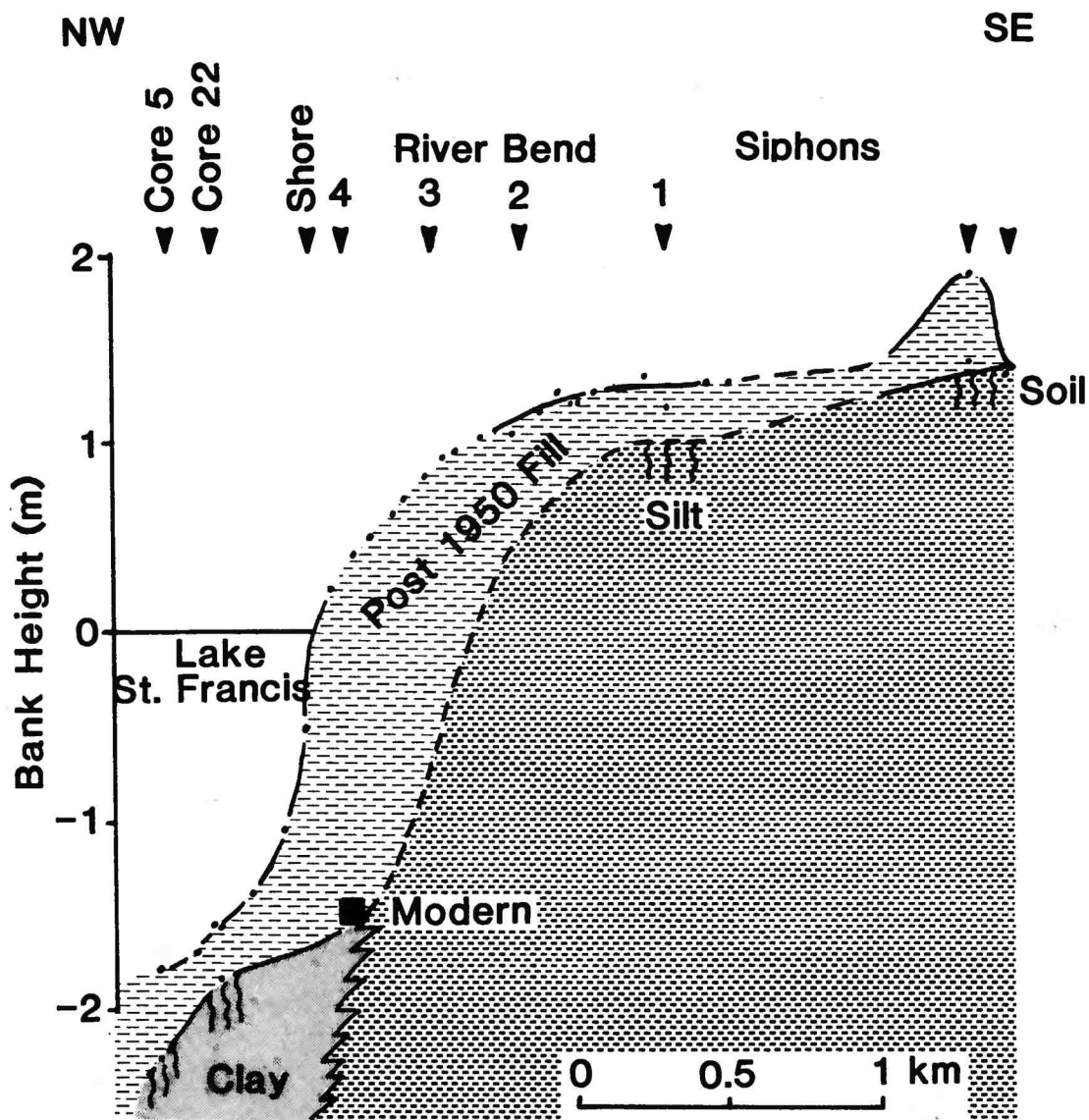
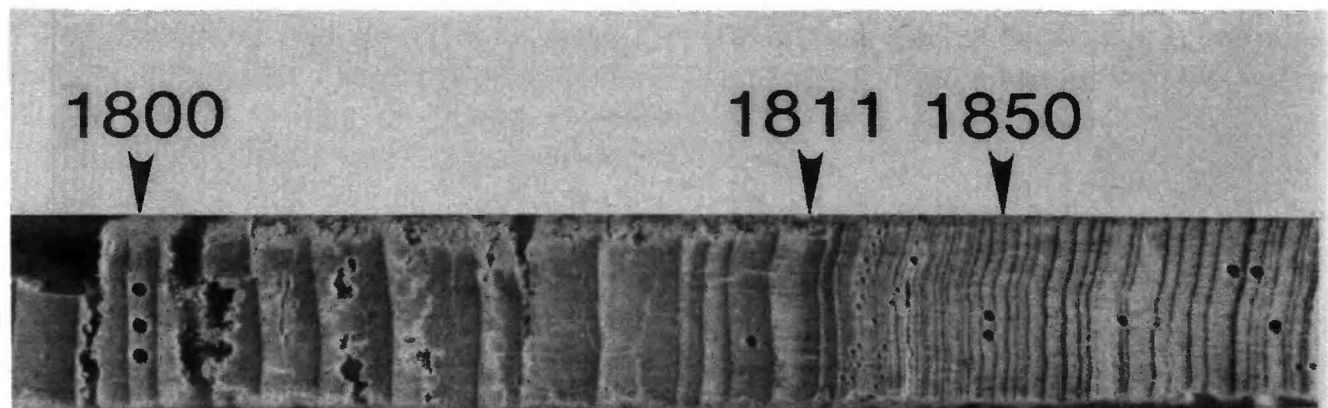


Figure 6. Cross section along the St. Francis River from the southern end of Lake St. Francis to 1 km south of the Siphons. Cross section is oblique to inferred trend of deformation (Figure 3).



**Figure 7.** Photograph of St. Francis Sunk Lands core 22B from one of the few trees that can be dated through the period immediately following the 1811-1812 earthquakes, which is characterized by many missing rings. Note that this tree grew less from 1812 to 1850 (39 years) than it did from 1807 to 1811 (5 years).

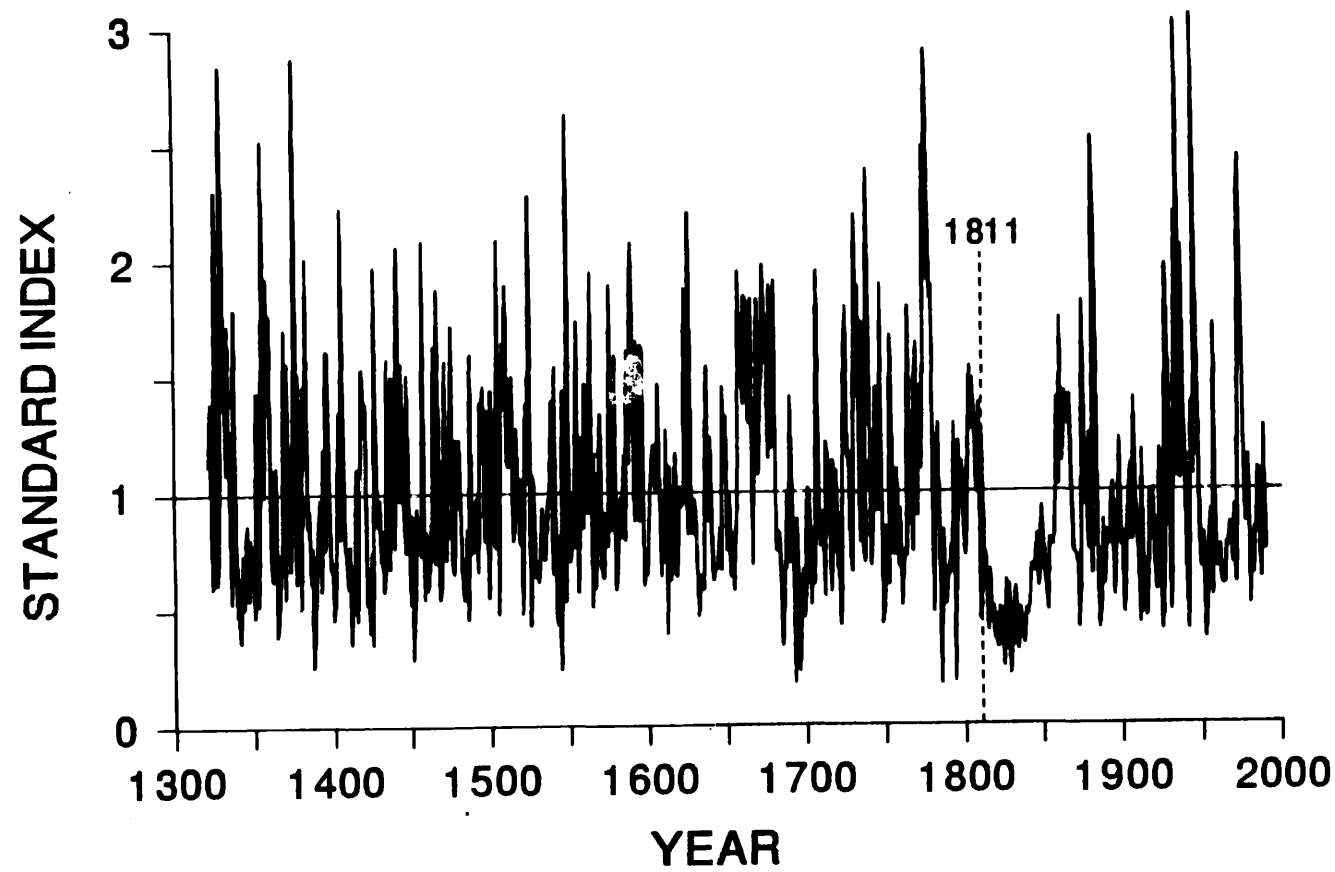


Figure 8. Plot of the St. Francis Sunk Lands tree-ring chronology 1321-1990.

## Paleoseismicity of the Castle Mountain Fault System

project number: 9310-23

Peter J. Haeussler  
 Branch of Alaskan Geology  
 U.S. Geological Survey  
 4200 University Dr.  
 Anchorage, AK 99508-4667  
 (907) 786-7447 office  
 (907) 786-7401 facsimile  
 pheuslr@tardaddy.wr.usgs.gov

Program element: PN:II:5 (Identify active faults, define their geometry, and determine the characteristics and dates of past earthquakes)

### Investigations

The Castle Mountain fault is located near half the population of Alaska (fig. 1), has historic seismicity—possibly up to magnitude 7, yet has only had a reconnaissance level of investigation. Early workers divided the Castle Mountain fault into two physiographic segments—the Talkeetna Mountains segment and the Susitna Lowlands segment. There has been no unequivocal evidence of Holocene surface faulting on the Talkeetna mountains segment, but Holocene surface faulting is apparent along the Susitna Lowlands segment as indicated by a discontinuous right-stepping series of scarps. I worked to better assess the earthquake hazard of this fault in two ways: by mapping an important area between the two previously mapped segments of the fault, and by trenching across the Castle Mountain fault in the Susitna Lowland in order to place constraints on the timing of paleoseismic events.

#### *Mapping Between Houston and the Hatcher Pass Road*

USGS workers in the mid-1970's mapped much of the Castle Mountain fault, but left a 30-km long area near the population center of the Matanuska Valley unmapped. I examined this area for surface faulting by producing a surficial geologic map (fig. 1) using aerial photographs, and then field checking this map and examining suspicious linear features on the ground. Two previously unidentified faults were found with scarps 1.5- to 4.4-m high that have been active in late Quaternary and possibly Holocene time (fig. 1). These faults are located several kilometers north of the inferred trace of the Castle Mountain fault sensu strictu and indicate there has been active deformation and surface faulting over a larger area than previously appreciated. Also, the Castle Mountain fault sensu strictu was traced in the Houston area about 3 km farther to the east than previously recognized onto an abandoned terrace of the Little Susitna River.

#### *Trenching Across the Castle Mountain Fault in the Susitna Lowland*

One trench by USGS workers in the early 1970's indicated there had been surface faulting on the Castle Mountain fault between 2349 and 1287 calibrated radiocarbon years before present and 225 yr BP based on dendrochronology. Two additional trenches across the fault in the late 1970's did not yield any additional information about the timing of ancient earthquakes. In order to better constrain the age of paleoseismic events nine trenches were dug across the Castle Mountain fault in the summer of 1994 (fig. 1). Trenching sites were dictated in part by access, and in part by where permission could be obtained to conduct trenching. Trenching sites were located in a range of soil types, with varying scarp heights, and different right-stepping segments of the fault. Some

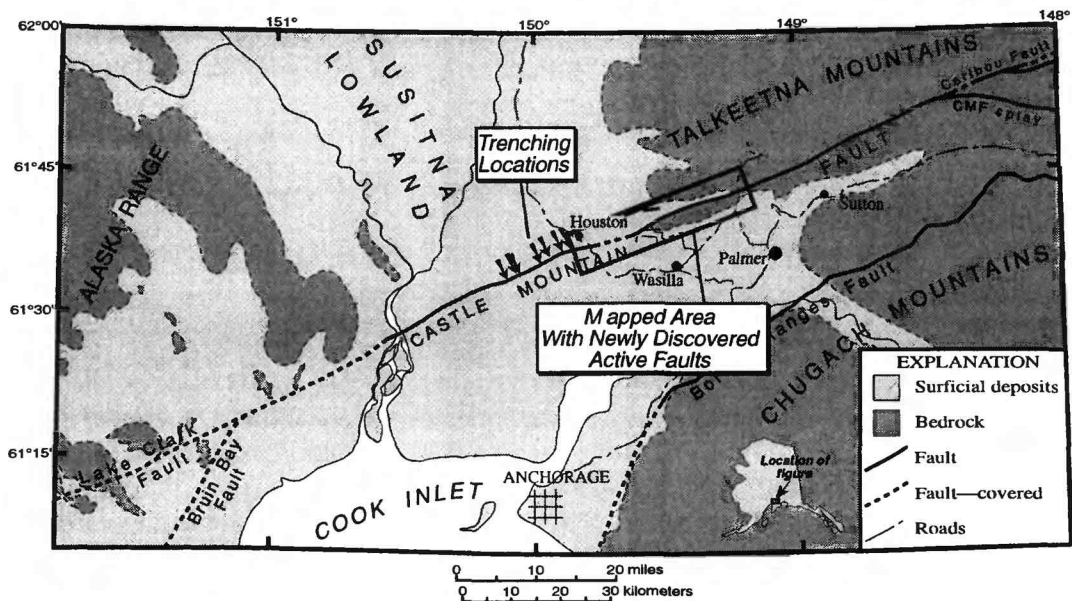


Figure 1. Simplified geologic map of upper Cook Inlet region, showing regional extent of Castle Mountain fault and location of study area.

trenches were extremely wet, and water pumps were used to keep the trenches drained and stabilize the trench walls. The walls of the trenches were mapped at a scale of 1 to 12 or 24. Samples for <sup>14</sup>C dating, tephrachronology, and soil samples were collected from all trenches. Photomosaics of the walls of the trenches and 8 mm video were also taken.

Results of trenching show: 1) Thrust motion across the fault of up to 4 feet since deposition of till, approximately 10,000-13,000 years ago. There was evidence for some thrust deformation in 7 of the 9 trenches. There was strong evidence for strike-slip faulting in one trench and suggestions of it in four more. In most cases, the surface faulting was accompanied by liquefaction and a zone of disruption 3 or more meters wide. 2) There has been recent seismic shaking along the Castle Mountain fault, as indicated by abundant liquefaction features in most trenches, which intrude the base of the modern A soil horizon. Liquefied material that was extruded onto the Earth's surface and overlies a paleosol was observed in only one trench. 3) Liquefaction affected every sediment type. As might be expected, fluvial sand and gravel, and eolian sand showed abundant evidence of liquefaction. In addition, most trenches with diamicton (till) also exhibited evidence of liquefaction in the main region of faulting. Liquefaction of till is probably enhanced by freeze-thaw processes and downward translocation of clay- and silt-sized sediment. 4) Because liquefaction features intruded the base of the A soil horizon, the ground was not frozen at the time of seismic shaking. The geologic record of surface faulting in this subarctic region would look very different if the event occurred in the winter rather than the summer. 5) The modern root mat is strong and probably does not tear or break during surface faulting—at least when the ground is not frozen. The implication is that surface faulting in this heavily vegetated environment generally does not produce a fault scarp from which colluvium can be derived, and therefore, scarp-derived colluvium overlying a paleosol below a scarp face is rare. As a result, dating paleoseismic events is difficult. The one location where liquified material overlay a paleosol was in an unusual vegetative environment where there were atypical grassy tussocks without a coherent root mat, rather than the normal shrub tundra. 6) The effects of soil forming processes, liquefaction, and frost action are not always readily distinguished. In areas where the groundwater was within a meter of the ground surface these effects were amplified and parent sedimentary material in the modern soil is not

identifiable. In some cases, it could be shown that cobbles transported by liquefaction were later modified by frost action.

### Results

1. Finished a surficial geologic map of the Houston to Hatcher Pass Road area that shows active faults. The map is being prepared for publication.
2. Wrote a paper on "Possible active fault traces on or near the Castle Mountain fault between Houston and the Hatcher Pass Road," for a USGS Bulletin. The paper describes two previously unrecognized faults active in late Pleistocene and probably Holocene time.
3. Trenched across the Castle Mountain fault in the Susitna Lowland at nine locations. Preliminary results are outlined above, but constraints on the age of surface faulting events will be obtained in the near future when  $^{14}\text{C}$  dates are returned. Summarizing the results of the trenching for publication is in progress.

### Reports Published

Haeussler, P. J., in press, Possible active fault traces on or near the Castle Mountain fault between Houston and the Hatcher Pass Road, in Till, A., and Moore, T., eds., U.S. Geological Survey Accomplishments in Alaska, 1993, U.S. Geological Survey Bulletin 2107.

**PALEOSEISMIC INVESTIGATIONS OF THE SAN ANDREAS FAULT  
ON THE SAN FRANCISCO PENINSULA**

Contract No. 14-08-0001-G2114

N. Timothy Hall  
Geomatrix Consultants  
100 Pine Street, 10<sup>th</sup> Floor  
San Francisco, California 94111  
(415) 434-9400

Robert H. Wright  
Kevin B. Clahan  
Harlan Tait Associates  
1269 Howard Street  
San Francisco, California 94103  
(415) 626-0765

**INTRODUCTION**

This report summarizes progress on the third phase (FY 94) of a multi-year investigation of the late Quaternary paleoseismic history of the San Francisco Peninsula reach of the San Andreas fault (SAF). Our research has focused primarily on the Filoli Estate, where ongoing deposition on an alluvial fan has preserved a late Holocene paleoseismic record. To date, our detailed geologic investigations at this site include detailed topographic mapping, geomorphic analysis, and logging and interpretation of 980 meters of backhoe trenches and stream channel wall exposures.

The Filoli site is located approximately 1 km southeast of Upper Crystal Springs Reservoir and about 8 km northwest of the town of Woodside (Figure 1). The study area is on the western margin of the SAF zone, where the head of an active, eastward draining alluvial fan is cut by the 1906 trace of the SAF. The fan was constructed by Spring Creek, which drains an area of approximately 3 km<sup>2</sup> on the northeast flank of the Santa Cruz Mountains. The Spring Creek basin is underlain primarily by sandstone of the Butano Formation of Eocene age. Poorly indurated gravels, sands, and fine-grained units of the Santa Clara Formation of Quaternary age, which are present in the lower reaches of the basin, also contribute sediment to the Spring Creek fan. Elevations of the fan surface at the study site vary between about 355 and 350 feet above mean sea level. The currently active channel of Spring Creek is incised from 2 to 4 meters below the surface of the fan, probably as a result of logging and grazing within the drainage basin during the past 100 to 150 years.

The study area and vicinity have been modified by cultural activities that may have spanned several thousand years. The most recent activities include plowing the upper 20 to 30 cm of the fan surface for agricultural purposes during the past 80 years. Before Spanish colonization and extending back at least 2000 years (based on archaeological information from the site), the local Ohlone Indians developed a large midden immediately south of the study area, which is bisected by the 1906 trace of the SAF. The impact of ground

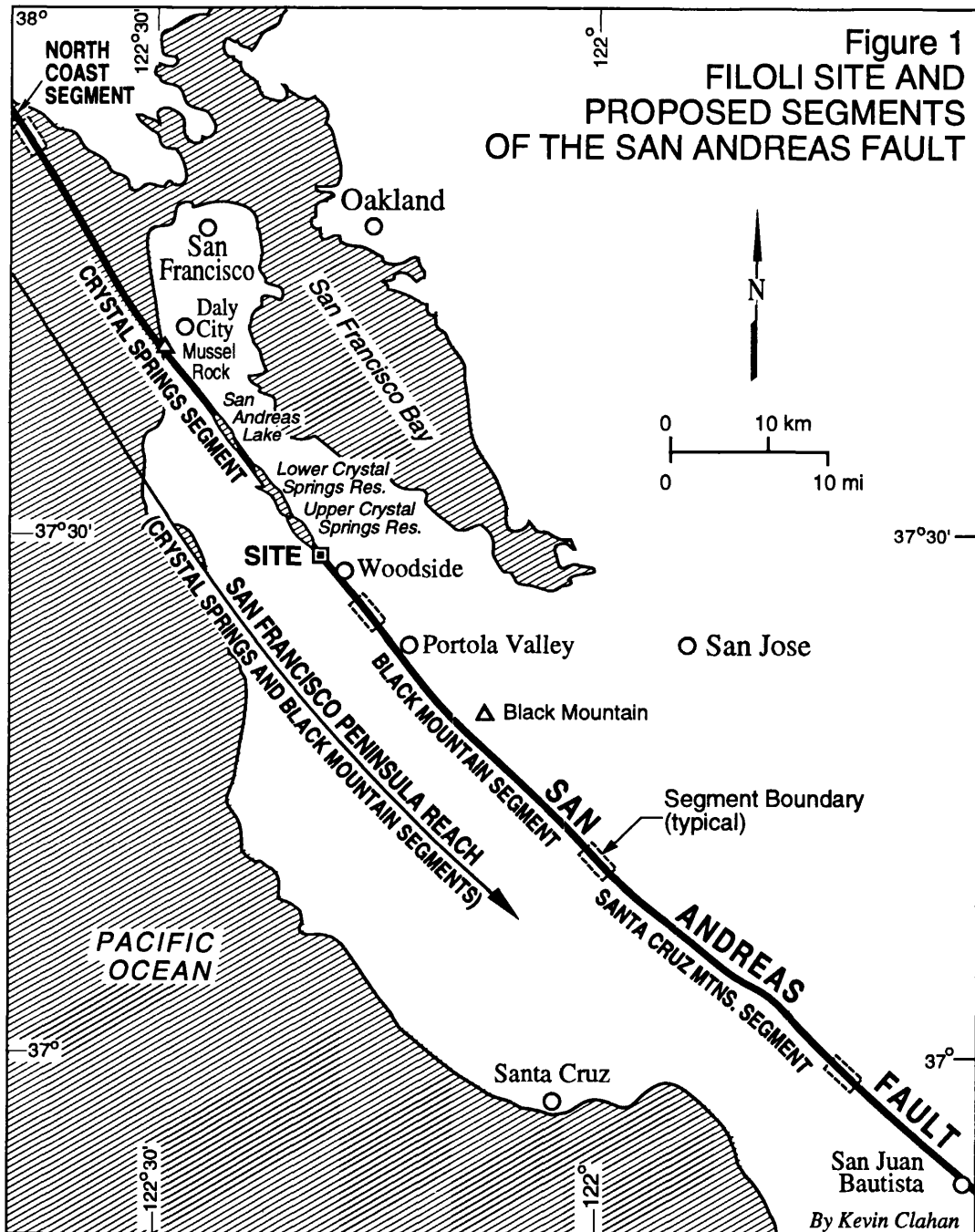
rupturing earthquakes on this settlement probably will be the subject of future research at the site.

## PROGRESS TO DATE

The field program for the final phase of this three-year investigation was recently completed. Preliminary conclusions are summarized below. During Phase 1 (FY92), we identified the Filoli Estate as a priority site on the San Francisco Peninsula having the potential to yield: (1) a late Holocene paleoseismic history and recurrence frequency of pre-1906 earthquakes; (2) an estimate of Holocene rates of slip; and (3) surface rupture characteristics for the San Francisco Peninsula reach of the SAF. Phase 2 (FY93) of our research involved excavating and logging 11 backhoe trenches, 5 that were oriented normal to the fault trace and 6 that were fault parallel. Results of the Phase 2 work included accurately locating and documenting the near-surface rupture characteristics of the SAF in the study area and documenting the location and morphology of buried channel deposits. We established a preliminary estimate of late Holocene slip, based on offset channel thalwegs and AMS radiocarbon ages. Subsequent geologic trenching during Phase 3 (FY94) research (Figure 2) focused on characterizing, sampling, and accurately locating buried channel deposits that intersect the fault at high angles and that have been dextrally offset by recurrent slip (Figure 3).

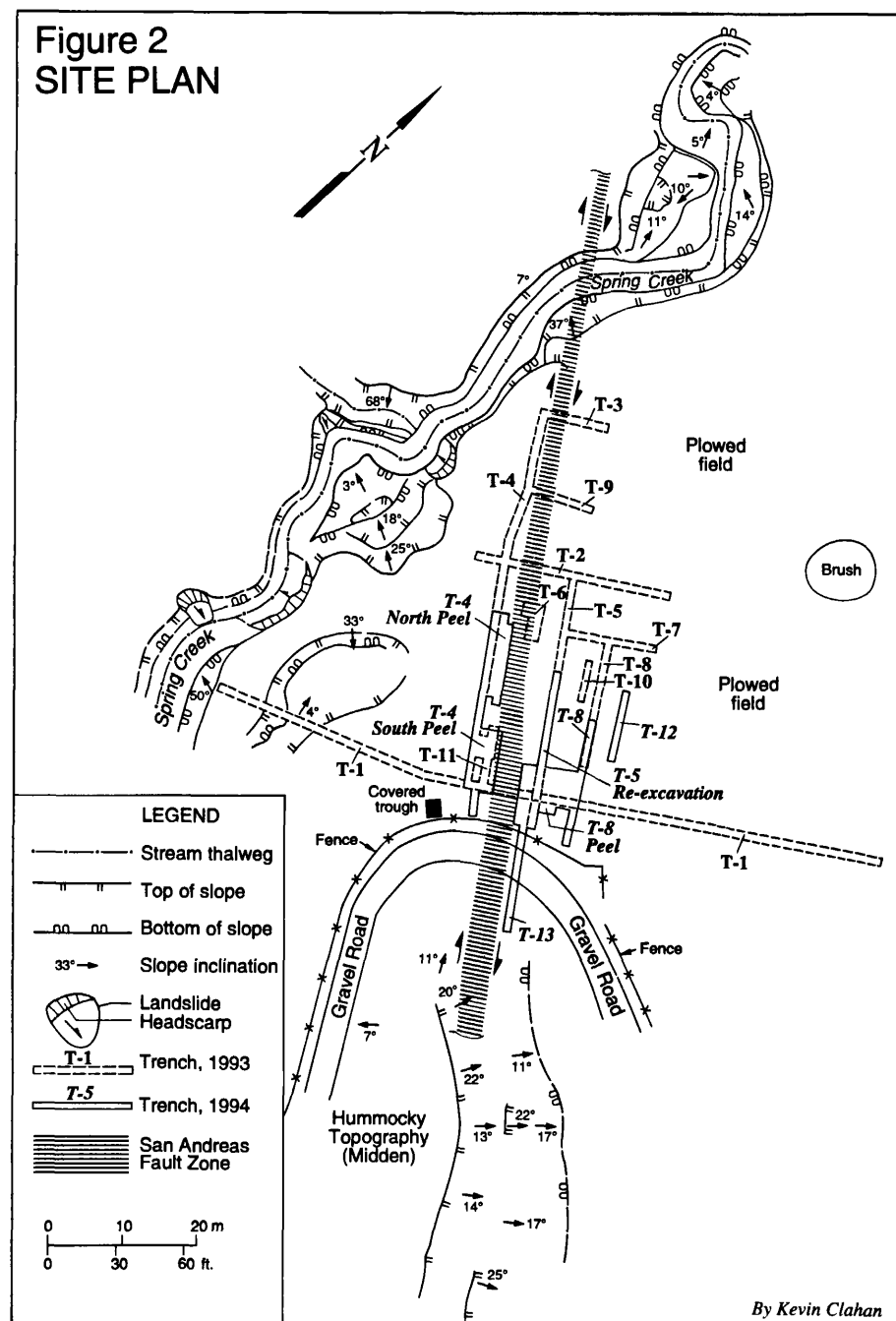
As a result of Phase 3, we have refined our estimates of slip rate and recurrence intervals. Several offset buried stream channel deposits at this site can be matched across the N35°W-trending trace of the fault where it crosses the head of Spring Creek fan. One channel having an AMS radiocarbon age of  $580 \pm 60$  yr B.P. is offset dextrally  $10.9 \pm 0.5$  m, for a minimum slip rate of  $19 \pm 3$  mm/yr. At this rate, it would take approximately  $150 \pm 25$  yr to accumulate strain equivalent to the local maximum coseismic displacement of 2.7 m (9 ft) that was observed near Upper Crystal Springs Reservoir after the 1906 earthquake.

Other offset channel deposits that match across the fault trace are younger and probably record historical slip events. Two channels with AMS radiocarbon ages of  $150 \pm 60$  yr B.P. are offset 2.4 m (8 ft), which agrees with the amount of dextral slip observed after the 1906 event in Woodside a few kilometers to the south. However, another channel dated at  $200 \pm 60$  yr B.P. is offset dextrally 3.5 m across the 1906 trace, leading us to speculate that the 3.5 m of horizontal separation may be the combined offset of the 1906 earthquake and the San Francisco Peninsula earthquake of June 1838 described by Louderback (1947). Even though uncertainties inherent in radiocarbon analysis for these very young deposits may preclude confirmation of the 1838 event, this channel displacement indicates that surface displacements of about 1 m, which correspond to a magnitude  $M_w$  7 earthquake, also have occurred on the San Francisco Peninsula. If this is the case, based on our slip rate of 19 mm/yr, more than 1.5 m of dextral strain has accumulated since 1906, and an 1838-type ( $M_w$  7) event is overdue.



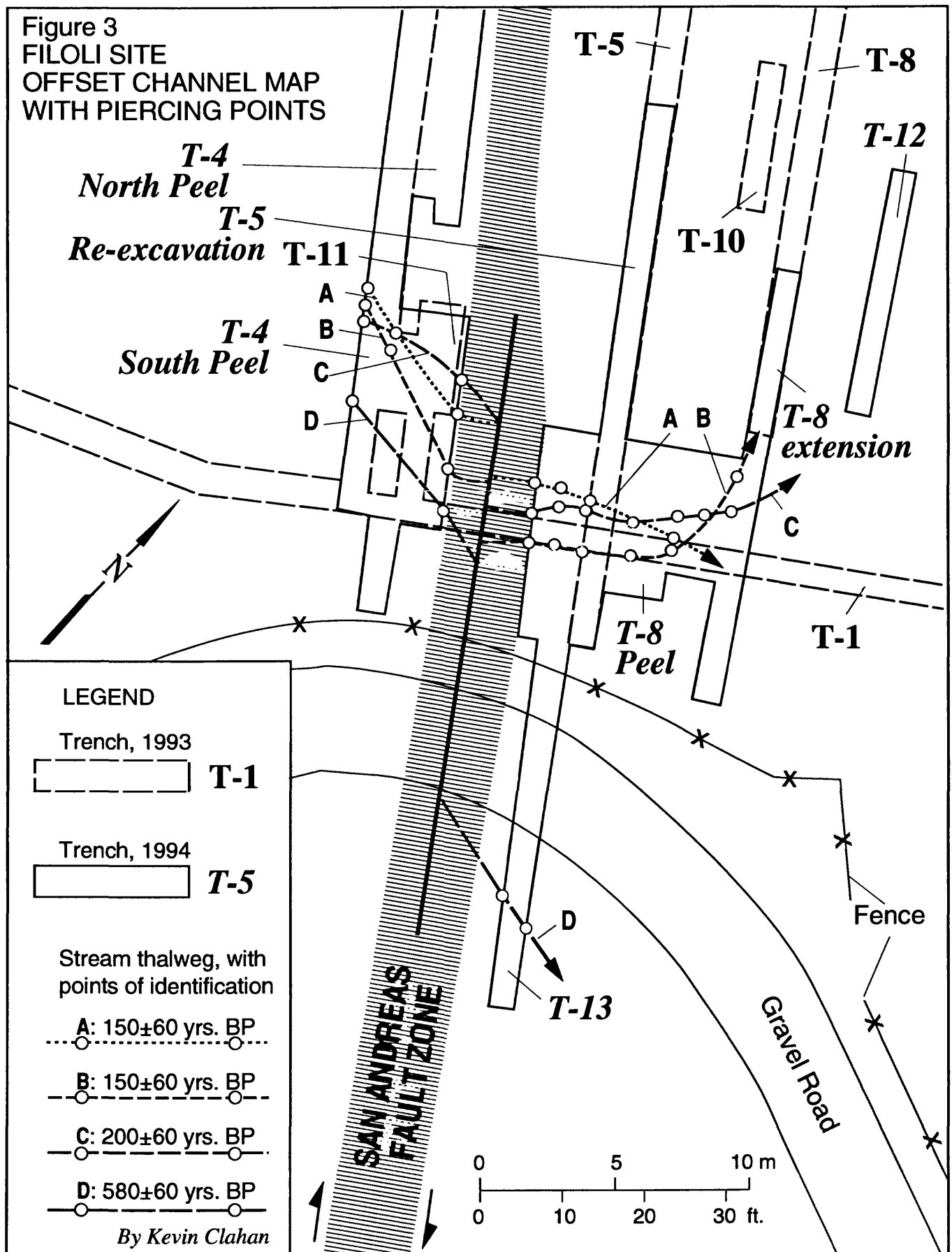
122°  
**Figure 1**  
**FILOLI SITE AND**  
**PROPOSED SEGMENTS**  
**OF THE SAN ANDREAS FAULT**

*By Kevin Clahan*



*By Kevin Clahan*

Figure 3  
FILOLI SITE  
OFFSET CHANNEL MAP  
WITH PIERCING POINTS



**INVESTIGATION OF STRUCTURAL DEFORMATION IN THE  
LAKE COUNTY UPLIFT AREA OF MISSOURI AND KENTUCKY  
USING HIGH-RESOLUTION SH-WAVE SEISMIC REFLECTION METHODS  
(Continuation)**

1434-94-G-2361

James B. Harris  
Kentucky Geological Survey  
University of Kentucky  
Lexington, Kentucky 40506-0107  
Phone:(606) 257-3016  
E-mail:super109@ukcc.uky.edu

Program Element:II.1

### **Investigation**

The relationship between geologic structure and recent seismicity is one of the most important topics of research related to seismic hazard evaluation in the New Madrid seismic zone (NMSZ). Determining the association of seismicity and structural deformation in the NMSZ is hindered by the presence of thick, water-saturated, unconsolidated sediments of the upper Mississippi embayment. The upward continuation of bedrock faults into the unconsolidated material is often masked by the inability of the soft sediments to propagate large fractures. This problem, along with erosional and depositional patterns associated with the Mississippi river, makes identification and age determination of near-surface faults difficult.

Seismic reflection methods have been used within the Mississippi embayment to determine the style, extent, and age of tectonic deformation. Although recent high-resolution P-wave (compressional wave) investigations have successfully imaged faults in the unconsolidated sediments (Schweig et al., 1992; Sexton et al., 1992; VanArsdale et al., 1992), "the critical Quaternary-to-Recent section could not be resolved (Johnston and Shedlock, 1992)." However, through the use of SH-wave (horizontally polarized shear-wave) reflection methods, deformation in this interval can be imaged.

The primary objective of the research is to collect high-resolution common-depth-point (CDP) SH-wave seismic reflection data across the Lake County uplift (LCU), a Quaternary deformational feature associated with active faulting and contemporary seismicity (Russ, 1982), through parts of southeastern Missouri and southwestern Kentucky. With increased resolution gained through the use of SH-wave reflection techniques, the location and magnitude of near-surface deformation in the LCU can be more thoroughly documented, and additional details associating shallow structure and modern seismicity can be determined.

## Results

In addition to reconnaissance profiling across the LCU (nearly 7 km of shear-wave reflection data has been collected to date), the research has generated several complementary projects including cooperative studies with researchers from William Lettis and Associates, Inc., the University of Memphis, and the Missouri Geological Survey.

Figure 1 shows a map of the central LCU focused on an area called Kentucky Bend, which lies inside a meander loop of the Mississippi River in extreme western Kentucky. New Madrid, Missouri, is located north of Kentucky Bend and Reelfoot scarp lies to the south. As part of a paleoseismologic trenching study of the Reelfoot scarp, shallow SH-wave seismic reflection data were collected over the scarp prior to excavation of the trench. The seismic line (600% CDP coverage) was collected using a sledge hammer/mass energy source and 30 Hz horizontal geophones. The interpreted section (Figure 2) shows several reverse faults beneath the scarp, and the updip projection of the easternmost fault corresponds with a low-angle reverse feature identified in the trench.

Additionally, a shallow shear-wave splitting experiment, located near the center of Kentucky Bend (Figure 1), shows the presence of near-surface azimuthal anisotropy believed to be associated with neotectonic deformation. A four-component data set, recorded using a hammer and mass energy source, displayed abundant shallow reflection energy on records made with orthogonal source-receiver orientations (Figure 3); an indicator of shear-wave splitting. Measurement of near-surface directional polarizations, produced by shear-wave splitting, may provide valuable information for identifying neotectonic deformation and evaluating associated hazards.

## References

- Johnston, A. C., and Shedlock, K. M., 1992, Overview of research in the New Madrid seismic zone: *Seismological Research Letters*, v. 63, p. 193-208.
- Russ, D. P., 1982, Style and significance of surface deformation in the vicinity of New Madrid, Missouri: in McKeown, F. A., and Pakiser, L. C., eds., *Investigations of the New Madrid, Missouri, earthquake region*: U. S. Geological Survey Professional Paper 1236-I, p. 95-114.
- Schweig, E. S., III, Shen, F., Kanter, L. R., Luzietti, E. A., VanArsdale, R. B., Shedlock, K. M., and King, K. W., 1992, Shallow seismic reflection survey of the Bootheel lineament area, southeastern Missouri: *Seismological Research Letters*, v. 63, p. 285-295.
- Sexton, J. L., Henson, H., Jr., Dial, P., and Shedlock, K., 1992, Mini-Sosie high-resolution seismic reflection profiles along the bootheel lineament in the New Madrid seismic zone: *Seismological Research Letters*, v. 63, p. 297-307.
- VanArsdale, R. B., Schweig, E. S., Kanter, L. R., Williams, R. A., Shedlock, K. M., and King, K. W., 1992, Preliminary shallow seismic reflection survey of Crowley's ridge, northeast Arkansas: *Seismological Research Letters*, v. 63, p. 309-320.

## Reports

Harris, J. B., Woolery, E. W., and Wang, Z., 1994, A shallow seismic investigation of Quaternary deformation on the Lake County uplift, central New Madrid seismic zone: Presented at the 1994 South-Central Section Meeting, Geological Society of America, March 21-22, 1994, Little Rock, Arkansas.

Kelson, K. I., Simpson, G. D., Haraden, C. C., Lettis, W. R., VanArsdale, R. B., and Harris, J. B., 1994, Multiple Holocene earthquakes along the Reelfoot fault, central New Madrid seismic zone: Presented at the 1994 Annual Meeting, Geological Society of America, October 24-27, 1994, Seattle, Washington.

VanArsdale, R. B., Kelson, K. I., Simpson, G. D., Lumsden, C. H., and Harris, J. B., 1994, Northern extension of the Reelfoot scarp, Kentucky and Missouri: Presented at the 1994 Annual Meeting, Geological Society of America, October 24-27, 1994, Seattle, Washington.

Harris, J. B., Shear-wave splitting in Quaternary sediments: Neotectonic implications in the central New Madrid seismic zone: submitted to Geophysics.

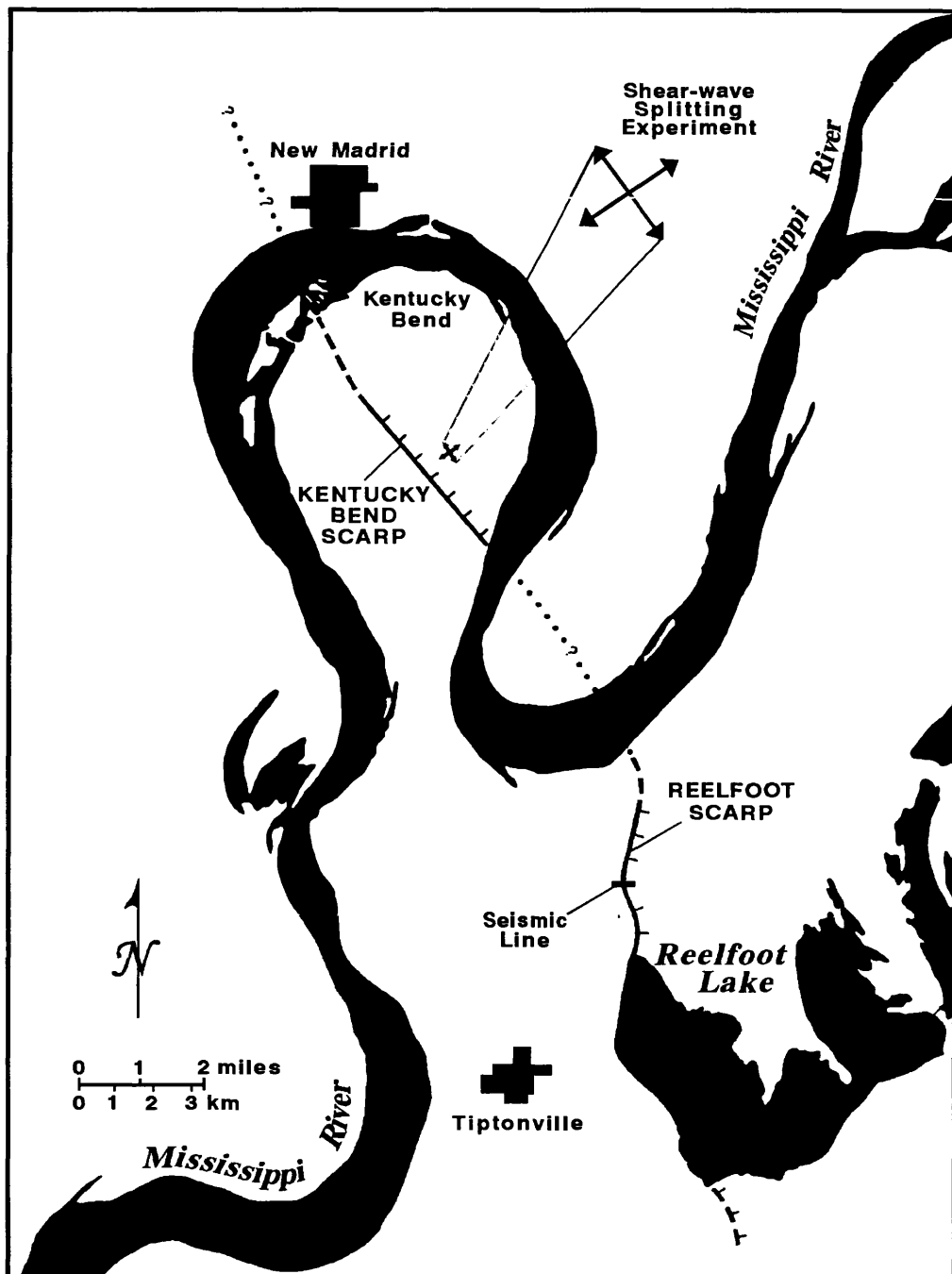


Figure 1. Map of Kentucky Bend showing locations of Reelfoot scarp seismic line and shear-wave splitting experiment.

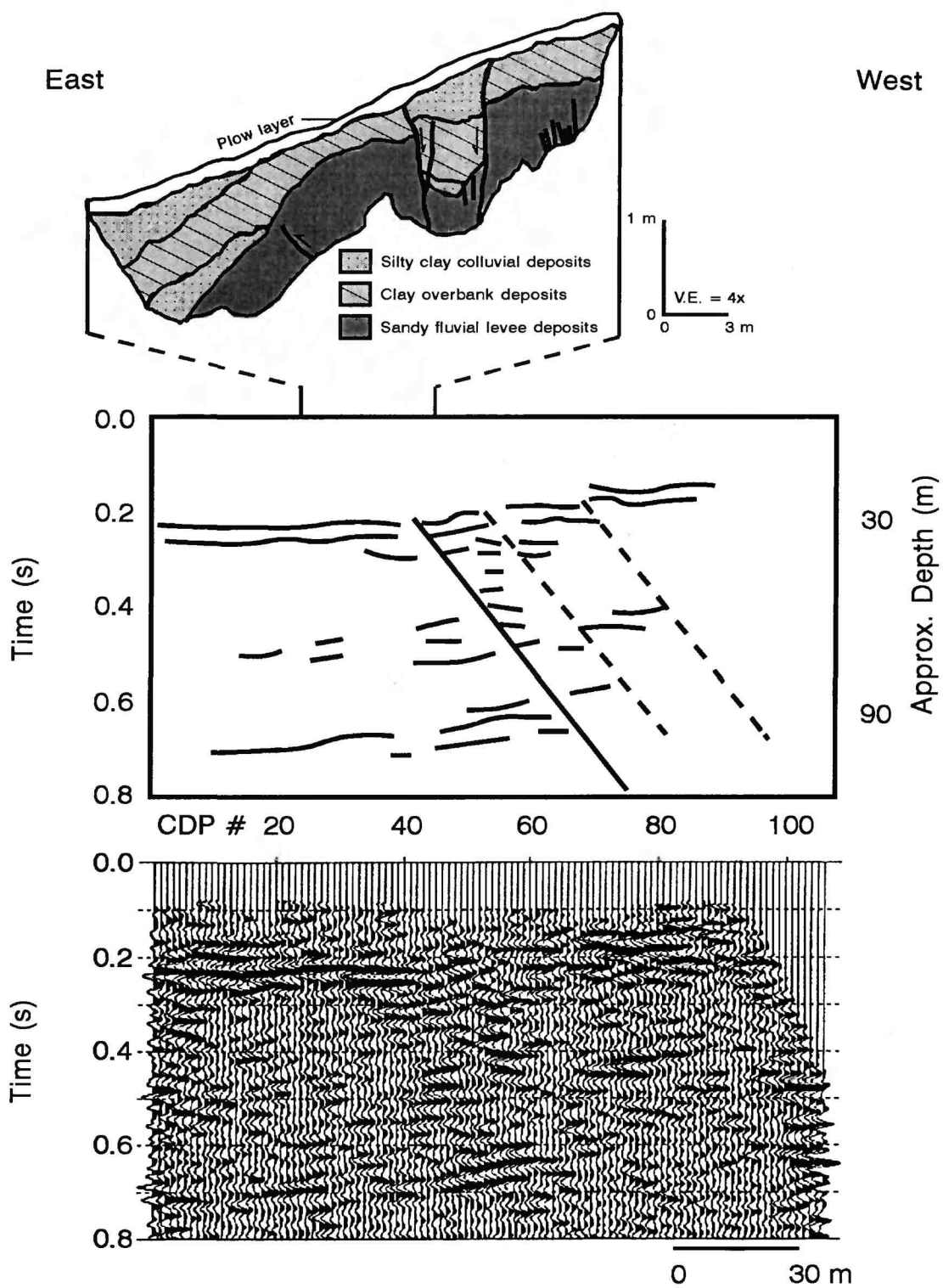


Figure 2. Reelfoot scarp seismic reflection line and trench log.

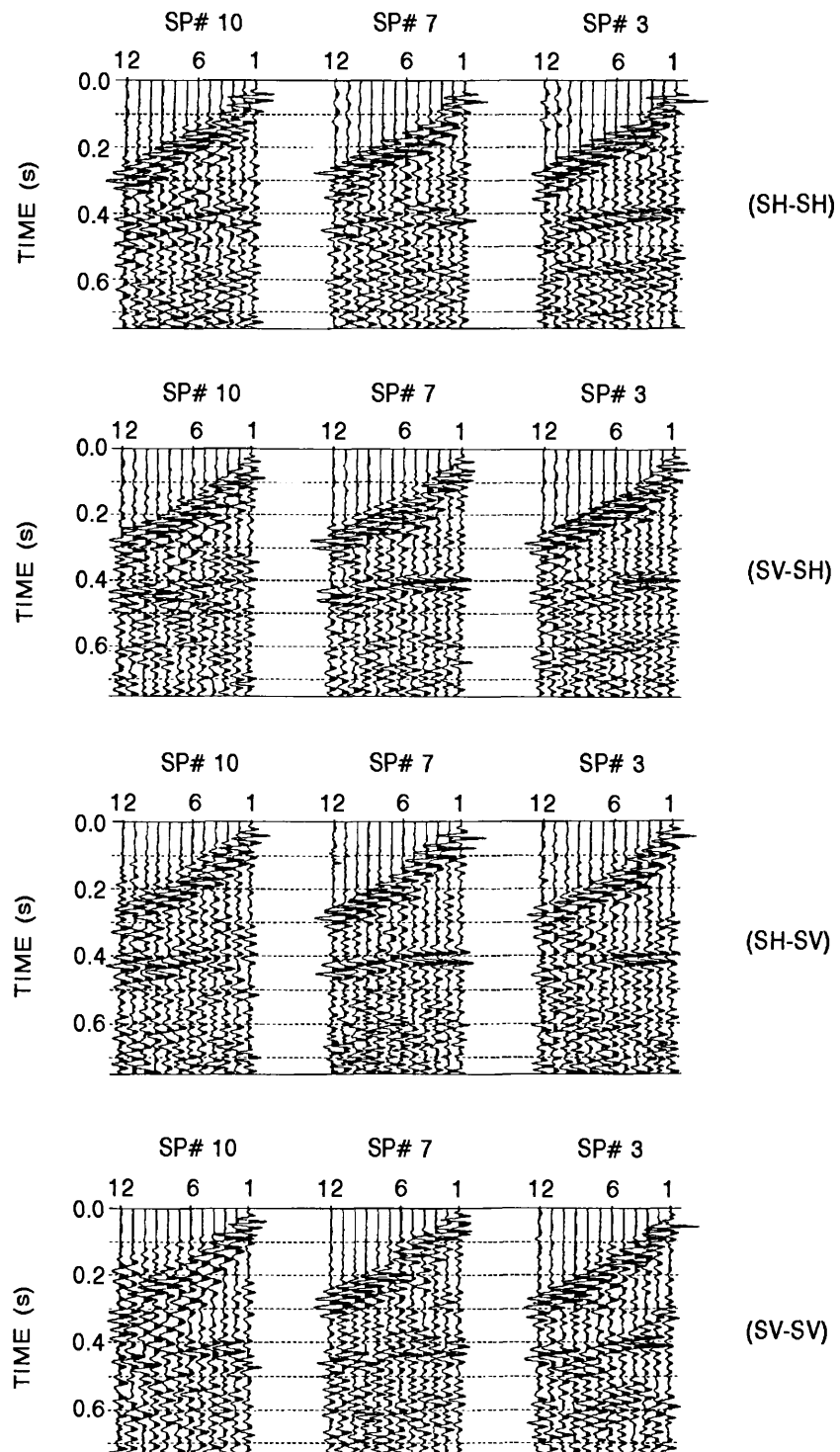


Figure 3. Field records from shear-wave splitting test.

**SURFICIAL GEOLOGIC MAPPING OF THE NEPHI SEGMENT,  
WASATCH FAULT ZONE, UTAH**

1434-93-G-2343  
Program Element II.5

Kimm M. Harty and William E. Mulvey  
Utah Geological Survey  
2363 South Foothill Drive  
Salt Lake City, Utah 84109-1491

**PURPOSE OF PROJECT**

This project consists of a geologic map and text that show and describe the surficial Quaternary deposits along the Nephi segment of the Wasatch fault zone (WFZ) in Juab Valley of north-central Utah. The discussion includes the size, age, and distribution of fault scarps. The purpose of this project is to provide the basic geologic data needed for accurate assessments of seismic history and earthquake hazards associated with this part of the WFZ. The map is a continuation of mapping initiated during the 1980s by the U.S. Geological Survey, and is the fifth in a series of 1:50,000-scale surficial geologic maps of the most active, central segments of the WFZ. The WFZ is recognized as the longest and most active normal-slip fault in North America, and the most likely source of future large, surface-faulting earthquakes to affect the populous Wasatch Front area of Utah. The 33-km-long Nephi segment of the WFZ exhibits some of the youngest looking fault scarps along the entire 370-km-long fault zone. Previous researchers estimate that the most recent surface-rupturing earthquake on this segment may have occurred within the past 1,000 years, and perhaps as recently as 300 to 500 years ago.

**INVESTIGATIONS**

Numerous surficial and bedrock geology, fault, and soils maps at various scales exist for the mapped area, and these were consulted for this project. We remapped much of the surficial geology along the fault trace and adjacent mountain and valley-floor areas, as most of the existing geologic maps are not sufficiently detailed, or the information is outdated. Mapping of the fault zone and surficial deposits was done on 1:20,000-scale black and white aerial photographs from 1950. Black and white, 1:12,000-scale low-sun-angle aerial photographs taken for the Utah Geological Survey in 1970 were also used in critical areas. Air-photo mapping was field-checked and has been compiled onto 1:24,000-scale topographic base maps using an International Imaging systems Alpha 2000 digital stereo plotter.

Field investigations included inspecting faulted Quaternary deposits and assigning relative ages based on geomorphic expression, landform preservation, soil development, and stratigraphic position. Fault scarps offsetting Quaternary deposits were measured and compiled onto the map for selected localities. Much of the scarp data (scarp heights and surface offsets) were derived from computer plots of surface profiles of scarps measured and provided by M.N. Machette, U.S. Geological Survey. Fault-scarp characteristics can be used to estimate slip rates and average recurrence intervals at various sites along the WFZ.

## RESULTS

Quaternary deposits along the Nephi segment of the Wasatch fault range in age from middle Pleistocene to late Holocene. Coalesced alluvial fans and Lake Bonneville deep-water deposits dominate Juab Valley. Pleistocene- and Holocene-age alluvium and alluvial fans form an apron of sediment that covers much of the valley along the mountain front. These deposits thin toward the center of the valley, exposing underlying deposits from the last cycle of Lake Bonneville (known as the Bonneville lake cycle) between 30,000 and 10,000 years ago.

Other Quaternary deposits in the mapped area include large, pre-Bonneville-age landslides (earth slides and flows); late Holocene debris-flows; glacial sediments deposited early in the Bonneville lake cycle; and older, inactive alluvial fans that were abandoned as the climate changed and movement on the Nephi segment altered the local base level and streams incised the fans.

The map text describes characteristics of the WFZ and its relationship to offset Quaternary deposits at several sites including North Creek, Pole Canyon, Willow Creek, Gardner Creek, Red Canyon, Nephi, and at the northern and southern fault-segment boundaries. In addition to providing new information on Quaternary deposits and fault-scarp heights and estimated slip rates, the text also summarizes information from previous workers who have mapped or trenched specific sites along the fault segment. As of October 1, 1994, the project is approximately 85 percent complete; computerized mapping is nearly finished and we are writing the map text.

## Analysis of Earthquake Data from the Greater Los Angeles Basin and Adjacent Offshore Area, Southern California

#1434-94-G-2440

Egill Hauksson  
 Seismological Laboratory, California Institute of Technology,  
 Pasadena, CA 91125  
 Tel.: 818-395 6954; Email: [hauksson@seismo.gps.caltech.edu](mailto:hauksson@seismo.gps.caltech.edu)  
 FAX: 818-564 0715

### INVESTIGATIONS

The goals of this project are: (1) seismotectonic analysis of earthquake data recorded by the CIT/USGS, TERRAscope, and USC seismographic networks during the last 18 years in southern California; (2) improve models of the velocity structure to obtain more accurate earthquake locations including depth and to determine focal mechanisms; and (3) studies of the earthquake potential and the detailed patterns of faulting along major faults in the metropolitan area and adjacent regions.

The ( $M_w$ 6.7) 1994 Northridge earthquake sequence that began on 17 January is the most substantial earthquake sequence to occur in the last 22 years in Los Angeles. We have synthesized aftershock data from this sequence recorded by the SCSN to provide a detailed three-dimensional picture of the deformation. The results appear in three papers; one was published in *Science*, one was published in *SPECTRA* special volume and one was submitted to *JGR*.

### RESULTS

#### The 1994 Northridge Earthquake Sequence in California: Seismological and Tectonic Aspects

The  $M_w$ 6.7 Northridge earthquake occurred on January 17, 1994 beneath the San Fernando Valley. Two seismicity clusters, located 25 km to the south and 32 km to the north-northwest, preceded the mainshock by 7 days and 16 hours, respectively. The mainshock hypocenter was relatively deep, at 19 km depth in the lower crust. It had a thrust faulting focal mechanism with the actual fault plane dipping  $35^\circ$  to the south, striking  $N75^\circ W$  with a rake of  $100^\circ$ . Because the mainshock did not rupture the surface, its association with surficial geological features remains difficult to resolve. Nonetheless, its occurrence reemphasized the seismic hazard of concealed faults associated with the contractional deformation of the Transverse Ranges. The Northridge earthquake is part of the temporal increase in earthquake activity in the Los Angeles area since 1970.

The mainshock was followed by an energetic aftershock sequence. Eight aftershocks of  $M \geq 5.0$  and 48 aftershocks of  $4 \leq M < 5$  occurred between January 17 and September 30, 1994. The aftershocks extend over most of the western San Fernando Valley and Santa Susana Mountains. They form a diffuse spatial distribution around the mainshock rupture plane, illuminating a previously unmapped thrust ramp, extending from 7-10 km depth into the lower crust to a depth of 23 km. No flattening of the aftershock distribution is observed near its bottom. At shallow depths, above 7-10 km, the thrust ramp is topped by a dense distribution of aftershock hypocenters bounded by some of the surficial faults. The dip of the ramp increases from east to west. The west side of the aftershock zone is characterized by a dense, steeply dipping, and north-northeast striking planar cluster of aftershocks that exhibited mostly thrust faulting. These events coincided with the Gillibrand Canyon lateral ramp. Along the east side of the aftershock zone the aftershocks also exhibited primarily thrust faulting focal mechanisms. The focal mechanisms of the aftershocks were dominated by thrust faulting in the large aftershocks, with some strike-slip and normal faulting in the smaller aftershocks. The 1971 San Fernando and the 1994 Northridge earthquakes ruptured partially abutting fault surfaces on opposite sides of a

ridge. Both earthquakes accommodated north-south contractional deformation of the Transverse Ranges. The two earthquakes differ primarily in the dip direction of the faults and the depth of faulting. The 1971 north-northeast trend of left-lateral faulting (Chatsworth trend) was not activated in 1994.

#### Focal Mechanisms of the Mainshock and $M \geq 4$ Aftershocks.

The first motion focal mechanism of the mainshock exhibited one nodal plane striking  $N75^\circ \pm 10^\circ W$  and dipping  $35^\circ \pm 5^\circ$  south-southwest with a rake of  $100^\circ \pm 10^\circ$  (Figure 1). Other determinations of the mainshock focal mechanism based on teleseismic and regional broadband waveforms show a more northerly strike of  $N50-60^\circ W$  and a somewhat steeper dip of  $40-45^\circ$  to the south-southwest [Dreger, 1994; Thio and Kanamori, 1994]. This difference in the mainshock focal mechanism determined with different frequency waves suggests a small increase in dip along strike and possibly a curved rupture surface. Such an increase in dip along strike can also be seen in the distribution of aftershocks.

Although no surface rupture has been found [USGS and SCEC Scientists, 1994], several preliminary interpretations of the mainshock faulting have been offered. One interpretation suggests that the Oak Ridge fault, mapped to the west in the Ventura basin, extends into this region [Yeats, 1994]. Another interpretation could be that some of the surficial faults exposed farther north, such as the Holser fault, are responsible for the earthquake. A third interpretation models the earthquake as slip on a south-dipping thrust ramp beneath the San Fernando Valley [Davis and Namson, 1994]. The seismological evidence for the mainshock faulting, the focal mechanism and the spatial distribution of aftershocks, are consistent with all three interpretations.

The available focal mechanisms of 57 aftershocks of  $M_L \geq 4.0$  and of the mainshock are shown in Figure 1. Nearly all of these focal mechanisms showed thrust faulting with only a few strike-slip and normal faulting events. The largest aftershock of  $M_L 5.9$  followed the mainshock within a minute and was located 10 km to the east-northeast of the mainshock. No focal mechanism is available for this event. The second largest aftershock of  $M_L 5.6$  occurred 11 hours later and was located about 20 km to the northwest of the mainshock. This aftershock had a thrust-faulting focal mechanism similar to the mainshock. This and two other thrust-faulting aftershocks of  $M > 5$  located near the trace of the Santa Susana fault could be associated with either south- or north-dipping fault structures.

Strike-slip deformation has occurred during the late Quaternary along faults such as the Northridge Hills fault and the Mission Hills fault. Three of strike-slip faulting  $M \geq 4$  aftershocks are located near the surface trace of the Northridge Hills fault. No large aftershocks were located near the Mission Hills fault, even though significant ground deformation in this region was caused by the Northridge mainshock [USGS and SCEC Scientists, 1994]. Only one of the eight  $M_L > 5.0$  aftershocks showed a strike-slip focal mechanism, and was located between the surface traces of the Northridge Hills and the Santa Susana faults. Most of the strike-slip and normal faulting aftershocks occurred at shallow depth above the main rupture surface where strike-slip or extensional deformation of the hanging wall may be expected.

#### Strike-Normal Cross Sections

In map view the aftershocks form a 45 km long and 40 km wide zone (Figure 2). The mainshock rupture as determined from waveform data [Wald and Heaton, 1994], started at the southeastern corner of this zone and extended about 15 km west-northwest from the mainshock epicenter and about 20 km up a  $35-42^\circ$  dipping surface to the north-northeast, covering less than one third of the aftershock zone.

Four cross sections extend from south-southwest to north-northeast (Figure 2). The focal mechanisms of the mainshock and representative large aftershocks are included in map of epicenters and the cross sections. Nearly all of these focal mechanisms are thrust, with only one strike-slip and one normal mechanism.

The cross section D-D' shows aftershocks that occurred along the eastern edge of the mainshock rupture surface. These hypocenters form a south-southwest-dipping distribution in the depth range of 5-15 km with a small number of aftershocks extending down to 20 km depth. The lower depth bound to the densest part of the aftershock distribution appears to coincide with the steeply dipping Northridge Hills fault. Most of the shallow aftershocks were located near the surface trace of the Santa Susana and Verdugo faults.

The cross section C-C' includes the hypocenter of the mainshock and shows the 35-40° dipping zone of aftershocks from 23 km to about 7 km depth, located mostly under the San Fernando Valley. If the 35° south-southwest dipping nodal plane of the mainshock is extended to shallower depths, the rupture surface is located near the lower surface of this dipping aftershock zone. The deep end of this zone is defined by a few aftershocks that extend as deep as 23 km. Above approximately 7 km depth, the aftershock zone is less well expressed as a southwest-dipping tabular feature but is rather a cloud of aftershocks representing diffuse deformation of an overlying anticlinal fold. The San Gabriel fault limits the northeast spatial extent of most of the shallow aftershocks. The southwestern edge of the distribution of shallow aftershocks is located further to the southwest, above the mainshock rupture surface.

Farther to the west, in cross section B-B', the western edge of the mainshock rupture surface is outlined by the south-southwest dipping zone of aftershocks. More distributed deformation of the hanging wall is evident in this section, including shallow events south of the mainshock. A north dipping trend of aftershocks, in the 5-8 km depth range, may be related to the north dipping Santa Susana fault. The only M>5 strike-slip aftershock lies at the eastern edge of this section at shallow depth.

The aftershocks in cross section A-A' occurred west of the mainshock rupture surface. They form a diffuse distribution beneath the Santa Susana Mountains and appear to be on different faults that did not rupture in the mainshock. There is some indication in the cross section of a wedge-shaped structure illuminated by both south and north dipping trends of aftershocks in the depth range of 13-18 km. This wedge-shaped structure coincides with the Gillibrand Canyon lateral ramp. The Northridge Hills fault brackets the distribution to the south while the northern edge of the distribution is midway between the Santa Susana and Holser faults.

## PUBLICATIONS and REPORTS

Hauksson, E., L. M. Jones, K. Hutton, and D. Eberhart-Phillips, The 1992 Landers Earthquake Sequence: Seismological Observations, *J. Geophys. Res.*, 98, 19835-19858, 1993.

Hauksson, E., State of stress from focal mechanisms before and after the 1992 Landers earthquake sequence: *Bull. Seismo. Soc. Amer.*, 84, 917-934, 1994.

Hauksson, E., and L. M. Jones, The Northridge Earthquake of January 17, 1994  
SPECTRA Special Report (contributed), Seismological Aspects, J. Hall (ed), EERI, December 1994.

Hauksson, E., The 1991 Sierra Madre earthquake sequence in southern California:  
Seismological and tectonic analysis, *Bull. Seismol. Soc. Amer.*, 84, 1058-1074, 1994.

Scientists of the U. S. Geological Survey and the Southern California Earthquake Center,  
The magnitude 6.7 Northridge, California, earthquake of January 17, 1994, *Science*, 266, 389-397, 1994.

# Northridge 1994 $M \geq 4.0$

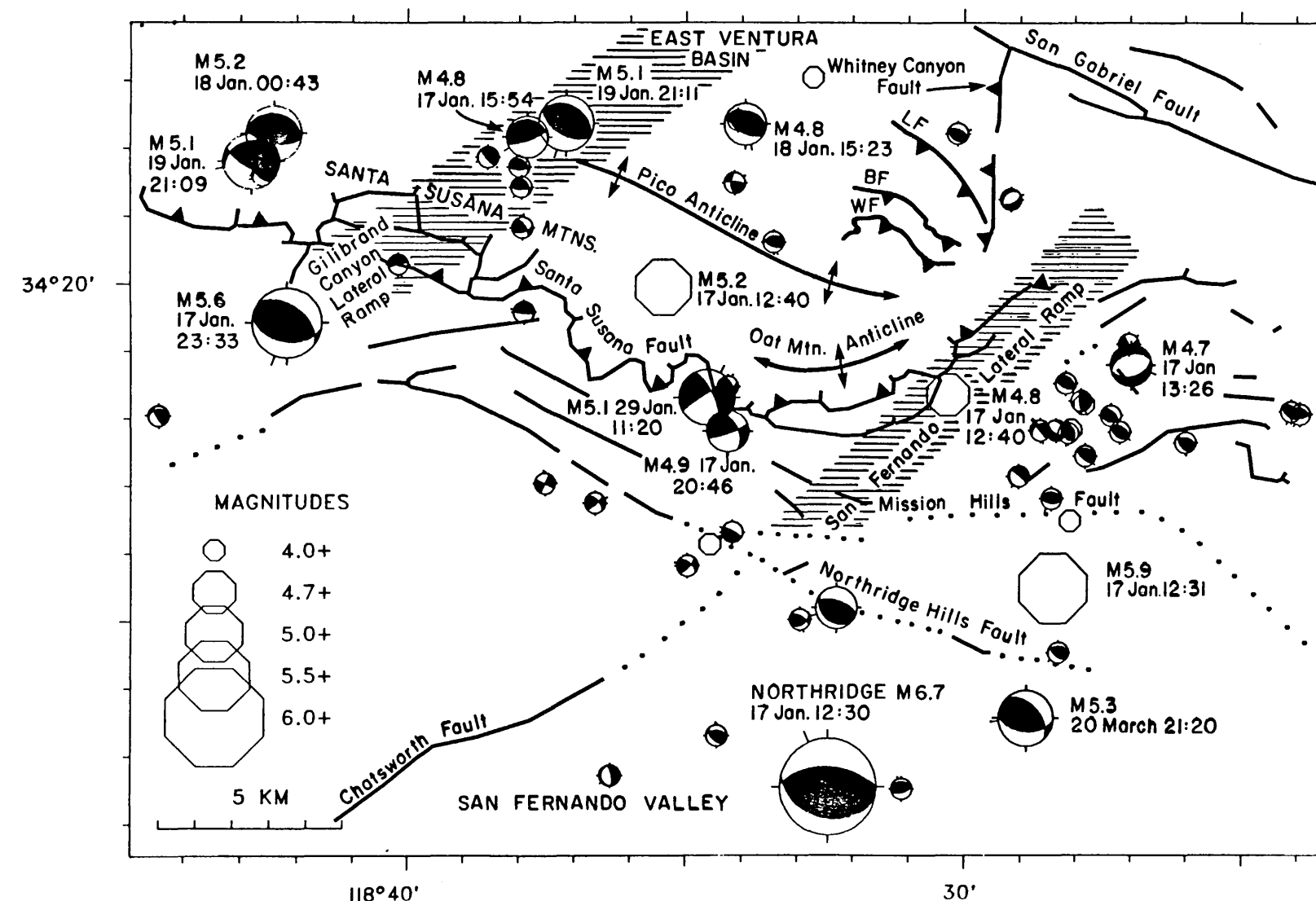


Fig. 1. Northridge aftershock region showing lower-hemisphere, first-motion focal mechanisms of  $M \geq 4$  earthquakes recorded by the SCSN from January through September 1994, and major faults (dotted where inferred) from Jennings [1975]. Because the M5.9 aftershock occurred too closely in time to the Northridge mainshock or, in several cases, aftershocks were preceded by immediate foreshocks, their focal mechanism could not be determined.

# 1994 Northridge Earthquake Sequence

January -- September  
NHC\_03402F DEF 0000014.LD 0-OCT-94 18:43:48

II

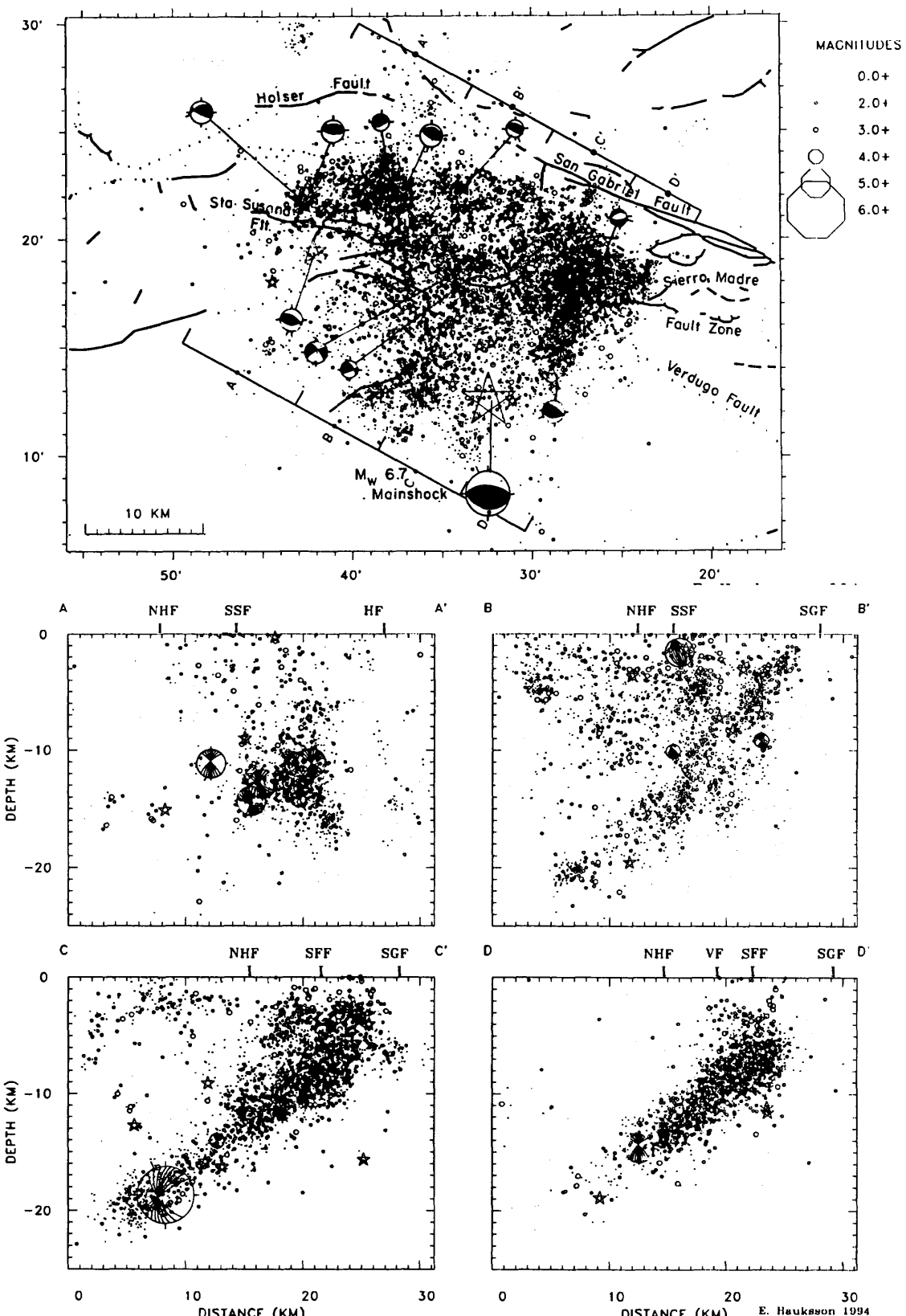


Fig. 2. (a) Map of the 1994 Northridge earthquake, its aftershocks, and major late Quaternary faults (dotted where inferred). Focal mechanisms for the mainshock and significant aftershocks are included. Symbol size is scaled with magnitude and earthquakes of magnitude greater than 4 are shown as stars. (b) Depth cross sections taken orthogonal to strike, A-A', B-B', C-C', and D-D' include all events in each box having horizontal and vertical errors less than 2 km. NHF, Northridge Hills fault; SSF, Santa Susana fault; SGF, San Gabriel fault, HF, Holser fault; VF, Verdugo fault; CWF, Chatsworth fault, and SFF, San Fernando fault.

## PREDICTION ALGORITHMS

9960-10066

John H. Healy

Branch of Earthquakes Geology and Geophysics  
 U. S. Geological Survey  
 345 Middlefield Road, MS/977  
 Menlo Park, California 94025  
 (415) 329-4848

### Investigations

We are continuing the evaluation of the M8 earthquake prediction algorithm in the Circum-Pacific region. During this period we have an important successful prediction of a large earthquake in the southern Kuril Islands. This prediction is described in the following abstract prepared by the four collaborators in this work (V.G. Kossobokov, International Institute for Earthquake Prediction Theory and Mathematical Geophysics, Russian Academy of Science; J.H. Healy, U.S. Geological Survey, Menlo Park, California, J.W. Dewey, U.S. Geological Survey, Denver, Colorado; and I.N. Tikhonov, Institute for Marine Geology and Geophysics, Russian Academy of Science).

### Results

#### *Precursory Changes of Seismicity Before the October 4 South Kuril Islands Earthquake*

According to the Harvard determination the October 4 Southern Kuril Islands earthquake is the largest ( $M_o = 3.7 \times 10^{21}$  Nm) worldwide since the Sumba earthquake of 1977. This earthquake provides a new case history of advance prediction by an intermediate-term earthquake prediction algorithm M8 (*Phys. Earth and Planet. Inter.*, 1990, 61, 73-83). In July 1992 the Time of Increased Probability (TIP) was diagnosed by M8 in a course of the real-time research prediction of magnitude 7.5+ earthquakes in Circum Pacific (Healy *et al.*, 1992, U.S. Geol. Surv. Open File Rep. 92-401). The results were confirmed using the data from the local seismic network of the Institute for Marine Geology and Geophysics, Far East Division, Russian Academy of Sciences. The prediction was transferred to the Ministry of Emergency Situations of Russia calling for "special attention of seismologists and civil defense to the area of the Southern Kuril Islands and Eastern Hokkaido as an area where magnitude 7.5-8.5 earthquakes are likely to occur before July 1997". The prediction was a part of a presentation at the AGU Western Pacific Geophysics Meeting (Hong Kong, July 25-29, 1994) and published. Using the NEIC Global Hypocenters Data Base through July 1, 1994, the "Mendocino Scenario" algorithm (Kossobokov *et al.*, 1990, *J. Geophys. Res.*, 95(B12), 19,763) reduces the territory of the TIP to the area of 210 by 160 km which coincide with the aftershock zone of the October 4 earthquake. This work was in part supported by International Science Foundation Grant MCI000.

**ANNUAL REPORT  
SOUTHERN CALIFORNIA EARTHQUAKE PROJECT  
94-9902-11010**

T. Heaton, J. Mori, L. Jones, D. Wald, S. Hough  
D. Given, R. Dollar, C. Koesterer, L. Wald, S. Perry, L. Curtis

Branch of Seismology, Office of Earthquakes, Volcanoes, and Engineering  
U.S. Geological Survey  
525 S. Wilson Ave. Pasadena CA 91106

818-405-7814  
heaton@bombay.gps.caltech.edu

**INVESTIGATIONS**

This project encompasses the USGS personnel that work together on the Southern California Seismic Network to ensure that earthquakes are well-recorded and archived in southern California, and that reliable seismic information is communicated to government agencies, scientific groups, media, and the public. The routine analyses and archiving of data involves close cooperation with Caltech and the Southern California Earthquake Center (SCEC). With the recent emphasis on providing rapid information, the project provides the necessary coordination of developing automated computer systems and organizing people that quickly respond to significant earthquakes. The project also includes the scientists' individual research topics that are closely tied to seismic data collected by the network. Tasks for FY1994 were divided into 3 categories.

- Seismic Data Collection
- Earthquake Hazards Monitoring and Public Information
- Earthquake Research

**Seismic Data Collection**  
(Elements II.2, II.7, III.1, IV.1)

A major responsibility of the project is to maintain and operate the large seismic network, thus a substantial part of the project's resources are used for instrument maintenance. The network consists of over 300 channels of data from 225 sites and provides the primary data for hazard monitoring in southern California and data for much of the research done by the project scientists. Responsibilities for hardware (instrument sites, radio telemetry, microwave and telephone links, computer cluster) and software (on-line recording system, off-line data processing, real-time earthquake information systems) are shared jointly with Caltech.

In addition to maintaining the network, we continue to improve our seismic recording capabilities by installing new sites in sparsely instrumented areas, adding Force-Balance-Accelerometers (FBA) to improve on-scale recordings of larger earthquakes, and installing broadband TERRAscope instruments with large dynamic range. FBA components and the TERRAscope

data are crucial for both the development of better real-time information systems and the on-going research of seismic waveforms.

Routine analysis of the data is also carried out cooperatively with Caltech and includes, interactive timing of phases, location of hypocenters, calculation of magnitudes and preparation of the final catalog. Phase data are stored on magnetic disks and waveform data are archived on an optical mass storage device operated by the SCEC Data Center. These data are readily available to other USGS and university users over INTERNET connections.

### **Earthquake Hazard Monitoring and Public Information (Elements II.1, IV.2)**

An important part of monitoring earthquakes in a populated region such as southern California, is the ability for scientists to have access to quick and accurate locations and magnitudes. This enables them to release timely information to government officials and the media following felt and damaging earthquakes. Also, real-time locations and magnitudes are useful for watching large aftershock sequences and providing possible information on forthcoming activity. Our current systems have performed fairly well during the numerous felt events over the past year and scientists have been able to quickly announce hypocentral information to government agencies and the media. To further increase our response capabilities, we are working to improve the reliability and speed of applications to improve the automated event locations and magnitudes. In addition to hypocenters and magnitudes of the earthquakes, we are developing further real-time utilizations such as, alarms for unusual activity in special study areas, designation of likely areas of damage from future large earthquakes, and rapid assessment of earthquake probabilities.

### **Earthquake Research**

Project scientists pursue a diverse range of seismological research topics which contribute to studies of the earthquake Source (I), Potential (II), and Effects (III). Many of these studies utilize the large database of seismicity and waveforms that is collected and archived by the seismic network.

#### ***Earthquake Rupture Processes (Elements I.2, III.2) D. Wald, Heaton***

We are studying the source process of the 1994 Northridge earthquake by inverting strong motion and teleseismic waveforms as well as geodetic data for the three dimensional rupture history of the earthquake. In addition we are developing ground motion time histories for sites located close to large earthquakes.

#### ***Foreshock and Aftershock Statistics (Elements II.2, II.8) Jones***

Based on the statistical properties of foreshock and aftershock distributions, short-term probabilities of future large events can be estimated from any earthquake occurrence, as possible foreshock or expected aftershocks. A computer program has been developed to evaluate and display the probability of damaging earthquake shaking ( $> 10\%g$ ) for the next 24 hours based on the long term estimates from geologic information modified by the probability that recent earthquakes recorded by the Network are foreshocks or will have aftershocks. The spatial/temporal characteristics of earthquakes in the Los Angeles region are a particular focus of this research because of the high level of activity in the past 7 years.

*Source Parameters of Small Earthquakes* (Element II.2) Mori

We are studying the pattern of Northridge aftershocks by simultaneously inverting for hypocentral location and 3-dimensional velocity structure. In addition, phase data from portable instruments deployed after the 1971 San Fernando earthquake are being used to find the spatial relationship between the San Fernando and Northridge earthquakes. In a separate study, the importance of shear-wave Moho reflections in the distance range of 60-120 km is being studied using aftershocks of the 1992 Landers earthquake.

*Teleseismic Network Waveform Studies* (Element II.4) L. Wald, Heaton, Mori

We have been using surface waves and body wave from teleseisms recorded on over 500 stations of the southern and northern California arrays to study velocity structures of the Earth. The surface wave data consisted of 10 to 20 sec Rayleigh waves that travel complicated paths across California. We have tried to identify the anomalies that are complicating the surface wave propagation by tracing their paths across the arrays. We are also studying body waves, such as the core reflection Pcp, to determine velocity structures of the Earth's deep interior.

## RESULTS

1. This Project (in cooperation with Caltech) provided the basic information for seismicity in southern California. Data collection during FY1994 included locating and archiving (with Caltech) over 20,000 earthquakes, with the activity dominated by aftershocks of the M6.7 Northridge earthquake. Relatively high aftershock activity also continued for the M7.5 Landers and M6.5 Big Bear earthquakes; in southern California there have been 28 earthquakes larger than M5 and about 200 earthquakes larger than M4 in the past two years. Seismicity and network operations are summarized in the 1993 (L. Wald et al., 1994) and 1994 (in preparation) Network Bulletins. In addition, this project provides software support for the Caltech/USGS Seismic Processing system (CUSP), which is the primary data processing system operated by the Northern California Seismic Network, the Univ. of Nevada Seismic Network, the Hawaii Volcano Observatory Network, the Parkfield downhole systems, the University of Southern California Seismic Network, and the Idaho National Engineering Lab Network.

- Data accessibility has improved with preliminary earthquake locations and magnitudes available to USGS and university researchers within a few minutes following an event. Hand-timed phase data are available within 24 to 48 hours. Using INTERNET connections to the Southern California Earthquake Center Data Center (SCEC-DC), waveform data are now usually available within a week. Because of the extremely high recent seismic activity, a second 300-Gbyte optical jukebox has been added to the SCEC-DC.
- Portable instrument data collected by USGS instruments (47 Reftek recorders and 5 continuous 5-Day recorders) following Landers have been played back and organized. Procedures have been developed to associate this data and the other portable data collected by various universities with the network data. Integrated phase and waveform data are available on the SCEC-DC mass storage device.
- Six short-period vertical stations were added in the Northridge aftershock region and 5 7-channel temporary stations were also added to the aftershock region.

2. Project personnel responded to felt earthquakes and sonic booms throughout the year, ensuring uninterrupted data recording and providing information immediately following the events.
  - We made significant improvements to the software systems which automatically determine and broadcast earthquake locations and magnitudes. In FY93, we replaced our existing 64-station real-time processor (RTP) with ISAIAH (Information from a Seismic Array In A Hurry). The new system works with all 300 channels of data and has an improved phase associator that can better distinguish multiple events that occur closely spaced in time. ISAIAH operates within the framework of the CUSP seismic data management system that has been developed over the past 15 years. Both CUSP and ISAIAH development continued throughout FY94. New software was implemented that shares real-time exchange of phase data between Pasadena and Univ. of Nevada, Reno. New software was developed to determine Wood-Anderson magnitudes within several seconds. Code was developed to automatically send phase data to NEIC and procedures have been implemented to broadcast data over the California Emergency Digital Information System (EDIS). Project staff also contributed heavily to the Caltech/USGS Broadcast of Earthquakes Project (CUBE) which is developing real-time systems for the broadcast of earthquake information to help agencies coordinate emergencies following earthquakes. Approximately 15 agencies are currently receiving earthquake locations and magnitudes within minutes of an earthquake. CUBE participation has recently been expanded to include radio and television stations. Together with Caltech we have begun procedures to provide very rapid checking of information by seismologists on a 24-hour basis.
  - We coordinated the deployment of portable seismographs by USGS, SCEC, Kinematics, and other universities following the Northridge earthquake. More than 85 instruments were deployed in the aftershock zone in the month following the earthquake. We also organized the dense re-deployment of 30 instruments in the Northridge area to record ground motions at spacings of a few hundred meters. The data are being analyzed for local site response and short-period coherence studies. The Pasadena Office also served as a base of operations for many USGS scientists who were temporarily stationed in southern California to study the effects of the Northridge earthquake.
  - Project scientists gave over 100 talks and participated in a number of community fairs to communicate to various civic and educational groups the importance of earthquake hazards in southern California. In addition we responded to more than 2,000 telephone requests for earthquake information.
3. The Pasadena Office served with Caltech as joint organizers of the 1994 Annual Meeting of the Seismological Society of America. This was the largest SSA yet held with 470 participants registering for the 3-day meeting. A 1-day symposium on the significance of thrust faults in the Los Angeles area was jointly presented with the Earthquake Engineering Research Institute (EERI) and a total of 1,325 earthquake professionals attended this session.
4. Most of the scientific results for the year centered on the Northridge earthquake activity. A general summary paper for Science has been prepared under the leadership of Lucy Jones (1994) and project scientists contributed to the EERI Northridge Earthquake Preliminary

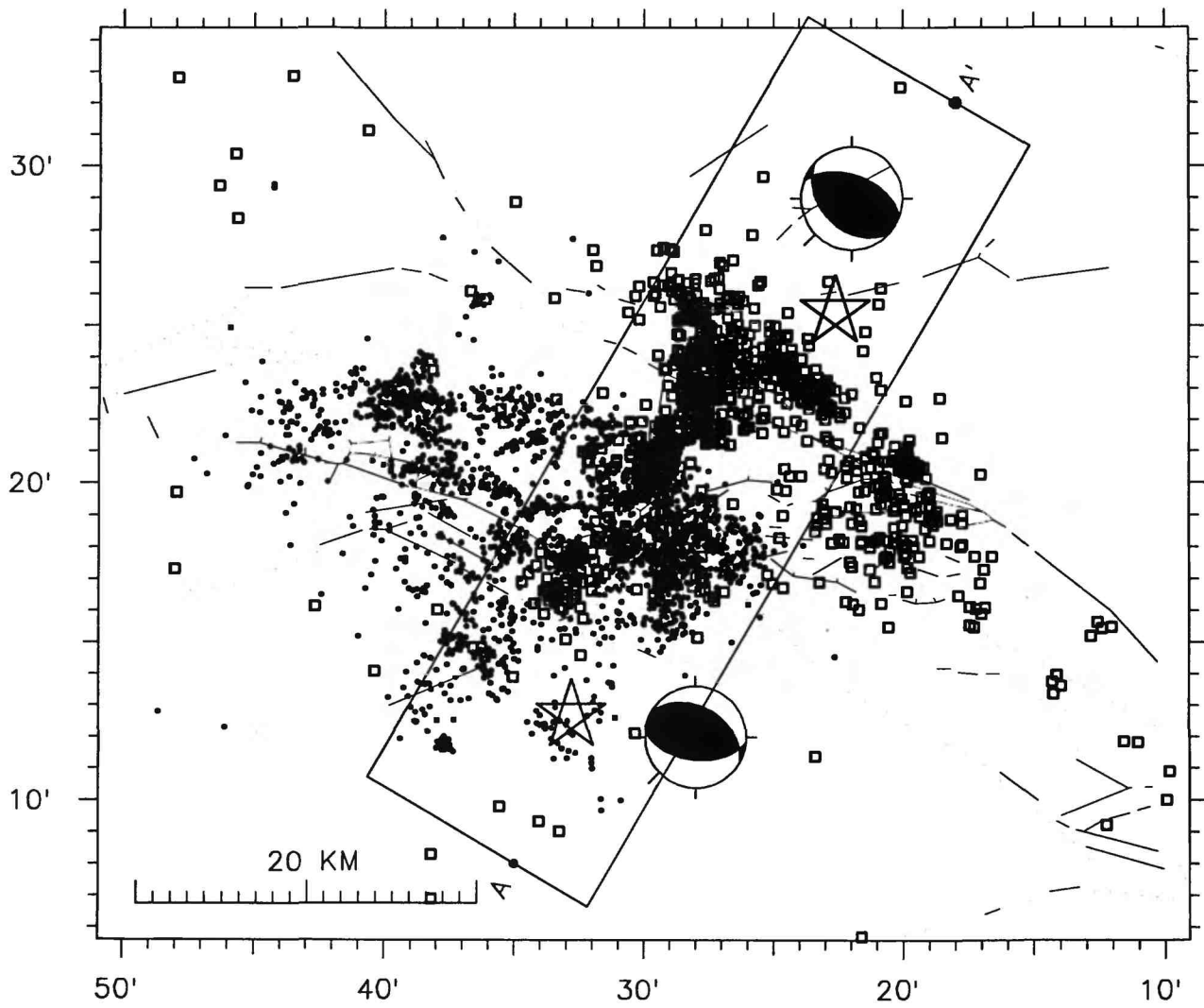
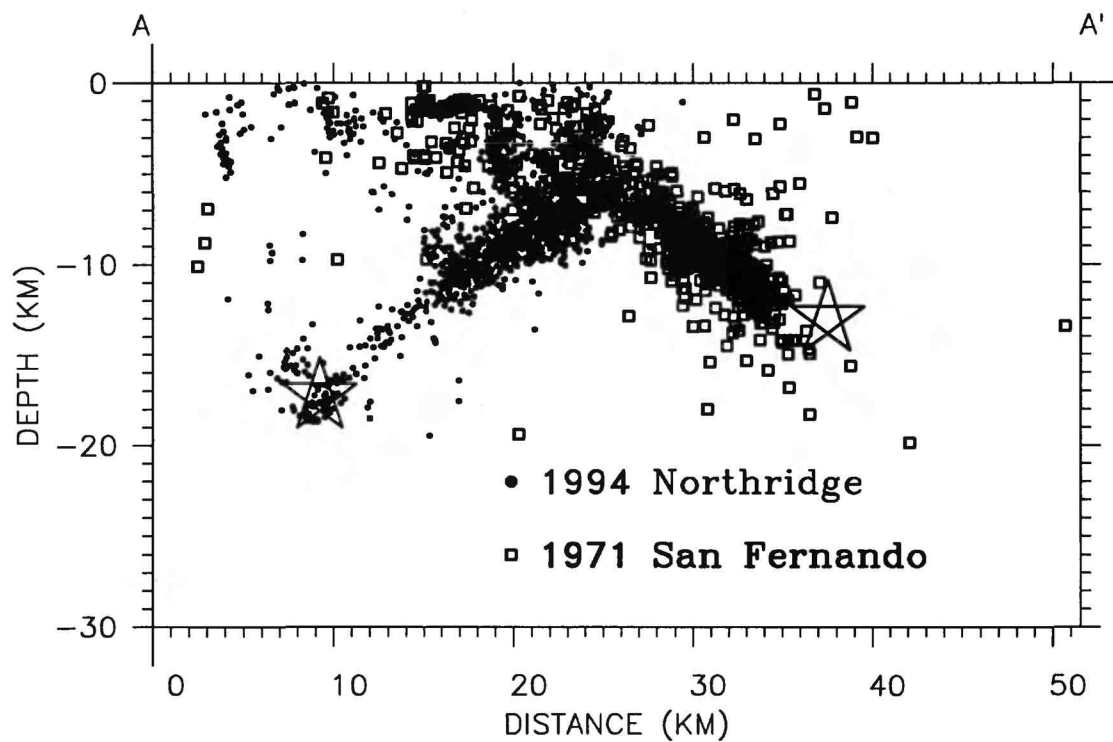
Reconnaissance Report and to the NCEER on Northridge. Jim Mori analyzed phase data from a portable deployment of seismometers following the 1971 San Fernando earthquake to obtain a far clearer picture of the spatial distribution of this earthquake than has been previously available. Aftershocks of the Northridge earthquake were also relocated to show the spatial relationship of these two sequences. A 3-dimensional velocity inversion was used to locate the events and the resulting aftershock distribution clearly shows that the 1971 fault plane appears to truncate the 1994 fault plane in the region that the two aftershock sequence overlap. Dave Wald and Tom Heaton are currently constructing a comprehensive model of the rupture process for the Northridge earthquake by modeling strong ground motions, teleseismic body waves, and geodetic deformations. Lucy Jones has studied the statistical properties of the Northridge sequence as well as general southern California seismicity which has been extraordinarily high for the past several years.

5. Work continued on the 1992 Landers earthquake sequence. Susan Hough continued her analysis of the seismotectonics of this sequence, including: 1) fault zone wave investigations in the southern Joshua Tree region; 2) dense array analysis of strong motion data from Landers and an early M 5.7 aftershock, focused on investigation of surface rupture to the south of the Landers epicenter; 3) empirical Green's function analysis of Joshua Tree aftershocks; and 4) broadband studies of the M6.5 Big Bear earthquake. Jim Mori's research included: 1) an empirical Green's function analysis of the Joshua Tree foreshock showing that it ruptured northward. The Joshua Tree mainshock initiated near the edge of the foreshock rupture zone. 2) work on a 3-D velocity inversion of the Landers fault area using explosions and earthquakes recorded on 40 portable stations along the fault. 3) Work continued on analyses of strong SmS phases, which are often 2 to 5 times larger than the direct S phase. The large amplitudes are attributed to the simple velocity structure in the Mojave Desert that does not complicate the Moho reflections. Dave Wald and Tom Heaton completed finite fault inversions of teleseismic, strong motion, and geodetic data for the Landers mainshock. A movie was made to show the temporal and spatial development of rupture.
6. Tom Heaton and Dave Wald produced estimates of broadband strong motions for hypothetical earthquakes in the Los Angeles basin. These estimates were used by John Hall (Caltech structural engineering) to show that large pulses of ground displacement could potentially cause the failure of high-rise and base-isolated buildings.
7. Dave Wald initiated analysis of a series of M7 earthquakes and one M8 earthquake in the Puerto Rico/ Dominican Republic region (1943-1953). Study of these damaging earthquakes will help to define the plate motions in a complex transition from frontal subduction to transcurrent faulting.
8. Lisa Wald and Tom Heaton continued analysis of 15 to 30-sec teleseismic Rayleigh waves observed on the dense short period California seismic networks. This study shows systematic differences in crustal structure and also demonstrates the complex nature of multipathing for these wavetrains.

## REPORTS

Abercrombie, R. and J. Mori, Initial onset of the M7.3 Landers Earthquake, Bull. Seismol. Soc. Am., 1994, 74, 725-734.

- Benz, H.M., J.E. Vidale, and J. Mori, Studies of the Earth's deep interior using an ultra-large aperture seismic array, EOS, 1994.
- Dolan, J.F., D. J. Wald, N. Breen, H.T. Mullins (1994). Strain accumulation and seismic energy release localized along collisional asperities: the 1946 and 1943 North-Central Caribbean earthquakes, *Geol. Soc. Am. Bull.* submitted for publication.
- Heaton, T.H. and D. J. Wald (1994). Ground Motion Estimates From a Magnitude 7, Blind Thrust Earthquake Under Los Angeles, Earthquake Engineering Research Institute, 1994 annual meeting abstracts.
- Heaton, T.H., J.F. Hall, D.J. Wald, and M.W. Halling (1994), Response of high-rise and base-isolated buildings to a hypothetical M 7.0 blind-thrust earthquake, submitted to *Science*.
- Hough, S.E., Y. Ben-Zion, and P.C. Leary (1994). Tectonic Structure of the Southern end of the 4/22/93 Joshua Tree earthquake rupture zone from analysis of fault zone waves, *Bull. Seism. Soc. Am.*, 84, 761-767.
- Hough, S.E. (1994), Southern surface rupture associated with the M7.3 1992 Landers, California, earthquake, *Bull. Seism. Soc. Am.* 84, 817-825.
- Jones, L.E. and S.E. Hough (1994). Analysis of broadband recordings of the 6/28/92 Big Bear Earthquake: Evidence for a multiple-event source, submitted to *Bull. Seism. Soc. Am.*
- Jones, L.M. (1994). Foreshocks, aftershocks, and earthquake probabilities: accounting for the Landers Earthquake, *Bull. Seism. Soc. Am.*, 84, 892-899.
- Jones L.M., and Scientists of the USGS and SCEC (1994). The Magnitude 6.7 Northridge, California, earthquake of January 17, 1994, submitted to *Science*.
- Jones, L.M., E. Hauksson, and J. Mori, The Landers earthquakes, *Earthquakes and Volcanoes* in press, 1994.
- Wald, D. J. and T. H. Heaton (1994). Spatial and temporal distribution of slip for the 1992 Landers, California earthquake, *Bull. Seism. Soc. Am.*, 84, 668-691.
- Wald, D. J. and J. Dolan (1994). Seismic waveform and tectonic analysis of the 1943-1953 Hispaniola earthquake sequence, *Seismological Research Letters*.
- Wald, D. J. and T. H. Heaton (1994). A dislocation model of the 1994 Northridge California, earthquake determined from strong ground motions, USGS Open-file Report 94-278.
- Wald, D.J. and P. Somerville (1994), Variable slip rupture model of the great 1923 Kanto, Japan earthquake: Geodetic and Bodywaveform analysis, submitted to *Geophysical Journal International*, 1994.
- Wald, L. A., S. Perry-Huston, D. Given (1994). The Southern California Network Bulletin; January-December, 1994. U.S. Geological Survey Open-File Report 94-199, 49p.



**Broadband Modeling Local and Regional Seismograms**  
**Grant No. 1434-93-G-2322**

**Program Element 1.2**

Donald V. Helmberger  
 Seismological Laboratory  
 California Institute of Technology  
 Pasadena, CA 91125  
 Tel (818)356-6998  
 Fax (818) 564-0715  
 email [helm@seismo.gps.caltech.edu](mailto:helm@seismo.gps.caltech.edu)

**Investigations**

The large number of recent events associated with the Big Bear-Landers earthquake sequence is providing a unique set of broadband data. This data set can be used in deriving detailed source characteristics and earth structure. In addition many of the historic events occurring along this extended zone have been recorded locally by relatively low gain long-period and short-period torsion instruments operated by Caltech (1930 to 1960) and by standard strong motion instruments.

To understand these seismograms and separate propagational distortions from source properties is relatively easy at teleseismic distances, but becomes more difficult at regional and local distances. Fortunately, the digital systems used in the TERRAscope array provide observations that greatly aid in establishing the nature of regional wave propagation. For example, the wide dynamic range allows motions from small events (aftershocks) to be compared with large events at the same site even though the motions can differ by several orders of magnitude. Signals at these distances have not suffered mantle attenuation and thus the broadband features of this system allow us to see obvious propagational effects (headwaves and critical reflections) and detailed source characteristics (near-field and source complexity).

**Results**

Several papers involving the waveform modeling of recent earthquakes have been published or are in press:

**PRELIMINARY WORK ON AN EARLY WARNING AND A RAPID RESPONSE  
 PROGRAM FOR MODERATE EARTHQUAKES**

by Craig W. Scrivner and Don V. Helmberger  
 Seismological Laboratory 252-21  
 California Institute of Technology, Pasadena, CA 91125

*Abstract.* Warning of imminent ground shaking due to a large earthquake would be useful to a variety of agencies. This kind of ground motion prediction is possible in southern California for events with magnitude less than 6, where path effects dominate. A test case for this is found in records for the June 28, 1991 Sierra Madre earthquake. A single station inversion of the record from the Pasadena station 20 km SW of the epicenter produces reasonable source parameters for the event. With these source parameters and a library of Green's functions calculated for an average southern California crustal model, ground motions can be predicted throughout the region. In particular, since the peak displacement for the Sierra Madre event occurs at Pasadena before ground motion begins at a station near the San Andreas in San Bernardino, ground motions near the San Andreas can be calculated before the seismic energy has propagated into the area. Considering this scenario in the reverse direction, records from a station near an earthquake on the San Andreas could be used to predict ground motions in the

metropolitan Los Angeles area. Broadband, high-dynamic-range seismic instruments produce high quality records for events over a wide magnitude range. Thus, the development of a warning system can be approached in stages starting with small events. With path effects determined by modeling moderate size events, work can begin on developing distributed fault models to predict ground motions of great earthquakes.

### SOURCE ESTIMATION OF FINITE FAULTS FROM BROADBAND REGIONAL NETWORKS

by Xi J. Song and Don V. Helmberger  
 Seismological Laboratory 252-21  
 California Institute of Technology, Pasadena, CA 91125

Fast estimation of point-source parameters for earthquakes has witnessed much progress in recent years, thanks to the development of broadband seismic networks. The expansion of these networks is now providing the opportunity to address source directivity and finiteness. Making this practical motivates the development of methods to quickly generate synthetic seismograms for finite sources. This proves possible when the fault dimension is small compared to the source-receiver distance and when the structure around the source region is relatively simple. To achieve this, we discretize the fault region into a set of elements represented as point-sources. We then generate and store the generalized rays separately for the best-fitting point-source location relative to the various stations and derive for each ray the response for neighboring point-sources with power series expansions. In this manner, each point-source contributes an element far-field source time function, a delta function in the case of step dislocation, to the total far-field source time function of a generalized ray. Finally, each ray is convolved with the corresponding far-field source time function and the results are summed up to form the total response. A simple application of this method is demonstrated with the tangential motions observed from the 1991 Sierra Madre earthquake. For this event, we are able to constrain the fault dimension by comparing data with synthetics for different source dimensions. Thus we simulate the faulting process as a 5 km-long line source propagating in the direction perpendicular to itself for 4 km with a constant velocity 3.0 km/sec. We then search the rupture direction on the fault plane by comparing corresponding synthetics with data. A southwestward rupture up-dip produces the best synthetic fit to the data which is compatible with other observations, Wald [1992].

### 2-D HYBRID METHOD STUDY OF LOS ANGELES BASIN EFFECTS FOR MODERATE AND POTENTIAL GREAT EARTHQUAKES

by L. Wen, C. W. Scrivner, and D. V. Helmberger  
 Seismological Laboratory 252-21  
 California Institute of Technology, Pasadena, CA 91125

A 2-D SH hybrid method was developed that combines finite-difference applied in the inhomogeneous region and an analytic method, GRT, outside this region. GRT enables us to study the basin effects for different types of incident energy. The comparison of hybrid method seismograms, GRT seismograms, and regular finite-difference seismograms yields good agreement. We applied this method to study Los Angeles basin effects for several moderate earthquakes to the NE of the basin by modeling the observations at USC station, which is located in the north part of the basin. Records at this station cannot be explained by 1-D models alone. 2-D models are more effective in fitting the amplitude, surface wave development and timing of phases at the station. For this study, a 2-D model for the NE edge of the Los Angeles basin (Scrivner and Helmberger, 1994) was combined with a 1-D model found by fitting waveforms recorded at the hard-rock site PAS. Local events could be fit with a layer (shear velocity 2.95 km/s, thickness 7 km) over a half space (shear velocity 3.7 km/s).  $S_n$ ,  $SmS$ , and  $sSmS$  times from events with greater than 100 km epicentral distance from PAS were then used to constrain the Moho depth. Comparisons of data and synthetic waveforms for 1-D and 2-D models were

made. The peak amplitude of the synthetics for both hard-rock and basin receivers match the data to within a factor of two. The synthetics accurately match the ratio in the data of the amplitudes of the basin waveforms to the hard-rock waveforms. The synthetic waveforms fit best for sources at mid-crustal depths. Shallow sources produce complicated cudas. For such sources, the synthetics underestimate the coda length by a factor of 2 and the coda amplitude by an order of magnitude. The general character of the coda can be matched by the inclusion of micro-basins in the shallowest portions of the basin model. Deep sources increase the amplitude of Moho reflection phases, and these can produce complex basin waveforms. Both observations and simulations indicate that the waveshape in the basin is controlled more strongly by the receiver's relative position in the basin than by the epicentral distance. In order to apply this method to large earthquakes, the hybrid method code was modified to be capable of handling large earthquakes with complex source kinematics. We use the slip description of the great 1906 San Francisco earthquake inferred by Wald et al. (1991) as a source on the southern San Andreas fault and predict the ground motions in the basin for a potential great earthquake in Southern California.

**MODELING OF AFTERSHOCKS FROM THE 1992 LANDERS, JOSHUA TREE AND BIG BEAR SEQUENCES, SOUTHERN CALIFORNIA**

by Laura E. Jones and Don V. Helmberger  
 Seismological Laboratory 252-21  
 California Institute of Technology, Pasadena, CA 91125

*Abstract.* The Joshua Tree, Landers and Big Bear sequences began on April 23, 1992 at 02:25 GMT with a  $M_w$ 4.3 foreshock which preceded the  $M_w$ 6.1 Joshua Tree mainshock by approximately 2 hours and 25 minutes. Aftershocks from the Joshua Tree mainshock (now considered precursory to the larger  $M_w$ 7.3 Landers earthquake) were distributed north of the Pinto Mountain fault into regions ruptured by the Landers sequence. The Landers earthquake consisted of rupture on six separate faults, if rupture south of the Pinto Mountain fault (on the Eureka peak fault) is included. Its aftershock sequence comprised earthquakes in many regions unassociated with primary rupture: aftershocks below the Pinto Mountain fault, in the Big Bear region, and an energetic cluster of aftershocks north of the city of Barstow. In this paper, we present source parameters, depths and durations, for sixty  $M_w > 3.8$  earthquakes from the Joshua Tree Landers, and Big Bear sequences. These events occurred between April of 1992 and November of 1994; the list of events presented comprises nearly every aftershock above  $M3.8$  for which we could obtain coherent TERRAscope data and accurate timing and location information. It includes a related, high stress-drop  $M5.3$  earthquake which occurred along the Garlock fault on July 11, 1992. Stress drops for these earthquakes appear to vary systematically with location, with respect to previous seismic activity, proximity to previous rupture (i.e., relative to the Landers rupture), and with tectonic province. In general, for areas north of the Pinto Mountain fault, stress-drops of aftershocks located off the faults involved with the Landers rupture are higher stress-drop than those located on the fault, with the exception of aftershocks on the newly recognized Kickapoo (Landers) fault. South of the Pinto Mountain fault, where there is a history of seismic swarms, but no single through-going fault, stress-drops are not usually high. For the Big Bear region, stress-drops appear to correlate with depth, with the deepest events yielding the highest stress-drops. Further, events in this region overall yield higher stress-drops than in the Mojave, associated with the Landers and Joshua Tree sequences.

## Quaternary Deformation Between Coyote Point and Lake Merced on the San Francisco Peninsula: Implications for Evolution of the San Andreas Fault

U.S Geological Survey  
 National Earthquake Hazard Reduction Program  
 Fiscal Year 1994 Award No.1434-94-G-2426

**James V. Hengesh**, Dames and Moore, 221 Main Street, Suite 600,  
 San Francisco, CA 94105  
 (415) 243-3819, FAX (415) 882-9261, E-mail: [sfojvh@dames.com](mailto:sfojvh@dames.com); and,  
**John Wakabayashi**, Consultant, 1329 Sheridan Lane,  
 Hayward, CA 94544 (510) 887-1796

Program Element: II.5 *Identify active faults, define their geometry and determine rates of earthquakes*

### INVESTIGATIONS

This investigation was conducted to evaluate potential hazards associated with the Coyote Point and Hunters Point fault zones, originally reported by Mann and others (1993). These two fault zones were identified based on numerous apparent displacements of Holocene Bay Mud observed on high resolution seismic reflection profiles acquired in south San Francisco Bay. The fault zones were interpreted to be several kilometers wide, projected onshore near Colma Valley and at Hunters Point, and across the densely populated San Francisco Peninsula. However, recent seismic reflection data and reinterpretation of data from Mann and others (1993), indicate that inferred fault-related features in the Bay were artifacts of the energy source and processing used during this survey. New data show strong evidence for unfaulted Holocene Bay Mud along the previously inferred Coyote Point fault zone (Marlow and others, 1994). Therefore, based on the most recent offshore reflection data, the Holocene active Coyote Point fault, as previously inferred, does not appear to exist.

The initial goal of this study was to evaluate the location and activity of onshore extensions of the inferred Coyote Point and Hunters Point fault zones, and if possible, to identify sites for future paleoseismic investigations: this project was conducted prior to acquisition of the new offshore data by Marlow and others (1994). Our investigation concentrated onshore of the inferred Coyote Point fault because the extensive Quaternary stratigraphic section in this area provided a means to evaluate the style and rate of deformation over the last ca 1.5 My. Our scope of work included: 1) compiling and reviewing existing data; 2) examining the earliest available aerial photography of the area; 3) constructing profiles of streams and geomorphic surfaces from existing topographic and geologic maps; 4) mapping Quaternary geologic units; 5) examining borehole data to assess Quaternary stratigraphy and evidence of deformation; and 6) analyzing deformation in a local and regional tectonic context.

### RESULTS AND DISCUSSION

#### Evidence for Late Quaternary Deformation

Investigations conducted for this study concentrated on the area between San Francisco International Airport and Ocean Beach, as shown on Figures 1 and 2. Our investigation identified: differential uplift

of Merced and Colma formations; presence of minor Quaternary faults in Merced Formation on the west side of San Francisco Peninsula; lineaments and topographic steps in Colma Formation in Colma Valley; and tonal lineaments in marshes on the west shore of San Francisco Bay. In addition, as a result of our investigation of Quaternary deformation, we have developed a model that relates deposition of the Pleistocene Merced and Colma formations to evolution of the San Francisco Peninsula segment of the San Andreas fault. This model helps explain Quaternary deformation and faulting observed in the Lake Merced area and elsewhere in Colma Valley, and relates occurrence and temporal variation in activity of secondary faults to migration of secondary extensional and contractional domains along the San Andreas fault.

Evidence of late Quaternary faulting and deformation was identified along Colma Valley, the northwest-trending topographic trough that lies southwest of San Bruno Mountain. Several photo-lineaments, expressed in Colma Formation sediments (< 70 to 130 ka; Clifton and others, 1988), trend northwestward through this trough, as shown on Figure 2. The lineaments consist of both downslope and upslope facing topographic steps and breaks in slope. Many of the downslope-facing topographic steps persist, but upslope-facing steps appear to have been modified by subsequent development. Changes in stream gradients noted in thalweg profiles coincide with some of these lineaments, and occur in reaches of drainages incised into Colma Formation and younger deposits, shown on Figure 3. Tonal lineaments were also identified in marshy areas on the Bay margin, but field examination could not determine their origin. One set of lineaments coincides with changes in stream gradient along the base of the southern slopes of San Bruno Mountain and may correspond to the Hillside fault zone (Figure 3), a Franciscan nappe bounding shear zone (Wakabayashi, 1992) originally mapped by Bonilla (1971). However, both the lineaments and breaks in stream gradient diverge significantly south from the basement fault trace. Other lineaments nearer to the axis of the trough or valley approximately correspond with the San Bruno fault of Bonilla (1964), but may also be due to fluvial processes. The lineaments, geomorphic surface, and stream gradient changes could also be due to erosional rather than tectonic processes.

A detailed total station survey of the sea cliff below Fort Funston was completed to investigate evidence of deformation in the Pleistocene Merced and Colma formations across the northwest projection of the Coyote Point Fault. The survey showed a significant angular unconformity between the Merced Formation and overlying Colma Formation, consistent with Hall (1964) and Clifton and others (1988). As shown on Figure 4, the upper Merced Formation dips up to 55 degrees to the northeast and is displaced by a fault with 20 m of down to the northeast vertical separation. A monocline adjacent to the fault may accommodate an additional 50 m of vertical separation and appears to fold Colma Formation, which changes dip from 10 degrees to 17 degrees across the fold axis. Displaced upper Merced Formation is estimated to be 200 to 400 ka (Clifton and others, 1988), yielding a vertical separation rate (including the monoclinal flexure) of 0.18 to 0.35 mm/yr. It is not clear whether this fault has normal or reverse separation, although dips of Merced strata on either side of the fault appear to be more compatible with a normal fault. This fault is a continuation of a linear down to the northeast topographic step that, in part, bounds the west side of Lake Merced basin.

Evidence for potential deformation onshore of the previously inferred Coyote Point fault zone has been identified. However, because recent offshore profiles provide evidence of no Holocene faulting along track lines that cross the inferred Coyote Point fault, features observed during this study may be: a) non-tectonic in origin, b) inherited structures from other structural domains, c) related to the Peninsula Fold and Thrust Belt, or d) related to deformation on an older bedrock fault inferred based on a prominent magnetic anomaly along western San Francisco Bay. Subsequent studies are proposed to clarify the deformational history of this area.

## Tectonic Subsidence, Emergence and Deformation of the Merced and Colma Formations

The Merced Formation and the overlying basal part of the Colma Formation are interpreted to have been deposited as a result of transgressive-regressive cycles related to eustatic sea level fluctuations superimposed on a subsiding basin, with deposition keeping pace with tectonic subsidence (Clifton and others, 1988). The subsidence rate is estimated at 1.3 mm/yr from the inception of Merced deposition (1.6 to 1.2 Ma) to 0.4 Ma, and 0.8 mm/yr after 0.4 Ma (Clifton and others, 1988). The Merced Formation dips and youngs to the northeast, suggesting that subsidence was controlled by a down to the southwest fault along the northeast margin of the basin. This interpretation is consistent with location of the basin axis, determined from depth to bedrock maps that show the axis to lie northeast of exposed Merced Formation (Bonilla, 1964). Rapid Quaternary subsidence represented by deposition of Merced and Colma formations appears inconsistent with exposures at 200 meters above sea level (e.g. Brabb and Pampeyan, 1983).

We believe that changes in localized extensional and contractional domains along the San Andreas fault may explain the opposing senses of deformation recorded in the Merced Formation. North of where the San Andreas fault enters the Pacific Ocean at Daly City, the fault must step or bend to the right to connect with its northwest continuation in Marin County. This geometry suggests a releasing or extensional bend in the fault, and is consistent with extensional focal mechanisms for earthquakes in this area (Zoback and Olsen, 1994). The extensional regime in the step-over region indicates that a pull-apart basin should be forming offshore of San Francisco and the Golden Gate. Such a basin may be the depo-center of the Merced Formation and future equivalents. Merced Formation exposed on San Francisco Peninsula (Peninsula) may have been translated southward along the San Andreas moving from a subsiding extensional domain offshore, to a dominantly contractional domain east of the San Andreas fault on the Peninsula. Similarly, Merced Formation west of the San Andreas fault may have been translated northward from its place of deposition to exposures 130 meters above sea level west of the fault in Marin County (Wagner and others, 1990).

The apparent high rate of Quaternary subsidence recorded by the Merced and Colma Formations (0.8 mm/yr between 0.4 to 0.2 Ma) is inconsistent with uplift of the Merced and Colma formations on San Francisco and Marin Peninsulas. Merced Basin appears to have formed as a localized extensional feature associated with a releasing bend in the San Andreas fault, and is progressively emerging onto San Francisco Peninsula as contractional deformation associated with a restraining bend in the San Andreas migrates northward into the "wake" of the migrating pull-apart. Merced Formation may be emerging on Marin Peninsula due to local contraction related to intersection of the Seal Cove and San Andreas faults.

Possible relationships between accumulation and deformation of the Merced Formation and evolution of the San Andreas fault are discussed below.

### Implications for Evolution of the San Andreas Fault in the San Francisco Bay Area

Mapping by Brabb and Pampeyan (1983), Wakabayashi and Moores (1988), Wakabayashi (1992, and unpublished mapping), indicate that distinctive limestone-bearing Franciscan nappes are displaced 27 km by the San Andreas fault on the Peninsula. This segment of the San Andreas fault has a late Holocene slip rate of about 20 mm/yr (Clahan and others, 1994). Based on offset basement rocks and an assumed constant slip rate, the Peninsula segment of the San Andreas fault may have initiated movement at 1.35 Ma. This age is similar to the 1.2-1.6 Ma age estimate for the basal Merced (Clifton and others, 1988), and suggests a genetic link between deposition of Merced and Colma formations,

onset of Merced pull-apart basin formation, and initiation of movement on the San Francisco Peninsula Segment of the San Andreas fault.

Although reports of a Holocene active Coyote Point fault in San Francisco Bay were based on an apparent mis-interpretation of geophysical data (Marlow and others, 1994), the initial report of Mann and others (1993) drew our attention to possible relationships between Franciscan Complex structures and late Quaternary deformation. Although the most recent reflection profiles from the area offshore of Coyote Point provide evidence of no Holocene faulting, the geometry and distribution of Franciscan structures may offer some constraints regarding development of the San Andreas fault system in the San Francisco Bay Area. Wakabayashi (1992) interpreted Bay Area Franciscan Complex as a stack of coherent thrust nappes bounded by melange zones. Some melange zones contain serpentinite and correspond to strong magnetic anomalies (Jachens and Roberts, 1993). This nappe stack formed from 165 to 60 Ma and comprises a series of gentle folds (Wakabayashi, 1992), the limbs of which define regional northeast or southwest-dipping domains. The folded nappe stack is cut by several faults: One of these faults appears to trend northward west of the Coyote Hills, as shown on Figure 5. The Coyote Hills are composed of a coherent Franciscan nappe that is equivalent to the Marin Headlands terrane in central San Francisco (Wakabayashi, 1992). In both areas the Marin Headlands terrane is structurally overlain by serpentinite-bearing melange, however the nappes dip southwest at Coyote Hills and northeast in San Francisco. Clearly the Coyote Hills and San Francisco are not part of the same fold limb. The location of the probable fault in the folded nappe sequence may be west of the Coyote Hills and coincide with a deflection of the linear magnetic anomaly pattern that appears to mark the southeastward continuation of the Hunters Point shear zone (Jachens and Roberts, 1993), the serpentinite-bearing melange that structurally overlies the Marin Headlands terrane in San Francisco. The offset part of the southwest-dipping fold limb on the west side of the fault is probably located west of Red Rock, west of Point Richmond (Wakabayashi, 1992). Restoration of the fold limb yields a dextral offset of 35-40 km. This fault may strike to the north and pass through an alluvium-filled gap east of Point Richmond (Wakabayashi, 1992). Another significant break in the nappe sequence passes through the topographic trough south of San Bruno mountain. Because this fault is parallel to the strike of the nappe contacts it is difficult to estimate the separation, but it appears to be significant (perhaps tens of kilometers) based on the mismatch of Franciscan structures and lithologies across the fault. The timing of movement on these faults is at present poorly constrained. They must post-date the assembly of the nappe stack, so they are post-60 Ma. These faults may have played a role in the evolution of the San Andreas fault system as will be discussed below.

As noted above, the Peninsula segment of the San Andreas fault displaces the Franciscan Complex only 27 km. The late Cenozoic dextral slip on the San Andreas fault system in central and northern California is estimated to be about 300 km (see Powell, 1993 for review). This leaves over 270 km of dextral displacement, when offset along the Peninsula segment of the San Andreas fault is subtracted from the total. This large amount of residual offset led some researchers to place over 250 km of dextral slip on the Pilarcitos fault (Jachens and Griscom, 1989; Powell, 1993), a fault that marks the contact between the Franciscan Complex and the Salinian Block. The original contact between the Salinian Block and Franciscan Complex in this area is a zone of mylonites over a kilometer wide, and clasts of mylonite are found in Eocene sandstones that overlap the old basement fault zone (Wakabayashi and Moores, 1988). The late Cenozoic Pilarcitos fault that displaces Tertiary rocks on the Peninsula west of the San Andreas fault must also cut across either the Salinian Block, Franciscan Complex or the contact mylonite zone. The distinctiveness of Franciscan Complex, mylonite zone and Salinian block lithologies preclude more than a few kilometers of late Cenozoic displacement along the Pilarcitos fault.

Wakabayashi (1992) suggests that most of the residual dextral slip along the San Andreas fault system occurred in the eastern San Francisco Bay Area, based on the 190 km post-10 Ma dextral offset of the Tolay and Quien Sabe volcanics proposed by Curtis (1989). This would distribute 190 km of post-10 Ma dextral displacement on the Hayward fault other faults to the east. Most of the displacement may have been accommodated on an inactive fault a few kilometers east of the Hayward fault, based on mismatches of Cretaceous conglomerate assemblages (Seiders, 1988; V. M. Seiders pers. comm., 1991). If we accept the 190 km dextral offset for the eastern faults of the San Andreas system, a residual of about 80 km still remains. It is possible that the fault west of Coyote Hills (35-40 km dextral separation) and the fault southwest of San Bruno mountain may have accommodated much of the remaining residual dextral offset. Late Cenozoic movement along the fault west of the Coyote Hills may have resulted in formation of a pull apart basin west of San Leandro that is marked by a major gravity low (Jachens and Roberts, 1993). If the dextral faults in the Bay are indeed late Cenozoic, they have accommodated high slip rates in the past based on their large separation. Even averaged over the entire post-subduction period (about 10 Ma at the latitude of the Bay) the long term slip rates on these faults would be comparable to major strike slip faults of the San Andreas fault system. As noted above there is evidence for no Holocene faulting along the surveyed part of the inferred Coyote Point fault and minimal seismicity, so bedrock structures in this part of the Bay are probably inactive or have extremely low slip rates.

## REPORTS PUBLISHED

Preliminary results of this investigation were presented at the June 7, 1994 CONCERT Workshop, are reported in the following abstracts, and will be presented at the 1994 AGU Fall Meeting and the 1995 AAPG/SEPM Spring Meeting:

Hengesh, J. V., and Wakabayashi, J., in review, Dextral translation and progressive emergence of the Pleistocene Merced basin and implications for timing of initiation of the San Francisco Peninsula segment of the San Andreas fault: accepted for the 1995 AAPG/SEPM Spring Meeting.

Hengesh, J. V., and Wakabayashi, J., 1994, Quaternary deformation along the onshore projection of the Coyote Point fault zone: EOS, v. 75, p. 681.

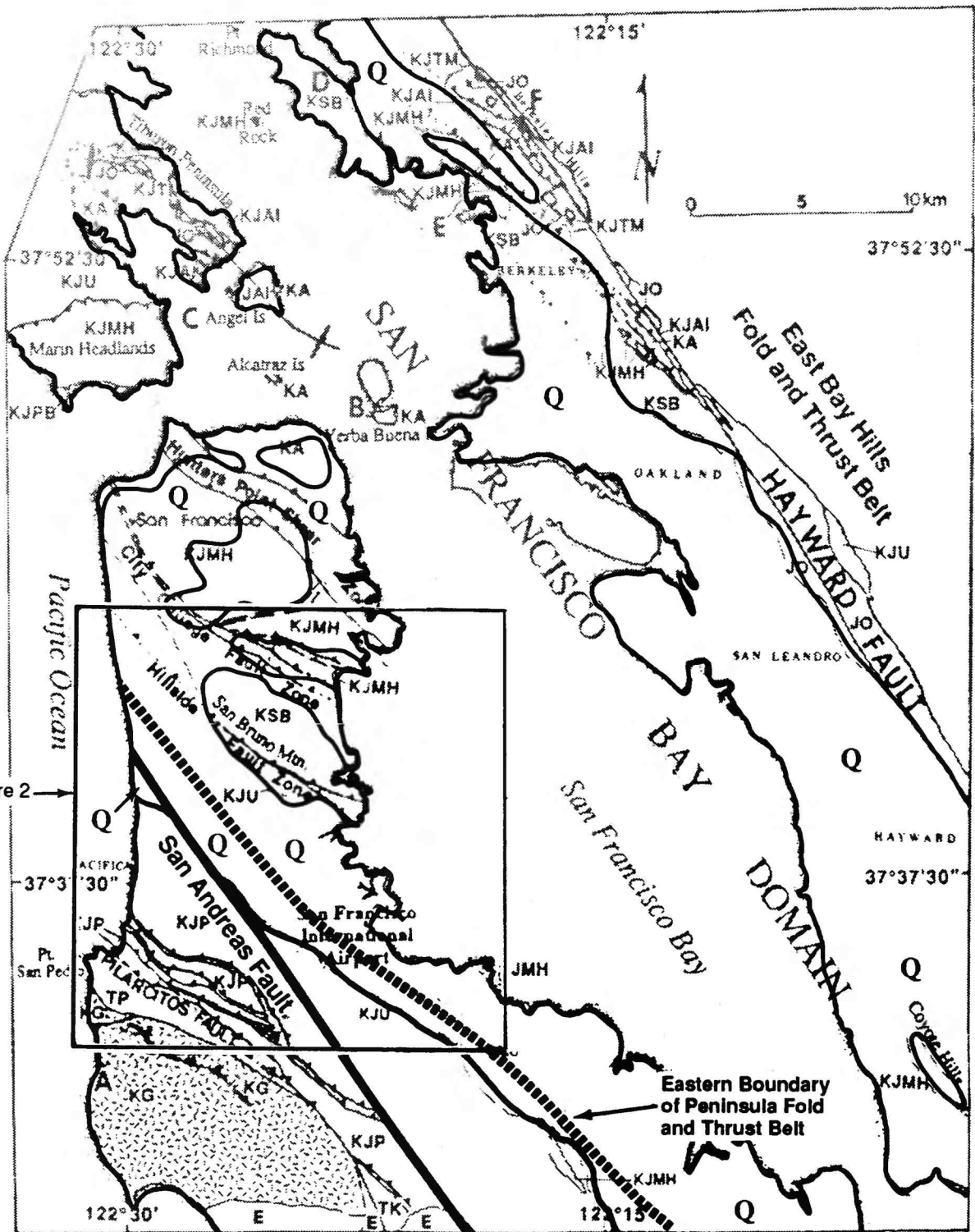
Wakabayashi, J., and Hengesh, J. V., 1994, The influence of basement structural grain on Holocene faulting, San Francisco Bay, California: EOS, v. 75, p. 681.

Some of the results are being prepared for publication as part of an SEPM special publication on neotectonics of the San Francisco Bay region, and manuscripts are being prepared for submission to peer-reviewed journals.

## REFERENCES

- Bonilla, M.G., 1964, Bedrock-surface map of the San Francisco South quadrangle, California: San Francisco Bay Region Environment and Resources Planning Study, Basic Data Contribution 26, scale 1: 31,680.
- Bonilla, M.G., 1971, Preliminary geologic map of the San Francisco South quadrangle, California: U.S. Geological Survey Miscellaneous Field Studies Map MF-311, scale 1:24,000.
- Brabb, E. E., and Pampeyan, E. H., 1983, Geologic map of San Mateo County, California: U.S. Geological Survey Miscellaneous Investigation Series Map I-1257.

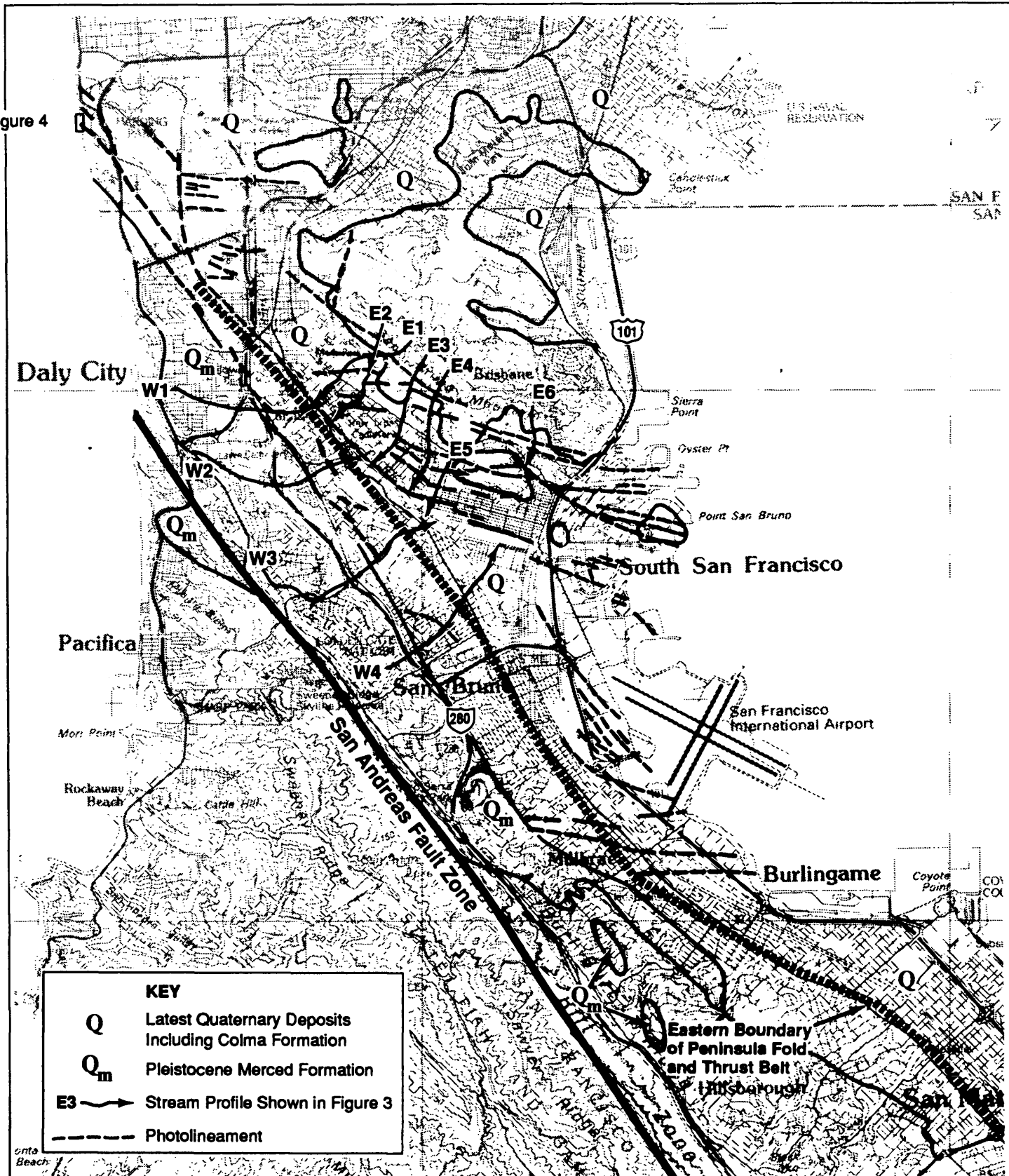
- Clifton, H.E., Hunter, R.E., and Gardner, J.V., 1988, Analysis of eustatic, tectonic, and sedimentologic influences on transgressive and regressive cycles in the late Cenozoic Merced Formation, San Francisco, California: in Paola, C., and Kleinspehn, K.L., eds., *New perspectives of basin analysis*: Springer Verlag, New York, p. 109-128.
- Curtis, G.H., 1989, Late Cenozoic volcanic rocks of the central Coast Ranges: in Wahrhaftig, C., and Sloan, D., eds., *Geology of San Francisco and Vicinity, International Geological Congress Field Trip Guidebook T105*, p. 33-35.
- Griscom, A., and Jachens, R. C., 1989, Tectonic history of the north portion of the San Andreas fault system, California, inferred from gravity and magnetic anomalies: *Journal of Geophysical Research*, v. 93, p. 3089-3099.
- Hall, N.T., 1965, Petrology of the type Merced Group, San Francisco Peninsula, California: unpub. M.A. thesis, University of California, Berkeley, 126 pp.
- Jachens, R. C., and Roberts, C. W., 1993, Aeromagnetic map of the San Francisco Bay Area: U.S. Geological Survey, Geophysical Investigations Map GP-1007, scale 1: 286,500
- Mann, G.M., Marlow, M.S., and Brabb, E.E., 1993, Newly discovered strike-slip faults in south-central San Francisco Bay: *EOS*, v. 74, p. 693.
- Marlow, M.S., Hart, P.E., Carlson, P.R., Childs, J.R., Mann, D.M., Anima, R.J., and Kayen, R.E., 1994, High-resolution seismic-reflection profiles and interpretation pitfalls created by acoustic anomalies from Holocene muds beneath south San Francisco Bay: U.S. Geological Survey Open File Report OFR 94-639
- Powell, R.E., 1993, Balanced palinspastic reconstruction of pre-late Cenozoic paleogeology, southern California: Geologic and kinematic constraints on evolution of the San Andreas fault system: in Powell, R.E., Weldon, R.J., II., and Matti, J.C., eds., *The San Andreas fault system: displacement, palinspastic reconstruction, and geologic evolution*: Geological Society of America Memoir 178, p. 1-106.
- Seiders, V. M., 1988, Origin of conglomerate stratigraphy in the Franciscan assemblage and the Great Valley Sequence, northern California: *Geology*, v. 16, p. 783-787
- Wagner, D.L., Bortugno, E.J., and McJunkin, R.D., compilers, 1990, Geologic map of the San Francisco-San Jose quadrangle: California Division of Mines and Geology, Regional Geologic Map Series, Map No. 5A, scale 1:250,000.
- Wakabayashi, J., 1992, Nappes, tectonics of oblique plate convergence, and metamorphic evolution related to 140 million years of continuous subduction, Franciscan Complex, California: *Journal of Geology*, v. 100, p. 19-40
- Wakabayashi, J., and Moores, E. M., 1988, Evidence for the collision of the Salinian Block with the Franciscan subduction zone: *Journal of Geology*, v. 96, p. 245-253.
- Zoback, M. L., and Olson, J.A., 1993, Faulting complexity in the 1906 San Francisco earthquake epicentral area: *EOS*, v. 74, p. 411.



**FIGURE 1: Location Map**

Quaternary deposits (Q) are shown, as well as the eastern boundary of the Peninsula fold and thrust belt. Quaternary deposits from Schlocker (1974), Bonilla (1971), Brabb and Pampeyan (1983), Basement geology adapted from Wakabayashi (1992).

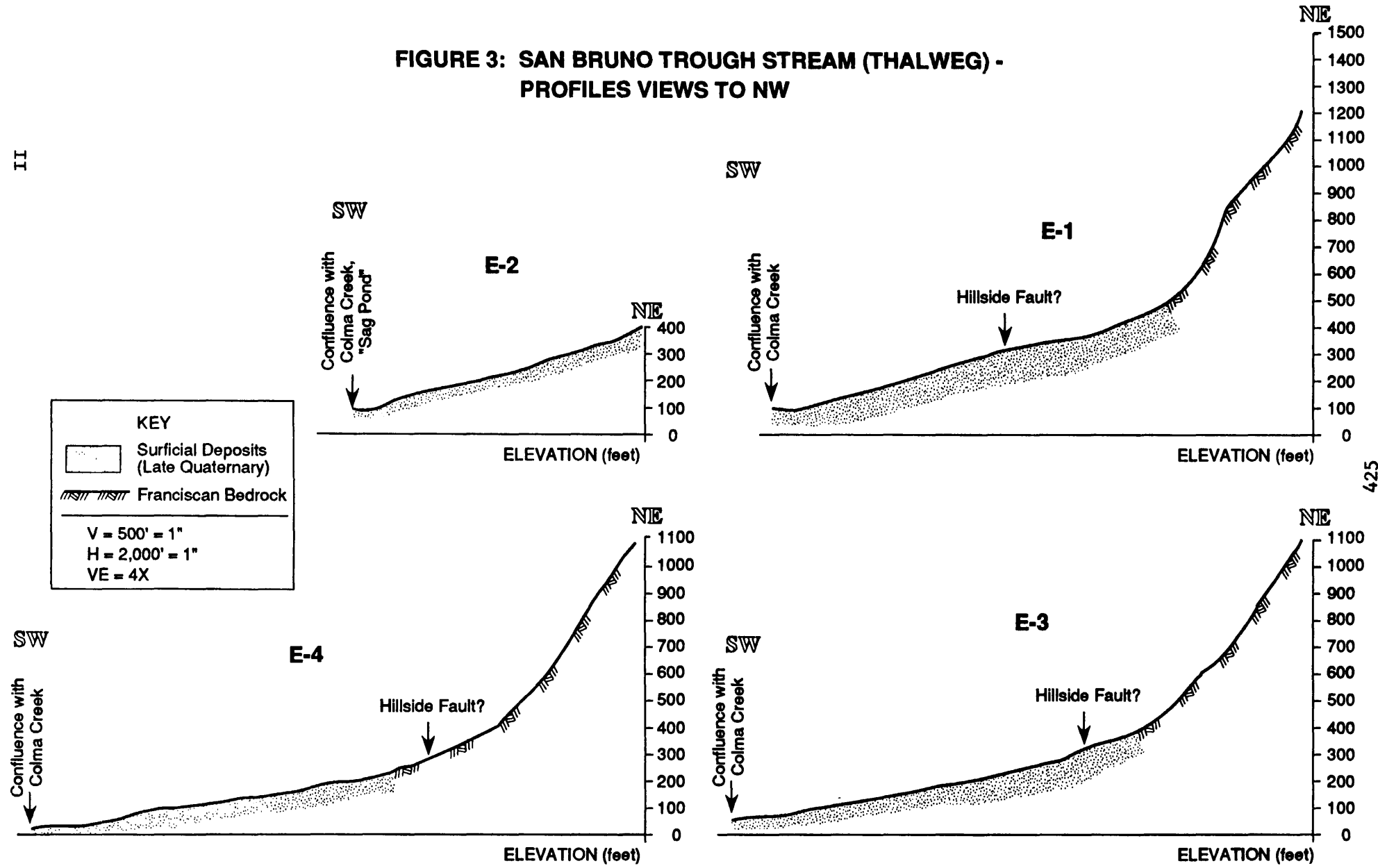
Figure 4



**FIGURE 2: Photolineament Map; Trough South of San Bruno Mountain**  
 Location of Figure 4, shown. Quaternary deposits from Schlocker (1974),  
 Bonilla (1971) and Brabb and Pampeyan (1983).

II

**FIGURE 3: SAN BRUNO TROUGH STREAM (THALWEG) -  
PROFILES VIEWS TO NW**



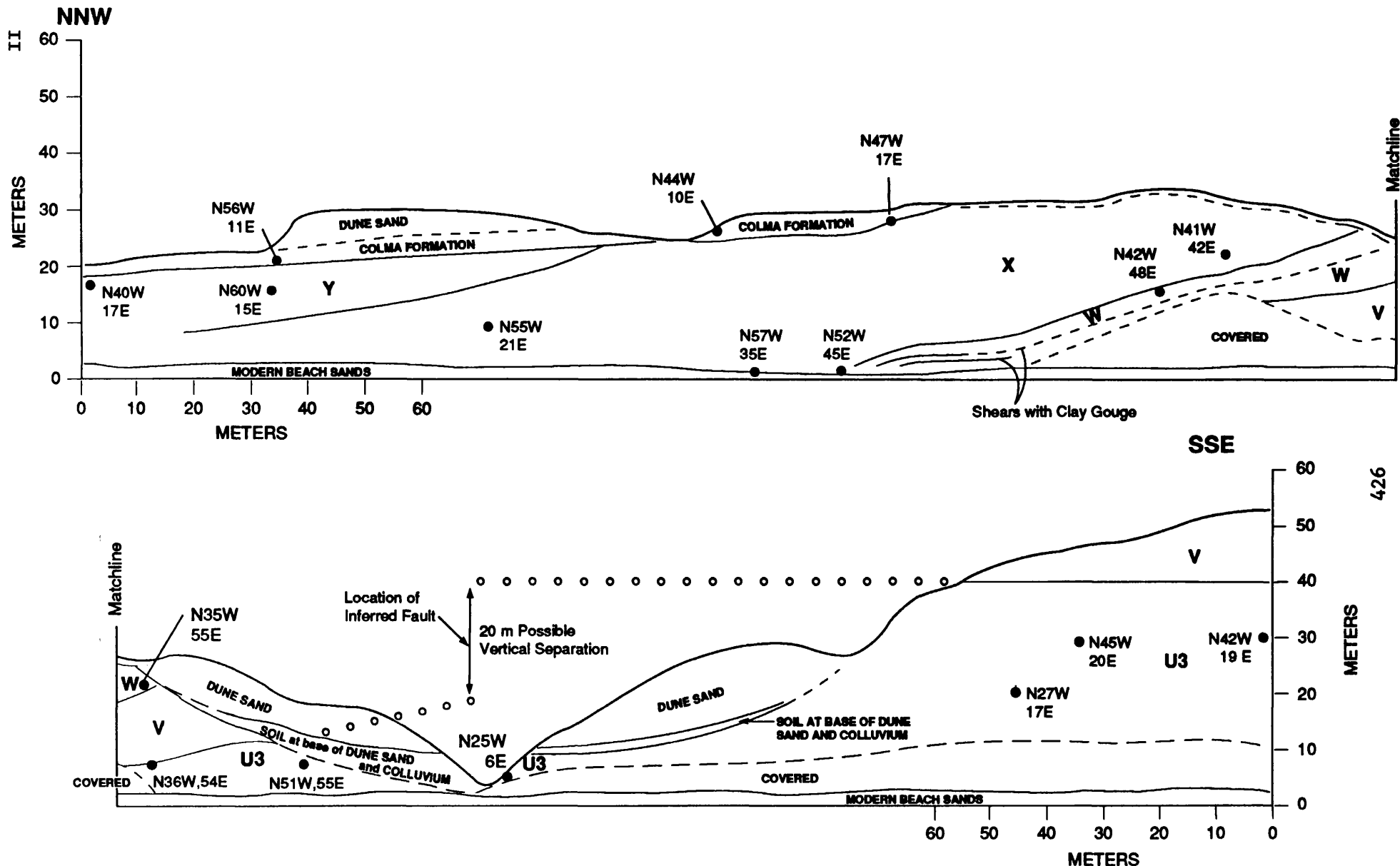
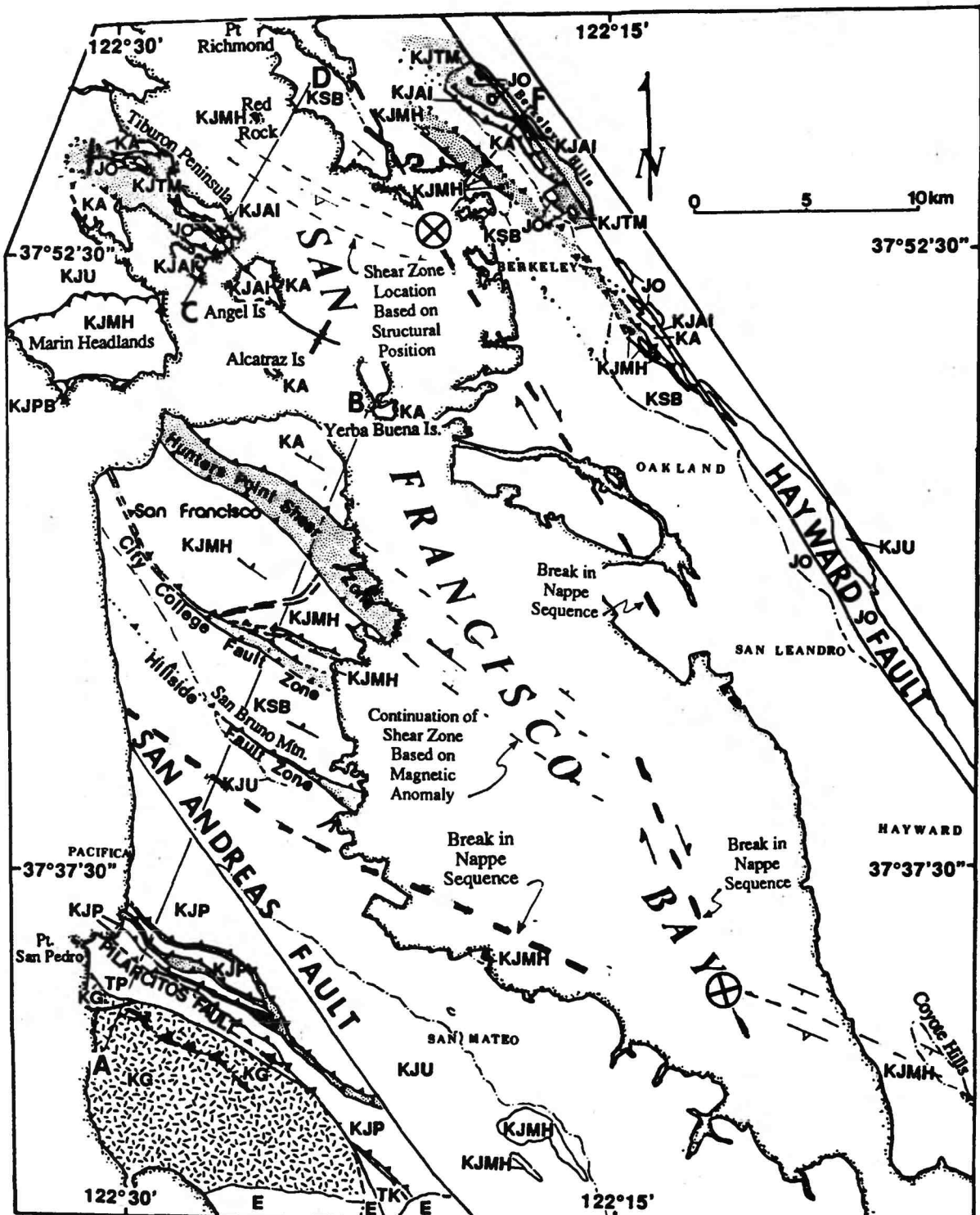


FIGURE 4: BEACH CLIFF, FORT FUNSTON, WEST OF LAKE MERCED

Contacts from total station survey data projected onto a vertical plane parallel to the beach. Note the change in orientation in bedding on the northern part of the profile in both the Merced Formation and overlying Colma Formation. This part of the beach cliff is the northernmost part of Clifton et al.'s (1988) Figure 6.4

Y, X, W, V, U3 = Stratigraphic units of the Merced Formation - units defined according to Clifton et al. (1988).  
 N54W, 36E = Strike and dip of bedding



**Figure 5.** Franciscan Complex structural grain showing dip of nappe sheets and faults that cut the nappe stack. Adapted from Wakabayashi (1992) with continuation of Hunters Point shear zone from Jachens & Roberts (1993). Denotes approximate location of offset northern margin of SW-dipping equivalent of Hunters Point shear zone.

Potential-field Study  
of the New Madrid Seismic Zone

9380-10101

Thomas G. Hildenbrand and Victoria Langenheim  
U.S. Geological Survey MS 989  
345 Middlefield Road  
Menlo Park, CA 94025  
(415) 329-5303  
(415) 329-5133 (FAX)  
[tom@laplace.wr.usgs.gov](mailto:tom@laplace.wr.usgs.gov)  
Element: II

### Investigations Undertaken

This project addresses the geophysical setting of the New Madrid seismic zone (using regional potential-field data) and characterizes seismic source zones (using high-resolution aeromagnetic and gravity data). The regional geophysical study delineates fundamental structures and their possible effect on the release of seismic energy. The local geophysical study identifies faults and other factors responsible for the concentration of earthquakes (e.g., igneous intrusions).

### Results

Past magnetic and gravity studies have primarily concentrated on the regional geophysical setting of the New Madrid seismic zone. FY 94 studies have focused on two particular geophysical features that appear to be intimately related to faulting: Missouri gravity low and the Arkansas to Illinois magnetic lineament.

The Missouri gravity low (MGL) trends SE across Missouri towards the Reelfoot rift. Filter applications and a processing called "terracing" have shown that the northeast border of the MGL extends across the rift. The significance of this result is that at the intersection of the rift and MGL lies the New Madrid seismic zone (NMSZ). An explanation has long been sought for the instability only along a 100-km-long segment of the rift axis in SE Missouri and NE Arkansas; yet the rift extends for at least 400 km from central Arkansas to western Kentucky. The crustal block created at the intersection of the Reelfoot rift and the source of the MGL includes the region of intense earthquake activity of the NMSZ. Why is this block unstable? What is the source of the MGL? What does this zone of intersection imply about earthquake potential?

- These questions are presently being addressed. Ideal body theory suggests that the top of the source of the MGL is shallow (<5 km). Simultaneous inversion of magnetic and gravity data along profiles across the 120-km-wide

source of the MGL reveals that the 35 mGal low is related to an upper crustal granitic body (depth to 12 km) with flanks dipping outward to suggest emplacement by intrusive activity.

These preliminary interpretations thus suggest that the MGL reflects a granitic batholith (herein called the Missouri batholith) that intersects the NMSZ (Fig. 1). Mechanical models are being studied that incorporate rigidity contrasts between a granitic batholith and flanking more competent metamorphic terranes. The presence of the weak granitic zone may be a contributing factor in restricting the lateral extent of the seismic zone along the rift's axis and in evaluating earthquake potential.

Another regional study includes the source of the Arkansas to Illinois (magnetic) lineament, which trends NE along the NW margin of the graben for at least 300 km. The AIL corresponds strongly with an exceptionally strong lineament as mapped on aerial photographs. This photo-lineament may be a southwestern continuation of the Commerce Fault from its mapped location at Thebes Gap, Illinois. The magnetic data suggest both normal and left-lateral movement along the AIL. The AIL crosses the Bloomfield pluton (M, Fig. 1) and apparently offsets its edges left-laterally about 5 km.

Modeling across the AIL and other NE-trending features just south of the Bloomfield pluton indicates a horst and graben topography, implying normal faulting. Because the AIL is probably caused by magnetic Precambrian crystalline rocks at depth, the close correlation in position between the AIL and the mapped location of the Commerce fault would imply that the Commerce fault is nearly vertical. The presence of this extremely linear, northeast-trending feature offset ~45 km northwest from the edge of the Reelfoot rift suggests that it is somehow related to the formation of the graben and may be susceptible to the same stress and earthquake potential as the Reelfoot rift.

On a more local scale, investigations continued on the strong relation between strain and igneous intrusions expressed in the magnetic field. Magnetic and gravity data were simultaneously inverted to provide a 3-D description of plutons N and N', Fig. 1. Seismicity correlates with plutons N and N' in three ways: (1) seismicity rate is higher NE of the plutons than within the plutons, (2) seismicity forms a cluster against the NE wall of pluton N' and decreases inside, and (3) seismicity is concentrated in a band NE of the plutons but is diffuse within the plutons. These patterns can be explained by higher fault strength where the rift fault passes through plutons and higher elastic module of the plutons compared to the surrounding crust:

- (1) If the top edge of the active rift fault is a dislocation loop expanding upward from NE of the plutons, then the highest seismicity rate may be where slip rate is highest, as observed. To the SW the high strength of plutons generally impedes the upward propagation of the main fault.
- (2) High strength of pluton N' impedes fault slip locally, and the high elastic rigidity of N' tends to repel and expel slip encroachment (edge and

screw dislocations near the fault edge). Thus pluton N' is nearly devoid of seismicity.

(3) Seismicity within pluton N may be diffuse for two reasons. First, high strength of igneous rocks may slow upward penetration of the fault, diverting slip sideways onto horizontal detachments at mid-crustal depth (10-20 km). Second, the high elastic rigidity of igneous rocks above and surrounding the fault tends to broaden the shear stress induced by the fault.

A secondary activity in FY 94 was to write a summary of the Geophysical Workshop held in Golden, CO, February 1993. The various presented data were synthesized within a promotional document of NEHRP's New Madrid efforts for EOS. Geophysicists involved in New Madrid NEHRP are coauthors.

#### Reports Published

Hildenbrand, T.G., Langenheim, V.E., and Stuart, W.E., 1993, Fault characteristics inferred from aeromagnetic data—Applications to the New Madrid Seismic Zone: 1993 Western Meeting of the American Geophysical Union, Technical Program and Abstracts, p. 223.

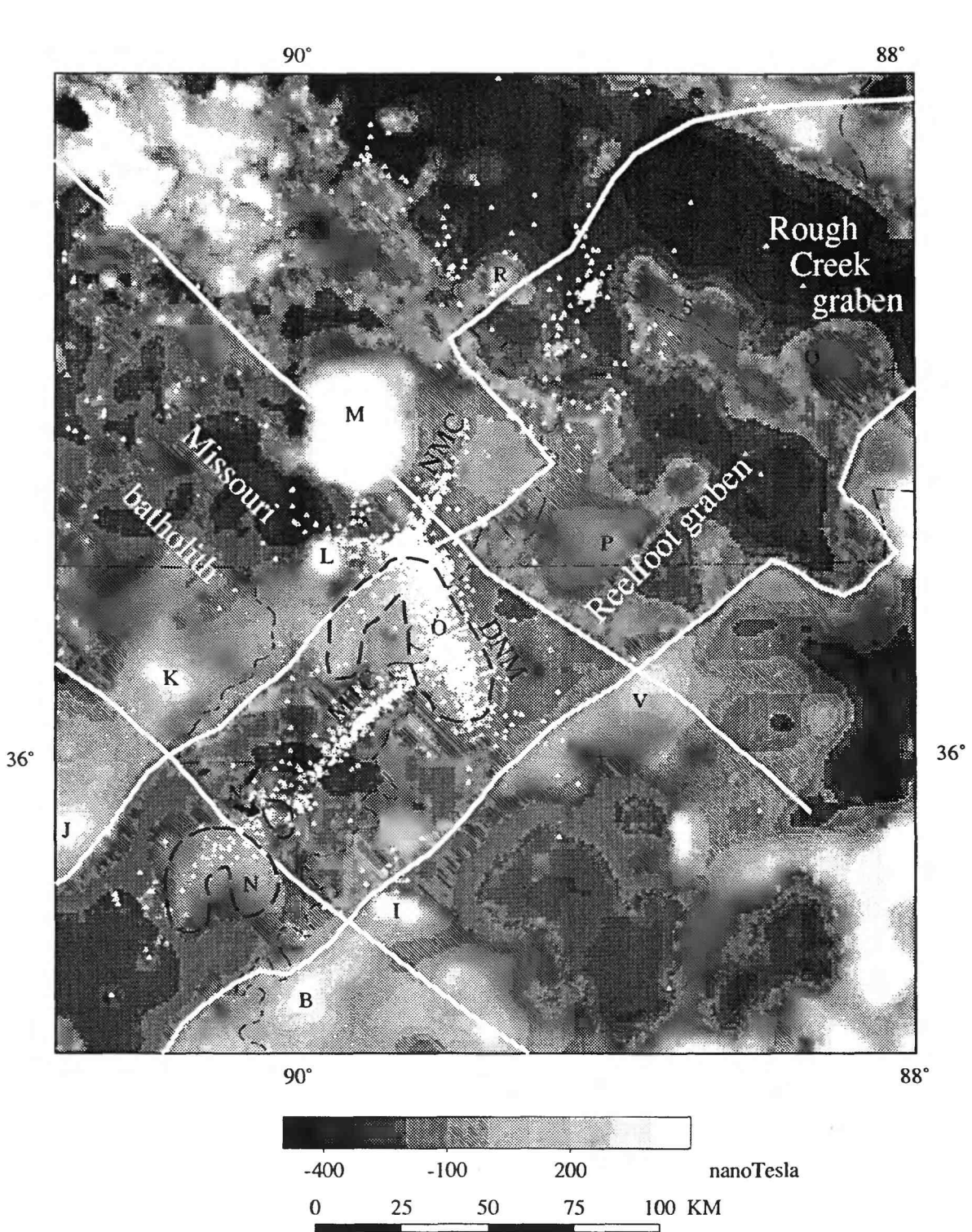


Figure 1 Magnetic-anomaly map showing two dense, magnetic igneous complexes (N and O) within the Reelfoot graben. Dashed lines delimit boundaries of complexes. (Note: N' is a secondary body of complex N). Small white triangles are earthquake epicenters. Several particularly interesting correlations between igneous bodies and earthquake occurrence exist: (1) earthquakes concentrate in the eastern limb of complex O, (2) earthquakes cluster at the edge of body N', and (3) earthquakes become more dispersed within the two igneous complexes, O and N.

## LONG VALLEY CALDERA MONITORING

9930-12073

D.P. Hill and A.M. Pitt  
Branch of Seismology  
U.S. Geological Survey  
345 Middlefield Road, MS 977  
Menlo Park, CA 94025  
(415-329-4795, FAX: 415-329-5163; email: hill@andreas.wr.usgs.gov)

### Investigations

This project is the hub of the USGS monitoring effort in the Long Valley caldera - Mono Craters area in eastern California. The Project Chief serves as Chief Scientist for Long Valley caldera and the Mono-Inyo Craters "observatory". As spelled out in Open-File Report 91-270, the objectives of the associated effort involve coordinating USGS monitoring, hazards assessment, and information dissemination activities focused on the ongoing unrest in the Long Valley-Mono Craters volcanic system. This project also systematically reviews the seismicity data from the subset of the Northern California Seismic Network (NCSN) stations covering the Long Valley caldera-Mono Craters region of the eastern Sierra Nevada and interprets their significance in terms of magmatic and tectonic processes.

### Results

#### *Long-Period Earthquakes*

Most earthquakes occurring near Long Valley caldera since the onset of recurring swarm activity in 1980 have the broad-band signature typical of tectonic (or volcano-tectonic) earthquakes with impulsive, high-frequency P and S waves. With the 6-month-long Mammoth Mountain earthquake swarm that began in May 1989, we began detecting occasional events with a marked deficiency in energy above 5 Hz, a feature typical of long-period (LP) volcanic earthquakes. These events occur beneath the southwest flank of Mammoth Mountain at focal depths ranging from 10 to 28 km, distinctly deeper than the 2- to 10-km depth range for tectonic earthquakes in the area. The LP events occur at intervals ranging from weeks to months. Individual occurrences typically consist of several events within 2 to 5 minutes where the largest event has never been first. Magnitudes range from 0.5 to 1.8. The mid-crustal focal depths of the LP events are similar to occurrences at a number of areas with Holocene volcanism in Japan and the western United States. They may indicate the movement of magmatic fluids but do not necessarily indicate an imminent volcanic eruption.

#### *Triggered Response of Long Valley Caldera to the 1992 Landers mainshock.*

Of the many sites in the western United States responding to the 28 June 1992 Landers earthquake ( $M=7.4$ ) with remotely triggered seismicity, only Long Valley caldera is monitored

by both seismic and continuous deformation networks. A transient strain pulse and surge in seismicity recorded by these networks began within tens of seconds following arrival of the shear pulse from Landers. The cumulative strain and number of triggered earthquakes followed the same exponentially decaying growth rate (time constant 1.8 days) during the first six days following Landers. The strain transient, which was recorded on a borehole dilatometer at the west margin of the caldera and a long-base tiltmeter 20 km to the east, peaked on the 6th day at about 0.25 ppm and gradually decayed over the next 15 to 20 days. The absence of a clear strain signal exceeding 0.4 ppm in data from the two-color geodimeter deformation lines, which span the central section of the caldera, indicates that the strain transient cannot be due solely to pressure changes in the concentrated pressure source 7 km beneath the central part of caldera that accounts for most of the uplift of the resurgent dome since 1980. The triggered seismicity occupied the entire seismogenic volume beneath the caldera. Focal mechanisms, the frequency-magnitude distribution, and the spatial distribution of the triggered earthquakes are typical of other swarms in Long Valley caldera. The cumulative seismic moment of the triggered earthquakes through the first two weeks after the Landers earthquake corresponds to a single  $M=3.8$  earthquake, which is too small by nearly two orders of magnitude to account for the 0.25 ppm peak amplitude of the observed strain transients. Evidently the strain transient represents the dominant response mode, which precludes direct triggering of local earthquakes by the large dynamic stresses from Landers as an important process here. Conditionally viable models for the triggering process beneath the caldera include 1) the transient pressurization of magma bodies beneath the resurgent dome and Mammoth Mountain by the advective overpressure of rising bubbles, 2) a surge in fluid pressure within the seismogenic zone due to upward cascading failure of isolated compartments containing super-hydrostatic pore fluids, 3) relaxation (fluidization) of a partially crystallized magma body in the deep crustal roots of Long Valley magmatic system, or 4) aseismic slip on mid-crustal faults. Only the deep, relaxing-magma body satisfies all the strain observations with a single deformation source. This model admits the possibility that large, regional earthquakes can trigger the episodic recharge of the deep roots of crustal magmatic systems.

## Publications

- Hill, D.P., (1994) Evidence for the depth to the brittle-plastic transition zone and the 400°C isotherm beneath the LVEW site in the Long Valley caldera, California (abs.), Abstracts of the VIIth International Symposium on the Observation of the Continental Crust through Drilling, Santa Fe, April, 1994.
- Hill, D.P., M.J.S. Johnston, J.O. Langbein, and R. Bilham (1994) Response of Long Valley caldera to the  $M=7.3$  Landers earthquake: tweaking a magma body? (abs.), Annual meeting of the Seismol. Soc. America, April 1994.
- Hill, D.P., M.J.S. Johnston, J.O. Langbein, and R. Bilham, Response of Long Valley caldera to the  $M=7.3$  Landers, California, earthquake, in Hickman, Sibson, and Bruhn , eds., Special Issue on the Material Involvement of Fluids in Faulting, *J. Geophys. Res.*, (in press).
- Hill, D.P., and P.A. Reasenberg (1994) Remotely triggered seismicity [abstract for invited

paper in the Frontiers of the Physical Sciences at the Annual AAAS meeting in San Francisco, February 1994].

Linde, A.T., S. Sacks, M.J.S. Johnston, D.P. Hill, and R.G. Bilham (1994) Increase pressure from rising bubbles as a mechanism for remotely triggered seismicity, *Nature*, v. 371, pp. 408-410.

Pitt, A.M., and D.P. Hill, (1994) Long-period earthquakes in the Long Valley caldera region, eastern California, *Geophys. Res. Lett.*, v. 21, pp. 1679-1682.

Thatcher, W. and D.P. Hill (1994) A simple model for the fault-generated morphology of slow-spreading mid-oceanic ridges, *J. Geophys. Res.*, (in press).

9930-12473  
*Hill, Vidale, and Benz*  
Branch of Seismology  
United States Geological Survey  
345 Middlefield Rd. - MS 977  
Menlo Park, California 94025  
(415) 329-4795

## Investigations

In the last few years, we established the software and communications to assemble recordings of distant earthquakes from up to 1500 short-period vertical-component stations across North America. With this very large aperture array, we are currently probing the deep structure of the Earth, investigating the crust and mantle beneath California, and examining the earthquake rupture process. In addition, we have begun efforts to understand the properties of fault-zone guided waves, which may be the most sensitive probe of the internal structure of faults. We are continuing efforts to understand the effect of deep sedimentary basin on earthquake strong motions.

The papers summarized below have been the result of this past year's effort. In addition, 16 abstracts were presented at various meetings.

## Results

### *Physics of earthquakes*

J.E. Vidale, W.L. Ellsworth, A. Cole, and C. Marone, 1994. Variations in rupture process with recurrence interval in a repeated small earthquake, *Nature*, 368, 624-626.

H. Houston and J.E. Vidale, 1994. The temporal envelope of short-period radiation during deep earthquake rupture, *Science*, 265, 771-774.

C.J. Ammon, T. Lay, A.A. Velasco, and J.E. Vidale, 1994. Routine estimation of earthquake source complexity: The October 18, 1992 Columbian earthquake, *Bull. Seism. Soc. Am.*, 84, 1266-1271.

J.E. Vidale, S. Goes, and P.G. Richards. Near-field deformation seen on distant broadband seismograms, in press, *Geophysical Research Letters*.

### *Fault zone structure*

Y.-G. Li, J.E. Vidale, K. Aki, C. Marone, W.H.K. Lee, 1994. Fine structure of the Landers fault zone; segmentation and the rupture process, *Science*, 265, 367-370.

*Mantle structure*

J.E. Vidale, 1994. A snapshot of whole mantle flow, *Nature*, 370, 16-17.

J.E. Vidale, 1994. A mystery in the mantle, *Nature*, 371, 288.

*Effect of basins on strong motion*

J. E. Vidale, The influence of basins on long-period ground motion amplitude and duration in the 1971 San Fernando earthquake, submitted to *Annali di Geofisica*.

A. Frankel, and J.E. Vidale, 1994. A three-dimensional simulation of seismic waves in the Santa Clara Valley, California, from an aftershock, p. 197-217, Loma Prieta Professional Paper, Strong Ground Motion Chapter.

**LATE QUATERNARY FAULTING, BENTON HILLS, SOUTHEASTERN MISSOURI,  
NEW MADRID SEISMIC ZONE**

David Hoffman, James R. Palmer and James D. Vaughn  
 Missouri Department of Natural Resources  
 Division of Geology and Land Survey  
 111 Fairgrounds Road  
 P. O. Box 250  
 Rolla, Missouri 65401  
 314-368-2144, 2182, and 2185

Award No.: 1434-94-G-2482  
 Program Element: II.5

**INTRODUCTION**

The Benton Hills are the northeastern-most segment of Crowley's Ridge and are located at the head of the Mississippi Embayment in southeastern Missouri. Geologic mapping in the Benton Hills has shown them to be structurally complex with numerous faults and folds (Stewart 1942, Stewart and McManamy 1944, Johnson 1985, Harrison 1994, Harrison and Schultz 1994). At English Hill, along the southeastern escarpment of the Benton Hills, Stewart identified the English Hill Fault(s) and an associated graben where there is clear evidence of post-late Eocene (Plio-Pleistocene?) deformation and loess is faulted against Tertiary sediments with up to 10 m (30 ft) of displacement. Some other geologists have assumed Stewart's displaced loess is a result of landsliding not faulting.

Geomorphic relationships of drainage areas, drainage divides and stream profiles suggest that the Benton Hills have been truncated at their southeastern escarpment (Palmer and Hoffman 1993). Equal-sized alluvial fans along the southeastern escarpment of the Benton Hills derived from similar-sized drainage areas in the Hills are on top of different-aged, Ohio and Mississippi River terraces suggesting a recent date for the formation of the escarpment (Palmer and Hoffman 1993). The southeastern escarpment of the Benton Hills is also directly above a prominent lineament, which extends from northeastern Arkansas to the Illinois-Indiana border, shown on a magnetic anomaly map by Hildenbrand and Hendricks (1994).

A shallow, high resolution seismic reflection survey (Mini-Sosie) conducted collaboratively with the USGS last year at the English Hill site identified 11 or 12 faults in the subsurface along the 2.5 km (1.6 mi) long line. Several of these faults have been correlated with nearby mapped faults (Harrison, pers. comm.). The seismic profile did not image materials above a depth of about 75 m (250 ft), so the minimum date of fault movement could not be determined but faulting is present under the escarpment.

**INVESTIGATIONS**

The current investigations are still underway. They are aimed at trying to locate and date faulting at or very near the ground surface and to date

the most recent movement. Surface geologic mapping, drilling, trenching and geophysical techniques are being used to accomplish this.

Seventy-one hand auger exploration holes 1 m (3 ft) deep and 29 machine drilled holes 2 m (6 ft) to 21 m (70 ft) have been completed. A 90 m (295 ft) shear wave seismic reflection profile with 1.5 m (5 ft) geophone spacing was run, courtesy of James B. Harris of the Kentucky Geological Survey, in order to image as near to the ground surface as possible. Five 2 m (6.5 ft) wide trenches 24 m (80 ft) to 165 m (540 ft) long and 1 m (3 ft) to 7 m (23 ft) deep were excavated up the escarpment. The trench walls were examined for evidence of faulting and the longest, deepest trench was logged. Mapping of surface exposures in adjacent erosion ravines is also being conducted and correlated with the trench exposures. Four ground penetrating radar profiles were run, courtesy of Nicholas Tibbs of the Southeast Missouri State University Department of Geosciences. Two profiles with different antennas were run in each of two trenches.

## RESULTS

Date collection, compilation and analysis is still underway so final results are not available at this time. Preliminary results show that faulting extends to the ground surface where Tertiary and Cretaceous sediments are at the ground surface. Faulting of the Quaternary loess has not been demonstrated but fracture zones within the loess suggest tectonic movement. A .6 m (2 ft) thick gravel bed 2.4-3.0 m (8-10 ft) above the base of the loess indicates a high energy event occurred post-Sangamon and pre-Roxana. No evidence for deep-seated landsliding has been found although a small 2 m (6 ft) deep slump has been mapped. A 3 m (10 ft) thick fluvial interbedded gravel, sand and silt deposit that fines upward is present at the current stream divide. This fluvial deposit is probably post-Mounds and may be post-Sangamon. A high energy stream drainage is inferred from a no-longer-existing drainage source south of the present escarpment. This indicates significant post-middle Wisconsinan truncation of the southeastern escarpment which may be related to tectonic movement.

## REFERENCES

- Harrison, R. W., 1994, Geology of the Thebes 7-1/2' quadrangle, Missouri and Illinois, scale 1:24,000, U. S. Geological Survey, Misc. Field Investigation Map, in press.
- Harrison, R. W., and A. Schultz, 1994, Strike-slip faulting at Thebes Gap, Missouri and Illinois: Implication for New Madrid tectonism: Tectonics, v. 13, no. 2, p. 246-257.
- Hildenbrand, T. G., and J. D. Hendricks, 1992, Geophysical setting of the Reelfoot rift and relations between rift structures and the New Madrid seismic zone, in Investigations of the New Madrid Seismic Zone, edited by K. M. Shedlock and A. C. Johnston, U. S. Geological Survey Prof. Paper 1538E, in press.
- Johnson, W. D., 1985, Geologic map of the Scott City quadrangle and part of the Thebes quadrangle, Scott and Cape Girardeau Counties, Missouri: U. S. Geological Survey, Miscellaneous Field Studies Map MF-1803.

- Palmer, J. R., and D. Hoffman, 1993, Possible late Quaternary faulting in the Benton Hills, southeastern Missouri (abs.): North-Central Section, Geol. Soc. Amer., Abstracts with Program, v. 25, no. 3, p. 72.
- Stewart, D., 1942, The Mesozoic and Cenozoic geology of southeastern Missouri: Missouri Geological Survey, unpublished manuscript, 122 p.
- Stewart, D., and L. McManamy, 1944, Early Quaternary or late Tertiary folding in the vicinity of Commerce, Scott County, southeastern Missouri: Missouri Academy of Science, Rolla, Missouri, 1944.

## The Kinematics of Southern California

1434-94-G-2455

W. E. Holt

Dept. of Earth and Space Sciences  
 State University of New York at Stony Brook  
 Stony Brook, NY 11794-2100  
 (516) 632-8215  
 wholt@seism1.ess.sunysb.edu

### INVESTIGATIONS

Using the method of Haines and Holt [1993] we determine the horizontal velocity gradient tensor associated with Quaternary deformation rates (Figure 1). This enables us to determine the role that individual structures are playing in taking up the plate motion. Strain rates associated with the active structures are determined within a uniform grid and modeled with continuous spline functions (Figure 2) in order to recover the velocity field. Velocities can be calculated within any frame of reference (Figure 3) and can be compared with expected plate motions (Figure 4) or geodetic observations. Geodetic observations can also be modeled or used as a constraint.

### RESULTS

Preliminary results indicate that the geologic strain rates yield a motion of the Pacific plate relative to North America that deviates from the expected NUVEL-1A plate motion (Figure 4). This preliminary result is consistent with the findings of Humphreys and Weldon [1994]. The difference between the expected plate motion and the calculated motion could potentially be explained by compression offshore. We are also calculating the expected slip rates, with formal estimates in uncertainty, that will account for the full plate motion. Assuming that the slip is taken up seismically, the expected moment rates, partitioned as pure strike-slip and pure thrust components, are also calculated.

### REPORTS PUBLISHED

Holt, W. E. and A. J. Haines, On the kinematics of California and New Zealand, *Eos Transactions, AGU*, 73, p. 588 - 589, 1993.

Holt, W. E., The kinematics of southern California determined from the inversion of Quaternary strain rates, In preparation and to be submitted to Bulletin Seismological Society of America.

### References Cited

Haines, A. J., and W. E. Holt, A method to obtain the complete horizontal motions within zones of distributed deformation from the inversion of strain rate data, *J. Geophys. Res.*, 98, 12,057-12,082, 1993.

Humphreys, E. D. and R. J. Weldon, Deformation across the western United States: A local estimate of Pacific-North America transform deformation, In Press, *J. Geophys. Res.*, 1994.

Jennings, C. W., Preliminary Fault Activity Map of California, California Department of Conservation, Division of Mines and Geology, DMG Open File Report 92-03, 1992.

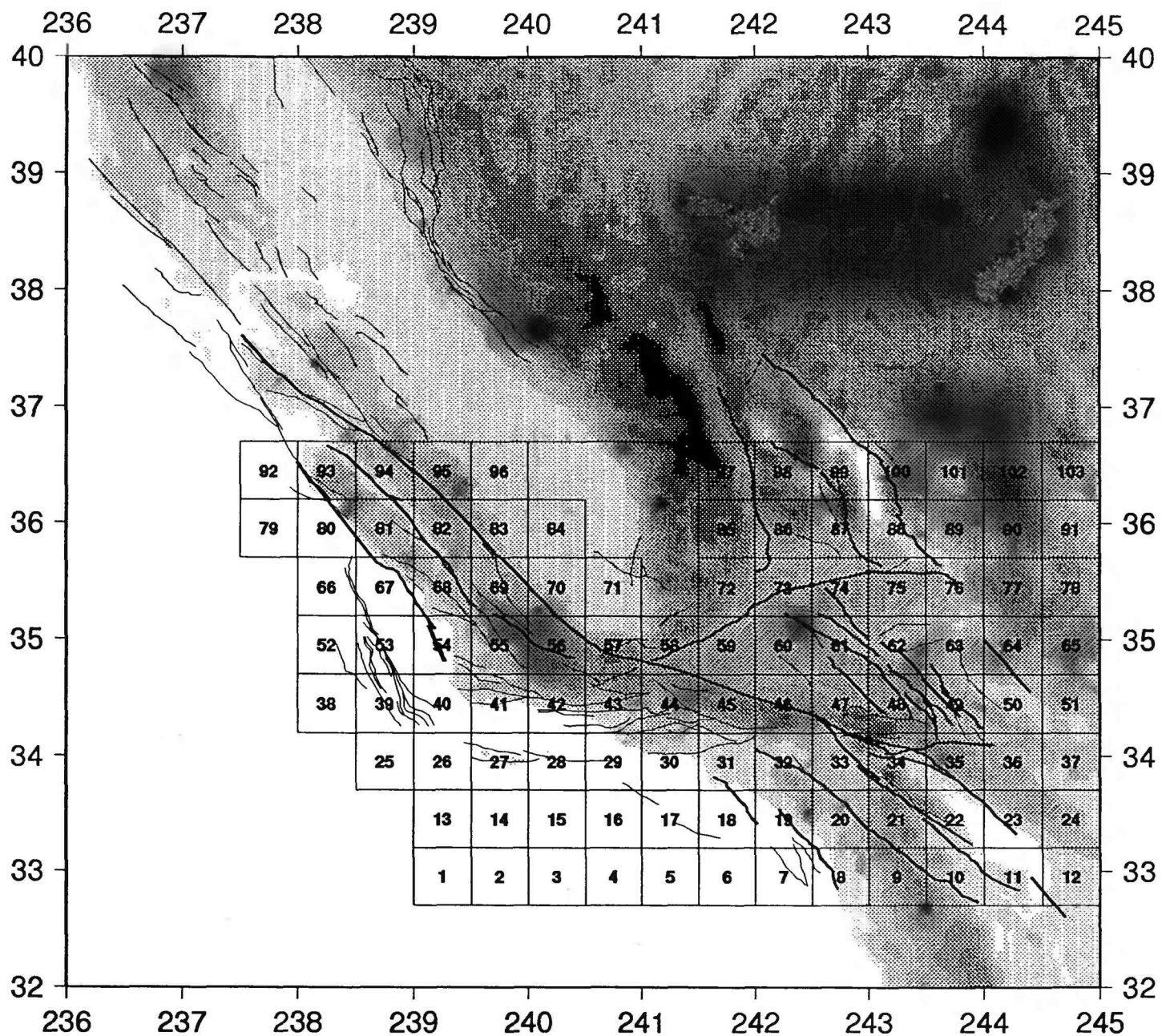


Figure 1: Quaternary Faults from Jennings (1992) used to obtain strain rates shown in Figure 2.

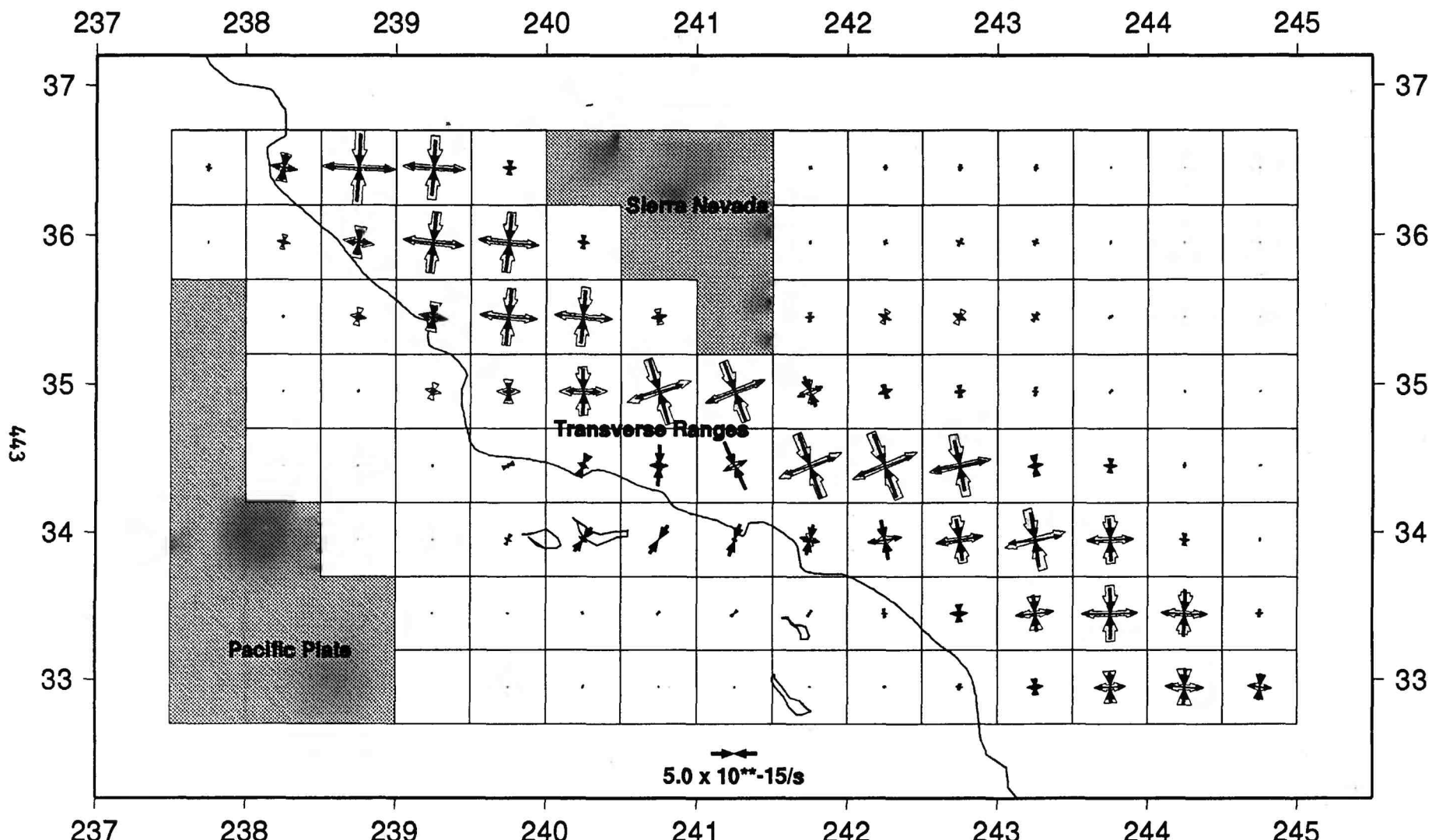


Figure 2: Average observed strain rate values within  $0.5^\circ \times 0.5^\circ$  regions (fat shaded principal strain axes) obtained from Quaternary slip rate estimates. The predicted average strain rate values (solid principal strain axes) are obtained from continuous spline functions that are matched to the observed strain rate distribution in a formal least-squares inversion. Shaded regions (Pacific Plate and Sierra Nevada) are constrained to behave rigidly.

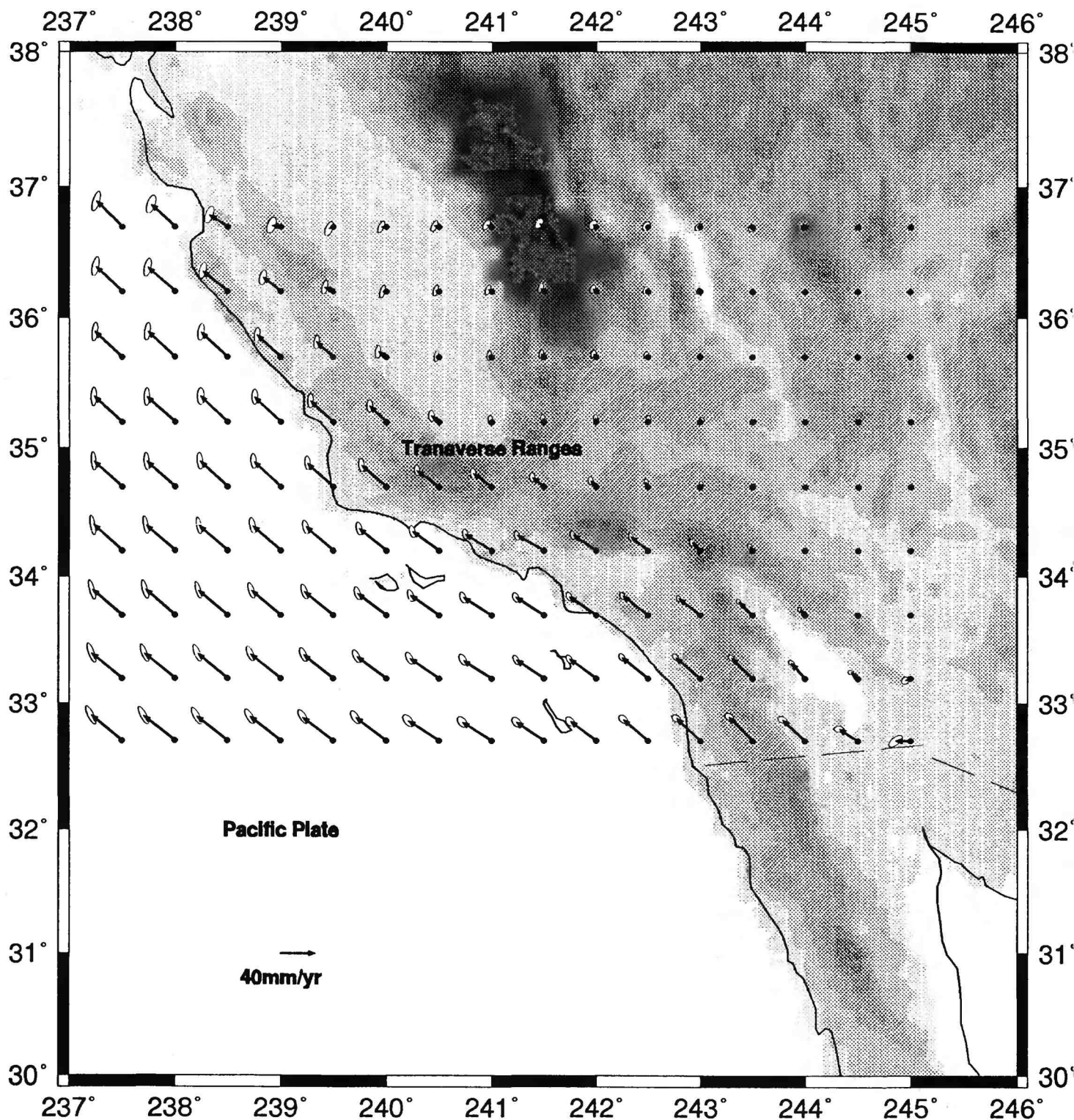


Figure 3: Horizontal velocity field associated with the Quaternary deformation rates calculated relative to North America. Error ellipses are for one standard deviation.

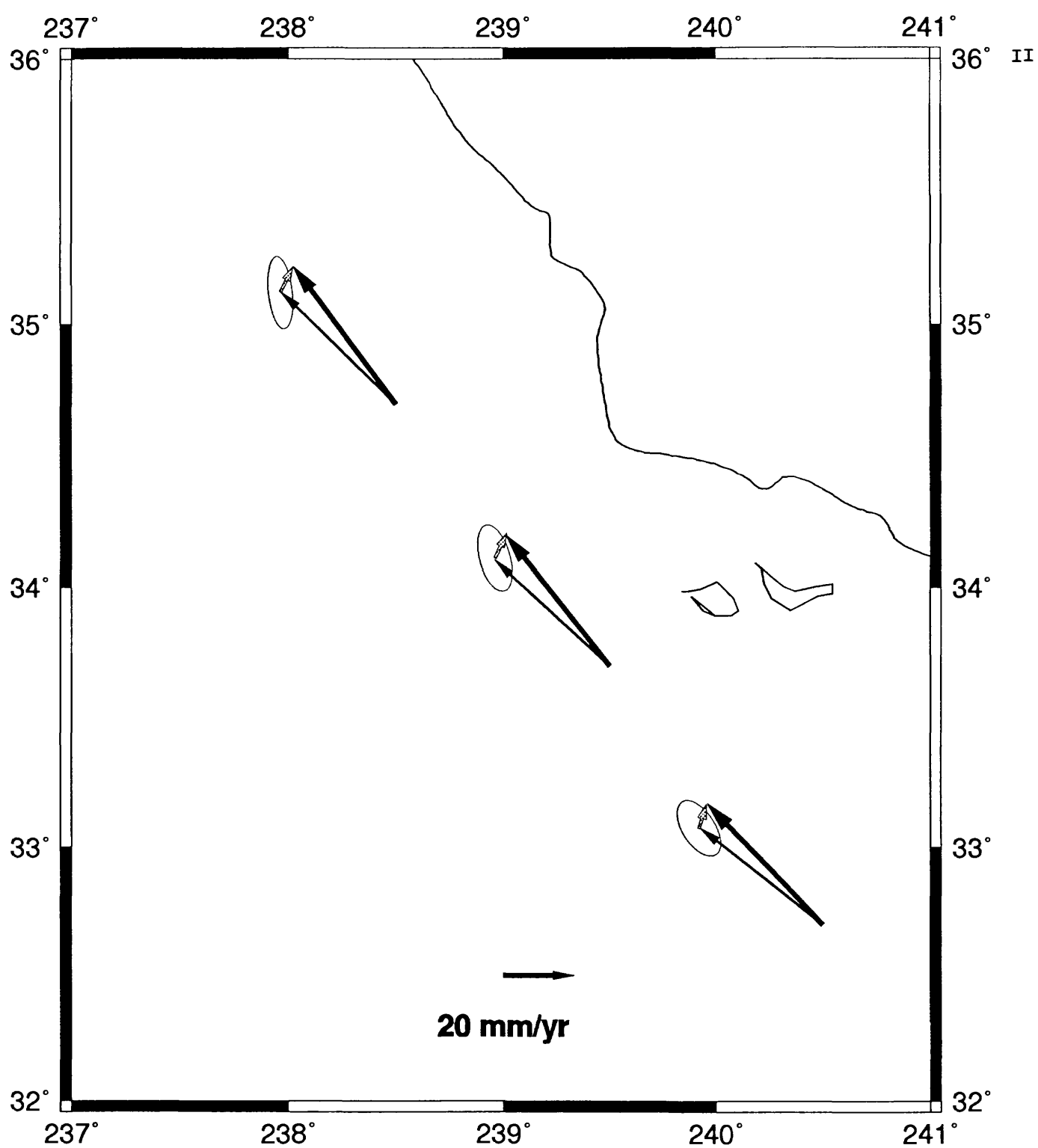


Figure 4: Motion of Pacific Plate relative to North America as provided by the estimated Quaternary slip rates. Also shown is the NUVEL-1A velocity vector (no error ellipse) and the difference vector (shaded).

## Geologic Strain Partitioning in the Eastern California Shear Zone

4-9540-10330

Keith A. Howard  
U.S. Geological Survey  
Branch of Western Regional Geology  
345 Middlefield Road MS-975  
Menlo Park, CA 94025-3521  
(415) 329-4943  
fax (415)329-4936  
khoward@isdmnl.wr.usgs.gov

### Investigations:

1. Faults showing evidence of Quaternary movement in the eastern Mojave Desert area within 50 miles of the proposed Ward Valley radioactive waste disposal site were compiled and summarized. These include newly discovered sites in the Needles and Topock areas where no young faults were previously known.
2. Two pairs of broad topographic troughs and swells 200- to 250-km long were studied along and north of the big bend of the San Andreas fault in the Mojave Desert. On the California 1:750,000-scale geologic map the two WNW-striking, 45-km-wavelength troughs (Bristol-Danby and Lucerne-Dale troughs) appear as mostly Quaternary deposits, while the crests appear as mostly older bedrock units.

### Results:

1. More than 15 small faults with known or suspected Quaternary movement are identified within 50 miles of the proposed Ward Valley radioactive waste disposal site in the eastern Mojave Desert.. These include faults in the Whipple Mountains area (Carr,1991), the New York Mountains (Miller and others, 1991), Chemehuevi Valley (Southern California Edison Company, 1974), Cadiz Lake playa (Bassett and others, 1959; Howard and Miller, 1992), and lineaments in Bristol Lake playa (Kupfer and Bassett, 1962; Sugiera and Sabins, 1980). Two newly discovered north-striking vertical faults cut Pleistocene fluvial deposits near Topock, and a newly discovered normal fault near the Needles airport dips gently northeast and cuts alluvium assigned to the Pleistocene.

The Bristol-Danby Trough (Thompson, 1929; Bassett and Kupfer, 1964; Gardner, 1980; Glazner, 1981) lies at the eastern boundary of the eastern California shear zone (Dokka and Travis, 1990). Tectonic analysis suggests several reasons to suspect that tectonic activity in the trough is continuing or geologically young. These include stratigraphic evidence from drill holes that faulting has deepened the Bristol Lake basin in Quaternary time (Rosen, 1989; Jachens and Howard, 1992), the existence of several Quaternary faults along the flanks of the trough (Bassett and others, 1959; Howard and Miller, 1992), projected alignment of deep parts of the trough with tectonically active Death Valley, and a steeper gradient of tributary Ward Valley near the trough than upstream. Holocene deposits cover much of the trough and could conceal evidence of Pleistocene faults.

These results were presented in an informal report:

Howard, K.A., 1994, Seismicity and tectonics, in Wilshire, H.G. and 9 others, Ward Valley proposed low-level radioactive waste site, Presentations made to the National Academy of Sciences review panel, July 7 to 9 and August 30 to September 1, 1994, Needles, California, September, 1994, Chapter 12, 10 p.

2.K. A. Howard and W.D. Stuart (1992) tentatively interpreted two sets of topographic waves along and north of the eastern Big Bend of the San Andreas fault as regional neotectonic buckle folds induced by horizontal NNE compression of the Mojave block. Thrust and reverse faulting accentuates structural relief of the waves.

Previous neotectonic analyses of the Mojave desert have focused largely on sets of strike-slip faults that segment the Mojave block like a sliced loaf of bread. We contend that the buckled waves and oblique shear of these smaller slices both represent manifestations of the regional stress and strain regime in the Mojave block. The historic Palmdale bulge is even broader.

The 45-km wavelength may be controlled by thickness of a folded layer of granitic continental crust. The folded layer may be 7-10 km thick if analogy can be made to scale modeling of buckled oceanic lithosphere in the Indian Ocean (Bull and others 1992). This thickness matches that of the seismically active brittle upper crust in the Mojave block.

#### References Cited:

- Bull, J.M., Martinod, John, and Davy, Phillip, 1992, Tectonics, v. 11, p. 537-548.
- Bassett, A.M., Kupfer, D.H., and Barstow, F.C., 1959, Core logs from Bristol, Cadiz, and Danby Lakes, San Bernardino County, California: U.S. Geological Survey Bulletin 1045-D, p. 97-138.
- Carr, W.J., 1991, A contribution to the structural history of the Vidal-Parker region, California and Arizona: U.S. Geological Survey Professional Paper 1430, 40 p.
- Dokka and Travis, 1990, Late Cenozoic strike-slip faulting in the Mojave Desert: Tectonics, v. 9, p. 311-340.
- Gardner, D.L., 1980, The Barstow-Bristol trough, central Mojave Desert, California, in Fife, D.L. and Brown, A.R., Geology and mineral wealth of the California desert: South Coast Geological Society, p. 204-214.
- Glazner, A.F., 1981, Tectonic significance of the stratigraphy and distribution of Cenozoic volcanic rocks in the central Mojave Desert, in Howard, K.A., Carr, M.D., and Miller, D.M., eds., Tectonic Framework of the Mojave and Sonoran deserts, California and Arizona: U.S. Geological Survey Open-File Report 81-503, p. 39-40.
- Howard, K.A. and Miller, D.M., 1992, Late Cenozoic faulting at the boundary between the Mojave and Sonoran blocks: Bristol Lake area, California, in Richard, S.M., ed., Deformation associated with the Neogene Eastern California Shear Zone, southeastern California and southwestern Arizona: Redlands, California, San Bernardino County Museums Special Publication 92-1, p. 37-47.
- Howard, K.A., and Stuart, W.D., 1992, Compressive origin of topographic waves in the Mojave Desert, California, abstract in Chapman Conference on Tectonics and Topography, Aug. 31-Sept. 4, 1992: American Geophysical Union, p. 28.
- Jachens, R.C., and Howard, K.A., 1992, Bristol Lake basin--a deep sedimentary basin along the Bristol-Danby trough, Mojave Desert, in Reynolds, R.E., ed., Old Routes to the Colorado: Redlands, California, San Bernardino County Museum, Special Publication 92-2, p. 57-59.

- Kupfer, D.H. and Bassett, A.M., 1962, Geologic reconnaissance map of part of the southeastern Mojave Desert, California: U.S. Geological Survey Mineral Investigations Field Studies Map MF-205, scale 1:125,000.
- Miller, D.M., Miller, R.J., Nielson, J.E., Wilshire, H.G., Howard, K.A., and Stone, Paul 1992, Preliminary geologic map of the East Mojave National Scenic Area, California: U.S. Geological Survey Open-File Report 91-435, scale 1:100,000.
- Rosen, M. R., 1989, Sedimentologic, geochemical, and hydrologic evolution of an intracontinental, closed-basin playa (Bristol Dry Lake, CA): A model for playa development and its implications for paleoclimate: Austin, University of Texas, Ph.D. thesis, 266 p.
- Southern California Edison Company, 1974, Information concerning site characteristics, Vidal nuclear generating station, Vol. 2, p. 2.5-142.
- Sugiera, Ray and Sabins, Floyd, 1980, The evaluation of 3-cm-wavelength radar for mapping surface deposits in the Bristol Lake/Granite Mountain area, Mojave Desert, California, in Radar geology: An assessment, Report of the Radar Geology Workshop, Snowmass, Colorado, July 16-20, 1979: Pasadena, California, Jet Propulsion Laboratory, National Aeronautics and Space Administration, p. 439-456.
- Thompson, D.G., 1929, The Mohave Desert region of California: U. S. Geological Survey Water-Supply Paper 578, 759 p.

## NEHRP Annual Technical Summary

Title:	<b>So. Calif. Fault Zone Tectonics</b>
Account Number:	9902-11030
Investigator:	Kenneth W. Hudnut
Institution:	USGS
Address:	525 South Wilson Ave. Pasadena, CA 91106
Phone #:	(818) 583-7232
E-mail:	hudnut@seismo.gps.caltech.edu
Program Element:	NEHRP / So. Calif. / II.3

### Investigations Undertaken and Results

During 1994, much of the work on this project involved response to the Northridge earthquake in several forms. First, measurements performed within days to months following the event were analyzed and modelled. This work has been reported already (USGS & SCEC, 1994), and further work is in progress. A paper will be presented at the Fall AGU meeting special session on Northridge, and submitted to the BSSA Special Issue on the Northridge earthquake. Initial results were posted on internet within 9 days after the earthquake. Current best estimates of displacements at 45 GPS stations are now openly available through mosaic and anonymous ftp. Second, I have collaborated with Ross Stein on performing extensive post-earthquake measurements with FEMA funding, using results of those measurements to further refine the earthquake source model.

Third, the main new effort of this project during 1994 was the expansion of continuous GPS monitoring across the Los Angeles Basin in cooperation with NASA (JPL) and SCEC (Scripps, MIT and UCLA). After the Northridge earthquake, this project received supplemental funds to establish up to 11 new continuous GPS stations in the Los Angeles region. Through our collaboration with other agencies and university groups, a total of about 25 continuous GPS stations will be established by spring 1995. At this time, four of the new stations are operational, monumentation has been completed at 8 of the sites, and 2 of the non-operating sites are fully prepared for equipment installation. We are awaiting award of contract on the hardware, and completing site preparation work at this time. We have established a cooperative project with Los Angeles County to monitor deformation of Pacoima Dam in near real-time with continuous GPS (and digital broad-band seismic equipment). The USGS office in Pasadena will be made a downloading and data analysis center, and data will be incorporated with the real-time earthquake information system here.

In addition, we have continued the other aspects of our monitoring work, including transfer of operations and upgrading of several creepmeters along the Coachella Valley segment of the San Andreas fault (in conjunction with Kerry Sieh at Caltech and Roger Bilham at Univ. of Colorado).

## Reports Published (and Submitted)

### Received Director's Approval:

- BOCK-Y; AGNEW-DC; FANG-P; GENRICH-JF; HAGER-BH; HERRING-TA; HUDNUT-K; KING-R; LARSEN-S; MINSTER-JB; STARK-K; WDOWINSKI-S; WYATT-F  
DETECTION OF CRUSTAL DEFORMATION FROM THE LANDERS EARTHQUAKE SEQUENCE USING CONTINUOUS GEODETIC MEASUREMENTS  
**NATURE**, 1993, 361(6410) 337-340
- BODIN, P.; R. BILHAM; J. BEHR; J. GOMBERG; K. HUDNUT  
SLIP TRIGGERED ON SOUTHERN CALIFORNIA FAULTS BY THE 1992 JOSHUA TREE, LANDERS, AND BIG BEAR EARTHQUAKES  
**BULL. SEIS. SOC. AMER.**, V. 84, #3, 806-816, 1994.
- HUDNUT, K. W., Y. BOCK, M. CLINE, P. FANG, J. FREYMUeller, K. GROSS, D. JACKSON, S. LARSEN, M. LISOWSKI, Z. SHEN, AND J. SVARC  
COSEISMIC DISPLACEMENTS IN THE 1992 LANDERS EARTHQUAKE SEQUENCE  
**BULL. SEIS. SOC. AMER.**, V. 84, #3, 625-645, 1994.
- HUDNUT, K. W. AND S.C. LARSEN  
SLIP DISTRIBUTION OF THE 1992 LANDERS, CALIFORNIA EARTHQUAKE SEQUENCE, DETERMINED FROM GEODETIC DATA  
**SUBMITTED, JGR**
- HUDNUT, K. W.  
EARTHQUAKE GEODESY AND HAZARD MONITORING  
**SUBMITTED, U. S. NATIONAL REPORT TO THE IUGG; 1991-1994**  
(TO BE PUBLISHED AS A SUPPLEMENT TO *REVIEWS OF GEOPHYSICS*)
- HUDNUT, K.W.; MURRAY, M.; DONNELLAN, A.; ET AL.  
COSEISMIC DISPLACEMENTS OF THE 1994 NORTHRIDGE, CA, EARTHQUAKE  
**SEISMOLOGICAL RESEARCH LETT.**, V. 65, NO. 1 (SUPPLEMENT), ABSTR #40, 1994 (ABSTR)
- HUDNUT, K.W.; BOCK, Y.; ZHANG, J.  
COMPRESSION ACROSS THE LOS ANGELES BASIN, CA, DETECTED BY CONTINUOUS GPS MEASUREMENTS  
**SEISMOLOGICAL RESEARCH LETT.**, V. 65, NO. 1, PG. 59, 1994A (ABSTR)
- PELTZER, G., K. HUDNUT, AND K. FEIGL  
ANALYSIS OF COSEISMIC SURFACE DISPLACEMENT GRADIENTS USING RADAR INTERFEROMETRY: NEW INSIGHTS INTO THE LANDERS EARTHQUAKE  
**JGR**, V. 99, #B11, PP. 21971-21981, 1994.
- SIEH, K., L. JONES, E. HAUSSON, K. HUDNUT, D. EBERHART-PHILLIPS, T. HEATON, S. HOUGH, K. HUTTON, H. KANAMORI, A. LILJE, S. LINDVALL, S. MCGILL, J. MORI, C. RUBIN, J. SPOTILA, J. STOCK, H.K. THIO, J. TREIMAN, B. WERNICKE, AND J. ZACHARIASEN  
NEAR-FIELD INVESTIGATIONS OF THE LANDERS EQ. SEQUENCE, APRIL TO JULY, 1992  
**SCIENCE**, V. 260 (APRIL 9), PP. 171-176, 1993.
- USGS AND SCEC (K. HUDNUT - CONTRIBUTOR)  
THE MAGNITUDE 6.7 NORTHRIDGE, CALIF., EARTHQUAKE OF JANUARY 17, 1994  
**SCIENCE**, V. 266 (OCT. 21), PP. 389-397, 1994.

### Director's Approval Not Requested:

- ALVARADO, G. E., M. CARR, H.-U. SCHMINCKE, AND K. W. HUDNUT  
POLYBARIC MAGMA MIXING AT IRAZU VOLCANO, COSTA RICA  
SUBMITTED TO *J. VOLCANOLOGY AND GEOTHERMAL RESEARCH* AUG. 28, 1993.

## Geophysical Framework San Francisco Bay Earthquake Hazards

9380-10105

Robert C. Jachens and Andrew Griscom  
U.S. Geological Survey MS 989  
345 Middlefield Road  
Menlo Park, CA 94025  
Tel. (415) 329-5300, FAX (415) 329-5133,  
e-mail [jachens@fourier.wr.usgs.gov](mailto:jachens@fourier.wr.usgs.gov)

### Element II

#### Investigations Undertaken

- 1) Continued our interpretation efforts in the East Bay Region with particular emphasis on the Hayward and Calaveras Faults and the Livermore Valley and San Pablo Bay. Our new gravity data set is essentially complete in these areas and is of a quality to effectively complement the detailed magnetic data available. Complimentary structural pictures emerging from the potential field interpretations and the detailed geologic mapping of Brabb, Jones, and the Berkeley graduate students in the area immediately east of the Hayward and Silver Creek faults promise to reveal much about the young faulting history of this area, including significant thrusting. Analysis of the shallow anomalies produced by the disruption of young magnetic sandstones in the Livermore Valley should help delineate buried faults in an area notably poor in outcrops. A better understanding of the relationship between the active Calaveras Fault and the older faults with which it apparently coincides may help explain other active faults whose microseismicity seems to deviate from the fault as defined by lithologic contrast.
- 2) Determined depth to pre-Tertiary basement in the northwestern San Francisco Peninsula based on an inversion of gravity data.
- 3) Determined the intermediate-depth crustal structure of the California Coast Ranges, with a focus on the San Francisco Bay area.
- 4) Collected new gravity data in San Francisco Bay area to address problems related to location and structure of concealed faults.
- 5) Designed and contracted for new aeromagnetic survey of south San Francisco Bay and vicinity with funds from a number of programs. This survey will fill in the last remaining hole in the greater San Francisco Bay area with aeromagnetic data conforming to modern standards of line-spacing, flight height, and data quality. The survey will address problems of the mud faults beneath the bay, the northern Hayward Fault, the northern San Gregorio Fault, stratigraphy and structure in the Cenozoic rocks of the east bay, possible channels for contamination into the bay, Franciscan geology of the San Francisco Peninsula, and general problems of wedge tectonics in the Bay area.

6) Began an interpretation of the relationship between magnetic anomalies, Coast Range ophiolite slabs, and mud faults beneath San Francisco Bay. Preliminary efforts included modeling the Hunters Point anomaly, searching for disruptions and truncations of magnetic bodies that could indicate faults, and establishing the spatial relationship between the mud faults and magnetic sources.

### **Results Obtained**

- 1) Magnetic data from the Great Valley and adjacent Coast Ranges in the Bay area indicate westward continuation of Great Valley basement beneath the Franciscan Complex rocks at least as far west as the Hayward Fault, and possibly to the San Andreas Fault. The basement appears to be cut by the Hayward Fault at mid-crustal depth. This interpretation has important implications regarding the geologic evolution of the eastern Bay region in terms of tectonic wedging, and concerning the numerous and varied models for the plate boundary in the Bay area. Specifically, the interpretation argues against a major decollement at or above the basement surface along which to accommodate Late Cenozoic compression, and suggests that the major 6-sec reflector seen by the BASIX seismic work may be Great Valley basement.
- 2) Depth-to-basement map of the northwestern San Francisco Peninsula based on an inversion of gravity data suggests a thick young sedimentary section northeast of the San Andreas Fault in the South San Francisco-Colma area, one that could reach a thickness >1 km along the fault where it passes out to sea.
- 3) A new detailed gravity map of the central Hayward Fault shows a strong gravity high near San Leandro. Comparison of the map with Jim Lienkaemper's detailed map of the fault trace and with magnetic data suggests that the local fault position is influenced by detailed structure within the Coast Range ophiolite (CRO) exposed along the fault. The fault appears to be deflected by a large block of mafic CRO (gravity high west of fault) and displays a right step-over southeast of the gravity high. The gravity high corresponds to a change in slip rate along the fault, may correspond to the north end of slip during the 1868 earthquake, and may reflect a geologically identifiable asperity in the fault zone. Magnetic data, although of limited quality in this area, indicate that highly magnetic, low density ultramafic (?) rocks of the CRO lie east of the fault in this area, suggesting that internal structure within the CRO may be an important local control of the fault position. New, detailed magnetic data being collected this year will complement these new gravity data and will form the foundation for a detailed examination of the 3-dimensional relationship between the Hayward Fault and the Coast Range ophiolite.
- 4) New gravity data collected in the central and southern San Francisco Peninsula indicate that:
  - a) the Pilarcitos Fault, a former strand of the San Andreas Fault system, is nearly vertical in the vicinity of San Carlos, and that the sliver of Permanente Terrane of the Franciscan Complex caught between the Pilarcitos and San Andreas Faults extends to mid-crustal depth as a steep-sided block.

b) the Monta Vista Fault zone, a zone of southwest-dipping reverse faults in the Cupertino/Saratoga/Los Altos area and associated with the San Andreas Fault, is clearly expressed by both gravity and magnetic anomalies. These anomalies permit the Monta Vista Fault zone to be traced from its exposure in the Los Altos area southeast toward Los Gatos through a developed area where it is mostly concealed beneath alluvium.

5) Many of the strong aeromagnetic anomalies in the east Bay are caused by magnetic sedimentary rocks, especially in the Livermore Valley and adjacent areas. The fact that sedimentary rocks are magnetic opens the possibility that the magnetic data can be used to define folds and faults that affect the young sedimentary deposits, and can contribute to the effort to identify active folds and blind thrusts in the S.F. Bay area.

6) Initial results from examining the relationship between the mud faults beneath San Francisco Bay and the magnetic anomalies indicative of possible fault zones in the basement rocks suggest that the spatial correlation between the mud faults and the magnetic sources may not be as good as first thought. Many of the mapped faults lie considerable distances from the magnetic sources. The relationship between the mud faults and basement fault zones will become clearer as the validity of the individual faults is re-examined and the new magnetic data come in.

#### Reports Published

1. Anonymous, 1994, Gravity point value data base for greater San Francisco Bay area available on Anonymous FTP. To access this file, ftp to mojave.wr.usgs.gov, logon as anonymous-password 'your id', cd to pub/sfbay, and copy files bayarea.grav and gravity.info.
2. Jachens, R.C., 1994, Aeromagnetic map of the Stockton 1:100,000 quadrangle, California: U.S. Geological Survey Open File Report 94-613, 1 sheet, scale 1:100,000 (descriptive text).
3. Jachens, R.C., Griscom, Andrew, and Roberts, C.W., Regional extent of Great Valley basement west of the Great Valley, California: Implications for extensive tectonic wedging in the California Coast Ranges: (submitted to Journal of Geophysical Research).
4. Jachens, R.C., Roberts, C.W., and Griscom, Andrew, 1993, Tectonic framework of California based on a merged aeromagnetic data base: Transactions American Geophysical Union, v. 74, p. 221.
5. Roberts, C.W., and Jachens, R.C., 1993, Draped aeromagnetic map of California—A new tool for regional structural and tectonic analysis: Transactions American Geophysical Union, v. 74, p. 379.

**San Andreas Fault  
Northern Gabilan Range Drill Site Geophysics**

9380-10107

Robert C. Jachens  
U.S. Geological Survey MS 989  
345 Middlefield Road  
Menlo Park, CA 94025  
Tel. (415) 329-5300, FAX (415) 329-5133,  
E-Mail [jachens@fourier.wr.usgs.gov](mailto:jachens@fourier.wr.usgs.gov)

**Element II**

**Investigations Undertaken**

- 1) Conducted gravity survey in vicinity of San Andreas Fault along the northern Gabilan Range, California, at one of two candidate locations for a proposed 3-km deep drill-hole to investigate the shallow structure, properties, and conditions of an active fault zone.
- 2) Designed and awarded a contract for a new aeromagnetic survey of the northern Gabilan Range site intended to trace the distribution at depth of the magnetic Etchegoin sandstone, especially along its contact with the granitoids of the Gabilan Range. These data should provide an independent test of whether the contact between the Cretaceous granitoids of the Gabilan Range and the Cenozoic sedimentary rocks (the geologic San Andreas Fault) dips to the southwest under the Gabilan Range as implied by the gravity data.

**Results Obtained**

- 1) With substantial help from Seth Stiles (a volunteer) new gravity data have been collected at critical locations along the San Andreas Fault at the candidate site. Modeling of these data support the earlier interpretation by Pavoni based on gravity data farther north that the Cretaceous granitoid-Cenozoic sedimentary rock contact dips steeply southwest along the northeast side of the Gabilan Range. This contact coincides at the surface with the trace of the active San Andreas Fault but apparently conflicting interpretations based on gravity data and seismicity suggest that the two may not coincide at depth. Resolving this apparent discrepancy will be an important part of the site characterization studies.

**Reports Published**

none

# ABSOLUTE DATING of PREHISTORIC EARTHQUAKES by TREE-RING ANALYSIS in CALIFORNIA

Award No.: USGS 1434-93-G-2367

Gordon C. Jacoby  
Tree-Ring Laboratory  
Lamont-Doherty Earth Observatory  
Palisades, New York 10963  
Phone: 914 365 8616  
FAX: 914 365 3046  
e-mail: druid@lamont.ideo.columbia.edu

## Program Objective II-5

### 1. San Andreas Fault (near San Francisco)

Studies of the effects of the 1906 earthquake on coast redwoods reveal the effects of the event in the annual tree-ring record. At two locations we have identified specific effects of the 1906 event and at a third site we hypothesize that an effect seen in a tree core from an old stump may be due to a prehistoric earthquake.

Plantation is a ranch just south of the primary study area near Gualala, California. It is one of the few locations where uncut old-aged trees grow on and near the fault zone. We took increment cores from 14 trees near the fault and detected definite of the 1906 event in the rings of 5 of the trees and possible effects in five others. Two of the trees were unworkable due to decay or anomalous growth. One tree is locally called the "split" or "earthquake" tree. It was reported on by LaMarche and Wallace in 1972. A small part of the tree was actually split off and slightly displaced by the 1906 earthquake. The displacement here is about half a meter. There are other traces of the 1906 rupture in the vicinity so this is only part of the total 5 meter displacement estimated for this area. Redwoods are known for their ability to regrow from stumps or damaged areas. In this case the part of the split portion regrew where the cambial layer survived and has now covered over one end of the knob. Six cores were taken from this tree and split knob. Core 1 A went through the outer years into the original pre-1906 growth rings. The ring widths show a substantial increase and reaction wood (a response to tilting after the 1906 damage. Core 1' B went completely through the split knob and shows the typical curved callus growth covering over the damaged area. It was deliberately taken close to the end of the split section. The innermost ring of this core is partial 1906

growth. This growth ring does not necessarily date the damage but it does show that the damage had to occur before much of the 1906 growing season was over. The other end of the core shows that it took until 1930 before regrowth reached that spot of the split. Trees PR05, PR08, PR09 and PR13 show definite damage due to the 1906 earthquake. Among all these trees is an abrupt increase in the variability of ring widths between trees and cores. This variability indicates unusual trauma causing widely varying growth response.

We also found 1906 damage in a redwood tree on the Kelly-Thompson Strawberry Ranch near Watsonville, California and documented the effects of the 1906 earthquake on Douglas fir [*Pseudotsuga menziesii* (Mirb.) Franco] at two locations. Since we have not found any old-aged Douglas fir that would be of use in our paleoseismic studies in this area, further study of this species was given lower priority.

The results of the analog studies described above indicate that in addition to severe trauma, disturbance by earthquake accelerations and displacement can produce varying effects in the annual rings on different sides of the same tree. That is the ring widths can be diminished on one side and enlarged on the other. If several cores or radii are measured from one tree, the result of these types of disruption of the normal growth pattern is to increase the standard deviation and thus coefficient of variation of the ring widths for a few to many rings after the event. In the extreme case growth rings can be missing on the damaged side of the tree. Insertion of zeros to account for the missing rings also increases the coefficient of variation for those years. The resulting time series of standard deviations for the ring-width indices for multiple cores from one tree or for several disturbed trees would show an unusually large increase beginning at the time of disturbance.

A large number of samples were taken in 1989 and 1991. The best samples are from along the fault at two locations near Gualala, California. At the first location the fault appears to be concentrated within a single, well-defined trace. A small creek drainage was offset approximately three times the estimated displacement of about 5 meters for this area due to the 1906 earthquake. A second location is about 2 km north of the offset creek area. Several samples from here are beside sag ponds or appear to be directly on the or very near the surface rupture. All of these samples have now been surfaced and ring widths of several radii measured. The resulting data are now being analyzed for clues to possible seismic disturbance.

For detection of unusual growth disturbance in fault-zone trees we need to have a control chronology of normal undisturbed growth for comparison. The abandoned logs from previous logging on a ridge a few

kilometers northeast of the sites mentioned above have been worked into the regional control chronology. These logs yielded full sections with good circuit uniformity for most of the rings. These sections served to strengthen the control chronology as a dating reference for the fault-zone samples and were also important contributors to a control chronology of undisturbed redwood growth. We made more progress in crossdating between the logs, modern trees, and some of the fault-zone trees. The preliminary control chronology extends from the present back to 361 AD. This date is reinforced by a radiocarbon date for the center of the oldest control tree, WFF17. Calibration of the radiocarbon date of the central 60 rings of the oldest tree indicates the center of mass for the radiocarbon sample is about 400 AD. The tree-ring date is well within one sigma error.

There is a definite reduction in growth in one redwood sample taken in 1993 from Grizzly Flat near Watsonville, California. A radiocarbon date for the wider rings just before the abrupt decrease in ring widths is 1670 AD (+/- 30). Although the tree-ring sample is not absolutely dated to calendar year, the disturbance in growth for this tree located right on the San Andreas fault is obvious and the disturbance is placed in time by the radiocarbon date. This date is in agreement with some radiocarbon dates from trench studies by D. Schwartz at this same location.

## 2. Cascadia Subduction Zone (CSZ): Mad River Slough and Eel River

We crossdated root portions from nine different trees submerged at Mad River slough near the Mendocino Triple Junction at the southern end of the CSZ. Among the samples at Mad River slough one can see that the deaths or end of final cell formation took place over 4 growing seasons. Trees, having no central nervous system, often do not die all over at once. If growth hormones and carbohydrates reach a cambial site, with appropriate temperatures, cell division can persist until these substances are exhausted. Even within one tree there can be several years difference in when cell division stops at different parts of the tree. The closely-spaced death of these trees indicates a rapid subsidence event leading to their deaths (Jacoby et al. 1994). Radiocarbon dates for the Mad River roots indicate the outer rings to be about 1700 A. D. Thus far we have not been successful in crossdating these specimens with living-tree series to produce a calendar date.

Samples from drowned trees at nearby Eel River have been analyzed but results indicate they are not the same age as the Mad River trees. Further tree-ring and radiocarbon analyses are underway. The Eel River samples are of much better quality than the Mad River samples.

There is much better agreement between samples and trees. The Eel River roots have much less distortion than the Mad River samples. There are higher correlations between the ring-width variations of the Eel River roots. These sites are important parts of the larger question of major subduction zone earthquakes in the CSZ.

Reports:

Jacoby, G. C., Carver, G. and Williams, P. L. 1993. Tree deaths and Earthquakes in the Cascadia Subduction Zone. (abst.) EOS Oct. 1993 Fall AGU Meeting. p. 199.

Jacoby, G. C., Carver, G. and Wagner, W. S. 1994. Tree-ring and plant evidence of rapid subsidence at Mad River slough, Humboldt Bay, CA about 300 years ago near the southern end of the Cascadia subduction zone. Geology (in press).

# Tree-Ring Dating of Coseismic Coastal Subsidence in the Pacific Northwest Region

Award No.: USGS 1434-94-G-2471

Gordon C. Jacoby  
Tree-Ring Laboratory  
Lamont-Doherty Earth Observatory  
Palisades, New York 10963  
Phone: 914 365 8616  
FAX: 914 365 3046  
e-mail: druid@lamont.ideo.columbia.edu

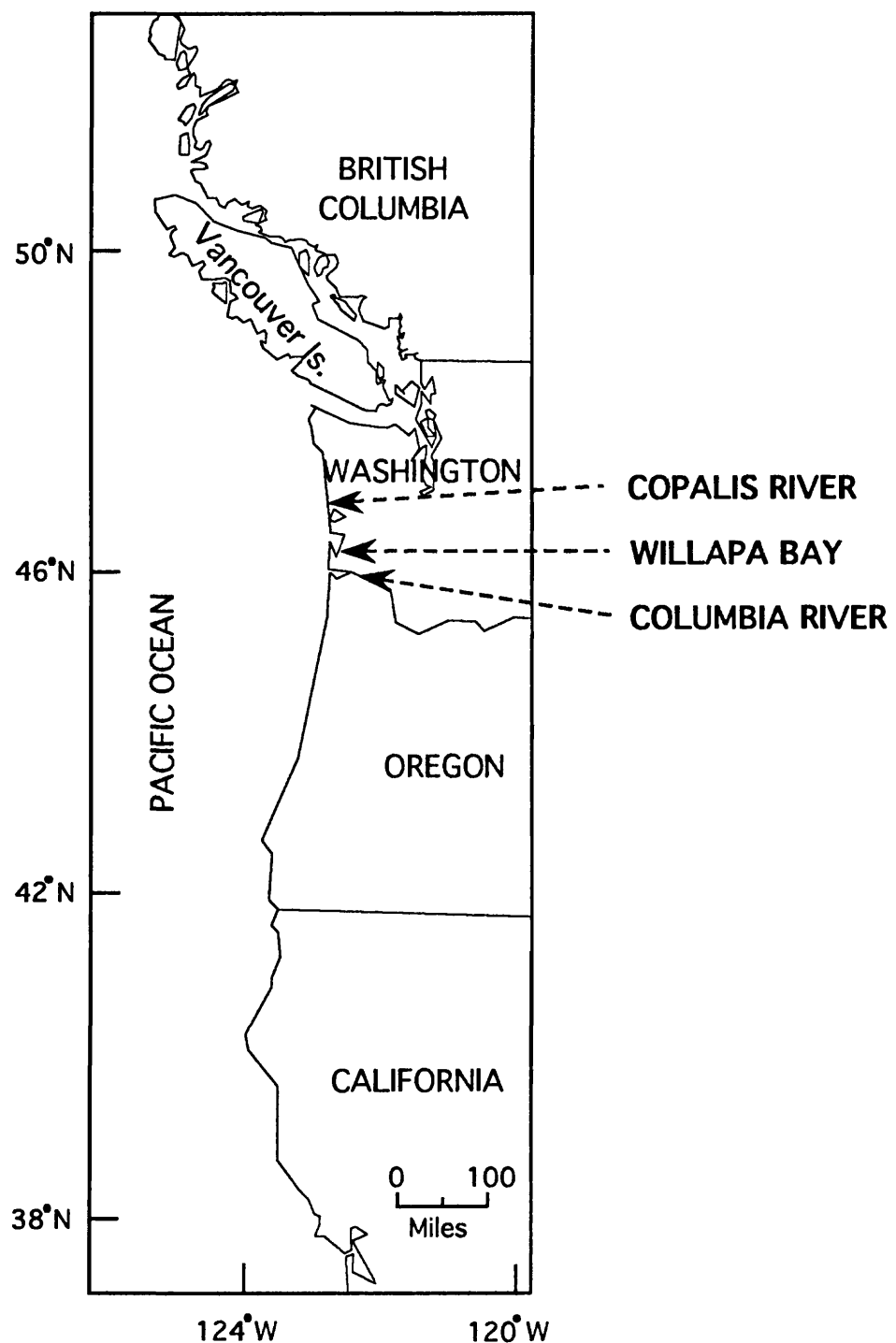
## Program Objective II-5

The purpose of this project is to use the high resolution capabilities of annual tree-ring analysis to determine whether some or any of the subsidence events documented along the Cascadia Subduction zone around 300 years ago may have occurred at the same time. These events are interpreted as being due to earthquake(s). Simultaneous occurrence would imply a large devastating event; differing times would mean several smaller, less damaging events.

Efforts were made to try and assemble information from previous tree-ring sampling and observations of subsided trees and remnants of trees along the coastal areas from northern California to Vancouver Island, Canada. Dave Yamaguchi, Brian Atwater and Boyd Benson were extremely helpful in aiding this effort. All specimens from these previous samplings and new sampling in the spring of 1994 made up a considerable amount of material for analysis. All were measured, dated and examined for evidence of disturbance and/or crossdated to determine the time of death.

The primary sampling sites are the Copalis River, Willapa Bay and Columbia River (Figure 1) with reconnaissance sampling at other sites ranging from the Tofino area on Vancouver Island to the Coquille River in southern Oregon. We have crossdated some material between Copalis River and Willapa Bay.

There are three categories of samples. 1. Trees that were killed by submergence and drowning. 2. Trees that were damaged by possible temporary inundation or partial burial but survived. 3. Newly established trees on recently deposited alluvium or post the estimated time of the most recent subsidence event. Unfortunately, the majority of samples were in the third category. In 1994 forty one new trees were sampled. All of the total of 134 trees and 38



roots were processed and thus far we have successfully dated 18 of the cores from living trees that are old enough to be considered survivors (300 years or older). The primary target event is the most recent event placed about 300 years BP or 1700 AD according to radiocarbon measurements.

We have dated 24 of the 38 roots. Only 4 of them have calendar dates and extend back to 1700. The 12 roots from Bay Center are crossdated relative to each other but not to calendar years yet. Continuing analysis will more accurately determine relative death dates but preliminary results indicate all deaths within a few years of each other.

In the survivor trees we are using the coefficient of variation for ring widths as well as actual changes in individual tree samples to identify times of disturbance. At a given site, trees tend to vary somewhat coherently in response to year-to-year climate variations with competition and other individual factors adding noise to this general response. A disturbance event will cause some trees to change growth rate according to the individual tree location and damage. The amount of disagreement in ring-width variation for each year is expressed in the coefficient of variation for rings widths of that year. These two parameters, ring width change in individual trees and coefficient of variation among trees form the basis of interpretation.

Dating and analyses of what we presume to be survivor trees indicate a change in ring width and increase in coefficient of variation in the early 1700's for some trees growing at the Copalis River and Willapa Bay locales. These analyses are ongoing and results from samples in hand should be achieved early in 1995. The interpretation of the onset of disturbance is complicated by trees reserving growth substances and utilizing them in the following year's growth. It is the onset of unusual growth and not the most damaged, usually narrowest, ring that must be identified. The early 1700's timing is encouraging as it fits within previous radiocarbon dating of subsidence trees.

The field location and collection of samples is greatly aided by other geologists working in the region who have suggested locations where trees and subsidence are in evidence.

## Instrument Development and Quality Control

9930-01726

E. Gray Jensen

Branch of Seismology

U.S. Geological Survey

345 Middlefield Road - Mail Stop 977

Menlo Park, California 94025

Voice: (415) 329-4729 Fax:(415) 329-5163

E-mail: [gjensen@andreas.wr.usgs.gov](mailto:gjensen@andreas.wr.usgs.gov)Investigations

This project supports other projects in the Office of Earthquakes, Volcanoes and Engineering by designing and developing new instrumentation and by evaluating and improving existing equipment in order to maintain high quality in the data acquired by the Office. Tasks undertaken during this period include construction and deployment of digital seismic telemetry units, participating in the development of new realtime seismic event picker and maintaining the Seismic Group Recorder system, among other things.

Results

An array of 12 digital seismic telemetry (DST) field stations was completed and has been installed to monitor volcanoes in Hawaii. Monitoring continued on the four units that have been deployed in the San Francisco Bay area. Two units have been operating in Alaska. These units have been telemetering 16-bit seismic data as much as 600 kilometers via radio and microwave links. Work is continuing on real-time merging of digital and analog telemetered data, as well as improving dynamic range and bandwidth.

A system to replace the RTP realtime seismic picker, dubbed Earthworm, is under development. This project has been providing support services for the Earthworm development, including building filters and special circuits needed as accessories to the A/D. Field tests of high-speed (38.4 Kbaud) telemetry radios for use with the Hayward Fault digital network were performed. Modifications have been ordered for improved performance. A new voltage-controlled-oscillator board was designed and built for use in retransmitting seismic data. One hundred are currently under construction. A modification was designed for the RTP which permits easier programming of station list updates.

The 190-unit Seismic Group Recorders were used in seismic refraction experiments in the Las Vegas area and the Los Angeles area (LARSE). This project supported these operations with instrument maintenance, enhancement and field support. Five Master Clock III precision chronometers were completed in time for the LARSE experiment and similar clocks were installed in the eight new blasters used for detonation of explosive charges in the experiments. Maintenance and repairs were made to two digital seismic monitoring arrays in Parkfield.

## SEISMIC LANDSLIDE HAZARD MAP OF LOS ANGELES REGION

Randall W. Jibson

Edwin L. Harp

Branch of Earthquake and Landslide Hazards

U.S. Geological Survey

Box 25046, MS 966

Denver, Colorado 80225

Jibson: (303) 273-8577, Fax 273-8600, [jibson@gldvxa.cr.usgs.gov](mailto:jibson@gldvxa.cr.usgs.gov)

Harp: (303) 273-8557, Fax 273-8600, [harp@gldvxa.cr.usgs.gov](mailto:harp@gldvxa.cr.usgs.gov)

NEHRP/SC/I.2,II.A, & II.B

### Investigations Undertaken

The 1994 Northridge earthquake triggered tens of thousands of landslides over a 10,000-km<sup>2</sup> area. These landslides destroyed dozens of houses, blocked roads, disrupted pipe and power lines, blocked streams, and generated dust that triggered an epidemic of valley fever that caused three fatalities. The area of greatest landslide concentration was the Santa Susana Mountains, an area of extreme landslide susceptibility on the edge of the developed metropolitan area. Many parts of the Santa Susanas are slated for residential development, and development pressure there will continue to increase as the metropolitan area expands. Landslides also caused considerable damage in parts of the Santa Monica and San Gabriel Mountains. The investigations being conducted in this project are twofold:

1. *Document in detail landslides triggered by the Northridge earthquake.* This involves field and airphoto mapping of landslides over a broad area and characterization of landslide types and distribution. The initial product will be an open-file digital map showing landslide locations and types. This will be followed by a formally published map accompanied by detailed analysis and narrative describing landslide types and distribution with respect to strong shaking, bedrock and surficial geology, and topography.
2. *Produce a GIS seismic landslide hazard map of the Los Angeles 1:100,000 sheet.* The landslide inventory described above will be used to calibrate a seismic landslide hazard model that will be applied to the Los Angeles 1:100,000 sheet. The model will combine data on material strength, slope steepness, and strong ground motion to predict seismic landslide displacement using Newmark's sliding block analysis. Displacements generated will then be used to estimate the probability of slope failure in each cell of the GIS model.

As the project progresses, contact is being maintained with experts in the private consulting community, geologists with the state geological survey, and county geologists and planners to assure the final product meets the needs of the end users.

## Results

We have mapped the precise locations and shapes of more than 10,000 individual landslides. This has involved extensive fieldwork and detailed examination of U-2 photography taken the day of the earthquake. Landslide locations have been digitized in ARC/INFO and, and the computer-generated inventory map will be released digitally as well as in paper form. This landslide inventory is nearly complete and will most likely be released in January 1995.

For the hazard mapping effort, digital elevation models (DEM's) have been purchased for the affected area to plot contours and calculate slope. Arrangements are proceeding to acquire digital geology for use in the hazard analysis. Also, strong-motion parameters (Arias intensities) are being calculated as strong-motion records become available for use in a dynamic analysis related to developing susceptibility and hazard categories.

## Reports Published

Harp, E.L., Jibson, R.W., Keefer, D.K., and Wilson, R.C., 1994, Landslides triggered by the January 17, 1994, Northridge California earthquake—Implications for future hazards [abstract]: Geological Society of America, Abstracts with Programs, v. 26, no. 7, p. A-217.

Jibson, R.W., Harp, E.L., Keefer, D.K., and Wilson, R.C., 1994, Landslides triggered by the 17 January 1994 Northridge, California, earthquake: Japan Landslide Society, Landslide News, no. 8, p. 7-10.

Jibson, R.W., Harp, E.L., Keefer, D.K., and Wilson, R.C., 1994, Landslides triggered by the 17 January 1994 Northridge, California, earthquake: Earthquakes and Volcanoes, U.S. Geological Survey [in press].

Jibson, R.W., Harp, E.L., Keefer, D.K., and Wilson, R.C., 1994, Landslides triggered by the 1994 Northridge earthquake [abstract]: Southern California Academy of Sciences, Annual Meeting, Proceedings, Irvine, California, p. 10.

Jibson, R.W., Harp, E.L., Spiegel, R.A., Hajjeh, R.A., Schreider, E.E., Marshall, G.A., and Stein, R.S., 1994, Landslides can be hazardous to your health [abstract]: An outbreak of coccidioidomycosis (valley fever) caused by landslides triggered by the 1994 Northridge, California earthquake: Geological Society of America, Abstracts with Programs, v. 26, no. 7, p. A-318.

## TILT, STRAIN, AND MAGNETIC FIELD MEASUREMENTS

9960-10146, 9960-11146, 9960-12146, 9960-15146

M. J. S. Johnston, R. J. Mueller, G. D. Myren  
 Branch of Earthquake Geology and Geophysics  
 U. S. Geological Survey  
 Menlo Park, California 94025  
 E-mail [mal@thebeach.wr.usgs.gov](mailto:mal@thebeach.wr.usgs.gov)  
 415/329-4812

### Investigations

- [1] To investigate the mechanics of failure of crustal materials using data from both deep borehole tensor and dilatational strainmeters and near surface strainmeters, tiltmeters, and arrays of absolute magnetometers.
- [2] To develop physical models of incipient failure of the earth's crust by analysis of real-time records from these instruments and other available data.

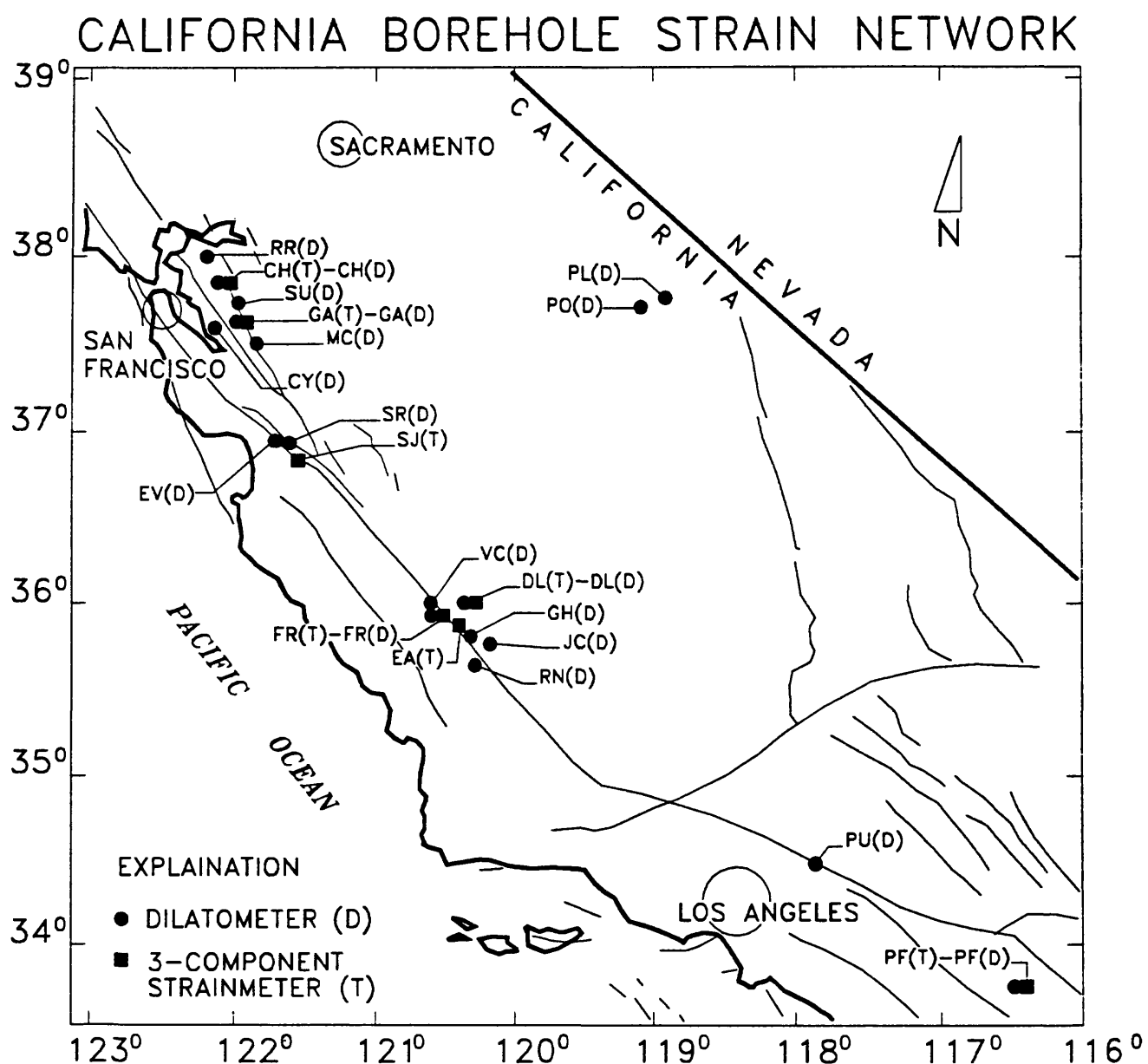
### Results

#### **[1] BOREHOLE STRAIN ARRAY IN CALIFORNIA**

A network of 23 borehole strainmeters along the San Andreas fault zone and in the Long Valley Caldera continues to be monitored and maintained (Figure 1). All instruments are installed at depths between 117-m and 324-m and all are between 1-km and 5-km from the the surface trace of the fault. High frequency dilatometer data in the frequency range 0.005 Hz to 100 Hz are recorded on 16-bit digital recorders with least count noise less than  $10^{-11}$ . Low frequency data from zero frequency to 0.002 Hz are transmitted through the GOES satellite to Menlo Park, CA, using a 16-bit digital telemetry system. At the USGS in Menlo Park the data are displayed in "almost real time" and are continuously monitored with detection algorithms for unusual behavior. Least-count noise is about  $5*10^{-12}$  for the on-site digital recordings, and about  $2*20^{-11}$  for the satellite telemetry channels. Earth strain tides, strain transients related to fault creep and numerous strain seismograms from local and teleseismic earthquakes with magnitudes between -1 and 6 have been recorded on these instruments. Static moments and total earthquake moments are determined from the co-seismic strains and total strain changes observed with the larger events.

#### **[2] TRANSIENT DEFORMATION DURING TRIGGERED SEISMICITY FROM THE JUNE 28, 1992, $M_w=7.3$ LANDERS EARTHQUAKE AT LONG VALLEY VOLCANIC CALDERA, CALIFORNIA.**

Continuous records from a borehole strainmeter and a long baseline tiltmeter in the Long Valley caldera (Figure 2) provide critical insights into the origin of at least one episode of minor seismicity in volcanic regions triggered by the June 28, 1992,  $M_L$  7.3 Landers, California, earthquake. A strain transient reaching a peak of 0.25 microstrain occurred in the few days following the Landers event and decayed over the next 20 days. A tilt perturbation during the same time reached a peak amplitude of 0.2 microradians. These signals correspond approximately in time to the primary seismic moment release across a 50 km<sup>2</sup> region of the south part of the caldera at depths between 2 and 10 km. Corresponding strain transients in 5-km geodetic lines across the south caldera are not apparent above the 95% confidence limits of about 0.4



microstrain in daily sampled data during this same period. These data rule out models involving single localized inflation sources within the upper crust beneath the caldera, including that responsible for the current rapid inflation of the resurgent dome. They also preclude models involving aseismic slip on single strike-slip or normal faults in the caldera. A single source in the form of a relaxing magma body at a depth of 50 km beneath the caldera can account for the deformation data, but whether the small stress changes are sufficient to drive the triggered seismicity is not clear. An alternate possibility involves distributed deformational sources triggered by the passage of the 10 microstrain peak amplitude surface waves from the earthquake. This distributed deformational source could result from either rupturing of overpressured fluid or gas chambers commonly encountered in volcanic regions or from advective gas overpressure during release of gas bubbles in hydrothermal or magmatic fluids.

### [3] NEAR-SILENT EARTHQUAKES ON THE SAN ANDREAS FAULT NEAR SAN JUAN BAUTISTA, CALIFORNIA, DECEMBER 10-15, 1992.

Moderate sized near-silent earthquakes were recorded on a small network of three borehole strainmeters near San Juan Bautista, California, from December 10 to December 15, 1992. The events had an associated earthquake swarm, an "aftershock" sequence and 3.7 mm of surface creep several days later. Fault parallel shear and dilatational strain changes of 1.1 microstrain and 0.1 microstrain were observed starting about 0700 UT on a borehole tensor strainmeter installed about 1.2 km from the San Andreas fault near San Juan Bautista while dilatational strains of 0.65 microstrain and 0.15 microstrain were observed on two borehole dilatometers, five kilometers to the northwest at distances of about 1 km and 7 km from the San Andreas fault starting at about 0730 UT on December 11, 1992. Three magnitude 3 events occurred at 0512, 0729, and 0804 on December 11 and these were followed by two magnitude 3.7 and numerous smaller events from 1553 UT on December 12. These seismic events form an approximate donut shape with a diameter of about 5 km from 3 km to 8 km beneath the strainmeters. Surface creep started late on December 14 and continued until December 18. Initial quasistatic modeling indicates aseismic moment release for the events was about  $10^{16}$  Nm, equivalent to a magnitude 4.7 earthquake. The total moment release for all the seismic events was an order of magnitude smaller. We use forward quasi-static modeling to estimate the physical parameters of the slow events. Examination of the strain time histories leads us to model the sequence as 3 slow events; one has duration of several days and the other 2 are relatively short (minutes and hours). The very slow event can be modeled as non-uniform slip over some  $60 \text{ km}^2$  of fault, with 6 mm of right-lateral slip together with an additional 1.3 cm of slip over about a quarter of that patch. The first of the sub-events requires a smaller amount of slip similarly distributed, but with a much shorter time scale. The remaining sub-event has a more complicated time history and can be approximately satisfied by 8 cm of slip on a  $2 \text{ km}^2$  patch of fault on which the rupture propagates slowly upward. Initiation of all 3 sub-events is closely correlated with the larger earthquakes. Our inferred slow slip distributions correspond with the area which experienced increased seismicity during this time interval. In particular, that part of the fault which experienced most of the earthquakes, including the larger ones, also had the greatest slow slip. Such slow earthquakes are very difficult to detect: deformations decrease with the cube of distance from the source and surface displacements are usually much too small to be detected by geodetic techniques. Here we have unambiguous detection of large slow earthquakes rupturing the fault down to a depth of 5 -- 8 km, and these slow ruptures occurred in the same location that experiences earthquakes up to  $M_L = 5.2$ .

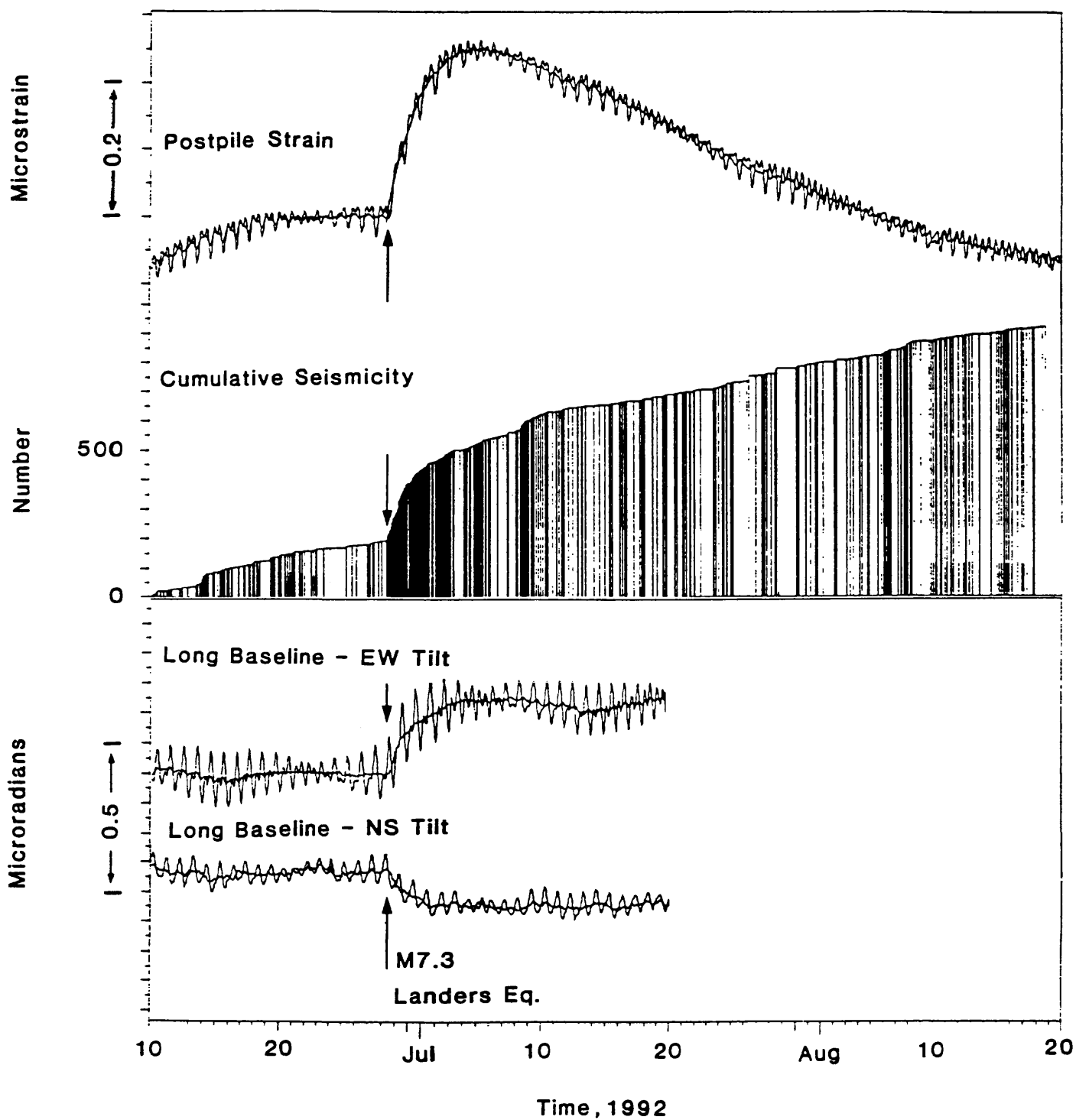


Fig. 2. Plot of strain (upper plot), cumulative seismicity (2nd plot), and tilt (3rd

and 4th plots) from June 10 to Aug 20, 1992. The occurrence time of the Landers earthquake is shown with an arrow on each record.

**[4] CONTINUOUS BOREHOLE STRAIN BEFORE, DURING AND AFTER THE JAN 17, 1994, M6.7 NORTHRIDGE, CALIFORNIA, EARTHQUAKE.**

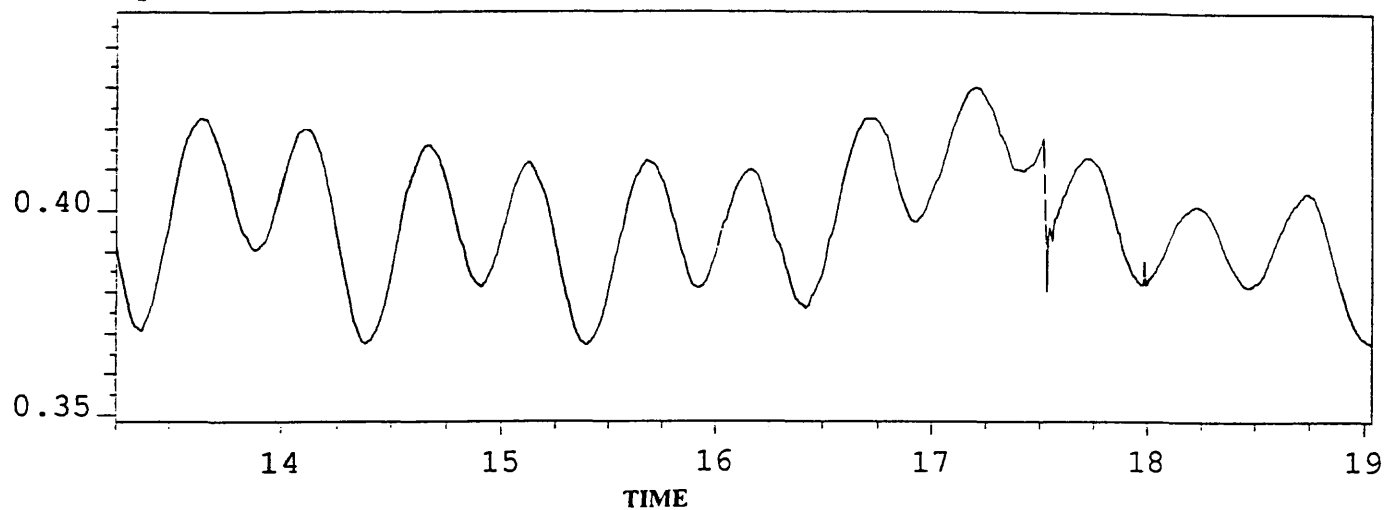
High precision strain was observed before, during, and after the 12:30 UT Jan 17, 1994, M6.7 with borehole dilatational strainmeters in the Devil's Punchbowl (PUBS) and at Pinon Flat (PCIA) 74 km and 196 km respectively, from the Northridge epicenter. These instruments operate at a sensitivity of better than a nanostrain. Precursive strain or changes in strain rate from days to seconds prior to the earthquake are not apparent at the nanostrain level in the data from the closest instrument. Offsets in the regional strain field, generated by the earthquake, were observed at PUBS (21 nanostrain extension) and at PCIA (7 nanostrain compression) (see Figure 3) with marginal signals on instruments at greater distances ( $\approx$ 260 km) in the Parkfield area. These few data are insufficient to solve for the location and physical parameters of the earthquake, but by also using the measured displacement changes in the epicentral area (courtesy of the many groups making geodetic measurements), we are able to invert for a source model consistent with all available observations of crustal deformation. The source model obtained indicate a moment of  $1.1 \times 10^{19}$  Nm on a fault that has a strike and dip of about N113°E and 46° down to the south, respectively. The rupture surface has a length of 9.1 km, a width of 12.7 km and extends downward from a depth 6.0 km. The onscale straingram at PUBS indicates peak dynamic strains in excess of 10 microstrain occurred during the first 20 seconds of the earthquake at this location. Ground displacement spectra calculated from these broadband borehole strain data indicate a corner frequency of about 1 Hz.

**[5] NUCLEATION SIZE OF MODERATE EARTHQUAKES AND KINEMATICS OF THE SAN ANDREAS FAULT IN CALIFORNIA FROM SUBMICRO HZ TO 30 HZ STRAIN MEASUREMENTS**

Popular views of the earthquake nucleation process and fault kinematics have included suggestions of: 1) non-linear deformation prior to rupture in regional-scale "preparation zones" of earthquakes, 2) strain redistribution by "crustal block interaction", 3) propagating aseismic slip waves, and 4) variation in the material properties of near-fault materials with time and location. In contrast, submicro-Hz to 30 Hz high-resolution strain through many moderate earthquakes in California and Japan indicate: 1) short-term non-linear precursive strains greater than nanostrain rarely occur in the eventual epicentral region prior to rupture, 2) fault patches that initiate large scale failure are apparently less than a few hundred meters in size, 3) strain redistribution from earthquakes is transmitted largely elastically through the complex geology and fault geometry in these regions, 4) aseismic slip at depth is apparently largely uniform in time at seismogenic depths but episodic in the near-surface material, and 5) material properties are invariant on timescales of days to years. Only one unambiguous example of a deep slip episode (slow earthquake?) with aftershocks and subsequent surface rupture has been detected. These results are supported by near-field continuous strain data during more than 50 recent events on the San Andreas and associated faults with magnitudes ranging from 7.3 to 4.5 and continuous strain records during numerous surface fault slip episodes. Similar events in Japan have similar characteristics. The apparent small size of the rupture initiation moments compared to the total earthquake moments suggests that there is no scaling of the nucleation process with earthquake magnitude. The basic failure process thus apparently involves rupture nucleation and runaway. High pore pressure fluids may be associated with this process but pore pressure redistribution must also be limited in extent. Detection of rupture nucleation apparently will require these highly sensitive and stable instruments be installed even closer to the hypocenters of large earthquakes.

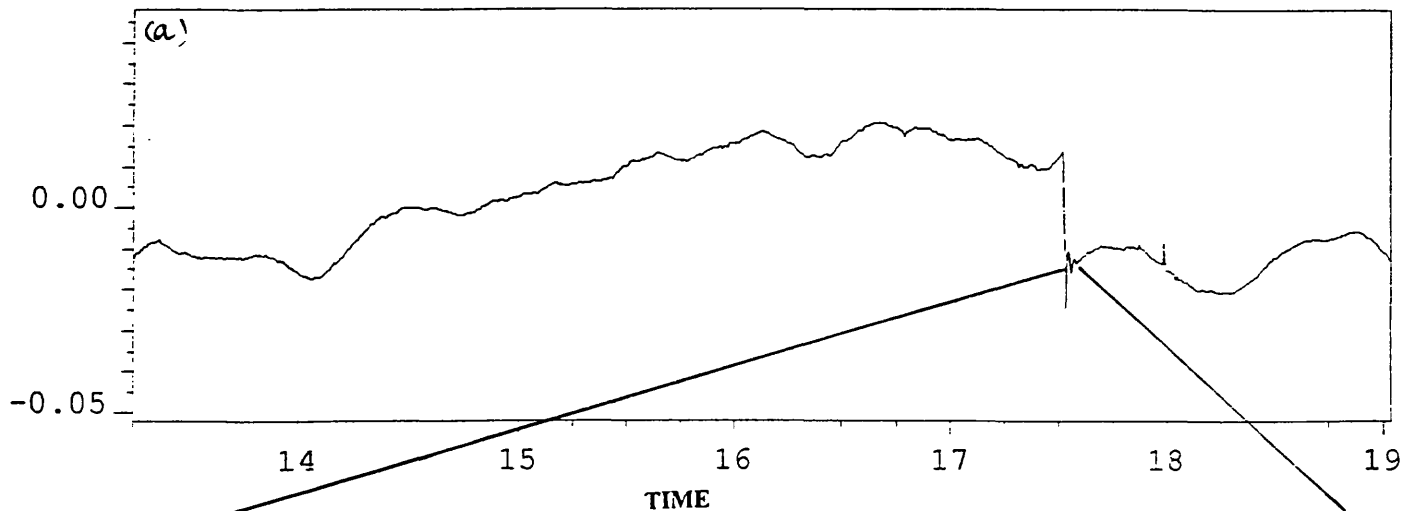
spua: 06:00 13 Jan 1994 013 - 00:50 19 Jan 1994 019

MICROSTRAIN



ppuba: 06:00 13 Jan 1994 013 - 00:50 19 Jan 1994 019

MICROSTRAIN



MICROSTRAIN

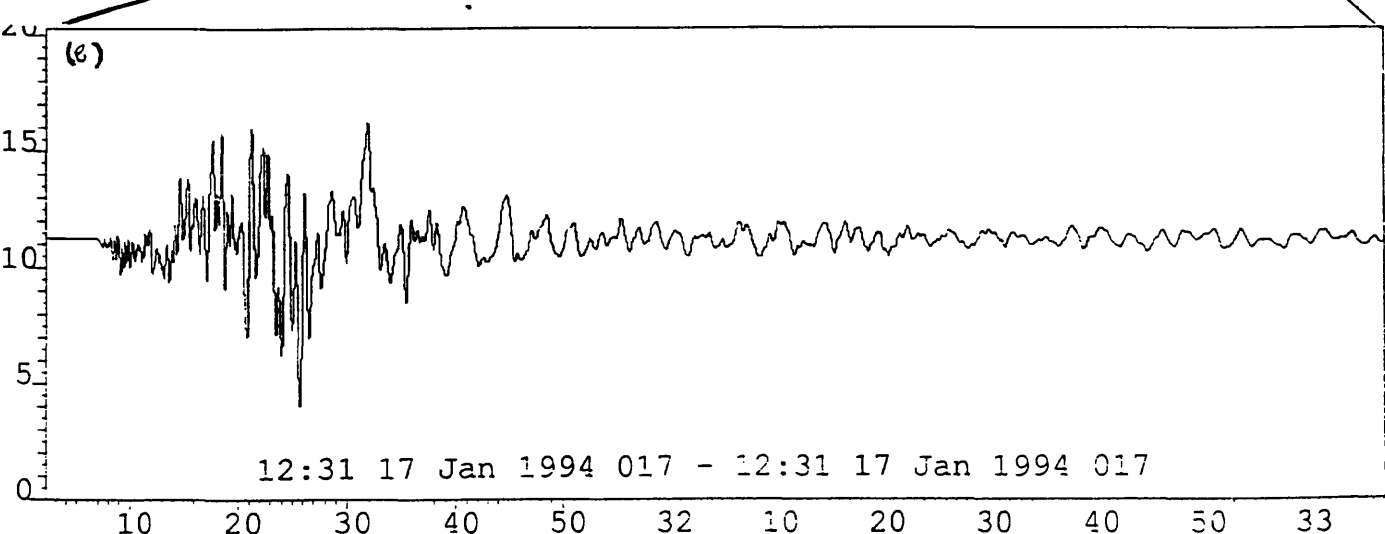


Fig. 3. Strain recorded at PUBA during the Jan 17, 1994 M6.6 Northridge earthquake.

**[6] MAGNETIC FIELD OBSERVATIONS IN THE NEAR-FIELD OF THE JUNE 28, 1992  $M_L$  7.5 LANDERS, CALIFORNIA, EARTHQUAKE.**

Two continuously operating proton magnetometers, LSBM and OCHM, at distances of 17.3 km and 24.2 km, respectively, from the epicenter of the June 28, 1992,  $M_w$  7.3 Landers earthquake, recorded data through the earthquake and its aftershocks. Seismomagnetic offsets of  $-1.2 \pm 0.6$  nT and  $-0.7 \pm 0.7$  nT were observed at these sites. In comparison, offsets of  $-0.3 \pm 0.2$  nT and  $-1.3 \pm 0.2$  nT were observed during the July 8, 1986  $M_L$  5.9 North Palm Springs earthquake which occurred directly beneath the OCHM magnetometer site. The observations are generally consistent with seismomagnetic models of the earthquake in which fault geometry and slip have the same form as that determined by either inversion of the seismic data or inversion of geodetically determined ground displacements produced by the earthquake. There is no indication of diffusion-like character to the magnetic field offsets that might indicate these effects result from fluid flow phenomena. There are no indications of enhanced low-frequency magnetic noise before the earthquake at frequencies below 0.001 Hz.

**[6] COSEISMIC AND TRIGGERED FAULT SLIP NEAR PAJARO GAP, CALIFORNIA DURING AND FOLLOWING THE 1989  $MSUBL$  7.1 LOMA PRIETA EARTHQUAKE**

Deformation along a 15 Km segment of the San Andreas fault, from the southern end of the October 18, 1989 Loma Prieta earthquake rupture, has been measured with an 11 station geodetic network since 1981. Line lengths ranging from 4 Km to 10 Km are measured with laser ranging equipment using end point meteorology. This limits the precision to between 6 mm and 12 mm. Two surveys conducted 7 years prior to the Loma Prieta earthquake and three surveys in the 2.5 years after the earthquake show clear coseismic and postseismic displacement along this segment of the San Andreas fault. When our data are compared with displacements predicted by other models of coseismic slip, we find additional slip is required to fit our measurements near Pajaro Gap. Continuing postseismic displacements are observed in these data between February and October 1990. During this period the largest Loma Prieta aftershock (Chittenden  $M_L$  5.4), and a major aftershock sequence, occurred beneath the geodetic network in April, 1990 along with increased shear and dilatational strain on borehole strainmeters within the network and increased creep rate on the San Andreas fault. The observed Loma Prieta coseismic displacements cannot be explained by slip in the main rupture zone. Slip on an extension of the rupture zone at depth to the southeast along the San Andreas under the network, together with some triggered slip on the Sargent fault, are required to explain the geodetic data. The geometry of this slip is consistent with the occurrence of aftershocks in this region in the first month following the Loma Prieta earthquake. The postseismic changes are consistent with continued shallowing of slip on the San Andreas with time as indicated by increased rates of crustal strain and fault creep in the region.

**[7] ELECTROKINETIC EFFECTS ASSOCIATED WITH CHANGES IN HIGH PORE PRESSURE COMPARTMENTS IN FAULT ZONES - APPLICATION TO THE LOMA PRIETA ULF EMISSIONS**

We have determined the electric and magnetic fields generated during failure of faults containing sealed compartments with pore pressures ranging from hydrostatic to lithostatic levels. Exhumed fault studies and strain measurement data limit the possible size of these compartments to less than 1 km in extent. Rupture of seals between compartments produces rapid pore pressure changes and fluid flow and may create fractures that propagate away from the high pressure compartment, along the fault face. Non-uniform fluid flow results from pressure decrease in the fracture from crack generated dilatancy, partial blockage by silicate deposition, and clearing as pressure increases. The direct consequences of this turbulent fluid flow are associated transient magnetic signals caused by electrokinetic, piezomagnetic, and magnetohydrodynamic

effects. Models of these processes for fault geometries with 1 km high pressure compartments show that electrokinetic effects are several orders of magnitude larger than the other mechanisms. The electrokinetic signals produced by this turbulent flow are comparable in magnitude and frequency to the magnetic signals observed prior to the ML 7.1 Loma Prieta earthquake of 18 October 1989 provided fracture lengths are less than 200 m.

#### **[8] DIFFERENTIAL MAGNETOMETER ARRAY IN CALIFORNIA**

We investigate crustal generation of local magnetic fields and their relationship to strain and seismicity in the Parkfield region and in southern California. The network consists of 9 stations which are all sampled synchronously every 10 minutes and transmitted with 16-bit digital telemetry to Menlo Park, CA through the GOES satellite. Data are monitored daily with particular attention to the seven stations operating in the Parkfield region of central California and the three stations operating in the Long Valley caldera. At these latter sites a magnetic field anomaly first became obvious in late 1989 and in continuing to the present in concert with anomalous 2-color geodetic strain measurements and spasmodic swarms of minor earthquakes.

#### **[9] USING SATELLITE TELEMETRY FOR NEAR REAL-TIME MONITORING OF SEISMIC EVENTS AND STATUS OF PORTABLE DIGITAL RECORDERS.**

Near real-time monitoring of seismic events and status of portable 16-bit digital recorders has been established for arrays near Parkfield, Mammoth Lakes and San Francisco, California. This monitoring system provides seismic event identification (rough location and magnitude) and a cost effective means to maintain arrays at near 100% operational level. Principal objectives in the design of this telemetry system have been portability and low cost. The system has been developed to utilize portable digital seismic recorders (GEOS-General Earthquake Observation System) and portable data collection platforms (DCP) for the Geostationary Operational Environmental Satellite (GOES) telemetry system. Data are transferred asynchronously from the GEOS seismic system through a microprocessor controlled interface every 10 minutes. The interface stores, determines priority, converts, and synchronously transfers these data to a Sutron Corp. Model 8004 DCP for transmission through the GOES satellite telemetry system. Event parameters include trigger time, peak amplitude, time of peak amplitude and event duration. Instrument configuration parameters, transmitted at system start up time and every 24 hours, include recording parameters, trigger parameters, GEOS software version, clock reference and location parameter. Instrument status includes battery voltage, number of events and percentage of tape usage. These data are transmitted as appropriate to the U.S. Geological Survey satellite downlink and computers located in Menlo Park, California where they are processed and displayed.

#### **[10] ANOMALOUS ULF SIGNALS AT PARKFIELD DURING DECEMBER 1993 AND JANUARY 1994**

Following observations of unusual ULF signals during the 1989 M7.1 Loma Prieta earthquake, two ULF monitoring stations were installed at Parkfield in 1991. The two sites are located about 5 km apart on Haliburton and Varian Ranches, respectively. Most signals seen by these stations are generated in the upper atmosphere, and generally the data at these, and other stations, track well. In December 1993 and January 1994, unusually signal levels occurred at 0.01-10 Hz initially at both stations but only at Haliburton after December 10, which were 10-30 dB higher than normal. To provide independent verification, proton precession magnetometers (0.1 nT sensitivity) covering the frequency range from DC to 0.05 Hz were deployed at the two ULF sites and a third site near a nearby permanently recording magnetometer on December 16. Although the proton and ULF instruments measure total magnetic field and NS component rate respectively, comparable amplitude time histories at Varian agree. Noise power at all proton sites agree and generally agree within 5 dB with Varian ULF noise

power in the overlap frequency band. ULF noise power at Haliburton is 20-30 dB higher and appears to be generated by aliasing of higher frequency noise spikes of local but not of instrument or tectonic origin. The Haliburton noise level gradually decreased after January and is now back to normal. The origin of the anomalous signals remains a mystery.

#### [11] RESPONSE OF LONG VALLEY CALDERA TO THE $M_w=7.3$ LANDERS, CALIFORNIA, EARTHQUAKE

Of the many sites in the western United States responding to the 28 June 1992 Landers earthquake ( $M=7.4$ ) with remotely triggered seismicity, only Long Valley caldera is monitored by both seismic and continuous deformation networks. A transient strain pulse and surge in seismicity recorded by these networks began within tens of seconds following arrival of the shear pulse from Landers. The cumulative strain and number of triggered earthquakes followed the same exponentially decaying growth rate (time constant 1.8 days) during the first six days following Landers. The strain transient, which was recorded on a borehole dilatometer at the west margin of the caldera and a long-base tiltmeter 20 km to the east, peaked on the 6th day at  $\approx 0.25$  ppm and gradually decayed over the next 15 to 20 days. The absence of a clear strain signal exceeding 0.4 ppm in data from the two-color geodimeter deformation lines, which span the central section of the caldera, indicates that the strain transient cannot be due solely to pressure changes in the concentrated pressure source 7 km beneath the central part of caldera that accounts for most of the uplift of the resurgent dome since 1980. The triggered seismicity occupied the entire seismogenic volume beneath the caldera. Focal mechanisms, the frequency-magnitude distribution, and the spatial distribution of the triggered earthquakes are typical of other swarms in Long Valley caldera. The cumulative seismic moment of the triggered earthquakes through the first two weeks after the Landers earthquake corresponds to a single  $M=3.8$  earthquake, which is too small by nearly two orders of magnitude to account for  $\approx 0.25$  ppm peak amplitude of the observed strain transients. Evidently the strain transient represents the dominant response mode, which precludes direct triggering of local earthquakes by the large dynamic stresses from Landers as an important process here. Conditionally viable models for the triggering process beneath the caldera include 1) the transient pressurization of magma bodies beneath the resurgent dome and Mammoth Mountain by the advective overpressure of rising bubbles, 2) a surge in fluid pressure within the seismogenic zone due to upward cascading failure of isolated compartments containing super-hydrostatic pore fluids, 3) relaxation (fluidization) of a partially crystallized magma body in the deep crustal roots of Long Valley magmatic system, or 4) aseismic slip on mid-crustal faults. Only the deep, relaxing-magma body satisfies all the strain observations with a single deformation source. This model admits the possibility that large, regional earthquakes can trigger the episodic recharge of the deep roots of crustal magmatic systems.

#### Reports

Johnston, M. J. S., R. J. Mueller and Y. Sasai, 1994, Magnetic Field Observations in the Near-Field of the June 28, 1992,  $M_L 7.5$  Landers, California, Earthquake, *Bull. Seis. Soc. Am.*, **84**, 792-798.

M. J. S. Johnston, A. T. Linde, G. D. Myren, M. T. Gladwin, K. S. Breckenridge. 1993, A Slow Earthquake on the San Andreas Fault near San Juan Bautista, California, December 10-15, 1992. *Trans. Am. Geophys. Un.*, **74**, 182.

Fenoglio, M. A., M. J. S. Johnston, and J. D. Byerlee, 1994, Magnetic Fields Associated with Changes in High Pore Pressure in Fault Zones - Application to the

Loma Prieta ULF Emissions, Proceedings USGS Redbook Conf. on the Mechanical Involvement of Fluids in Faulting, USGS Open-File Report 94-228, 623pp.

M. J. S. Johnston, 1994, Nucleation Size of Moderate Earthquakes and Kinematics of the San Andreas Fault from Submicro Hz to 30 Hz Strain Measurements Abstracts 27th General Assembly IASPEI, Wellington, New Zealand, p324.

Johnston, M. J. S., and A. T. Linde, 1994, Continuous Borehole Strain in the San Andreas Fault Before, During and After the June 28, 1992 M<sub>w</sub> 7.3 Landers, California, Earthquake. *Bull. Seis. Soc. Am.*, **84**, 799-805.

Hill, D.P., P.A. Reasenberg, A. Michael, W.J. Arabasz, G. Beroza, J.N. Brune, D. Brumbaugh, R. Castro, S. Davis, D. DePolo, W. L. Ellsworth, J. Gomberg, S. Harmsen, L. House, S.M. Jackson, M. Johnston, L. Jones, R. Keller, S. Malone, L. Munguia, S. Nava, J.C. Pechmann, A. Sanford, R.W. Simpson, R.S. Smith, M. Stark, M. Stickney, A. Vidal, S. Walter, V. Wong, and J. Zollweg, 1993, Seismicity in the Western United States Triggered by the M 7.4 Landers, California, Earthquake of June 28, 1992. Proc. 8th Joint Meeting of U.S.-Japan Conference on Natural Resources, Nov 16-25, 1992. U.S. Geol. Surv. Open-File Rep. 93-542, 238-276.

Fenoglio, M. A., M. J. S. Johnston, and J. D. Byerlee, 1994, Magnetic Fields Associated with Changes in High Pore Pressure in Fault Zones - Application to the Loma Prieta ULF Emissions, Hickman, S., R. Sibson, and R. Bruhn (eds), Special Issue on the Mechanical Involvement of Fluids in Faulting, *J. Geophys. Res.*, (in press).

Hill, D. P., M. J. S. Johnston, J. O. Langbein, and R. Bilham, 1994, Response of Long Valley Caldera to the M7.4 Landers Earthquake: Tweaking a Magma Body. *Seis. Res. Lett.* **65**, 58.

Mueller, R. J., M. Lee, M. J. S. Johnston, R. D. Borcherdt, G. Glassmoyer, and S. Silverman, 1994, Near Real-Time Monitoring of Seismic Events and Status of Portable Digital Recorders using Satellite Telemetry, *Bull. Seis. Soc. Am.*, (in press).

Johnston, M. J. S., and A. T. Linde, 1994. Continuous Borehole Strain in the San Andreas Fault Before, During and After the June 28, 1992 M<sub>w</sub> 7.3 Landers, California, Earthquake. *Seis. Res. Lett.*, **65**, 53.

Johnston, M. J. S., and A. T. Linde, 1994. Continuous Borehole Strain Before, During and After the Jan 17, 1994 M 6.7 Northridge, California, Earthquake. *Seis. Res. Lett.*, **65**, 43.

A. T. Linde, M. J. S. Johnston, M. T. Gladwin, and K. S. Breckenridge, 1994. Modeling of a Slow Earthquake Sequence Near San Juan Bautista, California, in December 1992 *Trans. Am. Geophys. Un.*, **75**, 113.

B. H. Armstrong, C. M. Valdes-Gonzalez, M. J. S. Johnston, and J. D. Leaird, 1994, Low Strain Level Acoustic Emission Due to Seismic Waves and Tidal/Thermoelastic Strains Observed at the San Francisco Presidio, *J. Acoustic Em* (in press)

- Johnston, M. J. S., D. P. Hill, A. T. Linde, J. Langbein, and R. Bilham, 1994. Transient Deformation during Triggered Seismicity from the June 28, 1992,  $M_w=7.3$  Landers earthquake at Long Valley Volcanic Caldera, California. *Bull. Seis. Soc. Am.*, (in press).
- Hill, D. P., M. J. S. Johnston, A. T. Linde, and R. Bilham, 1994. Response of Long Valley Caldera to the  $M=7.3$  Landers, California, earthquake, *J. Geophys. Res.*, **xx**, (in press).
- Linde, A. T., I. S. Sacks, M. J. S. Johnston, D. P. Hill and R. Bilham, 1994. Remote Triggered Seismicity Following the Landers Earthquake - A Bubble Mechanism, *Nature*, **371**, 408-410.
- Jones, L., K. Aki, D. Boore, M. Celebi, A. Donnellan, R. Harris, E. Hauksson, T. Heathon, K. Hudnut, K. Hutton, M. Johnston, W. Joyner, G. Marshall, A. Michael, J. Mori, M. Murray, D. Ponti, P. Reasonberg, L. Seeber, A. Shakal, R. Simpson, H. Thio, J. Tinsley, M. Trifunac, D. Wald, and M. L. Zoback, 1994. The Magnitude 6.7 Northridge, California, Earthquake of January 17, 1994, *Science*, **266**, 389-397.
- M. J. S. Johnston, 1994. Nucleation Size of Moderate Earthquakes and Kinematics of the San Andreas Fault from Submicro Hz to 30 Hz Strain Measurements, *Trans. Am. Geophys. Un.*, **75**, 470.
- R. J. Mueller, M. J. S. Johnston, and M. Lisowski, 1994. Coseismic and Triggered Fault Slip near Pajaro Gap, California, During and Following the 1989  $M_L 7.1$  Loma Prieta Earthquake. *Trans. Am. Geophys. Un.*, **75**, 180.
- C. Teague, M. J. S. Johnston, A. C. Fraser-Smith, P. McGill, R. Mueller, and W. Wiegand, 1994. Anomalous ULF Signals at Parkfield During December 1993 and January 1994. *Trans. Am. Geophys. Un.*, **75**, 470.
- A. T. Linde, M. J. S. Johnston, M. Gladwin, and K. Breckenridge, 1994. A Sequence of Three Slow Earthquakes Near San Juan Bautista and Related Seismicity *Trans. Am. Geophys. Un.*, **75**, 446.

**Annual Technical Report  
1434-93-G-2305**

**Title:** Systematic Monitoring of Slow Earthquakes in the Los Angeles Basin

**Investigators:** Hiroo Kanamori and Robert W. Clayton

**Institution:** California Institute of Technology

**Address:** Seismological Laboratory, California Institute of Technology,  
Pasadena, California 91125

**Telephone number and E-mail address:** (818) 395-6914,  
hiroo@seismo.gps.caltech.edu

**Program Element:** I.1

**Investigations:**

**Continuous Monitoring of Seismic Energy Release Associated with the 1994 Northridge earthquake**

**Result:**

We have developed a method to continuously monitor long-period signal recorded with TERRAscope stations. We divided a continuous long-period (LP) TERRAscope record (1 sps) into a series of overlapping time windows, each 30 min long with 10 min overlap, and computed the spectrum over a frequency band of 0.0005 to 0.1 Hz. The result is shown as a time-frequency plot (spectrogram) for each station-day.

Figure 1 shows the result for the Pasadena TERRAscope station for a time window from January 17 to 18, 1994, which includes the 1994 Northridge earthquake ( $M_w=6.7$ ). Our objective is to see whether there was any slow deformation in the epicentral area of the Northridge earthquake just before it. Many recent studies demonstrated that slow precursory slip, if any occurs, is very small, probably less than 1 % of the mainshock in terms of seismic moment (e.g. Johnston et al. 1989, 1990, 1994; Agnew and Wyatt, 1989; Linde and Johnston, 1989). Modelling studies using velocity weakening constitutive relations predict that such precursory changes on time scales of minutes are very small, less than 1 % (in moment) of the main shock (e.g. Tse and Rice, 1986; Lorenzetti and Tullis, 1989). However, some precursory slow slip has been reported for the 1960 Chilean earthquake (Kanamori and Ciper, 1974; Kanamori and Anderson, 1975; Cifuentes and Silver, 1989), the 1944 Tonankai earthquake (Sato, 1970, 1977; Mogi, 1984) and the 1989 Macquarie ridge earthquake (Thmle et al., 1993). In particular, the levelling data before the Tonankai earthquake suggest a precursory tilt of as large as 30% of that of the mainshock for a few hours before the mainshock. This result is one of the very bases of the Japanese short-term prediction program. Unfortunately the data are very limited for both the Chilean earthquake and the Tonankai earthquake. Also, Kedar et al. (1994) saw no direct evidence for the precursor for the Macquarie ridge earthquake. Hence whether such slow precursory deformation occurs under certain circumstances or not is presently unresolved. It is thus important to investigate into such precursory deformation for other earthquakes.

Figure 1 shows the spectrogram for the mainshock of the 1994 Northridge earthquake and many aftershocks recorded at Pasadena (epicentral distance=35 km). The window position is adjusted so that the origin time of the mainshock is at the beginning of the time window that includes the mainshock. All the aftershocks with  $M>4$  are clearly seen over the entire frequency band. Most aftershocks with  $M>3.8$  are also seen, but those with  $M<3.5$  can be seen only at periods shorter than 20 sec. For the time period before the earthquake, no event can be identified at long-period, except an event at about 8:00 AM on January 17. This event exhibits only long-period energy, and its spectral pattern is different from that of the aftershocks. In a way, it has the characteristics of slow

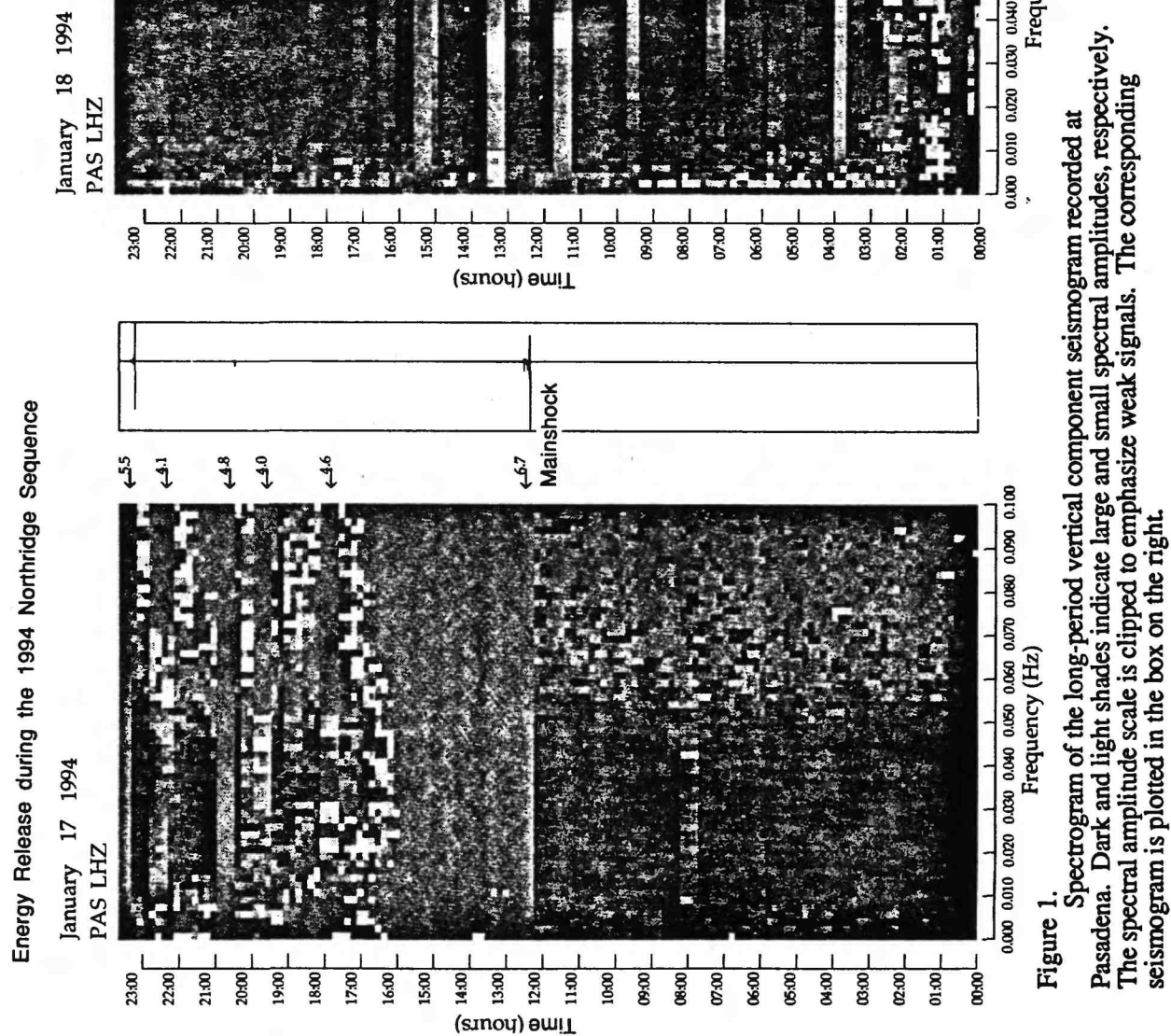


Figure 1. Spectrogram of the long-period vertical component seismogram recorded at Pasadena. Dark and light shades indicate large and small spectral amplitudes, respectively. The spectral amplitude scale is clipped to emphasize weak signals. The corresponding seismogram is plotted in the box on the right.

Energy Release during the 1994 Northridge Sequence  
 January 17 1994  
 PAS LHZ

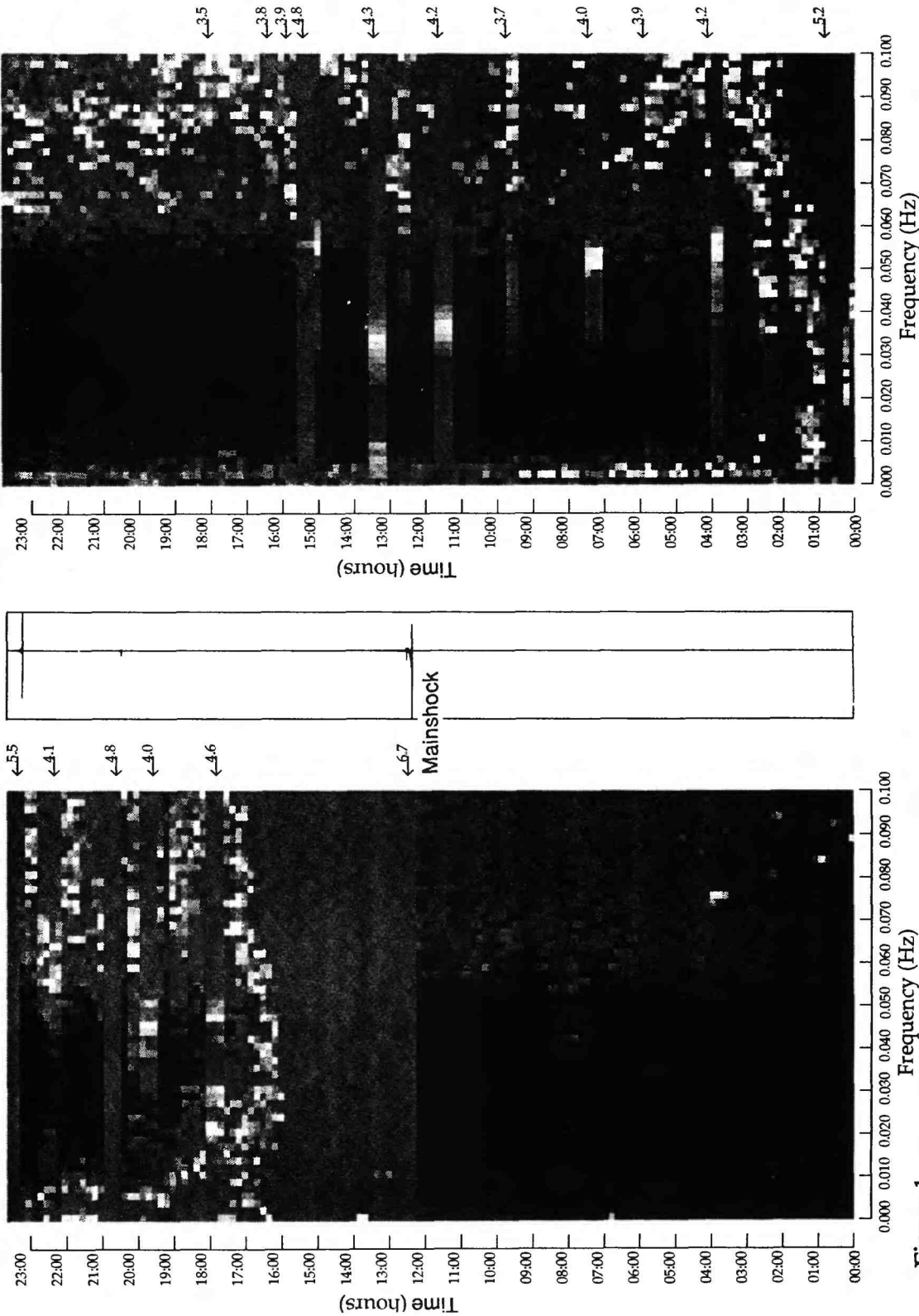


Figure 1. Spectrogram of the long-period vertical component seismogram recorded at Pasadena. Dark and light shades indicate large and small spectral amplitudes, respectively. The spectral amplitude scale is clipped to emphasize weak signals. The corresponding seismogram is plotted in the box on the right.

**Annual Technical Report  
1434-93-G2287**

**Title:** Earthquake and Seismicity Research Using SCARLET and CEDAR

**Investigators:** Hiroo Kanamori

**Institution:** California Institute of Technology

**Address:** Seismological Laboratory, California Institute of Technology,  
Pasadena, California 91125

**Telephone number and E-mail address:** (818) 395-6914,  
hiroo@seismo.gps.caltech.edu

**Program Element:** I.1

**Investigations:**

1. Moment tensor inversions for local earthquakes using surface waves recorded at TERRAscope stations
2. Source complexity of the 1994 Northridge earthquake and its relation to aftershock mechanisms

**Results:**

1. We have already reported on this project; now we have completed the study and the result is summarized in a paper to be published in the Bulletin of the Seismological Society of America.

We have developed a method to determine moment tensors for local earthquakes using short-period (10-50 s.) surface waves recorded at TERRAscope stations. To correct for the substantial lateral variations in crustal structure we applied phase corrections to the data using a regionalized phase velocity model. We have determined moment tensors for over 180 events in the last three years in Southern California for magnitudes as small as 3.2 and as large as 6.5. The results are consistent with those obtained from first-motion data as well as other waveform inversions. When continuous data telemetry from the stations becomes available this method can yield moment-tensors for earthquakes in Southern California and adjacent regions within minutes after the occurrence of an event. Our results confirm the relation between  $\log M_0$  (seismic moment) and  $M_L$  (local magnitude) obtained by an earlier study.

2. We studied the source process of the 1994 Northridge earthquake and the mechanisms of its aftershocks. To study the source complexity of the mainshock, we inverted the  $P$  and  $SH$  waveforms recorded by the IRIS and IDA/IRIS networks, using the method of Kikuchi and Kanamori (1992) in which the rupture is represented by a series of discrete subevents with varying mechanisms. The waveforms show that the rupture consisted of several subevents with about two seconds in between. Our best solution consists of three subevents with the first two having very similar mechanisms viz. 134/42/114 (strike/dip/slip) and the third event slightly different, 126/43/128. However, we found that this difference in mechanism is not significant and we subsequently modelled the earthquake using a single mechanism, 130/42/116. The first subevent occurred at a depth of about 19 kilometers, followed after 2 seconds by the second and largest subevent at a depth of 17 kilometers and the third subevent again two seconds after the second at a depth of about 13 kilometers. The total moment from the body-waves of this sequence amounts to about  $1.14 \times 10^{26}$  dyne.cm ( $M_w=6.7$ ) with a source duration of seven seconds. The depths of these subevents explain the lack of any surface rupture. Furthermore, the upward propagation of the subevents is consistent with the depth of the hypocenter and the

distribution of the aftershocks which are shallower and more northerly than the mainshock hypocenter. The aftershocks were analyzed using data from the TERRAscope network. We inverted short-period surface waves to determine the moment tensor for events with  $M_w > 3.5$ , which amounts to over 60 events. The aftershocks can be grouped into three regions based on the mechanisms; the eastern part of the aftershock zone, where we find thrust events with mechanisms very similar to the main event, a central area with predominantly strike-slip events and an area to the west where we find oblique thrust events but with more northerly P-axes than in the eastern region. This distribution suggests that the fault system on which the Northridge earthquake occurred is segmented, and that the extent of the Northridge rupture is controlled by a change in geometry of the fault. We find a high stress-drop for the Northridge mainshock.

Publications:

Thio, H. K., and H. Kanamori, Moment tensor inversions for local earthquakes using surface waves recorded at TERRAscope stations, in press, Bull. Seismol. Soc. Am., 1994.

Thio, H. K., and H. Kanamori, Source complexity of the 1994 Northridge earthquake and its relation to aftershock mechanisms, to be submitted to Bull. Seismol. Soc. Am., 1994.

PALEOSEISMIC EVALUATION OF THE  
EAST FRANKLIN MOUNTAINS FAULT ZONE, EL PASO, TEXAS

Grant No. 1434-94-G2382  
AGRA Job No. E93-4149

Jeffrey R. Keaton

AGRA Earth & Environmental, Inc.  
125 Montoya Road, El Paso, Texas 79932  
(915) 585-2472; Fax (915) 585-2626  
E-mail: 74503.1060@compuserve.com

Program Element: II.5

#### Investigations Undertaken

Geomorphic mapping of an area approximately 12 km long and 1.5 km wide along the eastern flank of the Franklin Mountains in the northern part of El Paso, Texas, was conducted to identify locations where the East Franklin Mountains fault could be exposed by shallow trenching. Numerous discussions have been held with representatives of the City of El Paso in order to secure permission to excavate trenches for the study. An archaeological survey of the selected trench sites and access routes has been performed. Trenching will be done as soon as final permission is obtained from the City and archaeological clearance has been granted. Trenching is anticipated to occur in mid-December 1994.

#### Results

The geomorphic model used as a basis for mapping in the project area was developed at the Desert Project (Gile and others, 1981) near Las Cruces, New Mexico, about 50 km to the north. The geomorphic features in the project area appear to be explained reasonably well using the general geomorphic framework of the Desert Project. The elements of the geomorphic model consist of Doña Ana alluvium (> 400 ka), Jornada I alluvium (400 to 250 ka), Jornada II alluvium (150 to 25 ka), Isaack's Ranch alluvium (25 to 12 ka), and Organ alluvium (12 ka to present). Topographic position, relative degree of soil development, and induration were the primary features used to correlate surfaces in the study area with the Desert Project geomorphic framework. Evidence has been found supporting subdivision of Jornada I into an older Jornada Ia and a younger Jornada Ib, and Jornada II into an older Jornada IIa and a younger Jornada IIb. Where Jornada IIb and Isaack's Ranch alluvium cannot be distinguished, they are mapped together. Similarly, where Isaack's Ranch and Organ alluvium cannot be distinguished, they are mapped together. Work by Machette (1987) inferred a Holocene age of most recent displacement because of a scarp in Isaack's Ranch alluvium. Current mapping indicates that the alluvium at that location probably is Jornada II and, therefore, the scarp would be late Pleistocene in age.

Fault scarps are distinct and well preserved along the East Franklin Mountains fault. Two trench sites were selected; one across a faulted Jornada II surface, and one across a nearby projection in apparently unfaulted Isaack's Ranch/Organ alluvium. Colluvial wedge stratigraphy will provide the basis of interpretation of slip history in the faulted Jornada II deposits. Excavation deep enough in the apparently unfaulted Isaack's Ranch/Organ alluvium to expose faulted Jornada II deposits will be attempted. This will provide a basis for interpretation of slip history in the younger sediments, and the age of the youngest displacement in this area.

The amount of time and effort required to secure access permission for trenching was severely underestimated. The land where trenching is planned is under control of the El Paso Public Service Board, and is located near the boundary of Franklin Mountain State Park. Detailed plans of equipment access, trench geometry, and stockpile location were required to be developed and presented at several levels of city government. The study area presently is undeveloped, but residential development is encroaching from the southeast. The land currently is part of a wilderness-development buffer zone. Some members of the City Council were concerned that the research trenches would be the first step in urbanization of an area that many would like to remain undeveloped. Cactus plants must be removed and transplanted; this will be done by volunteers from the community. Archaeological resources must be protected; this will be done by avoidance. An archaeological survey had to be commissioned; it was paid for with research funds.

#### Reports Published

No reports have been published as of November 1994. The 90th Annual Meeting of the Seismological Society of America will be held on the campus of the University of Texas at El Paso on March 22-24, 1995. An abstract will be prepared for this meeting; abstracts are due in January 1995. Other reports will be prepared as appropriate as soon as possible.

#### References

Gile, L.H., Hawley, J.W., and Grossman, R.B., 1981, Soils and geomorphology in the Basin Range area of Southern New Mexico - guidebook to the Desert Project: New Mexico Bureau of Mines and Mineral Resources Memoir 39, 222 pp.

Machette, M.N., 1987, Preliminary assessment of paleoseismicity at White Sands Missile Range, southern New Mexico: Evidence for recency of faulting, fault segmentation, and repeat intervals for major earthquakes in the region: U.S. Geological Survey Open-file Report 87-444, 46 pp.

## Multiple Late Holocene Earthquakes Along the Reelfoot Fault, Central New Madrid Seismic Zone

U.S. Geological Survey  
National Earthquake Hazards Reduction Program  
FY94 Award Number 1434-93-G-2293

**K.I. Kelson, G.D. Simpson, C.C. Haraden, and W.R. Lettis**  
William Lettis & Associates, Inc., 1000 Broadway, Suite 612, Oakland, CA 94607  
(510) 832-3716, fax (510) 832-4139, e-mail: [wla@netcom.com](mailto:wla@netcom.com)

**R.B. Van Arsdale**  
Department of Geological Sciences, University of Memphis, Memphis, TN 38152  
(901) 678-4356, fax (901) 678-2178

### Program Element I: *Understanding the Earthquake Source*

#### **Investigations**

Because of the potential for widespread strong ground motions generated by future earthquakes within the New Madrid seismic zone (NMSZ), identifying specific seismogenic sources and evaluating their paleoseismic behavior is required to assess seismic hazards in the central United States. In particular, assessing the number and timing of paleoearthquakes within the seismic zone and along specific potential seismogenic sources is a critical step in evaluating seismic hazard. The primary purpose of this research is to refine the number, timing, and recurrence of late Holocene tectonic deformation along the Reelfoot fault in northwestern Tennessee, and thus to provide paleoseismologic information on a specific seismogenic source within the central NMSZ.

Investigations conducted during 1994 included excavation of three shallow trenches and collection of shallow-borehole data from a site along the Reelfoot scarp about 2 km north of Reelfoot Lake in northwestern Tennessee. This site near Proctor City is between sites previously excavated by Russ<sup>1</sup> and Kelson and others<sup>2</sup>. Analysis of aerial photography and field reconnaissance also was conducted along the northern extension of the Reelfoot scarp in westernmost Kentucky. The investigations summarized herein were conducted from March through June, 1994, and data were analyzed and integrated with previous results during July through September, 1994.

---

<sup>1</sup>Russ, D.P., 1982, Style and significance of surface deformation in the vicinity of New Madrid, Missouri: U.S. Geological Survey Professional Paper 1236-I, p. 95 -114.

<sup>2</sup>Kelson, K.I., VanArsdale, R.B., Simpson, G.D., and Lettis, W.R., 1992, Assessment of the style and timing of late Holocene surficial deformation along the central Reelfoot scarp, Lake County, Tennessee: Seismological Research Letters, v. 63, no. 3, p. 349-356.

## Results

Our investigation of the Proctor City site provides data on the style of surficial deformation associated with the Reelfoot fault as well as data on the number and timing of late Holocene paleoearthquakes on the fault. These data enable estimation of late Holocene earthquake recurrence. Trenches and shallow boreholes show that the scarp morphology mimics the style of near-surface deformation of fluvial strata. Fluvial deposits identified via trenches and boreholes across the scarp define an 8-m-high, east-facing monocline and show that the majority of near-surface deformation along the Reelfoot scarp is accommodated via folding rather than faulting. The base of the scarp coincides with the up-dip projection of a west-dipping reverse fault interpreted from shallow seismic reflection data and contemporary microseismicity<sup>3</sup>. We interpret that the scarp is a fault-propagation fold developed over this fault.

Deposits exposed in the three trenches provide evidence of multiple late Holocene earthquakes along the Reelfoot fault. Two trenches exposed a linear graben on the upthrown side of the scarp. In addition to down-dropped fluvial sediments, the graben is associated with fine- to medium-grained sand that was extruded onto an existing scarp during an AD 1811-12 event. The trench exposures and 19 radiocarbon age-estimates from displaced and undisplaced sediments provide evidence of three episodes of deformation along the Reelfoot fault within the past approximately 2,400 years. We estimate that these earthquakes occurred at about AD 900, about AD 1400, and AD 1812. Based on the likely age ranges for each earthquake, our best estimate of recurrence for deformation along the Reelfoot scarp is  $450 \pm 50$  years. These results compare well with the interpretations by Russ<sup>1</sup> of two pre-1811 events in the past approximately 2000 years, and by Kelson and others<sup>2</sup> of an episode of surficial deformation between about AD 1380 and 1450.

Based on several trench exposures at the Proctor City site and the sites studied by Russ<sup>1</sup> and Kelson and others<sup>2</sup>, each of the late Holocene earthquakes had a slightly different style of deformation. The third-most-recent event produced a small graben a few tens of centimeters deep in the hanging wall of the reverse fault. The second-most-recent earthquake produced about 1 m of throw in the graben, as well as folding along the up-dip projection of the reverse fault and development of the scarp. These relations suggest that graben development increased through time concomitant with growth of the monocline, or that the events are of different magnitude. Lastly, the 1811-12 events produced abundant liquefaction, prominent folding of fluvial strata along the scarp, and minor faulting in the graben.

Analysis of aerial photography and field observations conducted during this study show that the scarp extends to the northwest of its previously mapped location<sup>2</sup>. In westernmost Kentucky, there are possibly as many as three fluvial geomorphic surfaces formed by the Mississippi River that have different amounts of vertical separation, suggesting repeated late Holocene uplift of the Tiptonville dome. Continuation of the scarp along this more northwesterly course suggests that it is at least 27 km long and extends from the southern end of Reelfoot Lake, across the Mississippi River, and perhaps into southern Missouri directly west of the town of New Madrid. If so, the Reelfoot fault crosses the Mississippi River at three locations. If surface deformation occurred along the Reelfoot fault during the mb7.2 New Madrid earthquake of 23 Jan 1812, uplift along the scarp may have been responsible for historical accounts of "waterfalls" and "upstream flow" along the river immediately following the earthquake.

---

<sup>3</sup>Chiu, J.M., Johnston, A.C., and Yang, Y.T., 1992, Imaging the active faults of the central New Madrid seismic zone using PANDA array data: *Seismological Research Letters*, v. 63, p. 375-393.

## Reports Published

Kelson, K.I., Simpson, G.D., Haraden, C.C., Lettis, W.R., VanArsdale, R.B., and Harris, J.B., in review, Multiple late Holocene earthquakes along the Reelfoot fault, central New Madrid seismic zone: Submitted to *Journal of Geophysical Research-Solid Earth*, September, 1994.

Kelson, K.I., Simpson, G.D., Haraden, C.C., Lettis, W.R., VanArsdale, R.B., and Harris, J.B., 1994, Multiple Holocene earthquakes along the Reelfoot fault, central New Madrid seismic zone: in Proceedings of the Workshop on Paleoseismology, U.S. Geological Survey, Open File Report 94-568, p. 92-93.

Kelson, K.I., Simpson, G.D., Haraden, C.C., Lettis, W.R., VanArsdale, R.B., and Harris, J.B., 1994, Multiple Holocene earthquakes along the Reelfoot fault, central New Madrid seismic zone: Geological Society of America Abstracts with Programs, v. 26, no.7, p. 189.

Kelson, K.I., and VanArsdale, R.B., 1994, Holocene surficial deformation associated with the Lake County uplift, northwestern Tennessee: Geological Society of America Abstracts with Programs, v. 26, no. 3, p. 20.

VanArsdale, R.B., Kelson, K.I., Simpson, G.D., Lumsden, C.H., and Harris, J.B., 1994, Northern extension of the Reelfoot scarp, Kentucky and Missouri: Geological Society of America Abstracts with Programs, v. 26, no.7, p. 189.

## Previous Related Publications

Kelson, K.I., VanArsdale, R.B., Simpson, G.D., and Lettis, W.R., 1992, Assessment of the style and timing of late Holocene surficial deformation along the central Reelfoot scarp, Lake County, Tennessee: Seismological Research Letters, v. 63, no. 3, p. 349-356.

Kelson , K.I., VanArsdale, R.B., Simpson, G.D., and Lettis, W.R., 1993, Late Holocene episodes of deformation along the central Reelfoot scarp, Lake County, Tennessee: Proceedings, 1993 National Earthquake Conference: Earthquake hazard reduction in the central and eastern United States: Central United States Earthquake Consortium, Memphis, v. 1, p. 195-203.

# Holocene Slip Rate and Recurrence of the Northern Calaveras Fault at Leyden Creek, Eastern San Francisco Bay Region

U.S. Geological Survey  
National Earthquake Hazards Reduction Program  
FY94 Award Number 1434-93-G-2338

**Keith I. Kelson, Gary D. Simpson, William R. Lettis, and Colleen C. Haraden**

William Lettis & Associates, Inc.  
1000 Broadway, Suite 612, Oakland, CA 94607  
(510) 832-3716, fax (510) 832-4139, e-mail: [wla@netcom.com](mailto:wla@netcom.com)

## Program Element I: *Understanding the Earthquake Source*

### **Investigations**

The Calaveras fault is a major, northwest-striking component of the San Andreas fault system and is a significant potential seismic hazard to the heavily populated eastern San Francisco Bay region. Information on geologic slip rate and earthquake recurrence is required to assess seismic hazards associated with the 48-km-long northern Calaveras fault, which extends from Calaveras Reservoir on the south to about the town of Danville on the north. The fault traverses a heavily populated area in the eastern San Francisco Bay region, and has not had a large-magnitude earthquake in more than 130 years. To obtain data on the number, timing, and recurrence of large-magnitude paleoearthquakes, we conducted paleoseismologic investigations at Leyden Creek, which crosses the fault 1.4 km north of Calaveras Reservoir. The objectives of this research are to assess the Holocene slip rate and earthquake recurrence along the northern Calaveras fault. This information provides direct input for estimating time-dependent probabilities of large earthquakes on the northern Calaveras fault and contributes to the understanding of the rates of strain accumulation along the fault. In addition, this research provides preliminary data on the rupture segmentation of the fault.

This research builds on previous work by Kelson and others<sup>1</sup> on the Holocene behavior of the northern Calaveras fault at Leyden Creek. This second phase of research was designed to further constrain the Holocene slip rate on the fault and the timing of late Holocene surface-faulting earthquakes. During the two phases, we interpreted aerial photography of the site vicinity, delineated late Quaternary deposits and landforms at the site, and conducted subsurface investigations that included six exploratory trenches, 28 small-diameter boreholes, and 2 large-diameter boreholes. Data developed during both phases provide: (1) an evaluation of Holocene slip rate based on the amount of offset and age of a buried paleovalley margin, and (2) an assessment of the number and timing of surface ruptures based on the recognition and dating of displaced and undisplaced fluvial and colluvial deposits.

---

<sup>1</sup>Kelson, K.I., Lettis, W.R., and Simpson, G.D., 1992, Late Holocene paleoseismic events at Leyden Creek, northern Calaveras fault: *in* California Division of Mines and Geology Special Publication 113, p. 289-298.

## Results

The northern Calaveras fault at Leyden Creek is marked by a prominent west-facing scarp and the juxtaposition of serpentine on the east against Cretaceous sandstone and siltstone on the west. At the site, five fluvial terraces are preserved on the western (upstream) side of the fault. On the eastern (downstream) side of the fault, the creek flows through a narrow bedrock canyon. This canyon constricts the modern valley and has constrained the location of former late Pleistocene and Holocene paleovalleys. The borehole data show that the margin of a buried bedrock valley west of the fault trends nearly perpendicular to the fault and is offset  $54 \pm 5$  m in a right-lateral sense from the narrow bedrock canyon. Based on radiocarbon ages for alluvial sediments pre-dating and post-dating this paleovalley margin, we estimate an age of  $11 \pm 1$  ka for the valley margin and a Holocene slip rate of  $5 \pm 1$  mm/yr for the fault at Leyden Creek.

Five trenches excavated across the fault provide information about the style and timing of deformation at this site. Slickensides show that the most-recent sense of movement was predominantly lateral with a minor component of down-to-the-west separation, which is consistent with the west-facing fault scarp and the net slip vector derived from the offset valley margin. Multiple displaced scarp-derived colluvial deposits are interpreted as results of five to six episodes of surface rupture within the past 2,600 years. Twenty-one radiocarbon samples from scarp-derived colluvium and interfingering alluvial deposits suggest an average interval between surface-rupture events of  $450 \pm 50$  years. We postulate that the most-recent earthquake at Leyden Creek likely occurred between 1670 (the minimum age of the youngest faulted deposit) and about 1830 (when the population of the eastern San Francisco Bay region was sufficient to record a large earthquake).

The Leyden Creek site lies adjacent to or within a 1.5- to 3.0-km-wide, 7-km-long releasing double bend at Calaveras Reservoir that may act as a rupture-segment boundary between the southern and northern sections of the Calaveras fault. Surface-rupture events at Leyden Creek may therefore reflect earthquakes along either the southern end of the northern Calaveras fault, or the northern end of the southern Calaveras fault, or both.

## Reports Published

Kelson, K.I., Simpson, G.D., Lettis, W.R., and Haraden, C.C., 1994, Holocene slip rate and recurrence of the northern Calaveras fault at Leyden Creek, eastern San Francisco Bay region, California: Submitted to *Journal of Geophysical Research-Solid Earth*, September, 1994.

Kelson, K.I., Simpson, G.D., Lettis, W.R., Haraden, C.C., Williams, C. R., and Thompson, S. C., 1994, Holocene slip rate and recurrence of the northern Calaveras fault at Leyden Creek, Alameda County, California [abstract]: in Prentice, C.S., Schwartz, D.P., and Yeats, R.S. (compilers), Proceedings of the Workshop on Paleoseismology, U.S. Geological Survey Open-file Report 94-568, p. 94-95.

Kelson, K.I., Lettis, W.R., and Simpson, G.D., 1994, Calaveras fault, Leyden Creek paleoseismic site: in Lettis, W.R., (ed.) Transpressional Deformation in the San Francisco Bay Region: 1994 Fall Field Trip, Friends of the Pleistocene Pacific Southwest Cell, p. 19-26.

Kelson, K.I., Simpson, G.D., Lettis, W.R., Haraden, C.C., Williams, C.R., and Thompson, S.C., 1994, Holocene slip rate and recurrence of surface-faulting earthquakes on the northern Calaveras fault at Leyden Creek, Alameda County, California: Final Technical Report, U.S. Geological Survey National Earthquake Hazards Reduction Program, Award Number 1434-93-G-2338; July, 1994.

**Related Publications**

Kelson, K.I., Lettis, W.R., and Simpson, G.D., 1992, Late Holocene paleoseismic events at Leyden Creek, northern Calaveras fault: *in* California Division of Mines and Geology Special Publication 113, p. 289-298.

Kelson, K.I., Lettis, W.R., and Simpson, G.D., 1992, Progress report on paleoseismic investigations at Leyden Creek, northern Calaveras fault zone [abs.]: Second Conference on Earthquake Hazards in the Eastern San Francisco Bay Area, Abstracts and Program, California Division of Mines and Geology, p. 38.

Kelson, K.I., and Simpson, G.D., 1994, Late Pleistocene deformation of the southern East Bay Hills based on fluvial terraces along Alameda Creek, Sunol Valley to Fremont, California: EOS Supplement, American Geophysical Union, v. 75, n. 44, p. 682.

Simpson, G.D., Lettis, W.R., and Kelson, K.I., 1992, Segmentation model for the northern Calaveras fault, Calaveras Reservoir to Walnut Creek: *in* California Division of Mines and Geology Special Publication 113, p. 253-260.

## HAWAIIAN EARTHQUAKE STUDIES

USGS Project number: 9930-10213  
 NEHRP program element II.2, II.4

*Fred Klein  
 Mail Stop 977  
 345 Middlefield Road  
 Menlo Park, California 94025  
 (415) 329-4794*

*Paul Okubo and Laura Kong  
 Hawaiian Volcano Observatory  
 Hawaii National Park, Hawaii 96718  
 (808) 967-7328*

### **Investigations:**

The project estimates the recurrence and quantitative hazard from ground shaking from large earthquakes near the island of Hawaii. M 7+ earthquakes on the flanks of the Volcanoes cause damage by shaking and have the potential for triggering catastrophic submarine landslides and tsunamis. Through studies of seismic structure and contemporary seismicity, we attempt to evaluate the short term potential of a M7 earthquake on Kilauea Volcano's South Flank and the relation between the flank and Loihi submarine Volcano. The project also publicizes the current seismicity and long term earthquake hazard with an interactive computer accessible to the public. Our work utilizes the 52 station seismic network operated by the Hawaiian Volcano Observatory with funding from the volcano hazards program.

To study the three-dimensional seismic structure of Kilauea's South Flank and Loihi Volcano, a high resolution active-source seismic data set was collected in February, 1994, in a cooperative study with NSF scientists from the Scripps Institute of Oceanography and the University of Hawaii. Over 200 km of seismic shot line were collected over the submarine portion of Kilauea's south flank using a 4-element marine source fired every 100-150 m to ocean-bottom instruments, sonobuoys, and a 6-channel seismic streamer in the ocean, and to the USGS/HVO permanent seismic network supplemented with 3 portable stations.

### **Results:**

(1) Intensity 5 earthquakes are common on Hawaii Island and include several historically damaging M7 earthquakes, especially the M~8 great Kau earthquake of 1868 (figure 1). Large earthquakes in south Hawaii generally do not occur on faults that break the surface, but on often near-horizontal buried faults. The volcano flanks move seaward on a basal fault at 9-13 km depth. The seismic hazard on the active southern sides of Kilauea and Mauna Loa Volcanoes is comparable to that on the San Andreas Fault and the Gulf of Alaska. Historic earthquakes (since 1823) and the best HVO catalog (since 1970) indicate recurrence intervals of M8 events similar to the 1868 Kau earthquake of 120-190 years. The peak acceleration which has a 90% probability of not being exceeded in 50 years exceeds 1.0 g on the south sides of both volcanoes (figure 2).

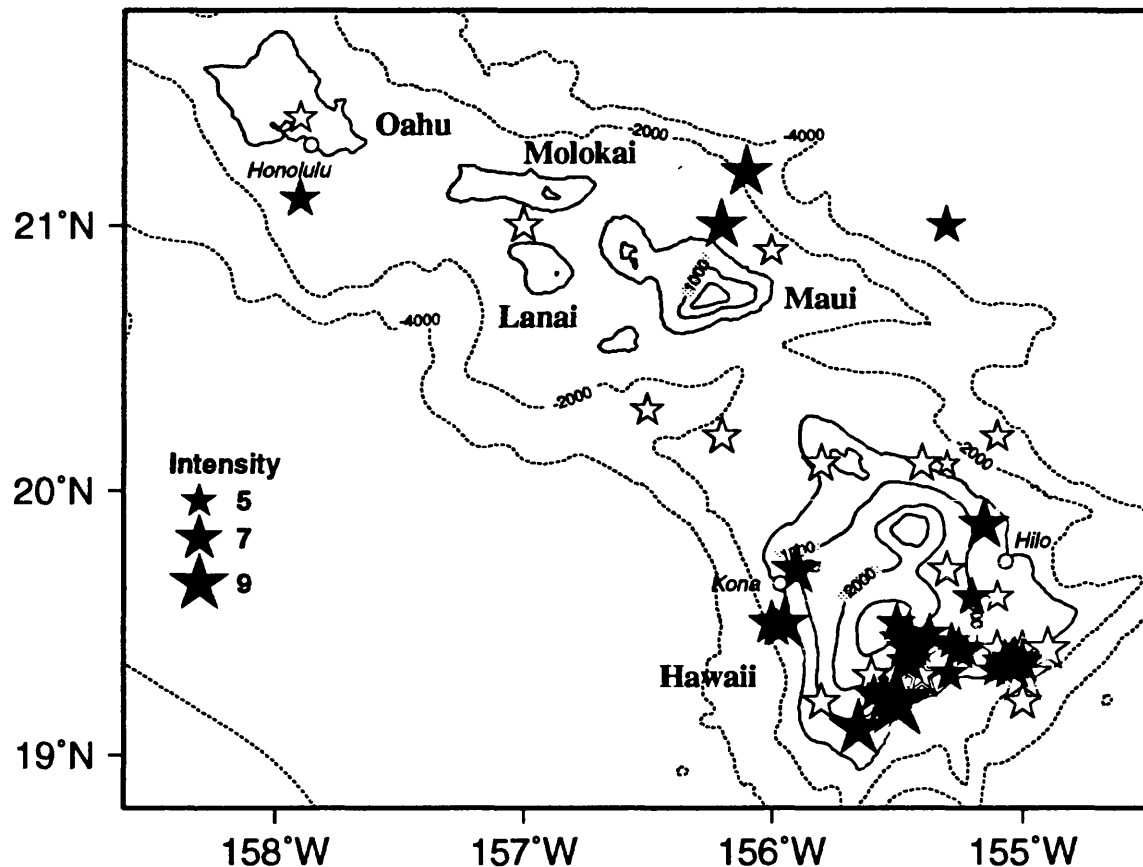
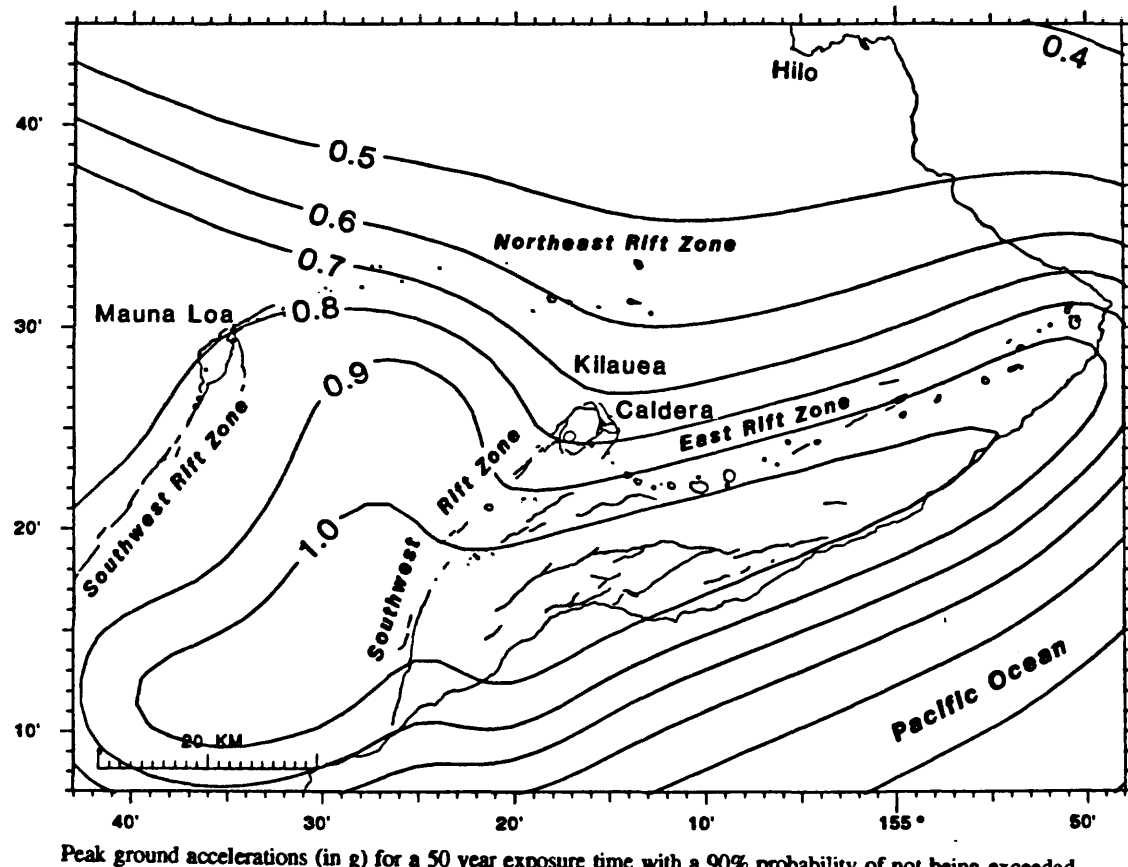


Figure 1. Moderate to large earthquakes with felt reports since 1823. The most destructive was the great 1868 M 7.9 Kau earthquake (Modified Mercalli intensity XII). Open symbols are estimated locations from historical accounts. Symbol size scaled to maximum intensity.



Peak ground accelerations (in g) for a 50 year exposure time with a 90% probability of not being exceeded.

(2) Research done in collaboration with J Dieterich has documented recent periods of seismic quiescence in the epicentral region of the 1975 M7.2 Kalapana earthquake. We have continued to analyze seismicity patterns in the Kalapana region of the south flank of Kilauea in greater detail to establish additional characteristics of earthquakes there. A manuscript which describes our work has been submitted to *Geophysical Research Letters*.

(3) During FY 1994, the CUSP ISAIAH (Information on Seismic Activity In A Hurry) real-time automatic earthquake analysis system was installed at HVO. Preliminary locations are typically available within 40 seconds of the event. For large earthquakes, an alarm module sends electronic mail to responsible officials. To provide better and more timely information on large Hawaiian earthquakes, HVO began in July, 1994, to send ISAIAH earthquake information to the NOAA/Pacific Tsunami Warning Center on Oahu, whose responsibility is to provide rapid location and evaluation of potentially tsunamigenic earthquakes in Hawaii.

(4) We have completed the first stage of establishing automated magnitude determinations for our CUSP on-line system. This is based on the coda duration magnitude. We have begun compilation of a data set to re-establish and improve amplitude magnitude estimation based on the digital data collected and analyzed with the HVO CUSP system. Much of this work is tied to upgrades in our field instrumentation and establishing and updating calibration information for new equipment.

(5) Version 1.0 of an Interactive Display of Earthquake Activity (IDEA) was completed for Amiga computers at HVO and Menlo Park. The computer display is controlled by a touch screen. It is designed both for monitoring of near real-time seismicity by scientists and education of the public in a museum or public location. Several maps, cross sections, time series plots, plots of catalog data from prior years and time-lapse animations are available.

(6) Preliminary data reduction and playback of the different types of seismic data from the active-source seismic experiment are being compiled for an Open File Report. Preliminary playbacks of the HVO network data show clear arrivals on the majority of stations out to 40-50 km range. Rays at these ranges sample the lowermost crust and upper mantle and will provide a seismic image of the postulated decollement, which is thought to be the source area for large earthquakes and the surface on which the south flank is sliding. Laura Kong has submitted a proposal, *Hawaii Crustal Imaging Experiments*, to NEHRP for support to analyze this data set.

(7) Documentation of the marked increase since 1984 in Loihi Volcano earthquake swarm seismicity and its possible relationships to volcano flank tectonism and magmatism, was begun. Data from the HVO catalog data were assembled and an overview presented at the 1994 SSA Meeting. To better constrain the earthquake hypocenters, we collected active source seismic data over Loihi's summit and rift zones (see above) in order to derive a realistic velocity structure for use in relocating the HVO- recorded seismicity.

**Products:**

- Denlinger, R.P. and P. Okubo, 1994, A huge landslide structure on Kilauea Volcano, Hawaii, submitted to J. Geophys. Res.
- Dieterich, J.H. and P. Okubo, 1994, An unusual pattern of recurring seismic quiescence, submitted to Geophys. Res. Let.
- Gillard, D., M. Wyss, and P. Okubo, 1994, Stress tensor orientations in the south flank of Kilauea Volcano, Hawaii estimated from fault plane solutions, submitted to J. Geophys. Res.
- Klein, F.W. and P. Okubo, 1993, Hazards from earthquakes, submarine landslides and expected levels of peak ground acceleration on Kilauea and Mauna Loa Volcanoes, Hawaii (abstract), EOS Transactions Am. Geoph. U. v. 74, p. 634.
- Klein, F.W., 1994, Seismic hazards at Kilauea and Mauna Loa Volcanoes, Hawaii, USGS Open File Report 94-216, 94 pp.
- Kong, L.S.L. and P. Okubo, 1994, Seismicity at Loihi Seamount, Hawaii (abstract), Seis. Res. Let., v. 65, p. 55.
- Kong, LSL, PG Okubo, WC Crawford, JA Hildebrand, MA McDonald, SC Webb, FK Duennebier, and GF Moore, Crustal imaging of Kilauea volcano and Loihi seamount, EOS Trans. Am. Geophys. Union, v. 75, 1994 Fall Meeting abstracts, p. 645.
- Okubo, P., 1994, Seismicity associated with the continuing eruption at Kilauea Volcano, Hawaii (abstract), Seis. Res. Let., v. 65, p. 55.
- Okubo, P., D. Seidel and M. Hellweg, 1994, The broadband wavefield at the Puu Oo vent of Kilauea Volcano, Hawaii, EOS Trans. Am. Geophys. Union, v. 75, 1994 Fall Meeting abstracts, p. 714.
- Turner, B, L Kong, PG Okubo, Automated location of earthquakes for tsunami alerts in Hawaii, EOS Trans. Am. Geophys. Union, v. 75, 1994 Fall Meeting abstracts, p. 358.

## CASCADIA SUBDUCTION ZONE: NEOTECTONICS OF THE CONTINENTAL SHELF OFF OREGON AND WASHINGTON

CONTRACT 1434-94-G-2489  
CONTRACT 1434-93-G-2319

Principal Investigator: LaVerne D. Kulm\*  
Co-Principal Investigator: Robert S. Yeats\*\*  
Research Associate (Post-Doctoral): Chris Goldfinger\*  
Graduate Research Assistant: Lisa C. McNeill\*\*  
\*College of Oceanic and Atmospheric Sciences  
\*\*Department of Geosciences  
Oregon State University  
Corvallis, OR 97331  
Telephone: (503) 737-5211  
Fax: (503) 737-2064  
E-mail: lkulm@oce.orst.edu  
Program Element II

### Investigations

The objective of our study is to use geologic and geophysical data from the submerged Cascadia forearc to investigate the nature and extent of forearc deformation, and to relate this deformation to the problem of great earthquakes in Cascadia. We are using a regional approach to the collection and integration of data, combined with field investigations of critical areas from which we can collect detailed tectonic information, and also ground-truth remotely-sensed data.

In May 1994, we installed a raster-based Geographical Information System (GIS), called ERDAS Imagine 8.1, on our UNIX workstations. With this system, we can integrate and visualize many different types of data in order to see the spatial relationships among them. We have created a GIS database containing much of the available geologic and geophysical data for the Cascadia forearc. In the early phases of this project, we focused on basic mapping of the submarine system using available and concurrently gathered data from related research programs. We now have the ability and sufficient data to begin to apply the collective geological and geophysical database to the problem of great earthquakes in Cascadia.

We have generated a gridded topographic/bathymetric dataset that covers the Oregon portion of the margin from east of the Cascade Range to the abyssal plain. We used all available land and marine data at maximum resolution to produce a complete, high resolution 2D surface. This data allows us to study the morphology of the margin in a single dataset that will be extended to California and Washington in the coming year. In collaboration with the University of New Brunswick, we are using and assisting in development of a 3D software package that allows real-time fly-throughs of this surface data. The surface data can also be combined with any geophysical or geologic datasets for 3D analysis.

In September 1994, we conducted a NOAA Undersea Research Program (NURP)-sponsored sidescan/submersible cruise using a high-resolution AMS 150 kHz sidescan sonar and the submersible DELTA on the northern Oregon and southern Washington continental shelf. This region is located within the Washington Study Corridor, the subject of a collaborative NEHRP-USGS Deep Continental Studies Program investigation of the structure of the Cascades subduction zone and volcanic arc, mentioned as a Regional Focus in RFP Announcement 8064. We mapped several active Holocene normal, flexural-slip, and strike-slip faults to determine their role in the deformation of the shelf and adjacent coastal region. (The NURP program is a complementary

marine data acquisition program running concurrently with our NEHRP research program described herein.)

We recently gained access to a proprietary industry dataset of high-resolution migrated multichannel seismic reflection profiles in the Washington Study Corridor through the cooperation of the Minerals Management Service. The entire dataset of closely space lines, covering the entire Cascadia system, will greatly improve our ability to map and understand the structural geology of the forearc region.

## **Results**

### *1. Active Strike-Slip Faults of the Abyssal Plain and Accretionary Wedge*

Using combinations of high-resolution AMS 150 kHz and SeaMARC-1A sidescan sonar, swath bathymetry, seismic reflection profiles and submersibles, we have surveyed in detail nine suspected zones of oblique strike-slip faulting on the abyssal plain, continental slope and shelf off Oregon and Washington (Figures 1, 2a). In our 1990-1992 studies of the Cascadia subduction zone, we mapped three left-lateral strike-slip faults which cut both the Juan de Fuca and North American plates, extending from the abyssal plain to the upper slope-outer shelf region (Goldfinger et al., 1992). During 1993, six new left-lateral strike-slip faults were discovered, three in Washington and three in southern Oregon, totaling nine left-lateral faults. The six faults mapped in Oregon and three in Washington strike 298° to 283°, with obliquity to the margin increasing to the south. Mapped lengths of the nine faults range from 40 to 95 km (Goldfinger, 1994). The faults are often expressed in swath bathymetry as irregular ridges composed of en echelon folds, and sigmoidal bends of throughgoing accretionary wedge folds. SeaMARC-IA sidescan records of these structures reveal steep scarps cutting accretionary wedge folds and commonly show straight traces, reversals of vertical separation, and left-lateral horizontal offsets of submarine channels and other crossing structures.

Of the nine oblique strike-slip faults in the Cascadia subduction zone, five occur on both the Juan de Fuca and North American plates, crossing and offsetting the deformation front. In seismic reflection and sidescan records they offset eastward thickening trench deposits left-laterally from 2.0 to 5.5 km and extend 8 to 18 km seaward into the abyssal plain (Goldfinger, 1994). At least one fault apparently cuts the subducting plate based upon vertical separation of the basaltic crust and modeling of the associated magnetic anomaly (Applegate et al., 1992). Five of these Quaternary faults range in age from 600 to 300 ka and have an average calculated slip rate of 5.5 to 8.5 mm/yr (Figure 1; Goldfinger, 1994). Latest Pleistocene/Holocene slip rates for two of these faults range from 5 to 12 mm/yr based upon the left offset of submarine channels in sidescan images and the age of channel development (Goldfinger et al., 1992; Goldfinger, 1994; Goldfinger et al., in press). Four oblique faults are mapped solely on the North American plate and also exhibit a left slip (e.g., see Figure 5). Several additional oblique faults are inferred, off northern Washington and southernmost Oregon, based upon interpretation of free-air gravity anomalies on the continental slope.

### *2. Active Strike-Slip Faults of the Continental Shelf and Slope*

One of the major left-lateral strike-slip faults, the 110-km long Daisy Bank fault, is best expressed adjacent to a structural uplift called Daisy Bank, on the upper slope and outermost shelf (Figures 1, 2b). Sidescan imagery shows this fault is a wide structural zone, within which Daisy Bank is a large horst uplifted between two strands of the main fault. The main fault zone is 5-6 kilometers wide northwest of Daisy Bank, widening around the oblong bank, then narrowing to a single strand to the southeast. Multiple scarps are evident, with both up-to-the-north and up-to-the-south strands occurring in close proximity southeast of the bank. Northwest of the bank, two main strands are evident, both up to the north, which is the same sense of motion observed on the

abyssal plain. Typical strike-slip morphology is evident in sidescan imagery and also at outcrop scale from the submersible. The traces of the multiple strands of the fault are straight, implying a near vertical fault. Reversals of vertical separation along strike, a characteristic common only to strike-slip faults, are well imaged at many locations. Probable drag folding of Tertiary strata, with a left-lateral sense of motion, is visible southeast of the bank in sidescan images. This supports the evidence for left-lateral motion inferred for this fault through stratigraphic offset on the abyssal plain and structural offsets mapped on the upper slope (Goldfinger et al., 1992a; Goldfinger et al., in press). Individual scarps observed from DELTA range in height from tens of centimeters to 47 m. The main scarp is a steep (25°-50°) debris covered slope. Carbonate deposition and active faulting were observed at most locations along the Daisy Bank fault. Spectacular carbonate chimneys, donuts, and slabs, derived from the venting of methane-rich fluids along active fault zones, are located within 100-150 m of the fault traces (Figure 3). The carbonate slabs are often broken and disrupted like a parking lot excavated by a bulldozer. This pattern of disruption appears tectonic in nature (as opposed to observed fishing trawl disruption), since it only occurs adjacent to major fault zones. We speculate that this breakage occurs during the high ground accelerations accompanying large earthquakes.

From the DELTA submersible, we traced one of the Daisy Bank scarps into an area of low relief and flat-lying Holocene mud deposition. In this area, we found a fresh scarp striking 290° across the unconsolidated mud. This fresh break averages 0.5 m in height, dips steeply south with its south side up, and offset cohesive grey late Pleistocene clays as well as the overlying unconsolidated olive-green Holocene muds (Figure 4). This sharp change in sediment color is radiocarbon dated at about 12,000 ka (Barnard and McManus, 1973), indicating Holocene motion on the fault. Continuous color video images and still photographs show that the scarp probably represents multiple late Pleistocene events, indicated by abrupt vertical changes in oxidation color of the Pleistocene clay, and corresponding abrupt upward increases in bioturbation by animals inhabiting the scarp face. At the outcrop scale, we observed both right- and left-stepping en-echelon morphology, although left-stepping was dominant. Dominant left steps suggest a compressional component of motion along the Daisy Bank fault, also suggested by the 80-90° south dip observed on this segment of the fault. While we could identify the major traces of the fault zone in sidescan sonar images, the most compelling and detailed evidence of recent faulting was obtained with DELTA.

### *3. Forearc Deformation, Interplate Rupture Geometry, and Great Earthquakes*

The occurrence of great subduction zone earthquakes has been linked to properties of the subduction system such as convergence rate, plate dip, and plate age. On the basis of comparison of subduction parameters such as plate age and convergence rate, investigators have inferred that the Cascadia subduction zone is comparable to other subduction zones where great  $M > 8.2$  have occurred in historic times. Recent analyses of subduction zone earthquakes show that forearc rheology and convergence rate are important controls on the generation of great earthquakes in oblique subduction settings (McCaffrey, 1992, McCaffrey, 1994). Significant rates of arc-parallel forearc deformation are negatively correlated with  $M > 8.2$  earthquakes in subduction zones worldwide, regardless of obliquity of subduction. The Oregon and Washington Cascadia forearc is undergoing a significant degree of along-arc deformation in the form of oblique strike-slip faulting and folding described above (Figures 1, 2, 5). The cumulative extension of the forearc by the nine strike-slip faults we have mapped is similar to the total arc-parallel component of plate convergence, and thus the Cascadia forearc may be fully strain partitioned. Thermal constraints (Hyndman and Wang, 1993) suggest that the position of the locked plate interface underlies the submarine forearc traversed by the extensive oblique deformation we have mapped. We therefore infer a direct connection between the zone of interplate coupling and the observed shearing of the forearc. The highly deformed and strain-partitioned nature of the Cascadia submarine forearc suggests that Cascadia is unlikely to generate earthquakes greater than magnitude 8.2 because the

forearc is not capable of storing the required elastic strain energy (Goldfinger, 1994, McCaffrey and Goldfinger, in revision). We are continuing to investigate the connection between forearc deformation and great earthquakes in collaboration with Rob McCaffrey of Rensselaer Polytechnic Institute.

We are also investigating the connection between rupture zone geometry and the generation of great earthquakes. Using the same thermal constraints suggested by Hyndman and Wang (1993), we are trying to improve estimates of potential rupture area through the addition of structural data from the accretionary wedge. We can then compare this estimate of Cascadia seismogenic zone geometry to data on rupture widths and lengths from great circum-Pacific earthquakes of this century. Preliminary comparisons suggest that rupture length is moderately dependent on downdip width of the locked zone, and that the aspect ratio of the seismogenic plate boundary has an empirical upper limit. If correct, this may allow us to estimate the maximum likely rupture length for a Cascadia interplate earthquake.

#### 4. Outreach Programs

We have produced a 20-minute video summarizing much of the above information about the Cascadia subduction zone, as well as basic information about the mechanics of subduction earthquakes, that is available for teaching purposes. We expect to collaborate with a Sea Grant outreach initiative in which a version of this video could be produced specifically for the public.

We have established a World Wide Web server in our mapping facility from which anyone with Internet access can download our Oregon-Washington Neotectonic Map. This map was published in 1992, but is constantly revised as our mapping project continues, and the latest version is made available on the server. The map is available in a variety of formats for MAC, DOS, and UNIX platforms. We also have created topographic/bathymetric grids for Oregon at 100 m and 300 m grid spacing. These grids utilize all available land and marine data at maximum resolution, and cover Oregon from 121° W to 126° W, 42° N to 46° N. Information on obtaining these grids and derived shaded relief maps of the Cascadia margin (e.g., Figure 5) is on the server. The URL (Universal Resource Locator) for this service is <http://pandora.oce.orst.edu>. These data and products can also be obtained by anonymous ftp to [pandora.oce.orst.edu](http://pandora.oce.orst.edu) in the pub directory.

#### Reports(\*) and References

\*Appelgate, B., Goldfinger, C., Kulm, L.D., MacKay, M., Fox, C.G., Embley, R.W., and Meis, P.J., 1992. A left lateral strike-slip fault seaward of the central Oregon convergent margin: Tectonics, v. 11, p. 465-477.

Barnard, W.D., and McManus, D.A., 1973. Planktonic foraminiferan-Radiolarian stratigraphy and the Pleistocene-Holocene boundary in the northeast Pacific: Geological Society of America Bulletin, v. 84, p. 2097-2100.

\*Goldfinger, C., Kulm, L.D., Yeats, R.S., Mitchell, C., Weldon II, R., Peterson, C., Darienzo, M., Grant, W., and Priest, G.R., 1992. Neotectonic map of the Oregon continental margin and adjacent abyssal plain: Oregon Department of Geology and Mineral Industries, Open File Report 0-92-4, 17 pages and 2 map sheets.

\*Goldfinger, C., Kulm, L.D., Yeats, R.S., Appelgate, B., MacKay, M., and Moore, G.F., 1992a. Transverse structural trends along the Oregon convergent margin: implications for Cascadia earthquake potential: Geology, v. 20, p. 141-144.

- \*Goldfinger, C., Kulm, L.D., Yeats, R.S., Applegate, T.B., Cochrane, G. and MacKay, M.E., Active strike-slip faulting and folding of the Cascadia plate boundary and forearc northern and central Oregon: in Rogers, A.M. et al., eds., Assessing and reducing earthquake hazards in the Pacific Northwest, U.S. Geological Survey Professional Paper 1560, in press.
- \*Goldfinger, C., 1994, Active deformation of the Cascadia forearc: Implications for great earthquake potential in Oregon and Washington [PhD Thesis]: Oregon State University, Corvallis, OR, 202 p.
- \*Goldfinger, C., Kulm, L.D., and Yeats, R.S., 1994. An estimate of the maximum earthquake magnitude on the Cascadia subduction zone, Abstracts with Programs: Geological Society of America Annual Meeting, Seattle, WA, p. A-525.
- Hyndman, R.D., and Wang, K., 1993. Thermal Constraints on the Zone of Major Thrust Earthquake Failure: The Cascadia Subduction Zone: *Journal of Geophysical Research*, v. 98, p. 2039-2060.
- \* Kulm, L.D., Goldfinger, C., Yeats, R.S., 1994. Diagenetic carbonates and fluid expulsion along a strike-slip fault in the Cascadia accretionary wedge, Abstracts with Programs: Geological Society of America Annual Meeting, Seattle, WA, p. A-457.
- McCaffrey, R., 1992. Oblique plate convergence, slip vectors, and forearc deformation: *Journal of Geophysical Research*, v. 97, p. 8905-8915.
- McCaffrey, R., 1993. On the role of the upper plate in great subduction zone earthquakes: *Journal of Geophysical Research*, v. 98, p. 11,953-11,966.
- McCaffrey, R., 1994. Global variability in subduction thrust zone-forearc systems: *Pure and Applied Geophysics*, v. 142, p. 173-224.
- \*McCaffrey, R., and Goldfinger, C., Forearc deformation and great earthquakes: Implications for Cascadia offshore earthquake potential: *Science* (in revision).
- \*McNeill, L.C., Goldfinger, C., Kulm, L.D., and Yeats, R.S., 1994. Tectonics of the Washington continental margin, Cascadia subduction zone, Abstracts with Programs: Geological Society of America Annual Meeting, Seattle, WA, p. A-523.
- \*Tréhu, A., Lin, G., Maxwell, E., and Goldfinger, C., A seismic reflection profile across the Cascadia subduction zone offshore central Oregon: New constraints on the deep crustal structure and on the distribution of methane in the accretionary prism: *Journal of Geophysical Research*, In press.
- \*Yeats, R.S., Yamazaki, H., Taira, A., Goldfinger, C., and Kulm, L.D., 1994. Seismotectonics of the Cascadia and Nankai subduction zones, Abstracts with Programs: Geological Society of America Annual Meeting, Seattle, WA, p. A-456.

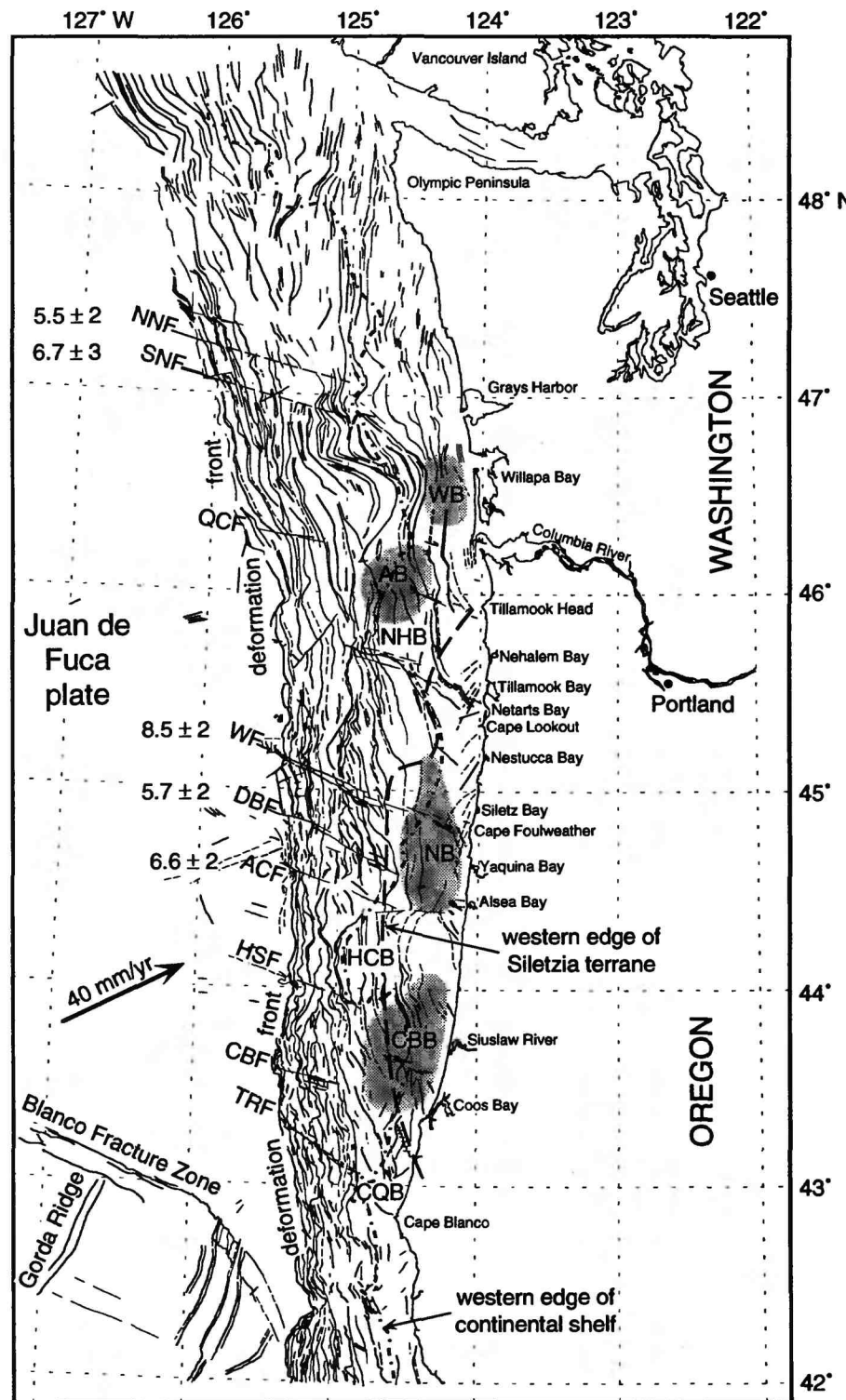
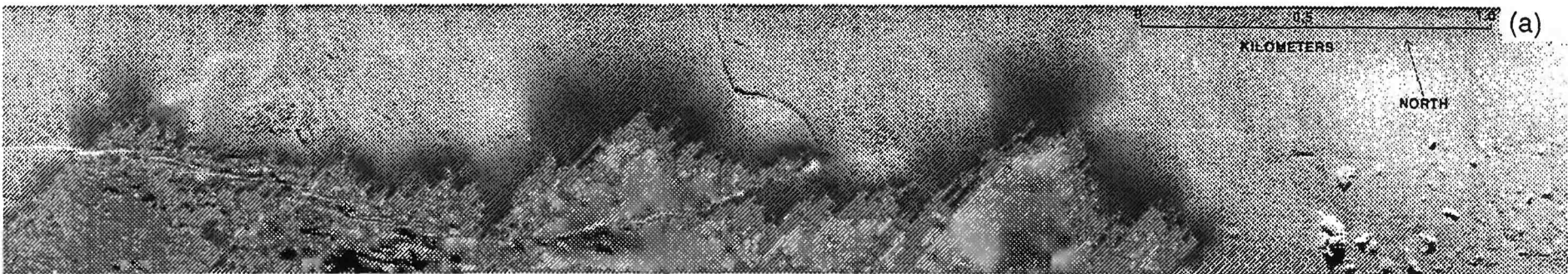
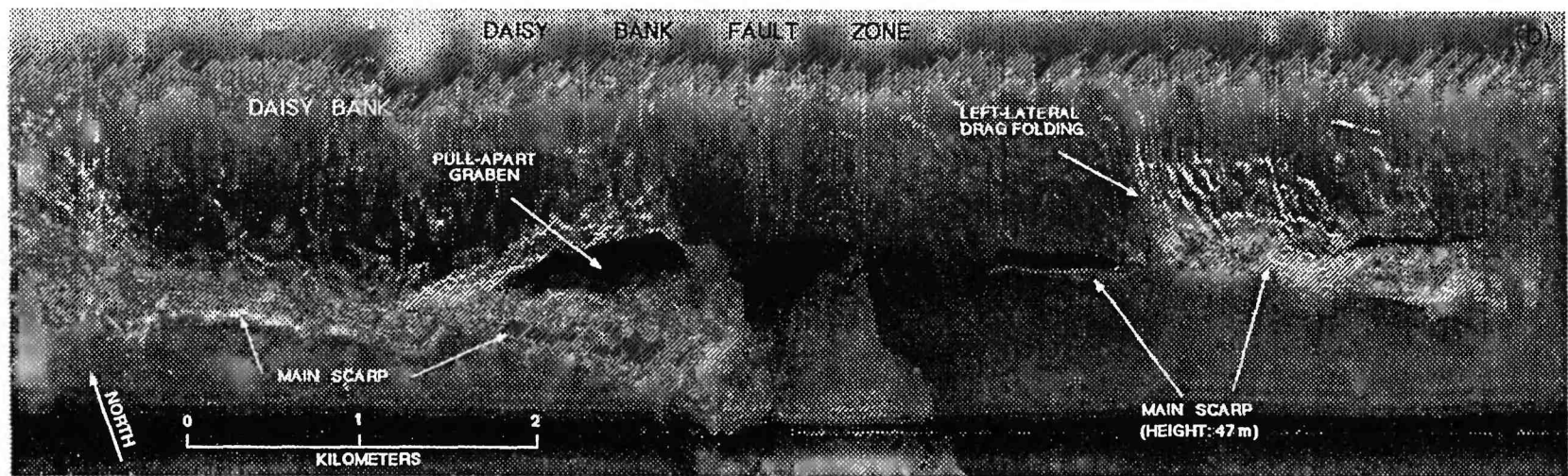


Figure 1. Map of Quaternary and Pliocene structures of the Oregon and Washington continental margin. For simplicity, only faults and anticlines are shown. Western edge of continental shelf is shown by the dash-dot line. Western edge of Siletzia terrane is shown by the dashed line. Abbreviations for WNW-trending left-lateral strike-slip faults, from north to south: NNF = North Nitinat fault; SNF = South Nitinat fault; QCF = Quinault Canyon fault; WF = Wecoma fault; DBF = Daisy Bank fault; ACF = Alvin Canyon fault; HSF = Heceta South fault; CBF = Coos Basin fault; TRF = Thompson Ridge fault. Slip rates for five of the left-lateral strike-slip faults are given, in mm/year. Major depocenters (stipple pattern): WB = Willapa basin; AB = Astoria basin; NB = Newport basin; CBB = Coos Bay basin. Major submarine banks: NHB = Nehalem Bank; HCB = Heceta Bank; CQB = Coquille Bank.



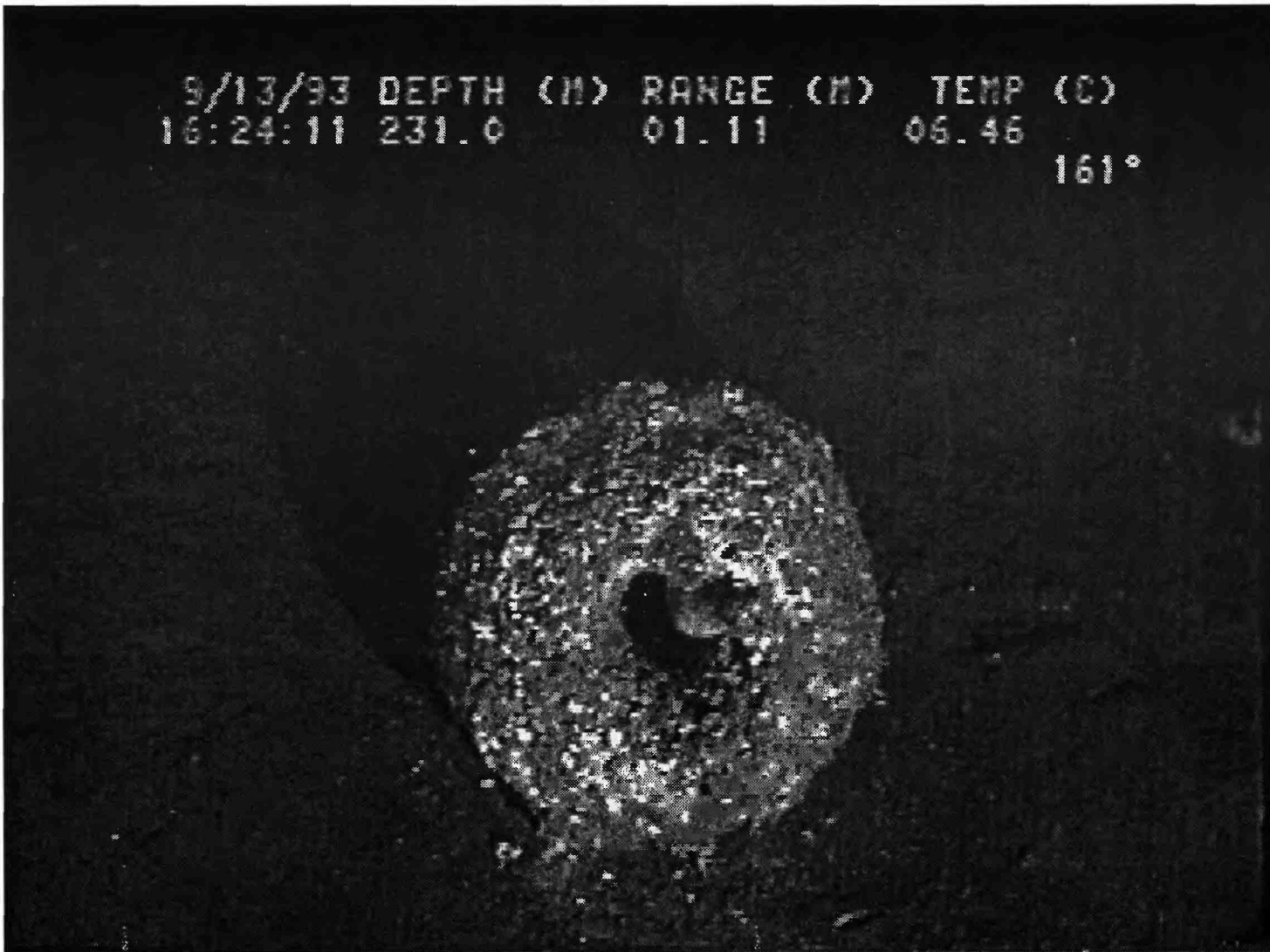
(a)



II

Figure 2. SeaMARC 1A sidescan sonar images of two left-lateral strike-slip faults on the Oregon/Washington continental margin. (a) 2 km swath along the North Nitinat fault, Washington continental margin, abyssal plain. See Figure 1 for location. The uneven texture at the west end of the image is a mud volcano. At the center of the image is the base-of-slope channel. (b) 5 km swath along the Daisy Bank fault, Oregon continental margin, at Daisy Bank. See Figure 1 for location.

9/13/93 DEPTH (M) RANGE (M) TEMP (C)  
16:24:11 231.0 01.11 06.46  
161°



500

II

Figure 3. Video from DELTA submersible shows a carbonate chimney formed by fluid venting on an active strand of the Daisy Bank fault. Chimney is about 40cm in diameter. The chimney's hole is occupied by a fish. Extensive carbonate deposition characterizes active faults on the Oregon continental shelf. These dense carbonates produce high backscatter patterns in sidescan images which are used to trace the active fault zones, in particular where only horizontal separation occurs (i.e., no vertical scarps).

— 9/13/93 DEPTH (m) RANGE (m) TEMP (°C)  
15:45:04 244.2 01.14 06.46  
99°

501



H

Figure 4. Video from Delta submersible shows a recent scarp on a subsidiary fault to the Daisy Bank fault. The scarp is up to the south, with a maximum height of ~1 m. A thin layer of Holocene olive-gray clay is cut by the fault. The underlying late Pleistocene gray clay is exposed in the fault scarp. This constrains the age of the fault to be post-12,000 years B. P. White dots are 20 cm apart.

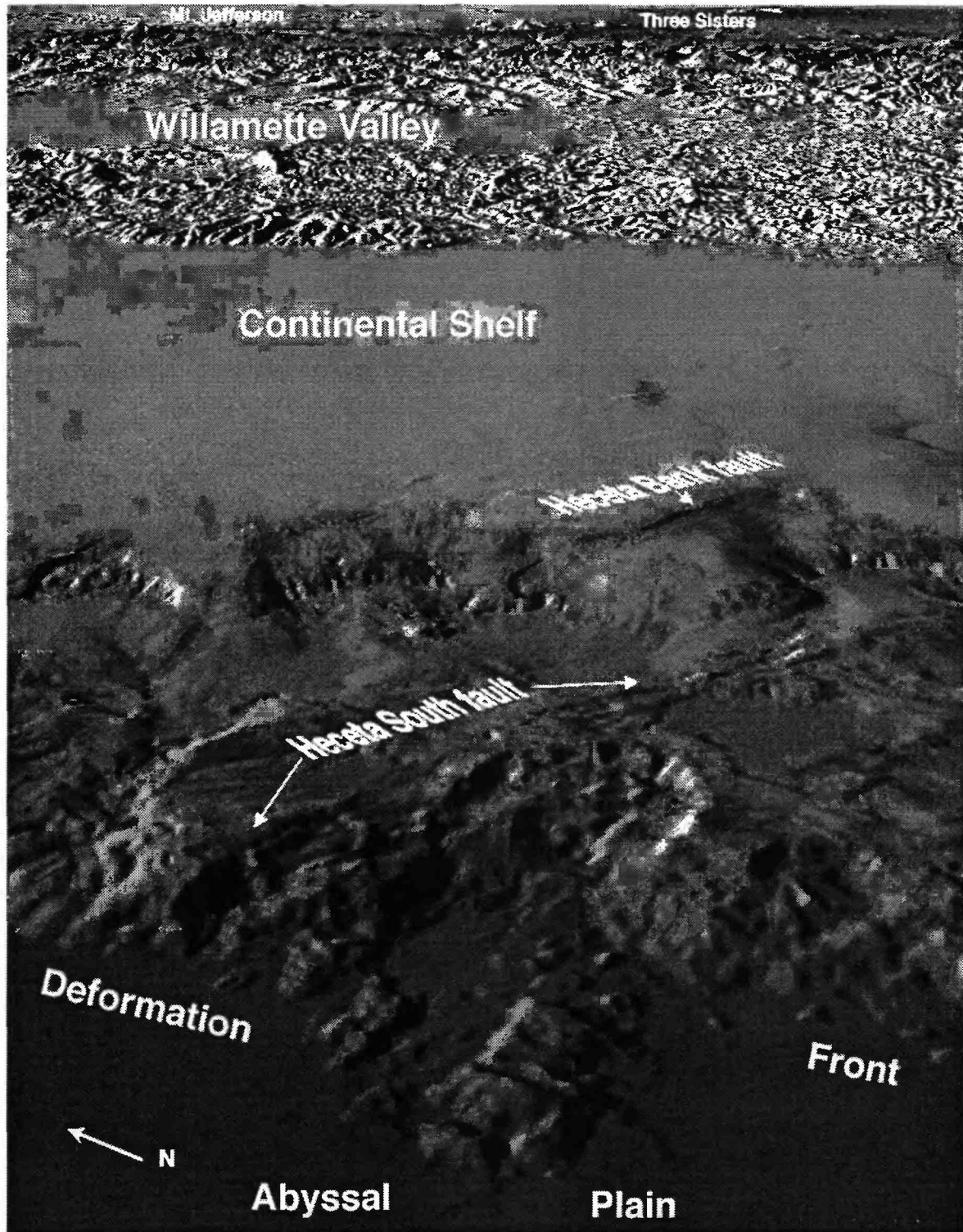


Figure 5. This image shows the topography of the central Oregon continental margin, and west-central Oregon, looking east from the abyssal plain. The bathymetric and topographic data were combined from several sources, and are shown with a grid spacing of 100 meters. The accretionary wedge is cut by a series of WNW-trending left-lateral strike-slip faults, including the Heceta South and Heceta Bank faults. Where the Heceta South fault cuts the deformation front, a large slump (8 km across) has slid from the first thrust ridge of the accretionary wedge. The left-lateral faults accommodate some of the oblique convergence between the Juan de Fuca and North American Plates.

## Alaska Seismic Studies

9930-13023

John C. Lahr\*, Christopher D. Stephens,

Robert A. Page, Kent A. Fogleman

Branch of Seismology

U. S. Geological Survey

345 Middlefield Road, Menlo Park, California 94025

Ph: (415) 329-4752 FAX: (415) 329-5143 Email: [stephens@ags.wr.usgs.gov](mailto:stephens@ags.wr.usgs.gov)

\*P.O. Box 757320, Fairbanks, AK 99775

Ph: (907) 474-7997 FAX: (907) 474-5618 Email: [lahr@fm.gi.alaska.edu](mailto:lahr@fm.gi.alaska.edu)

NEHRP: Pacific Northwest: Task II.2 (90%) and III.1 (10%)

Investigations undertaken

1. Cooperated with the Geophysical Institute of the University of Alaska (GIUA) and the USGS National Earthquake Information Center (NEIC) in the operation of the Alaska Earthquake Information Center (AEIC) in Fairbanks. The AEIC is responsible for recording and analyzing Alaskan earthquake data and disseminating earthquake information and advisories to government agencies and to the public. As part of AEIC, continued lead role in collection and analysis of data from the high-gain short-period seismograph network extending across southern Alaska from the volcanic arc west of Cook Inlet to Yakutat Bay, and inland across the Chugach Mountains.
2. Cooperated with the Branch of Igneous and Geothermal Processes, the GIUA, and the Alaska Division of Geological and Geophysical Surveys in conducting the seismic activities of the Alaska Volcano Observatory (AVO). Under this program, we have principal responsibility for monitoring the seismicity of Redoubt and Spurr, the recently active northern Cook Inlet volcanoes.
3. Cooperated with the Branch of Earthquake and Geomagnetic Information and the GIUA in operating 13 strong-motion accelerographs in southern Alaska, including 11 between Icy Bay and Cordova in the area of the Yakataga seismic gap.

Results (October 1993 - September 1994)

1. For the time interval October 1993-September 1994, AEIC processed more than 7,000 event triggers, of which 4,310 were caused by earthquakes in southern and central Alaska (Figures 1 and 2). Thirteen of these earthquakes had magnitudes of 4.5 or greater. The largest, a 5.7  $M_L$  (5.4  $m_b$ , NEIC) shock on April 25, was located 70 km southwest of Anchorage (near 61.8°N, 151°W) at a depth of 50 km. This event was felt widely throughout southern Alaska, with MM intensity V reported in Anchorage and intensity II as far as Fairbanks. The focal mechanism determined from P-wave first motions is compatible with normal faulting on a nearly vertical plane striking north-northeast, which is typical for events in the Wadati-Benioff zone (WBZ) of the subducted Pacific plate beneath southern Alaska. However, the aftershock sequence -- 22 events of magnitude 1.5 to 2.3 within 24 h -- was unusually strong for a WBZ

source. Another shock of note is a  $4.1 M_L$  shock ( $4.1 m_b$ ) located 10 km deep beneath the southern Kenai Peninsula (near  $59.8^\circ N$ ,  $150^\circ W$ ) which has a well-constrained focal mechanism showing almost pure normal faulting on either of two moderately dipping, NNW-striking planes. This observation is consistent with previous studies of recent seismicity in this area which indicate that the shallow crust above the interplate thrust is in tension (Stephens and others, 1982). An unusual crustal shock of magnitude  $4.3 M_L$  ( $4.0 m_b$ ) was located near  $61^\circ N$ ,  $140.2^\circ W$  in an area devoid of mapped Neogene and younger faults (Figure 1). Among other features of note is the moderate level of shallow seismicity east and northeast of Kodiak Island where a belt of NE-trending submarine faults of Quaternary age is mapped. No unusual seismicity patterns were noted in and around the Yakataga seismic gap. Two new stations, one three-component and one single-component vertical, were installed near Anchorage to help investigate the nature of persistent seismicity associated with the fold and thrust belt of northern Cook Inlet.

2. The use of composite focal mechanisms to infer the stress orientation within the subducting Pacific plate was tested with artificial data and the results compared to the FMSI stress inversion method (Gephart and Forsyth, 1984). For the distribution of stations in southern Alaska and for the variety of mechanisms occurring within the WBZ, the T- and P-axes derived for the composite solutions are closely aligned with the least and greatest principal stress directions if more than about 2,000 first motions are included. The composite mechanism approach is a useful adjunct to FMSI because it provides greater spatial resolution of the stress orientation in regions such as southern Alaska where only a small fraction of earthquakes have well-constrained single-event mechanisms.

In the WBZ extending from beneath Prince William Sound (PWS) to below Cook Inlet the least compressive stress trends W-E to NW-SE and plunges subparallel to the local dip of the WBZ (Lahr and others, 1994b). The relation between the orientation of the greatest compressive stress and the plate geometry is more varied. Beneath northern PWS and northern Cook Inlet, the orientation is nearly normal to the upper surface of the plate. To the south, beneath the western Kenai Peninsula and southern Cook Inlet, the greatest compressive stress is subhorizontal and trends N-S.

3. Page and others submitted a manuscript to *Geology* that presents a seismotectonic model for east-central Alaska to explain the occurrence of magnitude 7.2-7.3 earthquakes in the Interior. Geologic and seismic data (for example, see Figure 1) reveal a set of parallel, active, strike-slip faults in east-central Alaska between the Denali and Tintina fault systems. The faults strike northeast to north-northeast, at a high angle to the bounding dextral fault systems, and exhibit sinistral slip. The authors hypothesize that this set of faults divides the crust into elongate blocks that are rotating clockwise in response to northerly compression resulting from Pacific-North American plate convergence, and suggest that these faults have produced most of the large historical earthquakes in east-central Alaska between the Alaska Range and the Yukon River.

4. The responsibility for routine network operations has been shifted from Menlo Park to Fairbanks in conjunction with stationing of John Lahr at the Geophysical Institute. Beginning with January, 1994, all routine analysis, data quality control, submission of data to NEIC, and cataloging are being conducted at the AEIC in Fairbanks. A multi-PC/Sun computer data-acquisition system to replace the aging, high-expense Masscomp computers at the AEIC has been

designed and implemented. The PC's in the system run PC-SEIS, a program modified by John Rogers from the IASPEI software XDETECT to address the specific needs of a large network. The new system continuously digitizes and stores on DAT tapes 155 analog and 35 digital channels of data. Event detection is based on 127 channels; the remaining channels, both analog and digital, are automatically added to the event directories within a few minutes of the end of each triggered event. Calibrations from the 78 components using USGS A1VCO field units are detected, stored, and processed routinely to keep track of battery voltage, system gain, and other parameters. Final testing is now under way and the new system is expected to go on-line on January 1, 1995.

5. The USGS participated in a two-day Workshop on Seismic Hazard Preparedness that was held at the Geophysical Institute in April 1994. In conjunction with this workshop, a wooden model with flexible oceanic plate was designed and built to help illustrate and explain the relationship between sea floor spreading, magnetic stripes, transcurrent faults, subduction, volcanoes, and earthquakes. At the USGS Menlo Park Open House a poster and computer-based display illustrated the seismicity and tectonics of Alaska. A working wooden model was designed and built to illustrate the block-rotation hypothesis for the origin of large earthquakes and sinistral faulting in central Alaska. A lecture was given to about 150 people on the Northridge earthquake and possible implications for Alaska at the EERI Northridge Earthquake Technical Briefing held on May 23, 1994, in Anchorage. A paper on earthquake potential in Alaska was presented at the Applied Technology Council/USGS Special Session on Regional Earthquake Potential in the United States at the Fifth U.S. National Conference on Earthquake Engineering in July 1994.

6. SMA records with calibrations but no earthquake signals were recovered from thirteen sites, of which all but three were operating. All SMA sites were operational upon departure. The three failures were due to defective batteries, and all batteries of this type were removed from service.

### References

- Gephart, J. W., and Forsyth, D. W., 1984, An improved method for determining the regional stress tensor using earthquake focal mechanism data: Application to the San Fernando earthquake sequence, *J. Geophys. Res.*, v. 89, 9305-9320.
- Stephens, C.D., Lahr, J.C., and Rogers, J.A., 1982, Review of earthquake activity and current status of seismic monitoring in the region of the Bradley Lake Hydroelectric Project, southern Kenai Peninsula, Alaska: November 27, 1980 - November 30, 1981, *U.S. Geol. Surv. Open-File Report 82-417*, 26 p.

### Reports (published or submitted)

- Chouet, B.A., Page, R.A., Stephens, C.D., Lahr, J.C., and Power, J.A., 1994, Precursory swarms of long-period events at Redoubt volcano (1989-1990), Alaska: their origin and use as a forecasting tool, *J. Volc. Geoth. Res.*, v. 62, p. 95-125..
- Fisher, M.A., Brocher, T.M., Plafker, G., Bruns, T.R., Geist, E.L., Page, R.A. and Stephens, C.D.,

- 1993, Deep seismic reflections from a young suture zone and the asperity of the great 1964 Alaska earthquake (abs.), *EOS, Trans. Amer. Geophys. Union*, v. 73, no 43 Supplement, p. 95.
- Fogleman, K.A., Lahr, J.C., Stephens, C.D., and Page, R.A., 1993, Earthquake locations determined by the southern Alaska seismograph network for October 1971 through May 1989, *U.S. Geol. Surv. Open-File Rept. 93-309*.
- Fogleman, K.A., Lahr, J.C., Stephens, C.D., and Page, R.A., 1993, Earthquake locations determined by the southern Alaska seismograph network for October 1971 through May 1989, in Habermann, R.E., P.K. Dunbar and L. Whiteside, eds., *Earth Systems Data: Natural Hazards -- Proceedings of the Wadati Conference on Large Subduction Zone Earthquakes*, CD-ROM, USDOC/NOAA/National Geophysical Data Center, Boulder, CO.
- Fogleman, K.A., Rowe, C., Stephens, C.D. and Hammond, B., Earthquakes in Alaska, *Alaska State Seismologist's Reports* (Periodical series. 12 issues/year: reports # 91-01 to 91-08 and 93-01 have been published to date).
- Jolly, A.D., Page, R.A., and Power, J.A., 1994, Seismicity and stress in the vicinity of Mt. Spurr volcano, south-central Alaska, *J. Geophys. Res.*, v. 99, n. B8, p. 15,305-15,318.
- Hammond, W.R., Lahr, J.C., Rowe, C.A. and Benoit, J.P., 1993, The Salcha seismic zone near Fairbanks, Alaska (abs.), *EOS, Trans. Amer. Geophys. Union*, v. 74, n. 43, p. 417.
- Lahr, J.C., Chouet, B.A., Stephens, C.D., Power, J.A., and Page, R.A., 1994a, Earthquake classification, location, and error analysis in a volcanic environment: implications for the magmatic system of the 1989-1990 eruptions at Redoubt volcano, Alaska, *J. Volc. Geoth. Res.*, v. 62, p. 137-151.
- Lahr, J.C., Fogleman, K.A., Stephens, C.D., and Page, R.A., 1993, Stresses within the Pacific Plate of southern Alaska (abs.), *EOS, Trans. Amer. Geophys. Union*, v. 74, n. 43, p. 417.
- Lahr, J.C., Stephens, C.D., Page, R.A., and Fogleman, K.A., 1994b, Characteristics of the Aleutian Wadati-Benioff zone seismicity beneath southern Alaska (extended abs.), SUBCON, An interdisciplinary conference on the subduction process, June 12-17, 1994, Avalon, California, p. 301-303.
- Page, R.A., 1994, Comparison of knowledge of earthquake potential in the San Francisco and Anchorage regions, in *Earthquake Alaska - are we prepared?* *U.S. Geol. Surv. Open-File Rept. 94-218*, p. 31-42.
- Page, R.A., Brocher, T.M., Stephens, C.D., Lahr, J.C., Fogleman, K.A., and Fisher, M.A. 1994, Piggyback subduction at the eastern end of the Aleutian trench and the giant asperity that ruptured in the great 1964 earthquake (extended abs.), SUBCON, An interdisciplinary conference on the subduction process, June 12-17, 1994, Avalon, California, p. 152-154.
- Page, R.A., Lahr, J.C., Chouet, B.A., Power, J.A., and Stephens, C.D., 1994, Statistical forecasting of repetitive dome failures during the waning eruption of Redoubt volcano, Alaska, February-April 1990, *J. Volc. Geoth. Res.*, v. 62, p. 183-196.
- Page, R.A., Plafker, G. and Pulpan, H., Block rotation in east-central Alaska: A framework for evaluating earthquake potential?, submitted to *Geology*.
- Plafker, G., Gilpin, L.M., and Lahr, J.C., 1994, Neotectonic map of Alaska, in Plafker, G., and Berg, H.C., eds., *The geology of Alaska*: Boulder, Colorado, Geological Society of America, *The Geology of North America*, v. G1, plate 12, scale 1:2,500,000.
- Power, J.A., Jolly, A.D., Page, R.A., and McNutt, S.R., 1994, Seismicity and forecasting of the 1992 eruptions of Crater Peak vent, Mt. Spurr, Alaska: An overview, *U.S. Geol. Surv. Bull.* [in press].

- Power, J.A., Lahr, J.C., Page, R.A., Chouet, B.A., Stephens, C.D., Harlow, D.H., Murray, T.L., and Davies, T.N., 1994, Seismic evolution of the 1989-90 eruption sequence of Redoubt volcano, Alaska, *J. Volc. Geoth. Res.*, v. 62, p. 69-94.
- Rogers, J. and Stephens, C.D., 1995, SSAM: Real-time seismic spectral amplitude measurement on a PC and its application to volcano monitoring, *Bull. Seism. Soc. Am.* [in press].
- Stephens, C.D., Chouet, B.A., Page, R.A., Lahr, J.C., and Power, J.A., 1994, Seismological aspects of the 1989-1990 eruptions at Redoubt volcano, Alaska: the SSAM perspective, *J. Volc. Geoth. Res.*, v. 62, p. 153-182.

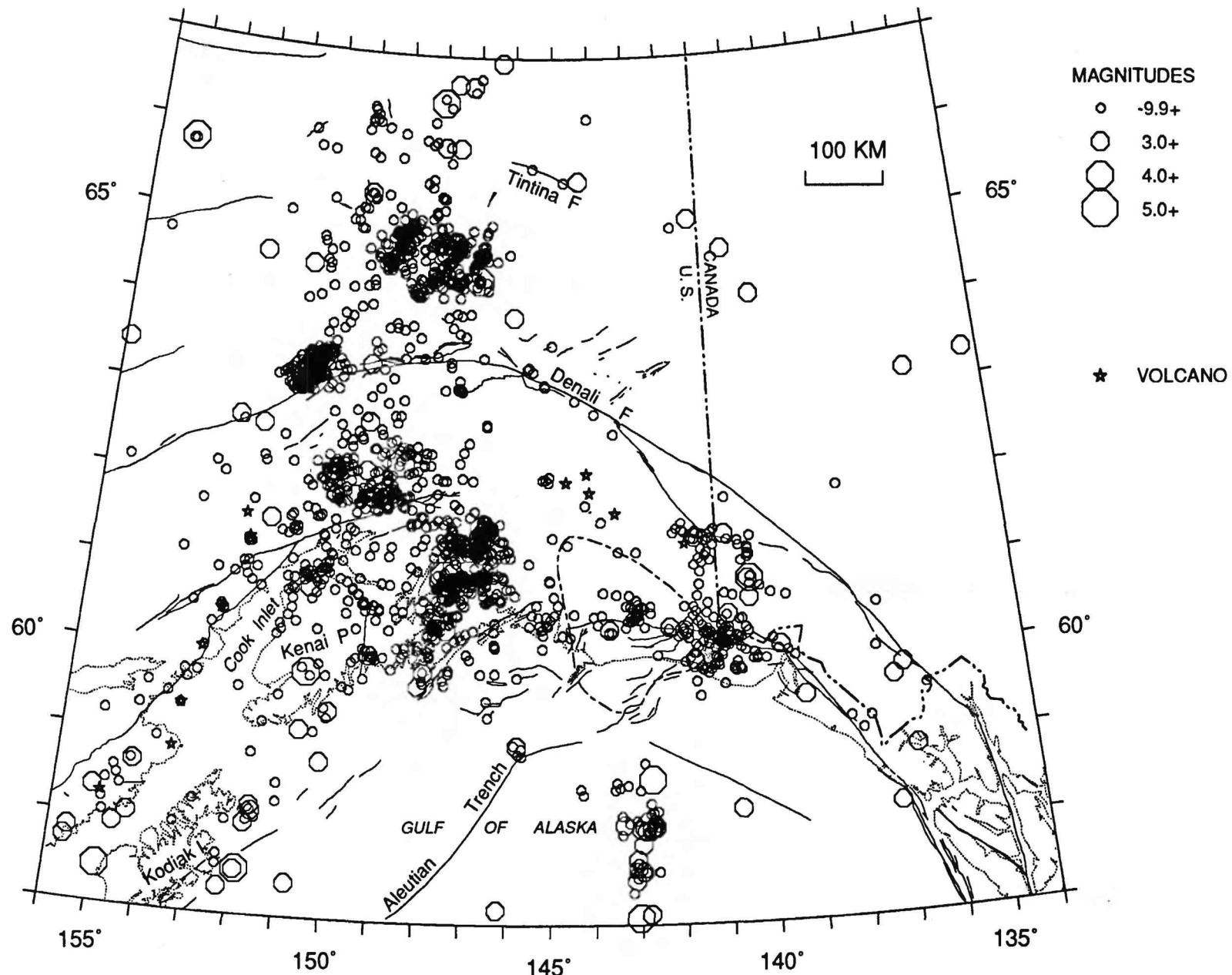


Figure 1. Shallow earthquakes (depths above 30 km) from October 1993 to September 1994 located by AEIC in southern and central Alaska. Solid lines show Neogene and younger faults after Plafker and others (1994), and heavy dashed contour indicates approximate extent of Yakataga seismic gap.

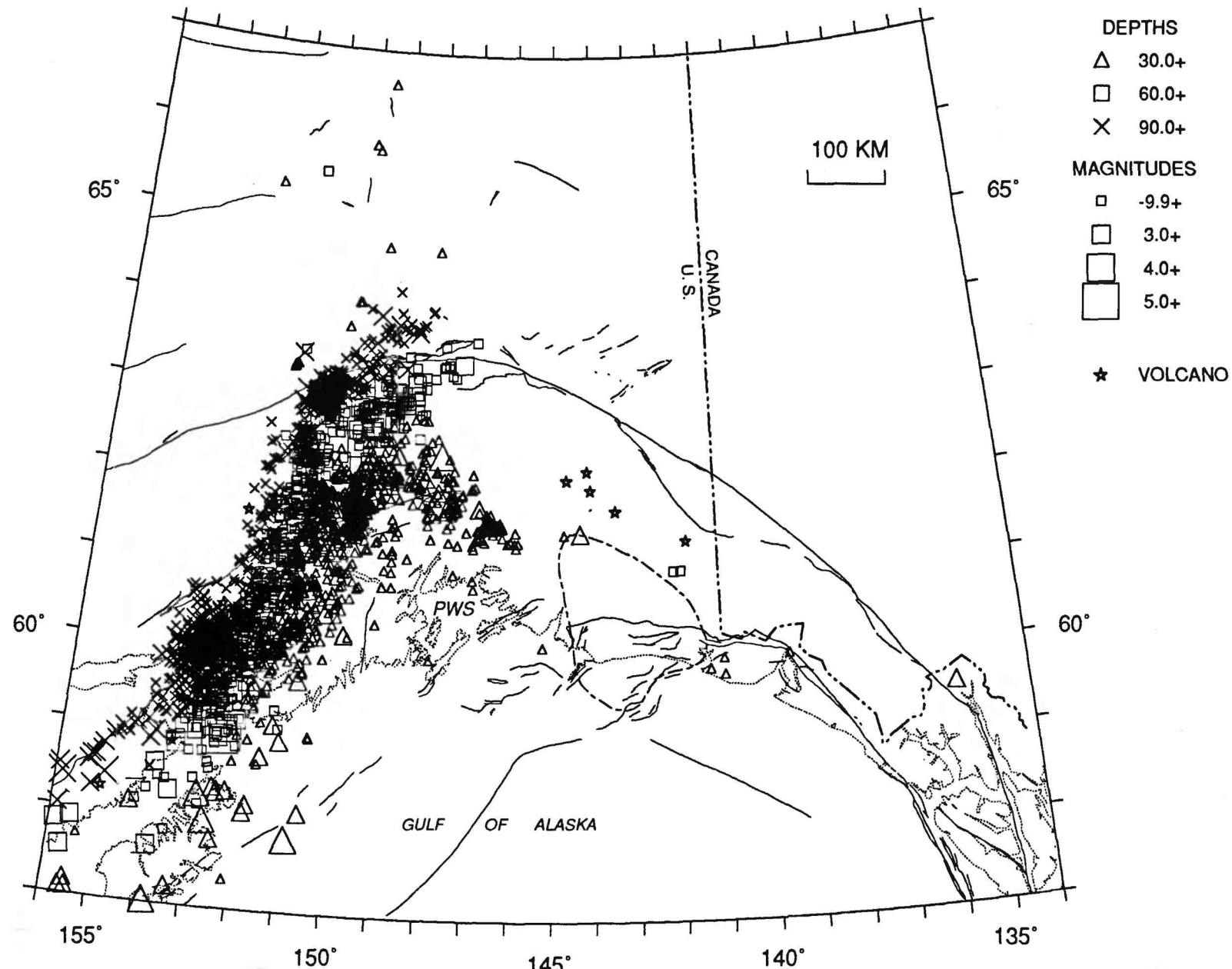


Figure 2. Earthquakes from October 1993 to September 1994 located at depths of 30 km and greater by AEIC in southern and central Alaska. Most of these events occurred within the subducted Pacific plate. PWS - Prince William Sound. Other map features are labelled in Figure 1.

## Surface Ruptures Produced by Landers 6/28/92 Earthquake

9960-11276

Kenneth R. Lajoie

Branch Earthquake Geology and Geophysics  
U. S. Geological Survey  
345 Middlefield Road MS 977  
Menlo Park, California 94025  
(415) 329-5641 phone, (415) 329-5163 FAX  
klajoie@isdmnl.wr.usgs.gov E-mail

### Investigations

1. **Landers ruptures:**  
The original goal of this project was to map surface ruptures produced by the 1992 Landers earthquake on aerial photographs (1:2.4k to 1:6k), to rectify and merge the resultant images using computer techniques, to field check the resultant rupture maps, and to publish a strip map at 1:12k of the rupture pattern. However, owing to dispersal of budgeted OE for overhead expenses (space, etc.) this project could not be completed as proposed. Consequently, a more modest goal of completing a 1:100k map of horizontal slip based on early field work was adopted.
2. **Vertical crustal deformation in the San Francisco bay region:**  
Following the Northridge earthquake a CONCERT working group was organized to assess the seismic hazard from active folding and blind thrusting in the bay region. As part of this effort, a collaborative study with Robert Simpson and Dave Oppenheimer was initiated to investigate the style and rates of vertical crustal deformation in the San bay region using computer-based geomorphic analysis.
3. **Electron-spin resonance (ESR) dating of Quaternary marine shells:**  
A broadly applicable dating technique that covers the last million years is badly needed for studying Quaternary tectonics. The goal of this study is to help fill this need. Tracy Furutani (University of Washington, previously USGS) completed a study investigating the feasibility of dating Quaternary marine shells by the Electron-Spin Resonance (ESR) technique. This study was initiated and partially funded by the USGS Coastal Tectonics project.
4. **High-precision Argon 40-39 dating of rhyolitic tephra in Mono Basin, California:**  
The Argon 40-39 laser-probe dating technique holds considerable promise for directly dating Holocene volcanic materials. However, the lower age limit of the technique has not been established. To address this problem a collaborative study was initiated with Derek York and Yanshao Chen (University of Toronto) to

analyse sanidine from 24 independently dated (36ka to 1ka) rhyolitic tephra deposits in Mono Basin.

## Results

### 1. Landers ruptures:

Slip data acquired during field investigations immediately following the Landers earthquake were not collected systematically. Consequently, coverage is not uniform and some field measurements cannot be reasonably interpreted. The reliable data yield relative displacements, which can be used to construct displacement profiles of the main, overlapping fault strands. Summing these profiles across the entire rupture zone yields an overall profile of lateral displacement.

### 2. Vertical crustal deformation in the San Francisco Bay region:

The ratio of fault-normal to fault-parallel interplate motions is roughly 1:10 in the San Francisco Bay region, in marked contrast to a 1:2 ratio in the Transverse Ranges of southern California. This contrast suggests that the seismic hazard from thrust-type earthquakes is roughly five times lower in the San Francisco region than in the northern Los Angeles basin, where the recent Northridge earthquake caused fifteen billion dollars in structural damage. However, the six billion dollars in damage caused by the Loma Prieta earthquake demonstrates that the hazard from thrust-type earthquakes is still considerable in the San Francisco Bay area. To assess this hazard, a CONCERT working group was recently organized to study active folding and blind thrusting in the San Francisco Bay region. As part of this effort, a collaborative study of the general geomorphology of the bay area was initiated with Robert Simpson and Dave Oppenheimer. The goal of the study is to define the broad, active structures of the area using generalized topography derived from computer analysis of 1:250k DEM data. In active tectonic belts such as the California coast ranges relative topographic relief generally reflects relative vertical crustal uplift during Quaternary time. In turn, the uplift reflects crustal thickening produced by earthquake-induced folding and related thrust faulting. The generalized topography of the area reflects the broad, active folds expressed in a few places by coseismic and interseismic deformation. Topographic profiles across the northwest trending mountain ranges in the bay area reveal relative uplift and subsidence of the structural blocks between strands of the San Andreas fault system. Upwarped Tertiary and Quaternary sediments along the flanks of some of these ranges reflect the time and rate of broad folding between the fault strands. Longitudinal profiles of the range crests reveal the structural lows and highs within each structural block, and collectively reveal the broad structural low occupied by the bay and the drainage from the Central Valley. Previous drainages, such as the wind gaps at Pacheco Pass and Pajaro Gap, are progressively higher to the southeast, suggesting that the bay area structural low is migrating northwestward, possibly in the wake of the triple junction.

3. Electron-spin resonance (ESR) dating of Quaternary marine shells:  
Vertical sequences of emergent marine terraces cut into coastal slopes along much of the Pacific Coast of the conterminous United States reflect vertical crustal movements in this tectonically active region. Dating these terraces yields rates of tectonic uplift and fault displacement. Unfortunately, there is no widely applicable dating technique that covers the probable age range of the terraces, roughly 100ka to 1my. In the past decade, however, Electron-Spin- Resonance (ESR) dating of fossil marine shells in Japan and Europe has shown promise of covering this broad time span. Accordingly, a study was initiated within the USGS Coastal Tectonics Project to assess the feasibility of dating fossil marine shells from emergent marine terraces along the Pacific Coast of the United States and Central Chile. Tracy Furutani, formerly with the project, expanded the study into his Phd dissertation at the University of Washington. A major impediment to testing this or any other new technique is that there are few independent dates that can be used for evaluation and calibration of new techniques. This shortcoming notwithstanding, Furutani's study produced encouraging results. The effective age range of the technique appears to be Holocene to Mid Pleistocene, roughly 0 to 900ka, with the error estimates of 7 to 20 percent for ages greater than 100ka.
4. High-precision Argon 40-39 dating of rhyolitic tephra in Mono Basin, California:  
Until recently volcanic materials younger than about 50ka could not be dated directly. The newly developed Argon 40-39 laser-probe dating technique, developed by Derek York at the University of Toronto, yields reasonable dates on sanidine down to about 10ka. But, because this technique has not been evaluated in a controlled experiment, its accuracy and its lower age limit are not known. A dating project using sanidine from rhyolitic tephra in Mono Basin, California was recently initiated with Derek York to address these uncertainties. Around the margins of Mono Lake twenty rhyolitic tephra deposits derived from the nearby Mono Craters occur in lake sediments ranging from 36ka to 12ka in age, as determined by radiocarbon analyses of algal tufa and ostracodes. In Crooked Meadow, 15km southeast of Mono Lake, twenty-two rhyolitic tephra deposits, also derived from the Mono Craters, occur in peat deposits ranging from 11ka to 1ka in age, as determined by radiocarbon analyses on peat. These forty-two indirectly dated tephra deposits yield a virtually complete eruptive history of the Mono Craters over the past 36ka. Twenty four of deposits yield sanidine grains suitable for laser dating. If the initial laser-probe results are promising, carbonate or peat samples from beneath each tephra deposit will be dated by the accelerator radiocarbon technique at the University of Toronto to improve independent age control of the tephra deposits. All carbonate and peat samples for this phase of the project have been collected and prepared. Results from this project have many potential applications beyond testing the reliability of the Argon 40-39 technique. For example, the history of eruptions from the Mono Craters and the history of fluctuations of Mono Lake over the past 36ka will be more firmly established. No USGS funds or time have been used on this project.

## Reports

Simpson, R.W., Lajoie, K.R., and Oppenheimer, D.H., 1994, Inferring blind thrusts in the San Francisco bay region from earthquake focal mechanisms and averaged topography: Eos, Transactions, American Geophysical Union, v. 75, p. 681.

## Geodetic Strain Monitoring

9960-11166  
9960-12166

*John Langbein*

Branch of Earthquake Geology and Geophysics  
U.S. Geological Survey  
345 Middlefield Road MS/977  
Menlo Park, California 94025  
(415) 329-4853  
langbein@shasta.wr.usgs.gov

Program element: II

### Investigations

Two-color geodimeters are used to survey, repeatedly, geodetic networks within selected regions of California that are tectonically active. This distance measuring instrument has a precision of 0.1 to 0.2 ppm of the baseline length. Currently, crustal deformation is being monitored within the south moat of the Long Valley caldera in eastern California, across the San Andreas fault at Parkfield, California, at three locations near Palmdale, California on a section of the San Andreas fault that is within its Big Bend region, and at two locations near Pinon Flat, California. Periodic comparisons with other other two-color geodimeters are conducted both at Parkfield and at Mammoth Lakes. These intercomparisons measurements serve as a calibration to monitor the relative stabilities of these instruments.

### Results

#### 1. Parkfield

Frequent measurements of length of 17 baseline are made for a geodetic network near Parkfield, California (Figure 1). Approximately one-half of these baselines straddle the San Andreas Fault along the segment that last ruptured in 1966. The data from these baselines are shown in Figure 2. This data are contaminated by both systematic dilatations due to drift in the instrument and localized displacements of monuments due to ground swelling from the seasonal rainfall. Computer routines have been written to remove systematic dilatations which can be compared with the periodic calibration measurements using the Parkfield based, two-color geodimeter and the portable, two-color geodimeter.

To address the issue of monument stability, we made arrangements with Frank Wyatt of UC San Diego to install additional monuments at two sites which have exhibited large seasonal variations. We have selected MIDE and POMO (Figures 1 and 2). The monument consists of 5, 10 to 15 meter long, 2.5 cm dia pipe where 4 of the pipes are installed into drill-holes oriented at 45° angles with respect to the ground's surface, and the fifth pipe is vertical. All 5 pipes are welded together at a point 1

meter above the ground to establish rigidity. The results of monitoring the lengths of these two pair of baselines are shown in Figure 3 and show that these new monuments, termed MIDA and POMM attenuate the seasonal variations. The residual variations observed with the new monuments are likely due to localized displacement of the central monument.

To test whether localized displacement of the central instrument monument is responsible for the variations in the new baselines, MIDA and POMM, and other baselines within the Parkfield network, we have adjusted the data using least squares estimates of the displacement of the central monument, CARR. Examination of 5 years of data spanning the 1989 to 1994 interval show that the accounting for the displacement of CARR yields a significant reduction in noise on these baselines.

**Reduction of baseline noise from  
displacement of central monument, CARR**

BASELINE	Baseline length km	Nominal precision mm	Standard Deviation about a linear trend in mm	
			No displacement of CARR	With displacement of CARR
MIDA	4.65	0.63	1.87	0.63
BUCK	2.90	0.46	1.68	0.61
NORM	1.06	0.33	1.46	0.39
HUNT	2.72	0.44	1.26	0.65
TURK	2.16	0.40	1.31	0.53
MASON	6.27	0.81	1.64	0.95
HOGS	5.00	0.67	1.44	0.75
LANG	4.08	0.57	1.05	0.99
POMM	5.60	0.74	3.11	0.81

## 2. Southern California

With nearly 14 years of geodetic measurements at Pearblossom, it is worthwhile to examine both the line-length changes and inferred strain changes from this 12 baseline network that straddles the locked section of the San Andreas fault. Using power spectral techniques shown in Figure 4, we can observe that the line-length variations are composed of 2 components; a frequency independent part that reflects the 0.12 part-per-million precision of the two color geodimeter and; a frequency dependent part that scales with  $f^{-2}$  and is approximately equal to  $0.75\text{mm/yr}^{0.5}$ . In addition, we have used simulated line-length change data with appropriate partition of the error budget between random walk monument noise and white noise due to the actual precision of the instrument and compute strain changes as we would normally process real data. We conclude that most of the inferred strain changes from real data that appears significant when compared to a white is actually a result of random walk noise in the geodetic monuments. We will need to modify the data correlation matrix to include non-diagonal terms in the inversion for strain.

## 3. Northern California, SF Bay

We now have two sets of observations of a network shown in Figure 5 that straddles the junction between the Hayward, Calaveras, and Mission Faults.

## 5. Publications

Langbein, J., D. Dzurisin, G. Marshall, R. Stein, and J. Rundle, Shallow and peripheral volcanic sources of inflation revealed by modeling two-color geodimeter and leveling data from Long Valley, Caldera, California, 1988-1992. *submitted, J. Geophys. Res.*

Roeloffs, E., J. Langbein, The earthquake prediction experiment at Parkfield, California, *Rev. of Geophysics*, 32, 315-336, 1994.

## Two-color Geodimeter Network at PARKFIELD

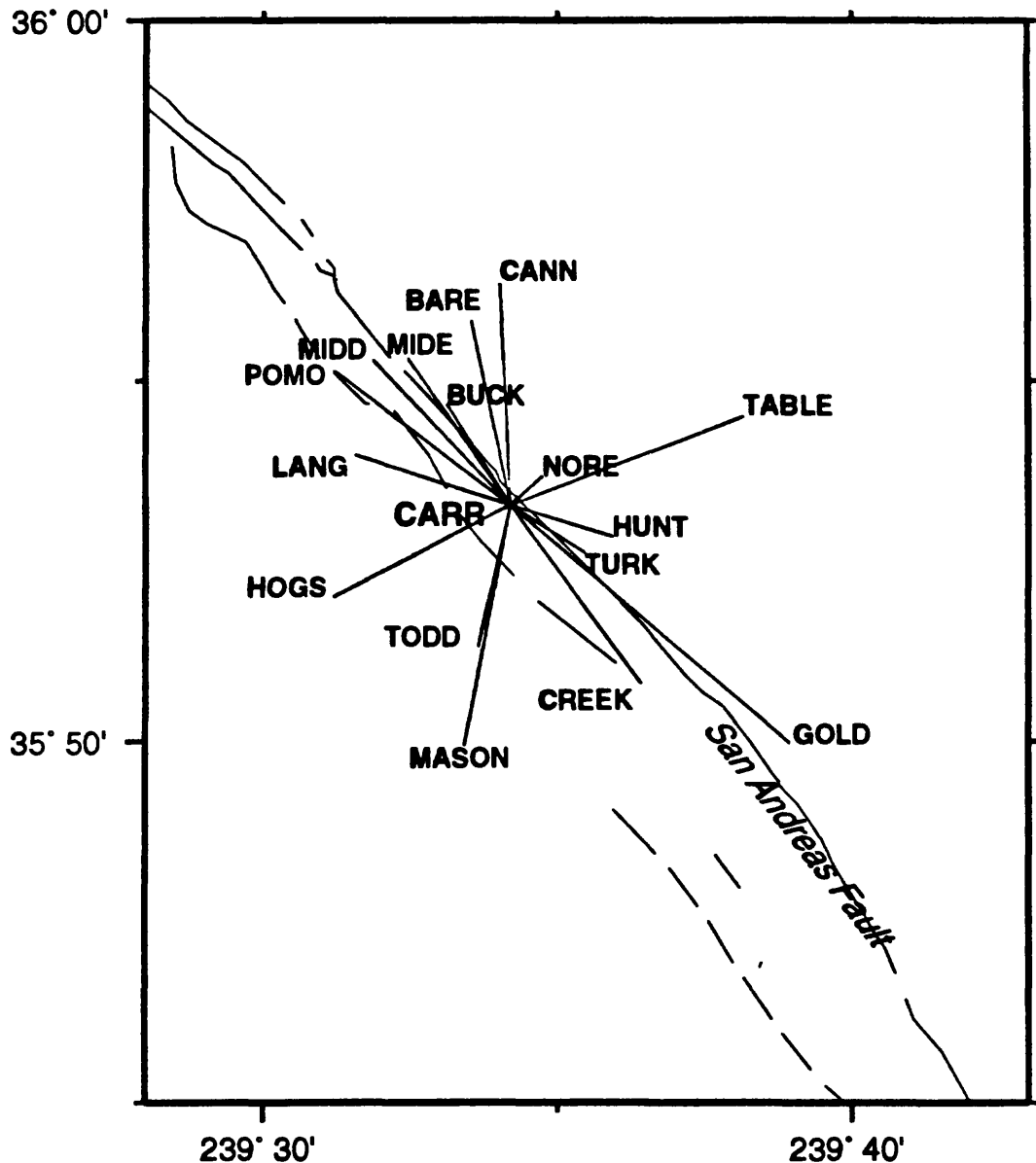


**FIGURE 1.** A map showing the locations of baselines measured at Parkfield using a two-color geodimeter. Measurements using the common station at CARR are made approximately 3 times each week.

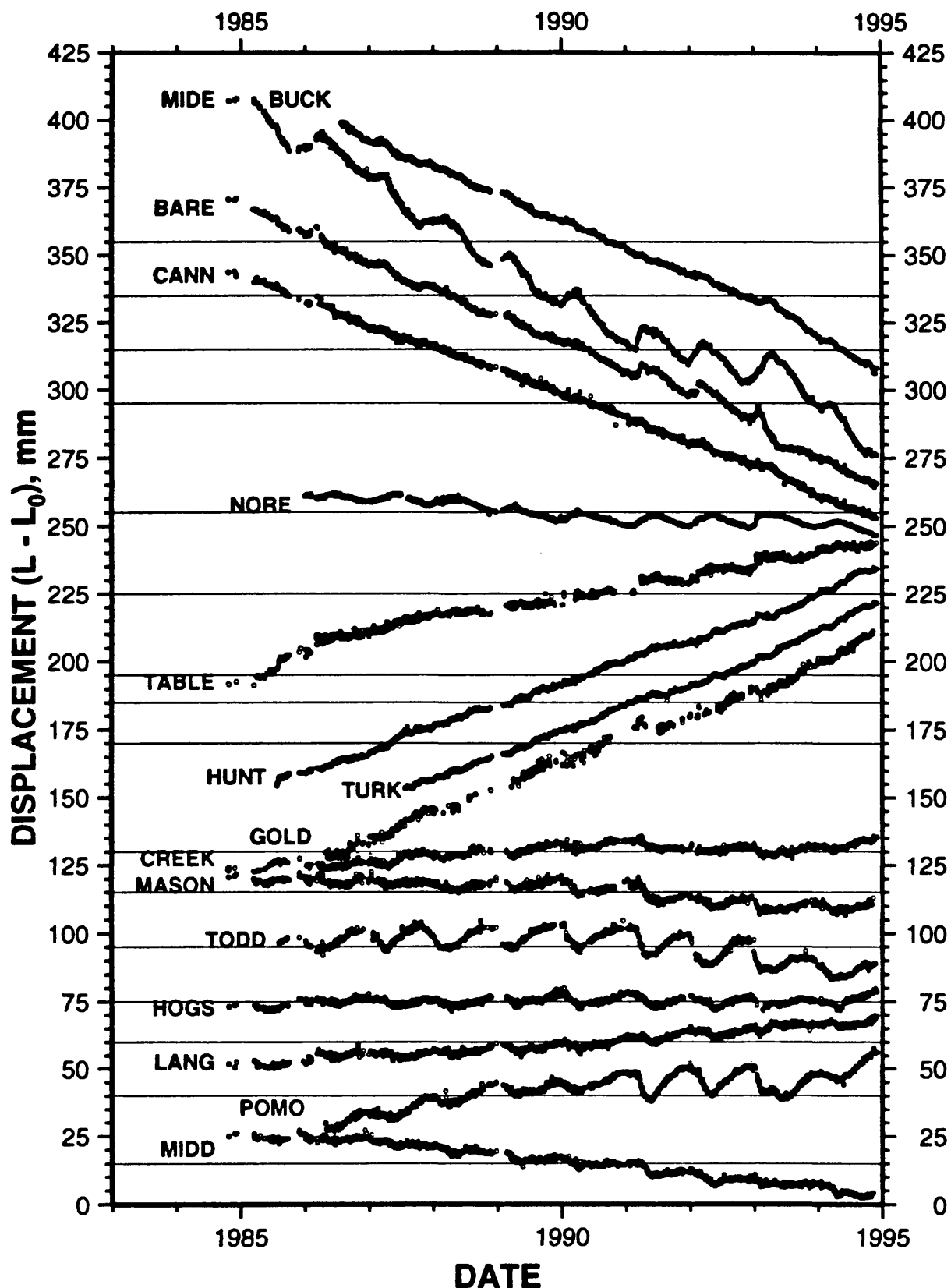


**FIGURE 2.** Plot of two-color geodimeter data for measurements of line-length changes using the common station at CARR at Parkfield.

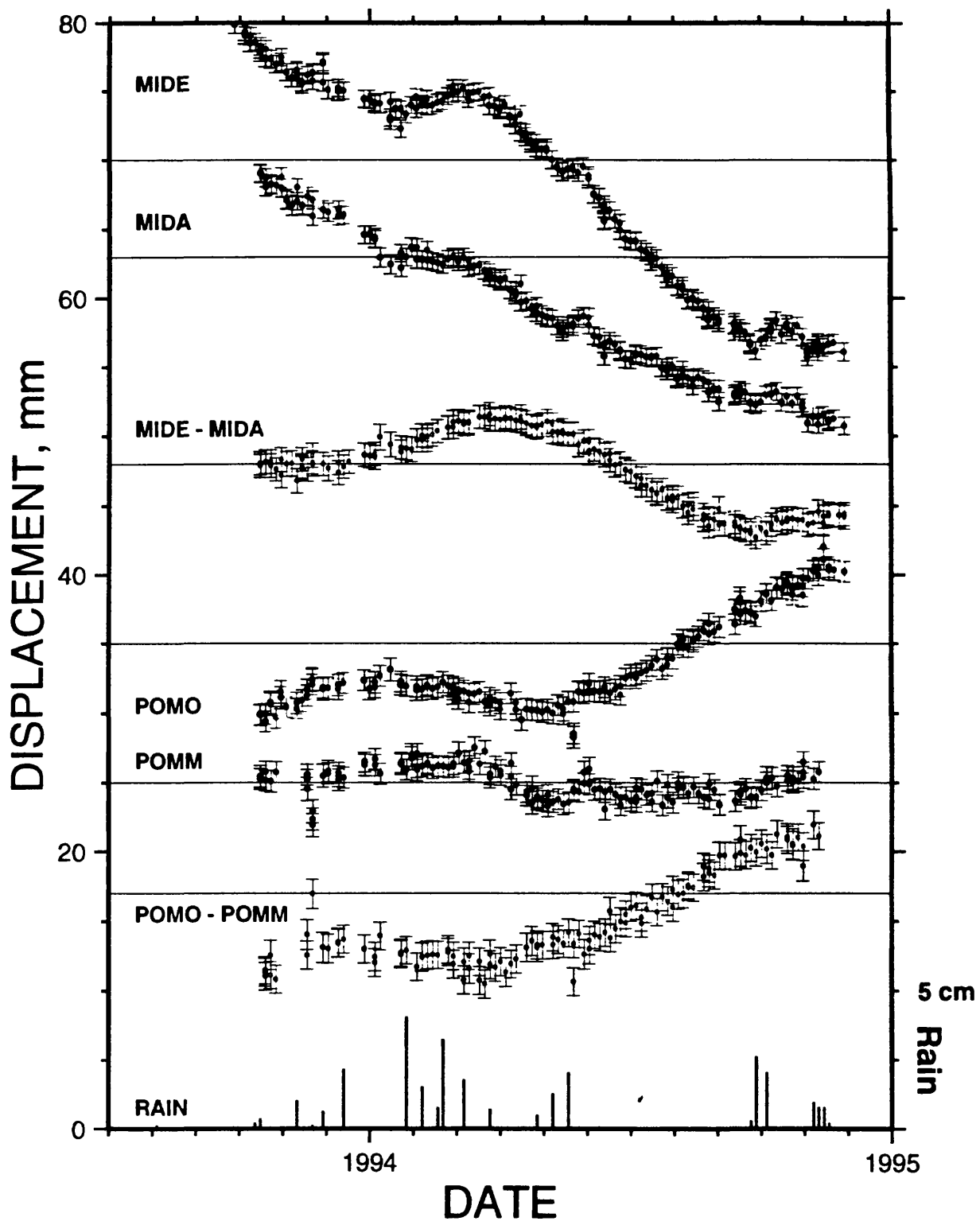


**FIGURE 3.** Comparison of line-length changes between 2 pairs of baselines. The baselines MIDE and POMO use *old* style monuments to 2 meter depth and their neighboring baselines, MIDA and POMM use deeply anchor monuments to 10 meter depth. The data show that the deeply anchored monuments have less seasonal variations.

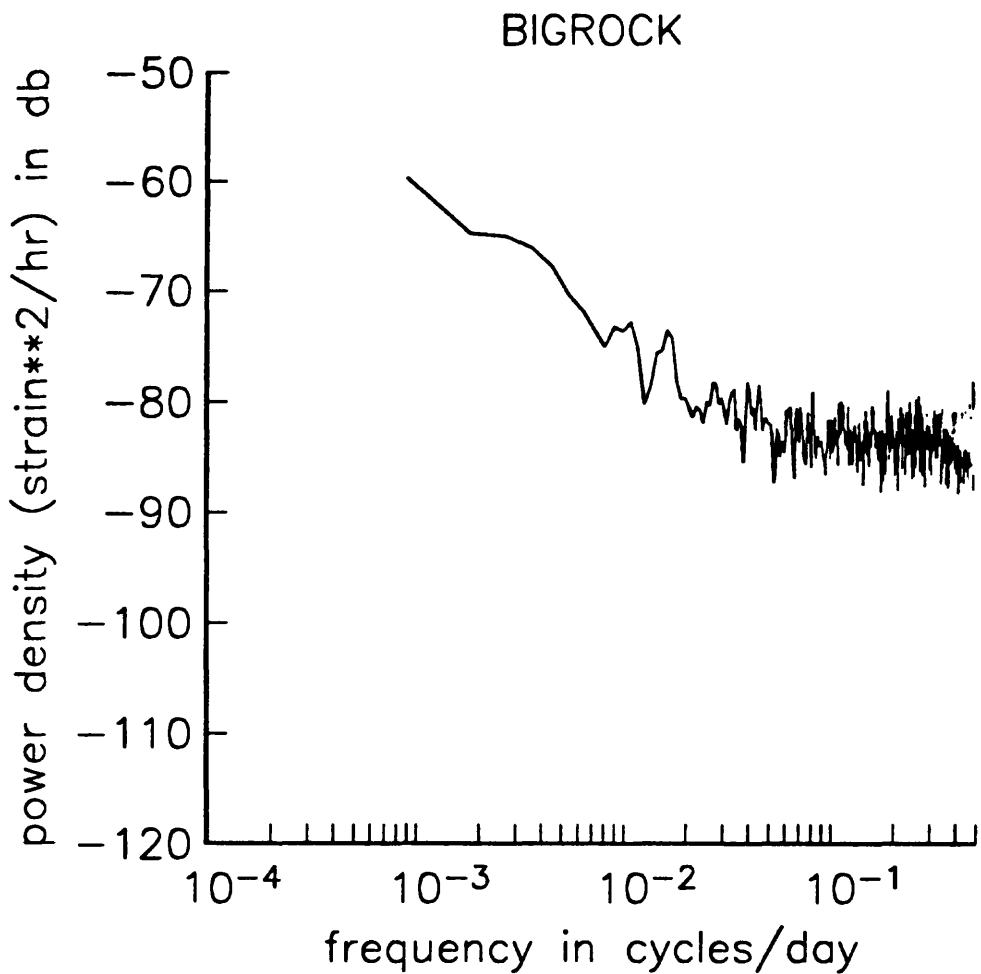


**FIGURE 4.** A power density spectrum of one of the baselines in the Pearblossom network.

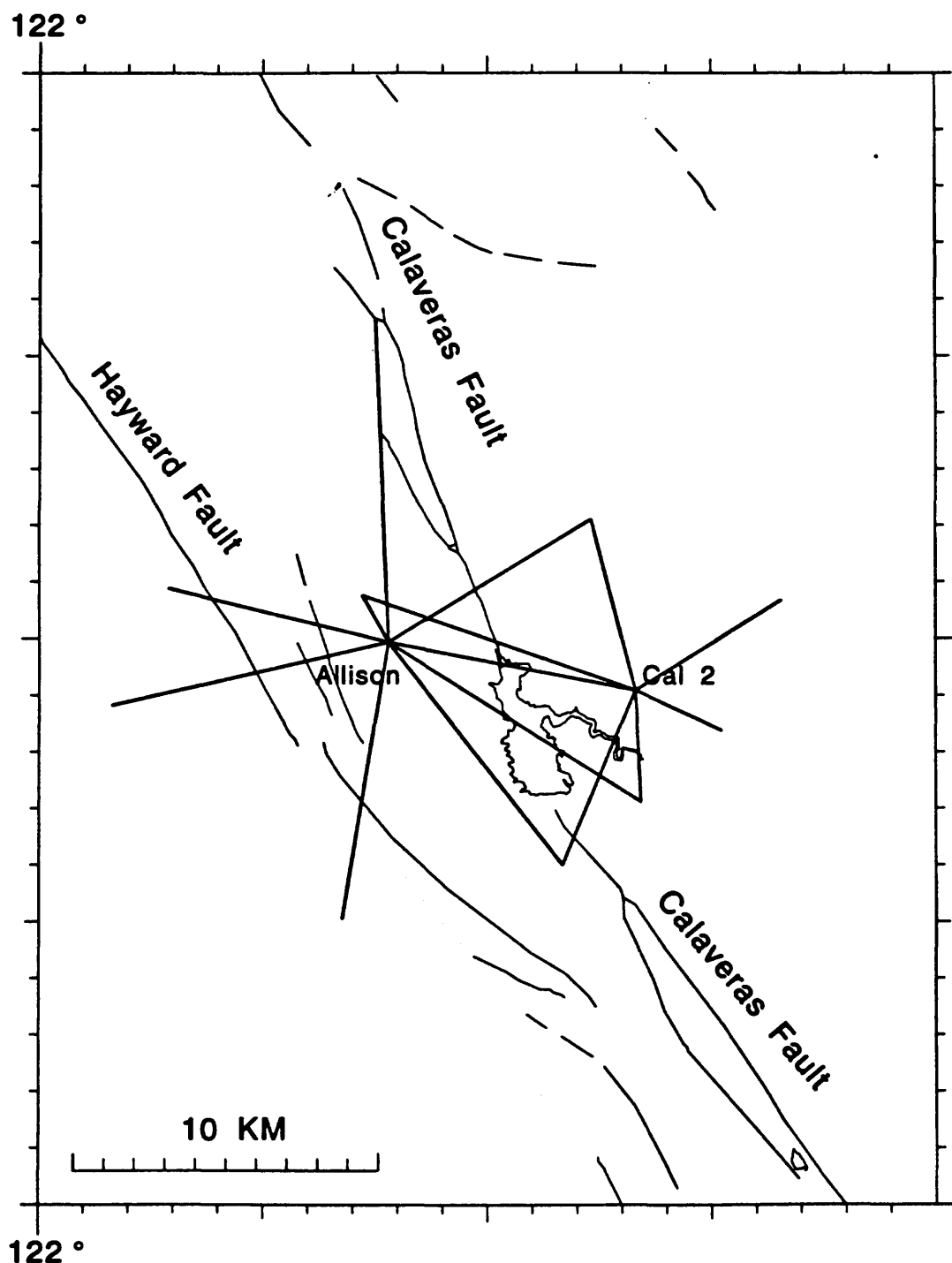


**FIGURE 5.** A map showing the location of baselines near Mission Peak used to detect strain accumulation at the junction of the Hayward and Calaveras faults.

## Parkfield Prediction Experiment

9960-12246

*John Langbein*

Branch of Earthquake Geology and Geophysics  
 U.S. Geological Survey  
 345 Middlefield Road MS/977  
 Menlo Park, California 94025  
 (415) 329-4853  
 email: langbein@shasta.wr.usgs.gov

Program element II

### Investigations

This project coordinates the different experiments at Parkfield run by both USGS and non-USGS investigators. Some of the experiments are focused on the prediction in the short-term of the next Parkfield earthquake. Other experiments will document pre-seismic, the co-seismic, and post-seismic events. Both data from seismicity and from deformation are examined for significant events. This project has been examining the formal rules used in either calling an "alert" or "status-level".

### Results

#### 1. Significant Signals

The table summarizes the events in the past 1.75 years that meet established criteria to be called either an "alert" or "x-level status". For purposes of semantics, low-level signals which meet the "C" and "D" levels are called "status-levels", and the larger signals which meet the "A" and "B" levels remain as "alerts".

#### 2. A-level alert of November 1993

In mid-November 1993, the Parkfield earthquake experiment had its second A-level alert where we advised the CA. Office of Emergency Services of a significant likelihood of a M6 earthquake at Parkfield. Figure 1 shows the location of the M4.8 earthquake that triggered this alert and its spatial relation with the previous A-level earthquake and the 1966 M6 mainshock.

#### 4. Publications

Roeloffs, E., J. Langbein, The earthquake prediction experiment at Parkfield, California, *Rev. of Geophysics*, 32, 315-336, 1994.

National Earthquake Prediction Evaluation Council (NEPEC) Working Group, Earthquake research at Parkfield, California, 1993 and beyond; Report of the NEPEC working group to evaluate the Parkfield Earthquake experiment, *US Geological Survey Circular*, 1116, 1994.

Table. 1993 Parkfield alerts.

Date	Location	Description	Size	Level	Comments
930212	Middle Mtn.	Earthquakes	M1.1	D	2 events in 72hrs
930215	Middle Mtn.	Earthquake	M2.5	C	
930216	Simmler	Earthquake	2.5	D	
930304	Middle Mtn.	Creep	0.6mm	D	at XMM1
930304	Middle Mtn.	Water Well	12.6cm	D	familiar combo
930313	Middle Mtn.	Earthquake	M3.5	B	Same loc. as 921026
930313	Parkfield	2-color		D	net contraction
930316	Parkfield	2-color		D	continuation
930403	Middle Mtn.	Earthquake	M4.4	B	2 km shallower than 921020
930406				D	step-down from B
930408	Middle Mtn.	Earthquake	M2.9	C	
930412	Middle Mtn.	Earthquake	M>2.4	C	2 events
930416	Middle Mtn.	Creep	0.7mm	D	at XMM1
930502	Middle Mtn.	Earthquake	M3.1	C	
930531	Middle Mtn.	Creep	<1mm	C	2 events >0.5 in 1 hour at XMD1 & XMM1
930715	Middle Mtn.	Earthquake	M1.8	D	
930804	Slack Canyon	Earthquake	M2.5	D	PKF region
930812	Middle Mtn.	Earthquake	M1.5	D	
930822	Middle Mtn.	Water Well	-6.5cm	D	minor creep xmd1
930823	Middle Mtn.	Earthquake	M1.2	C	2 events and combo rule
930827	Middle Mtn.	Earthquake	M1.9	D	
930927	Gold Hill	Earthquake	M3.5	C	
930929	Middle Mtn.	Water Well	4.7cm	D	
931017	Middle Mtn.	Creep and water	1.5mm	D	XMR1
931110	Middle Mtn.	Earthquake	M1.6	D	
931113	Middle Mtn.	Earthquake	M2.8	C	
931114	Middle Mtn.	Earthquake	M4.8	A	within 1km of 66 event
931115	Middle Mtn.	Earthquake	2 events M>1.5	C	
931118	Middle Mtn.	Earthquake	2 events M>1.5	C	
931122	Middle Mtn.	Earthquake	M1.5	D	
931126	Middle Mtn.	Earthquake	M1.6	D	
931130	Middle Mtn.	Earthquake	2 events M>1.5	C	
931201	Middle Mtn.	Water well	-10.6cm	C	combines with eq.
931204	NW of Middle Mtn.	Earthquake	M2.3	D	
931205	Middle Mtn.	Earthquake	M1.1	D	
921205	Middle Mtn.	Earthquake	M1.6	C	combine with 921204 event
931206	Middle Mtn.	Earthquake	M1.7	C	
931230	Middle Mtn.	Creep	1.2mm	D	XMD1

Note. Right lateral creep, water level rises, and compressive strain are positive.

1993 Combined Alert Totals: 1 A alert 2 B alert, 14 C alert, 20 D alerts.

Total alerts since beginning experiment: 2 A alert 4 B alert, 49 C alerts, 116 D alerts.

Table. 1994 Parkfield alerts.

Date	Location	Description	Size	Level	Comments
940104	Middle Mtn.	Earthquake	M1.5	D	
940125	Middle Mtn.	Earthquake	M1.5	D	
940128	Gold Hill	Earthquake	M2.5	D	
940211	Middle Mtn.	Earthquake	M2.1	D	
940215	Parkfield	Earthquake	M2.7	D	too shallow for C
940224	Middle Mtn.	Creep	0.7mm	D	XMM1 and water drop
940301	Middle Mtn.	Earthquake	M2.1	D	
940408	Middle Mtn.	Creep	0.6mm	D	XMM1
940420	Middle Mtn.	Earthquake	M2.5	C	
940427	Middle Mtn.	Creep	1.1mm	D	XMD1 and water drop
940531	Middle Mtn.	Earthquakes	M1.3	D	2 events >M1
940710	Middle Mtn.	Water level	13cm	D	0.4mm creep xmd1
940801	Middle Mtn.	Creep	0.8mm	D	XMM1
940901	Middle Mtn.	Creep	0.7mm	D	XMD1
940907	Middle Mtn.	Earthquake	M3.3	D	at 4km depth
941005	Middle Mtn.	Water level	5cm	D	
941107	Middle Mtn.	Creep	1.1mm	D	20ns change, too

Note. Right lateral creep, water level rises, and compressive strain are positive.

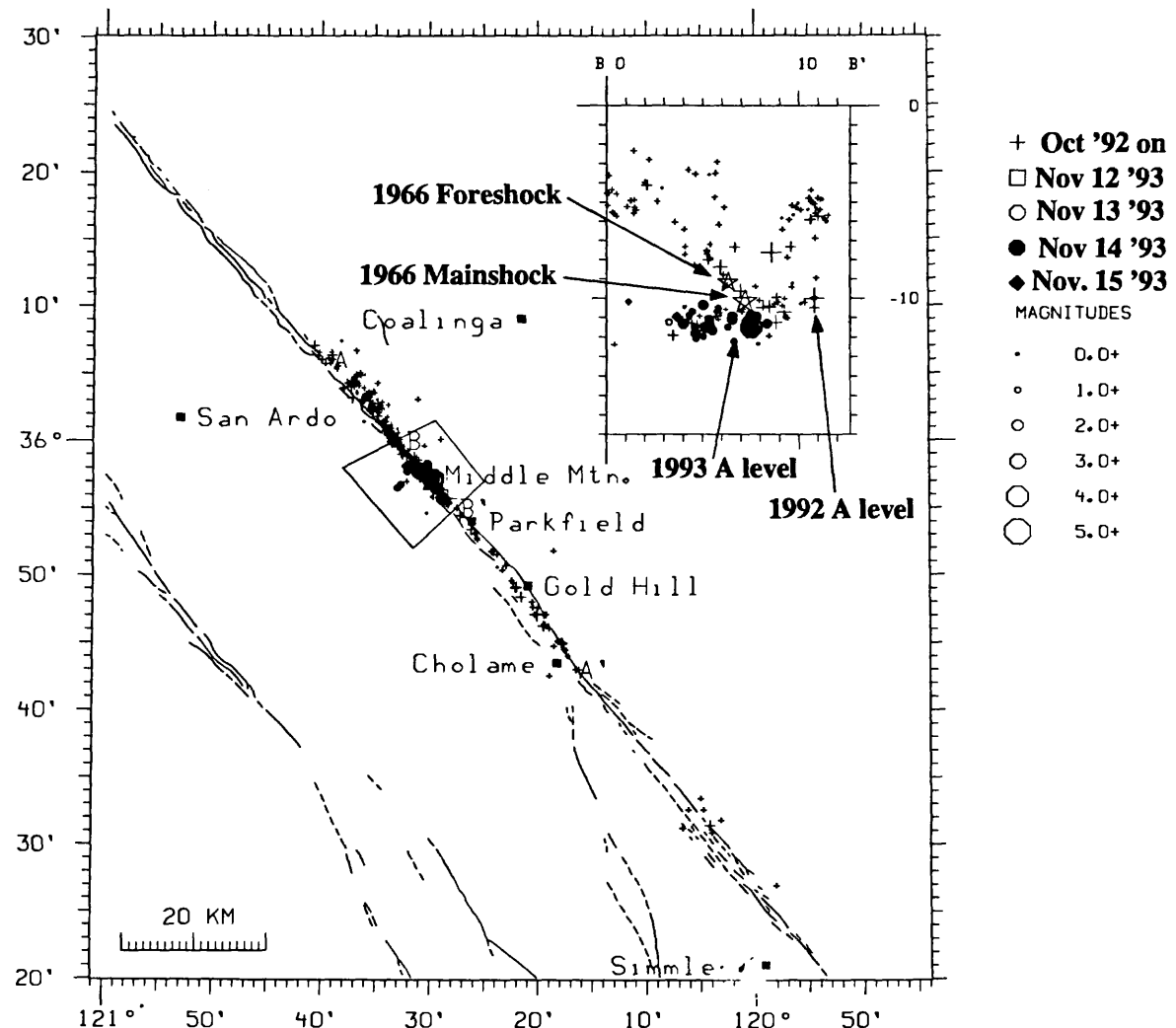
1994 Combined Alert Totals: 0 A alert 0 B alert, 1 C alert, 16 D alerts.

Total alerts since beginning experiment: 2 A alert 4 B alert, 50 C alerts, 132 D alerts.

This plot shows the seismicity associated with the two A level alert events in October 1992 and November 1993. This year's event is closer to the 1966 hypocenter than last year's event. The new seismicity in this plot stays within the aftershock pattern defined in the first few hours after the largest event. The magnitude of today's A level event is from 4.7 (USGS, NCSN) to 5.0 (UCB synthetic W-A). This plot is complete until 931115 1423. UT.

Andy Michael, USGS

October 1992 to Nov 15 '93 1423 UT



## RAPID QUANTIFICATION OF EARTHQUAKE FAULTING IN THE WESTERN U.S.

Award # 1434-94-G-2442

P.I.: Thorne Lay

University of California, Santa Cruz

Earth Sciences Department  
 Earth and Marine Science Building, UCSC  
 Santa Cruz, CA 95064

Phone: 408-459-3164  
 Fax: 408-459-2127  
 e-mail: thorne@earthsci.ucsc.edu

Program Element: II

## Investigations Undertaken:

Under this project, source parameters of moderate to large size ( $M_w > 4.5$ ) earthquakes in the western United States from 1992 to 1994 were determined by point-source moment tensor inversion of complete long-period ( $T > 35-50$  s) ground motions recorded at regional distances ( $1^\circ$  -  $12^\circ$ ). Stable long-period signals are obtained by lowpass filtering records from the very broad band seismometers recently deployed in several networks in western states (TERRAscope, operated by Caltech; BDSN, operated by U.C. Berkeley; and IRIS-University Stations). These filtered signals are dominated by fundamental mode Rayleigh and Love waves, which have very simple waveforms due to the limited dispersion on the short paths to regional stations. Since long-period motions are relatively insensitive to the attenuation model and crustal structure used in the inversion, they provide robust constraints on the seismic moment and faulting geometry as long as adequate azimuthal coverage is available.

Comparisons of solutions for 21 events with results of other regional and teleseismic wave inversions were made to assess the model dependence and uncertainties of our Regional Centroid-Moment Tensor (RCMT) solutions. RCMT inversion has limited source depth resolution for shallow crustal events, but the focal mechanism and seismic moment determinations prove quite stable over a range of source depths in the crust, as well as over a range of crustal propagation models. Simultaneous waveform inversion of shorter period body wave signals can improve the source depth resolution. By applying path corrections for heterogeneous crustal structure, shorter period surface wave energy can also be inverted, allowing the methodology to be extended to lower magnitude regional events as well. The RCMT procedure requires minimal signal processing, only a sparse broadband network, and a simple laterally homogeneous propagation model, thus it can readily be automated and applied in near real-time to events in the magnitude range from 4.5 to 7.5 distributed over an area as large as the western U.S.. We are presently collaborating with broadband array operators in Mexico, Japan, and Alaska to implement our methodologies in their local routine analysis of regional faulting.

An additional detailed analysis of the 21 September, 1993 Klamath Falls earthquake sequence in Oregon was undertaken in collaboration with researchers at the University of California, Berkeley. A variety of waveform analysis methods was applied to the mainshock/aftershock sequence, for events ranging in size from  $M_w = 3.8-6.0$ . An empirical Green function inverse method was applied to estimate kinematic source parameters of the two  $M_w = 6.0$  mainshocks. Both events were found to have ruptured northwestward on adjacent segments of the Lake of the Woods system of normal faults. The two mainshocks abut in the vicinity of a  $10^\circ$ - $20^\circ$  clockwise rotation of the fault system, which may have initially acted as a barrier, preventing a larger through-going event.

## Results:

The Regional Centroid Moment Tensor (RCMT) procedure is the regional counterpart to the teleseismic CMT method used by Harvard, as it involves moment tensor inversion of long-period seismic waveforms stabilized by simultaneous relocation of the epicenter and a centroid time shift. The basic theoretical framework for such moment tensor inversions is unchanged from the CMT development. The theoretical seismograms are computed by either normal mode summation or wavenumber integration, and various source velocity models have been considered. Regional long-period ( $T > 35-50$  s) ground motions such as in Figure 1, are dominated by  $P_{nl}$  and fundamental mode surface waves. The overlap of body wave phases and fundamental mode surface waves in the filtered regional waveforms complicates a separate windowing of body waves and surface waves, as in teleseismic CMT inversions, so complete long-period ground motions are inverted in RCMT. Three component recordings are used to exploit the radiation patterns of Rayleigh and Love waves and the relative excitation of long-period surface waves and body waves.

The data going into the inversion are bandpass filtered VBB displacement records of 10-15 minute duration from BDSN, TERRAscope and IRIS/University stations for western United States earthquakes with  $M_w > 4.5$ . Earthquakes with  $M_w > 5$  excite seismic periods longer than 50 s well above noise levels, so a lowpass filter with this cut-off is usually used, although for events larger than magnitude 7 it is useful to filter more heavily. Recordings at distances up to 1500 km span less than 7 wavelengths for  $T > 50$  s so that effects of dispersion, attenuation and focusing are relatively small. Therefore accurate simulation of regional long-period waves can be achieved even with laterally homogeneous velocity models as simple as a layer over a halfspace. Smaller magnitude earthquakes ( $M_w = 4.5-5.1$ ) can be analyzed using somewhat shorter periods ( $T > 35$  s) without requiring a detailed crustal model by restricting to stations within 300 km of the earthquake. Given the numerous VBB stations available in the western U.S., we select the highest quality waveform data, eliminating noisy traces, and retaining about 4-6 well distributed stations to ensure stable inversions. Adequate sampling of the Love and Rayleigh wave radiation patterns is critical to obtaining a stable solution. Inclusion of additional stations is straightforward, but typically has little effect on the solutions.

Errors in origin time, earthquake mislocation, effects of source finiteness, and inaccurate velocity model cause phase misalignments between observed and point-source synthetic seismograms, complicating accurate estimation of the moment tensor with time domain inversion methodologies. The Centroid Moment Tensor (CMT) inversion strategy effectively reduces phase misalignments by combining the inversion for moment tensor with an optimization of "centroid location", which includes epicenter and origin time. RCMT inversions using the PREM model typically yielded epicentral relocations of 5-15 km and positive origin time shifts of 8-12 s, with the time shifts being fairly uniform throughout the region. These systematic biases result from the 21.4 km thick crust and 3 km thick water layer in PREM, which is a poor approximation to the shallow structure in the western United States. The origin time shift absorbs most of the phase misalignments caused by using the PREM model while the epicentral relocations are relatively unimportant in the inversion optimization given the low frequency signals that are used. Of course it is not necessary to use PREM, and we have now incorporated more realistic regional crustal models.

For the applications in this project, we omit optimization of epicentral location, based on an analysis of the stability of our long period inversions for various crustal models and focal mechanisms, but we still optimize the centroid time by cross correlation of waveforms or waveform envelopes. Source depth is estimated by searching over trial depths, as in most inversion methods. We use a wavenumber integration method to construct the complete regional synthetics, since it is cumbersome to compute complete normal mode data sets for various crustal models. For all of the earthquakes studied we perform RCMT inversions using three models; WUS, SC and PREM. Model WUS, developed from phase velocity measurements of surface waves through the western U.S (Charles Ammon, personal communication, 1993), and model SC (developed in Southern California) differ in average crustal velocities by 5%, but nonetheless result

in very comparable moment tensor solutions and variance reductions. Model PREM, with a thinner crust than WUS and SC, results in somewhat poorer waveform fits although the best-fitting focal mechanisms are very similar to those obtained with WUS and SC. The effects of the velocity model on the estimates of source depth and seismic moment can be best understood by considering inversion results for the various models.

Inversions for a selection of 21 earthquakes in 1992-1994 (Table 1) are considered. These events are well-distributed throughout the western United States, range in magnitude from 4.5 to 6.6 and have variable mechanisms (Figure 2). Examples of the waveform fits achieved for two of the larger events in the Western U.S. in the last two years are shown in Figure 3. The simple long-period signals can be very well modeled and give good resolution of the source parameters without the need for detailed crustal structure information on each path (which is not available for most paths). Solutions from other regional wave inversion methods and the Harvard teleseismic CMT solutions for the larger earthquakes are available for comparison. In general, we find (Figure 4) quite good agreement in the overall focal mechanism geometry between the results of different methods. Many of the isolated cases of significant disagreement have been investigated and can be attributed to poor signal quality, limited azimuthal coverage, or other limitations that may apply to either all or specific methodologies. We have analyzed in the detail the relative estimates of source depth and seismic moment, finding that scatter of around 5 km in source depth and 50% in seismic moment exist between different methods (Figure 5). The results of the RCMT method are generally intermediate, and appear to be particularly stable due to the excellent quality of the data used in each inversion. We use model WUS for most events, but model SC is used for some southern California events (Table 2).

Preliminary results have been obtained using regional short-period phase velocity tomography models to develop path specific corrections, which are introduced into the waveform inversion. This appears to hold promise for enabling inversion of periods as short at 10-20 s in the RCMT procedure, as long as a suitable phase velocity model is available. We have also performed simultaneous inversion of the long-period information and windowed broadband shorter-period body wave signals, such as Pnl, which has the potential to improve both source depth and focal mechanism resolution. Work on these areas is continuing.

The work described here has been submitted for publication in two articles:

Ritsema, J., and T. Lay, Long-period regional wave moment tensor inversion for earthquakes in the Western United States, *J. Geophys. Res.*, submitted August 18, 1994.

Dreger, D.S., J. Ritsema, and M. Pasmanos, Broadband analysis of the 21 September, 1993, Klamath Falls earthquake sequence, *Geophys. Res. Lett.*, in press, 1994.

## St George-Utah at ANMO

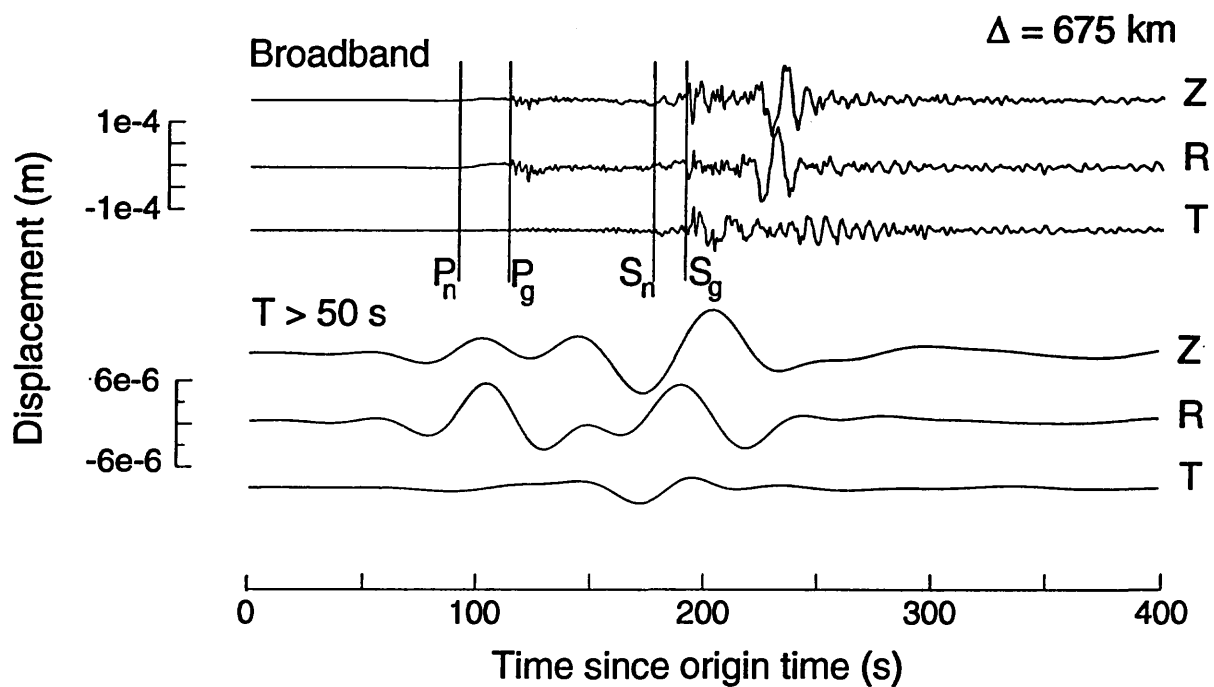


Figure 1. Vertical (Z), radial (R), and transverse (T) component recordings of the St. George, Utah earthquake at station ANMO (Albuquerque, New Mexico). Top: Broadband displacements. Bottom: low pass ( $T > 50$  s) filtered displacements.

## Western United States earthquakes 1992-1994

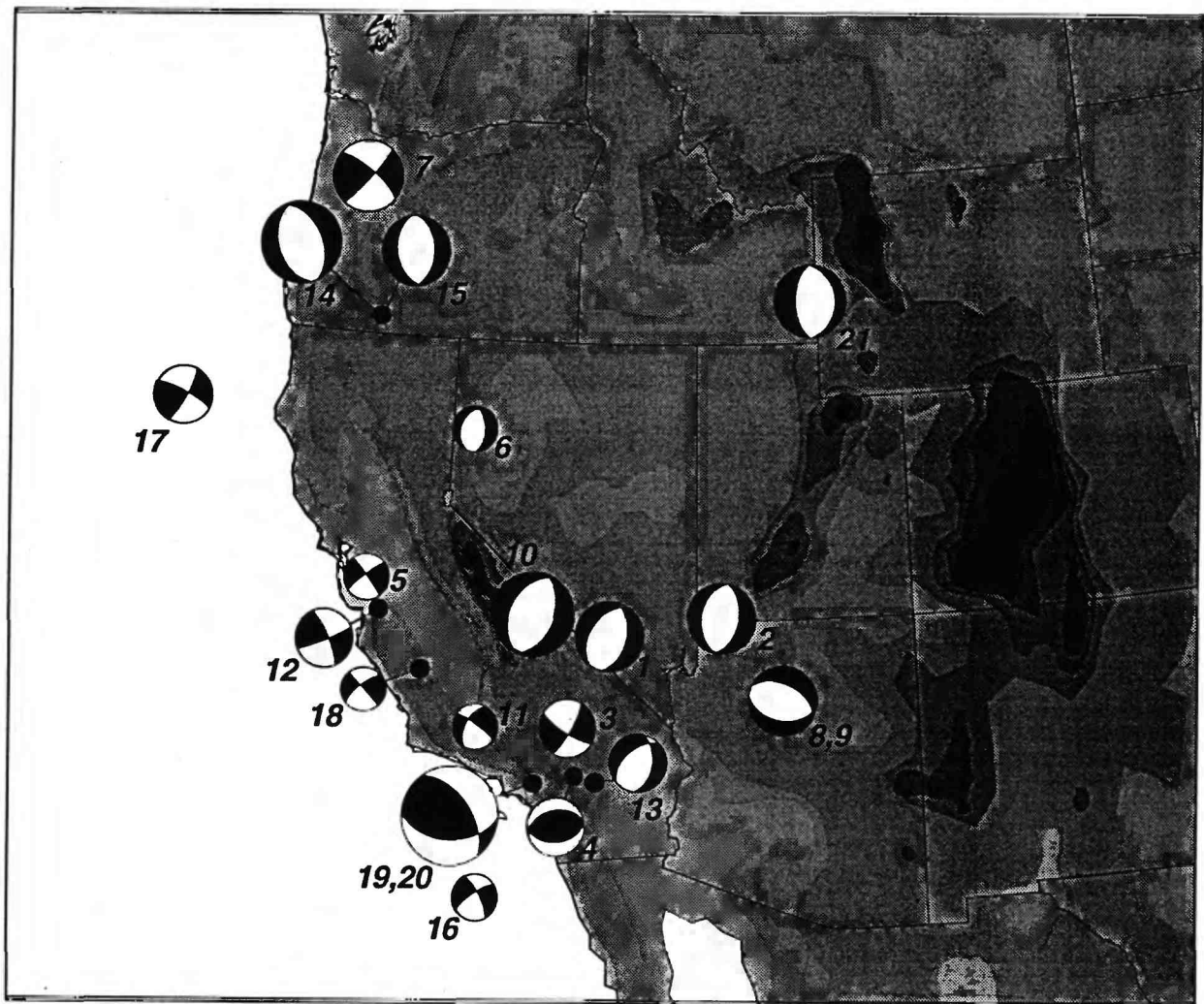


Figure 2. Focal mechanism and epicentral location of earthquakes studied.

## Event 10: Eureka Valley, 17 May 1993

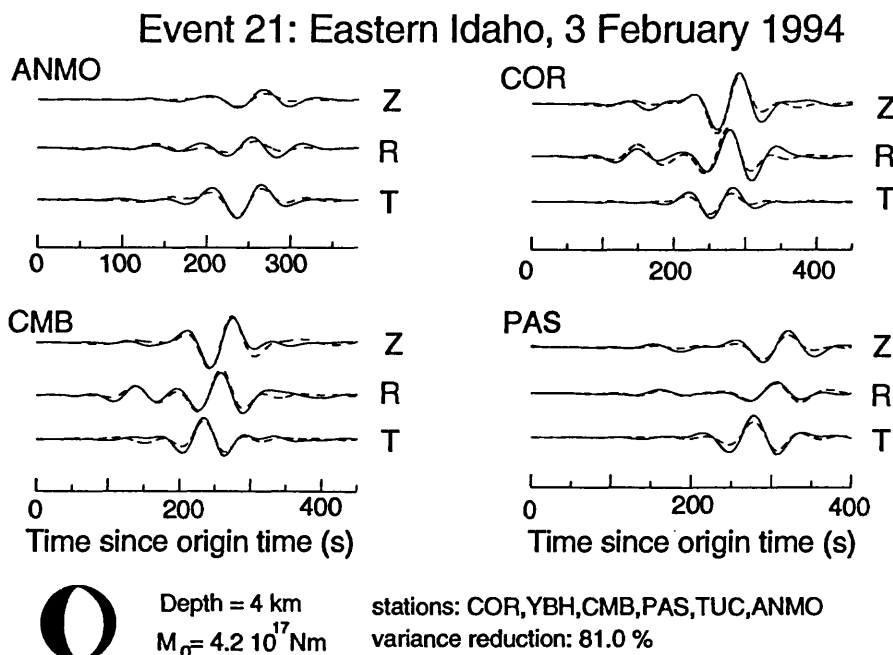
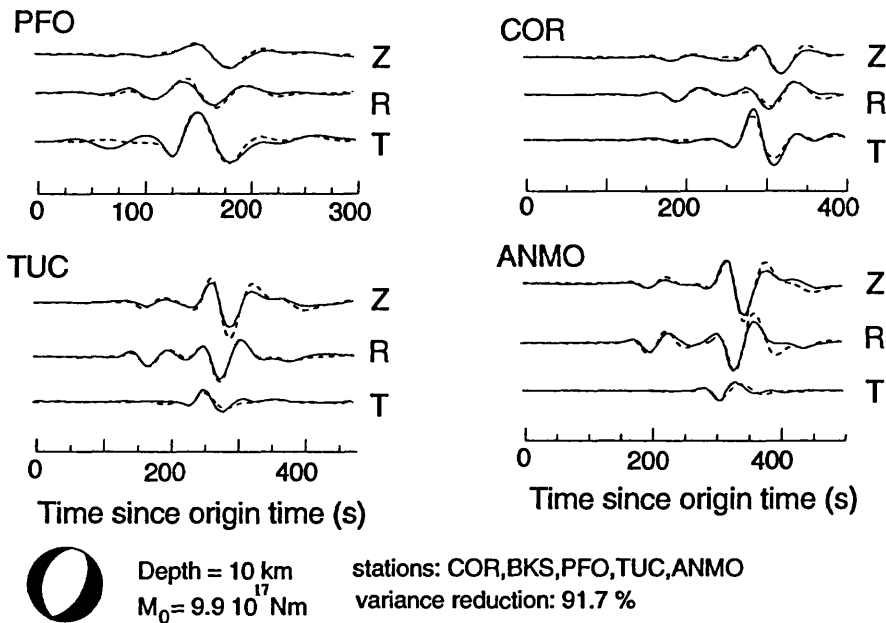


Figure 3. Waveform fit (dotted lines) to observed (solid lines) vertical (Z), radial (R) and transverse (T) component waveforms of events 10 and 21. Waveforms are analyzed at  $T > 50$  s. Best fitting source mechanism is given below the waveform fit.

## Comparison of focal mechanism

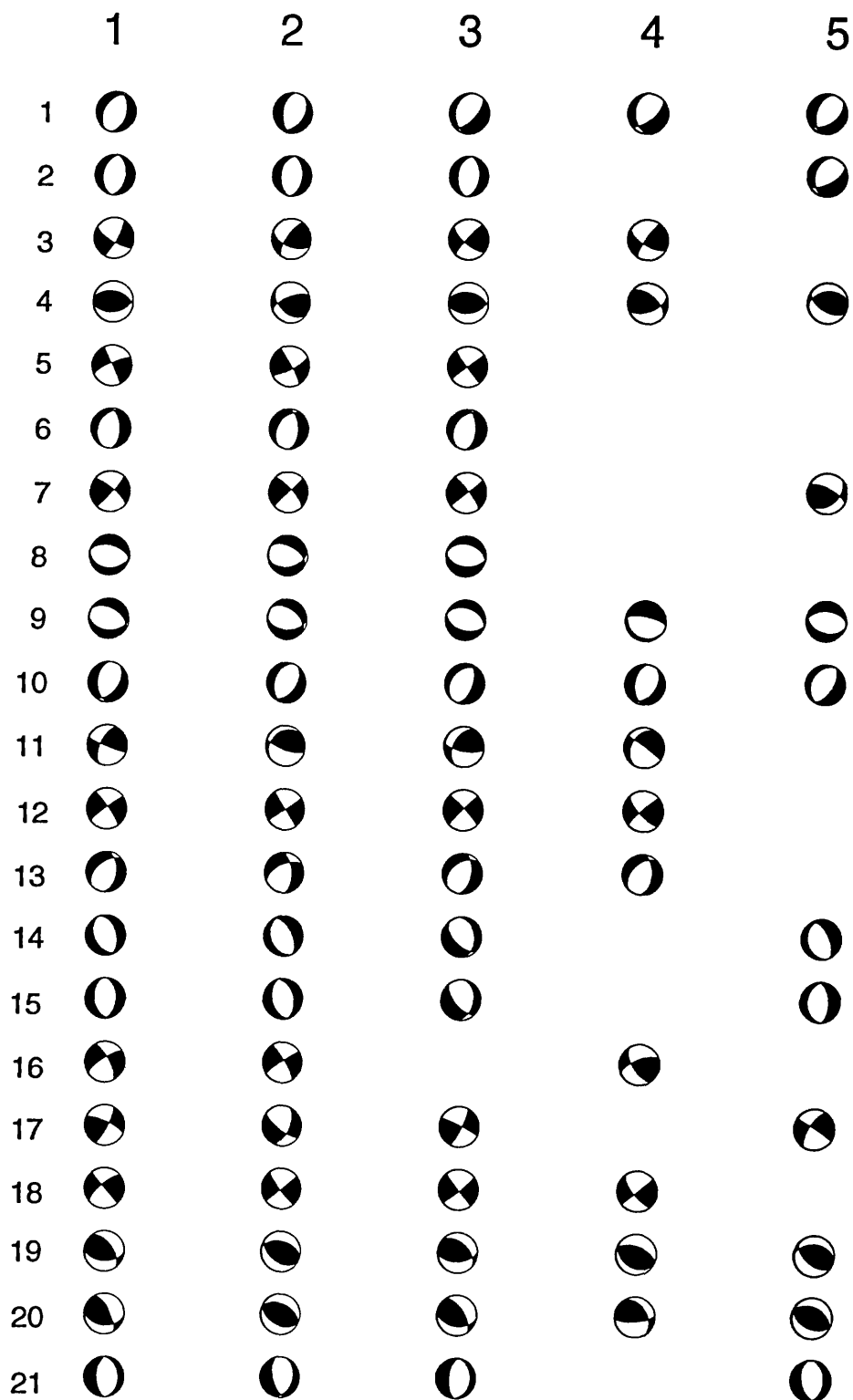


Figure 4. Comparison of best double couple focal mechanisms obtained with method 1 (RCMT), method 2 (time domain body waveform inversions by Doug Dreger), method 3 (short-period surface wave spectral inversions by Mike Pasyanos), method 4 (short-period surface wave spectral inversions by Hong-kie Thio), and method 5 (Harvard CMT).

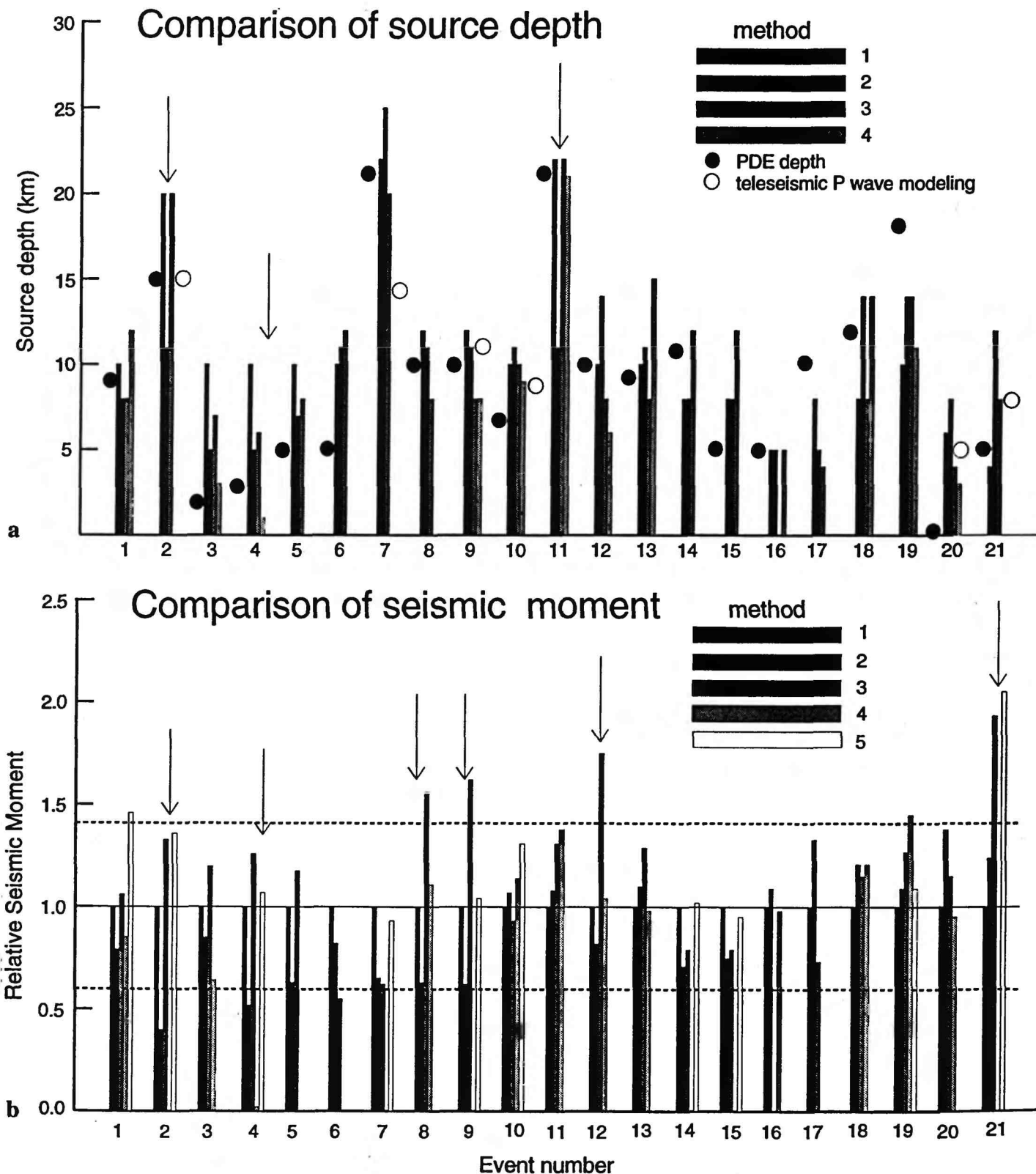


Figure 5. a. Comparison of source depth estimates from methods 1, 2, 3, 4, 5, PDE depths, and depths estimated by teleseismic body waveform modeling (see Figure 4 for definition of methods). Arrow highlight significant discrepancies. b. Comparison of seismic moments relative to RCMT (solid horizontal line). The dotted line represents an estimated 40% seismic moment uncertainty for RCMT.

## Microearthquake Data Analysis

4-9930-10053

W. H. K. Lee  
U.S. Geological Survey  
Branch of Seismology  
345 Middlefield Road, Mail Stop 977  
Menlo Park, California 94025  
(415) 329-4781

### Investigations

The primary focus of this project is the development of state-of-the-art computation for analysis of data from microearthquake networks. For the past twelve months I have been involved in:

- (1) Northridge Aftershocks. Shortly after the January 17, 1994 Northridge, California earthquake, a dense seismic array was deployed to study the site response in the Northridge area using the aftershocks as natural sources and also explosives and a shear wave generator as artificial sources. three sites were occupied: Tarzana, VA Hospital, and Potrero Canyon. We found large variations of ground motion on scale of tens of meters, especially at Tarzana. The processed data were released in May, 1994, in Lee et al. (1994), and were used in papers presented in (Spudich et al, 1994, Lee et al. 1994, and Spudich, Hellweg and Lee, 1994).
- (2) San Francisco Bay Faults. A search of San Francisco Bay Faults using on-shore high-resolution seismic imaging along the San Mateo Bridge, Foster City, California was conducted in collaboration with R. D. Catchings and M. Rymer. A paper summarizing the preliminary results is given by Catchings et al. (1994). The high-resolution seismic imaging was conducted using a PC- based seismic system designed by me.
- (3) Site Response in Santa Cruz. I also provided a PC-based seismic system to Williams et al. (1994) to conduct site response study in Santa Cruz, California.
- (4) Landers Fault Zone Studies. A joint experiment with the Southern California Earthquake Center was conducted to study the Landers Fault Zone using a dense seismic array designed by me. Some results of this study have been published in Li et al. (1994a; 1994b).
- (5) Design and Implementation of a Prototype Earthquake Warning System for Taiwan. Under a cooperative program between USGS and the Taiwan Central Weather Bureau, a prototype earthquake warning system has been implemented. A modern digital seismic network with rapid response time (10-20 sec after an earthquake occurred) was installed in the Hualien area of Taiwan by Nanometrics of Canada under my supervision. At the same time, Quanterra is under contract to supply three broad-band digital seismic stations of our specification. The Hualien network and the broad-band stations have been in operation since summer of 1994. We are now testing the reliability of hardware and software.
- (6) Training Course on PC-Based Seismic Systems. A one-week training course on how to design, implement, and operate PC-based seismic systems was conducted by me in October, 1994. The course was attended by over 30 seismologists from seven countries, including about 10 professors.

### Reports

- (1) Lee, W. H. K., (1994). A project implementation plan for an advanced earthquake monitoring system in Taiwan, Report submitted to the America Institute in Taiwan, 89 pp., May 1993; U. S. Geological Survey Open-File Report, 94-004, 89 pp.
- (2) Lee, W. H. K., White, D. H., Harlow, D. H., Rogers, J. A., and Spudich, P., (1994). Digital Seismograms of selected aftershocks of the Northridge earthquake recorded by a dense seismic array on February 11, 1994 at Cedar Hill Nursery in Tarzana, California, U. S. Geological Survey Open-File Report, 94-234, 78 pp.

- (3) Spudich, P., Harlow, D., Lee, W. H. K., Rogers, J., and White, R., (1994) . Strong site effects observed at the Tarzana accelerograph site using aftershocks of the 1994 Northridge, California earthquake: Implications for microzonation (Abstract), SSA 94 Program for Northridge Abstracts, No. 55.
- (4) Lee, W. H. K., Catchings, R. D., Gibbs, J. F., Spudich, P., and White, R. A., (1994). Observations of Northridge aftershocks and artificial sources in Tarzana, California, using a dense seismic array (Abstract), EOS, V75, No. 44, p. 167.
- (5) Spudich, P., Hellweg, M., and Lee, W. H. K., (1994). Directional site resonances and topographic effects observed at the Tarzana accelerograph site using aftershocks of the 1994 Northridge, California earthquake, (Abstract), EOS, V. 75, No. 44, p 167.
- (6) Williams, R. A., Pratt, T. L., Cranswick, E., Carver, D. L., Worley, D. M., and Lee, W. H. K., (1994). Preliminary site response in Santa Cruz, California, using controlled seismic sources, (Abstract), EOS, V.75, No. 44, p. 447.
- (7) Catchings, R. D., Kohler, W. M., Rymer, M., and Lee, W. H. K., (1994). A search for San Francisco Bay faults using on-shore high-resolution seismic imaging along the San Mateo Bridge, Foster City, California, EOS, V. 75, No. 44, p. 684.
- (8) Li, Y. G., Aki, K., (1994a). Seismic guided waves trapped in the fault zone of the Landers, California earthquake of 1991, Journal. Geophys. Res., V. 99, p 11705-11722.
- (9) Li, Y. G., Vidale, J. E., Aki, K., Marone, C. J., and Lee, W. H. K., (1994b). Fine structure of the Landers fault zone: segmentation and the rupture process. Science, V. 265, p. 367-370.

# Investigation of Stress Regimes and Crustal Fracturing in the Los Angeles Basin Based on Shear-Wave Splitting Data

1434-94-G-2462  
Program Element I

Yong-Gang Li  
University of Southern California  
Southern California Earthquake Center  
Los Angeles, CA 90089-0740  
213-740-3556; Fax: 213-740-8801  
e-mail: [ygli@coda.usc.edu](mailto:ygli@coda.usc.edu)

## INVESTIGATION

Our investigation has two main objectives: 1. to map subsurface stress regimes in the Los Angeles basin and 2. to evaluate the crustal crack density beneath the basin using shear-wave splitting data. We also search for probable temporal changes of shear-wave splitting associated with major earthquakes in the Los Angeles basin and adjacent areas.

The Los Angeles basin is located at the juncture of the east-west trending Transverse Ranges and the northwest trending Peninsular Ranges (Figure 1), and is currently undergoing the N-S compression. It consists of a deep central basin, with folded and uplifted eastern, northern and southwestern flanks. The basin is filled with a thick section of Tertiary and Quaternary sedimentary rocks (up to the depth of 9 km in the central basin). The major Holocene surficial faults in the basin are the Newport-Inglewood fault and Whittier fault; both of them are strike-slipping at depth. The Santa Monica and Sierra Madre fault systems are northward dipping reverse faults. Many strands of these systems do not break the earth's surface, instead being draped with fault propagation folds. Thus, apparently the style of deformation in the basement beneath the Los Angeles basin may be distinctly different from that in the sedimentary section and cannot be easily inferred from near-surface observations.

Within this tectonic framework, the relatively high seismicity of the Los Angeles basin is characterized by scattered foci. Most of the large earthquakes in the basin area appear to be located below the sedimentary layers, with the maximum depth of the seismogenic zone at about 18 km. Recent major seismic events in the great Los Angeles basin area, including the 1971 M6.6 San Fernando, 1987 M5.9 Whittier Narrows, 1989 M4.6 Montebello, 1990 M5.5 Upland, 1991 M5.8 Sierra Madre and 1994 M6.8 Northridge earthquakes, attest the existence of active faulting in apparent response to regional N-S compression. This compression can be expected to preferentially open vertical microcracks whose long dimensions are in the N-S direction.

Geological observations in various tectonic regimes demonstrate the existence of near-vertical planes of fluid-filled cracks which are aligned parallel to the direction of the maximum compressive stress as determined by macrostructural criteria. Microcracks are

opened by crustal fluids and remain open in the direction of the least principal stress. Because of their small dimensions and low elastic stiffness, microcracks can, in principle, respond to changes in regional or local stress and strain. This relationship between microcracks and crustal fluids and their potential response to contemporary crustal stress and strain has been mentioned as a possible precursor of earthquake. A prominent feature of fracture-related rock is effective seismic anisotropy due to aligned fractures and microcracks. In the cracked medium, the shear wave is retarded if the shear displacement vector is normal to planes of weakness that exist for aligned microcracks. In contrast, the shear wave with displacement parallel to planes of weakness is advanced.

In the present research, we use shear-wave splitting data from earthquakes occurring beneath the Los Angeles basin to investigate the stress regimes and crustal fracturing at depth, and to search for evidence of temporal variations in shear-wave splitting associated with major earthquakes in the region.

## RESULTS

We completed a systematic analysis of three-component seismograms from earthquakes occurring beneath the Los Angeles basin during a period from 1988 to the present. The data used in this study are recorded at ten three-component stations of the USGS/USC Los Angeles Basin Seismic Network which has seventeen stations in the basin and adjacent areas, including twelve three-component stations (Fig. 1, top). Most three-component stations are changed from single-component stations recently. Stations SCS, LNA and SAT are located in the sedimentary basin. Stations DHB, IPC, LCL and RCP are located along the Newport-Inglewood fault. Station PVP is located near the Palos Verdes fault. Station FLA is located in the vicinity of the Whitter fault. Station GFP is located on the border of the Santa Monica fault. DHB, FLA, LCL, PVP, SAT are borehole stations at depths of 415 m, 436 m, 98 m, 25 m and 396 m, respectively. SCS is a multi-station site in the campus of USC.

In this study, we examined seismograms from ~500 earthquakes occurring within shear-wave windows (Within the shear-wave window, the affect of S-P conversion at ground surface on shear-wave splitting observation can be avoided.) of ten stations using the ratio method for an objective analysis of shear-wave splitting data. This method is defined as the ratio of the total projections of particle displacements onto a pair of orthogonal axes in a time window between the two split shear wave arrivals. It is calculated as a function of azimuth on a plane perpendicular to the direction of wave propagation. The maximum ratio indicates the azimuth of the most linear particle motion. The results from three-component data recorded at site SCS during 1988 to 1993 have been reported in our paper (Li et al., 1994).

Fig. 3 and Fig. 4 show new results from a systematic analysis of the data recorded at ten stations. The data show 20 to 160 ms shear-wave splitting for earthquakes occurring at depths 5 to 20 km beneath the Los Angeles basin. Shallow events exhibit little splitting, while deeper events show progressively greater splitting with depth (Fig. 2). The preferred polarization of the fast shear wave is either nearly in N-S which is consistent with the direction of the regional maximum horizontal compressive stress or in the direction of local subsurface fault strikes at station GFP and PVP (Fig. 1, bottom). We interpret that the shear-wave splitting is caused by liquid-filled crustal microcracks

aligned in the N-S direction or macrofractures associated with the local faulting. The subsurface stress axes inferred from the shear-wave splitting data are consistent with results from geological mapping and fault plane solutions in the Los Angeles basin area. The shear-wave splitting observed in the Los Angeles basin area is ~2-8 ms/km, with the higher value at the north end of the Newport-Inglewood fault.

Ray-trace modeling (Li et al., 1994) indicates that observations of shear-wave splitting can be explained in terms of an anisotropic crust containing vertical cracks with the crack density of 0.03-0.06, with a higher crack density at the northwestern part of the Los Angeles basin. It infers the northwestern part of the basin is undergoing a higher stress level than the other part of the basin.

Shear-wave splitting data also show fairly rapid changes in delay times of the slow shear wave during the Montebello earthquakes of 1989 (Fig. 4), which occurred within the shear-wave window of station SCS. The delay time sharply decreased from 70 ms to less than 20 ms after the mainshock and then returned to the average level gradually. This rapid variation of shear-wave splitting might be resulted from stress-induced modification to crack geometry and changes in pore-fluid velocity near the source region. The aspect ratio of fluid-filled cracks might abruptly decrease in response to the local stress relaxation during the mainshock. We also observed somewhat changes of shear-wave splitting (~2 ms/km) before and after the Northridge earthquake of 1994 at stations IPC, SCS and DHB which are located in the northwestern Los Angeles basin about 20 to 30 km away from the source region (Fig. 4). We plan to conduct a systematic examination of the data recorded by portable instruments deployed at San Fernando Valley before and after the Northridge mainshock for further understanding if the shear-wave splitting may be a possible earthquake precursor.

## PUBLICATIONS AND REPORTS

- Li, Y. G., T. L. Teng and T. L. Henyey, Shear-wave splitting observations in the Northern Los Angeles basin, southern California, Bull. Seism. Soc. Am., V84, No. 2, 307-323, 1994.
- Li, Y. G. and T. L. Henyey, Shear-wave splitting observations in the source area of the Northridge, California, earthquake of 1994, Seis. Res. Lett., V65, No.1, Program for Northridge Abstract, p18, 1994.
- Li, Y. G. and T. L. Henyey, Observations of shear-wave splitting in source areas of 1992 Joshua Tree and Big Bear Earthquakes, EOS, Trans. Am. Geophys. Union, V73, No. 42, p382, 1992.
- Li, Y. G. Shear-wave splitting in the Los Angeles basin, California, in preparation.

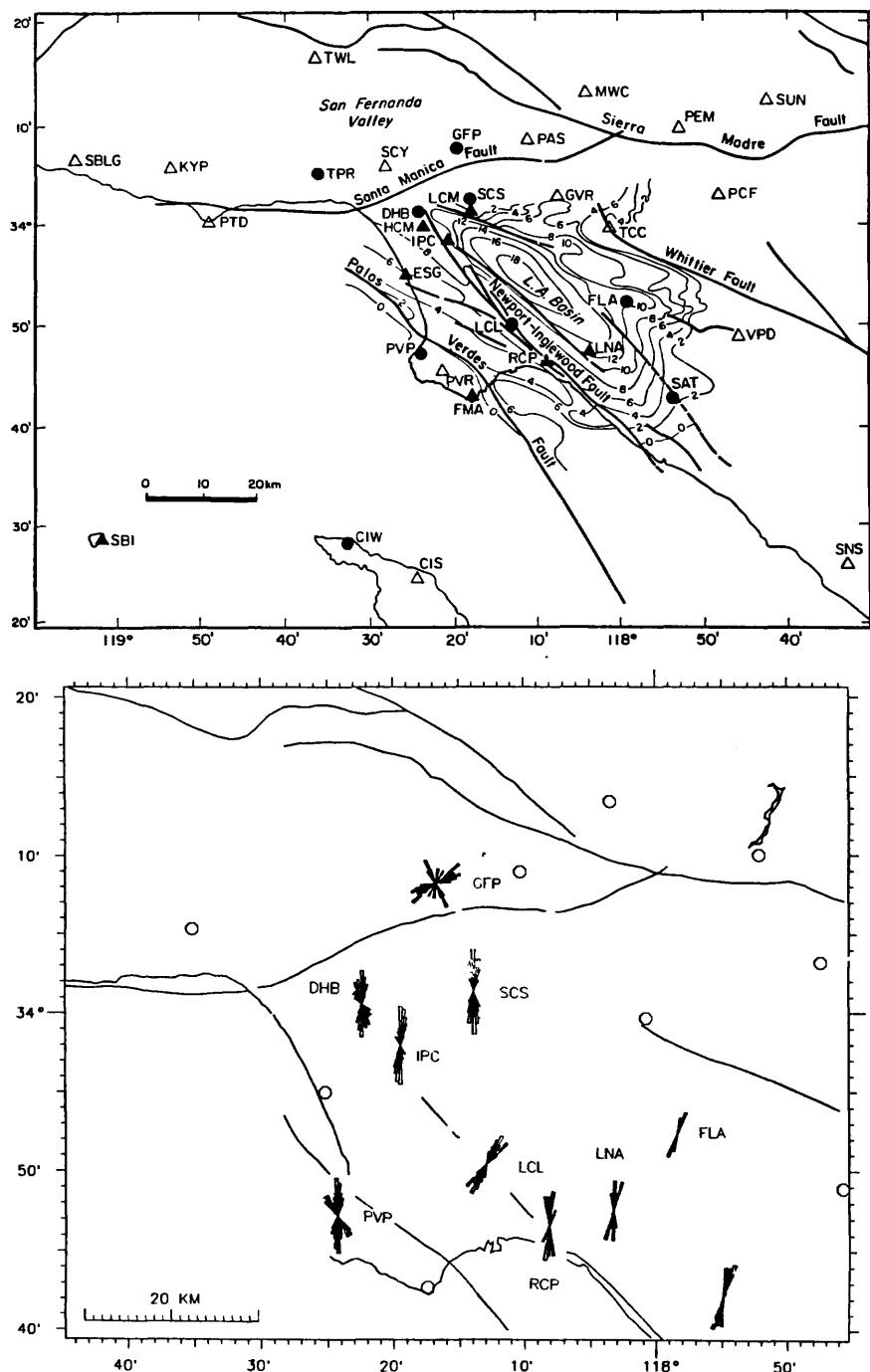


**Fig. 1** Top: An overview of the Los Angeles basin and adjacent areas. The major surficial faults in this area are plotted by solid lines. Structure-contours on base of Repetto formation, a lower Pliocene horizon (ca. 4.5 Ma) are plotted by thin lines with the contour interval of 2000 ft (adapted from Wright, 1991). Solid circles and triangles are three-component and single stations of the Los Angeles basin seismic network, respectively. Open triangles are stations of the USGS/Caltech southern California seismic network. Bottom: The map shows rose diagrams of polarizations of fast shear waves for earthquakes within shear-wave windows of ten three-component stations on the lower hemisphere out of 50°.

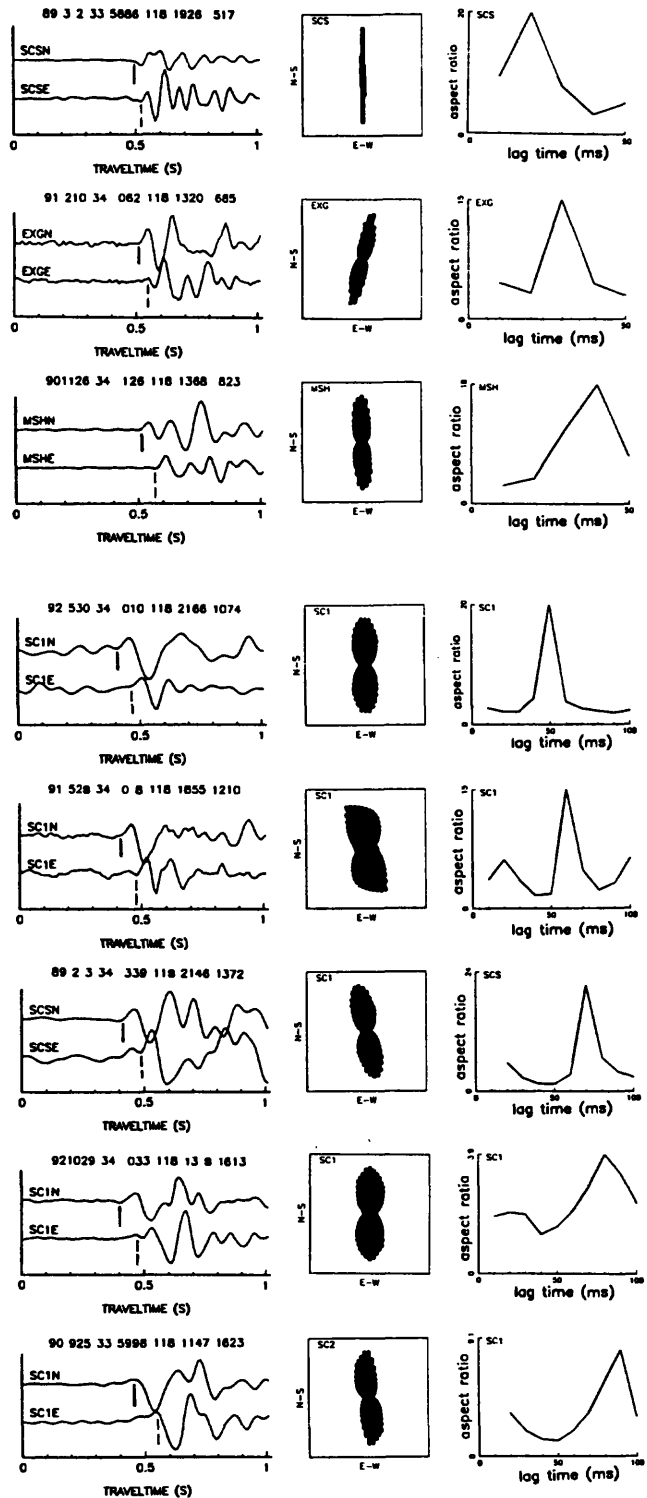


**Fig.2** Left: Horizontal components of seismograms from earthquakes within the shear-wave window of station SCS, and with increasing focal depths from 5.2 km to 18.2 km (from the top to bottom frame). Solid lines denote onsets of the fast shear waves while dashed lines denote onsets of the slow shear waves. Middle: Ratio diagrams corresponding to seismograms to left. Right: Plots of ratio vs. lag time for these events. The peak ratio corresponds to the time separation between two split shear-waves.

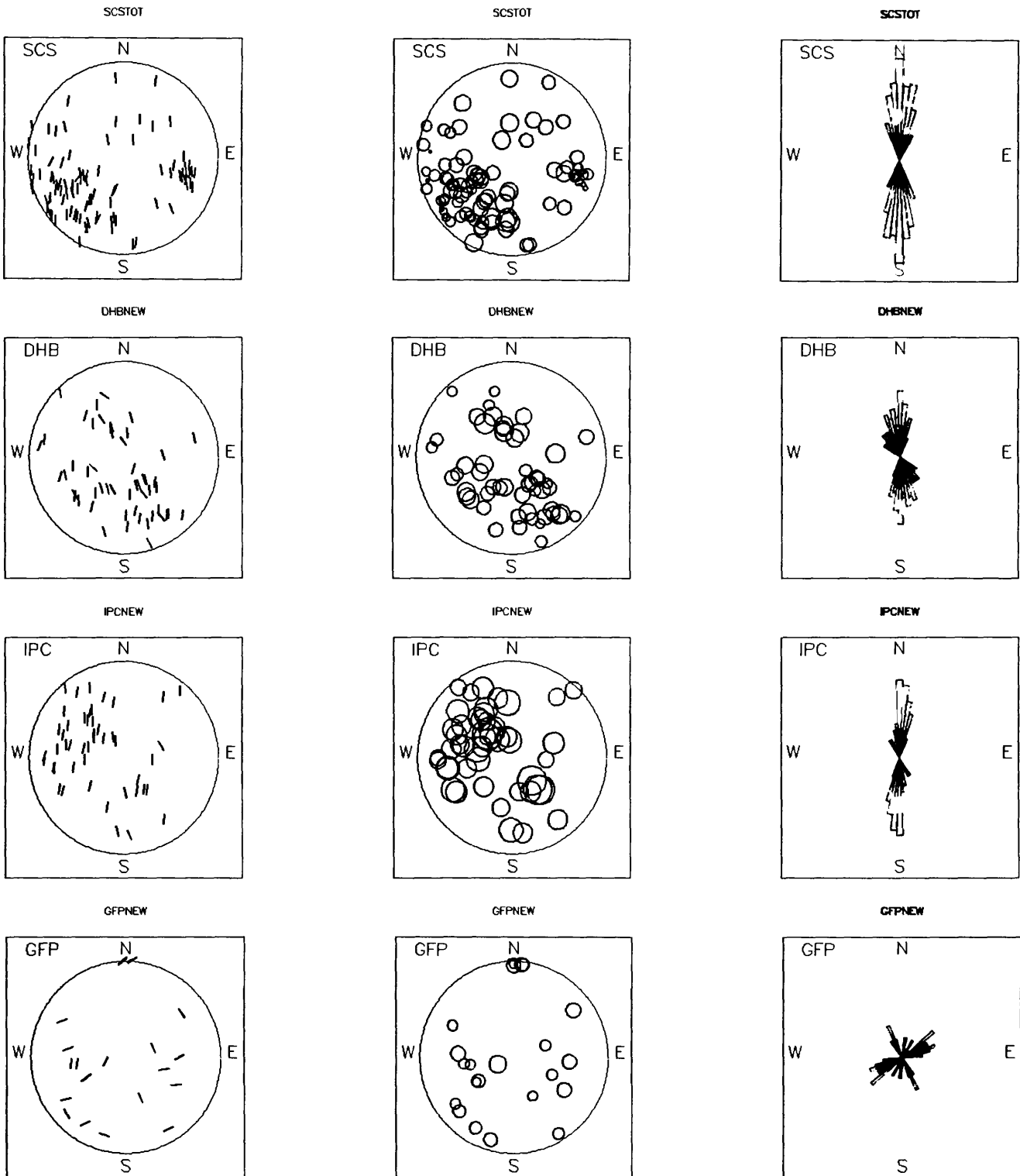


**Fig. 3** Left: Equal-area projections of polarizations of the fast shear waves from earthquakes within shear-wave windows of eight stations SCS, DHB, IPC, GFP, PVP, LCL, LNA and RCP (from the top to bottom frame). Middle: Equal-area projections of normalized time separations between two split shear waves from events within the eight shear-wave windows on the lower hemisphere out of 50°.

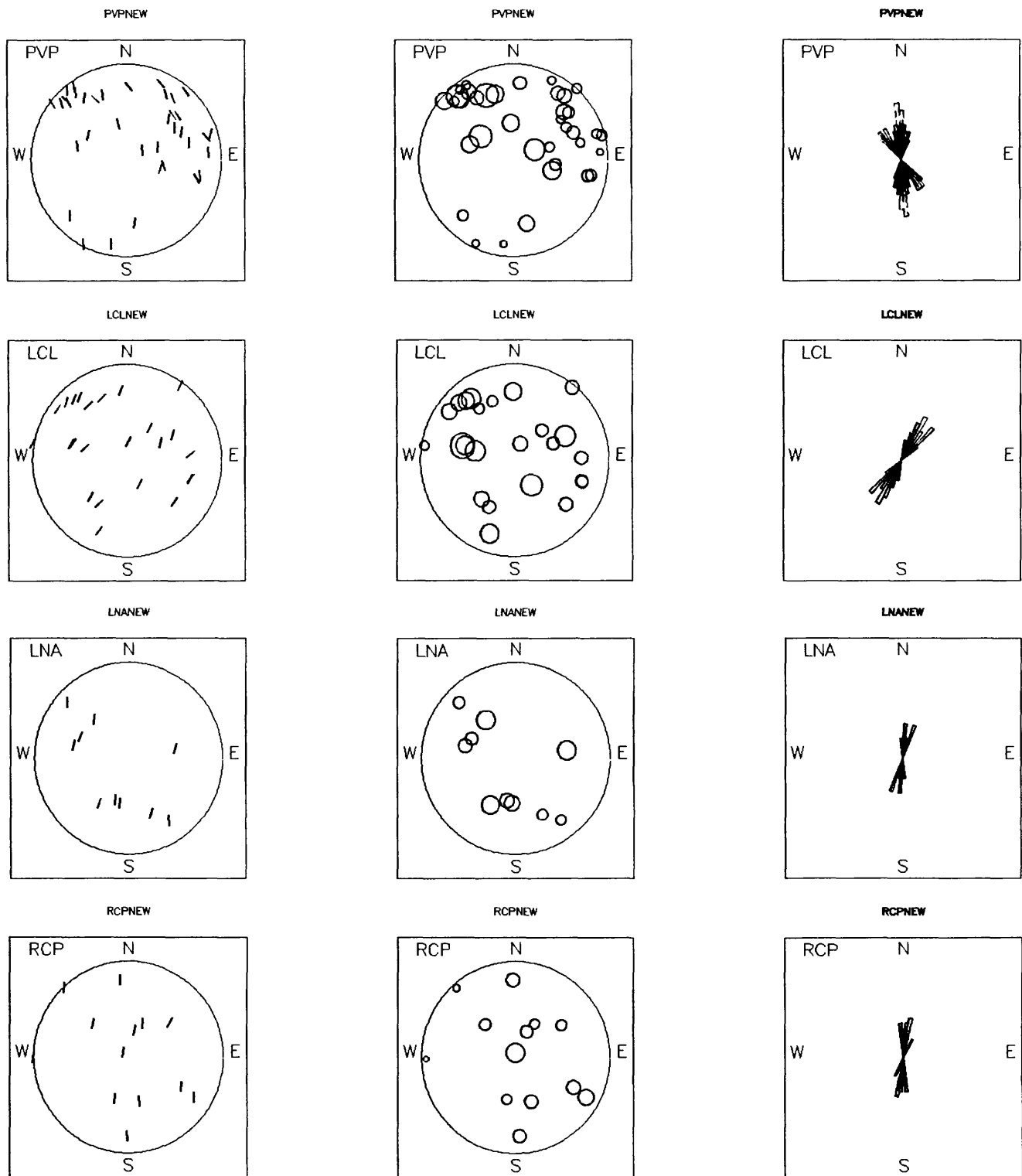


**Fig. 3** (Continue) Circles indicate the time separations normalized by hypocentral distances of events, radii of the circles are proportional to the length of the time separation. Right: Rose diagrams of polarizations on the lower hemisphere out of 50° with the centers at these eight stations.

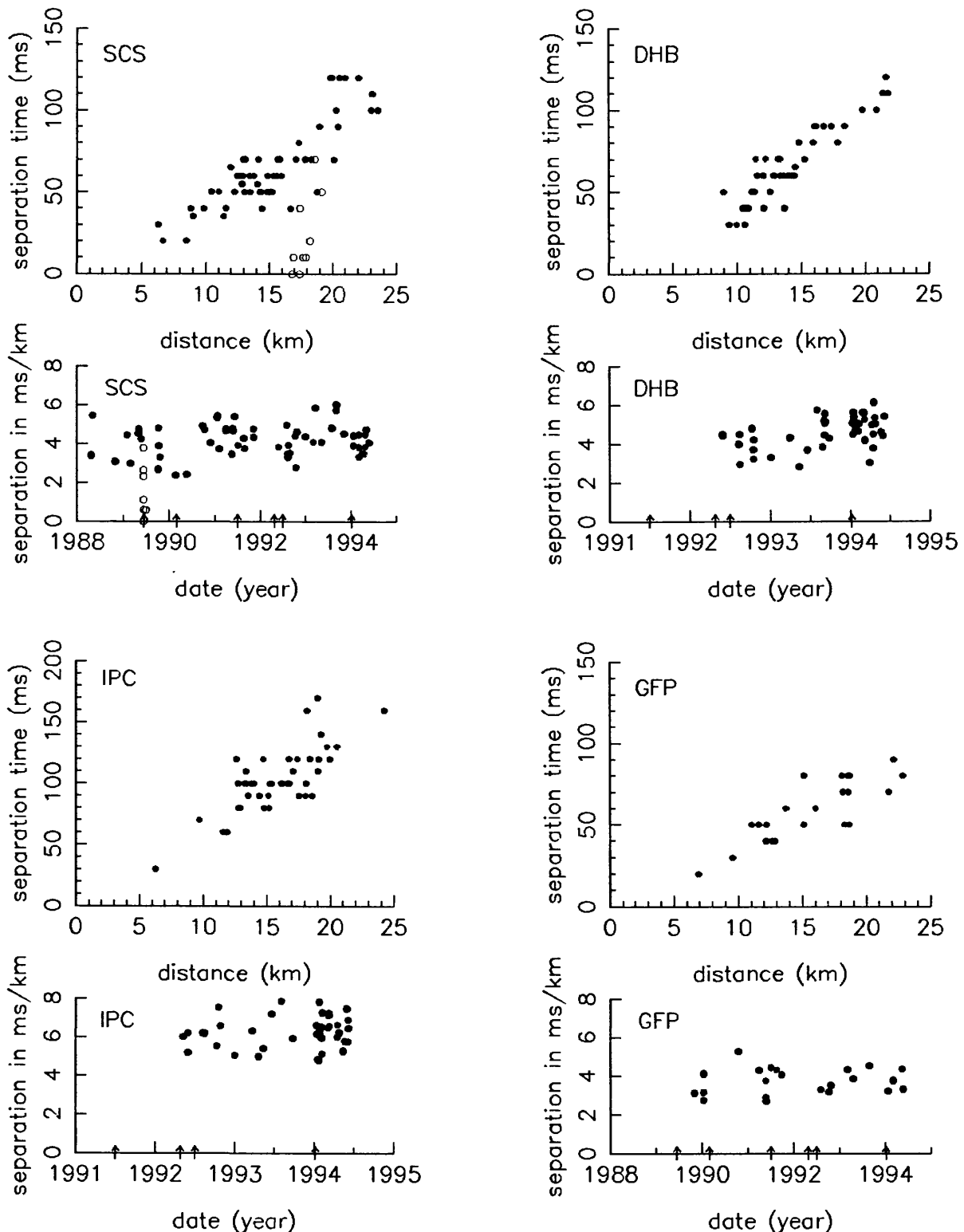


**Fig. 4** Results from eight stations SCS, DHB, IPC, GFP, PVP, LCL, LNA and RCP. Top frame for each station: The plot of time separations between two split shear waves versus hypocentral distances for earthquakes within the shear-wave window of the corresponding station. The raypaths from events have incident angles to the station smaller than 38°. The data from the Montebello earthquakes are denoted by open circles.

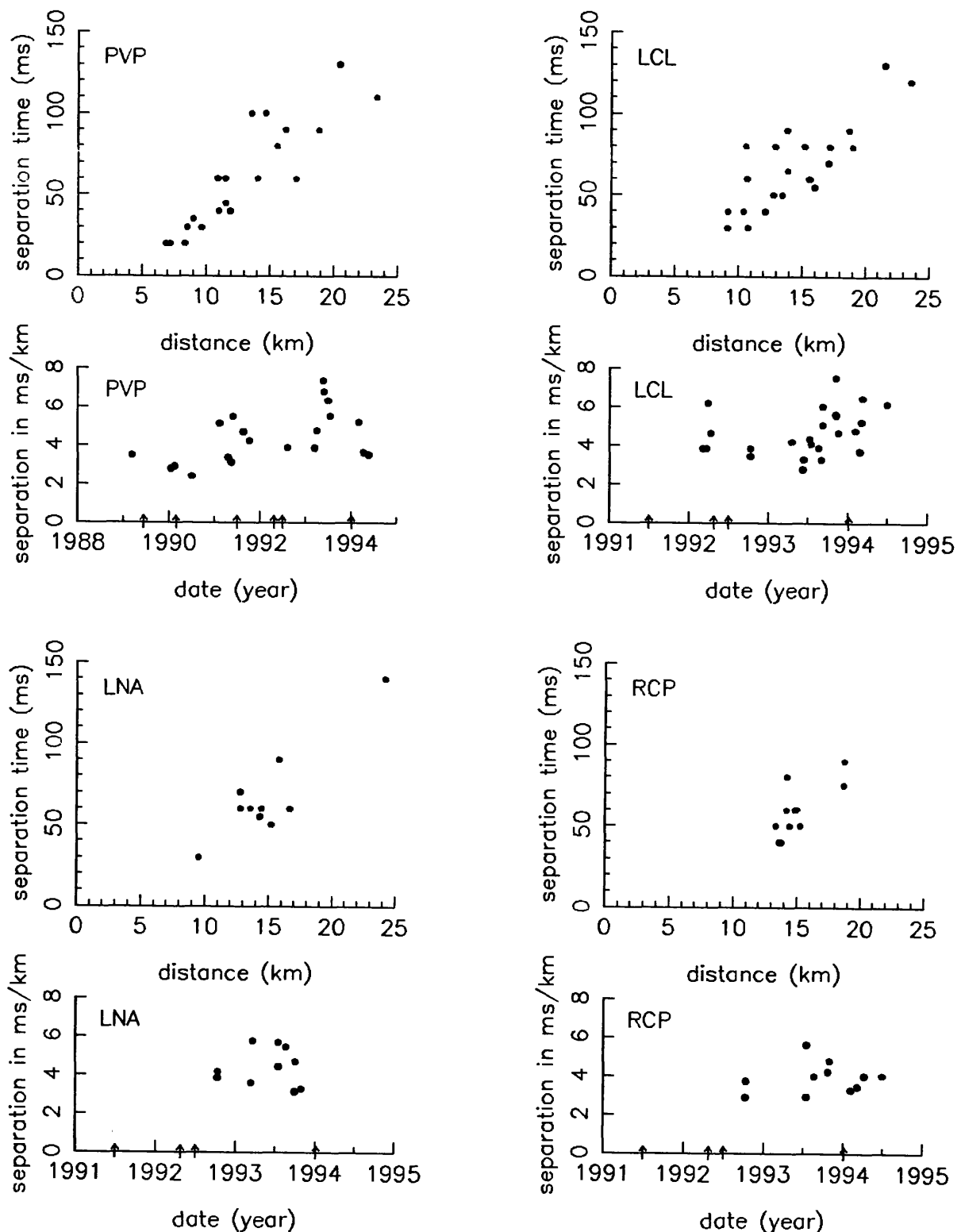


**Fig. 4** (Continue) Bottom frame: The plot of normalized time separations between two split shear waves from earthquakes having raypaths with incident angles to the station smaller than  $38^\circ$  versus date. The delay times are normalized by hypocentral distances of these events. The data from the Montebello events are denoted by open circles. Arrows denote the occurrences of the Montebello, Upland, Sierra Madre, Joshua Tree, Landers, Big Bear Lake and Northridge earthquakes.

## Slip History of San Andreas and Hayward Faults

9960-12376

J. J. Lienkaemper  
 Branch of Engineering Seismology and Geology  
 U.S. Geological Survey, 345 Middlefield Road, MS 977  
 Menlo Park, California 94025  
 jlienk@isdmnl.wr.usgs.gov; (415) 329-5642  
 Program Element II

### Investigations

Determine slip rates and earthquake recurrence times on San Andreas and Hayward Faults. Compare rates of geologically determined surface slip to rates of historic creep and geodetically determined deep slip. Analyze effects of structural complexity and fault segmentation upon inferring recurrence from slip rate.

### Results

1. Creep Rates, Hayward Fault. With two surveying teams from USGS and SF State University, we measured 33 Hayward fault arrays during a 5 day sweep in late Summer 1994. We confirmed and revised the interesting results on creep rate for the initial 3 years (1989-1992) of precision monitoring of about 20 arrays established for observing afterslip expected in the next major earthquake on the Hayward Fault [Lienkaemper, Galehouse, and Simpson, 1993]. Creep rate along most of the fault since the 1989 Loma Prieta Earthquake (LPE) until summer of 1992 averaged only  $70 \pm 10$  percent of the long-term rate. At the southeast end where long-term rates have been about 9 mm/yr right-lateral, the post-LPE creep rate continues until December 1993 at 0-2 mm/yr left-lateral. This reversal in the direction of creep rate is a predictable effect of modelled static stress changes and can be expected to continue for at least another year at our southernmost array. From central Fremont northward, creep rate has at most sites returned to normal (where long-term rate is 5-6 mm/yr), but at some sites creep is still retarded (where long-term rate is 3.5-5 mm/yr). Detailed results and scientific summaries of these recent and other longterm creep investigations will become available next year in various written and digital formats.

2. Holocene Slip Rates, Masonic Site. This work was completed and submitted to a special paleoseismology issue of Journal Geophys. Res. (January 1996) [Lienkaemper and Borchardt, submitted]. Archival field logs were digitized and are available on optical disks for the cost of reproduction. A new paleoseismology site on the Hayward Fault, Montclair Park in Oakland, was permitted during this period and trenched during the next period. Results will be reported during next period.

3. Hayward fault, telemetered creepmeter siting and installation with R.G. Bilham and K.S. Breckenridge. We chose several sites for a 3-yr installation program that began in November-December 1993 with installation of the first device in southern Fremont using 30-m deep concrete piers that will also be monitored for pier tilt. A second instrument has been installed at Palisade Dr in Hayward and permitting for other sites is in progress.

**Reports**

**Lienkaemper, J.J., and G. Borchardt, submitted, Holocene slip rate of the Hayward Fault at Union City: [submitted to *Jour. Geophys. Res.*]**

**Lienkaemper, J.J., J.S. Galehouse, R.W. Simpson, and K.S. Breckenridge, 1993, Creep slowdown since the 1989 Loma Prieta earthquake (LPEQ) continues on the Hayward fault, California: *EOS, Transactions, Am. Geophys. Union*, v.74, 192.**

## CRUSTAL STRAIN

9960-10076, 11076, 12076, 13076, 15076, 60076

M. Lisowski, J.C. Savage, N.E. King, J.L. Svart, M.H. Murray, W.K. Gross  
 Branch of Earthquake Geology and Geophysics  
 U.S. Geological Survey  
 345 Middlefield Road, MS/977  
 Menlo Park, California 94025  
 (415) 329-4832  
 e-mail: [nking@eratos.wr.usgs.gov](mailto:nking@eratos.wr.usgs.gov)

### Investigations

The principal subject of investigation was the measurement and analysis of crustal deformation within tectonically active areas of the United States. Almost all measurements were made with Global Positioning System (GPS) receivers. All data was archived and reduced by personnel from the Crustal Strain project. In Table 1 we list the networks surveyed during FY 1994 along with details about the data collected by personnel from the Crustal Strain project.

In the San Francisco Bay Area, we surveyed a series of profiles, including one spanning the rupture zone of the Loma Prieta earthquake. We also observed our Farallon-Sierra arc. We carried out several studies in the East Bay, near the Hayward fault. We re-surveyed several small-aperture networks spanning the Hayward fault. We also performed GPS surveys of alignment arrays put in by Jim Lienkaemper (USGS) and John Galehouse (San Francisco State University). In cooperation with Malcolm Johnston (USGS), Doug Myren (USGS), and Rich Clymer (U.C. Berkeley), we set GPS monuments near borehole strainmeters in the East Bay.

In southern California, we continued surveys of the Bessemer profile in order to monitor post-seismic strain diffusion after the Landers earthquake. We also surveyed several monitor networks, the Salton profile, and the Barstow and Garlock networks. Northridge dominated much of our southern California effort. In cooperation with Ken Hudnut, the Southern California Earthquake Center, JPL, the Scripps Institution of Oceanography, and various Los Angeles city and county agencies, we participated in GPS monumentation and observation.

In July 1994, we observed the Fallon/Excelsior and Mammoth networks. We re-surveyed our Pacific Northwest GPS networks just before the September 1, 1994 earthquake (M 7) on the Mendocino transform fault. In cooperation with Stanford University, we carried out a post-seismic survey in late September.

The Bay Area Regional Deformation (BARD) permanent GPS array continued to expand in 1994. The network is a cooperative effort between the USGS, University of California at Berkeley (Barbara Romanowicz, Rich Clymer), Lawrence Livermore (Shawn Larsen), Trimble Navigation (Brian Frohring), and Stanford University (Paul Segall, Jeff Freymueller). Table 2 shows the institution, start date, and receiver type at each BARD

Table 1. Field Surveys FY 1994

Project	Program/Region	Start Date	Finish Date	Peo ple	Field Days	Tra vel Days	Geod olite Lines	GPS Station Days	Local Ties	GPS Sta tions	Local Sta tions
BARD	NEHRP-SF	91/09/12	Continuous								9
Bessemer Mine	NEHRP-SC	93/10/05	93/10/06	5	2	1		13			11
S. Cal Monit	NEHRP-SC	93/10/07	93/10/12	5	6	1		30	2	28	2
Geodolite/GPS	NEHRP-SF	93/10/26	93/10/26	3	1		2	3			3
Loma-Monit	NEHRP-SF	93/11/02	93/11/02	5	1		5	6			6
Geodolite/GPS	NEHRP-SF	93/11/03	93/11/03	3	1		2	4			4
Geodolite/GPS	NEHRP-SF	93/11/23	93/11/23	4	1		2	4			4
Small Nets + AA	NEHRP-SF	93/12/07	94/01/10	5	8			43		43	
Loma-Profile	NEHRP-SF	94/01/11	94/01/13	5	3			15		15	1
Northridge Resp.	NEHRP-SC	94/01/19	94/01/23	5	5	2		33	3	14	3
Northridge Resp.	NEHRP-SC	94/02/01	94/02/02	5	2	1		16	3	13	3
Salton Profile	NEHRP-SC	94/02/03	94/02/08	5	5	1		33	2	24	
Northridge Resp.	NEHRP-SC	94/02/14	94/02/16	5	3	1		12	1	12	1
Farallon-Sierra	NEHRP-SF	94/02/28	94/03/04	5	5	1		26	6	17	4
Northridge Resp.	NEHRP-SC	94/03/14	94/03/15	5	2	1		14	3	13	3
Garlock/Barstow	NEHRP-SC	94/03/17	94/03/24	7	7	1		26	3	20	3
Tolay	NEHRP-SF	94/04/06	94/04/06	3	1			6			6
Strainmeter Ties	NEHRP-SF	94/04/12	94/04/12	4	2			9			9
NBay-Profile	NEHRP-SF	94/04/18	94/04/20	5	3			19		17	
GG-Profile	NEHRP-SF	94/04/21	94/04/21	5	1			5		5	
CBay-Profile	NEHRP-SF	94/04/25	94/04/26	5	2			12		12	
Profile-Ties	NEHRP-SF	94/04/28	94/04/28	5	1						
SBay-Profile	NEHRP-SF	94/05/02	94/05/04	5	3			17		15	
Loma-Profile	NEHRP-SF	94/05/05	94/05/06	5	2			14		13	
S. Cal Monit	NEHRP-SC	94/05/09	94/05/14	4	6	1		26		26	
Bessemer Profile	NEHRP-SC	94/05/15	94/05/16	5	2			15	1	15	1
Northridge Resp.	NEHRP-SC	94/05/17	94/05/18	5	2	1		11		10	
Loma-GPS	NEHRP-SF	94/05/31	94/05/31	5	1			7	1	6	1
Monterey-Profile	NEHRP-SF	94/06/01	94/06/03	5	3			7	1	6	1
L.A. Monument	NEHRP-SC	94/06/07	94/06/17	5	9	2					
Fallon/Excelsior	Core	94/07/06	94/07/18	6	11	2		63		54	1
Mammoth	Volcano Hazards	94/07/26	94/08/03	6	7	2		53	1	44	1
Pacific Northwest	NEHRP-PN	94/08/08	94/08/25	5	15	3		97	3	73	
Mendocino Resp.	NEHRP-PN	94/09/13	94/09/19	5	5	2		33		24	
		Total			128	23	11	672	30	571	25

station. Each institution maintains and downloads its receivers. USGS processes the data using JPL's precise orbits and GIPSY-OASIS software. UCB runs the data archive (Northern California Data Center).

**Table 2**  
**Bay Area Regional Deformation (BARD) Permanent GPS Array**

Station	Operated by	Start date	Receiver type
Briones	UCB	09/03/1993	Ashtech Z-12
Chabot	USGS	09/12/1991	Ashtech M-12
Columbia	UCB	12/11/1993	Ashtech Z-12
Farallon	UCB	02/03/1994	Ashtech Z-12
Molalte	USGS/Trimble	10/15/1993	Trimble 4000SSE
Nunes	USGS/Trimble	10/15/1993	Trimble 4000SSE
Stanford	Stanford	04/21/1994	Trimble 4000SSE
Tiburon	UCB	06/18/1994	Ashtech Z-12
Winton	USGS	09/12/1991	Ashtech M-12

#### *GPS Data Reduction and Data Archives*

We are able to process GPS data with Bernese (University of Berne), GAMIT (MIT and Scripps), and GIPSY-OASIS (JPL) software packages. Until 1993, we processed most data with the Bernese software. Mark Murray used GAMIT to process data from the Pacific northwest and Northridge (in collaboration with Ken Hudnut). In 1993 we began to process data with GIPSY-OASIS II. UNIX scripts, written at USGS, allow us to automate much of the processing. The BARD processing is almost completely automated. Various utilities allow us to combine solutions obtained with different software packages.

We are developing a UNIX database for easy data retrieval and inspection. As of December 1994, raw and RINEX data files for 1991 through 1994 are on optical cartridges, and can be made available upon request. An index file for the raw data is available now, via anonymous FTP, in directory `/pub/outgoing/gpsdata` on the USGS machine `andreas.wr.usgs.gov` (IP 130.118.4.120). This index gives campaign name, station name, 4-character code, raw and RINEX file names, start and end times, file length, sample interval, station position, receiver type, and comments for each raw data file. The index is complete for 1991 through 1994. We have also submitted our most recent data from southern California to the SCEC archive. Eventually all our data will be available via anonymous FTP from the USGS-UC Berkeley data archives. For more information, send e-mail to `kwendt@isdmln.wr.usgs.gov`.

#### **Results**

##### **1. Changes in Long-Term Extension Rates Associated With the Morgan Hill and Loma Prieta Earthquake in California**

Frequent measurements since mid-1981 of the distances from a geodetic monument located about 100 km south-southeast of San Francisco to three monuments 30 to 40 km distant provide an unusually complete record of the deformation before and after two nearby earthquakes, the 1984 Morgan Hill ( $M_L = 6.2$ ) and 1989 Loma Prieta ( $M_s = 7.1$ ) earthquakes. Except possibly for the first few months postseismic, the extension rates indicated by these measurements appear to be steady over the four or five years both preceding and following those earthquakes. However, the preseismic and postseismic rates differ significantly for at least one of the distances measured for each earthquake. The data

over the four to five year postseismic records available are not adequate to demonstrate that the postseismic rates are relaxing back to the preseismic rates.

## 2. *Geodetic Monitoring of the Southern San Andreas Fault, California, 1980–1991*

Five geodetic arrays (10 to 40 km aperture) located along the San Andreas fault have been surveyed frequently (several times in most years) over the 1980–1991 interval to detect possible fluctuations in the deformation rate. In each survey of an array the distances between the same four to seven pairs of geodetic monuments were measured. The distances measured (with corresponding standard deviation) range from 8.4 km (3.4 mm) to 38 km (8.2 mm). The data are displayed as plots of measured distance as a function of time. Linear fits in such plots furnish a satisfactory representation of the data. That is, the scatter of the data about the linear fits is within the range expected for the estimated standard deviations in measurement. However, there are coherent low-amplitude (within the observational error) fluctuations apparent in some of the measured distances. Those fluctuations need not be tectonic effects but rather may be either random patterns or artifacts introduced by systematic drift in instrument calibration or wander of the geodetic monuments. We conclude that the measurements are consistent with steady deformation of the arrays over the 1980–1991 interval, and we find no convincing evidence in the data for fluctuations in the rate of deformation.

## 3. *Strain Accumulation in Owens Valley, California, 1974–1988*

Strain accumulation observed over the 1974–1988 interval in a  $25 \times 100$  km aperture trilateration network spanning Owens Valley is adequately described by a strain rate that is uniform in space and time. The tensor strain rate components referred to a coordinate system with the 2 axis directed N18°W (parallel to the trend of the valley) and the 1 axis N72°E are  $\dot{\varepsilon}'_{11} = 0.042 \pm 0.014 \mu\text{strain/yr}$ ,  $\dot{\varepsilon}'_{12} = -0.058 \pm 0.007 \mu\text{strain/yr}$ , and  $\dot{\varepsilon}'_{22} = 0.002 \pm 0.014 \mu\text{strain/yr}$ ; quoted uncertainties are standard deviations and extension is reckoned positive. Across the 25 km breadth of the network this amounts to  $1.0 \pm 0.3$  mm/yr extension normal to the axis of the valley,  $2.9 \pm 0.4$  mm/yr right-lateral shear across the axis, and no extension parallel to the axis. If the measured strain accumulation is attributed to slip on the deeper section of the Owens Valley fault with the uppermost 10 km of the fault locked, the observed right-lateral deformation would imply about 7 mm/yr right-lateral slip on the buried fault, much greater than the geologic estimate of  $2 \pm 0.5$  mm/yr right-lateral secular slip (Beanland and Clark, 1994). Nor is the observed uplift profile across the valley consistent with continuing normal slip on just the deep segment of the Owens Valley fault; normal slip at depth on the Sierra frontal fault also seems to be required. The observed deformation across Owens Valley apparently implies processes more complicated than those represented by the conventional model of strain accumulation along a throughgoing fault.

The dislocation model of the 1986 Chalfant Valley earthquake just north of Owens Valley has been revised. Gross and Savage (*Bull. Seismol. Soc. Am.*, 77, 306, 1987) originally proposed an oblique-slip mechanism, but leveling data that became available subsequently showed that no appreciable dip slip was involved. The revised model requires right-lateral slip on the main rupture and left-lateral slip on a conjugate plane (rupture plane of the principal foreshock).

#### 4. Interseismic Deformation Along the San Andreas Fault in Southern California

Eight trilateration networks located along the San Andreas fault in southern California have been surveyed 8 to 19 times within a 14 to 17 year interval between 1971 and 1992. The data, measurements of distances between the same 10 to 32 pairs of geodetic monuments within a network in each of the surveys, have been corrected for coseismic offsets from nearby earthquakes calculated from dislocation models. The corrected data, a total of 2027 measurements, are displayed in the form of plots of measured distance versus time for each of the 167 lines measured. The hypothesis that the interseismic deformation is steady is tested by examining whether deviations from linear fits to the data in the plots are within the range expected for observational error. A significant deviation from steady deformation is found only for the network located near Palmdale, California. In that network, many of the measurements made in the survey of early 1982 deviate from the trend defined by the measurements in other surveys. The deviations are not of the form (fixed proportional error) one would generally expect from systematic survey error. If the survey of early 1982 is excluded, the remaining data at Palmdale are consistent with steady deformation. Thus, the apparent strain event observed near Palmdale in 1982 was transient.

The data for each network were also analyzed by principal component analysis to represent the observed changes in line length as a superposition of individual modes:

$$L_{ij} - L_i = \sum_k A_{ik} C_k(t_j)$$

where  $L_{ij}$  is the length of the  $i^{\text{th}}$  line measured at the time  $t_j$ ,  $L_i$  is the average length of the  $i^{\text{th}}$  line, and  $A_{ik} C_k(t_j)$  is the  $k^{\text{th}}$  mode. Each mode is described by a common time function  $C_k(t_j)$  that is evaluated only at the times  $t_j$  of the surveys, and the participation of each line in that mode is described by a constant amplitude  $A_{ik}$  for that line. For all networks the deformation is largely described by the first mode, and the first-mode time function is essentially linear in time. That is, the deformation in each of the networks appears to be steady. Two anomalies in the accumulation of deformation were observed: In the network near Palmdale a transient strain event occurs in the second mode in early 1982, and in the network within Cajon Pass fluctuations in the accumulation of deformation somewhat greater than would be attributed to measurement error were found. Although both anomalies are formally significant given the estimated measurement error, we are not confident that either anomaly is real. The principal conclusion is that the accumulation of interseismic deformation in the southern California trilateration networks is, within the precision of measurement, either steady or almost steady.

#### 5. Strain Accumulation 1973-1994 Across the Nevada Seismic Zone

A trilateration network extending 200 km along the Nevada seismic zone (1915 Pleasant Valley,  $M=7.3$ ; 1954 Dixie Valley,  $M=6.8$ ; 1954 Fairview Peak,  $M=7.1$ ; 1932 Cedar Mountain,  $M=7.2$ , earthquakes) has been surveyed six times since 1973, five times by Geodolite and most recently (1994) with GPS. The average annual principal strain rates measured by these surveys are shown in the table below.

The strain rates are shown for two fault segments (Cedar Mountain and Fairview Peak) as well as for a historically unbroken segment (Stillwater Gap) between the Dixie Valley and Pleasant Valley segments. We have also calculated strain rates south of the Cedar Mountain fault segment into the Long Valley Caldera of eastern California (Excelsior network).

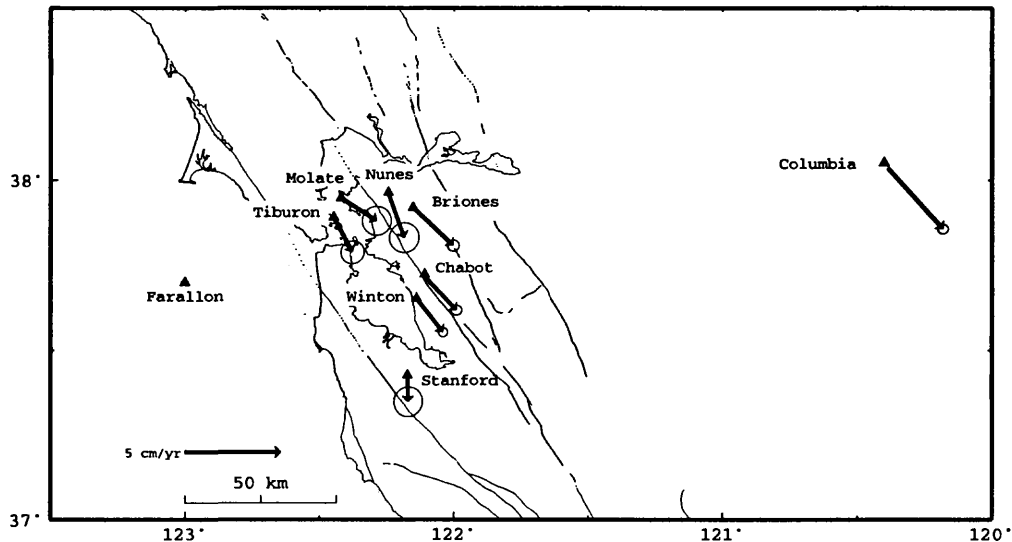
With the most recent survey the strain rates are well defined. They are very consistent from segment to segment with possibly more extension to the south. Moreover, the orientation of the principal axis of strain accumulation is relatively well defined ( $N52^\circ W \pm 5^\circ$  extension). That orientation is consistent with that of the stress axes deduced by Zoback and Zoback.

Segment	Principle Strain Rates $\mu\text{strain/yr}$	Ext. Axis
Stillwater Gap	$0.047 \pm 0.012$	$N61^\circ W \pm 5^\circ$
Fairview Peak	$0.034 \pm 0.010$	$N61^\circ W \pm 4^\circ$
Cedar Mountain	$0.032 \pm 0.009$	$N52^\circ W \pm 5^\circ$
Moho	$0.058 \pm 0.009$	$N60^\circ W \pm 3^\circ$
Hunton	$0.067 \pm 0.009$	$N59^\circ W \pm 3^\circ$

## 6. *The Bay Area Regional Deformation (BARD) Permanent GPS Array*

As of December 1994, we routinely process data from nine BARD stations and three tracking stations (Goldstone, Vandenberg, and Quincy). Daily solutions show that offsets sometimes occur after equipment swaps, firmware changes, or electronic changes. This suggests that results from traditional surveys may be contaminated with such errors. For baselines between BARD stations, rms scatter about the best-fitting straight line (with offsets removed, if necessary) is typically 10 to 20 mm in the vertical, and 2 to 3 mm in length, north, and east. Baselines between BARD and Goldstone, Vandenberg, or Quincy have large outliers and non-linear features. This is clearly related to the precise orbits from JPL, since these features disappear when we re-process the data with precise orbits from other agencies. These problems are probably related to the onset of anti-spoofing in January 1994. However, problems appear only in baselines longer than 400 km, so we can use baselines between the BARD stations to estimate station velocities. The velocity solution (next page) shows 42 mm/yr across the entire array (Farallon to Columbia). The velocity vectors for Stanford, Molate, and Nunes appear anomalous. There are significant gaps in the time histories of these stations. Furthermore, station Stanford is on top of a building. However, the 95 percent error ellipses for these stations are sufficient large that the velocity vectors are consistent with the vectors from other sites. We rotated the velocity vectors into  $S35^\circ E$  (fault-parallel) and  $S55^\circ W$  (fault-normal) components, and used the  $S35^\circ E$  velocities to estimate deformation across faults. The difference between Farallon and the weighted mean of Tiburon, Molate, and Winton provides an estimate of the deformation across the San Andreas fault. To estimate the deformation across the Hayward fault, we used the difference between the weighted mean of Tiburon, Molate, and Winton and the weighted mean of Briones, Chabot, and Nunes. Finally, the difference between Columbia and the weighted mean of Briones, Chabot, and Nunes provides an estimate of the deformation across the Calaveras fault and the shear zone to the east. The table on the next page shows the results.

Segment	S35°E velocity, mm/yr
San Andreas fault	$22.2 \pm 0.7$
Hayward fault	$4.7 \pm 1.1$
Calaveras fault + shear zone	$15.2 \pm 1.7$



## 7. Regional Crustal Deformation Near Long Valley Caldera, California

We observe radial expansion and domal uplift across Long Valley caldera at average rates exceeding 30 mm/yr in the 1989–1993 interval. Fluctuations in the rate of deformation are apparent, with higher rates during the 1989–1990 and 1992–1993 intervals. We use Mogi point sources embedded in an elastic half-space to approximate the surface deformation produced by an inflating magma chamber. We use Monte Carlo techniques to find the locations and rates of expansion of one or two Mogi sources that will best reproduce the observed average rates of deformation. A single Mogi source 8 km beneath the center of the resurgent dome and expanding at a rate of  $0.014 \text{ km}^3/\text{yr}$  fits the data within the caldera, but underpredicts deformation observed outside of the caldera. We can fit the far-field data significantly better by adding a deep Mogi source. In the two source model, the shallow source is 4 km beneath the center of the resurgent dome and expands at a rate of  $0.0036 \text{ km}^3/\text{yr}$  and the deep source is 10 km southwest of the center of the resurgent dome at a depth of 31 km and expands at a rate of  $0.09 \text{ km}^3/\text{yr}$ . The location and rate of expansion of the deep source is poorly resolved. Our results and the occurrence of long-period earthquakes (first detected beneath Mammoth Mountain by M. Pitt in 1989) suggest injection of magma beneath the resurgent dome and at depth below the southwestern edge of Long Valley caldera.

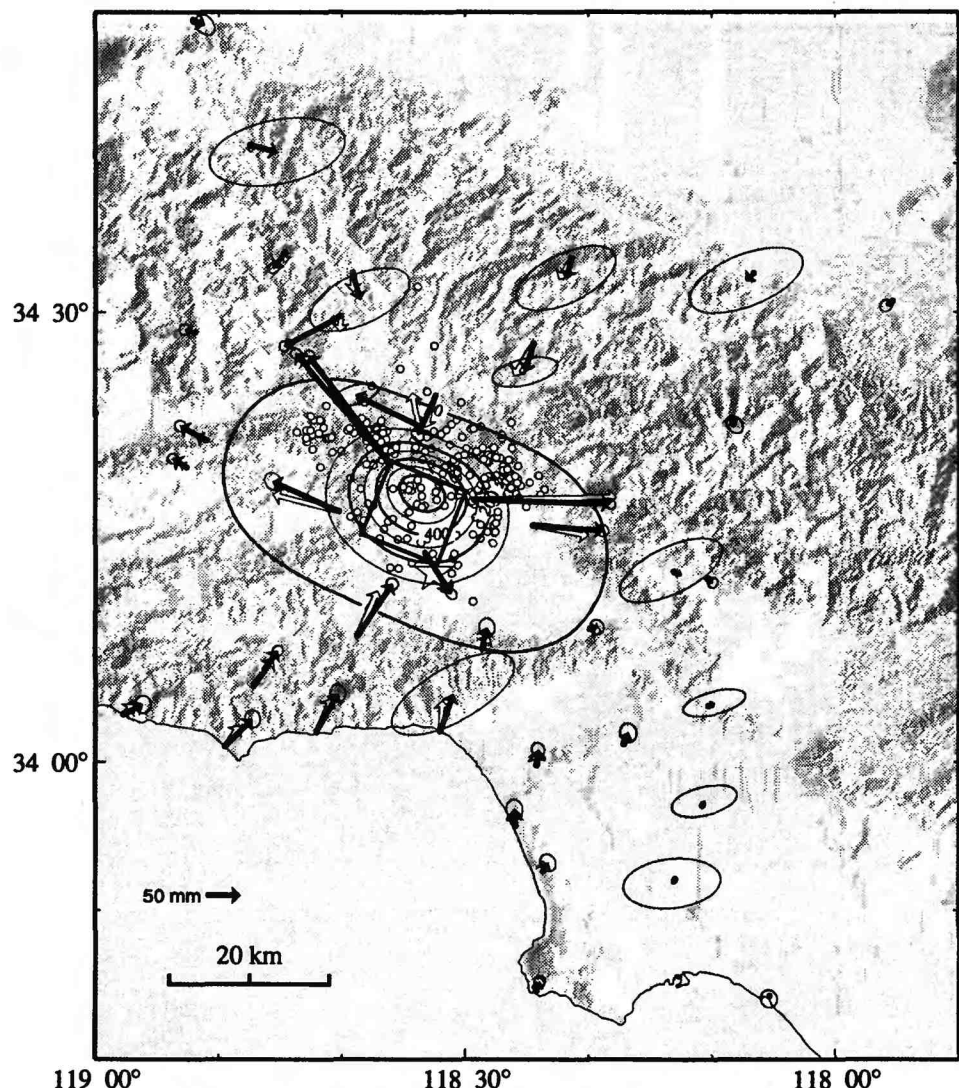
## 8. Strain Accumulation Along the Cascadia Subduction Zone

We combine observations from triangulation during the last century, Geodolite trilateration during 1972 - 1989, and the Global Positioning System (GPS) since 1989 to determine

present-day horizontal strain accumulation along the Cascadia subduction zone. All networks west of the Cascade Range show significant strain accumulation with maximum contraction nearly parallel to the direction of Juan de Fuca/North America plate convergence. Shear-strain accumulation from GPS recovery of historical triangulation networks is observed in coastal northern California, near the mouth of the Columbia river, and across the Strait of Juan de Fuca ( $0.16 \pm 0.07$ ,  $0.09 \pm 0.03$ , and  $0.11 \pm 0.03 \mu\text{rad/yr}$ , respectively). Nearly uniaxial contraction in the direction of plate convergence from Geodolite trilateration is observed near Cape Mendocino, Seattle, and on the Olympic Peninsula ( $0.19 \pm 0.03$ ,  $0.03 \pm 0.01$ , and  $0.09 \pm 0.03 \text{ mstrain/yr}$ , respectively), and from GPS observations in southwestern Oregon ( $0.07 \pm 0.02 \text{ mstrain/yr}$ ). Networks within or east of the Cascade Range, near Mt. St. Helens and the Hanford Reservation, do not show measurable strain accumulation. These deformation rates are consistent with a model proposed by Savage et al. (1991) for northwestern Washington in which the megathrust underlying the continental slope and outer continental shelf currently is locked but is free to slip farther landward. These results are consistent with a locked segment that extends along the entire subduction zone, which presumably will eventually rupture in one or more great thrust earthquakes. We have begun to survey some of the significant gaps between the networks to detect variations in strain accumulation, in particular along the central Oregon coast where lower rates of strain accumulation are suggested by leveling and tide gauge measurements.

#### 9. *Coseismic Displacements of the 1994 Northridge, California, Earthquake*

The January 17, 1994 Northridge, California, earthquake permanently deformed the earth's crust by at least one centimeter throughout a 3,000 to 5,000 km<sup>2</sup> area around the epicentral region. Displacements of 62 survey stations determined from Global Positioning System (GPS) observations made before and after the earthquake show that stations were uplifted by as much as 50 cm, and displaced horizontally by up to 20 cm. Modeling these displacement data, we have determined a uniform-slip model assuming a single rectangular dislocation embedded in a homogeneous elastic half space. The fault geometry and slip are estimated independent of seismological information using Monte Carlo optimization techniques that minimize the misfit between the observed and predicted horizontal and vertical displacements. The estimated slip vector is 2.6 m with a rake of  $6^\circ$  for the optimal fault model (dip= $42^\circ$ , strike= $112^\circ$ , down-dip width=13 km, along-strike length=10 km, centroid location= $34.277^\circ\text{N}$ ;  $118.570^\circ\text{W}$  at 10 km depth), which extends from 5 to 14 km depth. The geodetic moment is  $1.0 \times 10^{26}$  dyne-cm. Displacements predicted by this model are generally in good agreement with geodetic observations in the epicentral region. Further modeling to determine the pattern of distributed slip indicates that a high-slip patch occurred up-dip and northwest of the main shock hypocenter, and that little slip occurred within the uppermost 5 km of the crust, consistent with the lack of surface rupture. In some areas, such as the Ventura basin, there is significant misfit to either model that does not appear to simply be caused by aftershocks. If the fault that ruptured during the Northridge earthquake has ruptured repeatedly in the past, the geomorphology of the region should mimic the coseismic deformation. The Northridge earthquake uplifted the Santa Susana range, in agreement with this prediction. However, it also uplifted the northern edge of the San Fernando valley, which



suggests that post-seismic relaxation or slip on other faults may also contribute to the long-term patterns of uplift in the region.

#### Reports Published in FY 1993 (excluding abstracts)

Jones, Lucile M., Aki, Keiiti; Boore, D. M.; Celebi, Mehmet; Donnellan, Andrea; Hall, J. R.; Harris, R. A.; Hauksson, Egill; Heaton, T. H.; Hough, S. E.; Hudnut, K. W.; Hutton, L. K.; Johnston, M. J. S.; Joyner, W. B.; Kanamori, Hiroo; Marshall, G. A.; Michael, A. J.; Mori, J. J.; Murray, M.; Ponti, D. J.; Reasenberg, P. A.; Schwartz, D. P.; Seeber, Leonardo; Shakal, A. F.; Simpson, R. W.; Thio, Hong-Kie; Tinsley, J. C.; Todorovska, M. J.; Trifunac, M. D.; Wald, D. J.; Zoback, M. L. The magnitude 6.7 Northridge, California, earthquake of 17 January 1994 *Science*, 266, 389-397, 1994

- Savage, J.C., Comment on "Evidence for near-frictionless faulting in the 1989 Loma Prieta, California, earthquake and its aftershocks", *Geology*, 22, 278–279. 1994.
- Savage, J.C., Empirical earthquake probabilities from observed recurrence intervals, *Bull. Seismol. Soc. Am.*, 84, 219–221, 1994.
- Savage, J.C., Probability of one or more  $M > 7$  earthquakes in southern California in 30 years, *Geophys. Res. Lett.*, 21, 313–315, 1994.
- Savage, J.C., and Lisowski, M., Strain accumulation north of Los Angeles, California, as a function of time, 1977–1992, *Geophys. Res. Lett.*, 21, 1173–1176, 1994.
- Savage, J.C., Lisowski, M., and Svarc, J.L., Postseismic deformation following the 1989 ( $M = 7.1$ ) Loma Prieta, California, earthquake, *J. Geophys. Res.*, 99, 13,757–13,765, 1994.
- Savage, J.C., Lisowski, M., Gross, W.K., King, N.E., and Svarc, J.L., Strain accumulation near Yucca Mountain, Nevada, 1983–1993, *J. Geophys. Res.*, 99, 18,103–18,107, 1994.
- Savage, J.C., Lisowski, M., King, N.E., and Gross, W.K., Strain accumulation along the Laguna Salada fault, Baja California, Mexico, *J. Geophys. Res.*, 99, 18,109–18,116, 1994.

## U.S. MAP AND DATABASE OF MAJOR ACTIVE FAULTS

9950-10215

Michael N. Machette  
 Branch of Earthquake and Landslide Hazards  
 U.S. Geological Survey, Box 25046, MS 966  
 Denver, CO 80225-0046  
 (303) 273-8612; fax 273-8600  
 (machette@gldvxa.cr.usgs.gov)  
 NEHRP Element II

### PURPOSE OF PROJECT

This project is part of the larger "World Map of Major Active Faults", which is co-sponsored by the International Lithosphere Program (ILP) and co-chaired by Machette. The main goal of the NEHRP-funded project is to compile a digital map and accompanying computer database of active (Quaternary) faults and folds in the United States in order to extend the modern seismic record into past (*i.e.*, Quaternary paleoseismic activity). Paleoseismic data are fundamental to understanding how strain is accumulated and released on faults and for improving the amount and quality of geologic input to seismic hazards analyses. The main project members are Michael N. Machette, Richard L. Dart, and Kathleen M. Haller.

### INVESTIGATIONS

We are continuing to coordinate efforts on and compile data for the World, Regional (*e.g.*, North American), and United States maps of major active faults in support of their new Global Seismic Hazards Assessment Program (GSHAP). Our involvement in this project began in mid-1992, but we are still enlisting technical experts from the United States and Mexico/Central and South America that are known to be both productive and knowledgeable, and which have strong national contacts. For the United States, the compilation will be supervised by the USGS in Denver, under the direction of this project. In addition, the USGS will assist compilers in the other regions with digitization and technical aspects of the data base.

Our strategy is to assemble a large body of data on Quaternary faults and folds in the U.S. Although many authors have compiled maps, few have taken the time to fully document their maps with supporting databases; thus, fault data in catalog form is relatively sparse. Overall, we suspect that there is existing catalog data for about 20 percent of the faults and folds in the U.S. About 75 percent of our time is spent on compiling data pertinent to the project.

### RESULTS

1. During FY 94, we conducted several planning and progress meetings for the project. At the 1993 AGU meeting in San Francisco, we held an initial meeting for the Caribbean and Central American maps of active faults, and were partly successful in gaining further commitments. The main problem here is the lack of ongoing research in active tectonics, particularly in Central America and parts of the Caribbean. During the year, we have been corresponding with project participants and plan to present draft versions of maps of the Caribbean region at the 1994 AGU meeting. At the Sept. 1994 ILP/USGS Paleoseismology Conference in Marshall, California, we discussed areas of responsibility for California (and other areas in the Western Hemisphere) and made some limited progress with gaining further commitments. The main problems with California are the large number of faults and folds and the overwhelming amount of data that must be compiled (see also item 3). In addition, in Nov. 1993, we organized and chaired our first meeting for the Active Fault Map of Mexico. During the year, the Mexican group was organized by Fernando Ortega (UNAM) and they agreed to hold a second formal meeting of this group at the Mexican Geophysical Union in Nov. 1994. And finally, for the 1994 GSA meeting in Seattle in

October, we organized a meeting to discuss the status of compilations for most of the western states, and to gain further commitments for the Pacific Northwest and Canada.

2. By the end of FY 94, we will have obtained satisfactory to excellent digital data for Quaternary faults in California, Nevada, Utah, the west half of Montana, east-central Idaho, west Texas, and the central U.S. (see Table 1). The California faults were scanned from a specially prepared version of Jennings' 1992 fault map (1:750,000 scale). This file has been edited and is being used by USGS personnel. However, we are revising these files to reflect changes made on the 1994 version of Jennings' map (release date ca. Dec. 1, 1994). There is considerable concern at CDMG about release of their data, which they treat as proprietary; thus, the USGS and CDMG are discussing how and when such data can be released. The files for most other states come from sources within the USGS or from cooperative efforts with state geological surveys. In addition, we are acquiring new data for the 100-km region surrounding Yucca Mountain and for Oregon as a Oregon DOT-sponsored study.

3. Discussions are ongoing with Angela Jayko (USGS-Menlo Park) concerning research on active folds and blind thrusts in the San Francisco Bay region, which is being conducted by a CONCERT working group (under NEHRP). We are trying to assure that the CONCERT effort will directly interface with our larger project, and if this is successful we will promote cooperation on similar efforts that are underway in Southern California as a result of special Northridge earthquake funding. Jayko's group is helping modify our guidelines; although these were developed for faults, folds have special considerations in terms of rates of uplift, geologic setting (*i.e.*, blind thrusts), and geomorphic expression.

4. We have tested our methods of digitization and data compilation for western Montana (where we had previous knowledge of faulting) and west Texas (where Collins and Raney have completed their work). At this point we are ready to "freeze" the input fields and start actual construction of the database structure in FoxPro. This aspect of the project involves a fair amount of programming, and we don't want to change the data input fields from this point on. The results of the Montana pilot study were presented at the 1994 GSA meeting in Seattle, and we received many favorable comments. In addition, preliminary versions of the California Nevada, and Utah fault maps were presented at the GSA meeting in Seattle. The response to these poster sessions indicates a high demand for the digital products, especially in on-line form such as over the Internet via World Wide Web. We anticipate further changes or considerations as to product release as we approach completion of the project in 1996(±). The Montana and Texas products are nearly complete, and we intend to submit the maps and text data for USGS review in late 1994.

## REPORTS

Crone, A.J., and Machette, M.N., 1993, A paleoseismic view of seismic hazards in stable continental regions—Similarities between the 1993 Latur, Southern India earthquake and Australian and North American intraplate earthquakes: *Eos*, 1993 Fall Meeting Program, p. 218 and 222 (late submittal poster session).

Hutton, J.T., Prescott, J.R., Bowman, J.R., Dunham, M.N.E., Crone, A.J., Machette, M.N., and Twidale, C.R., 1994, Thermoluminescence dating of Australian palaeo-earthquakes: *Quaternary Geochronology (Quaternary Science Reviews)*, v. 13, p.143-147.

Machette, M.N., 1994, A new digital map and database for major active faults and folds in the United States: *Geological Society of America Abstracts with Program*, v. 26, no. 7, p. A-304 (poster).

Machette, M.N., and Crone, A.J., 1994, Geologic investigations of Australian Earthquakes: Paleoseismicity and the recurrence of surface faulting in stable regions of continents: *Earthquakes and Volcanoes (USGS/OEVE publication)*, v. 24, no. 2, p. 74-85.

Machette, M.N., Haller, K.M., and Dart, R.L., 1993, A new digital map and database for major active faults in the United States: *EOS*, v. 74, no. 43, p. 66, Oct. 23, 1993/Supplement (poster).

- Machette, M.N., 1994, Plans for a new digital map and database for major active faults of the Caribbean and Central America: *Eos*, v. 75, no. 44, p. 610, Nov. 1, 1994/Supplement (poster).
- Machette, M.N., Haller, K.M., and Dart, R.L., 1994, A new digital map and database for major active faults (and folds) in the United States [abs.], in *Proceedings of the Workshop on Paleoseismology*: U.S. Geological Survey Open-File Report 94-569, p. 110-111 (poster).
- Machette, M.N., and Thenhaus, P. C., Paleoseismicity of the basin and range—Examples of slip rates, recurrence intervals, and patterns of faulting: *Proceeding of the Fifth U.S. National Earthquake Engineering Conference*, Chicago, Illinois, July 10-14, 1994, 34 ms. p., 13 figs, 2 tables, in press.
- Zoback, M.L., Zoback, M.D., Crone, A.J., Machette, M.N., and Richardson, R.M., 1994, Processes and patterns of intraplate seismicity: *Geological Society of America Abstracts with Program*, v. 26, no. 7, p. A-382.

**TABLE 1. Status of Quaternary fault data for the United States**  
*[Data quality: A, good; B, adequate; C, poor or nonexistent]*

State/region	Map and Type	Database and Type	Main Sources
Alaska	<b>A.</b> Digital, 1994 (in prep.).	<b>B.</b> Text, unpub., 1985-94.	Plafker and Gilpin
Arizona	<b>A.</b> Nondigital, 1986.	<b>A.</b> Partial, text; 1983-85.	Pearthree and Menges
California	<b>A.</b> Digital, 1994 (in prep.) nondigital, 1984, 1992.	<b>B.</b> Partial, text; 1984, 1994.	Consortium (USGS, CDMG, and others)
Colorado	<b>B.</b> Digital, ca. 1986.	<b>B.</b> Partial, text; 1975, 1980, 1986.	Colman, Kirkham, Rogers, and USBR
Eastern U.S.	<b>C.</b> Uncompiled.	<b>C.</b> Uncompiled.	Amick, Talwani and Tuttle (?)
Hawaii	<b>C.</b> Uncompiled.	<b>C.</b> Uncompiled.	None
Idaho	<b>A.</b> Digital for north half, 1994 (in prep.).	<b>A.</b> Text, 1975, 1994 (in prep.).	Hilt, Breckenridge, and Haller
Mid-Continent	<b>A.</b> Digital, 1994 (in prep.).	<b>A.</b> Text, 1994 (in prep.).	Crone, Obermeier, Schweig, and others
Montana	<b>A.</b> Nondigital, 1975, 1984, 1987; digital, 1994 (in prep.).	<b>A.</b> Text, 1975, 1984, 1994 (in prep.).	Johns and others, Witkind, Haller, Stickney, and USBR
Nevada	<b>A.</b> Digital, 1991; needs revision.	<b>B.</b> Partial, 1994 (in prep.).	Dohrenwend, Reheis, Piety, and Haller
New Mexico	<b>B.</b> Part digital, ca. 1987.	<b>B.</b> Partial; text, 1987, 1994.	Machette and Kelson
Oregon	<b>A.</b> Non-digital, 1992; digital, 1993, 1994.	<b>B.</b> Partial, text; 1992, 1994.	Pezzopane, Geomatrix, Yeats, and DOGAMI
Texas (West)	<b>A.</b> Digital, 1994 (in prep.).	<b>A.</b> Text, 1994.	Collins and Raney
Utah	<b>A.</b> Digital, 1993.	<b>A.</b> R-base, 1993.	Hecker and Jarva
Washington	<b>B.</b> Non-digital, 1991.	<b>C.</b> Uncompiled.	Walsh and others
Wyoming	<b>B.</b> Nondigital, 1975, 1991, 1994 (in prep.).	<b>B.</b> Text, 1975, 1991, 1994 (in prep.).	McCalpin, Pierce, and Case

**Earthquake Hazards Assessment for  
Northwestern Oregon.**

Award # 1434-93-G-2324

Ian P. Madin and Dr. Matthew A. Mabey  
Oregon Department of Geology and Mineral Industries  
800 NE Oregon St. # 28  
Portland, OR 97232

**ELEMENT II.4**

**Investigations**

This project consists of 5 separate tasks. Progress on each is summarized below. Progress has been slow because one of the P.I.'s lost much of 1994 to a family medical crisis. The project has been extended to April 1995.

**Task 1. Publication of the Damascus 1:24,000 quadrangle.**

Largely complete. Print proofs are expected to be available on November 1, 1994.

**Task 2. Publication of Charleston 1:24,000 quadrangle.**

Map is ready to go to review. Will go to cartography department January 1, 1995.

**Task 3. Publication of the Liquefaction map of the Portland quadrangle.**

Complete, map is available as Oregon Department of Geology and Mineral Industries GMS-79.

**Task 4. Shallow seismic profiling of potential Quaternary faults.**

This task involved the purchase of seismic reflection hardware (geophones and cable) and software (Eavesdropper) and collection of seismic reflection lines across faults in Beaverton, Hillsboro and the northern Willamette Valley. Our strategy was to reoccupy industry seismic lines which positively identified faults at depths of hundreds of meters, to determine whether these faults extended into shallow Quaternary deposits. The ultimate goal is to identify targets for future trenching. Acquisition has been completed on 3 of the 4 proposed seismic profiles and they are currently being processed. Processing is nearly complete on two of the lines with no offset of bedding being immediately apparent in the deposits near enough the surface to be reached with a trench. The processing of the third line is not yet to a point where a preliminarily interpretation can be made. Refinement of the processing of all lines needs to be completed for final interpretation. The fourth profile is being offset to a street adjacent to the original oil industry seismic line due to steady, heavy traffic on the original street.

**Task 5. Collection of shear wave velocity data through co-ops.**

Complete. This funding was used in co-ops that resulted in collection of shear-wave velocity profiles from over 680 m of cone pentrometer sounding and over 1600 m of purpose-drilled boreholes. The velocity data will be published in 1995 as a DOGAMI Open-File Report.

**Instrumentation to Improve the Washington Regional Seismograph Network**  
**1434-92-G-2195 S.D. Malone and R.S. Crosson, P.I.s**

Geophysics Program  
University of Washington  
Seattle, WA 98195  
(206) 543-8020

e-mail: steve or bob@geophys.washington.edu  
Oct. 1, 1993 - Sept. 30, 1994

### **Investigations undertaken**

This contract is for the purchase and installation of four new, high quality broad-band three-component digital seismograph stations as an addition to the Pacific Northwest Seismograph Network (PNSN; see the report for Joint Operating Agreement 1434-92-A-0963). It also includes funding to develop software for recovering and integrating the broad-band data into our routine data analysis procedures. In addition to the four stations supported under this contract, a prototype station (LON), situated on the same pier as the DWWSSN station at Longmire WA (near Mount Rainier), has been operating since early 1993. By the end of the contract period, there will be a total of 10 high quality seismograph stations operating in the Pacific Northwest (5 operated by the PNSN, two by USNSN, one by IRIS/USGS -- COR, and two by the University of Oregon; PIN and DBO).

### **Results**

In addition to the LON prototype, three of the new stations are fully operational, and data from them are routinely merged with PNSN short-period data. Since July of 1993, we have recovered 5,400 broad-band data traces for 2,800 different events. Installation of the final station (with on-site recording) will be completed in early 1995 on Marrowstone Island, Washington. Figure 1 shows the current PNSN network configuration (both broad-band and short-period).

During this contract period, we upgraded two of the four installed broad-band three-component stations. All installed recorders now have GPS time-code receivers and 24 bits/sample dynamic range. Three of the stations (LON at Longmire, LTY at Liberty, and SSW at Satsop; all in Washington) time-stamp, digitize, and record data on-site. We recover selected broad-band data from these stations via phone lines using automated procedures that run late at night (to minimize long-distance charges). The fourth station, (TTW) near Tolt, Washington, also digitizes and time-stamps data on-site, but continuously telemeters data to the UW Seismology Lab where it is recorded as a continuous data stream. Individual events are extracted from the data stream and, with data from other broad-band stations (including COR, PIN, and DBO as well as LTY, SSW, and LON), are merged and archived with data from PNSN short-period stations. The broad-band event data are also translated to IRIS-SEED format and submitted to the IRIS Data Management Center for archive and distribution.

To allow broad-band data to be merged into the PNSN short-period data stream, the PNSN has modified both trace data and pickfile (phase arrival times) formats, and associated data-processing software. The new working trace data format (UW-2) allows us to accommodate data of varying durations, sample rates, start times, and formats (e.g., integer, floating point, etc.), is extensible without affecting existing processing programs, and is backward-compatible with our original (UW-1) format.

The new UW-2 pickfile format provides full support for three-component stations, flexibility to represent arbitrary phase types (our old UW-1 format could only represent P and S phases) such as Pn and PmP, and a number of other advantages, and is also backward compatible. Interactive viewing of both trace and pickfile data is provided through **Xped** (X pick editor), an X window application that allows the user to display trace and pick information, modify picks, run location programs, and perform other data analysis functions.

We are receiving data from the USNSN via VSAT and recording it continuously. We are currently developing software that will allow the USNSN data to be merged into our event data files. Eventually, the data from our continuously transmitting site (TTW) will be reformatted into USNSN format and transmitted to the National Seismic Network in Golden, CO via VSAT.

One of our students, Gia Khazaradze, has developed a technique to generate synthetic Wood-Anderson records from the broad-band data. This provides several independent measurements of local magnitudes from the broad-band data, and should improve our ability to provide more robust magnitude estimates.

#### Abstracts

Khazaradze, G. and S.D. Malone, 1994, Determination of local magnitude using Pacific Northwest Seismic Network Broadband Data, EOS, Vol. 75, Supplement to No. 44, p. 460.

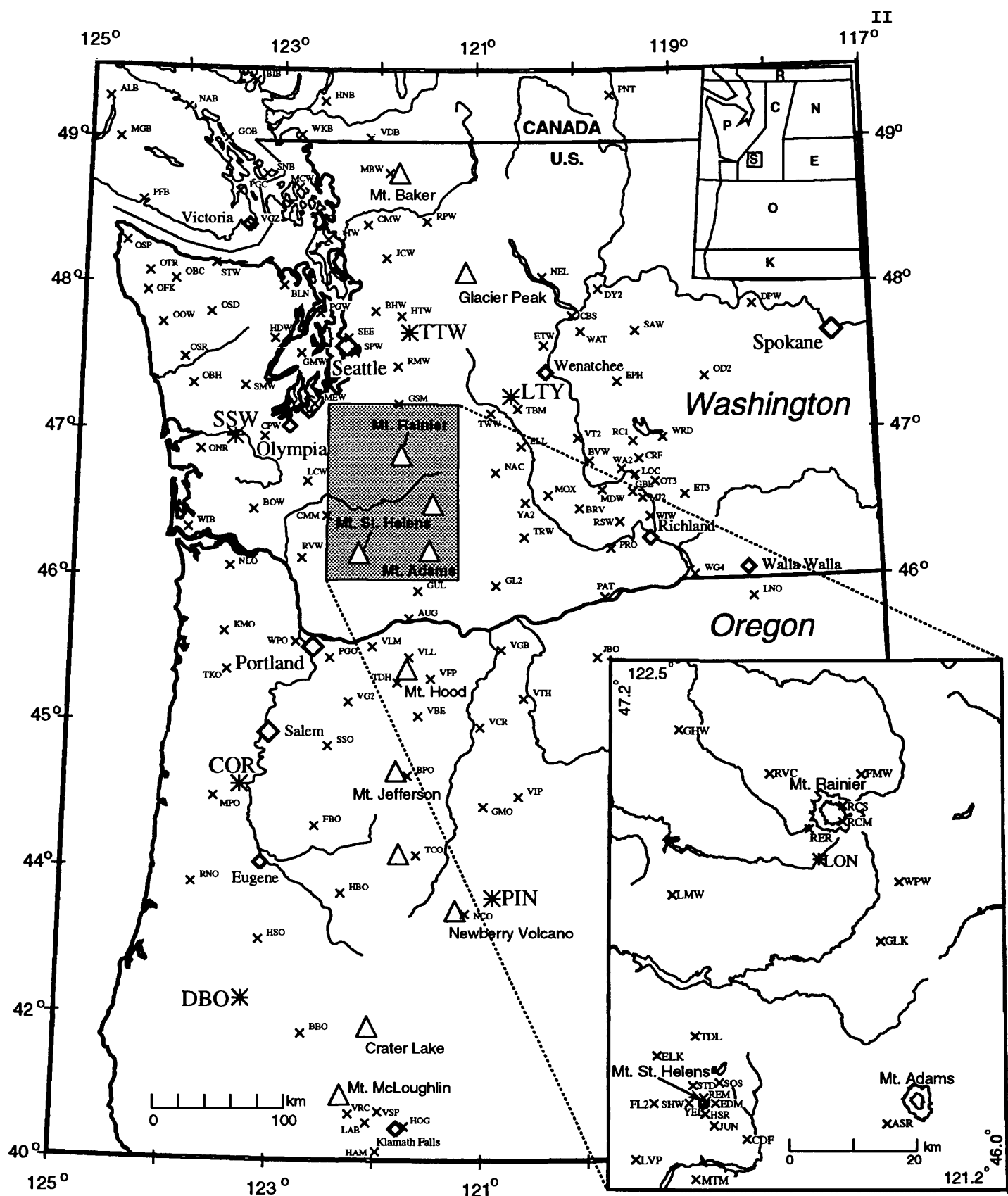


Figure 1. Locations of stations operating in the Pacific Northwest at the end of 1994. Short-period stations are shown by the "x" symbol, while broad-band stations are designated by the larger asterisks. The locations of volcanic centers are shown by triangles, and cities are indicated by white-filled diamond shapes. Most stations are operated by the PNSN, but station COR is operated by Oregon State University, and stations DBO and PIN are operated by the University of Oregon. The upper inset shows the eight regions in which different crustal velocity models are used to locate hypocenters (P, Puget Sound; C, Cascades S, Mt. St. Helens; N, northeast Washington; E, southeast Washington; O, northern Oregon; K, southern Oregon; and R, regional velocity model). The lower inset shows station locations in the vicinities of Mts. Rainier, St. Helens, and Adams.

**PALEOSEISMIC INVESTIGATION OF THE NORTH AMERICA-CARIBBEAN STRIKE-SLIP PLATE BOUNDARY, DOMINICAN REPUBLIC**

**Award Number: 1434-93-G-2341**

**Paul Mann**

**Institute for Geophysics, University of Texas at Austin, 8701 Mopac Blvd., Austin, Texas 78759**

**Telephone: 512-471-0452; FAX: 512-471-8844; email: paulm@utig.ig.utexas.edu**

**NEHRP II.5**

**Investigations undertaken**

The Septentrional fault zone is the major left-lateral strike-slip fault separating the North America and Caribbean plates in Hispaniola (Fig. 1). Much of the active, 3000 km long left-lateral plate boundary is submarine or crops out in pre-Quaternary rocks that do not preserve a record of recent activity. However in northern Hispaniola (Dominican Republic), the Septentrional fault zone forms a prominent scarp in alluvium and provides an opportunity to study the Quaternary behavior of the plate boundary and to quantify the seismic hazard it represents to the densely populated islands of Hispaniola and neighboring Puerto Rico.

Collaborative work involving Mann, Carol Prentice (USGS/Menlo Park) and George Burr (NSF Accelerator Facility, Univ. of Arizona/Tucson) in 1994 consisted of three efforts: 1) continued analysis of trench data and radiocarbon dating of samples collected in 1993 from the Septentrional fault zone in the Cibao Valley; 2) improved mapping of fault traces in the western part of the Cibao Valley using aerial photographs and field observations; and 3) integration of information gained from previous and ongoing fault trench work into the design of a new northeastern Caribbean GPS network funded by NSF.

**Results**

**1) Continued analysis of fault data and radiocarbon dating.** Trenching in 1991 at site 91-2 revealed folded and faulted Holocene deposits that provide evidence for an earthquake on the Septentrional fault zone that occurred before 1260 AD (Prentice et al., 1993). In 1993, trenching at site 93-2 was carried out to better constrain the age of this event (Fig. 2). Evidence for this event included the folding of units 70 and below and the presence of a sand-blow deposit indicating paleoliquefaction. Radiocarbon dates on charcoal samples

from this excavation (Fig. 3) confirm that this is the same earthquake as seen in trench 91-2 and this this earthquake occurred between AD 1150-1230 or about 760-840 years ago.

3-D excavation of a buried channel at site 93-2 showed that the AD 1150-1230 ground-breaking earthquake on the central Septentrional fault zone was accompanied by about 5 m of left-lateral offset and about 2 m of vertical displacement (Fig. 4). This offset shows that the earthquake was large,  $\geq M7.5$ .

If all motion is concentrated on the central Septentrional fault and assuming the minimum predicted plate rate of 5 mm/yr, several meters of slip have accumulated in the  $800\pm40$  years since the last groundbreaking earthquake seen in our trenches. The absence of ground rupture in such a long period suggests a high earthquake potential for the Hispaniola-Puerto Rico segment of the North America-Caribbean strike-slip boundary.

**2) Improved mapping of fault traces.** Studies of aerial photographs and field mapping in 1993 revealed that the westward continuation of the fault trenched at 91-2 and 93-2 splays into an inactive, but geomorphologically prominent, northern branch striking 110 and a less conspicuous southern branch striking 100. Fault features are less pronounced or obscured along the southern branch because this area of the Cibao Valley is heavily sedimented by late Holocene fluvial sediments of the Yaque River. Discontinuous scarps of the southern branch align with the active submarine extension of the fault mapped with sidescan sonar along the northern margin of Haiti. Field studies of the northern branch of the fault show that its trace is covered at one locality by late Quaternary terrace and fan deposits and that stream channels, terraces and other marker features have not been disturbed by faulting. Based on these observations, we conclude that the southern branch is the more active strand and that the northern branch has been abandoned. The southward shift of the fault trace has transferred a small sliver of the Caribbean plate to North America.

We are currently preparing maps of the fault scarps and fault-related features of the entire Septentrional fault zone including the two western strands.

**3) Expansion of the Hispaniola GPS network.** In May of 1994, 11 GPS instruments were operated by DeMets, Mann, Calais, UNAVCO personnel and Dominican collaborators in the Dominican Republic as part of an 18 instrument northeastern Caribbean plate regional network (CANAPE) funded by NSF (Ambeh et al., 1994). The network includes four "core" sites occupied in 1986 as part of one of the first regional GPS experiments. Data quality for both the 1986 and 1994 data is good and comparisons should yield the first direct measurement of the rate of Caribbean-North America plate motion through the island of Hispaniola. These rates will be used to better constrain our previous calculation for the amount of slip accumulation along the central Septentrional fault zone (Prentice et al., 1993).

Four new benchmarks were built and surveyed in a north-south line crossing the area of the central Septentrional fault known from trenching not to have ruptured in  $800 \pm 40$  years. This line is part of a longer across-strike line that spans the entire island and is tied to stable sites on the North America plate in the Bahamas and Florida and to a presumably stable site Aves Island in the eastern Caribbean Sea.

### References cited

Prentice, C. S., Mann, P., Taylor, F. W., Burr, G., and Valastro, S., 1993, Paleoseismicity of the North America-Caribbean plate boundary (Septentrional fault), Dominican Republic: *Geology*, v. 21, p. 49-52.

Ambeh, S., Saleh, J., Bilham, R., Kozuch, M., and 10 others, 1994, Caribbean GPS networks: *Transactions of the American Geophysical Union, EOS*, v. 75, p. 612.

### Reports published

Prentice, C. S., Mann, P., Burr, G., and Peña, L. R., 1994, Timing and size of the most recent earthquake along the central Septentrional fault zone, Dominican Republic: in Prentice, C., et al., *Proceedings of the Workshop on Paleoseismology*, USGS Open-File Report 94-568, p. 158-160.

Mann, P., Prentice, C., Burr, G., and Peña, L. R., 1994, A splayed, late Quaternary trace of the North America-Caribbean strike-slip fault in northern Hispaniola and its seismotectonic implications: *Transactions of the American Geophysical Union, EOS*, v. 75, p. 611.

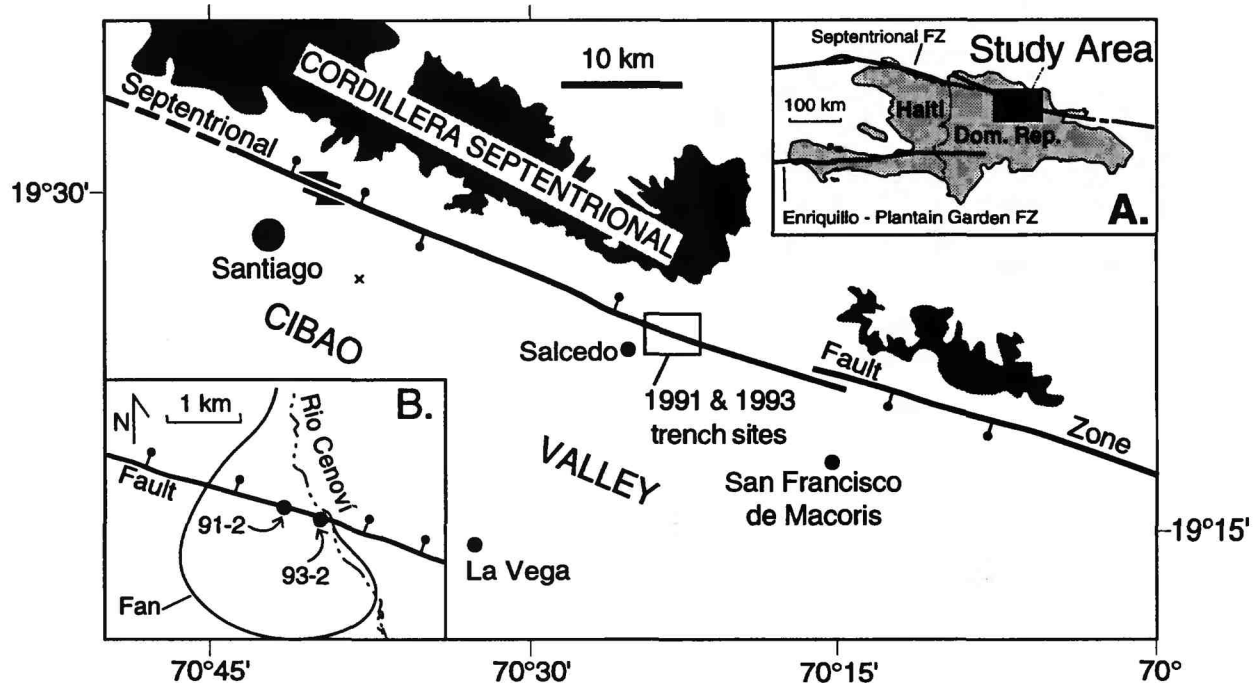


**Figure 1.** Map showing location of 1991 and 1993 trench sites along the central Septentrional fault zone in Hispaniola. Inset A shows location of study area (black rectangle). Area of trench sites 91-2 and 93-2 on Cenovi fan burying the scarp of the Septentrional fault zone are shown in inset B.

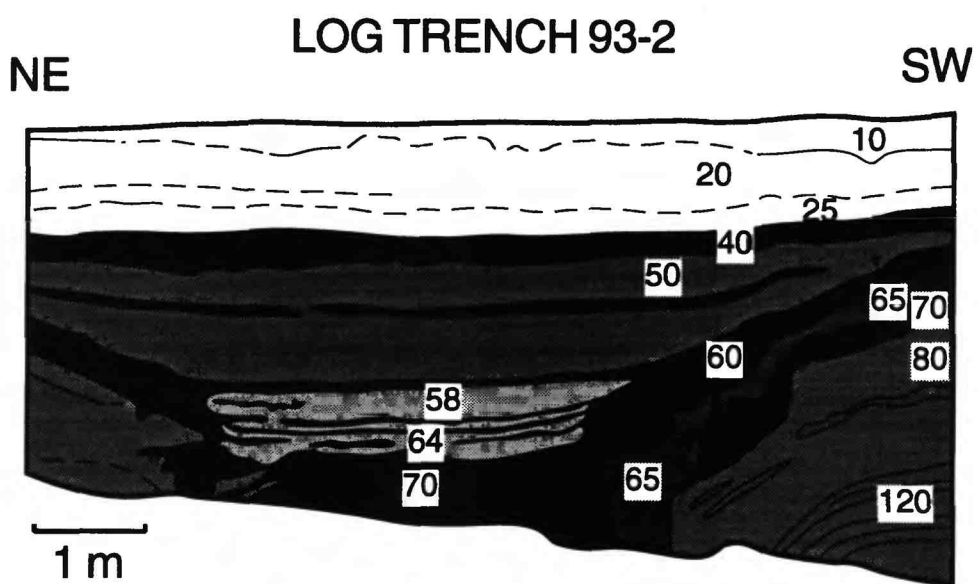


**Figure 2.** Partial log of trench 93-2 on Cenovi fan (see Figure 1, inset B for location). Earthquake occurred when unit 70 was the ground surface. This event caused liquefaction of unit 65 and tilting of horizons 70-120. Upper units are unfaulted and fill in depression created by syncline.

## ALL DATES TRENCH 93-2

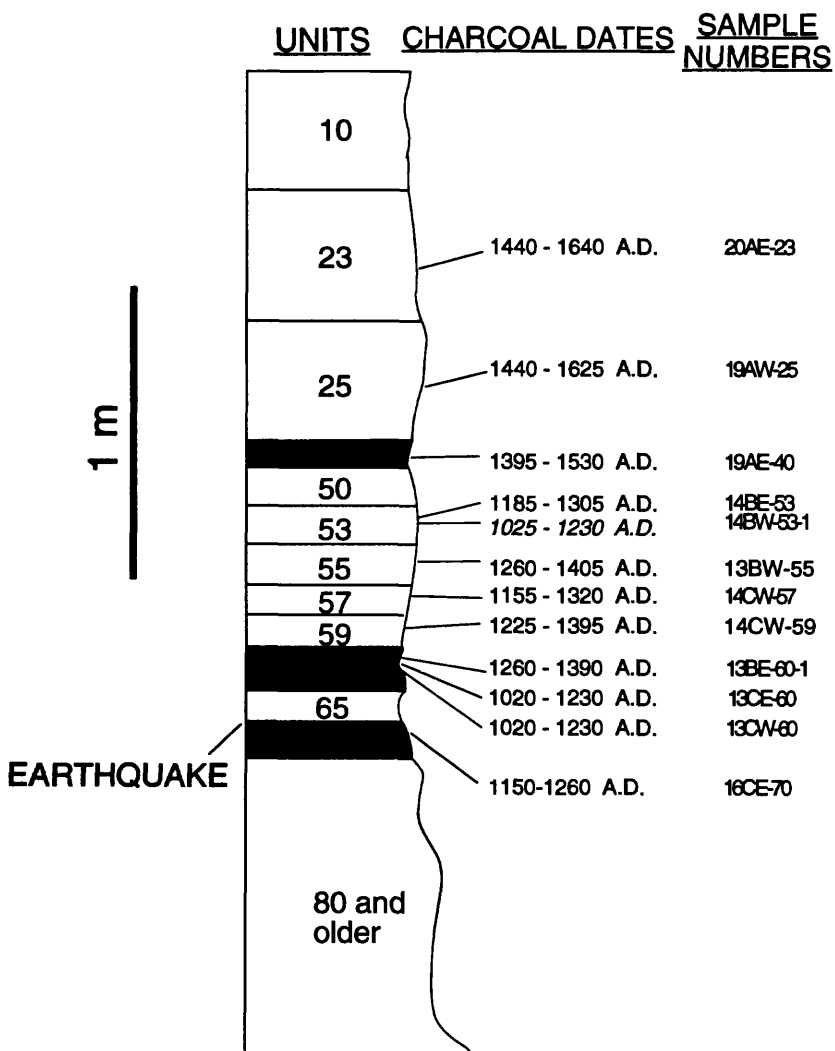


**Figure 3.** Stratigraphic column showing dendrochronologically-calibrated radiocarbon dates (2 sigma) of samples collected from trench 93-2. Note the relation of dated units to earthquake horizon indicated. Radiocarbon dates indicate that this earthquake occurred between AD 1150 and 1230. Age results from trench 93-2 are consistent with our earlier results from study of trench 91-2 (Prentice et al., 1993).

### 3-D EXCAVATION AT TRENCH 93-2

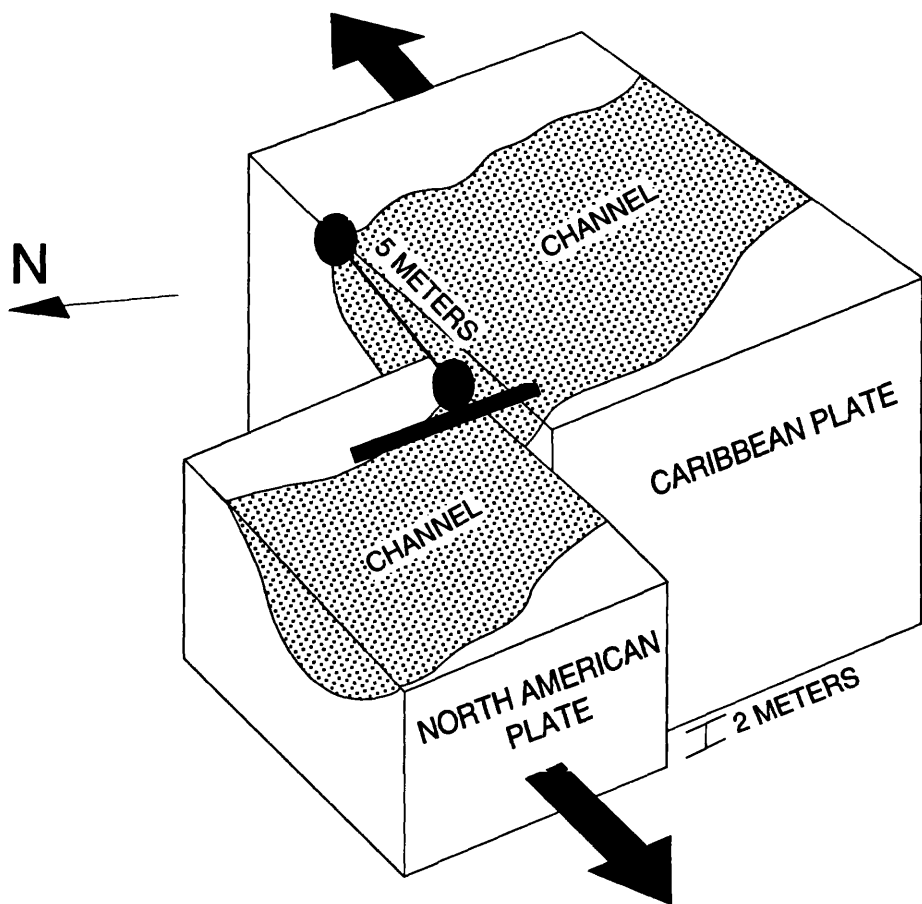


**Figure 4.** Schematic block diagram showing offset of buried Holocene channel deposit (stippled area) that was excavated using 3-D techniques to determine horizontal and vertical offset of approximately 2 and 5 meters, respectively. This offset occurred as the result of the earthquake of AD 1150-1230 and indicates that this event was a large (M7.5). Black bar shows location of exposure.

# ACTIVE MARGIN TECTONICS, PACIFIC NORTHWEST REGION

## 9960-13416

Patricia A. McCrory  
 Branch of Earthquake Geology and Geophysics  
 U. S. Geological Survey  
 345 Middlefield Road, MS 977  
 Menlo Park, California 94025  
 telephone: 415.329.5677  
 telefax: 415.329.5163  
 pmccrory@isdmnl.wr.usgs.gov

### Program Element II

#### **Investigations Undertaken:**

The active Cascadia subduction zone is situated adjacent to densely populated areas in the Pacific Northwest region of North America mandating evaluation of its potential for generating damaging earthquakes. However, low ambient seismicity along most of the Pacific Northwest margin hampers evaluation of its seismic potential. The lack of large historic ( $>M7.5$ ) earthquakes and several unique features of the Cascadia subduction boundary (*e.g.*, minimal slab-pull forces driving megathrust earthquakes; conditions favoring ductile deformation of the overriding plate; partitioning of crustal strain reflecting segmentation of the margin) preclude using a simpler subduction system as a modern analog for modeling future seismic behavior. Because of the lack of such an analog, deciphering the record of recent tectonism offers one of the few means by which the seismic potential of the Cascadia subduction margin can be evaluated. This research project uses the record of cumulative Quaternary crustal deformation to provide a context in which to interpret the Holocene record of coseismic subsidence and the modern geodetic record of interseismic strain accumulation.

Several estuaries along the Cascadia margin record episodes of abrupt Holocene subsidence. A model of great megathrust earthquakes recurring about every 500 y is inferred from these subsidence records. However, the structural setting of many of these estuarine sites is unknown, making this inference of a megathrust source ambiguous. Regional geodetic data is consistent with a model of interseismic elastic strain accumulation above locked portions of the megathrust; however, geodetic results display a more complicated pattern of interseismic strain accumulation than the estuarine model postulates. In particular, these data show variations in uplift rates parallel to the margin which suggest a component of N-S contraction contributes to deformation of the margin. Also, the longer Quaternary geologic record onshore and subsurface seismic data offshore demonstrate that strain accumulation within the coastal zone is not entirely elastic. Oblique convergence between the Juan de Fuca plate and the overriding Washington margin is partially dissipated by internal deformation within the accretionary prism. Geodetic data together with Quaternary geologic data collected by this project suggest a more complex dynamic setting for deformation within this convergent margin and a more complex relationship between deformation and significant seismic events.

Previous project research focused on reconnaissance mapping of Quaternary deformation along 70 km of sea cliffs between Copalis River and Browns Point. This initial mapping established that although, in general, the 83-ka shore platform forming the sea cliffs has been gently uplifted and warped; several sites have undergone more intense folding and faulting. This

style of intense localized deformation overprinted on modest regional deformation suggested the presence of active crustal structures deforming the coastal zone.

In FY 1994, project research focused on mapping the distribution of these young crustal structures and relating their activity to subduction-boundary dynamics. Quantifying the rates and style of crustal faults and folds addresses several key questions regarding seismic hazard along the Cascadia margin: (1) What mechanism(s) cause the Holocene subsidence events? (2) What seismic hazard is associated with N-S compression of the margin? (3) How is strain partitioned between ductile (aseismic) and brittle (seismic) rupture? Project research aims to quantify deformation rates over several time periods and to provide insights into the processes controlling modern rates of shortening, Holocene rates (past 10 ky), and Quaternary rates (past 500 ky).

## Results

**Data Collection.** During FY 1994, this project continued field work aimed at documenting the style and recency of deformation at several sites along the coast. For example: (1) Langely ridge (Figure 1, Site A), just south of Copalis River, trends N65°E, is at least 9-km long, and rises 75 m above sea level. Field investigation of surface exposures reveal both steeply dipping glaciofluvial strata (up to 80° E) and several late Quaternary thrust faults with offsets ranging from 0.5 to 2.5 m. Field data suggest an active ENE-trending fault-propagation fold beneath Langely ridge. FY 1994 field work documented the distribution of young deformation along the ridge and attempted to collect charcoal for radiocarbon analyses (unsuccessful to date) to constrain timing of the most recent slip. Quantifying the slip history of the primary thrust fault beneath Langely ridge is vital for resolving whether the sources of the Copalis River seismic events are megathrust sources, crustal sources or both. (2) Preliminary field investigation of steeply tilted glaciofluvial deposits (up to 65°E) adjacent to Quinault River (Figure 1, Site B) provides evidence of both young folding and thrust faulting. The pattern of folding and minor thrust faulting (offsets range from 0.2 to 0.5 m) is consistent with an underlying fault-propagation fold trending NNW. This fault-propagation fold is part of a 100-km long thrust system which parallels the coast. (3) Completed a high resolution leveling survey across another part of the NNW-trending thrust system with evidence of Holocene movement ( $\leq 2$  mm/y) near the Raft River (Figure 1, Site D) (in collaboration with M. Lisowski and M. Murray). Raw data indicates a surveying error of 0.9 mm and preliminary corrections indicate minimal refraction error. Thus, a planned re-survey in FY 1997 should be able to document rates of ductile deformation across one of the Holocene structures in this area. This experiment is aimed at determining the relative contributions to ductile strain accumulation from (i) elastic strain along a locked megathrust and (ii) inelastic strain from crustal shortening.

**Data Reduction.** (1) Preliminary compilation of a coastal and nearshore structure map in central Washington in order to discern blocks with differing structural fabrics. (2) Initial comparison of the pattern of post-83 ka deformation of the shore platform with the pattern of modern geodetic deformation. (3) Initial geomorphic analysis of coastal central Washington in order to identify and evaluate active structures. (4) Preliminary reconstruction of Juan de Fuca plate with respect to Washington margin during last 20 My (in collaboration with D. Wilson, U.C. Santa Barbara) in order to gain insight into how shortening associated with oblique convergence is distributed within the margin.

**Research Results.** Although the Cascadia subduction system has received increasing scrutiny in recent years, it is still unclear what portion of the 30 to 50 mm/y oblique convergence across the plate boundary is dissipated as aseismic deformation; what portion is locked along the megathrust; and what portion is represented by seismic deformation within the overriding crust. This information is crucial to understanding the relative frequency of megathrust and crustal

earthquakes. The complex pattern of onshore and nearshore Quaternary structures within the upper crust is characterized by broad folds and tear faults trending ENE, overprinted on tighter folds also trending ENE and thrust faults trending NNW. The regional pattern of Quaternary subsidence in the Queets River and Grays Harbor areas and uplift in adjacent areas broadly agrees with the regional geodetic pattern of uplift. This coherence between late Quaternary deformation and modern interseismic deformation suggests that ongoing crustal shortening may result from coupling between the subducting Juan de Fuca plate and the accretionary rocks along the central segment of the Cascadia margin. These results also suggest that the Holocene estuarine-subsidence events along this portion of the margin may be partially controlled by ongoing deformation within major crustal structures. If some of these Holocene seismic events have a crustal source, the recurrence interval of great megathrust earthquakes needs to be reevaluated.

A crustal structural source for any of the subsidence record in the Copalis-Grays Harbor-Willapa Bay area was previously rejected because of the lack of evidence for surface rupture that could account for coeval subsidence at sites 55 kilometers apart (Atwater, 1992, JGR). However, the lack of recognized surface rupture does not preclude a crustal source in a region of compressional tectonism. It is widely recognized that many active folds are cored by "blind" thrust faults which are capable of generating regional coseismic vertical displacements of 1 to 2 meters (e.g., the Loma Prieta and Northridge earthquakes). In fact, the 7-m uplift of a Holocene terrace in Puget Sound is attributed to such a blind-thrust mechanism (Buckman *et al.*, 1992, Science). The possibility of similar structures elsewhere in coastal Washington cannot be ruled out without additional study of deformed Quaternary deposits onshore and offshore.

## Reports Published in FY 94

McCrory, P. A., Wilson, D. S., Ingle, J. C., Jr., and Stanley, R. G., 1994, Neogene geohistory analysis of Santa Maria basin, California and its relationship to transfer of central California to the Pacific plate: U. S. Geological Survey Bulletin 1995-J.

McCrory, P. A., 1994, Measuring the Earth's pulse, Spirit leveling: Quinault Natural Resources, v. 17, n. 2, p. 30-31.

McCrory, P. A., 1994, Quaternary crustal shortening along the Cascadia margin, Washington [abs.]: Geological Society of America Abstracts with Programs, v. 26, n. 7, p. 523.

McCrory, P. A., 1994, Late Quaternary thrust faulting along the Cascadia margin, Washington: Implications for partitioning of strain [abs.]: Eos Transactions, American Geophysical Union, v. 75, n. 44, p. 622.

McCrory, P. A., Wilson, D. S., Ingle, J. C., Jr., and Stanley, R. G., 1995, Neogene Transfer of Central California to the Pacific Plate: Evidence from Santa Maria Basin, California [abs.]: American Association of Petroleum Geologists, Program & Abstracts, Pacific Section.

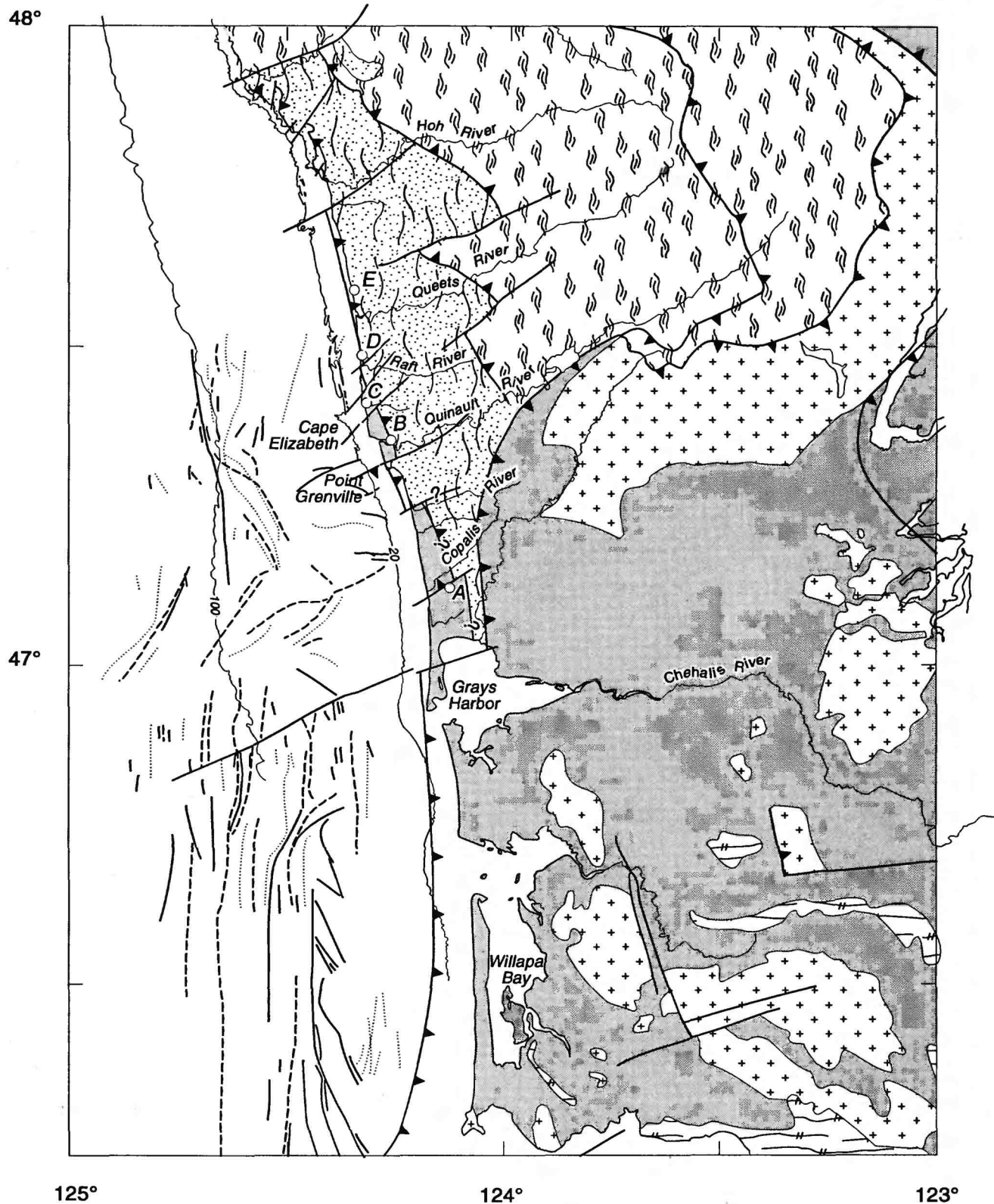


Figure 1. Map showing generalized bedrock geology; location of field sites; 20- and 100-m bathymetric contours offshore. Barbs on upper plate of thrust faults; dashed lines, anticlines; dotted lines synclines. (Modified from Rau, 1973; 1975; 1979; 1980; Rau and MacFarland, 1982; Tabor and Cady, 1978; Wagner *et al.*, 1986; Snavely, 1987; Snavely and Kvenvolden, 1989; Walsh *et al.*, 1987; Orange *et al.*, 1993)

## INDEX 1

### INDEX ALPHABETIZED BY PRINCIPAL INVESTIGATOR

	Page
Agnew, D. C.	234
Aki, K.	1
Aki, K.	855
Andrews, D. J.	3
Arabasz, W. J.	4
Archuleta, R.	856
Aster, R. C.	239
Atwater, B.	246
Atkinson, G. M.	860
Austin, W. J.	248
Bell, E. J.	1051
Bennett, R.	249
Beroza, G.	7
Black, B. D.	257
Black, G. L.	863
Blakely, R. J.	263
Boatwright, J.	13
Boatwright, J.	17
Bock, Y.	267
Bohlen, S.R.	21
Boore, D. M.	864
Borchardt, G.	273
Braile, K. W.	277
Bray, J. D.	867
Breckenridge, R. M.	286
Breckenridge, K. S.	870
Bucknam, R. C.	288
Bufe, C. G.	1055
Butler, H. M.	290
Campbell, N. P.	291
Catchings, R.	23
Catchings, R.	25
Celebi, M.	875
Chen, Y. J.	27
Chester, F. M.	31
Chiu, J. M.	307
Choy, G. L.	1060
Clark, M. M.	310
Clayton, R. W.	37
Crone, A. J.U.S.	312
Crosson, R. S.	42

Crosson, R. S	Washington, University of	317
Delaney, P.	U.S. Geological Survey	47
Dewey, J. W.	U.S. Geological Survey	1064
Dieterich, J.	U.S. Geological Survey	765
Dmowska, R.	Harvard University	51
Dreger, D.	California, University of, Berkeley	319
Dusseau, R. A.	Wayne State University	878
Ebel, J. E.	Boston College	58
Ebel, J. E.	Boston College	882
Ebel, J. E.	Boston College	1068
Eldredge, S. N.	Utah Geological Survey	1070
Elgamal, A-W	Rensselaer Polytechnic Institute	890
Ellsworth, W. L.	U.S. Geological Survey	64
Endo, E. T.	U.S. Geological Survey	329
Engdahl, E. R.	U.S. Geological Survey	331
Etheredge, E.	U.S. Geological Survey	775
Frost, J. D.	Georgia Institute of Technology	914
Forster, C. B.	Utah, University of	71
Frankel, A.	U.S. Geological Survey	907
Frankel, A.	U.S. Geological Survey	909
Frankel, A.	U.S. Geological Survey	911
Frankel, A.	U.S. Geological Survey	912
Frost, J. D.	Georgia Institute of Technology	914
Galehouse, J. S.	San Francisco State University	335
Gee, L. S.	California, University of, Berkeley	1071
Genrich, J.	California, University of, San Diego	347
Gephart, J. W.	Cornell University	352
Gephart, J. W.	Cornell University	360
Gibbs, J. F.	U.S. Geological Survey	918
Gladwin, M. T.	Queensland, University of	364
Gomberg, J. S.	U.S. Geological Survey	85
Goter, S. K.	U.S. Geological Survey	877
Graves, R. W.	Woodward-Clyde Federal Services	919
Graves, R. W.	Woodward-Clyde Federal Services	927
Guccione, M. J.	Arkansas, University of	373
Haeussler, P. J.	U.S. Geological Survey	386
Hall, N. T.	Geomatrix Consultants	389
Hall, W.	U.S. Geological Survey	87
Harp, E. L.	U.S. Geological Survey	937
Harris, J. B.	Kentucky, University of	393
Harris, R. A.	U.S. Geological Survey	89
Harty, K. M.	Utah Geological Survey	399
Hartzell, S. H.	U.S. Geological Survey	91
Hauksson, E.	California Institute of Technology	401

Healy, J. H.	U.S. Geological Survey	406
Heaton, T.	U.S. Geological Survey	407
Helmberger, D. V.	California Institute of Technology	414
Hengesh, J. V.	Dames & Moore	417
Herrmann, R. B.	Saint Louis University	95
Herrmann, R. B.	Saint Louis University	99
Herrmann, R. B.	Saint Louis University	939
Herrmann, R. B.	Saint Louis University	942
Hickman, S. H.	U.S. Geological Survey	101
Hildenbrand, T. G.	U.S. Geological Survey	428
Hill, D.	U.S. Geological Survey	432
Hill, D.	U.S. Geological Survey	435
Hoffman, D.	Missouri Department of Natural Resources	437
Holt, W. E.	New York State University at Stony Brook	440
Holzer, T. L.	U.S. Geological Survey	945
Howard, K. A.	U.S. Geological Survey	446
Hudnut, K. W.	U.S. Geological Survey	449
Hylland, M. D.	Utah Geological Survey	948
Hyndman, R. D.	Pacific Geoscience Centre	108
Jachens, R. C.	U.S. Geological Survey	451
Jachens, R. C.	U.S. Geological Survey	454
Jacoby, G. C.	Lamont-Doherty Earth Observatory	455
Jacoby, G. C.	Lamont-Doherty Earth Observatory	459
Jarva, J. L.	Utah Geological Survey	1078
Jayko, A. S.	U.S. Geological Survey	392
Jensen, E. G.	U.S. Geological Survey	462
Jibson, R. W.	U.S. Geological Survey	463
Johnson, S. Y.	U.S. Geological Survey	122
Johnston, M. J. S.	U.S. Geological Survey	465
Kanamori, H.	California Institute of Technology	476
Kanamori, H.	California Institute of Technology	479
Keaton, J. R.	AGRA Earth & Environmental, Inc.	481
Keefer, D. K.	U.S. Geological Survey	950
Keefer, D. K.	U.S. Geological Survey	956
Keller, G. R.	Texas, University of, El Paso	433
Kelsey, H. M.	Western Washington University	444
Kelson, K. I.	William Lettis & Associates, Inc.	483
Kelson, K. I.	William Lettis & Associates, Inc.	486
King, C.-Y.	U.S. Geological Survey	126
Klein, F.	U.S. Geological Survey	489
Kulm, L. D.	Oregon State University	493
Lahr, J. C.	U.S. Geological Survey	503
Lajoie, K. R.	U.S. Geological Survey	510
Langbein, J.	U.S. Geological Survey	514

Langbein, J.	U.S. Geological Survey	522
Lay, T.	California, University of, Santa Cruz	526
Lee, W. H. K.	U.S. Geological Survey	534
Lester, F. W.	U.S. Geological Survey	474
Li, Y-G.	Southern California, University of	536
Lienkaemper, J. J.	U.S. Geological Survey	545
Lisowski, M.	U.S. Geological Survey	547
Lin, J. S.	Pittsburgh, University of	957
Liu, H. -P.	U.S. Geological Survey	963
Liu, H. P.	U.S. Geological Survey	964
Lockner, D.	U.S. Geological Survey	966
Logan, J. M.	Texas A&M University	131
Machette, M. N.	U.S. Geological Survey	557
Madin, I. P.	Oregon Department of Geology and Mineral	560
Madin, I. P.	Oregon Department of Geology and Mineral	1081
Malone, S. D.	Washington, University of	561
Mann, P.	Texas, University of, Austin	564
Marone, C.	Massachusetts Institute of Technology	134
Masse, R. P.	U.S. Geological Survey	1084
McCrory, P. A.	U.S. Geological Survey	571
McEvilly, T. V.	California, University of, Berkeley	575
McEvilly, T. V.	California, University of, Berkeley	582
McLaughlin, R. J.	U.S. Geological Survey	586
McMechan, G. A.	Texas, University of, Dallas	135
McMechan, G. A.	Texas, University of, Dallas	140
McNutt, S. R.	Alaska, University of, Fairbanks	588
Mortensen, C. E.	U.S. Geological Survey	594
Mortensen, C. E.	U.S. Geological Survey	1085
Nelson, A. R.	U.S. Geological Survey	595
Noller, J. S.	William Lettis & Associates, Inc.	600
Noller, J. S.	William Lettis & Associates, Inc.	602
Obermeier, S. F	U.S. Geological Survey	606
Oppenheimer, D. H.	U.S. Geological Survey	144
Park, S. K.	California, University of, Riverside	610
Perkins, D. M.	U.S. Geological Survey	974
Perkins, J. B.	Association of Bay Area Government	1087
Person, W. J.	U.S. Geological Survey	977
Pollard, D. D.	Stanford University	149
Pollard, D. D.	Stanford University	620
Ponti, D. J.	U.S. Geological Survey	623
Potter, C. J.	U. S. Geological Survey	627
Powell, C. A.	UNC, Chapel Hill	158
Pratt, T. L.	U.S. Geological Survey	631
Prentice, C.	U.S. Geological Survey	634

Qamar, A. I.	Washington, University of	1091
Rice, J. R.	Harvard University	162
Richards, M. A.	California, University of, Berkeley	636
Richardson, R. M.	Arizona, University of	642
Roecker, S. W.	Rensselaer Polytechnic Institute	644
Roeloffs, E.	U.S. Geological Survey	646
Rogers, A. M.	U.S. Geological Survey	986
Romanowicz, B.	California, University of, Berkeley	659
Romanowicz, B.	California, University of, Berkeley	667
Rosenberg, L. I.	Staal, Gardner & Dunne, Inc.	673
Roy, D. C.	Boston College	674
Rudnicki, J. W.	Northwestern University	168
Rymer, M. J.	U.S. Geological Survey	681
Safak, E.	U.S. Geological Survey	989
Sarna-Wojcicki, A.M.	U.S. Geological Survey	684
Satake, K.	Michigan, University of	172
Sato, M.	U.S. Geological Survey	687
Schultz, A.	U.S. Geological Survey	692
Schwartz, S. Y.	California, University of, Santa Cruz	696
Schweig, E. S.	Memphis State University	705
Shaw, H. R.	U.S. Geological Survey	710
Shearer, P. M.	California, University of, San Diego	711
Shennan, I. Durham,	University of, United Kingdom	718
Sherrod, D. R.	U.S. Geological Survey	1092
Shires, P. O.	William Cotton and Associates, Inc.	1093
Silverman, S.	U.S. Geological Survey	722
Simpson, G. D.	William Lettis & Associates, Inc.	724
Simpson, R. W.	U.S. Geological Survey	990
Sipkin, S. A.	U.S. Geological Survey	1094
Sleep, N. H.	Stanford University	176
Smalley, R.	Memphis, University of	179
Smalley, R.	Memphis University of	181
Smith, R. B.	Utah, University of	183
Smith, R. B.	Utah, University of	726
Snoke, J. A.	Virginia Polytechnic State University	189
Snyder, D. L.	Rogers/Pacific, Inc.	731
Somerville, P. G.	Woodward-Clyde Federal Service	993
Spitz, W. J.	Ayres Associate	735
Spudich, P.	U.S. Geological Survey	739
Spudich, P.	U.S. Geological Survey	1000
Stein, R. S.	U.S. Geological Survey	741
Stevens, J. L.	S-CUBED	1002
Stock, J.	California Institute of Technology	745
Street, R. L.	Kentucky, University of	1013
Suppe, J.	Princeton University	750
Swanson, D. A.	U.S. Geological Survey	756
Sylvester, A. G.	California, University of, Santa Barbara	760

Tarr, A. C.	U.S. Geological Survey	1097
Teng, T.	Southern California, University of	195
Thorson, R. M.	Connecticut, University of	763
Thurber, C. H.	Wisconsin-Madison, University of	767
Thurber, C. H.	Wisconsin-Madison, University of	1015
Tinsley, J. C.	U.S. Geological Survey	1022
Toksoz, M. N.	Massachusetts Institute of Technology	201
Toksoz, M. N.	Massachusetts Institute of Technology	771
Tubbesing, S. K.	Earthquake Engineering Research Institute	1100
Tullis, T. E.	Brown University	208
Tumarkin A. G.	California, University of, Santa Barbara	1024
Tuttle, M.	Maryland, University of	782
Tworzydlo, W. W.	The Computational Mechanics Company	216
Uba, O. G.	Spangle Associates	1044
Unruh, J. R.	William Lettis & Associates, Inc.	794
VanArsdale, S.	Memphis, University of	221
VanSchaack, J.	U.S. Geological Survey	797
Vernon, F.	California, University of, San Diego	798
Walsh, T. J.	Washington Geology and Earthe Resources	799
Weaver, C. S	U.S. Geological Survey	800
Weber, G. E.	Weber, Hayes and Associates	805
Weber, G. E.	Weber, Hayes and Associates	808
Wentworth, C. M	U.S. Geological Survey	810
Wesnousky, S. G.	Nevada, University of, Reno	813
Wesnousky, S. G.	Nevada, University of, Reno	815
West, M. W.	Michael West & Associates, Inc.	817
Wheeler, R. L.	U.S. Geological Survey	1101
Williams, C.	U.S. Geological Survey	223
Woodward, R. L.	U.S. Geological Survey	1048
Wyatt, F. K.	California, University of, San Diego	828
Wyatt, F. K.	California, University of, San Diego	832
Yeats, R. S	Oregon State University	838
Yerkes, R. F.	U.S. Geological Survey	1050
Zoback, M. D.	Stanford University	846
Zoback, M. L.	U.S. Geological Survey	852

## INDEX 2

### INDEX ALPHABETIZED BY INSTITUTION

		Page
AGRA Earth & Environmental, Inc.	Keaton, J. R.	481
Alaska, University of, Fairbanks	McNutt, S. R.	588
Arizona, University of	Richardson, R. M.	642
Arkansas, University of	Guccione, M. J.	373
Association of Bay Area Government	Perkins, J. B.	1087
Gail M Atkinson	Atkinson, G. M.	860
Ayres Associates	Spitz, W. J.	735
Boston College	Ebel, J. E.	58
Boston College	Ebel, J. E.	882
Boston College	Roy, D. C.	674
Brown University	Tullis, T. E.	208
California Institute of Technology	Clayton, R. W.	37
California Institute of Technology	Hauksson, E.	401
California Institute of Technology	Helmburger, D. V.	414
California Institute of Technology	Kanamori, H.	476
California Institute of Technology	Kanamori, H.	479
California Institute of Technology	Stock, J.	745
California, University of, Berkeley	Bray, J. D.	867
California, University of, Berkeley	Dreger, D.	319
California, University of, Berleley	Gee, L. S.	1071
California, University of, Berkeley	McEvilly, T. V.	575
California, University of, Berkeley	McEvilly, T. V.	582
California, University of, Berkeley	Richards, M. A.	636
California, University of, Berkeley	Romanowicz, B.	659
California, University of, Berkeley	Romanowicz, B.	667
California, University of, San Diego	Agnew, D. C.	234
California, University of, San Diego	Bock, Y.	267
California, University of, San Diego	Genrich, J.	347
California, University of, San Diego	Shearer, P. M.	711
California, University of, San Diego	Vernon, F.	798
California, University of, San Diego	Wyatt, F.	828

California, University of, San Diego	Wyatt, F.	832
California, University of, Santa Barbara	Archuleta, R.	856
California, University of, Santa Barbara	Tumarkin, A. G.	1024
California, University of, Santa Barbara	Sylvester, A. G.	760
California, University of, Santa Cruz	Lay, T.	526
California, University of, Santa Cruz	Schwartz, S. Y.	696
California, University of, Riverside	Park, S. K.	610
Connecticut, University of	Thorson, R. M.	763
Cornell University	Gephart, J. W.	352
Cornell University	Gephart, J. W.	360
Dames & Moore	Hengesh, J. V.	417
Durham, University of, United Kingdom	Shennan, I.	718
Earthquake Engineering Research Institute	Tubbesing, S. K.	1100
Geomatrix Consultants	Hall, N. T.	389
Georgia Institute of Technology	Frost, J. D.	914
Harvard University	Dmowska, R.	51
Harvard University	Rice, J. R.	162
Idaho Geological Survey	Breckenridge, R. M.	286
Kentucky, University of	Harris, J. B.	393
Kentucky, University of	Street, R. L.	1013
Lamont-Doherty Earth Observatory	Jacoby, G. C.	455
Lamont-Doherty Earth Observatory	Jacoby, G. C.	459
Louisiana State University	Austin, W. J.	248
William Lettis & Associates, Inc.	Kelson, K. I.	483
William Lettis & Associates, Inc.	Kelson, K. I.	486
William Lettis & Associates, Inc.	Noller, J. S.	600
William Lettis & Associates, Inc.	Noller, J. S.	602
William Lettis & Associates, Inc.	Simpson, G. D.	724
William Lettis & Associates, Inc.	Unruh, J. R.	794
Maryland, University of	Tuttle, M.	782
Massachusetts Institute of Technology	Bennett, R.	249
Massachusetts Institute of Technology	Marone, C.	134

Massachusetts Institute of Technology	Toksoz, M. N.	201
Massachusetts Institute of Technology	Toksoz, M. N.	771
Memphis State University	Chiu, J. M.	307
Memphis State University	Schweig, E. S.	705
Memphis State University	Smalley, K.	179
Memphis State University	Smalley, K.	181
Memphis State University	VanArsdale, S.	221
Michigan, University of	Satake, K.	172
Missouri Department of Natural Res.	Hoffman, D.	437
Nevada, University of, Reno	Wesnousky, S. G.	813
Nevada, University of, Reno	Wesnousky, S. G.	815
New York State University at Stony Brook	Holt, W. E.	440
Northwestern University	Rudnicki, J. W.	168
Oregon Department of Geology and Mineral	Black, G. L.	863
Oregon Department of Geology and Mineral	Madin, I. P	560
Oregon Department of Geology and Mineral	Madin, I. P.	1081
Oregon State University	Kulm, L. D.	493
Oregon State University	Yeats, R. S.	838
Pacific Geoscience Centre	Hyndman, R.	D.108
Pittsburg, University of	Lin, J-S.	957
Princeton University	Suppe, J.	750
Purdue University	Braile, K. W.	277
Queensland, University of	Gladwin, M. T.	264
Rensselaer Polytechnic Institute	Roecker, S. W.	644
Roger/Pacific, Inc.	Snyder, D. L.	731
Saint Louis, University of	Chester, F. M.	31
Saint Louis, University of	Herrmann, R. B.	95
Saint Louis, University of	Herrmann, R. B.	99
Saint Louis, University of	Herrmann, R. B.	939
Saint Louis, University of	Herrmann, R. B.	942
S-Cube	Stevens, J. L.	1002

San Francisco State University	Galehouse, J. S.	335
Soil Tectonics, Berkeley, California	Borchardt, G.	273
Southern California, University of	Aki, K.	1
Southern California, University of	Aki, K.	855
Southern California, University of	Li, Y-G.	536
Southern California, University of	Teng, T.	195
Spangle Associates	Uba, O. G.	1044
Staal, Gardner & Dunne, Inc.	Rosenberg, L. I.	673
Stanford University	Beroza, G.	7
Stanford University	Pollard, D. D.	149
Stanford University	Pollard, D.	D.620
Stanford University	Sleep, N. H.	176
Stanford University	Zoback, M. D.	846
Texas A&M University	Logan J. M.	131
Texas, University of, Austin	Mann, P.	564
Texas, University of, Dallas	McMechan, G. A.	135
Texas, University of, Dallas	McMechan, G. A.	140
The Computational Mechanics Company	Tworzydlo, W. W.	216
UNC, Chapel Hill	Powell, C. A.	158
U.S. Geological Survey	Andrews, D. J.	3
U.S. Geological Survey	Atwater, B. F.	246
U.S. Geological Survey	Blakely, R. J.	263
U.S. Geological Survey	Boatwright, J.	13
U.S. Geological Survey	Boatwright, J.	17
U.S. Geological Survey	Bohlen, S. R.	21
U.S. Geological Survey	Boore, D. M.	864
U.S. Geological Survey	Breckenridge, K. S.	870
U.S. Geological Survey	Bucknam, R. C.	288
U.S. Geological Survey	Bufe, C. G.	1056
U.S. Geological Survey	Butler, H. M.	290
U.S. Geological Survey	Catchings, R.	23
U.S. Geological Survey	Catchings, R.	25
U.S. Geological Survey	Celebi, M.	875
U.S. Geological Survey	Choy, G. L.	1060
U.S. Geological Survey	Clark, M. M.	210

U.S. Geological Survey	Crone, A. J.	312
U.S. Geological Survey	Delaney, P.	47
U.S. Geological Survey	Dewey, J. W.	1064
U.S. Geological Survey	Ellsworth, W. L.	64
U.S. Geological Survey	Endo, E. T.	329
U.S. Geological Survey	Engdahl, E. R.	331
U.S. Geological Survey	Frankel, A.	907
U.S. Geological Survey	Frankel, A.	909
U.S. Geological Survey	Frankel, A.	911
U.S. Geological Survey	Frankel, A.	912
U.S. Geological Survey	Gibbs, J. F.	918
U.S. Geological Survey	Gomberg, J. S.	85
U.S. Geological Survey	Haeussler, P. J.	386
U.S. Geological Survey	Hall, W.	87
U.S. Geological Survey	Harp, E. L.	937
U.S. Geological Survey	Harris, R. A.	89
U.S. Geological Survey	Hartzell, S. H.	91
U.S. Geological Survey	Healy, J. H.	406
U.S. Geological Survey	Heaton, T.	407
U.S. Geological Survey	Hickman, S. H.	101
U.S. Geological Survey	Hildenbrand, T. G.	428
U.S. Geological Survey	Hill, D. P.	432
U.S. Geological Survey	Hill, D. P.	435
U.S. Geological Survey	Holzer, T. L.	945
U.S. Geological Survey	Howard, K. A.	446
U.S. Geological Survey	Hudnut, K. W.	449
U.S. Geological Survey	Jachens, R. C.	451
U.S. Geological Survey	Jachenc, R. C.	454
U.S. Geological Survey	Jensen, E. G.	462
U.S. Geological Survey	Jibson, R. W.	463
U.S. Geological Survey	Johnson, S. Y.	122
U.S. Geological Survey	Johnston, M.J.S.	465
U.S. Geological Survey	Keefer, D. K.	950
U.S. Geological Survey	Keefer, D. K.	956
U.S. Geological Survey	King, C. -Y.	126
U.S. Geological Survey	Kline, F.	489
U.S. Geological Survey	Lahr, J. S.	503
U.S. Geological Survey	Lajoie, K. R.	510
U.S. Geological Survey	Langbein, J.	514
U.S. Geological Survey	Langbein, J.	522
U.S. Geological Survey	Lee, W. H. K.	534
U.S. Geological Survey	Lienkaemper, J. J.	545
U.S. Geological Survey	Lisowski, M.	547
U.S. Geological Survey	Liu, H. -P.	963
U.S. Geological Survey	Liu, H. -P.	964
U.S. Geological Survey	Lockner, D.	966
U.S. Geological Survey	Machette, M. N.	557
U.S. Geological Survey	Masse, R. P.	1084

U.S. Geological Survey	McCrory, P. A.	571
U.S. Geological Survey	McLaughlin, R. J.	586
U.S. Geological Survey	Mortensen, C. E.	94
U.S. Geological Survey	Mortensen, C. E.	1085
U.S. Geological Survey	Nelson, A. R.	595
U.S. Geological Survey	Obermeier, S. F.	606
U.S. Geological Survey	Oppenheimer, D. H.	144
U.S. Geological Survey	Perkins, D. M.	974
U.S. Geological Survey	Person, W. J.	977
U.S. Geological Survey	Ponti, D. J.	623
U.S. Geological Survey	Potter, C. J.	627
U.S. Geological Survey	Pratt, T. L.	631
U.S. Geological Survey	Prentice, C.	634
U.S. Geological Survey	Roeloffs, E.	646
U.S. Geological Survey	Rogers, A. M.	986
U.S. Geological Survey	Rymer, M. J.	681
U.S. Geological Survey	Safak, E.	989
U.S. Geological Survey	Sarna-Wojcicki, A. M.	684
U.S. Geological Survey	Sato, M.	687
U.S. Geological Survey	Schultz, A.	692
U.S. Geological Survey	Shaw, H. R.	710
U.S. Geological Survey	Sherrod, D. R.	1092
U.S. Geological Survey	Silverman, S.	722
U.S. Geological Survey	Simpson, R. W.	990
U.S. Geological Survey	Sipkin, S. A.	1094
U.S. Geological Survey	Spudich, P.	739
U.S. Geological Survey	Spudich, P.	1000
U.S. Geological Survey	Stein, R. S.	741
U.S. Geological Survey	Swanson, D. A.	756
U.S. Geological Survey	Tarr, A. L.	1097
U.S. Geological Survey	Tinsley, J. C.	1022
U.S. Geological Survey	Van Schaack, J.	797
U.S. Geological Survey	Weaver, C. S.	800
U.S. Geological Survey	Wentworth, C. M.	810
U.S. Geological Survey	Wheeler, R. L.	1101
U.S. Geological Survey	Williams, C.	223
U.S. Geological Survey	Woodward, R. L.	1048
U.S. Geological Survey	Yerkes, R. F.	1050
U.S. Geological Survey	Zoback, M. L.	852
Utah Geological Survey	Black, B. D.	257
Utah Geological Survey	Eldredge, S. N.	1070
Utah Geological Survey	Harty, K. M.	399
Utah Geological Survey	Jarva, J. L.	1078
Utah, University of	Arabasz, W. J.	4
Utah, University of	Forster, C. B.	71
Utah, University of	Hylland, R. D.	948

Utah, University of	Smith, R. B.	183
Utah, University of	Smith, R. B.	726
Virginia, Polytechnic Institute	Snoke, J. A.	189
Washington, University of	Bell, E. J.	1051
Washington, University of	Crosson, R. S.	42
Washington, University of	Crosson, R. S.	317
Washington, University of	Malone, S. D.	561
Washington, University of	Qamar, A. I.	1092
Washington Geology & Earth Resources	Walsh, T. J.	799
Wayne State University	Dusseau, R. A.	878
Weber, Hayes and Associates	Weber, G. E.	805
Weber, Hayes and Associates	Weber, G. E.	808
Michael West & Associates, Inc.	West, M. W.	817
William Cotton and Associates, Inc.	Shires, P. O.	1093
Wisconsin-Madison, University of,	Thurber, C. H.	767
Wisconsin-Madison, University of	Thurber, C. H.	1015
Woodward-Clyde Federal Services	Graves, R. W.	919
Woodward-Clyde Federal Services	Graves, R. W.	927
Woodward-Clyde Consultants	Somerville, P.	993
Yakama Indian Nation	Campbell, N. P.	291